TID-24190

meteorology and atomic energy 1968

David H. Slade, Editor
Air Resources Laboratories

Prepared by
Air Resources Laboratories
Research Laboratories
Environmental Science Services Administration
United States Department of Commerce

For the
Division of Reactor Development and Technology
United States Atomic Energy Commission

July 1968

Reprinted by the
Technical Information Center
U. S. Department of Energy

U. S. ATOMIC ENERGY COMMISSION Office of Information Services

DISCLAIMER

Available as TID-24190 for $6.00 from

National Technical Information Service
U. S. Department of Commerce
Springfield, Virginia 22161

Library of Congress Catalog Card Number: 68-60097

July 1968; latest printing, October 1977

Foreword

The first edition of *Meteorology and Atomic Energy* has found wider use throughout the world, by both nuclear and nonnuclear technologists and also over a longer span of time, than those who were connected with its production would have dared predict. The pace of research in this field has continued to be vigorous, however, and the present edition is entirely new. Most of the material, especially the experimental basis for the estimates of atmospheric diffusion and deposition, has been developed during the intervening period.

The Atomic Energy Commission is grateful to the scientists who have contributed to this book and proud of its share in supporting their efforts. We hope that the new edition will be as useful in the future development of peaceful nuclear power as the first one has been in the past and that it will also contribute to the conservation of our atmospheric environment generally.

Glenn T. Seaborg, Chairman
U. S. Atomic Energy Commission

Preface

At the time that this volume was conceived, the question of its ultimate nature arose. It was not clear whether its content and style should be that of a guide, a handbook, or a textbook. As the work progressed, it became apparent that the book would have some of the characteristics of each of the three.

The reader requiring a general knowledge of the factors relating the atmosphere and the nuclear industry may view this book as a guide, a publication that will introduce him to the concepts and terminology of the meteorologist and the health physicist and permit him to hold a more meaningful dialogue with experts when the occasion arises. As a greater variety of professional disciplines becomes involved in the relation between meteorology and the nuclear industry, the need for a timely guide increases.

Professional workers in the various fields in the nuclear industry may find this volume of use as a handbook since it contains equations, graphical aids, and an extensive bibliography.

The student can use the book as a text in the sense that it contains an outline of some of the principles of a subject of study. It does not, as most textbooks do not, comprise a complete and self-contained discussion of the field but must be used with a variety of other publications in the same field and in allied fields.

Finally, in addition to the traits of a guide, handbook, and textbook, this volume also has the characteristics of a research report. In many sections the information includes reports of recent work, the implications of which are not yet fully evaluated.

The large number of authors who have contributed to this volume guarantees that there will be some diversity of views and orientation. This diversity constitutes an accurate picture of an expanding technical field in which coincidence of approach and opinion is not always found and, indeed, may not as a general rule be possible.

The reader should not expect to find hard and fast rules for the evaluation of a specific problem. The treatment of a practical situation usually involves the use of specific quantitative techniques along with a broad variety of assumptions engendered by the imperfect knowledge of the atmosphere and the pollutant-producing device. Although these assumptions may be justified on scientific grounds, their selection can be rationally made only by someone with a broader range of experience and knowledge than can be garnered from even a careful reading of the following pages.

David H. Slade

Silver Spring, Maryland
April 1968

Acknowledgments

The preparation of this manual was supported by the Division of Reactor Development and Technology, U. S. Atomic Energy Commission.

Contributors to this volume include J. K. Angell, R. E. Baker, H. Bernard, A. B. Bernstein, H. Booth, N. Bowne, G. A. Briggs, S. B. Carpenter, J. E. Carson, P. M. Cork, W. M. Culkowski, N. Delver, C. R. Dickson, R. J. Engelmann, J. J. Fuquay, F. E. Gartrell, F. A. Gifford, Jr., G. C. Gill, J. Halitsky, J. W. Healy, C. H. Huber, N. F. Islitzer, J. M. Leavitt, P. A. Leighton, H. Moses, A. E. O'Keeffe, D. H. Pack, E. Robinson, B. Shull, I. A. Singer, D. H. Slade, M. E. Smith, G. H. Strom, F. W. Thomas, I. Van der Hoven, R. L. Waterfield, and E. M. Wilkins.

Reviewers of various sections and chapters include J. K. Angell, A. B. Bernstein, K. L. Calder, H. E. Cramer, A. N. Dingle, C. C. Gamertsfelder, P. B. MacCready, Jr., L. Machta, D. H. Pack, F. Pasquill, G. H. Strom, and I. Van der Hoven.

All of the diagrams were drafted by Mrs. Barbara F. Ritchie. Mrs. Helen Marks and Mrs. Pauline Fuhr contributed materially to the preparation of the text and bibliography. Mrs. Joan Roberts and Marian C. Fox, Editorial Branch, Division of Technical Information Extension, USAEC, edited the entire manuscript.

Contents

Chapter 1

Introduction to the Meteorology–Atomic Energy Relation

1-1 INTRODUCTION

The waste products of our civilization must be disposed of. Receptacles for this debris are the earth's land masses, water bodies, and atmosphere. The science of meteorology is important in the study of the disposition of waste products in the atmosphere.

Wastes that are released to the atmosphere consist of particles and gases. Atmospheric residence times for some of these materials may be very short, hours or even minutes. For other materials residence times may be measured in terms of years. Regardless of the residence time, the movement of gases and particles in the atmosphere will be, in large measure, governed by the motions of the atmosphere. Some atmospheric motions dictate the paths to be followed by airborne contamination; other motions determine the extent to which the contaminants will be diluted. The study of the effects of atmospheric motions on suspended pollutants is a branch of the science of meteorology variously categorized under the headings "air-pollution meteorology" or "atmospheric diffusion."

The total amount of debris released during routine atomic processes and conceived as possible from accidents is minuscule when compared with the amount of pollutants produced throughout the world by combustion. The extraordinarily poisonous nature of the radioactive materials involved, however, dictates that even small quantities be treated with respect. For instance, it has been estimated that some of the radioactive materials found in a reactor are 3 million to 2 billion times as toxic as chlorine, the most common poison used by industry. It has been calculated that, if it were possible for all the many controls and safety features in a large power reactor to fail so as to produce a disastrous release of radioactivity, this release could conceivably kill thousands of people and cause economic losses of billions of dollars. Although, in actual practice, such an accident is made to have a vanishingly small probability of occurring, the theoretical potential for such an accident is probably greater than for any work of man other than the explosion of a fission or fusion weapon.

The nuclear safety criteria that have evolved in the United States are therefore elaborate and comprehensive. Every facet of the safety problem is given a searching examination in which conservatism is the keynote. The examination starts during the design of the particular facility, continues through site selection and extends through construction and actual operation. This degree of care is exercised in the review of proposals for both routine and experimental operations. The examination is performed by individuals and groups drawn from a number of disciplines. Physicists, chemists, and a variety of engineers contribute to the safety analysis of the design and construction phases of the facility. Legal experts are alert for any inadvertent violations of the regulations governing atomic energy programs and for infringements on the health and safety of the general public. Finally, specialists in health physics, biology, hydrology, seismology, and meteorology examine the environmental aspects of the atomic facility. Virtually the entire safety analysis is performed at least twice: once by the proposing organization, which develops the detailed information, and again by the licensing agency, which critically reviews every step.

The basic question to which both the first edition of Meteorology and Atomic Energy and the present edition are addressed remains: "How can the available knowledge of the atmosphere be used to aid in solving problems of health, safety, and economics which arise in the peaceful exploitations of nuclear fission or fusion processes?" Although the answer to this question is categorical in part, there is still a tentative and even speculative remainder.

1-2 METEOROLOGY, DIFFUSION, AND ATMOSPHERIC POLLUTANTS

Recorded evidence of man's concern with the extent and effects of air pollution caused by his activities goes back several centuries. The increasingly heavy use of coal for home heating as well as for industrial power in Great Britain has led to episodes of extreme pollution in cities such as London. Luke Howard, the author of a number of books dealing with the weather in the vicinity of London, has described one of the cases of severe pollution which occurred in 1812:

> London was this day involved, for several hours, in palpable darkness. The shops, offices, etc. were necessarily lighted up; but the streets not being lighted as at night, it required no small care in the passenger to find his way, and avoid accidents. The sky, where any light pervaded it, showed the aspect of bronze. Such is, occasionally, the effect of the accumulation of smoke between two opposite gentle currents, or by means of a misty calm. I am informed that the fuliginous cloud was visible, in this instance, for a distance of forty miles. Were it not for the extreme mobility of our atmosphere, this volcano of a thousand mouths would, in winter be scarcely habitable.

The problem of air pollution from sources "of a thousand mouths" continued to gain in importance with the continued growth of the large metropolitan areas. Shortly after the beginning of this century, the large urban areas became the primary sources and receptors for these contaminants. The increase in size and diversity of the myriad of industrial processes in our civilized society guarantees the contribution of a steadily growing quantity of unpleasant or even toxic pollutants to the already overburdened urban atmosphere.

The increasing level of environmental air pollution has not gone unobserved. There have been numerous instances in the last few hundred years of attempts at pollution-level control by legislation aimed at restricting the emission of pollutants at the source. It has only been in the last half century, however, that the meteorologist has become directly involved in the study of the atmospheric problems in this field. The advent of the atomic energy industry during this period has provided a major focus for the development of air-pollution meteorology because prediction and control before the fact are essential in this new field.

The air-pollution meteorologist, much as his other meteorological colleagues, is interested in the movement of the atmosphere over scales from fractions of a second to a number of years and from a fraction of a meter to the circumference of the earth. He is interested in the mean motions of the atmosphere, i.e., those which indicate the direction and rate of bulk transport of atmospheric pollutants. He is also interested in turbulent fluctuations about these means. These turbulent eddies are the motions that disperse a pollutant as it travels with the mean motion.

The sources of atmospheric pollutants occur over an equally broad range of scales. Smoke from forest fires in British Columbia has darkened skies in western Europe. Dust from the 1883 volcanic eruption at Krakatoa was observed in the atmosphere over a period of many months during which it spread from the source near the equator to cover most of the northern hemisphere. The accumulated pollutants from an aggregation of human activities have darkened skies over cities and occasionally have caused widespread sickness and death. Noxious materials released from small industrial complexes, or even from a single stack, have resulted in human indisposition and economic penalty.

Air-pollution meteorology is concerned with all scales and types of releases of material to the atmosphere. The air-pollution meteorologist associated with the atomic energy industry draws on the experience and experimental evidence provided by the broad field of air pollution but concentrates his interest and effort in specific problem areas. These areas are dictated by the characteristics of the possible

radionuclide releases, planned or accidental, from existing or proposed facilities. Some of the special characteristics frequently associated with the release of contaminants to the atmosphere from nuclear energy facilities are given in the following paragraphs.

Most, although certainly not all, pollutant releases from atomic facilities can be approximated by a continuous flow or an instantaneous puff from a point or small-volume source. These source configurations have been the subject of numerous investigations, both theoretical and experimental, dealing with the resulting downstream concentration and exposure patterns. Much of the information in subsequent chapters will be devoted to this topic. Problems associated with larger scale or more complex sources, such as those characteristic of urban pollution, are not yet generally encountered in the nuclear field.

Most releases originate from sources in the first hundred meters above the ground, and virtually all receptors for atmospheric pollutants are located within this same layer. Natural lids to vertical dispersion in the atmosphere frequently guarantee that surface-released pollutants will remain near the surface for protracted periods. It is not surprising therefore that much of the meteorological development for the atomic energy field has dealt with the lowest thousand meters of the atmosphere with particular emphasis on the lowest hundred meters. The very lowest layer of the atmosphere is of particular interest for other, purely meteorological reasons, which will be discussed in Chap. 3. Applications of atomic energy to provide auxiliary power for space vehicles, of course, create problems involving possible high-altitude sources, and this is an area into which air-pollution meteorology will expand in the future.

Because of various engineering and conceptual safeguards, postulated ground-level releases from atomic facilities, even under the worst assumed conditions, are usually sufficiently small that concentrations of interest would not extend to great distances from the source. Much attention has been concentrated therefore on the time history of these releases within the first few kilometers from the source. Interest in longer range travel has been increasing in recent years, but techniques for dealing with these longer range (>10 to 20 km) problems are still in a relatively undeveloped state.

Thus many of the past and present requirements of the atomic energy industry have resulted in meteorological investigation that is largely confined to transport and diffusion over a limited horizontal, vertical, and temporal range. Exceptions to this broad generalization will be noted in the appropriate chapters.

1-2.1 The Role of the Meteorologist in the Atomic Energy Industry

From a meteorological viewpoint all atomic facilities fall into two broad and overlapping categories: (1) those which have a planned and predictable effluent to the atmosphere and (2) those in which any significant effluent would be due solely to an accident. In the first category are such diverse systems as boiling-water reactors, fuel-processing plants, and any one of a large number of atomic experimental systems. A primary representative of the second group is the well-contained pressurized-water reactor. The magnitude of any of the releases can vary greatly in theory if not in practice. Simply stated, the role of the meteorologist is to evaluate the effects of weather and terrain on the concentration of the effluent as it travels from source to receptor. Assuming that limiting levels have been established for concentration of the released radioactive species, the meteorologist participates in the engineering by providing answers to the questions: "To what extent can the atmosphere be effectively utilized to dispose of pollutant materials?" for the first category of facilities and "How much of a safety factor can the atmosphere provide?" for the second.

The first consideration of meteorology in the atomic energy field was probably the "meteorological reconnaissance" of the Hanford, Wash., area, now the site of the Pacific Northwest Laboratory of the Battelle Memorial Institute. Dr. Arthur Compton of the Metallurgical Laboratory of the University of Chicago asked Dr. Phil Church, now Chairman of the Department of Atmospheric Sciences of the University of Washington, to make a meteorological survey of the Hanford area in preparation for the installation of the production reactors. The request was made in January of 1943. By March of that year, the first surveys

of the area had been completed, the sources of existing data had been investigated, and plans had been formulated for an experimental study. In preparation for this study, a wind and stability measurement network was installed and balloon wind measurements to heights of 1000 m were conducted. Oil fog generators were soon installed, and a massive program of diffusion experiments was initiated. By December of 1944, a 120-m tower had been installed. This tower is still in use.

It is to the credit of the founders of this new technology that the potential problem was realized very early in the U. S. program and early action was initiated to study and forecast the geophysical aspects of the movement of radionuclides in the atmosphere, in the ground, and in water bodies. The primary motivation for these at times costly studies has been the extreme interest and concern for the safety and well-being of workers in the nuclear industry and the general population.

The science of meteorology enters the atomic energy field at three reasonably distinct phases in the life history of any typical facility: (1) during the choice of site and adaptation of design and operating procedure to its special characteristics, (2) during routine operations, and (3) in the unlikely event of an accident.

The choice of the site for a nuclear reactor is a complicated decision that depends not only on the factors that govern site selection for conventional industries, such as the availability of land, water, and labor and a market for the product in the general region under consideration, but also on such factors as the nature of the particular facility in regard to its potential for routine or accidental releases of radionuclides, the population distribution about the site, and, finally, the environmental characteristics of the surrounding area. Among these characteristics are meteorology, hydrology, and seismology. The final choice of the site is not usually based solely on any one of these characteristics. As an example, a particular site might be extremely undesirable from a meteorological point of view alone. The possible risk from an accidental release, however, could be very small if the region were neither populated nor farmed or if the reactor were of a type with which there existed much operating experience at other locations over many years and whose inherent stability and safety were very well established. Moreover, additional engineering safeguards might be incorporated to balance the deficiencies of the site. Again, if proximity of the site to the nearest populated areas were an important economic factor, meteorology would be one of the tools used to decide just how great a distance between the facility and the population would be necessary to ensure safety in the case of the most severe credible accident.

The choice of the site may depend on the routine release of radionuclides from the facility rather than on accidental release. Here again the dispersive capacity of the atmosphere at the location can be considered to determine the usefulness of the site. Further, the release of normal effluents can sometimes be carried out under positive meteorological control; i.e., the release can be adjusted to the current state of the atmosphere so that the effluent is diluted to previously determined safe levels. Because the atmosphere is usually enormously efficient in diluting material released into it, it would be, within limits, economically unwise to ignore completely or to fail to utilize properly this dispersive capacity.

Thus from this cursory treatment of the subject it would appear that the extent of the program necessary to evaluate the environment of a given site is not subject to any simple set of rules. Many of the small facilities of conventional design that are in operation have had minimal site-evaluation programs. In many cases these evaluations were carried out without the direct participation of meteorological specialists. On the other hand, some of the large reactors or those with unique problems of population distribution or unconventional design have had site evaluation studies that involved rather large staffs of meteorologists, long series of observations at the site, and rather detailed research into some of the characteristics of the environment. Often these studies continued for periods as long as a few years before the actual commencement of operations at the facility.

Once the atomic facility has been completed and routine operations have begun, the role of the meteorologist is usually considerably reduced. Again, with many of the smaller or more conventional reactors, meteorological aid has been completely dispensed with. The experience gained in running the systems in these

cases has indicated that the effect of any routine effluent is negligible; thus the plant has little effect on its environment. However, there are atomic facilities, primarily at the various national laboratories and test sites, from which routine releases may be large enough that continuous meteorological advice is required. It is not unusual for particularly high release processes or experiments to be carried out under meteorological control. Usually in such cases the meteorologists at the particular sites will have prepared in advance forecasting schemes that will allow the rapid computation of the expected wind direction and diffusion conditions. Most civilian power or test reactors, however, have been designed so as to require no further meteorological assistance once they are operative.

The third function meteorology must be prepared to perform in the interest of safety would occur during an unplanned release of radionuclides from any nuclear system. Presumably, if the estimate of the possible release of material made during the site evaluation is not exceeded and if the weather conditions at the time of the accident are not more limiting than had been postulated, the safety of the surrounding population and environment will not be threatened. Even in such cases, however, immediate prediction of the direction of movement and the rate of diffusion is extremely useful if only to assist the radiological-monitoring organization to establish promptly and fully the actual extent of environmental contamination. Such information may frequently be estimated by a meteorologist from the simplest instrumentation at the site or even from the weather data that could be furnished by the nearest U. S. Weather Bureau station. The use of such raw data by a staff prepared by a minimal meteorological training program will be much better than no meteorological input at all. A meteorologist at a well-equipped weather station can offer considerably greater help in an accident situation by making rapid quantitative estimates of the extent and severity of contamination and by effectively utilizing early radiological-survey results to reassess the situation. Moreover his services may be of great use in the postmortem evaluations of some of the details of the accident, including deductions regarding the magnitude of the release based on the observed contamination patterns. In the unlikely event of a really severe accident, the services of the meteorologist would be invaluable for carrying out any large-scale countermeasure programs.

Of the three areas encompassing the use of meteorology in the interest of safety, the initial site evaluation is currently the area of greatest meteorological involvement. This is certainly due in part to the legal requirement made in the interest of safety that the environment of the proposed site be carefully scrutinized and that a formal hazards evaluation be prepared for submission to the Atomic Energy Commission.

1-2.2 A Brief History of the Meteorology–Atomic Energy Relation

1-2.2.1 History of the Atomic Energy Industry. The atomic energy industry had its beginning in the published reports of Hahn and Strassman and Meitner and Frisch in 1938 and 1939 on the discovery of fission. By 1942, with the help of Enrico Fermi and a number of other scientists, a pile of graphite and uranium was made to go "critical" (have a sustained chain reaction by fissioning with neutrons) under the stadium at Stagg Field in Chicago. This first reactor, known as a critical assembly because of its low power level, was called Chicago Pile 1 (CP-1). It was later moved to the grounds of the Argonne National Laboratory. The initial work was performed under the code name Manhattan Engineer District. Because of its low power (about 200 watts), this reactor generated a small inventory of fission products; so its inherent hazard potential was not great. Nevertheless the probability of an accident should have been considered rather high in view of the lack of knowledge and experience on the part of the designers and the extremely experimental nature of the reactor.

In 1943 the X-10 air-cooled graphite reactor was built at Oak Ridge, Tenn., also by the Manhattan Engineer District. This reactor operated at a power of 1.0 to 2.0 Mw and served as a prototype for the plutonium-production reactors on which construction was begun at Hanford, Wash., during the following year. This reactor had a rather large fission-product inventory, and, because of its experimental nature and

the lack of knowledge and experience, the probability of an accident was rather large. However, because of the inherent slow response of this type of reactor and because the control system was designed to make it even slower, safe operation was an important consideration from the start.

In 1944 construction of the Hanford reactors for the production of plutonium began. Because these reactors were designed to generate pound quantities of an element in a short period of time by the formation of individual atoms, they had to operate at comparatively large powers. These reactors were somewhat different from the Oak Ridge Graphite Reactor; so engineers did not have a sufficient foundation of knowledge and experience to have confidence in the reactor behavior. Also built at this time was the Hanford 305 Test Reactor, a 30-watt graphite test reactor that was used to make certain tests of the graphite moderator and of the uranium slugs.

As soon as a charge of fuel came out of the plutonium-production reactors, a large source of gaseous effluents was encountered. For the plutonium produced to be removed from the uranium and other fission products, it was necessary to dissolve the fuel by various chemical reactions. During the early stages of this process, all the noble-gas fission products, notably radioactive isotopes of xenon and krypton, were released. It was not feasible to remove them by a filter system; they were released to the atmosphere in rather large quantities.

As part of this same separation process, large quantities of radioactive iodine were also evolved. In time methods were developed for filtering or otherwise removing most of the iodine from the effluent. Iodine remained one of the most important elements in the effluent as far as biological effect was concerned. Because of the high volatility of its oxide, ruthenium was also occasionally lost in large quantities in the gases from the chemical-separation plants at Hanford.

The reactors at Hanford were operated in such a manner that the loss of fission products from the fuel during normal operation was minimal. There was some production of ^{14}C and ^{41}Ar in the gases used to cool the graphite at various stages in the development of the reactors. These effluents never acquired great importance, however, because there was no way in which a large unexpected release could occur. Carbon-14 and ^{41}Ar were always released as fast as they were formed, and the rate of formation was known and controlled.

Another source of radioactive effluent from the Hanford reactors was created in the process of changing the fuel. The fuel was changed by pushing new fuel slugs into one end of the horizontal process tubes and forcing the spent fuel out the other end into a canal of water. Owing to the heat generated by the fission products and to the pyrophoric nature of the uranium and plutonium contained in the fuel, however, a fuel element would occasionally catch fire while it was falling from the process tube to the canal. When the fuel caught fire, krypton, iodine, and other fission-product elements were driven off, and the release occurred in an area in which ventilation control and efficient filtering were difficult. Therefore great care was taken to prevent these fuel fires.

In 1944 two experimental reactors were built to investigate other configurations for producing chain reactions. One of these was a homogeneous water-boiler reactor at Los Alamos (HYPO) operated at a power level of 5.5 kw. From such a reactor the xenon and krypton are released as they are formed once the ability of the water to dissolve them has been exceeded. The volume of these gaseous nuclides is extremely small; so they can be stored for extended periods while they decay, and thus the residual radioactivity in the final effluent is minimal.

Also in 1944 a heavy-water-moderated reactor (the CP-3) was built at Palos Park, Ill. It operated at a power level of 300 kw. Because this reactor employed clad fuel that was never removed from water while the fuel was hot, there was little effluent from it. Its fission-product inventory, which was, of course, proportional to its power level, was the largest accumulated up to that time. The risk was accepted as necessary at the time because of the national-defense aspects. What was learned from this reactor helped in the design and construction of the Savannah River production reactors in the 1950's.

In 1946 the Atomic Energy Commission was formed to carry out the research and development required to obtain useful power by means of atomic energy. In this year the first reactor

designed to produce power was built at the Los Alamos Scientific Laboratory. Called "Clementine," it operated at a power level of 20 kw on plutonium fuel with mercury for coolant. Even by today's standards this would be an unusual reactor of advanced design with unknown properties which should be treated with caution and respect. The location at Los Alamos provided the degree of isolation that was deemed appropriate at the time. The potential effluent from an accident included plutonium and radioactive mercury as well as the volatile fission products. Although plutonium is not at all volatile, its relative biological hazard is so great that its effective hazard is often on a par with the products that it produces during fission.

In 1948 an assembly known as PPA was constructed at Knolls Atomic Power Laboratory (KAPL) near Schenectady, N. Y. This was the first critical experiment in the military reactor program. The same year the Advisory Committee on Reactor Safeguards was established by the AEC to evaluate sites for new reactors, and the role of meteorology in the atomic energy program took on more importance.

In 1950 the AEC reactor program expanded greatly. A number of reactors were completed that year including the Los Alamos Water Boiler (SUPO), the 20-Mw gas-cooled graphite reactor at Brookhaven National Laboratory, the Low Intensity Training Reactor (LITR), the Bulk Shielding Reactor, and a homogeneous critical facility at Oak Ridge National Laboratory.

In 1951 KAPL built the Thermal Test Reactor No. 1 (TTR-1), and Argonne built the Experimental Breeder Reactor–I (EBR-I) at the National Reactor Testing Station (NRTS), which had been established in Idaho. The latter reactor produced the first electricity generated by atomic energy in this country. Los Alamos also built their "Little Eva" that same year.

In 1952 the Materials Testing Reactor (MTR) was completed at NRTS, and engineering testing in addition to physics testing for reactors was made possible. The same year two additional small homogeneous reactors were built, including one at a new site, the Atomics International Critical Experiment Laboratory at Santa Susana, Calif. The foundations of the atomic energy industry were now laid, and the industry was ready to expand rapidly. During this same period the naval reactors program was initiated at KAPL and at Bettis, the Atomic Power Division of Westinghouse, and there were naval and aircraft reactor programs, both operating at NRTS. Research reactors were being built at universities, and more production reactors were constructed at Savannah River. The number of locations was increasing, the types of reactors were increasing, and the power level of each unit was increasing. The hazard of effluent from the reactors during normal operation and in the event of an accident was becoming of greater importance to the public.

The experience meteorologists gained at the government facilities furnished the information that enabled them to make an intelligent appraisal of conditions at new locations where privately owned reactors were being built. Most of these reactors have contributed insignificant amounts of radioactivity to the environment because of the nature of their operation. The necessity for removing air and radiolytic gas from the primary system presents the problem in some reactors of avoiding the release of fission products by the same process. Attempts to control the fission-product release by delaying the effluent en route to the stack have only been partially successful, and considerable quantities of short-lived fission products may be released when delays of only a few minutes are used. The problem can be essentially eliminated by using holdup tanks that delay the release for a day or two.

During the past decade there has been a continuing increase in the number and type of reactors and, most important, a significant increase in power levels. Thermal power levels of 500 to 1000 Mw and higher are becoming relatively common for reactors designed to generate electricity. Furthermore there has also been a significant upsurge in the construction of large reactors for electrical power on a private-ownership basis at sites in no way connected with AEC operations.

In addition to the direct increase in reactor number and power level, there has been a diversification of reactor types, particularly in the power-reactor-prototype power range. These types include those with a variety of coolants including high-temperature gas, liquid metals, organics, and heavy water. Advanced types with liquid or slurry fuels and continuous

fission-product removal systems have been designed. The gaseous effluents from these new reactors are not likely to be different in kind but will probably be different in quantity and mode of release.

It appears that in the future three major developments will influence the need for knowledge of atmospheric transport and dilution of reactor-produced effluents: (1) the increase in the number of large power reactors located close to large population centers and the concurrent proliferation of potential sources; (2) the entry of private industry into the fuel-processing field at several U. S. locations; and (3) the possibility that very large reactors, perhaps in excess of 10,000 Mw(t) power, will be advantageous for some applications, such as combined desalinization and power production. The waste-disposal requirements, including the safe and judicious use of atmospheric dispersal, can only increase.

1-2.2.2 The Development of Diffusion Theory. The early theoretical framework for atmospheric diffusion was based on macroscale analogies to the molecular processes of heat and momentum transfer. In such systems the diffusion transfer of a property is described by the product of the gradient of the property and a coefficient of diffusivity. Transport is assumed to occur along the gradient from regions of high values of the property to regions of lower values. The estimation of diffusion then resolves itself into a search for representative values of the coefficient of diffusivity and a search for the solutions of differential equations that represent the distribution of the property in space and its variation in time. The use of the gradient-transfer approach revealed that the diffusion coefficients varied with the space scale of the phenomena as well as with height above the surface and physical state of the atmosphere. In spite of these and other shortcomings, the description of diffusion by gradient-transfer processes has found considerable application in both research and studies oriented to practical problems.

In the early 1920's the British scientist G. I. Taylor introduced the concept of diffusion by continuous motion, which suggested that the final position of an elementary particle in a turbulent medium could be determined from a knowledge of the turbulent velocities acting upon it during its travels from source to destination. If the particles were those in a smoke cloud and were expected to faithfully follow the motions of the air in which they were embedded, the statistical time history of smoke concentration within the cloud could be forecast from a knowledge of the spectrum of the existing atmospheric turbulence. Although this essentially kinematical–statistical approach does not concern itself with the dynamical and thermodynamical causes of the turbulent motions, it has been responsible for furnishing many of the working diffusion techniques that will be discussed in the remainder of this volume. The well-known Sutton equations of diffusion are a direct result of Taylor's theorem. Another technique currently gaining favor in applied diffusion studies uses wind-speed and direction-fluctuation measurements and the Taylor hypothesis to yield a direct indication of atmospheric diffusion. Both the techniques resulting from gradient-transfer considerations and those based on the Taylor theorem will be discussed in considerable detail in Chap. 3.

Progress in diffusion meteorology has always been intimately associated with progress in the fundamental studies of atmospheric turbulence. Throughout the development of the classical diffusion theory, there has been the recognition that these semiempirical and statistical representations of turbulence would eventually yield to more direct physical approaches. Currently there is great interest in studies of the dynamic and thermodynamic mechanisms of the generation, distribution, and decay of atmospheric turbulence. Working directly with basic physical qualities, such as heat flux, kinetic energy, and surface configuration, turbulence specialists are today rapidly constructing an edifice of theory that may be expected to produce the next generation of practical diffusion techniques.

1-2.2.3 The Development of Diffusion Experiments. The first large-scale organized effort in the field of diffusion experiments began in England in 1921 when the Meteorological Department of the Chemical Defense Experimental Station at Porton was opened. Until this date there had been no accurate and comprehensive assessments of the rate of diffusion as measured by the dispersal of gases and smokes in the atmosphere. The pioneering work of this department

in the use of smoke plumes and puffs led directly to the most important result of published studies carried out during the first 10 years of diffusion experiments: the determination of the shape of the crosswind distribution of material released from a point source. The Gaussian character of the average crosswind concentration distribution was rapidly established by the use of techniques that are quite primitive by today's standards.

Experimental determinations of diffusion processes have increased significantly in number and sophistication during the last 20 years. These experiments have been of three very general types. First are the studies of the very largest scale of diffusion and transport which use as source material the products of nuclear detonations or natural cataclysms injected into the troposphere or stratosphere. The second group contains the smaller man-made sources. These consist of instantaneous or continuous point, line, or area sources, usually observed to horizontal distances of about 10 km and typically represented by the release of effluent from an industrial process via a stack or fissure in a container. Finally, there are the primary micrometeorological experiments, the goal of which is the understanding of basic atmospheric processes. Although the practical interest in this volume is focused on the second of these groups, the contributions from micrometeorological studies are essential to the theory and suggest much of the practice for the applied investigations.

As will be evident from the detailed discussion in Chap. 4, one of the outstanding features of many of the experiments on man-made sources has been the large sampling grid networks, containing hundreds of samplers mounted on towers and at the surface. Quantitative values of the downstream concentration of emitted tracer are therefore available over the entire horizontal as well as over some of the vertical extent of the emitted plume or puff. Extremely sensitive techniques were developed for identifying and measuring these concentrations, and the concurrent observations of the meteorological variables then furnished the necessary data for evaluating the various theoretical or empirical formulations. Most of the diffusion measurements have been made within the first few kilometers from the source. There have, however, been experiments at greater distances, including some as far as 100 km from the source. Transport and diffusion at distances greater than 10 km is still a field for further experimentation, and detailed studies at distances greater than 100 km have yet to be carried out.

Many large diffusion experiments have been conducted in the United States and abroad. They can be divided into two major types: (1) experiments to determine the characteristics of a particular site and (2) experiments to gain basic meteorological knowledge. Some of these experiments have been designed to furnish additional values of Sutton's coefficients. Other experiments have yielded greater insight into the relations between wind fluctuation and pollutant dispersal. The rate at which airborne material is deposited on surface features has also been the subject of some series of experiments, and a number of important experiments have been conducted to clarify some of the basic physical processes of atmospheric turbulence. On a very large scale, high-level debris from the various nuclear-weapon tests has been used to delineate some of the characteristics of transport and diffusion in the stratosphere. In these cases the space scale has been global, and the time scale has been a few years.

Although much has been learned from the various experiments, there are still areas that have received no more than cursory attention. Experiments in long-range diffusion from surface sources are still largely in the future. Diffusion in the vicinity of topographic inhomogeneities, such as land–water boundaries or irregular terrain, needs experimental research. The increasing interest in placing power reactors in locations dictated by economic necessity indicates that the atmospheric characteristics over cities will receive increasing experimental attention.

1-2.2.4 The Development of Sensors for Turbulence and Diffusion Estimates. The equipment used in atmospheric diffusion studies has also become more advanced during the last 20 years or so. It may be said that there have been no basically new meteorological sensors developed in this period. Rather, progress has been most apparent in the fields of sensor engineering. As a result the instruments available as off-the-shelf items today have accuracies and sensitivities that were available only in specially en-

gineered systems a few years ago. Moreover many of the high-precision instruments have been designed to allow continuous operation with a minimum of recalibration and repair.

Great strides have been made in the methods of accumulating and processing the data generated by the large and rapidly growing numbers of instrumental systems. Recent advances in electronics enter into every phase of the data-handling problem. It is not unusual to find instrumental systems that read out directly in terms of the processed data necessary for a specific application rather than in the raw data supplied from the sensor. Finally, the electronic computer has entered into virtually every phase of data processing in both research and operational diffusion studies.

1-2.2.5 Development of Working Techniques. The working techniques referred to in the title of this section, one of the major subjects of this volume, are those dealing with the estimation from readily available meteorological data of the diffusive potential of the atmosphere.

Of the many techniques that have been advanced to estimate diffusion in the lower atmosphere, only those of Sutton and, more recently, Pasquill have found more than limited acceptance. Both involve substitutions in a Gaussian interpolation formula that relates the downwind concentration to the vertical and horizontal concentration-distribution function in a plume or a puff as a function of travel time or distance. In both techniques these concentration-distribution functions are evaluated from actual tracer-release tests and are related to meteorological measurements taken at the time of the smoke release. Sutton's technique relates the downwind-concentration values to the vertical gradient of the wind speed, atmospheric "gustiness," and a measure of surface roughness. Pasquill relates concentration to wind-direction fluctuations and wind speed only. This approach has been adopted by an increasingly large audience. A discussion of the theory behind Pasquill's technique appears in Chap. 3; many corroborating measurements may be found in Chap. 4.

It is unfortunately true that theory has not advanced to the point at which precise diffusion estimation can be made directly from meteorological measurements. It is therefore frequently necessary to perform those diffusion experiments discussed in the last section in order to verify the theoretical predictions in those situations where the assumptions of the theory are reasonably well fulfilled and to obtain estimates of the values of the diffusion parameters in the remaining situations. The diffusion parameters measured in this way have been categorized by the meteorological conditions existing at the time of the experiment, and these empirically determined values can be used as a "working technique" that requires no atmospheric knowledge other than that available from comparatively simple instrumentation. When such parameters are used under conditions similar to those under which they were derived, fairly good estimates of downstream concentration can be obtained. A reasonably high degree of subjective skill and basic meteorological acumen is necessary if diffusion is to be estimated under anomolous conditions.

A fairly large number of diffusion-estimation techniques are based on a subjective appreciation of diffusion theory but utilize an empirical approach to the determination of the actual diffusion parameters. Although frequently successful, hopefully such techniques will become increasingly unnecessary as the physical theory of atmospheric diffusion develops.

1-2.2.6 Advances in General Meteorology. The most common question asked of meteorologists by any lay or professional group deals with the future state of the weather. Although this question is only one of a number that are asked by the atomic industry, it is both a basic and an important query. It is only fair to say that the accuracy of a typical forecast for a period of perhaps 24 hr in the future has not shown any marked improvement in the last 20 years although there has been a considerable increase in the ability to use forecast information more efficiently.

The overall situation is not, however, quite as bleak as it would seem on the basis of this information alone. For one thing the atomic energy industry depends heavily on climatological estimates of both surface and upper-air variables, and here there have been major advances in the years since World War II. There are over 14,000 surface weather observing stations currently operating in the United States and producing data that are used to com-

pile climatologies. One thousand of these stations collect all the normally observed meteorological data, and the remaining stations collect a more limited sample. This great mass of information would be of little use if some central clearing house were not available for storing it. Fortunately the National Weather Records Center of the Environmental Science Services Administration (ESSA) not only stores but also processes this great mass of weather data in many ways that are useful to those working with atomic–meteorological problems. Therefore a great fund of climatological data is readily available for many locations in the United States and abroad.

The daily weather forecast may not have shown a great deal of improvement, but many other meteorological areas have. Fewer than 15 years ago, forecasts of severe weather, tornadoes, and violent thunderstorms were of the most general and rudimentary kind. Today this branch of prediction is highly developed with accuracy approaching a few hours in time and less than 150 km in space. Forecasts of upper-air flow patterns by numerical techniques utilizing the latest computers have also shown a very significant increase in accuracy. This information may be of considerable help in nuclear aerospace operations. Finally, data dissemination techniques have improved markedly. It is comparatively simple and frequently inexpensive to receive current data in both raw and analyzed form at any point in the country served by telephone lines.

1-2.2.7 How Much Meteorology Is Necessary? The answer to the question posed by the heading of this section is dependent on the particular site and on the nature of the facility to be operated on it. In the early days of the nuclear industry, accumulated experience in operating atomic facilities and in assessing the environment was less than it is today; so it was frequently deemed necessary to perform long and costly site evaluations for each new facility. This approach was justified by the normal caution felt when first embarking on the unknown. With increased experience in both atomic operations and diffusion meteorology has come a discernible tendency on the part of the meteorologist to identify, early in the planning stages, the salient meteorological features of the location and to concentrate on these in his analysis. This streamlining of the analytical procedure, reflecting greater confidence, is justified meteorologically by experimental experience and theoretical advances in the fields of atmospheric turbulence and diffusion.

An increase in knowledge has also taken place in the fields of atomic physics and engineering. In fact certain types of reactors and other atomic facilities have become so standardized that the meteorological evaluation can be considered of minimal importance.

On the other hand, the increase in understanding of the biological results of the uptake of radionuclides has indicated the need for increased attention to meteorological processes other than diffusion. Deposition and washout processes for instance are currently fields of increasingly strong interest. Long-term dosage calculations and dosages at great distances from the sources have also been the subject of increased attention. The quickening interest in the use of atomic power sources in the aerospace industry also results in meteorological programs of completely different scope than those for surface-based sources. Many of the problems in this field have not been identified; so the extent of meteorological involvement in these studies has yet to be fully delineated.

We have not then given a definite answer to the question of how much meteorology is necessary. We have only outlined the trends. An answer, if it exists at all, is contained in the discussions of meteorology and health physics computations in subsequent chapters and may only be realized by the application of this information to a particular problem.

1-3 OUTLINE OF THE REMAINING CHAPTERS

Chapter 2, entitled "Meteorological Fundamentals for Atmospheric Transport and Diffusion Studies," is intended as an introduction to the general field of meteorology with emphasis on those characteristics of particular interest to the study of diffusion, transport, and atmospheric pollution. This chapter should be useful to those who are coming upon the subject of meteorology for the first time. A bibliography of selected textbooks and other publications dealing in greater detail with the information in this chapter is included.

Chapter 3, "An Outline of Diffusion Theories for the Lower Layers of the Atmosphere," contains in some mathematical detail the basic physical formulations behind the practices of diffusion meteorology. This chapter is divided into three parts dealing, respectively, with the mean flow in the planetary-boundary layer, diffusion theories, and diffusion models. It should be useful both to meteorologists receiving their first exposure to this specialized field and to technicians in other disciplines. Some mathematical knowledge is assumed of the reader.

The fourth chapter, "Diffusion and Transport Experiments," describes some of the more important diffusion experiments accomplished primarily over the last 10 years. The motivation for these experiments was in many cases the necessity for practical answers to questions of local diffusivity at particular sites. As a result, the complete range of meteorological data ideally required for investigating a variety of approaches to diffusion estimation is not always available. An attempt is made in this chapter, however, to categorize diffusion data in terms of some objective measure of wind fluctuation whenever possible.

Chapter 5, "Processes Other Than Natural Turbulence Affecting Effluent Concentration," deals with those effects which reduce or otherwise change the distribution of airborne pollutants. Included in this chapter are discussions of plume rise, deposition, and washout as well as diffusion in the vicinity of structures.

Meteorological instruments and techniques are the subject of Chap. 6. Particular stress is given to the measurement of the various features of the wind in view of the current trend toward the use of wind-fluctuation techniques for the prediction of diffusion.

Chapter 7, "Radioactive-cloud Dose Calculations," introduces the reader to the aspects of nuclear technology necessary for radioactive-cloud dosage calculations. Included are discussions of terms and concepts in this field, sources of radioactive gases and aerosols, and external and internal dosage computation methods.

In Chap. 8, "Environmental Safety Analysis," the radiological information developed in Chap. 7 is used with the meteorological information presented in earlier chapters in discussions and illustrations of methods of environmental safety analyses.

An appendix listing diffusion equations, various constants, conversion factors, and other information useful to the reader and the references for the various chapters are included at the end of the volume.

Chapter 2

Meteorological Fundamentals for Atmospheric Transport and Diffusion Studies

2-1 INTRODUCTION

The science of meteorology is composed of a variety of subdisciplines, all of which have some bearing on the understanding of transport and diffusion processes in the atmosphere. One of the purposes of this chapter is to present some of this peripheral information to those readers who are not meteorologists. Another purpose is to introduce the reader to the concepts and terminology used in atmospheric transport and diffusion studies.

The early sections of the chapter deal with some of the basic physical atmospheric processes and the weather systems that result from these processes. One section is devoted to climatology and conventional weather data. The later sections deal, in a generally qualitative way, with the fundamental concepts related to transport and diffusion studies. Many of these topics are developed in a more rigorous mathematical form in Chap. 3. The reader who wishes to go further in his study of basic meteorology, turbulence, and diffusion will find a list of standard textbooks at the end of this chapter.

2-2 THE PHYSICAL BASIS OF LOCAL CLIMATE

2-2.1 Solar Radiation and the Earth's Energy Balance

The present atmosphere of the earth is the result of various geophysical, biological, and chemical processes, some of which are still going on. The chief constituents of the atmosphere are nitrogen and oxygen, which make up 75% and 23%, respectively, of its total mass. In addition, there are very small quantities of argon, neon, helium, and other inert gases, methane, nitrogen dioxide, and hydrogen, as well as small, variable amounts of water vapor, carbon dioxide, and, in the upper atmosphere, ozone.

The permanent constituents of the atmosphere are found in the same proportion throughout a region called the homosphere, which extends from the surface to a height of about 85 km; the chief variable constituents, water vapor and carbon dioxide, are found primarily in the lowest few kilometers. For practical purposes air may be treated as if it were a single gas with its own physical and chemical properties. For thermodynamic considerations air is assumed to be an ideal gas.

The sun is the primary source of energy for the earth–atmosphere system, and its influence is felt in the radiant energy that is the basic source of heat to the atmosphere. The sun radiates energy approximately as if it were a blackbody at a temperature of about 6000°K. (The intensity of blackbody radiation is proportional to the fourth power of the temperature, and the wavelength of maximum intensity is inversely proportional to the temperature.) About 99% of the sun's radiation is in the 0.15- to 4.0-μ wavelength range, with maximum intensity at about 0.5 μ in the visual portion of the spectrum. A small portion of this radiant energy is intercepted by the earth; the exact amount reaching the earth's surface depends on time of year, time of day, latitude, topography, and weather conditions.

Were it not for the presence of the atmosphere and the complexity of the earth's surface, the distribution of solar energy would be a simple matter. The intensity of solar radiation reaching any point on the earth's surface would be greatest where the sun was directly overhead

and would diminish with zenith angle, becoming zero where the sun was below the horizon. The total amount of solar energy received at the surface in the course of a day would be the same at every point around a parallel of latitude and, owing to the tilt of the earth's axis, would display a seasonal variation. The distribution of radiant energy would be determined solely by the relative positions of the earth and the sun. On June 22 the duration of sunlight would, if there were no atmosphere, vary from zero south of 66°30'S to 12 hr at the equator and 24 hr north of 66°30'N. At this time the total daily radiation would have a maximum value in the Arctic, where the sun would be continuously above the horizon. On December 22 the opposite situation would prevail with the Antarctic receiving the greatest daily radiation. On March 21 and September 22, when the earth's axis is perpendicular to the solar beam, the total daily radiation would be greatest at the equator, diminishing to zero at both poles. Radiation values during the summer would be greatest in the southern hemisphere because the earth is closest to the sun in January. If the year as a whole is considered, the greatest total insolation would be found at the equator with insolation values decreasing toward each pole.

In the presence of the atmosphere, the picture changes. The solar energy is depleted by reflection from cloud tops, scattering by airborne particulates, and absorption by atmospheric gases with subsequent reradiation both to space and to the ground. The greatest relative depletion takes place near the poles where the sun is at a low angle and its rays must pass through the greatest thickness of atmosphere. Therefore the primary effects of the atmosphere are to reduce the values of insolation, generally, and to displace the summer maximum in the northern hemisphere from the pole to about 35°N.

Of the solar energy reaching the earth's surface, a portion is reflected back to space, and the remainder is absorbed at the surface. The absorbed energy may be converted to heat energy, either directly by raising the surface temperature or indirectly by causing water to evaporate, or it may be converted to mechanical, electrical, or chemical energy. This energy may set up convective motions within the atmosphere, or it may be stored in the earth for lengthy periods, such as occurs when chemical energy resulting from photosynthesis is stored in fossil fuels for many millennia before being converted to heat. The earth has an average surface temperature of about 280°K to 300°K and radiates approximately as if it were a blackbody in that temperature range, over a range of wavelengths extending from 4 to 80 μ with maximum intensity at a wavelength of about 10 μ in the infrared range. A large portion of this energy is absorbed and reradiated by the atmosphere, which does not behave as a blackbody but absorbs and radiates in various wavelength bands. Water vapor and carbon dioxide are the chief absorbing gases although both are nearly transparent to wavelengths from 8.5 to 11 μ, in the vicinity of the peak of the curve. Since these two gases are concentrated in the lowest layers of the atmosphere, most of the absorption takes place there.

Because the oceans occupy a major portion of the earth's surface (70%), absorption of solar radiation at the surface is accompanied by evaporation of seawater. The latent heat used in evaporation is released when the vapor condenses, usually at higher levels, in storm and cloud systems. Through rather complex mechanisms this energy becomes available for driving the various atmospheric wind systems—tropical hurricanes, subtropical anticyclones or high-pressure systems, mid-latitude cyclonic storms, the jet stream, and smaller circulations of all sizes. The well-ordered large-scale air motions are accompanied, especially near the surface, by irregular small-scale motions called turbulence. These motions exist in a continuous range of sizes extending down to fractions of a centimeter. The large turbulent whirls, or eddies, are thought to transmit energy to the small ones until ultimately this energy is dissipated as heat. The complex interrelations among the various atmospheric motions have the effect of transporting poleward the excess solar energy received in the tropics and thus of maintaining the heat balance of the atmosphere.

Highest air temperatures are found at 0° to 20°S in January and at 10° to 30°N in July. The isotherms do not lie along parallels of latitude as they would if solar radiation were the determining factor; rather, they show a tendency to follow continental outlines, with higher temperatures occurring over the oceans in winter and over the continents in summer. The belt of

highest temperature appears to lie near the belt of strongest insolation over land areas, but it is displaced toward the equator over the oceans.

These discrepancies result from the nonuniformity of the earth's surface. Different surfaces reflect and transmit solar radiation in different degrees, depending upon the properties of the soil or surface material. The ability of a surface to reflect solar radiation determines the amount of solar energy available for absorption by the soil and subsequent transmission to the atmosphere. In general, light-colored dry surfaces are the best reflectors; dark moist surfaces reflect poorly. Figure 2.1 shows some typical values of the percent reflectivity (albedo) of different surfaces. The average albedo of the northern hemisphere is estimated as 10%.

The qualities of the soil that permit the transmission of energy depend on the physical properties of the soil material rather than on the surface features. The two physical properties of importance are thermal conductivity, or the rate of heat flow through a substance under steady temperature gradient, and specific heat, or the amount of heat necessary to raise the temperature of a given quantity of the substance by a fixed amount. When the thermal conductivity is high, heat is transmitted through the soil to great depths during the day, and little energy is available at the surface. At night this stored energy flows upward through the soil and

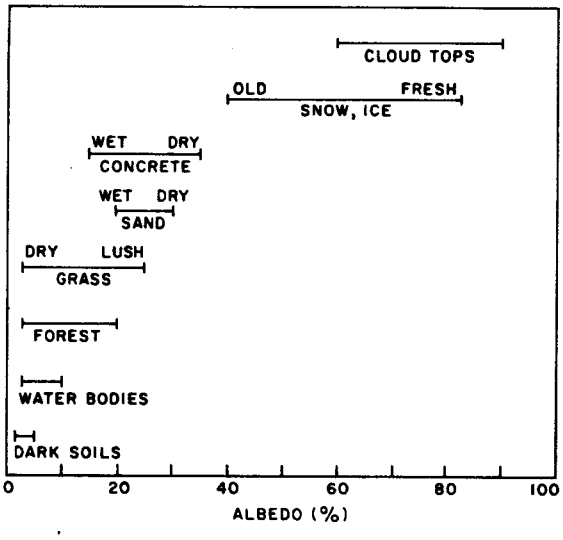

Fig. 2.1—The albedo (percent reflectivity) for various surfaces.

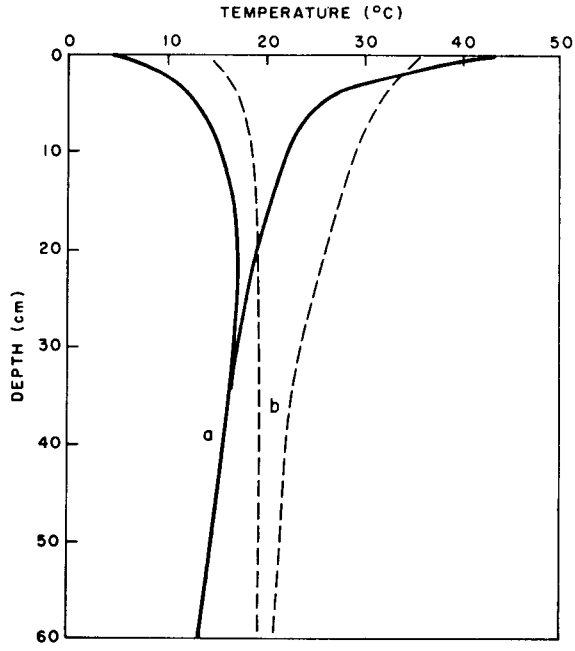

Fig. 2.2—The diurnal extremes of temperature change with depth below the land surface. (a) Soil of low specific heat and conductivity. (b) Soil of high specific heat and conductivity.

warms the atmosphere at the surface. When the specific heat of the soil is large, the addition of a given amount of heat produces a much smaller temperature change than when the specific heat is small. When both thermal conductivity and specific heat are large, a considerable amount of energy is stored to comparatively great depths in the soil, and the daily temperature range at the surface is small. When both values are small, little heat energy is stored, and the temperature range of the ground surface as well as the temperature range of the air near the surface is quite large.

Figure 2.2 shows the typical daily temperature range in soils having high and low thermal properties. The general slope of the profiles to the left with increasing depth is typical of a period of general atmospheric warming. A dry sandy soil with low specific heat and conductivity due to the large amount of air trapped in the interstices between the grains (Fig. 2.2, curve a) exhibits the typical temperature variations associated with soils having low thermal properties. Deserts are frequently composed of such a material and are known for their daily temperature extremes. A densely packed rocky

soil might be expected to show the more limited range of temperature variation (Fig. 2.2, curve b). There is, however, some depth in any soil at which the temperature does not display a diurnal variation. This depth is greatest in soils with high thermal properties.

In an evaluation of the overall effect of surface type on the radiation climate, both albedo and thermal properties must be considered. High values of both albedo and thermal properties contribute to small diurnal temperature ranges, whereas low values contribute to large diurnal ranges. Sometimes the two factors oppose each other, as in the case of fresh snow, which has a high albedo but low thermal properties. Since the albedo is effective only during periods of sunshine, a snow surface displays the effect of high albedo by day and low thermal properties by night; thus the surface does not become very warm during the day but does become very cold at night. Nonuniform surfaces may be very difficult to evaluate. Estimates of the thermal properties of such "surfaces," for example, forests, which present surfaces of intermixed wood, leaves, and air, are made as a rule from consideration of the complete energy budget.

Turbulent water has extremely high thermal properties, high enough, in fact, to outweigh its low albedo. Deep turbulent currents provide mixing, which transmits heat from the surface to great depths. Because of their tremendous capacity to transmit and store heat, the oceans serve as immense heat sinks or sources. When land surfaces warm rapidly (in summer), the ocean surfaces warm comparatively little and quite slowly, and, when the land cools (in winter), the oceans retain much of their warmth. This phenomenon accounts for the higher temperature of air over land in summer and over water in winter. A similar variation may be found over small bodies of water from day to night. This picture must be modified slightly to include the role of the major ocean currents in transporting heat from one area to another within the oceans. The tendency for the highest air temperatures to occur near the equator rather than in the belts of maximum insolation can therefore be attributed to the thermal lag exercised by the oceans. The high thermal properties of water have an effect in land areas as well: wet soils tend to be good heat conductors with small temperature ranges.

Up to this point the discussion has centered on an atmosphere of uniform composition. Actually, however, the atmosphere contains several variable components, such as carbon dioxide, water vapor, dust, and, most important when considering radiation, clouds composed of liquid water droplets. When clouds are present, the incoming solar radiation is greatly depleted, largely by reflection from the cloud tops. When cloud cover is randomly distributed over a large area of the earth's surface, the average insolation over this area for some long period of time is reduced everywhere by the same amount. There are, however, types of cloud systems that reduce the insolation over certain specific locations from those values found outside of these locations. Stationary and persistent cloud systems are frequently found along the windward side of mountain ranges. As air flowing toward the mountains is forced to rise over the mountain barrier, it experiences a temperature drop to the condensation point, and orographic cloud decks are formed. Over the lee slopes, the air sinks and warms, and the clouds are dissipated. A different sort of phenomenon is the moving cloud system associated with extratropical or tropical cyclones. These storms tend to occur in certain areas and to move along roughly defined tracks; consequently the regions containing these storm tracks experience an overall increase in cloudiness.

The effects of cloud systems can be seen in Fig. 2.3, which shows the normal annual number of hours of sunshine in the United States. Lowest values occur along the western slopes of the Appalachians and the Rocky Mountains and in the Pacific Northwest; highest values occur in the deserts of the Southwest. In the absence of cloudiness, these isopleths, connecting areas of equal hours of sunshine, would lie along parallels of latitude.

The average air temperature at a given location is the result of the energy balance of the atmosphere at that location and depends on the factors just discussed as well as advection over the location from colder or warmer regions and the elevation of the site. The resulting temperature patterns can be quite complicated, as shown in Fig. 2.4, a map of the average daily maximum air temperature for January constructed from hourly observations taken a few feet above the surface. On a still smaller scale, the effects of soil type, ground cover, cities,

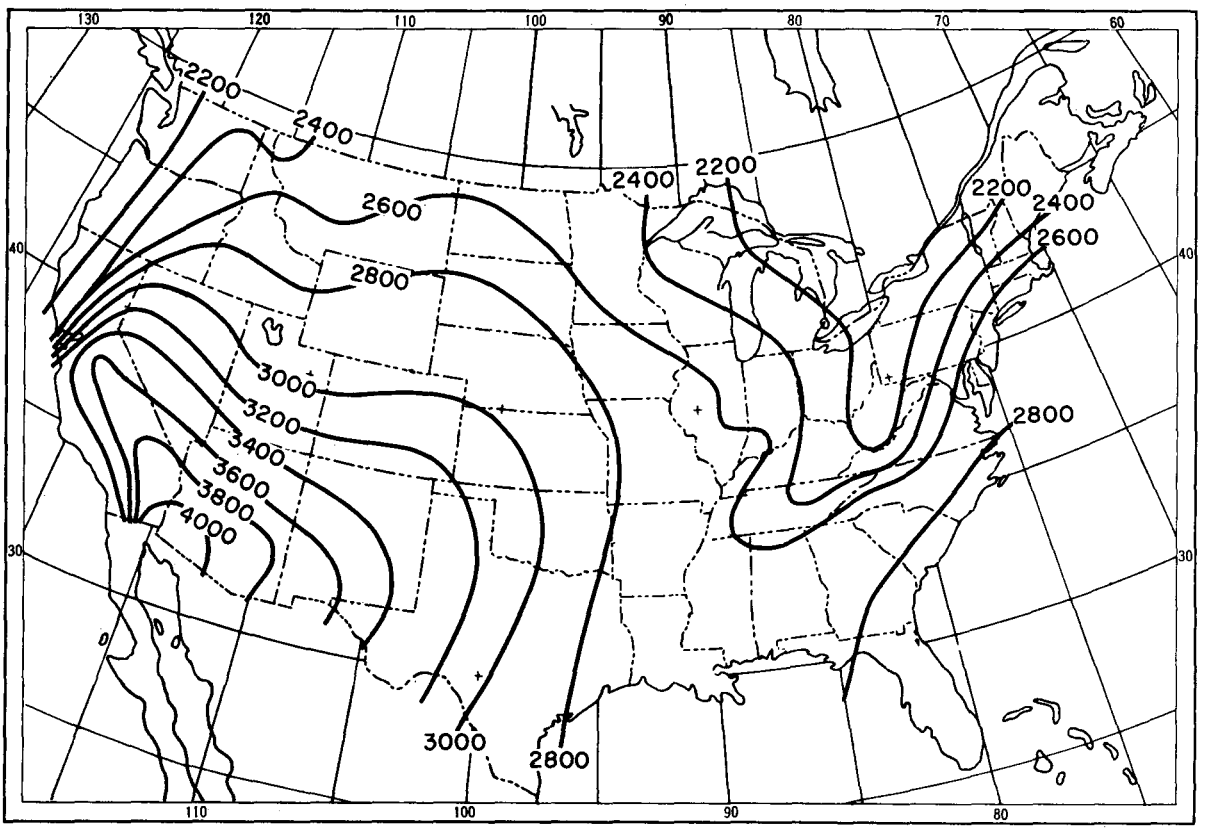

Fig. 2.3—Normal annual hours of sunshine in the United States.

and small water bodies further increase the complexity of the energy balance and the resulting air temperature.

2-2.2 The Local Energy Balance

At noon, on an average day, the energy balance might resemble that in Fig. 2.5. A variety of physical processes acting simultaneously will on a sunny day produce a net increase in the temperature of the surface layers of the earth and of the atmosphere. Figure 2.5 represents average conditions. Under different conditions of cloudiness, wind speed, soil type, or moisture supply, the same processes will operate, but the fraction of the total energy used in each will differ.

At night, when solar radiation is absent, the picture changes. The earth, radiating approximately as a blackbody, is the source of energy. Because the surface temperature drops only slightly (from 300°K to 280°K, for example) and radiant emission is proportional to the fourth power of the temperature, the earth radiates outward at a rate only slightly less than that during the day.

The earth emits energy over a continuous spectrum of wavelengths, but the atmosphere absorbs and radiates energy in certain wavelength bands only. Thus only part of the energy radiated outward by the earth is intercepted by the atmosphere. The result is a net loss of energy to space. A typical nighttime energy balance is shown in Fig. 2.6. This figure represents conditions of average cloudiness. If the sky is overcast, very little radiant energy can be lost to space. Instead, this energy is absorbed by the clouds and is reradiated downward, and the surface temperature remains relatively constant. On clear nights less energy is returned to earth by the atmosphere; as a result the loss to space is large, and the surface temperature drops considerably. Thus the picture at night is the opposite of that during the day.

One atmospheric process that has not been considered in any detail is the change of state

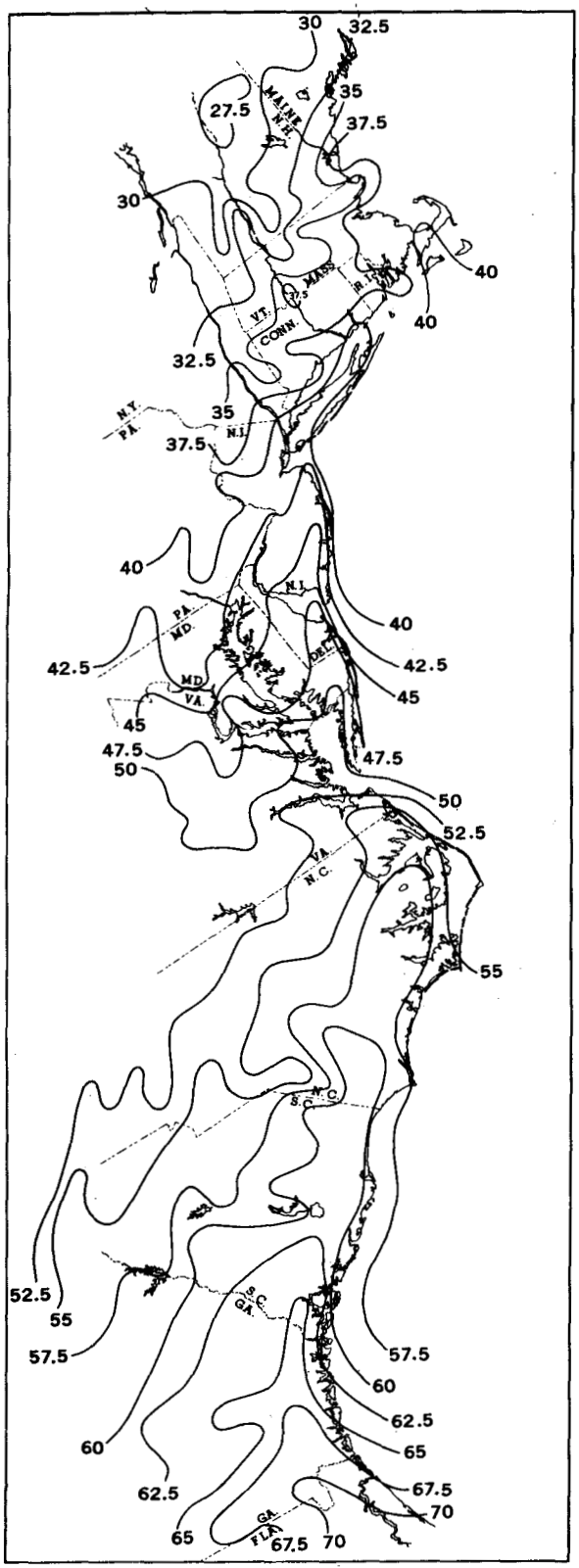

of water. Water changes from liquid to solid or vapor form under suitable conditions of temperature, pressure, and density provided certain other factors, e.g., condensation nuclei, are present. Although this process is of prime importance in general meteorology, especially in the fields of cloud and precipitation physics and in the study of dew, frost, and fog formation, it is not usually a major factor in the study of atmospheric diffusion.

2-3 WEATHER SYSTEMS

Although the physical characteristics of a site may vary with time (presence or absence of leaves on trees, snow on the ground, ice on lakes, etc.), they are for the most part unchanging and may be thought of as relatively constant. Such characteristics as latitude, location within the landmass, altitude, slope of the ground, type of soil, nature of the ground cover, and proximity to areas of different geographical properties determine the evolution of meteorological conditions at a given location in response to the large-scale meteorological conditions to which that location is exposed. It is this local response that results in the turbulent fluctuations of the air motions, which are, in turn, the determining factors in the diffusion of atmospheric properties and pollutants.

The atmosphere is a continuum in space and time. Like any turbulent fluid it has a wide variety of perturbations on all possible time and space scales. Certain of these perturbations repeat themselves again and again with sufficient similarity to permit them to be regarded as members of a discrete family of systems with fairly well defined boundaries and characteristics. Table 2.1 shows some of the common families. In addition to these patterns, there is an infinite variety of wind patterns that do not fit into any discrete categorization but can be considered as random perturbations in the mean wind field and therefore are studied statistically rather than in terms of discrete systems. These fluctuations, including mechanically and thermally induced motions, range in size from a fraction of a centimeter upward.

Fig. 2.4—Average daily maximum temperature along the Atlantic Coast in January (°F). (Bernstein and Hosler, 1959)

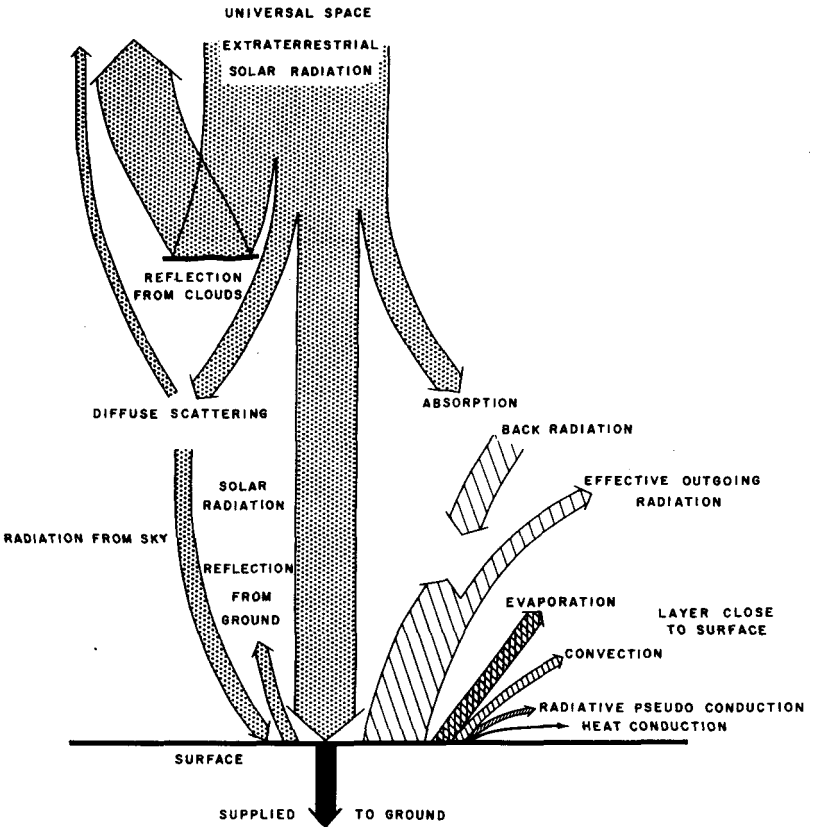

Fig. 2.5 — Energy balance at noon on a sunny day. The width of the arrows is proportional to the amount of energy transfer. (From R. Geiger, *The Climate near the Ground*, Fig. 1, Harvard University Press, Cambridge, Mass., 1957)

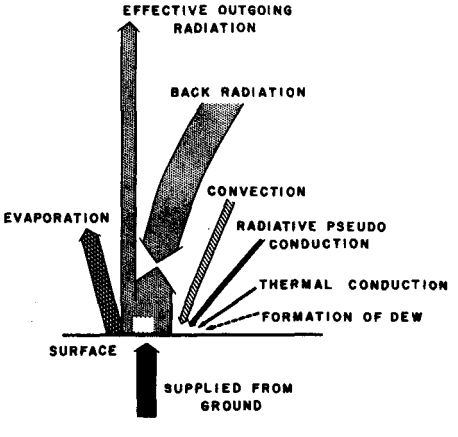

Fig. 2.6 — Energy balance at night drawn to the same scale as Fig. 2.5. (From R. Geiger, *The Climate near the Ground*, Fig. 7, Harvard University Press, Cambridge, Mass., 1957)

Table 2.1 — FAMILIES OF WEATHER SYSTEMS

Scale	Size
Very large:	
Long waves	Thousands of kilometers
Large:	
Cyclones	Many hundreds to a few thousand kilometers
Anticyclones	
Jet stream	
Hurricanes	
Fronts	
Monsoons	
Medium or mesoscale:	
Meso highs and lows	Tens to a few hundred kilometers
Squall lines	
Land–sea breezes	
Mountain and valley breezes	
Small:	
Tornado	Less than 1 km

These "chaotic" fluctuations are in great part responsible for turbulence and diffusion on scales of importance in local air-pollution problems.

The wind patterns associated with all systems on all time and space scales, both those with a recognizable identity and those of less obvious characteristics, make some contribution to the movement and diffusion of matter injected into the atmosphere and are therefore of some interest here.

Weather systems may be divided into six main categories:

1. The general circulation.
2. Phenomena associated with a particular type of air mass.
3. Isolated phenomena occurring at random locations within an air mass.
4. Phenomena associated with the boundaries of air masses of different types.
5. Stationary phenomena associated with some particular geographic feature occurring at a fixed location.
6. Chaotic systems.

2-3.1 The General Circulation

Above the surface layer large-scale air movement is determined by the general heat balance of the earth. Air receives heat from the ground at the equator and rises; air loses heat near the poles and sinks. Dynamical considerations indicate that, if no other factors operated, the resulting circulation would consist of two convective cells, one between the equator and each pole. In each cell air would flow from the pole to the equator near the surface; there it would rise and flow aloft back to the pole. Because the earth is a rotating spheroid, however, other factors, such as centrifugal and Coriolis forces, modify this simple picture.

In north temperate latitudes the surface winds generally blow from southwest to northeast, whereas in polar latitudes they generally blow from northeast to southwest. The region between the cold polar and warm tropical air masses where these two flows meet is the spawning ground for major mid-latitude storms. These storms generally move in an easterly direction, transporting cold polar air southward and thus forcing the warm tropical air to rise and move northward.

This crude description does little justice to the actual phenomena, which are far more complex than suggested here. It does indicate, however, that the large-scale wind pattern is dynamically related to the global energy balance and is generally independent of local features of the terrain.

2-3.2 Air-mass Weather

An air mass is formed when a large portion of the atmosphere remains over an extensive area of uniform surface features long enough for the air to take on certain characteristic values of temperature, moisture, and stability. These values are determined by the underlying surface and show little horizontal variation within the mass. An air-mass source region has rather vague boundaries and may extend over millions of square kilometers. Air masses are generally classified according to their source regions, e.g., continental polar and maritime tropical. When the large-scale circulation changes, the air mass moves away from its source region. As it passes over different types of surfaces, its properties are modified until gradually the mass loses its identity as a recognizable system. For example, a cold continental polar air mass moving southward over a warmer surface becomes warmer in its lower layers; a dry continental air mass moving out to sea becomes moist. While this modification is occurring, the circulation pattern may change again, and conditions over the source region may become conducive to the formation of a new air mass.

Within an air mass, owing to the general uniformity of the atmosphere, every locality receives the same "input" from the large-scale weather regime. If the winds are light, relatively little horizontal mixing will occur and differences in the microweather of the various locations will be due primarily to the differences in the local features. If the winds are strong, conditions will tend to be horizontally homogenecus.

One characteristic of air-mass weather is the subsidence inversion usually associated with regions of high pressure. Inversions, which are discussed more fully later in this chapter, may be simply defined as an atmospheric state in which temperature increases with height. Such a vertical stratification tends to inhibit turbu-

lence and thus to reduce the extent of atmospheric mixing. At the earth's surface air generally flows radially outward from high to low pressure. This flow is compensated by the sinking of the air within the high-pressure system. When a layer of air sinks, the temperature at the top of the layer increases more than the temperature at the bottom. If the layer sinks far enough, a subsidence inversion will be formed. Subsidence inversion layers are not normally based at the ground.

Subsidence inversions are generally present in the eastern regions of the semipermanent oceanic high-pressure systems found at about 30°S and 30°N. In these locations they are reasonably permanent and stationary systems. Los Angeles is in one such location. The subsidence inversion associated with the Pacific High combines with local topography and pollutant emissions to cause the smog problem in that city.

Subsidence inversions are also found in high-pressure systems associated with polar air masses. These are moving masses of cold air formed, in this hemisphere, over the northern parts of the American and Asian continents. Since these are moving systems, no one locality is generally under the influence of the inversion for more than a few days.

The surface-based radiation inversion is another type of inversion frequently associated with high-pressure systems. The radiation inversion is a nocturnal phenomenon associated with clear nighttime skies and light winds. Both subsidence and radiation inversions may be widespread phenomena extending over areas ranging from tens of thousands to hundreds of thousands of square kilometers. The major difference between them is that the radiation inversion depends on the time of day, nature of the surface, and local cloud cover, whereas the subsidence inversion depends only on the large-scale sinking motion of the air mass.

2-3.3 Isolated Disturbances Within an Air Mass

The primary characteristic of isolated disturbances is the apparent randomness with which they occur within the air mass. Small, patchy clouds caused by local anomalies of heating are typical visible systems of this type. Small perturbations in the wind and temperature field on the same scale as these clouds are also included in this category. These perturbations are not usually regarded as discrete entities but are treated statistically and are categorized by such statements as "scattered cloudiness" or "gusty winds." The air-mass thunderstorm is a possible exception. These thunderstorms do have an identifiable circulation, and this circulation may exist for a period of an hour or more.

2-3.4 Air-mass Boundary Systems

The major sources of inclement weather in the temperate latitudes are the boundaries between air masses (fronts) and the cyclonic storms that form on these boundaries. Although it is common knowledge that the air temperature decreases as one moves from tropical locations northward toward the temperate latitudes and, finally, to the Arctic, it is not so well-known that this transition usually occurs in reasonably discrete steps. As one proceeds northward from the equator, air temperatures remain fairly constant until the polar front is reached. In winter the mean position of this front is somewhere in the southern United States. The actual position of the front is highly variable although it can usually be traced around the world. At any one time there may be numerous breaks in the front and areas where it is a thousand or more kilometers north or south of its mean winter position. In any case, along this boundary separating the cold polar air masses from the warmer tropical air, the major cyclonic storms of the northern hemisphere develop and move. In summer the polar front will be found farther north, in the latitudes of southern or central Canada.

A typical winter surface weather map is shown in Fig. 2.7. The polar front meanders irregularly from the Atlantic to the Pacific oceans, the cold air always north of the frontal lines. The passage of a low-pressure center, such as that north of New York State, is accompanied by falling pressure and increasing cloudiness ahead of the center and rapid clearing and colder weather after the center has passed. The upper-air map accompanying this surface map is illustrated in Fig. 2.8.

Routine weather data, such as are measured at a typical U. S. Weather Bureau Station, are the data that are conventionally thought of as describing the weather or climate of a location

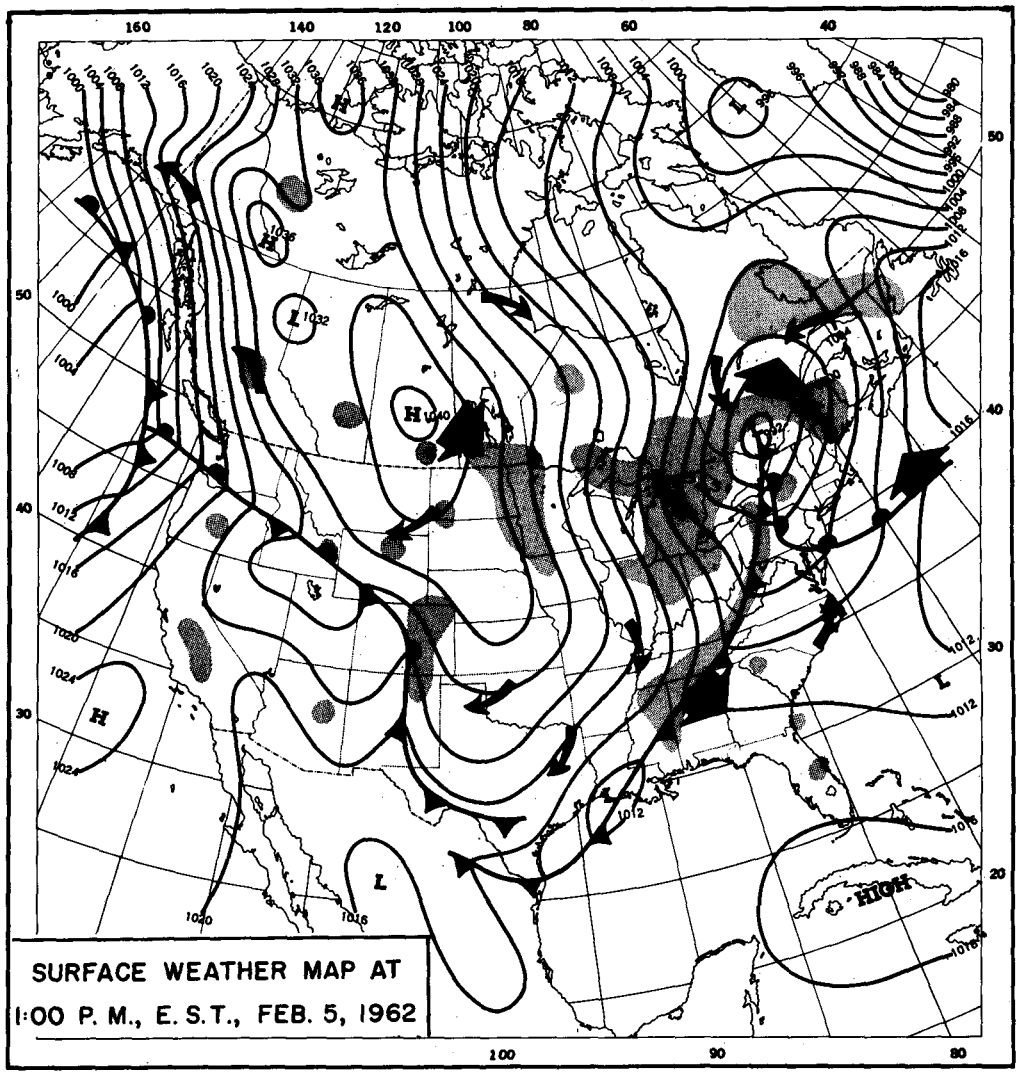

Fig. 2.7—An example of a typical surface weather map. The thin solid lines are isobars connecting points of equal atmospheric pressure. The heavier lines with pips are fronts separating air masses of different characteristics. The thin arrows depict the general surface-wind flow about the pressure systems, and the broad arrows indicate the direction of motion of the highs (H) and lows (L). Areas of precipitation are indicated by shading.

for most general purposes. The data are used to construct weather maps called synoptic maps because all the observations were taken at the same time and thus represent a synopsis of the weather at that time. The data are also used in many other types of analyses necessary for understanding and predicting the large-scale general state of the atmosphere.

The surface map shown in Fig. 2.7 is based on observations made at hundreds of weather stations. On the basis of these observations of temperature, dew point, pressure, wind velocity, cloud cover, and occurrence of weather phenomena, the map has been analyzed; i.e., the observations have been interpreted in terms of weather systems (the lows, highs, and fronts), which have been drawn on the map. Lines of constant pressure (isobars) have been drawn to delineate the pressure systems. Precipitation patterns have been indicated. The variation of the weather parameters from place to place on these maps can be noted. In addition, the tem-

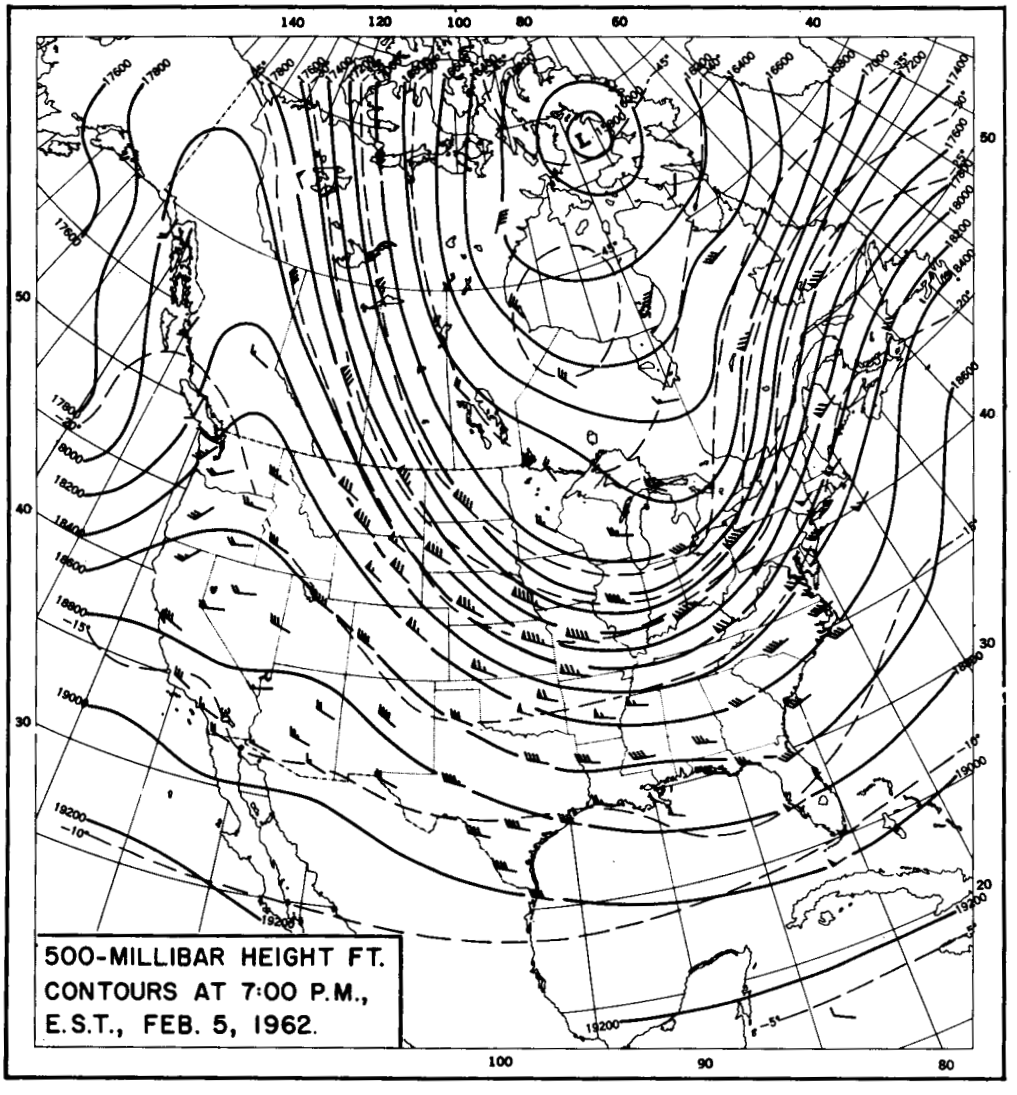

Fig. 2.8 — Upper-level (500 mb) weather map corresponding to the surface weather map in Fig. 2.7. The contours of this constant-pressure surface map are labeled in feet above mean sea level. The barbed arrows represent measured wind speeds and directions at this level.

poral variation of these same parameters is apparent from the change and movement of the systems on a sequence of weather maps.

The upper-air charts (500-mb charts) are constructed for a fixed-pressure surface, and instead of isobars lines of constant height above sea level (isohypses) are drawn. These lines are frequently called "contours" because of their similarity to contours on topographic charts. The contours delineate highs and lows just as the surface isobars do. At this altitude closed patterns are much less common than they are at the surface. Regions of low height are frequently identified as troughs, and regions of great height, as ridges. The wind at these heights generally blows along the contour lines. Considerably less variation in the weather parameters is evidenced on these high-level charts. This uniformity is due to two factors: the absence of surface effects (a true physical cause) and the greater spacing between upper air stations, which may result in a simplicity that more-complete data would show to be unwarranted.

Other types of charts commonly used to display the spatial and temporal variations of weather conditions are vertical soundings that show the wind and temperature as a function of pressure or height above an individual station and cross sections that show these variables as well as clouds as a function of height and time or of height and horizontal distance. Depending on the need, weather charts may be analyzed by drawing lines of constant density (isosteres), lines of constant wind speed (isotachs), lines of constant wind direction (isogons), lines showing the instantaneous flow patterns (streamlines), and lines showing the path of travel for a fluid particle (trajectories).

The weather maps described above are typically subjective evaluations of the weather patterns. Until the early part of the 1940's, these maps and the skill of the individual meteorologist constituted the major forecasting tools. At about this time basic theoretical advances coupled with the then new numerical computers resulted in the radically new method of routine forecasting of the pressure and flow patterns usually referred to as numerical weather prediction. This method called for the interpretation of the map in terms of the fields of the various variables and for the extrapolation of these fields by theoretically derived formulations. These techniques have become quite sophisticated today and have achieved their greatest success in the prognosis of upper-level flow patterns. Because of the complexity of the surface of the earth, however, these theoretically based, objectively implemented techniques have not yielded equal success in the forecast of the surface flow patterns or the prediction of actual weather conditions, e.g., clouds, fog, visibility, and precipitation.

The study of large-scale weather, in general, and of air-mass boundary systems, in particular, only briefly touched on here, constitutes the great bulk of past and present meteorological effort. Detailed discussions of these topics are given in the books noted in the bibliography at the end of this chapter.

The significance of air-mass boundary systems on local climate lies in the effects produced by extensive cloud cover, precipitation, and strong winds. While a storm is passing, local weather is dominated for a period of 1 to 3 days by large-scale dynamic processes and is, in large part, independent of local features. At other times the local weather is more likely to be dependent on local topographic conditions superimposed upon the generally more placid large-scale weather pattern.

A discrete system that is usually found in conjunction with frontal systems, particularly the cold front, is the squall line, an extremely active line of violent thunderstorms that occasionally forms in the warm air prior to a strong and moving cold front. This line of activity is usually about 100 km long and a few kilometers wide and moves in a direction perpendicular to its long axis. Thus its duration at any location is short, but its activity may result in local damage. The most violent of all the systems of the atmosphere, the tornado, is frequently found in squall lines as an appendage to the larger thunderstorms making up the lines.

The hurricane, a system of infrequent occurrence even in areas prone to hurricane visitations, is an air-mass storm that exhibits some of the outward characteristics of a mid-latitude frontal cyclone. Hurricanes usually form in the warm oceanic region near the equator and travel in a westerly direction, curving north into temperate latitudes to the east of the American continent and finally northeast. At this time they generally lose their tropical characteristics.

2-3.5 Weather Systems Associated with Fixed Geographic Features

Weather systems associated with fixed geographic features do not travel in space. They are the result of influences on the airflow produced by differing, juxtaposed geographic configurations, such as mountains and valleys, land and water, or cities and countryside. The many resulting weather systems are extremely varied in nature and size, e.g., the monsoon, sea breeze, mountain–valley wind, coastal fog, glacier wind, cloud and precipitation systems on the windward side of mountain ranges, foehn and chinook winds as well as standing waves and eddies on the leeward slopes, and the heat island over cities, a man-made feature. Although these disparate systems are often described in terms of one meteorological variable, a change in one variable must be associated with changes in the others.

One such system quite common in the warm seasons along oceanic coastlines is the sea breeze. Since water warms more slowly than

land, the daytime air temperature over the ocean during the warm season is usually lower than that over the land. As a result, if the general wind flow is weak, a circulation develops from the sea to the land at low levels and from land to sea aloft. The entire system is rather shallow (usually limited to the lowest 1000 m) and may be detected as far as 40 to 80 km inland. The sea breeze is important to diffusion studies at seaside locations because of the associated changes in atmospheric stability, turbulence, and transport patterns. Moreover its almost daily occurrence at many seaside locations during the warmer seasons results in significant differences in diffusion climatology over rather short distances.

During the midmorning hours of a clear summer day with light winds, the sea breeze will develop first as a gentle breeze felt to a distance of only a few hundred meters in from the shoreline. As the sun rises, the sea breeze increases in inland penetration, depth, and speed. By midafternoon, the sea breeze is at its greatest development and, as the sun sinks, begins to weaken. Frequently, at night after the sea breeze has dissipated, a weak land breeze forms when the land is cooler than the water surface. This is more likely to occur during the winter season, at which time the land breeze reaches its maximum development. The land breeze is usually much weaker than the sea breeze.

The term "sea breeze" is something of a misnomer because a similar circulation will be set up at the shores of any body of water that is at a temperature significantly different from that of the adjoining land surface. The magnitude of the circulation, however, is much smaller for smaller bodies of water.

Another common local wind pattern is known variously as the mountain–valley or slope–valley wind. During clear nights when the prevailing wind is light, the wind in a valley frequently assumes a configuration after sunset similar to the one shown in Fig. 2.9. As the slopes of the valley cool by radiation, the air immediately adjacent to the slopes cools also and becomes more dense than the air over the center of the valley at the same elevation. This dense air drains down the slopes toward the valley axis. The drainage flow from the slopes at various points along the valley will combine into a general flow toward the valley mouth.

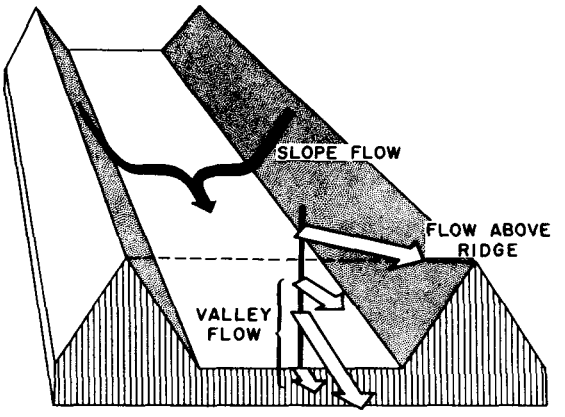

Fig. 2.9 — Idealized representation of the circulation that might be expected in a typical valley on a clear night.

Although greatly dependent on the slope and configuration of the valley, on the ground cover, and on the prevailing large-scale meteorological situation, down-valley flows of perhaps 5 m/sec are not uncommon. The slope–valley circulation, once established, will usually extend to the height of the ridge tops. This pattern will be destroyed after sunrise by the heating of the slopes and valley floor.

On clear days with light winds, an opposite circulation pattern may develop. This upvalley, upslope flow is due to the heating of the air adjacent to the sun-warmed slopes and valley floor. This phenomenon is not as marked as the night flow. At night, turbulence in the valley is suppressed by a thermal inversion (Sec. 2-5); thus the flow in the valley is comparatively undisturbed. By day, however, the turbulence induced by the heated land surface can be expected to stir the air within the valley and to cause mixing with the free flow above the ridges. This turbulence constitutes a general disruptive mechanism and hinders the establishment of any sensitively balanced circulation patterns. Therefore, although daytime upslope, upvalley patterns undoubtedly exist, they are not so common or so well marked as the down-valley flow at night.

Heating or cooling of the earth's surface by incoming or outgoing radiation results in other circulation patterns. These patterns may not be quite so distinct as the sea breeze or slope–valley wind, but they too are important in assessing local variations of atmospheric transport and diffusion.

Heating of the earth's surface tends to induce circulation patterns having large vertical components; radiational cooling, however, results in air motions that are primarily horizontal or parallel to the slope of the land. This is not restricted to definite mountain–valley configurations but may be observed over any sloping land provided the general wind over the area at night is light. This drift of air is frequently called a drainage wind. In many localities of pronounced slope, the drainage-wind direction, which is reasonably similar on succeeding nights since it depends on the invariant ground contours, will determine the climatological mean wind direction. The large ice-cap continents of Greenland and Antarctica display during their long winter nights an almost continuous drainage wind that is disturbed only by the passage of a storm.

Another large class of stationary atmospheric circulation patterns is caused by the passage of the air over topographic or man-made obstacles. These circulation patterns display a rotational or oscillatory motion in the vertical when the air is forced to flow over the obstacle and may be associated with clouds or even precipitation if the air is sufficiently moist.

On the large scale, mountain ranges frequently produce widespread uplifting of air moving toward the barrier. The Olympic and Cascade mountains in the state of Washington, which are situated in a westerly flow of moist air, furnish a dramatic example of large-scale uplifting. Figure 2.10 shows the average annual precipitation over the state of Washington in relation to the major mountain ranges.

The variety of topographic obstacles and the great diversity of weather situations create an unlimited range of local circulation patterns. Under appropriate meteorological conditions the disruption of an air stream by even a small hill can extend many kilometers vertically or horizontally downstream from the point of generation. Considering only the lower layers of the atmosphere, (a) of Fig. 2.11 shows a cross section of a topographic barrier perpendicular to the general wind flow. Either of the two patterns shown is possible, but the pattern showing lee separation of the flow is more likely to occur during periods when the atmosphere is unstable in the lower layers. The flow in a valley perpendicular to a wind stream is shown in (b) of Fig. 2.11. Again, the resulting state is determined by a balance between the existing

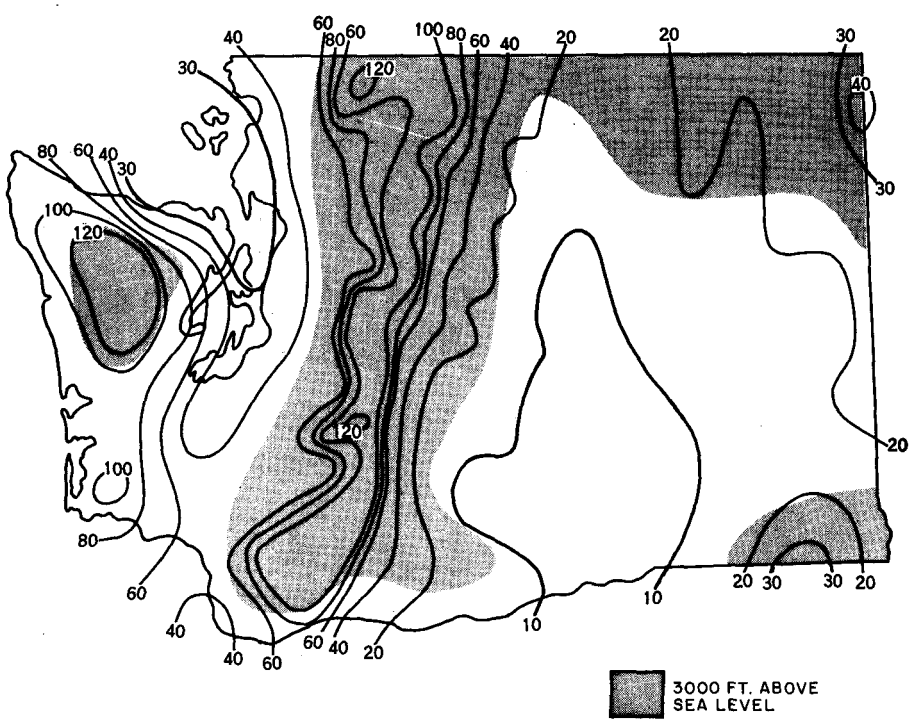

Fig. 2.10—Annual rainfall (in inches) for the state of Washington.

topographical and meteorological conditions. Moreover, if these conditions are not strongly defined, it may be possible for the circulation pattern to change back and forth as first one, then another, balance is struck among the acting forces. The pattern shown in (c) of Fig. 2.11 is found when stable air lifted over a barrier begins to oscillate about some equilibrium value and gives rise to lee mountain wave phenomena. When the amplitude of these waves is large, the pictured rotor forms, and quite violent up and down drafts and rapid diffusion result. Local diffusion conditions vary rapidly from point to point when complicated patterns such as these exist.

The horizontal, as well as the vertical, circulation is affected by barriers in the flow. Figure 2.12, a composite of many observations, depicts the perturbation in the wind field due to a simple hill.

Many different configurations are possible when the air flows at some angle to a valley. One such configuration is shown in (a) of Fig. 2.13. The thermally produced up- or down-valley flow may enhance or subtract from the component of the wind in the valley caused by channeling. Another common situation, (b) of Fig. 2.13, shows high or even severe local winds produced by a rather gentle flow through a pass in a mountain barrier. The Santa Ana wind of Southern California and the Columbia Gorge winds are examples of these phenomena in the United States.

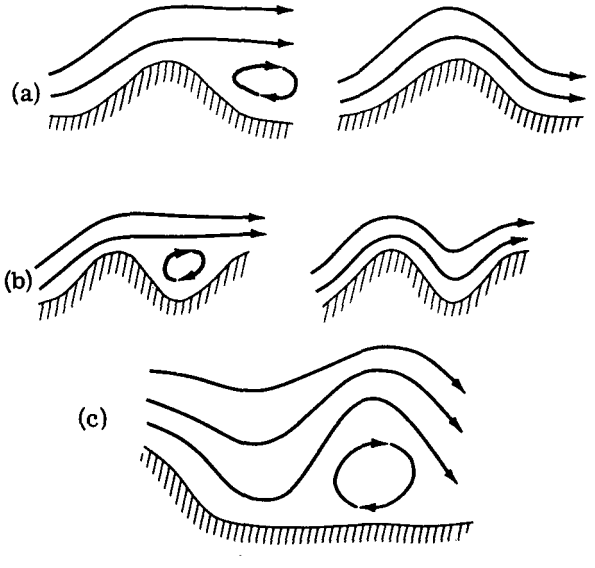

Fig. 2.11 — Various flow patterns over topographic obstacles. (a) Over hills. (b) Over valleys. (c) A rotor in the lee of a mountain.

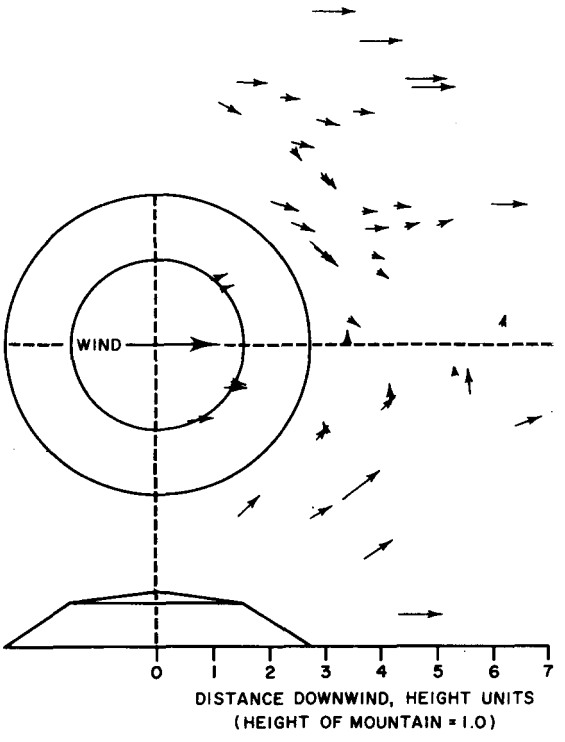

Fig. 2.12 — The airflow in the vicinity of an idealized hill. The small arrows indicate horizontal wind directions about the plan view of the hill. (Halitsky, 1961)

2-3.6 "Chaotic" Systems

The weather systems discussed in the previous sections may all be categorized by the facts that they are repetitive and that each repetition of a particular system has the family characteristics of all the other systems of that type. Each system lies within a certain size range, and each has thermal and circulation patterns similar to others in that family. If the wind patterns associated with these systems were to be subtracted from a highly detailed weather map, the resultant motion pattern would be difficult for the meteorologist to explain physically. The upper limit of size or duration of such patterns is somewhat obscure, but the patterns would certainly be evident on scales of hours and of tens of kilometers and down to the smallest size instruments can measure. Some of these systems are due to differential heating or cooling of the earth's surface; others are mechanically induced by the wind blowing against ob-

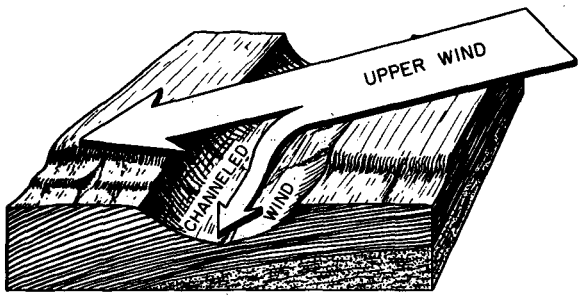

(a)

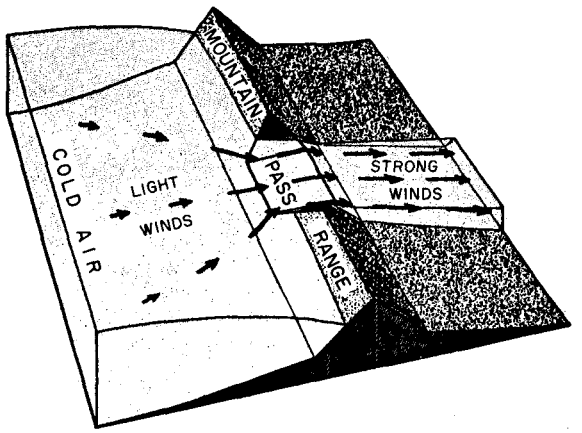

(b)

Fig. 2.13—Distortions of the wind flow by topographic obstacles. (a) Channeling of the wind by a valley. (b) The effect of a mountain pass on the wind flow.

stacles both man-made and natural; still others may be generated by differential motions within the atmosphere itself. These are the fluctuations in the wind that are responsible for most of the diffusion and for a large part of the transport of materials in the atmosphere out to distances ranging up to tens of kilometers. The impossibility of ascribing a physical cause to each small perturbation in the wind has dictated the adoption of statistical methods by meteorologists interested in relating wind fluctuations to diffusion in the atmosphere.

2-4 CLIMATOLOGY AND CONVENTIONAL WEATHER DATA

Before we proceed from the earlier discussions of general meteorology to those of specific interest in diffusion studies, we will give some attention to climatology and the use of conventional weather data (that data collected routinely by national weather services) in climatological analyses.

2-4.1 Climatology

Over a period of years, the fluctuations of the various meteorological variables at a given location result in distinctive patterns of average and extreme values of these variables, usually referred to as climatological statistics. Any number of such statistics can be constructed; e.g., considering temperature, one can compute:

1. Average temperature for each day of the year.
2. Average daily maximum.
3. Average daily minimum.
4. Average monthly, seasonal, or annual temperature.
5. Average monthly, seasonal, or annual maximum temperature.
6. Average monthly, seasonal, or annual minimum temperature.

The temporal changes of wind direction and speed resulting from the weather systems just discussed can be combined to determine the wind climatology of a particular site. Of all the climatological data, those on the wind are of greatest interest and use in atmospheric transport and diffusion studies. One of the most common yet useful of these climatological presentations of wind data is the wind rose, a circle from the center of which emanate lines representing the direction from which the wind blows. The length of each line is proportional to the frequency of the wind from that particular direction; the frequency of calm conditions may be entered in the center. Many variants of the wind rose exist. Some wind roses indicate the range of wind speed from each direction; some relate wind direction to other weather occurrences. Figure 2.14 shows a typical wind rose.

Figure 2.15 shows a composite night and day wind rose for New York City during the summer months. This wind rose was constructed from observations made during five summer seasons. The contribution of the sea breeze to the daytime wind distribution during the summer season is quite evident. Figure 2.16 shows a collection of wind roses for the hilly area adjacent to the Oak Ridge National Laboratory in Tennessee. The channeling caused by this moun-

tain–valley configuration is evident from the skewness of some of the individual roses.

Another way to introduce more detail on diurnal variability into a pictorial presentation is shown in Fig. 2.17. The lines in this figure connect all points of equal wind speed; the shaded areas represent the frequency with which a particular wind direction occurred at a particular time of day.

Figures 2.15, 2.16, and 2.17 are examples of the information that can be presented on the seasonal and diurnal variation of the wind. It is frequently of interest to specify the directions and speeds associated with various weather conditions. The presence or absence of inversions or precipitation can be used to derive inversion and precipitation wind roses. Vertical temperature data are needed for the construction of an inversion wind rose. If such data are not available, a good approximation may be made by constructing a night wind rose.

2-4.2 The Use and Collection of Available Weather Data

Gross estimates of the diffusion or engineering climatology of a particular site can frequently be made by the proper use of so-called available data. These data include any observations taken by federal, state, municipal, or private organizations which are considered to be representative of the site in question. Such data exist in great profusion.

The U. S. Weather Bureau, now part of the Environmental Science Services Administration, has been charged by act of Congress with the responsibility for observing, recording, and forecasting the weather over the United States and its possessions for the use of the general public. The responsibility for collecting weather data for solely military purposes has been assumed by the armed services. Other weather data are collected by commercial and educational organizations for operational and research purposes. The great bulk of the raw information collected by the governmental agencies, both civilian and military, is available to the interested public, some routinely at negligible cost and the rest by special request.

The Weather Bureau operates or is involved in weather-data collection at some 14,000 locations within the United States and its possessions. Of these, approximately 300 are locations

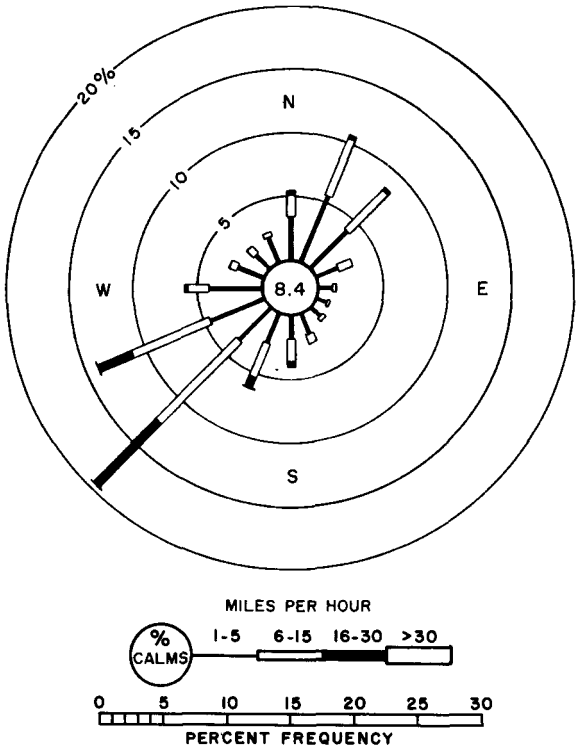

Fig. 2.14—A typical wind rose with wind-speed information.

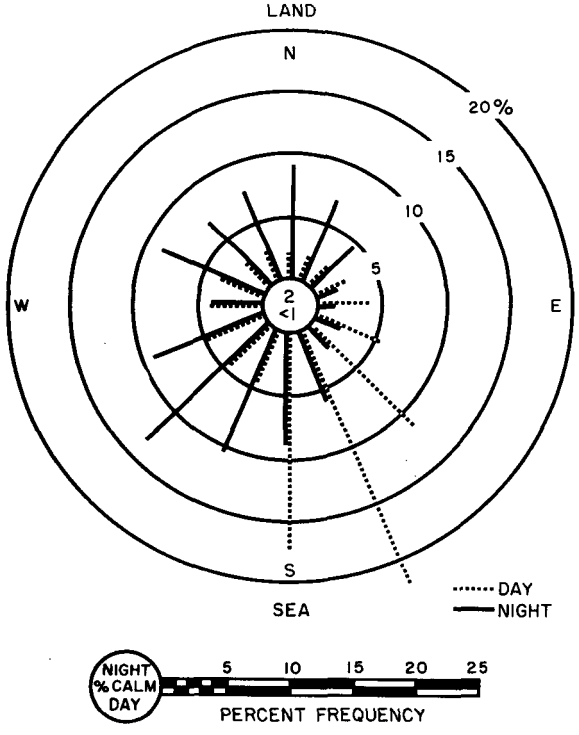

Fig. 2.15—A day–night wind rose showing, in this case, the diurnal effect of the sea breeze.

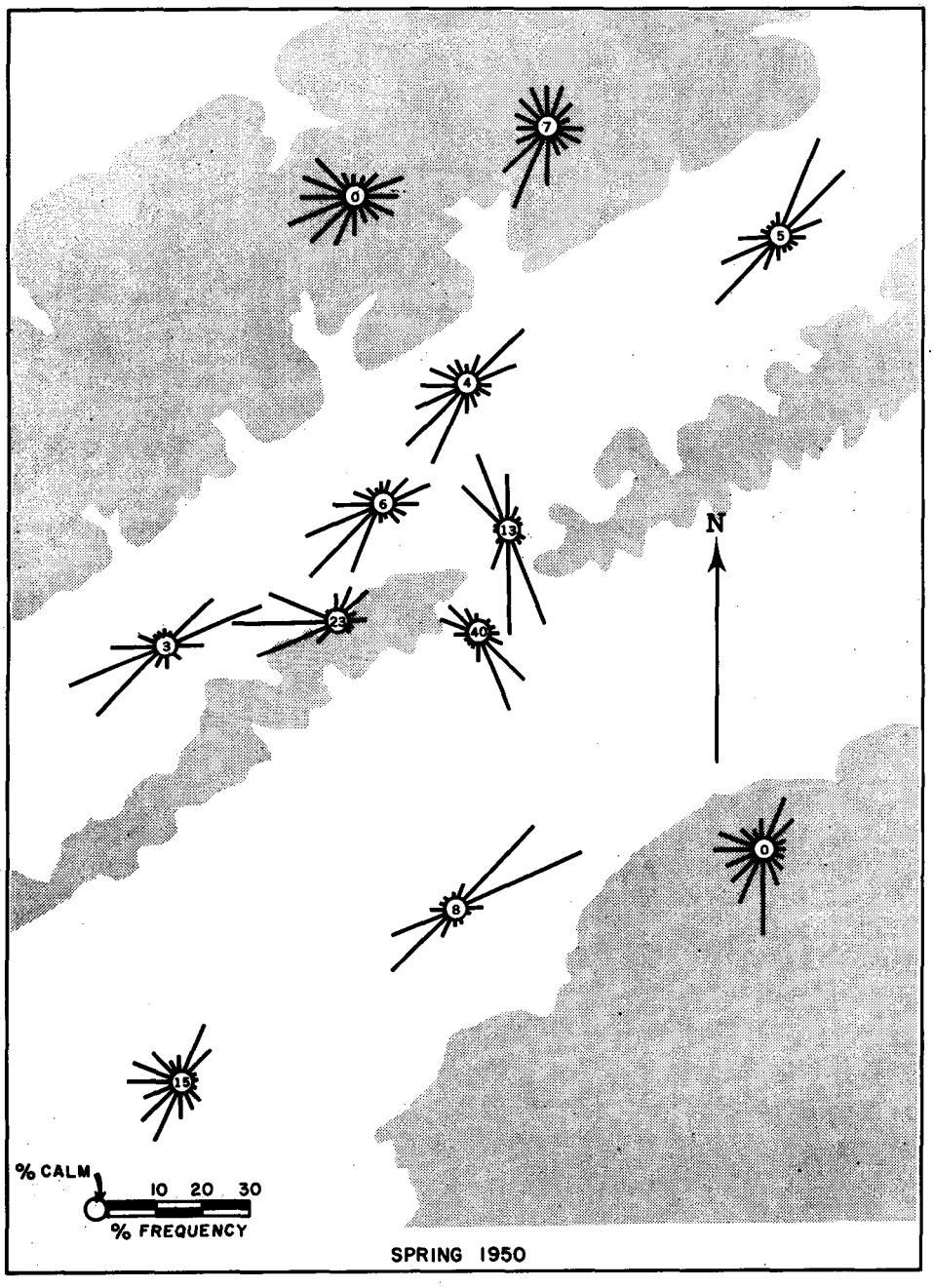

Fig. 2.16—Map of the hilly area about the Oak Ridge National Laboratory showing the wind flow in this region by means of massed wind roses. The shaded areas represent elevated terrain.

at which a complete record of all the surface-observed weather elements is kept as a routine matter. Observations including sky cover, visibility, pressure, temperature, humidity, wind velocity, precipitation, and various special elements are made hourly or even more frequently at times of rapid weather changes. These data are disseminated by teletype within an hour of the observation time. In addition to these stations, almost 700 other weather stations are operated either partially or entirely by personnel who are not employed by the Weather Bu-

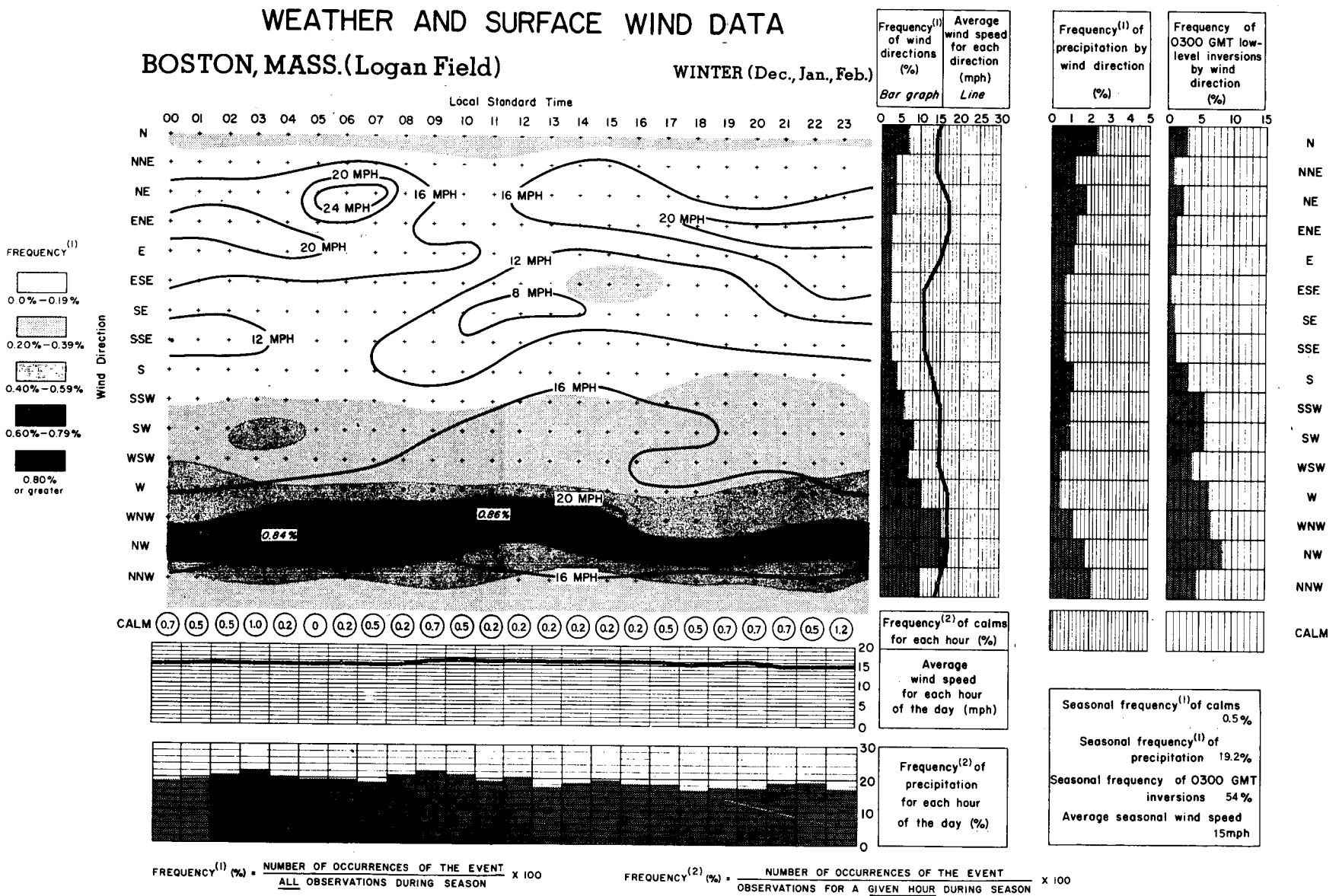

Fig. 2.17—An alternate form of presenting wind data and other weather statistics. Average wind speed and direction frequency of occurrence are presented for each hour of the day. All frequency computations based on 5 years of data.

reau but who cooperate with the Weather Bureau in more-limited observational programs. The data from many of these stations are also routinely available over the teletype networks. Finally, there are 13,000 other weather observation points primarily devoted to measuring temperature and precipitation. These stations do not report over the established teletype circuits. The data from all three weather-station categories are available from the National Weather Records Center (NWRC), an organization discussed in Sec. 2-4.4.

In addition to the surface observations, approximately 50 of the stations recording all surface-observed weather also routinely observe the wind, temperature, and humidity structure of the atmosphere up to heights of more than 25,000 m. These data are taken twice a day and are also disseminated by teletype.

Much of the surface and upper-air data just described is available from the NWRC on punch cards. Other data are available in log form (Weather Bureau Form WBAN 10a and 10b) or as analog traces where the original chart records have been retained.

In addition to this basic information, the Weather Bureau observes many special phenomena, such as solar radiation, radar echoes from rain areas, and river stages. Again, most of these data for past years are available from the NWRC.

The last group of weather data sources is so diverse as to defy any general attempt at classification. Meteorological research projects have frequently gathered large bodies of specialized meteorological data. Project reports are occasionally rich sources of weather data. Some of these, dealing primarily with diffusion, are noted in Chap. 4. Other sources of data for particular locations may be found in the literature from turbulence, aviation, agricultural meteorology, hydrology, and fire weather studies. A familiarity with these fields is necessary for determining the data sources since no single inclusive list of data compilations is available.

The requirement of the Atomic Energy Commission for a safety analysis of most sites proposed for a nuclear facility has resulted in about 200 safety analyses. The analyses for these sites frequently present weather data in considerable detail. Copies of these reports are not generally available; they are kept at the AEC Public Document Room in Washington, D. C.

Many municipal and state agencies, particularly those involved in pollution, conservation, and port management, take series of limited or comprehensive weather observations. Educational institutions, particularly the colleges and universities with meteorological curricula, are also sources of weather data.

A large body of usually unprocessed wind and temperature data has been collected at various industrial locations, particularly at chemical and petroleum sites. As an instance, a recent, rather cursory, survey identified over 45 wind-recording systems within 40 miles of New York City.

Recently, the archival facilities of the NWRC have been offered to any organization that wishes to preserve its weather records provided the station location and instrumentation are properly documented.

2-4.3 Summarized Meteorological Data

Although raw meteorological data are useful in many applications, their reduction to climatological statistics is time-consuming and costly. In many applications climatological summaries prepared by the U. S. Weather Bureau or other agencies may be found useful. A wide variety of these exists for both surface and upper-air observations. Some sources of these summaries are described in the following paragraphs.

The U. S. Weather Bureau has prepared a publication titled *A Selective Guide to Published Climatic Data Sources Prepared by the U. S. Weather Bureau.* It is sold by the Superintendent of Documents, U. S. Government Printing Office, and is an invaluable source of data summary information. Both surface and upper-air data are represented.

The Department of the Navy has published a volume titled *Guide to Standard Weather Summaries* (Navaer 50-1C-534). This document contains a list of standard weather summaries prepared by the Navy, Air Force, and Weather Bureau as well as sample formats from each. A second part of the volume lists the summaries available for approximately 9000 weather stations around the world. This publication is currently for sale by the Superintendent of Documents as catalog number D 202.6/7:W37.

The following summaries of Weather Bureau data are routinely available from the Superintendent of Documents, U. S. Government Printing Office, Washington, D. C. 20402, at nominal cost. In some cases only recent issues are available.

Climatography of the United States, No. 82 (Decennial census of the United States Climate-Summary of Hourly Observations, 1951-1960): This series is the most generally useful single summary prepared for a wide variety of uses. When completed, this series will treat approximately 150 major cities. Since most weather stations are at airports, these summaries may represent either urban or rural statistics. The "82" series replaces a similar series, *Climatography of the United States, No. 30,* which was based on 5 years of data from approximately 100 weather stations.

Local Climatological Data Summary (including monthly supplement): This publication summarizes the weather for a particular month rather than the mean of many repetitions of that month. The data are presented for each day of the month and for each hour of each day. The supplement includes a portion of the surface observation for every third hour of each day. An annual summary is also prepared.

A complete list of governmental weather-data summaries is given in the price list *Weather, Astronomy, and Meteorology,* 48th Edition (May 1960), which is distributed at no cost by the Superintendent of Documents, U. S. Government Printing Office, Washington, D. C. 20402.

2-4.4 The National Weather Records Center

The National Weather Records Center is operated by the Environmental Science Services Administration at Asheville, N. C. Since the various functions of the Center are described by Barger (1960), only a brief summary will be given here.

The Center contains over 400,000,000 punched cards bearing meteorological data. Every effort is made to ensure that a copy of each meteorological record collected in the United States and its possessions is stored in the NWRC depository. In addition to the cards, various meteorological observation forms and a wide variety of original recorder charts are stored. The Center is manned by about 500 employees who operate a wide variety of accounting machines and digital computers. At the Center observations are checked and prepared for publication. The facility provides, at cost, hand and machine computations, charts and map analyses, relationship studies, etc. to the general public, industry, agriculture, and other government agencies. The records are held officially as a designated extension of the National Archives. Navy climatological data are also processed, and an Air Force contingent, working primarily with its own data, carries out requests of its own service or of contractors.

Copies of all the raw data, including cards, various observation forms, and autographic records can be obtained from the Director, National Weather Records Center. Data other than those on cards are usually available in photocopy, Ozalid, or microfilm form. Unpublished data summaries including upper-air and surface data, Navy summaries (SOMAR and SMAR), and Air Force summaries (A, B, C, D, E surface weather observations) are also available. The Center will prepare, on request, a summary of all pertinent data available for a given small geographical area. For areas larger than a standard metropolitan statistical area, for example, it would be best to discuss data-acquisition problems with the Director, National Weather Records Center, before requesting a list of all available data. The Center also prepares the Weather Bureau summaries referred to in Sec. 2-4.3.

In addition to storing data and preparing routine summaries, the Center will also prepare data according to the client's requests. Although each such task is unique, a copy of the resulting tabulation is kept in information files. New requests are reviewed in the light of these previous summaries, and copies are provided to the client at the cost of the reproduction if the information is pertinent to his problem.

2-5 THE VERTICAL TEMPERATURE STRUCTURE OF THE LOWER ATMOSPHERE

Atmospheric turbulence, the state of chaotic motion discussed in Sec. 2-3.6, has been found to depend in large measure on the vertical

gradient of temperature, one response of the atmosphere to the energy balance in the earth–atmosphere system. The nature of the temperature structure in the first approximately 1000 m of the atmosphere is the subject of the following sections.

The fact that atmospheric pressure decreases with height was established during the middle of the 17th century. If by some unspecified process a parcel of air is carried upward in the atmosphere, the pressure of that parcel will decrease in response to its surroundings. The decrease of pressure within the parcel will be associated with an increase in volume and a decrease in temperature. If the process is assumed to be adiabatic, i.e., without any exchange of heat between the rising parcel and its surroundings, the rate of temperature change may be calculated from the first law of thermodynamics. Because atmospheric motions generally occur too rapidly to permit heat exchange with the surroundings the assumption of an adiabatic process is commonly made in meteorology. The rate of change of temperature with height, as determined from this adiabatic process, is referred to as the adiabatic lapse rate, the term lapse rate referring to the rate of change in the value of an element with height.

The lapse rate in the real atmosphere over any given location usually differs from the adiabatic. Owing to a variety of physical processes, the observed lapse rate in the atmosphere will differ in magnitude, and occasionally even in sign, in different layers above the surface. Thus the lifted parcel may at some particular level be warmer or cooler than its surroundings. If, after moving upward for some distance and experiencing a fall in pressure and an associated drop in temperature, the parcel were at a lower temperature than its surroundings, its density would be greater than that of the surroundings, and buoyancy forces would accelerate it downward. Unless some other force is operating, the air, once the lifting process has been terminated, will sink until it returns to its original level. If, however, the parcel, having risen, were at a higher temperature than its surroundings, buoyancy forces would accelerate it upward, and it would continue to rise. These two conditions are known as thermal or static stability and instability, respectively. An exactly similar situation would prevail for a parcel of air forced downward from its initial position. When the atmosphere is thermally stable, turbulent motions are suppressed; when it is thermally unstable, turbulence is enhanced. Buoyancy alone is not sufficient to account for the motions that actually occur, but the vertical temperature structure, together with its associated buoyancy effects, is a necessary consideration in determining the energy of atmospheric fluctuations.

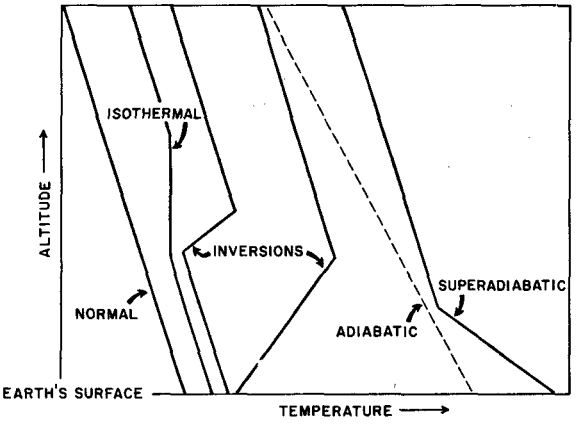

Fig. 2.18—Examples of low-level vertical temperature structure. In this figure the choice of surface temperature is arbitrary.

The normal or standard lapse rate of temperature in the atmosphere (e.g., U. S. Standard Atmosphere) is specified as a decrease of 3.5°F/1000 ft or 0.65°C/100 m. A layer displaying no temperature change with height is described as isothermal; a stratum in which the temperature increases with height is called an inversion. These conditions are illustrated in Fig. 2.18.

The unique atmospheric lapse rate in which an element of air is displaced from one level to another yet still maintains the same temperature or density as the surrounding air is the adiabatic lapse rate noted previously. Here the warming or cooling of a parcel during its downward or upward trip is exactly matched by the temperature gradient of the environment. Numerically the adiabatic, or neutral, lapse rate is equal to about 1°C/100 m or 5.4°F/1000 ft.

If the temperature in the atmosphere decreases at a rate greater than the adiabatic rate, the lapse rate is termed superadiabatic. During superadiabatic conditions all vertical

motions are accelerated because a mass of air that is forced to rise is warmer and less dense than the surrounding air and thus continues to rise whereas one that is forced downward is cooler and more dense and continues to fall.

2-5.1 The Diurnal Cycle of the Vertical Temperature Structure

The daily cycle of vertical temperature pattern is typically as shown in Fig. 2.19, which was constructed from data taken during a late summer and early fall period in the eastern United States. At 0600 EST and 0700 EST a typical surface radiational inversion is evident. By 0800 EST the heating effect of the sun results in the destruction of the lowest part of the inversion, and by 1000 EST no trace of the nocturnal inversion exists. The daytime hours show an unstable layer nearest the ground and a gradual heating of the entire layer of air represented by these traces. The return of the nocturnal inversion is evident at 1800 EST, and cooling of the entire layer progresses through the night. The presence of a cloud cover will reduce the intensity of the radiation inversion since the clouds will absorb the energy leaving the ground and reradiate it back to the ground; thus a higher temperature will be maintained than that realized during clear sky conditions. Furthermore strong pressure-gradient-induced winds give rise to mechanical turbulence, which also reduces the inversion intensity.

Figure 2.20 shows an interesting example of the effects of wind speed and cloudiness on the temperature difference between 11 m and 110 m. It can be seen that inversion formation at this site in central Long Island was completely suppressed by winds in the 6.0 to 9.0 m/sec range.

2-5.2 Seasonal Variations in the Vertical Temperature Structure

Actual profiles of temperature are affected by local conditions and will vary greatly, but, in general, the seasonal differences in solar

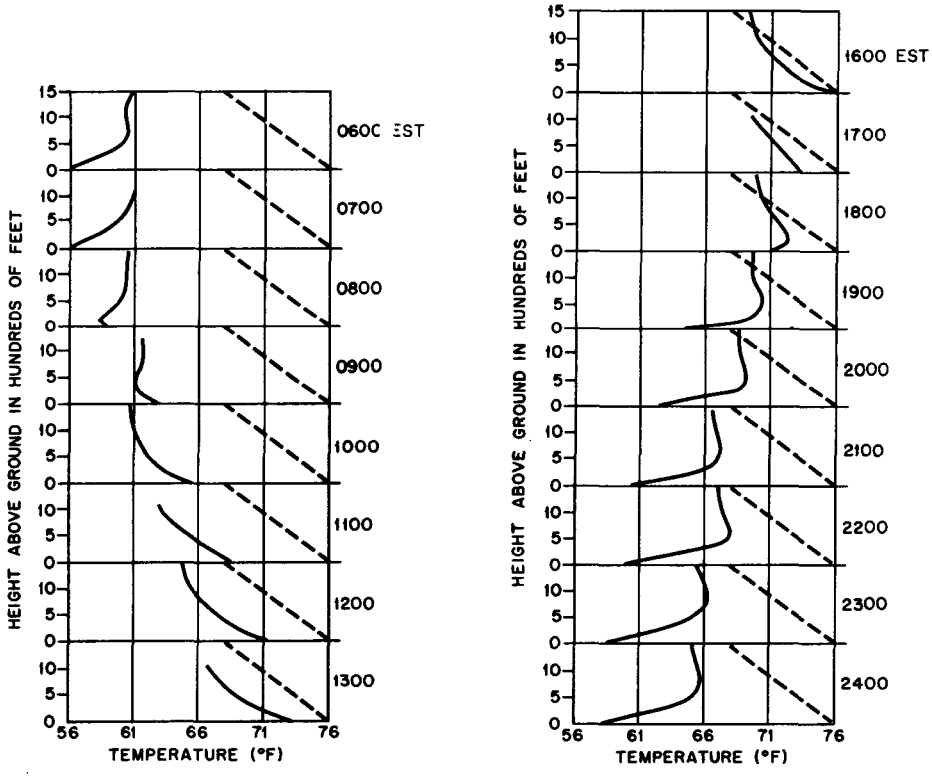

Fig. 2.19—The average diurnal variation of the vertical temperature structure at the Oak Ridge National Laboratory during the period September–October, 1950. The data were obtained from captive-balloon temperature soundings. The dashed line in each panel represents the adiabatic lapse rate. (Holland, 1953).

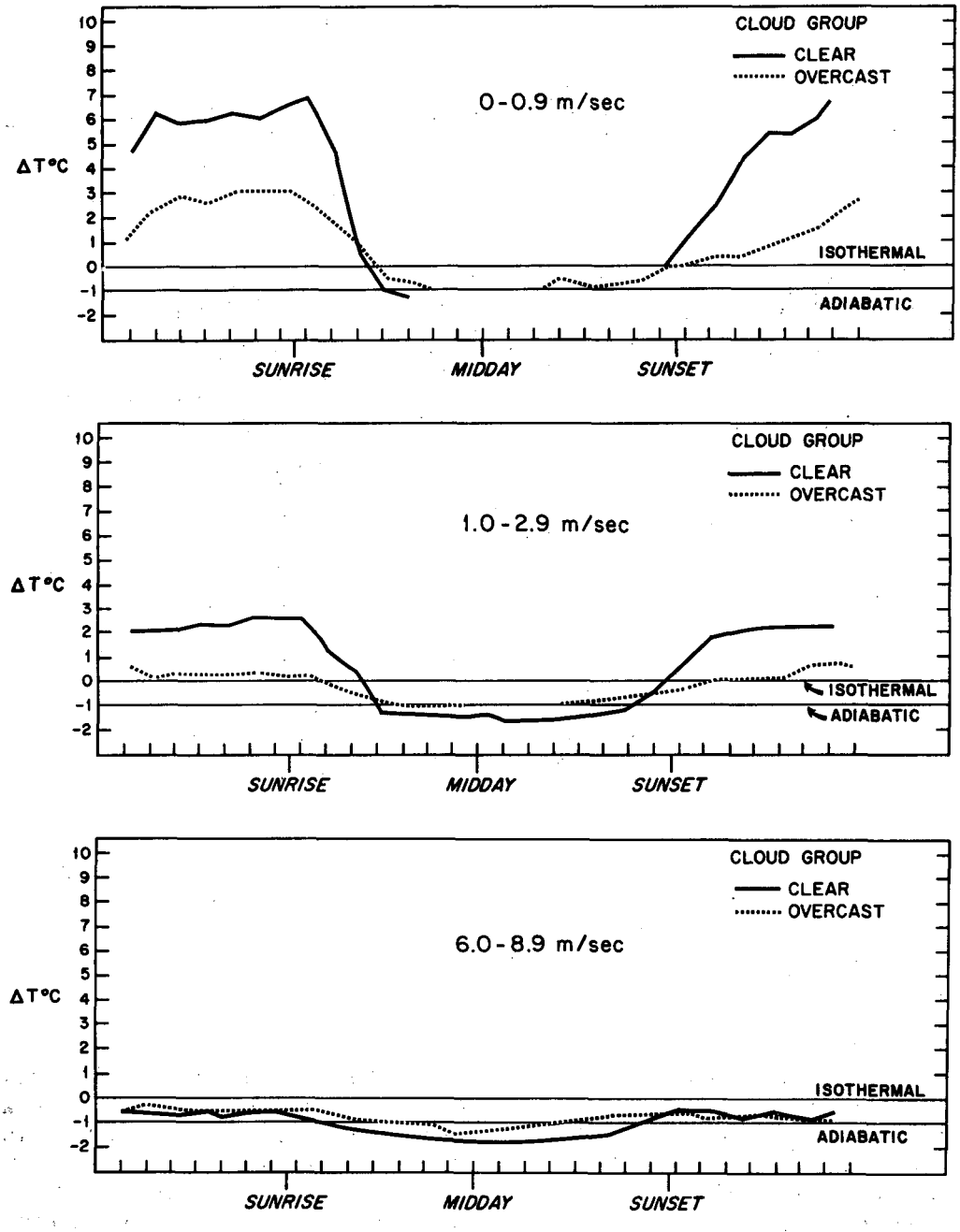

Fig. 2.20—Diurnal variation of the temperature difference between 11 m and 110 m as a function of cloud cover and wind speed at 11 m. These data were obtained at the Brookhaven National Laboratory over a 2-year period. (Singer and Raynor, 1957)

radiation will favor longer inversion periods during cold months. At a continental station with pronounced seasonal effects, a maximum of only a few consecutive hours of definitely superadiabatic conditions will occur during midwinter, whereas sometimes an unbroken period of inversion conditions will occur for several days. At the same station throughout the summer months, superadiabatic conditions will be the rule during daylight hours.

Figure 2.21 shows the vertical temperature difference between 1.5 and 120 m in south-

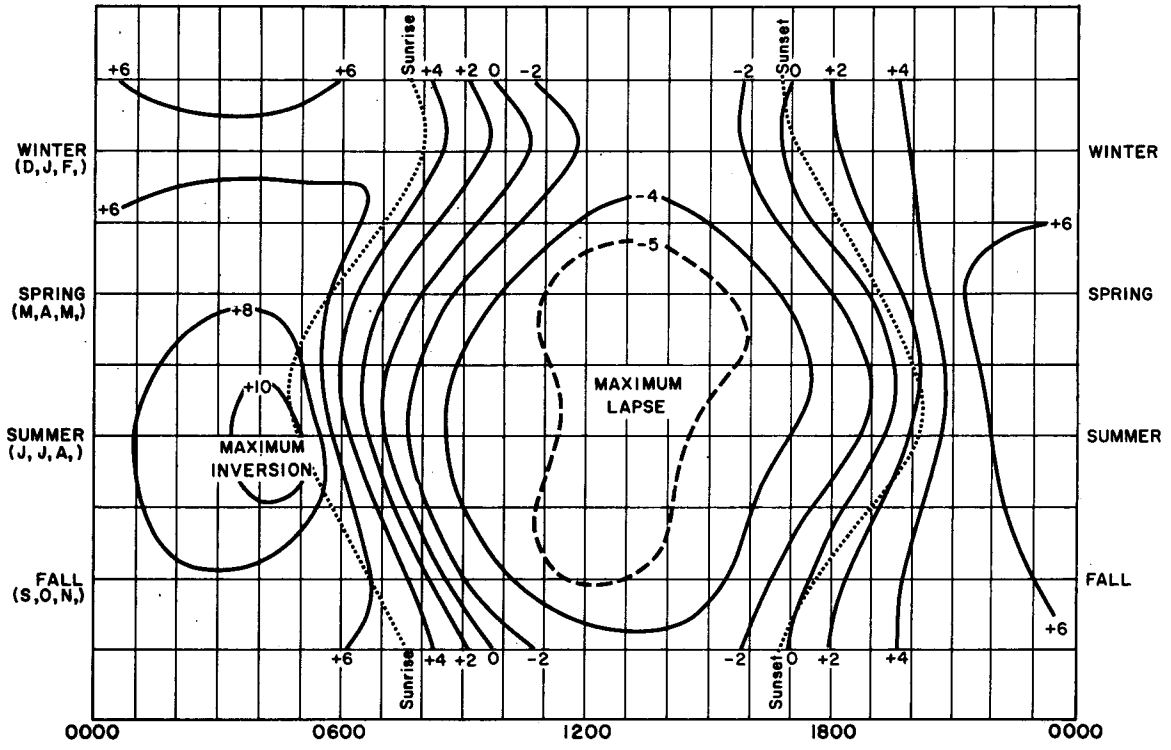

Fig. 2.21—Seasonal variations in the vertical temperature difference (°F) between 1.5 and 120 m for each hour of the day. These data were collected over a 2-year period at the National Reactor Testing Station at Idaho Falls, Idaho. (DeMarrais and Islitzer, 1960)

eastern Idaho over a desert location. It can be seen that the *average* maximum intensity of inversions occurs during the summer. The individual maximums usually occur during the winter, but these larger values are obscured in the mean by the greater number of inversions of lower intensity associated with the increased frequency of high winds and clouds at this and most locations in winter. Inversions of greatest persistence, however, occur during the winter. The most unstable conditions usually occur during the summer, the late spring and early fall values being somewhat lower.

A comparison of the frequencies of low-level inversions, as estimated from winter and summer radiosonde data, is shown in Fig. 2.22. Although the seasonal patterns are basically similar, the increased frequency during the winter at most locations is evident.

Caution should be used in direct comparisons of vertical temperature-difference data from different sources. Since the temperature changes most rapidly close to the ground, small differences in the heights of the observations can cause surprisingly large variations in temperature difference or gradient statistics.

2-5.3 Atmospheric Stability and Pollution

The diffusion meteorologist's interest in the vertical temperature structure of the atmosphere stems from the fact that the turbulent structure of the atmosphere is intimately related to the temperature structure. Since it is much more difficult to measure atmospheric turbulence than to measure the accompanying vertical temperature gradients, the latter has frequently been used as an index to the former.

On clear days with light winds, superadiabatic lapse rates are usually found in the lowest few hundred meters of the atmosphere. A high level of turbulence exists within the unstable layer, and these motions guarantee rapid lateral and vertical mixing between an emitted pollutant and the clean air. Above a few hundred meters,

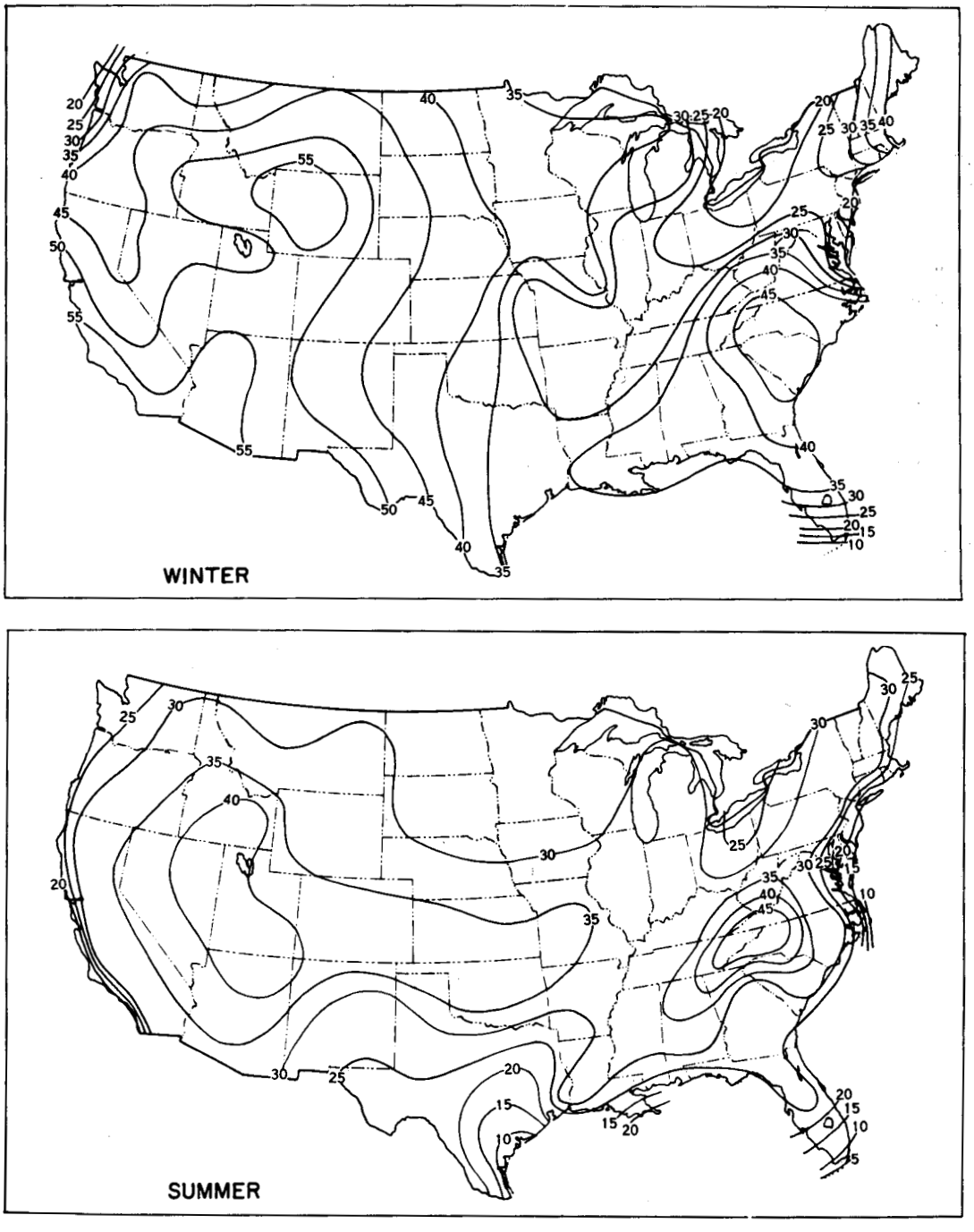

Fig. 2.22—Percentage frequency (percent of total hours) of the occurrence of inversions or isothermal conditions based below 500 ft during the winter and summer. (Hosler, 1961)

the lapse rate is usually less unstable, and the chaotic low-level turbulence shows some organization into discrete columns of rising and falling air. The ascending columns may be topped by convective clouds (cumuli) if the moisture supply is sufficient and if the rising air cools until the condensation temperature is reached. The height of the tops of the cumulus clouds can be used as an estimate of the height of the top of the mixed layer.

Even in the absence of cumulus clouds, a sharp demarcation is not uncommon between the mixed, turbid air below and the clean air above. This boundary is usually associated with an upper-level inversion, such as a subsidence inversion, and marks the limit of ground-based mixing. The mixed layer is usually 300 to 3000 m deep although, under conditions of large-scale dynamically induced instability, it may extend many thousands of meters higher. A pollutant released near the ground, e.g., from a stack, will under unstable conditions spread rapidly in both the lateral and vertical directions. The vertical spread will eventually cease when the top of the mixing layer is encountered. Figure 2.23 shows the mean maximum mixing-depth patterns for January and July. When there are multiple sources of pollution below the mixing lid, as in an urban area, the layer between the ground and the base of the lid may become quite polluted. When this lid is low and is maintained for a few days and the horizontal air motion is small, a potential for air pollution is established. This potential will manifest itself if the pollutant sources are available.

When considering pollutant materials released near the earth's surface, one should remember that the night hours are marked by restrictions to turbulent diffusive spreading. The development of the surface-based inversion inhibits both lateral and vertical turbulence. Thus material released from a stack into the nocturnal radiation inversion will rise until its initial buoyancy and vertical momentum are dissipated. It will then drift downstream, frequently as a thin undisturbed ribbon. It is possible to follow such ribbons released from stacks for many tens of kilometers downstream. As the sun rises, turbulence levels will also rise, and the thin concentrated plumes will usually be dissipated within 2 hr after sunrise on a clear morning. If a fog layer should develop within a nocturnal inversion, a not uncommon situation, the morning breakup of the inversion may be considerably retarded since the top of the layer will reflect much of the sunlight incident upon it. In extreme cases an inversion accompanied by fog may last for the entire daylight period.

During periods of strong winds, the atmosphere is well mixed by mechanical turbulence, and lapse rates nearly equal to the dry adiabatic rate are observed throughout the mixed layer. Since the dry adiabatic lapse rate is generally greater than that of most of the atmosphere, a turbulence inversion will form at the upper limit of the mixed layer. Under strong inversion conditions gentle mechanically induced mixing will tend to stir the air and cause the nocturnal inversion to be deeper and less intense.

2-6 THE LOCAL WIND STRUCTURE

2-6.1 The Mean Vertical Structure of the Horizontal Wind

In the first thousand or so meters above the earth's surface, the wind speed and direction are determined primarily by three forces: the force due to the horizontal pressure gradient, the Coriolis force due to the earth's rotation, and the frictional force due to the nearness of the earth's surface.

The pressure-gradient force is induced by the horizontal pressure differences between any two points, greater pressure differences being associated with stronger winds. The close spacing of the isobars over the Great Lakes in Fig. 2.7, compared with the wide spacing over the Dakotas, indicates stronger winds in the former than in the latter location. The pressure gradient alone would cause the air to flow from regions of high to regions of low pressure. However, since the earth is turning beneath this flow, an observer on the earth's surface in the Northern Hemisphere would notice an apparent turning of the flow to the right. The force postulated to explain this turning is the Coriolis force. The net result of the pressure gradient and Coriolis forces in equilibrium is a flow that is parallel to the isobars with low pressure to the left of the direction of motion in the Northern Hemisphere. The wind resulting from this balance is called the geostrophic wind.

In the upper layers of the atmosphere, observed winds are often quite close to geostrophic winds, indicating that only the pressure gradient and Coriolis forces are operative in determining the flow. Near the surface, however, a third force due to the frictional drag exerted on the atmosphere by the surface enters the picture. This force is analogous to that arising in a viscous fluid flowing smoothly over a fixed plane surface. Such a fluid has a speed

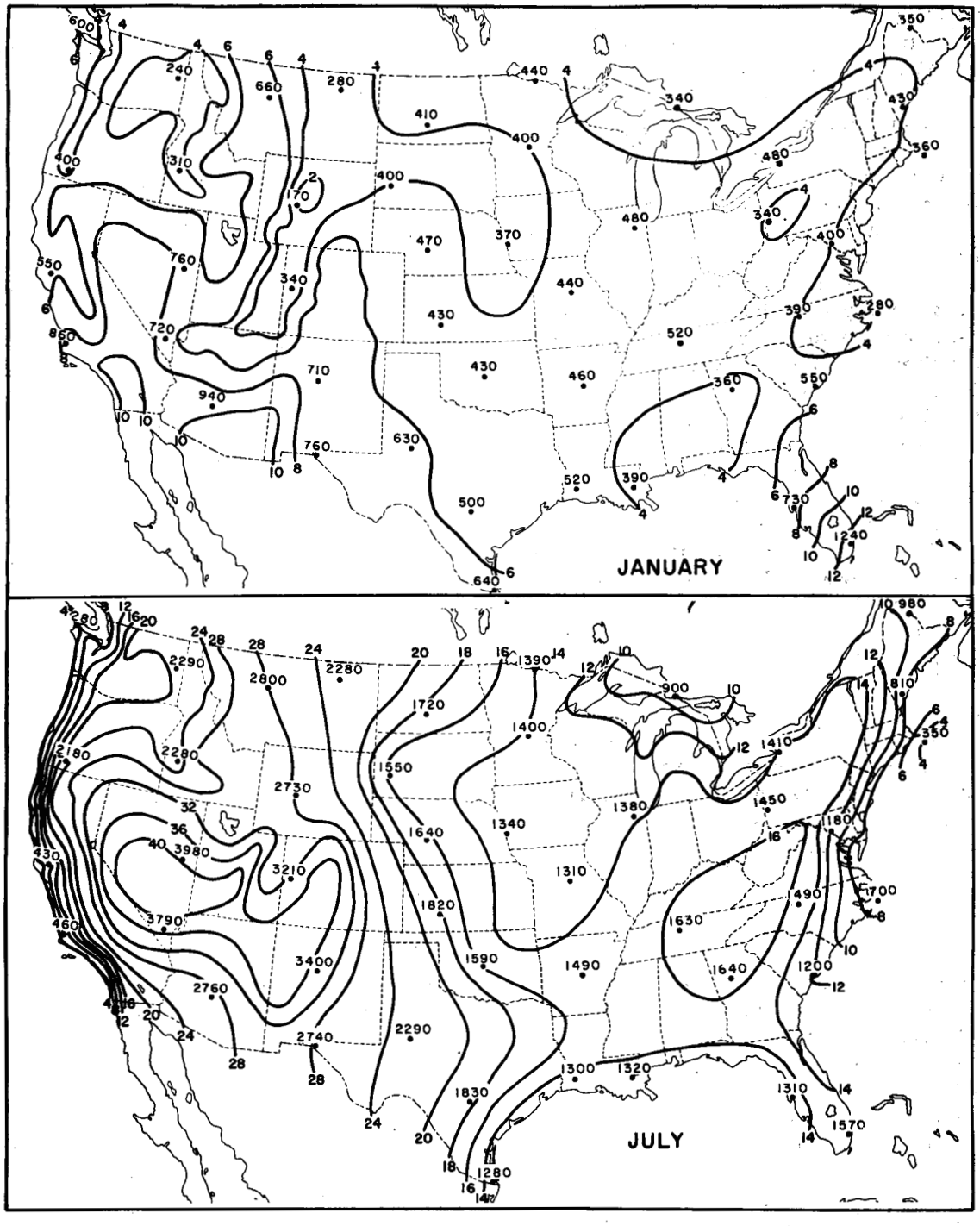

Fig. 2.23—The mean maximum mixing depth (m) for January and July. These data were computed from atmospheric temperature soundings obtained at 45 points in the United States. (Holzworth, 1964)

of zero just at the plane surface but an increasingly higher speed at increasingly greater distances from the plane. If the unretarded fluid some distance from the plane is moving in response to a given balance of forces, then the flow near the surface can be explained by the introduction of an additional force due, in this case, to molecular viscosity. This force becomes progressively larger as the fixed surface is approached. In the atmosphere the role played by molecular viscosity near the surface of the earth is small in comparison with what is called the eddy viscosity. This is an apparent viscosity due to turbulent whirls that bring rapidly flowing air from aloft and transport the slowly moving air near the surface to greater heights. The term "eddy" is purely descriptive and refers in a general way to any of the infinite variety of turbulent motions that transfer momentum or other properties from regions rich in that property to regions deficient in it. The nature of these fluctuations and the methods by which they are measured are discussed in subsequent sections.

The eddy viscosity, then, gives rise to a frictional force which decreases with height and must be added to the balance of the pressure gradient and Coriolis forces. This frictional force not only reduces the wind speed near the surface but also changes the vector balance of forces so that the air near the surface moves at some angle to the geostrophic wind. In Fig. 2.7 the small arrows representing the wind direction spiral inward toward low pressure and outward from high pressure rather than being aligned parallel to the isobars. This is due to the frictional forces.

In general, the air flow at the earth's surface is directed to the left of the geostrophic flow at an angle that varies from about 15° by day over a smooth surface to about 50° at night over rough terrain. Above the surface the observed wind usually turns slowly in a clockwise manner so that the angle between the wind and the geostrophic wind (or between the wind and the isobars) gradually decreases with height until, at roughly 1000 m above the ground, the observed wind is parallel and equal in magnitude to the geostrophic wind. The portion of the atmosphere below this level is the layer in which surface frictional effects have a substantial effect upon the wind (the planetary boundary layer).

Above the top of the planetary boundary layer, the characteristics of the wind, such as average speed, direction, vertical structure, and turbulence, are divorced from surface influences and are reflections of upper-level pressure forces.

Since eddy viscosity, unlike molecular viscosity, is not a permanent characteristic of the fluid but depends upon the amount of turbulent mixing present, it can be associated not only with mechanical features, such as the roughness of the surface, but also with other factors. A major factor to be considered is the presence of buoyancy forces associated with the occurrence of heating or cooling at the surface. By day, when the earth's surface is heated by the sun, turbulent mixing is enhanced, and the influence of the surface may be detected to a comparatively great height. At night, however, the stable stratification of the air limits mixing and produces a situation in which the surface effects are limited to the very lowest layers. Thus some level in the atmosphere will be subjected to frictional retardation by day but not at night. Above such a level the average wind speed may be expected to be higher at night than during the day. Below this level, in the region affected by the nocturnal temperature inversion, highest wind speeds occur during the day when the faster moving air aloft is mixed downward toward the surface. A typical diurnal pattern is shown in Fig. 2.24. These data from the Oak Ridge National Laboratory in Tennessee are based on anemometer measurements in the lower levels and balloon trajectories at the higher levels. Another example of this type of data, taken entirely from anemometers on a tower, is shown in Fig. 2.25.

Since both wind speed and direction vary with height near the surface, a vector diagram is frequently used to illustrate this combined change. Figure 2.26 shows average vectors constructed from data obtained during a number of summer nights and days at a location in central Nebraska. During the day the lowest level wind (16 m) is much closer in both direction and magnitude to the upper-level wind (1000 m), which may be assumed to be geostrophic, than it is at night. This is due to the greater degree of vertical mixing associated with daytime unstable conditions, which tends to establish greater homogeneity in the vertical.

The nighttime situation shows a wind-speed maximum somewhere in the middle of the plan-

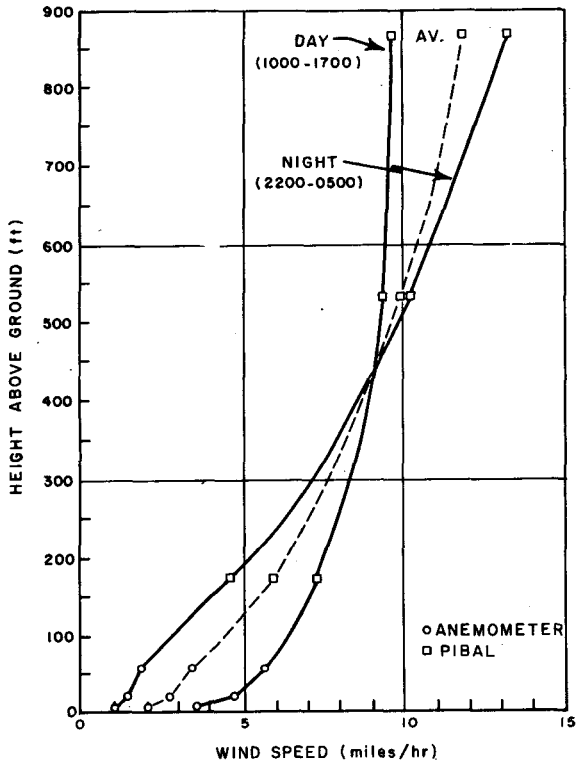

Fig. 2.24—Average wind-speed profiles constructed from measurements made during a 1-year period at the Oak Ridge National Laboratory. (Holland, 1953)

etary boundary layer. This phenomenon, known as a low-level jet, has been the object of much study in recent years. It is thought to be due largely to the "decoupling" of the upper layers of the planetary boundary layer from the surface and the setting up of an inertial oscillation. A full and widely accepted explanation of the low-level jet has yet to be advanced.

Even in the absence of turbulent mixing, the wind speed and direction may change with height owing to the change with height of the large-scale pressure distribution. This variation, coupled with the smaller scale frictional effects, results in a vertically varying wind structure that cannot be simply specified.

2-6.2 Atmospheric Turbulence

The interaction of all weather systems on all scales results, at a given point of observation, in a three-dimensional wind direction and speed that vary continuously in time. This continuous fluctuation, or turbulence, is the characteristic of the atmosphere that causes the diffusion of pollutants introduced into it.

The fluctuating wind, observed at a point, can usually be divided into a mean motion and superimposed fluctuating motions with components along the direction of the mean wind and in the vertical and lateral perpendicular directions. The distinction between the mean and turbulent motion may be determined on the basis of the dimensions of the diffusing system, e.g., a puff of smoke. Wind fluctuations larger than the puff tend to move it in its entirety and thus contribute to the mean motion. Fluctuations considerably smaller than the dimensions of the puff tear it apart and thus can be regarded as turbulent. On the scales involved in most practical diffusion problems, the discrete weather systems mentioned earlier usually contribute to the mean motion and the chaotic systems make their greatest contribution to the turbulent motions.

Turbulence is dependent upon three factors: the mechanical effects of objects protruding

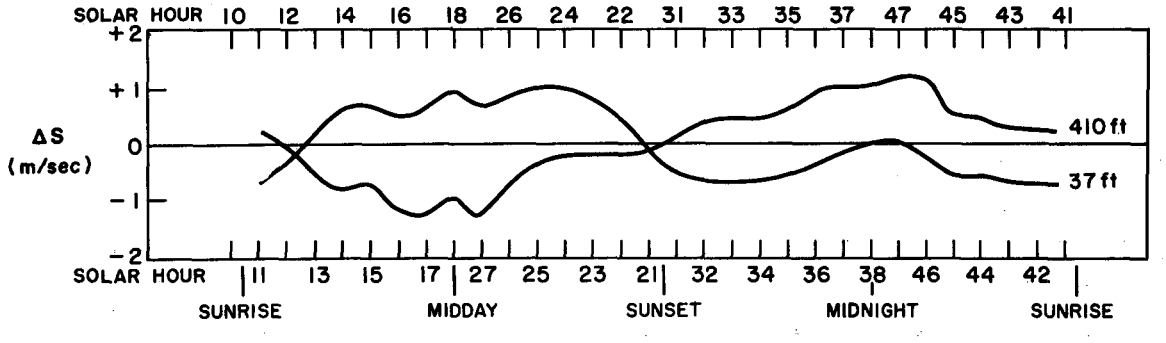

Fig. 2.25—The deviation of the mean hourly wind speeds from their respective daily averages at 37 ft and 410 ft. The data were collected at the Brookhaven National Laboratory. (Singer and Raynor, 1957)

into the air stream, such as the roughness of the earth's surface, the vertical rate of increase of wind speed, and the vertical temperature structure of the atmosphere.

When the ground is smooth over a large area, the air flow will tend to be similarly smooth.

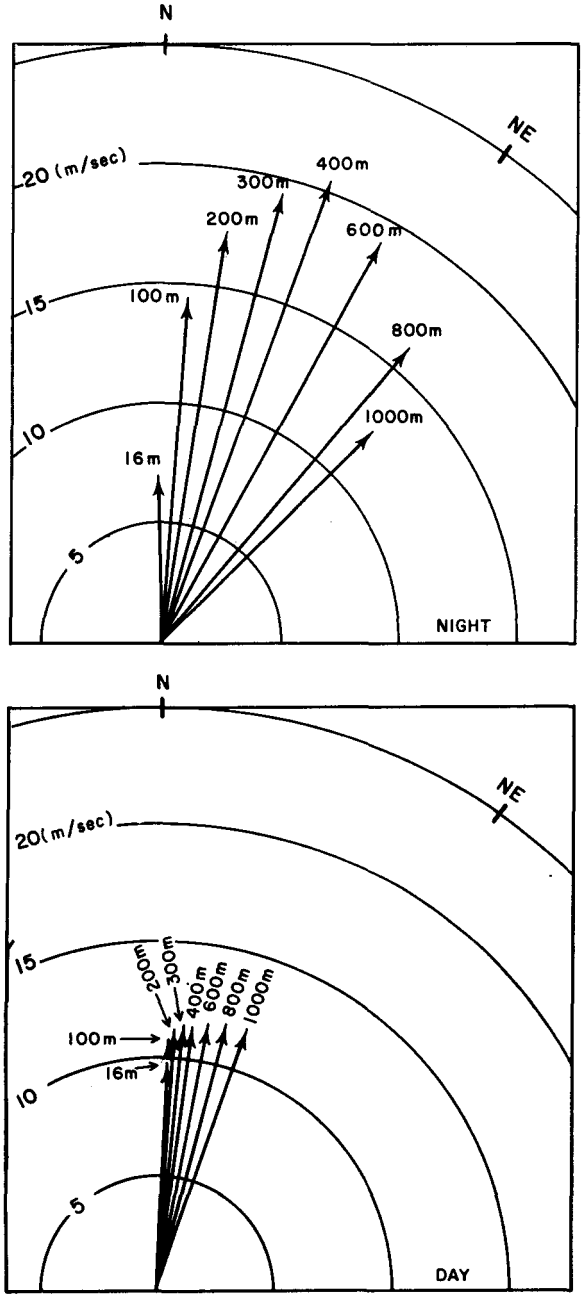

Fig. 2.26—Average vectors constructed from night and day wind observations obtained during the Great Plains Turbulence Field Program in central Nebraska. (Lettau and Davidson, 1957)

When the ground is rough, the air passing over it will rise and fall in response to the surface undulations. Thus vertical turbulence is generated. Since the air will also flow around some of the objects, horizontal turbulence is also generated. This mechanically generated turbulence is greater with higher wind speeds and, being generated at the surface, characteristically exhibits a decrease with height. If the mean wind vector in the atmosphere were constant with height, the turbulence would consist entirely of small displacements of this mean flow by the surface configurations. However, no matter what the wind vector may be at some upper level, it must be zero at the immediate surface of the earth. The wind vector characteristically increases in magnitude with height as well as usually changing direction. Thus, if a particle of air is displaced from one level to another, it will arrive at the new level with some of its initial momentum and will constitute a perturbation in its new surroundings. Any vertical fluctuations existing in a fluid with vertical shear will result in a chaotic field of vertical and horizontal turbulence. The existence of a vertical shear itself will initiate or enhance turbulence when the shear is great.

Properties other than momentum may also be transferred by turbulence. If the air next to the ground is heated until it is warmer than the air above, a heat-energy gradient will exist above the ground. A particle moving upward will carry more heat energy than a particle from an upper level moving downward. Thus there will be a net upward flux of heat due to turbulent motion. This mechanism is described by the principle that states: air properties are transferred by turbulence in the direction of decreasing values of these properties, i.e., down the gradient. Obviously the greater the turbulence or gradient, the greater the rate at which this transfer, or mixing, can take place. If a mass of smoke is injected into the atmosphere, there will be both vertical and horizontal components of the gradient between the smoke and the unpolluted air, and, in the presence of turbulence, smoke transport down the gradient will result in the dilution and spreading of the smoke mass.

It is not always clear where the line should be drawn between transport by mean motion and transport by turbulence. The scale of averaging and the nature of the phenomenon being studied

must enter into the decision. On a sufficiently large scale, the mean wind may turn out to have its own turbulent fluctuations; then the puff, instead of simply being transported downwind, will be transported along an irregular, meandering path. Although both mean transport and turbulence are of importance in horizontal transfer, turbulence is largely responsible for vertical transfer.

The mean structure of the wind, in spite of the many complicated features that have been noted or suggested, is simpler than the actual structure of the observed wind. The actual wind consists not only of the mean part but also of seemingly random variations about the mean. The study of these turbulent variations has usually proceeded via the application of statistical techniques rather than the dynamical methods that have characterized much of the progress in other fields of atmospheric physics.

The statistical study of turbulence frequently requires data that are in the form of a digital or analog time series, and many of the techniques that relate diffusion to wind fluctuations involve the processing of such time series. Section 2-6.2.1 presents definitions of some terms used in the discussion of time series and the less frequently encountered space series.

2-6.2.1 The Random Process. The concept of a random process has been applied with considerable success to problems in turbulence and diffusion in spite of the fact that meteorological occurrences are not strictly random (the wind speed at a given instant is correlated with the speed at the previous instant). The time trace shown in (a) of Fig. 2.27 could represent the horizontal or vertical wind direction measured by a wind vane during a particular regime of meteorological conditions. The specific features

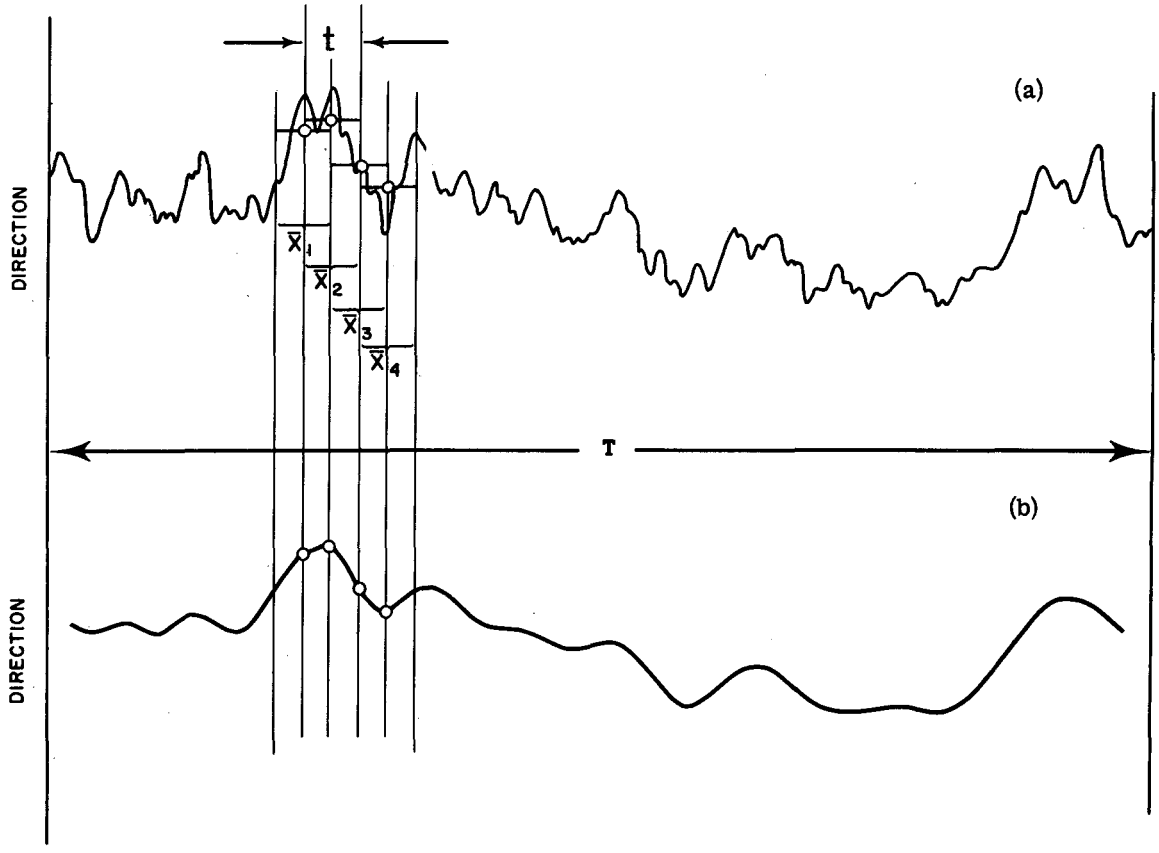

Fig. 2.27—An instantaneous wind-direction trace (a) and the time-averaged trace derived therefrom (b). The time interval t represents the averaging time, and T represents the total length of record, or the sampling time.

of a second trace taken under the same conditions would be different, but there might well be a decided resemblance in some of the statistical characteristics, such as mean value, total range, and variance or variance distribution as a function of wavelength. The ensemble statistics resulting from numerous repetitions of this experiment could be offered as a physical representation of turbulent wind structure. Since the statistical characteristics derived from any one of these traces would bear a distinct family resemblance, it is frequently only necessary to study one or a few of these individual traces to derive some of the characteristics of the entire ensemble.

A type of random process that has found frequent application in turbulence and diffusion studies can be described as being stationary, homogeneous, isotropic, and Gaussian. The property of stationarity implies that the statistical properties derived for a time series do not vary with time. Thus a variance computed from 1 hr of data would be similar to that computed from the next hour of data if the turbulence were stationary. Major changes in the meteorological regime such as occur during the diurnal cycle or with the passage of a front would mitigate against stationarity. The concept is, however, generally fulfilled during periods of several hours duration when the large-scale pattern is not changing.

If the random process is homogeneous, its statistical properties will not vary in space; that is, a measurement taken at a particular point will display statistical characteristics identical to those taken at some neighboring point in space. Horizontal homogeneity is usually assumed in regions of not dissimilar topography, such as flat plains or rolling countryside. Owing to the vertical forces of gravity and buoyancy and to the presence of the physical boundary of the earth's surface, vertical homogeneity is a rarity in the real atmosphere.

Isotropy can be defined by the condition that the statistical properties of the field being studied are independent of the rotation of the coordinate axes. Thus the variances of the various normal velocity components are equal in an isotropic field. Although this condition may be met in a limited way in the atmosphere, such is not generally the case.

A Gaussian random process is one in which the frequency distribution of values of the variable of interest follows the familiar Gaussian, or normal, curve. The distribution is completely specified by the mean and standard deviation. Many atmospheric variables have been found to be distributed in a Gaussian manner. Thus a histogram of 1-sec mean wind directions accumulated over 10 min can usually be fitted quite accurately by a Gaussian curve with the mean and standard deviation of the histogram.

2-6.2.2 Measurement of Wind Fluctuation. Atmospheric turbulence in the context usually encountered in diffusion literature consists of seemingly random fluctuations of the three-dimensional wind vector which act in a highly organized manner to dilute an effluent or tracer injected into the atmosphere. Before these fluctuations can be discussed, some base value must be defined; the deviations from this value then can be considered as turbulence. The base value is usually the time-averaged value of the particular wind statistic and is given by

$$\overline{W} = \frac{1}{T}\int_0^T W d\tau \qquad (2.1)$$

where W represents any characteristic of the wind, i.e., speed, direction, or value of any one of the components, and T is the sampling time.

If, in an orthogonal coordinate system, u is the component of the wind along the x-axis (usually assumed to coincide with the mean vector wind direction), v is the component in the y-direction, and w is the component along the z-axis (assumed to be vertical), then the actual wind components at any instant can be thought of as being composed of mean values and deviations from the mean:

$$\begin{aligned} u &= \overline{u} + u' \\ v &= \overline{v} + v' \\ w &= \overline{w} + w' \end{aligned} \qquad (2.2)$$

The fluctuation quantities u′, v′, and w′ can be represented as time series that pass through positive and negative values. These series can be subjected to variance, spectral, and autocorrelation analyses.

At this point we will confine our attention to some of the problems inherent in the measurement and calculation of the variance, or standard deviation, of the wind fluctuations. To facilitate the discussion, we will introduce sev-

eral concepts that will appear frequently on following pages: the intensity of turbulence and the standard deviation of the horizontal (azimuth) and vertical angles of the wind vector.

The intensity of turbulence along each axis is defined by

$$i_x = \left(\frac{\overline{u'^2}}{\bar{u}^2}\right)^{1/2} = \frac{\sigma_u}{\bar{u}} \qquad (2.3)$$

$$i_y = \left(\frac{\overline{v'^2}}{\bar{u}^2}\right)^{1/2} = \frac{\sigma_v}{\bar{u}} \qquad (2.4)$$

$$i_z = \left(\frac{\overline{w'^2}}{\bar{u}^2}\right)^{1/2} = \frac{\sigma_w}{\bar{u}} \qquad (2.5)$$

where σ is the standard deviation of the velocity distribution. These statistics of turbulence bear a direct relation to the diffusing power of the atmosphere.

Another statistic of wind fluctuation that has found wide use in diffusion-estimation techniques is the variance, or standard deviation, of the azimuthal wind-direction angle (σ_θ^2 or σ_θ) where θ is the angular direction of the horizontal wind. This can be measured directly from the output of a wind vane. It is related to the intensity of turbulence in the crosswind direction (i_y) since, as shown in Fig. 2.28,

$$\tan\theta' \approx \theta'(\text{radians}) = \frac{v'}{\bar{u} + u'}$$

$$\overline{\theta'^2} = \frac{\overline{v'^2}}{(\bar{u} + u')^2} = \frac{\overline{v'^2}}{(\bar{u})^2}\left(1 + \frac{u'}{\bar{u}}\right)^{-2}$$

which, expanding and neglecting the higher order terms, gives

$$\overline{\theta'^2} = \frac{\overline{v'^2}}{(\bar{u})^2} \quad \text{or} \quad \sigma_\theta = \frac{\sigma_v}{\bar{u}} \qquad (2.6)$$

Vertical wind-direction fluctuation data may be treated similarly. Such data are obtained as an output of a vane that is free to pivot in the vertical plane as well as in the horizontal (bivane wind sensor). The standard deviation of the vertical-direction trace is usually denoted by σ_φ.

It is important to recognize that the numerical values of i_x, i_y, i_z, σ_θ, and σ_φ are not constants for a particular set of meteorological conditions. Their values depend on sampling and averaging times that are inherent characteristics of a sample of data (See Sec. 2-6.2.3).

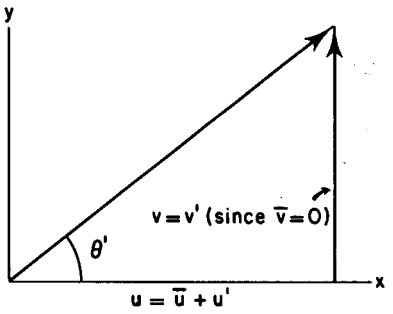

Fig. 2.28 — Deviation of the instantaneous wind from the mean wind.

2-6.2.3 Sampling and Averaging Times. The wind-direction trace shown in (a) of Fig. 2.27 could represent the wind direction measured by a wind vane at a particular point, in which case it would be called a Eulerian time series. It could, however, represent the path of a particle following the wind, in which case it would represent a Lagrangian series.

Considering the curve as a Eulerian time series produced by a wind vane, we can define the sampling and averaging times as follows: the sampling time, T, is that interval during which the data are measured and is represented in (a) of Fig. 2.27 by the total period of the record; the averaging time, t, is some time interval over which the continuously varying trace may be represented by a constant (average) value. If the illustration represents the trace taken directly from a wind-direction recorder, the averaging time will be that resulting from the inertia of the wind vane and recorder system and their resulting inability to respond faithfully to the very highest frequency fluctuations impressed upon them. This averaging time is usually in the range of a few seconds or less for the high-response instruments used in diffusion work. It will be shown in later chapters that it is frequently necessary to smooth the instrumental time trace. This can be done by constructing a digital series from the analog series. The digital series might be composed of the average values of the trace over successive overlapping equal intervals of time, t, where t is the averaging time. Connecting these average values produces the time-averaged, or time-smoothed, trace shown in (b) of Fig. 2.27. The application of the averaging time has the effect of removing those fluctuations of periods shorter than t.

The standard deviation of wind-direction fluctuations, whether horizontal or vertical, normally increases with increasing sampling time up to some point. Further, the standard deviation decreases with increasing averaging time. The increase of standard deviation with increasing sampling time follows because more of the long-period fluctuations are sensed during the longer sample periods. On the other hand, the increase in averaging time damps out the contribution of the shorter-period fluctuations to the total standard deviation. The application of a sampling and averaging process to a time series therefore constitutes a filter, or window, through which only a portion of the total energy in the spectrum of wind fluctuations can be observed.

The standard deviation of the wind direction may be computed by hand, by computer from suitable digital data, or by comparatively simple electronic equipment that computes the standard deviation directly from the signal generated by the wind vane. A rather simple, if gross, estimate of the horizontal standard deviation may be obtained from the wind-direction range, or total width of the direction trace over some given time interval. Individual range values, e.g., the range over a 1-hr interval, give only a crude estimate of the standard deviation for the same 1-hr interval because one extreme oscillation of the vane, lasting perhaps for only a second, can cause a great change in the value of the range but contribute little to the standard deviation. The average of a great many range values, however, has been shown to be closely related to the average of the standard deviation for those intervals (Markee, 1963). In general, the range divided by about 6.0 has been found to give a good approximation to the horizontal standard deviation for the same data sample period when an averaging time of the order of 1 to 10 sec is used. Range statistics are particularly helpful for climatological estimates from large quantities of data taken from ordinary recording wind systems.

Atmospheric diffusion is related not only to the value of the standard deviation, or variance, of wind direction but also to the frequency or range of frequencies in the spectrum that makes the greatest contribution to the total standard deviation. Although two records of the fluctuation of a wind component may have the same standard deviation, this could be caused in one case by a few oscillations of long period and in the other by more numerous oscillations of shorter period. Since long-period oscillations tend to transport a small mass of atmospheric pollutant in its entirety whereas short-period fluctuations tend to tear it apart, the distribution of the energy within the different fluctuation periods is of great interest. This distribution has been studied by spectrum analysis methods.

Meteorological spectra are usually computed from time- rather than space-series data. A typical meteorological spectrum will present an estimate of the variance of a meteorological element per frequency interval as a function of frequency. Although spectra can be determined for any meteorological variable that can be presented quantitatively by a continuous or discrete-value time series, the spectra of the various wind statistics are of primary concern in turbulence and diffusion research. The spectra of the orthogonal wind components have received considerable attention in turbulence literature, and diffusion studies have frequently concentrated on the spectra of lateral and vertical wind directions. A typical wind-direction spectrum has the units of direction variance in degrees^2 or radians^2. When the spectral estimates [S(n)] are multipled by frequency (n) and plotted as a function of the logarithm of frequency, the area under the curve in each frequency range will give the contribution of that frequency range to the total variance. Most published spectra are in this form.

Figure 2.29 presents typical spectra of vertical and lateral wind directions in which the individual spectra for the series of experiments have been grouped by categories of thermal stability (Walker, 1963). The vertical-direction spectra, (a) of Fig. 2.29, show quite clearly the typical features of vertical wind fluctuations. The stable curves show small variance, the small peaks that do exist being at rather high frequencies. Under stable conditions at the observation height of 15 m, the turbulence is mechanically generated at the surface by the air passing over the surface irregularities. During instability the warm ground introduces a thermal component into the turbulence. This thermal contribution results in the shifting of the peak to lower frequencies. Because of the proximity of the surface to the observation level, individual vertical turbulence elements

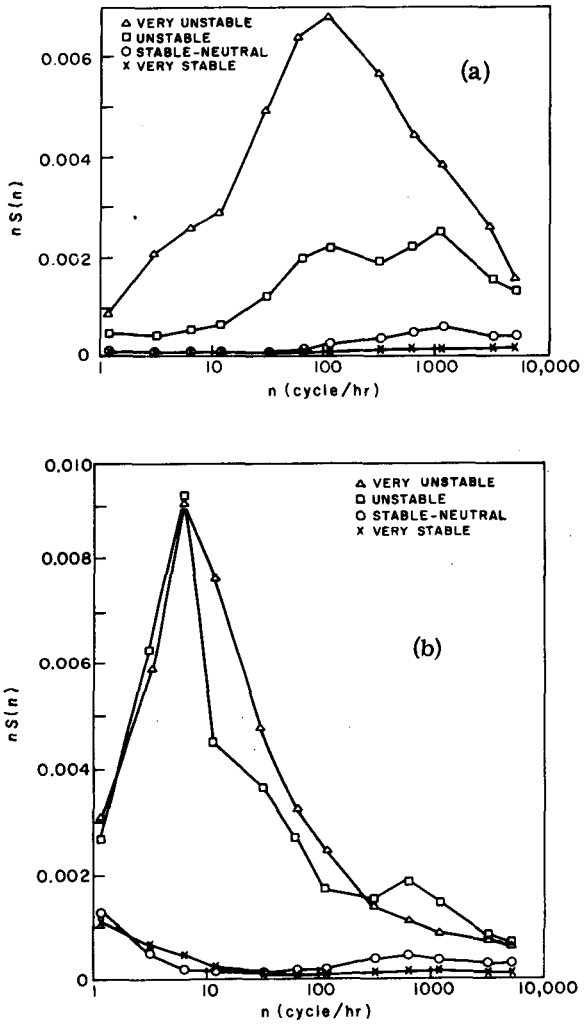

Fig. 2.29—Spectra of the vertical (a) and horizontal (b) wind-direction fluctuations (σ_φ^2 and σ_θ^2) at 15 m grouped by atmospheric stability. (Walker, 1963)

are limited in extent, and a rapid decrease in the variance at the lower frequencies results. Data taken at higher elevations would show a pattern similar to that in (a) of Fig. 2.29 except that the unstable curves would be of greater magnitude and at lower frequencies whereas the stable spectra would be flatter.

Lateral-direction spectra are presented in (b) of Fig. 2.29. Both the stable and the unstable curves show two peaks, one at a comparatively high frequency and one at lower frequencies. The high-frequency peaks are due to fluctuations in the lateral wind direction initiated by surface roughness. The magnitude of these peaks increases with increasing wind speed and decreases with height above the surface. The low-frequency peak during unstable conditions reflects the wind fluctuations due to thermally induced eddies. The magnitude of this latter peak increases with increasing incoming radiant energy and decreases with increasing wind speed. The existence of a low-frequency peak during night (stable) conditions although established by observational evidence cannot be explained simply. The long-period oscillations contributing to this peak are probably due to slow-moving systems, which are imbedded in the stable air and have horizontal dimensions ranging from hundreds to a few thousands of meters. For longer sampling times the low-frequency peak would probably be displaced toward even lower frequencies. These systems are of considerable importance in predicting dispersion at night since they may lead to a much greater degree of horizontal effluent spreading than might normally be expected during inversion conditions.

2-6.3 Fluctuation of the Wind

The continuous fluctuation of the atmosphere on time scales of hours or less can be visualized from the time traces of wind speed and direction shown in Figs. 2.30 and 2.31. These rather typical traces were obtained from wind instruments mounted on masts or towers at the heights indicated in the figures. Part (a) of Fig. 2.30 shows a typical change from night to day wind conditions under clear skies at a rural location near Washington, D. C. From 4:00 a.m. to about 5:30 a.m., a light wind speed associated with inversion conditions resulted in a wind-direction trace averaging 10° to 15° in width. At the time of sunrise (5:30 a.m.), the wind dropped to almost the instrumental threshold, but even this was sufficient to cause the vane to meander for the next half hour. A thin ground fog prevented the destruction of the inversion until about 7:00 a.m. At this time the wind speed began to pick up slowly, and the direction fluctuations increased to fairly typical daytime values, which persisted for the rest of the period.

Part (b) of Fig. 2.30, taken in mid-July in the desert area of central Washington State, shows a transition from a light-wind thermally unstable flow to a less unstable high-wind regime. The extremely variable nature of the wind is

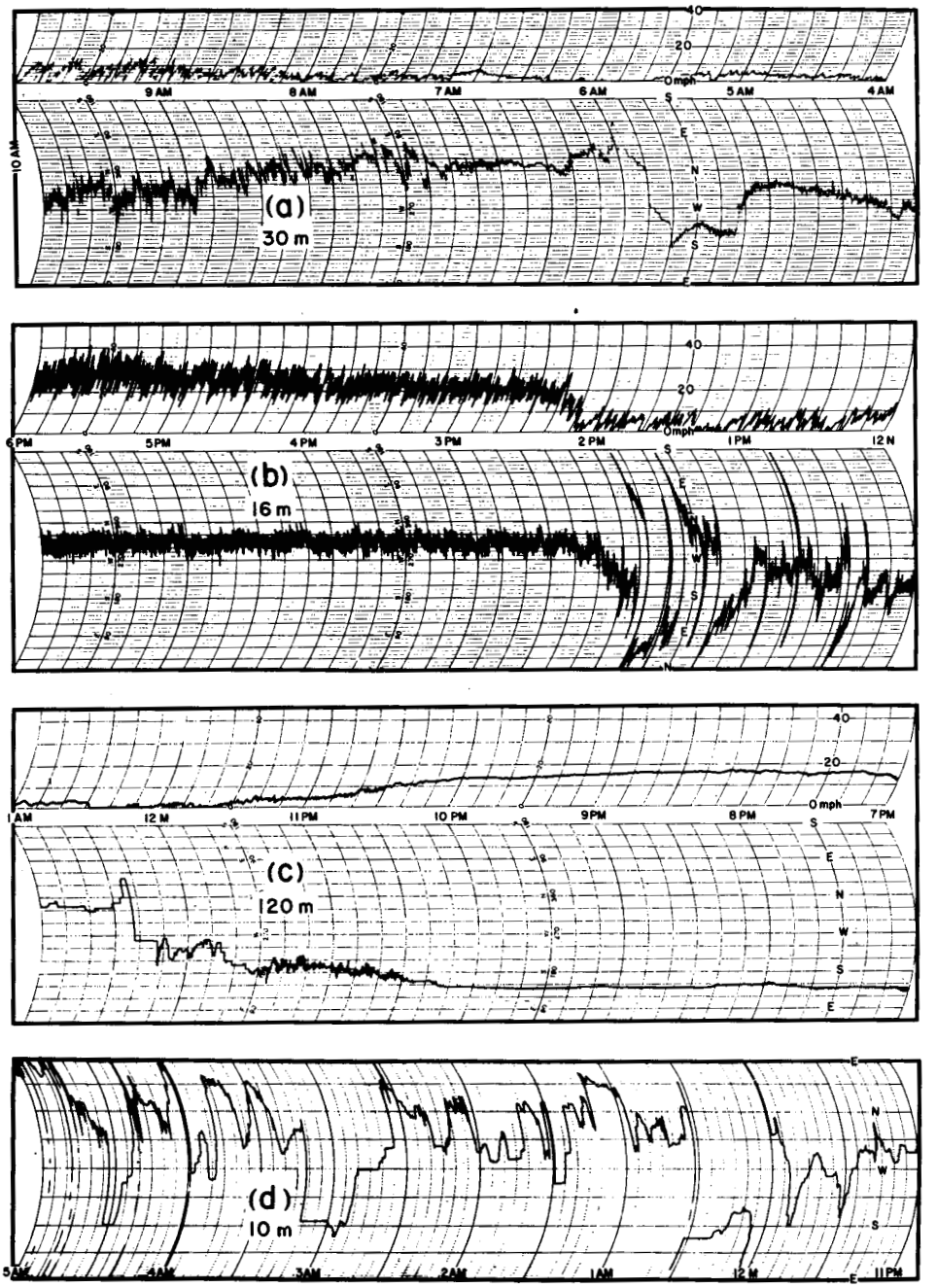

Fig. 2.30 — Typical horizontal wind-speed and -direction traces at various heights. Chart speed, 3 in./hr. (a) Night to day change. (b) Light wind, unstable flow followed by a cold frontal passage. (c) Upper-level flow during an intense inversion. (d) Low-level flow during an intense inversion.

evidenced by the fact that between the hours of 1:00 and 2:00 p.m. the wind blew from every direction of the compass under clear skies and therefore under strong solar radiation. At about 2:00 p.m. the passage of a front caused a narrowing of the direction range and high wind speeds. This part of the direction trace shows the result of mechanical turbulence caused by the high winds blowing over surface obstacles superimposed on a thermally unstable regime.

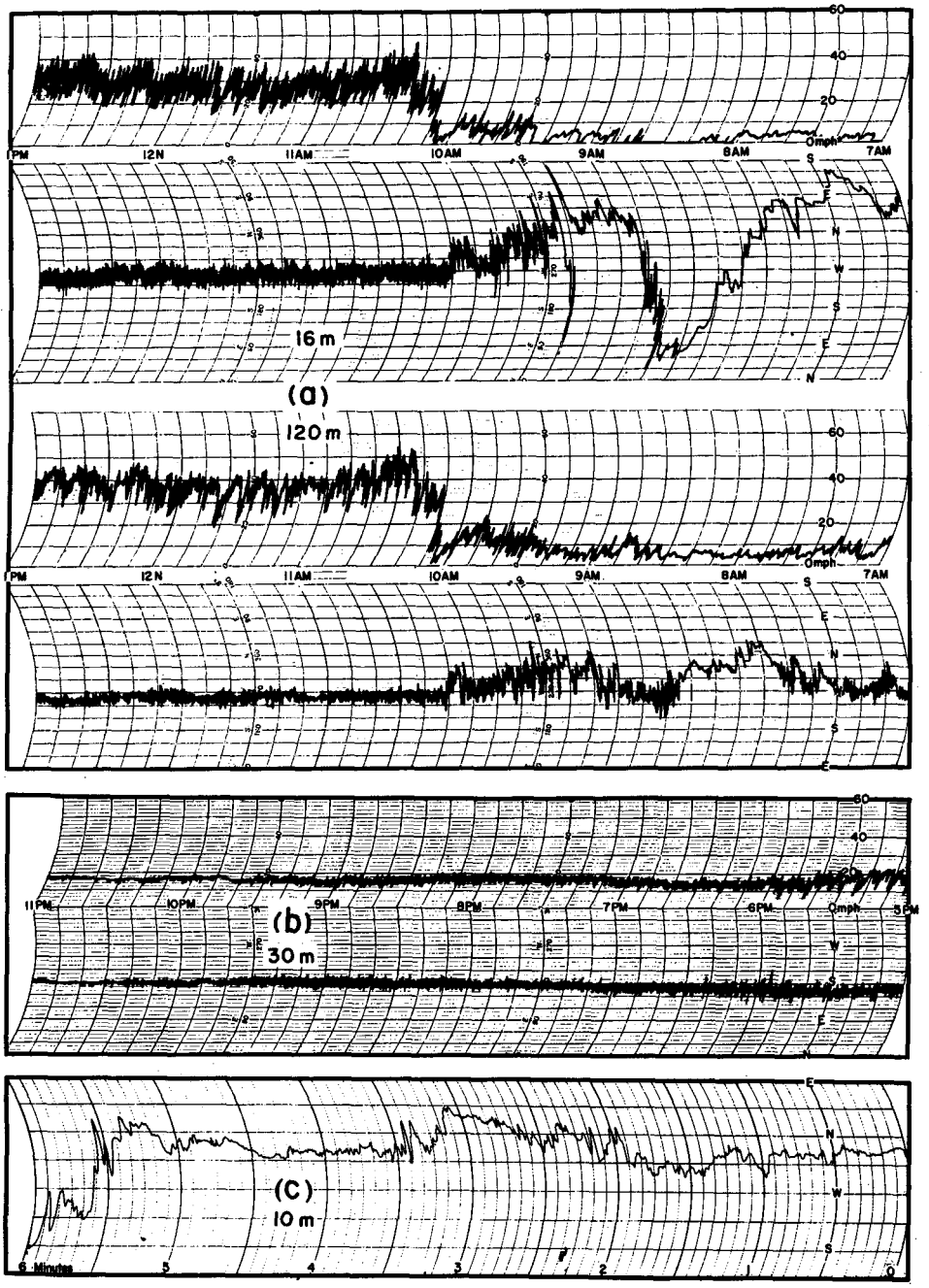

Fig. 2.31—Typical horizontal wind-speed and -direction traces. (a) Differences in characteristics for simultaneous recordings at 16 and 120 m (chart speed, 3 in./hr). (b) Example of a very steady wind trace (chart speed, 3 in./hr). (c) High-speed trace (chart speed, 3 in./min).

Part (c) of Fig. 2.30, taken at the same location in Washington State but at 120 m above the surface, shows the wind pattern existing during an intense inversion in mid-March. During the early part of the period, a wind speed averaging 15 mph was accompanied by a direction almost devoid of oscillation. As the wind speed began to drop, shortly after 10:00 p.m., the direction fluctuations increased. When the wind speed reached a few miles per hour, the direction

meander typical of very light speeds became evident. The squared appearance of the oscillations is probably due to pen friction on the paper chart combined with a vane movement that started and stopped as the wind speed rose above and fell below the starting speed of the vane.

Part (d) of Fig. 2.30, again observed at a rural location near Washington, D. C., at 10 m above the surface, is an example of the extreme direction meander frequently associated with wind speeds on the threshold of detectability. These low speeds are most frequently experienced close to the surface, and therefore this type of direction trace is usually, although not necessarily, confined to about the lowest 30 m. The wind-speed trace is not given since the speed was below the starting speed of the anemometer during most of the period. The abrupt direction changes occurring exactly at midnight and again at about 12:32 a.m. were due to movement of the wind vane through east, the boundaries of this particular chart.

Part (a) of Fig. 2.31 has been included to show the difference in wind-speed and direction fluctuations at 16 m and 120 m. The meander at 16 m in the first part of the trace is considerably reduced at 120 m. The amplitude of the higher frequency fluctuations at the 120-m level is reduced by about one-third over the 104-m vertical interval.

Part (b) of Fig. 2.31 shows a case of quite steady wind direction and speed in mid-April near Washington, D. C., under cloudy conditions. The wind direction changes very evenly and slowly, and the direction fluctuations decrease slowly during the late afternoon and early evening.

Finally, (c) of Fig. 2.31 is a high-chart-speed section of a direction record taken at 10 m. During this run the chart was moving 60 times faster past the pens than the charts were in the other illustrations. Records such as these are of use in studying the very-fine-scale atmospheric oscillations. At this end of the atmospheric fluctuation spectrum, the instrumental response determines the highest frequency fluctuations that can be seen. Fluctuations of significantly shorter period than those shown in the diagram occur and have been measured by specially designed high-response instrumentation.

Figure 2.32 shows the vertical wind-direction trace taken from a typical bivane wind sensor at 10 m above the ground. It is immediately seen that the mean direction taken over any length of time longer than a few minutes is 0° (horizontal). During the predawn hours the trace shows typical mechanical turbulence associated with moderate wind speeds and inversion conditions. At 5:30 a.m., the wind speed dropped, and the vertical-direction fluctuations decreased in magnitude. Sunrise (6:40 a.m.) was accompanied by slowly increasing direction fluctuations, which reached a rather steady value by 8:30 a.m. and persisted for the rest of the period. The magnitude of the fluctuations was greatest during the midafternoon period (not included in this illustration).

Figure 2.33 is an example of a horizontal wind-direction range climatology taken from recorder charts similar to those in the last section over a broad plain in southeast Idaho. The raw data used to construct this chart were the absolute range measurements taken for a period of 15 min once each hour. The greatest values of the range are associated with the most intense instability during summer days; the minimum values of the range occur during the winter nights. The isopleths of range in

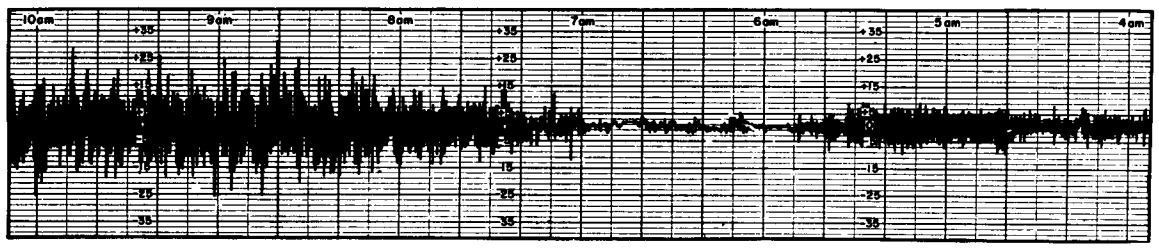

Fig. 2.32—Example of a vertical wind-direction trace (chart speed, 3 in./hr). The bivane sensor was mounted 10 m above the surface.

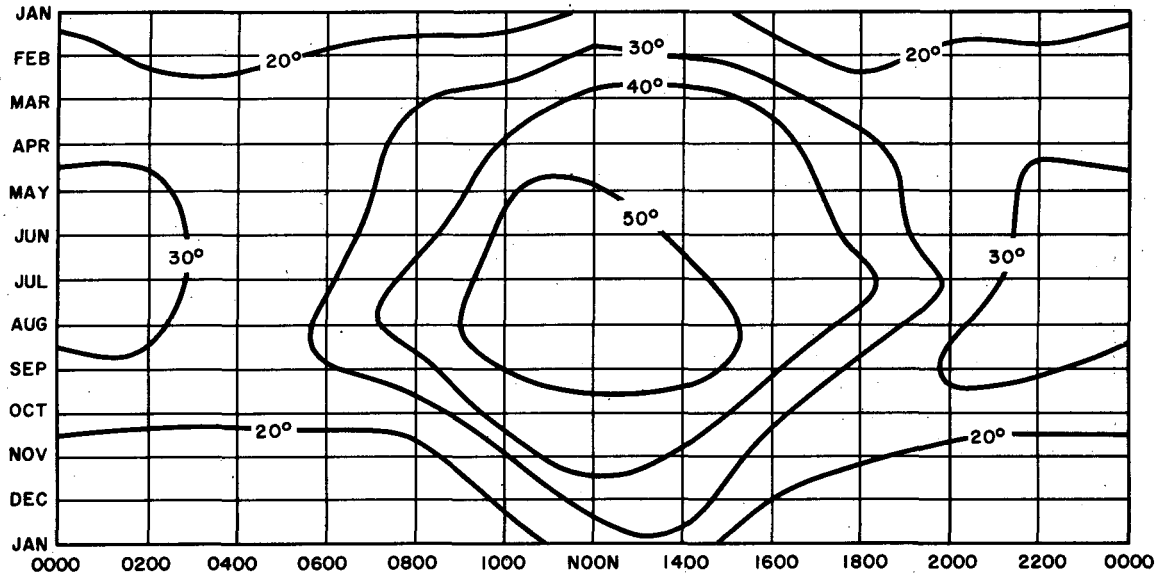

Fig. 2.33—Wind-direction range climatology compiled from data observed at 75 m above the National Reactor Testing Station in Idaho. The total range was measured over a sampling time of 15 min.

Fig. 2.33 may be compared with those for vertical temperature structure in Fig. 2.21 to relate wind fluctuation to stability.

Figures 2.34 and 2.35 present a general picture of the vertical variation of the standard deviation of the horizontal and of the vertical wind directions, respectively, with height and stability. The data used to construct these diagrams were drawn from a variety of experimental determinations. The original data were either in the form of velocity-component variance, direction standard deviation (variance), or direction range. The velocity-component variance and direction range were converted into direction standard deviation to permit data comparison.

The approximate thermal-stability categories used to stratify the data represent different temperature gradients at different heights, as may be inferred from the profiles of temperature in Fig. 2.19. Thus the term "very stable" may represent a temperature increase with height of 8°C in the first 30 m above the surface but only a degree or less in a 30-m layer well above the surface. The values presented in these two figures are only approximate. The factors that were not controlled by the various experimenters contribute to a large spread of possible values for a particular stability category, height, etc.

Figure 2.34 shows the variation of the lateral-wind-direction standard deviation for a sampling time of about 10 min as measured up to about 400 ft and extrapolated to 600 ft. For a given stability condition, values of σ_θ for sampling times greater than a minute or so will always be greater when the wind is light than when it is strong. This is most noticeable in the lowest layers. The line in Fig. 2.34 representing very

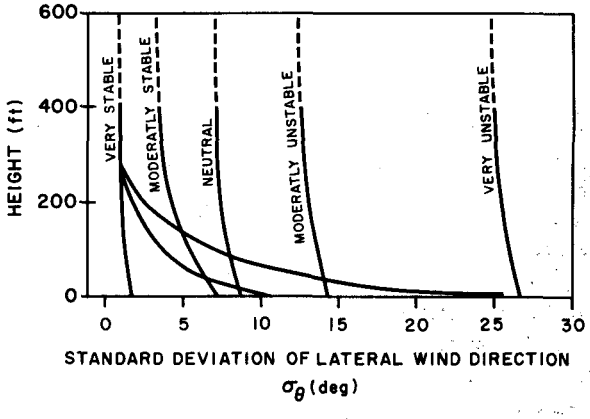

Fig. 2.34—The vertical variation of the lateral wind-direction standard deviation (σ_θ) for various stability regimes. The curves represent average or typical conditions with the exception of the two outer "very stable" lines, which represent extremes. Sampling times of the data used in the construction of this diagram averaged about 10 min, and averaging times were on the order of a few seconds.

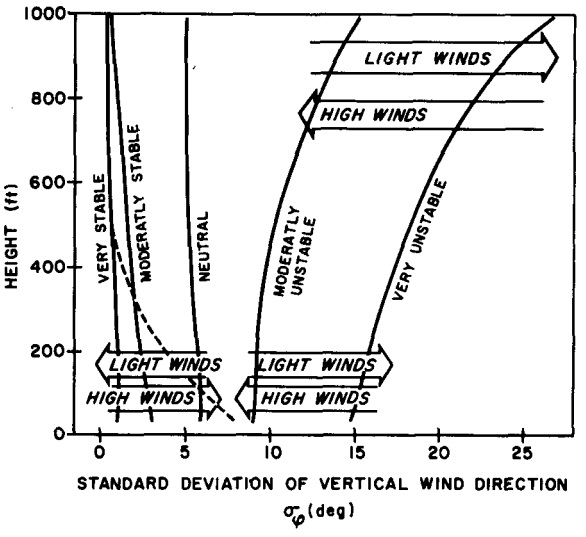

Fig. 2.35 — The vertical variation of the vertical wind-direction standard deviation (σ_φ) for various stability regimes. The relations shown represent sampling times of at least 3 min at the lowest levels and up to 30 min at the greater heights.

stable conditions (which by their nature are associated with light winds) branches into three separate lines near the ground. The curve at the left represents the smallest values of σ_θ usually observed. The curve that branches off to the right reflects the contribution of very-low-level wind-direction meander to the total 10 min standard deviation. These meandering oscillations decrease in amplitude very rapidly with height under stable conditions. The central curve represents typical inversion conditions.

The large surface values of σ_θ for unstable conditions do not decrease very rapidly with height. As in the case of very stable conditions, the greatest lateral fluctuations during a very unstable thermal structure occur with very light winds. As a general rule, for a given insolation condition, increasing wind speeds are associated with profiles of σ_θ that tend toward neutral stability.

If the value of σ_θ for a given sampling time T_0 is known, the value of σ_θ may be crudely estimated for a different sampling time by the following empirical formula:

$$\sigma_\theta(T_1) = \left(\frac{T_1}{T_0}\right)^p \sigma_\theta(T_0) \qquad (2.7)$$

where the subscripts 0 and 1 refer to the known and required values of sampling time, respectively. The value of p varies with stability, wind speed, and height above the surface, but a value of p = 1/5 can be used for a working approximation.

Although there are not as yet definitive data on the vertical structure of σ_θ above the heights given in Fig. 2.34, it is not likely that there will be any dramatic change in the higher levels from the values given in the 400- to 600-ft layer.

Turbulence and diffusion studies frequently require a knowledge of the standard deviation of the crosswind component distribution (σ_v) as well as of σ_θ. Since, from Eq. 2.6, $\sigma_v = \sigma_\theta \bar{u}$ and since the wind speed increases with height above the surface, the variation of σ_v with height cannot be simply inferred from Fig. 2.34. The following are general statements concerning the variation of σ_v with wind speed, stability, and height:

1. At a given height during neutral conditions, σ_v is proportional to wind speed.

2. For a given wind speed and height, σ_v is greater during unstable than during stable conditions.

3. For a given stability condition and at a given height, σ_v increases with wind speed and surface roughness, most markedly during stable conditions.

4. The value of σ_v changes rather little with height during any stability condition. This may be inferred from the nature of the height variation of σ_θ and wind speed. During stable conditions σ_θ decreases rather rapidly with height whereas the wind speed increases comparatively rapidly over the same height interval. During unstable conditions the decrease of σ_θ with height is slow, and the increase in wind speed is slow.

It is important to realize that the last statement is quite general and that a marked vertical gradient of σ_v might exist under some particular conditions of wind speed and direction fluctuation.

Figure 2.35 presents the vertical profiles of the vertical wind-direction standard deviation (σ_φ) for averaging times of a few seconds. In the case of the vertical fluctuation of the wind at heights below 1000 ft, it is not essential to consider sampling time if the period is longer than 20 min. Vertical wind fluctuations are restricted because of the proximity of the earth's surface and are therefore smallest in magni-

tude, on either a time or length scale, near the surface and increase with height. Even at 1000 ft, however, they are still influenced by the solid boundary of the earth, and vertical oscillations of periods longer than 20 min are unusual. Thus the standard deviation of vertical wind direction will show very little increase for very long sampling times. This is in sharp contrast with the standard deviation of horizontal wind direction, which increases continuously with sampling time.

During nighttime inversions, when the predominant vertical turbulence is mechanically induced at the surface, sampling times of less than 10 min would be more than sufficient to obtain standard deviations that would not increase with increasing sampling length. During unstable day conditions 10-min sampling times are probably adequate in the lowest few hundred feet, but this adequacy may decrease with height, and at 1000 ft a 10-min sampling time may result in standard deviations of the vertical wind direction which are too low.

The effect of wind speed is somewhat different on the vertical fluctuations than on the horizontal. Light winds at the lower levels are associated with large values of σ_φ during unstable conditions and small values during stable conditions. Strong winds result in mechanical mixing, which prevents the development of strong stable or unstable vertical temperature gradients. Therefore during strong-wind periods σ_φ values will tend toward those marked "neutral" in Fig. 2.35. Mechanical vertical turbulence decreases with height above the surface whereas thermally induced vertical motions characteristically increase with height.

During strong surface-based radiational inversions, the vertical shear of the horizontal wind may become large enough to overcome the effects of thermal stability and cause turbulence. This phenomenon can be described in terms of the Richardson number, which quantitatively relates the vertical wind-velocity profile to the vertical temperature profile. Turbulence caused by strong wind shear at night is usually evident as short bursts of heightened vertical motion.

It is sometimes desirable to consider the variability of σ_w as well as of σ_φ. As in the case of σ_v, we may write $\sigma_\varphi \bar{u} = \sigma_w$ and make the following general statements:

1. Under neutral conditions σ_w is proportional to wind speed and displays little variation with height.

2. In a stable atmosphere σ_w generally decreases with height.

3. During unstable conditions σ_w increases markedly with height through some large, but as yet unspecified, fraction of the friction layer.

The along-wind component of turbulence, σ_u, has not received as much experimental attention as have the vertical and lateral components. The along-wind component is of particular interest in instantaneous-release processes as is explained in subsequent sections. Some general characteristics of σ_u are:

1. At a fixed height σ_u is proportional to wind speed.

2. At a fixed height σ_u increases with increasing instability but probably not as markedly as σ_v.

3. The value of σ_u is generally independent of height during neutral and unstable conditions, but it decreases with height during stable conditions. Thus $\sigma_u/\bar{u}$ may be expected to decrease with height at all times.

2-6.3.1 Long-period Variability of the Wind. It is frequently necessary, in environmental studies, to make some estimate of the length of time that the wind will remain within given direction boundaries. A computer program designed to operate on conventional weather-station wind observations has recently been developed (Gordon, 1963). The program was designed to answer the question, "What is the probability that the wind, once having turned into a given direction sector, will remain in that sector for 2, 3, 4, etc., hours?" Since the raw data were available for 16 points of the compass (16 sectors of 22.5° each), the program has been designed to furnish the information for one sector, three sectors (with the sector of interest at the center), or five sectors. Figure 2.36 shows a typical graph compiled from wind data gathered at Corpus Christi, Texas, over a period covering five summers. This graph may be interpreted by recourse to a typical point, such as the point on the 10% line enclosed within the small circle. This point indicates that 10% of the total number of times that the wind turned to the east it was observed to remain in that 22.5° sector for at least 5 hr. Thus the directions for which the 10% and the 50% lines are

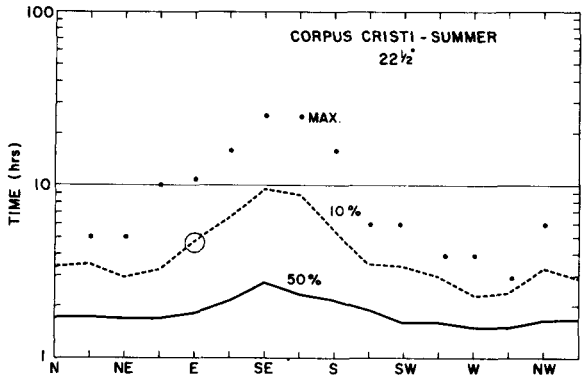

Fig. 2.36—An example of a wind-direction persistence diagram based on a 16-point compass. Interpretation of a typical point on the diagram (in small open circle) is as follows: 10% of the times during the summer that the wind turned to the east, it was observed to remain in that 22.5° sector for at least 5 hr. The irregular row of dots indicates the maximum number of hours that the wind was observed to come continuously from the given directions.

high are the directions of greatest wind persistence. The upper row of points on the diagram represents the maximum number of hours for which the wind remained in the indicated direction. This program using five years of data for the four seasons has been run at 64 locations in the United States.

2-6.3.2 Spatial Variability of the Wind. Simultaneous measurements of the wind variation in the vertical have been made by many investigators (see the bibliography at the end of this chapter). Thus it is possible to estimate the wind at some distance above or below a measurement at a given level if the topography, time of day, and weather conditions are known. The variation of the wind in the horizontal, at least on a microscale or mesoscale, has not received nearly the same study. However, in transport and diffusion work the extent to which a single wind observation represents conditions at various distances from the measurement point is important. The results of one investigation of the variability of simultaneous wind measurements at different locations are shown in Table 2.2. Hourly wind data from four standard weather stations in the San Antonio, Texas, area were used. The average distance between stations was 12 miles. The direction data were given to 16 compass points and the wind speed to 1 mph. The data were processed to determine the average standard deviation of the wind speed and direction differences between the six possible pairs of unlike station combinations.

Similar data were collected in the hilly area around the Oak Ridge National Laboratory. In this case a central station was compared to 16 satellite stations at an average distance of 2.5 miles from the central station (range from 0.3 to 7.5 miles), and the percentage of the time that the wind direction at the central station and at each satellite station agreed within one compass point was tabulated. Data collected over a period of about 1 year were used to prepare the averages for all 16 combinations of stations. The data showed the following percentages:

Table 2.2—WIND DIFFERENCES BETWEEN FOUR WEATHER STATIONS NEAR SAN ANTONIO, TEXAS

Station	Standard deviation of wind-direction differences,* compass points	Standard deviation of wind-speed differences,* mph
1–2	1.70	4.7
1–3	1.70	4.5
1–4	1.60	4.8
2–3	1.60	4.2
2–4	1.75	4.9
3–4	1.50	4.0
Average	1.65	4.6

* Based on 10 years of data.

Light winds (day)	43.4%
Light winds (night)	38.3%
Strong winds (day)	72.6%
Strong winds (night)	68.6%

On the basis of the discussion presented earlier in this chapter, the greater variability with light winds seems reasonable. It is quite possible that similar data comparisons in very regular terrain, such as the Great Plains area, would show more spatial homogeneity at all times and for all ranges of wind speed.

2-7 ATMOSPHERIC DIFFUSION

Knowledge of the configuration of the source of an effluent is a necessary starting point for diffusion estimates. For purposes of description it will be assumed in the following discussion that the effluent is composed of a gas or of particles that faithfully follow the motions of the atmosphere. This implies that the effluent

is neither negatively nor positively buoyant if it is a gas and that it has a negligible settling velocity if it is composed of discrete particles.

2-7.1 The Instantaneous Point Source

The instantaneous point source is the conventional approximation to the type of release associated with a very short venting of material to the atmosphere, e.g., an explosion. The term "instantaneous point" is, of course, fiction since even a small rapid explosion will have finite time and space dimensions. The puff, once formed, moves away from the source with a speed and direction determined by the wind at the moment of release. The mean speed and direction of the puff can be expected to change from the original values during its travel as the wind pattern in which it is imbedded changes with time. As the puff moves, it will expand about its center owing to the action of turbulent fluctuations. Part (a) of Figure 2.37 shows an idealized circular smoke cloud imbedded in a uniform turbulent field in which all the turbulent elements are smaller than the cloud. Both the puff and turbulent elements may be carried along with some large-scale motion (indicated by the arrow). This puff will, as indicated, grow slightly as its edges are mixed with the pure air by the small eddies. This growth is accompanied by a proportional decrease in concentration of the smoke within the puff. In (b) of Fig. 2.37, a puff is imbedded in a field of turbulent elements that are considerably larger. In this case the puff will experience transport and little dispersion or decrease in concentration. Finally, (c) of Fig. 2.37 shows a puff imbedded in eddies of approximately the same size. In this case diffusion will be quite rapid, and the concentration within the puff will decrease rapidly.

In the real atmosphere, turbulence is the composite result of all the motion systems discussed earlier. The turbulent elements are not regular circles. They are best visualized by traces such as those in Fig. 2.30 or 2.31. A puff of smoke released into the atmosphere will always grow larger since there almost always will be eddies smaller than or of the same size as the puff.

The amount of material in a puff from an instantaneous point source is usually given as the total quantity of material released (curies, grams, etc.), and the downwind distribution of the material after it has been dispersed is frequently expressed in terms of exposure, or the time integral of the concentration as the puff passes the point of observation.

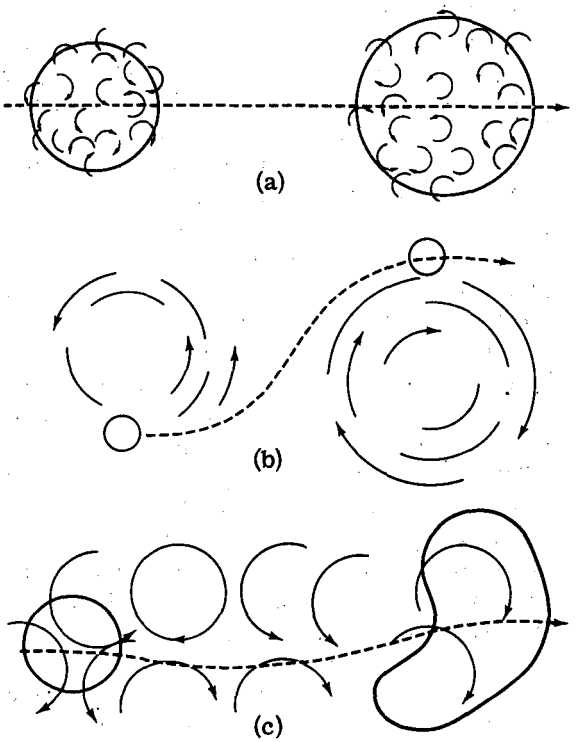

Fig. 2.37—Idealized dispersion patterns. (a) A large cloud in a uniform field of small eddies. (b) A small cloud in a uniform field of large eddies. (c) A cloud in a field of eddies of the same size as the cloud.

2-7.2 The Continuous Point Source

Diffusion meteorologists have paid more attention to the continuous point source release than to any other type. It is a good approximation to releases from stacks, from small fissures in structures containing pollutants, and from small spills of volatile materials. The approximation of the true source configuration by a point becomes increasingly better as the distance at which the concentration is observed grows increasingly large compared with the dimensions of the source.

A continuous plume may be considered to be made up of an infinite number of puffs released sequentially with a vanishingly small time interval between puffs. Initially each puff moves with the wind direction at the moment of release. The quantity of material released is usu-

ally expressed in terms of a release rate (curies per second, kilograms per hour, etc.), and the downwind material distribution is usually expressed in terms of average concentration over the period of release (curies per cubic meter, etc.). Linear dimensions of the plume perpendicular to the plume axis are often given in terms of the standard deviation of the concentration distribution since the average cross-plume distribution is usually close to a normal curve with boundaries at infinity.

The left side of Fig. 2.38 denotes, schematically, the boundaries of a smoke plume as it would appear at any given instant (such as in a snapshot) or as it would appear having been averaged over 10 min or 2 hr (as in a time exposure). The right side of the figure represents the distributions of the concentration for each of the three plume types. The snapshot shows an irregularly varying plume, which gradually expands with distance from the source. The corresponding concentration distribution is irregular and quite peaked. The 10-min average shows a smooth and regular boundary that can be considered as the envelope containing all the short-period fluctuations of the plume. The average concentration distribution perpendicular to the axis of such a plume has been found to resemble a normal (Gaussian) distribution about the center line, as shown on the right side of the figure. The 10-min cross-plume average concentation distribution is broader and smoother than in the instantaneous case but has a lower peak value. The 2-hr plume is wider yet with an even flatter average concentration pattern.

If the time-averaged diagrams of the plume were extended to distances quite far from the source, the boundaries of the time-smoothed plume would themselves meander because the longer length of plume would be under the influence of eddies that are quite large in area (as well as in time necessary to pass an observer). The averaging time used originally therefore would be too short to show a time-averaged picture of these larger fluctuations. A longer time average appropriate to this greater distance would, again, be too short for distances greater yet. It is important to recognize that fluctuations in the wind that are larger than the plume dimensions tend to transport the plume intact whereas those that are smaller tend to tear it apart. Thus, as the plume reaches greater and greater distances and gro ' in size, larger and larger turbulent eddy sizes become effective in diffusing the cloud, and smaller eddies become increasingly ineffective.

Since the time-averaged plume from a continuously maintained point source expands both laterally and vertically with downwind distance from the source, the center-line concentration within the plume will decrease continuously with distance. The rate at which the center-line concentration decreases varies with atmospheric stability or, equivalently, with the magnitude and scale of the turbulence. Much of the dis-

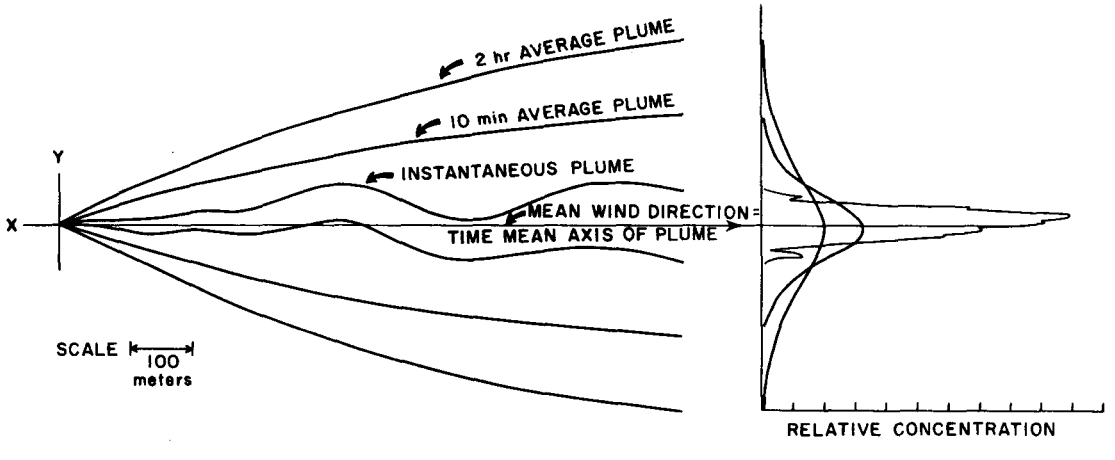

Fig. 2.38—The diagram on the left represents the approximate outlines of a smoke plume observed instantaneously and of plumes averaged over 10 min and 2 hr. The diagram on the right shows the corresponding cross-plume distribution patterns.

cussion in the following two chapters is concerned with this subject.

Although continuous sources located at the earth's surface may be postulated, the elevated source represented by a continuously emitting chimney is a more common occurrence. The surface-concentration pattern from an elevated source is typically like that shown in Fig. 2.39. The concentration is essentially

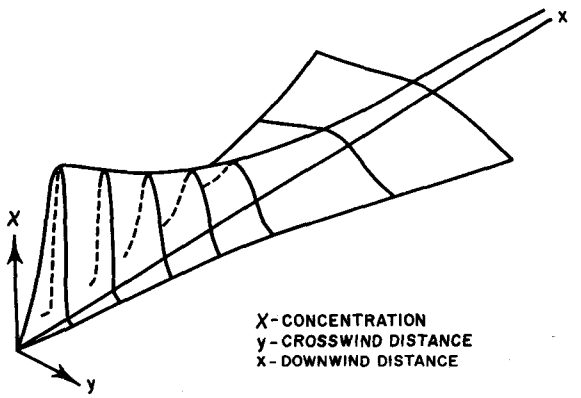

Fig. 2.39—The surface-concentration pattern downwind from an elevated source.

zero near the base of the chimney, rises rapidly to a peak value at some downstream distance, and decreases regularly thereafter. The concentration is always higher along the projection of the plume axis on the ground than on either side.

Many formulations have been advanced for estimating the concentration distribution within a continuously emitted plume from a knowledge of the values of the accompanying meteorological variables. Some of these formulas are given in Chap. 3. The various measures of wind-velocity fluctuation discussed earlier have found considerable application in estimating the downstream concentration distribution from a variety of effluent source configurations including the continuous point source. Such techniques have been particularly useful over the range of distances that are usually of interest in reactor safety analyses, i.e., from a few hundred meters to about 10 km.

The horizontal spreading of a continuously released plume may be estimated from the magnitude of the wind fluctuations, in terms of σ_θ, presented in Fig. 2.34. If σ_y is the standard deviation of the horizontal concentration distribution within a continuous plume, then, as is shown in subsequent chapters, $\sigma_y \approx \sigma_\theta x$, where σ_θ is the horizontal wind-direction standard deviation (radians) and x is the distance from the source. The wind-fluctuation data in Fig. 2.34 can on the basis of this relation be interpreted directly in terms of plume spread.

During unstable and neutral conditions, both the mean wind velocity and the fluctuations about the mean change rather little with height, and a measurement made at any one level is representative of a rather deep layer. During stable conditions, however, both these variables change rather rapidly with height, and lateral diffusion may proceed quite differently, its behavior depending on the height of the source above the surface. Near the surface the instantaneous inversion plume may be quite narrow, but slow meandering of the wind results in a similar meandering of the plume; therefore the time-averaged plume may appear quite broad. At greater heights the stable values of σ_θ are quite small, but the plume is likely to encounter large values of wind speed and direction shear that act as nonturbulent diffusive mechanisms.

It was noted earlier in this section that the width of a time-averaged plume increases with increasing sampling time. If a plume were emitted continuously over a period of many weeks or months, it would move many times during this period through all the directions of the compass; the concentration distribution therefore would not fall into some finite sector but, rather, would be represented by isopleths about the source. Such a distribution shows the average concentration decreasing in all directions from the source but most slowly in the directions of greatest wind frequency.

Although the characteristics of horizontal spreading of time-averaged smoke plumes are difficult to observe, the vertical appearance of a real plume makes no demands on the observer; it offers considerable information on the thermal and dynamic state of the lower atmosphere. Some typical patterns of vertical smoke spreading are presented in the next paragraphs and illustrated in Fig. 2.40.

2-7.2.1 Fanning. The characteristics of fanning are those that would be expected from a consideration of σ_φ described in Sec. 2-6.3. Since the vertical component is very small, the plume will expand very little in depth over long distances. The vertical shear of the horizontal

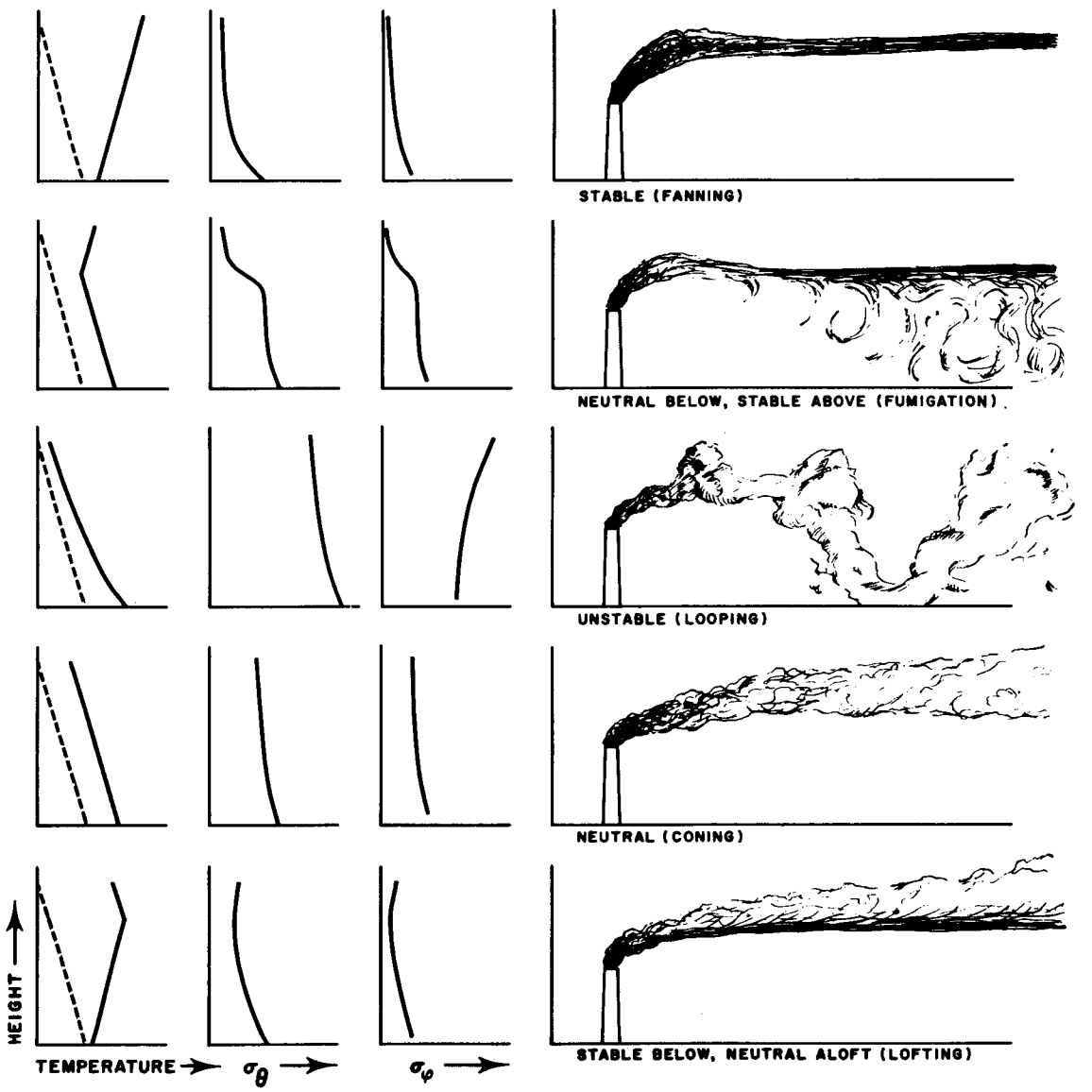

Fig. 2.40 — Various types of smoke-plume patterns observed in the atmosphere. The dashed curves in the left-hand column of diagrams show the adiabatic lapse rate, and the solid lines are the observed profiles. The abscissas of the columns for the horizontal and vertical wind-direction standard deviations (σ_θ and σ_φ) represent a range of about 0° to 25°.

wind, which may be quite large at night, is frequently sufficient to cause rather great horizontal spreading of this shallow plume. Further, if the wind is very light, the horizontal meandering of the low-level wind, as shown in (d) of Fig. 2.30, might result in a very sinuous plume path, similar to a shallow meandering river that widens slowly with distance from the source. Since the diffusion is very small, however, a plume under an inversion may be visible to hundreds of times the distance that it could be seen under better daytime mixing conditions.

The prediction of concentration in a fanning plume is one of the weakest points in statistical diffusion-forecasting schemes because the meandering motions are often in response to particular topographical configurations and unique atmospheric variable patterns.

In many cases the fanning behavior of plumes is not considered an unfavorable condition for

stack releases even though the effluent undergoes little vertical dilution after leaving the stack. The important feature is that an effluent of neutral buoyancy tends not to spread to the ground during inversion conditions. This situation might be unfavorable, however, in the following circumstances:

1. Where the stack is short with respect to surrounding buildings or terrain requiring freedom from pollution.
2. Where the effluent plume contains radioactive materials, the radiation from which could deliver a ground-level exposure even with zero ground-level air concentrations.
3. Where there is a group of stacks of various heights and the resulting cloud of effluent is extensive.
4. Where lateral spread and variability of plume direction are restricted (as by a deep, narrow valley) so that effluent passes repeatedly over the same places.

It is quite rare that the wind will be truly calm. Usually there is some drift that cannot be measured by an anemometer but is shown by the movement of smoke. Therefore it would be unusual for an effluent released over a period of an hour or more to remain in the immediate vicinity of the source.

2-7.2.2 Fumigation. Shortly after the sun comes up on a clear morning, the existing radiational inversion begins to dissipate and is slowly replaced by a neutral or unstable layer that usually begins at the ground and works its way upward. At some time after sunrise, the inversion is present just above the top of the stack and acts as a lid while the newly developed convective eddies mix the effluent plume within the shallow unstable layer next to the ground. This condition may also develop in sea-breeze circulations during late morning or early afternoon.

This condition can give rise to the greatest ground-level concentrations observed in the neighborhood of a stack over periods of about 30 min because of the high inversion-like concentrations brought rapidly to the ground. Moreover, if the growth of the neutral or unstable layer is slow or if it does not grow at all, as in the case of the sea breeze, fumigation conditions may persist for many hours along a considerable length of the plume.

2-7.2.3 Looping. During the warmer seasons, when the skies are clear, a condition known as looping is frequently evident by midday. The temperature structure at such times is likely to be very unstable, at least in the lower layers (see Fig. 2.19), giving rise to large, vertical, thermally induced eddies that bring the plume to the ground close to the source in intermittent puffs. Because of the higher degree of turbulence, both in the vertical and horizontal, these puffs are of a somewhat lower concentration at a given distance from the source than under fumigation conditions. Furthermore, the concentration of the puffs that may reach the ground will decrease very rapidly with distance from the stack. However, since the puffs reach the ground close to the source, average ground-level concentrations during looping conditions are likely to be quite high for the given stack height. The horizontal wind pattern associated with looping is typically like that during the 12:00 a.m. to 2:00 p.m. interval in (b) of Fig. 2.30.

2-7.2.4 Coning. Coning occurs with a vertical temperature gradient between isothermal and adiabatic. The effluent plume is shaped like a cone with a horizontal axis. The distance from the stack at which the effluent first comes to the ground is greater than with looping conditions because of the lower level of thermally induced turbulence. Coning usually accompanies cloudy, windy conditions and can occur during the day or at night. In dry climates it may occur infrequently and, conversely, in cloudy climates it may be the most frequently observed plume.

The typical coning plume shown in Fig. 2.40 might be associated with the wind conditions in the latter part of (b) of Fig. 2.30.

2-7.2.5 Lofting. Lofting occurs with the transition from unstable to inversion conditions and is most often observed near sunset. Depending upon the height of the stack and the rate of deepening of the inversion layer, the lofting condition may be very transitory or may persist for several hours. It may infrequently persist throughout the night. The zone of strong effluent concentration is caused when the inversion traps the effluent carried into the stable layer by turbulent eddies that penetrate the layer for a short distance. Other than when the inversion is very shallow, the lofting condition may be considered as the most favorable diffu-

sion situation. The inversion prevents effluent from reaching the ground, and, at the same time, the effluent is diluted in the layer above the inversion.

2-7.2.6 Limits of Vertical Plume Spread. The vertical patterns of smoke plumes discussed in the last sections are those that have been observed in the first few tens of stack lengths from the source. The rate of vertical growth that is observed over such distances cannot be maintained indefinitely. The lower boundary of the plume is, of course, fixed by the surface of the earth, and the top of the plume is bounded even during the most unstable low-level temperature patterns by more-stable layers aloft. The day temperature profiles in Fig. 2.19 show the average trend toward greater stability with height. On a clear summer day, the superadiabatic lapse rate will rarely extend more than a few hundred to a thousand meters above the surface. Above this there may be a smooth transition to less unstable structure, or there may be a sharp change to stable conditions. These changes may arise because of subsidence or more subtle large-scale meteorological processes. As a result of the stabilization aloft, a distinct lid is placed on the further vertical growth of a plume, and any future decrease in concentration must be due to horizontal spreading. This condition is frequently referred to as "trapping." Estimates of diffusion at distances 5 or 10 km or more from the source must take account of this fact. The existence of a lid to vertical diffusion is one of the main factors in assessing the extent of pollution from a multisource region, such as a city. If the wind speeds and the lid are both low, the available volume through which the accumulated pollution from the city may be dispersed is comparatively small, and high pollutant concentrations may be reached.

2-7.3 Other Source Configurations

Although instantaneous and continuous point sources have traditionally been of the greatest interest in diffusion meteorology, a number of other source configurations have claimed some attention also. The instantaneous line source is a fairly common type that can be approximated by a continuously emitting, rapidly moving system, such as a crop-spraying aircraft. Such a line is usually thought of as extending to infinity in both directions so that along-line diffusion may be neglected, and the diminution of concentration with travel distance is entirely explained by diffusion in the vertical and along-wind directions.

Another source type, the continuous line source, may be approximated by a busy highway or a line of closely spaced vents. Since the release is continuous, the sampling time is germane.

The continuous area source, although as yet of minor importance in nuclear problems, is receiving increasing attention in the urban air-pollution field. A city, with its multitude of pollutant-emitting sources, is the most common and characteristic representative of the area source.

2-7.4 Nonideal Plume Characteristics

A number of features of real smoke plumes have been disregarded in the previous discussion. These frequently must be considered in actual computations. Real plumes from real stacks have some exit velocity, perhaps small but frequently large enough to ensure that the plume will travel upward in bulk to some height determined by the exit speed, volume of effluent, wind speed, and stability condition. Similarly, the plume may be above ambient temperature at emission and thus have a buoyant component of upward motion in addition to the mechanical effect. It has also been assumed that the plume particles are of the same density as the air. Again, in practice, the particles may be more dense, and thus the plume would have some constant downward motion superimposed on the turbulent mixing. If portions of the plume are in contact with the ground, deposition of the particulates on or absorption of the gases by surface features can cause a decrease in downstream concentrations. Resuspension of the deposited material must also be considered in assessing concentrations. Pollutants may vent from a variety of openings other than stacks. Material leaking from a crack in a vessel will experience an initial diffusion, which is dependent on the airflow about the vessel and its associated structures. Wind-tunnel modeling is used to study these situations. Finally, predictions of downstream concentration may be in error if the pollutant material is

such that it reacts with atmospheric constituents or changes composition owing to solar irradiation. Radioactive decay, which depends on the half-lives of the radioactive materials involved, will diminish the concentration of radioactive material downstream. All of these mechanisms are discussed in subsequent chapters.

BIBLIOGRAPHY OF METEOROLOGICAL PUBLICATIONS

ELEMENTARY TEXTS (A more complete bibliography may be found in the October 1967 issue of *Weatherwise*):

Sutton, O. G., *The Challenge of the Atmosphere*, Harper & Brothers, New York, 1961, 227 pp. One of the best concise summaries of meteorology available. Most fields of meteorological endeavor are discussed.

ADVANCED TEXTS:

Brooks, C. E. P., and N. Carruthers, *Handbook of Statistical Methods in Meteorology*, British Information Services, New York, 1953, 412 pp. Thorough treatment of application of statistics to climatological or meteorological problems.

Byers, H. R., *General Meteorology*, 3rd ed., McGraw-Hill Book Company, Inc., New York, 1951, 540 pp. A textbook covering the large-scale features of the atmosphere as well as meteorological observing and forecasting.

Haltiner, G. J., and F. L. Martin, *Dynamical and Physical Meteorology*, McGraw-Hill Book Company, Inc., New York, 1957, 470 pp. Another meteorological textbook with somewhat more emphasis than most on the theory of the planetary boundary layer, classical diffusion theory, and diffusion of atmospheric pollutants.

Panofsky, H., and G. W. Brier, *Some Applications of Statistics to Meteorology*, Pennsylvania State University, University Park, Pennsylvania, 1958, 224 pp. Aims at serving as textbook for meteorology students and acquainting active forecasters and research personnel with modern statistical techniques.

Petterssen, S., *Weather Analysis and Forecasting*, 2nd ed., Vol. 1, Motion and Motion Systems, 446 pp., Vol. 2, Weather and Weather Systems, 284 pp., McGraw-Hill Book Company, Inc., New York, 1956. A revision and expansion of an earlier work which brings thinking on this subject up to date.

SPECIAL TEXTS:

Geiger, R., *The Climate near the Ground*, rev. ed., Harvard University Press, Cambridge, Mass., 1959, 494 pp. A comprehensive survey of micrometeorological problems. Valuable both for the researcher and the general reader. Includes revised bibliography.

Huschke, R. E. (Ed.), *Glossary of Meteorology*, American Meteorological Society, Boston, Mass., 1959, 638 pp. Defines all important meteorological terms.

Kendrew, W. G., *The Climates of the Continents*, Oxford University Press, New York, 1961, 608 pp. A standard descriptive text of the main features of world climate.

Lumley, J. L., and H. A. Panofsky, *The Structure of Atmospheric Turbulence*, John Wiley & Sons, Inc., New York, 1964, 239 pp. In the authors' own words, "The purpose of this book is twofold: first to summarize the basic characteristics of turbulence (derived from hydrodynamics and pertinent to the meteorological problems) ... and to bring observational material up to date with particular emphasis on recent Russian observations."

Middleton, W. E. K., and F. A. Spilhaus, *Meteorological Instruments*, 3rd ed., University of Toronto, Toronto, 1953, 286 pp. Contains information on automatic weather stations, airplane reconnaissance, mobile weather stations, radiosondes and rawinsondes, and the uses of radar meteorology as well as full discussion and critique of traditional instruments.

Pasquill, F., *Atmospheric Diffusion*, D. Van Nostrand Company, Ltd., London, 1962, 297 pp. This book must be required reading for any serious student of atmospheric diffusion.

Saucier, W. J., *Principles of Meteorological Analysis*, The University of Chicago Press, Chicago, 1955, 438 pp. Detailed textbook on meteorological analysis discussing theory and methods of presentation.

Stern, A. C. (Ed.), *Air Pollution*, Vol. 1, 656 pp., Vol. 2, 586 pp., Academic Press Inc., New York, 1962. A comprehensive discussion of many of the aspects of the air-pollution problem.

Sutton, O. G., *Atmospheric Turbulence*, 2nd ed., John Wiley & Sons, Inc., New York, 1955, 111 pp. Pocket-size textbook dealing with turbulence, in general, the meteorology of the lower atmosphere, and diffusion theory and applications.

Sutton, O. G., *Micrometeorology: A Study of Physical Processes in Lowest Layers of the Earth's Atmosphere*, McGraw-Hill Book Company, Inc., New York, 1953, 333 pp. A standard textbook dealing with turbulence, diffusion, evaporation, and local heating in the lowest layers of the atmosphere.

PERIODICALS

United States

American Meteorological Society, 45 Beacon Street, Boston 8, Mass.
Bulletin of the American Meteorological Society (monthly)
Journal of Applied Meteorology (bimonthly)
Journal of the Atmospheric Sciences (bimonthly)
Meteorological Monographs (irregular)
Meteorological and Geoastrophysical Abstracts (monthly)
Weatherwise (bimonthly)

American Geophysical Union, 1515 Massachusetts Avenue, N. W., Washington, D. C.
Geophysical Monographs Series (irregular)
Journal of Geophysical Research (semimonthly)
Reviews of Geophysics (quarterly)
Transactions of the American Geophysical Union (quarterly)

U. S. Weather Bureau, Superintendent of Documents,

U. S. Government Printing Office, Washington, D. C.
Monthly Weather Review (monthly)

Mount Washington Observatory, 87 Canal Street, Salem, Mass.
Mount Washington Observatory Bulletin (quarterly)

Great Britain

Royal Meteorological Society, 49 Cromwell Road, London SW 7, Eng.
Quarterly Journal of the Royal Meteorological Society (quarterly)
Weather (monthly)

British Meteorological Office, British Information Services, New York, N. Y.
Meteorological Magazine (monthly)

Pergamon Press, Oxford, Eng.
International Journal of Air and Water Pollution (bimonthly); name changed January 1967 to *Atmospheric Environment*

Chapter 3

An Outline of Theories of Diffusion in the Lower Layers of the Atmosphere

Franklin A. Gifford, Jr.*

LIST OF SYMBOLS

Symbols used frequently in Chaps. 3 and 4 are listed here. (The dimensions mass, length, time, and temperature are abbreviated as *M*, *L*, *T*, and *D*, respectively. Equation or section numbers indicate where the symbol first appears or where additional clarification may be found.)

A	Turbulent or eddy viscosity or "Austausch" coefficient ($ML^{-1}T^{-1}$), Eq. 3.7
A	Refers to average concentration value in discussions of peak-to-average ratio, Eq. 3.137
A	Area within a concentration or exposure isopleth (L^2), Eq. 3.150
C_x, C_y, C_z	Sutton's virtual diffusion coefficients ($L^{n/2}$), Eqs. 3.78 and 3.80
c_p	Specific heat of air at constant pressure ($L^2T^{-2}D^{-1}$), Eq. 3.26
D	Distance along y- or z-axis of center of meandering plume (L), Eq. 3.119
D	Depth of laminar sublayer (L), Eq. 3.11
d	Zero-plane displacement (L), Eq. 3.16
$d_{max.}$	Distance to point of maximum ground concentration from an elevated source (L), Sec. 4-4.1.2
F(n)	Lagrangian eddy-energy-spectrum function (T), Eq. 3.66
f	Coriolis parameter (T^{-1}), Eq. 3.34
g	Gravitational acceleration (LT^{-2}), Eq. 3.18
H	Eddy heat flux [$(ML^2T^{-2})L^{-2}T^{-1}$], Eq. 3.26
h_i	Depth of the mixing layer (L), Eq. 3.133
h	Height of a source above the ground (L), Eq. 3.115
i_u, i_v, i_w	Intensity of turbulence in the x-, y-, and z-directions (dimensionless), Eq. 4.26, Chap. 2, Sec. 2-6.2.2
K	Eddy diffusivity coefficient (L^2T^{-1}), Eq. 3.45
K_H	Eddy heat conductivity coefficient (L^2T^{-1}), Eq. 3.26
K_M	Kinematic eddy-viscosity coefficient (L^2T^{-1}), Sec. 3-1.2.5
k	Von Karman's constant ≈ 0.4 (dimensionless), Eq. 3.12
L	Stability-dependent length introduced by Lettau, Monin, and Obukhov (L), Eq. 3.28
$\mathscr{L}$	Lagrangian integral time scale (T), Eq. 3.70
l	A length scale (L), Table 3.2
n	Frequency (T^{-1}), Eq. 3.66
n	Sutton's parameter associated with stability (dimensionless), Eq. 3.76
P	Refers to peak-concentration value in discussions of peak-to-average concentration, Eq. 3.137
p	Atmospheric pressure ($ML^{-1}T^{-2}$), Eq. 3.17
Q	Source strength; total amount of material released from a point source (M or other units of quantity), Eq. 3.49
Q′	Source strength; time rate of material emission from a continuous point source (MT^{-1}), Eq. 3.91
Q_L	Source strength; total amount of material emitted per unit length from a line source (ML^{-1}), Sec. 3-3.5.8
Q'_L	Source strength; time rate of material emission per unit length from a continuous line source ($ML^{-1}T^{-1}$), Sec. 3-3.5.3
q	Mean value of a conservative air property per unit mass of air, Eq. 3.45

*Atmospheric Turbulence and Diffusion Laboratory, Environmental Science Services Administration, Oak Ridge, Tennessee.

R(t)	Velocity autocorrelation coefficient (dimensionless), Eq. 3.65
Re	The Reynolds number (dimensionless), Eq. 3.5
R_f	Flux form of the Richardson number (dimensionless), Eq. 3.27a
Ri	The Richardson number (dimensionless), Eq. 3.22
T	Temperature (D), Eq. 3.17
t	Time (T); appears in various equations; in special applications T is also used , Eq. 3.108
u,v,w	Components of the wind in the x-, y-, and z-directions, respectively (LT^{-1}), Eq. 3.2
$\vec{V}$	Total wind-motion vector (LT^{-1}), Eq. 3.1
v_d	Deposition velocity (LT^{-1}), Eq. 4.14, Chap. 5, Sec. 5-3.2.1
v_*	Friction velocity (LT^{-1}), Sec. 3-1.2.6
x,y,z	Positions in a Cartesian coordinate system which is usually oriented so that the x-axis is in the direction of the mean horizontal vector wind, the y-axis is crosswind, and the z-axis is vertical (L), Eq. 3.2
Y	A distance between particles (L), Eq. 3.96
z_0	Roughness length (L), Eq. 3.14
β	Lagrangian–Eulerian time-scale ratio (dimensionless), Eq. 3.104
Γ, γ	Dry adiabatic temperature lapse rate and existing temperature lapse, respectively (DL^{-1}), Eq. 3.21
ϵ	Rate of eddy energy transfer (L^2T^{-3}), Sec. 3-2.2.6
ζ	Dimensionless ratio = z/L, Eq. 3.32
Θ	Potential temperature (D), Eq. 4.19
θ	Lateral wind-direction angle or width of sector (expressed as degrees, radians, etc.), Eq. 3.122
μ	Dynamic viscosity coefficient ($ML^{-1}T^{-1}$), Eq. 3.4
ν	Kinematic viscosity (L^2T^{-1}), Eq. 3.5
ρ	Atmospheric density (ML^{-3}), Eq. 3.5
σ_y, σ_z	Standard deviation of the distribution of material in a plume in the y- and z-directions (L), Eq. 3.113
σ_{xI}, σ_{yI}, σ_{zI}	Standard deviation of the distribution of material in a puff in the x-, y-, and z-directions (L), Eq. 3.154
σ_θ	Standard deviation of lateral wind-direction distribution (degrees or radians), Sec. 3-3.4.1
σ_φ	Standard deviation of vertical wind-direction distribution (degrees or radians), Table 4.2
τ	Tangential stress on a unit area of fluid ($ML^{-1}T^{-2}$), Eq. 3.4
τ_0	Tangential stress in the lowest air layers ($ML^{-1}T^{-2}$), Eq. 3.8
φ	Geographical latitude, vertical wind-direction angle or width of sector (degrees or radians), Sec. 3-1.3
$\chi(x,y,z,t)$	Concentration at a point (x,y,z) at time t (ML^{-3}), Eq. 3.89
$\bar{\chi}$	Average concentration (ML^{-3}), Eq. 3.91
χ_{CWI}, $\bar{\chi}_{CWI}$	Crosswind integrated concentration (ML^{-2}), Eq. 3.143
$\bar{\chi}_F$	Fumigation concentration (ML^{-3}), Eq. 3.133
$\bar{\chi}_{max.}$	Maximum concentration on the ground from an elevated source (ML^{-3}), Eq. 3.135
χ_p, $\bar{\chi}_p$	Peak or center-line concentration values (ML^{-3}), Eqs. 3.155 and 3.91
ψ	Exposure (MTL^{-3}); subscripts p and CWI have the same meaning as for concentration (also referred to as the concentration time integral), Eq. 3.156
ω	Angular velocity of earth's rotation [(radians)T^{-1}], Sec. 3-1.3
$^-$ (overbar)	Space, time, or statistical average, Sec. 3-2.3
$\langle\ \rangle$	Running mean average, Eq. 3.75
$'$ (prime)	Superscript referring to deviation from the mean, i.e., $x \equiv \bar{x} + x'$, Eq. 3.1; also used in source-strength notation to indicate a release rate, Eq. 3.91
A, P	Subscripts referring to conditions surrounding a parcel of air and within the parcel, respectively, Eq. 3.18
G	Subscript referring to geostrophic flow
x,y,z	Subscripts referring to coordinate axes

Other subscript notation accompanies the notation found in the preceding portion of this table.

3-1 MEAN FLOW IN THE LOWER LAYERS OF THE ATMOSPHERE

3-1.1 Introduction

The problem to be considered is the description, by means of mathematical–physical models, of the role of the earth's lower atmosphere in redistributing and diluting the radioactive gases and particles that may be introduced into it as a result of various activities of the atomic energy industry. Although most interest is centered on the problem of isolated, more or

less continuously emitting sources at or near the ground level, such as fixed nuclear reactors and their associated chemical processing plants, the problem of quasi-instantaneous sources, such as might result, for example, from a nuclear rocket launch-pad accident, will also be considered. The special problems created by the radioactive nature of these various sources are most conveniently dealt with separately. Therefore the results described in this chapter apply equally to nonradioactive air contamination, such as that created by large conventional power plants and many other activities of an industrial society.

The symbols most frequently used in this chapter and in Chap. 4 are listed and defined in the List of Symbols at the beginning of the chapter.

The atmosphere disperses gases and particles rapidly because it is turbulent. Turbulence is the property, easy to recognize but difficult to define, of irregular, chaotic motion possessed by almost all natural fluid flows. In fact, for practical purposes we can best define a turbulent fluid flow as one that has the ability to disperse particles embedded within it quite rapidly, at a rate orders of magnitude greater than can be accounted for by molecular diffusion. Most of the meteorological problems (as well as certain other technical fluid-flow problems, such as heat transfer) of the power, chemical, and atomic energy industries center themselves around the phenomenon turbulent diffusion.

Osborne Reynolds (1895) suggested in 1883 a device by which such a complex phenomenon as a turbulent flow could be reduced to a relatively manageable mathematical form. Reynolds' idea was that the total wind-motion vector, $\vec{V}$, can be thought of as being composed of a constant mean part $\bar{\vec{V}}$ and a fluctuating, or turbulent, part $\vec{V}'$, such that

$$\vec{V} = \bar{\vec{V}} + \vec{V}' \qquad (3.1)$$

or, considering the three orthogonal wind components separately,

$$\begin{aligned} u &= \bar{u} + u' \quad \text{(in the x-direction)} \\ v &= \bar{v} + v' \quad \text{(in the y-direction)} \\ w &= \bar{w} + w' \quad \text{(in the z-direction)} \end{aligned} \qquad (3.2)$$

Components of the natural wind can be measured by a sensitive anemometer. Figure 3.1 is a sample of one such measurement made at 35 m above the ground surface. Notice that the fluctuating, or turbulent, component of the wind is of the same order of magnitude as the fixed, or mean, part; i.e., u' is about as large as $\bar{u}$. This is characteristic of atmospheric turbulence and distinguishes it sharply from wind-

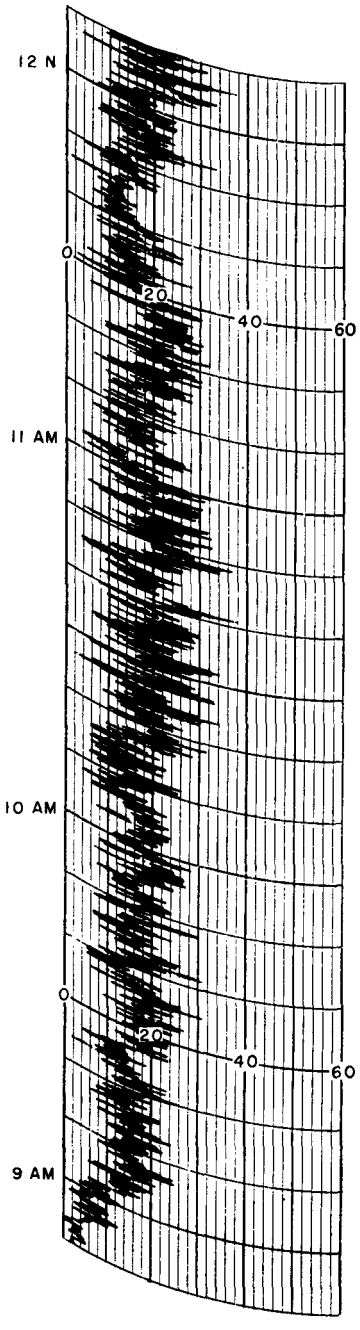

Fig. 3.1 — Portion of anemometer record, u(t), made at an elevation of 35 m in the atmosphere.

tunnel turbulence, where $\bar{u}$ is more likely to be 10^2 to 10^3 times u′.

Equation 3.1 or 3.2 tells us that to specify atmospheric turbulence we must first be able to specify the mean state of atmospheric motions. Some consideration of the mean state of the atmosphere is also necessary because the energy supply for atmospheric turbulence lies in the organized large-scale mean atmospheric motions. Moreover the strength of the mean wind is directly related to the capacity of the atmosphere for diluting pollutant materials injected into it. Finally, in the layers of air nearest the earth's surface, extending to elevations of several kilometers, the mean wind pattern itself is determined primarily by turbulence arising from frictional drag at the air–earth interface. Thus it appears that the analysis of atmospheric turbulence is deeply involved with the mean field of motion on four separate counts. A discussion of the mean wind structure in the lower layers of the atmosphere is clearly required as a preliminary to the treatment of the diffusion problem. Although it is convenient to proceed as though this mean wind can actually be defined over some suitable space or time domain, it should be noted that in the atmosphere, in contrast to the wind tunnel, the method of doing this is neither simple nor obvious. Fluctuations of the wind having a wide range of periods can and do occur, but just how to define the average value is not always clear. This problem is discussed at some length in Sec. 3-2.3.

3-1.2 The Mean State of the Wind in the Lowest Layers

3-1.2.1 Viscosity. Assuming for the moment a horizontal, straight, parallel, steady mean wind flow, $\bar{u}(z)$, at some level z, fairly near the surface (just how near will be determined subsequently), let us try to determine the mean wind structure. Upon what quantities should it depend? Obviously $\bar{u}$ must increase with height, z, for at least some distance above the earth's surface since just at the surface it must equal zero. This means that adjacent horizontal layers of air must be in motion relative to one another, and so certainly $\bar{u}(z)$ must be expected to depend also on the viscosity of the atmosphere.

Imagine a small volume of air next to the surface to be symbolized by a deck of smooth new playing cards resting on a table (Fig. 3.2). If the top card is slid parallel to the deck while the cards are held firmly in contact, the bottom card remains fixed, but the remainder of the deck is tilted forward, or sheared, in such a way as to deform the deck into a uniform parallelepiped. The horizontal force on the top card represents the horizontal (in general,

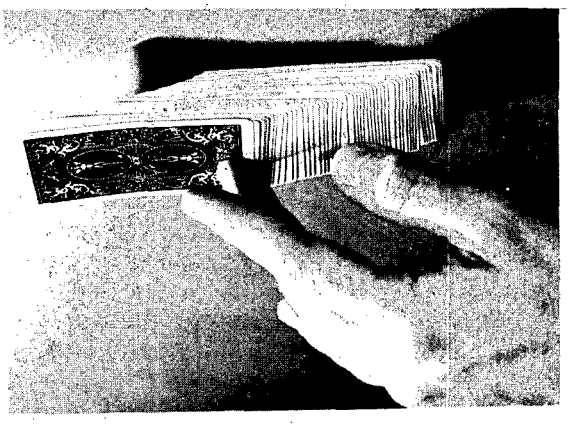

Fig. 3.2—Illustration of shear due to a tangential force.

tangential) shearing stress on any small air volume. The resistance of the cards to vertical hand pressure symbolizes ordinary (normally directed) air pressure, and the resistance to horizontal slippage of cards symbolizes the viscosity of the air. Just as the bottom card sticks to the table, so the lowest air layer sticks to the surface of the earth.

3-1.2.2 Shearing Stress. A tangential shearing force, or stress, applied for a certain time to the top card produces a certain deformation of the deck, symbolizing a vertical shear of the horizontal wind $[d\bar{u}(z)/dz]$; the smaller the viscosity is the greater this effect will be. It is reasonable to suppose that

$$\frac{d\bar{u}}{dz} \propto \frac{\text{shearing stress}}{\text{viscosity}} \qquad (3.3)$$

or, using the symbols ordinarily assigned to these quantities and rearranging terms,

$$\tau = \mu \frac{d\bar{u}}{dz} \qquad (3.4)$$

This is Newton's law for molecular fluid viscosity; τ is the tangential stress on a unit area of the fluid, and μ is called the dynamic viscosity coefficient because it is a measure of the resistance of the fluid to volume distortion resulting from the stress.

3-1.2.3 Mechanical Turbulence. Fluid viscosity, which is described in Sec. 3-1.2.1, depends on molecular structure; it is a bulk property of the fluid, which, however, is determined by internal microscopic fluid characteristics. In fact it is sometimes called internal friction, and its detailed nature can best be elucidated by the arguments of kinetic theory, involving transfer of momentum from layer to layer of the fluid by individual molecules. Molecular viscosity accounts adequately for transfer of fluid properties very near flow boundaries and, in general, in any small volume of fluid. Considering the situation for the flow as a whole, however, we have to deal in the lower atmosphere with a structure much more complex than the simple layered parallel flow we have so far conceived, namely, a turbulent flow. For the time being let us regard this turbulence next to the surface as purely mechanical in origin and as deriving its energy somehow from the mean flow of the air at greater elevations in a way that does not depend on the action of thermal buoyancy forces.

3-1.2.4 The Reynolds Number. What is the nature of low-level turbulent atmospheric motions? In a nonturbulent flow, such as water issuing at low velocity from a tap, paths of adjacent fluid "particles" are essentially parallel, as illustrated in (a) of Fig. 3.3. (By a fluid particle, we have in mind a small volume of the fluid. Such a volume would contain a very large number of molecules, but the molecular nature of the fluid does not concern us here. We regard the fluid as being microscopically continuous, an assumption that permits us to apply the definitions and limiting processes of ordinary differential calculus to the fluid motions.) This nonturbulent flow is called laminar, the connotation being that adjacent layers of fluid remain distinct and identifiable (laminated) and do not intermix. Physically, the laminar stream of water appears smooth and coherent; small irregularities remain small or are rapidly damped. Under these conditions Newton's law for viscosity would be obeyed. If the velocity of the stream is increased slowly, no change may occur at first, but at some point the nature of flow will be observed to change radically and suddenly. The smooth appearance turns to a rough, irregular one, as shown in (b) of Fig. 3.3. It is obvious that adjacent

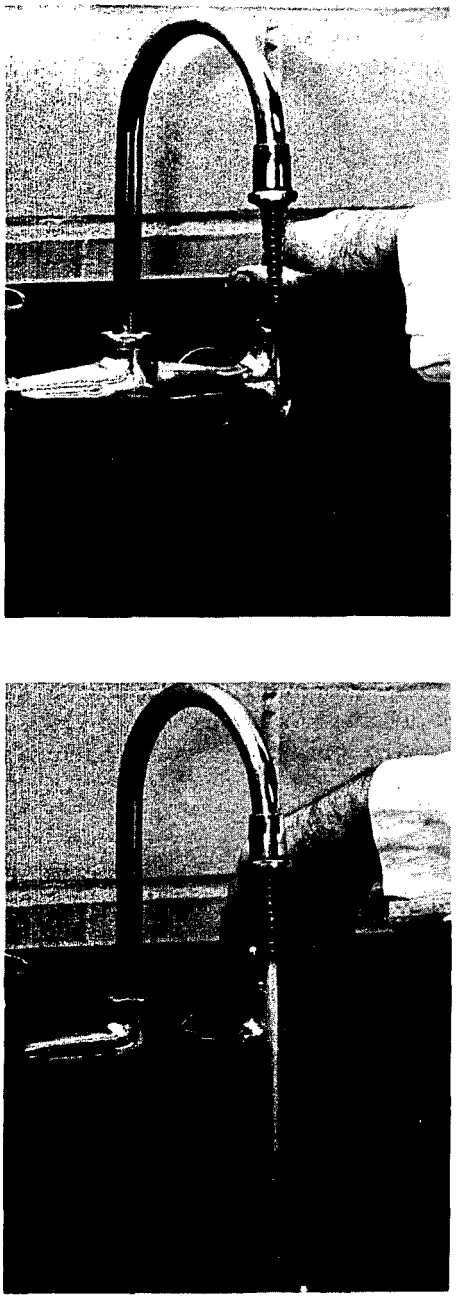

Fig. 3.3—(a) Laminar flow of water from a laboratory faucet. (b) Turbulent flow of water issuing at a higher speed from the same faucet as in part (a). (Courtesy J. E. Westcott)

particle paths no longer are parallel but are intermingled in a highly irregular way. The water churns and splatters. We immediately recognize the new state of the fluid as turbulent and can readily grasp the importance of the turbulent fluid state in problems involving the transfer of such properties as heat and momentum.

It is possible to learn more from this simple experiment. By repeating it with taps having openings of different sizes, we would find that the water flow issuing from a smaller opening stays laminar up to a higher velocity. For example, the very fine stream of water issuing from a laboratory wash bottle is nearly always smooth, i.e., laminar, for considerable distances from its tip [(a) of Fig. 3.4]. On the other hand, the flow from a fire hydrant is invariably turbulent [(b) of Fig. 3.4]. Now consider an experiment otherwise identical but performed with some thick liquid, e.g., heavy oil or molasses, substituted for water as the fluid. We would find that the velocity required to produce turbulent flow is in each case higher than for water.

We have now in a highly qualitative way established the facts about turbulent flows that were found to be significant by Reynolds, who made the first systematic study of the onset of fluid turbulence:* to change a laminar flow into a turbulent flow one must either increase the velocity, increase a characteristic reference length associated with the flow, or decrease the viscosity of the fluid. These factors can be combined into a dimensionless ratio known as the Reynolds number, Re:

$$\text{Re} = (\text{a characteristic flow length}) \times (\text{a characteristic flow velocity}) \times (\text{dynamic viscosity/density})^{-1} \qquad (3.5)$$

The denominator of this expression is called the kinematic viscosity, ν (square centimeters per second), and is related to the dynamic viscosity by $\nu = \mu/\rho$, where ρ is air density. The kinematic viscosity is a measure of how the intrinsic fluid stickiness, i.e., the dynamic viscosity, affects the overall flow geometry, and consequently it must depend on the inertia

*The word "turbulence," designating a state of fluid flow exceeding a certain critical threshold, was introduced by Lord Kelvin in 1887 according to Rouse and Ince (1957).

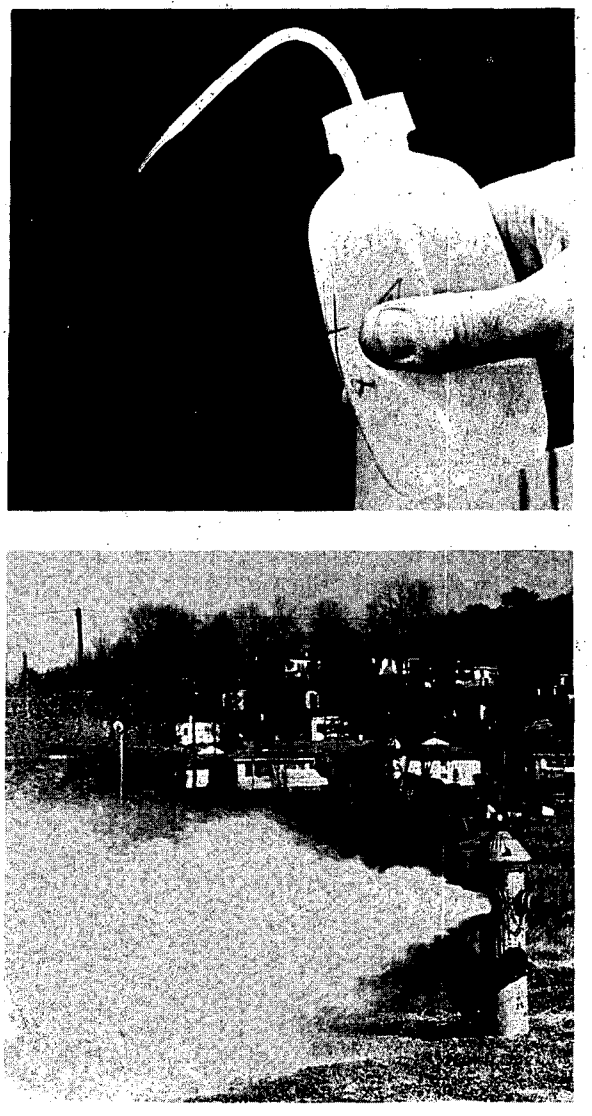

Fig. 3.4—(a) Laminar flow of water from laboratory wash bottle with a small nozzle. (b) Turbulent flow of water from a fire hydrant. (Courtesy J. E. Westcott)

of the fluid and hence on the density. The Reynolds number can also be thought of as the ratio of the inertial to the viscous forces acting on a small volume of fluid,

$$\text{Re} \propto \frac{\text{inertial force}}{\text{viscous force}} \qquad (3.6)$$

The inertial force on a unit volume of fluid is equal to the product of density and acceleration; the viscous force equals the viscous stress per unit area.

The way in which a length characteristic of the flow should be specified in the atmosphere

is not by any means self-evident. In pipe flows, such as those Reynolds studied, the pipe diameter provides a natural reference length, as did the size of the opening in the example with which the discussion in this section began. In airfoil theory the wing chord is a suitable reference length; in wind tunnels the size of a wire mesh or grid used to induce turbulence likewise defines a length. With any of these definitions, flows characterized by Reynolds numbers above about 10^2 or 10^3 are always turbulent.

What length scale applies in the atmosphere? In the atmosphere there is no particularly obvious macroscopic external length scale associated with the turbulence phenomenon. In fact it seems that fluctuating motions can occur over a very wide size range. For any reference length we might choose as a matter of expediency (height above the ground, for example), we are bound to conclude that the Reynolds number of the atmosphere will be very large because typical velocities are of the order 10^2 cm/sec and ν equals about 0.15 cm^2/sec. Consequently we find that atmospheric flows are ordinarily turbulent. The degree of turbulence of the atmosphere can vary over wide limits and depends primarily on the vertical temperature structure, i.e., upon stability. Nevertheless the atmosphere is normally turbulent. In laminar flow the rate of diffusion of molecules or particles is proportional to the coefficient of molecular viscosity, or diffusivity, μ. Because atmospheric flows are turbulent, diffusion in the atmosphere occurs at a rate which is rarely less than several orders of magnitude greater than the molecular rate and which may be many orders of magnitude greater than this value.

3-1.2.5 Eddy Viscosity. By analogy with the Newtonian law of molecular viscosity (Eq. 3.4), Boussinesq (1877) proposed that the effect of turbulent viscosity be taken into account by introducing an augmented viscosity,

$$\tau = (\mu + A)\frac{d\bar{u}}{dz} \qquad (3.7)$$

The turbulent, or eddy, viscosity, A, was termed by Schmidt (1925) an "Austausch," or exchange, coefficient. It was, of course, realized much earlier than this that the Newtonian, or molecular, viscosity, μ, was orders of magnitude too small to account for the observed transfer of heat or momentum in fluids. An interesting historical account of the subject by Bateman (1956) mentions the studies by Dalton in 1799 and Count Rumford in 1806. Convection over heated ground was described as early as 1749 by Benjamin Franklin, according to Middleton (1965). The meteorologist Espey in 1840 also used the idea of convective mixing of wind currents to explain the diurnal variation of the wind. In line with the molecular analogy, it is convenient to define a kinematic eddy-viscosity coefficient K_M in terms of A and ρ, $A = \rho K_M$; K_M thus has the same dimensions as ν but is, as we shall see, normally several orders of magnitude larger. The subscript M indicates that this eddy-exchange process involves transfer of momentum.

Notice that a significant new concept, that of an eddy,* has just been introduced. An eddy is thought of as an irregular but somehow identifiable material wind structure, perhaps similar to a "puff of wind" or to a "cat's paw" over open water, having the ability to transfer air properties across the flow in a way that can conveniently be thought of as analogous to transfer by the air molecules on a much smaller scale. At this point we need not try to make this idea very much more precise; indeed to do so will turn out to be impossible in most respects although we shall freely discuss from time to time various properties of eddies. To prevent such looseness of argument from becoming too great a mental or aesthetic obstacle, we need only recollect how much of physical theory can be rationalized by assuming that molecules behave like little hard balls.

Assume then an eddy viscosity K_M that controls, through the properties of turbulent eddies, the mean structure of the wind over the earth's surface. Very near the surface, height above the ground must limit the vertical size of eddies. At greater and greater elevations, eddies that are larger and larger in their

*The concept of an eddy is new, of course, only at this point in the present discussion. The intuitive idea of relating turbulent fluid motion to such an entity seems to be very old. Rouse and Ince (1957) reproduced a sketch drawn by Leonardo da Vinci clearly illustrating eddies in the wake of an obstacle in a water channel (he, however, attributed properties to these eddies that we would not today).

vertical dimension can be present, and so it is reasonable to expect that K_M should depend upon z. Moreover K_M is related to the tangential shearing stress by Eq. 3.7, which may be rewritten

$$\tau_0 = (\rho K_M)\frac{d\bar{u}}{dz} \tag{3.8}$$

where the subscript zero indicates that this is to apply in the lowest air layers and μ is neglected as small.

3-1.2.6 The Logarithmic Wind Profile. In general, the tangential shearing stress, τ_0, will vary with height in the lower layers of the atmosphere. As a simplification we can, however, limit the discussion to a layer of air just next to the surface through which the vertical variation of τ_0 is small enough that τ_0 can be considered constant. Then the vertical structure of the mean wind, $\bar{u}$, for the flow we are considering appears to depend on the following quantities, which can be chosen as fundamental to the flow: the kinematic air viscosity, ν; height above the surface, z; air density, ρ; and frictional stress, τ_0. The quantity K_M can be expressed in terms of these through Eq. 3.8.

In particular, the vertical gradient of the mean velocity in a uniform, straight, parallel flow of air next to the ground, for which the energy of the air turbulence is purely mechanical in origin, involves relations among five dimensional quantities: $d\bar{u}/dz$, ν, z, ρ, and τ_0. If ordinary principles of dimensional analysis are applied to this problem (see Bridgman, 1931), the well-known Π theorem tells us that two independent dimensionless ratios can be formed from these (namely, the number of quantities, 5, minus the number of fundamental dimensions involved, 3) and that a single unknown function of these two ratios may be set equal to zero. Of these remaining quantities, only τ_0 and ρ involve mass, and so they must enter any dimensionless product as the ratio τ_0/ρ, which has the dimensions of velocity squared. Its square root is often termed the friction velocity and is given the special symbol v_*. One dimensionless ratio can thus be written as $(d\bar{u}/dz)(z/v_*)$, and the second, as zv_*/ν. Consequently the dimensional analysis provides the following result:

$$f_1\left(\frac{d\bar{u}}{dz}\frac{z}{v_*}, \frac{zv_*}{\nu}\right) = 0 \tag{3.9}$$

Since our object is to determine $d\bar{u}/dz$, we can solve for the ratio containing it:

$$\frac{d\bar{u}}{dz} = \frac{v_*}{z} f_2\left(\frac{zv_*}{\nu}\right) \tag{3.10}$$

Although simpler than Eq. 3.9, Eq. 3.10 nevertheless contains a function f_2 about which it is not yet possible to speculate on the basis of the assumptions made so far; f_2 may be a simple linear function, or it could equally be highly transcendental. This is a common impasse when dimensional analysis is applied to a complicated problem and can only be resolved by invoking some additional principle or physical understanding of the problem. Let us see what can be accomplished.

Very close to the earth's surface the vertical structure of $\bar{u}$, the vertical velocity profile, must mainly be governed by molecular viscosity because close enough to the surface the turbulence due to eddies must become negligible, there being insufficient height for the eddies to come into play. Let us assume that this situation holds up to some fixed elevation, z = D, and attempt to estimate D. If we substitute D into the second of the dimensionless ratios, which we should recognize as a form of Reynolds number, we see that for a given flow (i.e., a constant value of v_*)

$$Re = Dv_*/\nu = \text{constant} \tag{3.11}$$

Because flows for which $Re \geq 10^2$ are ordinarily turbulent, it follows that an upper limit to D, the depth of the laminar sublayer of the atmosphere, will be of the order of a millimeter since v_* is known from observations to be of the order of 100 cm/sec and ν equals about 10^{-1} cm^2/sec.

This means that blades of grass, grains of dirt, sticks, twigs, people, and so forth, all protrude through the laminar sublayer. In fact, except perhaps for flow over very smooth ice or still water, we may ignore the effect on $d\bar{u}/dz$ of zv_*/ν. Then the equation for the gradient of the wind profile near the earth's surface simplifies to

$$\frac{d\bar{u}(z)}{dz} = \frac{v_*}{kz} \tag{3.12}$$

which will apply to fully turbulent flow over a rough surface, i.e., one whose roughness ele-

ments protrude through the laminar sublayer. Such a surface is sometimes called aerodynamically rough; an aerodynamically smooth surface is, in contrast, one whose roughness elements are contained within the laminar sublayer, a case that does not as a rule apply in the atmosphere. The universal proportionality constant, k, is called von Karman's constant and has been found by experimentation to equal 0.4.

Equation 3.12 can be integrated to obtain the wind profile near the earth's surface in the constant-stress layer:

$$\bar{u}(z) = \frac{v_*}{k} \ln z + \text{constant} \qquad (3.13)$$

The integration constant is usually defined so as to introduce the effect of surface roughness by requiring that $\bar{u} = 0$ when $z = z_0$; z_0 is called the roughness length because it expresses the effect of varying ground surface roughness on the wind profile:

$$\bar{u}(z) = \frac{v_*}{k} (\ln z - \ln z_0) = \frac{v_*}{k} \ln \left(\frac{z}{z_0}\right) \qquad (3.14)$$

Written in this form, the result indicates the role of the integration constant, which is to translate the wind profile without changing its form. This equation is valid only for $z \geq z_0$ since the dimensional argument applies only above the laminar sublayer.

Sometimes z_0 is chosen so that $\bar{u}(z) = 0$ when $z = 0$. If this is done, the wind profile equation takes the form

$$\bar{u}(z) = \frac{v_*}{k} \ln \left(\frac{z + z_0}{z_0}\right) \qquad (3.15)$$

Since, as a practical matter, interest is ordinarily centered on wind at heights where $z \gg z_0$, the two forms are substantially equivalent. It is sometimes necessary to take account of the possibility that the actual zero-plane datum level used in an experiment may differ from the zero-plane implied by Eq. 3.14 either arbitrarily for experimental convenience or because the level down to which the effect of the wind profile extends (e.g., over thick vegetation) does not coincide with the ground surface. This is done by formally introducing a zero-plane displacement, d,

$$\bar{u}(z) = \frac{v_*}{k} \ln \left(\frac{z - d}{z_0}\right) \qquad (3.16)$$

Such precision is not often required in field work. The existence of a logarithmic wind profile next to the earth, such as these equations predict, has been confirmed in numerous experiments for the type of flow that we have specified, i.e., purely mechanical turbulence. Values of z_0 and v_* found from such experiments appear in Table 3.1.

Table 3.1— TYPICAL VALUES OF PARAMETERS GOVERNING THE LOGARITHMIC WIND PROFILE NEAR THE EARTH'S SURFACE*

Type of surface	z_0, cm	v_*, m/sec†
Smooth mud flats; ice	0.001	0.16
Smooth snow	0.005	0.17
Smooth sea	0.02	0.21
Level desert	0.03	0.22
Snow surface; lawn to 1 cm high	0.1	0.27
Lawn, grass to 5 cm	1–2	0.43
Lawn, grass to 60 cm	4–9	0.60
Fully grown root crops	14	1.75

*Based on Sutton (1953), Priestley (1959), and Pasquill (1962).
†For $\bar{u}(2\text{m}) = 5$ m/sec.

3-1.2.7 Effect of Buoyancy. The effect on the wind profile of departures from purely mechanical turbulence must be considered, and we should begin by trying to clarify what is meant by mechanical turbulence. Because of the weight of air, i.e., because of the vertical force exerted on any air volume by gravity, the pressure of the atmosphere decreases with elevation. This vertical pressure variation implies a certain vertical temperature structure governed by the atmosphere's equation of state,

$$p = \rho RT \qquad (3.17)$$

where ρ is the density, R is the gas constant for air, and T is the Kelvin temperature. Specifically, the temperature of a volume of dry air displaced upward by a process that does not add or remove sensible heat will decrease at the linear rate of 1°C per 100 meters, the so-called "dry adiabatic lapse rate."

The mean vertical temperature structure of the lower layers of the atmosphere may under certain circumstances happen to possess a dry adiabatic lapse rate; if so, a small isolated

volume of air, an air parcel, that is undergoing adiabatic vertical motion will at all times adjust itself so that it will experience no buoyancy force tending to restore it to its original elevation. It will always possess just the temperature of its environment. Mechanical turbulence in the atmosphere is conceived to have just this essential property that, no matter how irregular the individual eddy motions of which it consists may appear, there are no net buoyancy forces on fluid elements, or eddies, due to departure from an average adiabatic lapse rate.

This restriction to mechanical turbulence has simplified the analysis considerably up to this point, but in the lower atmosphere an adiabatic lapse rate is present only a small fraction of the total time. This seriously restricts the utility of the results obtained thus far. Figure 2.19 of Chap. 2, illustrating the normal clear-day diurnal variation of temperature structure of the lower atmosphere, demonstrates that the adiabatic state can ordinarily be expected only just after dawn and at dusk and will last perhaps for a few moments. The reason is that the flow of heat to and from the underlying surface by radiation, conduction, and convection causes the lapse rate in the lower air layers to vary from day to night over wide limits. During the day vertically displaced volumes of air undergoing adiabatic expansion must be acted upon by positive buoyant forces, and as a result turbulence is enhanced. During the night the converse effect tends ordinarily to suppress turbulence sharply. Of course, when the normal vertical heat flux in the lower layers is restricted markedly, for instance by a thick low cloud layer, the adiabatic state can persist for longer periods of time.

The buoyant force, F, on an air parcel is easily calculated, being equal to the weight of the displaced air volume, W_A, minus the weight of the air parcel, W_p, i.e.,

$$F = W_A - W_P = g\,V(\rho_A - \rho_P) \qquad (3.18)$$

where positive F indicates upward buoyancy, g is the gravitational acceleration, and V is the volume in question. The resulting acceleration, a, of the parcel, i.e., F divided by its mass, is

$$a = g\,\frac{\rho_A - \rho_P}{\rho_P} \qquad (3.19)$$

which, from the equation of state, can be written (bearing in mind that $p_A = p_P$)

$$a = g\,\frac{T_P - T_A}{T_A} \qquad (3.20)$$

where T_A and T_P are the air and parcel temperatures, respectively, in degrees Kelvin. Since the air parcel is conceived of as acquiring buoyancy by changing temperature dry adiabatically in a diabatic (i.e., nonadiabatic) environment, the last equation can also clearly be written as follows:

$$a = \frac{dw}{dt} = g\,\frac{(\gamma - \Gamma)\Delta z}{T_A} \qquad (3.21)$$

where γ = existing (in general, diabatic) lapse rate in the surrounding air
Γ = dry adiabatic lapse rate
Δz = height through which this process operates
w = vertical velocity acquired by the air parcel

The adiabatic lapse rate thus emerges as a natural standard of vertical temperature stratification in the atmosphere. It is of fundamental interest in connection with problems related to the turbulent structure of the lower layers of air because vertical displacements of air parcels, such as occur in turbulent flow, have the following character: (1) Vertical displacements have neutral stability, and displaced air parcels tend neither to fall nor to rise when

$$\gamma = -\frac{dT}{dz} = \Gamma;\ (T_P = T_A)$$

(2) Vertical displacements are unstable and are amplified by buoyancy when

$$\gamma > \Gamma;\ (T_P > T_A)$$

(3) Vertical displacements are strongly damped when

$$\gamma < \Gamma;\ (T_P < T_A)$$

3-1.2.8 The Richardson Number. Previous discussion has indicated that the energy of purely mechanical turbulence is associated with vertical wind shear, $d\bar{u}/dz$, through the

agency of an eddy stress, τ_0. In the presence of a diabatic lapse rate, it now appears that turbulent energy is also strongly affected by buoyancy forces. Richardson (1920) suggested that turbulence should occur in the atmosphere when the production of turbulent energy by the wind shear is just large enough to counterbalance its consumption by buoyancy forces. He proposed as a measure, or criterion, of the effect the dimensionless number Ri that has been given his name:

$$\text{Ri} \propto (\text{rate of consumption of turbulent energy by buoyancy forces}) \times (\text{rate of production of turbulent energy by wind shear})^{-1} \qquad (3.22)$$

There are several ways to derive the Richardson number. Let us once again view the problem from the dimensional standpoint, asking what are the relevant variables. We have seen that mechanical turbulence is controlled by the vertical shear, or gradient, of the mean horizontal wind, $d\bar{u}/dz$. From Eq. 3.19 we conclude that the effect of consumption of turbulent energy by buoyancy will be governed by gravity, g, air density, ρ, and the vertical density gradient. This follows because Eq. 3.19 can be rewritten in the essentially equivalent form

$$a = \frac{g}{T_A}\frac{d\Theta}{dz} \qquad (3.23)$$

where a is now to be interpreted as the restoring force on a unit mass of air resulting from its unit vertical displacement ($\Delta z = 1$) from an equilibrium position. From these four quantities, involving three fundamental dimensional units, a single dimensionless ratio can be formed, namely,

$$\text{Ri} = \frac{g}{T_A}\frac{(d\Theta/dz)}{(d\bar{u}/dz)^2} \qquad (3.24)$$

This can also be written

$$\text{Ri} = \frac{g}{T_A}\frac{(\gamma - \Gamma)}{(d\bar{u}/dz)^2} \qquad (3.25)$$

which follows from Eqs. 3.21 and 3.23 and shows the relation of the Richardson number to the departure from an adiabatic lapse rate.

A second form of the Richardson number is often used. In diabatic turbulent shear flow, the significant phenomenon has been shown to be the departure of the temperature of the eddies from that of the surrounding air in which they are conceived as embedded. It follows that, in addition to momentum, the eddies act to transport heat across the flow. An expression for this eddy heat transport, or flux, H, can be written by analogy with Eq. 3.8 for the momentum flux, or stress,

$$H = \rho\, c_p\, K_H\, (\gamma - \Gamma) \qquad (3.26)$$

where c_p is the specific heat capacity of the air at constant pressure and K_H is a coefficient of eddy heat conductivity. If Eqs. 3.8 and 3.26 are substituted into Eq. 3.25 for Ri, we find that

$$\text{Ri} = \frac{g\,H}{c_p\, T_A\, \tau_0\, (d\bar{u}/dz)}\frac{K_M}{K_H} \qquad (3.27)$$

Thus an alternate definition is the so-called "flux form" of the Richardson number, R_f, where

$$R_f = \text{Ri}\,\frac{K_H}{K_M} = \frac{g\,H}{c_p\, T_A\, \tau_0\, (d\bar{u}/dz)} \qquad (3.27a)$$

3-1.2.9 The Diabatic Wind Profile. The Richardson number, Ri, or R_f, has come to be used as a characteristic turbulence parameter rather than as an absolute criterion of turbulence. That is, it is regarded as broadly indicating the nature and to some extent the intensity of the turbulence rather than specifying an exact criterion for turbulence to occur. As such, the Richardson number indicates the quantities upon which the velocity profile will depend in the diabatic case, namely, $\bar{u}$ will involve z, z_0, v_*, and k, as before, and, in addition, the parameters characterizing the diabatic effects, g, ρ, c_p, H, and T_A. A direct dimensional attack on this problem by the method we have been employing will evidently be fruitless because of the large number of dimensionless ratios that can be formed from the quantities involved. An elegant simplification is, however, possible following the suggestion made (independently) by Lettau (1949) and by Monin and Obukhov (1953).

We are considering uniform, straight, parallel turbulent flow near the surface with constant stress and heat flux. We assume that this kind of flow will extend to some elevation above the surface, an elevation that has not yet been directly specified but will be approximated later on. For the time being the depth of the layer can be regarded as that depth through which the assumptions of constant heat and momentum fluxes are applicable. Within this region of applicability, which Lettau calls the surface layer, the turbulence properties, including the wind and temperature profiles, will at any point be under the control of the various physical parameters just enumerated. It is known from the form of the governing equations of motion (Lumley and Panofsky, 1964, for example) that the effect of thermal buoyancy enters this problem through the buoyancy parameter, g/T_A. The conditions of constant momentum flux and heat flux likewise lead (Monin and Obukhov, 1953) to dependence of the flow on the dimensional parameters v_* and $H/c_p\rho$, respectively. From these three parameters, which uniquely characterize the velocity and temperature profiles in the surface layer, Monin and Obukhov formed the unique length, L,

$$L = \left[\frac{v_*^3}{k(g/T_A)}\right]\left(\frac{-H}{c_p\rho}\right)^{-1} \qquad (3.28)$$

The quantity L is a constant, characteristic length scale for any particular example of the flow; it is negative for unstable conditions (upward heat flux), positive for stable conditions, and approaches infinity as γ approaches Γ. Of course L, being formed from the same parameters as the Richardson number, is closely related to Ri or R_f,

$$R_f = \frac{K_H}{K_M}\,Ri = \frac{v_*}{k}\,\frac{1}{L(d\bar{u}/dz)} \qquad (3.29)$$

as can easily be verified by substitution. It is more convenient to use L than Ri as a stability parameter characterizing the diabatic velocity profile because Ri must, from Eq. 3.29, vary with height.

Since all quantities having the dimension of length associated with this problem must be proportional to L, the diabatic wind profile is by dimensional analysis found to be

$$\bar{u}(z) = \frac{v_*}{k}\,f_3\left(\frac{z}{L}, \frac{z_0}{L}\right) \qquad (3.30)$$

Bearing in mind the boundary condition at the ground, $\bar{u} = 0$ when $z = z_0$ provided $z_0 > D$, the depth of the laminar sublayer, we usually express Eq. 3.30 in the equivalent form

$$\bar{u}(z) = \frac{v_*}{k}\left[f\left(\frac{z}{L}\right) - f\left(\frac{z_0}{L}\right)\right] \qquad (3.31)$$

because the role of z_0 as a constant of integration is only to shift the velocity profile without changing its form (Eq. 3.14).

In the past few years, a large amount of research has gone into evaluating the form of the universal function f for various regimes of atmospheric stability. Such a function can be evaluated by means, for example, of a carefully planned program of measurements of $\bar{u}(z)$, or auxiliary physical or mathematical assumptions and principles can be invoked. As experience, in the form of detailed observational and theoretical studies of the vertical transport of heat and momentum in the surface layer, has been accumulated, it has become clear that three physically more-or-less distinct regimes are involved in this problem: forced convection, free convection, and the inversion or stable regime. The forced-convection regime is characterized by the fact that buoyancy does not contribute appreciably to the vertical momentum or heat diffusivities, these being completely dominated by mechanical turbulence and accompanied by a nearly adiabatic lapse rate. In this kind of turbulence, both heat and momentum are transferred by the action of the mechanically driven eddies, and these might be expected to occur at approximately equal rates, i.e., $K_H \approx K_M$.

In free convection, on the other hand, the vertical flux is mostly produced by buoyant motions. Strictly speaking, the term "free convection" should be reserved for the case of no mean wind shear, i.e., the case in which turbulence arises solely from the action of buoyant eddies. In practice, the term is commonly used to describe a turbulence regime that is characterized by the presence of a certain amount of forced, or mechanical, turbulence, i.e., by some shear. As Webb (1962) pointed out, this kind of turbulence should probably be called mixed convection in recogni-

tion of its composite nature. The term "free convection" will be retained in this discussion on the grounds that it conforms to current usage, but the point is well taken. The immediate sources of the energy that drive both mechanical and free convection are located at the earth's surface, but, as Scorer (1958, pp. 140-141) points out, the character of the turbulent air motions involved is necessarily quite different. In forced convection the turbulent eddies appear to be most vigorous within the surface layer near the ground. These eddies feed turbulent kinetic energy both upward and downward but always in the direction of smaller fluctuations. The picture is probably similar to that advanced by Townsend (1956, p. 236) in describing the energy flow in a wind-tunnel boundary layer. On the other hand, buoyant elements associated with free convection characteristically grow larger as they ascend from the ground.

The entire subject of the structure of the diabatic surface layer is under study by a number of investigators, and it is possible to give here only a brief sketch of the main results that are available. As an asymptotic approximation to Eq. 3.31, valid under conditions sufficiently near adiabatic, the well-known log plus linear law has been derived by several workers,

$$\bar{u}(z) = \frac{v_*}{k}\left(\ln \frac{z}{z_0} + \alpha\zeta\right) \qquad (3.32)$$

where $\zeta = z/L$. This equation implies that $f(\zeta)$ in nearly adiabatic conditions is given by

$$f(\zeta) = \ln \zeta + \alpha\zeta \qquad (3.33)$$

Although it is usually associated with the similarity theory, the log plus linear wind profile was also deduced independently in the surface-layer study by Lettau (1949). In fact, a wind profile of this form was suggested by Halstead (1943) on empirical grounds.

Interpolation formulas for velocity profiles that provide a smooth transition between the forced-convection and the free-convection cases have been suggested by Kazansky and Monin (1958), Ellison (1957), Yamamoto (1959), Sellers (1962), and Businger (1959). Panofsky, Blackadar, and McVehil (1960) recently showed that Ellison's diabatic profile agrees well with observations made in unstable air. The results of these studies were summarized in the form of the so-called "KEYPS" function described in detail by Lumley and Panofsky (1964). The case of great stability remains, on the other hand, something of an enigma from the theoretical standpoint. The general conclusion from the above studies is that the log plus linear velocity profile, Eq. 3.32, agrees well with observations in both stable and forced convection conditions for $|\zeta| < 0.1$ if the value $\alpha = 6.0$ is used, but, on the side of considerable stability, this good agreement seems to fail. The suggestion made by Panofsky, Blackadar, and McVehil (1960) is that under very stable conditions the velocity profile no longer will depend simply on distance from the ground as is assumed by the similarity theory. Under very stable conditions there seems to be a decoupling of the direct linkage assumed in the similarity theory between the structure of surface-layer turbulence and the physical presence of the ground with the result that the surface-layer flow properties are primarily determined by the nature of the air flow at still higher elevations in the planetary boundary layer.

3-1.3 Wind Variation in the Planetary Boundary Layer

Restricting consideration to steady, straight, and parallel flow with constant stress and introducing complications serially makes it possible to analyze the average wind structure in the surface layer of the atmosphere in some detail and to isolate and emphasize the crucial phenomenon involved, i.e., that of eddy turbulence. When this has been done, the mean wind has been regarded as a given condition superimposed on the flow, so to speak, from above. A wind-speed profile showing an increase with height above the surface as a result of a net downward transport of momentum by turbulent eddies was found.

On the other hand, it is a matter of common experience (e.g., on airplane flights) that the effect of turbulence decreases with elevation in the lower atmosphere and is usually negligible above several thousand feet. Moreover the eddy stress has been found by analysis of wind-fluctuation observations to decrease with height above the surface layer. Furthermore the mean wind does not increase indefinitely with height.

In the model adopted here, however, both turbulence and the mean wind as a result of the assumption of constant stress must, according to Eqs. 3.8 and 3.12, increase with height. Consequently this model can apply only in the lowest part of this region, and the theoretical picture requires some modification and elaboration.

The equations of motion (i.e., the form of Newton's law, $\Sigma F = ma$) applicable near the earth's surface to a steady horizontal wind flow with parallel isobars, according to texts on dynamic meteorology, are

$$f\bar{v} - \frac{1}{\rho}\frac{\partial p}{\partial x} + \frac{1}{\rho}\frac{\partial}{\partial z}\tau_{zx} = 0 \qquad (3.34)$$

$$-f\bar{u} - \frac{1}{\rho}\frac{\partial p}{\partial y} + \frac{1}{\rho}\frac{\partial}{\partial z}\tau_{zy} = 0 \qquad (3.35)$$

where f is equal to $2\omega \sin \varphi$ and is called the Coriolis parameter (ω is the angular velocity of the earth's rotation and φ is geographical latitude), p is pressure, and the subscript zx on the eddy stress, τ, indicates that it acts to transport x-directed momentum in the vertical or z-direction. Stated in words, the average air motion is governed by the sum of three accelerations: the Coriolis acceleration (or the apparent acceleration due to the earth's rotation), the pressure-gradient acceleration, and the frictional acceleration. The sum of these is zero because the flow is assumed steady (unaccelerated). These equations are supposed to apply to a unit mass of the atmosphere, and so the accelerations are equally likely to be referred to as forces.

By analogy with Eq. 3.8, we might suppose that

$$\tau_{zx} = \rho K \frac{\partial \bar{u}}{\partial z} \qquad (3.36)$$

and

$$\tau_{zy} = \rho K \frac{\partial \bar{v}}{\partial z} \qquad (3.37)$$

In other words, the eddy viscosity can be generalized by breaking it up into x- and y-components. The K's will, in general, depend on height, z. Then Eqs. 3.34 and 3.35 become

$$f\bar{v} - \frac{1}{\rho}\frac{\partial p}{\partial x} + \frac{\partial}{\partial z}\left(K\frac{\partial \bar{u}}{\partial z}\right) = 0 \qquad (3.38)$$

$$-f\bar{u} - \frac{1}{\rho}\frac{\partial p}{\partial y} + \frac{\partial}{\partial z}\left(K\frac{\partial \bar{v}}{\partial z}\right) = 0 \qquad (3.39)$$

Since we expect the effect of turbulent friction to decrease with elevation, the third term in these equations, which represents the accelerations due to eddy turbulence, should become negligible at some height in the atmosphere. If we orient the x-axis in the direction of the wind at this level, $\partial p/\partial x = 0$, the above system simplifies to the following:

$$f\bar{u}_G = -\frac{1}{\rho}\frac{\partial p}{\partial y} \qquad (3.40)$$

where the subscript G is introduced to designate the level in question. The term $\bar{u}_G$ is called the geostrophic wind, from the Greek words meaning "earth" and "turning," and Eq. 3.40 is known as the geostrophic wind equation.

Assuming, as the simplest useful approximation, that below the geostrophic wind level the effect of eddy viscosity on the mean wind structure can be expressed by letting diffusivity be constant and that the pressure gradient is independent of height, the solution is

$$\bar{u}(z) = \bar{u}_G (1 - e^{-az} \cos az) \qquad (3.41)$$

$$\bar{v}(z) = \bar{u}_G e^{-az} \sin az \qquad (3.42)$$

where $a = (f/2K_M)^{1/2}$. This can easily be verified by substituting into Eqs. 3.38 and 3.39 and taking into account Eq. 3.40. Figure 3.5 is a plot of this wind distribution, which shows that near the ground friction causes the air to flow across the lines of constant pressure (isobars) in the direction of low pressure. This effect decreases with increasing height and disappears at the geostrophic wind level z_G, which can conveniently be defined as the lowest level at which $\bar{v} = 0$ and therefore the lowest level at which the wind is parallel to $\bar{u}_G$. This must occur when $az = \pi$, from which we can conclude since $f \approx 10^{-4}$ sec^{-1} and K_M is known to be of the order of 10^4 cm^2/sec, that the depth of the layer of frictional influence in the atmosphere is of the order of hundreds of meters. This layer is called the planetary boundary layer. Notice also that the eddy viscosity, K_M, is five

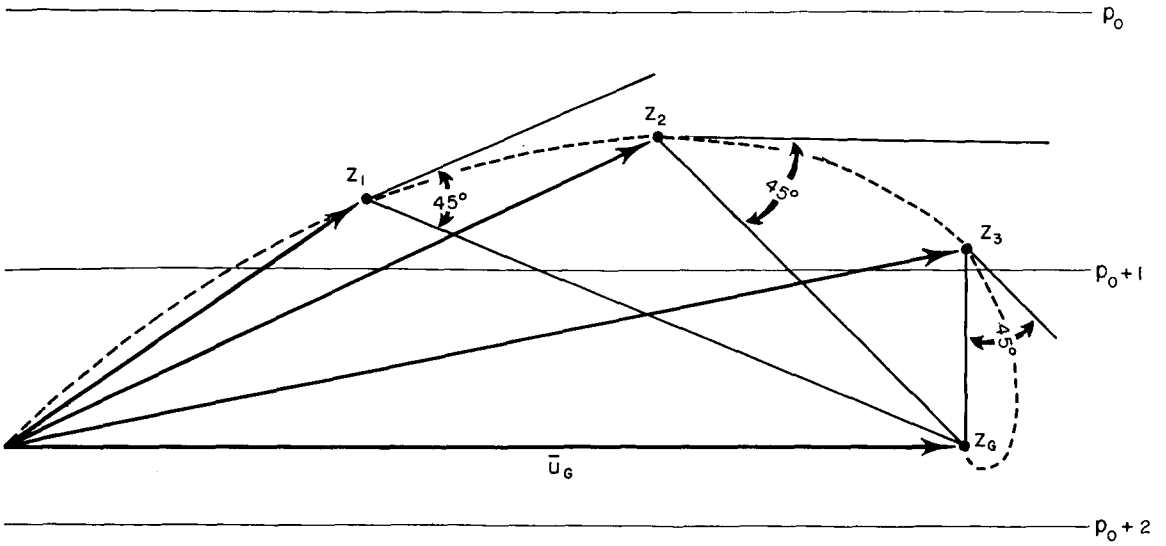

Fig. 3.5—Schematic wind distribution (Ekman's spiral) in the planetary boundary layer, assuming K_M = constant, according to Eqs. 3.41 and 3.42. Wind vectors are plotted from a common origin at increasing heights, z_i, i = 1, 2, etc.

orders of magnitude larger than ν, a fact which justifies neglect of the influence of molecular viscosity.

The frictional acceleration in the equations of motion is known to be of the same order of magnitude as the Coriolis acceleration, about 10^{-1} cgs units; i.e., $|(1/\rho)\,(\partial\tau/\partial z)| \approx 10^{-1}$. Consequently $\partial\tau \approx 10^{-4}\ (\partial z)$, which equals 0.1 dyne/cm^2 in 10 m of height. This will usually amount to about 10% of τ_0 as the following calculation shows. The magnitude of the total eddy stress is given by the sum of Eqs. 3.36 and 3.37 for the components. The value at the surface, τ_0, is, assuming constant K,

$$\tau_0 = \rho\, K_M(\partial\bar{u}/\partial z|_{z=0} + \partial\bar{v}/\partial z|_{z=0}) \qquad (3.43)$$

where the wind shears are to be evaluated at the surface. Substituting Eqs. 3.41 and 3.42 into Eq. 3.43, carrying out the differentiations, and letting z = 0, we find that

$$\tau_0 = 2^{1/2} a K_M \rho\, \bar{u}_G = \frac{z_G}{2^{1/2}\,\pi}\, f\, \rho\, \bar{u}_G \qquad (3.44)$$

Estimating that z_G is of the order of 10^4 cm and $\bar{u}_G \approx 10^3$ cm/sec, we find that τ_0 is of the order of 1 dyne/cm^2.

From this it can be concluded that the depth of the surface layer, i.e., the layer just next to the ground through which the stress τ_0 may be considered to be constant, is of the order of tens of meters, or about 10% of the depth of the planetary boundary layer. Through the surface layer the mean wind direction is approximately constant, and the speed increases with height according to equations derived in the preceding sections. Above the surface layer the mean wind turns to the right (in the northern hemisphere) and attains, provided the overlying flow is geostrophic (i.e., governed by Eq. 3.40), the direction and speed of the geostrophic wind at elevations of the order of hundreds of meters.

The solution to the wind distribution in the planetary boundary layer given by Eqs. 3.41 and 3.42 was first obtained by Ekman in 1902 and is known as Ekman's spiral. It provides a reasonably good qualitative explanation of the wind structure and an order of magnitude estimate of such quantities as z_G and K_M. But we have seen that eddy viscosity, K_M, must vary with height in the planetary boundary layer, increasing just above the ground as larger eddies become effective and then decreasing at greater elevations as the general influence on the airflow of the surface frictional drag decreases. Moreover we can expect, on the basis of analysis of the diabatic surface layer, that the eddy structure in the planetary boundary layer will also be strongly influenced by buoyant heat flux. In addition, for many important practical situations, it cannot be as-

sumed that the governing forces are in balance. The sea breeze and mountain and valley winds are examples of such accelerated flows. All these complicating factors and others are the subject of active research studies, and considerable progress has been made, which, however, would take us too far afield to summarize. As a practical matter, such effects are not normally evaluated quantitatively in connection with estimates of atmospheric diffusion, and so the qualitative discussion given in Chap. 2 provides an adequate guide. Readers interested in further development of this important subject will find useful discussions in the papers by Estoque and Yee (1963), Blackadar, Panofsky, McVehil, and Wollaston (1960), and Lettau (1962).

3-2 DIFFUSION THEORIES

Small particles or droplets released into the atmosphere will separate more or less rapidly from one another under the influence of turbulent eddies, a phenomenon called diffusion. We have already investigated the vertical diffusion of such intrinsic air properties as momentum and heat in Sec. 3-1. Indeed the two phenomena are closely related, differing only in that for particle diffusion the possibility exists of effects arising from the size and inertia of the particles involved. In Sec. 3-2 we are concerned with diffusion of particles from isolated sources in the lower atmosphere.

The problem of turbulent diffusion in the atmosphere has not yet been uniquely formulated in the sense that a single basic physical model capable of explaining all the significant aspects of the problem has not yet been proposed. Instead there are available two alternative approaches, neither of which can be categorically eliminated from consideration since each has areas of utility that do not overlap the other's. The two approaches to diffusion are the gradient transport theory and the statistical theory. Diffusion at a fixed point in the atmosphere, according to the gradient transport theory, is proportional to the local concentration gradient. Consequently it could be said that this theory is Eulerian in nature in that it considers properties of the fluid motion relative to a spatially fixed coordinate system. On the other hand, statistical diffusion theories consider motion following fluid particles and thus can be described as Lagrangian. Diffusion theories may be classified as either continuous-motion or discontinuous-motion theories, depending on whether this particle motion is postulated to occur continuously or as discrete events. There must necessarily be a close connection among all these approaches to the diffusion problem since obviously there is only one atmosphere. We will consider here those aspects of each of these approaches which have found application in the atmosphere.

3-2.1 The Gradient Transport Approach

3-2.1.1 Fickian Diffusion. Adolph Fick, a German physiologist, published a paper in 1855 (*Ann. Physik Chem.*, [2] 94: 59-86) entitled "Über Diffusion." These details are given because, although Fickian diffusion is spoken of quite familiarly by research workers in many disciplines, few appear to know who Fick was. His idea stated in his own words [*Phil. Mag.*, [4] 10: 30-39 (1855)] is: "It is quite natural to suppose that this law for the diffusion of salt in its solvent must be identical with that according to which the diffusion of heat in a conducting body takes place; upon this law Fourier founded his celebrated theory of heat, and it is the same which Ohm applied, with such extraordinary success, to the diffusion of electricity in a conductor." The mathematical statement of this hypothesis, Fick's law, has (in the one-dimensional case) the form of the classical equation of conduction,

$$\frac{d\bar{q}}{dt} = K \frac{\partial^2 \bar{q}}{\partial x^2} \qquad (3.45)$$

where K (in the atmosphere) is a constant eddy-diffusivity coefficient and $\bar{q}$ refers to the mean value of some conservative air property per unit mass of air. One of the many interesting applications of this useful equation is to describe the diffusion of thermal neutrons in a nuclear reactor.

The more general case of diffusion in three dimensions in which the diffusion coefficients, which are not necessarily equal, can vary with the three spatial coordinates, i.e.,

$$\frac{d\bar{q}}{dt} = \frac{\partial}{\partial x}\left(K_x \frac{\partial \bar{q}}{\partial x}\right) + \frac{\partial}{\partial y}\left(K_y \frac{\partial \bar{q}}{\partial y}\right) + \frac{\partial}{\partial z}\left(K_z \frac{\partial \bar{q}}{\partial z}\right) \qquad (3.46)$$

was first investigated independently by Richardson (1926) and by Schmidt (1925). The problem of atmospheric diffusion reduced to that of solving Eq. 3.45 or 3.46 under appropriate boundary conditions is often called the K theory. If K_x, K_y, and K_z are constants, the diffusion is called Fickian. The K can be thought of as measuring the flux of a passive scalar quantity $\bar{q}$, such as smoke [flux is defined as $K_x(\partial\bar{q}/\partial x)$ or by a similar expression in y or z]. This quantity, by definition, does not affect the dynamics of the air motions but is merely carried along by them. Consequently, when the turbulence is largely mechanical, $K = K_M$; but, when there is strong thermal convection, $K = K_H$ would be the better approximation. In view of our present limited ability to specify K_H, due largely to the difficulty of determining atmospheric heat flux, this distinction is somewhat academic. In practice K values are usually determined by reference to observed diffusion data.

For a stationary medium Eq. 3.45 in one dimension becomes

$$\frac{\partial \bar{q}}{\partial t} = K\frac{\partial^2 \bar{q}}{\partial x^2} \tag{3.47}$$

Boundary conditions specifying a point source are

(1) $\bar{q} \to 0$ as $t \to \infty$ $\qquad (-\infty < x < +\infty)$

(2) $\bar{q} \to 0$ as $t \to 0$

(for all x except $x = 0$) (3.48)

where $\bar{q} \to \infty$ such that

$$\int_{-\infty}^{\infty} \bar{q}\, dx = Q \tag{3.49}$$

where Q is the source strength (total release of $\bar{q}$). The solution may be obtained by various mathematical devices, in particular by the method of Fourier series. In fact it is probably fair to say that the existence of a large variety of solutions to Eq. 3.45 with various boundary conditions, from the classical theory of heat conduction, has been one of the greatest incentives to development of the K theory.

The fundamental solution of this problem is known to be a Gaussian function, i.e., it has the form

$$\frac{\bar{q}}{Q} = \frac{1}{at^{1/2}} \exp\left(-\frac{bx^2}{t}\right) \tag{3.50}$$

Notice that the factor x^2 implies a symmetrical cloud and that the factor t^{-1} in the exponent satisfies condition (2) of Eq. 3.48. By partial differentiation of Eq. 3.50, we can easily show that it satisfies Eq. 3.47, and, making use of the continuity condition, Eq. 3.49, we find that $a = (4K\pi)^{1/2}$ and $b = (4K)^{-1}$. Since condition (1) corresponds to an instantaneous point source at $t = 0$, the solution to Eq. 3.45 for an instantaneous point source of $\bar{q}$ with strength Q is

$$\frac{\bar{q}}{Q} = \frac{1}{(4\pi Kt)^{1/2}} \exp\left(-\frac{x^2}{4Kt}\right) \tag{3.51}$$

This solution would apply to an atmosphere in which $\bar{u}$ = constant, $v = w = 0$, and for which the coordinates are thought of as moving with the mean wind, $\bar{u}$.

Equation 3.51 may be extended to three dimensions and generalized to the case (nonisotropic diffusion) where $K_x \neq K_y \neq K_z$. The resulting solutions to Eq. 3.46 are, for $K_x = K_y = K_z = K$ and $x^2 + y^2 + z^2 = r^2$,

$$\frac{\bar{q}(r,t)}{Q} = (4\pi Kt)^{-3/2} \exp\left(-\frac{r^2}{4Kt}\right) \tag{3.52}$$

and, for the nonisotropic case,

$$\frac{\bar{q}(x,y,z,t)}{Q} = (4\pi t)^{-3/2}\,(K_xK_yK_z)^{-1/2} \times \exp\left[-\frac{1}{4t}\left(\frac{x^2}{K_x} + \frac{y^2}{K_y} + \frac{z^2}{K_z}\right)\right] \tag{3.53}$$

These are the fundamental building blocks of Fickian diffusion theory. Integration of one of these instantaneous-point-source solutions with respect to space yields equations for instantaneous volume sources (bomb bursts, for example). Integration of the instantaneous-point-source equation with respect to time gives the continuous-point-source solutions. These may, in turn, be integrated with respect to, say, the y-axis to give the crosswind infinite-line-source equation, or they may be integrated with respect to the horizontal plane, and so on. Probably because of the essentially tractable nature of the mathematics involved, almost every laborer in the vineyard of atmospheric

diffusion theory has worked out a solution or two for the Fickian case. As a result, this branch of the subject is now fairly complete.

3-2.1.2 The K Theory. The assumption of constant eddy diffusivity, although it may be of considerable use in the free atmosphere, can hardly apply to the planetary boundary layer, which, as we have seen, is characterized by pronounced shear of the mean wind and large variations in vertical temperature gradients due to heat flux. The K theory of diffusion has addressed itself to these problems.

Equation 3.46 may be simplified by assuming the steady state, i.e., $\partial\bar{q}/\partial t = 0$. If we take an infinite crosswind line source, for which, at ground level,

$$\frac{\partial}{\partial y}\left(K_y \frac{\partial \bar{q}}{\partial y}\right) = 0 \qquad (3.54)$$

(recalling that $\bar{w} = \bar{v} = 0$ if the mean wind blows along the x-axis) and assume, as is reasonable, that $\partial(K_x \partial\bar{q}/\partial x)/\partial x \ll \bar{u}\,\partial\bar{q}/\partial x$, i.e., the x-transport by the mean flow greatly outweighs the eddy flux in that direction, then we can reduce Eq. 3.46 to

$$\bar{u}\frac{\partial \bar{q}}{\partial x} = \frac{\partial}{\partial z}\left(K_z \frac{\partial \bar{q}}{\partial z}\right) \qquad (3.55)$$

This equation, together with the boundary conditions

(1) $\bar{q} \to 0$ as $z \to \infty$

(2) $\bar{q} \to 0$ as $x \to 0$ for all $z > 0$ but $q \to \infty$ as $x \to 0$, $z \to 0$ such that $\lim_{x\to 0} \int_0^\infty \overline{uq}\, dz = Q$

(3) $K_z\,\partial\bar{q}/\partial z \to 0$ as $z \to 0$ for all $x > 0$ (3.56)

the latter implying zero flux at the ground, has been used as the basis for many investigations.

The effect of shear of the mean wind was taken into account by Roberts, who solved Eqs. 3.55 and 3.56 together with a power-law form of K_z; the solution can be found in Sutton's (1953) book. On the basis of the assumption that the surface layer is about 10 m deep, it has been supposed that power-law solutions to Eq. 3.55 would be strictly valid to a distance of about 100 m from a ground-level source since beyond that the diffusing cloud would be likely to be growing out of the surface layer. It now appears from DeMarrais' (1959) study that as a practical matter such solutions may be valid to considerably greater distances. DeMarrais shows that wind profiles can be fit by power functions to elevations of about 100 m, which implies that K_z can also be represented by a power function to this height.

Extension of the K theory to account for surface-roughness effects was undertaken by Calder (1949), who assumed the power-law wind profile

$$\bar{u} = v_* r'\left(\frac{z}{z_0}\right)^{\alpha'} \qquad (3.57)$$

and chose the constants r' and α' so as to give the best fit to the logarithmic wind profile. His solutions are complicated, but over level uniformly rough ground good experimental verification is obtained to distances up to a kilometer from the line source in adiabatic conditions.

Varying atmospheric stability was introduced into the problem by Deacon (1949), who gave a solution for an infinite line source based at the surface, using

$$K(z) = kv_* z_0 \left(\frac{z}{z_0}\right)^{\beta}$$

$$\bar{u}(z) = v_* r^*\left(\frac{z}{z_0}\right)^{\alpha^*} \qquad (3.58)$$

and determining β and α^* from observed (diabatic) wind profiles. A solution for an infinite elevated crosswind line source has also been given, as has a solution for a finite line source oriented along the mean wind. Finite and infinite plane sources are considered extensively in evaporation theory; a review of much of this material can be found in the monograph by Anderson, Anderson, and Marciano (1950). Lettau (1952) developed a shearing advection correction to the K theory which takes into account the apparent diffusion that results from the presence of shear of the mean wind in the planetary boundary layer. Davies (1954), Gee and Davies (1963), and Saffman (1962, 1963) have also discussed the effect of shear. Some progress has recently been made on solutions to Eq. 3.46 for a continuous point source, both at the ground and aloft, by Rounds (1955) and

Smith (1957). This work has been extended in the papers by Godson (1958) and Davidson and Herbach (1962) to include stable conditions, elevated point sources, and the effect of particle settling.

The K theory has great appeal to research workers in atmospheric turbulent diffusion, judging by the papers just cited as well as many related ones found in the bibliographies that the papers contain. Because the fundamental differential equation involved, Eq. 3.46, can be considerably simplified by eliminating one or more of the space coordinates, K theory is widely applied in studies of evaporation and heat conduction from the earth's surface, which is considered to be an extended, horizontal, plane source. Study of the momentum distribution in the planetary boundary layer has likewise suggested the use of K theories. The abundant literature on this phase of the subject was reviewed by Priestley (1959) [see also Priestley, McCormick, and Pasquill (1958)].

Since, in planetary-boundary-layer heat conduction, the source, or driving term, is a sinusoidal time function, the mathematical complexity of some of these solutions is considerable. Staley (1956) described certain K theories quite accurately as "a mathematical extravaganza." It seems that the attraction exerted by the K theory may stem as much from the opportunity it provides for obtaining mathematically explicit results as from its intrinsic physical correctness. All ramifications of the K theory depend ultimately on the validity of the assumption of simple gradient transport, which is the notion that the flux of a quantity is proportional to the gradient of this quantity. Priestley (1959) points out that there is no precise physical basis for the use of this assumption as the foundation for a description of turbulent diffusion in the atmosphere, and consequently the validity of the K theory "is normally judged from the degree of success achieved in ... predicting particular diffusion phenomena." Calder (1965) studied the applicability of the diffusion equation to the atmospheric case and concluded that the standard K-theory form, Eq. 3.46, cannot be generally valid. Russian workers, e.g., Monin (1959), refer to K theory as a semiempirical theory of diffusion. The basic nature of K theory must be kept in mind as the chain of deductions from the original equation grows longer and more involved.

This being said, it must hastily be added that K theory provides many useful, practical results. For example, an approach to the difficult problem of the deposition of polydisperse aerosols (Davidson and Herbach, 1962) can be made via K theory. Barad (1951) presented a K theory of the complicated problem of diffusion of a bent-over stack plume in very stable atmospheres. There are many other examples. Corrsin has aptly summarized the situation by pointing out that K theory is not useful in principle but only in practice.

3-2.2 Statistical Theories of Turbulent Diffusion

Today the statistical theory of fluid turbulence comprises a large and important body of literature, and its results are applied in many areas from oceanography to cosmology. The study of turbulence by this method actually began, however, with the investigation of turbulent diffusion by Taylor (1921). The statistical approach to the diffusion problem differs considerably from K theory. Instead of studying the material or momentum flux at a fixed space point, one studies the histories of the motion of individual fluid particles and tries to determine from these the statistical properties necessary to represent diffusion.

3-2.2.1 Diffusion by Discontinuous Motion. Many of the essential characteristics of statistical diffusion theory can be introduced by the following classroom experiment in diffusion by discontinuous motion. The instructor takes a number of pennies and distributes them to the class as follows. He tosses one and, according to whether it comes up heads or tails, passes it out to the student on his right or on his left in the middle of the first row. The student, in turn, repeats this, passing the penny over his right or left shoulder, and so on, until finally the penny reaches the back row. The instructor continues tossing more pennies and passing them out. Of course, after a time the students in the back row of the classroom will receive pennies in some more or less regular pattern with most of the pennies going to students near the middle of the row and fewest to those near each end. This experiment, simple and obvious

as it is, nevertheless brings out a number of important features of the diffusion problem:

1. The stochastic, or probabilistic, nature of diffusion: this is illustrated by the process used to distribute the pennies.

2. Continuity: the diffusion process must satisfy a continuity condition (i.e., all the pennies should be returned at the end of the experiment).

3. Deposition: occurs if a penny is dropped.

4. Attenuation: at any step, a penny might be removed permanently from the diffusion process (for radioactive particles the analogy is radioactive decay).

5. Effect of sampling: the actual distribution of pennies at the back row is not a perfectly symmetrical distribution. It could be skewed or perhaps bi- or multimodal. Since only a relatively small sample (just a few pennies) was used, the observed distribution will depart from the ideal, symmetrical pattern.

This experiment can be formalized (see Chandrasekhar, 1943). The probability, P, that a penny will move right or left equals $\frac{1}{2}$. After n steps, the penny can be at any of the points $-n, -n+1, \ldots, -1, 0, 1, \ldots, n-1, n$. The number of possible paths in n steps is 2^n, and $P = 2^{-n}$, i.e., all are equally probable. Let $x = mh$ and $t = nk$; then the probability of a penny's reaching any given point mh, at step nk is $P(mh,nk) = 2^{-n}$ (number of possible paths). The grid spacing, h and k, can be chosen as unity and ignored. Let r equal the number of steps right and l equal the number of steps left in a path. Then $l = r - m$ (number to left = number to right minus total lateral distance), and $l = (n - r)$ (total number of steps minus number to right), i.e., $r - m = n - r$, or $m + n = 2r$, and $r = \frac{1}{2}(m + n)$. The number of paths equals $\binom{n}{r}$, i.e., the number of combinations of r elements or n; so

$$P = \frac{1}{2^n}\binom{n}{r} = \frac{1}{2^n}\frac{n!}{r!(n-r)!} = \frac{1}{2^n}\frac{n!}{\left(\frac{n+m}{2}\right)!\left(\frac{n-m}{2}\right)!} \qquad (3.59)$$

which is Bernoulli's distribution. For large values of n, this distribution approaches the normal distribution, normal error curve, or Gaussian distribution:

$$P(m,n) = \left(\frac{2}{\pi n}\right)^{1/2} \exp\left(-\frac{m^2}{2n}\right) \qquad (3.60)$$

If Eq. 3.60 is plotted for successive values of n, the familiar bell-shaped curves of the normal error law result. It is of interest that the coin-tossing, or Monte Carlo, method was originally developed by von Neuman and Ulam in connection with complex problems arising in the calculation of diffusion of neutrons through absorbing and shielding media.

The simple discrete-step stochastic diffusion model (sometimes called "the drunkard's walk") implied by the above discussion is far from irrelevant to the atmosphere. Its molecular analog describes Brownian diffusion. On the other hand, actual turbulent atmospheric motions tend to be rather highly self-correlated, in marked contrast with Brownian motion. The approximation that successive diffusion events are uncorrelated is not a good one in the case of atmospheric turbulence except when the time scale of the problem is large compared with the time scale of the diffusion process. The consequences of a direct application of the Brownian-motion analogy to atmospheric diffusion have been investigated by Obukhov (1959), Lin (1960), and Chadam (1962).

The uncorrelated kind of diffusion process described by Eq. 3.60 corresponds closely to Fickian diffusion; consequently it must be governed by a parabolic type of differential equation, such as Eq. 3.47. Physically, parabolic differential equations characterize equalization processes, of which the heat-conduction problem provides the classical example. Solutions of parabolic equations have the character that some effect is felt everywhere except at the initial instant, $t = 0$, as is shown by Eq. 3.51. The implication is that diffusion proceeds in some sense with infinite velocity. Generalizations to more realistic discrete-step diffusion models in which successive events are correlated (drunkard's walk with a memory) have been discussed by Taylor (1921), Goldstein (1951), Davies and Diamond (1954), Davies, Diamond, and Smith (1954), and Monin (1955). These studies indicate that atmospheric diffusion should obey the "telegrapher's equation" rather than a simple parabolic equation of the heat-conduction type. Since, in the diffusion application, the telegrapher's equation is hyperbolic like the wave equation rather than para-

bolic, it describes diffusion that proceeds at a finite velocity. Thus there will be a definite limit to the distance that fluid particles can disperse in a given amount of time in contrast to the conclusion from Eq. 3.51 that the effect of diffusion is felt everywhere to some extent for all values of $t > 0$. It cannot be denied that finite diffusion is physically more realistic although the practical difference, as shown in Sec. 3-3, is probably not great.

3-2.2.2 Diffusion by Continuous Motion. Taylor (1921) derived a fundamental diffusion theorem that has had very great influence on all subsequent work in this field, both theoretical and practical. Taylor's result applies to diffusion in one space dimension or to the projection onto a single space axis of two- or three-dimensional diffusion in a stationary, homogeneous turbulent flow. A homogeneous turbulent flow is one in which the statistical properties are independent of position. Stationary turbulence is homogeneous in time. Properties of the turbulence, such as the transverse (to the mean flow direction) root-mean-square velocity, $(\overline{v'^2})^{1/2}$, would be expected to be invariant anywhere in such a flow. Turbulence in the upper portion of the planetary boundary layer may approximate the homogeneous type, but surface-layer turbulence is decidedly inhomogeneous. The idea of turbulence homogeneity is a simplification introduced into the theory to permit further progress to be made.

Taylor's calculation involves the motion (continuous) of a fluid particle, which is assumed to be somehow identified or tagged. On the other hand, we might consider a dynamically and chemically inert particle of negligible size and mass which is being transported by the atmosphere. The distance, y, that this particle is carried away from an origin by turbulent wind fluctuations, v', during a time interval, t, is equal to

$$y(t) = \int_0^t v'(t_1)dt_1 \qquad (3.61)$$

(We will not introduce a separate symbolism to distinguish the particle-attached, or Lagrangian, motion from the fixed-point Eulerian motion since this would greatly complicate the notation. The distinction should always be kept clearly in mind, however.) This straightforward process is pictured in Fig. 3.6. By the transformation $t = x/\bar{u}$, we can also visualize the

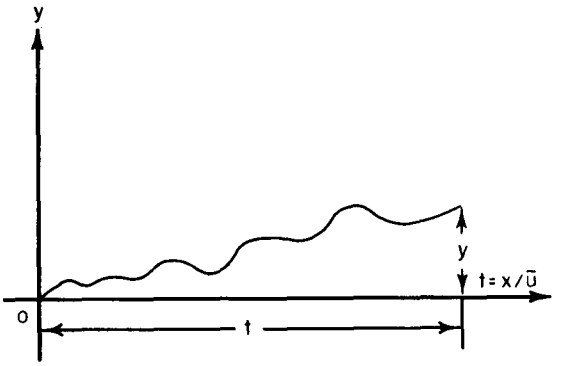

Fig. 3.6 — Path of a tagged particle displaced a distance y in time t by the action of random turbulence.

motion as taking place relative to a fixed space axis extending downwind from the origin. A physical example of this phenomenon would be the motion of a smoke particle emitted from a chimney in a steady mean wind.

The simplest meaningful statistical measure of this irregular, random process that we can compute is the mean-square diffusion that would result from a large number of independent repetitions, i.e., the variance, or second moment, of the resulting distribution of particles along the y-axis. By squaring both sides of Eq. 3.61 and taking the average over many repetitions of the experiment (the statistical, or ensemble, average), we are led to Taylor's result:

$$\overline{y^2}(t) = 2\,\overline{v'^2}\int_0^t \int_0^{t_1} R(\xi)\, d\xi\, dt_1 \qquad (3.62)$$

The mathematical steps are given in many references, e.g., Pasquill (1962).

The function $R(\xi)$ is called the one-point Lagrangian velocity correlation coefficient, Lagrangian because it refers to the velocity of a particle rather than the velocity at a fixed space point, and coefficient because it has been normalized, i.e., adjusted, by dividing by $\overline{v'^2}$ so that $R(0) = 1$:

$$R(\xi) = \frac{\overline{v'(t)\, v'(t+\xi)}}{\overline{v'^2}} \qquad (3.63)$$

Batchelor (1949) generalized Eq. 3.62 to three dimensions. In this form the mean-square diffusion becomes a tensor, δ_{ij}^2, with indices ranging from 1 to 3, and $\overline{y^2} \equiv \delta_{22}^2$. Computation of higher order moments, such as $\overline{y^3}$, could be carried out by the same straightforward process although with rapidly increasing complexity.

Since $R(0) = 1$ and, for sufficiently small diffusion time, $R(t) \approx 1$ because R is a correlation coefficient, it follows that when t is small

$$\overline{y^2}(t) \approx \overline{v'^2}\, t^2 \qquad (3.64)$$

When t is large, it may be supposed that the autocorrelation function, R, must approach zero sufficiently rapidly that

$$\overline{v'^2} \lim_{t\to\infty} \int_0^t R(t_1)\, dt_1 = K_1 \qquad (3.65)$$

where K_1 is some constant. The particle must ultimately "forget" its original motion. There are several ways to see why this should be true. Perhaps the most obvious is the one discussed in the following paragraphs.

Consider the Fourier cosine transform F(n) of R:

$$F(n) = 4 \int_0^\infty R(t) \cos(2\pi nt)dt \qquad (3.66)$$

where F(n) is called the Lagrangian eddy-energy spectrum. The eddy-energy spectrum expresses the distribution as a function of frequency, n, of turbulent kinetic energy corresponding to the various Fourier components of the (in this case) one-dimensional Lagrangian turbulent velocity field. The simpler term "eddy" will be used from now on to denote a Fourier component of the turbulent velocity field characterized by a certain time or length scale. Although it is always more convenient to speak of an eddy of some size (or of some time scale proportional to n^{-1}), it should not be inferred that such a Fourier component necessarily has a separate, identifiable material existence such as we have previously imagined is possessed by eddies. It must be remembered that two meanings of the term "eddy" exist and that they are often confused in the meteorological literature. The interested reader should consult Corrsin (1959) for a concise discussion of the meaning of the spectrum representation of a turbulent velocity field; a complete discussion of atmospheric energy-spectrum properties is contained in the books by Pasquill (1962) and by Lumley and Panofsky (1964).

At zero frequency (n = 0), we can see from Eq. 3.66 that

$$F(0) = 4 \int_0^\infty R(t)\, dt \qquad (3.67)$$

Even without further discussion of the properties of the energy spectrum, it seems clearly to be required that $F(0) \propto K_1 < \infty$. Otherwise the eddy kinetic energy would be in some sense infinite. Consequently we may derive the limit of Eq. 3.62 for large diffusion times:

$$\overline{y^2}(t) \approx 2K_1 t \qquad (3.68)$$

where K_1 is a constant.

The derivative of Eq. 3.68, i.e., $\frac{1}{2}\, \overline{dy^2}/dt$, has the dimensions of a diffusivity. It might be argued therefore that K_1 plays a part similar to that of the K of Fickian theory and that

$$\frac{1}{2}\frac{\overline{dy^2}}{dt} = K_1 = K \qquad (3.69)$$

where K has the original meaning assigned to it, an eddy diffusion coefficient. Comparing Eqs. 3.69 and 3.68, the conditions for the applicability of the K theory in the atmosphere can be appreciated. The quantity $\int_0^\infty R\, dt$ defines a time-scale characteristic of the turbulence called the Lagrangian integral time scale, $\mathscr{T}$:

$$\mathscr{T} = \int_0^\infty R(t)\, dt \qquad (3.70)$$

This argument makes it appear reasonable that Fickian theory, in which K is constant, should apply when the diffusion time, t, is large compared to $\mathscr{T}$.

There appears to be no basic way of evaluating the precise points at which the limits of Taylor's diffusion theorem for small and large times will apply in the atmosphere. If it were possible to measure the Lagrangian autocorrelation function, R, with precision, the applicable diffusion times could be determined, but this is very difficult to do. In fact most of the reliable knowledge of the form of R has been inferred, by applying Eq. 3.62 inversely, from diffusion experiments (Panofsky, 1962; Mickelsen, 1955; and Baldwin and Mickelsen, 1961).

Taylor's theorem can also be written in terms of the eddy-energy spectrum by combining Eq. 3.62 and the inverse transform of Eq. 3.66. It then follows that the mean-square diffusion, $\overline{y^2}$, is

$$\overline{y^2} = \overline{v'^2}\, t^2 \int_0^\infty F(n) \frac{\sin^2(\pi nt)}{(\pi nt)^2}\, dn \qquad (3.71)$$

It can be seen from this not only that $\overline{y^2}(t)$ depends on the entire energy spectrum, F(n), for any value of t but also that the larger t is, the more the diffusion is dominated by the low-frequency contributions to F(n). This follows because the spectrum in Eq. 3.71 is weighted by the function

$$W(n;t) = \left(\frac{\sin \pi nt}{\pi nt}\right)^2 \qquad (3.72)$$

which is largest for small values of nt and rapidly approaches zero for other values. The larger t is, the smaller n must become in order that this weighting factor differ much from zero. In other words, it appears that the large eddies (Fourier components of the motion having low frequency) dominate atmospheric diffusion when this is calculated with reference to a fixed source or axis. In this day and age of high-fidelity sound equipment, there will be general understanding of the statement that the diffusion process acts like a filter for high-frequency spectrum components, having the band-pass characteristic of Eq. 3.72.

3-2.2.3 Method of Moving Averages. Hay and Pasquill (1959) noticed that the integrand of Eq. 3.71 is similar in form to the expression by which a computed turbulence energy spectrum is corrected for the effect of averaging the raw data over a time interval a;

$$F(n)\left(\frac{\sin \pi na}{\pi na}\right)^2 = F_a(n) \qquad (3.73)$$

where $F_a(n)$ is the observed spectrum obtained from a wind-velocity-fluctuation record that has been averaged over the time interval a. The averaging might, for example, reflect the response characteristic of the particular anemometer used or the interval between diffusion measurements.

If the averaging interval is selected to be equal to the time of travel, or diffusion time, t, it follows that

$$\overline{y^2}(t) = \overline{v'^2}\, t^2 \int_0^\infty F_t(n)\, dn \qquad (3.74)$$

By definition $\overline{v'^2} \int_0^\infty F_t(n)\, dn$ is just the total turbulence energy contained in a velocity signal that has been subjected to a moving average over the time t. Thus Eq. 3.74 can be written

$$\overline{y^2}(t) = \langle \overline{v'^2} \rangle_t\, t^2 \qquad (3.75)$$

a form fully equivalent to the autocorrelation and spectrum forms, Eqs. 3.62 and 3.71. The symbol $\langle\ \rangle_t$ indicates that (one component of) the single-point Lagrangian velocity, v', is to be subjected to a moving average over t prior to computation of the variance.

3-2.2.4 Sutton's Diffusion Model. From the limiting cases for small and large diffusion times of Taylor's theorem, Eqs. 3.64 and 3.68, it appears that the limit for large diffusion time may not be attained very rapidly since there is room in the atmosphere, at least in the horizontal direction, for quite large eddies to come into play. This fact led Sutton to propose his well-known model of averaged plume diffusion. Sutton (1953) reasoned that the Lagrangian single-particle autocorrelation function, $R(\xi)$, must depend only on the intensity of turbulence, $\overline{v'^2}$, on viscosity, ν, and on ξ. Since $R(0) = 1$ and $R(\infty) = 0$, he proposed on dimensional grounds the following simple interpolation formula for R:

$$R(\xi) = \left(\frac{\nu}{\nu + \overline{v'^2}\xi}\right)^n \qquad (0 < n < 1) \qquad (3.76)$$

If Eq. 3.76 is combined with Eq. 3.62 and if terms of the order of ν are ignored, it develops that

$$\overline{y^2}(t) = \frac{2\nu^n}{(1-n)(2-n)\overline{v'^2}}\,(\overline{v'^2}t)^{2-n} \qquad (3.77)$$

Defining a constant C_y^2, called by Sutton a virtual diffusion coefficient,

$$C_y^2 = \frac{4\nu^n}{(1-n)(2-n)\overline{u}^n}\left(\frac{\overline{v'^2}}{\overline{u}^2}\right)^{1-n} \qquad (3.78)$$

we find that

$$\overline{y^2} = \frac{1}{2}\, C_y^2 (\overline{u}t)^{2-n} \qquad (3.79)$$

Sutton further introduced the concept of macro-viscosity, $N = v_* z_0$, to replace the molecular viscosity, ν, for flow in the atmosphere in which the effect of molecular viscosity can be ignored.

Sutton originally studied diffusion in the lower few meters, in what we now call the

surface layer. Since this region of the planetary boundary layer is characterized by marked vertical shear of the mean wind, the question might be raised whether Sutton's application of Taylor's result, which is based on the assumption of turbulence homogeneity, can conceivably be correct. Certainly the assumption of horizontal turbulence homogeneity at a fixed level is a reasonable one. Therefore it is also reasonable to expect that an expression of the form of Eq. 3.79 might apply in the atmosphere.

Sutton also assumed that similar expressions hold for $\overline{x^2}$ and $\overline{z^2}$. For example,

$$C_z^2 = \frac{4\nu^n}{(1-n)(2-n)\bar{u}^n}\left(\frac{\overline{w'^2}}{\bar{u}^2}\right)^{1-n} \qquad (3.80)$$

and

$$\overline{z^2} = \frac{1}{2} C_z^2 (\bar{u}t)^{2-n} \qquad (3.81)$$

Notice that since $n > 0$ Sutton's expressions for $\overline{y^2}$ and $\overline{z^2}$ grow with time at a rate much more rapid than is true for Fickian diffusion (Eq. 3.68). In view of Eq. 3.71, such behavior could very well be a generally desirable property for an atmospheric diffusion model to have in some suitably restricted range of t, as Batchelor (1949) pointed out.

In order to introduce the effect of stability on the wind profile, it was originally assumed that n could be determined from the following relation:

$$\frac{\bar{u}_1}{\bar{u}_2} = \left(\frac{z_1}{z_2}\right)^{n/(2-n)} \qquad (3.82)$$

where the subscripts refer to two different elevations. The justification for identifying n as a stability factor is that this exponent does exhibit a marked variation with stability. On the other hand, no satisfactory direct relation between n as defined by Eq. 3.82 and as defined by Eq. 3.76 is apparent since Eq. 3.76 assumes a homogeneous turbulence field that is true for Eq. 3.82 only if $n = 0$ and Eq. 3.76 involves Lagrangian wind statistics. Equation 3.82 involves the Eulerian wind field. Furthermore, for very large diffusion times, the autocorrelation defined by Eq. 3.76 must be questioned by the same argument that was used in deriving the limit for large time of Taylor's theorem. According to this argument the Lagrangian integral scale of turbulence corresponding to Eq. 3.76 is

$$\mathcal{I} = \int_0^\infty \left(\frac{\nu}{\nu + \overline{v'^2}t_1}\right)^n dt_1 = \infty \qquad (3.83)$$

which by Eq. 3.67 implies infinite eddy energy density at zero frequency, i.e., $F(0) = \infty$. This is in conflict with Eq. 3.68 as well as with observed power spectra.

Notwithstanding these purely theoretical difficulties, Sutton's model has been widely proved in practice and sanctioned by usage. It should certainly be regarded as something better in the sense of being more useful, theoretically oriented, or physically motivated than, say, a purely empirical interpolation formula. But it should not be accorded the unequivocal status of a law of nature; it should be used with due regard for its several ad hoc features, and verification over some restricted range of distance and meteorological conditions should not be taken as an open invitation to an uncritical, universal application. Good verifications of diffusion predictions by Sutton's method have been obtained for distances of the order of several kilometers under neutral or unstable conditions.

Attempts have been made to extend the applicability of Sutton's scheme empirically to greater distances by introducing the separate parameters, n_y and n_z, for each direction (Schmidt, 1960; Leonard, 1957; and Barad and Haugen, 1959). Barad and Haugen were able to improve agreement considerably with data on diffusion from a source very near the ground while at the same time emphasizing the basically empirical nature of such extensions to Sutton's formulation.

3-2.2.5 A Similarity Theory of Diffusion in the Surface Layer. The statistical diffusion methods discussed so far depend on stationary, homogeneous turbulence. The planetary boundary layer, particularly the surface layer, however, is characterized by marked inhomogeneity of turbulence in the vertical direction as a result of wind shear and stability. Vertical inhomogeneity of the surface layer is taken into account in the K theories of Calder (1949), Deacon (1949), Frost (1948), Rounds (1955), and Smith (1957) by assuming some variation of

$\bar{u}(z)$ and consequently of $K(z)$, usually a power law. This amounts to recognizing the problem of vertical inhomogeneity without solving it since the coefficients of the assumed power laws, or some related parameters of the problem, are invariably left to be determined from suitable observations. Ellison (1959), prompted by a remark by Batchelor (1959), applied a dimensional method to the determination of the diffusion downwind from a continuous point source in a logarithmic (adiabatic) surface layer. Batchelor (1959a) obtained the same results as Ellison (unpublished note; see also Batchelor, 1964). Subsequently Gifford (1962) attempted to extend the method to the diabatic surface layer, and Cermack (1963), Calder (1963), and Yaglom (1965) presented further results. The remaining paragraphs in this section outline the reasoning involved in these studies, which are important because they treat surface-layer diffusion without postulating a diffusivity.

The Eulerian (spatially fixed) characteristics of surface-layer turbulent flow are, as we have seen in the mean-wind field, particularly simple, being completely characterized by the friction velocity, v_*, and the stability length, L. Since any characteristic surface-layer velocity must therefore be proportional to v_* times a universal function of the dimensionless length, $\zeta = z/L$, Kazansky and Monin (1957) and Monin (1959) reasoned that the maximum vertical velocity of a smoke particle in a diffusing plume emanating from a source at ground level, w_*, must be given by

$$\frac{dz}{dt} = w_* = \lambda' v_* \, \varphi(\zeta) \tag{3.84}$$

where $\varphi(\zeta)$ is a universal function, λ' is a universal constant, and z refers to the motion of a smoke particle at the upper boundary of the plume. It is reasonable to suppose that the equation for the horizontal velocity of a smoke particle at the upper plume boundary is $dx/dt = \bar{u}$; the shape of the upper boundary of the plume can be described (recalling Eq. 3.31) by

$$\frac{dx}{dz} = \frac{1}{k\lambda'} \frac{[f(\zeta) - f(\zeta_0)]}{\varphi(\zeta)} \tag{3.85}$$

Monin evaluated the function $\varphi(\zeta)$ from the turbulent-energy-balance equation and found

$$\varphi(\zeta) = \left[1 - \frac{1}{f'(\zeta)}\right]^{1/4} \tag{3.86}$$

Using Eq. 3.86 and suitable equations for $f(\zeta)$, Monin integrated Eq. 3.85 numerically to obtain the shape of the upper boundary of the plume from an infinite crosswind line source at ground level as a function of stability. A result similar to Monin's was obtained by Kao (1960) with, however, differences in the numerical values involved.

The concentration distribution of a diffusing plume is a statistical function of the Lagrangian (particle-attached) fluid velocities. If Lagrangian statistical properties of the surface-layer flow are assumed to obey the hypothesis of dynamical similarity, as do the above Eulerian properties, then we may proceed as follows.

Let the mean position of a particle be $\bar{x}(t)$, $\bar{y}(t)$, $\bar{z}(t)$. (If we choose the downwind direction to coincide with $\bar{x}$, then $\bar{y} \equiv 0$.) Assume that

$$\frac{d\bar{x}}{dt} = \bar{u}(\bar{z}) \tag{3.87}$$

i.e., that at any point the horizontal part of the particle's motion equals the average wind speed (see, however, the discussion of this point by Yaglom, 1965). Following a dimensional line of reasoning, we can also conclude that the mean vertical velocity of a particle, $\bar{w}$, is given by

$$\frac{d\bar{z}}{dt} = \bar{w} = b \, v_* \, \varphi_1\left(\frac{\bar{z}}{L}\right) \tag{3.88}$$

where φ_1 is a universal function that has usually been assumed to coincide with φ of Eq. 3.86 although this cannot be justified a priori and b is a universal constant. As Ellison (1957) pointed out, the role of z_0 in surface-layer turbulence is restricted to that of a horizontal translation of the mean flow, as in Eq. 3.87. Consequently neither $\bar{z}$ nor the concentration depend on z_0.

Now apply dimensional reasoning to determining the probability of a particle's reaching some distance $r = (x^2 + y^2 + z^2)^{1/2}$ from the mean particle position $(\bar{x},0,\bar{z})$. This is the same as inquiring what the concentration distribution, χ, would be following the instantaneous release of Q particles from the coordinate origin, where χ is measured from the mean particle position and averaged over a very large num-

ber of repetitions of the experiment and the x-axis is oriented along the mean wind direction. In addition to χ and Q, the relevant variables are the displacements, $x - \bar{x}$, $y - \bar{y} = y$, $z - \bar{z}$; the parameters characterizing the turbulence, v_* and L; and the mean time of particle travel to point $(\bar{x},0,\bar{z})$, t.

For the special case of the axial ground concentration, y = z = 0. From the remaining variables we can form the following:

$$F_3\left(\frac{\chi\bar{z}^3}{Q}, \frac{x-\bar{x}}{\bar{z}}, \frac{\bar{z}}{L}, \frac{v_* t}{L}\right) = 0 \qquad (3.89)$$

Solving for the ratio containing χ, we find

$$\frac{\chi}{Q} = \frac{1}{\bar{z}^3} F_4\left(\frac{x-\bar{x}}{\bar{z}}, \frac{\bar{z}}{L}, \frac{v_* t}{L}\right) \qquad (3.90)$$

To find the continuous-point-source axial concentration, $\bar{\chi}_p$, we would have to integrate Eq. 3.90 with respect to time from 0 to ∞. Since all the remaining dimensionless ratios are functions of time and nothing whatsoever is known about F_4, this becomes a difficult problem. In the adiabatic case, however, $L = \infty$ and $\varphi = 1$, and the integration can readily be performed:

$$\frac{\bar{\chi}_p}{Q'} = \int_0^\infty \frac{F_4\left(\frac{x-\bar{x}}{\bar{z}}, 0, 0\right) dt}{\bar{z}^3} \qquad (3.91)$$

where Q′ is the continuous-source strength. By changing the integration variable, we find that

$$\frac{\bar{\chi}_p}{Q'} = \int_{-\infty}^\infty \frac{F_4\left(\frac{x-\bar{x}}{\bar{z}}, 0, 0\right) d\left(\frac{x-\bar{x}}{\bar{z}}\right)}{bv_*\bar{z}^2\left(\frac{x-\bar{x}}{\bar{z}} + \frac{d\bar{x}}{d\bar{z}}\right)} \qquad (3.92)$$

At a sufficient distance downwind, the diffusing particles will be swept past any point rapidly compared with the time taken to reach that point, and we may assume that $x \approx \bar{x}$. With this simplification it is easily shown that

$$\frac{\bar{\chi}_p}{Q'} b v_* \propto \frac{1}{\bar{z}^2[(\bar{x}/\bar{z}) + (1/kb)]} \qquad (3.93)$$

where, from Eqs. 3.87 and 3.88,

$$\bar{x} = \frac{1}{kb}\left[\bar{z}\left(\ln\frac{\bar{z}}{z_0} - 1\right)\right] \qquad (3.94)$$

This is the result found by both Ellison and Batchelor.

By evaluating Eq. 3.93, these authors showed that in the adiabatic surface layer the downwind concentration from a continuous point source varies as x^p, where p varies approximately in the range −1.8 to −1.9. For a continuous, infinite crosswind line source, the downwind concentration was found to vary as x^{-1}. These results are quite interesting. They provide an alternative to Sutton's solution that leads to essentially the same result and, in the adiabatic surface layer, is known to be in excellent agreement with data. It is also interesting to note that the surface-layer diffusion proceeds at a rate quite close to the limiting prediction for homogeneous turbulence, Eq. 3.64, i.e., as x^{-2} (since $x = \bar{u}t$).

In the diabatic case the last two of the dimensionless ratios of Eq. 3.90 cannot be expected to disappear so conveniently. By, in effect, assuming that even in the diabatic case the function F_4 does not depend strongly on these two ratios, Gifford (1962) proposed that

$$\frac{\bar{\chi}_p}{Q'} \propto [\bar{u}(\bar{z})\,\bar{z}^2]^{-1} \qquad (3.95)$$

which is the counterpart to Eq. 3.93 for a nonadiabatic surface layer. For a relation between axial ground concentration and downwind distance, $\bar{x}$, to be obtained, a relation between $\bar{x}$ and $\bar{z}$ must be established. This follows from integration of Eq. 3.85 for $d\bar{x}/d\bar{z}$. Details have been given by Gifford (1962), and the results are in reasonably close agreement with detailed experimental atmospheric-concentration measurements. Wind-tunnel diffusion studies by Cermak (1963) have provided additional verification.

3-2.2.6 Relative Atmospheric Diffusion. Taylor's expression for diffusion measured from a fixed origin or axis, Eq. 3.62, is completely characterized by the statistics of the motion of a single fluid particle. The statistical averaging that Taylor had in mind was independent of any single particular realization of the experiment, that is, of any single set of initial conditions of the turbulent flow. The

motions of any two or more fluid particles during a diffusion time t should be completely independent from the point of view of Eq. 3.62. But, if one is interested in the spreading out of an isolated cloud of fluid particles, this requirement cannot hold. Because the particles all start out together, the motions of particles in a cloud, puff, or cluster will at first be strongly correlated. In fact, if it is required that particles start out infinitely close together (an instantaneous-point-source condition), they will (in principle) never separate since at all times they are acted upon by the same fluctuation. Thus Richardson concluded that a spreading dot is unsuitable as a model for cloud diffusion. A second mode of diffusion, based on the rate of spreading of a cluster of fluid particles relative to their mutual center of gravity, must be calculated.

Consider two dispersing fluid particles, the simplest case of the diffusion of a cloud of n particles (Fig. 3.7). Stationary and homogeneous turbulence conditions are again assumed. One can calculate $\overline{Y^2}$, the mean-square value of the spreading, or the relative, diffusion. The procedure is exactly the same as for the calculation of $\overline{y^2}$ (Eq. 3.62), the single-particle dispersion parameter. The distance between the particles, Y, is given by

$$Y = y_1 - y_2 = Y_0 + \int_0^t v_1'(t_1)dt_1 - \int_0^t v_2'(t_1)dt_1 \qquad (3.96)$$

where Y_0 is the initial separation between the particles and the subscripts on y and v′ refer to the particles. The corresponding mean-square relative diffusion is

$$\overline{Y^2} = Y_0^2 + 2\,\overline{v'^2}\int_0^t\int_0^t R(t_2-t_1)\,dt_1\,dt_2 - 2\int_0^t\int_0^t \overline{v_1'(t_1)\,v_2'(t_2)}\,dt_1\,dt_2 \qquad (3.97)$$

The detailed steps are essentially the same as those for the one-particle case. Generalization to a cloud of particles is given by Batchelor (1952).

Comparison of Eqs. 3.97 and 3.62 shows that the separation between two particles depends on two factors in addition to the single-particle Lagrangian time correlation, $R(\xi)$. These are the initial separation, Y_0, and the relative (two-particle) Lagrangian correlation term, $\overline{v_1'(t_1)\,v_2'(t_2)}$. Notice that if two particles initially occupy the same position in the fluid then $Y_0 = 0$ and $v_1' = v_2'$. As a result $\overline{Y^2} = 0$, and the particles will never disperse relative to one another. By Taylor's diffusion theorem, Eq. 3.62, they will, however, disperse on the average with respect to a fixed axis.

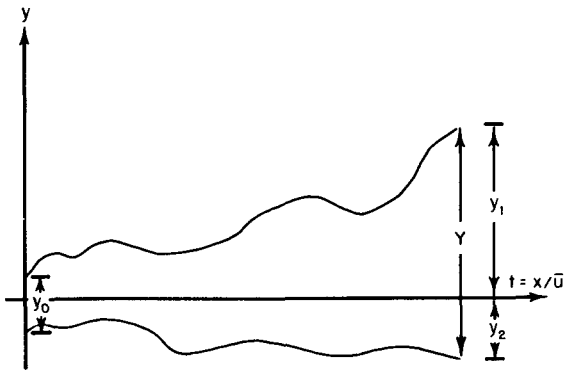

Fig. 3.7—Relative diffusion of two tagged particles (see Eq. 3.96).

From the foregoing arguments it appears that relative diffusion, that is, the spreading out of a cloud of fluid particles or the spreading of a plume from its center line, is described by the joint Lagrangian statistics of two dispersing particles. Single-particle Lagrangian statistics, on the other hand, describe the average spreading of a plume about a fixed axis. The plume photographs shown in Fig. 3.8 (Culkowski, 1961) may make the distinction between relative and average dispersion clearer. Part a, Fig. 3.8, is an instantaneous ($\frac{1}{50}$ sec) exposure of a plume. The spreading of this plume relative to its irregular, undulating center line is described by Eq. 3.97. Part b, Fig. 3.8, is a 5-min time exposure of the same plume. The average diffusion about the horizontal plume center line, which is obviously oriented in the direction of the mean wind, is appropriately described by Taylor's diffusion equation (Eq. 3.62).

Qualitatively, relative diffusion should depend on the action of eddies approximately as large as a puff or, as in (a) of Fig. 3.8, as large as the width of the instantaneous plume. We have, on the other hand, noticed (Eq. 3.71) that average plume diffusion rapidly becomes dependent on quite large eddies. This distinction, first made by Richardson, was reemphasized by Yudine (1946), Brier (1950), and particularly by Batchelor in his definitive theoretical treatment (Batchelor, 1949, 1950, 1952). Richardson

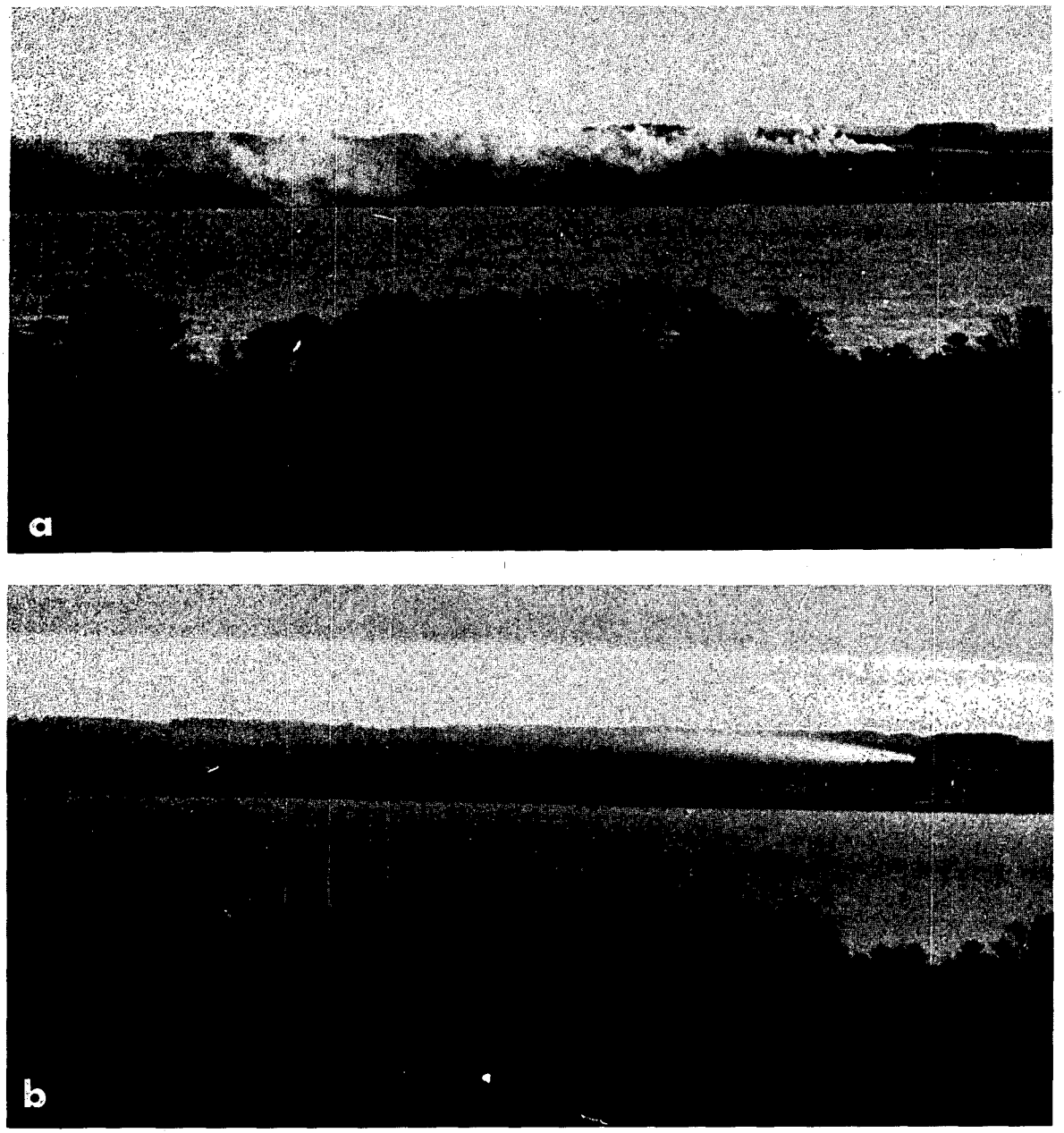

Fig. 3.8—Plume photographs. (a) Instantaneous ($\frac{1}{50}$-sec) exposure photograph of a plume. (b) Time exposure (5-min) of same plume. (From Culkowski, 1961.)

(1926) observed horizontal eddy diffusivities, K, of particle clusters with widely divergent sizes and arranged his K values according to a length scale, l, corresponding to the size of the clusters involved, as shown in Table 3.2. The K values clearly increase with l, and Richardson proposed the empirical equation $K = 0.2l^{4/3}$ to describe these observed values. Somewhat unexpectedly, the spreading of puffs or clusters appears to depend upon the scale of the diffusion event, i.e., on the separation between representative dispersing particles. A formal explanation for Richardson's discovery was given by Obukhov (1941), who pointed out that the law $K \propto l^{4/3}$ follows by a dimensional argument from the assumption that in the inertial range the structure of eddies governing cloud or cluster spreading is controlled by the rate of eddy-

Table 3.2—VALUES OF HORIZONTAL EDDY DIFFUSIVITIES AT VARIOUS SCALES*

Scale (l), cm	K, cm^2/sec	Source of data
5×10^{-2}	1.7×10^{-1}	Molecular diffusion
1.5×10^{3}	3.2×10^{3}	Low-level wind shear
1.4×10^{4}	1.2×10^{5}	Low-level wind shear
5×10^{4}	6×10^{4}	Pilot balloons, 100 to 800 m
2×10^{6}	1×10^{8}	Manned and unmanned balloons
5×10^{6}	5×10^{8}	Volcanic ash
1×10^{8}	1×10^{11}	Cyclonic storms

*From Richardson, 1926.

energy transfer, ϵ (cm^2/sec^3); K (cm^2/sec) must be proportional to $\epsilon^{1/3} l^{4/3}$.

The useful concept of an inertial range of eddies, i.e., a range of eddy sizes in which the properties of turbulence are dominated by the transfer of energy by inertial forces and are independent of viscous dissipation, was introduced by Kolmogorov (1941) and Obukhov (1941). Like so much of significance in atmospheric turbulence and diffusion theory, it has its origin in Richardson's early work. Richardson stated the basic idea in characteristically unorthodox form, the frequently quoted (Shaw, 1942; Sutton, 1949; and Batchelor, 1950, to give but a few examples) quatrain:

> Great whirls have little whirls
> That feed on their velocity;
> And little whirls have lesser whirls,
> And so on to viscosity.

These lines, a parody of a well-known verse by Swift, represent in all probability the only example of the statement of a fundamental physical principle in doggerel. There is ample room in the atmosphere for whirls (eddies) that are quite large, at least in their horizontal dimensions. Between the largest of these (possibly comparable to the scale of great cyclonic storms) and the smallest (the very small scale of viscous dissipation), there is a wide range of eddy sizes available for the eddy-energy cascade process described so neatly by Richardson's rhyme. In a sufficiently restricted portion of this size range, the turbulence properties must be independent of both the manner of energy supply to the large-scale eddies and the manner of eddy-energy dissipation at very small scales by viscosity. Consequently the turbulence properties in this range must be determined only by the rate of eddy-energy transfer, ϵ (cm^2/sec^3). This range of small-scale high-frequency eddies, lying in size just above the dissipative range of eddy sizes, is called the inertial range. The available evidence on the limits of the inertial range of eddy sizes in the atmosphere has been summarized by MacCready (1962). From his work we can conclude that eddies ranging in size from several times height above the surface down to well below the resolving power of ordinary wind-measuring equipment should be inertial in character.

Batchelor argued that in the inertial range the rate of relative diffusion, $d\overline{Y^2}/dt$, can depend only on the initial separation, Y_0, on the diffusion time, t, and on the rate of eddy-energy transfer per unit mass, ϵ. Furthermore, for t greater than some value t*, the diffusion rate will be independent of the initial separation. Provided this also occurs within the inertial range, purely dimensional considerations result in the following predictions concerning the rate of relative diffusion:

$$\frac{d\overline{Y^2}}{dt} \propto (\epsilon Y_0)^{2/3} t \qquad (t < t^*) \qquad (3.98)$$

$$\frac{d\overline{Y^2}}{dt} \propto \epsilon\, t^2 \qquad (t > t^*) \qquad (3.99)$$

$$t^* \approx Y_0^{2/3} \epsilon^{-1/3} \qquad (3.100)$$

Integrating Eqs. 3.98 and 3.99, we get

$$\overline{Y^2}(t) - \overline{Y^2}(0) \propto t^2 \qquad (t < t^*) \qquad (3.101)$$

$$\overline{Y^2}(t) \propto t^3 \qquad (t > t^*) \qquad (3.102)$$

Not much credence was attached at first to these predictions of relative diffusion since the extent of the inertial range of eddy sizes was thought to be quite small. Until very recently researchers have attempted to explain the diffusion of puffs near the surface or the instantaneous spreading of a plume by applying Eq. 3.62. Note that Eq. 3.64 should never predict diffusion any faster than t^2, in marked contrast to the prediction of Eq. 3.102. The reanalysis of data on puff spreading and concentration from several experiments by Gifford (1957) has confirmed the validity of the relative-diffusion predictions in the atmosphere.

By studying the relative accelerations rather than the velocities of particle pairs, Lin (1960, 1960a) derived a relative diffusion law of the same form as Eq. 3.102 without, however, making explicit use of the inertial-range concept. Lin found that

$$\overline{Y^2} = \frac{2}{3} Dt^3 \qquad (3.103)$$

where D is a quantity having the dimensions of energy dissipation (ϵ), i.e., cm^2/sec^3. The proof is quite similar to that of Taylor's diffusion theorem. Since Eq. 3.103 is not restricted to the inertial range, it is presumably valid over a greater spatial domain and may contain the explanation for Richardson's empirical diffusion law, which can be derived from it. Furthermore D is a Lagrangian parameter, i.e., it arises in a Lagrangian description of diffusion; whereas ϵ is Eulerian in nature. Consequently Lin's result appears to be a conceptual improvement. Smith and Hay (1961) also studied relative diffusion by assuming a certain form of the relative-velocity correlation and assuming that the material distribution in a cluster is Gaussian. They derived a particularly simple relative-diffusion formula that has been useful in several field studies (see Chap. 4).

It is interesting that the concept of relative diffusion has been employed by oceanographers to explain the spreading of dye patches on the sea surface (see the excellent summary of this area of research by Okubo, 1962). Relative diffusion has also been invoked in discussing the spreading of sodium vapor trails in the lower ionosphere (e.g., Coté, 1963, and Zimmerman and Champion, 1963).

3-2.3 The Problems of Averaging

Two distinct kinds of averages have so far been used in discussing diffusion: the time average of the instantaneous turbulent velocity field, on which Reynolds' average-wind definition was based, and the statistical, or ensemble, average, which was introduced in connection with Taylor's diffusion theory. In addition, a distinction must be made between two distinct systems of reference before averaging can be performed. These are the spatially fixed, or Eulerian, system and the particle-attached, or Lagrangian, system.

Eulerian coordinates can be fixed with respect to a certain location, e.g., an anemometer. Consequently the Eulerian fixed-point system is the natural system for experimentalists to use. On the other hand, the Eulerian reference frame can be thought of as attached to and moving along with the mean wind. In this system the mean wind components vanish, and only the turbulent components remain. Of these, fluctuations in either space or time or a combination of both can be discussed. Most of the statistical theory of turbulence is developed in the Eulerian space or space–time system.*

3-2.3.1 Taylor's Hypothesis. Because the mean wind speed in wind-tunnel flows is very large compared with the root mean square of the turbulent fluctuations, Taylor (1938) proposed transforming from the experimentally convenient Eulerian fixed-point coordinates to the Eulerian space scheme by introducing the transformation $x = \bar{u}t$, where x is the distance covered in t seconds. This transformation is valid in wind-tunnel work, where $\bar{u} \gg (\overline{v'^2})^{1/2}$. In

*A suitable designation of these various Eulerian frames of reference has caused meteorologists some difficulty. For example, it has been suggested that what we here call the "Eulerian time" system, in accordance with the usage of fluid-turbulence theoreticians, should be called a "pseudo-Lagrangian" system (Pasquill, 1963) or a "pseudo-Eulerian" system (Frenkiel, 1948). Adding to the confusion, what is here termed the "Eulerian fixed-point" system has commonly been designated the "Eulerian time" system in meteorological literature; Pasquill (1963), on the other hand, proposes calling it the "quasi-Eulerian" system.

Without pretending that it solves all possible problems of turbulence nomenclature, I urge that meteorologists use the system suggested in the text above for the following reasons:

1. The terms "Eulerian" and "Lagrangian" should refer only to the basis of the coordinate system. If this is particle attached, the term "Lagrangian" is appropriate; the term "Eulerian" is properly applied to all other cases without the need for qualifying prefixes of questionable relevance.
2. The term "fixed point" unambiguously characterizes the commonest type of Eulerian reference or measurement system, that in which the measuring probe is located at a fixed point in space.
3. The term "Eulerian time" should mean the same thing to specialists in both atmospheric and wind-tunnel turbulence; moreover, it should be intelligible as a special case of the term "Eulerian space–time," which is generally understood to apply to a reference system that is at rest with respect to the mean flow.

the atmosphere, where $\bar{u} \approx (\overline{v'^2})^{1/2}$ and the mean wind may vary, the applicability of this transformation is not so obvious although it has been widely employed. It is probably valid, at least for turbulence fluctuations of comparatively high frequency.

3-2.3.2 Eulerian–Lagrangian Averages. Before wind-fluctuation statistics can be applied to the diffusion problem, a method must be devised to convert these statistics, measured at a point by an anemometer, bivane, or other device, into the corresponding Lagrangian values that apply to the motion of a fluid particle. This problem, which in principle is a purely mathematical one, is notoriously difficult. Hay and Pasquill (1959) suggested as a working approximation that the Langrangian time, ξ, is approximately linearly related to the time, t, of the Eulerian fixed-point reference system, i.e.,

$$\xi = \beta t \tag{3.104}$$

where β is a dimensionless Lagrangian–Eulerian time-scale ratio. This proposal is closely related to the result of an earlier study by Gifford (1955), who showed that

$$\frac{n_E}{n_L} = \frac{\xi}{t} = \frac{1.12\,\bar{u}}{(\overline{v'^2})^{1/2}} + 1 = \beta \tag{3.105}$$

where n_E and n_L are Eulerian fixed-point and Lagrangian frequencies, respectively, referring to the corresponding energy spectra. It appears that by an order-of-magnitude approximation of the turbulence intensity, $(\overline{v'^2})^{1/2}/\bar{u}$, we can expect $2 \leq \beta \leq 12$. In fact Hay and Pasquill (1959), on the basis of a series of eight short-range low-level diffusion observations, computed values of β ranging from 1.1 to 8.5.

Values of β can be computed directly from diffusion observations by introducing the scale transformation Eq. 3.104 into Eq. 3.71,

$$\overline{y^2}(t) = \overline{v'^2}\, t^2 \int_0^\infty F_E(n) \left[\frac{\sin(\pi n t/\beta)}{\pi n t/\beta}\right]^2 dn \tag{3.106}$$

where $F_E(n)$ is the Eulerian energy spectrum corresponding to velocities v'(t) measured at a fixed point. The integrand in Eq. 3.106 is evidently equivalent to the spectrum of a fixed-point Eulerian velocity record that has been averaged over a time interval t/β. If the total Lagrangian turbulence energy, $\overline{v'^2}$, were equal to the corresponding value for the fixed-point Eulerian velocities, Eq. 3.106 would be equivalent to

$$\overline{y^2}(t) = \langle \overline{v'^2}(t) \rangle_{t/\beta}\, t^2 \tag{3.107}$$

by the same argument that led to Eq. 3.75. For incompressible, stationary, and homogeneous turbulence conditions, the equality was proved by Lumley (1957). Observations of diffusion can be compared to $\overline{y^2}(t)$ as calculated from the Eulerian fixed-point wind-fluctuation moving-average variances of Eq. 3.107, $\langle \overline{v'^2} \rangle_{t/\beta}$, for various values of t/β. Since the diffusion time, t, is known from the distance involved in the experiments ($x = \bar{u}t$), this procedure determines β.

In addition to data on diffusion over a length scale of several hundreds of meters, Hay and Pasquill (1959) also examined diffusion data on a scale of a thousand miles (Durst, Crossley, and Davis, 1957) and on the very small scale of wind-tunnel diffusion (Mickelsen, 1955). For both these sets of data, the computed β values lie in the range 1 to 10, and so it appears that β "is evidently at least of the same order for an enormous range in the scale of turbulence" (Hay and Pasquill, 1959). Thus the practical utility of this simple Lagrangian–Eulerian transformation seems on the whole to be quite well established. Further comparisons of atmospheric diffusion and wind-fluctuation data indicate that a lower limit, e.g., $\beta = 1$, should be employed in unstable conditions and a β value approaching an upper limit of 10, in stable conditions. Haugen (1960) has reported a tendency for computed β values to increase with distance from the source in stable conditions. Wippermann, Gburcik, and Klug (1962) found β values less than unity for diffusion on a hemispheric scale. Fortunately, as Pasquill (1962) pointed out, moderate departures from the average value of $\beta = 4$ have little practical effect on diffusion estimates.

3-2.3.3 Finite Sample–Infinite Sample Averages. It would seem, ideally, that samples obtained over very long times or throughout very large volumes might be substituted for the ensemble averages demanded by statistical turbulence theory provided the turbulence fluid flow possesses stationary, homogeneous statis-

tical properties. Practically, however, such ideally long samples are not ordinarily obtained in the atmosphere, either because of the difficulty of making and analyzing extensive observations or because some change in the external flow situation violates the stationarity condition. Frenkiel (1952a) discussed the latter problem and provided an interesting example of the marked changes that can actually occur. The lower layers of the atmosphere rarely maintain a state of turbulence that approximates a statistically stationary condition for more than, perhaps, a few hours. Even if gross changes in the large-scale wind field (passage of a front, onset of a sea breeze, etc.) do not occur, the duration of a quasi-stationary condition is limited to a few hours by the marked diurnal variation of low-level turbulence. For this reason it is essential to be able to form some idea about the effect of finite sampling periods on turbulence statistics.

The effect of finite sampling on turbulence statistics has been studied by Ogura (1957), Kahn (1957), Pasquill (1962), and Smith (1962) in terms of correlations or spectra. The principal result of these studies, given by both Ogura and Pasquill, is the following expression for the ensemble average diffusion over a diffusion time t computed with respect to a sampling period T:

$$\overline{y_T^2}(t) = \overline{v'^2}\, t^2 \int_0^\infty F(n) \left\{ \left[1 - \frac{\sin^2 \pi nT}{(\pi\, nT)^2} \right] \times \frac{\sin^2 \pi nt}{(\pi nt)^2} \right\} dn \qquad (3.108)$$

As T becomes large, this equation reduces to Eq. 3.71. Pasquill has pointed out that the term multiplying F(n), amounts to a filtering of the spectrum, which effectively suppresses the contributions to diffusion from spectral frequencies much higher than 1/t and lower than 1/T (see Pasquill, 1962, Sec. 1-4 for a complete discussion). The interpretation of finite diffusion in terms of spectrum filtering (Eq. 3.108) suggested to Jones and Pasquill (1959) the so-called "sigma meter," a very useful and practical device for estimating diffusion from wind-fluctuation records (Chap. 6, Sec. 6-4.2.2).

Some sort of assumption about the functional form of the turbulence statistics, i.e., autocorrelation, spectrum, or running-mean variance, must be made before more specific theoretical results can be obtained. (The reader is referred to Ogura's study for an idea of what can be accomplished along this line.) In such practical applications as the analysis of diffusion experiments, the opportunity to perform an averaging that corresponds even remotely to the ensemble average usually does not exist. Nevertheless the above discussion gives at least a qualitative idea of the effect on the mean-square diffusion, $\overline{y^2}$, of the relation between diffusion time and time of sampling so far as departures from ideal diffusion statistics are concerned.

The experimentalist, of course, wants to know how to interpret this discussion in practical terms. There seems to be no better guide than ordinary statistical sampling practice combined with common sense. For example, suppose we have a record of the transverse wind-velocity fluctuation, v′, over a period of time equal to T from which we wish to estimate the Eulerian fixed-point autocorrelation, $R_E(t)$. We would probably restrict t to values of about $1/20$ or $1/10$ of T at most in order to have reasonably well-behaved statistics; even so our confidence in the computations of R_E for t in the neighborhood of T/10 would be very low indeed. Naturally we would also require that no gross changes in the character of the turbulence had occurred during this period T that would violate the stationary condition. This means that the record should not reflect the passage of frontal systems, changes from land to sea breeze or valley to mountain wind regimes, changes from mechanical to convective turbulence or from stable to unstable conditions, or any other marked disturbance of the external forces driving the turbulence.

Similarly, we might wish to interpret measurements of the path of a single floating balloon in terms of Lagrangian turbulence statistics, as has recently been proposed by Angell (1963) and by Pack (1962). For this purpose we would probably employ segments no longer than $1/20$ to $1/10$ of the total length of an observed balloon trajectory so that the estimated autocorrelation, $R(\xi)$, or diffusion, $\overline{y^2}$, for example, would have reasonable statistical stability. We would likewise make certain that none of the occurrences that affect the external forces driving the turbulence had taken place during

the run. Furthermore, to combine various segments of a single trajectory statistically, we would have to ascertain whether or not the segments were located over similar underlying terrain. All these factors impose very serious and very real limitations on our ability to perform reproducible turbulence or diffusion experiments in the lower atmosphere, particularly at large scales, and it is essential to keep them in mind when planning, making, or interpreting such experiments.

3-3 ATMOSPHERIC DIFFUSION MODELS AND APPLICATIONS

3-3.1 The Gaussian Plume Diffusion Model

The object of all the preceding discussion has been to arrive at useful mathematical formulas describing atmospheric diffusion. The main theories of atmospheric diffusion have now been mentioned, and we have seen that the well-known normal, or Gaussian, distribution function provides a fundamental solution to the Fickian diffusion equation. The Gaussian distribution has been assumed as a continuous-source diffusion model by Sutton (1932), Frenkiel (1953), and many other workers. Combination of the Gaussian assumption with one of the following expressions for the mean-square particle diffusion,

$$\overline{y^2} = 2Kt \tag{3.109}$$

$$\overline{y^2} = \overline{(v')^2}\, t^2 \tag{3.110}$$

$$\overline{y^2} = \frac{1}{2} C_y^2 (\bar{u}\, t)^{2-n} \tag{3.111}$$

(and similar expressions for $\overline{x^2}$ and $\overline{z^2}$) forms the basis for most of the practical plume-diffusion formulas that are found in the literature on applications.

Strictly speaking, the Gaussian diffusion model applies only in the limit of large diffusion time and for homogeneous, stationary conditions, for which, we have observed, the diffusion problem may be stated in the form of the simple Fickian differential equation. Batchelor (1949) conjectured, however, that the Gaussian function may provide a general description of average plume diffusion because of the essentially random nature of this phenomenon by analogy with the central limit theorem of statistics. Lin and Reid (1963) pointed out that for very small diffusion times the distribution of particles should take the same form as the wind-fluctuation distribution since the particle trajectories coincide with the instantaneous wind; in the atmosphere this approximates a Gaussian distribution fairly closely. Moreover recent experimental diffusion studies by Hay and Pasquill (1957), Cramer, Record, and Vaughan (1958), and Barad and Haugen (1959) indicate that the Gaussian plume formula should have a wide area of practical applicability in the atmosphere.

The usual way of deriving average-plume-diffusion formulas starts with the assumption of an instantaneous point source of material diffusing in three dimensions. The source strength is Q in grams or curies; the concentration is $\chi = \chi(x,y,z,t)$; x, y, and z are the usual coordinate axes, the point (0,0,0) being a fixed origin; and t is the time of travel of the cloud. If σ_y^2 is the variance of the distribution and if it is assumed that $x = \bar{u}t$, which makes the σ's functions of x, then the Gaussian formula for an instantaneous point source of material is

$$\chi(x,y,z,t) = Q(2\pi\sigma_y^2)^{-\frac{1}{2}} \exp\,(-r^2/2\sigma_y^2) \tag{3.112}$$

where $r^2 = [(x - \bar{u}t)^2 + y^2 + z^2]$, and it is assumed, for the moment, that $\sigma_y = \sigma_x = \sigma_z$, i.e., that the diffusion is isotropic. If this may not be assumed, as is clearly the case under stable meteorological conditions or in the presence of boundary effects, it is usually assumed that the diffusion takes place independently in the three coordinate directions. Then

$$\chi(x,y,z) = \frac{Q(2\pi)^{-\frac{3}{2}}}{(\sigma_x\sigma_y\sigma_z)} \exp\left\{-\left[\frac{(x-\bar{u}t)^2}{2\sigma_x^2} + \frac{y^2}{2\sigma_y^2} + \frac{z^2}{2\sigma_z^2}\right]\right\} \tag{3.113}$$

Equations 3.112 and 3.113 have been written in terms of the standard deviation symbols σ_x, σ_y, and σ_z to stress the following point. According to its derivation Taylor's diffusion function, $\overline{y^2}$, specifically applies to the one-dimensional problem. When it is used to describe the average diffusion of a real three-

dimensional cloud, it correctly describes the diffusion of the marginal projection on the y-axis of this cloud. Likewise, $\overline{x^2}$ and $\overline{z^2}$ must be regarded as applying to marginal distributions on their respective axes. Consequently Eqs. 3.112 and 3.113 contain the implicit assumption that the distribution of the diffusing cloud is, in the terminology of mathematical statistics, jointly as well as separately normal. This is equivalent to the assumption that cross-product terms such as $\overline{yz}$ do not contribute to diffusion. As indicated in Sec. 3-2, Batchelor extended Taylor's theory formally to provide a general theoretical expression for the diffusion tensor, including such terms as $\overline{yz}$; but such terms will naturally depend on Lagrangian correlations more complicated than $R(\xi)$. If we assume joint normality, we may write the diffusion equations with $\sigma_y^2 = \overline{y^2}$, and so on.

A further restriction to the applicability of Eqs. 3.112 and 3.113 in connection with Eqs. 3.109, 3.110, and 3.111 follows from the discussion of the phenomenon of relative diffusion in Sec. 3-2. In principle these formulas may not be conceived as describing the spreading of a single puff of material or of an ensemble of puffs relative to their centers of mass. Application of these equations to such puff, or cluster, spreading is valid only when the average diffusion is calculated over an ensemble of puff experiments relative to a fixed axis. By Eq. 3.64 the maximum rate of average diffusion from a fixed axis is proportional to t^2, but by Eq. 3.102 the average diffusion about the center of mass of a puff can be as great as t^3 when it occurs in the inertial range. Consequently, in principle, quantitative errors can result if the two phenomena are confounded. In fact data summarized in Fig. 4.38 show that puffs do have a somewhat greater growth rate, particularly at shorter distances (i.e., at smaller times), than do plumes (Fig. 4.21).

The method of obtaining a continuous-point-source diffusion formula from Eq. 3.112 or 3.113 proceeds according to the principle of superposition. The plume is regarded as resulting from the addition of an infinite number of overlapping averaged puffs, carried along the x-axis by the mean wind, $\bar{u}$, as in (a) of Fig. 3.9. Each puff is in reality composed of the average over an ensemble of puffs which have diffused for a time t and consequently have reached the position (x,0,0). Mathematically this corresponds to integration of Eq. 3.113 with respect to t from 0 to ∞. This integration is not convenient because the values of σ, in general, depend on t and hence on x because $x = \bar{u}t$. As a practical matter, diffusion along the x-axis is always neglected by comparison with the gross transport along the x-axis by the mean wind, producing what Frenkiel (1953) has termed the spreading-disk diffusion model for a continuous point source, (b) of Fig. 3.9. With this simplifi-

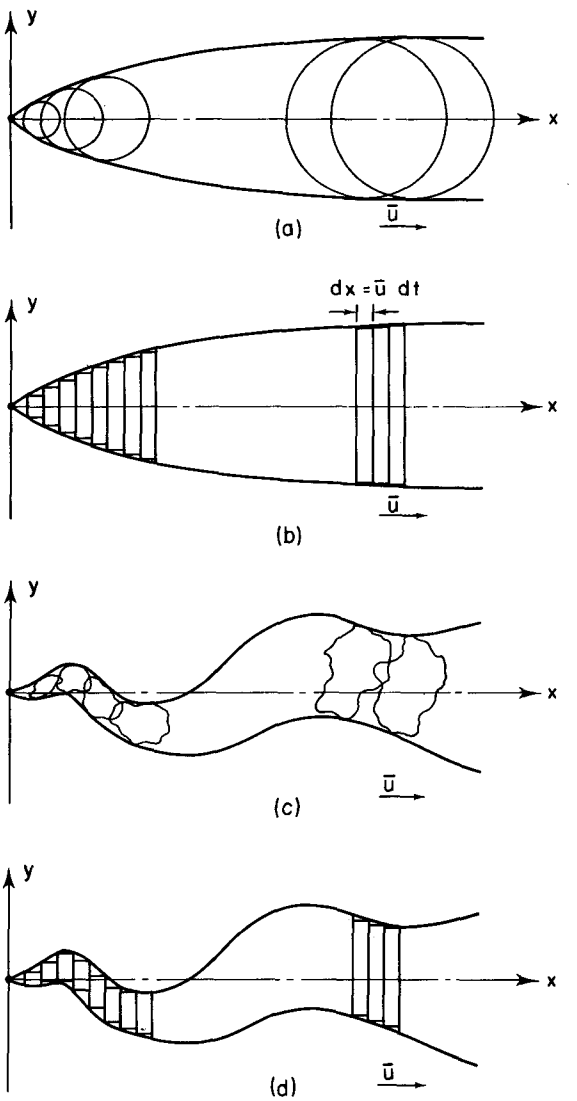

Fig. 3.9—(a) Schematic formation of plume from superposition of individual averaged elements. (b) Schematic spreading-disk plume model obtained by neglecting x-diffusion. (c) Appearance of naturally occurring plumes, with "real" puff elements indicated. (d) Fluctuating plume model.

cation integration of the equation can readily be carried out:

$$\frac{\bar{\chi}(x,y,z)}{Q'} = (2\pi\sigma_y\sigma_z\bar{u})^{-1} \times \exp\left[-\left(\frac{y^2}{2\sigma_y^2} + \frac{z^2}{2\sigma_z^2}\right)\right] \quad (3.114)$$

where $\sigma_y \equiv (\overline{y^2})^{1/2}$ and $\sigma_z = (\overline{z^2})^{1/2}$. The continuous-source strength, Q', is in grams or curies per second, and the quantities σ_y and σ_z can now be regarded as functions of x.

Since most isolated continuous sources are located at or near the earth's surface, it is necessary to account for the presence of this physical barrier to the flux. This has usually been done by the technique, borrowed from heat-conduction theory, of assuming an image source located symmetrically, with respect to the ground plane, to the actual source. The result is

$$\frac{\bar{\chi}}{Q'} = (2\pi\sigma_y\sigma_z\bar{u})^{-1} \exp\left(-\frac{y^2}{2\sigma_y^2}\right) \times \left\{\exp\left[-\frac{(z-h)^2}{2\sigma_z^2}\right] + \exp\left[-\frac{(z+h)^2}{2\sigma_z^2}\right]\right\} \quad (3.115)$$

where h is the elevation of the source above the ground plane. If the receptor is located at the ground level (z = 0), then

$$\frac{\bar{\chi}}{Q'} = \frac{1}{\pi\sigma_y\sigma_z\bar{u}} \exp\left[-\left(\frac{y^2}{2\sigma_y^2} + \frac{h^2}{2\sigma_z^2}\right)\right] \quad (3.116)$$

which is the form of the Gaussian plume model most usually used.

By combining Eqs. 3.109 through 3.111 with Eq. 3.114, we can obtain the continuous-point-source diffusion formulas of Roberts, Frenkiel, and Sutton. The same generalized Gaussian plume equation, moreover, serves as a useful interpolation formula for the interpretation of field diffusion trials, as in Cramer's studies (1957, 1959). Cramer combined Eq. 3.116 with the assumed power laws

$$\sigma_y \propto x^p \quad (3.117)$$

and

$$\sigma_z \propto x^q \quad (3.118)$$

and obtained best fits to the Prairie Grass and Round Hill diffusion data (Chap. 4, Sec. 4-4.2.1).

Barad and Fuquay (1962) compared several detailed plume-concentration measurements made under very stable atmospheric conditions with the bivariate normal distribution function. In their study the usual implicit assumption, discussed previously, that the distribution of diffusion in the y- and z-directions is jointly as well as separately normal, was not made. Their results indicate that the plume distribution was not jointly normal in this extreme case but that the vertical and horizontal distributions are separately normal.

3-3.2 A Fluctuating Plume Model

The spreading-disk plume model of Eq. 3.116 describes diffusion averaged over some period of time. Practical experience indicates that this period of time is at least several minutes (see Fig. 3.8). The appearance of real plumes is quite different from that predicted by this assumed model, especially during unstable conditions when the entire plume, at any instant, meanders or fluctuates about some mean position, as in (c) of Fig. 3.9. Accordingly, a fluctuating plume model has been proposed (Gifford, 1958, 1959a) which differs from Eq. 3.114 in that the centers of the disk elements are conceived of as distributed at random around their mean position, (d) of Fig. 3.9. The basic Gaussian equation for the instantaneous concentrations is

$$\frac{\chi}{Q'} = (2\pi\overline{Y^2}\bar{u})^{-1} \times \exp\left[-\frac{(y-D_y)^2 + (z-D_z)^2}{2\overline{Y^2}}\right] \quad (3.119)$$

In this equation D_y and D_z are distances to the center of the instantaneous plume from the axis; D_y and D_z are assumed also to possess Gaussian distributions with variances $\overline{D^2}$. As defined in Sec. 3-2, $\overline{Y^2}$ is a relative diffusion parameter.

The mean value of χ/Q', assuming $\overline{D_y^2} = \overline{D_z^2} = \overline{D^2}$, is found to be

$$M\left(\frac{\chi}{Q'}\right) = [2\pi\bar{u}(\overline{Y^2} + \overline{D^2})]^{-1} \times \exp\left[-\frac{r^2}{2(\overline{Y^2} + \overline{D^2})}\right] \quad (3.120)$$

where $r = (y^2 + z^2)^{1/2}$. A similar result was obtained by Hilst (1957). Extension to the case where $\overline{D_y^2} \neq \overline{D_z^2}$ is straightforward. The mean value of χ/Q' has exactly the same form as Eq. 3.114, but the diffusion has been separated into a mean and a fluctuating part. In addition to the mean values, more complex statistics, in particular the variance and the distribution of χ/Q', can be calculated (Gifford, 1959a). Further results based on this model have been presented in papers by Moore (1963) and Scriven (1965).

3-3.3 Remark on Non-Gaussian Diffusion Models

The virtues of the Gaussian distribution function are considerable, and the temptation to employ it exclusively is correspondingly great. Statistically it is completely determined by its second moment, i.e., by σ^2. It has many highly useful purely mathematical properties; for instance, it possesses a self-reciprocal Fourier transform. Moreover, as noted earlier, it agrees reasonably well with much, although not all, of presently available atmospheric diffusion data. Non-Gaussian diffusion distributions arise from the various K theories and also from the statistical diffusion theories of Goldstein, Monin, and Davies mentioned briefly in Sec. 3-2. It is natural to ask whether these may not be better than the Gaussian model discussed at some length in the previous section. For example, we might ask whether non-Gaussian diffusion models agree better with diffusion observations. Elliott (1960) compared the Prairie Grass data with Calder's non-Gaussian K theory diffusion model and with Sutton's Gaussian model. His conclusion is that, although Sutton's model gives a slightly better fit to the Prairie Grass data, the differences are quite small from any practical point of view. Pasquill (1962) also showed that the resulting plume center-line concentration formulas of Calder's model and Monin's (1959) limited-diffusion velocity model, differ but little.

On the other hand, the basic theoretical point emphasized by Monin (1959) and others, namely, that the speed of a real diffusion event like the spreading out of a smoke plume must necessarily be less than some finite value, such as the speed of sound, is certainly correct in principle. It should be clearly understood, however, that anomalies in diffusion data, such as those arising from the presence of marked wind shear (Barad and Fuquay, 1962) or the irregular departures from smooth concentration contours noted by Elliott (1959), are not to be explained as an effect of finite speed of diffusion. Because Gaussian plume models have proved to be, by and large, reasonably successful in explaining observed concentration patterns, it seems reasonable to continue to employ them in practice.

3-3.4 Estimation of Diffusion Coefficients

For practical use to be made of diffusion formulas numerical values for the diffusion coefficients σ_y and σ_z must be determined. Various theoretical expressions were derived for this purpose, particularly Eqs. 3.64, 3.68, 3.75, 3.79, and 3.81. Equation 3.64, corresponding to the limiting case of Taylor's formula for small diffusion times, has been used by Frenkiel (1952, 1952a, and 1953). It undoubtedly gives reliable predictions for diffusion times up to at least a few minutes. At the opposite limit Eq. 3.68, corresponding to the case of large diffusion times, has been used to solve the problem of diffusion on scales ranging from continental to global (Machta, 1958). Values of K appropriate to various scales were given in Table 3.2. Equations 3.79 and 3.81, Sutton's model, have frequently been applied in reactor-hazard analyses and air-pollution studies, and there has been considerable experience with Sutton's diffusion coefficients. The theoretical limitations of this model have been discussed in Sec. 3-2, and examples of observed parameter values are noted in Chap. 4.

Equation 3.75, the moving average variance method, seems a promising development in that (1) it specifies diffusion coefficients by a detailed analysis of atmospheric turbulence measurements, (2) it does not involve adjustable empirical constants, (3) it is comparatively free from debatable physical assumptions, and (4) it is not, in principle, limited to a particular range of diffusion times. It is, however, limited as are all applications of Taylor's theorem, Eq. 3.62, to stationary, homogeneous turbulence conditions. The condition of homogeneity in particular limits its effectiveness in estimating

vertical diffusion from sources near the ground. It also appears practically desirable to be able to estimate diffusion coefficients from meteorological data more universally available than detailed wind-fluctuation measurements or even just these 10% values. The 10% value is only an estimate. It may or may not apply to smoke plumes in general; the point has never been studied exhaustively. Moreover, since many of the clouds and plumes that interest us are in-

Table 3.3—RELATION OF TURBULENCE TYPES TO WEATHER CONDITIONS

A—Extremely unstable conditions
B—Moderately unstable conditions
C—Slightly unstable conditions
D—Neutral conditions*
E—Slightly stable conditions
F—Moderately stable conditions

Surface wind speed, m/sec	Daytime insolation			Nighttime conditions	
	Strong	Moderate	Slight	Thin overcast or ≥ 4/8 cloudiness†	≤3/8 cloudiness
<2	A	A–B	B		
2	A–B	B	C	E	F
4	B	B–C	C	D	E
6	C	C–D	D	D	D
>6	C	D	D	D	D

*Applicable to heavy overcast, day or night.
†The degree of cloudiness is defined as that fraction of the sky above the local apparent horizon which is covered by clouds.

to make diffusion estimates based on only a general knowledge of a location. The various series of field-diffusion experiments described in Chap. 4 provide considerable guidance for such estimates.

3-3.4.1 Pasquill's Diffusion Curves. On the basis of available data, including the Prarie Grass experiments, and guided by theoretical expectations, Pasquill suggested in an unpublished note in 1958 a practical scheme for the estimation of diffusion which is particularly suitable for practical applications. The substance of this note is contained in the papers by Meade (1959, 1960) and by Pasquill (1961, 1962). The general idea can, as well, be expressed in terms of σ_y and σ_z; moreover it can be related to results derived earlier in this chapter.

The visible edge of a diffusing cloud has often been assumed to coincide roughly with the lateral point at which the concentration falls to 10% of its axial value and could, in any event, be defined as this point, as was done by Pasquill (1961) and Holland (1953), for example. For smoke screens the visible smoke-plume edge is approximated by this figure (Gifford, 1959). Pasquill and Meade define a smoke-plume elevation, H, and an angular spread, θ, which are visible, there appears to be no special virtue to this definition. If, instead, we define plume concentration distributions in terms of their standard deviations, we find, in Pasquill's notation, that,

$$H = 2.14\ \sigma_z \tag{3.121}$$

and, for fairly small values of θ,

$$\theta = \frac{4.28\ \sigma_y}{x} \tag{3.122}$$

The numerical coefficient 2.14 is just the 10% ordinate of the normal error curve.

Figures 3.10 and 3.11 exhibit families of curves of σ_y and σ_z for various stability categories, based on the values of H and θ given originally by Pasquill. The manner of relating these curves to prevailing conditions of average wind speed and to the estimated radiation balance is set out in Table 3.3, which was also presented in the papers by Pasquill and Meade. An evaluation of Eq. 3.116 for various values of stack height, employing the σ_y and σ_z values of Figs. 3.10 and 3.11, has been carried out by Hilsmeier and Gifford (1962) (these results are reproduced in Sec. A.3 of the Appendix). The studies by Beattie (1961), Couchman (1961),

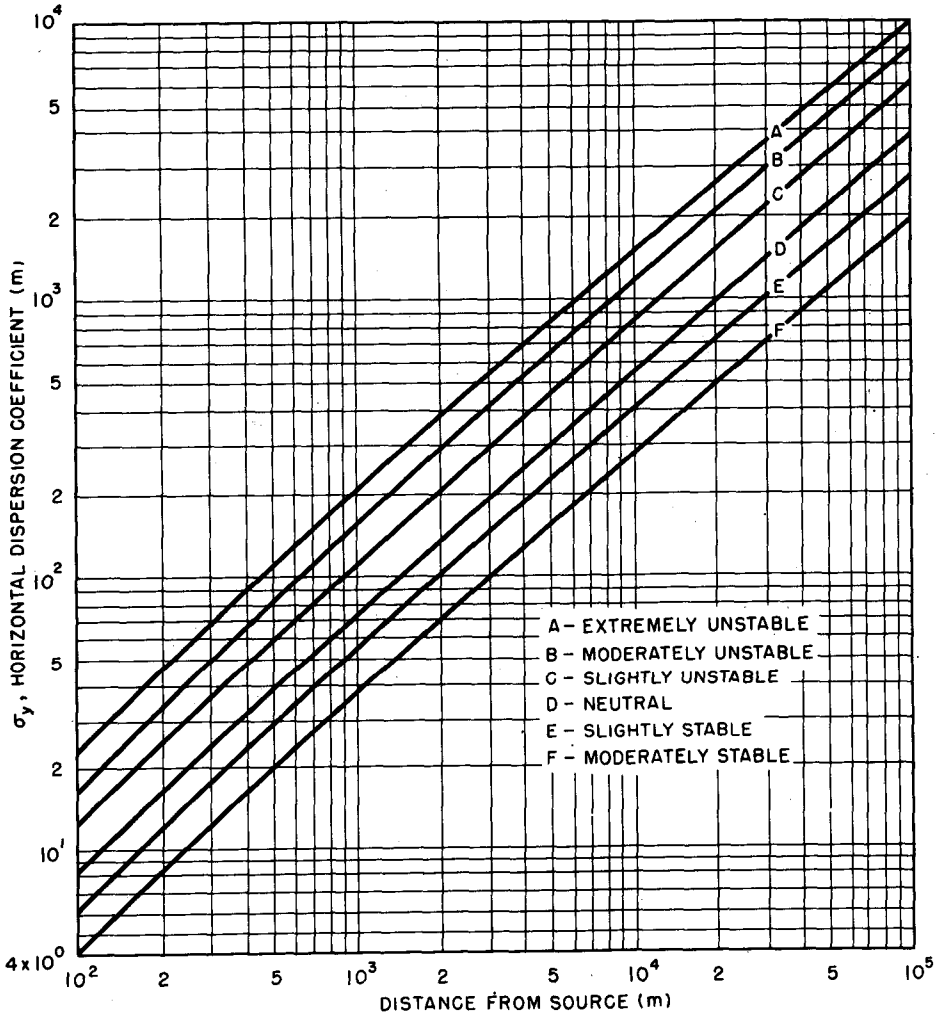

Fig. 3.10 — Lateral diffusion, σ_y, vs. downwind distance from source for Pasquill's turbulence types.

and Bryant (1964) have also employed these values of σ in plume diffusion analyses.

Sections 4-4.3 and 4-4.4 of Chap. 4 indicate that Pasquill's curves fit the experimental data collected since the Prairie Grass experiments quite well. Furthermore the experimental data discussed in these sections demonstrate that the standard deviation of the horizontal wind direction, σ_θ, for a short averaging time and for the sampling times used in these experiments (10 min to 60 min) can be related empirically to the measured values of plume width or to normalized average concentration or exposure from continuous sources. On the basis of these data, Pasquill's stability categories can be relabeled approximately in terms of measured values of σ_θ as follows:

Pasquill stability categories	σ_θ
A, extremely unstable	25.0°
B, moderately unstable	20.0°
C, slightly unstable	15.0°
D, neutral	10.0°
E, slightly stable	5.0°
F, moderately stable	2.5°

Pasquill's method of estimating diffusion is well suited to field use because a simple recording wind vane and anemometer erected at a proposed site can, when used with the wind-direction range theory (Chap. 2, Sec. 2-6.2.3),

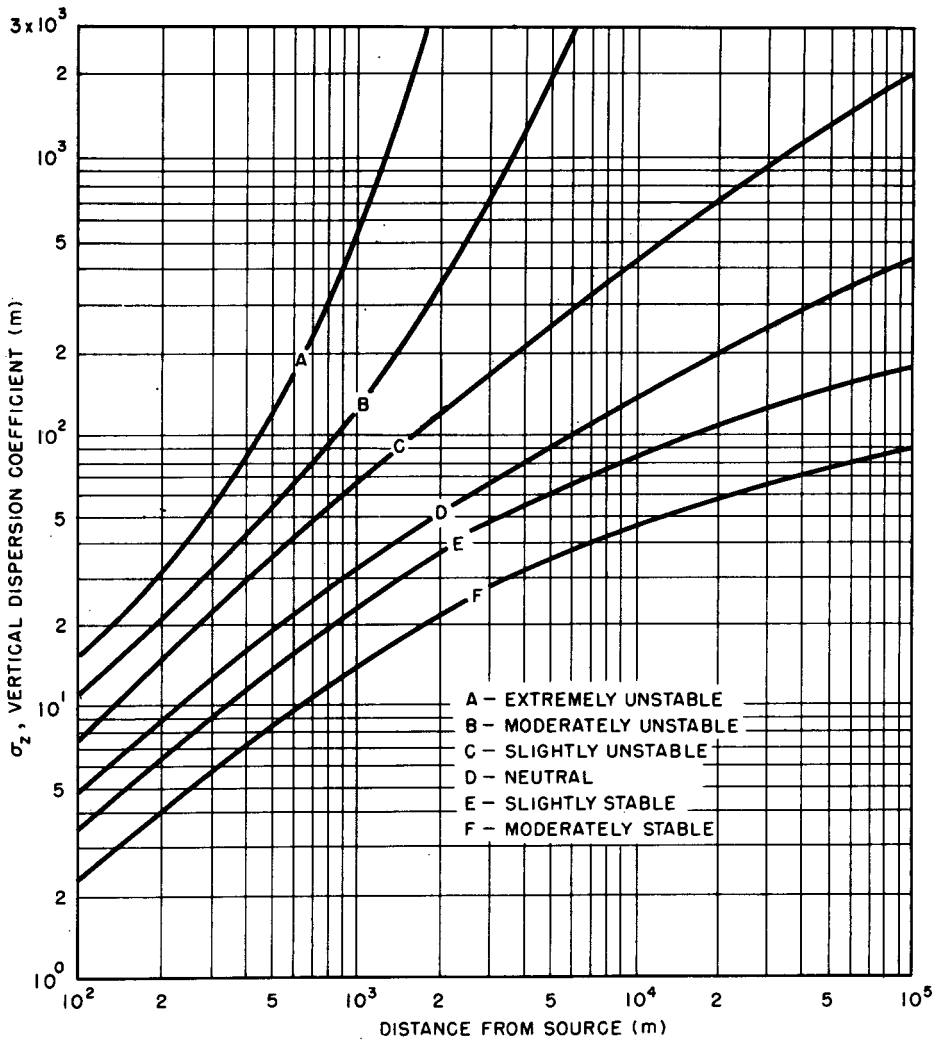

Fig. 3.11 — Vertical diffusion, σ_z, vs. downwind distance from source for Pasquill's turbulence types.

furnish climatologically useful estimates of σ_θ rapidly. Only simple manual data processing is necessary. The wind-measuring system will, moreover, furnish data for other climatological wind statistics for the site, such as wind roses, and will also serve as the necessary wind-velocity monitoring equipment for permanent installation when the reactor or other plant is in operation.

3-3.4.2 Quantitative Use of Smoke Observations to Determine Diffusion Coefficients. Visual and photographic observations of smoke plumes and puffs have always appealed to workers in atmospheric diffusion as a useful research tool. Characteristically Richardson (1920) worked with time-exposure photographs of smoke puffs very early in the history of diffusion study. The use of smoke as a diffusion index continues to be widespread to this day. Quantitative interpretations of smoke observations (Sutton, 1932, Holland, 1953, Kellogg, 1956, Frenkiel and Katz, 1956, Gifford, 1957, 1959, Saissac, 1958, Inoue, 1960, and Högström, 1964) have usually exploited Roberts' (1923) opacity theory in which the visible edge of the smoke plume or puff is supposed to represent a constant threshold density of smoke particles along the line of sight.

The total density of smoke particles is obtained, according to the opacity idea, by integration of the concentration-distribution equa-

tion along a line of sight. For the generalized Gaussian plume distribution, Eq. 3.116, assuming that the plume is being viewed from a fairly great vertical distance, this procedure would give

$$\int_0^\infty \bar{\chi}\, dz = \frac{Q' \exp\left(-y^2/2\sigma_y^2\right)}{2\pi\sigma_y\sigma_z\bar{u}} \times \int_0^\infty \exp\left(\frac{-z^2}{2\sigma_z^2}\right) dz \qquad (3.123)$$

If there is a fixed threshold value of the integrated concentration, χ_e, corresponding to the visible plume edge and located a distance $y_e(x)$ from the plume axis, then it can be shown, using the condition for a maximum value, that

$$(\sigma_y^2)_m = y_m^2 \qquad (3.124)$$

where y_m is the maximum value of $y_e(x)$. Then

$$(\sigma_y^2)_m = y_e^2\left\{\ln\left[\frac{e y_m^2}{\sigma_y^2(x/\bar{u})}\right]\right\}^{-1} \qquad (3.125)$$

where e is the base of natural logarithms. Figure 3.12 illustrates the meaning of the various lengths used.

An equation equivalent to Eq. 3.125 for the case of plume observations made at a great horizontal distance, following a line of sight integration in the y-direction, is

$$(\sigma_z^2)_m = z_e^2\left\{\ln\left[\frac{e z_m^2}{\sigma_z^2(x/\bar{u})}\right]\right\}^{-1} \qquad (3.126)$$

Corresponding equations for smoke puffs based on Eq. 3.125 have also been given (Gifford, 1958). All these transcendental equations can be solved for $\sigma_y(x/\bar{u})$ or $\sigma_z(x/\bar{u})$ if there are visual or photographic observations of smoke plumes from which y_e and z_e, the plume half-width and half-height, can be determined. The computations are facilitated by Fig. 3.13, which is a graphical solution of the equation ln p = ap. No assumption about the analytical form of σ_y or σ_z is necessary.

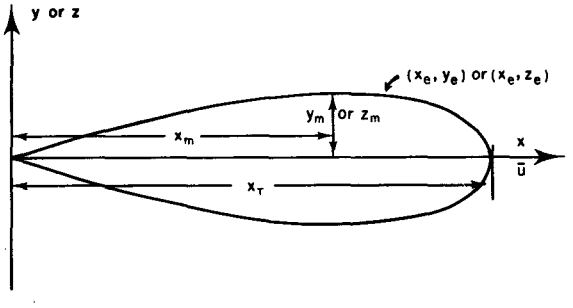

Fig. 3.12—Meaning of various quantities used in smoke-plume analysis.

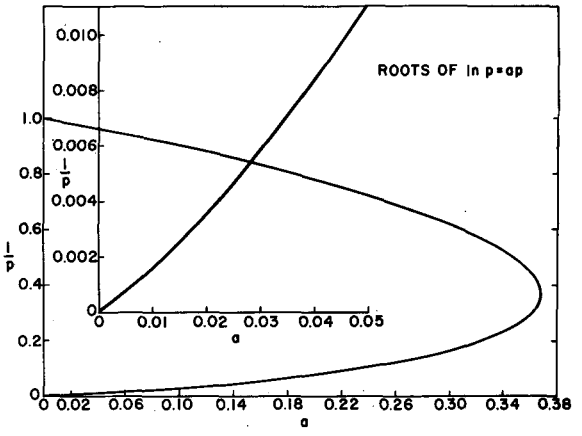

Fig. 3.13—Plot of the equation ln p = ap.

A simpler procedure when, as in the smoke studies by Sutton (1932), Kellogg (1956), Frenkiel and Katz (1956), Holland (1953), Moses and Clark (1956), and others, one is willing to choose in advance a specific form for the diffusion function, was suggested by Gifford (1959). It is to combine, for example, Eq. 3.109, 3.110, or 3.111 directly with Eq. 3.124. Systematic exploitation of this idea leads to a number of particularly simple pairs of formulas for diffusion coefficients:

$$K_y = \bar{u}\left(\frac{e}{2}\right)\left(\frac{y_m}{x_T}\right) y_m$$

$$K_z = \bar{u}\left(\frac{e}{2}\right)\left(\frac{z_m}{x_T}\right) z_m \qquad (3.127)$$

$$\overline{v'^2} = \bar{u}^2 e \left(\frac{y_m}{x_T}\right)^2$$

$$\overline{w'^2} = \bar{u}^2 e \left(\frac{z_m}{x_T}\right)^2 \qquad (3.128)$$

$$C_y^2 = 2x_T^n e \left(\frac{y_m}{x_T}\right)^2$$

$$C_z^2 = 2x_T^n e \left(\frac{z_m}{x_T}\right)^2 \qquad (3.129)$$

$$K_y = \left(\bar{u}\,\frac{y_m}{2}\right)\left(\frac{y_m}{x_m}\right)$$

$$K_z = \left(\bar{u}\,\frac{z_m}{2}\right)\left(\frac{z_m}{x_m}\right) \qquad (3.130)$$

$$\overline{v'^2} = \bar{u}^2\left(\frac{y_m}{x_m}\right)^2$$

$$\overline{w'^2} = \bar{u}^2\left(\frac{z_m}{x_m}\right)^2 \qquad (3.131)$$

$$C_y^2 = 2x_m^n\left(\frac{y_m}{x_m}\right)^2$$

$$C_z^2 = 2x_m^n\left(\frac{z_m}{x_m}\right)^2 \qquad (3.132)$$

In these equations x_T is the total plume length and x_m is the distance downwind from the source at which the maximum plume width or height, y_m or z_m, occurs. The utility of these formulas lies in the fact that many of the significant plume dimensions that need to be determined from visual observations or photographs appear as ratios and so do not need to be measured absolutely but only relatively; and certain of the remaining distances, e.g., x_T and x_m in Eqs. 3.129 and 3.132, appear as nth powers (roughly as fourth roots) and consequently need only to be approximated. A procedure somewhat similar to this but involving the K theory was used by Richardson and Proctor (1925), and further interesting results were derived by Inoue (1960, 1961), using an equivalent method in connection with his similarity theory of diffusion.

Examples of diffusion-coefficient determinations at nuclear-reactor sites by the ratio method, i.e., by one of Eqs. 3.127 through 3.132, have been given by Bowne (1961), Culkowski (1961), Gifford, Culkowski, and Hilsmeier (1963), and Hewson, Gill, and Walke (1963). When this method is applied to plume photographs, some form of time averaging of the smoke-plume observations is desirable. Time-exposure photographs of plumes through neutral density filters were described by Culkowski (1961), who has experimentally determined the necessary film reciprocity factors for quite long exposure times. Bowne (1961), Shorr (1952), Saissac (1958), Richardson (1920), and Inoue (1960) have also reported long-time-exposure smoke-plume photographs. It appears, on the basis of Culkowski's example, that a close approximation to the effect of time averaging can be achieved by estimating the smoothed envelope of the instantaneous photograph and basing the plume measurements on this envelope. In view of its real simplicity and economy and the measure of agreement with direct diffusion measurements reported in various of the above references, the ratio method seems a promising way to obtain plume diffusion coefficients.

3-3.5 Equations for Calculating Concentration and Exposure

The equations presented in the first edition of *Meteorology and Atomic Energy* for dealing with various practical diffusion problems that arise in reactor-hazard analysis and in other air-pollution problems were based on the widely used diffusion model formulated by Sutton. A list of these equations appears in the Appendix Sec. A.4. Many of these equations were first presented by Holland (1953). There is a need for a corresponding list of diffusion equations based on the simple Gaussian formula, Eq. 3.116. In this section a number of such equations will be considered. Most can be converted to the equivalent Sutton form by means of Eqs. 3.79 and 3.81.

3-3.5.1 Characteristic Continuous-source Plume Equations. Equations for the five characteristic continuous-source plume types described in Chap. 2, namely, fanning, fumigation and trapping, looping, coning, and lofting, can be developed as follows.

3-3.5.1.1 Fanning. Fanning is characterized by very slow vertical diffusion during stable conditions. Concentrations can be estimated from Eq. 3.116 with σ values corresponding to stable conditions, for which the horizontal diffusion, σ_y, considerably exceeds the vertical diffusion, σ_z. Figure 3.14 illustrates (a) fanning that commenced a very short distance from the source and (b) fanning that did not begin for some considerable distance from the source.

3-3.5.1.2 Fumigation and Trapping. Hewson and Gill (1944) introduced the term "fumigation" to describe the rapid mixing downward to the ground of material that has accumulated aloft during a period of atmospheric stability,

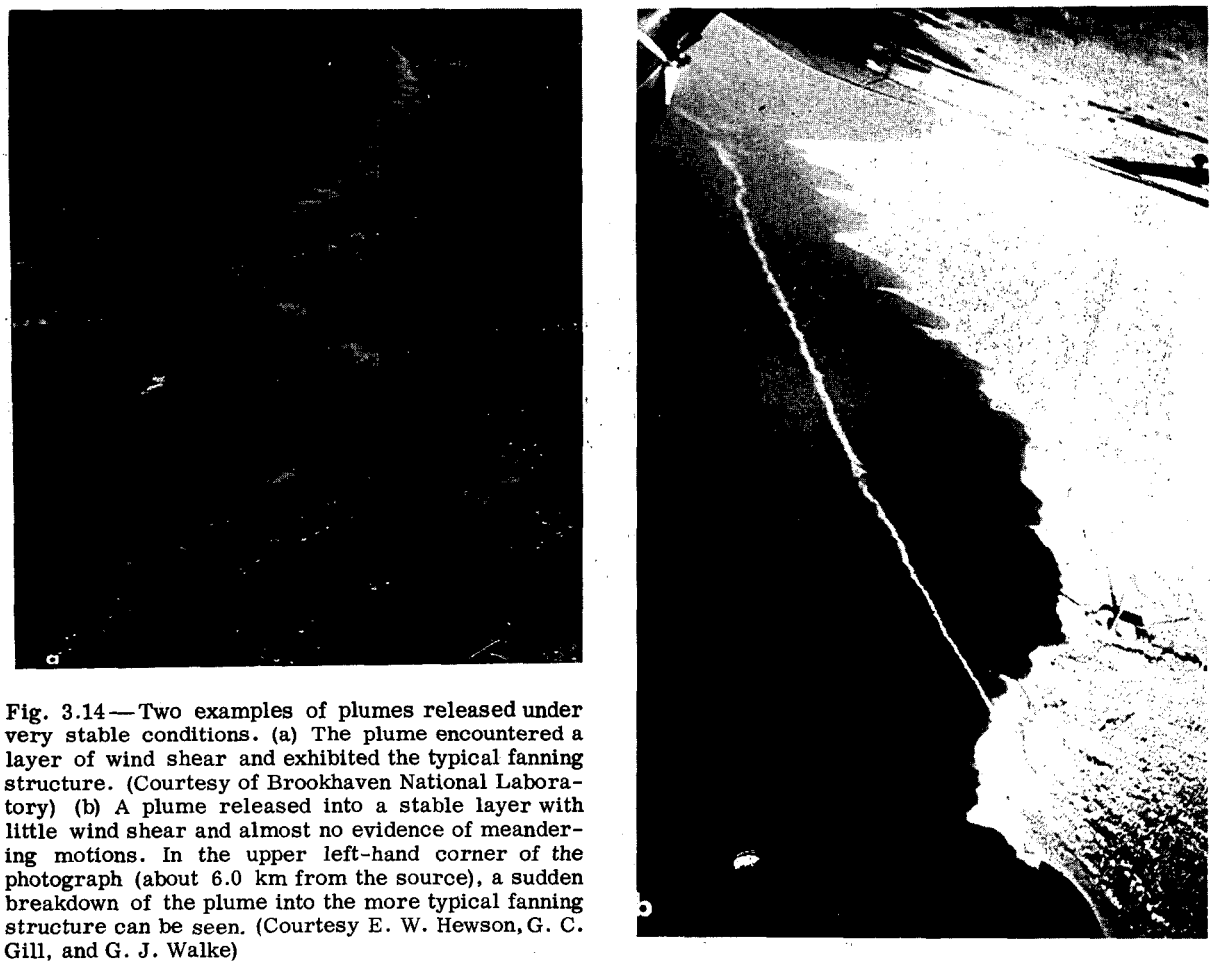

Fig. 3.14—Two examples of plumes released under very stable conditions. (a) The plume encountered a layer of wind shear and exhibited the typical fanning structure. (Courtesy of Brookhaven National Laboratory) (b) A plume released into a stable layer with little wind shear and almost no evidence of meandering motions. In the upper left-hand corner of the photograph (about 6.0 km from the source), a sudden breakdown of the plume into the more typical fanning structure can be seen. (Courtesy E. W. Hewson, G. C. Gill, and G. J. Walke)

an occurrence that is common after dawn when the nocturnal temperature inversion is rapidly dissipated by warming due to solar heating of the ground. Concentrations due to the fumigation effect can be estimated by integrating Eq. 3.115 with respect to z from 0 to ∞ and then considering the material in the cloud to be distributed uniformly through a layer of height h_i. The equation for the fumigation concentration, $\overline{\chi}_F$, is accordingly

$$\overline{\chi}_F = \frac{Q'}{(2\pi)^{1/2}\overline{u}h_i\sigma_y} \exp\left(-\frac{y^2}{2\sigma_y^2}\right) \qquad (3.133)$$

This equation can also be used to describe the trapping condition during which the effluent diffuses rapidly below the base of an elevated inversion but is prevented by the stable layer from diffusing to greater heights. For example, h_i could be taken as the height of the base of a persistent inversion aloft, such as the West Coast (California) subsidence inversion. Or h_i might be the height of the top of the planetary boundary layer or of the base of some other distinct inversion layer, such as a frontal inversion. Scorer (1959) says that a stable layer approximately equal to the elevation of ridge tops often marks the upper boundary of smoke diffusion in valleys; h_i could be identified with this level.

In the fumigating plume shown in Fig. 3.15, fumigation occurred within the stable air of a lake breeze, a situation analagous to that which might occur during a sea breeze. Plume trapping from an open burn and from a stack is shown in Fig. 3.16. Another instance of trapping, in this case of the combined detritus from natural and man-made processes operating over a large area, is shown in Fig. 3.17.

By considering both the ground and the inversion base to be reflecting barriers, Hewson,

Fig. 3.15 — An illustration of a fumigating plume near the shore of Lake Michigan. The plume was embedded in a very stable air flow originating over the lake during late afternoon on a summer day. As the cool stable air moved inland, it was heated from below, and a fumigation pattern was created. (Courtesy E. W. Hewson, G. C. Gill, and G. J. Walke)

Gill, and Bierly (1959) derived the following formula for trapping:

$$\frac{\bar{\chi}}{Q'} = \frac{1}{\pi\,\sigma_y\sigma_z\bar{u}}\left\{\exp\left(-\frac{h^2}{2\sigma_z^2}\right) + \exp\left[-\frac{(2h_i - h)^2}{2\sigma_z^2}\right] + \exp\left[-\frac{(-2h_i - h)^2}{2\sigma_z^2}\right]\right\} \quad (3.134)$$

where h_i is the height of the inversion base and the result is expressed in terms of σ_y and σ_z instead of the corresponding Sutton formula as given by these authors. This equation is a special case of a more general formula developed earlier by Hewson, which contains an infinite series of exponential terms corresponding to the plume reflections.

A similar result was developed by Albracht (Lindackers, Bresser, and Albracht, 1965). Gifford (1961), following proposals by Meade (1959) and Pasquill (1961), suggested that, in the event vertical diffusion is restricted by a strong inversion lid at some height h_i, diffusion could be computed directly from Eq. 3.116 by assuming that the value of σ_z involved is constant at distances beyond the point where $\sigma_z = h_i/2.15 \approx h_i/2$. This suggested treatment of trapping, offered purely on the basis of its simplicity, agrees very closely with Eq. 3.133, differing only by a small constant factor, at all downwind distances greater than a few stack heights. There are, as Lindackers, Bresser, and Albracht (1965) have shown by carrying out the calculations, differences between the results of trapping calculations based on such simple assumptions as these and the results based on the assumption of multiple reflections of the plume. Without experimental evidence it is not possible to make a choice between these alternatives now.

Two problems may be encountered in the application of Eq. 3.133 or Eq. 3.116 to trapping or fumigation calculations. First, there is no direct indication of the minimum distance from the stack beyond which these equations may be applied. Judging by qualitative discussion in the literature (for example, Bierly and Hewson, 1962, and Pooler, 1965), there seems to be some uncertainty about this point although there is no obvious reason why the distance should exceed a few stack heights. The second problem is encountered in the attempt to specify a value for σ_y. During the fumigation process the plume is mixed through the increasingly unstable layer below the inversion. Therefore the effective value of σ_y to be used in estimating fumigation concentrations should probably be somewhat greater than the inversion value to account for this augmented mixing.

3-3.5.1.3 Looping. Looping is the most spectacular of plume conditions in appearance.

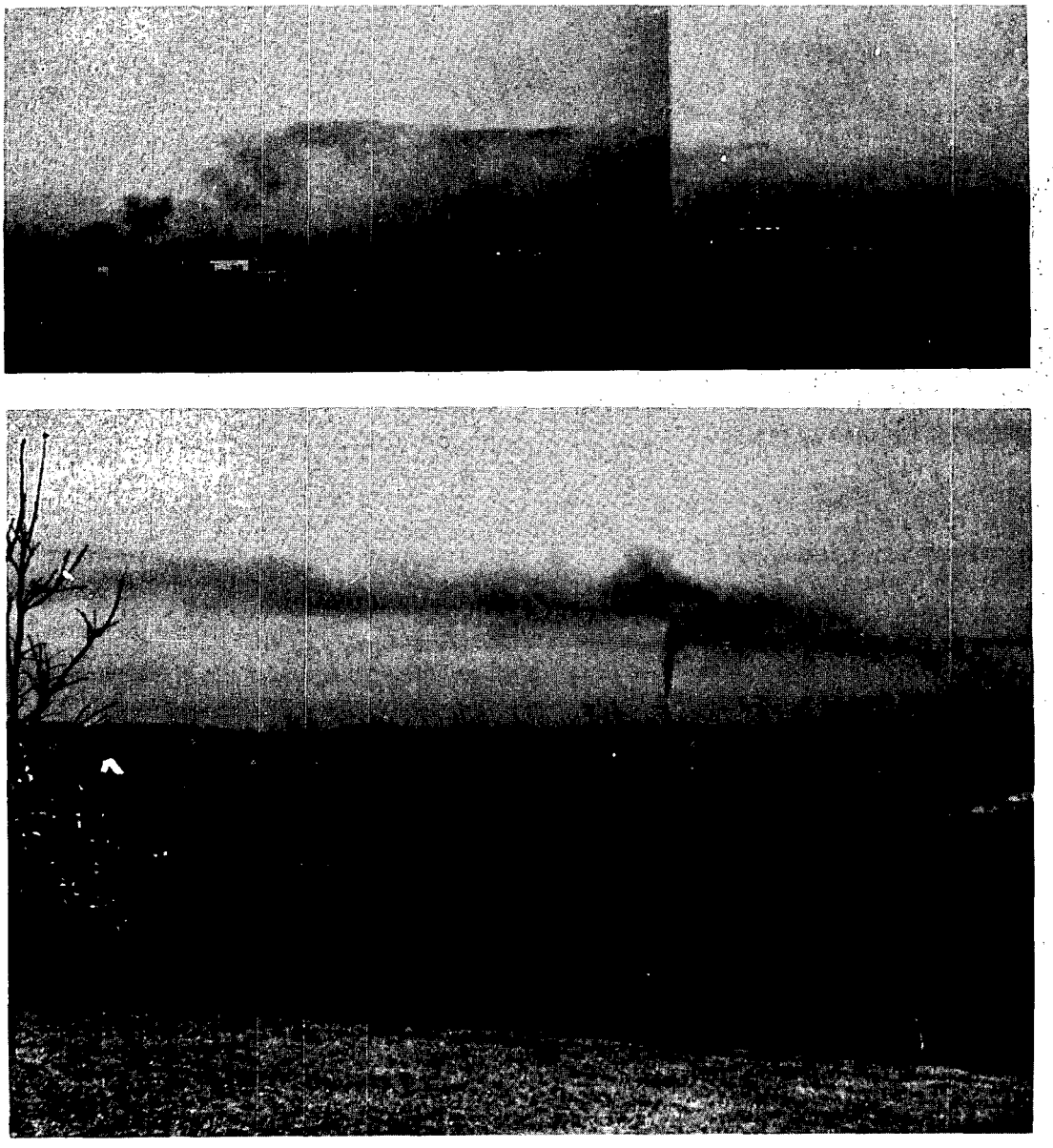

Fig. 3.16—Two illustrations of the trapping of smoke from an isolated source within the planetary boundary layer. (Courtesy D. H. Slade and W. M. Culkowski)

Large loops of the plume are carried down to the ground and cause momentary bursts of high concentration, only to be replaced by effluent-free air as corresponding loops go aloft. The average concentration during plume looping probably corresponds to a Pasquill type A condition and can thus be estimated from Eq. 3.116. Figure 3.18 illustrates looping. Holland (1953) suggested that the maximum ground concentration during looping, $\overline{\chi}_{max.}$, could be estimated from the usual plume equation expressed for the axial concentration, $y = 0$, due to a ground-level source, $h = 0$, where, however, the downwind distance from the source is redefined as $x' = (x^2 + h^2)^{1/2}$, x being the actual distance and h, the source height. Expressed in terms of Eq. 3.116, Holland's equation for the maximum concentration during looping is

$$\overline{\chi}_{max.} = \frac{Q'}{\pi\, \sigma_y(x')\, \sigma_z(x')\, \overline{u}} \qquad (3.135)$$

Fig. 3.17 — Trapping of smoke and haze, which has originated over a broad area, beneath the West Coast (California) subsidence inversion. (Courtesy W. M. Culkowski)

Because of the great variability of instantaneous concentration during looping, it is helpful to be able to estimate the peak to average concentration ratio. This can be done by means of the fluctuating plume model described in Sec. 3-3.2. In the fluctuating plume model, the mean-square diffusion, $\overline{y^2}$, is separated into two portions: a part due to the instantaneous spreading out of the plume, $\overline{Y^2}(t)$, and a part attributable to the meandering or looping, $\overline{D^2}(t)$, i.e.,

$$\overline{y^2}(t) = \overline{Y^2}(t) + \overline{D^2}(t) \qquad (3.136)$$

It can be shown (Pasquill, 1962, and Gifford, 1960) that for large travel times $\overline{D^2}$ approaches some constant value but, according to Batchelor (1952), $\overline{Y^2}$ will increase indefinitely with time. This follows from Eq. 3.97. From the ratio of Eq. 3.119 to Eq. 3.120, it is possible to compute the peak to average concentration ratio. The peak concentration occurs when $y = D_y$ and $z = D_z$, i.e., when the receptor is at the center line of the instantaneous plume. The result is

$$\frac{\text{Peak}}{\text{Average}} = \frac{P}{A} = \frac{(\overline{Y^2} + \overline{D^2})}{\overline{Y^2}} \exp\left[\frac{y^2}{2(\overline{Y^2} + \overline{D^2})} + \frac{z^2}{2(\overline{Y^2} + \overline{D^2})}\right] \qquad (3.137)$$

If $y = z = 0$, i.e., on the mean plume axis (or, equivalently, at the ground at a moderate distance downwind from the source),

$$\frac{P}{A} = \frac{\overline{Y^2} + \overline{D^2}}{\overline{Y^2}} = 1 + \frac{\overline{D^2}}{\overline{Y^2}} > 1 \qquad (3.138)$$

Since $\overline{D^2} \rightarrow$ constant, $P/A \rightarrow 1$ for large travel times.

The effect of stack height on P/A depends on the term $\exp[z^2/2(\overline{Y^2} + \overline{D^2})]$, which involves the total vertical plume diffusion $(\overline{Y^2} + \overline{D^2}) = z^2$. This exponential can be estimated, for example, from Eq. 3.81 or by reference to observations. For stack heights of interest, reasonable values of vertical diffusion indicate that P/A values at the ground fairly near the stack base may be one or two orders of magnitude greater

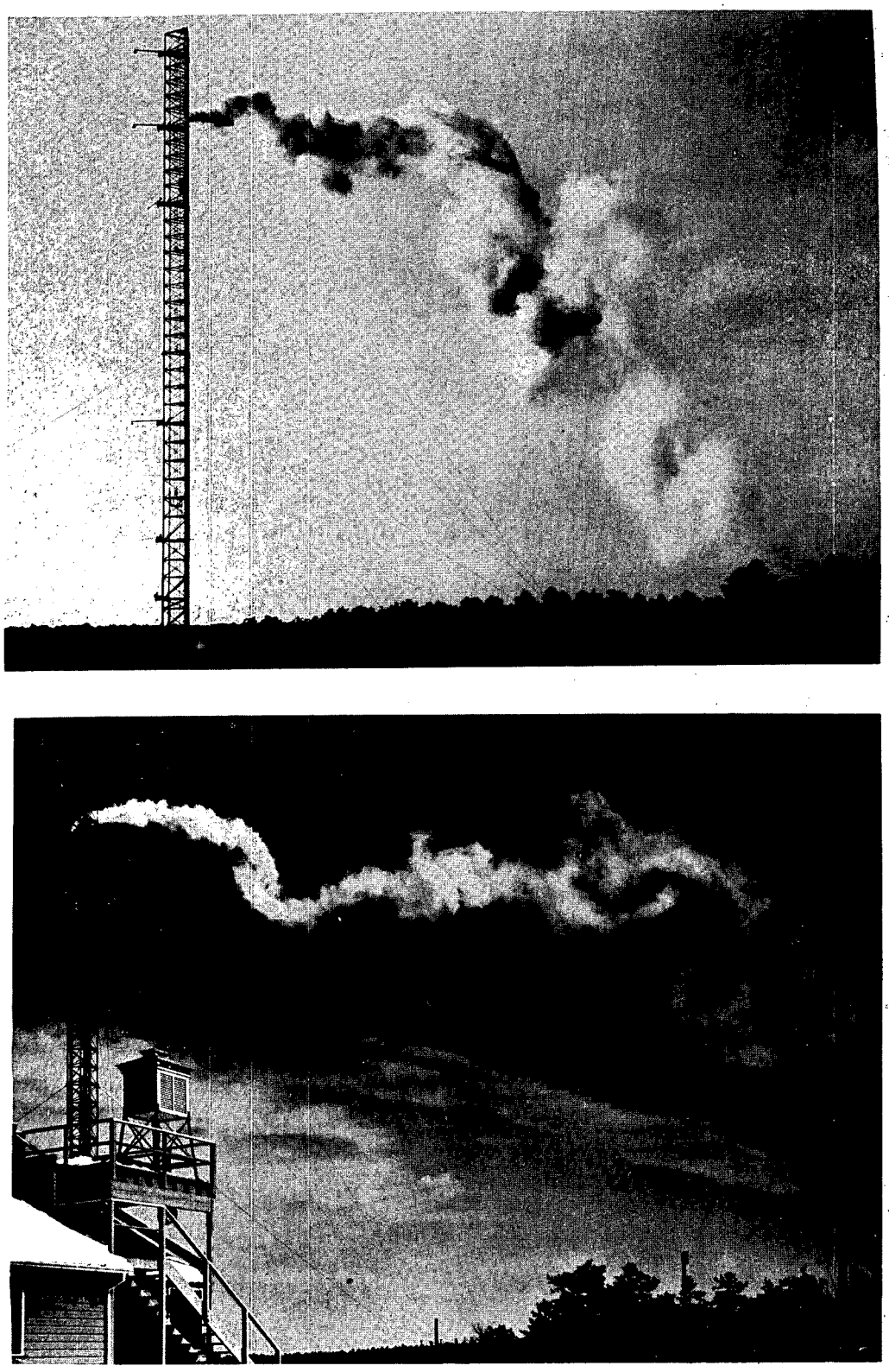

Fig. 3.18 — Two illustrations of looping plumes observed at the Brookhaven National Laboratory.

than those on the mean plume axis. Various observations of P/A as a function of distance from the source, the relative level of source and receptor, and the times over which the peak and average concentrations were obtained are discussed in Chap. 4.

In principle the theoretical results of Sec. 3-3.2 on fluctuating plumes and the above paragraphs apply equally to other diffusion conditions and not just to looping. The looping condition, however, makes visually evident the separation between plume spreading and meander.

3-3.5.1.4 Coning. Coning is the straightforward, relatively uncomplicated case of diffusion in a neutral or slightly stable atmosphere and is handled by means of Eq. 3.116, evaluated for the Pasquill type C or D conditions. Figure 3.19 shows an instantaneous photograph and a time exposure of a coning plume.

3-3.5.1.5 Lofting. Since a ground-based inversion prevents material from reaching the surface, lofting is of practical importance largely as the possible precursor of a fumigation. A reasonable scheme for estimating concentrations in the lofting plume might simply be to treat the inversion base as the level $z = 0$ and to apply Eq. 3.116 (with $h = 0$ to obtain concentrations along the plume center line) although there are no concentration observations confirming this suggestion.

3-3.5.2 Volume-source Formulas. Because of the possible emission of airborne radioactive material through leaks in a reactor-containment structure, Eq. 3.116 should be modified for the effect of a volume source. In a reactor-hazard analysis, the source generally consists of some fraction of the fission products contained in the reactor core, and the source material is assumed to be distributed uniformly throughout the volume of the building enclosing the reactor. For many power reactors the enclosure is a large pressure-tight dome designed to have, at most, some specified leakage rate under the postulated accident conditions. The source strength, Q', is defined, but the location of the leak and the effect of the building on the source geometry must be determined.

Reasoning that a reactor building must have a turbulent wake in its lee, Fuquay (1960) suggested treating the building effect as an initial dilution factor, D_B,

$$D_B = cA\bar{u} \tag{3.139}$$

where A is the cross-sectional area of the building normal to the wind. In other words, any material escaping from the containment building is assumed to be dispersed rapidly into a volume equal to c times the building cross-sectional area times the wind speed. The

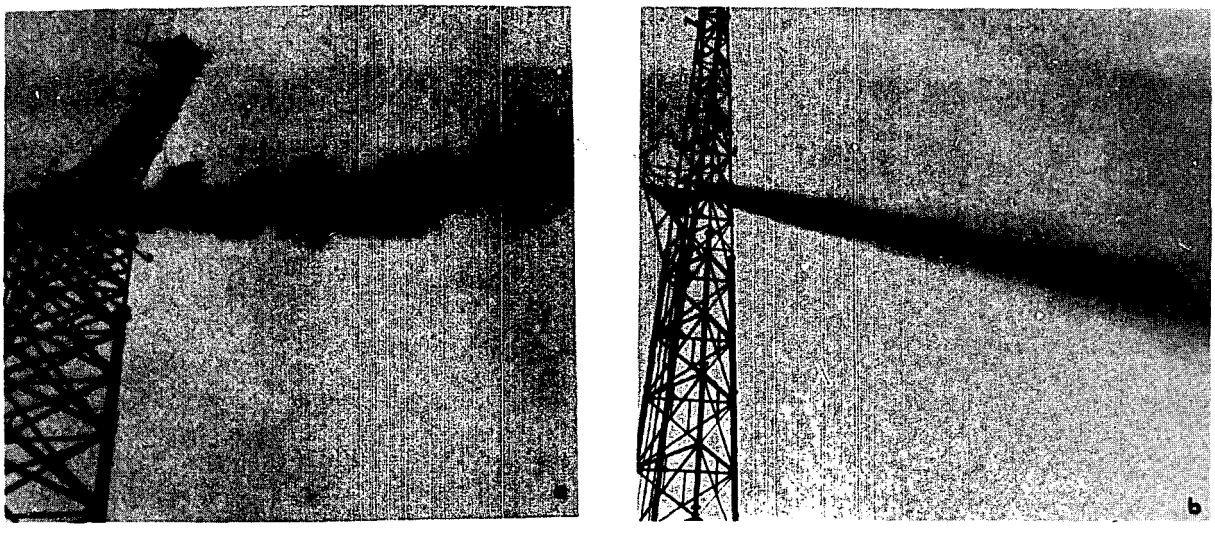

Fig. 3.19 — (a) Coning plume using an exposure of $\frac{1}{25}$ sec at the meteorological tower of the Big Rock Point reactor site near Charlevoix, Mich. (b) The same coning plume photographed with a time exposure of 5 min. (Courtesy W. M. Culkowski)

factor c represents an estimation of the relation of the cross-sectional area of the building to the size of observed pressure wakes, and its exact numerical value will have to be determined by suitable experiments. Gifford (1960) suggested that, as a reasonable estimate, $\frac{1}{2} \leq c \leq 2$. The reason for choosing these particular bounds, which were actually no more than a guess, was to provide, in the absence of suitable experimental data, usable numbers for concentration estimations. According to Barry (1964), who made an interesting and useful summary of the results of a number of recent experiments, studies with wind-tunnel models have suggested values of c near the lower of these limits, namely, c = 0.50 to 0.67. Of course, it is not impossible that larger values of c may be found if suitable full-scale atmospheric experiments are performed, particularly in unstable light-wind conditions. A comprehensive summary of relevant wind-tunnel measurements of building dilution effects is given in Chap. 5. A few atmospheric experiments have been reported by Islitzer (1965) and J. E. Martin (1965). A photograph from Martin's paper, Fig. 3.20, illustrates the building effect on the plume.

The building dilution factor, D_B, is combined with the atmospheric dilution factor, $D_A = Q'/\bar{\chi}$, in a way similar to Fuquay's (1958) handling of stack dilution,

$$D_{total} = D_B + D_A \qquad (3.140)$$

Combining Eqs. 3.116, 3.139, and 3.140, one can reasonably assume that, as suggested by Davidson (1965),

$$\frac{\bar{\chi}}{Q'} = (\pi \Sigma_y \Sigma_z \bar{u})^{-1} \exp\left[-\left(\frac{y^2}{2\Sigma_y^2} + \frac{h^2}{2\Sigma_z^2}\right)\right] \qquad (3.141)$$

where Σ_y and Σ_z are total diffusion factors given by

$$\Sigma_y = (\sigma_y^2 + cA/\pi)^{1/2}$$
$$\Sigma_z = (\sigma_z^2 + cA/\pi)^{1/2} \qquad (3.142)$$

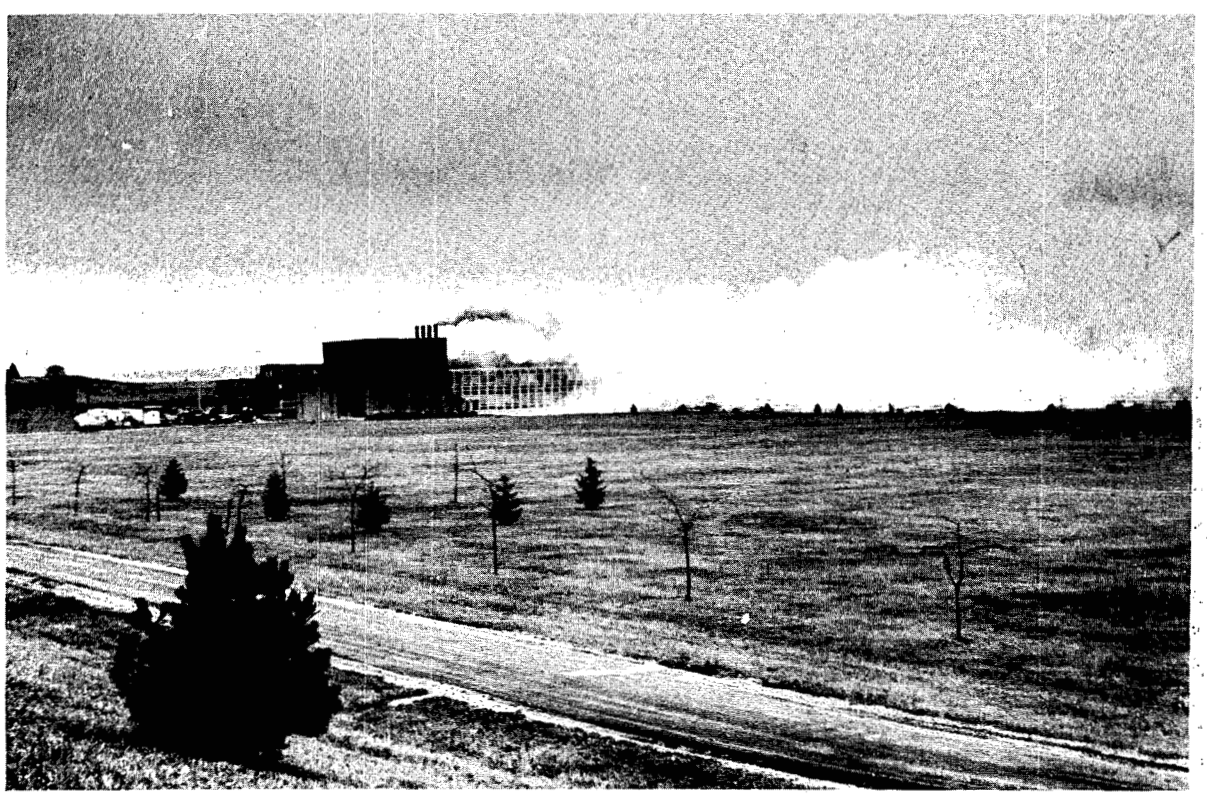

Fig. 3.20—A photograph of a smoke plume released from the top of a building during neutral conditions. (Courtesy J. E. Martin, 1965).

Equation 3.141 resembles the volume-source treatment proposed by Holland (1953) in that the volume effect is taken into account by adding a correction to the diffusion term of a Gaussian distribution. Holland achieved much the same result by defining a "virtual point source" that would produce a Gaussian plume, or puff, having a "width" equal to that of the actual volume source at the initial point.

Various other initial volume-source distribution functions were compared by Gifford (1955a) with the Gaussian initial distribution. The conclusions from this study are that the Gaussian initial volume leads to much simpler diffusion expressions and that it is conservative; that is, it leads to downwind concentrations slightly greater than for other volume-source distributions that were considered.

3-3.5.3 Crosswind Integrated Concentration. The crosswind integrated concentration, $\bar{\chi}_{CWI}$, from a continuous source is obtained by integrating Eq. 3.116 with respect to y from $-\infty$ to ∞:

$$\bar{\chi}_{CWI} = \frac{2^{1/2}Q'}{(\pi)^{1/2}\sigma_z\bar{u}} \exp\left(-\frac{h^2}{2\sigma_z^2}\right) \qquad (3.143)$$

This equation is particularly useful as an interpolation formula in connection with field-diffusion trials because it contains only one diffusion parameter, σ_z. The same equation describes the concentration due to a continuous infinite crosswind line source (source strength, Q'_L), which might be realized in practice by, for example, a heavily traveled highway. Some discussion of the problem of a line source of finite length has been presented by Elliott and Barad (1964) among others, and the problem of a crosswind line source oriented at some angle to the mean wind direction was discussed by Barad, Haugen, and Fuquay (1960). Equation 3.143 has also been used as an approximation for an area source (Turner, 1964).

3-3.5.4 Long-period Average Concentration. Over a period of time, the direction of the mean wind shifts. The wind rose, which gives the joint wind-speed and direction-frequency distribution, is therefore a useful indicator of the characteristic features of the climate of a particular place. To obtain an estimate of the average concentration over a period that is very long compared with that over which the mean wind is computed, multiply the integrated concentration formula, Eq. 3.143, by the frequency with which the wind flows toward a given sector and divide by the width of that sector at the distance of interest:

$$\bar{\chi}_{\text{long-term av.}} = \left(\frac{2}{\pi}\right)^{1/2} \frac{0.01\, f\, Q'}{\sigma_z\bar{u}(2\pi x/n)} \times \exp\left(-\frac{h^2}{2\sigma_z^2}\right) \qquad (3.144)$$

where the frequency, f, is expressed in percent, $2\pi x/n$ is the sector width, and Q', σ_z, and $\bar{u}$ are averages over the long time period. An expression equivalent to this forms the basis for the calculations by Meade and Pasquill (1958) of annual SO_2 concentrations in the vicinity of the Staythorpe Power Station (using the corresponding Sutton formula) and is similar to one proposed by Culkowski (1960) (see also Lowry, 1951)

3-3.5.5 Maximum Concentration and Its Distance from the Continuous Elevated Source. Because σ_y and σ_z are not necessarily the same functions of x, in general, it is not possible to obtain simple explicit formulas for the maximum ground concentration and its distance from the source. However, in the special case $\sigma_y = \sigma_z$, i.e., for neutral or slightly unstable conditions, these maximum values can be specified. Differentiating Eq. 3.116 with respect to x and setting the result equal to zero in the usual way gives

$$\bar{\chi}_{max.} = \frac{2Q'}{\pi h^2 e\bar{u}} \qquad (3.145)$$

when $h^2 = 2\sigma_z^2$. In the slightly more general case characterized by $\sigma_y = a\sigma_z$, $d\sigma_y/dx = ad\sigma_z/dx$, i.e., where the vertical and horizontal cloud growths are simply proportional, which again occurs when $h^2 = 2\sigma_z^2$, the result is

$$\bar{\chi}_{max.} = \frac{2Q'}{\pi h^2 e\bar{u}} \frac{\sigma_z}{\sigma_y} \qquad (3.146)$$

Because the maximum concentration occurs when $h = 2^{1/2}\sigma_z$, this formula may also be written in the following form

$$\bar{\chi}_{max.} = \frac{2^{1/2}Q'}{he\bar{u}(\sigma_y)_{max.}} \qquad (3.147)$$

where the notation indicates that the value of σ_y to be used is the one applying at the maximum concentration distance.

Alternatively, Fig. A.4 of the Appendix, which presents evaluations of Eq. 3.116 with the σ_y and σ_z values of Figs. 3.10 and 3.11, can be used.

3-3.5.6 Concentration Isopleths: Plume Width and Height Formulas. Practical computations with diffusion formulas often require the construction of concentration isopleths, for example, in connection with calculation of total population dosage (Gomberg, 1958). For this purpose it is convenient to know the distance z_p or y_p where the concentration has dropped to p% of its value on the plume axis, For the generalized Gaussian plume model, the following formulas are an obvious application of Eq. 3.116:

$$y_p = \left(2\sigma_y^2 \ln \frac{100}{p}\right)^{1/2} \tag{3.148}$$

and

$$z_p = \left(2\sigma_z^2 \ln \frac{100}{p}\right)^{1/2} \tag{3.149}$$

From these, with p = 10%, it can be seen that H, as defined by Eq. 3.121, is equal to $2z_p$ and that a similar relation exists between y_p and θ.

On the basis of plots of concentration isopleths, Hilsmeier and Gifford (1962) have computed areas enclosed by various concentration values, $\bar{\chi}$, for sources located at the surface. They followed the generalized Gaussian formula, Eq. 3.116, and used the diffusion-parameter values of Figs. 3.10 and 3.11. The results are shown in Fig. 4.32 of Chap. 4 together with observed isopleth areas from the Prairie Grass and Green Glow programs, as analyzed by Elliott (1959) and by Elliott and Nickola (1961).

An extensive numerical computation of areas within concentration isopleths, based on Sutton's diffusion model, Eq. 3.116 taken in combination with Eqs. 3.79 and 3.81, was undertaken by Rosinski (1958). Rosinski's computation allowed for the effect of varying deposition rates. A similar computation using Sutton's model was performed by Velez (1961), who allowed for the effects of varying source heights and radioactive decay of mixed fission products. Nishiwaka (1959) likewise employed Sutton's model to estimate concentration-isopleth areas and, in addition, provided several useful approximations to the isopleth area based on the areas of equivalent ellipses. His formulas, which give the area A within a concentration isopleth, $\bar{\chi}$ = constant, for a surface-level source, are:

$$A_1 \approx \frac{2\pi}{(2-n)} C_y \exp\left[-\frac{2-(n/2)}{2-n}\right] (\gamma)^{2-(n/2)} \tag{3.150}$$

$$A_2 \approx \frac{\pi}{2} C_y e^{-1/2} \quad (\gamma)^{2-(n/2)} \tag{3.151}$$

$$A_3 \approx \frac{\pi}{4} 2^{n/2} C_y (\ln 2)^{1/2} (\gamma)^{2-(n/2)} \tag{3.152}$$

where

$$\gamma \equiv \left(\frac{2Q'}{\bar{\chi}\bar{u}\pi C_y C_z}\right)^{n-2} \tag{3.153}$$

and the other parameters have their usual meanings. The error of these useful approximations is ≤3% for A_2 and A_3 and ≤6% for A_1, as compared with areas calculated directly from Sutton's formula.

3-3.5.7 Multiple and Area Sources. Many of the large nuclear installations already face the problem of emissions from several isolated sources. If there are only a few sources, it is a simple matter to compute their concentrations individually and sum these to obtain their joint effect. The arithmetic can in some cases be simplified by taking advantage of a circumstance that seems first to have been pointed out by Bosanquet and Pearson (1936). Because of symmetry with respect to the x-axis, Gaussian diffusion models possess the property that, if the source and receptor locations are interchanged, the numerical value of the concentration is not affected. This means that the concentration at a point downwind from a number of isolated sources can be computed by imagining all the sources to be combined and located at the receptor point and summing the resulting (computed) concentrations at the actual source points after reversing the mean wind direction, $\bar{u}$. Culkowski (1960) has shown that this scheme can also be applied to annual average concentrations from multiple sources. A plastic overlay, or template, of concentration isopleths expedites the calculation.

On the other hand, sources may be so numerous that they can be considered most effectively as an area source, and the point-source plume formula may be integrated over this area. This procedure was followed by Lucas (1958). If

there are a very large number of individual sources, it may be desirable, as Turner (1964) has done, to combine them into a smaller number of virtual area sources and then to sum the concentrations that result from these.

3-3.5.8 Instantaneous-source Diffusion Equations. In addition to procedures for average plume diffusion, a procedure for calculating the diffusion from sudden, explosive, or very short term releases of material to the atmosphere is often required. Although the so-called "hot-cloud" accident, an instantaneous release of all the nuclear and chemical energy of a reactor to the atmosphere, is no longer considered credible because of reactor-containment features, other possibilities for generating sources of this kind exist. Some examples are the short-term controlled release of fission products from a contained accident, explosive accidents occurring during nuclear-fuel reprocessing, accidental criticalities, launching-pad accidents involving nuclear (or chemical) rockets, and nonnuclear explosions of all kinds.

Equation 3.113 for the instantaneous puff concentration, χ, can be written

$$\chi(x,y,z) = Q\, 2^{-1/2}\pi^{-3/2}(\sigma_{xI}\sigma_{yI}\sigma_{zI})^{-1} \times \exp\left\{-\left[\frac{(x-\bar{u}t)^2}{2\sigma_{xI}^2} + \frac{y^2}{2\sigma_{yI}^2} + \frac{h^2}{2\sigma_{zI}^2}\right]\right\} \quad (3.154)$$

Here Eq. 3.113 has been multiplied by 2 to account for the assumed ground reflection so that it will be consistent with the plume equation, Eq. 3.116. For reasons discussed in Sec. 3-2.2.6, it is to be expected that, in general, the puff standard deviations σ_{yI} and σ_{zI} will differ from the corresponding plume σ_y and σ_z. Appropriate values based on recent experimental data are presented in Sec. 4-10.3.

Since the processes of puff creation are frequently associated with some degree of violent expansion (typically an explosion or short and rapid burning), it will usually be necessary to consider the diffusion of a puff that has some finite initial volume. This can be done by combining an initial volume dilution with the atmospheric value. In this case the equation for the concentration at the puff center, where $x = \bar{u}t$, $y = z = 0$, and V is the initial volume, is

$$\chi_p(x,y,z) = 2^{-1/2}\pi^{-3/2}Q\,(\sigma_{xI}\sigma_{yI}\sigma_{zI} + V)^{-1} \quad (3.155)$$

The consequence to a receptor subjected to the passage of an airborne cloud of radioactive or other contaminants is frequently expressed in terms of the integrated concentration, sometimes called the exposure, ψ. The exposure is the integral of the concentration over a specified time interval,

$$\psi_s = \int_{T_0}^{T_0+T} \chi_s \, d\tau \quad (3.156)$$

where T refers to the time of exposure and the subscript s is introduced as a reminder that sources of different types may be involved. The average concentration over the interval T is found by dividing ψ_s by T. This concept would be too obvious to belabor were it not for the following interesting fact. Consider a puff, i.e., an instantaneous point source, as specified by Eq. 3.154. The total exposure that would be experienced by a receptor at a point (x,y,0) when the puff passes by is given by

$$\psi = \int_{x/\bar{u}}^{\infty} \chi(x-\bar{u}t,y,0)\, dt \quad (3.157)$$

If the usual assumption is made that the puff passes rapidly overhead so that σ_{yI} and σ_{zI} will be effectively constant during the time of puff passage (compare with Eqs. 3.113 and 3.114), it follows that

$$\psi = Q(\pi\sigma_{yI}\sigma_{zI}\bar{u})^{-1} \exp\left[-\left(\frac{y^2}{2\sigma_{yI}^2} + \frac{h^2}{2\sigma_{zI}^2}\right)\right] \quad (3.158)$$

Thus the equation for the exposure is seen to have the same mathematical form as the equation for the continuous-plume concentration, and methods of calculation that provide the latter also can be used to compute the former.

The crosswind integrated concentration from an instantaneous point source may be obtained by integrating Eq. 3.142 with respect to y from $-\infty$ to ∞. The resulting equation is

$$\chi_{CWI} = \frac{Q}{\pi\sigma_{xI}\sigma_{zI}} \exp\left\{-\left[\frac{(x-\bar{u}t)^2}{2\sigma_{xI}^2} + \frac{h^2}{2\sigma_{zI}^2}\right]\right\} \quad (3.159)$$

The equation for the exposure from a crosswind integrated instantaneous point source follows from integration of Eq. 3.158:

$$\psi_{CWI} = \left(\frac{2}{\pi}\right)^{1/2} \frac{Q}{\sigma_{zI}\bar{u}} \exp\left(-\frac{h^2}{2\sigma_{zI}^2}\right) \quad (3.160)$$

A diffusion equation of possible interest is that for an instantaneous infinite crosswind line source. Although an actual source of this type can be conceived only by a considerable exercise of the imagination, this mode of release is approximated by the effluent from a rapidly traveling rocket or an airplane or by the exhaust from an automobile traveling along a highway. The equations for concentration and exposure from the instantaneous infinite crosswind line source are identical with Eqs. 3.159 and 3.160, respectively, with the exception that the source strength, Q (amount), must be replaced by the appropriate line-source value, Q_L (amount per unit length).

3-3.5.9 Nonideal Characteristics of Atmospheric Diffusion. In all the previous discussion, it has been assumed that particles or gases diffusing in the atmosphere behave as if they were identical with ideal fluid particles or points. The diffusing material is, in effect, identical in its physical properties with the assumed fluid continuum, possessing neither extension, inertial, nor buoyant properties of its own. For practical purposes gases and submicron particles can be assumed to behave in this way and can therefore be expected to obey laws of diffusion calculated on such a basis.

On the other hand, many diffusing particles of interest lie in a size range that does not encourage the ideal fluid-point assumption. Moreover there are certain removal processes, e.g., deposition, washout, and radioactive decay, that can significantly affect diffusion, and it is desirable to give these processes some consideration. In most cases it will not be possible to go much farther than a qualitative description of the significant physical processes, which are often characterized by considerable complexity and subtlety and for which in many cases an extended theoretical treatment is not yet available.

A heavy diffusing particle (i.e., one that does not follow the ideal fluid-point assumption) falls under the action of gravity. In the absence of turbulent mixing, the particle reaches a terminal velocity given quite accurately by Stokes' law. In the presence of turbulence, however, this orderly settling process is markedly changed. This conclusion follows from the readily observable fact that particles of various kinds are present in the atmosphere in equilibrium amounts, having diameters such that they would rapidly settle out if Stokes' law applied.

The problem of the diffusion of heavy particles in a turbulent fluid turns out to be very difficult in theory. Physically, the reason is that the path of such a particle is not a function of any particular set of boundary or initial conditions. Rather, the problem has to be formulated in a way that recognizes that the path of the particle at any instant depends continuously on its trajectory during its prior travel through the turbulent medium. The integro-differential equations resulting from this formulation are not easily simplified. In addition to gravitational settling, the effects of particle inertia, the inertia of the displaced air, and the possible boundary-layer effects on the particles come into play. It is not surprising that there are few reliable, practically useful results on the turbulent diffusion of heavy particles. The reader interested in fundamental aspects should be aware of Tchen's (1947) formulation and Lumley's (1957) discussion. Applied studies have been presented by F. B. Smith (1959), Yudine (1959), and Liu (1956).

Chapter 4

Diffusion and Transport Experiments

Norman F. Islitzer* and David H. Slade†

4-1 SCOPE

The goals of diffusion experimentation are diverse, and this diversity works against the simple comparison of experiment results. The purest diffusion experiments attempt to relate the dynamic and physical characteristics of the earth–atmosphere system to the mean and turbulent atmospheric structure and, in turn, to relate these characteristics to diffusion. In other experiments, instead of investigating the genesis of the mean and turbulent flow, effort is directed toward establishing the relation between a number of particular atmospheric states and the concomitant diffusion. Some experiments are mounted to establish the diffusion climate of a particular site. Finally, there are experiments designed to evaluate the effects of a particular pollutant-releasing process. These motivational differences are reflected in experimental techniques and the resulting data.

The purposes of this chapter are to illustrate the relation between measured meteorological data and diffusion and to establish a set of diffusion parameters that can be estimated from meteorological observations at a given site. When the first edition of *Meteorology and Atomic Energy* was published in 1955, a small number of diffusion experiments had been described in the literature. These field trials were limited in range and in the type of data collected. Since 1955 a variety of tests, conducted in many topographic regimes and during a wide range of stability and wind-speed conditions, has added significantly to the confidence with which the meteorologist can estimate diffusion from meteorological data.

Most of this chapter is devoted to a review and comparison of many recent diffusion experiments. A number of different criteria were observed in choosing the experiments to be discussed. Some experiments were included because of the broad range of meteorological conditions sampled, some, for the high quality and large quantity of data, and others, for the interesting features of the technique of relating meteorological data to diffusion data. A few experiments were included because they supplied measurements of diffusion during unusual or special conditions or at distances from the source at which no other measurements were available. Numerous small field studies that would add little to the discussion were excluded. Data that appeared to be presented in interim form or that were difficult to obtain owing to security restrictions were also excluded. The diffusion experiments noted in this chapter are listed in Tables 4.1a and 4.1b.

The primary concern in this chapter is the turbulent diffusion of gases and aerosols. Such effects as cloud rise, aerodynamics of flow around obstacles, deposition, washout, and changes in the effluent along its atmospheric path are discussed only when necessary to the interpretation of observed pollutant concentrations and cloud dimensions. These effects are discussed in Chap. 5.

4-2 PRESENTATION OF DATA

4-2.1 Sources and Limitations

For most continuous-source operational problems, the change of center-line axial con-

*Air Resources Field Research Office, Environmental Science Services Administration, Idaho Falls, Idaho.

†Air Resources Laboratories, Research Laboratories, Environmental Science Services Administration, Silver Spring, Maryland.

Table 4.1a—SUMMARY OF RECENT CONTINUOUS-SOURCE DISPERSION EXPERIMENTS

Experiment	Location of experiment	Number of releases* and maximum sampling distance	Sampled material and sampling method	Height of release and release or sampling duration	Type of terrain and stability condition	Initial source size and temperature	Parameters directly measured
				Elevated Sources			
Porton (Hay and Pasquill, 1957)	Porton Downs, England	19 releases; 500 m	Lycopodium spores; impaction on cylinders mounted on barrage-balloon cable	150 m; 30-min release	Gently rolling; slightly unstable to slight inversion	Small; ambient	Vertical concentration distribution
National Reactor Testing Station (Islitzer, 1961)	Idaho Falls, Idaho	16 releases; 1800 m	Uranin dye; aspirated samplers at 1.0 m	46 m; 30-min release	Flat desert; unstable	Small; ambient	Surface concentration distribution
Hanford (Hilst and Simpson, 1958)	Richland, Wash.	16 releases; 600 m	Fluorescent pigment and oil fog; impaction cylinders on blimp cable and photography	56 m; 60-min release	Flat desert; stable	Small; near ambient	Vertical concentration distribution and crosswind plume width
Harwell (BEPO) (Stewart et al., 1954)	Harwell, England	88 releases; 10^4 m	^{41}Ar; beta counters on blimp cable and counters at surface	68 m; 15- to 60-min sampling	Built-up area and open country; stable and unstable	Stack diameter of 3.5 m; 50°C above ambient	Crosswind and vertical concentration distribution (not simultaneously)
Brookhaven National Laboratory	Central Long Island, N. Y.	Many; 5×10^4 m	Oil fog, ^{41}Ar, and irradiated spheres; a variety of sampling methods	Surface and 115 m; short to about 1 hr	Low woods and open fields; stable and unstable	Variety; variety	Crosswind and vertical concentration distributions
Tennessee Valley Authority (Gartrell et al., 1964)	Northwestern Ala.	24 releases; 1.6×10^4 m	SO_2 in stack gases; titrilog and recorder mounted on aircraft	100 m; short sampling time during aircraft passes	Gently rolling; neutral and stable	Stack diameter of 5 m; 145°C	Crosswind and vertical concentration distribution

				Surface Sources			
Project Prairie Grass (Cramer, 1957, and others)	O'Neill, Neb.	70 releases; 800 m	SO_2; gas drawn through hydrogen peroxide solution	0.5 m; 10-min release	Flat prairie; stable through unstable	Small; ambient	Crosswind concentration distribution at 1.5 m and limited measurements of vertical concentration distribution
Project Green Glow and 30 series (Fuquay et al., 1964)	Richland, Wash.	46 releases; 2.56×10^4 m	Zinc sulfide; aspirated filters	1.5 m; 30-min release	Flat desert; stable and unstable	Small; ambient	Crosswind concentration distribution at 1.5 m and limited measurements of vertical concentration distribution
Project Ocean Breeze (Haugen and Fuquay, 1963; Haugen and Taylor, 1963)	Cape Kennedy, Fla.	76 releases; 4800 m	Zinc sulfide; aspirated filters	2.0 to 3.0 m; 30-min release	Sand dunes and dense scrub; unstable	Small; ambient	Crosswind concentration distribution at 1.5 and 4.5 m
Project Dry Gulch (Haugen and Fuquay, 1963; Haugen and Taylor, 1963)	Vandenberg AFB, Calif.	109 releases; 5665 m	Zinc sulfide; aspirated filters	2.0 to 3.0 m; 30-min release	Rough foothills; unstable	Small; ambient	Crosswind concentration distribution at 1.5 m
National Reactor Testing Station (Islitzer and Dumbauld, 1963)	Idaho Falls, Idaho	35 releases; 3200 m	Uranin dye; aspirated filters	1.0 m; 60-min release	Flat desert; stable and unstable	Small; ambient	Crosswind and limited vertical concentration distribution
United Kingdom (Hay and Pasquill, 1959)	Porton Downs, England	8 releases; 100 m	Lycopodium spores; adhesive cylinders	2 m; 3-min release	Downland; mixed	Small; ambient	Crosswind concentration distribution
United Kingdom (Pasquill, 1962a)	Cardington, England	10 releases; 7.5×10^4 m	Fluorescent pigment; rotating-drum filters mounted on aircraft	Surface; continuous release and short sampling by aircraft	Downland; unstable	Small; ambient	Limited crosswind and vertical concentration distribution

*The number of experiments used in analyses are frequently fewer than the total number performed owing to faulty equipment, unexpected wind shifts, etc.

Table 4.1b—SUMMARY OF RECENT QUASI-INSTANTANEOUS-SOURCE EXPERIMENTS

Experiment	Location of experiment	Number of releases and maximum sampling distance	Sampled material and sampling method	Height of release and release duration	Type of terrain	Initial source size and temperature	Parameters directly measured
(Smith and Hay, 1961)	Porton Downs, England	10 releases; 300 m	Lycopodium spores; impaction on adhesive cylinders	Surface; 1 sec	Downland	1 to 4 m; ambient	Surface dosage distribution
Sand Storm (Taylor, 1965)	Edwards AFB, Calif.	43 releases; 2400 m	Beryllium powder in rocket propellant; aspirated filters	Surface (plus initial height of rise); 2 to 8 sec	Flat desert	Diameter of 15 to 45 m; above ambient	Surface dosage distribution
(Högström, 1964)	Ågesta and Studsvik, Sweden	430 releases; ≈ 5000 m	Oil fog; photography from position upwind of source	24 to 87 m; 30 sec	Low hills	Small; close to ambient	Puff width and puff depth
Dugway (Cramer et al., 1964)	Dugway Proving Grounds, Utah	33 releases; 1100 m maximum used here	BW and CW gases and particulates	Surface; 3 and 26 sec	Flat desert	Finite but accounted for by authors; near ambient	Surface dosage distribution and limited measurements of vertical distribution
Point Arguello (Smith et al., 1964)	Naval Missile Facility, Pt. Arguello, Calif.	17 releases; $\approx 10^4$ m	Zinc cadmium sulfide; rotorods and aspirated filters	Surface; 1 min	Rugged coastline	Small; ambient	Dosage along irregular arcs
Reactor Destruction Test (Islitzer and Markee, 1964)	National Reactor Testing Station, Idaho Falls, Idaho	4 releases; 6100 m	Fission products; aspirated filters	Surface; <30 sec	Flat desert	10 meters; above ambient	Surface dosage distribution
Texas (MacCready, Smith, and Wolf, 1961)	Dallas TV tower, Cedar Hill, Tex.	37 releases; $\approx 10^4$m	Zinc cadmium sulfide; aspirated filters on tower	110 to 320 m; small (aircraft-released line source upwind of tower)	Rolling terrain	Finite but accounted for by authors; ambient	Vertical dosage distribution on tower

Table 4.2—SUMMARY OF DIFFUSION COEFFICIENTS*

Identification	Diffusion coefficients	Plume dimensions
Sutton	C_y, C_z, n_y, n_z	$\sigma_y = \frac{1}{2^{1/2}} C_y x^{2-n_y/2}$
		$\sigma_z = \frac{1}{2^{1/2}} C_z x^{2-n_z/2}$
Fickian	K_x, K_y, K_z	$\sigma_y = (2K_y t)^{1/2}$
		$\sigma_z = (2K_z t)^{1/2}$
Cramer	σ_θ, σ_φ, p, q	$\sigma_y = \sigma_\theta x^p$
		$\sigma_z = \sigma_\varphi x^q$
Pasquill	$\sigma_{\theta(T,t)}$, $\sigma_{\varphi(T,t)}$	$\sigma_y = \sigma_{\theta(T,t)} x$
		$\sigma_z = \sigma_{\varphi(T,t)} x$

*The symbols T and t represent the sampling time and averaging time, respectively.

centration must be known as a function of distance. In addition, the horizontal and vertical dimensions of the plume are usually required, and the ground surface area contained within a particular isopleth of air concentration or exposure may be required. The diffusion coefficients needed to compute these quantities from the various diffusion models for a continuous point source (discussed in Chap. 3) are listed in Table 4.2. Symbols used frequently in Chap. 4 are included in the list of symbols given at the beginning of Chap. 3.

For instantaneous-point- or instantaneous-line-source concentration calculations, diffusion along the direction of the mean wind also must be considered. This requires diffusion coefficients along the x-axis. Sutton's derivation actually considered a single value for n, but it has been shown by Barad and Haugen (1959) among others that different values of n along the y- and z-axes are needed to fit the measured diffusion data and that neither n_y nor n_z can be obtained from the wind profile. Therefore identification of the coefficients in Table 4.2 with Sutton is primarily for historical convenience since their original meaning has been lost by the use of empirical constants.

In some studies the data were not presented in a manner compatible with the format; so recomputation or replotting was necessary. However, every attempt was made to ensure that the findings and conclusions emphasized by the original authors were not violated.

A review of the diffusion experiments summarized in Tables 4.1a and 4.1b cannot but impress the reader with their overall inadequacy in some respects. This is not a criticism since, in most cases, the inadequacies were engendered by logistical and technical difficulties, funding limitations, operational requirements, and other similar problems that preclude truly comprehensive diffusion experiments. Some of these shortcomings are:

1. Limited extent of sampling grids. The diffusion experiments described later in the chapter can be divided into two types: those in which the sampling was carried out on geometrical grids involving hundreds of samplers and those in which sampling was carried out by a limited number of mobile sampling systems individually placed for each experiment. The former experiments usually have supplied the more comprehensive data. The data from dense surface sampling grids, except for a few percent of the observations, have been confined to distances of less than 5 km. This is probably a consequence of funding and manpower limitations since the technical feasibility of surface sampling has been demonstrated to distances of over 25 km and aircraft sampling using various tracers has been accomplished to distances in excess of 100 km.

Even the extensive horizontal grid experiments, however, lacked similarly extensive vertical measurements of turbulence and diffusion. Although the detailed description of the vertical plume distribution presents a probably insurmountable logistic and funding problem, a considerable amount of information can be obtained from the careful use of a limited number of tower and balloon- and aircraft-borne samplers.

In addition to limited vertical measurements, orientation of the grids in fixed directions frequently precluded sampling during conditions characterized by shifts and large angular changes in wind direction, conditions not described by theory but certainly within the realm of experimental measurements.

2. Diffusion during nonhomogeneous turbulence conditions. Although homogeneous turbulence is called for by most diffusion theory, the atmosphere never approaches vertical and infrequently approaches horizontal homogeneity. This is particularly true during radiational inversions, which are marked by strong vertical gradients of wind speed, wind direction, and turbulence. The limited angular extent of the grids and the paucity of elevated meteorological sensors and tracer samplers in most experiments limit the description of diffusion during just those times that diffusion is of greatest interest. Furthermore, diffusion experiments in regions of topographic complexity have not been of the scope necessary for general solutions.

3. Time interval of tracer release and sampling. The release of pollutants from single sources in the nuclear-energy industry varies from virtually instantaneous releases to continuous releases over periods of years. The major experimental studies have, with few exceptions, been conducted for release and sampling times in the range of a few minutes to a few hours. Only rarely has an experimental series been designed to furnish data over a variety of release and sampling times.

4. The effects of deposition. The data from most diffusion experiments conducted using sources in the lowest hundred or so meters of the atmosphere probably include the effects of deposition of the tracer used. Because of the difficulty of experimentally determining deposition, the study of this effect has not always been a part of a diffusion-experiment series. Since deposition will affect the absolute value of concentration, the rate of concentration decrease with distance, and the vertical concentration distribution, the lack of these data can be considered an important gap in experimental knowledge.

4-2.2 Concentration, Exposure, and Dosage

The diffusion data presented in this chapter will usually be discussed in terms of instantaneous concentration, χ, exposure ψ, or average concentration, $\bar{\chi}$. As noted in Chap. 3, Sec. 3-3.5.8, these quantities may be defined as:

$$\chi = \frac{\text{amount of pollutant}}{\text{volume of mixture}} \tag{4.1}$$

$$\psi = \int_{T_0}^{T_0+T} \chi \, d\tau \tag{4.2}$$

$$\bar{\chi} = \frac{1}{T} \int_{T_0}^{T_0+T} \chi \, d\tau \tag{4.3}$$

where χ in each case is the concentration at a given moment. Note that the definition of dosage as the product of exposure and flow rate is in wide use and will be adopted here.

In practice extensive measurements of χ are not at all common because the relative complexity of the real-time or sequential samplers required for such measurements usually prohibit their use in large numbers.

The major diffusion experiments, those with numerous sampling arcs and many hundreds of samplers, usually involved measures of exposure rather than of average concentration. In these experiments the samplers were actuated before the dispersing tracer arrived and were deactivated after the last of the tracer was assumed to have passed. These times were estimates only since real-time or sequential samplers were not in wide use. (The reason for this sampling mode in experiments which are considered to describe continuous-source characteristics over finite time intervals is that the cost of the equipment necessary to activate and deactivate hundreds of samplers simultaneously during the emission of a continuous plume is inordinately large.)

Among the detached plume surface-source experiments in the group just discussed are the Prairie Grass tests (Sec. 4-4.2.1), Green Glow and 30 tests (Sec. 4-4.2.2), Projects Ocean Breeze and Dry Gulch (Sec. 4-4.2.3), and the National Reactor Testing Station (NRTS) series (Sec. 4-4.2.4). In each of these experiments, one must assume some elapsed time interval in order to compute a value of $\bar{\chi}$. In the Prairie Grass and NRTS series, this time interval was assumed to be equal to the release time. For the comparatively short distances investigated during these experiments, this assumption is probably reasonable if the problem to be in-

vestigated is the average concentration in a continuous plume. Some error must be introduced, however, since the total time required for the passage of all the material in a detached plume at a point downwind must be greater than the release interval because of the effects of along-wind turbulent diffusion and the along-wind spreading introduced by vertical wind shear in a turbulent medium. Unpublished estimates indicate that, at measurement distances greater than those of the Prairie Grass and NRTS series, detached plumes may require as much as twice the release time to pass a given point. Dividing the exposure by a time interval equal to the release time will indeed give an average concentration in such cases of elongated plumes (as does the assumption of any time interval), but the meaning of such average concentrations must be very precisely known if they are to be related, for instance, to meteorological indices. If the entire elongated detached plume is sampled, however, one would expect nearly the same level of exposure as would be obtained by sampling a continuous-source plume for a period of time equal to the release time of the detached plume.

Since the experiments just noted were all performed in a similar manner, normalization of the exposure or the average concentration by the appropriate source strength (total amount of source or amount of source per unit time, respectively), as usually done in this chapter, yields values which are identical dimensionally and similar numerically and which therefore may be directly compared.

4-2.3 Summary Diagrams

The data from the various experiments discussed in this chapter are summarized in the nine diagrams listed below:

Fig. 4.5	σ_z, elevated continuous sources
Fig. 4.6	$\bar{\chi}_p\bar{u}/Q'$, elevated continuous sources
Fig. 4.21	σ_y/σ_θ, surface and elevated continuous sources
Fig. 4.22	σ_y, long travel time
Fig. 4.23	σ_y, long travel distance
Fig. 4.24	$\bar{\chi}_p\bar{u}/Q'$, surface continuous sources
Fig. 4.38	σ_{yI}, surface and elevated instantaneous sources
Fig. 4.39	σ_{zI}, surface and elevated instantaneous sources
Fig. 4.40	$\psi_p\bar{u}/Q$, surface instantaneous sources

These diagrams generally contain measured values of the data (reduced to some common basis) determined during the individual experiments. On occasion, where insufficient data are available, computed values have been entered. The effects of deposition and finite source size have been accounted for in certain cases. Such manipulations of observed data are noted in appropriate sections of the text.

4-3 DIFFUSION-ESTIMATION METHODS

Over the years three methods of estimating diffusion from a minimum of measured meteorological data have come into common use. The first of these, by Sutton, is described in Chap. 3, Sec. 3-2.2.4. The analytic form of the equations, the variety of equations for many specific calculations, and the body of experimentally determined values of the diffusion coefficients C_y, C_z, and n recommended this method to many.

In 1957 Cramer published a set of three graphs from which the plume dimensions σ_y and σ_z or the concentration, $\bar{\chi}$, for distances up to 1.6 km could be determined directly from a knowledge of the horizontal wind-direction standard deviation (Cramer's σ_A). The curves in these graphs were based on the Project Prairie Grass and the Round Hill data (Cramer, 1957). The completeness of this system (estimates could be made by simple reference to one or two graphs) and the simplicity with which it could be applied recommended this approach to an increasingly large audience. If σ_A (referred to as σ_θ) and σ_E the vertical wind-direction standard deviation (referred to as $\dot{\sigma}_\varphi$) are known, Cramer suggests that the equations credited to him in Table 4.2 be used.

An effort was made by Pasquill, in an unpublished note the substance of which was later presented in a paper by Meade (1959) and, again, by Pasquill (1961), to develop a simple system of downwind concentration estimation. Pasquill suggested that both σ_y and σ_z be estimated in accordance with the suggestions of Hay and Pasquill (1959). The Hay and Pasquill paper presented a convenient method of estimating both vertical and lateral cloud spread from measurements of wind-direction fluctuations made with a suitably responsive instrument. Recognizing that the data on vertical wind-direction fluctuation required by this

method were not generally available, Pasquill suggested values for the appropriate degree of vertical spreading which could be estimated from stability considerations. He suggested that stability be estimated from wind speed and the degree of insolation. He also indicated how the lateral spreading of the plume could be estimated from the range of the wind-direction trace for long (about 1 hr) pollutant releases and suggested a series of wind-direction-range values to be used in lieu of actual wind measurements for short releases during steady wind-direction conditions. These direction-range values were related to the same estimates of stability used to infer the vertical spreading.

As pointed out by Pasquill and also by Gifford (1961), the values of plume height (h) and width (θ) described by Pasquill can be expressed in terms of the diffusion coefficients σ_y and σ_z of the generalized Gaussian plume model. Gifford performed this conversion and presented the resulting curves (Gifford, 1961). In Gifford's scheme diffusion estimation is achieved by estimating both σ_y and σ_z from the appropriate curves representing the various thermal-stability values, which are, in turn, estimated from cloud cover, wind speed, and (by day) insolation intensity. These curves are presented in Sec. A-3 of the Appendix for comparison with experimental data in diagrams in this chapter. To date no one has systematically related the estimated stability categories to Cramer's σ_θ categories or to values of σ_θ and σ_φ computed as suggested by Hay and Pasquill in their 1959 paper.

The diffusion experiments described in this chapter will fall under one of two headings depending on whether the releases were instantaneous (or in practice quasi-instantaneous) or continuous. The experimental data were neither observed nor published in sufficient detail to allow the presentation of a complete selection of diffusion parameters as a function of meteorological conditions or height above the surface.

4-4 CONTINUOUS SOURCES

4-4.1 Continuous Elevated Releases

Continuous elevated releases are of interest in practical applications since many real releases take place at some distance above the earth's surface. Measurements of axial concentration are difficult to obtain because of the problem of positioning samplers at a sufficient distance above the surface. Elevated-source plume-center measurements have rarely been made from a grid of towers. Consequently axial concentration measurements have involved manually positioned samplers suspended from large balloons in the plume center or traverses by helicopters or light aircraft. Since the elevated plume will usually disperse toward the surface, the conventional surface sampling grids have been used successfully to infer the rates of crosswind spreading under all but very stable conditions.

In some cases, particularly during strong inversions, estimates of diffusion are simplified by the comparative unimportance of surface deposition of the plume material. In others, such as the Hanford elevated-source releases, the plume released under strong inversion conditions did not reach the ground for great distances, and thus deposition did not occur.

4-4.1.1 Porton, United Kingdom. Some of the first organized attacks on the problems of diffusion experimentation were initiated in 1921, the year that the Meteorological Department of the Chemical Defense Experimental Station at Porton, England, began operation. Some of the most important work done at the station during the 1920's and 1930's centered about determinations of the shape and magnitude of the downwind lateral diffusion from continuously maintained sources. These early measurements, by hand-operated instrumentation quite crude by today's standards, were adequate for describing the crosswind concentration distribution, the change of this distribution with distance, at least in the first few hundred meters, and the stability dependence of the magnitude of the spreading. An excellent summary of these early measurements, partially based on hitherto unpublished data, may be found on pp. 127-137 of *Atmospheric Diffusion* by Pasquill (1962).

In 1957 Hay and Pasquill published some of the first results of their various experiments designed to relate atmospheric diffusion directly to concurrent wind fluctuations. A continuous source of Lycopodium spores was generated at 150 m above the ground and sampled at distances from 100 to 500 m downwind by a series of samplers suspended along the cable

of a barrage balloon. Hay and Pasquill gave the results of 10 such experiments, each lasting approximately 30 min. It was found that σ_φ, measured in angular units at the height of the source, was remarkably similar to σ_z, the particle distribution, also measured in angular units, to distances of 500 m. This indicated to the authors that, to a fair approximation, the particles traveled in almost straight lines from the source to the samplers. From this fact they concluded that the Lagrangian correlation coefficient remained close to unity over the travel times of these experiments. The ratio σ_z/σ_φ varied from 0.94 to 1.25 in eight of the experiments; the other two experiments exhibited values outside this range owing to marked inhomogeneity in the turbulence. The arc average value of σ_z for essentially neutral conditions was about 3.9°. The average σ_z value is shown by the Hay-Pasquill line in the summary diagram, Fig. 4.5.

4-4.1.2 National Reactor Testing Station (NRTS), Idaho Falls. The NRTS test was a series of 16 releases of a fluorescent tracer, uranin dye in solution, made in unstable atmospheres from the top of a 46-m tower (Islitzer, 1961). The terrain at this site is fairly flat with desert characteristics. The tracer was released for 30-min periods over a dense grid consisting of six arcs of samplers extending 150 to 1800 m from the 46-m-tower release point. The meteorological tower was instrumented at several levels with bivanes and anemometers.

One of the most interesting aspects of the NRTS test was the direct evaluation of plume width from horizontal wind-direction-fluctuation data. The wind direction at the 46-m level was read as 5-sec end-to-end averages for the period of the test. The standard deviation of this series was computed, multiplied by the distance from the source, and plotted against the measured particle-distribution standard deviation values computed for each of the 16 releases at each of the six arcs. The result of this rather simple use of the wind-direction fluctuation is given by the expression

$$\sigma_\theta x = 1.23\ \sigma_y \qquad (4.4)$$

and is shown in Fig. 4.1. The horizontal component of the wind direction was also averaged over a time period equal to $x/\bar{u}\beta$ (where x is distance from source to arc, $\bar{u}$ is average wind speed, and β is 4.0) for each sampling arc. The improvement in correlation by equating the time-averaged σ_θ values to σ_y was not significant, partly because of the rather slow change of σ_θ with averaging time for the time scales in these experiments. A mean travel time of 100 sec for the 82 cases used implies a mean averaging time of only 25 sec. The effect of ignoring the variation of the wind-direction fluctuations with height may have also tended to prevent a better agreement.

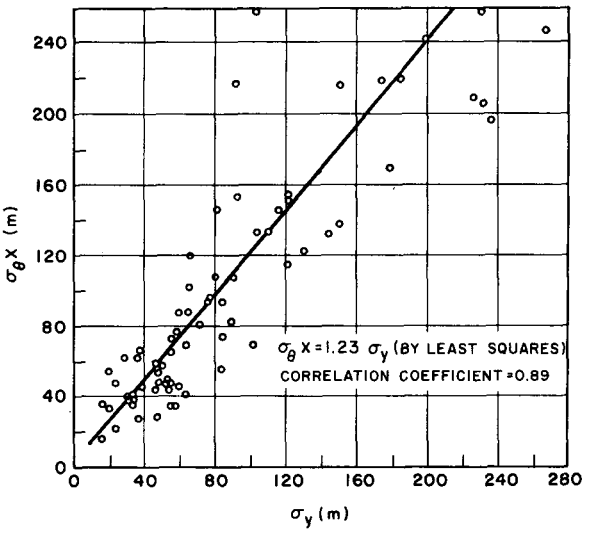

Fig. 4.1 — The relation between measured values of σ_y and those estimated from wind fluctuation data. The data are taken from elevated-source experiments. (From Islitzer, 1961.)

The mean value of the cloud standard deviations for the 16 releases is plotted in the summary diagram, Fig. 4.21. Islitzer also showed that, on the basis of measurements of the distance from the source to the point of maximum ground-level air concentration and assuming rectilinear dispersion,

$$\sigma_\varphi x = 1.23\ \sigma_z \qquad (4.5)$$

a direct use of the 5-sec averaged vertical wind-direction-fluctuation data at source height. The use of σ_y and σ_z values obtained from Eqs. 4.4 and 4.5 in the Gaussian plume-concentration formula results in downstream computed surface-concentration values closely matching the observed at all distances.

The measured meteorological data for each release including the distance to the point of maximum ground-level air concentration ($d_{max.}$) are shown in Table 4.3. There is a rather good

Table 4.3—METEOROLOGICAL DATA AND $d_{max.}$ FOR ELEVATED-SOURCE STUDIES DURING LAPSE CONDITIONS AT NRTS*

Test	$\bar{u}$(46 m), m/sec	ΔT (46 to 3 m), °F	σ_θ(46 m), deg	σ_φ (46 m), deg	$d_{max.}$, m
2	5.7	−2.5	6.9	4.5	700
3	6.5	−5.4	8.8	7.8	300
4	7.0	−1.6	5.4	3.5	800
5	8.9	−4.8	6.2	5.0	530
6	9.7	−3.5	7.0	4.6	650
7	7.8	−4.0	8.9	6.4	600
8	7.2	−4.0	12.6	6.8	560
9	10.0	−6.1	7.7	4.2	600
10	7.7	−5.3	7.9	5.0	800
11	6.7	−5.6	25.6	10.2	315
12	8.1	−3.4	4.2	4.1	940
13	11.3	−1.9	6.7	4.3	600
14	9.0	−5.4	8.4	6.0	480
15	6.5	−2.8	14.6	8.4	300
16	10.6	−3.9	6.6	4.4	730
17	6.5	−6.1	20.8	10.6	250
Mean	8.1	−4.1	9.9	6.0	572

*From Islitzer, 1961.

correlation between σ_φ and $d_{max.}$ in contrast to the poorer relation between the vertical temperature gradient and $d_{max.}$.

The problem of deposition, probably minor for these elevated source experiments, was not considered.

4-4.1.3 Hanford, Washington. Measurements of vertical diffusion in elevated plumes during various degrees of inversion intensity were made at Hanford, Wash. (Hilst and Simpson, 1958). A fluorescent pigment was emitted from the 56-m level of a tower for 60-min periods simultaneously with a continuous plume of smoke used to observe the visual width of the dispersing particles. The vertical concentration distribution of the fluorescent pigment was obtained from an array of cylindrical impaction samplers held aloft by tethered blimps and centered in the visible smoke plume during the tests. Simultaneous observations at a variety of distances to 600 m from the source permitted the empirical determination of the distance dependency of σ_z.

The horizontal spread of the smoke plume was photographed at 1-min intervals from an altitude of 1800 m. From these photographs both the horizontal width of the plume and the displacement of the plume center from the time-mean axis, as defined by the mean wind direction, were obtained. By making assumptions about the horizontal concentration distribution in a plume segment, Hilst (1957) deduced values for the short-period horizontal particle variance about the instantaneous-plume axis. This variance, when added to the meander, i.e., the variance of the plume center about the time-mean axis, gives the total horizontal particle-distribution variance.

The range of the σ_z data is summarized in Fig. 4.5, and the average of the σ_y data, in Fig. 4.21. Peak-to-average air-concentration values based on this experiment are presented in Sec. 4-5.

4-4.1.4 Harwell (BEPO), United Kingdom. Measurements of diffusion using the radioactive ^{41}Ar from the 68-m reactor stack of the Harwell Pile (BEPO) were reported by Stewart, Gale, and Crooks (1954). Vertical profiles of beta activity through the axis of the plume were measured out to 1000 m with a large blimp and an array of 10 beta counters on a cable. Ground-level surveys of both gamma and beta measurements were carried out to 10,000 m. A variety of meteorological conditions were sampled for times up to 60 min. The test site consisted of reactor buildings and built-up area to 500 m downwind from the stack with open country beyond. In addition to inhomogeneous terrain, the large finite size of the stack (3.5 m in diameter) and the efflux conditions of

the ^{41}Ar gas (50°C temperature excess above ambient air and 10 m/sec stack velocity) introduced mechanical turbulence and buoyant plume rise that influenced the sampling results.

From the vertical profiles of radioactivity, Stewart, Gale, and Crooks (1954) computed σ_z and then obtained σ_y from the air concentration, $\bar{\chi}_p$, in the plume center by

$$\sigma_y = \frac{Q'}{\pi \bar{\chi}_p \sigma_z \bar{u}} \tag{4.6}$$

The values of σ_z and σ_y found in this manner would be appropriate for computations of air concentration in the elevated plume. In addition, crosswind surveys of ^{41}Ar radioactivity were carried out to 10,000 m on the ground, and σ_y was determined. The σ_z values appropriate to diffusion from the elevated source to the ground could then be computed from Eq. 4.6 when σ_z and σ_y are interchanged. Apparently, simultaneous crosswind and vertical surveys were not attempted or were inadequate for the determination of σ_y and σ_z at the same time. The diffusion coefficients C_y and C_z derived by Stewart et al. from the measured σ_y and σ_z values (Table 4.4) are appropriate for a 40-min sampling time. Average values of σ_z are presented in Fig. 4.5.

The values for C_y and C_z in Table 4.4 were computed with the assumption that $n = 0.25$ for all conditions. The decrease of the diffusion coefficients with distance is attributed to the dying out of the mechanical turbulence downwind of the buildings, and Stewart et al. deduced that a value of $n = 0.16$ is appropriate for both C_y and C_z over the open country surrounding the BEPO installation. The decrease of C_y with distance in Table 4.4 is not surprising, but the relatively large values of C_z compared to computed values of C_y from elevated sampling, even during stable conditions, is contrary to experience at most sites. Stewart et al. ascribe these high C_z values to the mode of discharge of the ^{41}Ar from the stack. The effluent was measured to rise about 80 to 135 m above the stack with an inverse relation between effective stack height and wind speed.

The strong tendency for elevated plumes to remain aloft for large distances during stable conditions suggested by the studies at Hanford, Wash., was also found at Harwell. No area of ground-level ^{41}Ar concentration was found within 10,000 m of the stack during any of the six surveys under inversion conditions. The inversion plume rode above the region dominated by the building turbulence and undoubtedly experienced largely laminar flow instead of the vertical turbulence measured near the stack.

The average measured ground-level axial air concentrations for all the runs are shown in Fig. 4.2 for the Harwell and Idaho sites. The effect of different stack heights on $\bar{\chi}_{max.}$ and $d_{max.}$ is evident and in accord with theory. For instance, from Sutton equations assuming similar diffusion coefficients for both sites, one can derive the relations

$$\frac{\bar{\chi}_{max.,2}}{\bar{\chi}_{max.,1}} = \left(\frac{h_1}{h_2}\right)^2 \tag{4.7}$$

and

$$\frac{d_{max.,1}}{d_{max.,2}} = \left(\frac{h_1}{h_2}\right)^{2/2-n} \tag{4.8}$$

Table 4.4— EXPERIMENTAL DIFFUSION COEFFICIENTS*

Type of survey	Meteorological conditions	Sampling range, m	C_y		C_z	
			Computed	Measured	Measured	Computed
Vertical	Unstable	150 to 1000	0.16		0.27	
	Adiabatic		0.10		0.22	
	Stable		0.10		0.12	
Ground	Adiabatic	590 to 620		0.46		
	and	880 to 1050		0.28		0.32
	unstable	1200		0.33		
Ground	Adiabatic	2400 to 2800		0.26		
	and					
	unstable	6000 to 9700		0.18		0.19
Ground	Stable	1000 to 10,000				<0.04

*From N. G. Stewart, H. J. Gale, and R. N. Crooks, The Atmospheric Diffusion of Gases Discharged from the Chimney of the Harwell Reactor BEPO, *Intern. J. Air Pollution*, 1(1-2): 93 (1954).

The ratio of stack heights squared is $(61/46)^2 = 1.8$; $\bar{\chi}_{max.,2}/\bar{\chi}_{max.,1}$ from Fig. 4.2 is 2.8. If $n = 0.25$, $d_{max.,1}/d_{max.,2} = (61/46)^{1.14} = 1.4$, which is nearly the same as the measured value of this ratio from Fig. 4.2. Allowances for the effective stack height of the BEPO plume would improve the agreement.

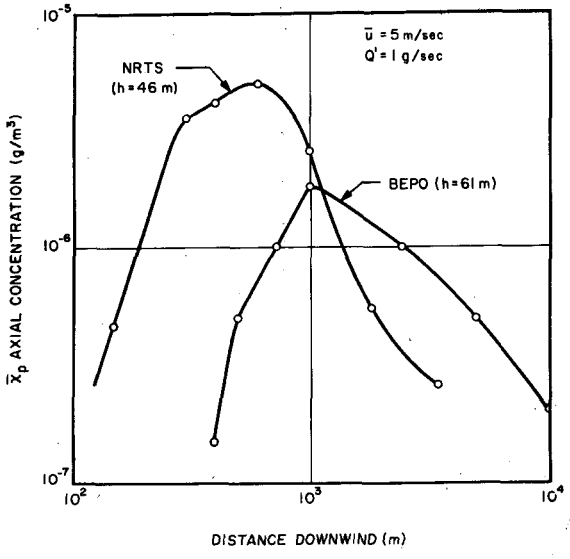

Fig. 4.2—Comparison of average normalized ground-level axial air-concentration measurements from elevated-source experiments conducted at Harwell (BEPO) and at the National Reactor Testing Station (NRTS).

4-4.1.5 Brookhaven National Laboratory, New York. Figures 4.3 and 4.4 summarize the results of atmospheric diffusion experiments conducted over a period of 15 years at the Brookhaven National Laboratory. The Brookhaven site is situated in central Long Island, N. Y., a region characterized by terrain rising to no more than 100 m above sea level with most relief being less than 50 m. The ground cover consists of alternating open fields and areas of scrub oak and pine extending to 10 m. A 130-m meteorological tower is instrumented with Aerovane and temperature instruments boomed toward the west-southwest.

The diffusion trials at this site can be divided into three groups: surface-release (2 m) diffusion–deposition tests to distances of about 100 m (Raynor and Smith, 1964), a series of elevated-source (110 m) diffusion experiments between 1949 and 1956 using oil fog (Smith, 1956), and aircraft sampling of the plume released from the Brookhaven reactor.

The data from the diffusion–deposition experiments are based on releases of irradiated ^{64}Cu particles, carefully elutriated to achieve a single size range. These particles and a solu-

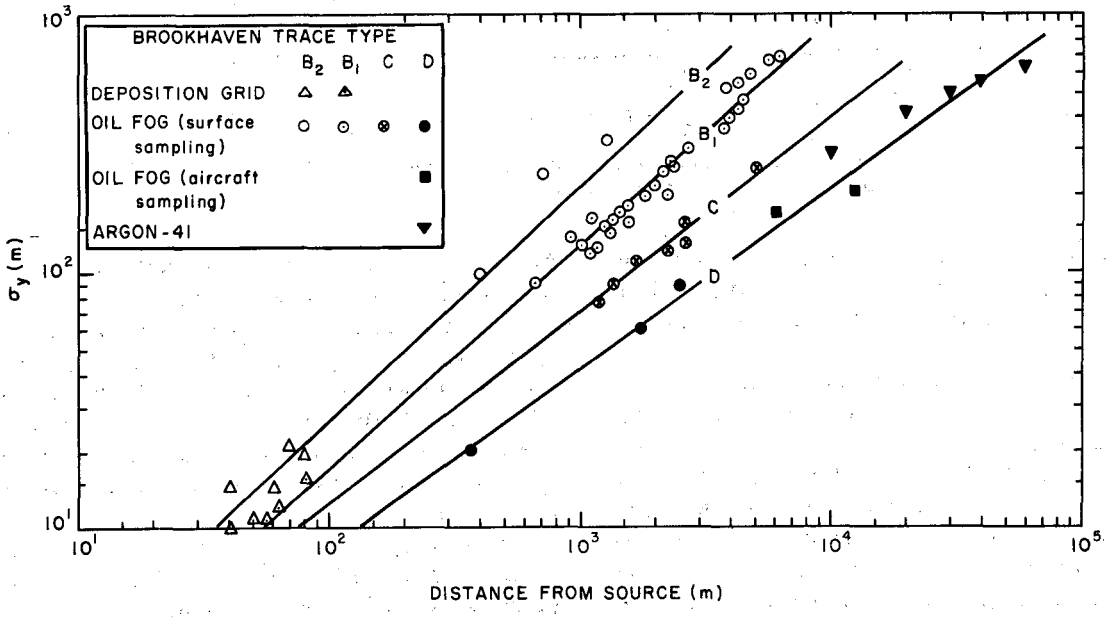

Fig. 4.3—Values of σ_y measured at the Brookhaven National Laboratory in a variety of continuous-source experiments. The trace types are based on the appearance of the wind records collected on the Brookhaven tower (See Sec. 4-4.1.5).

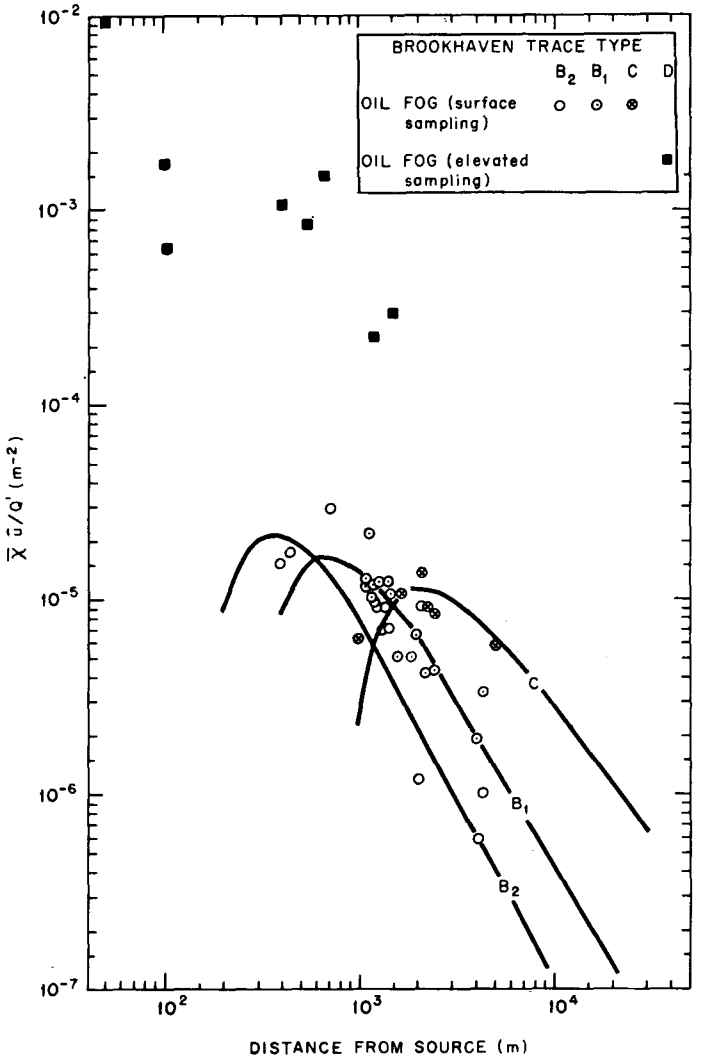

Fig. 4.4—Normalized concentration data from elevated oil fog releases at 110 m on the Brookhaven tower.

tion of uranin dye were sprayed from two separate nozzles over a 100-m square grid instrumented with 100 primary and 92 secondary samplers.

The oil fog experiments were generally conducted during daytime conditions when the existing turbulence was sufficient to carry the plume to the surface. The Brookhaven type D (stable) data in Fig. 4.4 were plume-center measurements made from an aircraft traversing the plume. The oil fog was measured by two different techniques. Photometric densitometers, operating on the principle of the 90-degree scattering of visible light, were used for continuous measurements at ground level. No more than three densitometers were in operation simultaneously in any of the experiments. A second method requiring a membrane filter was also used. This method permits measurements to be made at a large number of points but gives no indication of short-term variation in the concentration levels. Both systems were calibrated independently and against each other.

The two types of measurement systems were used in three different ways. The densitometers were used to provide continuous concentration data at a fixed point at times ranging from a few minutes to several hours. These data were used to obtain peak-to-mean values.

The densitometers were also transported crossplume to obtain ground-level concentration-distribution patterns. The third method consisted of mounting 10 or more filter samplers in a crossplume direction to obtain plume-width statistics.

The appropriately marked σ_y values in Fig. 4.3 were obtained during aircraft measurements of the ^{41}Ar in the reactor plume. The data were obtained during temperature inversions by equipping a light aircraft with dual Geiger-tube detectors mounted under the wings. The detectors were identical except that one permitted free passage of air through an aluminum shield container and the other did not. Thus the former detector responded to both gamma and beta radiation from the ^{41}Ar, whereas the latter was effectively shielded against beta radiation. Individual disintegrations as detected by the Geiger tubes were recorded on a stereo tape recorder.

The σ_y data in Fig. 4.3 are stratified by the Brookhaven gustiness types. These types are subjective estimates of the lateral intensity of turbulence determined from analogue wind-direction recordings. The trace types have been found to correspond in the mean to the values of σ_θ given in Table 4.5. No σ_θ value is given for type A since the wind direction as defined in this case is too variable for the computation of this statistic. Using the σ_θ values corresponding to the trace types, one can see in the σ_y summary diagram (Fig. 4.21) that the Brookhaven values fit the other data very well.

The $\bar{\chi}\bar{u}/Q'$ data points presented in Fig. 4.4 were fitted by the values of the Sutton diffusion coefficients given in Table 4.6.

4-4.1.6 Tennessee Valley Authority, Colbert, Alabama. During the period 1957 to 1962, the Tennessee Valley Authority under the sponsorship of the Public Health Service conducted a diffusion research project at the Colbert coal-fired generating station in extreme northwestern Alabama (Gartrell et al., 1964).

The Colbert plant has four 200-Mw units each served by a 100-m stack. Stack diameter is 5 m, flue-gas exit velocity is 14 m/sec, and gas temperature at exit is about 145°C.

Sampling was accomplished by helicopter-mounted instrumentation including a portable Titrilog and recorder for measuring SO_2 concentrations, temperature probes, an altimeter, and an air-speed indicator. The sampling procedure consisted of flights perpendicular to the plume axis at distances from 0.8 to 16.0 km from the source during stable conditions and from 0.8 to 3.2 km during neutral conditions. A sufficient number of traverses were made at different altitudes at each distance from the source to ensure a complete sample of the width and depth of the plume. The lateral standard deviation of the concentration distribution as well as the peak concentration was obtained from the pass showing the highest concentration. The vertical standard deviations at each distance from the source were obtained from all passes at that distance. The plume statistics derived by this method of sampling are representative of a sampling time of a few minutes at the most. The measurements of the releases from the four Colbert stacks were adjusted by Gartrell et al. to approximate a point-source (single-stack) release.

Representative values of the plume measurements σ_z and $\bar{\chi}_p\bar{u}/Q'$ are plotted in Figs. 4.5 and 4.6, respectively. During very stable conditions the σ_z values show no increase with distance. This observation, identical to the Hanford experience, reflects the almost complete lack of vertical turbulence during such conditions. The initial rather large values of σ_z are probably caused by strong vertical mixing

Table 4.5—VALUES OF σ_θ AND $\bar{u}$ CORRESPONDING TO THE BROOKHAVEN TRACE TYPES*

Trace type	σ_θ, deg	$\bar{u}$, m/sec
A		2
B_2	20	3
B_1	13	7
C	7	13
D	4	5

*Values were derived from wind measurements at 355 ft made with a 1-hr sampling time and a 6-sec averaging interval.

Table 4.6—VALUES OF SUTTON DIFFUSION COEFFICIENTS DETERMINED FROM BROOKHAVEN EXPERIMENTS

Trace type	n	C_y	C_z
B_2	0.15	0.48	0.50
B_1	0.26	0.44	0.38
C	0.48	0.54	0.32
D	0.57	0.41	<0.08

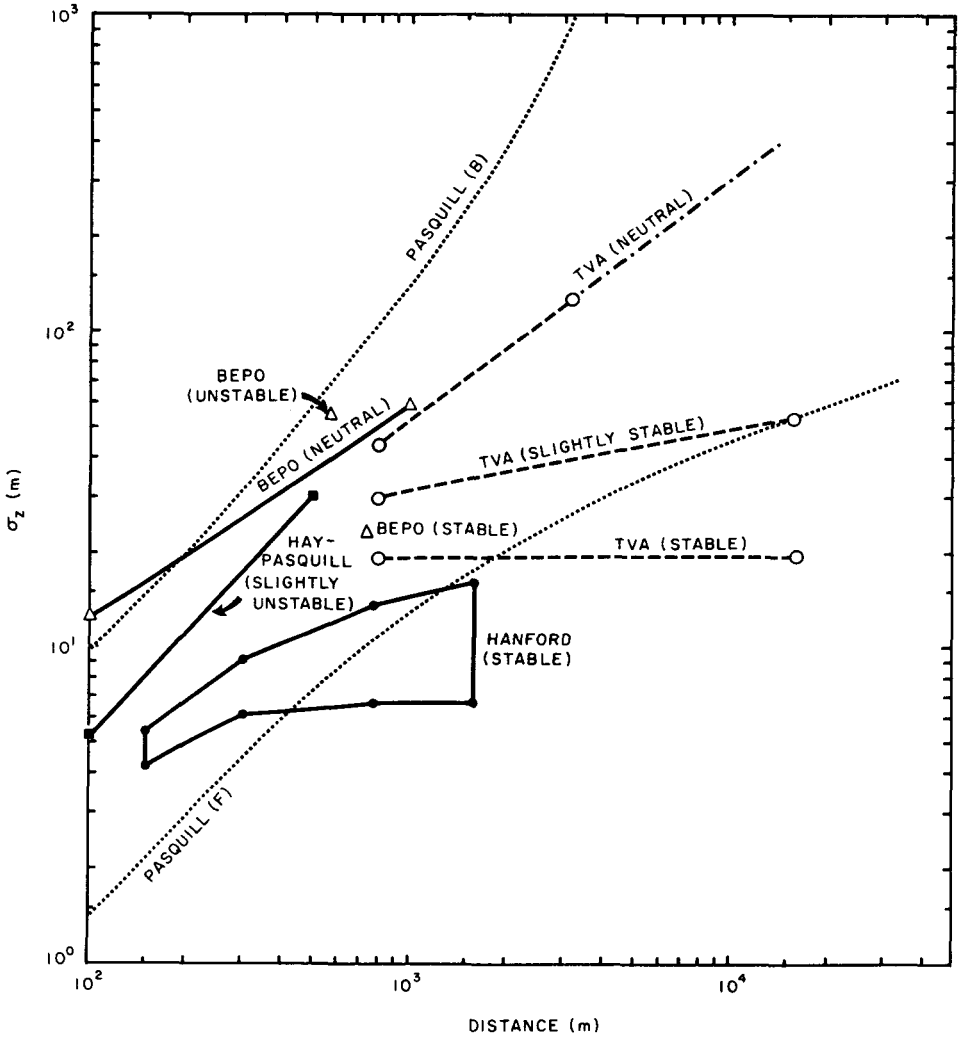

Fig. 4.5—Summary diagram for measurements of σ_z, the standard deviation of the vertical material distribution in continuously maintained plumes from elevated point sources. The dotted lines represent the Pasquill estimates discussed in the text (Sec. 4-3).

as the hot plume is ejected from the stack. The slightly stable and neutral σ_z values have slopes that seem consistent with other data from elevated releases. The values of σ_y (not plotted) are curious in one respect. Although the rate of increase of σ_y with distance for neutral conditions is only slightly less than that observed in other experiments, the stable values show a considerably smaller slope (i.e., 74 m at a distance of 0.8 km and 247 m at 16.0 km).

The values of normalized center-line concentration are shown in Fig. 4.6. The similarity of the three TVA values plotted at 0.8 km may, again, be due to the dispersive characteristics of the source configuration. The rather slow decrease of axial concentration with distance during the stable regimes is similar to observations at Hanford, and the neutral curve fits well with the other data.

4-4.1.7 Summary of Elevated Continuous-source Data. The elevated continuous-source data are summarized in Figs. 4.5 (σ_z) and 4.6 ($\bar{\chi}_p\bar{u}/Q'$). Where possible, the σ_y data measured in these experiments have been included in the σ_y summary diagram (Fig. 4.21).

The elevated-source σ_y data plotted in Fig. 4.21 agree quite well in slope and magnitude both with the surface σ_y data and with the

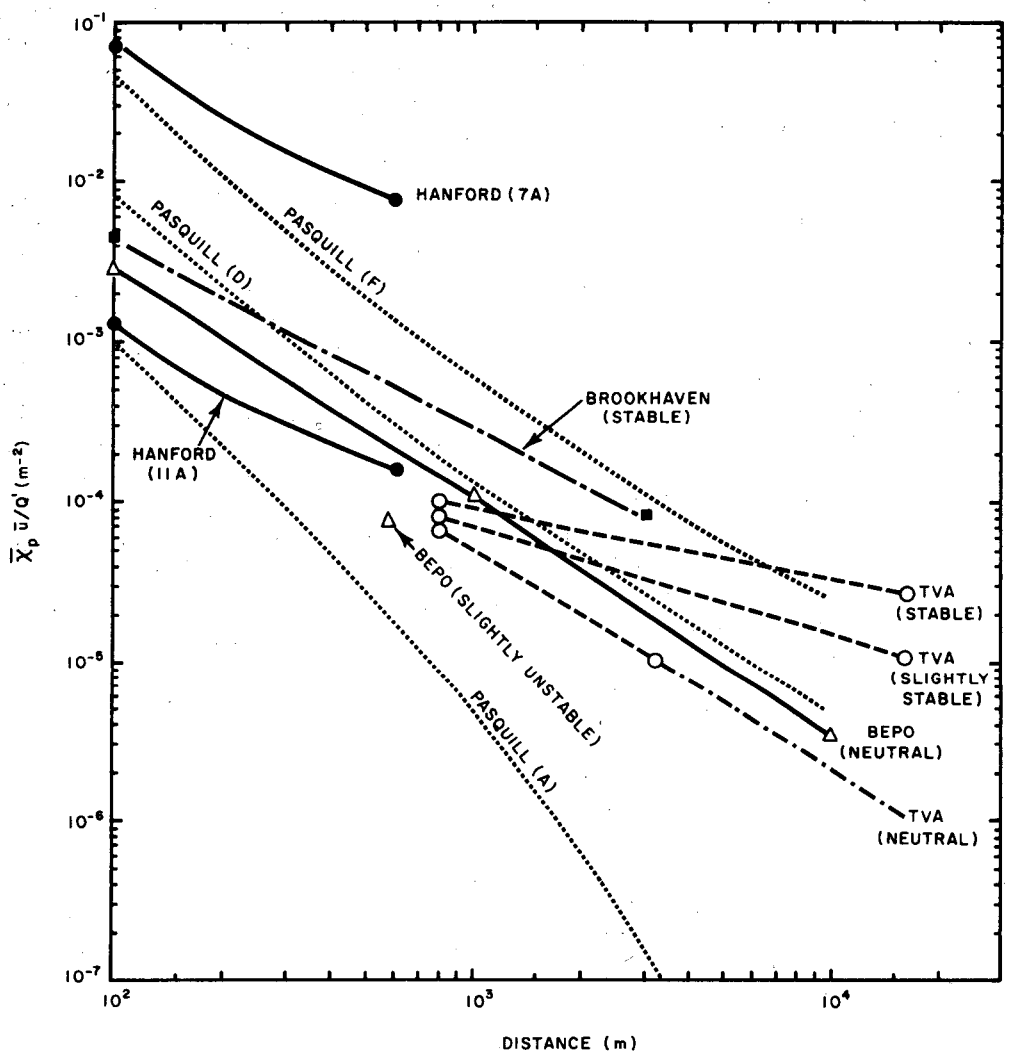

Fig. 4.6—Summary diagram for normalized axial-concentration measurements for elevated releases. The Pasquill estimates are shown as dotted lines.

generally held opinion that σ_y is approximately proportional to $x^{0.85}$.

The few measured values of σ_z in Fig. 4.5 do not show the consistency of the lateral data. The difficulty in vertical measurement and the effects of nonhomogeneity of wind characteristics in the vertical, particularly during stable conditions, work against the simple comparison of data taken under different conditions at different sites.

The most interesting feature of Fig. 4.5 is the apparent cessation of vertical plume growth during stable conditions. There is no way to compare the degree of stability between the Hanford and TVA experiments, but it appears from these experiments and from more subjective observation that vertical plume growth essentially ceases during strong inversions in the region above a few tens of meters over a rural area. The neutral curves from the Harwell and TVA experiments agree well with each other. The large values indicated at 100 m probably reflect the mode of emission from the large stacks.

The measured values of normalized concentration are presented in Fig. 4.6. The NRTS data did not include axial measurements and thus are not included. The most striking feature of Fig. 4.6 is the slow decrease of concentration with distance during stable condi-

tions when compared with the Pasquill curves. Again, the data representing warm jets from large stacks seem to show the effect of initial nonmeteorological dilution. The TVA (stable) and the Hanford (7A) curves indicate that the use of the Pasquill model might result in an underestimate of normalized axial concentration of an order of magnitude or more at distances of 10 km. The use of typical stable Sutton coefficients would similarly underestimate the measured data. It should be kept in mind, however, that wind speeds at typical stack heights during strong inversions will usually be considerably higher than those measured near the surface.

4-4.2 Continuous Surface Releases

The term "surface release" has been used to classify those experiments in which the height of release was within a few meters of the surface. More detailed diffusion data are available from continuous-source surface experiments than from any other type. Measurements of vertical distribution are noticeably lacking although effective vertical distribution data may be estimated from the excellent and copious measurements of the lateral spread and center-line (peak) concentration if an estimate of the deposition can be made.

A number of problems arise during surface-release experiments. During unstable (daytime) conditions the emitted plume disperses rapidly with distance from the source. Therefore measurement of tracer concentrations at the longer distances is difficult. Furthermore, the rapid vertical spreading rules out tower measurements of the vertical distribution of the tracer except at distances on the order of only a few hundred meters. Vertical distributions have been measured by aircraft- or tethered-balloon-borne sensors in such cases. However, the aircraft measurements, which are logistically the most flexible, provide only an instantaneous slice across the plume. Moreover, during extreme instability, such as might occur over a desert in summer, convective cells of sizes near the range of the total plume length can result in significant departures from the assumed state of turbulent homogeneity and thus preclude simple relations between turbulence information and concurrent diffusion.

During moderate instability the atmosphere is usually well mixed over reasonably regular terrain. Diffusion experiments conducted under such conditions usually provide regular and reproducible patterns.

A variety of important effects must be considered when estimates of diffusion during stable situations are studied. As noted in Chap. 2, Sec. 2-6.1, the mean horizontal wind vector shows a decided shear in the lower levels of the atmosphere during inversions. Furthermore, the horizontal wind-fluctuation characteristics vary considerably with sampling time (Smith and Abbott, 1961) and also with height (Chap. 2, Sec. 2-6.3). The effect of steady-state shear on diffusion has been discussed by Barad and Fuquay (1962). The problem of the various possible vertical configurations of horizontal wind fluctuations and their effect on diffusion near the surface has rarely been treated in a systematic way. During a strong surface-based nocturnal inversion, the horizontal wind fluctuations above 100 m, or even less, will be small, with the wind direction frequently appearing as an almost laminar trace on conventional wind-recording equipment. At the surface, however, wind fluctuations ranging from those which give a 10-min σ_θ value of a few degrees to those which touch momentarily at every point of the compass are possible. This variety of wind-fluctuation values and their vertical gradients are reflected in a wide range of possible center-line concentration values.

A final feature of diffusion from surface sources during stable conditions is the rather large rates of aerosol deposition or active-gas adsorption that are possible. Since much of the material released from a surface source will remain within the region of the surface-roughness elements, the opportunity for plume depletion is large. This depletion lowers the downstream concentration values from those computed on the basis of turbulent diffusion and further modifies the shape of the vertical distribution of the effluent.

For the reasons discussed above, it is likely that a definitive surface-source stable-atmosphere diffusion experiment has yet to be accomplished.

4-4.2.1 O'Neill, Nebraska (Project Prairie Grass), and Round Hill Field Station, Massachusetts. Project Prairie Grass, a comprehensive turbulence and diffusion research project, was carried out

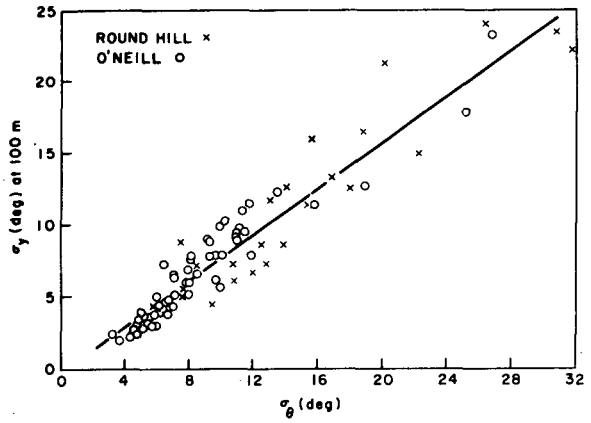

Fig. 4.7—The relation between plume width at 100 m and the standard deviation of the azimuthal wind direction. The data include both day and night experiments, and the regression line applies to both. (From Cramer, 1957.)

during the summer of 1956 over a large flat field in the Great Plains. A complete description of the experimental details and tabulations of diffusion and meteorological data has been presented (Barad, 1958, and Haugen, 1959). Numerous papers based on these measurements have been written (notably, Cramer, 1957, and Barad and Haugen, 1959). Cramer related the diffusion data taken during the experiments to the concurrent wind-fluctuation measurements (Table 4.2) and also summarized the results of a similar, although more limited, series of tests conducted at the Round Hill field station of the Massachusetts Institute of Technology.

The two studies present diffusion data for 90 field experiments: about 70 at the O'Neill site and 20 at the Round Hill station. Diffusion measurements at O'Neill were determined from sulfur dioxide gas released at 46 cm above the surface and sampled along semicircular arcs at from 50 m to 800 m from the source. The gas collectors were placed at a height of 1.5 m above the surface and were located along the arcs at 1- or 2-deg intervals. In addition, the vertical concentration distribution was available from six 20-m towers mounted along the 100-m arc. The tracer was released for 10 min in each experiment, sampling beginning prior to the arrival of the tracer at the first arc and ending after the last of the material had passed the last arc. The actual measurement was of exposure, but the authors assumed that the difference between the exposure and the average concentration computed for a 10-min sampling time was small and chose to use the concentration in their discussions. Similar measurements were made at the Round Hill site at arcs located 50 m, 100 m, and 200 m from the source. Here a continuous plume was sampled for 10 min. Meteorological measurements at both sites included the mean wind speed, the azimuth wind direction determined at a height of 2 m near the gas source, and vertical profiles of the mean wind speed and temperature. The O'Neill site is unusually smooth (z_0 less than 1.0 cm) with an unobstructed upwind fetch of at least 1.0 km. The Round Hill site is considerably rougher (z_0 greater than 10 cm) with roughness elements in the form of trees and small buildings. Differences in elevation on the order of 30 m were found within the first 0.5 to 1.0 km upwind from the test area.

The crux of Cramer's thesis is presented in Fig. 4.7. Of immediate interest is the very close dependence of plume width on σ_θ over the entire range of conditions sampled for the two dissimilar sites. This dependence of plume spreading on wind fluctuation is an interesting contrast to the fact that the value of σ_θ for neutral conditions at the rough site (Round Hill) is twice that at the smoother site (O'Neill).

Having established the relation between horizontal plume spreading and the horizontal wind-direction fluctuations, Cramer then investigated the distance dependency of σ_y, σ_z, and concentration (Cramer et al., 1964). These data are reproduced in Table 4.7 where p and q are the

Table 4.7—DISTANCE DEPENDENCY OF DIFFUSION COEFFICIENTS BASED ON PROJECT PRAIRIE GRASS DATA* IN WHICH $\sigma_y = \sigma_\theta x^p$ AND $\sigma_z = \sigma_\theta x^q$

σ_θ, deg	p (200 to 800 m)†	q (50 to 800 m)†
3	0.45	0.86
4	0.56	0.86
5	0.64	0.88
6	0.71	0.91
7	0.80	0.96
8	0.85	1.13
10	0.85	1.29
12	0.85	1.55
20	0.85	1.74
25	0.85	1.89

*From Cramer et al., 1964.

†Distance interval on which the estimates are based.

exponents noted in Table 4.2. Cramer relates all his diffusion data to σ_θ and makes no use of the collected vertical-fluctuation data except to show the quasi-dependence between the vertical and horizontal fluctuations. The distance dependency of normalized concentration and plume width for 46 of the O'Neill tests is shown in Figs. 4.8 and 4.9, where the data in each

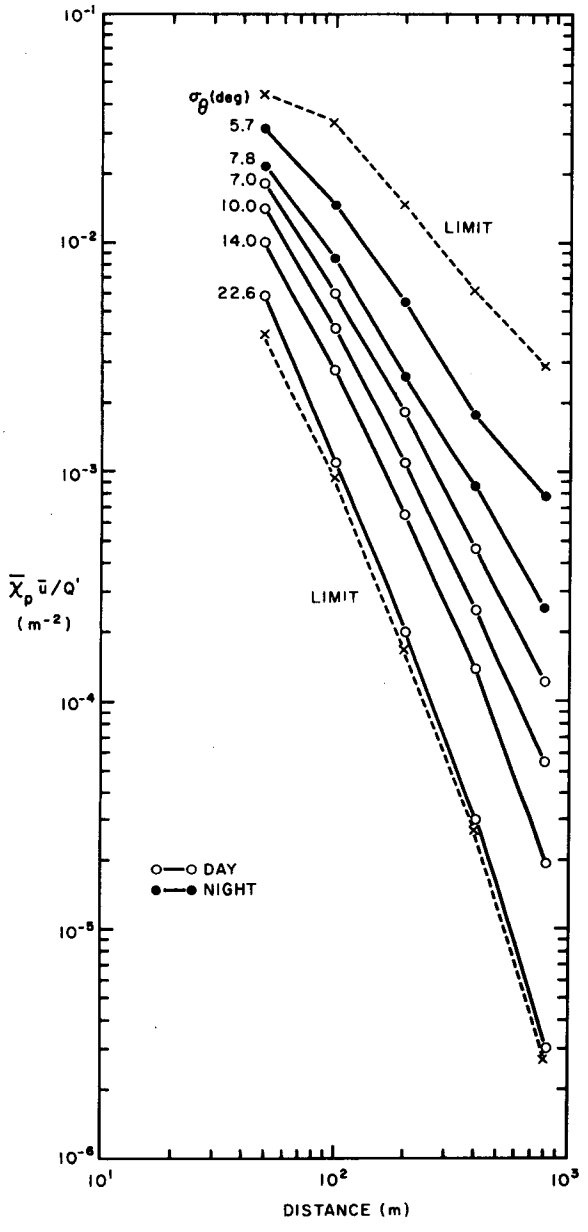

Fig. 4.8 — Normalized axial concentration measurements from the Prairie Grass experiments. The σ_θ values are averages for various groups of observed plume-spread data.

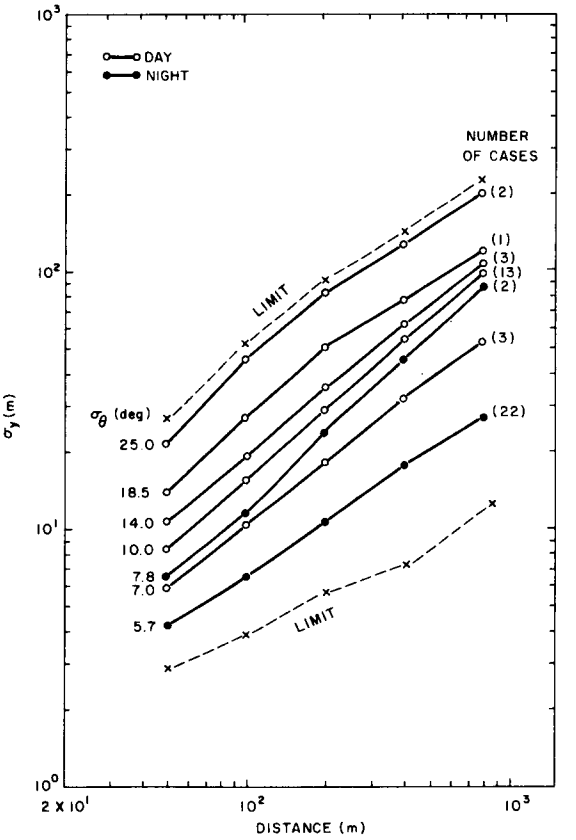

Fig. 4.9 — Measured values of σ_y observed during the Prairie Grass experiments and stratified by average σ_θ values.

diagram are indexed by σ_θ values. The scatter that may be expected about these averaged curves is discussed in Sec. 4.6.

Barad and Haugen (1959) showed that the slopes of the σ_y and σ_z curves with x could not be obtained from the wind profiles, one of the fundamental claims of the original Sutton theory. There has already been a growing tendency to recognize this in practical problems. In addition, they showed that $n_y \neq n_z$ in many cases, and thus the use of four adjustable diffusion parameters is required for an adequate fit of measured diffusion data to a Sutton type equation, i.e., C_y, C_z, n_y, and n_z.

4-4.2.2 Hanford, Washington (Project Green Glow-30 Series). During the period 1959–1962, a series of 66 diffusion experiments was carried out at Hanford, Wash. The results of analyses of 46 tests have been reported by Fuquay, Simpson, and Hinds (1964). Details of the early experiments in this series, as well as tabulations of

diffusion and meteorological data, have been described by Barad and Fuquay (1962). Other publications based on these experiments include discussions of tracer-deposition characteristics and computations of vertical diffusion (Simpson, 1961), the area contained within specified isopleths and tracer travel time (Elliot, Engelmann, and Nickola, 1961), diffusion during conditions of shear flow (Barad and Fuquay, 1962a), and other general descriptions of the experimental results (Fuquay, Simpson, Barad, and Taylor, 1963).

The fluorescent tracer, zinc sulfide, was sampled at 833 locations on arcs at 200, 800, 1600, 3200, 12,800, and 25,600 m from a source 1.5 m above the ground. The last two arcs were not operated during 26 of the 46 experiments analyzed. Drum samplers at the last two arcs were used to obtain the time of arrival of the tracer at these distances.

Vertical diffusion to heights of 62 m was measured at the first four arcs by five towers on each arc. Spaced 8 deg apart, each tower supported 15 samplers. The test site was quite flat to gently rolling with sagebrush cover some 1 to 2 m high. The tracer with water as a carrier was released for 30-min periods through two fog generators. The field samplers were in operation well before and after the passage of the tracer cloud, thus providing measures of exposure rather than average concentration. The fluorescent particles were collected on filters, and their total mass was determined by a technique that involved irradiating the particles with an alpha-emitting isotope and counting the scintillations with an automatic electronic counter.

The analysis techniques used on this project differed somewhat from those of other experiments. Although plume-spread data are commonly evaluated in terms of distance from the source, the data from these experiments are related to time of travel from the source. Fuquay et al. felt that this was closer to the concepts originally introduced by Taylor. The lateral spread of the plume was related to the

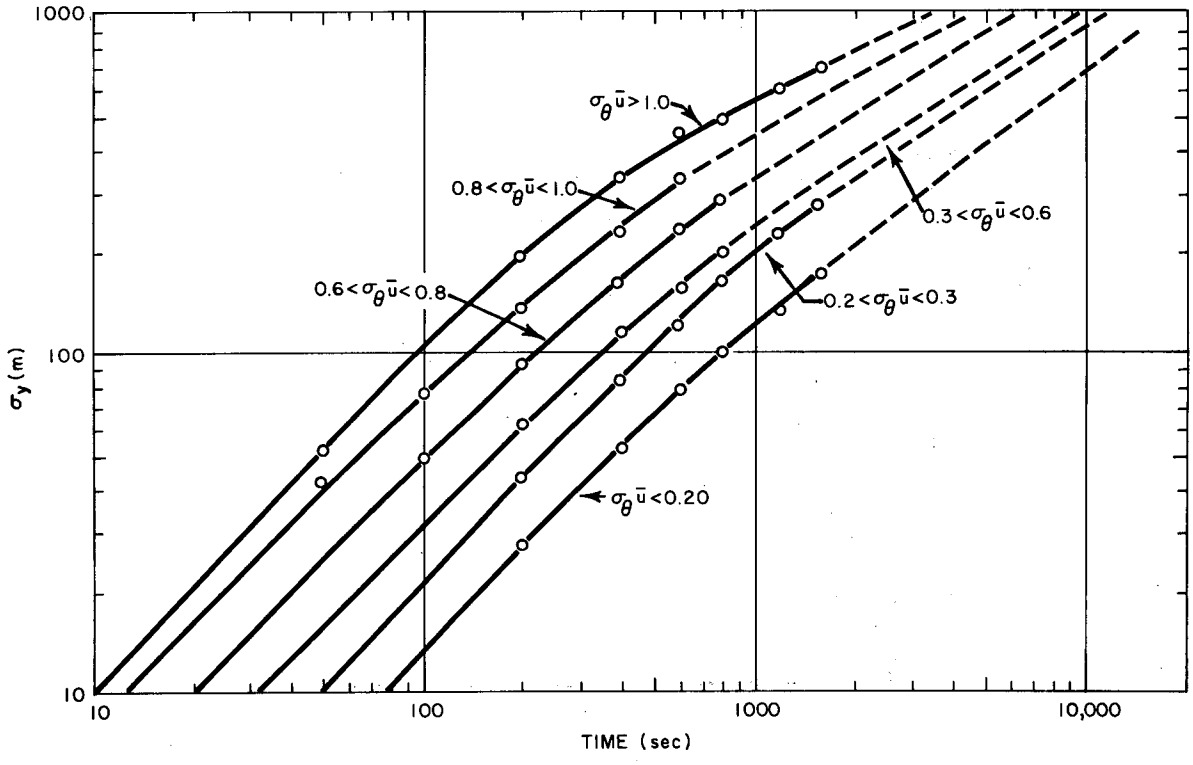

Fig. 4.10 — σ_y vs. travel time for various values of $\sigma_\theta \bar{u}$ based on the Green Glow and 30 series experiments. Solid lines are based on measured data and dashed lines are suggested extrapolations. (From Fuquay, Simpson, and Hinds, 1964.)

value of $\sigma_\theta \bar{u}$ (σ_θ being computed from wind records of 30-min duration with a 20-sec averaging interval). Measurements of the lateral spread of the plume, when expressed in terms of distance from the source rather than time of travel and stratified by values of σ_θ, agree with other data on lateral spreading from sources near the ground. These data are presented in Fig. 4.21.

Figure 4.10 presents observed values of σ_y for various classes of $\sigma_\theta \bar{u}$ as a function of travel time. The data indicate that the slopes for short times of travel are about unity but become smaller as the travel time increases. A slope of 0.5 appears likely at large travel times and corresponds to that deduced by Taylor from theoretical considerations. The dashed lines are speculative estimates of σ_y for large values of travel time. The data imply a convergence of the curves at some large travel time.

Figure 4.11 is a different representation of the growth–travel time relation. The irregular curvature in the region $0.25 < \sigma_\theta \bar{u} < 0.50$ separates the curves into two sets: one converging at $\sigma_y = \sigma_\theta \bar{u} = 0$ and the other set converging at negative values of these quantities. This irregularity is believed to be caused by differences in the wind-direction shear associated with $\sigma_\theta \bar{u}$. The greatest shear is observed during stable atmospheric conditions (i.e., large Richardson number), which, in turn, are associated with small values of $\sigma_\theta \bar{u}$. The shearing in stable atmospheres results in comparatively large values of the lateral spread, σ_y. At the travel times shown in Fig. 4.11, the plumes

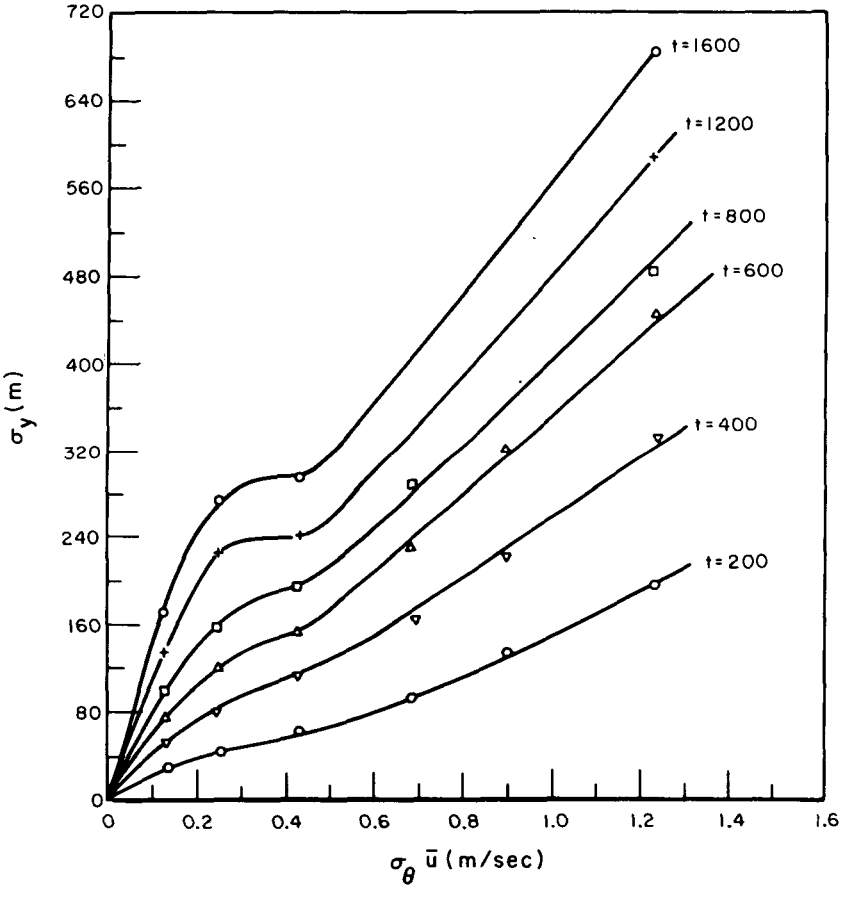

Fig. 4.11—σ_y vs. $\sigma_\theta \bar{u}$ for various travel times. The irregularity in the curves is believed to be due to wind shear during very stable conditions. (From Fuquay, Simpson, and Hinds, 1964.)

have usually spread upward so that this effect is amplified.

The observed normalized exposures are presented in Figs. 4.12 and 4.13. Curves representing the Pasquill moderately stable (F), neutral (D), and very unstable (A) conditions (with assumed typical wind speeds) have been entered for comparison and appear to bracket the observed data although there is the suggestion that, at travel times beyond 1000 sec, the observed data show a more rapid decrease with travel time than do the Pasquill curves.

Simpson (1961) computed by material balance methods rather large losses of tracer due to deposition within 3200 m of the source. These losses amounted to as much as 90% of the source for one test. The effect of deposition upon the air concentration is shown in Fig.

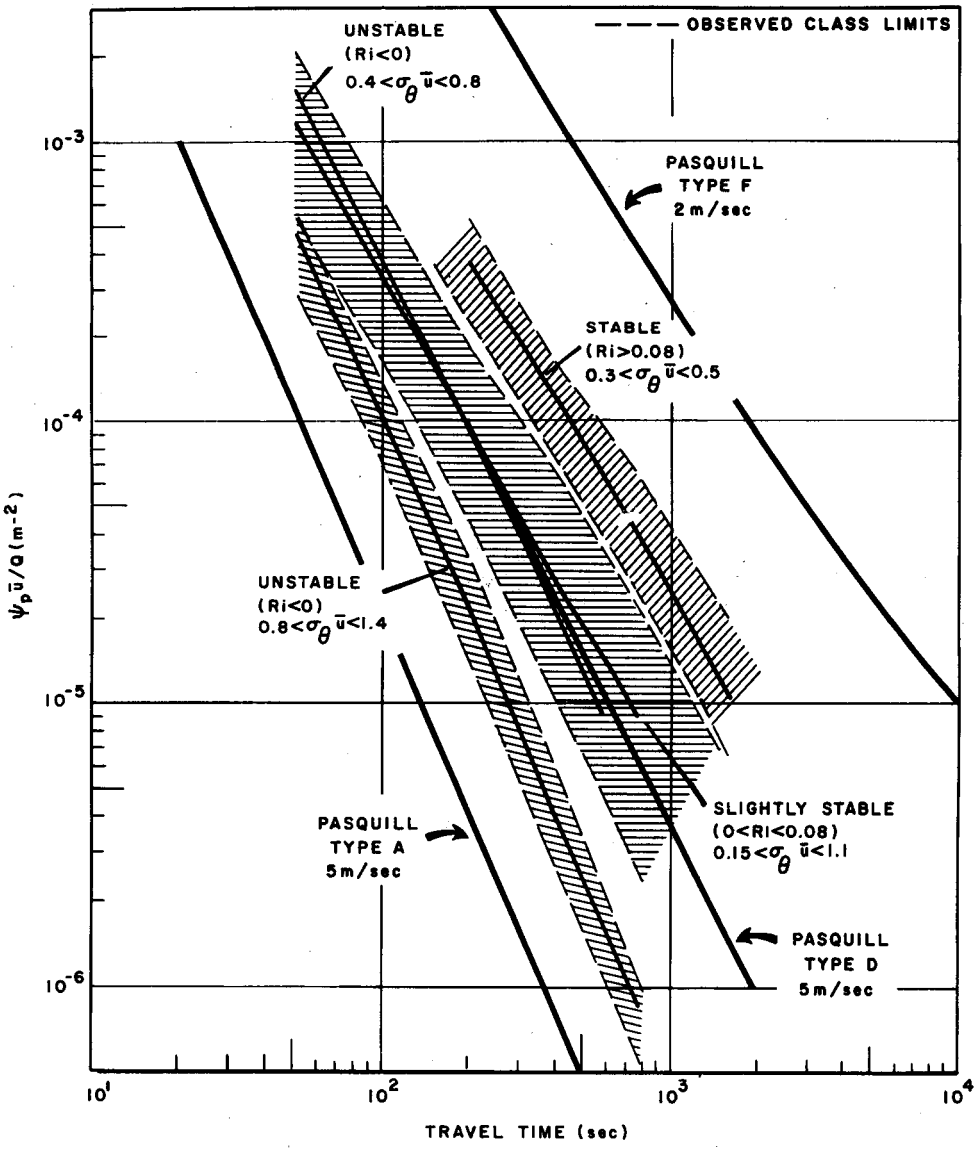

Fig. 4.12—Normalized exposure values as determined during the Green Glow and 30 series experiments. The data are presented in terms of travel time and are arranged according to observed values of Richardson number and $\sigma_\theta \bar{u}$. The Pasquill curves for typical conditions have been entered for comparison. (From Fuquay, Simpson, and Hinds, 1964.)

4.14, which relates the total mass transport, Q_x, past a certain distance to the total released tracer, Q_0, for four runs during stable conditions.

In order to compute σ_z, the standard deviation of the vertical tracer distribution in the absence of deposition, Simpson used flux concepts and the measured vertical distributions at the various towers along with mass-transport data in an iterative procedure. The resulting σ_z curves are shown in Fig. 4.15 for various degrees of stability. The limited vertical diffusion during stable conditions, as well as the tendency for a nonpower law relation between σ_z and x, is immediately apparent, just as Hilst and Simpson (1958) measured for the elevated source. The σ_z values derived by Simpson from the Green Glow data are, however, somewhat smaller than those found by Hilst and Simpson in spite of the fact that the releases by the latter workers took place at 56 m above the surface. It would be expected that the smaller values of the vertical turbulence during inversions at this elevated level would result in

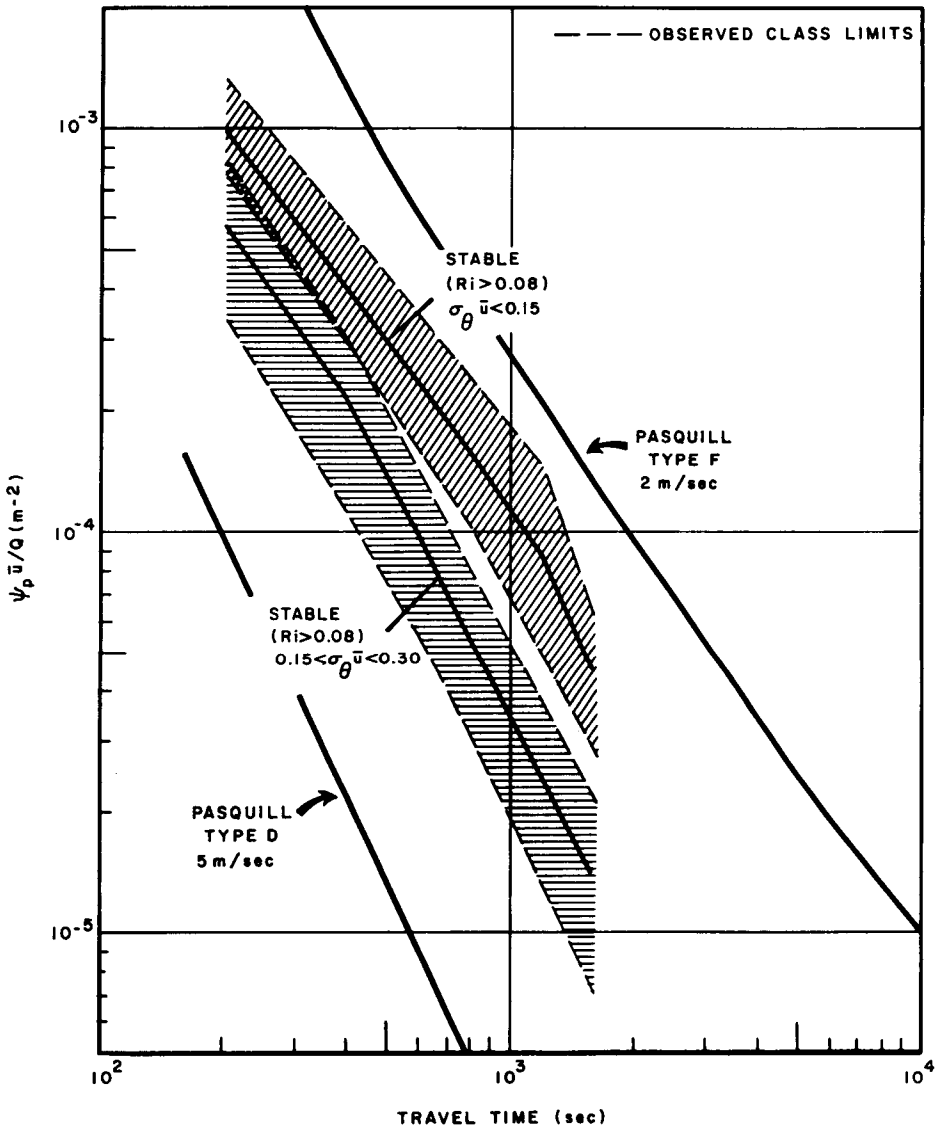

Fig. 4.13 — Similar to Fig. 4.12 but showing exposure values obtained during conditions of greater stability. (From Fuquay, Simpson, and Hinds, 1964.)

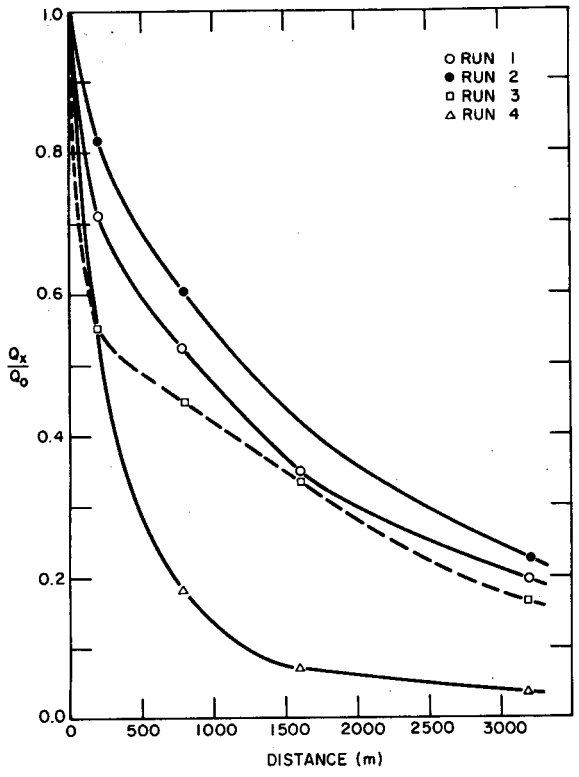

Fig. 4.14—Relative mass transport through vertical planes perpendicular to the average plume direction as observed during the Green Glow and 30 series tests. The decrease in the ratio Q_x/Q_0 indicates the extent of deposition processes operating during these four tracer releases. (From Simpson, 1961.)

smaller values of σ_z than would be found in releases near the surface.

Barad and Fuquay (1962a) discuss a diffusion model in which the tracer exposure at a point downwind from the source is given by the normal frequency function of two variables (the lateral and vertical coordinates of a point) and the correlation coefficient between the lateral and vertical coordinates of the tracer particles. The inclusion of the nonzero correlation coefficient results in elliptical isolines of exposure in the y–z plane which are inclined with respect to the horizontal. From inspection of the exposures received at towers mounted on the first four arcs of the grid, this model appeared to be a reasonable representation of the plume cross section during stable conditions when the plume is sheared by the clockwise turning of the wind with height (see Figs. 2 to 5, Barad and Fuquay, 1962a). Comparison of the total plume width or depth, as might be obtained from a vertical or lateral photograph of the plume, with the exposure-distribution standard deviations computed from the model and tower data indicates that the photographs might provide an overestimate of the plume dimensions and, thus, lead to a lower than actual exposure estimate.

Based on the experimental results of the Green Glow and 30 series and on experience

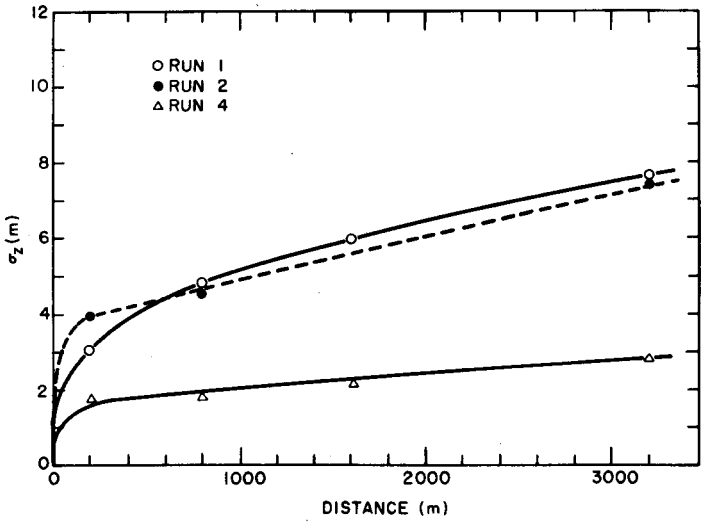

Fig. 4.15—Values of σ_z for three of the four tests shown in Fig. 4.14. These computed values are those expected in the absence of deposition. (From Simpson, 1961.)

and experiments of the last 20 years at the Hanford site, two forms of the bivariate normal model have been adopted to assess the consequences of releases to the atmosphere at this location. The Sutton formulations are used for unstable and neutral conditions, and the generalized Gaussian form is used for stable situations. Another deviation from general practice adopted at the Hanford location is the use of travel time rather than travel distance for organizing the diffusion data. Although these procedures have worked well at the Hanford site, caution should be observed before extrapolating this information to sites of different topography and wind regimes. A detailed description of the Hanford models is given in the following paragraphs.

In a stable atmosphere the exposure at ground level is determined from

$$\frac{\psi}{Q_0} = \frac{Q_x/Q_0}{\pi\sigma_y\sigma_z\bar{u}} \exp\left[-\left(\frac{y^2}{2\sigma_y^2} + \frac{h^2}{2\sigma_z^2}\right)\right] \qquad (4.9)$$

where $\bar{u}$ is the average wind speed at the height of emission, Q_0 is the total amount of material released, and Q_x is the apparent amount of material released as measured at a given downwind travel distance or travel time, i.e., the difference between the total amount of material released and the amount deposited on the surface between the source and the measurement point.

The value for σ_y in Eq. 4.9 is determined from

$$\sigma_y^2 = At - \frac{A^2}{2(\sigma_\theta\bar{u})^2}\left\{1 - \exp\left[-\frac{2(\sigma_\theta\bar{u})^2 t}{A}\right]\right\} \qquad (4.10)$$

where t is the travel time and A is a constant related to the scale of turbulence and is evaluated from the experimentally determined relation

$$A = 13.0 + 232\,\sigma_\theta\bar{u} \qquad (4.11)$$

Equations 4.10 and 4.11 are the relations used in constructing the smooth isopleths in Fig. 4.10.

The variance of the vertical distribution of exposure for stable conditions at the Hanford site is determined from

$$\sigma_z^2 = a[1 - \exp(-k^2t^2)] + bt \qquad (4.12)$$

where a, b, and k^2 are functions of the degree of stability. Values of these terms, derived for use at the Hanford site, are shown in Table 4.8.

Table 4.8—VALUES OF PARAMETERS USED AT HANFORD FOR DETERMINING THE VARIANCE OF THE VERTICAL DISTRIBUTION OF EXPOSURE

Parameter	Degree of stability	
	Moderate stability	Strong stability
a	97 m^2	34 m^2
b	0.33 m^2/sec	0.025 m^2/sec
k^2	2.5×10^{-4} sec^{-2}	8.8×10^{-4} sec^{-2}

During neutral and unstable conditions, the Sutton form of Eq. 4.9 is used:

$$\frac{\psi}{Q_0} = \frac{2Q_x/Q_0}{\pi C_y C_z \bar{u} x^{2-n}} \exp\left[-\frac{1}{x^{2-n}}\left(\frac{y^2}{C_y^2} + \frac{h^2}{C_z^2}\right)\right] \qquad (4.13)$$

The values of the Sutton parameters used at the Hanford site for unstable and neutral conditions are given in Table 4.9.

Table 4.9—VALUES OF SUTTON PARAMETERS USED AT HANFORD FOR UNSTABLE AND NEUTRAL CONDITIONS

Parameter	Release level	Wind speed, m/sec	Unstable	Neutral
C_y	Ground	1.0	0.35	0.21
		5.0	0.30	0.15
		10	0.28	0.14
	Elevated	1.0	0.30	0.15
		5.0	0.26	0.12
		10	0.24	0.11
C_z	Ground	1.0	0.35	0.17
		5.0	0.30	0.14
		10	0.28	0.13
	Elevated	1.0	0.30	0.15
		5.0	0.26	0.12
		10	0.24	0.11
n			0.20	0.25

The depletion factor, Q_x/Q_0, for use with depositing material is determined from the following equations for stable or neutral and unstable conditions, respectively:

$$\frac{Q_x}{Q_0} = \exp\left[-\left(\frac{2}{\pi}\right)^{1/2}\left(\frac{v_d}{\bar{u}_0}\right)\left(\frac{\bar{u}_0}{\bar{u}}\right)\bar{u} \times \int_0^t \frac{\exp(-h^2/2\sigma_z^2)}{\sigma_z}\,dt\right] \qquad (4.14)$$

$$\frac{Q_x}{Q_0} = \exp\left[-\frac{2}{C_z(\pi)^{1/2}}\left(\frac{v_d}{\bar{u}_0}\right)\left(\frac{\bar{u}_0}{\bar{u}}\right)\int_0^x x^{(n-2)/2} \times \exp\left(-\frac{h^2}{C_z^2 x^{2-n}}\right) dx\right] \quad (4.15)$$

where v_d is the deposition velocity, $\bar{u}_0$ is the wind speed at the surface, and $\bar{u}$ is the wind speed at the height of emission. The Hanford group have found it more practical to work with the ratio $v_d/\bar{u}_0$ and refer to this quantity as their deposition coefficient. Values of the deposition coefficient for very fine reactor particulates and for the halogens are presented in Table 4.10. This table also contains values of the wind-speed ratio, $\bar{u}_0/\bar{u}$. Interpolation of the shear factor for different levels can be accomplished by assuming either a logarithmic or power function relation for the wind profile.

Table 4.10—GROUND-DEPOSITION PARAMETERS USED AT HANFORD

Atmospheric conditions	Deposition coefficient ($v_d/\bar{u}_0$)		Wind-speed ratio ($\bar{u}_0/\bar{u}_{60m}$)
	Fine reactor particulates	Halogens	
Very stable	1.5×10^{-4}	2.4×10^{-3}	0.17
Moderately stable	2.2×10^{-4}	3.4×10^{-3}	0.35
Neutral	3.0×10^{-4}	4.6×10^{-3}	0.50
Unstable	6.0×10^{-4}	8.0×10^{-3}	0.70

Solutions for the deposition equations can be obtained with numerical techniques; so the entire system of equations can be programmed for any combinations of parameter values necessary. Solutions of this form permit the extensive calculations necessary for assessing the consequences of a broad variety of chemical or radioactive releases.

4-4.2.3 Cape Kennedy, Florida (Project Ocean Breeze), and Vandenberg Air Force Base, California (Project Dry Gulch). Field diffusion programs were conducted at Cape Kennedy, Fla. (Ocean Breeze), and Vandenberg Air Force Base, Calif. (Dry Gulch), during 1961 and 1962 (Haugen and Fuquay, 1963, and Haugen and Taylor, 1963). These programs were undertaken to establish quantitative prediction equations for use as safety tools at these missile-test ranges. The programs culminated at each range with the installation of an automatic computer-controlled meteorological-data acquisition and processing system. Tracer emissions were planned for periods of onshore flow which, at these seaside locations, were usually accompanied by daytime instability. In all, 76 experiments were carried out at Cape Kennedy and 109 at Vandenberg; not all, however, could be used in the analyses.

Zinc sulfide particles were released from ground-level sources for 30-min periods at both sites. The diffusion course at Cape Kennedy consisted of three concentric arcs 1.2, 2.4, and 4.8 km from the source. Samplers were positioned 1.5 and 4.5 m above the ground surface. The complexity of the terrain at Vandenberg led to sampling over two different courses. The first course, with samplers at arcs 2.3 and 5.7 km from the source, was oriented so that the flow from the source ascended in its path to the arcs. The other course consisted of three arcs at 0.85, 1.5, and 4.7 km with the radius connecting the midpoints of these arcs oriented approximately up a valley. Samplers were positioned at 1.5 m above the ground surface. The terrain at Cape Kennedy is fairly flat with thick vegetation extending to 5 m, whereas the Vandenberg site is quite rugged with elevations at the arcs varying by more than 60 m. Comprehensive supporting meteorological measurements were available at both sites. These measurements included σ_θ data for a variety of running averaging times and vertical temperature-difference data.

Early in the program the decision was made to develop a diffusion equation using statistical techniques, such as multiple regression analysis, rather than to work from physical principles. The technique involved combining half of the Prairie Grass, Ocean Breeze, and Dry Gulch diffusion data into one set and deriving the constants in a diffusion equation by machine analyses. The other half of the data from each of the three series could then be used to verify the predictions. The derived equation is

$$\frac{\bar{\chi}_p}{Q'} = 0.00211 x^{-1.96} \sigma_\theta^{-0.506} (\Delta T + 10)^{4.33} \quad (4.16)$$

where $\bar{\chi}_p/Q'$ = normalized peak concentration in sec/m^3

x = downwind travel distance in meters

σ_θ = standard deviation of azimuthal wind direction in degrees (15-sec running average over 30-min observational interval)

$\Delta T = T_{54ft} - T_{6ft}$

On the basis of tests with the independent data, this equation predicted 72% of the cases within a factor of 2 of the observed values and 97% within a factor of 4. Figure 4.16 is a graphical representation of the results based on this equation.

4-4.2.4 National Reactor Testing Station (NRTS), Idaho Falls, Idaho. A study of atmospheric diffusion and deposition from a surface source was reported by Islitzer and Dumbauld (1963). The grid was similar to that used in the elevated diffusion experiments except for the addition of five sampling towers 30 m high and 70 m apart installed at the 400-m arc to obtain mass-balance measurements for some releases. Direct measurements of deposition were also made at the 100- and 200-m arc on flat plates constructed to simulate a bare soil surface. The uranin dye tracer was released at a height of 1.0 m for 1-hr periods during a wide range of stability conditions.

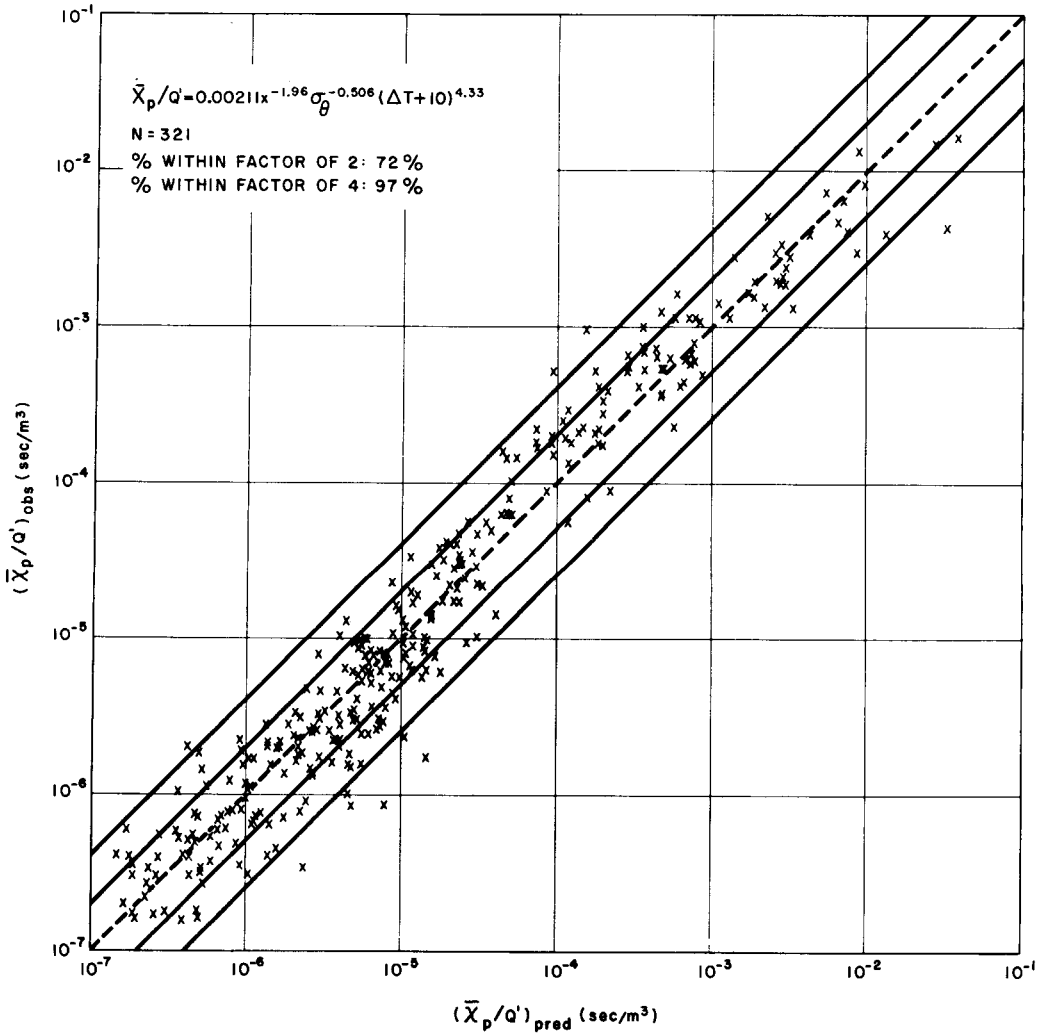

Fig. 4.16—Observed vs. predicted values of $\chi_p\bar{u}/Q'$ based on independent data from the Prairie Grass, Ocean Breeze, and Dry Gulch surface-diffusion experiments. (From Taylor, Nou, and Tucker, 1964.)

The measured lateral plume spreads during lapse conditions were related to the lateral wind-direction standard deviation for each measurement distance by an averaging time determined for $\beta = 5.0$, an experimentally determined average value. Measured vs. computed values of σ_y using the mean β factor are shown in Fig. 4.17 for lapse conditions.

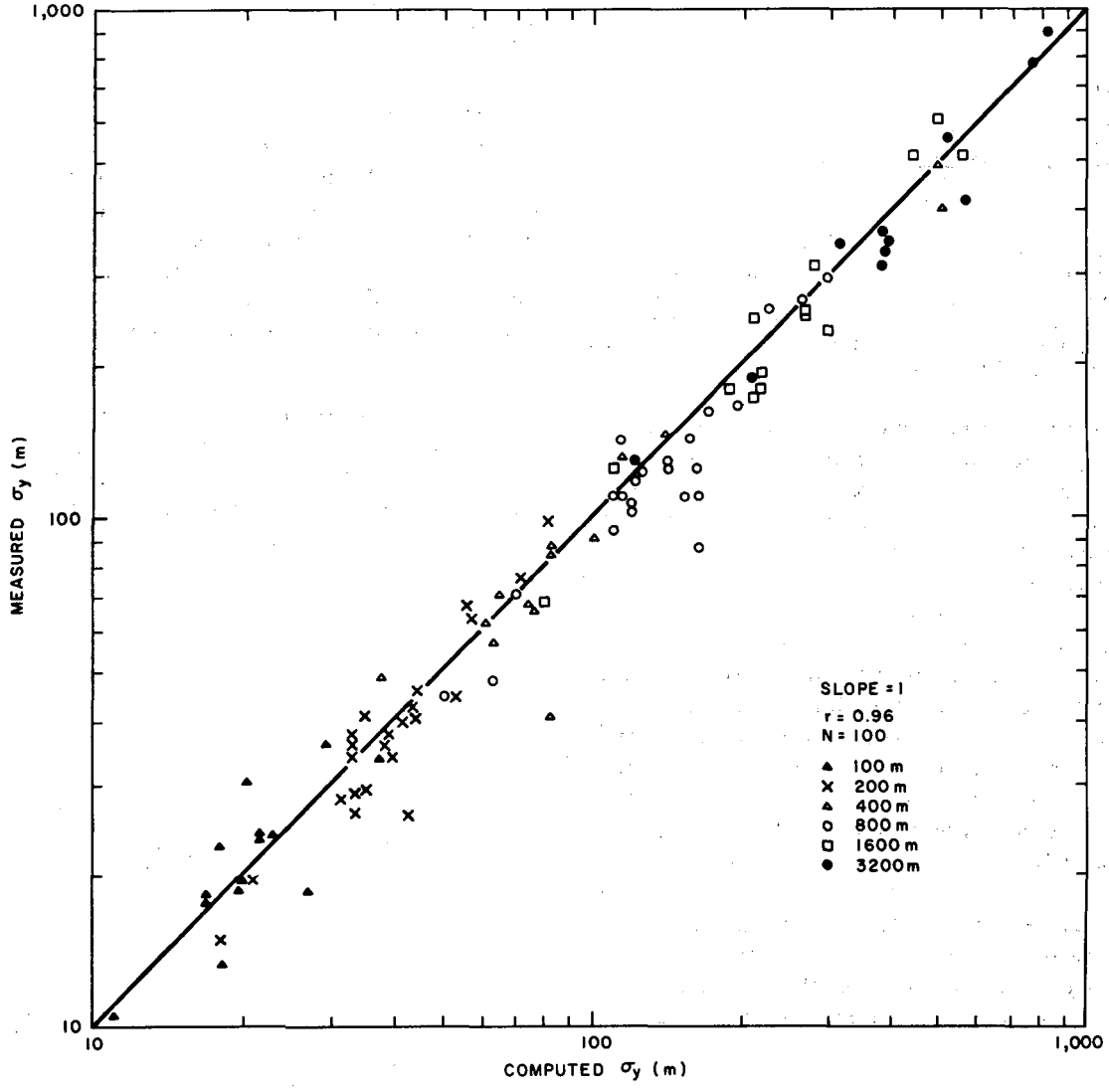

Fig. 4.17—Measured values of σ_y compared to those estimated from σ data computed with $\beta = 5.0$ during unstable conditions at the National Reactor Testing Station. (From Islitzer and Dumbauld, 1963.)

The prediction of lateral diffusion during stable conditions using a mean measured β was less successful. A 10-sec averaging time was found to give a better prediction of σ_y at all distances (Fig. 4.18).

Two different methods were used to compute σ_z from the vertical wind-direction fluctuations. These, together with the equations for σ_y, are shown in Table 4.11.

Lateral wind-direction standard deviations for 5.0-sec averaged data and 1.0-hr sampling times at 4.0 m above the surface are given in Table 4.12.

The normalized air-concentration measurements along the mean plume axis are shown in Figs. 4.19 and 4.20. These measured data are compared with the computations from the diffusion equation using the relations in Table

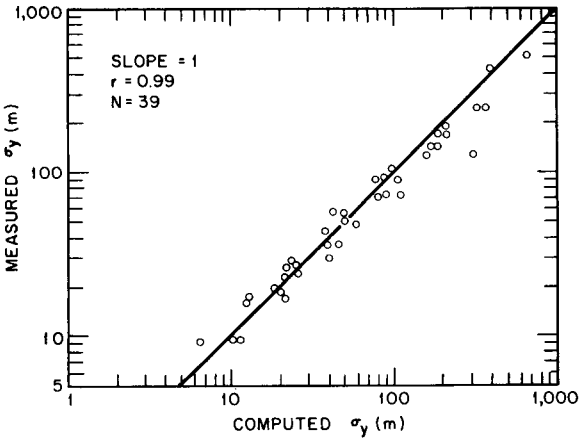

Fig. 4.18 — Measured values of σ_y compared to those estimated from σ_θ data during stable conditions at the National Reactor Testing Station. An averaging time of 10 sec was applied to the wind-direction trace before computation of σ_θ. (From Islitzer and Dumbauld, 1963.)

4.11 and assuming total reflection of the plume. This postulation overpredicts the measured concentrations in all cases, presumably because deposition was ignored although a similar result could occur if the models in Table 4.11 were incorrect.

Deposition velocities were determined for 11 of the diffusion tests by two different techniques. The first method was based on computations involving the total amount of released material deposited between the source and 400 m (as determined from tracer material-balance measurements). The results along with the concurrent meteorological data are given in Table 4.13. The results of the second technique, based on measured air concentration and the assumed relation for σ_z given in Table 4.11, are given in Table 4.14. The higher values of the deposition velocity during unstable conditions, as opposed to stable conditions, are

Table 4.11 — FORMULAS USED AT NRTS FOR COMPUTING σ_y AND σ_z*

Lapse	Inversion
$\sigma_y = \sigma_{\theta(x/\bar{u}\beta)}x$	$\sigma_y = \sigma_{\theta(10\ sec)}x$
$\sigma_z = \sigma_{\varphi(x/\bar{u}\beta)}x$	$\sigma_z = \sigma_{\varphi(x/\bar{u}\beta)}x$
$\sigma_z = \sigma_{\varphi(10\ sec)}x$	$\sigma_z = \sigma_{\varphi(10\ sec)}200$ (for $x \geq 200$ m)

*Subscripts refer to averaging times. The sampling time was 1 hr in each case.

Table 4.12 — WIND-DIRECTION STANDARD DEVIATIONS MEASURED DURING SURFACE-RELEASE TESTS AT NRTS*

	σ_θ, deg		σ_θ, deg	
	Range	Average	Range	Average
Lapse	5.6 to 22.6	11.7	1.7 to 4.5	2.4
Inversion	4.4 to 14.8	9.3	0.5 to 2.5	1.8

*Data from Islitzer and Dumbauld, 1963.

evident in the results of the two methods. This is the same trend noted at Hanford (Table 4.10). As a general rule, however, ground-level concentrations from surface sources are from one to two orders of magnitude larger during stable conditions than during instability; so the opportunity for depletion could be greater during stable conditions despite a perhaps smaller deposition velocity.

4-4.2.5 United Kingdom. This section includes two series of surface-release continuous-source experiments. The first, a short-range series (Hay and Pasquill, 1959), was designed to evaluate the factor β, ratio of the Lagrangian

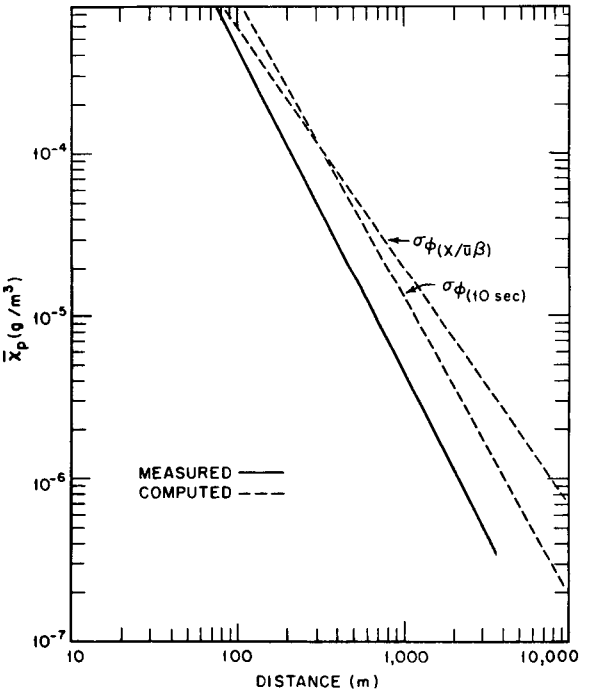

Fig. 4.19 — Computed and measured axial concentrations for unstable conditions at the National Reactor Testing Station. The quantities in parentheses refer to averaging times applied to the raw wind data. (From Islitzer and Dumbauld, 1963.)

Table 4.13—METEOROLOGICAL DATA AND DEPOSITION VELOCITIES COMPUTED FROM TRACER MATERIAL-BALANCE MEASUREMENTS AT NRTS*

Test	$\bar{u}_{4m}$, m/sec	$\Delta T_{16 \text{ to } 4 m}$, °F	Travel distance, m	σ_θ (measured), deg	σ_φ (measured), deg	Amount deposited, %	σ_z (measured),† m	σ_z (computed),‡ m	v_d, cm/sec
C	6.3	−0.3	400	5.6	2.1	54	14.6	10.8	9.2
D	4.9	+0.5	400	14.8	2.0	35	9.5	8.6	2.3
E	6.0	−2.4	200	15.9	3.9	32	13.5	13.0	8.0
F	4.7	−1.1	200	12.9	4.1	24	13.2	12.6	4.4
G	6.2	−1.9	200	15.3	2.3	22	13.7	8.1	5.4
I	6.0	−1.6	400	14.9	3.1	48	13.4	15.5	6.8
M	3.9	−0.7	400	12.2	2.7	32	12.2	13.3	2.4
N	4.7	+0.7	400	10.9	2.3	38	10.0	9.8	2.6
O	2.6	+3.4	400	12.1	0.8	10	5.0	4.7	0.2
Q	2.5	+4.1	400	5.9	0.5	14	5.5	3.5	0.2
S	8.4	−2.3	400	11.1	2.5	37	17.8	14.0	8.9

*From Islitzer and Dumbauld, 1963.
†σ_z measured at travel distance.
‡σ_z computed from $\sigma_{\varphi(x/\bar{u}\beta)}x$ for $\beta = 5.0$ and a sampling time of 1 hr.

and Eulerian autocorrelogram time scales, for use in the expression

$$\overline{y^2} = \overline{v'^2_{(T,t)}}\, t^2 \qquad (4.17)$$

where t, the averaging time, is given by $x/\bar{u}\beta$ (see Chap. 3, Sec. 3-2.3.2). The data from these experiments are summarized in Table 4.15. The average value of σ_y/σ_θ, although not plotted on summary diagram Fig. 4.21, falls on the daytime curve for Project Prairie Grass at 100 m.

A series of 10 long-range continuous-source releases has also been described by Pasquill (1962a). Fluorescent pigment was released during lapse conditions and sampled to distances

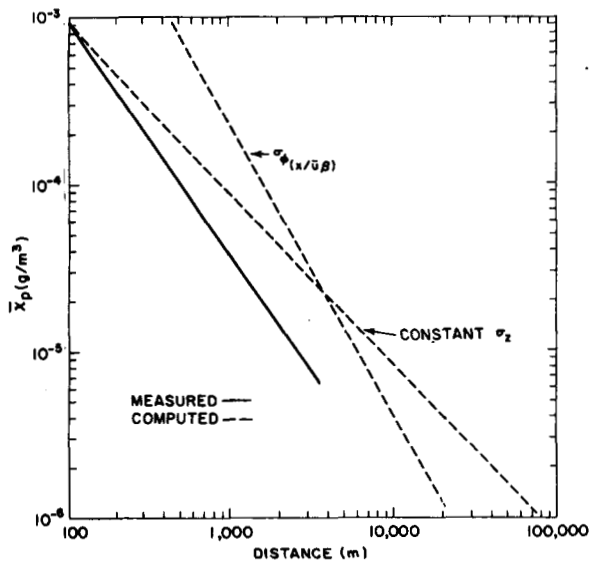

Fig. 4.20 — Computed and measured axial concentrations for stable conditions at the National Reactor Testing Station. (From Islitzer and Dumbauld, 1963.)

Table 4.14 — DEPOSITION VELOCITIES (IN CM/SEC) COMPUTED FROM MEASURED AXIAL AIR CONCENTRATIONS

Unstable $[\sigma_z = \sigma_{\varphi(10\ \text{sec})}x]$

	Distance, m					
	100	200	400	800	1600	3200
Mean*	6.4	5.3	4.0	4.5	5.2	5.6
Standard deviation	3.3	2.9	2.4	1.6	1.5	1.8
Number of observations	13	24	13	20	14	14

Stable $[\sigma_z = \sigma_{\varphi(x/5\bar{u})}x]$

	Distance, m					
	100	200	400	800	1600	3200
Mean†	2.6	1.6	1.3	1.1	1.0	0.80
Number of observations	39					

*Grand mean 5.2.
†Grand mean 1.5.

of about 75 km by aircraft equipped with rotating-drum samplers. Sampling extended from near the surface to about 1000 m and was accompanied by wind measurements through this layer taken with pilot balloons. Data on the crosswind spread are presented in Table 4.16, and the plume-width measurements are included in summary diagrams Figs. 4.22 and 4.23.

A number of elevated line-source releases are also discussed in Pasquill (1962a). The released material was sampled in this case by samplers strung along a balloon cable. These

Table 4.15 — DATA ON CROSSWIND SPREAD AND WIND-DIRECTION FLUCTUATION LEADING TO VALUES OF β*†

Experiment	1	2	3	4	5	6	7	8
$\bar{u}$, m/sec	4.4	5.3	8.3	3.8	3.3	4.3	3.8	2.8
Temp. diff. (23 ft to 4 ft), °F	−1.3	−1.1	−0.6	−1.3	0	0	0.7	1.5
σ_θ at source,‡ deg	7.9	6.3	8.2	15.3	6.8	7.2	5.4	4.8
σ_y at 100 m downwind, deg	6.8	5.4	5.6	12.8	5.5	6.7	4.6	3.1
β	3.5	5.4	1.1	1.6	5.2	8.5	4.3	3.2

*From J. S. Hay and F. Pasquill, Diffusion from a Continuous Source in Relation to the Spectrum and Scale of Turbulence, *Adv. Geophys.*, 6: 351 (1959).
†All wind measurements, as well as the particle release point, were at a height of 2 m.
‡The values of σ_θ refer to a sampling duration equal to the period of particle release and an averaging time of 1 sec.

Table 4.16—DATA ON CROSSWIND SPREAD*

Experiment	Distance downwind, km	Plume spread,† radians
8	18.5	0.33
9	14.9	0.23
10	15.3	0.19
11	16.5	0.38
13	14.4	0.23
14	33.8	0.23
15	27.4	0.31
16	16.1	0.21
17	72.5	0.21
18	18.5	0.49

*From Pasquill, 1962a.
†Defined as 4.3 σ_y.

experiments are discussed in greater detail in Sec. 4-8.

4-4.3 Summary of Continuous-source Lateral-diffusion Measurements

Figure 4.21 presents a summary of lateral-diffusion data for most of the experiments discussed in previous sections. The σ_y values for each test in each series were divided by the appropriate σ_θ values, and an average curve for each series was constructed. The data are ordered quite well when normalized by the use of the wind-fluctuation data. Averaging times for σ_θ range from 2.5 sec for the Prairie Grass

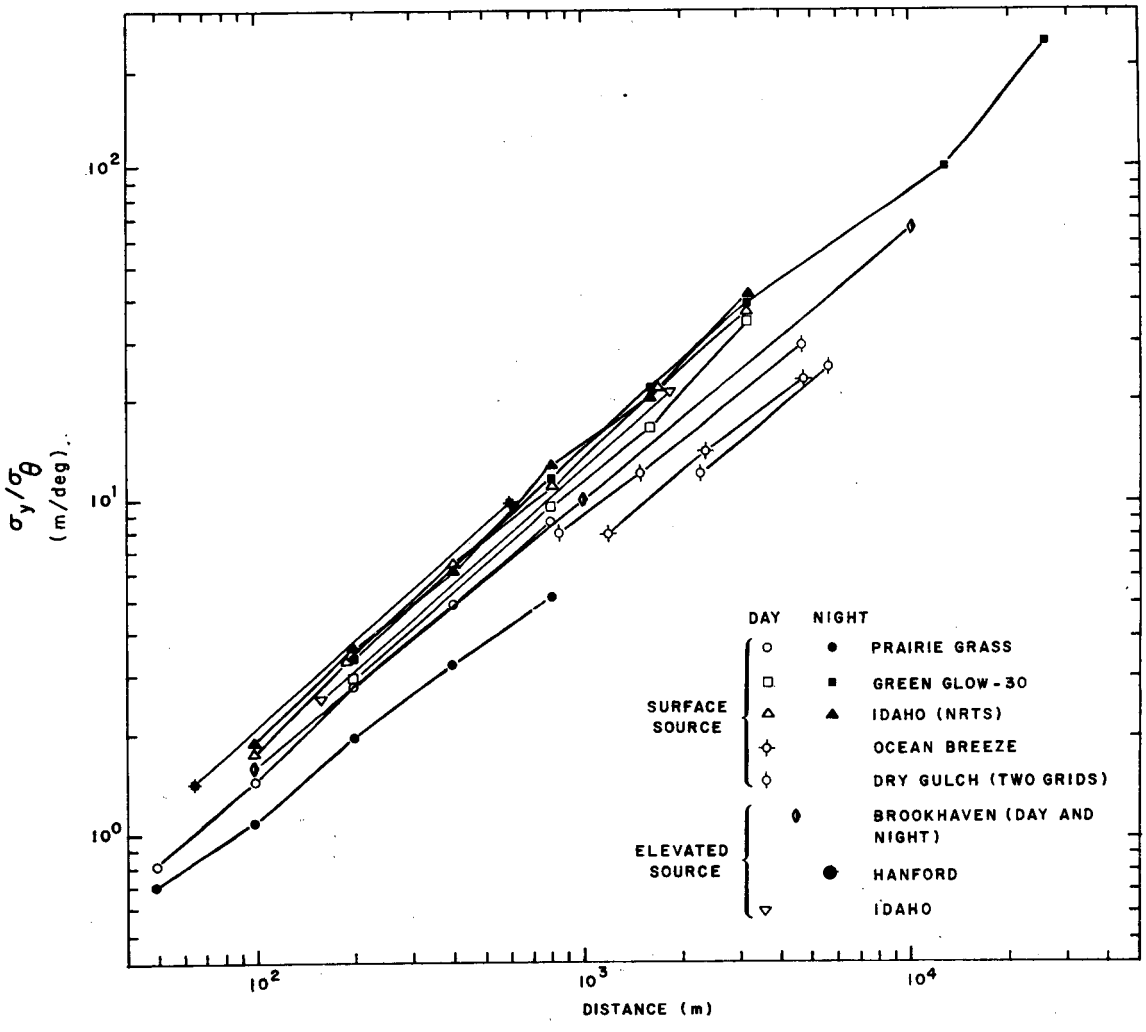

Fig. 4.21—Summary diagram for normalized σ_y measurements for both surface and elevated sources. Average curves are given for most of the experimental series discussed.

information to 20 sec for the Green Glow and 30 series. Sampling times range from 10 to 60 min, and both surface and elevated sources are considered.

The values of σ_y in Fig. 4.21 were obtained from the diffusion experiments on short distance or time scales, generally less than 10 km. Heffter (1965) has presented a summary of lateral-dispersion measurements for travel distances or times considerably in excess of those measured in the shorter range experiments. The summary material in Heffter's paper is presented in Table 4.17 and Figs. 4.22 and 4.23. The σ_y values shown in the two figures were obtained from a wide variety of sources including continuous smoke plumes, multiple balloon releases, and clouds from nuclear detonations. The diagrams include data for a wide range of release durations measured by many different techniques over a height

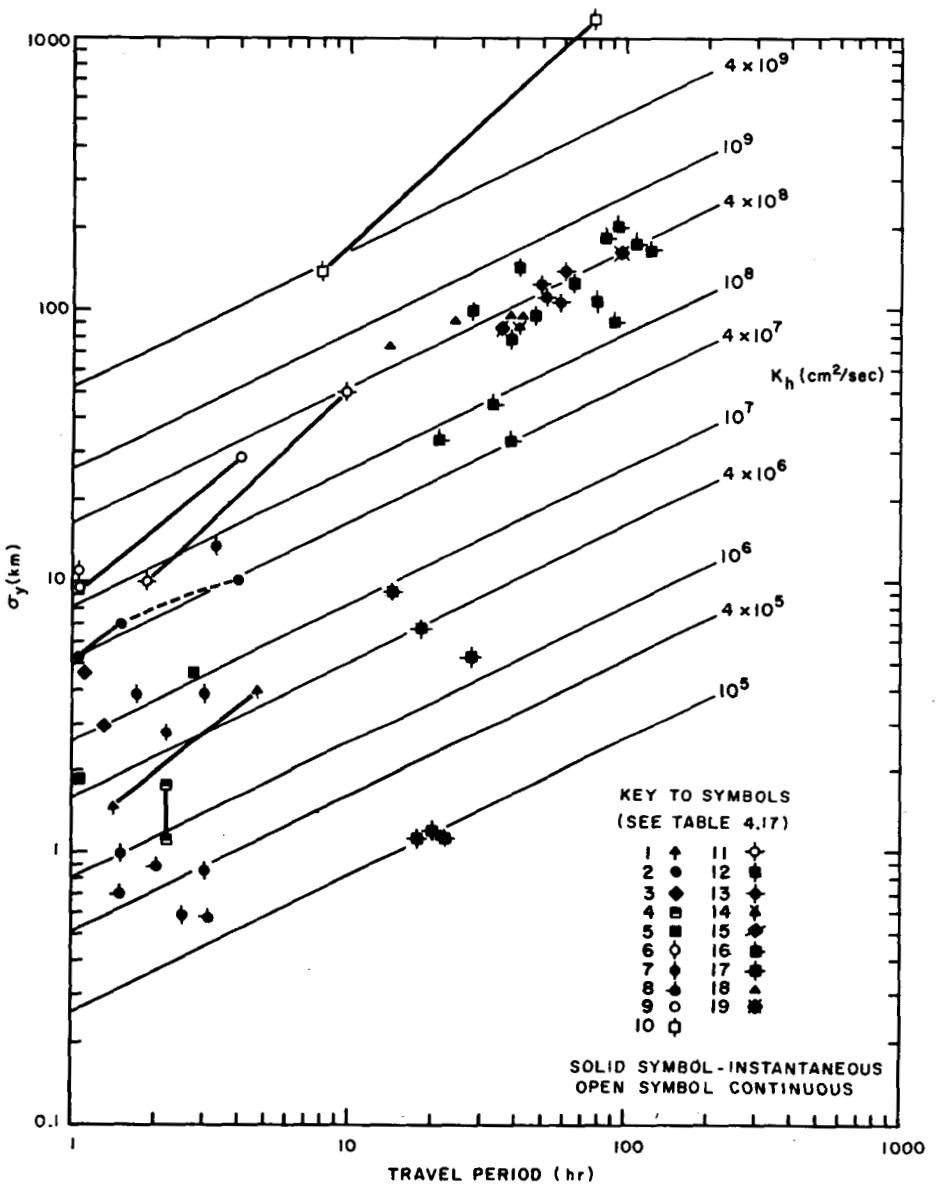

Fig. 4.22 — Long-distance individual and average σ_y values obtained from measurements described in Table 4.17 as a function of travel time. The lines of constant K_h have been computed from the relation $K_h = \sigma_y^2/2t$. (From Heffter, 1965.)

Table 4.17—A KEY TO THE SYMBOLS IN FIGS. 4.22 AND 4.23 INCLUDING REFERENCE, SOURCE AND MEASUREMENT INFORMATION, AND A GENERAL CLASSIFICATION FOR THE INDIVIDUAL AND AVERAGE σ_y VALUES*

Key	Reference	Classification of plotted σ_y value	Source		Measurement			General classification
			Continuous	Instantaneous	Continuous	Instantaneous	Height above surface, ft	
1	Gifford	Neutral conditions	Plume			Primarily stationary surface samplers	Primarily surface	Instantaneous
2	Braham et al.	Average	Plume			Aircraft samplers	Surface to 4000	Instantaneous
3	Crozier and Seely	Individual	Plume			Aircraft samplers	Surface to 5000	Instantaneous
4	Barad and Fuquay	Average	Plume			Stationary surface samplers (30 min)†	Surface	Instantaneous–continuous
5	Pasquill	Average	Plume			Aircraft or motor-vehicle samplers	Surface to 4000	Instantaneous
6	Pack and Angell	Average	Tetroons (12 hr)†		Separation distances		1500 ± 400	Continuous
7	Pack and Angell	Average		Tetroons		Separation distances	1500 ± 400	Instantaneous
8	Classified Project (I)	Individual	Plume			Aircraft samplers	1500	Instantaneous
9	Sakagami	Average	Balloons (1 hr)†		Separation distances		Surface (from flights at low levels to approx. 30,000)	Continuous
10	Angell	Average	Transosondes (24 hr)†		Separation distances		30,000 ± 1000	Continuous
11	Richardson and Proctor	Average	Balloons (10 hr)†		Separation distances		Surface (from flights at low levels)	Continuous
12	U. S. Weather Bureau (1957)	Individual		Nuclear clouds		Aircraft samplers	9000 to 16,000	Instantaneous
13	Allen et al.	Individual		Nuclear cloud		Aircraft samplers	7000 to 14,000	Instantaneous
14	Wilkins	Average		Nuclear clouds		Aircraft samplers	8000 to 25,000	Instantaneous
15	Machta et al.	Average		Nuclear clouds		Aircraft samplers	8000 to 30,000	Instantaneous
16	U. S. Weather Bureau (1954)	Individual		Nuclear clouds		Aircraft samplers	5000 to 25,000	Instantaneous
17	Moore et al.	Individual		Constant-level balloons		Separation distances	30,000	Instantaneous
18	Classified Project (II)	Individual	Plume			Aircraft samplers	1000 to 3000	Instantaneous
19	Ferber	Individual		Nuclear cloud		Aircraft samplers	50,000	Instantaneous

*Heffter, 1965.
†Duration for individual σ_y computations.

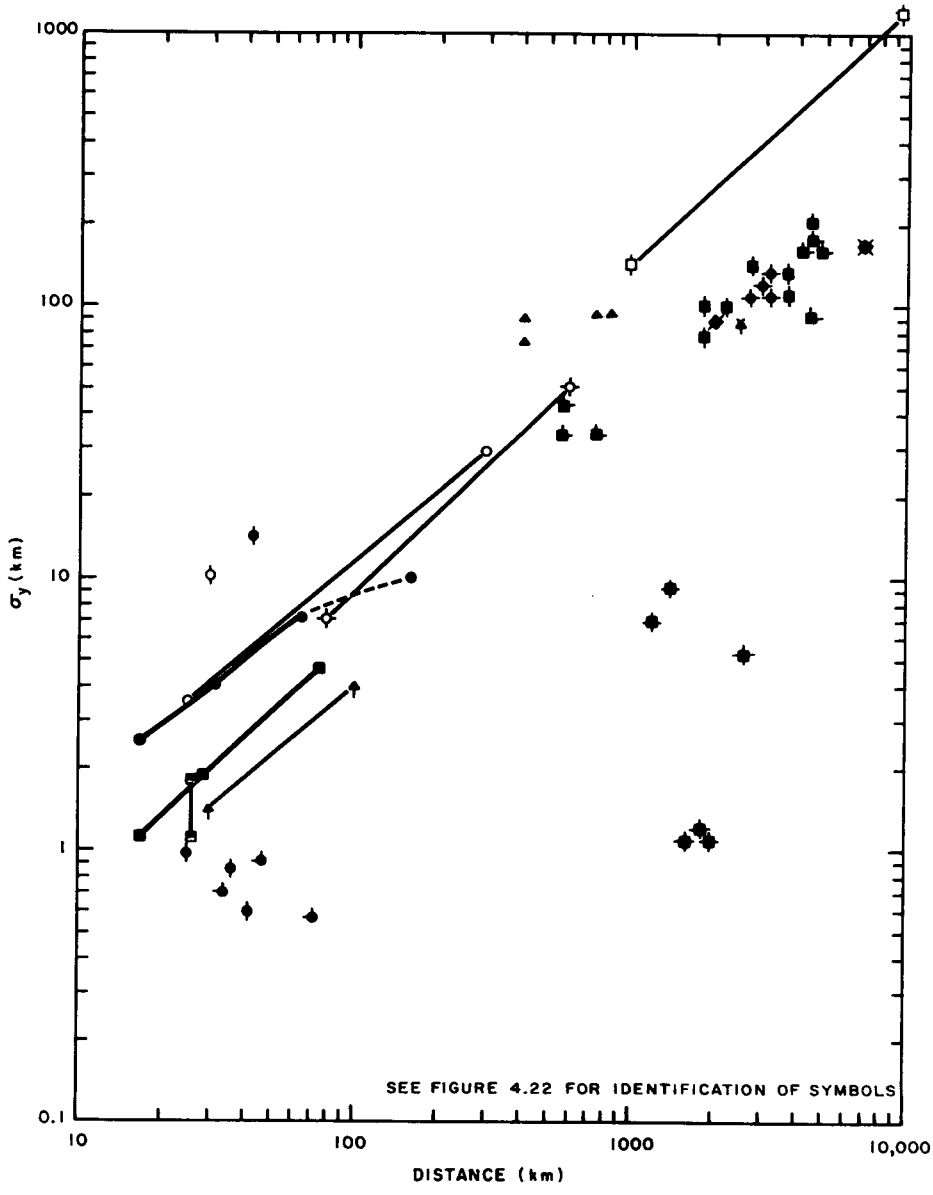

Fig. 4.23 — Long-distance σ_y values from Fig. 4.22 plotted as a function of travel distance from the source. (From Heffter, 1965.)

range of 50,000 ft above the surface. Examining the data from the viewpoint of the relation between K and statistical diffusion theories, namely,

$$K_h = \frac{\sigma_y^2}{2t} \qquad (4.18)$$

the author suggests that an average value of $K_h = 4 \times 10^8$ cm^2/sec seems to apply to travel periods of 1 to 4 days bearing in mind that fairly reliable values that are lower by a factor of 10 or more have been observed. A more detailed discussion of the sources and of the nature of the data presented, as well as the identification of the references noted in Table 4.17, can be found in the original paper.

4-4.4 Summary of Continuous-source Surface-concentration Measurements

There are many possible avenues for summarizing the diffusion experiments that have

been presented. In a useful summary the measurements of diffusion parameters should be related to objective meteorological measurements. Only in this way can the gains made in relating diffusion to meteorological parameters be realized in the direct utilization of meteorological data to estimate diffusion without further laborious and expensive diffusion experiments.

A variety of meteorological predictors were used in the various diffusion experiments. Specifically, σ_θ (for both fixed and varying averaging times), $\sigma_\theta \bar{u}$, σ_φ, ΔT, Ri, and $\bar{u}$ were used individually or in combination. The fluctuation data were computed for a variety of sampling and averaging times. Vertical temperature-difference data were computed over a number of different height intervals originating at different levels above the surface.

From the results of the various experiments, it appears that a measure of the horizontal wind-direction fluctuation (σ_θ) can be used to construct a set of diagrams for summarizing diffusion-experiment data. Such diagrams are also useful for estimating diffusion directly from the meteorological measurement. The use of σ_θ only results in more scatter than would be expected if some measure of stability or vertical wind-fluctuation were included. However, no variable of this type was measured in a consistent manner in most of the experiments.

Figure 4.24 shows the relation between normalized axial concentration and travel distance from the source for approximately 200 individual diffusion experiments selected from the Green Glow-30, Prairie Grass, National Reactor Testing Station, Ocean Breeze, and Dry Gulch series. The normalized concentration data for each travel distance were grouped according to the observed σ_θ values, and the median values of concentration for each 5-deg range of σ_θ were plotted. The Pasquill type A and F categories have been added for comparison. The relations for $\sigma_\theta \approx 2.5°$ and 25.0° are partially based on extrapolated data since there were but few occasions during which measured σ_θ values were either this small or large.

The observed data fit the broad band of values postulated by Pasquill quite well except during the more stable conditions (smaller values of σ_θ) at the longer distances. Here the observed values of normalized concentration are almost an order of magnitude lower than indicated by the Pasquill type F curve. However, the observed data associated with the smaller values of σ_θ probably reflect the effects of deposition, the results of which should be most evident during stable conditions and at the greater distances for the aerosol tracers used in these experiments. The Prairie Grass data, obtained with a nominally nondepositing tracer, are included in Fig. 4.24 for the first 800 m and generally show higher concentrations for the same meteorological conditions than the other experimental results. If the effect of deposition is removed from the observed data by techniques such as indicated in Chap. 5, Sec. 5-3.2.2, the six Pasquill curves are matched quite well by the six corrected σ_θ curves. This circumstance suggests that an estimate of the diffusion climatology at a site may be made directly from wind measurements obtained at that site. Accordingly the reproductions of the Pasquill curves given in Sec. A.3 of the Appendix have been labeled with the appropriate values of σ_θ (2.5° for type F, 5.0° for type E, etc.).

A diagram similar to Fig. 4.24 but using $\sigma_\theta \bar{u}$ as the meteorological index and travel time rather than travel distance could also be constructed. In practice there is little difference between results obtained with either of these two methods.

As noted in Sec. 4-4.1.7, the downstream concentration from elevated sources during stable conditions appears to decrease more slowly than the concentration from a surface source. Therefore the Pasquill curves associated with stable conditions may underestimate the average concentration from elevated sources. A curve labeled $F_{(elev)}$ has been added to Fig. A.1 in the Appendix to account for the cessation of vertical plume growth during strong inversions.

Editor's Note: A series of 43 field experiments using fluorescent-particle tracers was conducted between 1963 and 1965 to investigate the transport and diffusion of airborne material over urban areas [Francis Pooler, Jr., A Tracer Study of Dispersion over a City, *J. Air Pollution Control Assoc.*, 16(12): 677-681 (1966).]. St. Louis, Mo., meets two experimental criteria for such a study: (1) it is a reasonably flat city, remote from significant topographic influences on the large-scale airflow; so the influence of the city itself could be studied, and (2) the Weather Bureau Office there operates

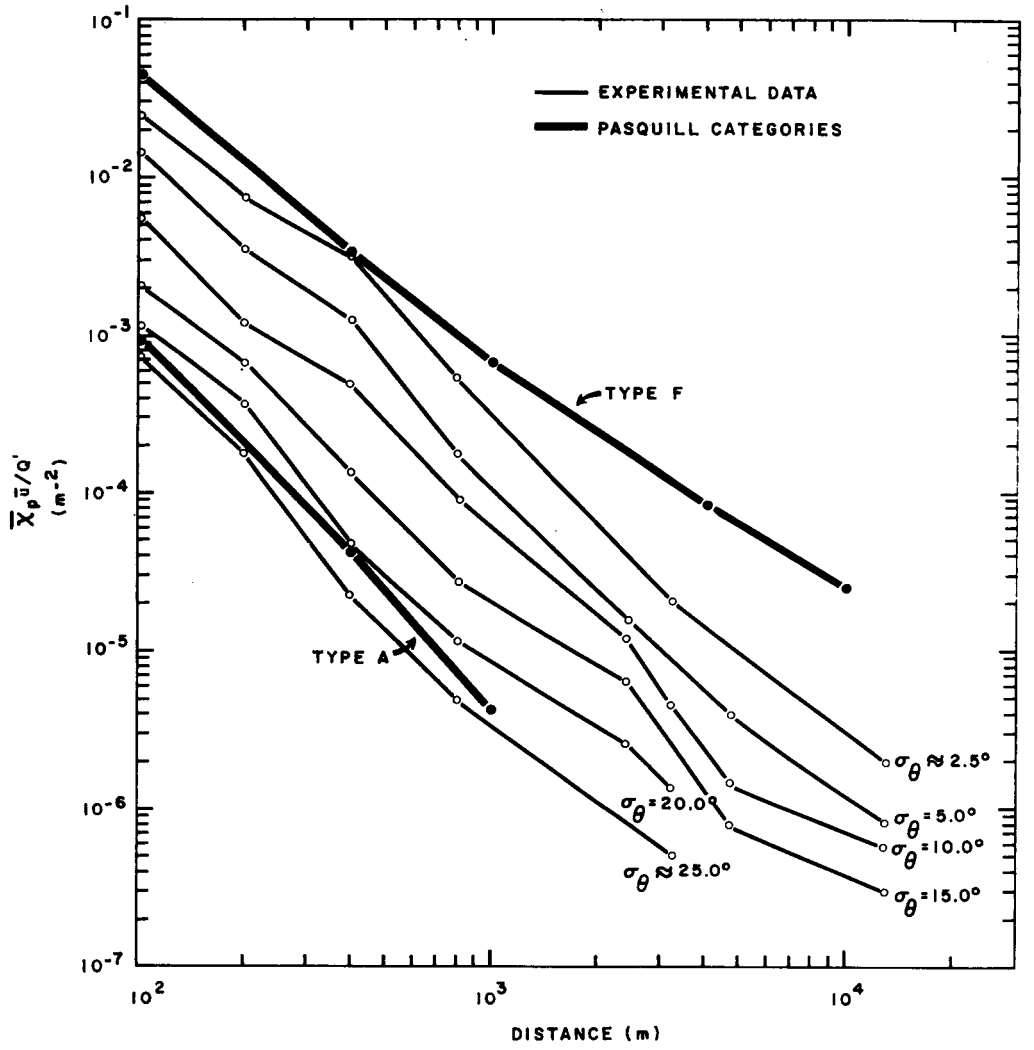

Fig. 4.24—Summary diagram for observed normalized surface-release axial-concentration measurements. The sloping lines connect median values of concentration for various ranges of concurrently observed σ_θ data. The experimental data include approximately 200 individual tests from the Green Glow-30, Prairie Grass, National Reactor Testing Station, Ocean Breeze, and Dry Gulch series.

a weather radar that could be modified to track transponder-equipped constant-level balloons.

Two tracer-release sites were selected, and sampling sites for three concentric 180° arcs were picked at nominal distances of ½, 2, and 4½ miles from the west site and at 1¼, 2½, 5, and, later, 10 miles from the south site. With these two release sites and associated sampling arcs, experiments could be conducted with winds from any quadrant except the northeast.

Although numerous analyses of the data from the St. Louis dispersion study remain to be completed, several results can be noted. Influences of the urban area on daytime dispersion patterns are not clearly evident; expressing the crosswind spread of the tracer cloud in terms of a root-mean-square length, or standard deviation, σ_y, yields no great departure from the results summarized in Sec. 4-4.4.

The St. Louis dispersion data indicate that the influence of the city brings about a slightly larger spread in the tracer cloud at shorter travel distances. Vertical dispersion over a city during the daytime is comparable to that observed over open country, particularly if an initial plume dimension on the order of typical building size is included.

The St. Louis data also indicate that the vertical spread of a plume can be expressed as a function of travel time with much greater confidence than as a function of travel distance. Data from the evening experiments indicate that vertical dispersion rates over a city are much greater than rates observed over open country; the St. Louis data suggest that

a limited weak convective overturn layer forms as air passes over a city. However, the data available from the St. Louis study are not adequate to specify either the depth or the overturning rate of the weak convective layer in terms of causative factors, i.e., wind speeds, preexistent structure of the air as it approaches the city, city roughness, and relative heating rates.

4-5 PEAK-TO-AVERAGE AIR CONCENTRATION

The discussion of the environmental hazards of many toxic materials requires a knowledge of the short-period or peak air concentration that can be experienced. The previous discussions of diffusion data dealt with average concentrations for sampling periods of 10 min to 1 hr. It is appropriate therefore to consider the effect of sampling time upon measured air concentrations and the ratio of peak-to-average air concentration.

The extensive ^{41}Ar radiation measurements from the Harwell stack, described in Sec. 4-4.1.4, yielded some information on the effect of sampling time. From a time history of the total integrated measured radiation, it was found that the measured average concentration decreased with the fifth root of sampling time. This relation was found to be the most appropriate for the 3- to 60-min range of sampling times reported by Stewart, Gale, and Crooks (1954).

An experiment to study the close-in ground hazard from an elevated source during convectively unstable conditions, commonly called looping, was conducted by Barad and Shorr (1954). An oil fog was emitted from a portable generator at the 56-m level of a tower while observers with theodolites noted the time, the position, and the relative intensity of the smoke puffs hitting the ground. Two tests indicating the wide spectrum of possibilities during convective instability are summarized in Fig. 4.25, which shows the cumulative distribution of the puffs hitting the ground as a function of radial distance from the tower. Of the 22 puffs coming to the ground during run 1, about half came down within 150 m from the tower. A later test with equally unstable atmospheric conditions but stronger and steadier winds was conducted. From a 51-min release of smoke, 42 puffs coming to the ground were counted (run 2). In this case, however, none were within 120 m of the tower, and only 28 were within 300 m of the tower. This indicates the effect of stronger winds, which tend to transport the pollutant farther from a stack before coming to the ground. The meteorological conditions for the two tests are listed in Table 4.18.

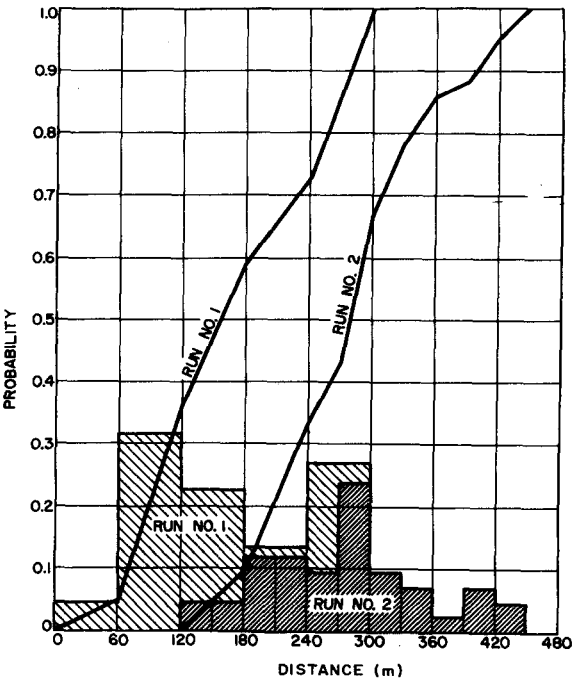

Fig. 4.25—Number of puffs from an elevated source at 56 m reaching the ground during unstable conditions. (From Barad and Shorr, 1954.)

During similar experiments (Shorr, 1953), a mobile air sampler was rushed to the area where a puff came to the ground, and measurements of the short-period peak air concentrations were made using the fluorescent properties of oil fog. A total of 172 puffs from a source at the 56-m level of the tower were sampled along a circular ring 120 to 180 m

Table 4.18—METEOROLOGICAL DATA FOR TWO DIFFUSION TESTS DURING LOOPING CONDITIONS*

	Run 1	Run 2
Sampling time	45 min	51 min
Temp. diff. (120 to 2 m)	−2.6° to −2.9°C	−2.4° to −2.9°C
Wind speed (60 m)	1.8 m/sec	4.9 m/sec

*From Barad and Shorr, 1954.

from the tower. The short-period sampling time in the 120- to 180-m sector ranged from 5 to 120 sec with a mean of 30 sec. It was observed that from 0 to 15 puffs per hour could be expected to reach the ground at this distance. A cumulative frequency distribution of the percentage of the puffs that exceeded a certain air concentration has been taken from Shorr's report and is shown in Fig. 4.26. Short-period peak concentrations of 10^{-3} for a unit release of 1 g/sec represent the likely upper limit. This is on the order of five times the longer term axial concentration at the measurement distance during unstable conditions.

Estimates of the peak-to-average air concentration in the center of elevated plumes during stable meteorological conditions were noted by Hilst (1957) based on his measurements of plumes described in Sec. 4-4.1.3. By forming the ratio of the crosswind particle variance measured with respect to the plume axis to the crosswind particle variance of the time-averaged plume, Hilst deduced estimates of the peak-to-60-min average air concentrations in the center of such elevated plumes. The results given by Hilst for three distances are shown in Table 4.19 for 16 diffusion trials. Generally the ratios are between 1.5 and 3, but they can be as high as 8.

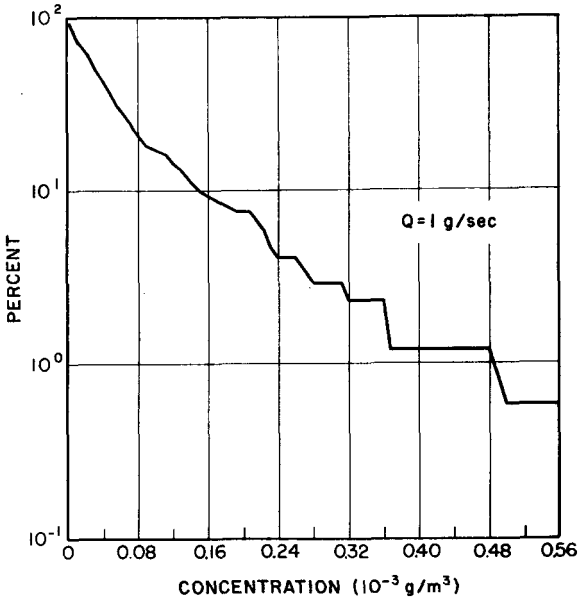

Fig. 4.26 — Percentage of puffs above a given concentration reaching the ground during unstable conditions. (From Shorr, 1953.)

Table 4.19 — RATIO OF PEAK TO 60-MIN MEAN AIR CONCENTRATIONS*

	Distance from source, m		
	200	400	600
Average value	2.28	2.39	2.51
Range	1.39 to 6.77	1.34 to 7.71	1.31 to 8.29

*From Hilst, 1957.

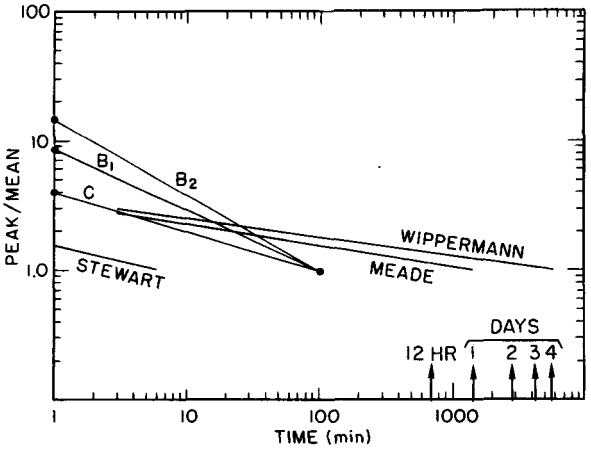

Fig. 4.27 — Peak-to-mean concentration ratio as reported by Singer, Kazuhiko, and Gonzalez del Campo. The lettered lines refer to Brookhaven data and the Brookhaven trace types. (From Singer, Kazuhiko, and R. Gonzalez del Campo, 1963.)

The lettered lines in Fig. 4.27 summarize experimental peak-to-average (P/A) concentration data collected at Brookhaven National Laboratory by Singer, Kazuhiko, and Gonzalez del Campo (1963) using an oil-smoke tracer from a 105-m stack. The slopes of the lines are functions of gustiness and stability. The greatest slope (line B_2) occurred with the most unstable conditions where large portions of the plume were brought down rapidly to the ground by convective turbulence. The smallest slope (line C) occurred with strong-wind conditions where fluctuations are smaller.

Singer, Kazuhiko, and Gonzalez del Campo (1963) obtained additional data that further affirm the existence of the power relation between P/A and sampling time. These data are also presented in Fig. 4.27. Others have also shown that a power function is valid. For short periods Stewart, Gale, and Crooks (1954) have demonstrated this, and for long periods Wipper-

mann (1961) and Meade (1960) have done likewise for periods of 4 days and 1 day, respectively.

Singer believed that the data of Wippermann and of Meade (Fig. 4.27) pertain to a city where short-term fluctuations might be smoothed out. In terms of roughness the city can practically obliterate all short-term fluctuations of concentration depending on the location of the receptor with respect to the source.

The problem of determining peak-to-average air concentrations owing to plume meander has been treated analytically by Gifford in his fluctuating-plume model (see Chap. 3, Sec. 3-3.2). Gifford (1960) also has analyzed peak-to-average data and discusses the results of many measurements. From his study Gifford cites the following guides that can be laid down for the estimation of peak-to-average air-concentration ratios (P/A):

1. For source and receptor located at the same level, P/A can be expected to be in the range from 1 to about 5.

2. For increasing difference in height between source and receptor or increasing distance from the plume axis, P/A increases, and values as great as 50 to 100 or greater may occur at the ground near a moderately tall (50- to 100-m) stack.

3. With increasing distance downwind from an elevated source, the ground-level P/A value will decrease toward its lower limit of unity but will attain values of this order only at considerable distances (perhaps 20 to 50 stack lengths or more) from the source.

4-6 EVALUATION STUDIES

4-6.1 Variability and Prediction of Diffusion

At the present time no comprehensive evaluation of the various diffusion models has been reported in the literature although numerous verification programs have been accomplished, usually with the data from one or a few experimental series. It is worthwhile to consider, at this point, the reason such a comprehensive evaluation might be very difficult.

An attempt is made in a diffusion model to relate meteorological variables to simultaneously measured diffusion statistics. Therefore the appropriate meteorological and diffusion information must be available for each attempted application of the model. However, in the experiments performed to date, a broad variety of meteorological and diffusion quantities have been measured. These, in many instances, are not reducible to some common set of values. Thus the vertical gradients of wind speed and temperature, for instance, called for by one model and collected during one experiment cannot be uniquely related to the wind-fluctuation data required and measured in another set.

Another major problem in the comparison of diffusion models arises because of the diversity of effects that may influence a particular tracer release, effects that are not usually accounted for explicitly in any one model. The downstream concentration in a diffusing plume will, over short distances, be well related to the degree of turbulent mixing. Thus the Prairie Grass data respond quite well to normalization by a surface-wind fluctuation criterion. As the plume moves to greater downstream distances, it spreads vertically and responds increasingly to the changes of the mean flow and turbulence with height. It may even encounter a lid to vertical mixing. During any part of the travel of most gas and all aerosol plumes, contact of the plume with the ground results in material depletion, which affects both the apparent rate of downstream concentration decrease and the vertical profile of the tracer. Finally, the meteorological situation accompanying a tracer test may change in either time or space over the measurement network. To date, no one model sufficiently general to treat all phases of this complex problem has been developed. The models in use give results that are not dissimilar when comparable meteorological values can be specified as inputs.

Since most working models make use of the Gaussian assumption coupled with some measure of thermal stability and wind fluctuation, a discussion of these criteria in terms of observed diffusion data is of interest. The σ_y measurements from the Idaho surface tests for all runs in which the Richardson number (Ri) ranged between 0 and −0.05 as computed from

$$\mathrm{Ri} = 2g\,(z_1\,z_2)^{1/2}\,\frac{(\Theta_2 - \Theta_1)\,\ln\,(z_2/z_1)^{1/2}}{\Theta_2\,(\bar{u}_2 - \bar{u}_1)^2} \qquad (4.19)$$

have been examined for scatter. The wind speed, $\bar{u}$, and potential temperature Θ (the temperature that a parcel of dry air would have if it were brought dry adiabatically from its initial level to the arbitrary standard level of 1000 mb) at 1.0 and 8.0 m were used to evaluate Eq. 4.19. The selected Ri values are appropriate for weak to moderately unstable conditions. The frequency distribution of the ratio of the measured σ_y at each arc to the average at that arc is shown in Fig. 4.28. More than 90% of the cases in Fig. 4.28 fall within a factor of 2 of the average value for this particular stability type. A similar frequency distribution for $\bar{\chi}_p$ is shown in Fig. 4.29 for moderate instability. Once again 90% of the cases fall within a factor of 2 of the average.

A similar type of study was made of the concentration and lateral-diffusion measurements of the Prairie Grass experiments, which cover a wider range of stabilities than the Idaho experiments. The lateral-diffusion data were grouped by different σ_θ values for stable and unstable conditions. The percentage frequency of the ratio of measured σ_y values for each test to the mean for all tests at an arc in an appropriate stability–σ_θ category is shown in Table 4.20. Four class intervals, encompassing most of the cases, are used. The scatter of $\bar{\chi}_p$, normalized to a unit source strength and $\bar{u} = 5$ m/sec, is also shown in Table 4.20. The variation of $\bar{\chi}_p$ about the mean is larger than the variation of σ_y about its mean. This apparently is due to the sensitivity of vertical diffusion to stability. However, separation of the concentration measurements into smaller ranges of stability by the appropriate σ_θ values reduces the scatter considerably. A similar study of Hanford measurements (Fuquay, Simpson, Barad, and Taylor, 1963) has been made using both Green Glow and 30 Series data. The results are shown in Table 4.21.

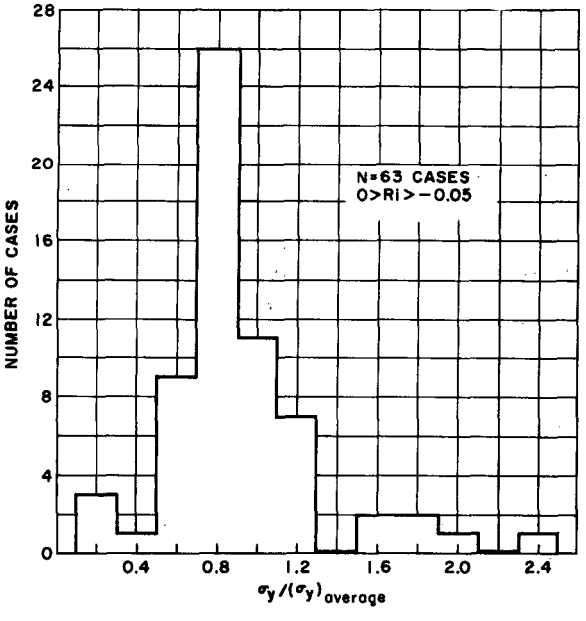

Fig. 4.28 — The distribution of ratios of individual σ_y measurements to the average value for tests during unstable conditions at the National Reactor Testing Station.

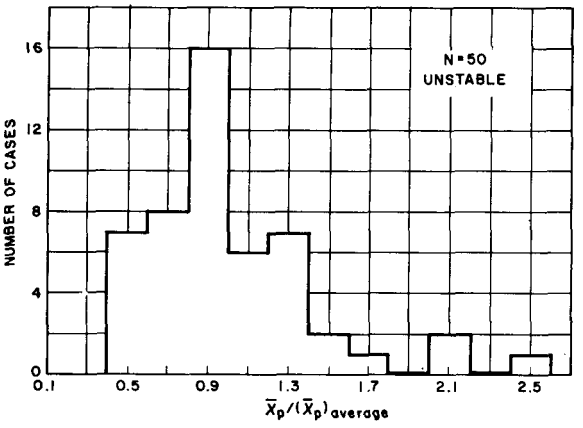

Fig. 4.29 — The distribution of the ratios of individual $\bar{\chi}_p$ measurements to the average value for all tests during unstable conditions at the National Reactor Testing Station. The concentration data are normalized to unit source strength and a wind speed of 5 m/sec.

4-6.2 Deviations from a Gaussian Model

Most of the practical methods for computing diffusion require a Gaussian distribution of the diffusing substance. In practice, deviations from a Gaussian distribution are common but in an apparently nonsystematic way. The concentration profiles through a plume may be too peaked, too flat, or too skewed to be classified as Gaussian curves. Since no single class of functions, however, seems to adequately describe all the possibilities, it appears practical to maintain the Gaussian interpolation formulas and to inquire into the magnitude of possible resulting errors.

Table 4.20—SCATTER OF PRAIRIE GRASS σ_y AND $\overline{\chi}_p$ VALUES ABOUT THE MEAN EXPRESSED AS PERCENTAGE FREQUENCY OF RATIO OF MEASURED VALUES TO AVERAGE IN A GIVEN CLASS INTERVAL

Unstable						Stable					
No. of cases	σ_θ, deg	Class interval 0.9–1.1	0.7–1.3	0.5–1.5	0.3–1.7	No. of cases	σ_θ, deg	Class interval 0.9–1.1	0.7–1.3	0.5–1.5	0.3–1.7
					σ_y						
30	>16	13	60	86	100	14	9 to 16	0	36	64	100
85	9 to 16	38	77	95	98	64	6 to 9	37	82	98	98
40	6 to 9	35	90	100	100	85	0 to 6	24	69	86	90
170	All cases	21	57	81	90	168	All cases	13	44	71	88
					$\overline{\chi}_p$						
24	>16	17	58	88	92	12	9 to 16	17	59	76	92
67	9 to 16	19	55	81	90	52	6 to 9	26	61	88	92
31	6 to 9	12	64	90	100	68	0 to 6	4	10	54	82
134	All cases	6	36	53	63	136	All cases	8	32	52	75

Table 4.21—SCATTER OF GREEN GLOW AND 30 SERIES σ_y AND ψ_p VALUES ABOUT THE MEAN EXPRESSED AS PERCENTAGE FREQUENCY OF RATIO OF MEASURED VALUES TO AVERAGE IN A GIVEN CLASS INTERVAL

Unstable						Stable					
No. of cases	σ_θ, deg	Class interval 0.9–1.1	0.7–1.3	0.5–1.5	0.3–1.7	No. of cases	σ_θ, deg	Class interval 0.9–1.1	0.7–1.3	0.5–1.5	0.3–1.7
					σ_y						
20	10 to 20	16	48	90	100	14	15 to 20	44	72	86	100
19	3 to 10	5	55	80	95	22	10 to 15	64	100	100	100
39	All cases	10	62	86	97	91	5 to 10	20	59	88	96
						37	<5	22	74	90	97
						164	All cases	28	68	89	96
					ψ_p						
20	10 to 20	15	40	65	85	15	15 to 20	20	40	53	60
20	3 to 10	15	35	50	65	22	10 to 15	23	78	97	100
40	All cases	15	37	58	76	93	5 to 10	17	44	65	79
						38	<5	18	53	66	83
						168	All cases	18	50	68	80

The Project Prairie Grass data were analyzed by Elliot (1960) in this regard. The crosswind integrated concentration, $\bar{\chi}_{CWI}$, the axial concentration, $\bar{\chi}_p$, and σ_y are related by

$$\bar{\chi}_{CWI} = (2\pi)^{1/2}\, \sigma_y \bar{\chi}_p \qquad (4.20)$$

if the crosswind distribution of particles is Gaussian. From the measured values of $\bar{\chi}_{CWI}$ and σ_y, $\bar{\chi}_p$ was computed and compared to the measured $\bar{\chi}_p$. The value of $\bar{\chi}_{CWI}$ is obtained by integrating the area under crosswind profiles of measured air concentration. The ratios of the computed to measured values of $\bar{\chi}_p$ for about 100 cases have been taken from Elliot's data, separated into lapse or inversion cases, and plotted as a frequency distribution in Fig. 4.30. These results show that computed values usually will not vary from measured results to a significant degree owing to the assumption of Gaussian distributions. The σ_y values used in Eq. 4.20 were found by Haugen (1959a) to be statistically stable. By eliminating every second sampler from the analysis, Haugen found virtually no effect on the computed diffusion.

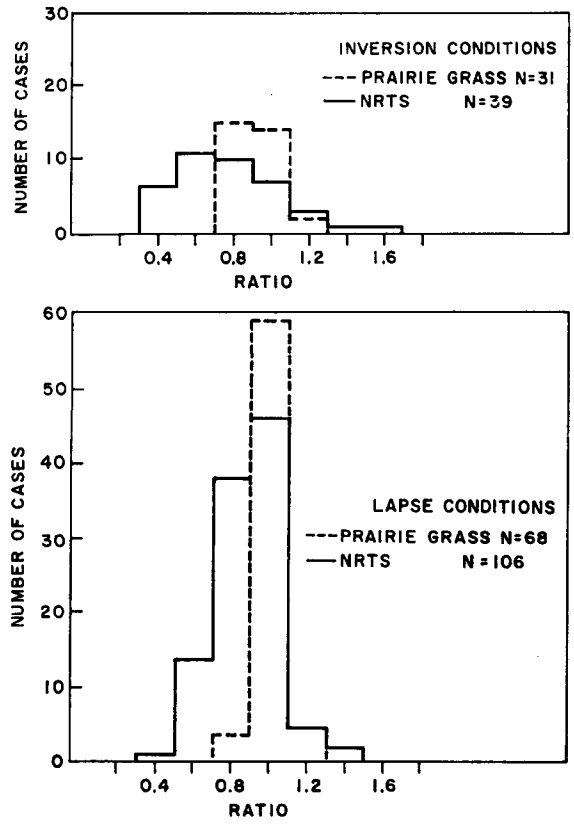

Fig. 4.30 — Ratios of computed to measured values of $\bar{\chi}_p$ for both lapse and inversion conditions under the assumption of a Gaussian distribution. Data are presented for the Prairie Grass and National Reactor Testing Station surface experiments.

A similar type of study was made from the ground-level-source data reported by Islitzer and Dumbauld (1963). The ratio of $\bar{\chi}_p$ computed from Eq. 4.20 to the measured $\bar{\chi}_p$ was determined. These results are also shown in Fig. 4.30.

4-7 AREA WITHIN AN ISOPLETH

In some pollution problems, such as those dealing with the concept of total population dosage, the area enclosed within a certain isopleth of air concentration or exposure must be estimated. The Prairie Grass and Green Glow data were analyzed by Elliot (1959) and by Elliot, Engelmann, and Nickola (1961) to determine the variation of measured areas within isopleths with changing meteorological conditions. Elliot found a high correlation between the area within a given isopleth of exposure, ψ, expressed in units of g sec/m^3, and the value of that isopleth normalized by source strength and wind speed for a range of stability conditions. Elliot derived empirically the relations between area and normalized exposure for the Green Glow and nighttime Prairie Grass data:

$$\text{(Green Glow) } A = 10.3\left(\frac{\psi\bar{u}}{Q}\right)^{-0.95} \qquad (4.21)$$

$$\text{(Prairie Grass) } A = 33.1\left(\frac{\psi\bar{u}}{Q}\right)^{-0.91} \qquad (4.22)$$

The plots of Eqs. 4.21 and 4.22 on log-log paper are virtually parallel lines displaced slightly from one another. Elliot surmises that this displacement may have resulted from the maximum air concentrations being frequently located some height above the ground during the Green Glow experiments but near the ground during the Prairie Grass experiments.

The Idaho elevated-source data (Islitzer, 1961) and ground-level-source data (Islitzer and Dumbauld, 1963) were analyzed in a similar manner, but the vertical and horizontal wind-direction standard deviations, σ_θ and σ_φ, also were introduced (Yanskey and Islitzer,

1962). The Prairie Grass data were also analyzed in this manner. All the cases for the entire range of stability could be well represented by a single straight-line plot of the logarithm of the area vs. the logarithm of $(\bar{u}\sigma_\theta\sigma_\varphi\bar{\chi}/Q')$; therefore the need for different curves for varying stability found necessary by Elliot was eliminated. Yanskey and Islitzer found that the correlation between area and predictor steadily improved as more meteorological variables were introduced into the predictor although the correlation was quite high for all the various selected predictors. The results given graphically in Fig. 4.31 show that the area within an isopleth is considerably less for ground-level concentrations from an elevated source than from ground-level sources. This is due to the reduced width of the plume at the ground from an elevated source. The slopes of the lines in Fig. 4.31 are fairly similar despite differences in the experimental and meteorological conditions of the three field studies. The correlation coefficients are all quite high for the various plots.

In an unpublished report Gifford (1962) compared measured area to computed area within a given isopleth. The ground-level air-concentration isopleths were computed from the generalized Gaussian diffusion model using the Pasquill diffusion categories as modified by Gifford (1961).

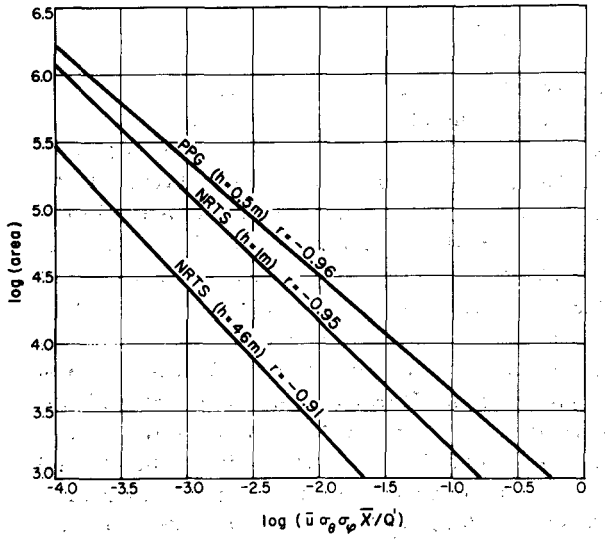

Fig. 4.31—Lines of best fit between the area within an isopleth of relative air concentration and meteorological predictors.

The results are shown in Fig. 4.32, which was taken from the original report. The range of Elliot's (1959) data from the Prairie Grass experiments is fairly well approximated by the range of computed curves, and the nighttime or stable cases tend toward the region of the figure occupied by Pasquill's cases E and F for slight and moderate stability. The line representing the Green Glow measurements, which represent moderate stability, tends to be most nearly represented by Pasquill's case C. Since case C is intended to apply to slightly unstable conditions, the agreement is poorer than for the Prairie Grass data. This may be due to such factors as the range of the measured data, i.e., 800 m for the Prairie Grass and 25.6 km for the Green Glow data, and differences in terrain.

4-8 SPEED AND DIRECTION OF TRAVEL

For very short distances of travel, perhaps in the range of a few hundred meters, the mean wind speed and direction measured at a source of pollution will provide a good estimate of the mean speed and direction of motion of the emitted effluent. For greater distances, i.e., of the order of kilometers and tens of kilometers, the speed and direction of the effluent will become increasingly dependent on the vertical profile of wind velocity. The arrival times of the fluorescent tracer released during the Green Glow tests at the 12.8 and 25.6 km arcs were obtained with rotating drum samplers and analyzed by Elliot, Engelmann, and Nickola (1961). The typical increase of wind speed with height resulted in travel times that were somewhat shorter than would have been computed from the wind at 1.5 m, the height of the source. The wind at 15 m was found, in the mean, to fairly represent the average travel speed of the tracer as measured at the surface.

The continuous-point-source and instantaneous-line-source data from the experiments discussed in Secs. 4-4.2.5 and 4-10.1.1 have furnished some information on particle travel speed and direction. Pasquill (1962a) gives the following mean deviations of particle travel speed and direction (averaged over all levels) from the average wind speed and direction as measured with pilot-balloon ascents and theodolite tracking: Direction: −17° to +4°, mean

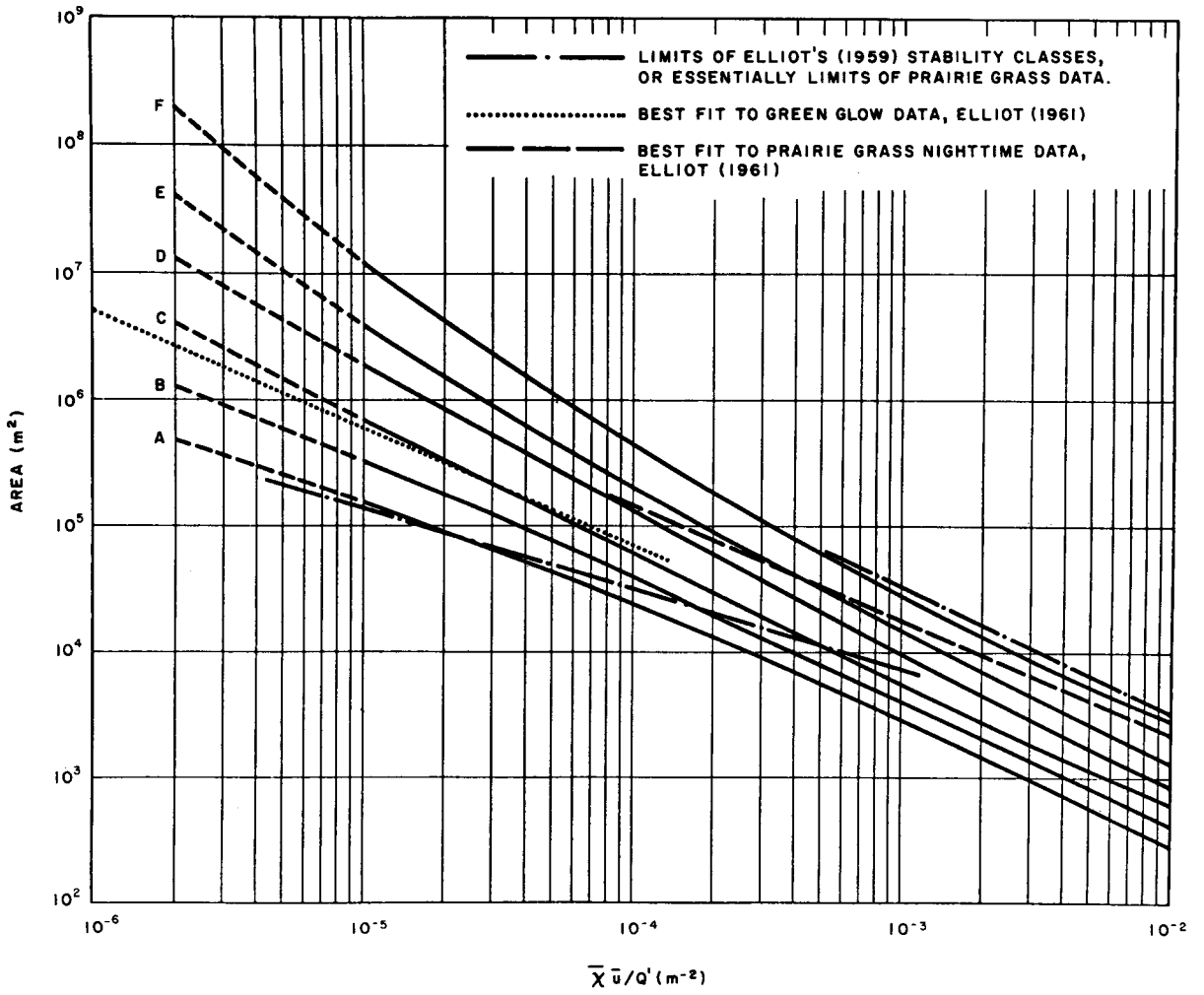

Fig. 4.32 — Comparison of measured area to computed area within a relative concentration isopleth.

−6° (point source; negative values are counterclockwise). Speed: −9% to +14%, mean +4% (line source).

A tendency was evident for the direction of particle travel to back (counterclockwise) somewhat from the average wind direction, averaged for 150-m layers, and for the particle speed to exceed the mean wind speed in the layer. However, there were some exceptions to this trend. One sampling cross section, 127 km downwind from a line source, showed a distinct lag of the passage of the bottom section of the cloud from the upper sections. Pasquill attributes this to the reduction of the vertical intensity of turbulence, i_w, from a midday value of 0.1 to near 0.02 by the time the plume passed the sampling point. With this reduction in vertical mixing as the particles traveled downwind, the decrease of wind speed with decreasing height in evidence during this experiment had a noticeable effect on the final stages of travel of the surface layer of the cloud. On the other hand, there was a lag in the passage of the cloud at higher levels during another test at 137 km from a line source. In this test the wind speed decreased with height above 300 m, and i_w decreased with time from 0.1 to 0.02 at the 900-m height by the time the cloud passed. Another experiment at 117 km showed more rapid travel of the cloud above 1200 m owing to stronger winds at 1800 m and a lower i_w (0.07 at 1800 m compared to 0.12 at 1200 m and 0.15 at 600 m). These were evidently all cases in which vertical mixing was insufficient to prevent some shearing of the cloud in accordance with the wind profile.

An attempt to determine an "effective" wind speed, a uniform wind speed throughout the diffusing cloud that will produce the same effect on the cloud as the actual wind profile, was made by Smith and Singer (1965). Assuming a Gaussian vertical concentration distribution and a power-law wind profile, Smith and Singer found that the effective wind speed may be found at the height given by

$$h = 0.62\sigma_z \qquad (4.23)$$

4.9 LONG-PERIOD AVERAGE AIR-CONCENTRATION MEASUREMENTS

The literature on diffusion experimentation shows that almost all the experiments have been concerned with release times of a few hours or, usually, less. Source–receptor relations for periods of days or months are important in pollution problems from continuously emitting industrial sources and also for the slow leak of fission products from reactors. Techniques of computing long-period average air concentrations or exposures with diffusion equations developed for shorter releases are discussed in Sec. 3-3.5.4.

A study of long-period average air concentrations was made by Meade and Pasquill (1958) from the routine surveys of sulfur dioxide in the neighborhood of power stations in the United Kingdom. Since Meade and Pasquill were dealing with low average concentrations superimposed on relatively high backgrounds, they analyzed the sulfur dioxide data with respect to the equation (in their notation)

$$p = a + \frac{b\, f(\theta)\, S}{\bar{u}} \qquad (4.24)$$

where p = the average concentration over any octant around a power station
a = the background concentration
S = the discharge rate of sulfur dioxide
$\bar{u}$ = the mean wind speed
$f(\theta)$ = the frequency of the wind direction in a given octant
b = the term containing the diffusion equation

In this case

$$b = \left(\frac{2}{\pi}\right)^{1/2} \frac{K}{x\sigma_z} \exp\left(-\frac{h^2}{2\sigma_z^2}\right) \qquad (4.25)$$

where a doubling due to ground reflection is introduced and the constant, K, depends upon the units used and the width of the sector over which the pollution is averaged.

From routine wind records values of $f(\theta)/\bar{u}$ were obtained for each octant for each season. Smooth isopleths of pollution were drawn in from the 14 observation sites available and then used to estimate the average pollution, p, on each 45-deg arc at a radius of 1500 m from the power station. The relation between measured and computed pollution is shown in Fig. 4.33, where p is given in units of deposition of sulfur on the lead peroxide candles used for the measurements. The conversion factor to sulfur in terms of concentration units would be included in the constant term in Eq. 4.25. Despite some scatter of points, the regression equations obtained by the method of least squares shown in Fig. 4.33 were found to be statistically significant. Moreover the values of the constant, a, from the regression equations in Fig. 4.33 were in good agreement with the seasonal background values of pollution observed at Staythorpe before the power station began to function. The higher values of p observed in wintertime are a reflection of the increased average atmospheric stability in that season as compared to summer. Studies such as the one described above indicate that reasonably reliable estimates of long-period average air concentration or exposure can be made from routine meteorological observations and the appropriate diffusion equations. Furthermore, from the slopes of the lines in Fig. 4.33, values of b can be obtained and used to determine σ_z by Eq. 4.25. Meade and Pasquill give mean values of σ_z as 90 m in winter and 150 to 180 m in summer.

In another form of the long-term average-concentration equation, the equation is applied for short time periods (perhaps an hour), and the resulting hourly concentrations are then totaled for each sector during the long period of interest. This form of the equation has been mentioned frequently in the literature, but experimental evidence is, as yet, meager.

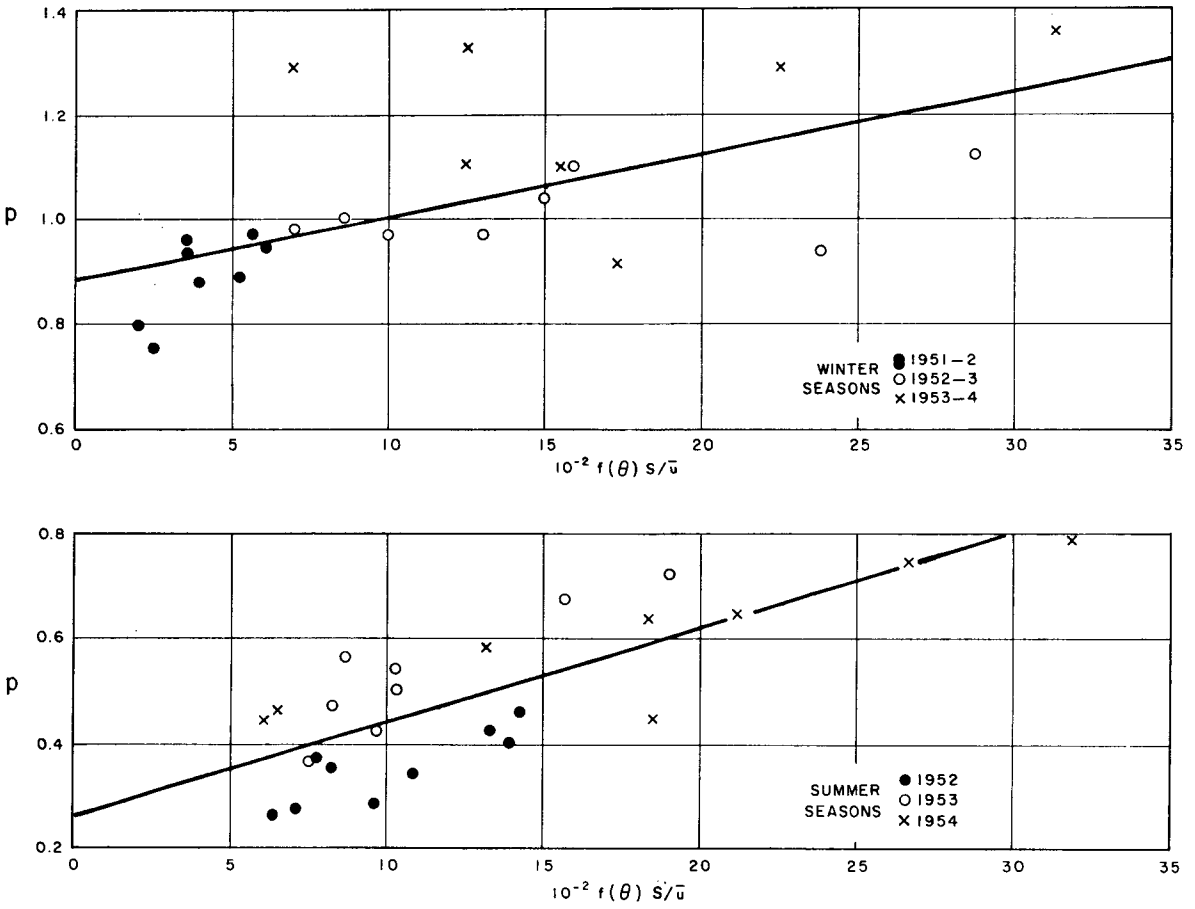

Fig. 4.33 — Measured vs. computed long-period average sulfur dioxide pollution. [From P. J. Meade and F. Pasquill, A Study of the Average Distribution of Pollution Around Staythorpe, *Intern. J. Air Pollution*, 1(1-2): 66-67 (1958).]

4-10 DIFFUSION FROM INSTANTANEOUS SOURCES

The practical evaluation of the diffusion parameters in the instantaneous-point-source diffusion equation, Eq. 3.118, has received little attention when compared with the effort expended in determining the characteristics of continuous point-source plumes. Certainly part of the reason for the paucity of instantaneous-source experiments has been the traditional interest in the vast number of continuously emitting chimneys. By comparison instantaneous sources are usually associated with accidents (by definition), unusual occurrences, and occasional military requirements.

It should be remembered in instantaneous-source diffusion problems that the instantaneous (snapshot) mass distribution of a puff or plume is a result of a finite number of discrete turbulent fluctuations. Turbulence theory deals statistically, not deterministically, with atmospheric motions. Therefore turbulence theory cannot be invoked to determine the details of an instantaneous observation of a diffusing pollutant. As indicated by the bar over the left hand side of Eq. 3.97, only the mean diffusion, the characteristics of an ensemble of puffs, can be discussed in terms of turbulence theory.

4-10.1 Instantaneous-point-source Experiments

Because of the difficulty of measuring the instantaneous values of concentration simultaneously at a sufficient number of positions, early observations of relative diffusion tended

to rely mainly on the visual methods and especially on the observation of the growth of puffs of smoke. Observations of smoke puffs were made by Kellogg (1956) and by Frenkiel and Katz (1956). In Kellogg's New Mexico experiments, vials of titanium tetrachloride and water were attached to trains of balloons and exploded at predetermined altitudes by small charges of cordite set off by baroswitches. The release altitudes ranged from 7.1 to 18.9 km, and the resulting puffs of smoke were observed by phototheodolites. From the records of the phototheodolites both the positions and visible sizes of the puffs were obtained. Eighteen usable sets of observations were reported in the form of graphs of visible diameter against time up to a maximum time between 3 and 11 min. The smoke puffs observed by Frenkiel and Katz were released within the first 100 m above the surface over a water surface during unstable conditions. The puffs were generated by exploding small charges of gunpowder carried aloft by a tethered balloon. Positions and sizes of the smoke puffs were obtained from photographs at 1-sec intervals, and the data on smoke-puff radius were tabulated by Frenkiel and Katz for 19 cases with total durations of observation ranging from 7 to 20 sec.

An interesting result from relative diffusion theory, as discussed in Chap. 3, is the prediction that the particle variances from an instantaneous source, σ_{xI}^2, σ_{yI}^2, or σ_{zI}^2, initially increase as the third power of the travel time. Gifford (1957) reexamined individual runs from Kellogg's data and found that the stratospheric data tended to support a t^3 regime initially and to change to a t^2 regime for particle-variance growth after some characteristic time of travel. The upper tropospheric smoke studies, however, best followed a t^2 dispersion regime throughout all travel times. A similar t^3 regime was found for the smoke-width measurements given by Frenkiel and Katz (1956) for about 12 sec with a definite transition to a t^2 law after that time. For Kellogg's stratospheric data the transition time was usually about 3 min.

4-10.1.1 Smith and Hay, United Kingdom. Current experiments designed to relate simply measured meteorological values to the diffusion of a puff have involved the use of the relation presented by Smith and Hay (1961),

$$\frac{\Delta\sigma_I}{\Delta x} = \frac{2}{3}\beta i^2 \qquad (4.26)$$

which relates the maximum spread of a cluster of dispersing particles to a meteorological variable. Here β is the Lagrangian–Eulerian time-scale factor, i is the intensity of turbulence along the appropriate coordinate, and σ_I is the standard deviation of the material distribution. Equation 4.26 applies strictly only in the case of homogeneous isotropic turbulence, conditions usually grossly violated near the ground. Smith and Hay state, however, that Eq. 4.26 can be applied in an empirical sense during conditions of inhomogeneous or anisotropic turbulence.

Smith and Hay carried out two sets of experiments to evaluate Eq. 4.26. The first set consisted in catapulting charges of Lycopodium spores to heights of 2 m above the surface and making measurements of σ_{yI} on crosswind arcs at distances to 300 m. Continuous measures of wind speed and direction were made during each experiment. These data are presented in Table 4.22.

The particle spread, σ_{yI}, had no obvious relation to the intensity of turbulence, but this is not surprising in view of the fact that the 3-min sampling time for the turbulence intensity included the effect of eddies much larger than those eddies which could possibly have contributed directly to the spread of the clouds. By comparing the measurements listed in Table 4.22 to the σ_y/σ_θ values in Fig. 4.21 for a continuous point source during lapse conditions, we see that the horizontal particle spread in a puff is considerably less than for releases on the order of 10 min or more.

A set of medium-range experiments is summarized in Table 2 of the Smith and Hay (1961) article. In these experiments zinc cadmium sulfide particles, which fluoresce when irradiated with ultraviolet light, were used as the tracer element. The particles were released from an aircraft flying on a crosswind track, the center of which was several miles upwind of sampling apparatus mounted on the cable of a captive balloon. Measurements of wind speed and vertical direction variation were made from instrumentation mounted on the cable.

The results of these two experiments are presented in Fig. 4.34. Equation 4.26 seems to furnish a fairly good estimate of the spread of

Table 4.22 — EXPERIMENTAL σ_{yI} DATA OBTAINED DURING NEAR-NEUTRAL CONDITIONS*

Experiment	σ_{yI},† m At 100 m	σ_{yI},† m At 200 m	σ_{yI},† m At 300 m	σ_θ,‡ radians	$\bar{u}$, m/sec
1	4.76	10.80	17.70	0.136	6.1
2	3.16	7.64		0.153	5.6
3	3.68	6.80	13.98	0.151	6.1
4	5.04	10.28	14.40	0.126	5.0
5	5.38	11.92		0.147	4.3
6		5.80	9.24	0.140	5.9
7	3.48			0.113	9.5
8	4.70			0.085	9.1
9	2.20			0.091	9.7
10	5.37			0.095	9.0

*From F. B. Smith and J. S. Hay, The Expansion of Clusters of Particles in the Atmosphere, *Quart. J. Roy. Meteorol. Soc.*, 87(371): 94 (1961).

†σ_{yI} is the standard deviation of the crosswind distribution.

‡σ_θ is the standard deviation of wind direction for an averaging time of 1 sec and a sampling time of 3 min. All wind measurements at a height of 2 m.

a cluster of particles over a tenfold range of the intensity of turbulence, a thousandfold range of distance, and a thousandfold range of cluster size.

Figure 4.34 indicates that a value of 4.5 for β gives a reasonable fit to the observed data. Thus Eq. 4.26 may be rewritten

$$\frac{\Delta\sigma_I}{\Delta x} = 3i^2 \qquad (4.27)$$

To date, this relation has been investigated in both the vertical and lateral directions but not in both directions simultaneously. Therefore there has been no direct verification of the usefulness of this formulation for estimating the exposure or concentration from an instantaneous point source.

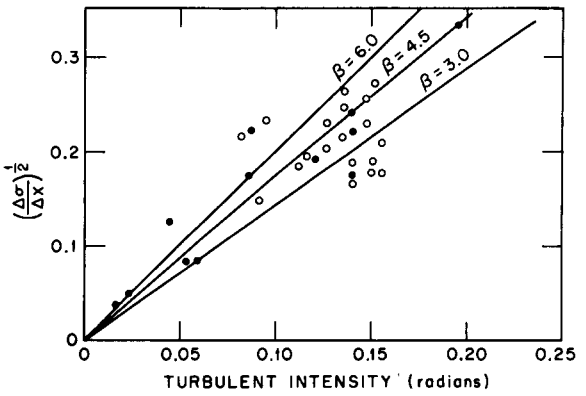

Fig. 4.34 — Experimental values for the spread of clusters of particles. Open circles represent crosswind spread from instantaneous point sources at distances to 300 m. Closed circles represent vertical spread from aircraft-released line sources at distances of 3 to 100 km. Lines through the origin are based on Eq. 4.26 for the indicated values of β. [From F. B. Smith and J. S. Hay, The Expansion of Clusters of Particles in the Atmosphere, *Quart. J. Roy. Meteorol. Soc.*, 87(371): 99 (1961).]

4-10.1.2 Project Sand Storm, California. Project Sand Storm, an atmospheric diffusion program aimed primarily at the development of quantitative statements of dilution rates of pollutants released as quasi-instantaneous volume sources, was carried out at the Air Force Rocket Propulsion Laboratory test facility at Edwards Air Force Base, Calif. (Taylor, 1965). All 43 experiments were carried out under unstable conditions. The sources consisted of solid-propellant rocket motors that contained known amounts of finely divided metallic beryllium in mixture with the propellant. Firing durations ranged from 2 to 8 sec, and puffs were produced with initial visible diameters of 15 to 45 m. The tracer was collected on membrane filters located along circular arcs about the firing point. Originally the grid consisted of 10 such arcs extending from 100 to 2400 m. After 14 experiments all the samplers were consolidated on six arcs extending from 200 to 2400 m, thus increasing the sampler density.

Meteorological data were obtained from a 60-m tower located 60 m upwind of the release point. Temperature sensors, as well as high-response wind systems and bivanes, were mounted on the tower. Information on the visual appearance of the puffs and some measurements of puff dimensions were available from phototheodolite camera photographs.

Using the equation for exposure from an instantaneous point source and the relation between instantaneous-source diffusion and meteorological data given by Smith and Hay (1961), Taylor reasoned that the equation

$$\frac{\psi_p}{Q} \propto [\pi(\sigma_\theta^2 x)\,(\sigma_\varphi^2 x)\bar{u}]^{-1} \qquad (4.28)$$

might describe the observed exposures. The first problem was the determination of the appropriate sampling and averaging times to apply to the horizontal and vertical direction-fluctuation data to ensure that the proper portion of the turbulent energy spectrum was used in computing the direction variances. After satisfying the Smith and Hay requirement that the initial size of the puffs was small in comparison with the length scale of turbulence, Taylor computed correlation coefficients between σ_θ^2 and $\Delta\sigma_{yI}/\Delta x$ using a variety of nontrivial values of sampling and averaging times and measured puff widths. The resulting matrices of correlation coefficients indicated that (1) of the four wind-measurement heights used, i.e., 4, 15, 30, and 60 m, the 4-m values furnished the highest correlation, (2) the shortest averaging time, 1 sec, gave correlations as high as or higher than those obtained with longer averaging times, and (3) there was a trend for higher coefficients to be associated with longer wind-sampling intervals at the greater puff-travel distances. For the range of travel distances in these experiments, a sampling time of 128 sec and an averaging time of 1 sec were adopted. No measurements of the vertical distribution of the tracer were made.

Since all the experiments were conducted under thermally unstable conditions, it was assumed that the vertical rate of growth was positively correlated with the lateral rate of growth. Therefore an attempt was made to use measured values of σ_θ^2, wind speed, and distance to estimate the normalized exposure. Regression analyses using the measured exposures and meteorological data yielded the somewhat surprising result that the inclusion of the wind speed and fluctuation data contributed little to the reduction of the variance obtained when distance was used as the sole criterion. The authors surmise that, since all the Sand Storm tests were conducted under thermally unstable conditions, the meteorological and diffusion data tended to occur within a very limited range. Had tests also been conducted under stable conditions, a greater range of data would have been observed, and it is quite likely that the correlations would have been higher.

Since the authors showed that most of the reduction of variance could be explained by distance from the source, a representation of the data in a probability framework (Fig. 4.35) was adopted. This format is well suited to operational usage. The data from the Sand Storm experiments are presented in summary diagrams Figs. 4.38, 4.39, and 4.40.

4-10.1.3 Högström, Sweden. An extensive set of measurements of the spreading of very short plume segments released from elevated sources was reported by Högström (1964). The tests were conducted at a coastal and an inland site near Stockholm, Sweden. Oil fog plumes were generated over a 30-sec period and released from masts at heights of from 24 to 87 m above the surface. Photographs of the plume segments taken from a point immediately upwind of the release point yielded measures of the vertical and lateral dimensions of plume segments that were assumed to be equivalent to those of an instantaneously generated point-source puff situated at the midpoint of the plume segment. The use of a 30-sec release time permitted photographic observation of the oil fog to much greater distances than would have been possible with true instantaneous releases.

The photographs were suitably enlarged, and the contours representing the visible edges were traced. These contours were assumed to represent some integrated value of concentration according to the tenets of opacity theory. The contours were usually elliptical. The lengths of the lateral and vertical axes of the ellipses were measured and related to standard deviations about the puff center by assumptions regarding the rate of change of

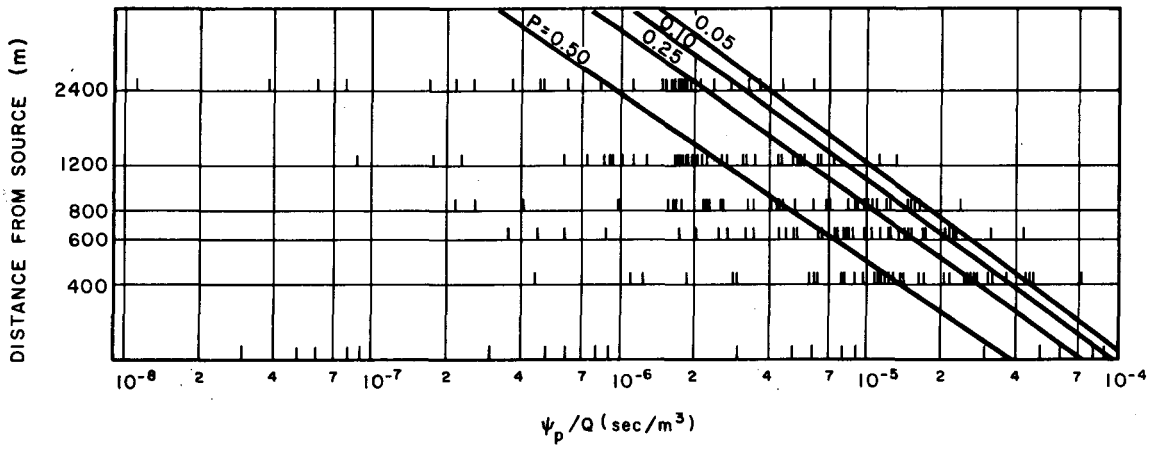

Fig. 4.35 — Normalized peak exposures plotted as a function of distance for 38 Sand Storm experiments. The curves represent the probability of observing a given value of exposure at a given distance. (From Taylor, 1965.)

the standard deviation with travel time and a process of successive approximation. The lateral and vertical motions of the puff centers were also measured. In all cases the downwind distance of the center of the released material was estimated from the mean wind speed at the height of release and the elapsed time. Högström discusses the magnitude of the possible error in this procedure.

The usual experimental procedure consisted of the sequential release of four to six puffs over an interval of an hour. Each interval was considered as one experiment. In all, 430 puffs were released during 111 separate experiments.

With few exceptions all the puffs were released during conditions ranging from near neutral to very stable. Högström developed the stability parameter, λ (the justification for which is discussed at some length in the portion of the paper devoted to theoretical development),

$$\lambda = \log_{10}\left(10^5 \frac{\partial\Theta/\partial z}{\bar{u}_f^2}\right) \qquad (4.29)$$

where $\partial\Theta/\partial z$ is the local vertical gradient of potential temperature between 30 and 122 m and $\bar{u}_f$ is the free wind. The free wind was obtained from twice daily rawinsonde ascents at a point over 100 km from the point of observation. The correlation of this stability parameter with the measured data was greater than for a variety of combinations of other predictors including potential temperature gradient, wind-speed gradient, and actual wind speed, all measured within the height range of the releases.

The basic measurements were of σ_{y_r} and σ_{z_r} (Högström's notation), the lateral and vertical standard deviations of the mass distribution within a puff relative to its moving center, and σ_{y_c} and σ_{z_c}, the standard deviations, in the appropriate directions, of the puff centers. The dispersion of the puff centers was computed from groups of about 25 individual puffs for each of the stability–distance combinations within the range of the measurements. The values σ_y and σ_z, the standard deviations applicable to a continuous release of the length of one of the experiments (about 1 hr), were computed from the relations

$$\begin{aligned} \sigma_y^2 &= \sigma_{y_r}^2 + \sigma_{y_c}^2 \\ \sigma_z^2 &= \sigma_{z_r}^2 + \sigma_{z_c}^2 \end{aligned} \qquad (4.30)$$

The author noted that all the terms in the above equations are stability dependent with the exception of σ_{y_c}. He suggests that the effect of stability is unimportant at the long wavelengths effective in the lateral dispersion of the puff centers. Both σ_{y_r} and σ_{z_r} data at the various distances show a high correlation with curves of the form

$$\sigma_r(x,s) = \frac{\sigma_r(x,0)}{1 + as} \qquad (4.31)$$

where $\sigma_r(x,0)$ is the value of σ_r at a given distance for neutral conditions, a is an experi-

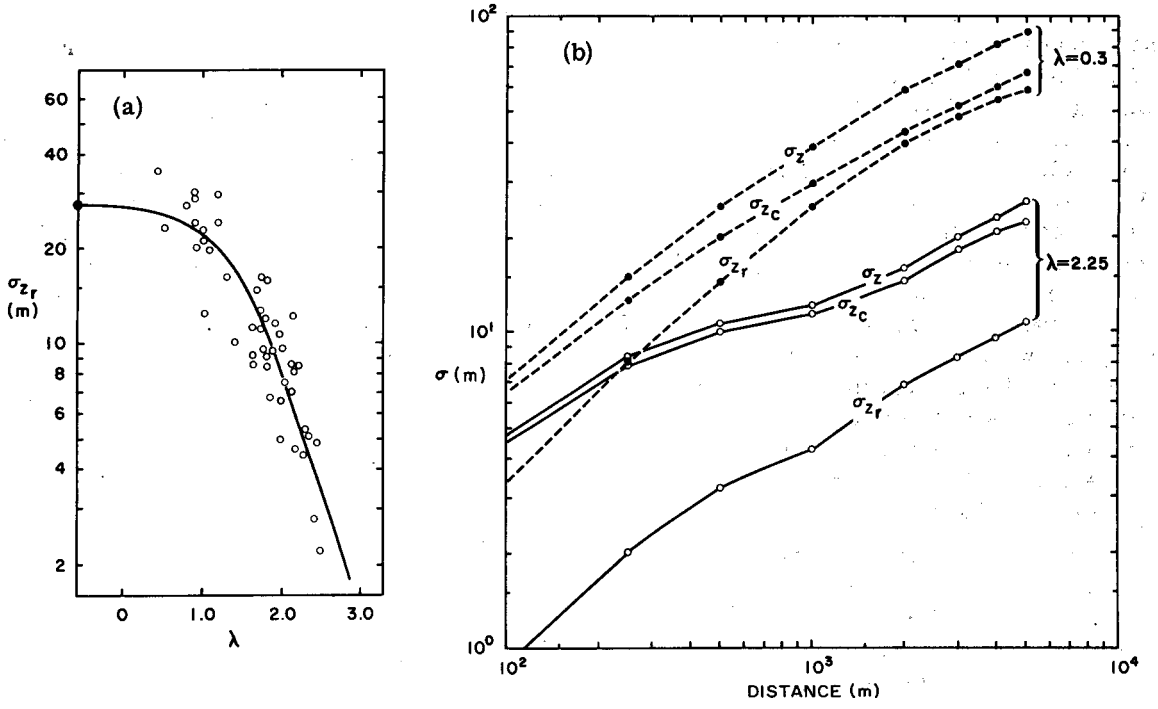

Fig. 4.36— (a) Measurements of σ_{z_r}, the vertical standard deviation of the puff concentration distribution, at 1000 m as a function of the stability parameter, λ. (b) The diffusion of a puff about its center (σ_{z_r}), the dispersion of the puff centers (σ_{z_c}), and the total dispersion (σ_z) as a function of distance for two different values of the stability parameter, λ. [From U. Högström, An Experimental Study on Atmospheric Diffusion, *Tellus*, 16(2): 213 (1964).]

mentally determined constant, and s is the quantity in parentheses in Eq. 4.29. In (a) of Fig. 4.36, σ_{z_r} is shown as a function of the stability parameter at a distance of 1000 m from the source. In (b) of Fig. 4.36, the values of σ_{z_r}, σ_{z_c}, and σ_z at various distances from the source are shown for two different values of the stability parameter, λ, corresponding to almost neutral and quite stable conditions. Equivalent data for σ_{y_r} are not given explicitly but can be inferred from some of the graphs presented.

The remainder of Högström's paper deals largely with the development of formulas for the variation of diffusion with height, distance from the source, and stability. General formulas for downstream concentration from surface and elevated sources are also developed. It is interesting to note that the variation of downstream concentration from continuous surface sources based on these formulas and the observed diffusion statistics compare quite well with the results of the other diffusion experiments reported in the literature. The last two sections of the paper deal with the effects of local terrain inhomogeneities and wind shear on diffusion.

The lateral and vertical puff-spread data from this experimental series are shown in summary diagrams Figs. 4.38 and 4.39.

4-10.1.4 Dugway Proving Grounds, Utah. A series of bomblet-produced puffs, both gaseous and particulate, released at the Dugway Proving Grounds in Utah were the subject of an intensive investigation by Cramer et al. (1964). The purpose of the investigation was the determination of an empirical generalized diffusion model that would have the property of separating the source parameters (initial size of the puff or plume cross section and release length) from the turbulence-induced spreading. Such a model would be expected to be of use with sources of a wide range of sizes, for release times ranging from the quasi-instantaneous to the continuous, and over a variety of different surface roughnesses.

Thirty-three different experiments were used in the analysis. These experiments consisted of

small explosive releases carried out primarily during the night over densely instrumented sampling grids extending to about 1700 m from the source in the case of the particulates and to over 100 m for the gaseous-release series. Release times were either 3 or 26 sec. Continuous records of wind speed and direction were available for each experiment and were used to furnish the values of σ_θ and $\bar{u}$ required by the models. No estimates of deposition or absorption were made. Since the efficiency of the various disseminators used in the tests varied widely, source strengths were estimated from measures of the flux of material through a dense array of towers surrounding and close to the source point.

Five diffusion quantities were observed directly or estimated from the experiments. The observed crosswind spread, σ_{yI}, and the observed crosswind integrated exposure, ψ_{CWI}, were computed from the observed sampler exposures at the various arcs. The vertical plume spread, σ_{zI}, was computed at the close-in distance from a two-dimensional grid of samplers mounted on the array of towers. An "observed" σ_{zI} at arcs further from the source was calculated from the inverse relation between σ_{zI} and the crosswind integrated exposure as a function of distance. The observed peak exposure, ψ_p, at any arc was defined as the highest exposure reported for that arc with no attempt at interpolation. The fifth quantity studied, the area enclosed within a given exposure isopleth, was computed from planimeter readings and, also, was checked by an independent method.

Prediction models were developed for each of the five observed quantities. The first step in the construction of these models was the specification of expressions for virtual-distance computations. Such expressions were necessary to account for the lateral and vertical puff dimensions at the source. Expressions for the two virtual distances were obtained by a rather complicated manipulation involving (1) the actual puff width or depth measured at the row of samplers and towers closest to the source, (2) the assumption of puff expansion rates for the region between the virtual source and the first measurement distance, and (3) estimates of the lateral wind-direction standard deviation applicable to short-term releases obtained from turbulence measurements made during each release.

As in the analysis of the Project Prairie Grass data, Cramer et al. (1964) used σ_θ as the sole meteorological predictor. Average 4-sec wind-direction values were obtained for 8.5-min intervals encompassing each release time. The σ_θ data were reduced to values appropriate to a 2.1-min sampling time via the results of an approximate spectral-analysis technique. These standard deviations were further reduced by the application of the formulation

$$\sigma_\theta(T) = \sigma_\theta(T_0)\left(\frac{T}{T_0}\right)^{1/5} \qquad (4.32)$$

where T_0 is an arbitrary sampling time, 2.1 min in this case, and T is the required sampling time, 3 or 26 sec in these experiments. Cramer et al. present considerable justification for this procedure. According to the authors, values of T larger than T_0 in the above formulation would result in estimates of σ_y appropriate to continuous releases.

The source configuration and turbulence formulations were combined to produce the model formulas. The models for the five diffusion quantities to be studied in the experiments were evaluated for each release on the basis of observed turbulence and initial puff size. The predictions for each of the quantities for each of the 33 experiments were compared on a case by case and on a statistical basis with the observed values.

The results of the comprehensive statistical comparison of the observed and measured diffusion data lead the authors to the general conclusion that, on the average, about 90% of the observations were within a factor of ±2 of the predicted model values. The model σ_{yI} furnished the best fits of the various models to the data with 90% of the data between the limits $0.65 < \sigma_{yI(obs)}/\sigma_{yI(mea)} < 1.38$. The limits for the area exposure were the widest (90% of the data between 0.40 to 2.52). Bias in some of the prediction models may be noted in the detailed graphs of the statistical comparisons.

In summary, the authors' contention that the models have demonstrated their ability to estimate quasi-instantaneous diffusion from measures of lateral turbulence and initial source configuration seems well supported. From other research accomplished by the authors,

Cramer in particular, it would seem that the basic premises involved in the construction of the models are useful for exposure estimation for a variety of release times at other sites.

In the interest of documenting the peak exposures and lateral and vertical plume spread observed during these experiments, average values of these data are presented in the summary diagrams Figs. 4.38, 4.39, and 4.40. The lines representing the average values of the two sets of longer range tests in each of the three diagrams contain the corrections for initial finite puff size derived by the authors. The two individual points at 100 m in Fig. 4.40 are averages of 14 stable and 3 unstable shorter range tests. These contain corrections for the initial puff widths, σ_{yI_0}, which were quite large in these tests.

4-10.1.5 Point Arguello, California. Another experiment that may be used to furnish instantaneous-source diffusion information was conducted at the Naval Missile Facility at Point Arguello, Calif. (Smith et al., 1964). This experiment consisted of both quasi-instantaneous and longer releases of zinc cadmium sulfide and uranin dye over an irregular network of sampling stations at the coastal California site. The site itself is quite irregular with individual ridges and peaks rising to well over 300 m. Sampling was conducted along irregular lines surrounding the release point. It was not possible to obtain puff dimensions and exposures at a number of distances downwind for each puff. However, the number of samplers was sufficient to obtain the width of a puff and an estimate of the maximum exposure at one distance for each release. The results of a number of 60-sec releases, which were not complicated by release or sampling in the vicinity of a pronounced ridge, are presented in Figs. 4.38 and 4.40 for puff width and exposure, respectively.

4-10.1.6 Reactor Destruction Tests (NRTS), Idaho. Islitzer and Markee (1964) report quasi-instantaneous releases that consisted of puffs of radioactive material emitted during reactor destruction tests at the National Reactor Testing Station in southeast Idaho. Release times for four tests were about 30 sec, and the resulting material was sampled over instrumented grids to 750 m in three cases and to over 6000 m in the fourth case. The lateral puff spread was found to be more closely approximated by the square, rather than the first power, of the lateral turbulence intensity. It is interesting to note that Smith et al., in their Point Arguello studies, also found such a relation. Although there is some doubt as to the sampling and averaging times to apply to the wind data to obtain the appropriate intensity of turbulence for the Smith-Hay (1961) expression $\sigma_{yI} = 3i_v^2 x$, there appears to be merit in the use of this formulation for predicting puff dimensions directly from wind-fluctuation measurements.

Since the source strength was not accurately known in these experiments, only relative exposure data were obtained. The plume-width measurements for the one long-distance experiment are given in Fig. 4.38.

4-10.2 Instantaneous-line-source Experiments

4-10.2.1 Dallas Tower, Texas. A series of diffusion tests using elevated line sources released from low-flying aircraft was carried out in the vicinity of the 430-m Dallas television tower at Cedar Hill, Tex. (MacCready, Smith, and Wolf, 1961). Thirty-seven tests were carried out in three two-week intervals in April, June, and August of 1961. Extensive use was made of wind and temperature measurements made by the Air Force at various levels of the tower. Mean-wind and turbulence information was obtained from Aerovane and bivane instrumentation. Vertical sampling of the zinc cadmium sulfide tracer material was accomplished by sequential filter samplers at various levels on the tower and by rotorod samplers located on the ground 1.6 km apart to a distance of about 48 km downwind of the release line. During a portion of the tests, a crosswind rotorod line was added near the downwind end of the main ground sampler line. All releases were made during the night. Source lines ranged between 14.5 and 42 km in length, between 1.6 and 11 km upwind of the tower, and between 110 and 320 m above the tower base.

The primary objective of the program was to relate the measured diffusion characteristics of the cloud to the observed turbulence, wind velocity, and temperature in a quantitative manner.

The principal analysis effort was concerned with the explanation of the observed vertical

cloud width on the tower, the distance from the release line to the first appearance of the cloud at the ground, and the location and magnitude of the maximum exposure at the ground. The basic theoretical relation investigated was that of Smith and Hay (1961) where i_w, the intensity of turbulence (vertical turbulence in this case), was estimated from tower measurements of σ_φ, the standard deviation of the vertical wind-direction distribution. The quantity σ_φ generally increases with the sample length up to some point where it becomes asymptotic to a maximum value. In the case of the Dallas tower data, it was found that almost all the increase occurred within 3 min.

The results of the tests showed that the vertical dimensions of the cloud, as given by σ_{zl}, were consistently larger than calculated from Eq. 4.27. One reason for this discrepancy was that the initial size of the cloud at release was appreciable because of the turbulence created by the releasing aircraft.

The rate of growth ($3i_w^2$) leads to a model of ground exposure given by

$$\psi = \frac{2Q}{3i_w^2 x\,\bar{u}\,(2\pi)^{1/2}} \exp -\left(\frac{H^2}{18i_w^4 x^2}\right) \quad (4.33)$$

where ψ = ground exposure at a distance x from the release
Q = source strength
$\bar{u}$ = mean speed in the layer from the ground to the release height
i_w = in this case, a weighted average of the vertical-turbulence intensity between the release height and the ground

Plots of the calculated and observed exposures are shown in Fig. 4.37. Observed ground exposures were in good agreement with the model described by Eq. 4.33 when the release was made within a well-developed turbulent layer above the ground. Observed maximum exposures averaged 23% higher than forecast for the 14 cases that satisfied this condition. For releases above this turbulent layer, ground exposures were much more erratic than predicted by the model.

Calculations of i_w for all tests were used to estimate the probability that a release would reach the ground. If a criterion is assumed which requires that the particle cloud reach the ground in reasonable quantity in the first 24 km, then this criterion would be satisfied 86% of the time for line-source releases at a height of 135 m, 37% of the time for releases at 225 m, and 3% of the time for releases at 315 m.

Dilution of the cloud from the ends of the release line was measured during nine of the tests in which adequate sampling was available along a crosswind line at the downwind end of the main sampler line. It was found that the cloud diluted laterally at a rate corresponding to

$$\frac{d\sigma}{dx} = i_v \quad (4.34)$$

where i_v was computed from the root-mean-square value of the horizontal direction variation over the period of interest. This rate is in marked contrast to the vertical spreading rate of $3i_w^2$.

4-10.2.2 Rough and Irregular Terrain, United States. Experiments similar to those conducted at the Dallas tower were carried out over sites in Oklahoma, Texas, Washington, and Nevada (Smith and Wolf, 1963). The most important difference between these tests and the Dallas experiments was the absence of a tall tower for measuring the turbulence values and the vertical distribution of tracer material from the aircraft-released line source.

In each of these four experiments, sampling was accomplished along a line of rotorods about 40 km in length oriented in a direction approximately normal to the aircraft line release of zinc cadmium sulfide. Meteorological information was obtained from a 30-m tower and two 10-m towers situated along the line of release as well as from a high-frequency turbulence-measurement system mounted on the tracer-releasing aircraft.

The experimental hypothesis consisted of the assumption that the effective turbulence computed for the Dallas experiments could be estimated from the more-limited meteorological measurements available during these experiments, and thus the estimate of the effective turbulence could be used to estimate the ground-exposure patterns. At the Oklahoma site, where the terrain was similar to that at Dallas, the computed exposures were in good agreement with those observed.

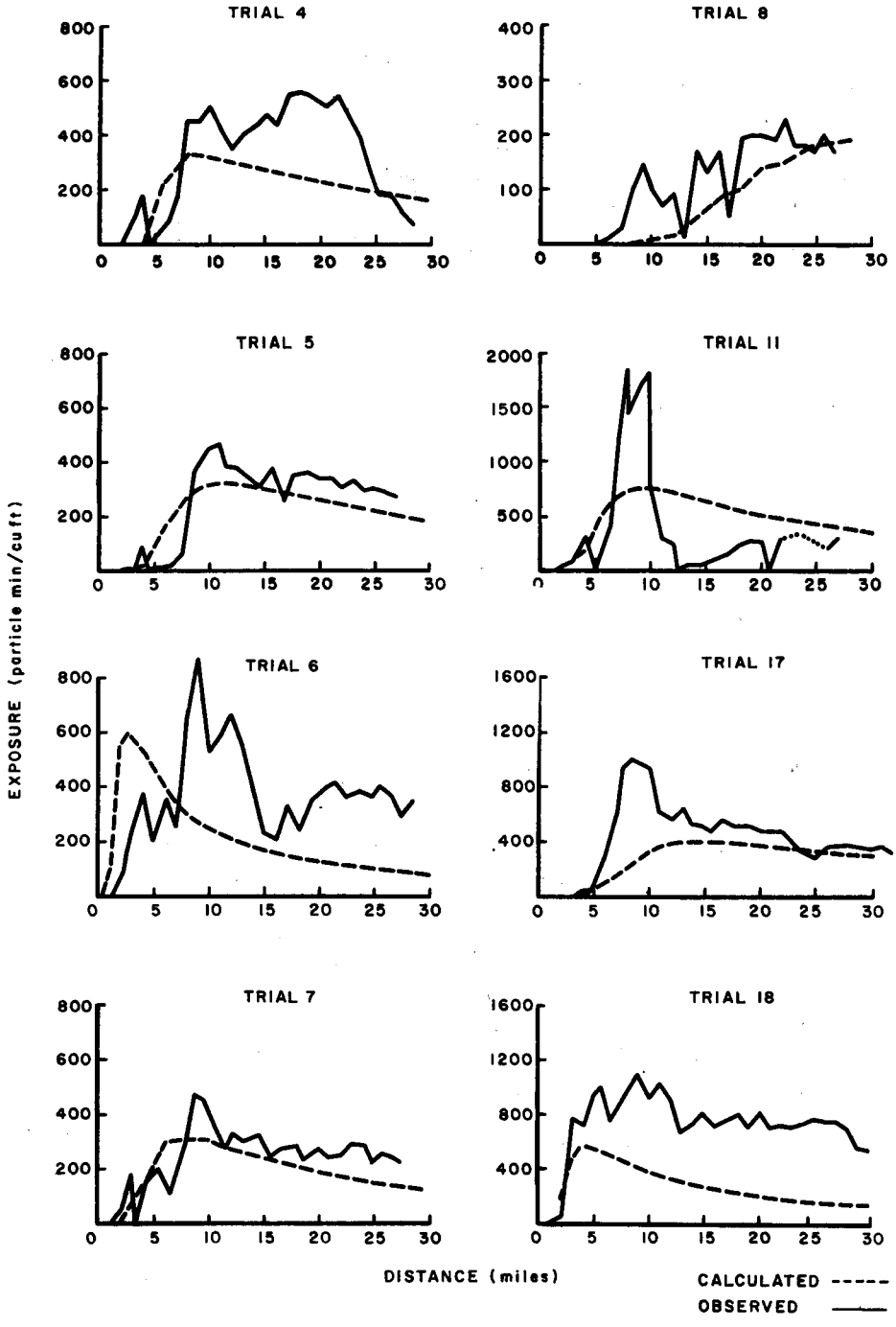

Fig. 4.37—Comparison of calculated and observed exposures from an elevated line-source release. (From MacCready, Smith, and Wolf, 1961.)

The Texas sampler line extended inward from the coast in the immediate vicinity of Corpus Christi. The observed exposure patterns bore little resemblance to those calculated. This result was ascribed to the possible existence of helical circulations in the air moving off the ocean over the very flat terrain. Two different results were obtained at the Washington site. During a few afternoon runs, atmospheric fluctuations of lower frequency

than could be sampled with the project instrumentation tended to bring higher than predicted exposure values to the ground. The remainder of the runs, taken at night, showed small ground exposures that were in accord with the small predicted values based on the low levels of turbulence.

Perhaps the most interesting of the four studies was that conducted at the Nevada site. The sampler line crossed a ridge with a maximum height of about 300 m above the lower land at each end of the line. During stable night conditions the highest ground exposures were invariably experienced on the lee side of the ridge. The authors surmised that the tracer, embedded in the stable flow, experienced an upward transport along the windward slope and little tracer reached the surface. The indications are that a more complex turbulence field in the lee of the ridge resulted in a greater degree of vertical mixing and thus in higher surface exposures.

These experiments point out with great clarity the effect of nonregular terrain on expected diffusion patterns. The classical methods, as well as those developed more recently over the flat diffusion grids, offer little help in estimating diffusion in the more complicated terrain. The meteorologist must in more complicated terrain use his total experience to assess, even qualitatively, the nature of the resulting diffusion.

4-10.3 Summary of Instantaneous-source Experiments

The data presented in this section, as can be seen from Table 4.1b, are quite inhomogeneous with respect to source configuration, release height, meteorological and terrain conditions, and, probably, scavenging effects. Since a variety of different meteorological predictors, which cannot be quantitatively compared, were used by the various investigators, the diffusion data in the summary diagrams are classified according to the broad categories of unstable, near neutral, and stable. Not all the data are plotted in the summary diagrams. Only those averages, regression lines, and, occasionally, individual runs that give some idea of the range of values encountered during these experiments have been used.

In general, the observed slopes of σ_{yI}, σ_{zI}, and $\psi_p \bar{u}/Q$ should not be expected to conform closely to any theoretical considerations unless such formulations include corrections for initial source size and deposition. Some of the data presented include corrections for initial source size, either given by the authors or estimated from other considerations. None, however, include any correction for deposition.

Figure 4.38 presents a summary of σ_{yI} values for quasi-instantaneous releases. The point labelled "approximate limit of most stable data" was estimated from a few of the most stable runs reported by Högström and from an extrapolation of his functional relation between σ_{yI} and his stability parameter, λ. The neutral

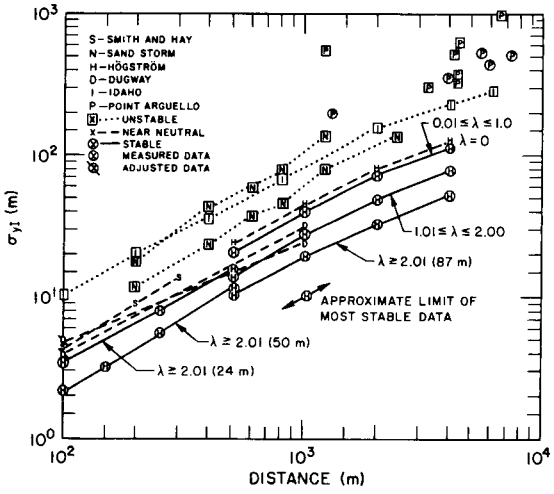

Fig. 4.38 — Summary diagram for measured σ_{yI} data. Note that measured data have been differentiated from those to which some adjustment has been applied.

curve for the Högström experiments appears to be an extension of that for the Smith and Hay data despite the source-height difference. The Point Arguello data represent individual determinations of σ_{yI} at various distances from the source over the rugged coastal site. The turbulence induced by the terrain may account both for the large individual values of σ_{yI} and for the similarity between the stable and unstable cases. In situations such as this, a measurement of turbulence or stability at the source may not be sufficient information to estimate the terrain-induced diffusion along the puff trajectory.

The Dugway measurements of σ_{yI} are represented by the regression lines for two test

series and contain a correction for lateral source dimensions. Two sets of Sand Storm curves are presented. The upper curve represents the average of the four highest values of σ_{yI} at each measurement distance, and the lower line is the average of all the data. It is interesting to note, in the original data, that the individual σ_{yI} curves generally increase quite steadily in comparison with the erratic decrease of exposure with distance. The observations of the vertical meander, or skipping, of the puffs during unstable conditions are consistent with this behavior.

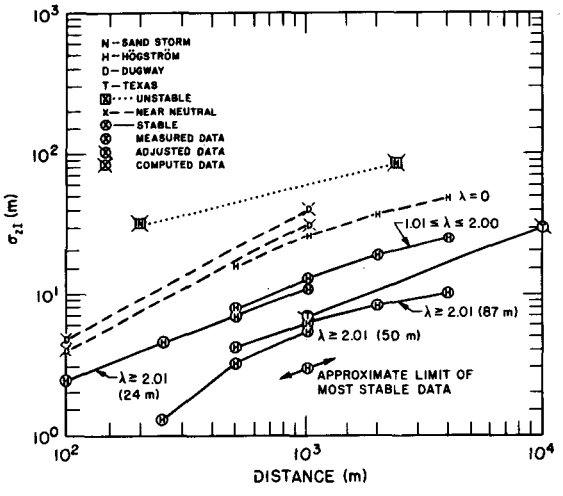

Fig. 4.39 — Summary diagram for measured σ_{zI} data. Computed data have been added for the Sand Storm series because of the lack of information on instantaneous-source vertical spreading during unstable conditions.

Considerably fewer direct measurements are available for instantaneous-release values of σ_{zI} (Fig. 4.39). By far the most numerous are those resulting from the photographic investigations of Högström. Again, an approximate lower limit for σ_{zI} at 1000 m is indicated. The regression line for the Dallas experiments is based on one measurement of σ_{zI} per experiment at source distances varying from about 10^3 to 10^4 m from the tower. The observed values have been reduced by factors indicated by the authors to remove the spreading due to the aircraft-induced turbulence. About 85% of the observations are included between the boundaries of ± 2 about the regression line. The data exhibit some dependence on the weighted vertical-turbulence intensity as derived from measurements made on the television tower. In practical applications this meteorological predictor cannot be measured unless a suitably tall tower exists.

The Dugway σ_{zI} data are basically computed values since they are based on measurements of σ_{zI} made at only one distance close to the source, and are derived from an adjusted crosswind integrated exposure at other distances. Although all the Dugway data presented in Fig. 4.39 were obtained during the night hours, the stability ratio and turbulence-intensity values indicate neutral or near-neutral conditions in every case.

The curve for σ_{zI} for the Sand Storm tests is a computed quantity and included in this summary of measurements only because of the lack of σ_{zI} observations during unstable conditions. The 90th percentile values of normalized exposure ($p = 0.10$ in Fig. 4.35) and the average value of Q, σ_{yI}, and $\bar{u}$ for all the tests were used to compute the average σ_{zI} values. The use of the 90th percentile values was based on the fact that the higher exposure values at each distance would be more likely to be estimates of puff-center values in situations where the puff exhibited some degree of vertical meander. The values obtained by this procedure were reduced to account for the initial vertical puff dimensions. The use of the median values of the Sand Storm exposure at each distance from the source results in a σ_{zI} curve higher by a factor of 3 to 4 with a slope more closely approaching that of neutral and stable conditions.

Measured values of normalized exposure are presented in Fig. 4.40. The numerous Högström data on puff dimensions were obtained photographically and thus do not include measured exposures. However, the approximate upper limit of normalized exposure has been computed from the appropriate values of σ_{yI} and σ_{zI} at 1000 m in Figs. 4.38 and 4.39.

The average observed value and range of the longer Dugway tests are presented along with average exposure values at 100 m for 17 shorter range tests. In these latter tests a correction was applied to the exposure data to account for the initial lateral puff width, which was frequently rather large.

The Sand Storm experiments are represented by two lines, the higher values representing the 90th percentile exposure data and the lower

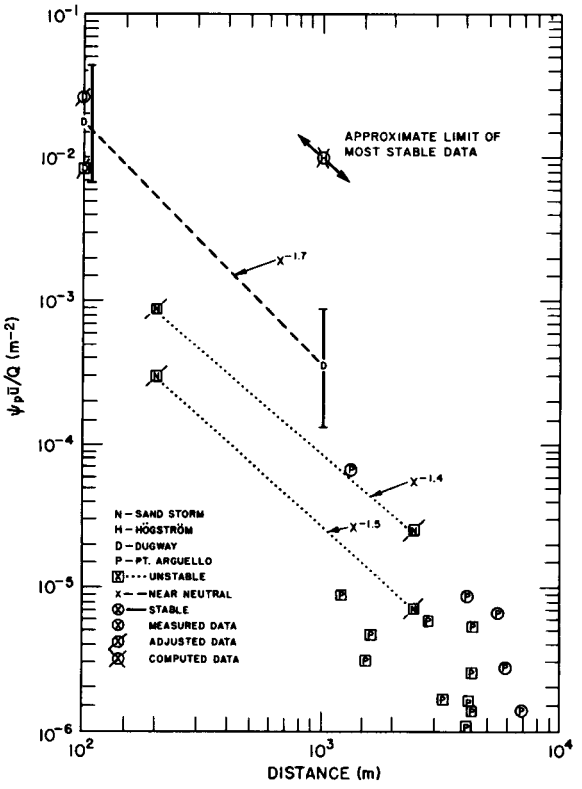

Fig. 4.40—Summary diagram for normalized axial exposure data. The point representing the approximate limit of most stable data is based upon the smallest values of σ_{yI} and σ_{zI} at 1000 m observed by Högström.

line, median values. In each case an adjustment for the initial vertical puff size was applied to the observations.

The Point Arguello data show some differentiation between stable and unstable exposures, but the stable values are still considerably smaller than would be expected on the basis of the other data that have been presented. Again, this may be due to the turbulence induced by the very rough terrain over which the experiments were conducted.

A set of suggested instantaneous-source values of σ_{yI}, σ_{zI}, and $\psi_p\bar{u}/Q$, based on the foregoing data, are presented in Table 4.23.

Editor's Note: An experimental program to study in detail the atmospheric diffusion of airborne aerosols over an isolated urban area was conducted at Fort Wayne, Ind. (Glenn R. Hilst and Norman E. Bowne, *A Study of the Diffusion of Aerosols Released from Aerial Line Sources Upwind of an Urban Complex*, Vols. I and II, Travelers Research Center, Hartford, Conn., 1966). Seventy aerial line-source releases were made in 21 separate experimental periods at night under various thermal stability conditions.

The city was expected to produce enhanced mixing because of increased surface roughness and, also, to show a heat-island effect. The tracer and meteorological sampling networks were designed to measure these effects quantitatively. Vertical tracer sampling on towers and a tethered balloon provided useful information on vertical motions around the city.

The following features of the atmospheric motion within and around an isolated city were identified:

1. In a large majority of situations, but particularly when the temperature lapse rate in the lower 61 m of the rural atmosphere is between dry adiabatic and isothermal, the axis of the tracer cloud descends toward ground level. The cloud was observed to enter the city with maximum dosages consistently at or near street level under these conditions. With inversion conditions the cloud remained at release height and diffused slowly in the vertical.
2. The enhanced surface roughness and thermal mixing caused by the city produced a 30 to 50% increase in the vertical mixing of the aerosol over the city as compared with the rural area.
3. An analysis of the mean and variance of tracer dosages at the surface sampling stations showed a random component of variability of about a factor of 2. No distinct differences of diffusion rates could be differentiated on the basis of land use within the city. These results suggest that a city of the size and structure of Fort Wayne can be considered a single-surface anomaly in predicting its effect on aerosol diffusion.

Table 4.23—SUGGESTED ESTIMATES FOR σ_{yI}, σ_{zI}, AND $\psi_p\bar{u}/Q$*

Parameter	Conditions	100 m	4000 m	Approximate power function
σ_{yI}, m	Unstable	10.0	300	$0.14(x)^{0.92}$
	Neutral	4.0	120	$0.06(x)^{0.92}$
	Very stable	1.3	35.0	$0.02(x)^{0.89}$
σ_{zI}, m	Unstable	15.0	220	$0.53(x)^{0.73}$
	Neutral	3.8	50.0	$0.15(x)^{0.70}$
	Very stable	0.75	7.0	$0.05(x)^{0.61}$
$\psi_p\bar{u}/Q$, m^{-2}	Unstable	2.12×10^{-3}	4.81×10^{-6}	$4.20(x)^{-1.65}$
	Neutral	2.08×10^{-2}	5.30×10^{-5}	$35.5(x)^{-1.62}$
	Very stable	3.26×10^{-1}	1.30×10^{-3}	$330(x)^{-1.50}$

*The power functions are applicable in the given range of distances only.

4-11 ESTIMATES OF TRAJECTORIES AND DIFFUSION (CONSTANT-LEVEL BALLOONS)

4-11.1 Use of Constant-level Balloons for Trajectory Estimation

In the past, estimates of the trajectory and spreading of pollutant releases to the atmosphere have usually been based upon wind statistics obtained at fixed points (Eulerian networks). Fundamentally, however, atmospheric diffusion depends on the movement of individual air parcels (Lagrangian statistics). In recognition of this fact, recent developments in the field of diffusion meteorology have emphasized ways of passing from the easily obtained Eulerian statistics to the desired Lagrangian statistics. It would appear that, although Eulerian wind statistics may be suitable for diffusion estimates over small times and distances, for the longer times and distances there are important difficulties inherent in this technique. For example, as a pollutant spreads vertically, it encounters wind-direction and speed changes that cannot be measured by a surface network of anemometers and are difficult and expensive to determine by existing fixed-point vertical wind-sounding methods.

The literature is replete with ingenious techniques for estimating air trajectories from Lagrangian observations. On the microscale one might mention the photographic positioning of soap bubbles by Edinger (1952), of dandelion seed by Badgley and Fleagle (1952), and of Kleenex lint by Miller (1952). However, even these tracers possessed some fall velocity with respect to the air. If a substance with a density equal to that of the air is introduced into the atmosphere, there is little doubt that it will follow the atmospheric motions. The difficulties arise in positioning such substances. With the exception of smoke, most of these substances are not visible to the naked eye and do not act as reflectors of electromagnetic radiation. Therefore their detection at a later time involves either a complex sampling network or a rapidly moving atmospheric probe such as an aircraft.

An alternative method of obtaining air trajectories involves placing a gas lighter than air within a visible container heavier than air so that the average density of the traceable object is equal to that of the air. A no-lift balloon satisfies this criterion, and through the years meteorologists such as Richardson and Proctor (1925), Koschmieder (1925), Gifford (1953), Lucas, Spurr, and Williams (1957), and Sakagami (1961) have made use of no-lift balloons to estimate air trajectories and atmospheric diffusion. In the following sections the use of a constant-volume balloon as a tracer of air motions, as first reported by Angell and Pack (1960), will be explored. The experiments reported are primarily those conducted by the personnel of the Environmental Science Services Administration (formerly the Weather Bureau).

The tetrahedron-shaped constant-level balloons (tetroons) are made of the nearly inelastic material, Mylar. Prior to flight, the tetroon is filled with a helium–air mixture to a pressure considerably higher than that at the expected flight (density) level. The advantage of the superpressured tetroon over expansible no-lift balloons is that the tetroon volume does not change appreciably with a change in temperature of the inflation gas. Thus there is little variation in buoyancy force, and the tetroon responds primarily to ambient density variations and to the three-dimensional wind patterns.

Since, in general, an air parcel moves vertically as well as horizontally, the fidelity with which a tetroon can trace air motions is a function of the fidelity with which the tetroon follows the vertical air motion. Inasmuch as there is always a restoring force tending to return the tetroon to its equilibrium floating surface, the amplitude of tetroon oscillations in the vertical will always be less than that of air parcels. There is, however, evidence that the three-dimensional tetroon trajectory represents a first approximation to the three-dimensional air-parcel trajectory. Thus Angell (1964) showed that at Cardington, England, in nearly calm conditions, the period of vertical oscillation of the tetroon was almost identical with the period of vertical oscillation of wind vanes attached to a barrage-balloon cable. Furthermore, at this same site the period and amplitude of the tetroon oscillations in the vertical were always greater in the afternoon when the atmosphere was relatively unstable than in the morning when the atmosphere was relatively stable, and indeed there was fair

agreement between the period observed and the period theoretically expected from a consideration of the lapse rate. Finally, at Cardington it was found that at the high-frequency end of the tetroon-derived vertical-velocity spectrum, the spectral density decreased approximately as frequency to the −2 power in agreement with theoretical expectations for Lagrangian-type data.

The tetroons have generally been positioned by radar, either through the use of passive reflectors or transponders (radio beacons) attached to the tetroons. The latter technique was first reported by Pack (1962) and was extensively used in the Los Angeles Basin by Pack and Angell (1963). Detailed descriptions of the various tetroon–transponder systems used may be found in the various references noted in this section. With an appropriate radar, tetroon positions can be obtained at intervals of a few seconds over distances well over 100 km.

A picture of the types of trajectories obtained in widely varying geographical areas is given by Figs. 4.41–4.43, which show tetroon trajectories from Cardington, England (Angell, 1964), Las Vegas, Nev. (Angell and Pack, 1961), and Los Angeles, Calif. (Pack and Angell, 1963). Cardington is located amongst gently

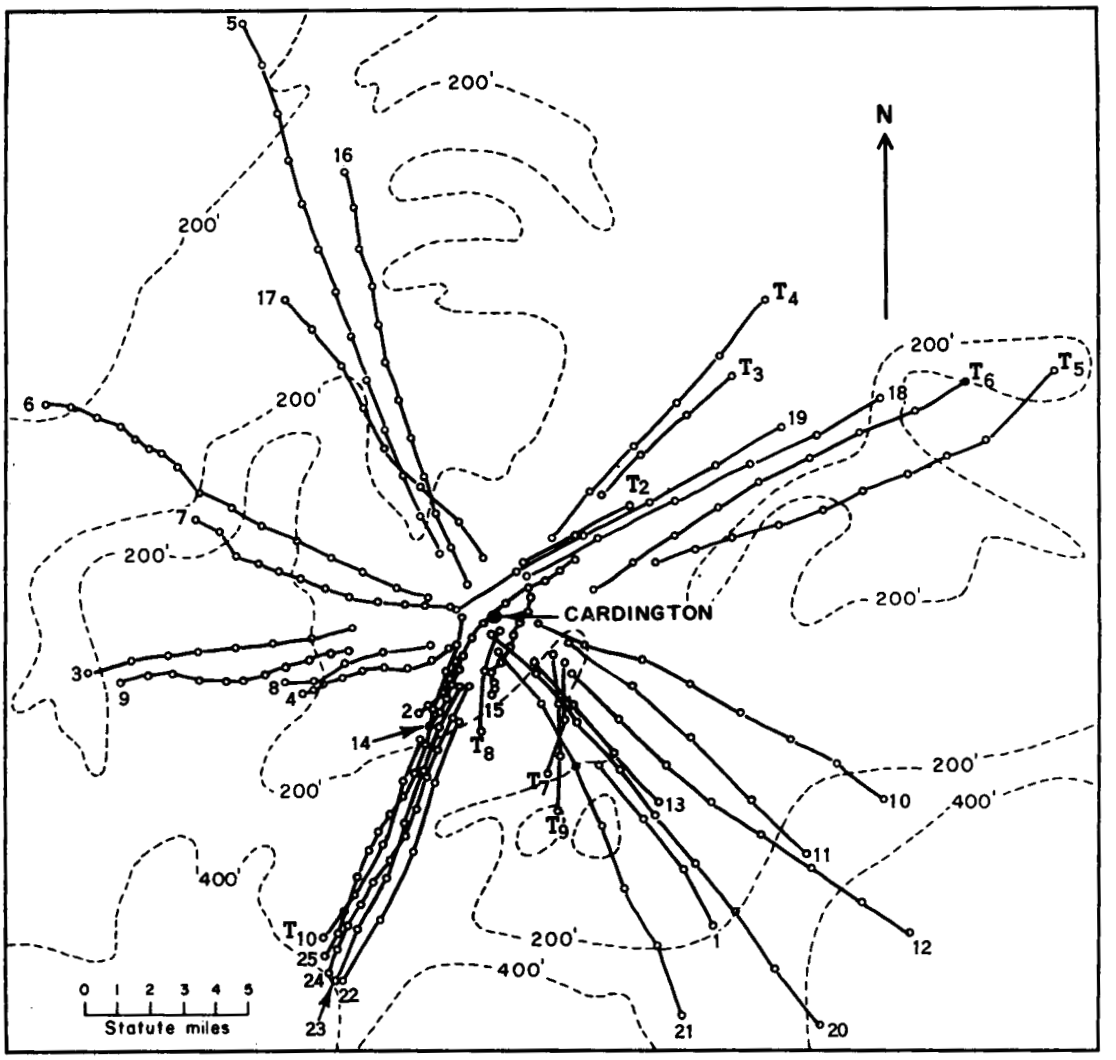

Fig. 4.41—Tetroon trajectories at Cardington, England, superimposed upon a simplified topographic map of the area. Tetroon positions indicated at 5-min intervals. Flights labelled T were made when the barrage balloon (with fixed-point wind instruments) could not be flown. (From Angell, 1964.)

rolling hills in south central England. Here the tetroons were flown at heights near 800 m. Very apparent from Fig. 4.41 is the straightness of trajectories in this region and, at this height, the lack of dependence of trajectories upon terrain features. The Las Vegas flights (Fig. 4.42) were launched from Yucca Flat and exhibited vertical height oscillations of as much as 3000 m during the daytime hours. The flights went upslope during the day and downslope (flights 6 and 13) during the night with some evidence that the veering of the trajec-

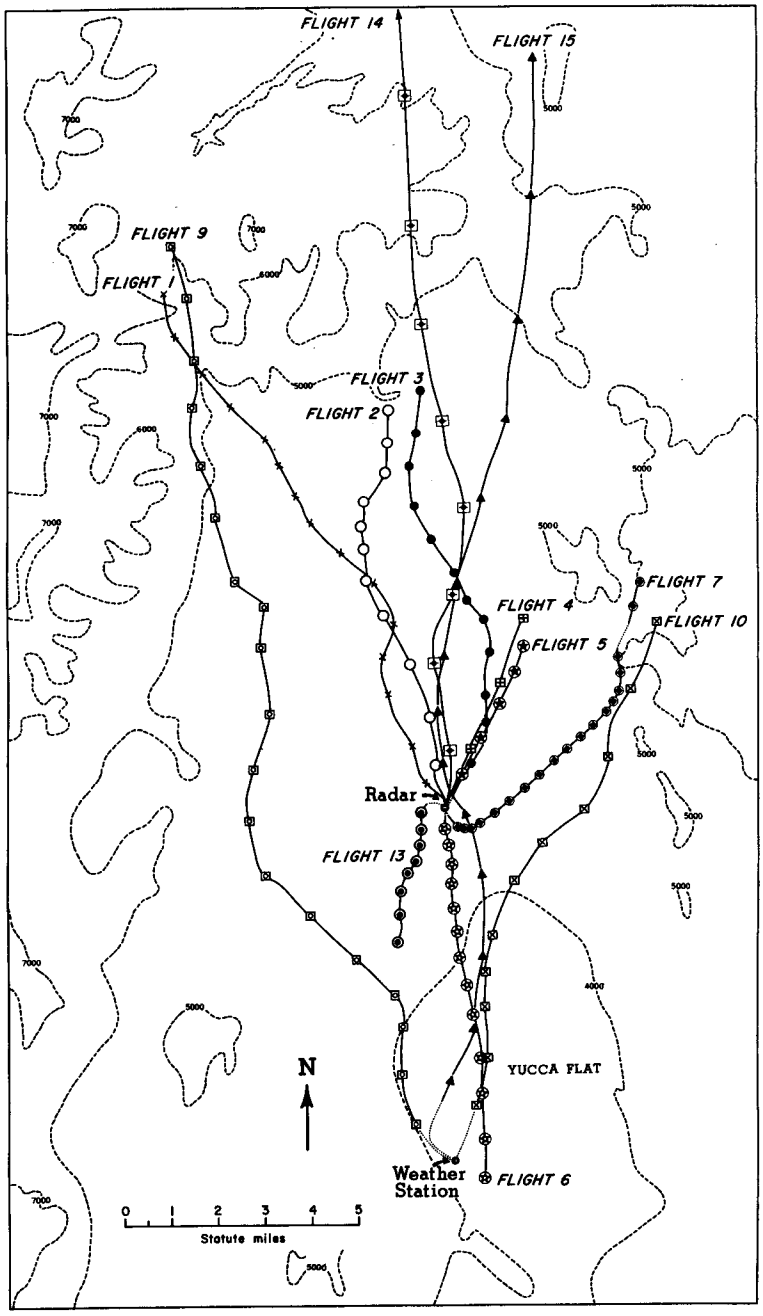

Fig. 4.42—Tetroon trajectories at Yucca Flat near Las Vegas, Nev., superimposed on a simplified topographic map of the area. Tetroon positions indicated at 5-min intervals. Dotted segments of trajectories estimated from visual sightings. (From Angell and Pack, 1961.)

tories during the day (flights 1, 2, 3, 4, 5, and flights 9 and 10) was associated with solar heating of the mountain slopes. Numerous flights have been made from various sites within the Los Angeles Basin, and Fig. 4.43 shows the flights from Long Beach at heights of 300 m to 600 m. Note the large directional shifts along the Long Beach flights, particularly in comparison with the Cardington flights.

4-11.2 Use of Tetroons for Estimating Atmospheric Diffusion

In addition to providing an estimate of the travel direction of a pollutant, tetroons can be utilized to yield an estimate of the diffusive capabilities of the atmosphere. In this section alternate ways in which this can be done are considered, and comparisons between the diffusion derived from tetroons and the diffusion derived by more-conventional techniques are recorded. Finally, mention is made of the use of tetroons to bridge the gap between the more easily obtained Eulerian statistics and the oftentimes desired Lagrangian statistics.

Within the atmosphere two different types of diffusion are of interest. The first type involves crosswind diffusion from a continuous point source (smoke-plume type diffusion), and the second involves so-called "relative" diffusion (smoke-puff type diffusion). Insofar as possible, both types of diffusion will be studied in both vertical and lateral dimensions.

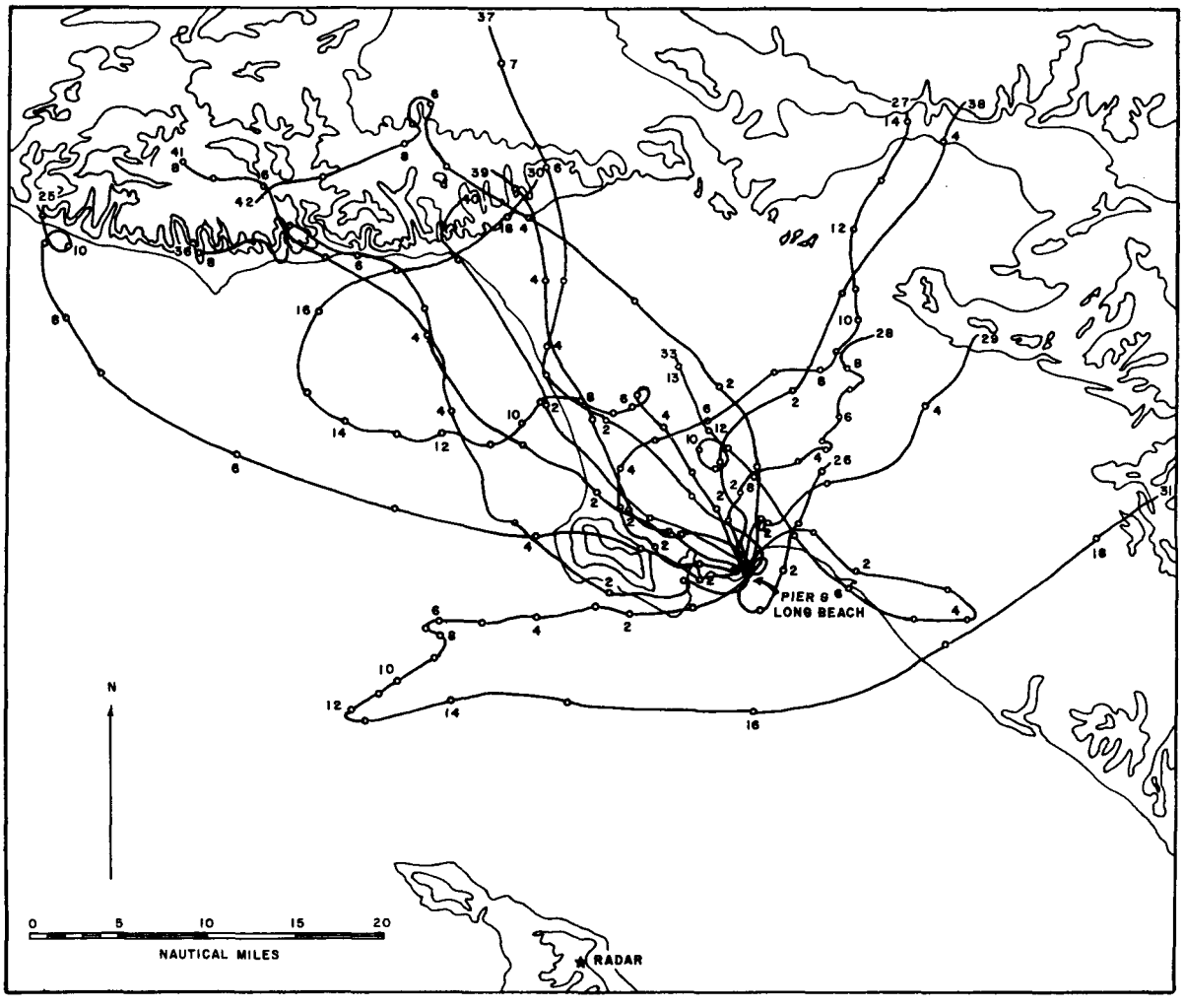

Fig. 4.43—Tetroon trajectories of 2-hr or more duration for releases from Long Beach, Calif. Tetroon positions are indicated at 1-hr intervals. (From Pack and Angell, 1963.)

In the following sections lateral atmospheric diffusion is estimated from tetroon data in three ways: (1) from successive tetroon releases, (2) from the lateral distance between pairs of nonsimultaneously released tetroons, and (3) from individual tetroon trajectories.

4-11.2.1 Lateral-diffusion Estimates from Successive Tetroon Releases. The most common measure of lateral diffusion, the lateral standard deviation, can be obtained from successive tetroon releases by evaluation at given downwind distances of the root-mean-square value of the distances between the mean trajectory and individual trajectories. Figure 4.44 shows the standard deviations so obtained for series of tetroon flights within the Los Angeles Basin and near Las Vegas, Nev. The series were selected so that a mean wind could reasonably be defined for each series. The time between the first and last tetroon release in each series varied from 8 to 48 hr. For these flights in the Los Angeles Basin, the lateral standard deviations were large, averaging 50% to 75% of the downstream distance because the tetroons were being used to simulate a continuous source sampled over periods of many hours. Thus the lateral standard deviations reflect not only what might be considered turbulent diffusion but also the effect of changes in the mean wind direction with time. The strength of the diurnal wind regime in the Los Angeles Basin is well known.

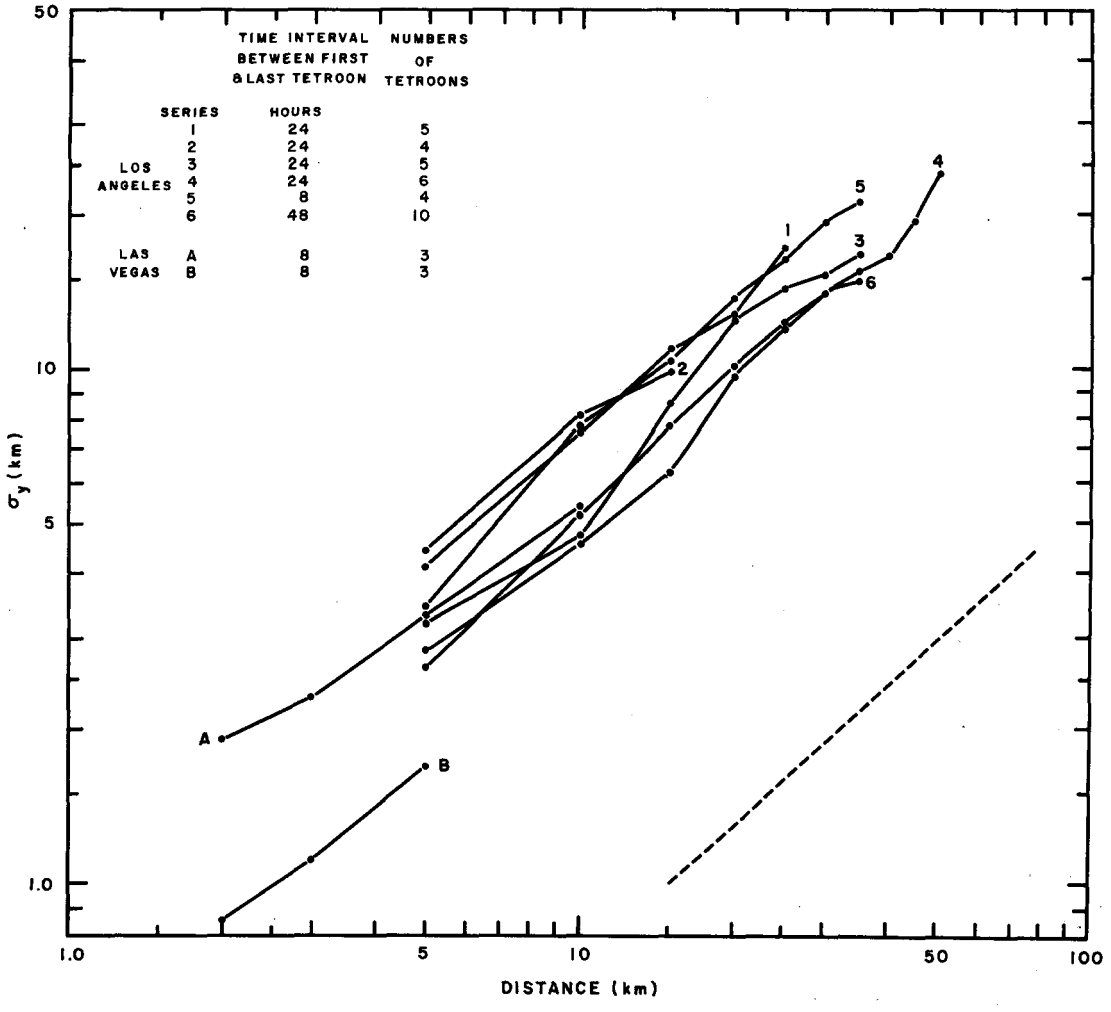

Fig. 4.44—Estimates of lateral diffusion from successive tetroon releases as a function of distance at Los Angeles, Calif., and Las Vegas, Nev. Dashed line gives typical values of σ_y obtained from 1-hr tracer diffusion experiments.

4-11.2.2 Lateral-diffusion Estimates from Tetroon Pairs. It has been indicated that diffusion estimates from successive tetroon releases so far available yield lateral standard deviations appropriate to a large sampling time. Also there is a certain subjectivity involved in deciding what flights should be included in a series and in defining the mean trajectory to be associated with that series. To some extent these difficulties may be circumvented by considering the lateral distance between pairs of nonsimultaneously released tetroons at various downwind distances. Panofsky and Brier (1958, p. 210) showed that the best unbiased estimate of the variance of the population (σ_y^2) is given by

$$\sigma_y^2 = (N-1)^{-1} \sum_{i=1}^{N} (Y_i - \overline{Y})^2 \qquad (4.35)$$

where N is the number of observations, Y_i is the individual position on the y axis, and $\overline{Y}$ is the mean position on the y axis. For the case of N = 2,

$$\sigma_y^2 = \left(\frac{Y_1}{2} - \frac{Y_2}{2}\right)^2 + \left(\frac{Y_2}{2} - \frac{Y_1}{2}\right)^2 \qquad (4.36)$$

but, since by definition the lateral distance, d, between a particle pair is $Y_1 - Y_2$, then

$$\sigma_y^2 = \frac{d^2}{2} \qquad (4.37)$$

Therefore, in principle at least, the lateral variance (and hence lateral standard deviation) can be estimated from a continuous point source through evaluation of the average of the square of the distances between pairs of nonsimultaneously released tetroons at various downwind distances. Furthermore, the effect on the lateral standard deviation of various release and sampling durations can be estimated by choosing tetroon pairs having different time intervals between release. This then is a particularly suitable method for estimating a diffusion climatology for various sites under given atmospheric conditions. Accordingly, at a variety of launch sites, circles with radii of 5, 10, 15 km, etc., were drawn, and the distance between points of intersection of pairs of trajectories with these circles was evaluated. This was done for all possible pairs of flights where the time interval between tetroon releases was less than 6 hr and less than 24 hr.

Based on the above procedure with 201 observations of tetroon pairs, Fig. 4.45 shows the mean lateral standard deviation as a function of downstream distance for various tetroon launch sites and for time intervals between releases of less than 6 hr (underlined symbols) and less than 24 hr. It is assumed, then, that these standard deviations are approximations to the standard deviations that would be obtained if one released a tracer material for periods of 6 hr and 24 hr and also sampled for the same periods. Thus, included in these standard deviations are meanderings of the tracer plume as well as what might be considered changes in the mean wind direction (meanderings on a much larger time scale). The asterisks at 5-km intervals in Fig. 4.45 indicate the mean of the 24-hour series (series 1, 2, 3, and 4) in Fig. 4.44. Inasmuch as these four series all involved flights from Long Beach, the similarity in the ordinate of the asterisks and the Long Beach designators implies that, basically, the two techniques are compatible.

It is of interest from the viewpoint of diffusion climatology that, for release periods of 6 hr, the lateral diffusion from the Long Beach and Venice sites is about three times the magnitude of the lateral diffusion from Cardington. This would be expected owing to the presence of a pronounced diurnal wind regime within the Los Angeles Basin. The tetroon flights from Marineland yield relatively small values of the standard deviation because flights were made only during the daytime sea-breeze regime and because many of the flights from Marineland involved the simultaneous release of two tetroons. The relatively rapid increase of lateral standard deviation with downstream distance for Wallops Island flights (Angell and Pack, 1962) released within 6 hr of each other suggests the predominance of large-scale eddies over the water during the winter period of the flights.

The adjacent dashed and solid lines in Fig. 4.45 indicate the mean values of lateral standard deviation as a function of downstream distance for all the tetroon launch sites and for time periods of release and sampling of less than 6 hr and less than 24 hr, respectively. It is emphasized that these mean values are not universally applicable owing to the preponderance of tetroon flights within the cyclic wind

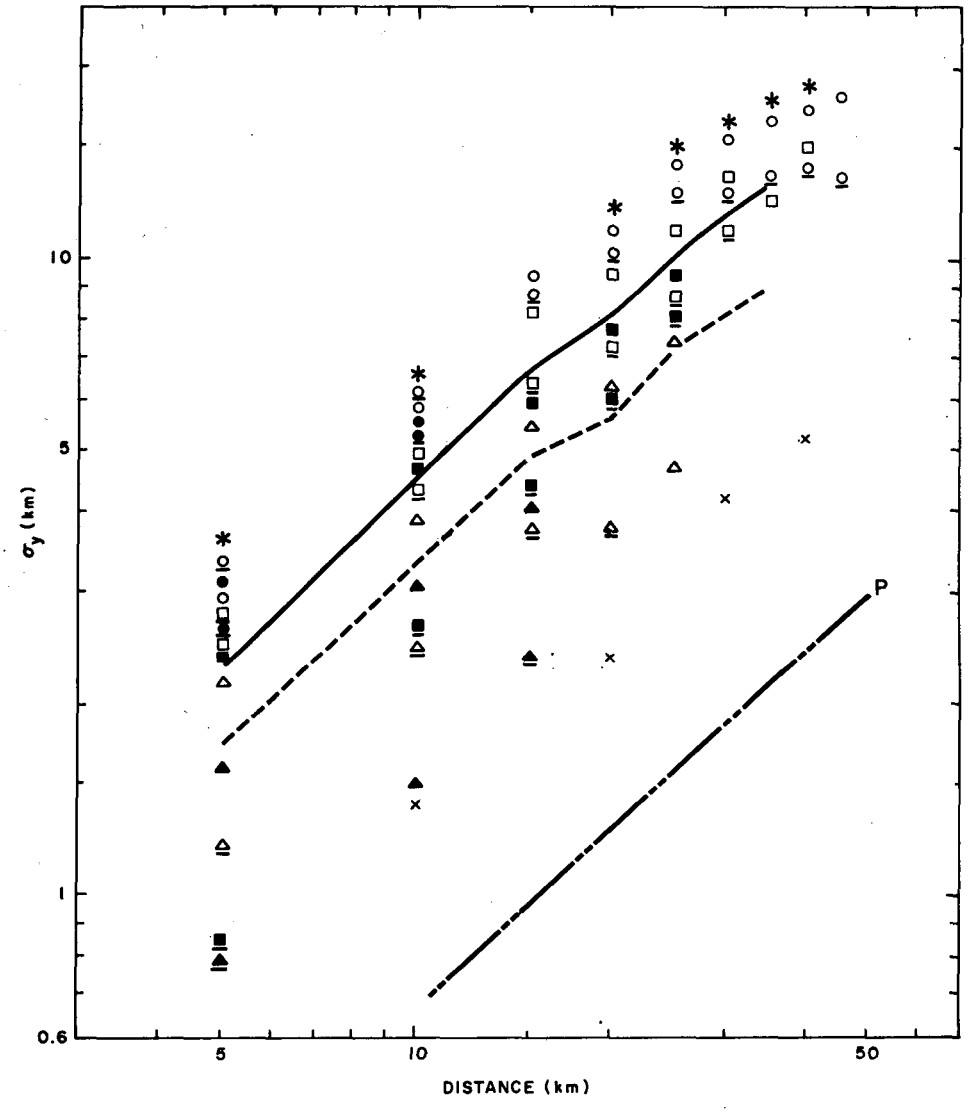

Fig. 4.45—Lateral standard deviation as a function of downstream distance based upon tetroon flights from Cardington (▲), from Las Vegas (●), from Wallops Island (■), and from Marineland (△), Long Beach (○), and Venice (□) within the Los Angeles Basin. Underlined symbols indicate tetroon releases within 6 hr of each other, plain symbols indicate tetroon releases within 24 hr of each other. The means for all flights are given by the adjacent solid and dashed lines for time periods of less than 24 hr and 6 hr, respectively. Asterisks represent means of the 24-hr series given in Fig. 4.44. Crosses represent values obtained from transosonde releases within 24 hr of each other (multiply ordinate and abscissa values by 100). P indicates values obtained by Pasquill at Porton.

regime of the Los Angeles Basin. Nevertheless the similar behavior of flights at Las Vegas (Yucca Flat) and Los Angeles suggests that such cyclic regimes are sufficiently widespread to be of practical interest.

The slopes of the adjacent solid and dashed lines in Fig. 4.45 indicate that, over downstream distances of 5 to 35 km, the lateral standard deviation is proportional to downstream distance to the 0.87 power for tetroon releases over 24 hr and proportional to downstream distance to the 0.84 power for tetroon releases over 6 hr. For all downstream distances between 5 and 35 km, the lateral stan-

dard deviation for the 24-hr releases is almost exactly 1.4 times the lateral standard deviation for the 6-hr releases. On the basis of this tetroon data, one would estimate that for a continuous point source the lateral standard deviation is proportional to sampling time to the 0.24 power. Cramer (1959) and Stewart, Gale, and Crooks (1954) have found that for sampling times of less than 30 min the concentration of a pollutant is inversely proportional to the one-fifth power. Inasmuch as concentration is inversely proportional to the product of lateral and vertical standard deviations, their results would indicate a lateral standard deviation proportional to the one-tenth power of the sampling time if both vertical and lateral dimensions are equally responsive to sampling time and a lateral standard deviation proportional to the two-tenths power of the sampling time if the vertical spread is assumed invariant with sampling time.

It is of interest to compare the tetroon results obtained at Cardington with the Pasquill (1962) results obtained at Porton (lower dashed line in Fig. 4.45) since the terrain is similar in the two areas. With the assumption that the lateral standard deviation is also proportional to the 0.24 power of the sampling time for sampling times shorter than 6 hr, Pasquill's aircraft probes of the plume from a continuous point source correspond to samples taken over an 8-min period. Although a slightly shorter sampling period might be more appropriate, the data are sufficiently consistent to suggest that successive tetroon pairs yield a useful approximation to the lateral diffusion to be expected over given time intervals of release and sampling. The advantage of the pair method is that even with existing radar facilities lateral diffusion can be estimated for sampling times ranging from a few minutes to many hours.

The crosses in Fig. 4.45 indicate lateral standard deviations as a function of downstream distance derived from transosondes released within 24 hr of each other. The transosondes were released from Iwakuni, Japan, for flight at about 300 mb (Angell, 1961). Note that the transosonde data refer to downstream distances and lateral standard deviations 100 times as large as the abscissa and ordinate values shown in Fig. 4.45. Thus, over downstream distances of 1000 to 4000 km, the lateral standard deviation varies from 140 to 520 km and indicates a lateral standard deviation proportional to nearly the first power of the downstream distance. Furthermore, for the transosonde flights the ratio of lateral standard deviation to downstream distance is only about half that found for the Cardington tetroon flights, the tetroon flights with the smallest value of this ratio in Fig. 4.45. However, owing to the great steadiness of the winds over Japan in winter, the transosonde results cannot be considered truly representative of the results that would be obtained from most release sites.

4-11.2.3 Continuous-point-source Diffusion Estimates from a Single Trajectory. Gifford (1960a), Pasquill (1961), and others have shown that the lateral diffusion can be estimated from running means of the lateral wind fluctuations and that this is, theoretically, fully equivalent to using Taylor's (1921) original formulation. The relevant formula is

$$\sigma_y = (\overline{v'^2}\, t^2)^{1/2} \tag{4.38}$$

where σ_y is the lateral standard deviation after travel time t and $\overline{v'^2}$ is the variance of the lateral wind fluctuation averaged over the diffusion (or travel) time t.

The use of Eq. 4.38 for diffusion estimation has been considered by Angell (1962). First, it should be noted that a single set of lateral wind-fluctuation (v') statistics of infinite length in a stationary homogeneous turbulence field would, in theory, provide complete information on lateral diffusion. However, for a finite length of v' information in a steady homogeneous turbulence field, we should expect the σ_y value to always be less than the true value. In the case of real atmospheric data, we should also expect differences in the observed turbulence field, owing to the manipulation of the data and to observational errors, which affect the v' statistics. On the other hand, the lateral standard deviations derived in this way refer to a sampling time corresponding to the travel time, which, in turn, is comparable to the sampling time utilized by previous investigators. Thus the lateral standard deviations derived from Eq. 4.38 might be expected to more closely resemble previously obtained continuous-point-source diffusion data than the lateral standard deviations obtained by either of the two methods discussed earlier.

The solid lines in Fig. 4.46 represent lateral standard deviations as functions of downstream distance derived from individual tetroon flights through the use of Eq. 4.38. In general, the tetroon flights were made at heights near 600 m. For clarity the solid lines in Fig. 4.46 have been drawn as straight lines even though there was some slight tendency for the lines to be concave downward. The lateral standard deviations were computed for travel times as large as 20% of the duration of the v′ statistics, but this is probably extreme, and, when longer tetroon flights are available, it would be desirable to limit evaluation to 10% of the duration of the v′ statistics. An obvious drawback of this method is that it requires very long tetroon trajectories to obtain diffusion data at even moderate distances downstream.

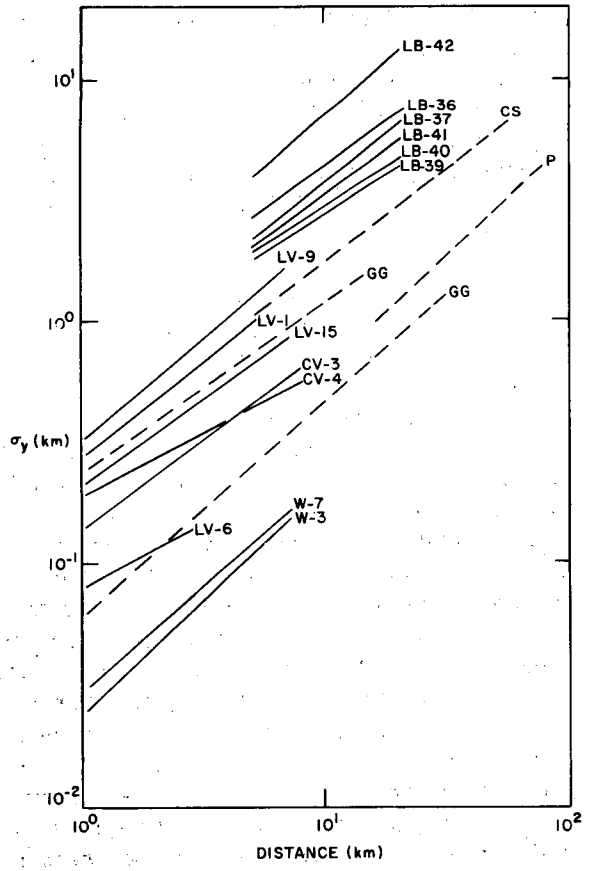

Fig. 4.46 — Lateral standard deviation as a function of downstream distance as derived from running means of the lateral velocity components along individual tetroon flights from Long Beach, Calif. (LB), Las Vegas, Nev. (LV), Covington, Ky. (CV), and Wallops Island, Va. (W). The dashed lines represent continuous-point-source lateral-diffusion estimates obtained by Crozier and Seely (CS), Pasquill (P), and from Project Green Glow (GG).

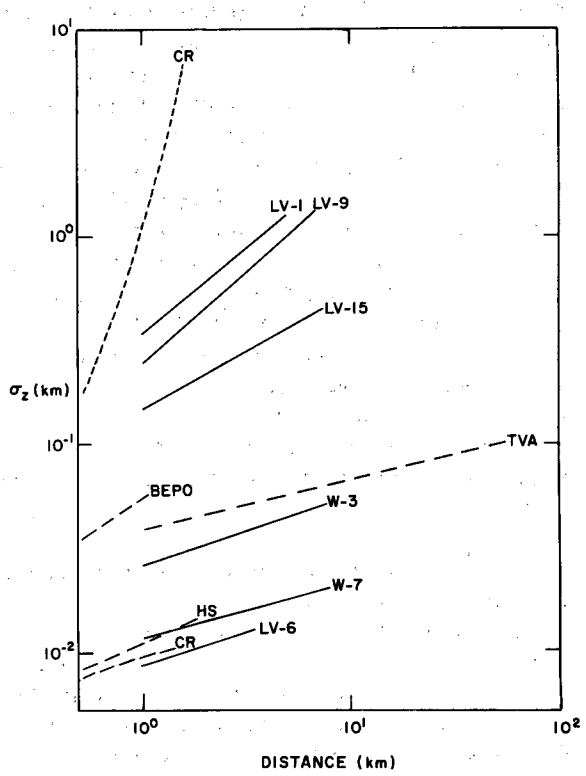

Fig. 4.47 — Vertical standard deviation as a function of downstream distance as derived from running means of the vertical-velocity components along individual tetroon flights from Las Vegas, Nev. (LV), and Wallops Island, Va. (W). The dashed lines represent continuous-point-source vertical-diffusion estimates obtained by Cramer (CR), Hilst and Simpson (HS), from Harwell (BEPO), and from the Tennessee Valley Authority (TVA).

For comparison, the dashed lines in Fig. 4.46 indicate the lateral standard deviations obtained by Crozier and Seely (1955) and other previously mentioned investigators. The variation reflects the meteorological or topographical conditions during the various flights with the Wallops Island data representing regular flow over a smooth surface, the Covington data representing regular flow over rolling hills, the Las Vegas data representing strong desert convection, and the Los Angeles data indicating the effects of the extreme longer period meander in a region of topographic complexity and light winds.

The solid lines in Fig. 4.47 represent the vertical standard deviation (σ_z) as a function of distance derived from tetroon flights through the use of an equation similar to Eq. 4.38. Be-

cause of the difficulties involved in obtaining accurate tetroon vertical velocities from the WSR-57 radar at Los Angeles (Long Beach flights) and Cincinnati (Covington flights), these data have been omitted from Fig. 4.47.

Figure 4.47 shows that on the basis of the tetroon flights the ratio of vertical standard deviation to downstream distance varies from a value of about 0.01 for daytime flights over the sea and nighttime flights over the desert to a value of 0.1 for daytime flights over the desert near Las Vegas. As in the case of Fig. 4.46, the appropriateness of the tetroon technique is indicated by the similarity in the rate of change of vertical standard deviation with downstream distance as derived from the tetroon flights and from conventional means.

4-11.2.4 Relative Diffusion Estimates from Simultaneous Releases. The second basic type diffusion investigated with tetroons is relative diffusion, which involves the rate of growth of an individual cluster of particles. Basically this puff type of diffusion depends on the increase in distance between pairs of particles, and therefore tetroon determinations require the use of two trajectories. Only a few cases are available for presentation. Obviously the tetroons must possess very nearly the same equilibrium floating surface, or the wind shear in the vertical will cause a misleadingly large rate of balloon separation with time.

Based upon four pairs of simultaneously released tetroons at Marineland, Calif., the lateral standard deviation was found to be proportional to $x^{0.38}$, which is less than the value derived from continuous point-source experiments. However, because of the small number of cases, this value may have little significance.

Of greater theoretical interest than the increase in separation distance between pairs of particles with respect to downstream distance is the increase in separation distance with respect to time. In particular, on the basis of the Kolmogorov similarity theory, Batchelor (1950) has predicted that at small time the square of the separation distance should be proportional to t^2 (with the assumption of negligible initial separation), and at intermediate time he has predicted that the square of the separation distance should be proportional to t^3. Gifford (1957) has synthesized the results of several experiments and has offered confirmation for Batchelor's hypothesis on a time scale of seconds and a few minutes.

Figure 4.48 shows the square of the distance between pairs of simultaneously released tetroons as a function of time after release of the tetroons. The numbered pairs of flights are from Marineland, Calif., the pair labeled CVG refer to flights at Covington, Ky., and the pair labeled LAX, to flights made from Los Angeles by Holzworth, Kauper, and Smith (1962). In the latter case tetroon positions were determined by observers following the balloons in automobiles. Included for comparison in Fig. 4.48 are no-lift balloon data obtained near the ground by Wilkins (1958) and smoke-puff data obtained in the stratosphere by Kellogg (1956). The long line represents the median value of the square of tetroon separation distances with respect to time. The median line suggests a power varying from 1.5 at a time of 10 min to a power of 2.5 at a time exceeding 100 min. However, on a few of the individual tetroon flights, the tetroons actually approached one another. This is particularly true for the Cincinnati data (Covington flights) and paired flights 75 and 76 in Los Angeles.

4-11.2.5 Estimation of Lagrangian Statistics from Eulerian Statistics. The foregoing discussion has dealt with ways of estimating atmospheric diffusion from Lagrangian type data. However, since Eulerian (fixed-point) statistics are still more readily obtained than Lagrangian (air particle attached) statistics, it is desirable to determine whether there is some consistent relation that would allow one to estimate Lagrangian statistics from Eulerian statistics. Indirect estimates of Lagrangian statistics have been made in recent years by sampling mass tracers, such as fluorescent aerosols. Comparison of the lateral standard deviation of particle diffusion of such mass tracers with the standard deviation of appropriately averaged wind directions at a fixed point has suggested to Hay and Pasquill (1959) that there is a basic scale relation between Eulerian and Lagrangian statistics such that, in the mean, the predominant period of oscillation following an air parcel is about four times the predominant period of oscillation noted at a nearby fixed point. Through the work of Barad (1959) and of Panofsky (1962), however, there have been indications that this scale

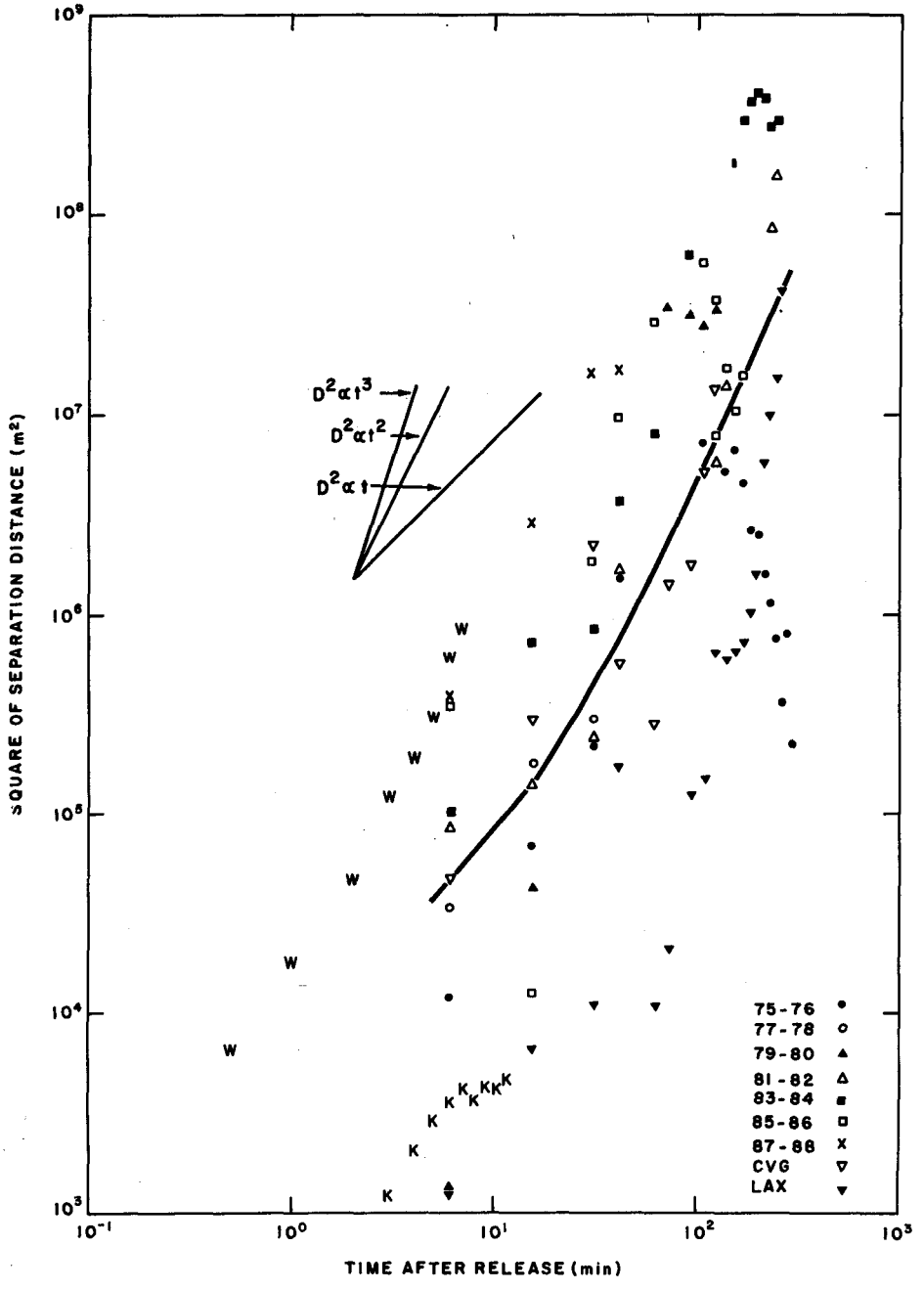

Fig. 4.48—Square of the separation distance between pairs of tetroons as a function of time. Numbered pairs represent simultaneous tetroon flights from Marineland, Calif., CVG indicates flights from Covington, Ky., and LAX indicates flights made by Holzworth, Kauper, and Smith over Los Angeles. Results obtained by Wilkins (W) with no-lift pibals near the ground and by Kellogg (K) with smoke puffs in the stratosphere are shown for comparison.

factor, β, is a function of turbulence intensity, stability, and perhaps travel distance.

Gifford (1955) utilized no-lift pibals and wind vanes mounted on the Brookhaven tower to investigate the problem of Eulerian–Lagrangian scale relations. The use of tetroons to estimate β is particularly appropriate at some distance above the ground where the erection of sampling stations for mass-tracer experiments is difficult and expensive. Consequently, during

the summer of 1962, tetroons were flown past instrumented barrage-balloon cables at Cardington, England, in an effort to obtain β values through comparison of the frequency at which the tetroon-derived vertical-velocity spectral density was a maximum with the frequency at which the fixed-point vertical spectral density was a maximum (Angell, 1964). Limiting the discussion to those tetroon flights which were accurately positioned by radar for at least 40 min at float altitude, an average β value of 2.4 was obtained. However, it appears from the top part of Fig. 4.49 that β tends to be relatively large when the turbulence intensity (in this case, the ratio of standard deviation of vertical velocity to mean wind speed) is relatively small, and vice versa. The bottom part of Fig. 4.49 shows the comparison between β and atmospheric stability, where the latter is estimated from the change in temperature over a 900-m depth centered on the tetroon flight level. Since all tetroon flights were made during the day, the variation in stability is not great, and, although there is some tendency for β to increase with increasing stability, the trend is not as striking as in the case of the turbulence intensity.

An alternative method of estimating β has been suggested by Smith and Hay (1961) and has been noted as Eq. 4.26. The average turbulence intensity indicated by the simultaneously released pairs of tetroon flights from Marineland is 0.34, and consequently, through the use of the information on $d\sigma_{yI}/dx$ derived from the Marineland flights, Eq. 4.26 yields an average β of 2.1. The similarity in β values derived by the two techniques although undoubtedly partly fortuitous is encouraging in its implication that fairly uniform results may be derived from very dissimilar methods.

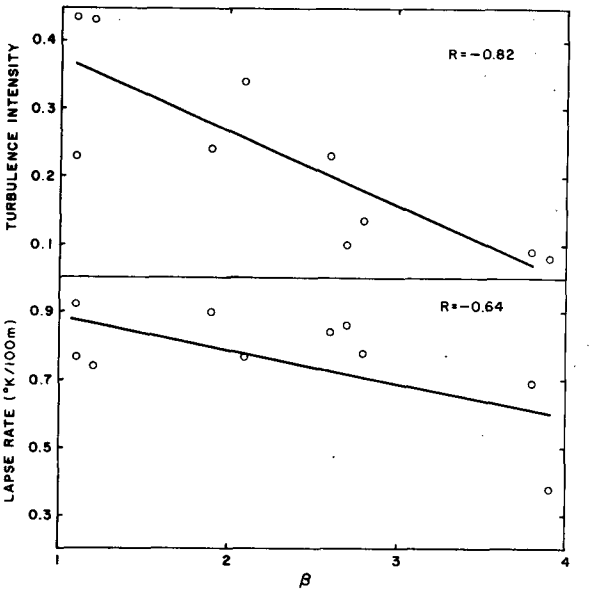

Fig. 4.49 — Variation of Lagrangian–Eulerian scale (β) with turbulence intensity (top) and with stability (bottom) as obtained from tetroon flights past instrumented barrage-balloon cables at Cardington, England.

4-12 RECAPITULATION

It would be most satisfying if this recapitulative section could consist of a framework in which the individual experimental series were small but distinct members. Although such an unequivocal construction cannot be presented, certain features of the current state of knowledge seem to be well documented by diffusion experiments.

The crosswind spread, σ_y, from a continuously maintained source in the first few hundred meters above the earth's surface has been the subject of repeated study and a summary such as is presented in Fig. 4.21 has broad features that are in agreement with most experimental results, namely, a power-function distance dependency (from about $x^{0.80}$ to $x^{0.90}$), a relation to the measured value of the low-level horizontal component of turbulence, and a dependence on the time period over which the average concentration distribution is measured.

The vertical spreading of material released from a continuous source has received comparatively little attention in diffusion experiments owing primarily to the difficulty and expense of adequately documenting this feature. Common practice has been to estimate the vertical diffusion from measurements of the ground-level crosswind spread and concentration distribution, a technique prone to some degree of error because of the effects of deposition. For release within a typical radiational inversion, it can be stated with considerable assurance that the vertical spreading will cease after some short travel from the source and the diffusion process will be dominated by the lateral spreading and the as yet not fully accounted for effects of vertical gradients

of the horizontal wind. Under unstable conditions the plume will spread rapidly until some vertical lid to mixing is reached. The existence of such a lid is common as amply verified by the work of Holzworth (1964). The implications of this lid are of great importance in any assessment of medium- and long-distance diffusion within the friction layer.

The downwind concentration distribution within a plume that in the course of its travel intersects the ground is well documented by surface sampling but is subject to some uncertainty because of the complex process of deposition. A continuous scavenging mechanism, such as deposition, can result in a measured decrease of concentration with distance quite different from that which would have occurred in the absence of deposition. The curves of normalized concentration variation with distance presented in Fig. 4.24 are quite representative of diffusion of the small particulates, but the magnitude of the correction factor necessary to remove the effects of deposition is in doubt, particularly at the greater travel distances during stable conditions. The conjecture that the correction for deposition would modify the concentration curves in Fig. 4.24 so as to approach the Pasquill curves appears to be a reasonable working hypothesis until theoretical studies and field experiments, both of which are currently being pursued, offer more quantitative alternatives.

With due cognizance of the experimental data presented in this chapter, there does not seem to be any strong argument favoring any one of the models or methods of continuous-source diffusion estimation presented in this chapter over any other for practical applications. The use of the horizontal wind-direction-fluctuation data and the relabeled Pasquill curves at locations of regular terrain are adequate for rapid assessments of the magnitude of a problem. The judicious use of these curves with various forms of the generalized Gaussian diffusion equation further broadens their utility. On the other hand, if machine processing of large amounts of data is indicated by the nature of the problem, the analytical forms of the diffusion parameters advanced by the Hanford group can be used. An attractive and useful statistical solution of the problems at a site requiring continuous diffusion estimates has been suggested by the Dry Gulch and Ocean Breeze studies. It is imperative to point out, however, that when the source and environmental characteristics point to a major pollution problem there is no alternative to the services of a diffusion meteorology specialist to assess the problem and suggest solutions.

The results of the instantaneous-source diffusion experiments summarized in Figs. 4.38, 4.39, and 4.40 and in Table 4.23 form a coherent picture despite the variety of experimental configurations. The Smith-Hay formulation (Eq. 4.27) has been used with some success (see Secs. 4-10.1.1, 4-10.1.6, and 4-10.2.1). Since the concentration or exposure from an individual puff is likely to be considerably more variable than that experienced from a continuous source, probability estimation techniques, such as developed from the Sand Storm data (Sec. 4-10.1.2), should be given serious consideration.

Finally, it should be mentioned once again that the diffusion experiments discussed in this chapter were carried out under relatively ideal conditions. When diffusion estimates are required over rugged terrain, at land–water boundaries, or during conditions of marked inhomogeneities of atmospheric structure, manipulation of the diffusion equations, as well as adjustment of parameter values, may be called for. In direct parallel to the weather-forecast problem, these procedures contain elements of both science and art, and here the inflexible guides of a handbook must yield to the acumen and imagination of a trained meteorologist.

Chapter 5

Processes Other Than Natural Turbulence Affecting Effluent Concentrations

Gary A. Briggs,* Isaac Van der Hoven,† Rudolf J. Engelmann,‡ and James Halitsky§

5-1 INTRODUCTION

A number of processes other than natural atmospheric turbulent diffusion can be significant in the fate of radioactive material emitted into the atmosphere. First is the effect of momentum and buoyancy due to the mode of emission. Thus, for example, the forced emission of a hot effluent from a stack will cause the plume to rise, depending on both the plume and the ambient-air characteristics. A second process is the surface deposition of airborne material composed of either particulate or gaseous matter with resulting depletion of the airborne cloud and quasi-permanent residence of material upon ground surfaces. In the case of radioactivity, surface deposition creates a fixed source of radiation exposure with its cumulative effect as opposed to the rather transitory effect of the airborne cloud. The mechanisms causing deposition are numerous and often not well understood. These include gravitational settling (fallout), precipitation scavenging (washout, snowout, and rainout), surface impaction, electrostatic attraction, adsorption, and chemical interaction. A further complication is the possibility of resuspension and redeposition of material. A third process is the modification of the natural flow by solid boundary constraints ranging from a building or complex of buildings to the topographic constraint of hills and ridges. The law of conservation of fluid mass states that the fluid must flow around or over the obstruction and that there will be subsequent changes of speed, pressure, and streamline configuration.

The variety of topics included in this chapter creates some overlap in the notation used in the various sections. Rather than arbitrarily changing some of this notation to ensure compatibility within the sections of this chapter and thus ensuring incompatibility with literature on the same topics, we have included a list of the symbols used in each major section at the beginning of the section.

5-2 MOMENTUM AND BUOYANCY EFFECTS (Gary A. Briggs)

Material released into the atmosphere is generally contained in a volume of gas having a velocity and buoyancy relative to the air; its behavior will differ from that of a passive volume of gas according to the magnitude of these parameters and the prevailing meteorological conditions. Although accidental releases are difficult to define in these terms, it is possible, on both theoretical and empirical grounds, to specify with some accuracy the behavior of the gases released as a continuous plume and as an instantaneous cloud.

*Atmospheric Turbulence and Diffusion Laboratory, Environmental Science Services Administration, Oak Ridge, Tennessee.

†Air Resources Laboratory, Environmental Science Services Administration, Silver Spring, Maryland.

‡Division of Biology and Medicine, Atomic Energy Commission, Washington, D. C. (formerly with Pacific Northwest Laboratory, Richland, Washington).

§Department of Meteorology and Oceanography, New York University, New York.

List of Symbols

Symbols used frequently in Sec. 5-2 on momentum and buoyancy effects are listed here. (The dimensions mass, length, time, and temperature are abbreviated as M, L, T, and D, respectively. Equation or table number indicates the first appearance of the symbol.)

c_p, c_{ps}	Specific heat at constant pressure of ambient and stack air ($L^2\ T^{-2}D^{-1}$), Eq. 5.11
d	Inside stack diameter (L), Eq. 5.1
F	Buoyancy flux = $g(\Delta T/T_s)\,wr^2$ ($L^4\ T^{-3}$), Eq. 5.11
F_i	Instantaneous buoyancy = $gQ_i/c_p\rho T$ ($L^4\ T^{-2}$), Eq. 5.22
F_m	Proportional to momentum flux = $(TM_s/T_sM)\,w^2r^2$ ($L^4\ T^{-2}$), Eq. 5.10
g	Gravitational acceleration ($L\ T^{-2}$), Eq. 5.6
h	Effective stack height = $h_s + \Delta h$ (L), Eq. 5.32
h_s	Actual stack height (L), Table 5.1
Δh	Plume rise (L), Eq. 5.1
K	Stümke regression coefficient = $\left(\frac{1}{N}\sum\frac{\Delta h\ \text{calculated}}{\Delta h\ \text{observed}}\right)^{-1}$, Eq. 5.14
L	Length parameter = $F/\bar{u}^3$ (L), Eq. 5.5
M, M_s	Average molecular weight of ambient and stack air, respectively, Eq. 5.10
Q_H	Rate of heat emission of a continuous source ($M\ L^2\ T^{-3}$), Eq. 5.2
Q_i	Heat emission from an instantaneous source ($M\ L^2\ T^{-2}$), Eq. 5.22
r	Inside stack radius (L), Eq. 5.6
s	Stability parameter = $\frac{g}{T}(\partial\Theta/\partial z)$ (T^{-2}), Eq. 5.9
t	Time after emission from the stack (T), appears in various equations
T, T_s	Absolute temperature of ambient and stack air, respectively (D), Eq. 5.1
ΔT	Stack effluent temperature minus ambient air temperature (D), Eq. 5.1
	Average value of the wind component in the direction of the mean horizontal wind vector ($L\ T^{-1}$), Eq. 5.1
$\bar{u}_c$	A critical wind speed ($L\ T^{-1}$), Eq. 5.29
w	Stack-gas efflux velocity ($L\ T^{-1}$), Eq. 5.1
ρ	Air density ($M\ L^{-3}$), Eq. 5.22
$\frac{\partial\Theta}{\partial z}$	Potential temperature gradient ($D\ L^{-1}$), Eq. 5.9

5-2.1 Behavior of Continuous Plumes

5-2.1.1 Qualitative Behavior. While a smoke plume quickly attains the wind speed in the horizontal plane, its rise is determined by its vertical momentum and buoyancy due to heat and molecular-weight difference. Rise of the plume is impeded by entrainment with air, which at first is due to turbulence generated by the relative motion of the plume. As this dies out, atmospheric turbulence dominates the mixing. In stratified air the buoyancy of the stack gases and entrained air is altered by the change of the relative density of the ambient air with height. In stable air this change acts as a restoring force on the plume, but in unstable air the plume may rise to unlimited heights. Plume behavior may be influenced by aerodynamic effects due to chimney phenomena, surrounding buildings, and terrain. The relation between the temperature profile and the appearance of plumes is shown in Fig. 2.40 (Chap. 2, Sec. 2-7.2), and a discussion of plume types appears in the accompanying text.

5-2.1.2 Height-of-rise Formulas. At least twenty formulas for calculating plume rise have been published since 1950.* None is universally accepted, primarily because of the lack of comprehensive data. This lack is due largely to observational difficulties, especially the difficulty of detecting the plume at large distances downwind. The fact that many plumes are still rising after becoming invisible through dilution has led to apparent contradictions in results when the final visible height was taken to be the ultimate rise. Some of the differences between transitional rise and ultimate rise are discussed by Scorer (1962). Published data are often based on an inadequate determination of lapse rate up to

*See Batchelor (1954), Bosanquet (1957), Bosanquet, Carey, and Halton (1950), Briggs (1965), Bryant and Cowdrey (1955), Csanady (1961), Danovich and Zeyger (1963), Davidson (1954), Hill, Thomas, and Abersold (1945), Lucas, Moore, and Spurr (1963), Morton (1959, 1959a), Morton, Taylor, and Turner (1956), Priestley (1956), Priestley and Ball (1955), Rupp et al. (1948), Schmidt (1957, 1963, 1965), Scorer (1958, 1959, 1959a), Scorer and Barrett (1962), Stümke (1961), Sutton (1950), Thomas (1954), and U. S. Weather Bureau (1953).

plume level and an insufficient number of runs for averaging in unstable conditions.

Four of the most commonly used formulas are presented in the following paragraphs. The Davidson–Bryant (1954) and Holland (U. S. Weather Bureau, 1953) formulas are completely empirical, and the Bosanquet (1957) and dimensional-analysis formulas (Batchelor, 1954, Briggs, 1965, and Scorer, 1958, 1959, 1959a) are semiempirical. Each author has his own criterion for final rise, but usually we are concerned with height of rise at the point where maximum ground concentration occurs.

1. The Davidson–Bryant Formula. Davidson (1954) suggested the formula

$$\Delta h = d\left(\frac{w}{\bar{u}}\right)^{1.4}\left(1 + \frac{\Delta T}{T_s}\right) \qquad (5.1)$$

stating that the factor $(w/\bar{u})^{1.4}$ is in fair agreement with Bryant's (1949) wind-tunnel data on plume rise due to momentum. To account for rise due to buoyancy, Davidson proposed using the multiplying factor $(1 + \Delta T/T_s)$. He indicates that this formula may be applied to "stacks of moderate or great height" but does not define these terms.

2. The Holland Formula. Rupp, Beall, Bornwasser, and Johnson (1948) give the height of rise of an effluent without buoyancy as $1.5\, d\, (w/\bar{u})$, which is based on wind-tunnel experiments with ammonium chloride as a tracer. Holland (U. S. Weather Bureau, 1953) added a buoyancy term to this to get closer agreement with photographs of plume trajectories of three power stations, whose parameters are shown in Table 5.1. The Holland, or Oak Ridge, formula is

$$\Delta h = 1.5\, d\, \frac{w}{\bar{u}} + 4.0 \times 10^{-5}\, \frac{Q_H}{\bar{u}} \qquad (5.2)$$

where Q_H is in calories per second and all other units are in the MKS system. To take stability into account, Holland suggests that the predicted rise be increased by 10 to 20% in unstable conditions and be decreased by an equal percentage in stable conditions.

Davidson presents no field data in his original paper. Although Holland does present such data, observations apparently were carried no further than 600 ft downwind (Hawkins and Nonhebel, 1955) and show much scatter. Both formulas have been criticized because they are empirical and their reliability is questionable when the ranges of variables are much outside those used in their formulation. Holland's formula has been further criticized because it includes a dimensional constant which is not based on the physical constants of air and thus must really be an averaged function of one or more variables.

Table 5.1—RANGE OF STACK AND METEOROLOGICAL PARAMETERS USED IN DERIVING HOLLAND FORMULA

	X-10 pile	X-10 steam plant	Watts Bar steam plant
h_s, ft	200	180	160
d, ft	5.8	9	14
w, mile/hr	45	5	34
T_s, °F	180	400	350
Q_H, cal/sec	8.3×10^5	7.1×10^5	6.6×10^6
$\bar{u}$, mile/hr	1 to 21	1 to 15	1 to 15
Number of observations	11	33	93
$\bar{u}\Delta h$, (mile/hr) ft			
Mean	620	452	2632
Standard deviation	410	324	2950

3. The Bosanquet Formula. Bosanquet, Carey, and Halton (1950) published a technique for calculating plume rise which has been widely used. Nonhebel (1957) reported that the Beaver Committee in England (Beaver, 1954) applied this formula to stack data and found it gave too high a thermal rise for large plants. Bosanquet was asked to reexamine his original calculations, and he published a revised technique (Bosanquet, 1957), which is described in the following paragraphs in somewhat altered form.

Bosanquet first considers a "cold" plume, i.e., one with a density the same as that of the ambient air. When $w/\bar{u} > 0.48$,

$$\Delta h = 3.14\, d\, \frac{w}{\bar{u}}\left\{1.31 - \frac{0.615}{[(w/\bar{u})^2 + 0.57]^{1/2}}\right\} \qquad (5.3)$$

When $w/\bar{u} < 0.48$,

$$\Delta h = 2.83\, d\left(\frac{w}{\bar{u}}\right)^{1.5} \qquad (5.4)$$

If the stack gases are similar to air in specific heat and molecular weight but are buoyant owing to heating, Bosanquet's formulation becomes

$$\Delta h = 29.6\ L\left\{F_1(X) + F_2(X_0) - \frac{0.615\ X_0^{1/2}}{[(w/\bar{u})^2 + 0.57]^{1/2}}\right\} \quad (5.5)$$

$$L = \frac{\Delta T\ gwr^2}{T_s \bar{u}^3} = \frac{F}{\bar{u}^3} \quad (5.6)$$

$$X_0 = 0.180\ \frac{T_s}{T}\left(\frac{\bar{u}^2 T}{dg\Delta T}\right)^2 \quad (5.7)$$

$$X = X_0 + 0.034\ \frac{x}{L} = 0.034\ \frac{\bar{u}t'}{L} \quad (5.8)$$

In the above equations L is the length parameter based on buoyancy flux and on wind speed, x is the distance downwind of the source, and the quantity within the parentheses in the definition of X_0 is proportional to the ratio of aerodynamic to buoyant accelerations at the chimney. Implicit in the equations is a turbulent diffusion coefficient assumed equal to 0.13. This formulation gives the rise trajectory rather than final rise; so it should be applied to the distance downwind of greater interest. Bosanquet presents tables of $F_1(X)$ and $F_2(X_0)$, which are condensed here in Table 5.2.

atmosphere $t' = 200$ sec might be appropriate for computing X.

4. Dimensional-analysis Formulas. When the relevant physical parameters and their units are specified, it is often possible to predict the outcome of a physical situation purely on dimensional grounds; Batchelor (1954) and Scorer (1958, 1959, 1959a) did this for plume rise. Briggs (1965) extended their work, and his work forms the basis of the presentation here. Since dimensional analysis cannot predict constants in the equations, these constants must be determined empirically. Analysis is simplified by replacing the chimney with a virtual point source with a height that can usually be approximated by the chimney's height. The point source is then entirely specified by some measure of its momentum flux and its buoyancy flux. The volume flux at the stack is $w(\pi r^2)$. Since only the density of the smoke relative to air affects rise, we can use momentum flux divided by π and ρ as the momentum parameter, i.e.,

$$F_m = \frac{TM_s}{T_s M}\ w^2\ r^2 \quad (5.10)$$

Buoyancy flux can be defined as the rate that buoyant force due to the effluent is added to a large volume of air divided by $\pi\rho$. It is given by

$$F = \frac{T}{T_s}\ g\ w\ r^2\left[\left(1 - \frac{M_s}{M}\right) + \left(\frac{T_s}{T} - 1\right)\left(\frac{c_{ps}M_s}{c_p M}\right)\right] \quad (5.11)$$

When the stack gases have nearly the same specific heat and molecular weight as air, the expression simplifies to

Table 5.2—VALUES OF $F_1(X)$ AND $F_2(X_0)$ IN BOSANQUET'S PLUME-RISE FORMULAS*†

X or X_0	$F_1(X)$	$F_2(X_0)$	X or X_0	$F_1(X)$	$F_2(X_0)$	X or X_0	$F_1(X)$	$F_2(X_0)$
0.1	0.170	−0.044	1	0.767	0.155	10	2.33	1.99
0.15	0.225	−0.046	1.5	0.965	0.296	15	2.70	2.73
0.2	0.274	−0.043	2	1.13	0.43	20	2.95	3.41
0.3	0.360	−0.030	3	1.39	0.69	30	3.33	4.56
0.4	0.434	−0.010	4	1.59	0.91	40	3.61	5.54
0.6	0.562	−0.041	6	1.90	1.32	60	4.00	7.24
0.8	0.671	−0.096	8	2.14	1.67	80	4.28	8.68

*From Bosanquet, The Rise of a Hot Waste Gas Plume, *J. Inst. Fuel*, 30: 326 (1957).
†Outside the range of the tables the following approximations are valid: when $X \geq 10^2$, $F_1(X) = \ln X - 0.12$; when $X_0 \geq 10^2$, $F_2(X_0) = 1.31\ X_0^{1/2} - 0.5 \ln X_0 - 1$.

In a stable atmosphere the plume reaches a limiting height in a time proportional to $s^{-1/2}$, s being a measurement of stability defined by

$$s = \frac{g}{T}\frac{\partial\Theta}{\partial z} \quad (5.9)$$

where $\partial\Theta/\partial z = (\partial T/\partial z) + 9.8$ °C/km, the potential temperature gradient. When $\partial\Theta/\partial z > 3.5$ °C/km, Bosanquet suggests that for final rise $t' = 2.16\ s^{-1/2}$ be used and that for a weakly stable

$$F = \frac{\Delta T}{T_s} g w r^2 \qquad (5.12)$$

which can be further approximated by

$$F = 3.8 \times 10^{-5} Q_H \qquad (5.13)$$

where F is in meters^4 per second^3 and Q_H in calories per second. When the wind is strong enough to bend the plume, the above quantities are diluted along the plume's length in proportion to $\bar{u}$, and the relevant parameters become $F_m/\bar{u}$ and $F/\bar{u}$. In the stable case the height is limited by the stability parameter, s, determined from the average potential temperature lapse rate through the layer in which the plume rises. In a neutral atmosphere rise is limited chiefly by $\bar{u}$ and depends to a lesser extent on the roughness of the ground and height. In all cases the trajectory before the final height is approached is not much dependent on stability; this will be called transitional rise.

With these assumptions we can derive the dimensional relations shown in Table 5.3. Where observations are available, the appropriate constants are estimated and included in the table. The constant for the neutral windy momentum-dominated plume is taken from the results of Rupp, Beall, Bornwasser, and Johnson (1948). In the buoyancy-dominated cases, the constant for the calm stable case is a compromise between the results of Morton, Taylor, and Turner (1956) and those of Crawford and Leonard (1962) [this is a correction of the value stated by Briggs (1965)]. The other constants are estimated from Figs. 5.1 and 5.2. Estimation of the constant for the windy neutral situation is particularly difficult since none of the plumes in Fig. 5.2 level off. The "constant" is also dependent on surface roughness and stack height; a conservative value would be about 400. The most pertinent atmospheric situation is the one whose formula gives the lowest value of rise; the momentum and buoyancy rises may be considered to add approximately linearly. Most hot plumes are buoyancy dominated.

5-2.1.3 Comparison with Observations. Data adequate to fully test the validity of the preceding and other proposed formulas do not exist. Nevertheless a number of investigations have been made in which available data were tested. The earliest studies comparing plume rise formulas with observations were made by Katz (1952), who compared the formula of Sutton (1950) with that of Bosanquet, Carey, and Halton (1950), and by Best (1957), who compared these two formulas and the one by Holland.

More recently, comparisons between observed and calculated plume rises were made by Moses and Strom (1961) using data taken at the Argonne National Laboratory in the United States, by Rauch (1962) using data taken at Duisburg and at Gernsheim in Germany, and by Stümke (1961, 1963) using data taken at Argonne, at Duisburg and Gernsheim, and at Harwell in England. Much of this work has been summarized by Moses, Strom, and Carson (1964). Additional comparisons will be made here, including a regression equation proposed by Stümke and the previous dimensional-analysis predictions.

Stümke defined a constant regression coefficient K by the formula

$$\frac{1}{K} = \frac{1}{N} \sum \frac{\Delta h_{calc}}{\Delta h_{obs}} \qquad (5.14)$$

where N is the number of observations. Thus, if K is calculated for a particular formula and set of observations, multiplying the calculated rises by K assures that their average ratio to observed values will be 1.0. A number of investi-

Table 5.3—DIMENSIONAL ANALYSIS PLUME-RISE PREDICTIONS

Wind	Type of rise	Momentum-dominated plume	Buoyancy-dominated plume
Calm	Transitional	Δh = constant $F_m^{1/4} t^{1/2}$	Δh = constant $F^{1/4} t^{3/4}$
	Stable	Δh = constant $F_m^{1/4} s^{-1/4}$	$\Delta h = 5.1\ F^{1/4} s^{-3/8}$
	Neutral	Δh = constant $F_m^{1/4} t^{1/2}$	Δh = constant $F^{1/4} t^{3/4}$
Windy	Transitional	Δh = constant $(F_m/\bar{u})^{1/3} t^{1/3}$	$\Delta h = 2.0\ F^{1/3} \bar{u}^{-1} x^{2/3}$
	Stable	Δh = constant $(F_m/\bar{u})^{1/3} s^{-1/6}$	$\Delta h = 2.6\ (F/\bar{u})^{1/3} s^{-1/3}$
	Neutral	$\Delta h = 3.0 F_m^{1/2} \bar{u}^{-1}$	$\Delta h \approx 10^3\ F\ \bar{u}^{-3}$

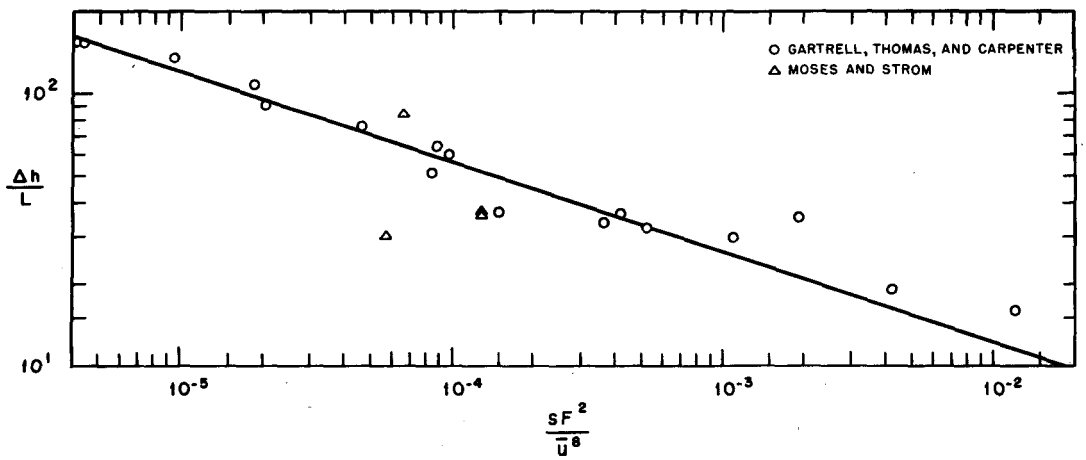

Fig. 5.1 — Observed plume rises for buoyant sources during stable windy conditions compared to $\Delta h = 2.6(F/\bar{u})^{1/3} s^{-1/3}$ (solid line; see Table 5.3) in nondimensional form. (From Briggs, 1965).

gators have made use of Stümke's correction factor.

Moses and Strom used least-squares techniques to compare the formulas of Davidson–Bryant, Holland, and Bosanquet, as well as those of Sutton, Scorer, and Bosanquet, Carey, and Halton. The plume-rise data used by Moses and Strom were obtained at the Argonne experimental meteorological stack using photogrammetric techniques. These measurements extended only to 60 m. The buoyancy in these experiments was very low, and it is likely, although not certain, that the plume rises were near their maximum since the angles between the smoke center line and the horizontal were 5° or less in 27 of the 31 cases studied. The weakness of the source may have made the plume more susceptible to variances due to atmospheric eddies. A statistical summary of three of the formulas considered is shown in Table 5.4. Also included are the plume rises obtained by applying Stümke's correction factor K. These data show that both the Holland and the Davidson–Bryant formulas yield values that are too low and that the Bosanquet formula yields values that are too high.

Rauch, using the same data used by Stümke from the Gernsheim and Duisburg stacks plus measurements taken later (for a total of 428 individual runs), compared Holland's formula with a K factor of 3.09 and a formula suggested by Lucas, Moore, and Spurr (1963) which states

$$\Delta h = 530\left[\frac{(Q_H)^{1/4}}{\bar{u}}\right] \qquad (5.15)$$

where units are in the MKS system and Q_H is the power in megawatts generated by the unit. Rauch concludes that for these two stacks the Lucas formula is superior to that of Holland. It does not take into account rise due to momentum, but for most hot plumes this factor is negligible compared to buoyant rise. The Lucas formula is an empirical fit to Priestley's theory (1956), in which the first phase predicts transitional rise approaching $\Delta h = 2.0\ F^{1/4}\bar{u}^{-1}x^{3/4}$ (MKS units) and differs from the dimensional prediction of Table 5.3 by a factor of only $(x/F)^{1/2}$ $(m/sec)^{1/4}$. The Lucas formula is equivalent to the above applied at a fixed distance of 800 m; actual measurements of balloons released into the plume (as tracers) were at distances of 1100 to 1800 m.

The most extensive tests of observed and calculated plume rise have been made by Stümke. In the first of his two papers, he used measurements by Stewart, Gale, and Crooks (1958) from a stack at Harwell, England, and by Rauch (1962) from stacks at Gernsheim and Duisburg, Germany, as well as the four sets of data presented in the paper by Bosanquet, Carey, and Halton. Stümke compared eight different formulas with these measurements, i.e., those of Bosanquet, Carey, and Halton, Davidson–Bryant, Holland, Scorer, Morton, two formulas of his own, and the Hill, Thomas, and Abersold formula (1945), which states that a 1° F temperature increase represents 2.5 ft of plume rise.

Stümke concluded that the Holland formula with a K factor of 2.92 gave the best representation of plume rise since the relative standard

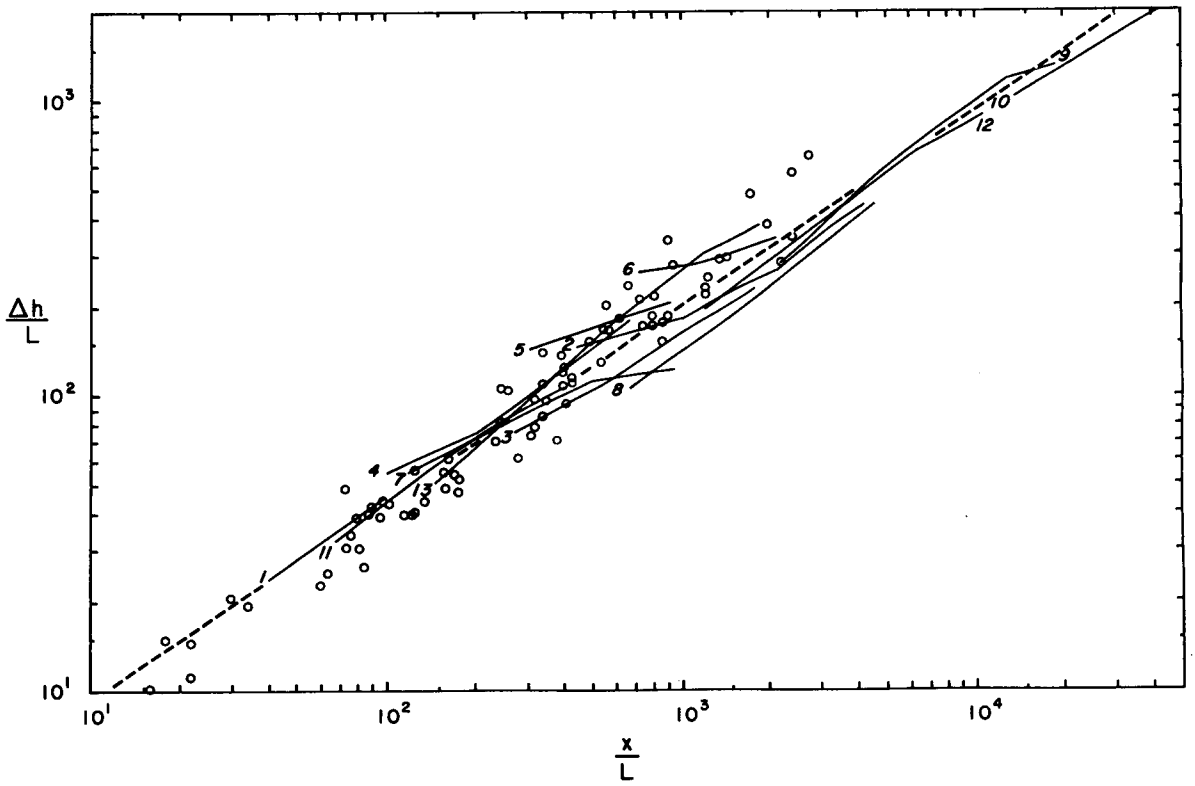

Fig. 5.2—Observed transitional plume rises for buoyant sources during windy conditions compared to $\Delta h = 2.0\ F^{1/3}\ \bar{u}^{-1}\ x^{2/3}$ (dashed line; see Table 5.3) in nondimensionalized form. (From Briggs, 1965.) Data on the sources of the trace lines are as follows:

Trace number	Source	Q_H, cal/sec	F, ft^4/sec^3	$\bar{u}$, ft/sec
1	Bosanquet	1.53×10^6	6,900	14
2	Bosanquet	1.53×10^6	6,900	33
3	Bosanquet	1.53×10^6	6,900	26.5
4	Bosanquet	1.53×10^6	6,900	19
5	Bosanquet	7.24×10^4	326	10
6	Bosanquet	7.24×10^4	326	13
7	Bosanquet	1.58×10^6	7,130	20.4
8	Harwell	1.10×10^6	4,830	21
9	Harwell	1.10×10^6	4,830	32
10	Harwell	1.10×10^6	4,830	46
11	Van Vleck & Boone	7.2×10^6	31,600	7 to 9
12	Van Vleck & Boone	7.2×10^6	31,600	16 to 19
13	Csanady	2.73×10^6	12,000	15 to 23
Circles	Ball	0.96×10^4	42.1	3 to 13

deviation of the ratio of calculated to observed height was the smallest. Also the correlation coefficient between observed and calculated values was largest. The results have been extended using Stümke's data to include the Bosanquet 1957 formula and are summarized in Table 5.5.

In his second paper Stümke used the data of Moses and Strom, of Stewart, Gale, and Crooks, and of Rauch (although Rauch's data appear to have been reevaluated) and derived a generalized formula of which the Holland and the Lucas, Moore, and Spurr formulas are special cases. Optimizing his adjustable parameters for best fit with data he gets

$$\Delta h = 1.5\frac{w}{\bar{u}}d + 65.0\frac{d^{2/3}}{\bar{u}}\left(\frac{\Delta T}{T_s}\right)^{1/4} \qquad (5.16)$$

where the units are in the MKS system.

Table 5.6 shows sample calculations, chosen for a wide variety of source strengths, for a comparison of the new Stümke formula and the dimensional-analysis formula for transitional rise ($\Delta h = 2\,F^{1/3}\bar{u}^{-1}x^{2/3}$) with the older formulas. Data of Bosanquet, Carey, and Halton (1950), of Rauch (1962) at Duisberg, and of Gartrell et al. (1964) at the Colbert plant in Alabama are pre-

Table 5.4—STATISTICAL SUMMARY OF CALCULATED AND OBSERVED PLUME HEIGHTS AT 60 M FROM EXPERIMENTAL SMOKESTACK AT ARGONNE NATIONAL LABORATORY*

		Calculated		
	Observed	Davidson–Bryant formula	Holland formula	Bosanquet formula
Without Stümke's K correction factor:				
Mean plume rise, m	6.1	3.5	2.6	7.3
Standard deviation, m	3.5	3.6	1.5	6.1
Root-mean-square observed height minus calculated height, m		4.2	4.7	5.2
Correlation coefficient (calc. vs. obs.)		0.52	0.46	0.52
With Stümke's K correction factor:				
Mean plume rise, m	6.1	5.7	4.8	5.5
Standard deviation, m	3.5	5.9	2.8	4.6
Root-mean-square observed height minus calculated height, m		4.9	4.3	4.0
Correlation coefficient (calc. vs. obs.)		0.52	0.46	0.52
Stümke's correction factor		1.63	1.86	0.753

*Moses, Strom, and Carson, 1964.

Table 5.5—STATISTICAL SUMMARY OF STÜMKE'S 1961 ANALYSIS BASED ON GERNSHEIM, DUISBURG, AND HARWELL DATA*†

		Calculated		
	Observed	Davidson–Bryant formula	Holland formula	Bosanquet formula
Average plume-rise height, m	65.4	66.7	65.4	66.1
Standard deviation, m	17.7	44.1	34.0	56.8
Stümke correction factor		6.69	2.92	0.75
Root-mean-square of observed height minus calculated height, m		37.4	26.5	51.7
Correlation coefficient		0.62	0.64	0.43

*Moses, Strom, and Carson, 1964.
†The Stümke K correction factor was applied.

Table 5.6—SAMPLE PLUME-RISE CALCULATIONS

(a) Observed Plume and Meteorological Data for the Case of Transitional Rise

Source*	Q_H, 10^6 cal/sec	$\bar{u}$, ft/sec	T, °C	d, ft	w, ft/sec	x, ft	Δh_{obs}, ft
Bosanquet (2)	0.072	10	25	4.1	28	300	67
Bosanquet (1a)	1.5	14	180	8.2	31	600	186
Bosanquet (1b)	1.5	33	180	8.2	31	800	84
Duisburg	2.7	24	114	11.5	38	1640	223
Colbert	7.2	30	126	16.5	47	10,560	1000

(b) Ratios of Calculated Δh to Observed Δh, Stümke Regression Coefficients (K), and the Product of the Data Standard Deviation and K

Source	Davidson–Bryant formula	Holland formula	Bosanquet formula	Stümke formula	Dimensional-analysis formula
Bosanquet (2)	0.28	0.30	0.82	1.04	0.92
Bosanquet (1a)	0.19	0.40	0.80	0.98	1.03
Bosanquet (1b)	0.12	0.37	0.37	0.92	1.17
Duisburg	0.13	0.34	0.59	0.91	1.16
Colbert	0.04	0.14	0.20	0.23	1.03
K	6.58	3.23	1.80	1.23	0.94
Standard deviation multiplied by K, %	53	29	43	36	9

*See legend of Fig. 5.2 for Bosanquet data.

sented. At Colbert the height of maximum SO_2 concentration for the two highest wind-speed runs are used.

Best results, with the lowest normalized standard deviation, were obtained from the dimensional-analysis formula for buoyant transitional rise (see also Fig. 5.2). This indicates that momentum rise for these plumes was probably unimportant and suggests that all the plumes were still rising, even the Colbert plume at 2 miles downwind. In fact, there are at present no data for neutral conditions in which the plume clearly levels off to a final height. In light of theoretical considerations, it is questionable whether there even exists an ultimate height of rise in these conditions. What are needed are observations of rise in neutral conditions at the point of maximum average ground concentration of effluent. Of the formulas for final rise, both the Stümke formula and the Holland formula times a factor of 3 seem to give good agreement for the moderate-sized sources but grossly underestimate rise in the case of the large Colbert plant.

To test the power law predicted by dimensional analysis for a stable windy buoyant source, Briggs (1965) plotted nondimensionalized height and stability parameter (Fig. 5.1). The data for inversion conditions at Colbert fit the law very well, especially at higher wind speeds. The most stable runs of Moses and Strom (1961) do not fit as well, but their source was three orders of magnitude weaker. The Colbert data show very definite leveling with the plume maintaining a constant height from ½ mile to as far as 9 miles downwind.

Figure 5.2 amply demonstrates the validity of the dimensional-analysis law $\Delta h = 2.0\, F^{1/3} \bar{u}^{-1} x^{2/3}$ since seven widely different sources seem to give reasonable agreement with the predicted rise. Observed rise and distance downwind are nondimensionalized in terms of $L = F/\bar{u}^3$. The stack-plume trajectories plotted are from Bosanquet, Carey, and Halton (1950), Csanady (1961), and Stewart, Gale, and Crooks (1958) at Harwell. Also plotted are rise data from lard-pail oil burners (Ball, 1958) and from exhaust clouds of horizontally fired rocket motors (Van Vleck and Boone, 1964). Because winds were measured much below the plume levels for the Harwell and the rocket-exhaust data, these wind speeds were adjusted by estimating roughness and assuming the logarithmic wind profile generally found in neutral conditions.

It was hoped that Fig. 5.2 would show evidence of a final height, but none of the observations went far enough downwind that a definite leveling was evident. However, a probably conservative estimate of final rise in neutral conditions is

$$\Delta h > 400 \frac{F}{\bar{u}^3} \qquad (5.17)$$

since traces from six of the seven sources approach or exceed this level.

In summary the Davidson–Bryant formula gives rises nearly 7 times too small for moderately large plants (Q_H about 10^6 cal/sec). Because this factor of underestimation varies from about 2 for a very small source to about 20 for a large source, with large standard deviations, this formula is not recommended. Both the Holland formula multiplied by a Stümke correction factor of 3 and Stümke's own formula give reasonable results for reported rises from moderate-sized plants but greatly underestimate rise for a large plant. The Bosanquet formula works well at short distances downwind but greatly underestimates rise at large distances downwind. The dimensional-analysis formulas for buoyant sources give consistently good results for all source sizes and distances downwind and take into account atmospheric stability. The formula for final rise in neutral conditions is necessarily conservative since there are few observations at large distances downwind, but it is not so severely conservative as the other formulas. Recommended then is whichever of the following formulas gives the minimum rise in a given situation:

Transitional:

$$\Delta h = 2.0\, F^{1/3} \bar{u}^{-1} x^{2/3} \qquad (5.18)$$

Final, neutral:

$$\Delta h = 400 \frac{F}{\bar{u}^3} + 3r \frac{w}{\bar{u}} \qquad (5.19)$$

Final, stable with wind:

$$\Delta h = 2.6 \left(\frac{F}{\bar{u}s}\right)^{1/3} \qquad (5.20)$$

Final, stable and calm:

$$\Delta h = 5.1\, F^{1/4} s^{-3/8} \qquad (5.21)$$

5-2.2 Behavior of Instantaneous Clouds

5-2.2.1 Qualitative Behavior. The rise of an instantaneous cloud, such as that originating from an explosion, is similar to the rise of a plume except that the cloud diffuses in three dimensions rather than just two. The cloud rises owing to its buoyancy and original vertical momentum, being carried along by the wind in the horizontal. Entrainment occurs at first because of the cloud's relative motion in the air and later because of the air's own turbulence. In stratified air the buoyancy of the cloud is altered by the relative density of the entrained air. In stable air a limiting height is reached when the buoyancy decays to zero; in unstable air the cloud will rise indefinitely.

5-2.2.2 Height-of-rise Formulas. The rise of a cloud from an instantaneous point source in a stable fluid is treated theoretically by Morton, Taylor, and Turner (1956) in agreement with Batchelor's dimensional analysis (1954). The point source is specified by the total buoyant force imparted to a large volume of entrained air divided by the density of air, given by

$$F_i = \frac{g\, Q_i}{c_p \rho T} \qquad (5.22)$$

This gives for a stable atmosphere

$$\Delta h \propto F_i^{1/4} s^{-1/4} \qquad (5.23)$$

For a neutral atmosphere, neglecting roughness effects, dimensionally we would have

$$\Delta h \propto F_i^{1/2} \bar{u}^{-1} \qquad (5.24)$$

but this formula has not yet been tested.

5-2.2.3 Comparison with Observations. Morton, Taylor, and Turner (1956) performed experiments in a stably stratified salt solution and found a 0.98 correlation factor between observed rises and a formula whose point-source atmospheric equivalent would be

$$\Delta h = 2.66 \left(\frac{Q_i}{c_p \rho \, \partial\Theta/\partial z} \right)^{1/4} = 2.66 \frac{F_i^{1/4}}{s^{1/4}} \qquad (5.25)$$

In Fig. 5.3 this formula is compared with the rise of clouds from nuclear detonations in Phase II of Operation Hardtack, where detonations ranged from 0.6 tons to 6 kt TNT equivalent (Telegadas and Nagler, 1960). The rises average about 30% higher than the above formula predicts, but this is not unexpected since the fireball at first rises as a bubble without mixing owing to the great density difference between it and the surrounding air; energy losses other than that of heating the air have not been accounted for. The potential temperature difference between the bottom and top of the rise layer was measured from the top to the ground inversion, when present, to allow for the bubble effect.

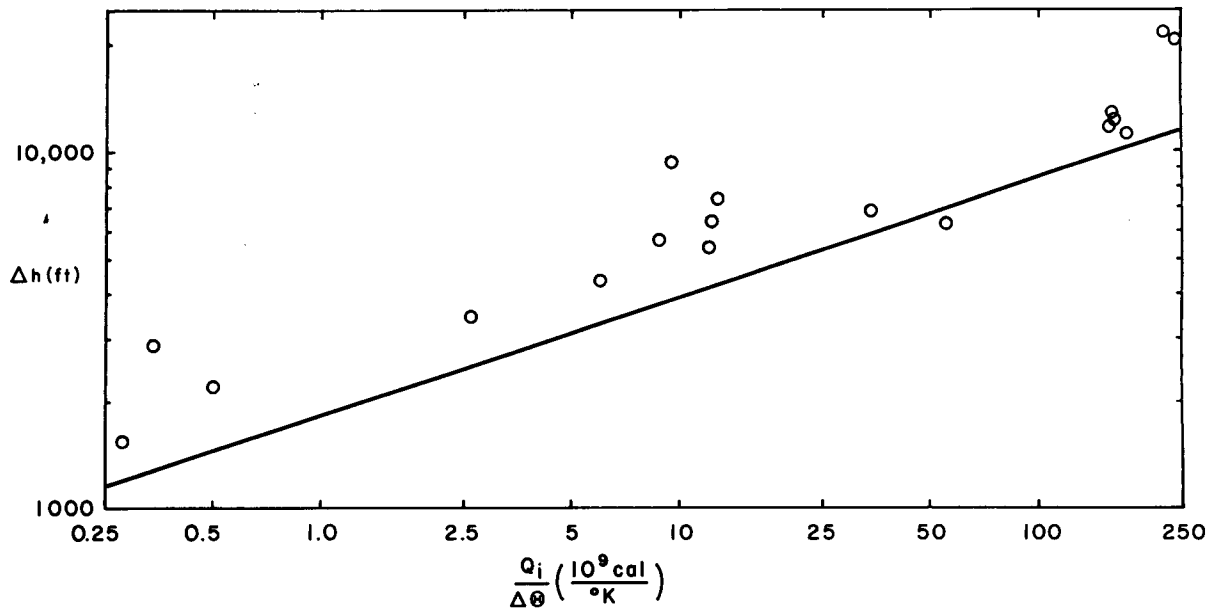

Fig. 5.3—Observed cloud rises from nuclear detonations vs. $\Delta h = 2.66\ F_i^{1/4}/s^{1/4}$ (solid line).

5-2.3 Effects on Ground-level Concentration

5-2.3.1 Practical Considerations. The general effect of efflux velocity and buoyancy is to raise the effective height of emission of gases, thereby reducing their ground-level concentration. Air-pollution meteorologists would like to know how to take best advantage of this to alleviate pollution at the ground. There are also undesirable aerodynamic effects that must be avoided, such as downwash at the chimney and large eddies due to surrounding buildings and terrain.

One obvious way to increase rise would seem to be to increase efflux velocity. Since the rise due to efflux velocity is only of the order 1.5 d $(w/\bar{u})$, however, the rise gained is generally much less than the total stack height and is therefore uneconomical. The TVA installed a nozzle on the stack of a 150-Mw unit increasing the efflux velocity from 45 to 90 ft/sec and found no significant increase in rise over adjacent unmodified units during pollution conditions (Thomas, Carpenter, and Gartrell, 1963). For a buoyant plume in stable conditions, it is even possible to get less rise with increased efflux velocity since this increase causes more vigorous entrainment at the chimney level (Morton, 1959).

A more effective way to increase rise is to make the heat efflux, Q_H, larger. When a single unit is involved, this method, too, is usually uneconomical since a higher stack would be cheaper than the long-run cost of added heat. When more than one pollutant-producing unit is available, however, combining the effluents into

one common stack results in a double advantage: first, for the same cost a single stack can be made taller than several individual stacks and, second, the buoyancies are additive so that the overall plume rise increases.

At two large London power stations, an attempt to reduce sulfur dioxide contamination was made by removing 90% of the gas through a washing process (Hawkins and Nonhebel, 1955). Unfortunately the process also reduced the temperature of the gas and saturated it with water vapor, causing the plume to lose its buoyancy and spread to the ground more quickly. Isopleths of SO_2 at the ground showed that the maximum concentration of the washed plume was comparable to that of the unwashed plume. One advantage gained by washing, however, was that the areas bounded by isopleths of relatively high concentration were substantially reduced.

When the wind is high, effluent may be drawn into the low-pressure area created on the leeward side of the chimney, a condition known as downwash. Wind-tunnel experiments by Sherlock and Stalker (1941) suggest that downwash is not serious as long as $w > \bar{u}$. Thus efflux velocity should exceed the wind speed at which the worst pollution is expected. One power-station stack in Bankside, England, is divided internally into four sections so that a partial load uses only part of the chimney and a sufficient efflux velocity is maintained. When efflux velocity is low, another way to eliminate downwash is to install around the chimney top a horizontal disk about one chimney diameter in width; such a disk is in use at St. Auban sur Durance, France (Scorer, 1959).

5-2.3.2 Prediction of Concentration. Once the possibility of extraneous aerodynamic effects has been eliminated, the usual method of predicting ground concentration is to calculate the total plume rise and to use this in the diffusion equations. This procedure is not simple to execute since a variety of meteorological situations must be accounted for and the best diffusion model and plume-rise formula must be chosen.

The meteorological complications are reduced if we consider only the average conditions (this treatment is given by Scorer and Barrett, 1962) and the worst situations, i.e., the windy neutral case and the low-wind fumigation case. In industrial areas the fumigation case is likely to be the worst since pollution from each source spreads and superimposes itself on that of its neighbors. These two situations were treated for maximum ground concentration from a buoyant source by Briggs (1965). A summary follows.

In the neutral case, assuming a Gaussian distribution and constant σ_z/σ_y for the pollutant, we find at the distance of maximum concentration

$$\bar{\chi}_{max.} = \frac{\sigma_z}{\sigma_y} \frac{2Q'}{\pi h^2 e\bar{u}} \qquad (5.26)$$

where the notation is that of Chaps. 3 and 4 (see Chap. 3, Eq. 3.146). If we assume that $\sigma_z/\sigma_y \approx 0.5$ in the neutral case and, further, assume a conservative rise given by $400F/\bar{u}^3$, a critical wind speed at which the highest concentration occurs is found by differentiation:

$$\bar{u}_c = 12.6(F/h_s)^{1/3} \qquad (5.27)$$

This results in a maximum ground concentration of approximately

$$\bar{\chi}_{max.} = a \frac{Q'}{F^{1/3} h_s^{5/3}} \qquad (5.28)$$

where $a = 0.0065$.

The corresponding equations for a nonbuoyant source whose plume rise is $1.5\, d\, (w/\bar{u})$ are

$$\bar{u}_c = 3\, w \frac{r}{h_s} \qquad (5.29)$$

$$\bar{\chi}_{max.} = 0.01 \frac{Q'}{w\, r\, h_s} \qquad (5.30)$$

For a large plant $\bar{u}_c$ may be 40 mph or more; so the maximum concentration predicted in Eq. 5.28 is rarely reached. Equations 5.27 through 5.30 best apply to about a half-hour average; peak concentrations for shorter averages may be higher owing to sustained eddies in the atmosphere. This is seen in the first three cases of Table 5.7 which shows some observed maximum ground concentrations expressed in terms of the dimensionless coefficient a in Eq. 5.28 for a buoyant source. Data are shown for ^{41}Ar at reactors in Oak Ridge, Tenn. (U. S. Weather Bureau, 1953), and in Harwell, England (Stewart, Gale, and Crooks, 1958), as well as for SO_2 at TVA plants. Since the TVA data involve multiple sources, observed concentrations were reduced by the factor plotted in Fig. 7 of Thomas,

Table 5.7—OBSERVED MAXIMUM GROUND CONCENTRATIONS IN NEUTRAL CONDITIONS

Plant	Type of average	Wind speed, m/sec	Height of wind-speed measurement, m	$\bar{u}_c$, m/sec	a
Oak Ridge	Peak 15-min average	6	47	10	0.019
	Average 15-min average	6	47	10	0.012
Harwell	Peak	12	35	11	0.012
	Peak 40-min average	5	1	11	0.006
TVA plant A	Peak 30-min average	8 to 12	55	17	0.006
TVA plant B	Peak 30-min average	9	67	18	0.007
TVA plant C	Peak 30-min average	12	98	20	0.005

Carpenter, and Gartrell (1963) showing maximum observed ground concentration vs. number of units operating.

In calm, stable conditions a buoyant plume rises to a limited height and stratifies, spreading horizontally over an increasing area. Fumigation occurs in the morning when convection due to ground heating builds up to the level of the stratified smoke and mixes it evenly down to the ground. Although highest ground concentrations usually occur during fumigation, as far as this author knows there is no quantitative model in the literature which predicts concentration at fumigation when there is no wind. Briggs suggested a simple model for a single source by assuming that during the inversion the smoke spreads horizontally at a constant rate of area increase and that this rate of spread is a function only of the buoyancy flux, F, and the stability parameter, s. Dimensionally, the area of spread must then be

$$b^{-1} F^{1/2} s^{-1/4} \Delta t \qquad (5.31)$$

where Δt is the time over which the smoke accumulates in the stratified layer and s is determined from the nighttime lapse rate through the layer of plume rise. The constant of proportionality, b, is estimated from data discussed in the next paragraph to be of the order 0.05. During calm, stable conditions we use the appropriate plume-rise formula to predict stratification at the height

$$h = h_s + 5.1 F^{1/4} s^{-3/8} \qquad (5.32)$$

If, at fumigation, the pollutant becomes evenly mixed down to the ground throughout the area of spread and edge effects are negligible, the concentration is given by

$$\bar{\chi}_{max.} = b \frac{Q'}{F^{1/2} s^{-1/4} (h_s + 5.1 F^{1/4} s^{-3/8})} \qquad (5.33)$$

Adequate data to test this formula do not exist, but the TVA observations were used to estimate b by assuming that a ground concentration of 0.1 ppm or more, occurring when the wind is not greater than 5 mph, is a case of fumigation. Since the temperature gradient at the plume level is not known, it was estimated from earlier TVA studies to be about 2.7° F/1000 ft. Fortunately this factor is not very critical, e.g., if it were as much as 10° F/1000 ft, b would be 30% smaller. Unfortunately the number of stacks, N, is greater than one at all three plants; so, for a conservative estimate of b, it was assumed that increasing N only increases the area of spread and does not affect the magnitude of concentration. This would be the case if the plumes merely displaced each other in spreading. The resultant estimates of b are shown in Table 5.8. Although this fumigation model looks promising, the assumption of a constant rate of horizontal spread is questionable and should be tested further.

In a valley of average width, W, and average drainage wind, $\bar{u}$, at night, we can use a simple channel model to predict fumigation downwind of buoyant sources that do not escape the valley. Assuming that the plume stratifies at the level given by the stable windy plume-rise formula and that it mixes evenly below this level at fumigation, we have

$$\bar{\chi}_{max.} = \frac{Q'}{\bar{u} W [h_s + 2.6 (\bar{u}s/F)^{-1/3}]} \qquad (5.34)$$

Table 5.8—MAXIMUM GROUND CONCENTRATION OF SO_2 DURING FUMIGATION AT TVA PLANTS (30-MIN AVERAGES)

	Plant A	Plant B	Plant C
F, ft^4/sec^3	23,000	31,000	67,000
h_s, ft	250	300	500
Q, tons/day	84	135	334
N (number of stacks)	8	4	2
Period of data	3/56 to 10/56	3/55 to 4/58	12/58 to 1/61
Number of fumigations	1	9	12
$\chi_{max.}$, ppm	0.4	0.6	0.6
Calc. h, ft	1350	1500	1900
b	0.05	0.06	0.05

5-3 DEPOSITION OF PARTICLES AND GASES (Isaac Van der Hoven)

List of Symbols

Symbols used frequently in Sec. 5-3 on the deposition of particles and gases are listed here. (The dimensions mass, length, time, and temperature are abbreviated as M, L, T, and D, respectively. The equation number indicates the first appearance of the symbol.)

C_D Drag coefficient (dimensionless), Eq. 5.35

C_y, C_z Sutton's virtual diffusion coefficients ($L^{n/2}$), Eq. 5.38

g Gravitational acceleration (LT^{-2}), Eq. 5.35

h Height of source above ground (L), Eq. 5.38

n Sutton's parameter associated with stability (dimensionless), Eq. 5.38

Q', Q'_0 Initial source strength (MT^{-1}), Eq. 5.38

Q'_x Depleted source strength at a distance, x, from the source (MT^{-1}), Eq. 5.42

r Particle radius (L), Eq. 5.35

$\bar{u}$ Average value of the wind component in the direction of the mean horizontal vector wind (LT^{-1}), Eq. 5.38

v_d Deposition velocity (LT^{-1}), Eq. 5.41

v_g Fall velocity (LT^{-1}), Eq. 5.35

λ Mean free path of air molecules (L), Eq. 5.37

μ Atmospheric dynamic viscosity ($ML^{-1}T^{-1}$), Eq. 5.36

ρ Particle density (ML^{-3}), Eq. 5.35

ρ_a Atmospheric density (ML^{-3}), Eq. 5.35

σ_y, σ_z Standard deviation of the distribution of material in a plume in the y and z directions (L), Eq. 5.44

$\bar{\chi}$ Average concentration (ML^{-3}), Eq. 5.38

ω Amount of aerosol removed per unit time per unit area ($ML^{-2}T^{-1}$), Eq. 5.39

5-3.1 Gravitational Settling

The earth's gravitational field plays an important role in the deposition of particulate matter on the earth's surface. The rate of descent of the particle depends upon a balance between the aerodynamic drag force and the gravitational force exerted by the earth. For a smooth spherical particle, neglecting the effect of slip flow, this balance may be expressed as

$$\rho_a \, v_g^2 \, C_D = \frac{8}{3} \, r \, g \, \rho \qquad (5.35)$$

where the notation is as given in the list of symbols. Equation 5.35 cannot be solved directly for the fall velocity because the drag coefficient is an empirical function of the Reynolds number, Re, and therefore also of velocity. McDonald (1960) has conveniently plotted this empirical relation for $Re \geq 1.0$ from which values of fall velocity vs. particle size can be computed. For the Reynolds number range between 10^{-4} and 10, the relation $C_D = 24/Re$ may be used, and, since $Re = 2\rho_a v_g r/\mu$, Eq. 5.35 reduces to the familiar Stokes equation

$$v_g = \frac{2 \, r^2 \, g \, \rho}{9\mu} \qquad (5.36)$$

The effect of the slip flow upon the fall velocity is a function of the ratio of the mean free path of the air molecules to the particle size. It can be expressed by multiplying the fall velocity by a slip correction factor (Davis, 1945)

$$1 + \frac{\lambda}{r}\left[1.26 + 0.4 \exp\left(-\frac{1.1r}{\lambda}\right)\right] \qquad (5.37)$$

where λ is primarily a function of altitude.

The effect of shape upon fall velocities is, on the average, to reduce the velocity by about $^2/_3$ from that of a smooth sphere. Smooth ellipsoidal particles theoretically will vary in fall velocities by factors ranging from 0.5 to 1.04.

At fall velocities less than about 1 cm/sec, the effect of sedimentation is negligible, and vertical movement of the particle is largely controlled by the larger vertical turbulent and mean air motions. Figure 5.4 (after Hage, 1964) shows the fall velocity of smooth spheres with a density of 5 g/cm^3 as a function of the altitude and particle diameter, with inertia terms and slip flow corrections taken into account where significant. It can be seen that the predominant

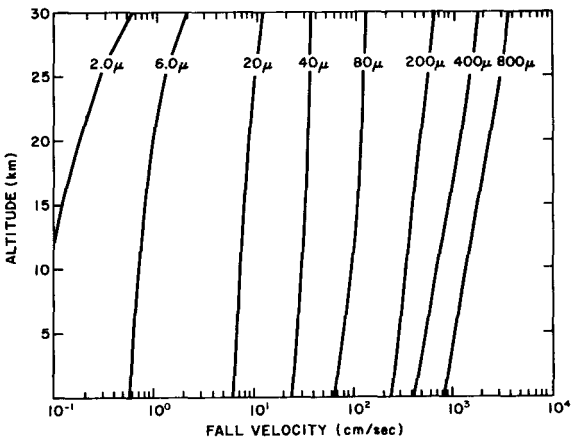

Fig. 5.4 — Fall velocity of smooth spheres with a density of 5 g/cm^3 as a function of altitude and particle diameter (microns). (From Hage, 1964.)

factor affecting fall velocity is the particle size. Similar fall-velocity computations for a particle with a density of 2.5 g/cm^3 are given by McDonald (1960a).

In the range where the sedimentation rate is significant, the vertical transport of an initially airborne particle (fall velocity greater than about 1 cm/sec) depends upon horizontal as well as vertical transport and diffusion. For fall velocities ranging from about 1 to 100 cm/sec, the diffusion of a cloud of particles under homogeneous horizontal transport (no wind shear with height) can be described by assuming that the particles are diffused according to a statistical diffusion model, such as that of Sutton (1953), and at the same time that they will settle with appropriate fall velocities. For the case of an elevated plume, the effect is essentially that of the downward tilt of the plume center line, which can be expressed by replacing the constant height of the plume center line in the Sutton equation by a variable expression such that

$$\bar{\chi}\,(x,y,0) = \frac{2Q'}{\pi C_y C_z \bar{u} x^{2-n}} \exp\left\{-x^{n-2}\left[\frac{y^2}{C_y^2} + \frac{(h-xv_g/\bar{u})^2}{C_z^2}\right]\right\} \qquad (5.38)$$

With the assumption that the particles are removed (deposited) when they reach the ground–air interface, the deposition pattern can be described by the expression

$$\omega = v_g \bar{\chi}\,(x,y,0) \qquad (5.39)$$

where ω is the amount removed per unit time per unit area and $\bar{\chi}$ is the volumetric concentration pattern of the air at the surface.

Van der Hoven (1963) used this tilted plume model to describe the observed deposition pattern of radioactive effluents and included a cloud depletion factor (Csanady, 1955) of

$$1 - \frac{1}{(1-n/2)(h_0\bar{u}/xv_g - 1) + 2} \qquad (5.40)$$

where n is one of Sutton's diffusion parameters. In practice the tilted plume model is only applicable in a well-mixed atmospheric layer, such as is typical of daytime adiabatic conditions within the lowest thousand meters.

The effect of horizontal wind-direction shear in the vertical becomes important as a diffusion mechanism if there is an initial distribution of particle sizes with height. With an initial cloud dimension of about 1000 m and particle fall velocities greater than 1 m/sec, the effect of turbulent diffusion on the ground deposition pattern can be neglected. The problem then becomes that of calculating particle trajectories using the appropriate fall velocity of each particle and the resultant wind vector of the atmospheric layer through which the particle falls. This technique as described by Kellogg, Rapp, and Greenfield (1957) has been applied primarily to the particle cloud resulting from surface nuclear-device detonations to calculate the fallout pattern for the first few hours after detonation.

5-3.2 Dry Deposition

5-3.2.1 Deposition Velocity. The observed fact that the deposition rate of small particles onto the ground can be greater than can be explained by the appropriate gravitational fall velocity has focused attention on nongravitational and nonprecipitation mechanisms, such as surface impaction, electrostatic attraction, adsorption, and chemical interaction. In analyzing the deposition of spores, Gregory (1945) concluded that the deposition rate was proportional to the immediate ground-level air concentration. Chamberlain (1953) defined the ratio of the deposition rate to the immediate ground-level air concentration as the deposition velocity, which, analogous to Eq. 5.39, can be stated as

$$\omega = v_d \bar{\chi}\,(x,y,0) \tag{5.41}$$

The interesting feature of such a formulation is that by using it as an experimental tool to compute v_d through the field or laboratory measurement of ω and $\bar{\chi}$, we can apply it to gases and vapors as well as to small particles. It in no way explains the physics of the deposition mechanism, but nevertheless it is a convenient way to express the whole complex and little-understood dry-deposition phenomenon.

5-3.2.2 Cloud Depletion. To account for the depletion of an airborne cloud because of dry deposition, Chamberlain (1953) modified Sutton's equation so that the original source term, Q_0', was replaced by an effective depleted-source term, Q_x'. Thus, for a continuous source at ground level, the depletion factor was expressed by Chamberlain as

$$\frac{Q_x'}{Q_0'} = \exp\left(-\frac{4v_d\,x^{n/2}}{n\bar{u}\pi^{1/2}\,C_z}\right) \tag{5.42}$$

Using Eq. 5.41 and the modified Sutton equation, we can express the deposition rate per unit time per unit area for a source at ground level as

$$\omega = \frac{2Q_0'\,v_d}{\pi\bar{u}\,C_yC_z x^{2-n}} \exp\left(-\frac{4v_d\,x^{n/2}}{n\bar{u}\pi^{1/2}\,C_z}\right) \times \exp\left(-\frac{y^2}{C_y^2\,x^{2-n}}\right) \tag{5.43}$$

Chamberlain further expressed the depletion factor for the case of an elevated source. Culkowski (1958) has presented graphical solutions to these equations.

The generalized Gaussian diffusion formula (in the notation used in Chap. 3) can also be modified for cloud depletion. The depletion correction for a continuous elevated source can be derived as follows:

$$\omega(x,y) = v_d\,\bar{\chi}(x,y,0) = \frac{v_dQ_x'}{\pi\sigma_y\sigma_z\bar{u}} \exp\left[-\left(\frac{y^2}{2\sigma_y^2}+\frac{h^2}{2\sigma_z^2}\right)\right] \tag{5.44}$$

where $\omega(x,y)$ is the surface deposition at (x,y) and Q_x' is the residual source at x meters downwind. The depletion of the source per unit distance is given by

$$\frac{\partial Q_x'}{\partial x} = -\int_{-\infty}^{\infty} \omega(x,y)\,dy = -\left(\frac{2}{\pi}\right)^{1/2} \frac{v_dQ_x'}{\bar{u}\sigma_z} \exp -\left(\frac{h^2}{2\sigma_z^2}\right) \tag{5.45}$$

which can be rearranged as

$$\int_0^x \frac{dQ_x'}{Q_x'} = -\left(\frac{2}{\pi}\right)^{1/2} \frac{v_d}{\bar{u}} \int_0^x \frac{dx}{\sigma_z \exp\,(h^2/2\sigma_z^2)} \tag{5.46}$$

If $Q_x' = Q_0'$ at $x = 0$, then

$$\ln\frac{Q_x'}{Q_0'} = -\left(\frac{2}{\pi}\right)^{1/2} \frac{v_d}{\bar{u}} \int_0^x \frac{dx}{\sigma_z \exp\,(h^2/2\sigma_z^2)} \tag{5.47}$$

and therefore

$$\frac{Q_x'}{Q_0'} = \left[\exp\int_0^x \frac{dx}{\sigma_z \exp\,(h^2/2\sigma_z^2)}\right]^{-(2/\pi)^{1/2}v_d/\bar{u}} \tag{5.48}$$

Since σ_z is not generally available as an analytical function of x in the generalized Gaussian form, the integral expression in Eq. 5.48 was evaluated numerically using the experimentally derived values of $\sigma_z(x)$ given by Hilsmeier and Gifford (1962). Figure 5.5 shows the depletion fraction, (Q_x'/Q_0'), as a function of distance from the source, diffusion category (in terms of Pasquill types or the corresponding values of σ_θ as given in Chap. 4, Sec. 4-4.4), height of release, a deposition velocity of 1 cm/sec, and a mean wind speed of 1 m/sec. To obtain depletion fractions for other deposition velocities and wind speeds, we may use the expression

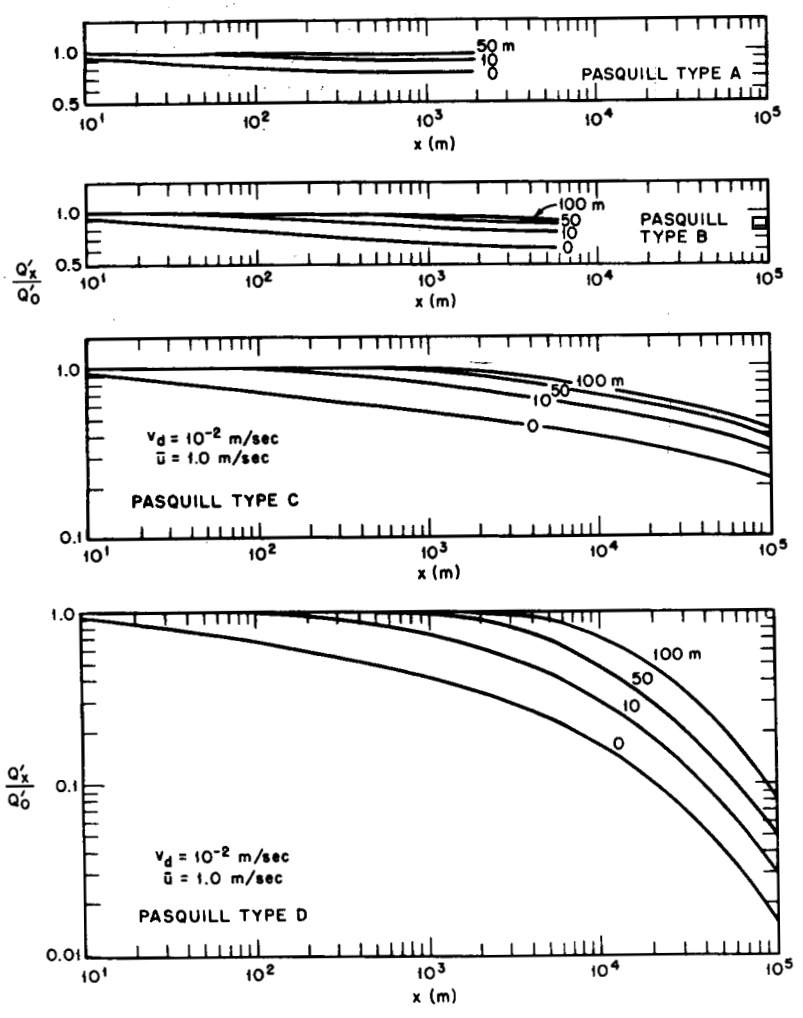

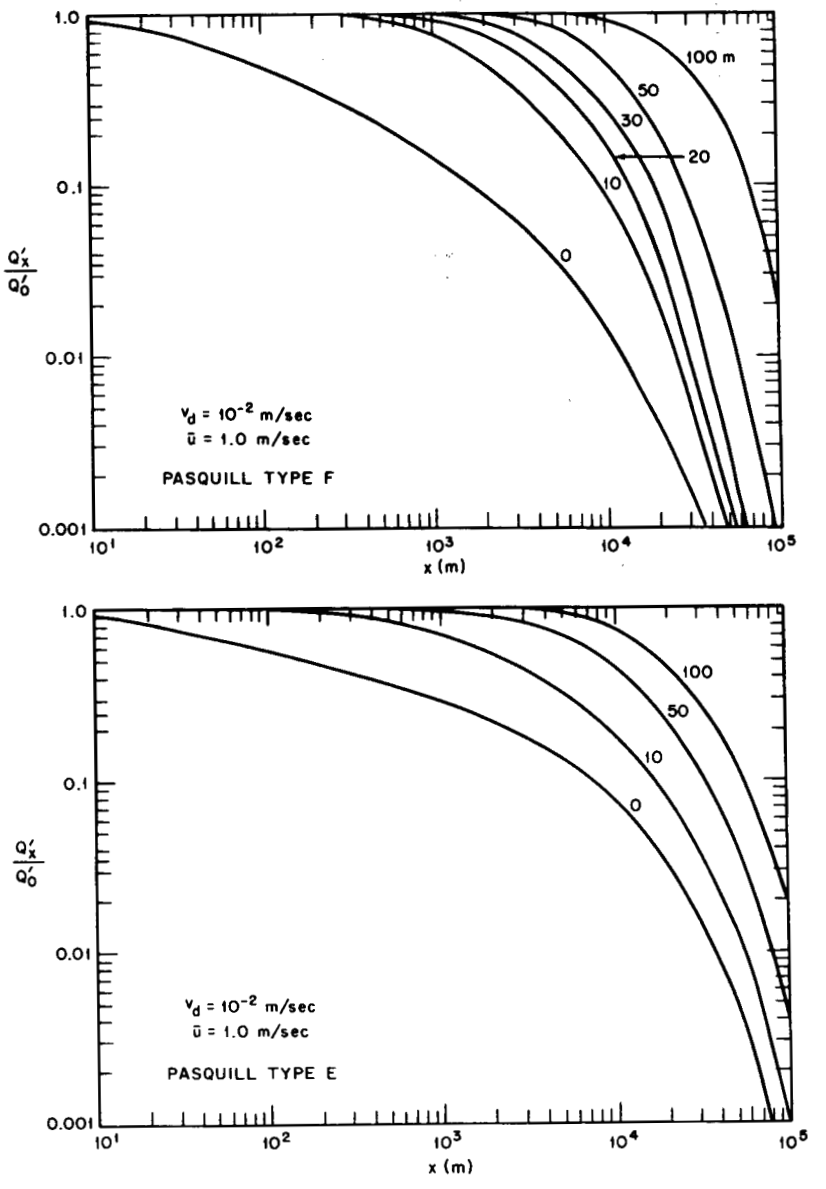

Fig. 5.5 — Source-depletion fraction, Q'_x/Q'_0, for a wind speed, $\bar{u}$, of 1.0 m/sec, a deposition velocity, v_d, of 10^{-2} m/sec, for source heights from 0 to 100 m above the ground and for various stability categories.

$$\left(\frac{Q'_x}{Q'_0}\right)_2 = \left(\frac{Q'_x}{Q'_0}\right)_1^{\bar{u}_1 v_{d2}/\bar{u}_2 v_{d1}} \qquad (5.49)$$

where the subscript 1 refers to values found in Fig. 5.5 and the subscript 2 refers to the desired values. Thus, for example, to find the depletion fraction at a distance of 10^4 m for a source 50 m high, a $\bar{u}_2$ of 1 m/sec, a v_{d2} of 0.1 cm/sec, and a type F diffusion category, first find, in Fig. 5.5, the value of $(Q'_x/Q'_0)_1$ for h = 50 m, $x = 10^4$ m, $\bar{u} = 1$ m/sec, and $v_d = 1$ cm/sec: $(Q'_x/Q'_0)_1 = 0.50$. Now substitute this value in Eq. 5.49,

$$\left(\frac{Q'_x}{Q'_0}\right)_2 = (0.50)^{0.1} = 0.93$$

The Chamberlain and the generalized Gaussian depletion models assume that the shape of the concentration profile in the vertical is unaltered by deposition. In an approach suggested by Calder (1961), K theory diffusion equations (see Chap. 3, Sec. 3-2.1.2) were used to describe the effect of deposition on a plume. In models of this type, the reduction of concentration caused by removing material from the cloud is not distributed evenly through the depth of the cloud but depends upon the profile of vertical mixing. Therefore the shape of the vertical profile of concentration will change as the computation proceeds. Smith (1962a) schematically illustrates the effect for a case where h = 0, $v_g = 0$, $v_d > 0$, and the exchange coefficient is constant with height. The net result is a more rapid depletion of the bottom portion of the plume; so downwind from the source the height of the maximum concentration is above the surface and increases in the downwind direction. Definitive field measurements to evaluate the statistical depletion model and the K-theory depletion model are not yet available. Computations show that the statistical models (Eqs. 5.42 and 5.48) give higher depletion factors than the K-theory models under stable conditions.

5-3.2.3 Deposition Measurements. Among the important measurements of the deposition of radioactive vapors and aerosols are the pioneering efforts of Chamberlain (1960) at Harwell. He was concerned with the fission products formed in reactors or by nuclear detonations. The isotope ^{131}I was one of the more important fission products studied. Although liberated as a vapor, ^{131}I is thought also to be adsorbed on condensation nuclei which are too small to have an appreciable gravitational settling velocity but which, nevertheless, deposit on surfaces under electrostatic, chemical, and other physical forces. Chamberlain's ^{131}I-vapor-release experiments were conducted both in the wind tunnel and in the free atmosphere and included simultaneous air concentration and deposition measurements on natural and simulated leaves and grass and on filter paper.

Recently, a series called Controlled Environmental Radioiodine Tests (Hawley, Sill, Voelz, and Islitzer, 1964) was conducted at the National Reactor Testing Station in Idaho to trace the radioiodine through the air–vegetation–cow–milk–human chain. The field results of both the Harwell and Idaho tests are summarized in Table 5.9a, which gives the existing meteorological conditions and the computed (from Eq. 5.41) deposition velocities for various collection surfaces. Similar results on the deposition of ^{131}I were obtained by Convair (1959, 1960) from the Fission-products Field Release Test I held in Idaho (NRTS) and Test II held in Utah (Dugway). Results are summarized in Table 5.9b. Chamberlain (1959) further computed an ^{131}I deposition velocity averaging 0.4 cm/sec on grass for the Windscale accident; Islitzer (1962) computed 0.2 cm/sec on sagebrush for the SL-1 accident, which occurred in the winter.

From these results one would conclude that the dry-deposition velocity of ^{131}I ranges over an order of magnitude and is dependent, to a large extent, upon the characteristics of the vegetation and ground surface. It is not clear if or how wind speed, thermal stability, or atmospheric turbulence affects the velocities. It is also possible that downwind distance has an effect because of a physical change in the iodine, for example, from a vapor to an aerosol. At present, without really having any information on the physical processes involved in the dry deposition of ^{131}I upon natural surfaces, a value of 2.0 cm/sec for grass or water surfaces appears appropriate as an average maximum, and somewhat smaller values ranging down to 0.5 cm/sec, for soil and snow surfaces.

The Convair (1959, 1960) studies essentially involved the release and downwind measurement of various radioactive isotopes from irradiated metallic reactor fuel elements, including isotopes of iodine, cesium, ruthenium,

Table 5.9a—SUMMARY OF ^{131}I DEPOSITION FIELD EXPERIMENT RESULTS*

	Harwell tests							Idaho tests		
	1	2	3	4	5	6	7	I	II	Snow
Deposition velocity, cm/sec										
Grass	1.9	2.6	1.8	3.7	1.7	1.8	1.1	0.6	1.0	
Soil								0.8	0.4	
Snow										0.2
Carbon								0.6	0.7	0.9
Clover leaves			1.3	0.9	0.5		0.3			
Paper leaves			2.0	1.5	1.0		0.6			
Filter paper	0.6	0.7	0.9	0.6	0.3					
Sticky paper								0.2	0.4	0.6
Wind speed, m/sec	5.2	4.3	5.2	4.1	1.6	2.3	3.9	7.1	9.3	6.0
Friction velocity, cm/sec	48	35	48	38	15	20	26	61	69	50
Roughness length, cm	2.8	1.5	1.2	2.4	2.4	5.0	1.0	3.1	1.5	2.1
Downwind distance, m	15	20	20	20	20	100	100	300	375	340
Grass cover, g/m^2	500	200	260	420	420	610	420	153	246	Snow cover
Stability	Lapse	Neutral	Lapse	Lapse	Neutral	Lapse	Neutral	Lapse	Lapse	Stable

*Chamberlain, 1960, and Hawley, Sill, Voelz, and Islitzer, 1964.

Table 5.9b—SUMMARY OF CONVAIR ^{131}I FIELD RELEASE TESTS*

	E	F	H	1	2	3	4	5	8	10	11
Deposition velocity, cm/sec											
Grass				2.1†						1.2‡	
Soil	0.5	1.4	0.5								
Sticky paper	1.1	0.7	1.5	0.4	0.3	0.1	0.2	0.2	0.3	0.2	0.6
Water	1.8†	2.3†	1.4†								
Wind speed, m/sec	6.8	5.3	4.0	5.0	4.2	3.2	2.4	4.4	2.7	2.6	4.4
Downwind distance, m	1,600	1,600	1,600	32,000	1,000	1,000	1,000	4,000	1,000	4,000	16,000
Stability	Lapse	Lapse	Stable	Stable	Stable	Stable	Stable	Stable	Stable	Stable	Stable

*Convair, 1959, 1960.
†Downwind distance of 2000 m.
‡Downwind distance of 1000 m or less.

zirconium, cerium, niobium, and tellurium for which deposition-velocity calculations were made. Meteorological conditions included both adiabatic and stable lapse rates, and measurements of ground deposition and air concentrations were made to distances of 3200 m. Some sticky-paper measurements were made out to 3.2×10^4 m. All particles were less than 10 μ in diameter. Table 5.10 summarizes the deposition-velocity calculations. Note that these values are averages and that there is considerable scatter in the data which cannot be explained by the meteorological parameters that were measured. For example, the average deposition velocity of 0.2 cm/sec for ^{137}Cs on a grass surface was computed from 21 values ranging from 0.04 to 0.4 cm/sec.

Table 5.10—SUMMARY OF CONVAIR RADIONUCLIDE FIELD RELEASE TEST DEPOSITION VELOCITIES

	Deposition velocities, cm/sec			
	Water	Soil	Grass	Sticky paper
^{137}Cs	0.9 (5)*	0.04 (15)	0.2 (21)	0.2 (117)
^{103}Ru	2.3 (9)	0.4 (16)	0.6 (20)	0.4 (98)
^{95}Zr, ^{95}Nb	5.7 (6)	2.9 (6)		1.4 (10)
^{141}Ce				0.7
^{127}Te, ^{129}Te				0.7 (8)

*Number in parentheses indicates the number of determinations.

Another technique used in calculating deposition velocities is material-balance measurements such as performed by Islitzer and Dumbauld (1963) in their fluorescent-particle studies. The technique involves the determination of the mass flux of material through a vertical plane perpendicular to the mean wind direction. The downwind decrease of this flux is attributed to a material loss through deposition. Using uranin particles with a median diameter of 1 μ and a fall velocity of less than 10^{-2} cm/sec, Islitzer and Dumbauld computed deposition velocities of 0.2, 2.4, and 7.1 cm/sec for inversion, neutral, and lapse conditions, respectively, for the arid terrain in Idaho. From data presented by Simpson (1961), these authors also computed a value of 0.5 cm/sec for four stable cases with zinc sulfide submicron particles over similar terrain at Hanford, Wash. These and other deposition data are quoted in a summary article by Gifford and Pack (1962).

Two conclusions seem apparent from the available field data on the deposition of vapors and submicron particles, i.e., that chemically active materials such as ^{131}I deposit more readily than inactive materials such as ^{137}Cs or nonradioactive fluorescent particles and that vegetation surfaces such as grasses and bushes provide removal rates that are greater than bare surfaces. At present, however, what effects atmospheric transport and diffusion parameters have upon deposition or what effect more complex surfaces, such as buildings and forests, have upon deposition rates is not clear.

5-4 THE CALCULATION OF PRECIPITATION SCAVENGING (Rudolf J. Engelmann)

5-4.1 Introduction

The scavenging process has three major divisions: (1) delivery or transport of the material to the scavenging site, (2) in-cloud scavenging by the cloud elements and precipitation, here called rainout and snowout, and (3) below-cloud scavenging by the precipitation, here called washout. Material from low-elevation sources will be transported with the low-elevation winds and diffused upward by low-level turbulence. Once in the vicinity of clouds it may be carried into those clouds by organized vertical motions. When the material is from high elevations (the stratosphere), the general circulation of the earth's atmosphere and the exchange mechanism at the tropopause have control of the delivery.

There are several good starting points for the study of scavenging. Junge (1963) and Facy (1962) have looked at in-cloud scavenging but with differing conclusions. Fletcher (1962) and Mason (1957) have published texts on precipitation and cloud physics with comprehensive bibliographies. Chamberlain (1953) appears to have attempted the first broad application of scavenging equations, and his approach is still used. Fuchs (1964) has presented an extensive volume on the mechanics of aerosols. Reiter (1964) and Danielsen (1964) serve as introductions to the controversy on stratosphere–troposphere exchange. There is increasing interest in the scavenging problem, and the reader should be alert for the very probable future measurements of rain spectra, washout coefficients, scavenging efficiencies, and other parameters discussed later in the section.

List of Symbols

Symbols used frequently in Sec. 5-4 on precipitation scavenging are listed here. (The dimensions mass, length, time, and temperature are abbreviated as M, L, T, and D, respectively. The equation or section number indicates the first appearance of the symbol.)

A	Cross-sectional area of drop of diameter D (L^2), Eq. 5.54
a	Particle radius (L), Eq. 5.52
D	Drop diameter (the collector) (L), Eq. 5.52
d	Particle diameter (the collected) (L), Eq. 5.56
E	Scavenging efficiency (dimensionless), Eq. 5.53
F	Flux density of drops (drops/area-time-diameter interval), Eq. 5.54
K	Impaction parameter or Stokes number (dimensionless), Eq. 5.52
k_1	Concentration of contaminant in cloud water (M/L^3), Eq. 5.60
L/ρ	Fraction of cloud space filled with liquid water (dimensionless), Eq. 5.60

M	Mass of aerosol particle of diameter d (M), Eq. 5.56
N	Concentration of drops in air (drops/volume-diameter interval), Eq. 5.55
Q, Q′	Plume source strength (M, M/T), Eq. 5.62
Re	Reynolds number of waterdrop (dimensionless), Eq. 5.58
Sh	Nusselt diffusion number or Sherwood number (dimensionless), Eq. 5.57
T	Age of cloud (T), Eq. 5.61
t	Time (T), Eq. 5.50
U	Obstacle (raindrop) speed (L/T), Eq. 5.52
$\bar{u}$	Average value of the wind component in the direction of the mean horizontal vector wind (L/T), Eq. 5.64
Y	Diffusivity of a vapor in air (L^2/T), Eq. 5.57
α	Radioactivity per mass of particle (curies/g), Eq. 5.56
ϵ	Rainout efficiency, $1-(\chi/\chi_0)$ (dimensionless), Eq. 5.60
Λ	Washout coefficient (T^{-1}), Eq. 5.51
μ	Dynamic viscosity of air (M/LT), Eq. 5.52
ν	Kinematic viscosity of air (L^2/T), Eq. 5.58
ρ	Density (M/L^3), Eq. 5.52
σ_θ	Standard deviation of horizontal-wind-direction distribution (radians), Sec. 5-4.11
σ_y	Standard deviation of plume concentration in the crosswind direction (L), Eq. 5.62
χ	Concentration of contaminant in air (M/L^3), Eq. 5.50
χ_0	Concentration at start of scavenging (M/L^3), Eq. 5.50
Ψ	Rainout coefficient (T^{-1}), Eq. 5.50
ω	Deposition rate by washout or total deposition in accordance with dimensions of Q′ or Q (M/L^2T or M/L^2), Eq. 5.62

5-4.2 Specification of the Problem

Quite obviously the intensity and location of the clouds and precipitation will determine the potential for scavenging and can usually be stated explicitly. However, fine details of the clouds and precipitation, such as entrainment, electrical charge, and snow-crystal shape, are also important but generally impossible to specify.

The nature of the material to be scavenged is fully as important as the nature of the precipitation and should be specified as to size, if particulate, and to solubility, if gaseous. Density is important for at least the larger particles. Characteristics of electrical charge and wettability can be quite important, and these effects are yet under debate and investigation. With increasing time and distance from the source, all these characteristics are modified by agglomeration and by attachment and adsorption onto natural aerosols. The material should then assume the nature of this host.

Now the natural aerosol is not a well-defined parameter either, varying with elevation, geography, and meteorology. In his extensive treatment of natural aerosols, Junge (1963) presents model size distributions that may be used in the absence of local measurements (Fig. 5.6). Although little is known about the density of natural aerosols, Junge concludes, from chemical composition, that most have densities of 1.0 to 2.0 g/cm^3.

The scavenging process consists of repeated exposures of particles and gases to cloud or precipitation elements with some chance of collection on the element for each exposure. The scavenging is, consequently, an exponential decay process obeying the equations

$$\chi = \chi_0 \exp(-\Psi t) \tag{5.50}$$

$$\chi = \chi_0 \exp(-\Lambda t) \tag{5.51}$$

where Ψ and Λ are called the rainout and washout coefficients, respectively. Because these coefficients are dependent upon many aerosol and scavenger characteristics, it is easier and generally as accurate to begin the solution of a problem by adjustment or modification of previously measured or predicted coefficients than with the more basic variables.

Note that Eqs. 5.50 and 5.51 and other equations in this section apply to instantaneous and space-averaged concentration fields but cannot apply to time-averaged concentrations since time is here used as an independent variable.

5-4.3 The Theory of Washout by Rain

When an obstacle (such as a raindrop) falls, it sweeps out a volume of air. This volume of air

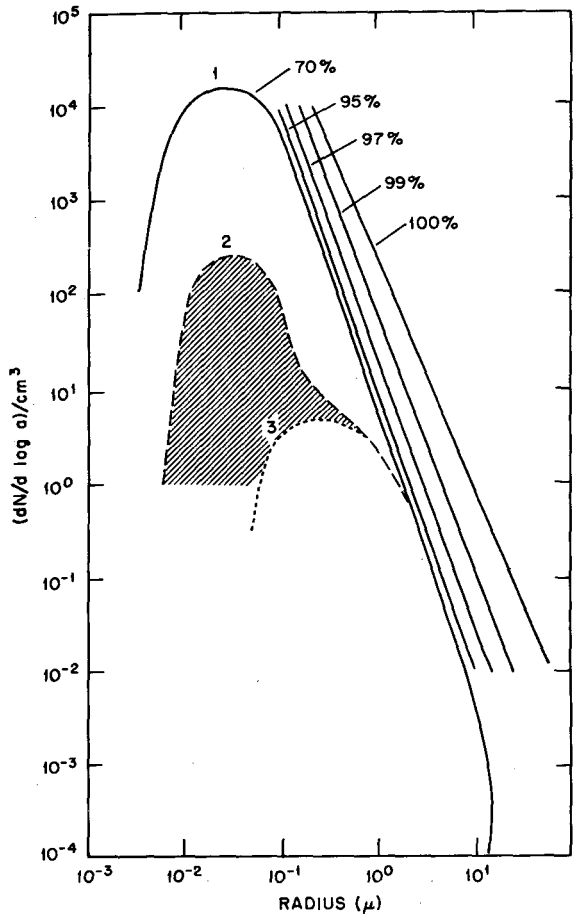

Fig. 5.6—Model size distributions for atmospheric aerosols. Curve 1 represents values over a continent, curve 2, over an ocean (the part of this curve below 1 μ is estimated), and curve 3, sea-spray component of the maritime aerosol. The hatched area between curves 2 and 3 represents the nonsea-spray component over the ocean. The straight lines indicate the shift of the continental log radius–number distributions curve due to particle growth by humidity for mixed particles of about 20% soluble material. (From C. E. Junge, *Air Chemistry and Radioactivity*, p. 124, Academic Press Inc., New York, 1963.)

must separate to allow the obstacle to pass, and particles therein will tend to follow the air. Owing to their inertia and electrical attraction and to molecular diffusion, however, some fraction of these particles will cross the streamlines of the air and intersect the obstacle. This fraction is the target or collision efficiency.

Contact with the obstacle does not ensure collection. Some particles may bounce off or be reentrained by the air. Of those particles making contact, the fraction remaining with the obstacle is the coalescence or retention efficiency.

The product of the target efficiency and the retention efficiency is the collection efficiency, E, of the obstacle for the particles considered. If 50 of the 100 particles in the path of a raindrop contact it, but only 20 are washed out, then the target efficiency is 0.5, the retention efficiency is 0.4, and the collection efficiency is 0.2.

The target efficiency is often presented as a function of the impaction parameter, which is derived from the equation of motion of a particle with drag resistance. The impaction, or inertial, parameter is

$$K = \frac{4\,a^2\rho U}{9\mu D} \qquad (5.52)$$

where a is the particle radius, ρ is the particle density, μ is the dynamic viscosity of the air, and U/D is the ratio of obstacle speed to diameter. In the case of rain, U and D are related and μ is nearly constant, therefore, approximately,

$$E = f(a^2\rho, D) \qquad (5.53)$$

Langmuir and Blodgett (1945) have calculated the target efficiencies for spherical collectors in potential and viscous flow fields, and Langmuir (1948) has provided an interpolation formula between the two flow types. In the past it has been generally assumed that this interpolation formula was applicable for raindrops; however, later measurements and theoretical predictions (e.g., Pearcey and Hill, 1957) cast doubt upon this.

Langmuir and Blodgett's target efficiencies were calculated for point-sized particles and did not allow for collection of a finite-sized particle whose center missed the drop but whose edge made contact. It may be that, if even the edge of some kinds of particles touch the drop, coalescence or collection may result. If so, the Langmuir efficiencies will be low. They may be approximately corrected by assuming a larger raindrop cross section of $(D+2a)^2/D^2$; this factor is to be multiplied by the Langmuir point-particle efficiency.

The Langmuir target efficiencies of raindrops at a pressure of 785 mb collecting particles of unit density appear in Table 5.11. Conversion

for particles of another density or at another altitude is made by equating $a^2\rho$ or K for the two particles in compliance with Eqs. 5.52 and 5.53.

Das (1950) and Fonda and Herne (Herne, 1960) have considered the finite size of the particles in later calculations of target efficiencies. The interception effect is noticeable for small raindrops and large particles. After adding to the calculations made by Fonda and Herne, Mason (1957) applied the Langmuir interpolation formula. The resulting target efficiencies for unit-density particles at 900 mb appear in Table 5.12. Approximate conversion to other densities can still be made by equating $a^2\rho$ for the two particles and multiplying the appropriate tabular efficiency by $(D + 2a_2)^2/(D + 2a_1)^2$ to allow for the change in interception area of the particle. It may be argued that, because of the uncertainties introduced by unknown retention efficiencies and by Langmuir's interpolation formula, there is little purpose in choosing Mason's efficiencies over Langmuir's or in considering corrections to these efficiencies for interception areas.

The effect on retention efficiencies of variations in the wettabilities of particles is a very unsettled question. McDonald (1963) and Owe Berg (1963) have published articles on the subject. Not only the effects of partial wettabilities but the actual wettability of natural airborne particles as well are in need of further definition. Even the coalescence of colliding water droplets is not assured. In the absence of wettability information, however, the assumption believed most likely to give correct results is that of perfect retention or coalescence. This is equivalent to equating target and collection efficiencies.

When airflow patterns other than viscous and potential are considered to exist about falling drops, calculated efficiencies can become very different. Efficiencies greater than 1.0 are predicted and observed for spheres with wakes (Pearcey and Hill, 1957). Whereas Langmuir's interpolation formula predicts a rather flat maximum in E at a drop diameter of 1.2 mm, Kinzer and Cobb (1958) and Engelmann (1963) have observed a peak in E for drops of about 0.4 mm diameter (Fig. 5.7).

When E is known as a function of drop size, the washout coefficient for a particular aerosol size and density can be computed from

$$\Lambda = \int_0^\infty \text{FEA}\, dD \qquad (5.54)$$

where A is the cross-sectional area of drops of diameter D and F is their flux density (drops/area-time-diameter interval). The flux density divided by the terminal velocity, U, yields the space density, N(D), which is the form most frequently used in presenting measured rain spectra. Equation 5.54 may, therefore, be written as

Table 5.11—COLLISION (TARGET) EFFICIENCY, E, FOR DROPS OF DIAMETER D FALLING THROUGH A CLOUD OF SMALLER DROPS OF RADIUS a*

D, mm	a, μ							
	2	3	4	6	8	10	15	20
0.03					0.092	0.269	0.500	0.643
0.05				0.050	0.277	0.411	0.613	0.724
0.08				0.205	0.394	0.510	0.690	0.782
0.14			0.035	0.340	0.500	0.608	0.750	0.834
0.2			0.133	0.418	0.564	0.660	0.793	0.862
0.3		0.010	0.245	0.498	0.631	0.713	0.829	0.887
0.4		0.085	0.326	0.564	0.684	0.756	0.859	0.908
0.6		0.213	0.425	0.643	0.749	0.810	0.892	0.929
0.8	0.040	0.303	0.500	0.698	0.793	0.849	0.919	0.950
1.2	0.121	0.355	0.530	0.731	0.827	0.876	0.939	0.963
2.0	0.140	0.358	0.535	0.738	0.834	0.886	0.944	0.966
2.8	0.168	0.360	0.534	0.735	0.840	0.890	0.950	0.970
3.6	0.117	0.288	0.456	0.680	0.800	0.865	0.935	0.965
4.8	0.075	0.220	0.372	0.606	0.743	0.823	0.920	0.950
6.0	0.050	0.170	0.306	0.546	0.690	0.785	0.900	0.940

*From I. Langmuir, The Production of Rain by a Chain Reaction in Cumulus Clouds at Temperatures Above Freezing, *J. Meteorol.*, 5(5): 182 (1948).

Table 5.12—COLLISION (TARGET) EFFICIENCIES FOR DROPS OF DIAMETER D COLLIDING WITH DROPLETS OF RADIUS a AT 0°C AND 900 mb*

D, mm	a, μ							
	2	3	4	6	8	10	15	20
0.03	0.03	0.05					0	
0.05	0.01	0.02	0.05	0.23				
0.08	0.004	0.01	0.04	0.29	0.55			
0.14	0.02	0.03	0.11	0.40	0.65	0.83	1.12	
0.2	0.03	0.07	0.18	0.47	0.67	0.83	1.08	1.26
0.3	0.07	0.14	0.28	0.55	0.72	0.84	1.04	1.16
0.4	0.10	0.21	0.35	0.61	0.76	0.86	1.01	1.11
0.6	0.15	0.31	0.45	0.68	0.80	0.89	1.00	1.06
0.8	0.17	0.37	0.51	0.72	0.84	0.91	1.00	1.06
1.2	0.17	0.40	0.54	0.74	0.85	0.91	0.99	1.02
2.0	0.15	0.37	0.52	0.74	0.83	0.90	0.97	1.00
2.8	0.11	0.34	0.49	0.71	0.83	0.89	0.96	0.96
3.6	0.08	0.29	0.45	0.68	0.80	0.86	0.98	0.95
4.8	0.04	0.22	0.39	0.62	0.75	0.83	0.93	0.97
6.0	0.02	0.16	0.33	0.55	0.71	0.81	0.91	0.95

*From B.J. Mason, *The Physics of Clouds*, p. 424, Oxford University Press, Inc., New York, 1957.

$$\Lambda = \int_0^\infty \text{NUEA } dD \qquad (5.55)$$

Russian authors call the product UEA the "coefficient of capture" of the drop of size D for the particle considered. Table 5.13 gives the terminal velocity of waterdrops near sea level

Table 5.13—TERMINAL VELOCITY OF FALL FOR DISTILLED-WATER DROPLETS IN STAGNANT AIR AT 20°C, 760 mm, AND 50% RELATIVE HUMIDITY*

Equivalent drop diameter, mm	Terminal velocity, cm/sec	Equivalent drop diameter, mm	Terminal velocity, cm/sec
0.1	27	3.2	826
0.2	72	3.4	844
0.3	117	3.6	860
0.4	162	3.8	872
0.5	206	4.0	883
0.6	247	4.2	892
0.7	287	4.4	898
0.8	327	4.6	903
0.9	367	4.8	907
1.0	403	5.0	909
1.2	464	5.2	912
1.4	517	5.4	914
1.6	565	5.6	916
1.8	609	5.8	917
2.0	649		
2.2	690		
2.4	727		
2.6	757		
2.8	782		
3.0	806		

*From R. Gunn and G. D. Kinzer, The Terminal Velocity of Fall for Water Droplets in Stagnant Air, *J. Meteorol.*, 6(4): 246 (1949).

as measured by Gunn and Kinzer (1949). Because waterdrops with a diameter greater than 1.2 mm are flattened, the diameter of a sphere of the same volume is listed as the equivalent diameter.

The washout coefficient for the entire aerosol is calculated by integrating Eq. 5.54 over particle size. If the aerosol characteristic of interest is size dependent, this relation can be inserted into the integral. For instance, for radioactivity uniformly distributed throughout the mass of aerosol,

$$\Lambda = \alpha \int_0^\infty \int_0^\infty \text{FEAM } dD\, dd \qquad (5.56)$$

where α is the activity per mass and M is the mass of the aerosol particle of diameter d.

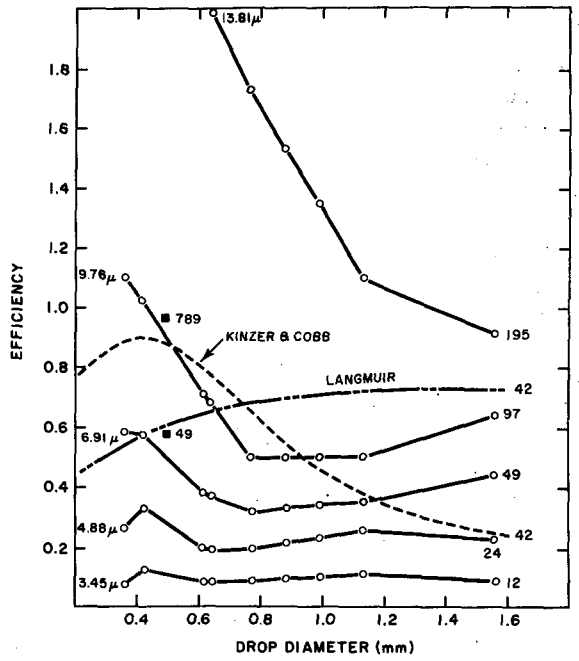

Fig. 5.7—Scavenging efficiencies vs. drop diameter and $a^2\rho$ (μ^2 g/cm^3), where a and ρ are the radius and density of the particles. The zinc sulfide experimental curves (solid lines) are labeled with $a^2\rho$ and the diameter in microns. The prediction by Langmuir (1948), when interpolating between viscous and potential flows, and the measurements of Kinzer and Cobb (1958) are entered as dashed lines. Two data points of Walton and Woolcock (1960) are entered as solid squares. (From Engelmann, 1965.)

5-4.4 Rain Spectra

Numerous measurements of rain spectra have been made, and several empirical equations have been fitted to them. Although rain spectra usually have peak frequencies between diameters of 0.5 and 1.0 mm, most empirical equations cannot fit peak frequencies. The distributions of Marshall and Palmer (1948) and Best (1950) have been most widely used, but these give excessive numbers of small droplets.

Levin (1954) has shown that several empirical space-density formulas are approximated by portions of a logarithmic-normal distribution. This distribution can fit a peak and can be argued to have a theoretical basis. It approximates, for example, rains sampled by Kelkar (1959) in India and a shower sampled by Engelmann in the semiarid climate of Sunnyside, Wash. (after somewhat arbitrary allowance for evaporation of the falling drops). The latter spectrum, uncorrected for evaporation, is shown

in Fig. 5.8 together with selected Kelkar spectra. Sims, Mueller, and Stout (1965) found that spectra from several locations were best fit with logarithmic-normal functions, but the function parameters did not seem to be ordered with rainfall rate.

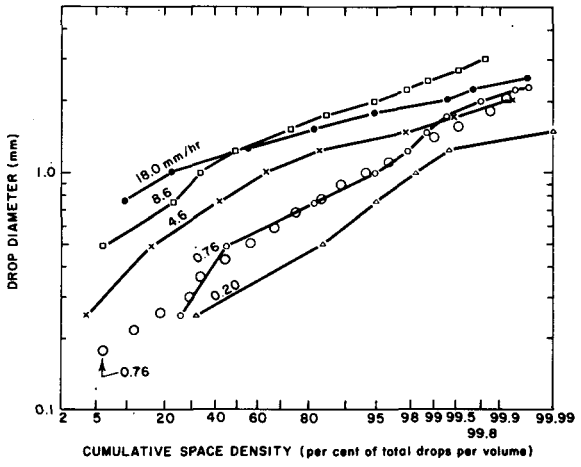

Fig. 5.8 — Selected rain spectra on logarithmic-normal probability paper. The large circles represent a spectrum from a semiarid region of Washington. The remaining curves were measured by Kelkar (1959) in India.

Users of measured rain spectra should consider the effects of evaporation as the rain falls between cloud and ground. Evaporation reduces the sizes of all drops and the number of the small ones. Splash droplets from the ground and equipment around rain samplers and breakup of drops on the entrance edge of rain samplers will increase the apparent number of small droplets. The errors introduced in spectra by these and other effects can be very large and frequently are not adequately discussed when the spectra are published.

5-4.5 Calculated Particle Washout Coefficients for Rain

Chamberlain (1953) used Langmuir's efficiencies and Best's (1950) fitted spectra to calculate washout coefficients for various rainfall rates and particle (cloud droplet) sizes. These coefficients are given in Fig. 5.9 as a function of $a^2\rho$.

Similar calculations have been made by May (1958) using the somewhat higher efficiencies of Mason, but these give coefficients only about 10% greater than Chamberlain's. May measured washout coefficients in natural rain using spores ($a^2\rho$ = 320 μ^4g/cm^3) and found Chamberlain's predictions "substantially correct."

A different result is obtained using the efficiencies of Kinzer and Cobb with the Washington State and Indian spectra as shown in Fig. 5.10. The two lines were fitted by eye to the co-

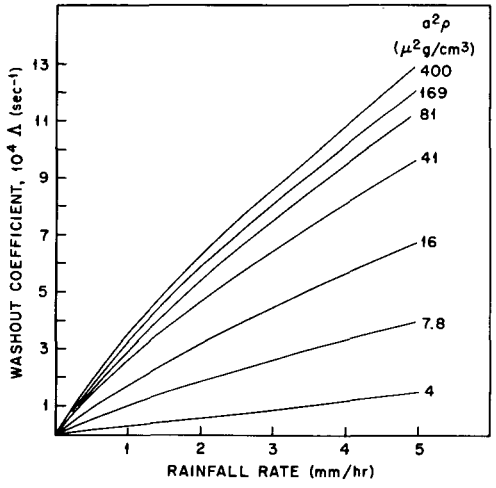

Fig. 5.9 — Washout coefficients for unit density particles vs. rainfall rate and $a^2\rho$. These calculations are based on Best's (1950) spectra and Langmuir's (1948) target efficiencies. (From A. C. Chamberlain, *Aspects of Travel and Deposition of Aerosol and Vapor Clouds*, British Report AERE-HP/R-1261, Fig. 1, Sept. 17, (1953.)

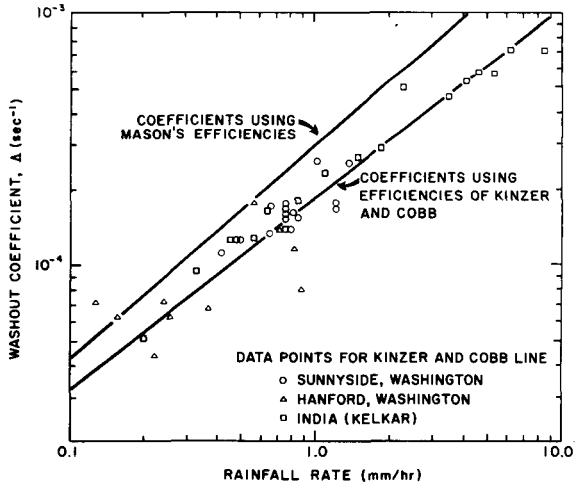

Fig. 5.10 — Washout coefficients for $a^2\rho$ = 42 only, calculated from spectra measured in Washington and India, using theoretical efficiencies from Mason (1957) and measured efficiencies of Kinzer and Cobb (1958).

efficients calculated for $a^2\rho = 42\ \mu^2\ g/cm^3$. A slightly convex line could be used. Only the plotted points for Kinzer and Cobb efficiencies are shown to prevent confusion; less scatter exists with the calculation using Mason's efficiencies.

Even though the Kinzer and Cobb efficiencies are greater than Mason's for the more numerous small drops, the calculated washout coefficients are lower. This is due to the greater contribution to the cross-sectional scavenging area made by the larger drops, where Mason's efficiencies are larger than Kinzer and Cobb's. The slopes of the lines show that the washout coefficient for large particles varies with about the 0.75 or 0.8 power of the rainfall rate. There is, however, a large amount of scatter within a single shower and between storms.

The coefficients calculated from the Langmuir or Mason efficiencies may be regarded as slight overestimates in the absence of significant electrical charges on the rain. Both the measurement of lower coefficients (actually collection efficiencies) by Kinzer and Cobb and by Engelmann and the possibility of retention efficiencies less than one support this view.

For particles less than about 1 μ in diameter, the calculations based only upon inertial effects in idealized flow patterns show negligible washout. They cannot be considered at all reliable, however, owing to the presence of electrical charges, which increase washout (e.g., see Byutner and Gisina, 1963). Solutions for selected particle and drop charges have been made by several workers (summarized by Fuchs, 1964), but there is insufficient information for safely extrapolating these predictions to other charge values. In addition, there is insufficient information on the normal charges existent in rain and clouds.

There are also no measurements on natural washout of these smaller particles although some current research plans do include them; e.g., Engelmann, Perkins, Hagen, and Haller (1966), and Georgii and Weber (1964). It is apparent that the problems of small-particle measurement, low collection efficiencies, and nonuniform raindrop charge will cause difficulty in the performance of these experiments.

5-4.6 Scavenging of Particles by Snow

There are no published scavenging coefficients, theoretical or measured, for snow. The large numbers of frozen cloud droplets occasionally attached to snowflakes establish that snow is an effective scavenger for at least large particulates. This effectiveness will vary with type of crystal, its shape, fall speed, and electrical charge.

For the same rate of precipitation, we expect a greater scavenging of smaller particles by the slower feathery snowflake, with its larger area and probable electrostatic charge, than by its equivalent waterdrop. Large numbers of Aitken particles (diameter $< 0.02\ \mu$) have been observed on snowflakes.

Hinzpeter's (1958) data show a lower specific radioactivity for snow water (about 0.4 to 0.6 as great as rainwater), at the same daily precipitation rates. The snow and rain were sampled at different times of the year, however, and the air activity has greater variation than this. Georgii and Weber (1964) found snow water to contain ammonia, nitrate, sulfate, and other ions at 1.7 to 2.9 times their concentration in rainwater. Reasoning that both precipitation types were originally snow within the cloud, they conclude that snow is a better scavenger than rain for these particles. Comparable results were found on radionuclides by Perkins and Engelmann (1966).

However, Facy (1962) suggests that the snowflake is less able to retain its scavenged materials and gases and will even reject material in its path during evaporation. Hinzpeter's data (1958) show increasing radioactivity in air following snow but decreasing radioactivity following rain. He interprets this as the release of adsorbed material when the flakes melt and evaporate on the ground.

In the absence of quantitative measurement in snow, the provision of specific scavenging coefficients for particulates is highly speculative. A few washout coefficients in rain and snow for submicron particles of silver iodide, scandium, and cesium salts have been published (Pacific Northwest Laboratory, 1967).

5-4.7 Scavenging of Gases by Waterdrops

Scavenging of gases is predicted on the basis of molecular diffusion to the drop or droplet in accordance with the vapor pressures and solubilities of the free and collected gases (Junge, 1963, Chamberlain, 1960, and Griffiths, 1963).

For fully soluble gases,

$$\Psi \text{ or } \Lambda = \int_0^\infty \pi Y Sh D N \, dD \qquad (5.57)$$

where Y is the coefficient of molecular diffusion (or diffusivity) and Sh is the Sherwood (or Nusselt diffusion) number. The Sherwood number for spheres is approximately

$$Sh = 2.0 + 0.6 \, Re^{1/2} \left(\frac{\nu}{Y}\right)^{1/3} \qquad (5.58)$$

where Re is the Reynolds number and ν is the kinematic viscosity of air. Because Eq. 5.57 is nearly linear in Y, scavenging coefficients for soluble gases are nearly proportional to their diffusion coefficients in a rain of given flux density. Theoretically trace quantities of insoluble gases may be treated as soluble in the scavenging process.

Figure 5.11 gives predicted coefficients for those gases* which are very soluble in water.

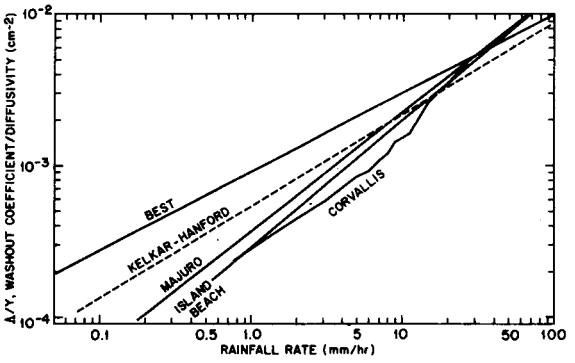

Fig. 5.11 — Washout coefficients divided by diffusivity for soluble gases as predicted from various rain spectra.

The upper line in the figure is based upon the fitted spectra of Best, which overestimate the number of small drops. The lower three curves were calculated from the spectra reported by Sims, Mueller, and Stout (1965) for Majuro in the Marshall Islands, Island Beach, N. J., and Corvallis, Oreg. These were measured with a raindrop camera and may underestimate the number of small drops when the rain is light. The dashed curve was calculated from the Washington State and Indian spectra, which were taken using water-sensitive paper.

The dashed curve is recommended for precipitation rates up to at least 20 mm/hr. At higher rainfall rates use of the raindrop camera spectra in calculations yields greater scavenging. How much of the increase is due to splash and is therefore erroneous is unknown. Differences in rain spectra affect the washout coefficients for gases more than for particles.

Recent laboratory work (Booker, 1965, Friedman, Machta, and Soller, 1962) confirms theoretical predictions of the exchange of deuterated and tritiated water vapor with monodisperse waterdrops in saturated air.

Three measurements of the washout of bromine gas by Engelmann, Perkins, Hagen, and Haller (1966) also verify the theoretical predictions in rain. The only three measurements available for iodine gas, however, yielded washout coefficients one and two orders of magnitude lower than those predicted in Fig. 5.11 and showed no relation to precipitation rate.

Engelmann et al. propose that the reaction rate with water, rather than the total solubility, determines washout rates. Figure 5.11 should then be used only for gases with reaction rates comparable to that of bromine after adjustment for the diffusion coefficient.

5-4.8 Washout Coefficients for Gases in Snow

The washout of bromine and inorganic iodine was also measured in snow. The six measurements of each show a great deal of scatter, and it is not possible to conclude from these data how the coefficients are related to precipitation rate or crystal type. The values for bromine and inorganic iodine were on the order of $3 \cdot 10^{-8}$ and 5×10^{-8} sec^{-1}, respectively, in powder snow of 0.2 mm/hr.

The lower coefficients in snow compared to rain support the importance of reaction rates. It appears that, although the large surface area and small terminal velocity of snow crystals may increase the scavenging of gases, these factors are not able to balance the lower adsorption rates on ice surfaces.

Washout coefficients for other gases with similar reaction rates should compare to those

*Very small particles that are unaffected by electrical charges and impaction can be regarded as gases, and their washout can be estimated from Fig. 5.11.

of bromine and iodine as the ratio of their diffusivities in air.

5-4.9 Washout Coefficients for Process-plant Iodine

A much higher washout rate was observed when process-plant inorganic radioiodine was used as a tracer (Engelmann, Perkins, Hagen, and Haller, 1966). Figure 5.12 shows three data points for columnar snow crystals, two for wet

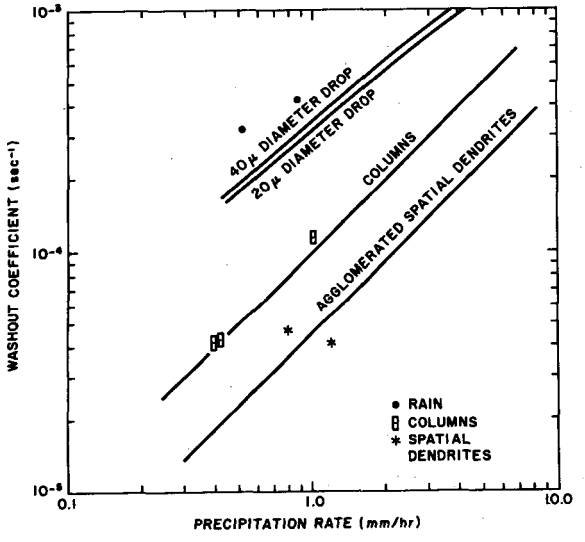

Fig. 5.12—Washout coefficients for inorganic iodine in process-plant stack gases in rain and snow. (From Engelmann, Perkins, Hagen, and Haller, 1966.)

agglomerates of spatial dendrites, and two for rain. The data points for rain are nearly 10 times higher than the theoretical predictions for soluble gases from Fig. 5.11.

In explanation of the high washout, it was noted that there was sufficient water vapor in the plant stack exhausts to produce a cloud of water droplets on a rainy day. If all the radioiodine (or other gas) in the stack exhausts were swept up by the cloud droplets during formation, subsequent washout of the iodine would be at the rate appropriate to cloud drops. Theoretical rain-scavenging rates of uncharged 20- and 40-μ-diameter cloud drops are shown in Fig. 5.12. Lines of slope 1.0 have been drawn through the data for snow for the assumption that increases in snowfall rate are due to increases in the number of crystals falling.

Similar washout rates may be expected for reactive gases in other stack exhausts with high water content. Again, reaction rates may influence the takeup during the condensation. In these tests washout coefficients for organic forms of iodine were about 1% as large as for the inorganic forms.

5-4.10 Rainout (In-cloud Scavenging)

Collection due to inertia becomes insignificant with small droplets in viscous flow and with very small particles. It is then necessary to use electrical effects, nucleation, diffusiophoresis, Brownian motion, and velocity gradients to explain rainout. These effects are also small, and calculations of rainout, such as those by Greenfield (1957), Junge (1963), and Chamberlain (1960), show long residence times for aerosols in nonfalling clouds. This is especially true in the aerosol range of 0.1- to 0.4-μ diameter, for which there seems to be no adequate scavenging mechanism.

Cloud elements do fall, however, and it may be that the inertia of a fine particle is sufficient to carry it into the boundary layer of the falling cloud element, where weak forces have opportunity to complete the collection. Facy (1962) considers the value of E in clouds to be at least 1.0. This yields high values for the rainout coefficient in the equations

$$\Psi = \int_0^\infty \mathrm{FEA}\, dD \qquad (5.59)$$

$$\chi = \chi_0 \exp(-\Psi t) \qquad (5.50)$$

Byutner and Gisina (1963) have calculated rainout coefficients in clouds composed of 100 drops per cubic centimeter, 10 μ in diameter. They assumed charges of 5×10^{-7} esu on the cloud droplets and 4.8×10^{-10} esu on ash particles and calculated separate coefficients for the several effects operating. The coefficients cannot be added together to obtain a total coefficient, but their values indicate that a minimum total rainout coefficient of about 3×10^{-5} sec^{-1} occurs near the 0.2-μ particle diameter. This corresponds to an efficiency of 0.1, which is less than 1.0 but quite significant. Smaller cloud drops will have higher efficiencies but may have lower flux densities.

Junge introduces the equation

$$k_1 = \chi_0 \epsilon \frac{\rho}{L} \qquad (5.60)$$

where k_1 = aerosol per volume of cloud water
χ_0 = aerosol per volume of unwashed air
ρ = density of water
L = mass of condensed water per cloud space volume
ϵ = rainout efficiency, or $1-(\chi/\chi_0)$

In Eq. 5.50 t is the time the air parcel is within the cloud. With this equation, the cloud air would eventually be cleansed, and ϵ would approach 1.0. Since most clouds entrain new air continuously, however, the aerosol contained in the cloud water increases as long as solubility allows and may be better represented by

$$k_1 = \chi_0 \Psi T \frac{\rho}{L} \qquad (5.61)$$

where T, the age of the cloud, is different from t.

The parameter ΨT at the onset of precipitation is quite possibly a characteristic of the cloud type since the cloud elements also grow by aerosol-collection processes. Both ϵ and ΨT can be estimated from measurements of χ_0/k_1 and estimates of L. The proper choice for L is debatable since it varies greatly with cloud type and precipitation amount, but reasonable values can be chosen which will keep ΨT or ϵ in the range 0.5-1.0. Table 5.14 lists such values.

The value of k_1 must be adjusted to allow for evaporation of the precipitation element as it falls. Aerosol scavenged or lost in the air below the cloud must also be added to k_1. These adjustments are implicit in the data of Small (1960) and Hinzpeter (1958) since their measurements were taken from air near the ground.

Because of the complexity of in-cloud scavenging, it would seem that particulate scavenging by rain and snow cloud elements is currently best estimated from data of the type given in Table 5.14. However, the near certainty that χ_0 varies with elevation must be considered when such data are used. As yet, little is known about the height variation of entrainment of outside air into convective clouds (aufm Kampe and Weickmann, 1957); also the height of the cloud water that contributes to the precipitation is uncertain.

5-4.11 Treatment of Precipitation Climatology

Preceding sections have provided the means of predicting scavenging when the precipitation characteristics are specified. We have considerable latitude when applying these techniques to uncertain future precipitation, and how we make this application will depend upon the particular problem at hand. We will now discuss, in general terms, the introduction of precipitation climatology into the applied problems.

A wide variety of prediction forms can be made according to the forms of the precipitation climatology and the contamination description.

Table 5.14—SELECTED MEASUREMENTS OF SURFACE AIR TO PRECIPITATION ACTIVITY RATIOS AND VALUES OF CLOUD-WATER CONCENTRATION CHOSEN TO PRODUCE RAINOUT EFFICIENCIES BETWEEN 0.5 AND 1.0

Data source	χ_0/k_1	k_1/χ_0	L/ρ	ϵ or ΨT
Small* (Norway)				
October 1956	0.25×10^{-6}	4.0×10^{6}	0.25×10^{-6}	1.0
September 1959	2.06	0.47	2.0	0.95
Average (3 year)	0.9	1.1	0.9	1.0
Hinzpeter† (Germany)				
Rain, mm/day				
0.1	0.8	1.25	0.5	0.62
1.0	1.4	0.71	1.0	0.71
10.0	2.5	0.40	2.0	0.8
Snow, mm/day (water equivalent)				
0.15	0.9	1.1	0.5	0.55
1.0	1.6	0.62	1.0	0.62
10.0	3.4	0.29	2.0	0.59

*S. H. Small, 1960.
†Hinzpeter, 1958.

For instance, we can obtain total washout-area isopleths, maximum possible washout—total or rate, return periods for washout rates, joint probabilities of accidental release and specified scavenging rates, and mean yearly and seasonal washout and rainout for continuous releases.

Unfortunately the accuracy of the estimated washout coefficient will usually be so poor as to allow the assumption that Λ is linearly related to the precipitation rate. In this case the washout can be estimated from the total depth of rain or snow. Area–depth relations (e.g., Court, 1961) can be superimposed on the predicted contaminant distribution to obtain total washout-area isopleths.

The reader is by no means restricted to considering area isopleths. Often a problem consists in determining whether some total deposition can be exceeded, and for this the centerline or peak exposure and the expected total depth of precipitation are sufficient.

Special consideration must be given to the climatology of plume widths, turbulence, and wind speeds during precipitation. At many locations the wind direction during precipitation differs noticeably from the mean direction for all weather types. The new region likely to be affected may be very significant in hazards appraisals.

In the special case of horizontally uniform precipitation over a continuous plume, the washout area may be obtained mathematically (U. S. Weather Bureau, 1955). Culkowski (1963) and Guthrie and Nichols (1964) have calculated the maximum washout possible at one particular distance with a rain that starts as soon as (or earlier than) the release. This washout rate for the Gaussian plume model* is

$$\omega_{max.} = \frac{Q'}{e\ x\ \sigma_y (2\pi)^{1/2}} \exp\left(-\frac{y^2}{2\sigma_y^2}\right) \qquad (5.62)$$

where ω is the maximum washout rate ($ML^{-2}T^{-1}$) for source strength Q' (MT^{-1}) [or total washout (ML^{-2}) for Q (M)].

*Owing to the practical difficulty of specifying the instantaneous concentration distribution in a plume from a continuous source, the instantaneous concentration must be estimated from the continuous-source equations and considered as an effective instantaneous concentration. Since the reader will likely deal with washout rates averaged over time, this should present no problem.

When calculating maximum possible washout, one must remember that the length of release and the duration of washout are often not the same. The washout rates at some distance from a source are generally greater when there is little or no intermediate precipitation.

The washout rate for precipitation just beginning is

$$\omega_0 = \Lambda \int_0^z \chi(x,y,z,Q')\, dz \qquad (5.63)$$

The upper limit for this integral is the height from which the rain falls. For the Gaussian plume model, Eq. 5.63 becomes

$$\omega_0 = \frac{\Lambda Q'}{\bar{u}\ \sigma_y (2\pi)^{1/2}} \exp\left(-\frac{y^2}{2\sigma_y^2}\right) \qquad (5.64)$$

Equation 5.64 assumes that the plume does not lean with elevation because of wind-direction shear.

If the rain cloud is stationary while the contaminant is moving, Eq. 5.64 will continue to apply on the upstream side of the rain cloud. Because of this, the continuous introduction of new material to an orographic precipitation cloud may result in washout rates that do not decrease in time. In this way Fuquay (1963) has explained greater radioactivity in the snow found on western mountain slopes.

Normally χ must be modified to account for previous scavenging upstream from x, which can easily reach 50% in 10 miles of rainfall. For instance, if the precipitation extends upstream to the source, Eq. 5.64 is modified to read

$$\omega = \frac{\Lambda Q'}{\bar{u}\ \sigma_y (2\pi)^{1/2}} \exp\left(-\frac{y^2}{2\sigma_y^2}\right) \exp\left(-\frac{\Lambda x}{\bar{u}}\right) \qquad (5.65)$$

from which Eq. 5.62 was derived.

In Eq. 5.65 the two washout coefficients are not necessarily the same. The first applies to the current precipitation, and the second, to the earlier precipitation extending back to the source. The area within a washout isopleth according to Eq. 5.65 has been obtained by numerical integration, and these results are presented in Figs. 5.13, 5.14, and 5.15 for three values of the stability parameter $\sigma_\theta \bar{u}$ (Chap. 4, Sec. 4-4.2.2) as a function of both the current and upstream washout coefficients.

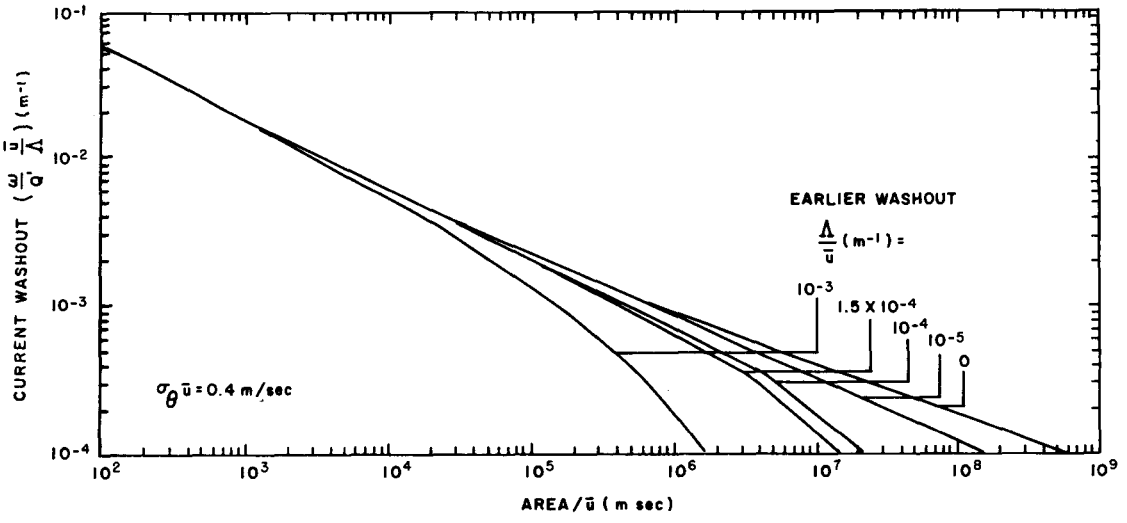

Fig. 5.13 — Area (divided by wind speed) within a current washout isopleth for various earlier washout rates. The curves are based on a Gaussian plume model with the crosswind concentration distribution determined from $\sigma_\theta \bar{u}$ = 0.4 m/sec (see Chap. 4, Sec. 4-4.2.2 for a discussion of the quantity $\sigma_\theta \bar{u}$). The use of this diagram is explained in the text.

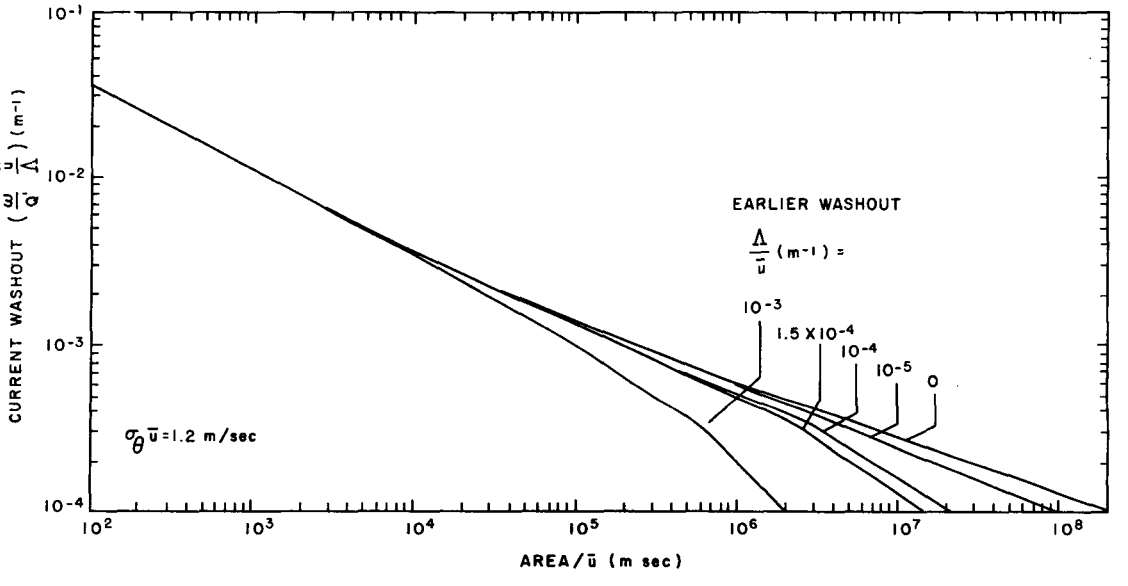

Fig. 5.14 — Same as Fig. 5.13 but for $\sigma_\theta \bar{u}$ = 1.2 m/sec.

As an example of the use of these figures, suppose that it had been snowing lightly for some time but that the snow had now intensified considerably. The reader wishes to know the area within a particular washout isopleth for the current stability and precipitation. He chooses the figure appropriate to the existing value of $\sigma_\theta \bar{u}$, then on the left side of the graph finds the value of ω/Q' of interest divided by the current washout, $\Lambda/\bar{u}$. He then moves his pointer to the curve labeled with the earlier washout, then down to the scale marked area/$\bar{u}$. He multiplies this by $\bar{u}$ to obtain the area of the washout isopleth in square meters.

As a matter of interest, the calculations have also been made for the plume described by

$$\sigma_y = 0.2\, x^{0.8} \qquad (5.66)$$

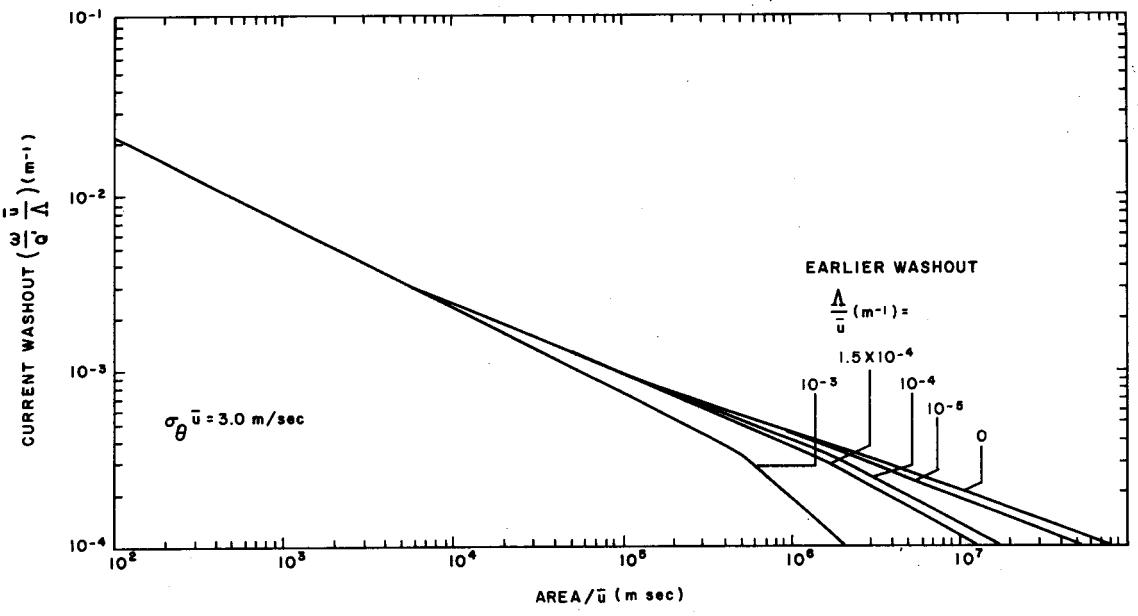

Fig. 5.15—Same as Fig. 5.13 but for $\sigma_\theta \bar{u} = 3.0$ m/sec.

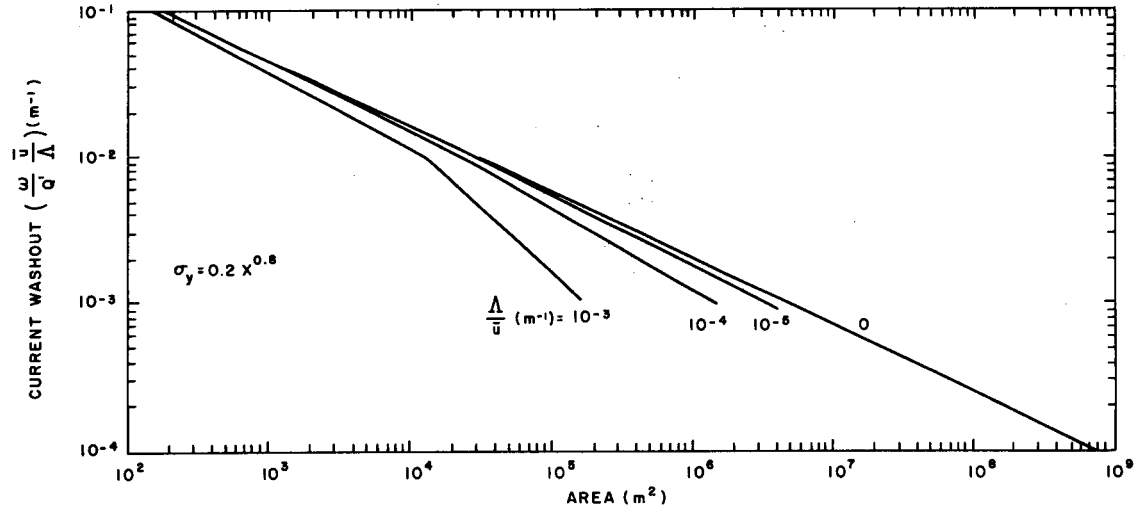

Fig. 5.16—Same as Fig. 5.13 but for $\sigma_y = 0.2x^{0.8}$.

(where σ_y and x are given in meters) and are shown in Fig. 5.16. Equation 5.66 is a composite of experimental data for 30-min releases at Hanford, Wash.

Comparison of the figures will show that the area is not only quite dependent upon the earlier washout coefficient but also upon the stability parameter. Some study of the climatology of $\sigma_\theta \bar{u}$ (or of σ_θ) vs. $\Lambda/\bar{u}$ should therefore be made before the figures are used in hazards appraisals.

5-4.12 Summary and Conclusions

Chamberlain's predicted washout coefficients in rain for particles larger than 1 μ in diameter (Fig. 5.9) are considered to be slight overestimates. In the case of particles smaller than 1 μ,

it is generally agreed that washout by rain is insignificant. This theory cannot be considered reliable for smaller particles, however, owing to uncertain electrical effects, and quantitative measurements of this washout are not yet available.

The washout of reactive gases can be predicted by using the theory of molecular diffusion to waterdrops. Newly calculated washout coefficients based on measured rain spectra rather than on fitted spectral equations are presented and recommended (Fig. 5.11). The prediction of washout of gases by snow must rely upon a few measurements for bromine and iodine gas since there are no theoretical predictions. In all cases the reaction rate of the gas with the rain or snow must be considered.

Snow apparently has about the same to three times the effectiveness of rain at the same precipitation rate for both washout and rainout of particles. However, definitive measurements are greatly needed.

Research is still inadequate on many of the complex in-cloud scavenging processes. Formal mathematical predictions of rainout due to various mechanisms are interesting but not decisive. It is therefore recommended that simultaneous measurements of contaminants in air and precipitation (e.g., Table 5.14) be used for prediction of rainout.

The manner in which the washout coefficient, Λ, and the ratio of surface air to precipitation activity, χ_0/k_1, vary with storm and cloud type is unknown. Therefore recommended values of Λ and χ_0/k_1 may be directly combined with precipitation rates to predict scavenging rates.

5-5 GAS DIFFUSION NEAR BUILDINGS (James Halitsky)

5-5.1 Introduction

The use of conventional diffusion formulas for the calculation of concentration fields produced by sources on or near buildings often gives misleading answers. Such formulas contain the implicit assumption that the flow field has straight streamlines that are parallel to each other and to the ground. Although this is reasonably accurate for flow over level uniformly rough ground, we know that flow near buildings contains curved streamlines, sharp velocity discontinuities, and highly nonhomogeneous and nonisotropic turbulence. The complexity of these fields is so great that analytical solutions of the differential diffusion equation in this context are not likely to be found in the near future. Computer solutions may, however, prove feasible when sufficient experimental data are collected to document the flow field in detail.

At the present time the optimum procedure for estimating concentrations near buildings is to obtain experimental data for a few configurations, to interpret such data in accordance with diffusion theory and flow-field fact and theory, and to extrapolate the data to other configurations. The following sections describe the current state of development along these lines.

The descriptions of the flow near structures are based upon observations of smoke patterns described in a variety of cited references as well as in many unreported experiments. The interpretation of the generating mechanism for the composite flow is a synthesis of a number of well-known explanations of aerodynamic phenomena described in such standard texts as Schlichting (1960). Most of the experimental data on concentrations close to buildings were obtained in low-turbulence wind tunnels; the extrapolation of such data to the full-scale natural atmosphere will introduce some unavoidable error. Nevertheless wind-tunnel tests will probably continue to be the principal source of data for these problems, and methods for reducing the error analytically or by modification of the test procedure will be required. For this reason a discussion on scaling criteria peculiar to flow near buildings will be presented. Sections 5-5.5, "Experimental Data on Concentrations near Buildings," and 5-5.6, "Applications," will be of particular interest to those concerned with practical pollution problems.

It should be understood that the study of diffusion near buildings is in its infancy and much work is needed to validate and refine the material presented herein. Until that time it is suggested that the data and calculation procedures be viewed as approximations suitable for preliminary estimates of mean concentration fields.

List of Symbols

Symbols used frequently in Sec. 5-5 on gas diffusion near buildings are listed here. (The

dimensions mass, length, time, and temperature are abbreviated as M, L, T, and D, respectively. The equation, figure, or section number indicates the first appearance of the symbol.)

A	Reference area (L^2), Sec. 5-5.3.1
A_e	Area of effluent aperture (L^2), Eq. 5.74
C_h	Total-pressure coefficient (dimensionless), Fig. 5.24
C_p	Static-pressure coefficient (dimensionless), Sec. 5-5.2.1.4
C_y, C_z	Sutton parameters ($L^{n/2}$), Eq. 5.72
D	Dilution (dimensionless), Eq. 5.73
D_0	Diameter of sphere or cylinder (L), Sec. 5-5.2.2.3
d	Distance normal to a surface (L), Eq. 5.85
Fr	Froude number (dimensionless), Eq. 5.80
Fr'	Modified Froude number (dimensionless), Eq. 5.81
f	Frequency (T^{-1}), Sec. 5-5.4.1
H	Characteristic height (L), Sec. 5-5.2.2.2
i	Local turbulence intensity = $\sigma/\bar{u}$ (dimensionless), Sec. 5-5.3.1
K_c	Concentration coefficient (dimensionless), Eq. 5.71
K_{ce}	Concentration coefficient at effluent aperture (dimensionless), Eq. 5.73
k	Von Karman's constant (dimensionless), Sec. 5-5.5.2
L	Reference length (L), Eq. 5.67
M	Coefficient in Clinical Center dilution formula (dimensionless), Eq. 5.87
n	Sutton parameter (dimensionless), Eq. 5.72
p	Pressure ($ML^{-1}T^{-2}$), Fig. 5.21
Q'	Source strength (L^3T^{-1} or MT^{-1}), Eq. 5.71
q	Resultant local velocity = $(u^2 + v^2 + w^2)^{1/2}$ (LT^{-1}), Sec. 5-5.2.2.1
Re	Reynolds number (dimensionless), Sec. 5-5.2.2.3
r	Radial-length coordinate = $(y^2 + z^2)^{1/2}$ (L), Sec. 5-5.2.2.1
r_w	Radius of wake boundary (L), Eq. 5.67
s	Curvilinear longitudinal length coordinate (L), Eq. 5.86
T	Temperature of the background flow (D), Eq. 5.78
T_e	Temperature in effluent aperture (D), Eq. 5.24
T_j	Temperature in jet (D), Fig. 5.24
T_1	Maximum temperature in flow field (D), Eq. 5.78
t	Time (T), appears in various equations
u_a	Velocity along axis of cavity (LT^{-1}), Sec. 5-5.2.2.1
V	Reference velocity (LT^{-1}), Sec. 5-5.2.2.1
V_e	Velocity in effluent aperture (LT^{-1}), Sec. 5-5.2.3
V_i	Velocity at air-intake aperture (LT^{-1}), Sec. 5-5.3.1
V_j	Velocity in jet (LT^{-1}), Fig. 5.24
v_*	Friction velocity (LT^{-1}), Sec. 5-5.5.2
z_0	Roughness height of ground surface (L), Sect. 5-5.2.2.2
μ	Dynamic viscosity ($ML^{-1}T^{-1}$), Eq. 5.78
ν	Kinematic viscosity (L^2T^{-1}), Sec. 5-5.6.1
ρ	Density (ML^{-3}), Eq. 5.78
σ_u, σ_v, σ_w, σ_q	Root-mean-square velocity fluctuations (LT^{-1}), Sec. 5-5.2.2.1
σ_θ	Root-mean-square lateral-gust angle (deg or radians), Sec. 5-5.4.1
φ	Angle between upwind axis and radius of a sphere or cylinder (deg or radians), Sec. 5-5.2.2.3
$\bar{\chi}$	Time average concentration [M/L^3 or $L^3(L^{-3})$], Eq. 5.71
$\bar{\chi}_e$	Time average concentration in the effluent aperture M/L^3 or $L^3(L^{-3})$, Eq. 5.73

Overbar ($\bar{}$) represents mean value
Prime (′) represents fluctuation
Asterisk (*) represents prototype

5-5.2 Structure of Flow Fields near Buildings

5-5.2.1 Origin and Characteristics of Flow Zones.

5-5.2.1.1 Aerodynamic Distortion. In discussing flow around buildings, we will, for convenience, establish a background flow from which deviations caused by the presence of the building can be measured. For the atmosphere we will assume that neutral stability conditions exist over flat ground of wide extent and produce

a logarithmic mean velocity profile, homogeneous turbulence, and uniform pressure. For the wind tunnel we will assume a uniform mean velocity profile, negligible turbulence, and uniform pressure.

The introduction of a building into either of the background flows causes a change in the velocity and pressure fields. The new fields will be called aerodynamically distorted, and the amount of distortion will be measured by the difference between the distorted and the background properties. It is characteristic of aerodynamically distorted fields that distortions decay with distance from solid surfaces. For practicability we will assume that velocity distortions less than 5% of the local background velocity or pressure distortions less than 10% of the local background dynamic pressure do not exist. These assumptions effectively limit the extent of the distorted field, which may now be considered as enclosed by an imaginary isolating surface. The isolating surface of a building on the ground resembles a bubble canopy. The isolating surface of a suspended object completely encloses the object in an ellipsoid-like shell.

Figure 5.17 shows the principal characteristics of the flow field near a sharp-edged building oriented with one face normal to a wind stream with little turbulence. The background flow is shown at station 1. The region of aerodynamic distortion, lying between the solid and isolating surfaces, has three zones: the displacement zone, the wake, and the cavity. The formation of the displacement zone is intuitively evident since the air must be displaced around the solid building. The formations of the wake and cavity are less evident; they result from the aerodynamic phenomenon of separation.

5-5.2.1.2 Separation and Wake Formation. Separation occurs when fluid in a boundary layer that is initially moving parallel to a solid surface suddenly leaves the surface and moves out into the flow field. The cause of separation is thought to be the loss of kinetic energy in the boundary layer, the loss being amplified when the pressure gradient is positive, i.e., when pressure increases in the direction of flow.

In flow around buildings the adverse pressure gradient is very important in fixing the location of the line of separation. At the onset of fluid motion, the pressure gradient is established by a quasi-potential flow that follows the contours of the building. In Fig. 5.17, for example, the pressure is high in the stagnation region near the center of the upwind face and diminishes and becomes negative near the roof and side edges. At the edges the flow bends sharply to adhere to the roof and side walls

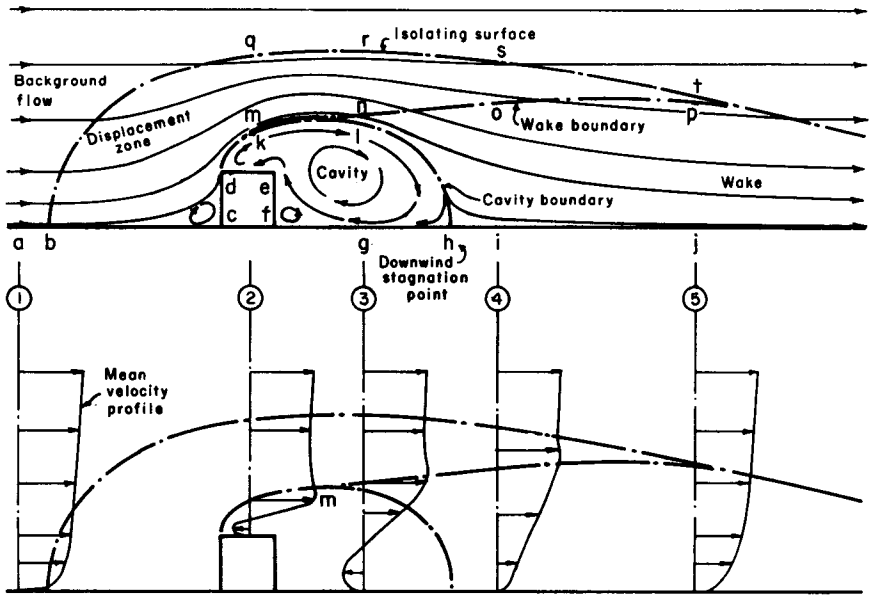

Fig. 5.17—General arrangement of flow zones near a sharp-edged building.

and thereby experiences high local centrifugal forces and extremely low pressures. After passing the edges the fluid streamlines straighten out, the centrifugal forces disappear, and the pressure rises. Therefore the pressure gradient is negative on the upwind face but becomes highly positive on the roof and side walls just downwind of their leading edges. Accordingly, the fluid adheres to the upwind face but separates from the building at the edges and continues its radially outward motion.

The character of the flow field after separation (which occurs almost immediately after onset of motion) is determined by the properties of the boundary layer at the periphery of the upwind face: outward directed momentum, low static pressure, and high vorticity. These properties are retained by the separated layer, which in its new role as a free jet in a transverse wind bends over downwind in a parabolic shell enclosing the building. If at this stage the fluid were to lose its viscosity and the separated layer were to lose its vorticity, the resulting flow field would be described as a classical wake in a potential flow. The speed and static pressure would be constant everywhere in the layer downwind to infinity. Between the layer and the solid surface (ground or building), the fluid would be completely stagnant, and the static pressure would be constant and equal to the layer pressure. On the other side of the separated layer, a potential flow would exist with velocities and pressures varying continuously from those of the layer to those of the background flow.

In a real, viscous, turbulent fluid, the classical wake cannot be achieved because the momentum in the separated layer diffuses into the wake and quasi-potential flow, sets the wake fluid in motion, and smooths out the sharp velocity discontinuity. Consequently the wake boundary is difficult to locate precisely. We will set the boundary on the imaginary surface along which the mean velocity is 95% of the local background-flow velocity and the velocity gradient is positive radially outward.

5-5.2.1.3 Cavity Formation. The viscous shears on the periphery of the initially stagnant wake cause the wake fluid to move downwind and thereby induce a return flow along the ground to replace the lost fluid. A toroidal circulation develops in the upwind portion of the wake, dividing it into two distinct subregions separated by the streamline d-k-l-h in Fig. 5.17. Fluid above and to the right of this streamline moves downwind continuously. Fluid in the closed region d-k-l-h-g-f-e-d recirculates. If it were not for diffusion transverse to streamlines, contaminants released into this region would be trapped, and concentrations would build up. Even with diffusion the level of concentration attained in many practical cases is high. Therefore the region is sufficiently important to be given a name. It has been called, variously, a bubble, an eddy zone, and a cavity. The term "cavity" will be used since it conveys the impression of a low-pressure hole in the wake. The term should not be confused with the classical cavity, which is the name given a classical liquid wake that has undergone a change of phase by virtue of low static pressure.

5-5.2.1.4 Velocities and Pressures. The mean flow characteristics of the displacement zone, the wake, and the cavity are given by the mean velocity profiles of Fig. 5.17. At station 2, moving from the free stream toward the building, the velocity is seen to increase to a maximum at m, reduce to zero at some point in the cavity, increase again to a smaller reverse maximum, and then decrease to zero at the roof. The same pattern occurs at station 3, but the maximum is not as high, and the gradients are less severe. At station 4 the flow is downwind everywhere, never exceeds the velocity in the background flow, and has a marked velocity defect near the ground in the vicinity of stagnation point h. At station 5 the velocity defect diminishes, but the height of the region of reduced velocity is greater.

The static-pressure coefficient C_p (local pressure change/nominal background-flow dynamic pressure) is negative at the separation edge, point d, remains constant along the separation streamline to point m, then increases gradually to zero at point o, and remains zero downwind. The static-pressure variation along the cavity boundary is a gradual rise from point d to a maximum (but still negative) value at stagnation point h. The static pressures within the cavity are lower than on its boundary. Outside the cavity, on a line downwind from h, the static pressure rises rapidly to the free-stream value.

Turbulence in the aerodynamically distorted region may originate either in the background flow or in the separated layer, or both. Close

to the building it seems likely that building-generated turbulence is predominant. As noted previously, the separated layer has a large amount of vorticity, created when the layer was still attached to the building. After separation the layer becomes unstable and breaks up into a vortex sheet consisting of discrete eddies that grow as they travel downwind. The smaller eddies transport momentum across streamlines, thereby smoothing the velocity discontinuity. Somewhat larger eddies are shed periodically, producing oscillations in the wake boundary. Very large eddies migrate down into the cavity, producing intermittent strong gusts. Farther downwind, building-generated turbulence has decayed and enough distance has been traversed for eddies in the background flow to have migrated well into the wake.

The interaction of the two types of turbulence has not been studied systematically. A few experiments (Halitsky, Magony, and Halpern, 1965) on flow downwind of a model of a mountain ridge in the wind tunnel with high and low turbulence in the background flow indicate that the aerodynamically generated turbulence intensity decays with distance from the ridge in the same manner in both cases, but the decay terminates when the intensity reaches that of the background flow. Therefore the dimensions of an aerodynamically distorted region, as determined by excess of turbulence over that of the background flow, appear to vary inversely with background-flow turbulence.

5-5.2.2 Flow near Characteristic Structures.

5-5.2.2.1 Suspended Flat Plate. The suspended flat plate is not a structure encountered in practical diffusion problems, but its flow field has been explored more thoroughly than those of buildings on the ground, and the test results are useful guides to the general magnitudes of velocities, pressures, and wake and cavity shapes that can be expected around buildings. In visualizing the plate as a building, assume for convenience that a horizontal ground boundary can be introduced through the center of the plate and that the upper half of the plate can be made coincident with the upwind face of the building. This will give the suspended square flat plate the same geometrical proportions as a building and its mirror image, with the building height being equal to one-half its width and its length (in the direction of the wind) being very small.

The actual introduction of a solid plane through the center of the plate would impose severe restrictions on the flow in the cavity since the velocity of real viscous fluids such as air must fall to zero at all solid boundaries. In general, the plate would exert a drag force on flow along the plate, and it would prevent the transverse movement of eddies from one side of the cavity to the other. These restrictions should be borne in mind when the suspended-plate data are to be applied to buildings on the ground.

According to Fail, Lawford, and Eyre (1957), the cavity and wake dimensions of axisymmetric plates suspended normal to the wind in a low-turbulence tunnel are not very sensitive to plate shape when referred to a characteristic dimension equal to the square root of the plate area. For a square plate of side L, the following properties were found to exist in the range of $0.5 < x/L < 5$ in a uniform stream of mean velocity V. The wake axis is coincident with the longitudinal (x) axis, and the origin is at the center of the plate.

1. The wake boundary originates at the edge of the plate and develops into a paraboloid of revolution. The curve of the boundary in a longitudinal section through the axis may be approximated by

$$\frac{r_w}{L} = \left(\frac{x}{L}\right)^{1/4} \tag{5.67}$$

where r_w is the radial distance from the axis at longitudinal distance x.

2. The mean velocity $\bar{u}_a$ at the center of the cavity is about 60% of the background-flow velocity and is opposite in direction.

3. The cavity boundary originates at the edge of the plate but develops into an approximate ellipsoid of revolution of length equal to 2.83L and radius at midlength equal to L.

4. The pressure coefficient is −0.42 all over the lee face of the plate, −0.66 at the center of the cavity, and −0.15 at the end of the cavity.

5. The longitudinal turbulence intensity, σ_u/V, at $x = 3.6L$ varies from 0.11 at the axis to 0.22 at $r = 0.8L$ and then falls to substantially zero in the background flow beyond the wake boundary (note that the local turbulence intensity, $\sigma_u/\bar{u}$, would be higher since $\bar{u} < V$ in a wake). Cooper

and Lutzky (1955) present the properties of square-flat-plate wakes in the range of $20 < x/L < 680$ in graphical form. Equations 5.68, 5.69, and 5.70 are approximations to their data.

6. The wake-boundary radius expands with distance downwind according to

$$\frac{r_w}{L} = 1.57 \left(\frac{x}{L}\right)^{1/3} \qquad (5.68)$$

7. The longitudinal variation of axial mean velocity is

$$\frac{\bar{u}_a}{V} = 1 - 0.32 \left(\frac{x}{L}\right)^{-3/4} \qquad (5.69)$$

8. The radial variation of mean velocity is similar at all stations; it has an axial minimum and increases to the free-stream value in a symmetrical bell-shaped curve.

9. The longitudinal variation of turbulence intensity is

$$\frac{\sigma_u}{V} = A \left(\frac{x}{L}\right)^{-2/3} \qquad (5.70)$$

where $A = 0.25$ at the axis and 0.32 at $r = 0.33\ r_w$.

10. The radial variation of turbulence intensity is similar at all stations; it has a maximum at $r = 0.33\ r_w$, a minimum at the wake boundary, and a secondary minimum at the axis.

Measurements of displacement flow around a plate are not available. Experience has shown, however, that approximations of the pressure and velocity fields at stations upwind of the center of the cavity and at large radial distances can be obtained by means of the potential-flow equations for flow around a solid object occupying the cavity.

Part (a) of Fig. 5.18 is a reconstruction of the flow near a suspended flat plate, based on potential theory and Fail's measurements. The displacement flow was obtained by first calculating the potential flow properties for a sphere of radius L placed with its center on the plate axis at station $x = L$ and then adjusting the properties near the surface of the sphere to conform to conditions at the plate and cavity boundaries.

Part (b) of Fig. 5.18 shows the relation between Cooper and Lutzky's and Fail's measurements with interpolated values in the range

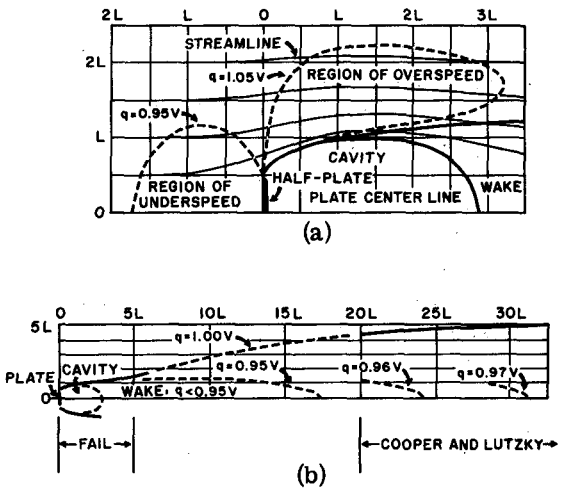

Fig. 5.18 — Flow around a suspended plate.

$5 < x/L < 20$. Cooper's wake boundary given by Eq. 5.68 was found by extrapolating the velocity defect in each transverse traverse to zero; therefore it can be considered as a limiting velocity contour extending downwind to ∞ and labeled $\bar{q}/V = 1.00$, where $\bar{q}$ is the local resultant mean velocity. All other velocity contours in the wake are closed and terminate at values of x/L given by Eq. 5.69. According to our convention the wake does not exist outside the $\bar{q}/V = 0.95$ contour, and consequently the length of the wake is effectively limited to about 17L from the plate. The ends of the velocity contours for $\bar{q}/V = 0.96$ and 0.97 are also shown to demonstrate the very slow change of axial velocity beyond $x/L = 20$ and the strong dependence of wake length on the convention employed.

5-5.2.2.2 Sharp-edged Buildings. Experiments to determine the cavity size of sharp-edged block buildings on the floor of a wind tunnel are reported by Evans (1957) and Holdredge and Reed (1956). The variables were height, length, width, roof pitch, and orientation of the buildings to the wind. Atmospheric turbulence was not simulated. It was found that cavity lengths and heights increase with building width (transverse to wind) and roof pitch. Small increases in building length (parallel to wind) do not affect the cavity greatly, but for long buildings the cavity boundary reattaches to the roof and walls, and a separate cavity is created at the downwind face.

(.ges in the orientation of the buildings to .ne wind produce marked changes in the cavity shape close to building surfaces. The corner orientation, in particular, produces a cavity that encloses the downwind walls and the lateral roof corners, leaving the center of the roof exposed to high-velocity flow (Figs. 5.19 and 5.20).

The sizes of real wakes and cavities associated with buildings in a natural wind may be expected to differ from those described above because of the presence of the ground boundary, the background-wind mean velocity profile, and the increased turbulence. Section 5-5.4.1 contains a discussion of the effect of profile and turbulence. Lettau and Kutzbach (1961) describe some experiments with bushel baskets at various spacings on a frozen lake. Wake lengths can be estimated from these data.

Pressure distributions on buildings were measured by Chien, Feng, Wang, and Siao (1951) and Holdredge and Reed (1956) using wind tunnels with uniform-velocity-profile airstreams. Jensen (1958) and Jensen and Franck (1965) made comparative pressure-distribution tests on a building in an open field and on a model of the building in a wind tunnel with various logarithmic velocity profiles produced by roughness elements on the tunnel floor and found considerable variation of pressure coefficient among the tests. Figure 5.21 shows the average pressure coefficient on various surfaces and the lowest value on the upwind roof as a function of building height/ground roughness, H/z_0. Agreement with field measurements was good at $H/z_0 = 170$, corresponding to field conditions, but the variation over the range of H/z_0 was considerable. Evidently the wind profile must be reproduced in order to obtain pressure-coefficient data from wind-tunnel tests that agree with field data.

Pressures on buildings and their dependence on building shape, mean wind velocity profile, and wind turbulence have been studied at the University of Toronto (Keffer and Baines, 1963, Hamilton, 1962, Baines, 1963, and Leutheusser, 1964, 1965). Discussion of the relation between pressure coefficients and flow conditions near building surfaces in these reports augment the foregoing descriptions.

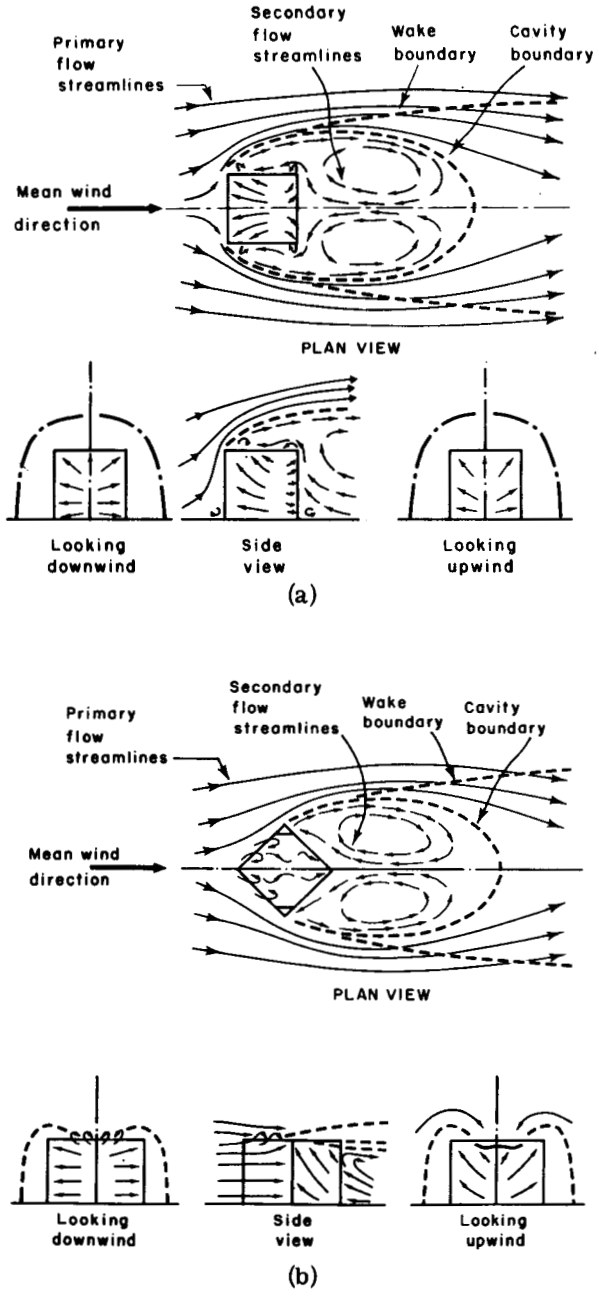

Fig. 5.19 — Flow around a sharp-edged building. (a) Normal orientation. (b) Diagonal orientation. [From J. Halitsky, Gas Diffusion near Buildings, *ASHRAE (Am. Soc. Heating, Refrig. Air-cond. Engr.) Trans.*, 69: 473 (1963).]

5-5.2.2.3 Rounded Buildings. A frequently used shape of containment structure for a nuclear power reactor is a vertical cylinder topped by a hemispherical dome. Although the rounded exterior surface lacks a sharp edge for a localization of the separation phenomenon,

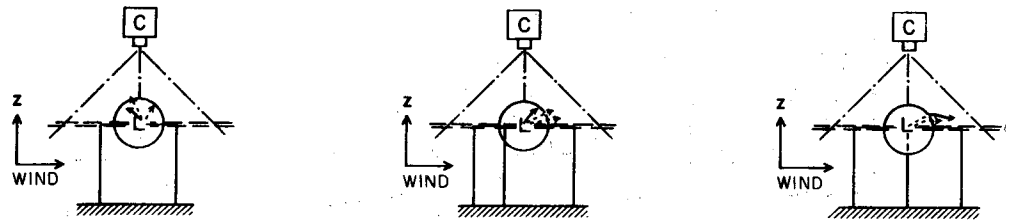

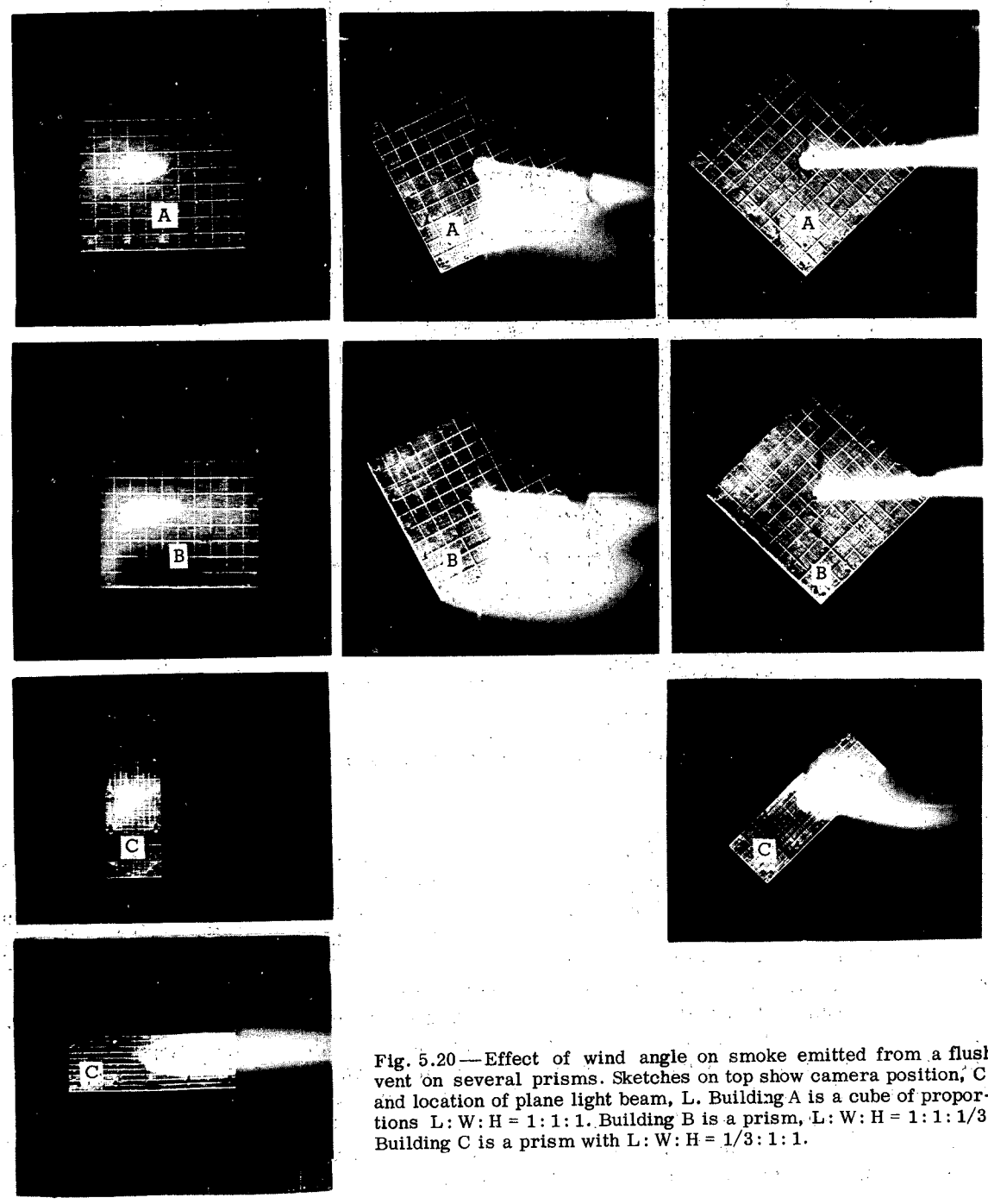

Fig. 5.20 — Effect of wind angle on smoke emitted from a flush vent on several prisms. Sketches on top show camera position, C, and location of plane light beam, L. Building A is a cube of proportions L: W: H = 1: 1: 1. Building B is a prism, L: W: H = 1: 1: 1/3. Building C is a prism with L: W: H = 1/3: 1: 1.

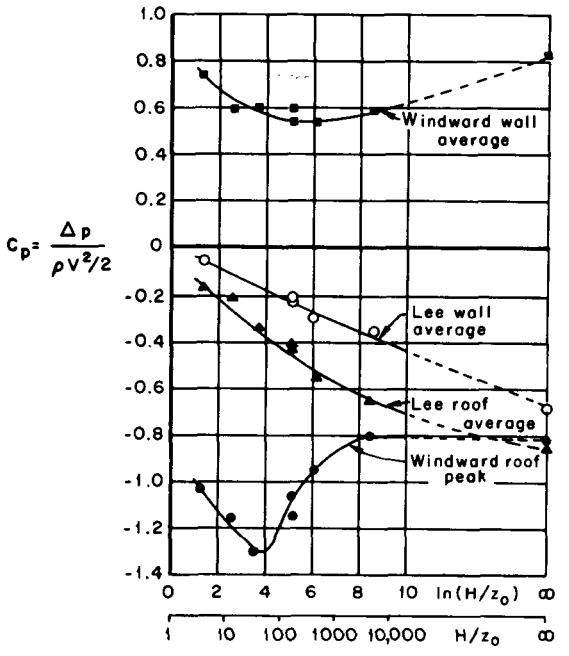

REPRESENTATIVE VALUES OF H/z_0

TERRAIN z_0 (FT)	SNOW 0.01	GRASS 0.1	OPEN TREES 1.0	DENSE 2-STORY BLDGS. 10
BUILDING HEIGHT H (FT)				
20	2,000	200	20	2
50	5,000	500	50	5
100	10,000	1000	100	10

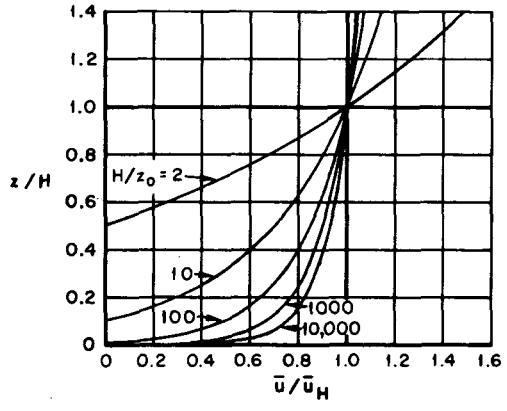

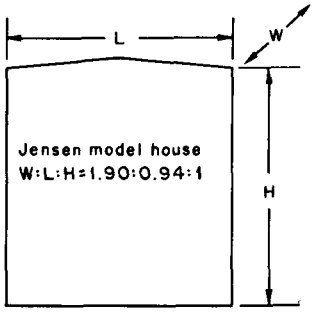

Fig. 5.21 — Effect of variation of mean-velocity profile on pressures on a sharp-edged building. (Based on data from Jensen, 1958.)

separation does occur, producing a wake and cavity. In contrast to the sharp-edged building, however, the location of the separation line varies.

Much available information about separation on curved surfaces comes from wind-tunnel tests in wind streams having turbulence intensities of less than 2.0%. These tests show that the controlling factor in separation is the Reynolds number, Re, which for the atmosphere is about 6000 LV, where L is a characteristic object dimension in feet and V is the wind speed in feet per second. For a sphere or cylinder, the characteristic dimension is the diameter D_0, and the location of the line of separation is specified by the angle φ between the radius to the line and the radius pointing directly upwind. At Re of the order of 1, no separation occurs at all. As Re increases, separation begins near $\varphi = 180°$ and moves upwind until the line becomes temporarily stabilized in the range of $75° < \varphi < 90°$ for $2000 < Re < 300{,}000$. At $Re \approx 300{,}000$ the line of separation moves abruptly downwind to $\varphi \approx 115°$, and φ increases slowly thereafter with large increases in Re. The abrupt shift in the line of

separation at Re ≈ 300,000 is produced by a transition from laminar to turbulent flow in the boundary layer.

For a Re of 300,000, the product D_0V must be at least 50. This is usually the case for most full-size buildings, and separation will occur at $\varphi \approx 115°$ in a steady wind. The angle may be expected to increase even more as the background flow becomes more turbulent. Therefore the wake will be attached to the downwind surface of the rounded structure, and the streamline distortion around the building and wake will be less than around a sharp-edged building. The condition is illustrated in Fig. 5.22.

The photographs of Fig. 5.23, taken during a model test of the EBR-2 reactor shell at Idaho Falls, show the movement of smoke released at

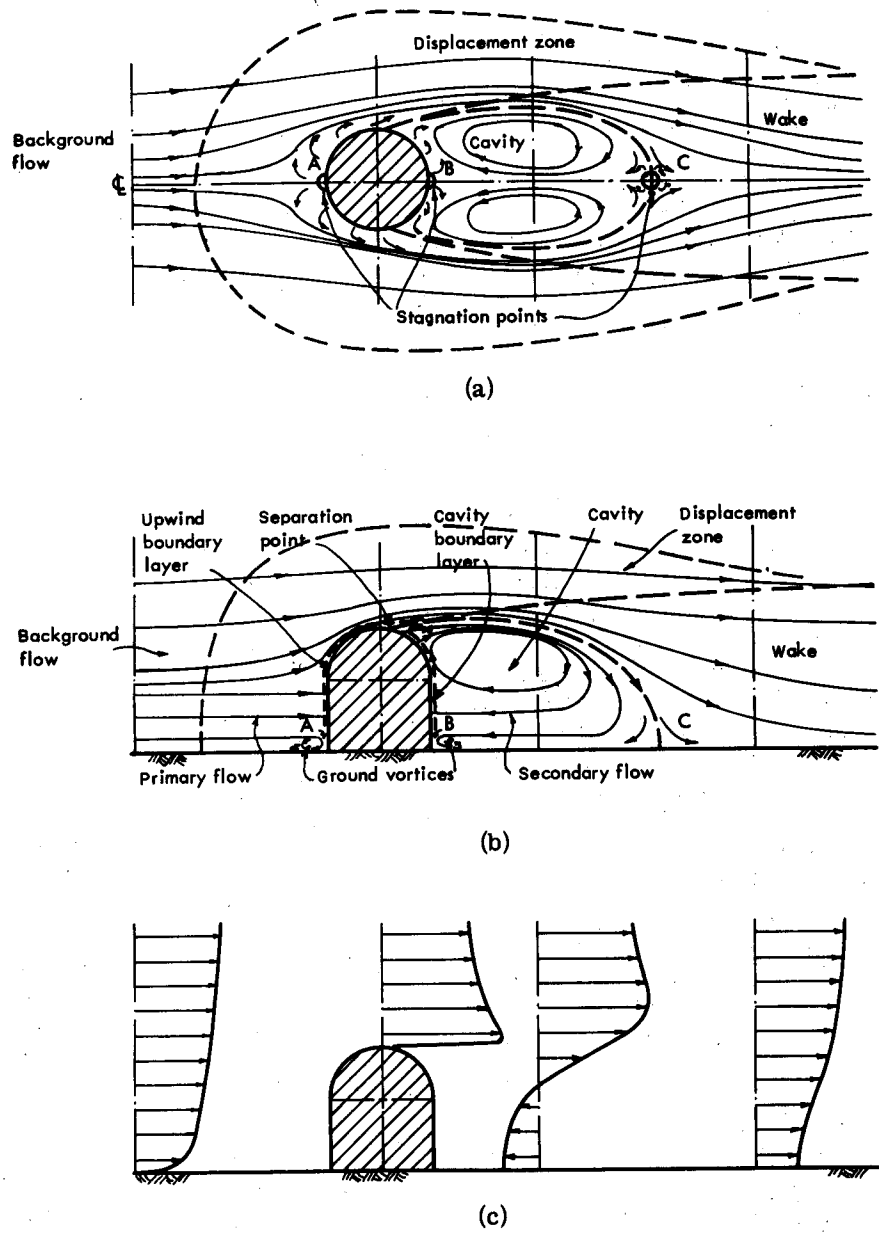

Fig. 5.22 — Flow around a rounded building. (a) Flow in a horizontal plane near the ground. (b) Flow in the longitudinal center plane. (c) Velocity profiles in the longitudinal center plane. (From Halitsky, Golden, Halpern, and Wu, 1963.)

various points on the surface of the shell or at the ground. Separation is seen to occur at φ somewhat larger than 90°. The stagnation point of the cavity-bounding streamline is seen in frame 14 to occur at $x/D_0 = 2.25$ from the center of the shell. Frame 4 shows the effect of placing an auxiliary building upwind of the shell. The cavity of the auxiliary building extends to the shell, and the downflow causes the smoke to recirculate back to and over the roof of the auxiliary building.

5-5.2.2.4 Walls. Flow approaching a wall encounters a positive pressure gradient along the ground since a stagnation zone exists on all building faces normal to the wind. Therefore the flow separates from the ground before reaching the wall and attaches to the wall at a higher elevation. A vortex is created at the base with horizontal axis normal to the wind and direction of rotation such that the upper part of the vortex is in the direction of the wind. This condition is illustrated at point c in Fig. 5.17. A weak vortex created by the return flow in the cavity also exists at point f.

Similar vortices are shown in Fig. 5.22 for the round building. Frame 2 of Fig. 5.23 shows that the upwind vortex can cause a contaminant discharged at the base of the shell to travel upwind along the ground a distance of about $D_0/3$. Frame 3 shows that the vortex also induces a strong downflow along the cylindrical wall of the shell.

Flow downwind of two-dimensional fences of various heights immersed in a wind-tunnel-floor boundary layer have been investigated by Nagabhushanaiah (1961). He found that the cavity length was 12 fence heights long and the cavity thickness was about 1.6 fence heights high. These proportions differ from those of the suspended plate in that the cavity is longer but not as deep. It is thought that the differences may be attributed to two causes: the presence of the ground boundary and the change from a three-dimensional to a primarily two-dimensional phenomenon. Insufficient information is available to separate the two effects.

5-5.2.2.5 Terrain Discontinuities. Brooks (1961) reviews various wind-tunnel experiments dealing with flow over a sudden drop of height H in terrain and over an abrupt change of surface roughness. A cavity is shown to exist for at least a distance of 6.0H downwind of the drop, and a new, stable wind profile is shown to be far from established at a distance of 7.5H. Also, a floating layer of high turbulence ($\sigma_u/V = 0.16$) exists and is still growing in intensity at x = 6.0H. The elevation of the turbulent layer at x = 1.5H is the same as the original terrain but at x = 6.0H the layer has descended to one-half the drop.

Changes in the mean velocity profile in the earth's surface boundary layer when the flow passes from a region of one uniform surface roughness to another were analyzed by Panofsky and Townsend (1964). They indicate that flow over the second region is divided into upper and lower parts by a fairly distinct surface originating at the juncture of the two roughnesses and pitching upward at a slope of about 1:10. The surface is characterized by velocities common to upper and lower flows. The lower flow is determined by the surface roughness in the downwind region. The upper flow retains the characteristics generated in passing over the upwind region. The authors conclude that the establishment of flow characteristics in a surface layer of height H does not require an upwind fetch of uniform roughness greater than 10H.

5-5.2.3 Transverse Jets. A common mode of gas release near a building surface is in an exhaust-air jet originating at a flush vent or stub stack on the building roof. The initial trajectory of the jet is important because fresh-air intakes are frequently located in nearby roof cupolas and the throw of the jet will determine whether the intake will be exposed to the relatively high concentration near the plume center line.

Although a number of theoretical solutions for transverse jet trajectories have been advanced, these are generally applicable only at large distances from the source. Near the aperture the jet takes on a semisolid character and creates a displacement flow, cavity, and wake in the transverse airstream. The reduced pressure at the sides of the jet cylinder causes the jet to expand laterally, and the reduced pressure in the cavity causes the jet cross section to warp into a horseshoe shape. Under these conditions simple momentum theories are not adequate to describe the initial trajectory.

Transverse jets have been studied in low-turbulence wind tunnels by Bryant and Cowdrey (1955), Jordinson (1956), Keffer and Baines

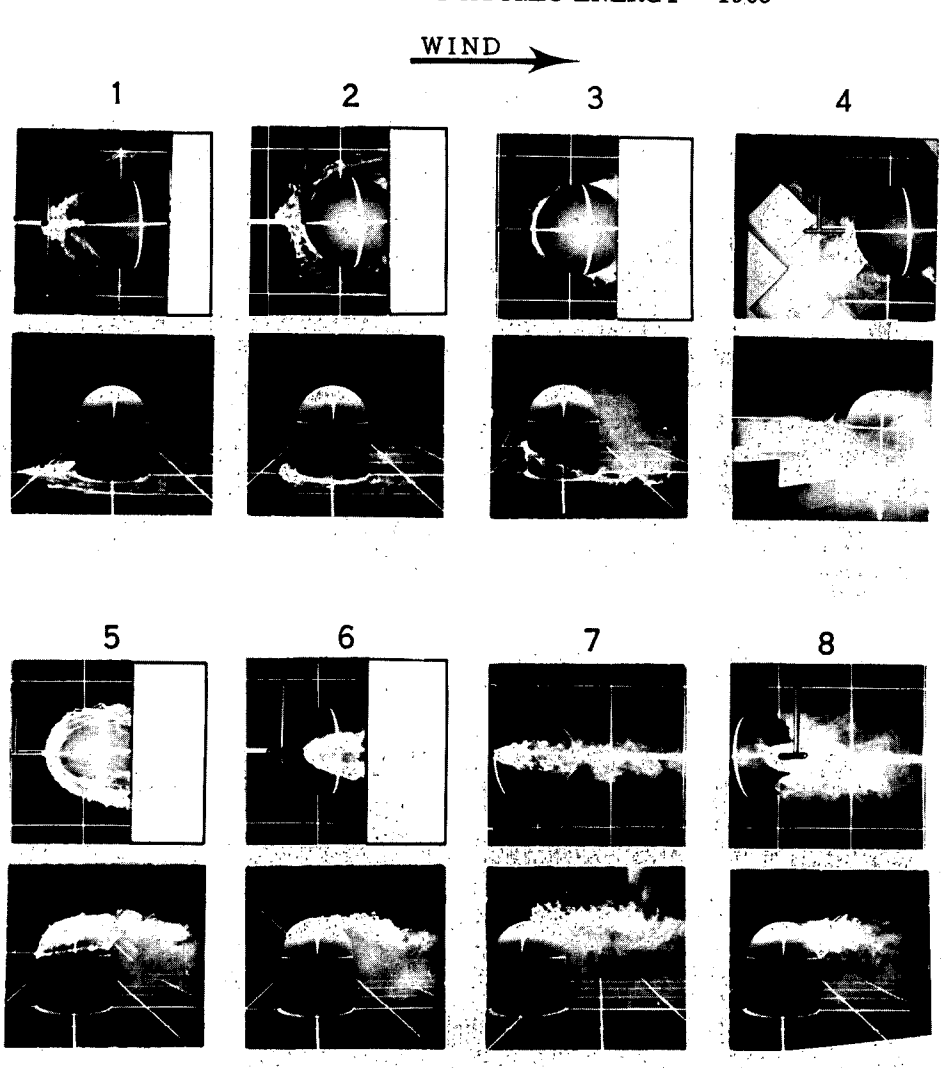

Fig. 5.23—Photographic sequence showing diffusion of smoke released at various points in the longitudinal center plane through a reactor shell. (From Halitsky, Golden, Halpern, and Wu, 1963.)

(1963), and Shandorov (1957). Jordinson measured total pressure in jets from a flush vent; typical cross sections and center-line trajectories are given in (a), (b), and (c) of Fig. 5.24. The negative total pressures are an indication of reduced static pressure in the cavity rather than reversed velocity. The jet center line is defined as the line of maximum total pressure. Bryant and Cowdrey measured temperatures in a vertical center plane through a heated chimney jet issuing at a [illegible]°F temperature excess. Temperature contours are shown in (d) of Fig. 5.24. A review of published data on transverse jets is given by Halitsky (1966).

Transverse jets in the cavity over a building roof are exposed to highly turbulent nonuniform mean-velocity flows. Figure 5.25 shows a flush roof jet under conditions of varying emission-velocity ratios, V_e/V, where V is the velocity of the external uniform nonturbulent flow. The shape of the jet is a reflection of the circulatory mean flow in the cavity. The jet bends upwind at low V_e/V, bends downwind at high V_e/V, and becomes forked at intermediate values. No quantitative measurements of jet characteristics in this type of flow field have been made.

5-5.3 Concentration Calculations

Because of the unavailability of explicit theoretical expressions to describe concentra-

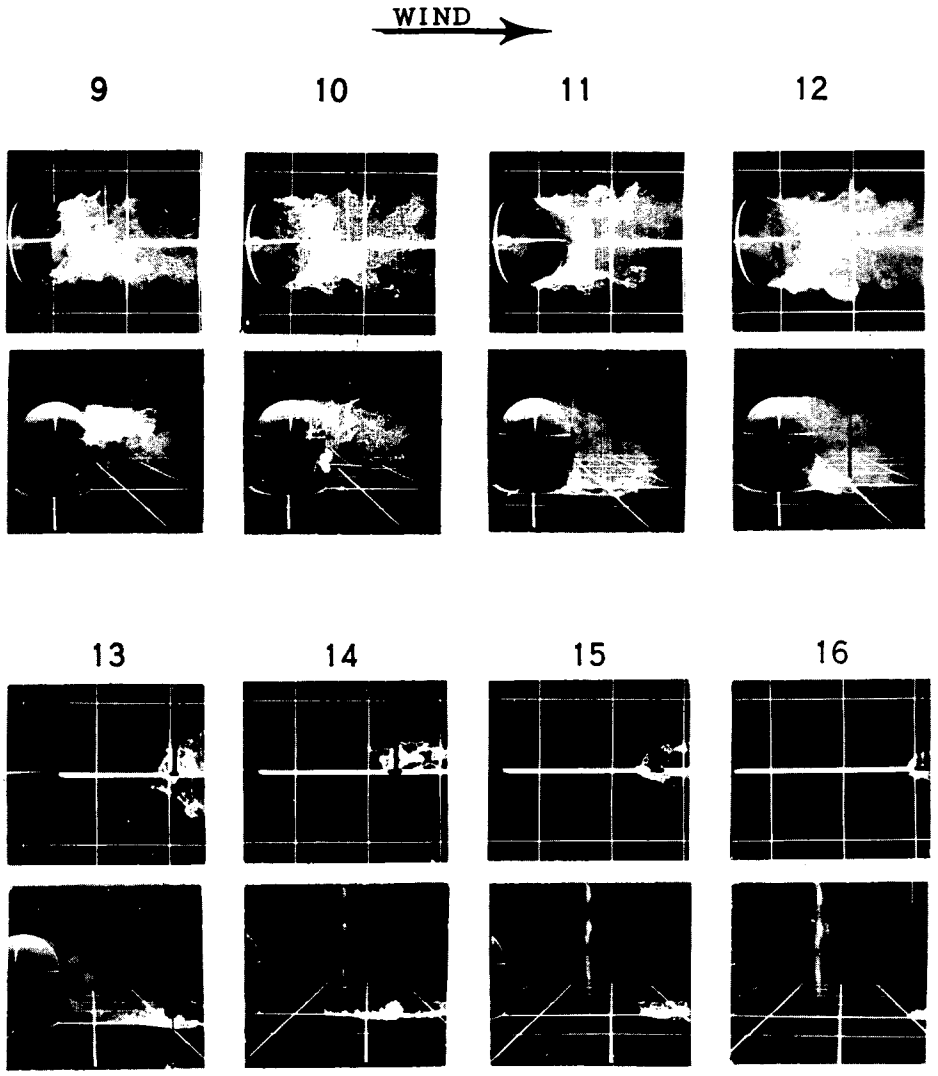

Fig. 5.23 — (Continued)

tion distributions in distorted flow fields and the impracticability of conducting a full-scale test for each problem, it is necessary to adopt an approach that combines the results of a few experiments with a method for extrapolation of the data to other than the test conditions.

A method that has proved successful in extrapolating pressures and forces on objects in a moving fluid stream is the reduction of data to nondimensional coefficient form. In this section we shall follow the same procedure: define a nondimensional concentration coefficient K_c for any concentration field, indicate the specifications needed to give it meaning, and show how characteristic values of K_c can be computed with a minimum of data for general types of problems.

5-5.3.1 The Concentration Coefficient and the Configuration. Any concentration field can be expressed nondimensionally by introducing reference parameters L for length, V for velocity, Q' for contaminant-release rate, and Q'/L^2V for concentration. We shall define the concentration coefficient K_c as the ratio of the actual concentration, $\bar{\chi}$, at any point in the field to the reference concentration, or

$$K_c = \frac{\bar{\chi}}{Q'/L^2V} = \frac{\bar{\chi}L^2V}{Q'} \qquad (5.71)$$

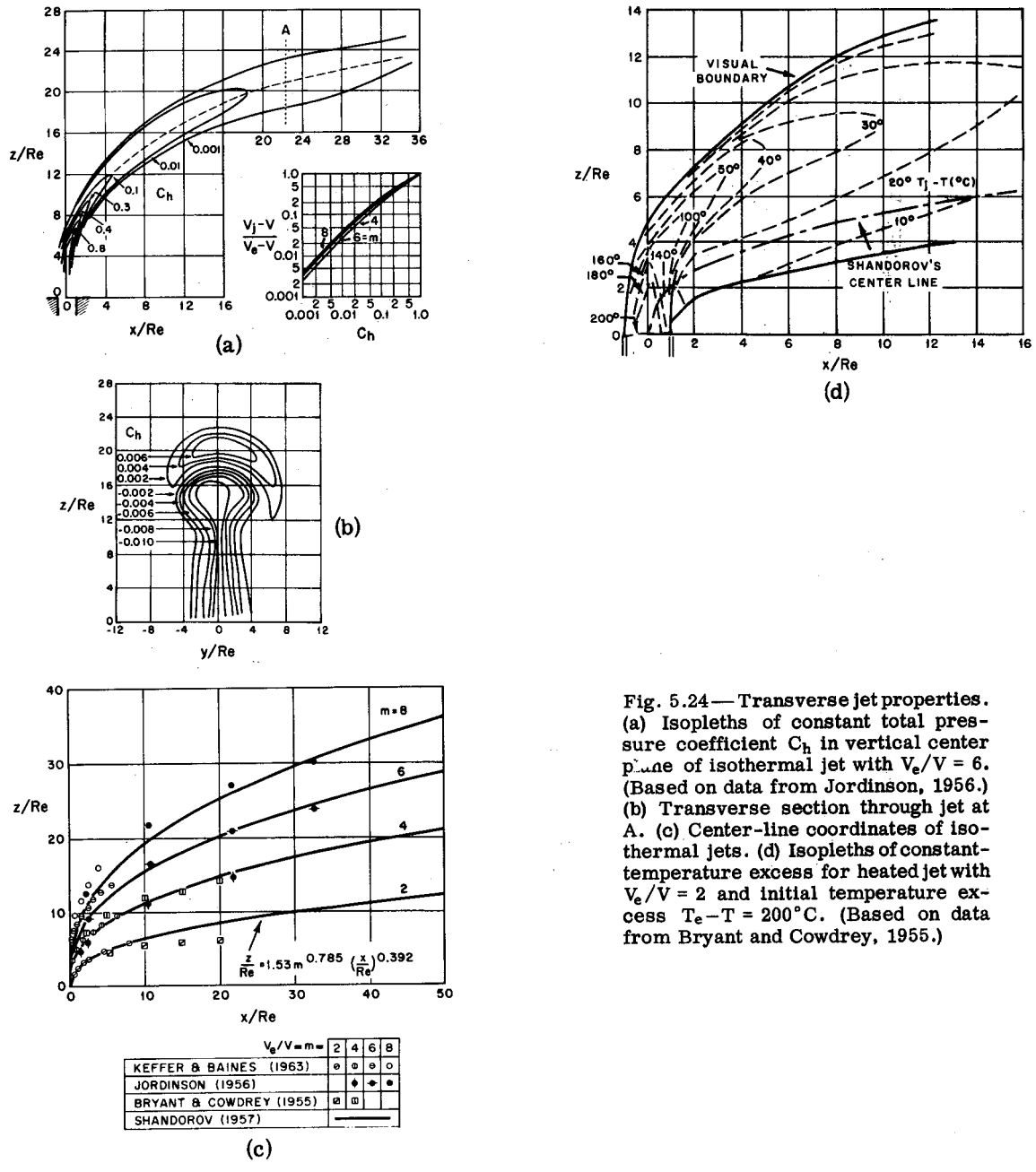

Fig. 5.24—Transverse jet properties. (a) Isopleths of constant total pressure coefficient C_h in vertical center plane of isothermal jet with $V_e/V = 6$. (Based on data from Jordinson, 1956.) (b) Transverse section through jet at A. (c) Center-line coordinates of isothermal jets. (d) Isopleths of constant-temperature excess for heated jet with $V_e/V = 2$ and initial temperature excess $T_e - T = 200°C$. (Based on data from Bryant and Cowdrey, 1955.)

In general, K_c is a function of nondimensional space coordinates x/L, y/L, and z/L, and other nondimensional parameters, collectively called the configuration.

These purely mathematical transformations are very useful in reporting concentration data in dynamically similar flow fields. If, as is generally accepted, the mechanism of contaminant diffusion is the eddy motion of the carrier fluid, then concentration fields should be similar and K_c fields should be identical in dynamically similar flow fields having similar source arrangements. The statement of the configuration contains those specifications which will guarantee the independence of a K_c field with respect to length, velocity, and source-strength scales.

In a few simple problems for which mathematical solutions of the concentration distribution have been found, K_c can be expressed

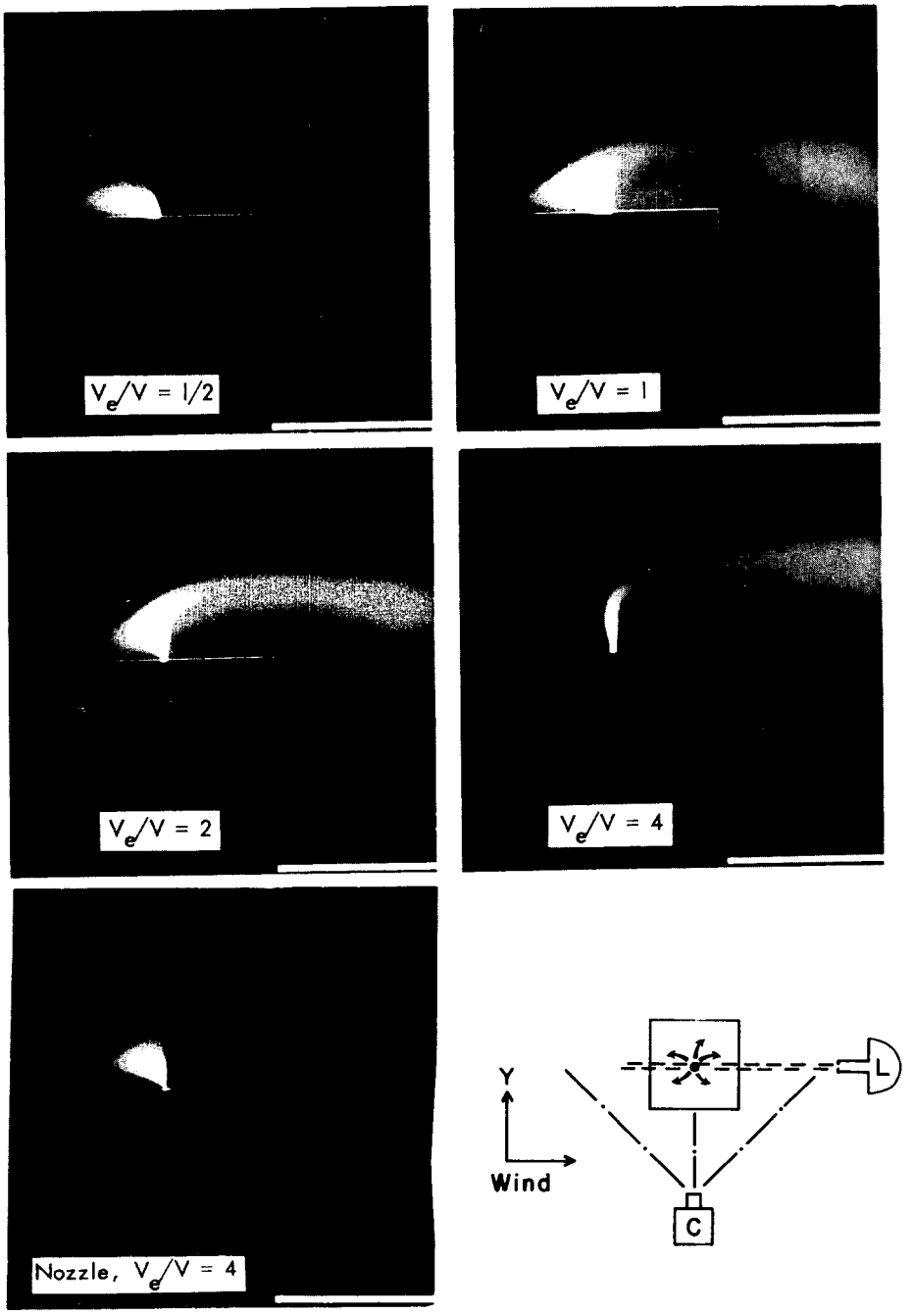

Fig. 5.25—Smoke patterns of jets discharging into a roof cavity. Cube side = L, aperture D_e = L/30, nozzle D_e = L/60, wind velocity = 4 ft/sec, wind profile is uniform, wind turbulence <1%. [From J. Halitsky, *Gas Diffusion near Buildings, ASHRAE (Am. Soc. Heating, Refrig. Air-cond. Engrs.) Trans.*, 69: 483 (1963).]

analytically. For example, the Sutton equation for a continuous point source at a large distance from the ground transforms into

$$K_c = \frac{1}{\pi\left(\frac{C_y}{H^{n/2}}\right)\left(\frac{C_z}{H^{n/2}}\right)\left(\frac{x}{H}\right)^{2-n}} \times \exp\left[-\frac{\left(\frac{y}{H}\right)^2}{\left(\frac{C_y}{H^{n/2}}\right)^2\left(\frac{x}{H}\right)^{2-n}} - \frac{\left(\frac{z}{H}-1\right)^2}{\left(\frac{C_z}{H^{n/2}}\right)^2\left(\frac{x}{H}\right)^{2-n}}\right] \quad (5.72)$$

where the reference parameters are Q' = source strength, V = mean wind velocity = $\bar{u}$ (uniform over field), and L = source height = H. Thus, K_c is seen to be a function only of nondimensionalized space coordinates x/H, y/H, and z/H, when the effective turbulence parameters n, $C_y/H^{n/2}$, and $C_z/H^{n/2}$ are given. The accompanying statement of the configuration would then read:

1. Mean flow consists of a uniform velocity field of semiinfinite extent with streamlines parallel to each other and to the plane of the ground.

2. Turbulence is homogeneous but not isotropic and is specified by the above effective turbulence coefficients.

3. Contaminant is emitted from a continuous point source at height H with temperature equal to the air temperature at the same height.

Simple algebraic expressions for K_c such as the above are possible only in flow fields having uniform mean velocity and homogeneous turbulence. This condition is satisfied approximately at large distances from the ground where emissions from tall chimneys experience the greater part of their diffusion. Many contaminant releases in distorted flow fields close to buildings, however, create concentration distributions that are so complicated that algebraic expressions are not practical even if they could be found. In such cases it is necessary to express the distribution in tabular or graphical form. Although this is not as elegant as an algebraic form, it is adequate for engineering use, and its accuracy is commensurate with that of the test data.

A K_c distribution for a specific building is easily determined experimentally by (1) releasing a quantity of contaminant at a known rate, Q', (2) measuring the concentration, $\bar{\chi}$, at a number of points in the space surrounding the building, (3) selecting a reference area $A = L^2$ related to the building size and a reference velocity V at a designated height above ground, and (4) dividing each concentration measurement by Q'/AV. Isopleths of constant K_c can then be drawn for the space surrounding the building. To use these K_c isopleths for a similar building on another scale, we need to nondimensionalize the coordinates, but the appropriate choice of a reference length is not immediately evident.

No method has been found for extracting a single reference length from the properties of a distorted flow field near a building which will guarantee similitude of the field on all turbulence, mean velocity, and length scales. We may, however, reason that the field properties are determined by the hydrodynamical equations of motion plus the initial and boundary conditions, and, if we are interested in the time-mean flow, the initial conditions are unimportant, and the boundary conditions alone should suffice. Therefore we should be able to extract a reference length from the boundary conditions.

The boundaries of a distorted flow field consist of the solid ground and building surfaces, the isolating surface between the distorted field and the background flow, and the holes in the solid surface through which air enters or leaves the distorted field. The simplest length that can be formed from the boundary conditions is a geometrical dimension of a recognizable feature of the solid boundary. Although any such feature will do, it is preferable to use one that has a controlling influence on the shape of the isolating surface. For a simple building on flat ground, the side area projected on a plane normal to the wind performs this function, and an appropriate length would be the square root of this area.

The use of a geometric reference length will scale the solid portion of the flow-field boundary properly, but this in itself does not guarantee that the shape of the isolating surface will be preserved. We may infer, however, from the previously cited tests on plates that the isolating surface surrounding a sharp-edged structure

in a low-turbulence flow will also scale geometrically. This assumption will be examined more closely later with respect to the influence of Reynolds and Froude numbers and turbulence in the background flow.

We must now make some statement that will define the shape of the boundary and the distribution of velocities on the boundary. The following specifications have been found to be important:

1. Building and terrain: dimensions and orientation to the wind.
2. Background wind: mean velocity and turbulence variation with height.
3. Air jets entering distorted flow region (exhaust vents and chimneys): mean velocity and temperature excess at aperture.
4. Air removed from distorted flow region (building air intakes): mean velocity at aperture.

These boundary conditions may be nondimensionalized by dividing all lengths by the reference length, L, and by dividing all velocities by a reference wind velocity, V, at a given elevation. This results in a background mean velocity profile $\bar{u}/V$ vs. z/L, exhaust- and intake-velocity ratios V_e/V and V_i/V, and the turbulence-intensity components $i_u = \sigma_u/\bar{u}$, etc., where σ_u is the root-mean-square turbulence velocity in the mean wind direction.

The configuration, then, will include the four specifications just mentioned, the statement of how A and V are to be measured, and the source distribution. In the present context the term "source" refers to the pure-gas component of an effluent. In ordinary problems involving the release of gas–air mixtures, the amount of pure gas is so small with respect to the volume of air in the jet that the presence of the gas does not influence the air motions in the flow field. The source distribution is important, however, because steep velocity gradients in the field, sometimes accompanied by flow reversals, may cause different portions of the source to disperse in different directions. The strength of the source affects the maximum concentration in the field, but it does not appear in the K_c term and is not properly a component of the configuration.

5-5.3.2 Dilution. In practical problems we may be given the rate of release of contaminant, Q', or the concentration in the effluent aperture, $\bar{\chi}_e$, and we wish to find the concentration, $\bar{\chi}$, at any point in the field or the dilution that will take place as the gas travels from the effluent aperture to the point. Evidently, if the concentration field is steady, each point may be assigned a given dilution, D, defined as the ratio of concentration in the effluent aperture to the concentration at the point. Using Eq. 5.71 to express the concentrations in coefficient form, we obtain

$$D = \frac{\bar{\chi}_e}{\bar{\chi}} = \frac{K_{ce}}{K_c} \tag{5.73}$$

5-5.3.3 Magnitudes of K_c and D for Isolated Buildings. The magnitude of K_c does not vary greatly among configurations in a few regions of practical importance, such as the side walls of a building and the nearby ground when gas is released into the cavity near the top of the building. On the other hand, K_c depends markedly on configuration in regions near the source. Thus fairly good estimates of concentration can be obtained for the former regions with only a small amount of information, but serious errors can be introduced if configuration details are not taken into account in the latter case, particularly when air intakes are located close to effluent apertures on the roof of the same building.

5-5.3.3.1 K_c and D in Effluent Apertures. Let the effluent at the source have velocity V_e and concentration $\bar{\chi}_e$ in an effluent aperture of area A_e. The source must then have strength $Q' = \bar{\chi}_e A_e V_e$, and, from Eqs. 5.71 and 5.73, the concentration coefficient and dilution at the source are

$$K_{ce} = \frac{AV}{Q'}\bar{\chi}_e = \frac{AV}{A_e V_e} \tag{5.74}$$

and

$$D_e = \frac{K_{ce}}{K_{ce}} = 1 \tag{5.75}$$

In most problems A_e and V_e are specified, but V and A must be selected. For V it is convenient to use the approach wind velocity at the elevation of the building roof. A suitable area is the side area of the building projected on a plane normal to the mean wind direction. Although basically correct, this formulation

makes computation difficult because a new area must be found for each wind direction. A more useful choice is the area of the building projected on a plane parallel to the largest side. Here A is a constant for a given building.

The release of a pure gas having $\overline{\chi}_e = 1$ produces $K_{ce} = AV/Q'$ at the effluent aperture. A representative configuration of an industrial laboratory building might be height, 40 ft; length, 200 ft; A, 8000 sq ft, and wind velocity V, 10 ft/sec. Here the numerator of Eq. 5.74 becomes 80,000. Let us assume that a laboratory experiment produces $Q' = 10$ cu ft/min = 0.167 cu ft/sec of pure gas. Then $K_{ce} = 480{,}000$. Such high values of K_{ce} are typical of small pure-gas releases.

If the gas is released in a fume hood, a large amount of initial dilution takes place prior to release to the atmosphere. Let us assume that the fume-hood air-flow rate is 1000 cu ft/min and that the discharge occurs through a 1 sq ft opening. Then $A_e = 1$ sq ft, $V_e = 16.7$ ft/sec, and $K_{ce} = 4{,}800$ according to Eq. 5.74. The decrease of K_{ce} from 480,000 to 4,800 represents the initial dilution of 100 in the duct system. Representative values of K_{ce} for single hood exhausts on large buildings usually fall in the range of 10^3 to 10^4.

If several fume-hood exhausts are combined and then released through a single effluent aperture, the product A_eV_e varies in direct proportion to the number of hoods, and K_{ce} varies in inverse proportion. Again, the decrease in K_{ce} is a reflection of internal dilution since it is presumed that the same amount of gas is released in either system (all hoods operate, but gas is released in only one).

5-5.3.3.2 K_c and D in the Wake at the End of a Cavity. A characteristic K_c value occurs in a cross section of the wake just downwind of the cavity when the cavity completely encloses a building having a roof exhaust. Because of high turbulence the contaminant spreads throughout the cavity and diffuses into the wake proper through the cavity boundary. In the indicated cross section, the concentration distribution is not uniform, but the entire wake is contaminated to some degree. An average concentration for the section may be estimated by dividing the source strength by the wake volume flow. For an average building the cross-sectional area of the wake is about twice the reference area, and the mean velocity in the cross section varies from a low value near the downwind stagnation point (point h in Fig. 5.17 or point C in Fig. 5.22) to the background-flow velocity V at the periphery of the wake, with an average value of about V/2. The average wake concentration then is

$$\overline{\chi} \approx \frac{Q'}{2A(V/2)} = \frac{Q'}{AV} \qquad (5.76)$$

which gives

$$K_c = \frac{\overline{\chi}AV}{Q'} \approx 1 \qquad (5.77)$$

This estimate has been borne out by measurements. For example, the stagnation point for the reactor shell in Fig. 5.23 (panels 9 to 16) is located 2.25 diameters downwind of the shell center line. Values of K_c in the same plane (see Fig. 5.29) for different source locations range from $K_c = 0$ to $K_c = 5$, with $K_c = 1$ being a rough average.

5-5.3.3.3 K_c and D at the Walls. The value of K_c at the downwind stagnation point has great significance for contamination of the downwind walls of a building. These surfaces are bathed by the return cavity flow, which appears to originate at the stagnation point and to move along the ground upwind toward the building, around the building sides, and upward toward the roof. Thus K_c values at the downwind building walls depend principally upon the K_c value at the stagnation point, or $K_c = 1$. The variation of K_c along the downwind walls is not large. It increases somewhat toward the roof owing to spillage of gas over the roof copings and short-circuiting of the upper cavity flow to the lower flow without making the full circuit along the cavity boundary. The upwind walls, being out of the cavity, are not contaminated.

5-5.4 Scaling Requirements

Since the mechanism of turbulent diffusion is the motion of air parcels, similarity of flow fields should result in similarity of concentration fields for similar sources. We shall take the view that flow similarity will exist in regions where aerodynamic effects predominate if the wind characteristics on the boundary of the distorted flow field are reproduced and the mean-flow hydrodynamic scaling criteria in the

interior of the field are observed (geometric similarity of the solid boundary being assumed). The important wind characteristics are the vertical profiles of mean velocity, turbulence intensity, and turbulence spectrum. The important scaling criteria are the Reynolds number and modified Froude number.

5-5.4.1 Wind Characteristics. The mean-wind-velocity profile is determined by upwind flow conditions. In an adiabatic atmosphere flow over level ground with uniform roughness produces a logarithmic variation of mean velocity with height, the controlling parameter being the roughness height z_0. In nonadiabatic conditions the profile is not logarithmic and cannot be adequately described by z_0 alone. In flow over nonuniform roughness, the profile will be affected by size, shape, and spacing of the roughness elements. When a nearby upwind ground irregularity is comparable in size to the building under consideration, the term "roughness" loses its meaning as a characteristic of the terrain, and the profile must be considered as part of an upstream wake. Excluding the last case and using the term z_0 in its broadest sense as some descriptive height based on physical dimensions of terrain and atmospheric stability, we may consider the general shape of the wind profile to be quasi-logarithmic and to originate at some point z_0 above the ground ($\bar{u} = 0$ at $z = z_0$).

Where a building of height H is immersed in a boundary layer characterized by z_0, the mean velocity distribution in a layer comparable to H will be very sensitive to the ratio H/z_0. Figure 5.21 shows velocity profiles calculated from $\bar{u} = (V_*/k) \ln (z/z_0)$ for a range of H/z_0 from 2 to 10,000. The table in Fig. 5.21 shows representative values of H/z_0 for several possible combinations of building height and terrain. Values of z_0 of 0.01 ft for snow and 0.1 ft for grass have been cited in several texts. A value of 10 ft for z_0 might occur in a densely built-up urban area. According to Jensen (1958) measurements of wind speed above Copenhagen extrapolated logarithmically to zero speed gave z_0 equal to about 40% of the average building height. A considerable difference is seen between profiles to which a four-story building may be exposed in a built-up region ($H/z_0 \approx 5$) and in a cleared isolated area ($H/z_0 \approx 500$).

The need for reproducing the full-scale velocity profile in model tests has not been carefully evaluated for diffusion close to buildings, but it appears to be important when H/z_0 is small. In such cases the velocity is reduced considerably over the lower part of the building, with the result that less air is provided for ventilation and the diffusion process is slowed. At the same time the wake cross section contracts since less air is displaced laterally and vertically by the building, and consequently the circulation patterns change in the cavity surrounding the roof and side walls. An indication of these effects is shown in Fig. 5.26. The streamline curvature in (b) and the wake boundary curvature in (d) of Fig. 5.26 for $H/z_0 = 60$ are less than in (a) and (c), respectively, for $H/z_0 \approx \infty$. Also, smoke released from a roof vent is seen to move upwind in the cavity in (c) but downwind in (d). These effects cannot be attributed entirely to the change in mean-velocity profile since the turbulence was greater in the case of $H/z_0 = 60$, but it is thought that the mean-velocity profile is the significant factor in controlling the shape of the wake boundary and the mean flow in the cavity. Similar behavior of the wake boundary with variation of wind-velocity profile was observed by Jensen and Franck (1965).

Two aspects of wind turbulence affect wake flow in characteristic ways. As discussed in Sec. 5-5.2.1.4, the intensity appears to influence the peripheral regions of the wake. On the other hand, if the spectrum shows considerable energy in the low-frequency range, the effect is that of a periodic change in mean wind direction, which strongly influences cavity flow. The degree of change may be seen in the change of smoke patterns in Fig. 5.20 when the wind angle changes by 22.5°. In the natural atmosphere under adiabatic conditions, the lateral turbulence intensity near the ground may be of the order of 0.15 corresponding to a root-mean-square lateral gust angle of about $\sigma_\theta = 9°$. In a normal distribution the effective range of gust angles is about 2.5σ with extreme gust angles of $\pm 22°$ produced. Therefore the time-average concentration pattern for a cube oriented with one face normal to the mean direction of a turbulent wind in an adiabatic atmosphere should be a weighted average of the concentration patterns shown in the two upper left photographs of Fig. 5.20 plus patterns for the intermediate

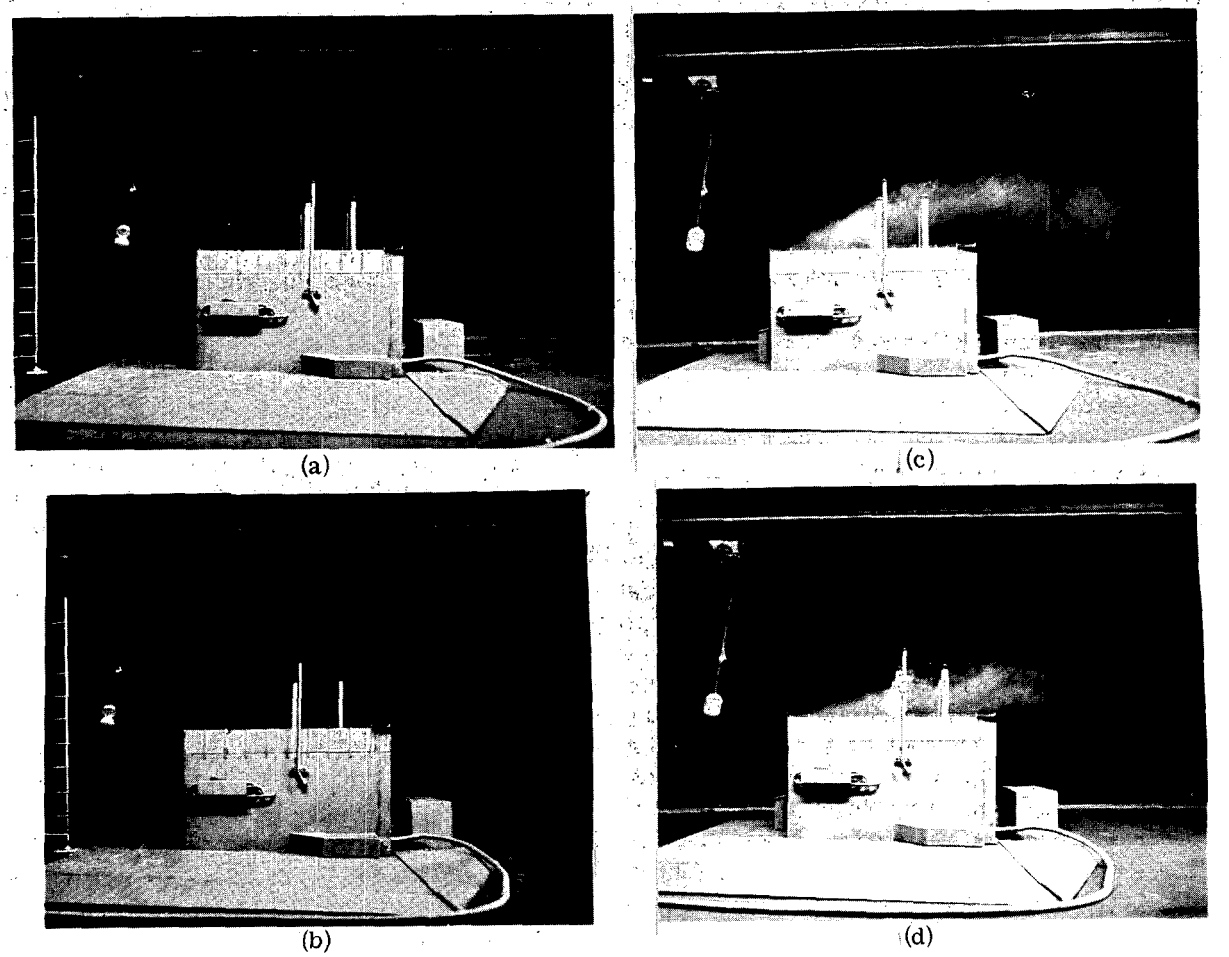

Fig. 5.26 — Effect of variation of mean-velocity profile and turbulence on streamline and cavity shape for a sharp-edged building. (a) Streamline flow. (b) Streamline flow. (c) Cavity flow for a uniform profile, $H/z_0 \approx \infty$ and $\sigma_u/\bar{u} \approx 0.005$. (d) Cavity flow for a logarithmic profile, $H/z_0 \approx 60$ and $\sigma_u/\bar{u} \approx 0.040$.

angles. The same principle applies to vertical gusts.

The transformation of cavity shape (and cavity flow field) with change in wind angle is also dependent upon the time available for the transformation to become complete. The minimum period for development of a recognizable cavity should be of the order of the time necessary for an air parcel to travel the length of the building, or $t = L/V$. In an adiabatic atmosphere it has been found (Pasquill, 1962) that the maximum energy per frequency decade in the spectrum of vertical oscillations occurs at a nondimensional frequency, $fz/V \approx 0.2$. At the roof level of a cube of side L, this corresponds to a period of $t = 1/f \approx 5L/V$. Therefore much of the energy of vertical oscillations is of long enough period to produce sustained changes in the cavity flow field. Lateral oscillation periods are of the same order.

An interesting conjecture concerning the interaction of wind turbulence and building-generated turbulence arises from observations that circular cylinders in a nonturbulent airstream shed periodic eddies whose frequency is given by the Strouhal number, $fD/V = 0.2$, for values of Reynolds number greater than 10^3 (Schlichting, 1960) and that measurements of pressure fluctuations on cubes in a wind tunnel show a Strouhal number for the dominant frequency around 0.25 to 0.5 (Keffer and Baines, 1963). The correspondence of eddy-shed frequency in the wake and maximum energy-carrying frequency in the atmosphere may tend to promote resonance effects and large oscillations in the cavity and wake proper.

In view of the above, it would appear that reproduction of the turbulence intensity and spectrum are both required for accurate modeling. It seems reasonable to assume that the distribution of intensity with height and the shape of the spectrum are less critical than the existence of the appropriate average intensity and the location of the maximum energy at the correct frequency.

The importance of wind scaling has not been evaluated thoroughly by field–tunnel correlation tests, but several recent experiments provide some indications of the effect of omitting wind turbulence in the tunnel.

In tests of diffusion from a flush vent on a building, Halitsky (1965a) found that the hourly mean field concentrations on the building surfaces were from 0.1 to 1.0 times the tunnel values, the greater discrepancies appearing on the roof near the point of emission. J. E. Martin (1965) reports that field and tunnel tests of diffusion from a short stack on a building show reasonably good correlation when the effluent is trapped in the cavity but that the field concentrations are lower than the tunnel concentrations by about the peak-to-mean ratio at larger distances. Islitzer (1965) reported that field tests of diffusion from a ground release in a building complex show K_c values on the ground just downwind of the complex to be about the same as the values found by Halitsky, Golden, Halpern, and Wu (1963) in tunnel tests of a different complex. At larger distances the measured concentrations approach those computed from a mathematical model of diffusion over flat terrain with coefficients appropriate to the atmospheric stability. The mechanical turbulence produced by the complex appeared to have substantially died out at a distance of 2800 ft from the source. Munn and Cole (1965) report that field tests on a heated effluent released from a short stack on a building in a complex show smaller concentrations at a distance of 500 ft than the values calculated by formulas derived from wind-tunnel tests.

These tests indicate that the conventional low-turbulence wind-tunnel test will probably yield sufficiently accurate data for making conservative estimates of full-scale time mean concentrations in the cavity. The introduction of scaled turbulence seems necessary if test data at large distances from the source are not to be overly conservative.

5-5.4.2 Hydrodynamic Scaling Criteria. Appropriate hydrodynamic scaling criteria for any given type of diffusion test have not as yet acquired the status of general acceptance. The approach described in the following paragraphs is intended for tests of diffusion in aerodynamically distorted regions. It represents a reasonable amalgam of theory and model experiments. Validation in the field must await more extensive tests.

The requirements for flow similarity can be derived by nondimensionalizing the boundary conditions and the differential equation of mean motion of a turbulent fluid. In the nondimensionalization process we use as reference quantities configuration reference length, L, wind velocity, V, air density, ρ, and viscosity, μ. The resulting equation of mean motion has the following form:

$$\begin{bmatrix}\text{accel-}\\ \text{eration}\\ \text{term}\end{bmatrix} = \begin{bmatrix}\text{pressure}\\ \text{term}\end{bmatrix} + \frac{\mu}{LV\rho}\begin{bmatrix}\text{shear}\\ \text{term}\end{bmatrix} + \begin{bmatrix}\text{turbulence}\\ \text{term}\end{bmatrix} + \frac{Lg(T_1 - T)}{V^2 T_1}\begin{bmatrix}\text{buoyancy}\\ \text{term}\end{bmatrix} \quad (5.78)$$

In the buoyancy term we have used the approximation $(\rho_1 - \rho)/\rho_1 \approx (T_1 - T)/T_1$, assuming that the gas component of most effluents discharged close to buildings is only a small fraction of the gas–air mixture. (Temperatures in this context are absolute.)

The coefficient of the shear term is the reciprocal of the Reynolds number, Re, and the coefficient of the buoyancy term is the reciprocal of a modified Froude number, Fr′. More specifically,

$$\mathrm{Re} = \frac{LV\rho}{\mu} \quad (5.79)$$

$$\mathrm{Fr} = \frac{V^2}{Lg} \quad (5.80)$$

$$\mathrm{Fr}' = \frac{V^2}{Lg}\frac{T_1}{(T_1 - T)} = \mathrm{Fr}\,\frac{T_1}{(T_1 - T)} \approx \mathrm{Fr}\,\frac{T}{(T_1 - T)} \quad (5.81)$$

Similar motions have identical nondimensional differential equations. This means that the numerical values of Re and Fr′ must be kept

constant if similarity is to be preserved. Let us examine the requirements for exact scaling if g, ρ, μ, and T_1 are kept constant. Let the prototype configuration be identified by the quantities L*, V*, T*, Re*, and Fr′*. If L* is changed to L the following changes must also be made:

To satisfy Re

$$V = V^* \frac{L^*}{L} \tag{5.82}$$

To satisfy Fr′

$$V = V^* \left(\frac{T_1 - T}{T_1^* - T^*} \frac{T_1^*}{T_1} \frac{L}{L^*}\right)^{1/2} \tag{5.83}$$

To satisfy both numbers simultaneously

$$T_1 - T = (T_1^* - T^*) \left(\frac{L^*}{L}\right)^3 \frac{T_1}{T_1^*} \tag{5.84}$$

When a temperature excess $T_1^* - T^*$ exists in the prototype, the temperature excess in the model must be larger by the factor $(L^*/L)^3 (T_1/T_1^*)$. Since T_1 and T_1^* are absolute temperatures, their ratio is of the order of 1. However, a prototype building 30 ft high may be modeled by a building 1 ft high; so $(L^*/L)^3 = 30^3 = 27{,}000$. Evidently any significant temperature excess in full scale will require prohibitively high model equivalents, and Re and Fr′ cannot be satisfied simultaneously.

We now wish to determine the effect on the flow field of a failure to observe Re and Fr′ scaling. Inspection of Eq. 5.78 shows that the shear and buoyancy terms become less important as Re and Fr′ increase and may be dropped when Re and Fr′ are very large. In such cases neither Re nor Fr′ scaling need be observed. Physically, large Re occur when lengths and velocities are large, and large Fr′ occur when $T_1 - T$ approaches zero. The problem now is to assign numerical values to "large Re" and "large Fr′."

5-5.4.2.1 Reynolds Number Scaling. Let us consider the isothermal case ($Fr' = \infty$) first. An average value of ρ/μ for the atmosphere is 6000 ft^{-2} sec, and a 30-ft-high building in a 10 ft/sec wind would have Re = 1,800,000. A model test on a 1-ft-high building in a 4 ft/sec wind would have Re = 24,000. Thus Re is smaller, and the influence of the shear term in Eq. 5.78 is greater in model tests than in the field. Whether this increase in influence is enough to produce significant changes in the K_c field must be answered by experiments. Golden (1961) measured K_c values on and near the roofs of sharp-edged cubes resting on a raised ground board in a uniform mean-velocity low-turbulence tunnel airstream and found that all K_c values were substantially constant above a Re of 11,000 in a test range of $2{,}000 < Re < 90{,}000$. As Re was decreased below 11,000, the K_c values at the roof surface changed systematically, but those in space above the roof remained invariant. This behavior may be attributed to the greater viscous stresses near the roof surface where the mean-velocity gradients are steep. Since the influence of the shear term in Eq. 5.78 decreases with increasing Re, it will be conservative to adopt Re = 11,000 as a diffusion-critical Re, above which changes in the flow field due to changes in Re will not produce significant changes in the K_c fields of sharp-edged buildings. A lower value may be used if measurements are restricted to regions away from the building surfaces.

With this criterion K_c fields will be invariant for LV products greater than about 2 sq ft/sec. This will be the case in full scale for all except almost-zero wind speeds. The same invariance will be expected in the tunnel if 1-ft-high models are tested at wind speeds greater than 2 ft/sec.

To determine if a diffusion-critical Re exists for rounded buildings, we can refer to tests of a model of a typical industrial nuclear-power reactor containment structure [Halitsky, Golden, Halpern, and Wu (1963) and Sec. 5-5.5.2]. Values for K_c isopleths were obtained for a leak at the top of the vessel at wind velocities of 3, 10, and 15 ft/sec, corresponding to a Re range of $15{,}800 < Re < 79{,}000$. Isopleth loops drew closer to the source as Re increased, showing that K_c at a fixed point was decreasing and that a diffusion-critical Re had not yet been reached up to a value of Re = 79,000.

It may be that boundary-layer tripping devices commonly used in aeronautical testing to produce a turbulent boundary layer and thereby to artificially increase Re can be employed in diffusion testing to stabilize the K_c field, but this possibility has not been explored.

In summary, then, there is reasonable assurance that Re scaling is not required when

determining K_c fields for sharp-edged buildings by model experiments as long as the LV product is greater than 2 sq ft/sec. The corresponding LV product for rounded buildings would be at least an order of magnitude higher, but an exact value cannot be specified as yet.

5-5.4.2.2 Modified Froude Number Scaling. Since the effect of a modified Froude number on the buoyancy term in Eq. 5.78 parallels that of the Reynolds number on the shear term, we may suspect that a diffusion-critical Fr′ exists above which Fr′ scaling need not be observed. To investigate this possibility, Golden (1961) conducted heated-effluent tests on 5-in. and 15-in. cubes in a wind tunnel, using a temperature excess of 200°F above ambient. He found that K_c isopleths did not change much as Fr′ (calculated with $T_1 - T = 200°F$) was varied between 0.8 and 3.9. Since we know that Fr′ scaling becomes unimportant at very large values, we suggest that the range of Fr′ in which Fr′ scaling need not be observed in this configuration only is $0.8 < Fr' < \infty$.

In terms of full-scale conditions where L is 30 ft, V is 10 ft/sec, and effluent aperture diameter is 1 ft, this configuration could tolerate a temperature excess $(T_1 - T)$ up to about 100°F without producing a Fr′ lower than 0.8. This temperature excess is high enough to ensure that ordinary ventilation problems, such as occur with laboratory fume-hood exhausts of the same proportions as those tested, do not require Fr′ scaling.

A common scaling problem occurs with hot effluents from power-plant chimneys. The exhaust from a chimney terminating above the wake boundary will pass initially through a distorted flow zone created by the chimney but thereafter will diffuse in a region of smooth flow. Since the model scale for buildings with tall chimneys is about 1:200, a 10-ft chimney diameter will scale down to 0.6 in. If Fr′ scaling is used without temperature scaling, Fr′ reduces to Fr, the velocity scale becomes $1:(200)^{1/2} \approx 1:14$, and a full-scale average wind of 14 ft/sec at chimney-top level would scale down to 1 ft/sec in the tunnel. In the distorted flow region near the chimney top, the characteristic dimension is the chimney diameter, and Re for the region becomes 300, well below the diffusion-critical value. Therefore these length and velocity scales would not give accurate modeling in this region. When the hot plume leaves the distorted flow region and enters the quasi-potential flow, the dominant forces are the plume buoyancy and turbulence. Here Fr′ scaling but not Re scaling is required. Since initial diffusion effects are relatively unimportant when measuring ground concentrations far downwind from the stack, a small amount of scaling distortion in the plume near the stack is acceptable. However, this problem should be given careful consideration when measuring plume spread in tunnel tests of diffusion from isolated stacks discharging effluents at high temperatures and high emission velocities.

5-5.5 Experimental Data on Concentrations near Buildings

Published experimental data on concentrations close to buildings in a form suitable for prediction of full-scale concentrations apparently consist only of the wind-tunnel experiments conducted since 1958 in the 3.5- by 7-ft low-speed wind tunnel at New York University. The three tests and their important characteristics are reviewed below, and the results are presented in graphs of concentration coefficient K_c as a function of nondimensional space coordinates.

5-5.5.1 Prism Tests. [Figures 5.20 and 5.27; (Halitsky, 1963).] The models consisted of two rectangular prisms having edge-length proportions of 1:1:1 or as given in the legend for Fig. 5.20. The reference area was the area of the largest wall that could be turned normal to the wind. If the long edge is L, the reference areas are L^2 for buildings A and C and $0.33L^2$ for building B. The actual model L is 1.25 ft. The effluent was released from a flush vent with a diameter of L/30 located in the center of the roof. The models were mounted on a ground board and were exposed to a low-turbulence wind with a uniform-mean-velocity profile. The emission-velocity ratio V_e/V was equal to 1 unless otherwise noted. Temperatures were isothermal.

In using the K_c diagrams (Fig. 5.27) remember that all these data were obtained in an essentially nonturbulent airstream and that effective full-scale K_c values will be different. The transformation from model to full-scale

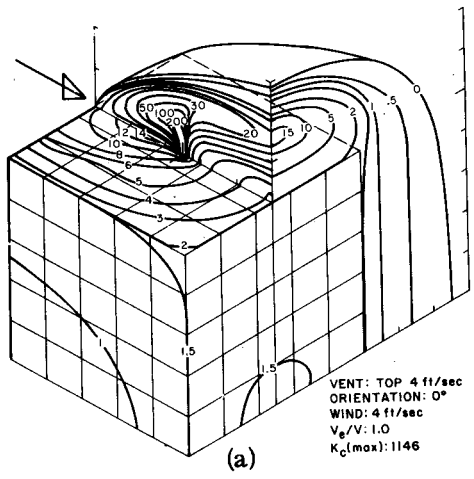
VENT: TOP 4 ft/sec
ORIENTATION: 0°
WIND: 4 ft/sec
V_e/V: 1.0
K_c(max): 1146

(a)

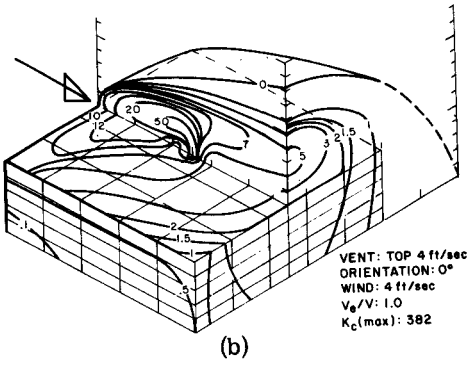
VENT: TOP 4 ft/sec
ORIENTATION: 0°
WIND: 4 ft/sec
V_e/V: 1.0
K_c(max): 382

(b)

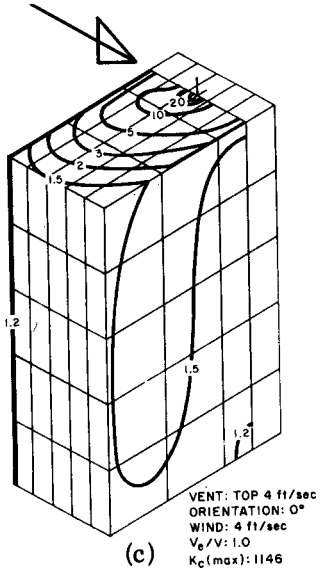
VENT: TOP 4 ft/sec
ORIENTATION: 0°
WIND: 4 ft/sec
V_e/V: 1.0
K_c(max): 1146

(c)

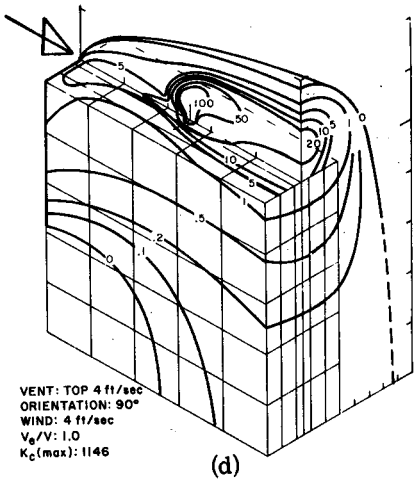
VENT: TOP 4 ft/sec
ORIENTATION: 90°
WIND: 4 ft/sec
V_e/V: 1.0
K_c(max): 1146

(d)

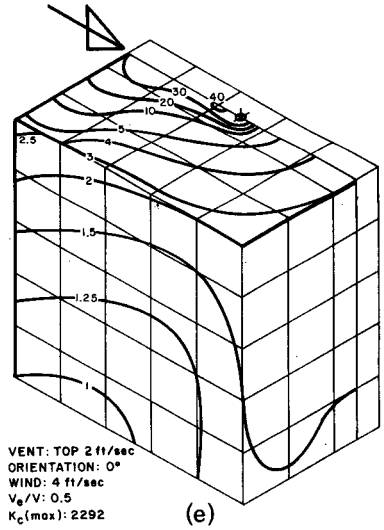
VENT: TOP 2 ft/sec
ORIENTATION: 0°
WIND: 4 ft/sec
V_e/V: 0.5
K_c(max): 2292

(e)

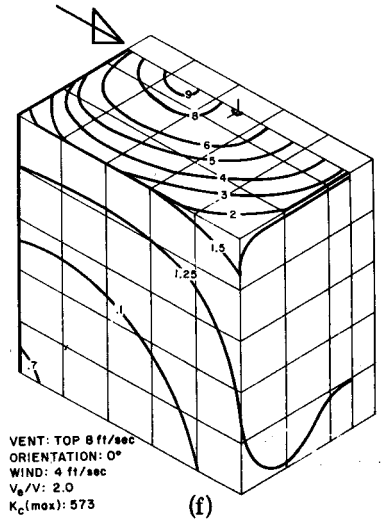
VENT: TOP 8 ft/sec
ORIENTATION: 0°
WIND: 4 ft/sec
V_e/V: 2.0
K_c(max): 573

(f)

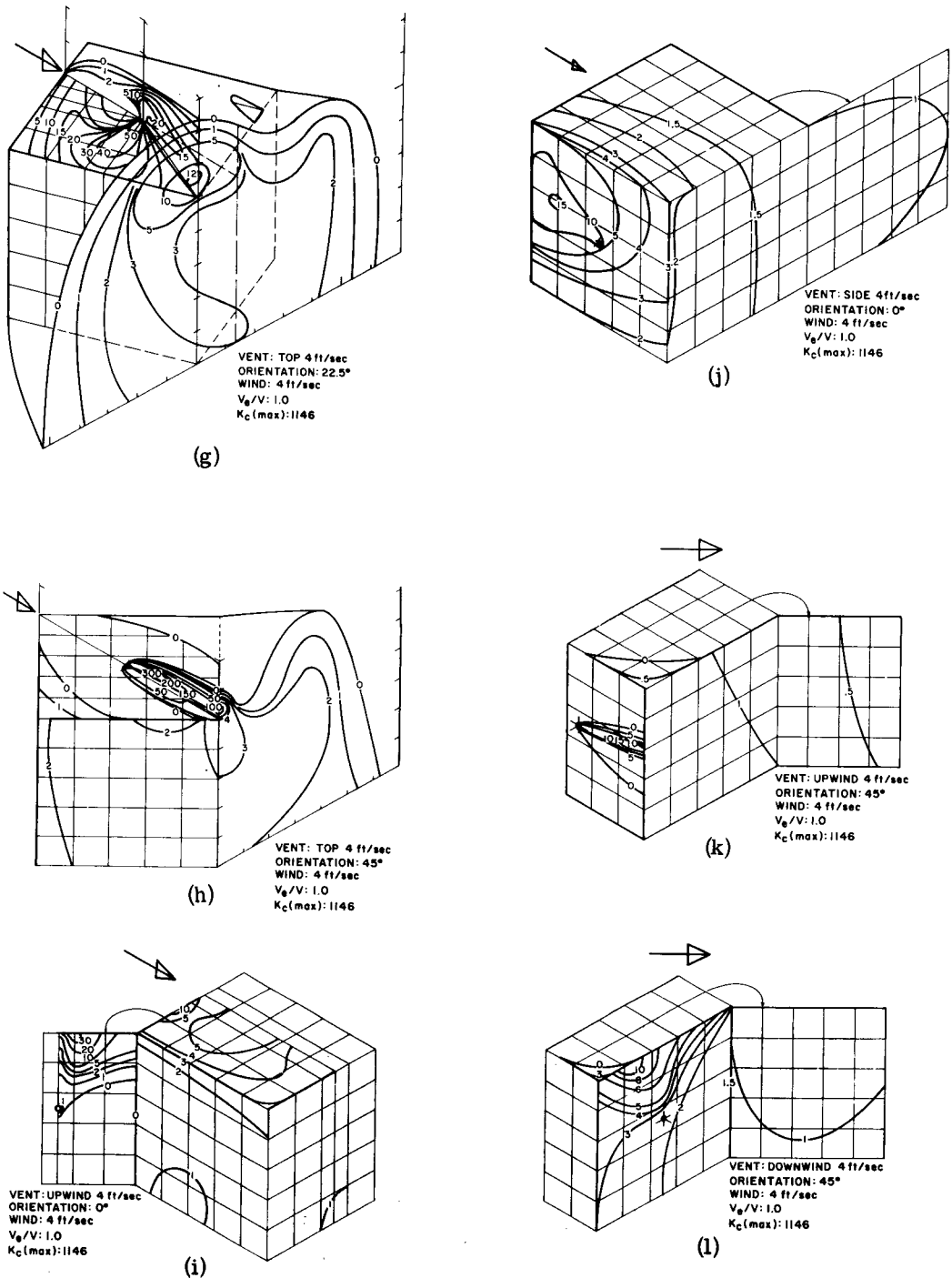

Fig. 5.27—K_c isopleths for tests of prisms with flush vents. Test data given in each panel. [From J. Halitsky, Gas Diffusion near Buildings, *ASHRAE (Am. Soc. Heating, Refrig. Air-cond. Engrs.) Trans.*, 69: 476-477 (1963).]

K_c values is currently being studied (Halitsky, 1965a). Preliminary results indicate that a full-scale K_c field can be approximated by weighting the test values of K_c at each point according to a probability distribution based on the variance of the wind angle for a given atmospheric condition. However, this requires the separate measurement of K_c fields at small increments of tunnel-wind angle. Since the data in the following tests were taken for only a few wind angles, study of the patterns combined with some intuition is needed to make an intelligent guess at the probable full-scale K_c field. In general, the K_c peaks and gradients on the roof will be smaller than those in the model, and concentrations will appear where none were indicated in a nonturbulent wind. On the side walls K_c values should be about the same as in the model if the wall is continually in the cavity and proportionally smaller if the wall emerges from the cavity for part of the time.

5-5.5.2 Nuclear-reactor Shell Tests. [Figures 5.23, 5.28, 5.29, and 5.30; (Halitsky, Golden, Halpern, and Wu, 1963).] The prototype of the reactor shell and auxiliary building was the EBR-2 complex at the National Reactor Testing Station, Idaho Falls, Idaho. The shell consisted of a hemisphere on a vertical cylinder of diameter D_0, overall height, H, 1.225 D_0, and reference area, A, 1.118 D_0^2. The actual model D_0 was 0.833 ft. The effluent was released at several points on the surface of the shell through holes of diameter 0.0063 D_0. The mean-wind profile represented a full-scale logarithmic profile given by $\bar{u} = (v_*/k) \ln (z/z_0)$ with $v_* = 25$ cm/sec and $z_0 = 1.5$ cm, scaled down according to a velocity scale of 1 : 3 and length scale 1 : 96. The emission velocity ranged from 0.2 to 8.1 ft/sec. The tunnel velocity was 5.54 ft/sec at an elevation of $2D_0$. Temperature gradients were isothermal.

In using the K_c graphs from this test, take into consideration the remarks in Secs. 5-5.2.2.3 and 5-5.4.2.1 on Reynolds-number scaling and the remarks in Secs. 5-5.4.1 and 5-5.5.1 on wind scaling. At the test wind velocity, the Reynolds number was not high enough to establish a fixed separation line. Also, even though the mean-velocity profile was logarithmic, the value of $\sigma_u/\bar{u}$ in the approach wind was probably about 0.04 at the midheight of the shell, corresponding to very low atmospheric turbulence.

In the isopleth graphs the maximum value of K_c that appeared on an imaginary surface surrounding the reactor shell at a distance d from the shell was found to be represented by the approximate relation

$$K_{c\,max.} = \frac{10}{(d/D_0)^2} \qquad (5.85)$$

where D_0 is the diameter of the base of the shell. Equation 5.85 was found to hold in the range $0.5 < d/D_0 < 3$ for all gas-release points in all wind directions and did not show much variation over a range of wind velocities from 3 to 15 ft/sec.

5-5.5.3 Clinical Center Test. (Halitsky, 1962) The prototype of the complex was the Clinical Center and surroundings at the National Institutes of Health, Bethesda, Md. The model was built to a linear scale of 1 : 240. The approach wind was the normal low-turbulence tunnel airstream with a mean velocity of 4 ft/sec, corresponding to a full-scale wind of 12 ft/sec, or a velocity scale of 1 : 3. The building air-intake and -discharge openings on the roof of the several wings functioned with volume flows scaled according to $1 : (240^2)\ (3) = 1 : 172{,}800$. The average emission-velocity ratio was $V_e/V = 2.22$ at the test wind velocity. Temperatures were isothermal.

This test was carried out in a different manner from the preceding two tests since the aim was not to determine K_c fields but to establish dilutions between specific exhaust and intake openings. The test procedure was to release gas in a given exhaust jet and to determine K_c at each intake opening in eight wind directions. The value of K_{ce} at the exhaust opening was calculated by Eq. 5.71, and the value of dilution, $D = K_{ce}/K_c$, was established for each combination. A simple mathematical model of a jet in a transverse airstream resulted in the following equation relating the dilution D to a nondimensional distance $s/(A_e)^{1/2}$, where s is the shortest arc distance from exhaust to intake and A_e is the area of the exhaust opening:

$$D = \left[\alpha + \beta \frac{s}{(A_e)^{1/2}}\right]^2 \qquad (5.86)$$

When the test data for all combinations of D and $s/(A_e)^{1/2}$ were plotted on a graph with D as

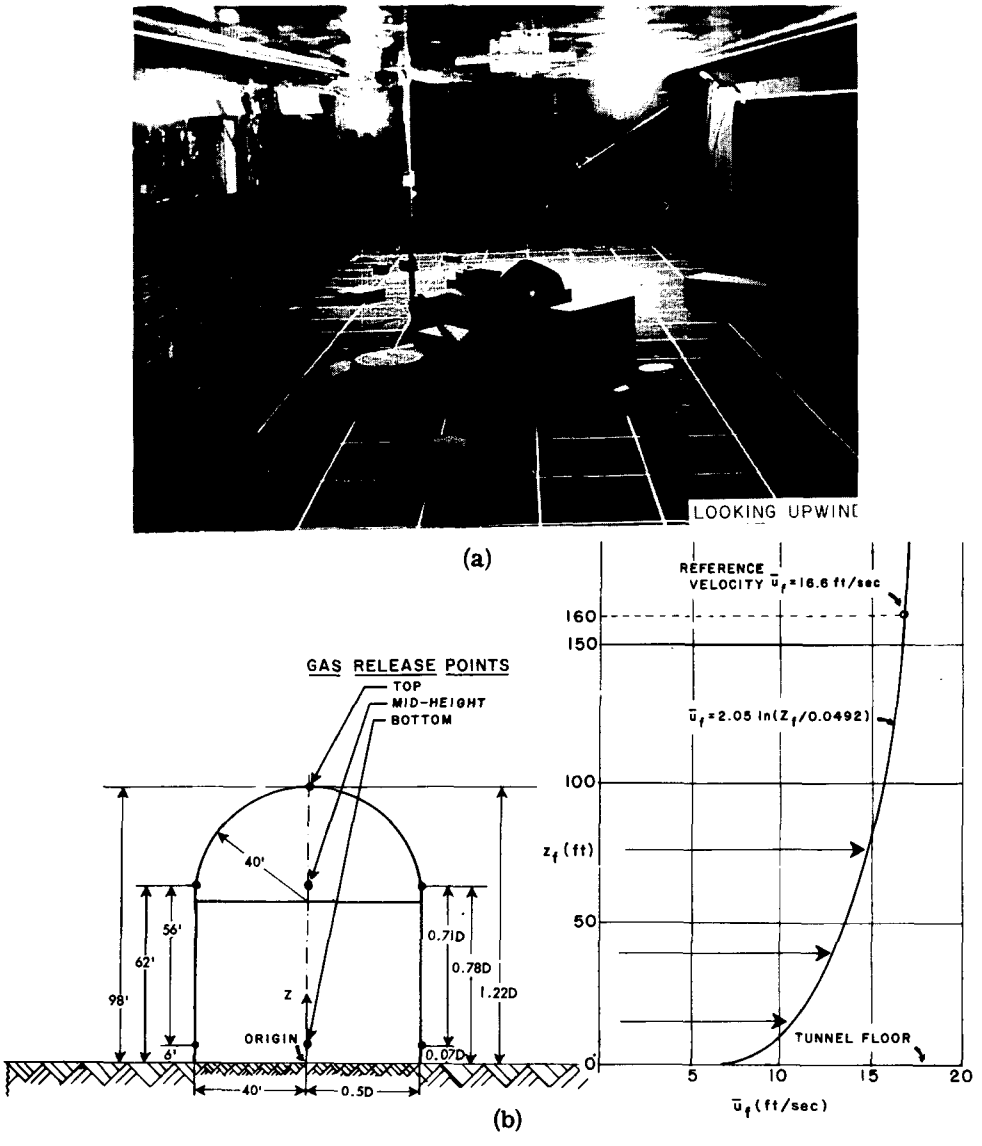

Fig. 5.28—Reactor shell test configuration. (a) Model and auxiliary buildings in the wind tunnel. (b) Full-scale dimensions (ft) and mean-velocity profile (ft/sec). (From Halitsky, Golden, Halpern, and Wu, 1963.)

ordinate, it was possible to select constants α and β that allowed Eq. 5.86 to be plotted as a parabola bounding the data from below. Although there was considerable scatter of the data above the curve, the absence of test points below the curve implied that at a given separation distance no dilutions less than those given by the curve had been found and therefore the curve could be used conservatively for design purposes.

The scatter above the curve, indicating greater dilution or lower concentration at the intake, was interpreted as resulting from the intake's not being on the plume center line for the given building orientation. In fact, for some combinations the intake would never be on the plume center line. This possibility was introduced into the formula by adding a factor M, which effectively displaced the curve upward and thereby provided some relief for different configurations. With an additional adjustment for emission-velocity ratio, the final equation became

$$D = 2.22\, M \left[3.16 + 0.1 \frac{s}{(A_e)^{1/2}}\right]^2 \frac{V}{V_e} \qquad (5.87)$$

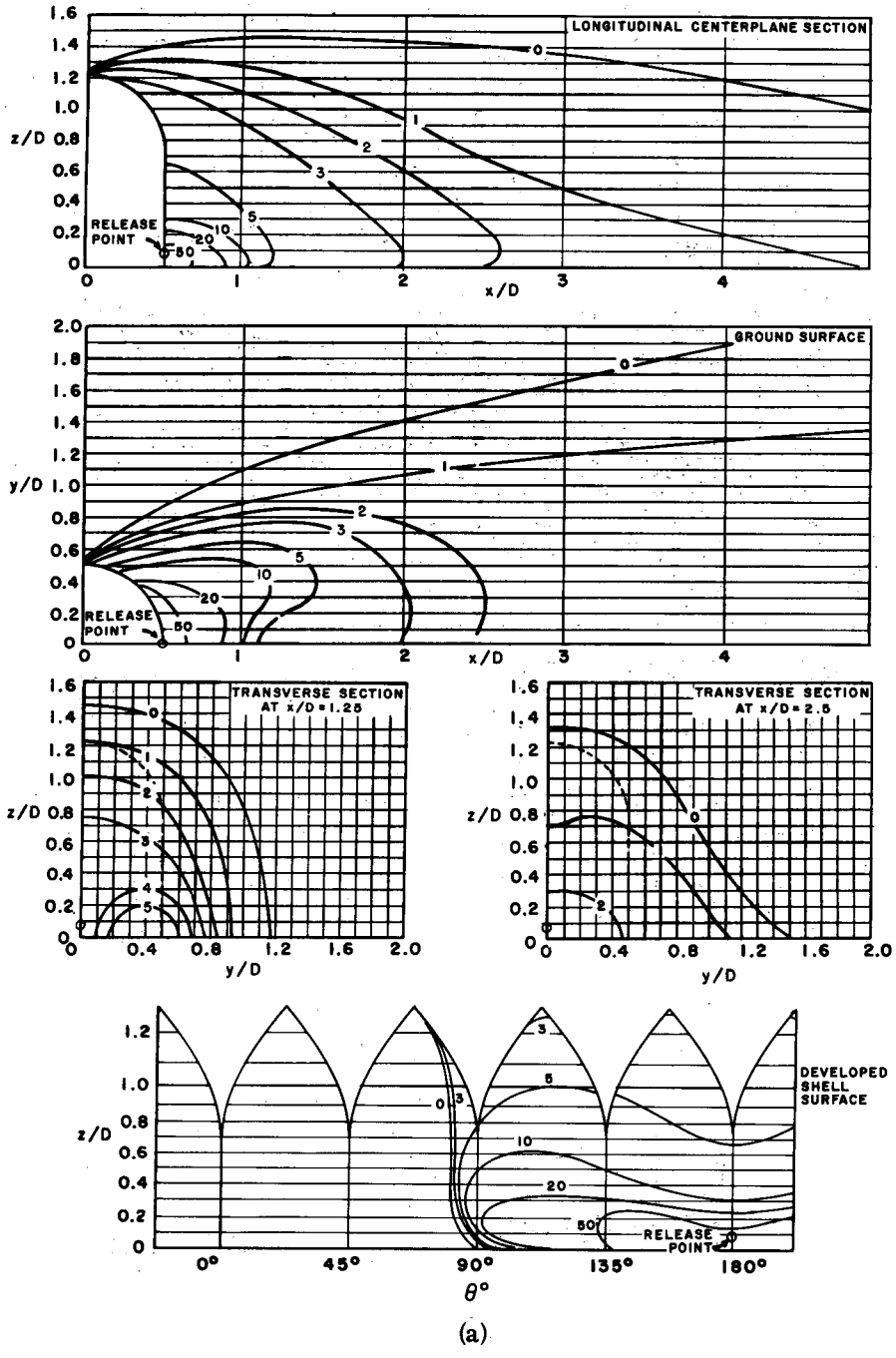

(a)

Fig. 5.29a—K_c isopleths for reactor shell with leaks. Logarithmic profile for wind. Release point, bottom and downwind. (From Halitsky, Golden, Halpern, and Wu, 1963.)

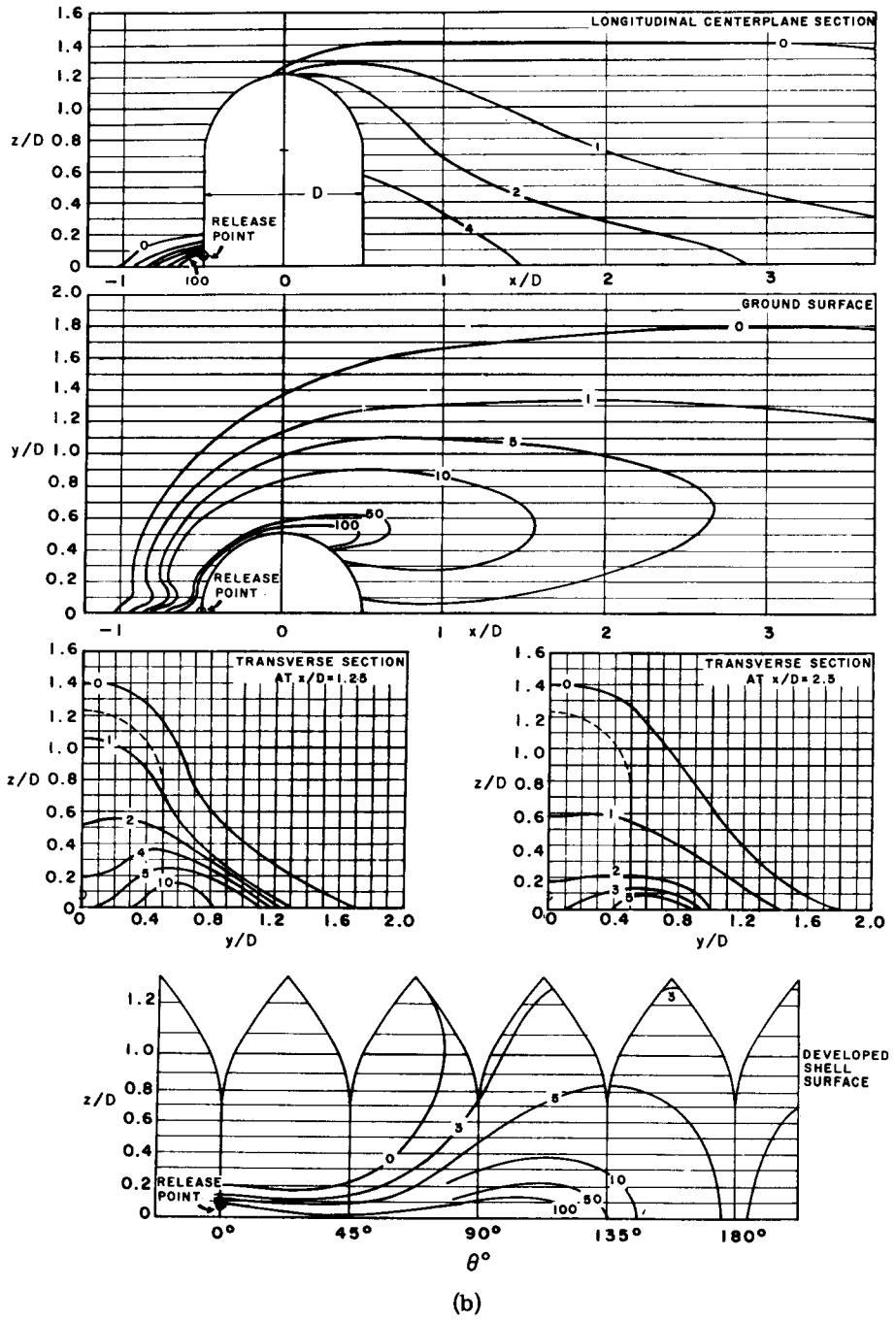

(b)

Fig. 5.29b—K_c isopleths for reactor shell with leaks. Logarithmic profile for wind. Release point, bottom and upwind. (From Halitsky, Golden, Halpern, and Wu, 1963.)

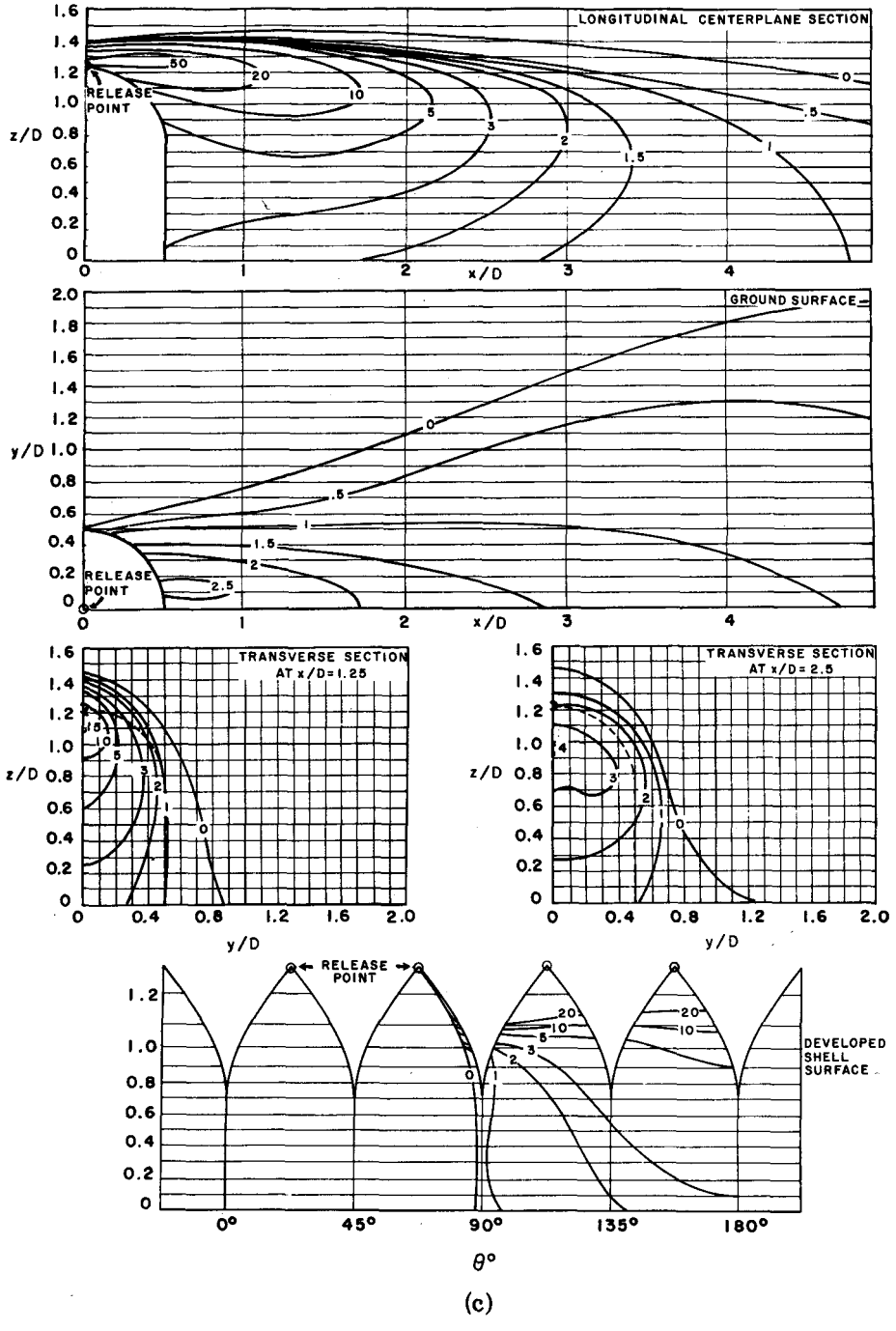

(c)

Fig. 2.29c — K_c isopleths for reactor shell with leaks. Logarithmic profile for wind. Release point, top. (From Halitsky, Golden, Halpern, and Wu, 1963.)

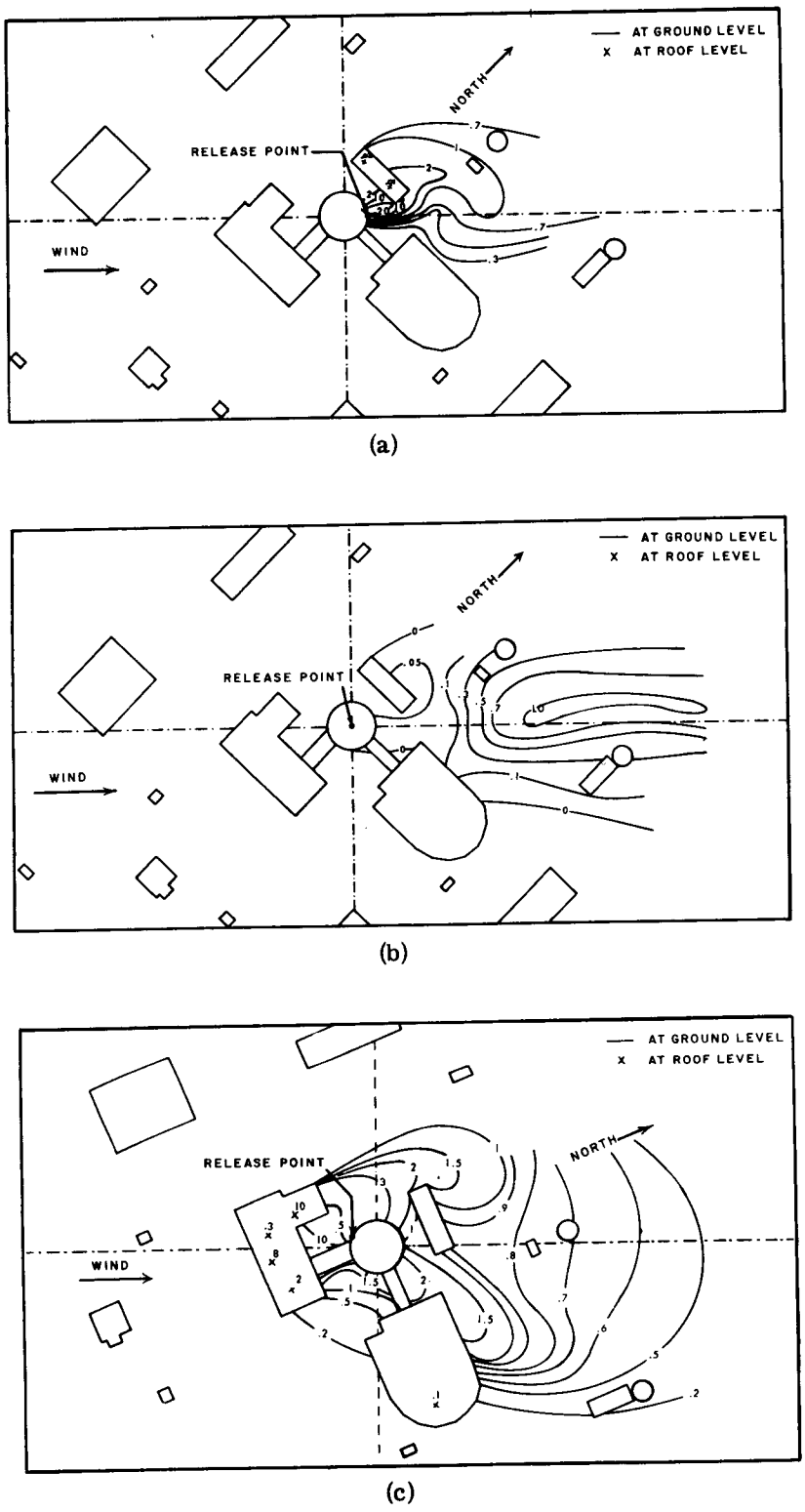

Fig. 5.30—K_c isopleths for reactor complex. (a) Downwind release. (b) Top release. (c) Upwind release. (From Halitsky, Golden, Halpern, and Wu, 1963.)

The suggested values of M were 1.5 for exhaust and intake on the same roof, 2.0 for exhaust and intake on wings separated by an air space, and 4.0 for exhaust on roof and intake in the cavity near ground level.

The factor V/V_e provides a correction for greater dilution at higher wind velocities. It does not, however, provide for changes in the vertical throw of the jet due to a change in velocity ratio. This can be quite important if the jet from a flush roof vent bends over and impinges on an intake in the side of a cupola. An increase of V_e/V may carry the jet axis over the cupola and produce low concentrations and an effectively higher dilution at the intake. The use of the V/V_e factor in Eq. 5.87 would show an opposite trend.

5-5.5.4 Dugway Urban Area Tests. (Kalinske, Jensen, and Schadt, 1945 and 1945a.) In 1945 wind-tunnel tests of diffusion from a continuous area source in the streets of an urban district were conducted in a 4- by 6-ft wind tunnel at the Iowa Institute for Hydraulic Research. The concentration field was measured vertically and horizontally among the buildings downwind of the source, and the results were converted to an equivalent K_c defined as $\bar{\chi}L^2V/Q'$. In the absence of a characteristic physical length, the reference length L was taken as 1 ft for the prototype and the equivalent scaled-down value for the model, and V was taken as equal to the airstream mean velocity above the boundary layer created by the buildings on the floor of the tunnel.

Although vertical diffusion was restricted in this case by the reduction of turbulence to zero at the top of the boundary layer, a method was developed whereby steady-state tunnel results could be correlated with field burst-type measurements, and discrepancies could be eliminated by selection of appropriate numerical coefficients. It was reported that "the accuracy obtained from such conversion is at least as good as the accuracy of single field measurements."

5-5.6 Applications

5-5.6.1 General Approach. The concentration at any point in a flow field can be expressed as the product of an average concentration Q'/AV and a concentration coefficient K_c. In a practical case the source strength Q′, reference area A, and velocity V are fixed by the design specifications, and the problem becomes one of determining the values of K_c at the point where the concentration is to be estimated.

At every point in the three-dimensional diffusion field around a source, K_c has a numerical value, and it has the same value at corresponding points of similar fields. If similarity can be established between two diffusion situations differing only in scale, the distribution of K_c obtained in one situation can be used for the calculation of concentrations in the other. Concentrations near buildings can thus be estimated from wind-tunnel data if similarity can be shown to exist. The similarity requirements are given in a statement of the nondimensionalized source distribution and the flow-field boundary conditions, called the configuration, and in hydrodynamic parameters of the flow field. Similarity is established if the configuration coefficients and certain hydrodynamic parameters have the same numerical value on all scales.

The important configuration specifications for concentration fields near buildings include the source distribution, a statement of how A and V are to be measured, the geometric characteristics of the building and terrain, the orientation of the building to the mean wind, the mean and turbulent velocities $\bar{u}$ and $\sigma_{u,v,w}$ in the background flow, the mean velocities in the exhaust and intake apertures V_e and V_i, and the maximum temperature excess in the flow field over the temperature of the background flow $(T_1 - T)$. The nondimensionalizing constants are V for velocities, $L = (A)^{1/2}$ for length, and the absolute temperature of the background flow, T, for temperatures. Under adiabatic conditions the logarithmic wind profile given by $\bar{u}/v_* = (1/k) \ln (z/z_0)$ will be reproduced if v_*/V and z_0/L are maintained constant.

The hydrodynamic parameters are the Reynolds number $Re = LV/\nu$, the modified Froude number $Fr' = V^2T/Lg(T_1 - T)$, and fL/V, where f is the peak frequency of the background-flow energy spectrum.

5-5.6.2 Sources Within the Cavity. Three techniques have evolved from experience in applying model data to full-scale conditions. The first is the order-of-magnitude approach using char-

acteristic values of K_c at various points near buildings without considering the details of the configuration (see Sec. 5-5.3.3). The second involves matching a given full-scale configuration to one of the model test configurations. The third seeks to specify the decrease in concentration in a hypothetical effluent jet or plume without considering the shape of the axis (see Secs. 5-5.5.3 and 5-5.6.4). It is often useful to compare the results from the three methods to judge the reliability of any one.

The accuracy of prediction of full-scale concentrations on the basis of K_c values in Sec. 5-5.5 is thought to be within a factor of 3 for short-period peak concentrations and for mean concentrations in very steady low-turbulence winds. On the basis of recent and as yet unpublished test data (Halitsky, 1965a), it would appear that the tunnel data overestimate the time-mean values in adiabatic conditions by factors up to possibly 10. The following discussions of testing procedures may be helpful in making the best choice of available K_c values and in conducting future tests with a minimum of procedural error.

In practical testing, Re and Fr′ cannot be maintained constant simultaneously over a change in scale, but the errors introduced into the K_c field by ignoring these criteria have been found to be negligible for sharp-edged buildings whose LV product is greater than 2 sq ft/sec and whose maximum temperature difference, $T_1 - T$, is less than 100°F. Rounded buildings have a considerably higher critical LV product, but such values have not been established. The turbulent wind energy peak at roof level (for vertical oscillations at least) occurs in the atmosphere at $f\,L/V \approx 0.2$. Therefore the time for one significant oscillation of the wind is $1/f \approx 5L/V$, and the distance traveled by an air parcel in this time is 5L. This is of the same order as the length of the cavity, a fact that indicates the time-mean cavity flow in the tunnel will not be similar if the frequency of the characteristic wind oscillation in the tunnel is greater than 0.2 V/L. With customary tunnel values of L = 1 ft and V = 5 ft/sec, the maximum characteristic frequency of tunnel oscillations should be about 1 cycle/sec. There is no lower limit to the characteristic testing frequency, but the sampling time required to obtain a true mean K_c value should be in excess of 1/f.

The model test data in Sec. 5-5.5 were obtained under isothermal conditions and with LV products varying from 5 to 10 sq ft/sec; therefore the prism and Clinical Center tests can be assumed to be free of Re and Fr′ inaccuracies. The nuclear-reactor shell test probably had a Re scaling defect. The approach-wind profile was different in each test, and this should be noted in using the data. The failure to scale the approach-wind characteristics in the Clinical Center test was mitigated by the presence of auxiliary buildings and trees, which introduced aerodynamic flow distortions comparable to those occurring in full scale. Long-period oscillations were not introduced in any of the tests.

5-5.6.3 Sources Above the Building Cavity. When the stack height is such that the effluent is discharged near the cavity boundary over the roof, the momentum in the effluent is usually sufficient to carry the gas outside the cavity, but the lower edge of the expanding plume may pass through the cavity boundary and thus provide a secondary source of building contamination. A method for calculating the stack height needed to limit the concentration at the building surface to a stated amount is given by Halitsky (1965).

Raising the release point still higher will prevent the plume from entering the cavity and thus prevent gas recirculation to the building, but, if the release point is not high enough, the combination of aerodynamic downwash and large wake turbulence can cause the gas to reach the ground closer to the stack and produce a higher maximum ground concentration than in the absence of the building.

If the mean velocity and turbulence in the wake can be defined, ground concentrations can be estimated by conventional diffusion equations. The plume is assumed to diffuse uniformly about a curved center line whose coordinates are calculated by procedures outlined in Sec. 5-2. However, the plume rise is referred to the curved streamline through the stack top rather than to a horizontal one. This system is feasible if the curvature is small and the turbulence is fairly homogeneous.

Another theoretical approach, suggested by Burger (1964), employs a hypothetical potential flow outside the cavity to simulate the streamlines and combines the flow properties

analytically with the Fickian diffusion equation. The flow used by Burger is that around a Rankine oval, suggested originally by Arie and Rouse (1956) but modified in proportions to represent a three-dimensional building. Burger illustrates his analysis by calculating the required stack height for various locations of a stack on a building such that a given ground concentration is not exceeded.

All theoretical approaches to this problem have in common a lack of information on streamline curvature and turbulence distribution in wakes. Even the data on the wake of a suspended flat plate (Sec. 5-5.2.2.1) contain a gap about $5 \leq x/L \leq 20$, which is particularly unfortunate since a rapid wake expansion seems to take place in this region, as evidenced by the discrepancies in wake-boundary radius given by Eqs. 5.67 and 5.68 and illustrated in (b) of Fig. 5.18. The wind-tunnel work of Arie and Rouse (1956) on wake flow measurements downwind of a two-dimensional fence in a uniform flow and that of Nagabhushanaiah (1961) in a floor boundary layer are helpful in this respect, but they should be augmented by three-dimensional studies in airstreams with controlled mean-velocity profiles and turbulence. Detailed wake measurements in the lee of buildings in a natural wind would, of course, be most desirable.

Wind-tunnel testing is a feasible method for determining ground concentrations for plumes that intersect the wake beyond the cavity, but greater care must be taken to introduce appropriate background turbulence than in the case of sources within the cavity. In both cases aerodynamically generated turbulence and background turbulence contribute to plume diffusion, but in the cavity the aerodynamic turbulence is dominant, and in the wake the background turbulence assumes increasingly greater control as the wake turbulence decays with distance downwind (Islitzer, 1965).

No wind-tunnel measurements of concentrations in plumes that have descended into the wake appear in the literature owing partly to the limited number of facilities available for this type of test and partly to the policy of industrial sponsors not to release such information. It would appear that a major contribution can be made by systematically measuring the K_c fields for medium-height stacks on top of or adjacent to buildings.

Many wind-tunnel tests of power plants discharging furnace effluents at high temperature and velocity through medium-height stacks have been conducted without concentration measurements. The height of the bottom of the plume at a specified downwind distance is used as a criterion for ground contamination. At low wind velocity the plume is usually high above the ground. As the wind velocity increases, the thermal and velocity rise are progressively reduced, and a velocity is reached at which the bottom of the plume just touches the reference level. This critical wind velocity is determined by test as a function of stack height, stack arrangement, emission velocity, emission temperature, and/or other configuration variables. A suitable arrangement is chosen by estimating from weather data the number of annual hours that the natural wind can be expected to have velocities in excess of the critical and thereby cause ground contamination at distances beyond the reference station. If the critical wind velocity is sufficiently high, the hours of contamination will be few and the concentrations small. The procedure can be made increasingly conservative by placing the sampling station farther downwind. Test results of this type are reviewed by G. H. Strom in "Atmospheric Dispersion of Stack Effluents" (Chap. 6, Stern, 1962). Lord, Baines, and Leutheusser (1964) have reported more generalized tests of stacks near box-shaped buildings with various criteria relating to the character of the bottom of the plume.

Full-scale ground concentration measurements of dye released in the stub stack of a building, such as those by Munn and Cole (1965), have practical interest in that they are representative of real configurations, but the data have limited applicability to isolated buildings since effects of heated plume rise and effects of multiple wake interactions with auxiliary buildings cannot be separated.

5-5.6.4 Sources in Transverse Jets. A configuration frequently encountered in laboratory buildings is a flush roof vent or short chimney discharging a transverse jet with insufficient momentum to break through the roof of the cavity or to pass over a nearby fresh-air intake. In this arrangement the intake is exposed not only to the general cavity concentration but also to the higher concentration

in the jet plume. When the distance from the effluent aperture to the intake is greater than about 10 or 20 diameters, the formula derived from the Clinical Center test data can be used to estimate the axial plume concentration (Sec. 5-5.5.3).

At closer spacings more attention must be given to the center-line trajectory and the influence of jet velocity on the rate of decay of concentration with distance along and normal to the jet center line. Halitsky (1966) treats this aspect in a semiempirical approach based on published data on transverse jet velocity and temperature distributions. Provision is made in the paper for extending the method to include the prism, Clinical Center, and reactor-shell test data and for estimating the location of the virtual point source for tall-chimney releases in an atmosphere with known diffusion coefficients.

Chapter 6

Meteorological Instruments for Use in the Atomic Energy Industry

Harry Moses*

With contributions from Elmer Robinson,†
Maynard E. Smith,‡ Gerald C. Gill,§
Eugene M. Wilkins,¶ and C. Ray Dickson**

6-1 INTRODUCTION

The type of meteorological-data acquisition system required for the nuclear-energy industry varies with the nature of the process contemplated, with the geographical and meteorological features of the site considered, and with quantity and type of potential receptors. The magnitude and diversity of the operations at, for instance, the Atomic Energy Commission site at Richland, Wash., have dictated a meteorological system that has at one time or another employed every type of sensor discussed in this chapter. In contrast, the observational requirements of many small facilities have been met by one or a few commercially available systems of the simplest variety, i.e., systems providing only relatively crude records of wind, temperature, and precipitation. No attempt will be made here, and indeed no attempt can be made, to specify the types and quantities of meteorological instruments and equipment required in particular situations. Instead a broad survey of appropriate instrumentation will be presented. In the case of wind instruments, the characteristics of the sensors will be discussed in some detail since a correct choice will depend in some measure on these features.

One of the most prominent uses of meteorological instrumentation in the atomic energy field is in the evaluation of sites for nuclear installations. Foregoing chapters have emphasized the problems involved, and here we need note only that when any substantial hazard is believed to exist it is prudent to examine the meteorology of the site. For this reason the Atomic Energy Commission requires that a meteorological site survey be made before a license to operate a reactor is granted. Meteorological information obtained in this manner provides a reliable basis for hazards evaluations by the Advisory Committee on Reactor Safeguards and by the Division of Reactor Licensing of the AEC. Thus a consideration of site meteorology is a routine feature of site evaluation, and it is not unusual for some meteorological measurements to be made in order to develop adequate detail.

The number of locations on a site at which meteorological measurements are necessary depends on the complexity of the terrain and the estimated distances to which abnormal behavior of the nuclear system would cause concern in the environs. For example, the study of a hill–valley complex that might

*Radiological Physics Division, Argonne National Laboratory, Argonne, Illinois.
†Stanford Research Institute, Menlo Park, California.
‡Instrumentation and Health Physics Division, Brookhaven National Laboratory, Upton, New York.
§Department of Meteorology and Oceanography, University of Michigan, Ann Arbor, Michigan.
¶Ling-Temco-Vought Research Center, Dallas, Texas.
**Air Resources Field Research Office, Idaho Falls, Idaho.

materially influence wind-flow patterns would require additional wind-measuring points. The same would be true for studies near bodies of water over which sea-breeze circulations may be formed, for large forested areas, and for cities. Decisions concerning the number and locations of on-site meteorological stations must depend on the judgment of a competent meteorologist working in close association with nuclear technologists and with health safety personnel.

After a nuclear facility has become operative, there may be a continuing need for reduced meteorological surveillance. In some cases this may be necessary to conduct operations in the safest possible manner; in others, to achieve a greater measure of operating efficiency. The operational modes of the facility should be kept in mind when selecting the meteorological equipment for the initial site survey since in all probability one set of instruments can be used to fulfill both functions.

6-2 THE MEASUREMENT OF METEOROLOGICAL VARIABLES IN THE ATOMIC ENERGY INDUSTRY

Most meteorological problems relating to nuclear energy concern the diffusion of airborne materials. This, in turn, implies that the basic operational data must include measurements of wind direction and wind speed and often an estimate of the turbulent nature of the flow. This latter can be measured directly with wind instrumentation, or it can be inferred from measurements of atmospheric stability, a function of both the wind flow and the vertical thermal stratification. Thus by far the greatest emphasis in this chapter will be placed on measuring and recording wind data and the vertical temperature structure.

Diffusion experiments, such as those discussed in Chap. 4, are not usually a part of the site evaluation or subsequent meteorological program at most reactor sites. However, to give some idea of the nature of diffusion-experiment technology to those who might consider such a program, we will include a section on atmospheric tracers and tracer techniques in this chapter.

It is occasionally necessary to measure meteorological variables which may be of secondary importance in the diffusion and transport problem but which are required in a variety of other contexts. Therefore discussions of equipment for observing precipitation, solar and net radiation, atmospheric pressure, and humidity are presented in later sections of this chapter.

Since many meteorological surveys involve considerable detail and therefore extensive processing of the data, it is important to consider at the outset the form of recording that is most desirable for each individual problem. Because of the large number of measurements made routinely, especially at the larger installations, the handling of data becomes a serious problem unless automatic techniques are adopted. For this reason all the meteorological groups at the national laboratories currently employ some form of automatic data-processing system. A section dealing with this subject emphasizes the relative capabilities and processing speeds of commonly used recording systems.

6-3 PLATFORMS FOR METEOROLOGICAL MEASUREMENTS

When elevated measurements of wind, temperature, or relative humidity are made, a platform is needed for mounting the meteorological sensors. Such platforms can take many forms, e.g., poles, towers of various cross-sectional sizes and of different types of lattice construction, and even buildings, though the latter form is seldom recommended.

Two types of poles can be used for mounting instruments: wooden poles, such as the conventional utility pole, having a diameter of about 1 ft near the ground and tapering slightly and metal poles generally made in a tubular construction with aluminum for relatively short poles and cold-rolled steel for tall ones.

Wooden utility poles are quite suitable for mounting anemometers to a height as great as 25 m above the ground. Such poles are often unguyed but are sunk about 3 m into the ground. Steel step bolts can be used for climbing. Unguyed tubular steel masts as high as 60 m

are commercially available for mounting radio and television antennas but might well be used for mounting meteorological instruments. Such masts are mounted on a concrete base and taper from 0.5 m near the bottom to 0.1 m at 60 m. They can be purchased with adjustable side arms for attaching sensors. Assembly of the sections, which range from 3 to 8 m, is generally made at the ground. Unguyed masts are quite expensive, and guyed masts can be used at a considerable saving.

A wide variety of towers is commercially available. Because of the need for mounting radio and television antennas, such towers are mass-produced and are comparatively inexpensive up to heights of about 25 m. These towers can be quite adequate for conducting a survey of several years' duration. They can be hinged and lowered for servicing or have ladder rungs. Some are telescoping in design. The cost of such towers varies linearly with their height.

Towers of intermediate size, i.e., from about 25 to 60 m, can be furnished either with or without guying. An unguyed tower, however, costs approximately three times as much as one with guying. In deciding upon a tower, one must be careful to determine the stresses to which it may be subjected. For example, some towers will withstand stresses from winds of about 30 m/sec; others will withstand stresses from 70 m/sec winds. The probability of high winds must always be considered in selecting a suitable platform.

Very high towers, i.e., those exceeding 100 m, are used only rarely and for special purposes, e.g., at a large national laboratory or for very special problems, such as the 470-m tower at the Nevada Test Site. For special research purposes television towers, such as the 430-m tower at Cedar Hill, Tex. (Gerhardt, Mitcham, and Straiton, 1962), have also been used.

It is interesting to note that, as of mid-1967, 188 television or radio towers taller than 300 m (with five slightly taller than 600 m), have been built in the United States and another 80 towers taller than 300 m are in the planning stage. In addition, there are at least as many towers in the height range from 150 to 300 m. Although the expense and complication of placing meteorological sensors on these tall towers are great, there will be instances that justify such an effort. A current listing of the heights and locations of television towers in the United States can be found in the *Television Fact Book*, an annual publication prepared by Television Digest, Inc. of Washington, D. C.

Side arms or booms extending from towers are generally about 3 m in length. The direction in which the booms extend should be selected with a knowledge of the least-frequent wind direction so as to minimize the tower wind-shadow effect (Moses and Daubek, 1961). A discussion of the errors in measurement of wind speed and direction for sensors mounted on openwork towers and on stacks is given by Gill, Olsson, and Suda (1966). At low speeds the tower effect can produce a substantial reduction in the measured wind. Anemometers are generally mounted some distance above the booms, and thermal elements are mounted below the booms. Humidity elements can be mounted on the booms.

Any high tower causes a deformation of the equipotential surfaces of the earth's electric field, especially if the tower is located in an unobstructed area. Since a high tower or even one of the order of 15 m may invite lightning strokes, it is essential to take necessary precautions to suitably ground the tower and avoid lightning damage to the meteorological instrumentation.

6-4 WIND MEASUREMENTS

6-4.1 Wind Speed

There are many types of instruments for measuring wind speed. The following classification given by Middleton and Spilhaus (1953) illustrates the different types that have been used at various times:

1. Rotation anemometers
   a. Propeller or windmill anemometers
   b. Cup anemometers
   c. Special types
2. Pressure-plate anemometers
   a. Plate allowed to swing
   b. Plate held normal to the wind
3. Bridled cup anemometers
4. Pressure-tube anemometers
5. Anemometers dependent on cooling
   a. The hot-wire anemometer
   b. The Kata anemometer
   c. The heated-thermometer anemometer

6-4.1.1 Commonly Used Wind-speed Systems. The most commonly used wind-speed measurement system is the cup anemometer revolving about a vertical shaft. High-quality instruments that meet U. S. Weather Bureau and Federal Aviation Agency specifications are durable and accurate and will give years of reliable service with little maintenance. Such instruments usually employ a cup wheel 38 to 45 cm in diameter from the center of rotation to the center of the cups and utilize conical beaded cups about 10 cm in diameter. Above speeds of 1 m/sec, the rate of rotation of the cups is essentially linear with wind speeds up to about 30 m/sec.

For accurate wind measurements at low speeds and for more sensitivity (more-rapid response to fluctuations in wind speed), small three-cup anemometers have been developed. These have an arm length, i.e., from the center of rotation to the center of the cup, of about 7.5 cm and a cup diameter of 5 cm. The cups are made of either plastic or very thin aluminum. The moment of inertia of such anemometers is appreciably smaller than that of the standard Weather Bureau or Federal Aviation Agency type. In addition, these instruments minimize friction with miniature ball bearings and frequently employ a light beam–photocell arrangement for transmitting information concerning the rotation of the cups. Several standard lightweight cup anemometers are shown in Fig. 6.1.

During steady rotation of a cup anemometer, the linear speed of the wind is about two or three times as great as the linear speed of a point on the center of a cup. When Robinson (1850) wrote about the cup anemometer, he indicated that this factor was equal to 3; later work by Brazier (1914), Patterson (1926), and others, however, indicates that this factor is neither constant over the range of speeds used nor is it a factor of 3 but that it varies between 2 and 3 depending upon such factors as the arm length, cup diameter, moment of inertia of the cups, ratio of cup diameter to arm length, and density of material of which the system is made.

Originally, four cups were used. Patterson indicated that a wheel of three cups was preferable because of the more uniform torque around the entire revolution. Furthermore, for a three-cup wheel with the same construction materials, a greater torque per unit weight is obtained, and the instrument is more sensitive to changes in wind speed since the moment of inertia is smaller.

Brazier describes the relation between wind speed and speed of the cup center as $U = a + bU_c + cU_c^2$. In this equation a, b, and c are constants, U is the speed of the steady wind,* and U_c is the linear speed of the cup centers. If this equation is divided by U_c, where $U/U_c = f$, the anemometer factor, we have $f = (a/U_c) + b + cU_c$. Brazier has found that when the ratio d/D is made approximately 0.5, where d is the diameter of the cup and D is the diameter of the circle described by the cup centers, the constant c goes to zero. In other words, the condition for constancy of the ratio is maximized. Work by Spilhaus (1934) indicates that the ratio d/D is also a function of the cup size for maximum linearity.

It might be expected that the maximum torque produced by a single cup occurs when the wind blows directly into the concave side of the cup. Patterson and later Brevoort and Joyner (1935) have shown that the maximum occurs when the concave side of the cup makes an angle of about 45° with respect to the wind direction. Figure 6.2 shows the relation between angle of attack of the cup and the normal force coefficient for hemispherical and conical anemometer cups.

The second most commonly used wind-speed measuring system is that in which a propeller or windmill revolves about a pivoted horizontal shaft that is oriented into the direction from which the wind is blowing by vanes. One example of the propeller-type anemometer is the Aerovane [(a) of Fig. 6.3]. The Aerovane uses a three- or six-blade propeller that is a modified helicoid made of durable plastic and has a diameter of about 38 cm. This is a dependable instrument for climatological measurements (Conover, 1946). Above speeds of

*In practice, the "steady" wind speed referred to here is that which might be observed in a well-maintained wind tunnel where most wind-sensor calibrations are performed. This steady speed fluctuates little about the mean speed, and the mean speed itself varies little over successive time intervals. The wind-tunnel type of steady flow is that which is represented by U in this and following equations. It is important to recognize that in the atmosphere this type of steady wind is not observed since atmospheric turbulence levels are greater and a wider range of fluctuation frequencies exists. As a result, in the atmosphere instantaneous departures of the wind from its mean are larger, and the mean itself will usually vary over successive time intervals.

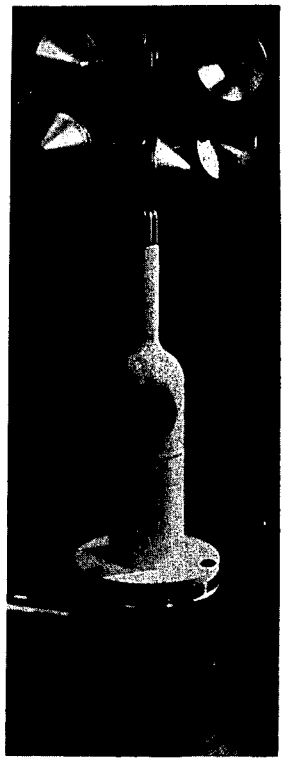

(a)

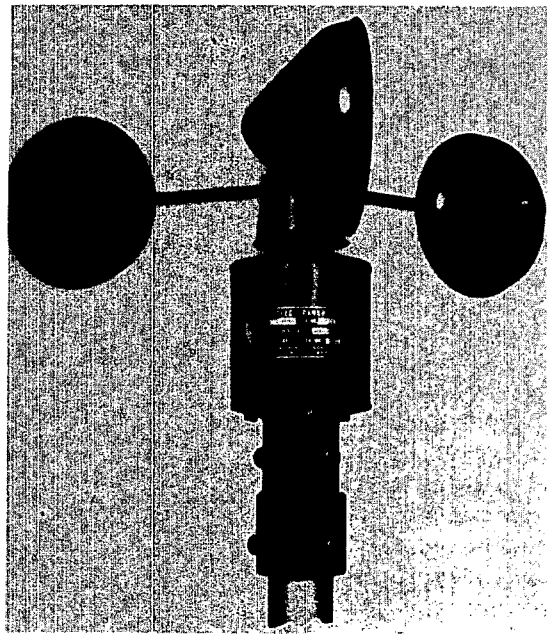

(b)

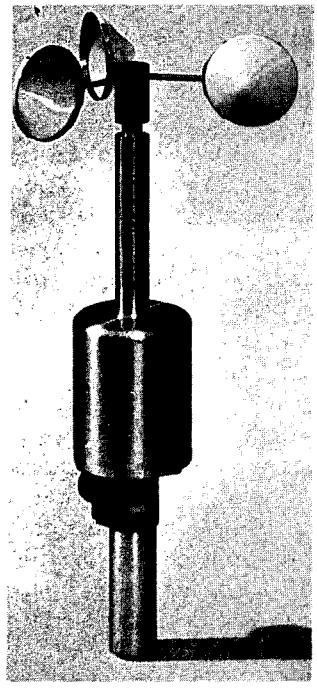

(c)

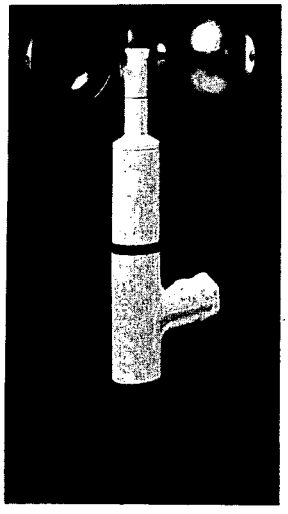

(d)

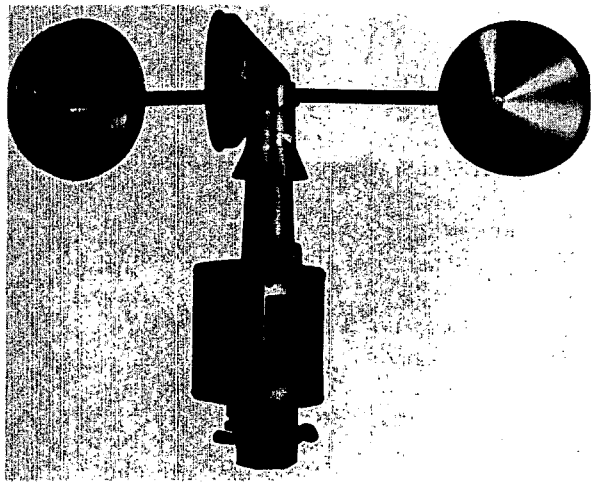

(e)

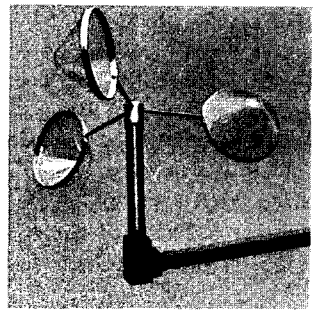

(f)

Fig. 6.1—Cup anemometers. (a) Beckman & Whitley, Inc. (b) Belfort Instrument Co. (c) Climet Instruments Inc. (d) R. M. Young Company. (e) Belfort Instrument Co. (f) C. W. Thornthwaite Associates.

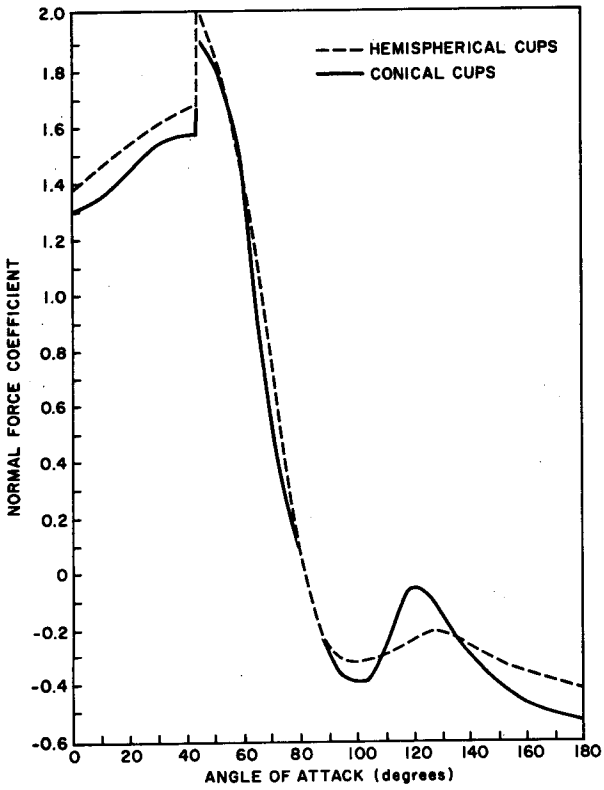

Fig. 6.2 — The variation of normal force coefficient with angle of attack for hemispherical and conical anemometer cups at a Reynolds number of 8×10^4. (Brevoort and Joyner, 1935.)

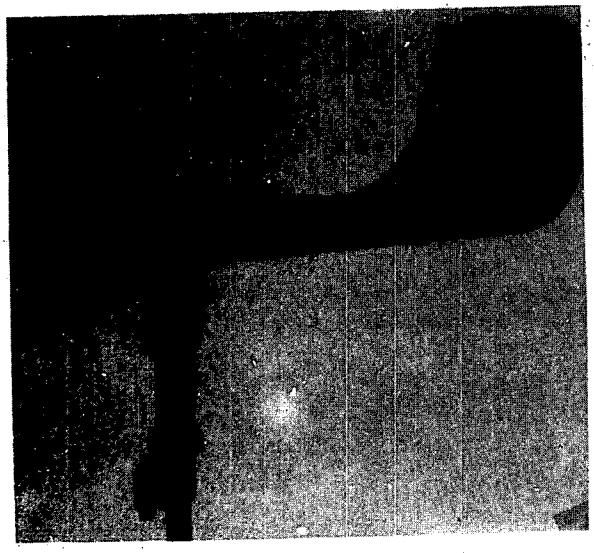

(a)

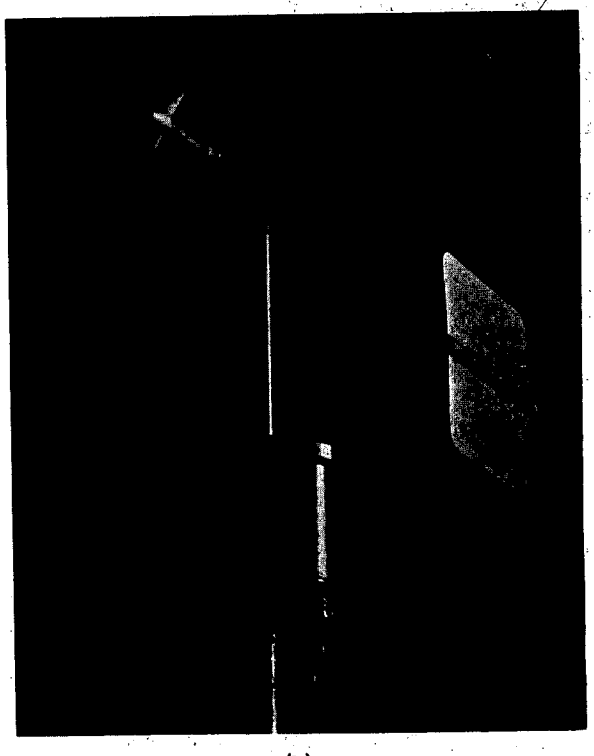

(b)

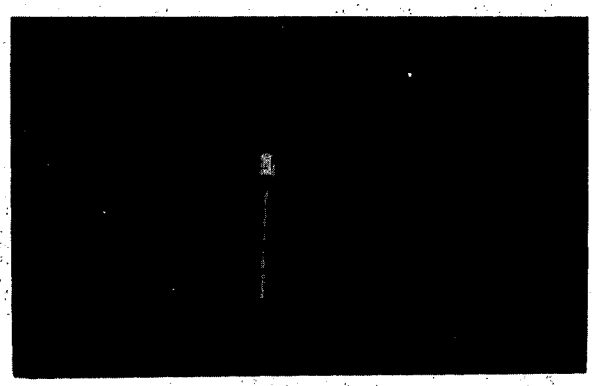

(c)

Fig. 6.3 — Propeller wind sensors. (a) An Aerovane wind sensor (Bendix Friez Instrument Division). (b) A Gill propeller vane (R. M. Young Company). (c) A vertical velocity propeller sensor (C. W. Thornthwaite Associates).

1 m/sec, the rate of rotation of the propeller is linearly proportional to the wind speed up to about 45 m/sec. An example of a lighter, more responsive propeller-type anemometer is shown in (b) of Fig. 6.3.

A propeller-type sensor for measuring the vertical component of the wind is shown in (c) of Fig. 6.3. The transmitter consists of a three-blade sensor mounted on a vertical shaft. The output indication of the system is proportional to the magnitude of the vertical component of the wind flow and at the same time indicates whether the vertical component is directed upward or downward.

The Aerovane and many of the standard three-cup anemometers drive a small permanent-field direct-current (d-c) generator that is connected electrically by two-conductor cable to a recording meter of the D'Arsonval type. The output of the generator is linearly proportional to the turning rate of the cup wheel or propeller. These transmitters have fairly low brush and bearing friction and need routine servicing two or three times per year. Brush and commutator maintenance is usually a minor problem. However, the friction is great enough to cause the starting speed to lie in the range of 1 to 2 m/sec. By means of a D'Arsonval galvanometer recorder and the d-c generator, a continuous trace of varying wind speed can be obtained.

Some manufacturers use alternating-current (a-c) generators instead of d-c generators to avoid using brushes and a commutator. This reduces friction considerably and eliminates the maintenance of brushes and dirty commutators. Two-, four-, six-, or eight-pole permanent-magnet rotors are usually employed, the larger number giving a correspondingly larger number of a-c pulses per revolution of the cup wheel and therefore a smoother record. The a-c pulses must be rectified, or a frequency meter circuit must be utilized for suitable recording. With normal rectifiers of the silicon type, the curve relating voltage and revolutions per minute is greatly compressed at the lower end of the scale; so speeds below 2 m/sec require correction. With the low frequency of impulses at these low speeds, each a-c impulse is individually recorded; thus spurious oscillations are produced on the wind-speed trace. Alternating-current generators are quite suitable for indicating or recording wind speed above 2 m/sec.

Another method of obtaining information from anemometers is to use the rotation of the anemometer to activate switches or relays. There are three general types of transmitters in this category: mechanical contacts similar to telephone relays, light interrupters, and magnet-actuated switches. In instruments of the mechanical-contact type, a rotating shaft is coupled through one or more gears to an eccentric cam that opens and closes a mechanical switch after the passage of a predetermined amount of wind (e.g., a fraction of a kilometer). This switch operates a suitable counter or recorder. An event recorder (Fig. 6.4) with suitable circuitry can be used to provide contacts for each 10-, 100-, and 1000-switch closure and simplify data extraction. Several transmitters can be used with a single time-of-event recorder; thus a single recorder can be used to economically obtain vertical wind profiles.

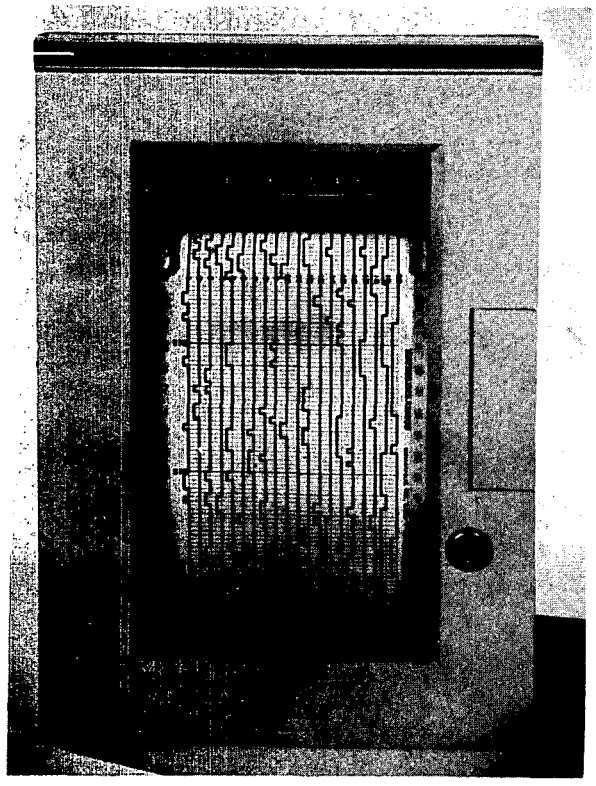

Fig. 6.4 — An event recorder (Easterline-Angus Instrument Co.).

To reduce mechanical friction (thereby permitting the measurement of low wind speeds) and also to increase the speed of response, the small three-cup anemometers often are used with the interrupted light beam – photocell technique. In this system electrical impulses are generated each time a perforation in the shaft rotates into a position that allows a light on one side of the shaft to shine on a photocell on the other side. The shaft can be drilled with one or many such holes. When only a few electrical impulses are generated for each rotation of the shaft–cup wheel assembly, counters or recorders are usually used for totaling. When many pulses originate with each revolution of the shaft, i.e., six or more, it is convenient to feed them to a frequency-measuring circuit that gives a voltage output directly proportional to the speed of rotation of the cup wheel. Recording this voltage provides a continuous record of the wind speed.

6-4.1.2 Types of Speed Systems Infrequently Used. The speed of air moving over a fine heated wire can be measured by the cooling effects produced. The hot wire used as an anemometer may range from 0.003 to about 0.01 cm in diameter and may be from about 0.1 to 10 cm in length. Various types of materials may be used, e.g., platinum, Nichrome, or tungsten. The wire may be heated over a range of from several hundred to well over 1000°C. The basic equations describing the theory of the hot-wire anemometer stem from the work of King (1914). An approximate equation relating electric current and wind velocity is

$$i^2 = i_0^2 + K\,(U)^{1/2} \qquad (6.1)$$

where U = steady wind speed
i = electric current in the wire at wind speed U
i_0 = electric current in the wire when U = 0
K = an experimental constant, which depends upon the units used

It is assumed in Eq. 6.1 that the hot wire is maintained at constant temperature, i.e., current is added or subtracted from the circuit as the wind speed varies to maintain a Kelvin bridge in balance. Electronic equipment has been developed which uses feedback amplifiers to automatically control the temperature of the hot wire and keep the bridge in balance. Hot-wire anemometers capable of measuring wind fluctuations up to several tens of thousands of cycles per second are commercially available.

With a hot-wire anemometer important variables of wind speed, such as the root-mean-square velocity or the correlation coefficient between two anemometers placed at different positions, or even lag correlations can be derived. Furthermore with suitable electronic circuitry the turbulence spectra can be obtained automatically.

Another type of hot-wire anemometer allows the temperature of the hot wire to vary, and the output voltage is read on a Wheatstone or a Kelvin bridge. This kind of instrument is calibrated to relate wind speed with bridge-imbalance to give wind-speed fluctuations. This technique is not used so frequently today as the constant-temperature technique. Although this technique is referred to as the constant-current technique, the current is not really constant.

Another technique for measuring wind speed utilizes three thermocouples in a T formation, as shown in Fig. 6.5. The thermocouple junctions A and B form the probe and face into the wind. Junction C acts as a temperature-compensating junction. This anemometer has been used by Cramer, Gill, and Record (1957) and is commercially available. The thermocouples are made of fine constantan–chromel P wires. Thermocouples A and B are heated by alternating current provided by a transformer; thermocouple C is unheated. The millivoltmeter, V, measures only direct current because the transformer is center tapped and the resistances of the heated thermocouples are equal.

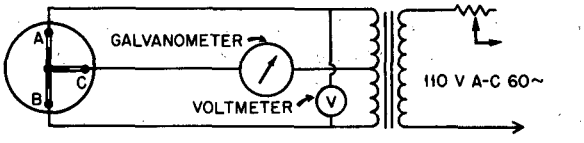

Fig. 6.5 — A schematic drawing of a heated-thermocouple anemometer. Thermocouple junctions are labeled A, B, and C.

Although hot-wire and thermocouple techniques can be extremely useful for turbulence studies both in wind tunnels and in the atmosphere, they are not usually used in operational diffusion studies because the instruments have the following disadvantages:

1. Deposits of dust and dirt necessitate frequent cleaning and frequent recalibration.
2. Zero shifts in the bridge can cause appreciable errors.
3. Rain or snow can cause very large errors.

If a rotation-type anemometer is prevented from rotating, it develops a torque proportional to the square of the wind speed. A measurement of this torque therefore provides a measure of the wind speed. An instrument based on this principle is called a bridled cup anemometer. Because of its insensitivity and inaccuracy at low speeds, as well as its distorted recording of gust speeds, it is no longer manufactured and is used rarely.

The response of the pressure-tube anemometer, a rarely used instrument, is based on the Bernoulli principle. Static and dynamic pressure holes lead to a float manometer that measures the pressure difference and transforms this difference into a linear displacement recorded on a chart wound about a clock-driven drum. Although the pressure difference is proportional to the square of the wind speed, the float manometer arrangement is designed to provide a linear relation between pen displacement and wind speed. Standard electrical transducers are also available to provide wind-speed readings based on the static and dynamic pressure difference. A disadvantage of the pressure-tube anemometer is that it must be oriented into the wind.

The force exerted upon a plate oriented perpendicularly to the wind direction is proportional to the square of the wind speed. Such pressure-plate anemometers have been used for detailed studies of the wind (Sherlock and Stout, 1931). Although such instruments offer the potential of high-frequency response and conceptual simplicity, they suffer from the difficulties of nonlinear drag coefficient and the necessity of orientation into the wind. This type instrument is not produced in the United States at the present time.

6-4.1.3 The Anemometer Distance Constant. Owing to moment of inertia and friction, a cup or propeller anemometer has appreciable lag, i.e., peaks and lulls are attenuated for frequencies greater than 1 cycle per several seconds. Schubauer and Adams (1954) have shown that the lag characteristics of this anemometer can be expressed by a length called the distance constant. If an instantaneous change in wind speed occurs, this constant represents the length of wind that must pass the anemometer before it indicates 1-1/e or 63% of the change. For example, if the anemometer was placed in a 10 m/sec wind but its rotational rate was retarded to correspond to a 9 m/sec reading and then the retarding force was removed, the distance constant would represent the distance the wind would have to travel before the anemometer indicates a value of 9.63 m/sec, i.e., 63% of the change. For any anemometer the distance constant is independent of the wind speed. Values of the distance constant range from about 0.7 to 8.0 m for commercially available anemometers (Table 6.1).

Table 6.1 — ANEMOMETER CHARACTERISTICS

Manufacturer and Instrument	Model	Distance constant, m
Beckman & Whitley, Inc.:		
3 cup	Series 50	1.22
Staggered 6	Series 50	0.98
Bendix Friez Instrument Division:		
Aerovane (3-blade prop.)	Model 120	4.6
Aerovane (6-blade prop.)		5.8
Climet Instruments Inc.:		
3 cup		1.0 to 1.5
4-blade prop.		0.45
Electric Speed Indicator Co.:		
3 cup	Type F-420C	7.9
R. M. Young Company:		
Gill anemometer, 3 cup		0.73
Belfort Instrument Co.:		
3 cup	Type M	6.4
Meteorology Research, Inc.:		
Velocity Vane	1057	1.7 to 1.8
C. W. Thornthwaite Associates:		
3 cup		1.07

Wind-speed data of sufficient accuracy for the evaluation of a reactor site, for day-to-day reactor operation, or for the rare accident can be obtained from an anemometer with a distance constant characteristic of the less sensitive but rugged instruments, such as the Aerovane. For installations where meteorological measurements are to be made over a period of many years, the economy gained from the rugged equipment is attractive.

The dynamic response characteristics of a cup or propeller anemometer, neglecting bearing friction, can be represented by the differential equation for a first-order system

$$\tau \frac{dU_i}{dt} + U_i = f(t) \qquad (6.2)$$

where τ = the time constant (i.e., the time for the system to respond to $1 - 1/e$ or 63% of a step change)
U_i = the indicated wind speed
t = time
f(t) = a time-dependent forcing function

For a forcing step function, assume that an anemometer is held fixed and is suddenly released in a steady wind of U m/sec. Its response can be described by

$$\tau \frac{dU_i}{dt} = U - U_i \qquad (6.3)$$

The solution of Eq. 6.3 can be written

$$U_i = U\left[1 - \exp\left(-\frac{t}{\tau}\right)\right] \qquad (6.4)$$

Let $L = U\tau$ and $x = Ut$, then

$$U_i = U\left[1 - \exp\left(-\frac{x}{L}\right)\right] \qquad (6.5)$$

It is readily seen that L is the distance constant or the length of travel of the wind before the anemometer attains 63% of a step wind change. Experiments by Schubauer and Adams (1954) and by MacCready and Jex (1964) indicate that the distance constant is independent of wind speed for cup and propeller anemometers over the usual range of atmospheric speeds. Since $L = U\tau$, τ must be inversely proportional to wind speed. Schubauer and Adams give the relation

$$\tau = \frac{Ik^2}{\rho Uc} \qquad (6.6)$$

where ρ = the density of the air
I = the moment of inertia of the anemometer
c = an effective drag coefficient appearing in the formula for the torque (T) exerted by an anemometer as shown by the relation $T = 1/2cU^2Ar$, where A is the blade or cup area and r is an effective radius
k = the anemometer factor U_c/U, where U_c is the linear speed of the center of the cup

Thus

$$L = U\left(\frac{Ik^2}{c}\right)\frac{1}{\rho}\left(\frac{1}{U}\right) = \frac{K}{\rho} \qquad (6.7)$$

or

$$L\rho = K = \text{constant} \qquad (6.8)$$

The distance constant is therefore inversely proportional to the air density and directly proportional to the moment of inertia of the cups.

If the forcing function is taken as

$$f(t) = U + A \sin bt \qquad (6.9)$$

where U is the steady wind speed, A is the amplitude of an imposed sinusoidal variation, and b is $2\pi f$, where f is the frequency in cycles per second and b is in radians per second, then Eq. 6.2 can be transformed to

$$\tau \frac{dU_i}{dt} + U_i = U + A \sin bt \qquad (6.10)$$

Neglecting transient effects, one can write a particular solution of Eq. 6.10 as

$$U_i = U + A\,(1 + b^2\tau^2)^{-1/2} \sin(bt - \beta) \qquad (6.11)$$

where β is a phase-lag angle and is equal to arctan bt. According to Eq. 6.11 the anemometer reading will show an amplitude reduced by a factor $(1 + b^2\tau^2)^{-1/2}$ and will lag a sinusoidally varying wind by an angle β. Although this equation indicates that the average indicated wind equals the steady wind, this is not strictly correct because the anemometer speeds up faster than it slows down and thereby gives a mean that is higher than the mean wind.

Since $b = 2\pi U/\lambda$, where λ is the gust wavelength, and $L = U\tau$, Eq. 6.11 can be written

$$U_i = U + \frac{A}{[1 + (2\pi L/\lambda)^2]^{1/2}} \sin(bt - \beta) \qquad (6.12)$$

Figure 6.6 shows the percentage of attenuation for a sinusoidally varying wind as a function of λ/L.

It should be emphasized that the above analysis is only approximate since equations for both the vane and cup anemometers are much more

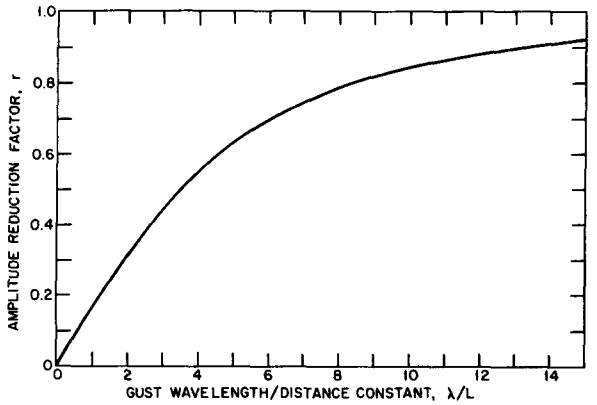

Fig. 6.6—Amplitude reduction of cup anemometers in a sinusoidally varying wind as a function of λ/L. The amplitude reduction factor, $r = \left[1 + \left(\frac{2\pi L}{\lambda}\right)^2\right]^{-\frac{1}{2}}$ (see Eq. 6.12). (Schubauer and Adams, 1954.)

complex than indicated (see MacCready, 1966, and Corcoran and Esau, 1964).

6-4.1.4 Errors in Wind-speed Measurements. There are many sources of error in wind-speed measurements. If an anemometer is mounted on top of a building, the Bernoulli effect will cause readings that are higher than the true reading. If an anemometer is mounted on a boom from a tower, the wind-shadow effect (Moses and Daubek, 1961) for certain directions will cause speeds that are lower or higher than the true speed. In addition to these errors due to poor exposure, a number of errors are inherent in the instrument itself. Errors due to lag, density variations, misalignment of the rotational axis, as well as those due to analysis technique, are discussed in the following paragraphs.

In Sec. 6-4.1.3 it was shown that the instantaneous reading lags behind the true reading for both a step function and a sinusoidally fluctuating wind. In addition, under the latter condition the amplitude is attenuated. Because the anemometer speeds up faster than it decelerates, the mean wind indicated may be slightly higher than the true speed. Schrenk (1929), Deacon (1951), and Schubauer and Adams (1954) discuss this type error. Figure 6.7 represents the errors that might be expected in a fluctuating wind. The K in this figure can be expressed as

$$K = \frac{A\rho TUa^2r^2}{4I} \qquad (6.13)$$

where A = a constant
ρ = air density
T = period of fluctuations
U = steady wind speed
a = cup radius
r = arm radius
I = moment of inertia of the cup rotor

Deacon used the value of 2.7 for the quantity A. For an air density of 1.2×10^{-3} g/cm^3, Deacon finds for a Sheppard cup anemometer that K = 0.031 UT, where U is in meters per second and T is in seconds. The dashed line in this figure shows the curves for a Sheppard anemometer, a type frequently used in this country.

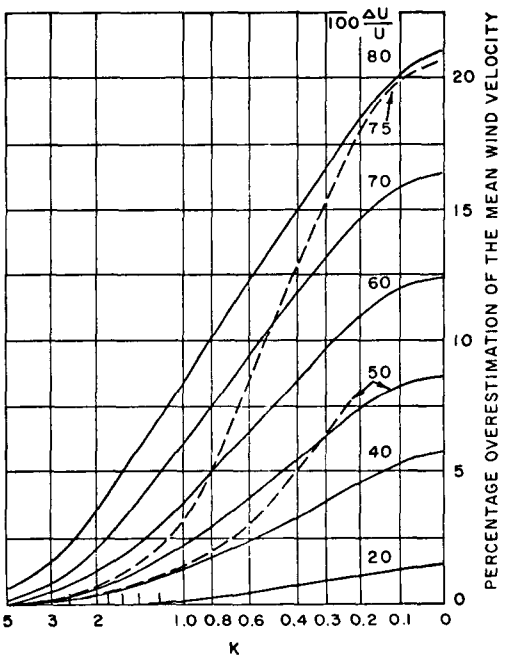

Fig. 6.7—The overestimation of the Sheppard anemometer (broken lines) compared with Schrenk's (1929) results (solid lines) for an anemometer with hemispherical cups for various values of K (see Eq. 6.13). The amplitude of the speed fluctuations as a percentage of the mean speed ($100\Delta U/U$) is indicated. (Deacon, 1951.)

Ower (1949) carried out an analysis for the errors expected from wind fluctuations of the order of 1 cycle/sec as indicated by a vane anemometer. He assumed that $U_i = U(1 + \Lambda \sin bt)$ and derived the relation

$$\overline{U}_i = U\left(1 + \frac{\Lambda^2}{2}\right) \qquad (6.14)$$

where $\overline{U}_i$ is the indicated mean wind speed, U is the true steady wind speed, and Λ is an amplitude parameter. It can be seen that the percentage of error is 100 $\Lambda^2/2$. This relation indicates that the errors are greater than those indicated by Shrenk. MacCready (1966) indicates that the errors due to fluctuating winds are ordinarily quite small, on the order of 1.0% or 2.0%. Additional experimental work of this nature for anemometers currently in use, especially for precision measurements, is in order.

For the usual variation of pressure and temperature, the changes in density are generally too small to materially affect the calibration of cup or propeller anemometers. Nevertheless one must remember that calibration does depend upon density and that density has a second order effect on the calibration.

MacCready (1966) made a study of the effects of turbulence on the measurement of horizontal mean wind speeds. He noted that various horizontal speed sensors respond differently to the vertical fluctuations of the real wind. Part (a) of Fig. 6.8 shows the vertical-angle effect for several representative mechanical sensors. Since the true horizontal wind speed would be V cos φ, where V is the total three-dimensional wind speed and φ is the angular departure of the total wind direction from the horizontal, it is seen that the conventional cup anemometer can give unrepresentative readings. MacCready indicated that the VectorVane and the VelocityVane respond to the cosine of the wind angle, and Mazzarella (1954) showed that the Aerovane-type of instrument responds to a $\cos^2$ relation. In a private communication Gill indicated that some vanes may respond to a $\cos^{3/2}$ law. Using data collected by Swanson and Cramer (1965), MacCready calculated that the error between the true and indicated horizontal wind speeds might be on the order of 6.0% for cup anemometers and negligibly small for a cosine propeller anemometer.

MacCready further discussed the error due to the inability of the vane-mounted propeller anemometer to faithfully follow the horizontal fluctuations of the wind. Again using the Swanson and Cramer data, he found that this error amounted to about 1.0%.

A third type of error discussed by MacCready was that due to along-wind turbulent fluctuations. A brief evaluation indicated that this

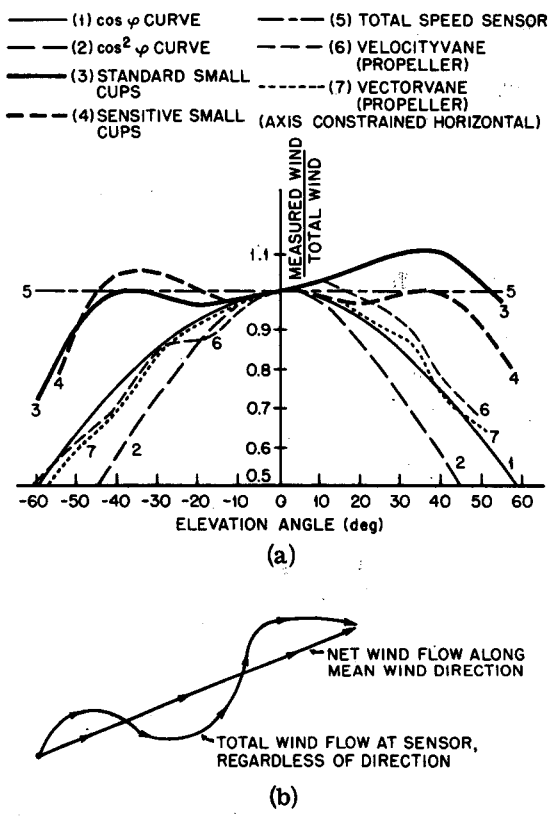

Fig. 6.8—(a) The response of a number of speed sensors to various vertical wind-direction angles. (b) An illustration of the data-processing error, i.e., the error that will arise in the measurement of the net wind flow along the direction of the mean wind with a sensor that measures the total wind flow. (MacCready, 1966.)

error could become increasingly important with typical sensors as the height of measurement approached the ground level.

In addition to instrumental errors, errors arise from the manner in which the data are analyzed. For a totalizing anemometer, i.e., one in which the wind is integrated over a changing horizontal direction, as shown in (b) of Fig. 6.8, the instrument reading differs from the horizontal component of the mean wind vector, i.e., obtained by averaging the vector components. This type of error can be circumvented by recording the wind components. The magnitude of this error applied to the White Sands data (MacCready, 1966) was calculated by MacCready to be 4.5%. Thus, even with low lag, a cup anemometer in a strongly fluctuating wind can produce a 10% difference between the indicated speed and the horizontal component of the mean vector speed.

Errors from recorder malfunctions, including drift in calibration, are always of concern. Procedures should be devised to check this source of error frequently.

6-4.2 Wind Direction

6-4.2.1 Wind Vanes and Bivanes. Wind vanes can take many different forms from the very ornate, as seen on some farmhouses, to the relatively simple rectangular flat plate. Flat plates are easy to construct and provide reliable data. For increased torque at low wind speeds, some splayed vanes, i.e., two vanes joined at their forward vertical edge and spreading out at an angle up to 20°, have been used. Sanuki (1950) has shown that the overall performance of the splayed vane is not superior to that of a single vane. Some manufacturers have used an airfoil as a vane. Gill (1959) indicates that up to 15% more torque is produced by this type with the same physical dimensions for certain ranges of attack angles, but, because of the added mass and therefore the increased moment of inertia of the airfoil, the improved torque is offset by poorer dynamic performance. Various wind-vane forms are shown in Fig. 6.9.

The vertical and horizontal components of the wind direction can be determined by means of a bivane. The bivane can take either of two forms. The first arrangement consists of two plates perpendicular to each other mounted on a gimbal so that the unit can rotate both horizontally and vertically. The plates are constructed of thin aluminum or expanded polystyrene. The second type consists of an annular fin, either an airfoil or a flat sheet of metal, with a similar gimbal arrangement. Various bivanes are shown in Fig. 6.10. Both types of bivanes, as well as bivanes with a propeller mounted on the shaft, are available commercially. The output from such an instrument can be used to determine all three components of the total wind vector.

6-4.2.2 Wind-direction Transmitters and Recorders. Perhaps the most trouble-free and reliable technique for recording the angular position of a vane is one that utilizes a synchro-motor system. The vane is coupled to the shaft of a synchro-transmitter, which can be located 100 m or more away from but is connected electrically to the synchro-receiver. The shaft of the synchro-receiver reproduces the rotation of the shaft of the synchro-transmitter and thereby locates the vane position. The shaft of the synchro-receiver can operate the pointer of a wind-direction-indicating dial or it can drive the pen of a strip-chart recorder.

Coupling to a recorder pen is frequently accomplished through a heart-shaped cam. The rotation of the vane from 0° to 180° effects a counterclockwise movement of the recorder pen from the left side of the chart to the right; a continued rotation from 180° to 360° results in a clockwise motion of the pen from the upper end to the zero position. Since each position of the pen represents two angular positions of the vane (except for the end points of the traverse) and therefore creates an ambiguity, a side marking pen is used to indicate whether the direction is east or west of north. Another scheme for recording uses a 540°-wide chart scale. When the pen reaches either the upper or lower end of the chart record, an electrical relay and mechanical system causes the pen to rotate in the appropriate clockwise or counterclockwise direction corresponding to 360° of vane rotation. Since a 540° chart is used, the pen in its new position, i.e., after the 360° change, operates about one-third of the distance from one end of the scale.

A less costly method of recording or indicating the rotation of the vane is accomplished with a potentiometer and a recording voltmeter. The potentiometer contact is coupled to the vane shaft; thus any angular position of the vane corresponds to a particular voltage that can then be applied to a suitably calibrated recording voltmeter. One drawback to this arrangement is the discontinuity that occurs when the contact moves across the gap in the potentiometer. If the wind direction oscillates about a position corresponding to this gap, the pen swings from one end of the chart to the other and causes a confusing record. This difficulty can be circumvented by using double-contact potentiometers and switching arrangements (M. E. Smith, 1959). Another disadvantage of the potentiometer system is the excessive wear produced as the contact moves along the wires. An advantage of this system is the low moment of inertia of the potentiometer system compared with that of the synchro-motor system. This is especially true if microtorque potentiometers are used.

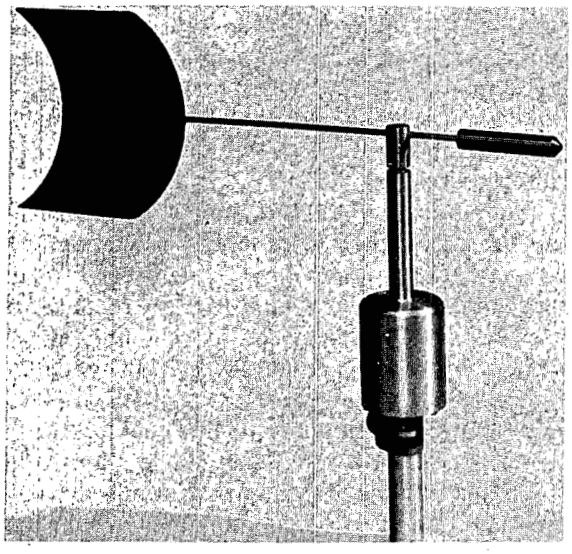

(a)

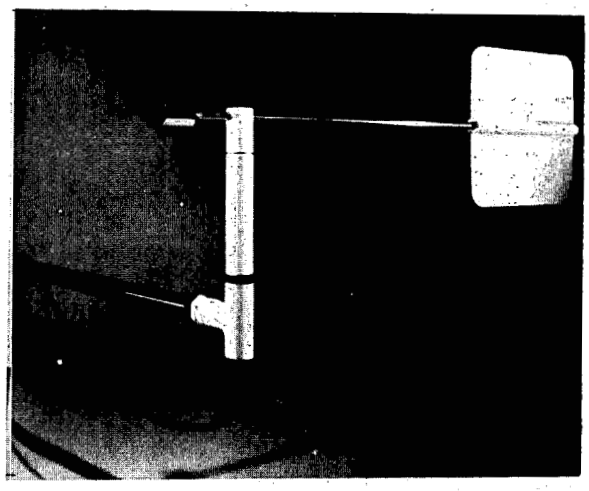

(b)

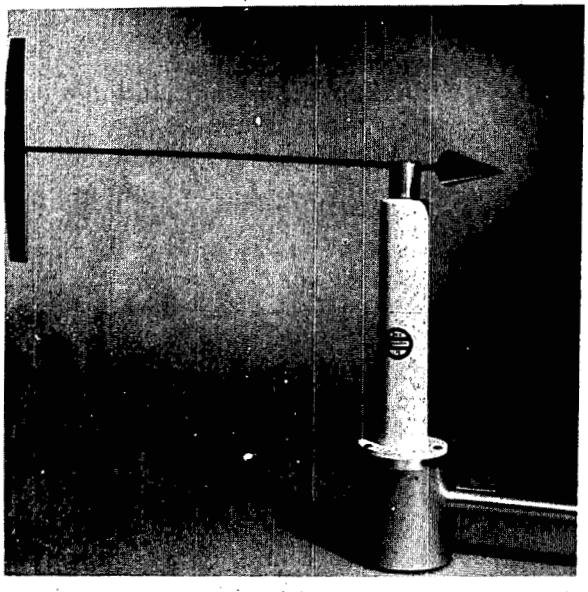

(c)

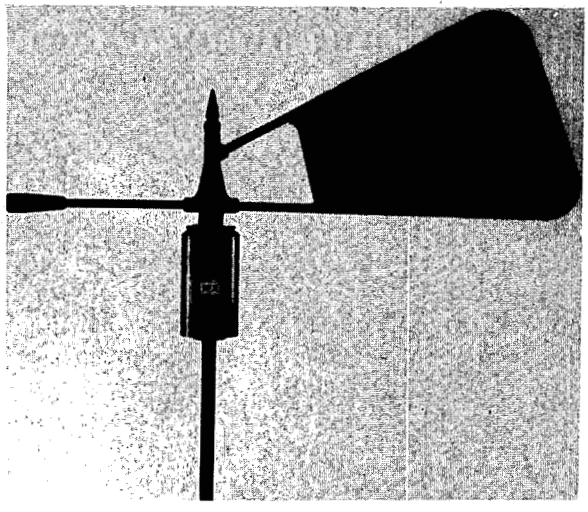

(d)

Fig. 6.9—Various wind vane forms. (a) Climet Instruments Inc. (b) R. M. Young Company. (c) Beckman & Whitley, Inc. (d) Belfort Instrument Co.

Another type of transmitter is the commutator system in which the vane is coupled to a unit that has two electrical contactors or brushes, spaced about 22.5° apart, making contact with one or two of eight 45° conducting sectors. Each of the sectors corresponds to 45° of wind direction, i.e., one point of an eight-point compass. When both brushes make contact in one sector, the direction corresponds to one of the eight compass points, e.g., north, northeast, east. When the brushes contact two of the sectors, the direction corresponds to an intermediate direction, such as north-northeast, east-northeast, or east-southeast. Thus direction to 16 points is obtained. This system can be used to energize light bulbs for visual reading or to operate electromagnetic relays that drive recorder pens. Similar systems can be used for dividing the compass into any other number of sectors.

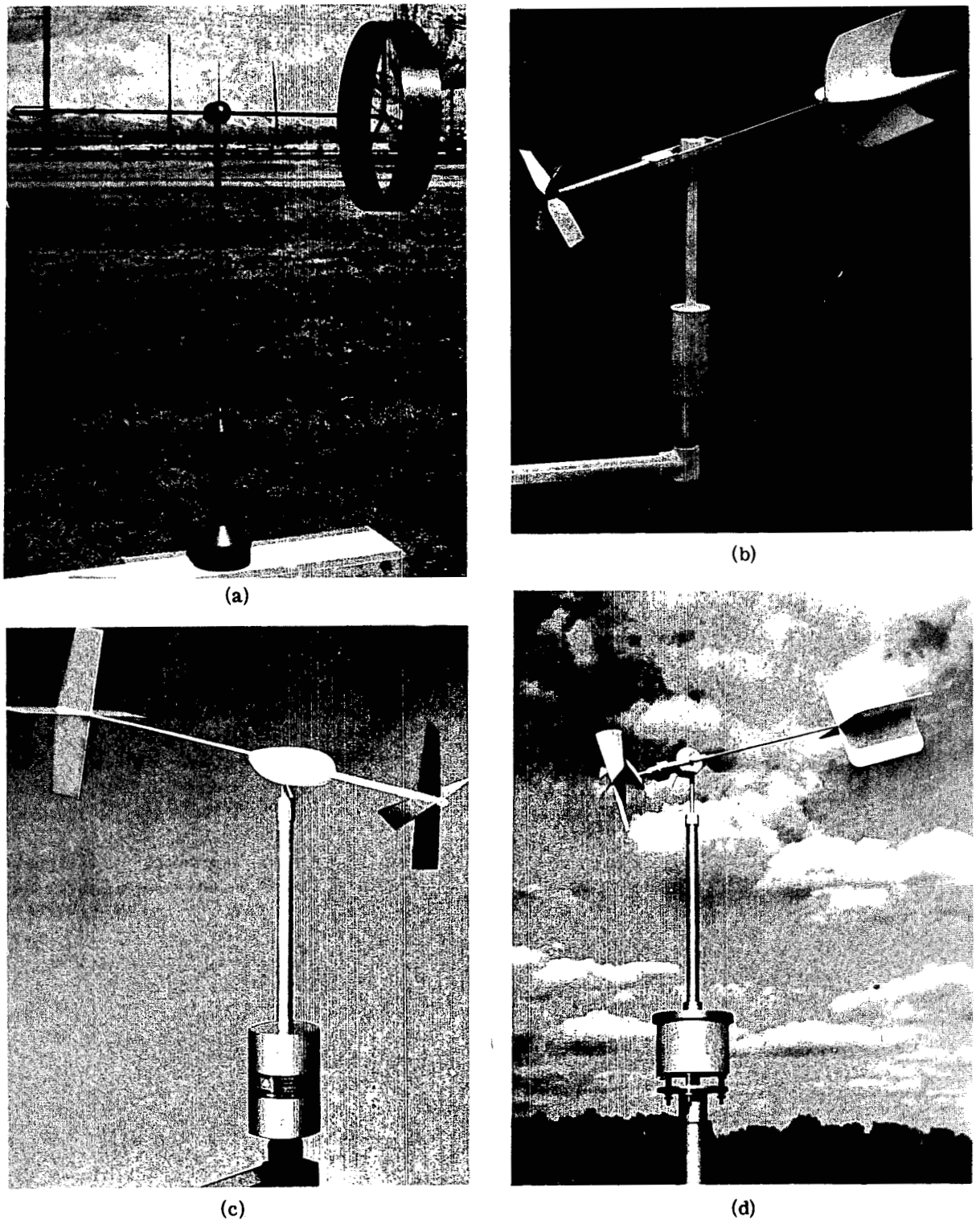

Fig. 6.10—Bidirectional-vane (bivane) sensors: (a) an annular fin bivane used at the National Reactor Testing Station. (b) the Axiometer Sensor by Climet Instruments Inc. (c) the VectorVane by Meteorology Research, Inc. (d) the Gill Anemometer Bivane by R. M. Young Company.

In some installations a switch operated by an anemometer is inserted in the circuit. A recording of wind then is made only when a given amount of air, such as 1 km, has passed, and thus there is a combined recording of both wind speed and wind direction. Although the data obtained under this scheme are difficult to reduce, the system is satisfactory for obtaining climatological data under some conditions.

The standard deviation of the wind-direction distribution (σ_θ or σ_φ) over time periods approximately equal to the length of a point-source release has been used in many experiments as an index of diffusion (see Chap. 4). These quantities can be computed from high-speed analog traces from wind-direction recorders or from other analog or digital data records. A simple electronic system, popularly called a sigma meter, which presents a continuous real-time record of the standard deviations of wind direction without recourse to an intermediate collection of the raw wind-direction data has been discussed by Jones and Pasquill (1959) and has been used in diffusion research studies (e.g., MacCready, Smith, and Wolf, 1961).

Using the nomenclature and notation of Jones and Pasquill, we find

$$\sigma^2_{T,t} = \sigma^2_\infty \int_0^\infty F(n)\left[1 - \frac{\sin^2 \pi nT}{(\pi nT)^2}\right] \times \frac{\sin^2 \pi nt}{(\pi nt)^2}\, dn \qquad (6.15)$$

where $F(n)$ = fraction of variance (σ^2_∞) occurring between (n) and (n + dn)
T = time interval of interest
t = incremental time of each sample ($t \ll T$)
$\sigma^2_{T,t}$ = the variance accounted for by the function $F(n)$ during the period T, as sampled from periods t

If the signal is a continuous one, e.g., the voltage from the wind vane, $t \to 0$ and Eq. 6.15 becomes

$$\sigma^2_T = \sigma^2_\infty \int_0^\infty F(n)\left[1 - \frac{\sin^2 \pi nT}{(\pi nT)^2}\right] dn \qquad (6.16)$$

Equation 6.16 shows that with a filter whose characteristics approach $1 - [\sin^2 \pi nT/(\pi nT)^2]$ one could feed the wind-vane signal through it and read the variance contained in $F(n)$ (the vane signal) directly.

The power factor (i.e., fraction of signal passed) of a two-stage resistance–capacitance network whose stages are isolated by a vacuum tube is

$$P = \frac{\omega^2 C^2 R^2}{1 + \omega^2 C^2 R^2} \qquad (6.17)$$

where ω is $2\pi n$, C is capacitance in farads, and R is resistance in ohms.

The square of Eq. 6.17 is mathematically similar to the expression in brackets in Eq. 6.16. At this juncture one could either employ squaring circuits to read the variance (σ^2) or employ a few simplifying assumptions (as did Jones and Pasquill) and read out the standard deviation (σ).

Basically the sigma meter is a high pass filter permitting passage of all frequencies above a set limit and attenuating other frequencies below this limit in accordance with Eqs. 6.16 and 6.17. The alternating current (across the capacitors) is passed to a simple voltmeter and read directly or, as is more often the case, is rectified to direct current and passed to a ripple filter to smooth the output signal into a more manageable form.

The device as described is limited by the performance of the capacitors. Even capacitors of very high quality cannot hold a charge reliably for more than a few minutes, hence T is limited to about 500 sec.

Since his original publication, Jones has published descriptions of various electronic filter designs for meteorological purposes (e.g., Jones, 1966). These include band-pass designs, cathode-ray-tube readout devices, and other ingenious applications. The sigma meter itself is now commercially available from several manufacturers and can be readily adapted to most telemetered systems, as well as to direct readout on charts or digital displays. For a list of manufacturers of this equipment, consult current issues of meteorological, air-pollution, and air-monitoring publications.

6-4.2.3 Dynamics of the Wind Vane. The behavior of a wind vane can be described by the differential equation for a second-order system

$$\frac{d^2\theta}{dt^2} + 2\omega_n \zeta \frac{d\theta}{dt} + \omega_n^2 \theta = f(t) \qquad (6.18)$$

where θ = angular displacement of the vane with respect to a fixed wind direction
ω_n = natural or undamped angular frequency of the system
ζ = damping ratio, the ratio of the actual damping to the critical damping (which produces no overshoot)
t = time
f(t) = a time-dependent forcing function

On the basis of the results of Corcoran (1962) and Garbell (1957), this equation can be expressed as

$$\frac{d^2\theta}{dt^2} + \frac{k\rho Ar^2U}{2I}\frac{d\theta}{dt} + \frac{k\rho ArU^2}{2I}\theta = f(t) \quad (6.19)$$

where k = an aerodynamic factor that depends on the geometry of the vane
ρ = density of the air
A = area of the vane
r = distance from the vane pivot to the vane centroid, i.e., arm length
U = steady wind speed
I = moment of inertia of the vane system.

From Eqs. 6.18 and 6.19, we see that the natural frequency of the vane is

$$\omega_n = U\left(\frac{k\rho Ar}{2I}\right)^{1/2} \quad (6.20)$$

and that the damping ratio is

$$\zeta = \frac{r}{2}\left(\frac{k\rho Ar}{2I}\right)^{1/2} \quad (6.21)$$

The dynamic characteristics of a wind vane are ordinarily determined by observing its behavior in a wind tunnel. A method frequently used is to displace the vane an angle θ_0 from the mean wind direction and then to release it. The resulting oscillations are recorded in terms of voltage output, which is proportional to the vane displacement. This allows one to determine the parameters of Eq. 6.18, ζ and ω_n.

If we take f(t) = 0 in Eq. 6.18, i.e., no forcing function is present, the equation will have three characteristic solutions depending on whether it is overdamped ($\zeta > 1$), critically damped ($\zeta = 1$), or underdamped ($\zeta < 1$). The most faithful response of a vane is obtained when ζ is about 0.6.

Assuming boundary conditions of $\theta = \theta_0$ and $d\theta/dt = 0$ at t = 0, we have for $\zeta > 1$

$$\theta = \theta_0 e^{-\zeta\omega_n t}\left[\cosh\ \omega_n(\zeta^2-1)^{1/2}\ t + \frac{\zeta}{(\zeta^2-1)^{1/2}}\sinh\ \omega_n(\zeta^2-1)^{1/2}\ t\right] \quad (6.22)$$

For $\zeta = 1$ we have

$$\theta = \theta_0 e^{-\omega_n t}(1+\omega_n t) \quad (6.23)$$

and for $\zeta < 1$ we have

$$\theta = \theta_0\frac{1}{(1-\zeta^2)^{1/2}}e^{-\omega_n\zeta t} \times \cos\left[\omega_n(1-\zeta^2)^{1/2}\ t - \beta\right] \quad (6.24)$$

where

$$\beta = \arctan\frac{\zeta}{(1-\zeta^2)^{1/2}} \quad (6.25)$$

It is customary to let

$$\omega = \omega_n(1-\zeta^2)^{1/2} \quad (6.26)$$

when ω is the observed angular frequency, i.e., 2π times the actual frequency. Then by substitution we have

$$\theta = \theta_0\frac{1}{(1-\zeta^2)^{1/2}} \times \exp\left[\frac{-\omega\zeta}{(1-\zeta^2)^{1/2}}\ t\right]\cos\ (\omega t - \beta) \quad (6.27)$$

Since Eq. 6.27 describes an oscillatory motion with a period of $2\pi/\omega$, the ratio of successive maximums can be expressed as

$$\frac{\theta_{n+1}}{\theta_n} = \frac{\exp\left\{-\frac{\omega\zeta}{(1-\zeta^2)^{1/2}}\left[\frac{2(n+1)\pi+\beta}{\omega}\right]\right\}}{\exp\left[-\frac{\omega\zeta}{(1-\zeta^2)^{1/2}}\left(\frac{2n\pi+\beta}{\omega}\right)\right]} = \exp\left[-\frac{2\pi\zeta}{(1-\zeta^2)^{1/2}}\right] \quad (6.28)$$

where n is an integer.

Figure 6.11 shows a typical record of a vane test. If the ratio of successive peaks is determined, ζ can be determined, and if the

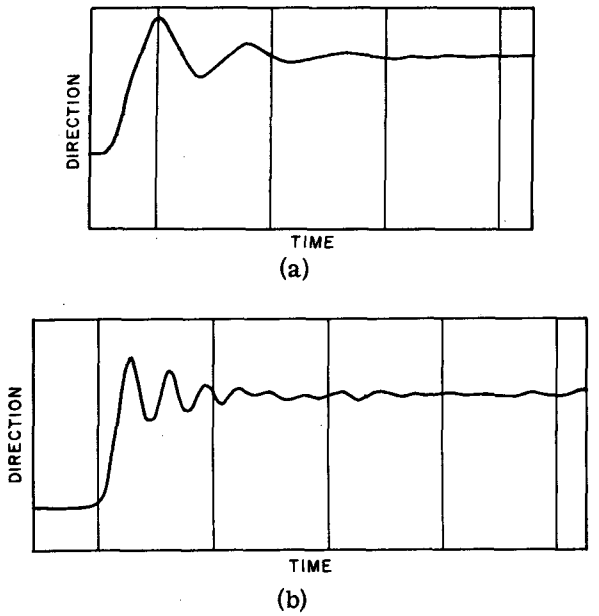

Fig. 6.11—Response of a wind vane to a step-function direction change. Time markers are at 1-sec intervals. (a) Displacement, 45°; wind speed, 4.5 m/sec. (b) Displacement, 45°; wind speed, 9.0 m/sec. (Courtesy of Beckman & Whitley, Inc.)

angular frequency, ω, is measured, Eq. 6.26 can be used to calculate ω_n, the natural frequency.

When the second-order system of Eq. 6.18 has a forcing function impressed on it, i.e.,

$$\frac{d^2\theta}{\omega_n^2\, dt^2} + \frac{2\zeta}{\omega_n}\frac{d\theta}{dt} + \theta = A \sin bt \qquad (6.29)$$

the general solution can be expressed as the sum of the complementary and particular solutions. Thus

$$\theta = C_1 \exp\left[-\omega_n\zeta - \omega_n(\zeta^2-1)^{1/2}\, t\right] + C_2 \exp\left[-\omega_n\zeta + \omega_n(\zeta^2-1)^{1/2}\, t\right] + \frac{A \sin(bt-\beta)}{\left[4\zeta^2\frac{b^2}{\omega_n^2} + \left(1-\frac{b^2}{\omega_n^2}\right)^2\right]^{1/2}} \qquad (6.30)$$

where

$$\beta = \tan^{-1}\left(\frac{2\zeta\omega_n b}{\omega_n^2 - b^2}\right) \qquad (6.31)$$

When $\zeta < 1$, the contribution of the first two terms will become negligibly small in a short time, and the motion can be described by

$$\theta = \frac{A \sin(bt-\beta)}{\left[4\zeta^2\frac{b^2}{\omega_n^2} + \left(1-\frac{b^2}{\omega_n^2}\right)^2\right]^{1/2}} \qquad (6.32)$$

The denominator of Eq. 6.32 is equal to 1/G, where G is referred to as the gain. Figure 6.12

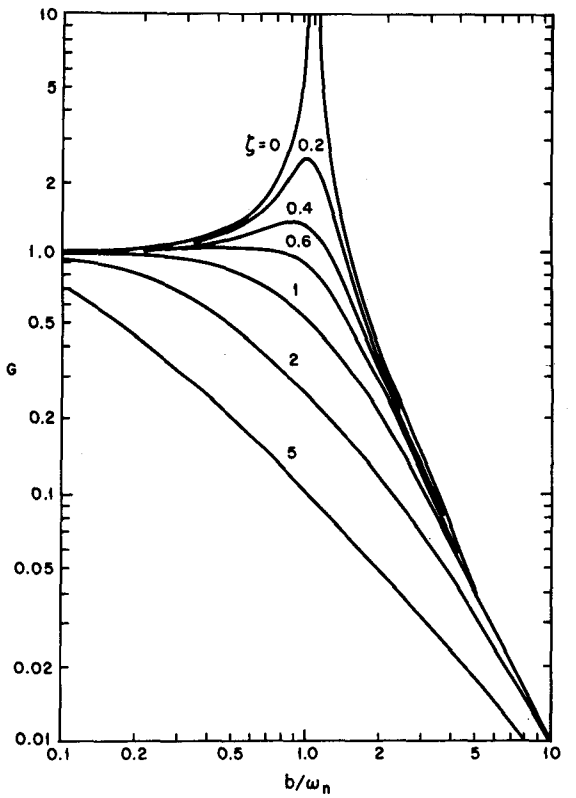

Fig. 6.12—Second-order gain characteristics. (Trimmer, 1950.)

shows the relation between the gain and the ratio of the forcing angular frequency, b, to ω_n, the natural angular frequency. When $b = \omega_n$, for ζ less than 0.5, amplification will occur since $G = (2\zeta)^{-1} > 1$ as can be seen from Eq. 6.30. Figure 6.12 indicates that for $\zeta = 0.6$, and $b/\omega_n < 0.8$, faithful response is to be expected.

The angle β is the phase lag between the forcing and response. This relation as a function of b/ω_n for a range of damping factors, ζ, is shown in Fig. 6.13. Even for a damping factor of $\zeta = 0.6$, the phase lag is appreciable.

The foregoing analysis is based on a sine wave of a given single frequency. The wind,

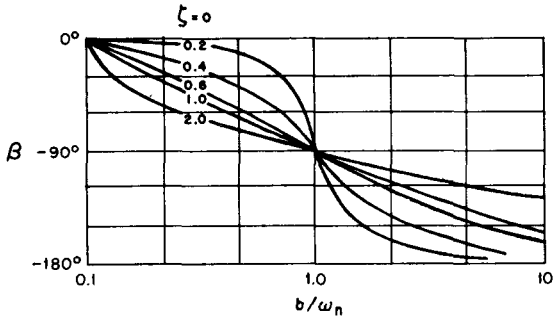

Fig. 6.13—Second-order phase characteristics. (Trimmer, 1950.)

however, as sensed by a wind vane is composed of sine waves having a spectrum of frequencies. Thus one might expect errors because the gain G, as well as the phase angle β, will be different for each frequency. Where the wind has frequency components comparable to or higher than the natural frequency of the vane, these will be attenuated as indicated in Fig. 6.12.

Figure 4.21 in Chap. 4 indicates the dependence of $\sigma_y(x)$ (the standard deviation of the plume concentration distribution in the horizontal transverse direction at a given distance, x, from the source) on σ_θ (the standard deviation of the azimuth-direction fluctuations). If data from different sites are to be compared or, alternatively, if graphs such as Fig. 4.21 are to be used as guides for estimating diffusion at a given site, one must be able to properly interpret the wind-vane readings.

In practice σ_θ is often estimated from a recorder trace by determining the range of fluctuations over an interval, such as 20 min, and assuming that this range is approximately equal to $6.0\sigma_\theta$. Others have suggested that a few of the largest deviations on either side of the mean be omitted and that the range be represented by $4.0\sigma_\theta$. These techniques may be satisfactory if the damping ratio is greater than 0.5 as seen from Fig. 6.12.

With data from a vane or bivane having a damping factor appreciably less than 0.4, the resonant oscillations must be removed mathematically by averaging the data over a 10- or 20-sec interval and using these averages for computing σ_θ. The most appropriate interval would depend on the characteristics of the vane and can be determined by the analysis of wind-vane dynamics presented in this chapter.

6-4.2.4 The Distance Constant of a Vane. The distance constant for an anemometer was defined as the distance over which the wind travels corresponding to (1 − 1/e) or 63% of a step function change. A similar concept can be used for the vane, but there is some difference in definition among different authors. MacCready and Jex (1964) suggest a 50% change for a step impulse from initial to final values; Gill (1959) suggests the length of wind trajectory necessary to complete an oscillation. Of course, wind vanes of less than critical damping are considered.

To show that for a given wind vane the distance concept is valid, i.e., that the fraction of the change from the initial to final position during the first oscillation is a function of wind distance rather than speed, we can rewrite Eq. 6.24

$$\frac{\theta}{\theta_0} = \frac{1}{(1-\zeta^2)^{1/2}}\, e^{-\omega_n \zeta x/U} \times \cos\left[\omega_n (1-\zeta^2)^{1/2}\, \frac{x}{U} - \beta\right] \qquad (6.33)$$

since t = x/U, where x is the distance of wind travel in time t.

From Eqs. 6.20 and 6.21, we see that

$$\omega_n = U\left(\frac{k\rho A r}{2I}\right)^{1/2} = \frac{2U\zeta}{r} \qquad (6.34)$$

Hence, when we substitute for ω_n in Eq. 6.33, the wind speed, U, cancels, and we have

$$\frac{\theta}{\theta_0} = \frac{1}{(1-\zeta^2)^{1/2}}\, e^{-2\zeta^2 x/r} \times \cos\left[\frac{2\zeta}{r}(1-\zeta^2)^{1/2}\, x - \beta\right] \qquad (6.35)$$

Since x is the only variable in the right-hand side of the equation, a distance constant can be defined. Thus the distance over which the wind must travel for the wind vane to adjust to (1 − 1/e) of its displacement, θ_0, is independent of the wind speed.

From Eq. 6.20 we have

$$2\pi f_n = U\left(\frac{k\rho A r}{2I}\right)^{1/2} \qquad (6.36)$$

where f_n is the natural vane frequency.

Multiplying both sides of the equation by λ_n, the natural gust wavelength, and using the relation $f_n \lambda_n = U$, we have

$$2\pi f_n \lambda_n = 2\pi U = \lambda_n U \left(\frac{k\rho Ar}{2I}\right)^{1/2} \qquad (6.37)$$

or

$$\lambda_n = 2\pi \left(\frac{2I}{k\rho Ar}\right)^{1/2} \qquad (6.38)$$

Thus we see that λ_n is also independent of the wind speed and is a useful vane parameter. Table 6.2 shows values of λ_n and ζ, the damping ratio, for some frequently used wind vanes.

since $\tan \beta = 2\zeta(b/\omega_n)/1 - (b/\omega_n)^2$. If the two phase angles are set equal to each other, then

$$bt = \frac{2\zeta b}{\omega_n} \qquad (6.41)$$

or

$$t = \frac{2\zeta}{\omega_n} \qquad (6.42)$$

In terms of the distance constant,

$$L = U\tau = \frac{2U\zeta}{\omega_n} = \frac{2U\zeta}{2\pi f_n} = \frac{\lambda_n \zeta}{\pi} \qquad (6.43)$$

since $U = \lambda_n f_n$ and $\omega_n = 2\pi f_n$, where λ_n is the wavelength corresponding to the natural frequency.

Table 6.2—VALUES OF THE DAMPING RATIO AND GUST WAVELENGTH FOR VARIOUS WIND VANES

Manufacturer	Model	Damping ratio (ζ)	Gust wavelength (λ_n), m
Beckman & Whitley, Inc.			
Quick One	Series 50	0.69	
Quick Two	Series 50	0.43	
Bendix Friez Instrument Division			
Aerovane		0.28	14.7
Climet Instruments Inc.	014-6	0.45	3.5
	014-51	0.60	2.3
Electric Speed Indicator Co.			
Splayed vane	F-420C	0.14	17.7
R. M. Young Company			
Gill Anemometer-Bivane		0.60	4.4
Belfort Instrument Co.			
Splayed vane	Type M	0.20	9.5
Meteorology Research, Inc.			
VelocityVane	1057	0.45 to 0.65	5.3
VectorVane	1053	0.60 to 0.66	3.2

6-4.2.5 Matching of Speed and Direction Sensors. In an Aerovane or an anemometer bivane, we can minimize wind-measuring error by matching the characteristics of the speed and direction sensors. This is done by making the phase lags of the two systems equal.

Because of phase lag, the vane or anemometer provides a reading corresponding to the wind some distance downstream. For large eddies, i.e., in the low-frequency region, the relation between phase angle and frequency is approximately linear.

For an anemometer, since $\beta = \arctan bt$,

$$\beta \approx bt \qquad \text{(for small bt)} \qquad (6.39)$$

Similarly, for a vane for $b/\omega_n \ll 1$,

$$\beta \approx 2\zeta b/\omega_n \qquad (6.40)$$

The speed lag refers to the propeller, and the direction lag, to the vane centroid. If there is an appreciable distance between the two, an additional correction equal to the distance d between the vane and propeller should be applied, i.e.,

$$L = \frac{\lambda_n \zeta}{\pi} + d \qquad (6.44)$$

MacCready and Jex (1964) indicated that this technique will provide a phase mismatch of less than 1° for eddies larger than five times the natural wavelength and 10° for eddies of the order of twice the natural wavelength.

The vane and propeller can also be matched by making the distance constants equal and cor-

recting for the separation between vane and propeller, i.e.,

$$L_{propeller} = L_{vane} + d \qquad (6.45)$$

According to MacCready and Jex, this technique will provide a better match at higher frequencies, i.e., a few degrees for eddies twice the natural wavelength and 10° for eddies only 1.4 times λ_n.

The preceding discussion on the dynamics of the vane applies to a vane without a propeller. When an instrument with a forward fin or propeller is considered, such as an anemometer bivane or an Aerovane, the analysis becomes considerably more complicated. It is then necessary to consider both downwash from the forward surface and the gradient of wind along the vane. The forward surface will reduce the natural frequency and increase the damping factor. Analyses of the dynamics of the vane with a propeller are given by MacCready and Jex (1964) and by Sanuki, Kimura, and Baba (1960).

6-5 TEMPERATURE MEASUREMENTS

At meteorological installations within the atomic energy industry, three types of temperature measurements are commonly made. The first and most frequent type measures the temperature of the air at about 1.5 m above ground. This is frequently referred to as the surface air temperature. The second type measures the temperature of the air at various elevations within about the first 100 m. The purpose of these measurements is to determine the thermodynamic stability of the atmosphere, which is of importance in assessing rates of turbulent diffusion. Such measurements, of course, are also used to establish general climatologies. The final type of temperature measurement is that of the soil at various levels below the surface.

6-5.1 Exposure of Temperature-sensing Equipment

When any object used as a thermal sensor is exposed in the atmosphere, it may assume a temperature quite different from that of the surrounding air. The temperature it assumes is the result of (1) the radiation it absorbs from the sun, sky, earth, and surrounding objects, (2) the radiation it emits (which, in turn, depends upon its own temperature and emissivity), (3) the heat transfer between it and the ambient air by convection and conduction, and (4) the heat conduction from surrounding materials, such as electrical lead wire or supporting mounts.

Usually the thermal sensor is placed in a well-ventilated enclosure to minimize unwanted radiation effects. At installations where only air temperatures are recorded, the enclosure is an instrument shelter such as shown in Fig. 6.14. Typical dimensions for this kind of

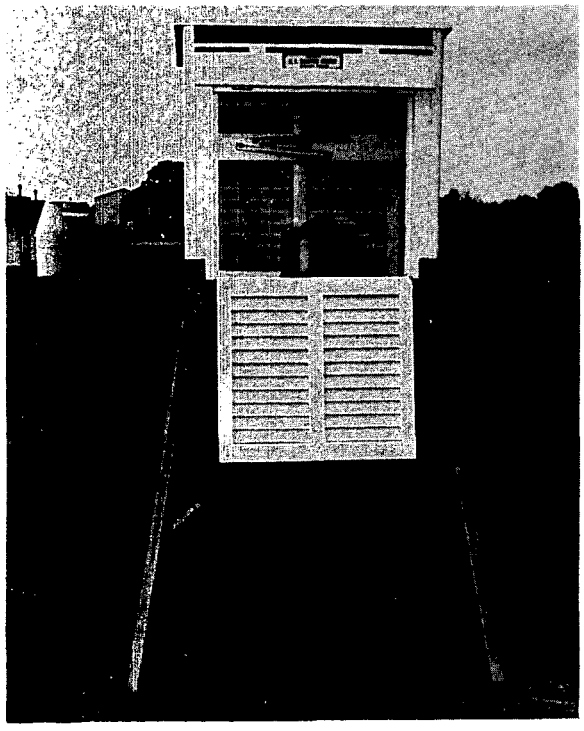

Fig. 6.14—Standard instrument shelter showing mounted minimum (upper) and maximum (lower) thermometers and a thermograph.

shelter are height, 83 cm, width, 73 cm, and depth, 52 cm. The shelter is painted white to enhance the reflectivity of impinging radiation. It is usually louvered on all four sides and has a double roof, with a 5.0- to 7.5-cm air space, and a slatted bottom. The shelter is mounted on an open framework so that the thermometer height above the ground is about 1.5 m. A door hinged at the bottom is placed on the side of the

shelter facing north so that when instruments are serviced the sun will not shine on them. This shelter is used to house not only mercury-in-glass thermometers for measuring ambient and wet-bulb temperatures but also hygrothermographs and maximum and minimum thermometers.

The shelter should be placed over a grass surface (never over hard gravel or cement) in an unobstructed area away from surrounding structures. A fan may be used to provide ventilation when taking hourly readings with a mercury-in-glass thermometer. Either a hand-driven or a motor-driven fan can be used. With the latter, precaution must be taken to assure that the heat from the motor does not influence the air passing over the sensing element.

The variation of temperature with height is a measure of the stability of the atmosphere. The thermal sensor must be placed on a platform to determine the temperature at various levels above ground. The platform may be a boom, 2 or 3 m in length, extending from a structure, such as an open-lattice tower. The use of building tops or hills as locations for determining vertical temperature gradients is strongly discouraged since the temperature near such objects may be quite different from that at the same height some lateral distance away.

Resistance thermometers or thermocouples are the most common thermal sensors used for measuring the variation of temperature with height. These sensors are generally enclosed in a radiation–ventilation shield (see Fig. 6.15). Fuchs and Tanner (1965) have made an extensive study of the emissivity characteristics of various materials used in radiation shields. The shield is often made of thin sheet metal, such as aluminum, and is in the form of two concentric cylinders about 15.0 cm long. The outer cylinder has a diameter of about 7.5 cm, and the inner one, a diameter of about 3.0 to 5.0 cm. The outer surfaces of these cylinders are made highly reflective. This shield is mounted from the end of a boom, and an aspiration blower is mounted at the other end. The blower draws in air through both the inner cylinder and the

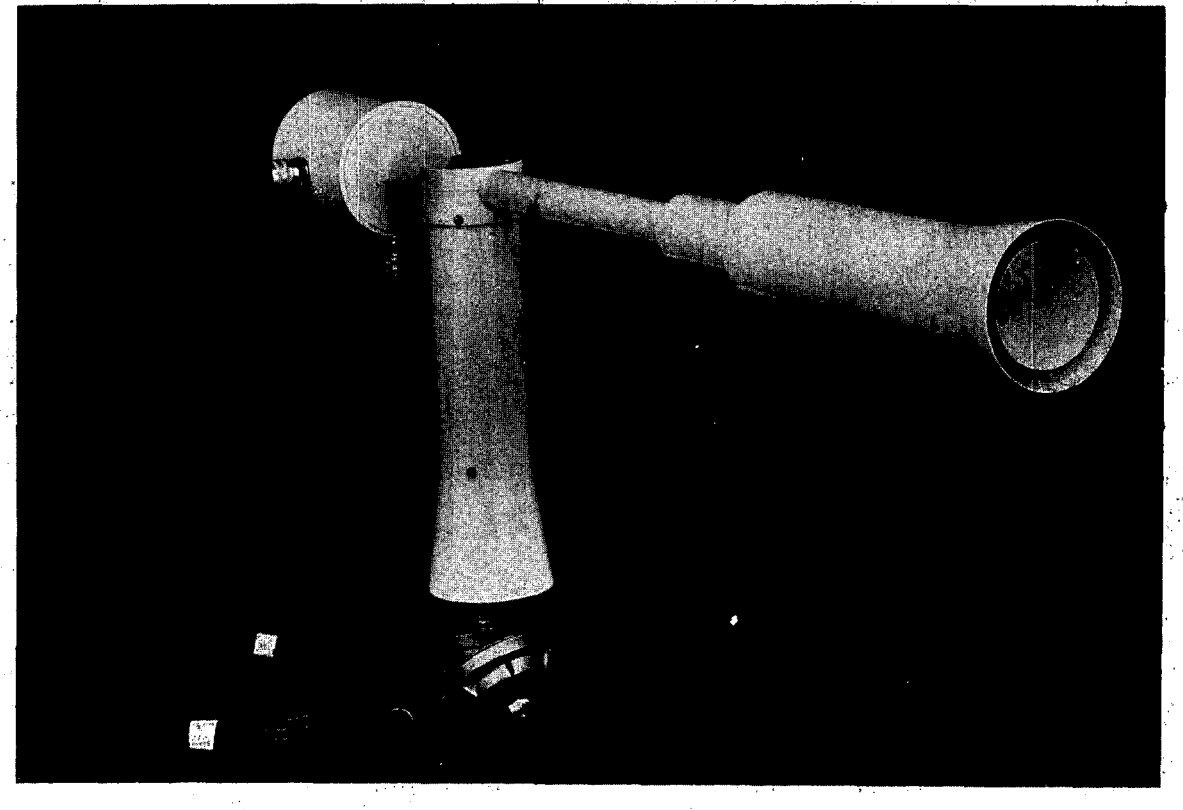

Fig. 6.15 — Photograph of a fan-aspirated radiation shield for housing temperature and dew-point sensors (Climet Instruments Inc.).

annular space. A baffle must be placed at the bottom of the shield to prevent reflected or emitted radiation from the ground from affecting the sensor. An umbrella-like shield is sometimes provided to protect against precipitation and, to a lesser extent, against radiation. In this way the radiation–ventilation shield minimizes the radiation effects and allows the thermal element to come into equilibrium with the ambient-air temperature. Tanner (1963) discusses other types of radiation shields and materials as well as the problems related to measurement of air temperatures and temperature profiles.

Aspiration can be obtained by either individual blowers or a centralized fan. On the meteorological towers at Brookhaven National Laboratory and at Battelle-Northwest, centralized blower systems provide the necessary ventilation. At Argonne National Laboratory individual blowers are used. Individual blowers are economical, will operate for 3 or 4 years with minimum maintenance, and are readily available commercially.

The airflow over the thermal sensor should be of the order of 5 m/sec. At typical atmospheric wind speeds, dynamic heating is not a problem.

A problem of importance in the measurement of vertical temperature profiles is the error that can result from the effects of rain or snow on the element or the electrical junctions. If the thermocouple junctions become wet, galvanic action may create spurious electromotive forces that produce errors.

For a continuous recording of soil temperatures, resistance thermometers or thermocouples are most frequently used. Resistance thermometers enclosed in a metallic shield welded to a lead-covered cable (which prevents moisture from entering the system) have proven satisfactory. For visual readings various forms of mercury-in-glass, mercury-in-steel, and bimetal thermometers have been used.

The World Meteorological Organization (Blanc, 1958) recommends that soil-temperature measurements be made at the following levels below the ground surface: 10, 20, 50, 100, 150, and 300 cm. When soil-temperature sensors are installed, the soil structure is usually altered. The soil above and around the sensor itself should be disturbed as little as possible so that such thermal properties as volumetric heat capacity, conductivity, and moisture content are not changed. Alteration of the soil profile can be minimized by the following procedure. First, with an auger dig a hole about 1 m in diameter to a depth slightly below the lowest level of soil-temperature measurement. Then drill a horizontal hole along a radius of the pit through the wall. This hole should be about 1 m in length with a diameter of about the same size as the protective shield of the soil thermometer. Drill similar horizontal holes at each level at which soil temperatures are to be measured. The soil thermometers should fit snugly into these horizontal holes. When the large pit is refilled, an effort should be made to restore each soil layer to its original position and compaction.

6-5.2 Types of Thermal Sensors

In general, any property of a substance that changes with temperature can be used for measuring temperature. In this section sensors based on the properties of thermal expansion, electrical resistance, and thermoelectricity will be discussed. Such properties as changes in the vapor pressure of liquids with temperature or dependence of the velocity of sound in air on temperature will not be discussed although thermometers based on these and other properties have been developed.

There are three commonly used types of temperature instruments that depend upon thermal expansion: the liquid-in-glass thermometer, the bimetal thermometer, and the Bourdon tube.

The liquid-in-glass thermometer consists of a bulb containing a liquid, e.g., mercury or alcohol, at one end of a capillary tube. The length to which the capillary tube is filled is a measure of the temperature of the bulb. Scale readings can be etched on the stem itself or on the mounting plate although the former procedure is to be preferred. Although the volumetric expansion of such organic liquids as ethyl alcohol is several times greater than that of mercury, the use of mercury is preferred because of its greater accuracy. Organic liquids must be used for very low temperatures since mercury freezes at $-38.9°C$ but organic liquids, such as ethyl alcohol, do not freeze until temperatures well below $-100°C$.

Although liquid-in-glass thermometers are simple to use and require little maintenance, they are subject to a number of problems, e.g., separation of the liquid in the capillary, distillation of the liquid, hysteresis, and secular changes. When the thermometer is exposed to high temperatures and then quickly placed in a cold environment, a calibration shift may occur, i.e., the 0°C point may change. After a few days, however, the readings will return to normal. Over a period of a year, a calibration change of the order of 0.1°C is not uncommon. Therefore annual calibration checks are desirable. A calibration check can be made by immersing the thermometer in a mixture of distilled water and ice made from distilled water.

Some liquid-in-glass thermometers are calibrated as partial-immersion thermometers, i.e., they read correctly only when the bulb and a few centimeters of the stem are immersed. Only total-immersion thermometers are suitable for meteorological measurements.

One special type of liquid-in-glass thermometer is the maximum thermometer (Fig. 6.16). For many purposes it is important to know the highest temperature that occurred over a selected time interval, such as 24 hrs. A maximum thermometer can be used to accomplish this.

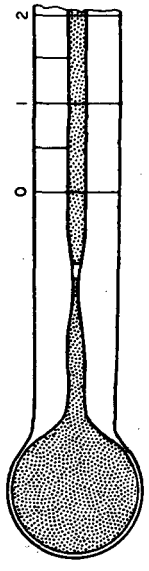

Fig. 6.16 — Details of a maximum thermometer showing the bulb and the constriction in the capillary tube. A mounted maximum thermometer is shown in Fig. 6.14.

This sensor is similar to the ordinary mercury-in-glass thermometer except for a constriction near the bulb. When the temperature rises, the liquid column remains intact; when the temperature falls, the column breaks at the constriction, the liquid above the constriction in the tube cannot return to the bulb, and thus the highest reading is retained. The ordinary fever thermometer used in medicine is an example of a maximum thermometer.

It is also possible to obtain minimum temperatures with a liquid-in-glass thermometer. In this case, the capillary tube contains a clear organic liquid and movable index (Fig. 6.17).

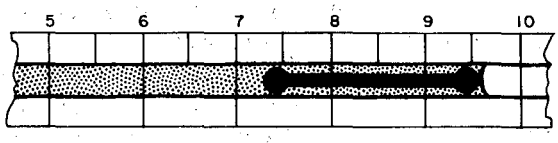

Fig. 6.17 — A section of the capillary tube of a minimum thermometer showing the sliding index that marks the lowest temperature reached by the meniscus of the fluid in the tube. A mounted minimum thermometer is shown in Fig. 6.14.

When the temperature falls, the surface tension of the liquid at the end of the capillary tube causes the index to move toward the bulb. When the temperature rises, however, the liquid flows around the index. Thus the position of the end of the index farther from the bulb provides a reading of the lowest temperature. For reliable results the minimum thermometer must be mounted at an angle of about 5° from the horizontal with the bulb end lower. Minimum and maximum thermometers mounted in a weather shelter are shown in Fig. 6.14.

The liquid-in-glass thermometer is essentially an indicating instrument. It can be used as a recording instrument but as such is uneconomical and cumbersome. The bimetallic sensor can be used in a recording system.

When two metallic strips of materials having different thermal-expansion coefficients, e.g., invar and brass or invar and steel, are welded together, the unit will bend with a change in temperature. If one end is fixed in position, the other end can be used for recording ambient temperature.

The welded strips can take the form of a simple strip several centimeters long and less than 2.0 cm wide or of a coil or helix. Its thickness is usually about 0.08 cm. Such an

instrument is insensitive to rough handling. A simple strip has greater sensitivity than does the coil or helix. Also, sensitivity varies inversely as the thickness but directly as the square of the total length and directly as the difference in the coefficients of expansion of the two metals. The greater the stiffness, the higher the torque available for driving the recorder pen.

The bimetallic sensor is frequently used in thermographs. With a suitable linkage, position changes of the free end of the bimetal sensor are recorded by a pen making an ink trace on a recorder chart wound on a clock-driven rotating drum.

The Bourdon tube is a thermal sensor consisting of a metallic enclosure filled with an organic liquid. The tube may be 5 cm or more in length and usually is of elliptical cross section. In its operation the Bourdon tube is similar to the bimetal thermometer. One edge of the tube is clamped, and the other is free to move. The movable edge is attached to a pen that provides a temperature–time record on a clock-driven rotating drum. The Bourdon tube is commonly used as the thermal sensor in commercial thermographs (Fig. 6.18). Although this type of equipment is subject to some sources of error, such as a calibration change due to polymerization of the organic liquid, inability to withstand rough handling, or temperature rises above design range, it nevertheless can be classed as a successful instrument. Such equipment in thermographs can operate for many years with only routine maintenance.

For remote recording, electrical thermometers are most suitable. They most frequently take either of two forms: resistance thermometers or thermal elements, depending on the thermoelectric effect.

The resistance of such metals as platinum, nickel, copper, silver, or iron increases with a rise in temperature. This property can be used to determine the temperature of the element and, in turn, the temperature of the medium in which it is immersed. This type thermal sensor can take several different physical forms. Frequently the element is a coil with enough wire to have a resistance of about 100 ohms at room temperature. If copper is used in a 100-ohm element, a 1.0°C change in temperature will provide an approximately 0.4-ohm change in resistance.

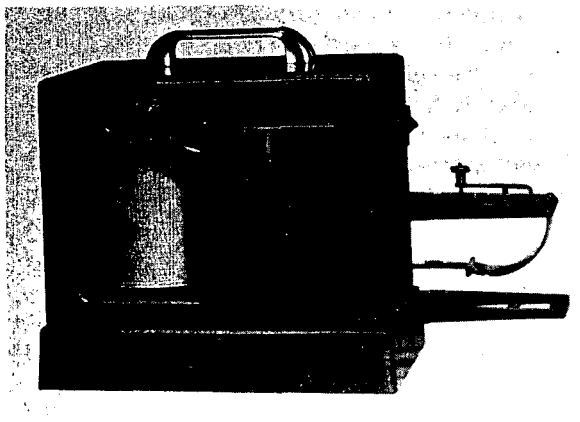

Fig. 6.18 — A thermograph. As the fluid-filled Bourdon tube (right) flexes with changes in temperature, the movement is transmitted through a series of linkages to the pen, visible in the window, which records the temperature on a calibrated chart wrapped around the clock-driven drum (Belfort Instrument Co.).

The relation between resistivity and temperature can be expressed as

$$R = R_0 \left[1 + a\,(T - T_0) + b\,(T - T_0)^2\right] \qquad (6.46)$$

where R is the resistance at temperature T, R_0 is the resistance at the reference temperature T_0, and a and b are calibration constants. Both copper and platinum show a fairly linear relation between temperature and resistance. Therefore the coefficient b is quite small. Copper is frequently used for soil thermometers that are completely enclosed in a metallic shield soldered to a lead-covered cable. Resistance thermometers of various physical sizes and resistance values are commercially available.

The output of a resistance thermometer is generally used with a self-balancing Wheatstone bridge and a strip-chart recorder.

A number of precautions must be observed in using resistance thermometers. Since the resistance change per degree is relatively small, contact resistances between electrical connections must be quite low. Changes in the temperature of the lead wire can cause problems, but these are usually compensated by making the lead wire part of the bridge. In addition, the current passing through the wires must be kept small so that the self-heating effects are kept to a minimum. With ordinary precautions these instruments will give years

of reliable service although calibration checks every 6 months to a year are necessary.

A second type of resistance thermometer is the thermistor, which is made from a mixture of metallic oxides compressed together and heat-treated. These sensors show a change of resistance with temperature that is one or two orders of magnitude higher than that of metallic resistance thermometers. Thermistors are available as rods, flakes, beads, or wafers of various sizes. The relation between resistance and temperature for the thermistor can be expressed as

$$R = a \exp\left(\frac{b}{T}\right) \tag{6.47}$$

or in differential form

$$\frac{1}{R}\frac{dR}{dT} = -\frac{b}{T^2} \tag{6.48}$$

Unlike metals, the metallic oxides exhibit the characteristic of decreasing resistance with increasing temperature. Recently metallic oxides have been developed with a positive temperature coefficient. In spite of the advantage of large resistance change with temperature, these elements have a number of deficiencies. First, the relation is extremely nonlinear, as can be observed from Eqs. 6.47 and 6.48. Second, the reliability is not so great as that of metallic resistors. These sensors may be satisfactory for short-term specialized studies where calibrations are frequently checked; however, attempts to use them for long-term climatological measurements have led to measurement errors.

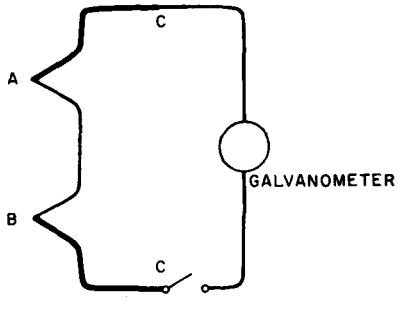

Fig. 6.19—A thermocouple. In operation the junctions A and B are at different temperatures, one of which is usually a known reference temperature. If neither metal is copper, the junctions C should be at the same temperature.

Another important class of temperature sensors includes thermocouples and thermopiles. When two dissimilar metals, such as copper and constantan (approximately 60% copper and 40% nickel with small amounts of manganese, iron, and carbon), are brought together as shown schematically in Fig. 6.19 and junction A is at a higher temperature than junction B, a current will be established. The relation between the potential difference ΔE between the two junctions and the temperature difference between junctions A and B can be expressed

$$\Delta E = c_1 (T_A - T_B) + c_2 (T_A - T_B)^2 \tag{6.49}$$

where T is temperature, c_1 and c_2 are coefficients, and the subscripts A and B refer to the thermocouples A and B. The electromotive force developed depends on the metal used. For copper–constantan at room temperature, about 40 μv/°C is generated. Thermopiles (several thermocouples in series) are often used to increase the signal per degree of temperature difference. The size of wires used in constructing thermocouples depends upon the degree of thermal lag desired in the measurements.

The output of a thermocouple is most frequently recorded by a self-balancing potentiometer. Except for precision work, a cold junction such as B is not necessary, but a compensating cold-junction spool in the potentiometer recorder is used. This consists of a thermocouple embedded in a resistance coil designed to compensate for the changes in the ambient temperature.

Thermocouples can be calibrated by immersion in a liquid bath of a low-volatility and preferably nonflammable liquid that can be cooled to low temperatures with dry ice and heated to temperatures of about 45°C with an electrical immersion heater. Ordinarily this is satisfactory for the range of meteorological conditions encountered.

The installation of a temperature-measuring system using thermocouples has many pitfalls, and consultation should be sought from those who have had previous experience in this area. For example, it is important to guard against induction currents from nearby a-c sources. Thermocouples can act as rectifiers and provide d-c potentials that are added to those generated from the temperature difference between the warm and cold junctions and thereby produce

an error that may be as much as 2° C. Proper electrical shielding can eliminate this type of error. It is also important to minimize the number of connecting junctions to avoid spurious contact potentials. During damp weather or rain, it is extremely difficult to eliminate all sources of the error even when extreme care is taken.

6-5.3 Thermometer Lag

Thermal sensors that must assume the temperature of the surrounding medium in their operation can be generally classed as first-order systems. Their behavior can be characterized by the first-order differential equation

$$\tau \frac{dT}{dt} + T = f(t) \qquad (6.50)$$

where τ is the time constant or lag coefficient, T is temperature, t is time, and f(t) is a time-dependent forcing function. The dynamic response of such thermal sensors to changing conditions is analogous to that of the cup or propeller anemometer.

When a thermal element at a temperature T_0 is suddenly placed in an environment of temperature T_e, the response is described by the differential equation

$$\tau \frac{dT}{dt} + T = T_e \qquad (6.51)$$

whose solution is

$$\frac{T - T_e}{T_0 - T_e} = \exp\left(-\frac{t}{\tau}\right) \qquad (6.52)$$

At time $t = \tau$, 63% of the change has already taken place.

The time constant, τ, is a function of the product of air density and wind speed raised to a power n. This relation can be expressed as

$$\tau = \frac{K}{(\rho U)^n} \qquad (6.53)$$

where ρ is the air density and U is the wind speed. The exponent n has a value of about $\frac{1}{2}$. The lag coefficient for a mercury-in-glass thermometer having a spherical bulb of 1.12-cm diameter is 56 sec for a ventilation rate of 5 m/sec (Great Britain, Meteorological Office, 1956).

Middleton and Spilhaus (1953) point out that for still air the lag coefficient for rising temperatures is slightly larger than for falling temperatures, but, even with a little ventilation, this difference becomes small. Peterson and Womack (1937) point out that at very high wind speeds, the exponent may approach the value of 1.

In addition to wind speed, the lag coefficient depends on other factors, e.g., the conductivity of the glass and mercury or organic material used, the specific heat and mass of the bulb and the liquid, and the geometric shape and roughness of the bulb. The latter two factors influence the turbulence and consequently the heat transfer from the sensor to the surrounding atmosphere.

When the temperature changes at a constant rate, a thermal sensor will lag behind the actual temperature. If we assume that the temperature of the environment is changing at a rate of α degrees per second, i.e.,

$$T_e = T_1 + \alpha t \qquad (6.54)$$

where T_1 is the initial temperature of the environment and α is the rate of change with time in degrees per second, then the differential equation describing this condition could be expressed as

$$\tau \frac{dT}{dt} + T = T_1 + \alpha t \qquad (6.55)$$

The solution of this equation is

$$T - T_e = -\alpha\tau + (\alpha\tau)\, e^{-t/\tau} \qquad (6.56)$$

Thus we see that for a period of time that is large compared to τ, the lag coefficient, the thermometer will lag the actual temperature by a difference equal to $-\alpha\tau$ degrees.

If the environment undergoes a sinusoidal fluctuation described by

$$f(t) = T_1 + A \sin \frac{2\pi}{P} t \qquad (6.57)$$

the differential equation can be given as

$$\tau \frac{dT}{dt} + T = T_1 + A \sin \frac{2\pi}{P} t \qquad (6.58)$$

and its solution is

$$T = T_1 + C_1 e^{-T/\tau} + \frac{A}{[1 + (2\pi\tau/P)^2]^{1/2}} \sin\left(\frac{2\pi}{P} t - \beta\right) \qquad (6.59)$$

where T_1 is the initial temperature, C_1 is a constant, A is the amplitude of the sinusoidal fluctuation, P is the period of the sinusoidal fluctuation, and β is the phase angle, which is given by

$$\beta = \tan^{-1} \frac{2\pi\tau}{P} \qquad (6.60)$$

Table 6.3 shows the relative attenuation of sinusoidal temperature fluctuations for various ratios of fluctuation period to lag coefficient. The phase shift β is also given. Middleton and Spilhaus (1953) recommended that for ordinary uses the thermal sensing element have a lag greater than 30 sec.

Table 6.3—RESPONSE OF THERMOMETERS TO FLUCTUATING TEMPERATURES*

Ratio of fluctuation period to lag coefficient (P/τ)	0.2	0.4	0.6	0.8	1.0	2.0	4.0	6.0	10.0
Ratio of response to time amplitude	0.04	0.06	0.09	0.13	0.16	0.31	0.54	0.69	0.85
Phase lag (β), deg	88	86	85	83	81	72	58	46	30

*Great Britain, Meteorological Office, Instruments for Surface Observations, in *Handbook of Meteorological Instruments, Part I*, p.92, Her Majesty's Stationery Office, London, England, 1956.

For ordinary needs at a reactor site, the 30-sec lag is quite acceptable, but, for special studies, such as those involving heat-flux determinations, where the quantity $\overline{w'T'}$ [i.e., the covariance of vertical wind (w') and temperature (T') fluctuation] must be determined, very low lags ($\approx$1.0 sec or less) are required. In addition, the wind and thermal-sensor response times must be matched.

6-5.4 Calibration and Testing of Thermometers

Equipment for the immersion testing and calibration of liquid-in-glass and electrical thermometers is available commercially. A thermometer calibrated by the National Bureau of Standards for use as a secondary standard is essential for carrying out thermometer calibrations.

The calibration procedure ordinarily consists in immersing the thermometer beside the reference thermometer in a large vessel (4 to 5 gal in volume is desirable) filled with a suitable liquid, such as one of the silicone oils, and comparing their readings at various temperatures. A sparkless stirring motor is used to provide uniform temperatures throughout the vessel. Its stirrer is enclosed in a metal case with suitable openings to allow liquid flow. Water can be used as the bath liquid for temperatures above freezing. A thermostatically controlled electric immersion heater is quite suitable for raising the bath temperature, and either cooling coils with circulating brine or dry ice can be used for lowering the temperature. Care must be taken to assure that equilibrium is reached during the comparison of the reference and test thermometers. If temperature comparisons are made for temperatures about 20°C above or below room temperature, the vessel should be insulated thermally to reduce heat transfer through the walls.

There are a number of pitfalls in the calibration of thermocouples or resistance thermometers. For example, when the temperature of the bath differs from that of the room, a sufficient length of the wire attached to the thermal element should be immersed in the bath or heat will be conducted through the wire and cause an error in the reading. If a thermopile that is not enclosed in a protective cover is used, the electrical conductivity of the liquid should be checked. If a liquid such as ethyl alcohol or water is used, dirt from the dry ice, as well as condensed water on the dry ice itself, will dissolve, raise the conductivity, and thus cause a serious calibration error. During cali-

bration the lead wire of the thermocouple should be shielded to avoid inductive pickup of alternating current. If a metallic vessel is used to hold the calibrating bath, it must be well grounded to minimize this source of error. The extent of the inductive a-c pickup can be determined by means of an oscilloscope connected to one of the input terminals of the recorder and the ground.

Thermographs using bimetals or Bourdon tubes are best calibrated in an air chamber. The reference thermometer must be placed as close as possible to the thermal element.

6-6 SOLAR AND TERRESTRIAL RADIATION MEASUREMENTS

In many instances the intensity of solar radiation or net radiation flux is closely correlated with the stability of the atmosphere and thus provides a measure of its diffusive capacity. Radiation measurements are also useful to indicate cloudiness at stations that are not manned on a 24-hr basis. This is especially true of the net-radiation-flux measurements, which are of value at night as well as during the day. Recent work on atmospheric chemistry has indicated that photochemical reactions in the atmosphere, producing ozone or other substances, are related to the production of smog. A measurement of the intensity of solar radiation is thus of value in air-pollution studies.

Two types of radiation instruments are most frequently used at atomic energy installations: the Eppley pyranometer (pyrheliometer) (Fig. 6.20) and the Beckman & Whitley net radiometer based on the design by Gier and Dunkel (Fig. 6.21).

The measurement of solar and sky radiation on a horizontal surface by an instrument such as the Eppley pyranometer is based on the temperature difference between two concentric rings, one coated with lamp black and the other with magnesium oxide. The temperature is measured by either a 10- or a 50-junction thermopile in thermal contact with the rings but electrically insulated from them. The entire assembly, consisting of the two rings and thermopile, is enclosed in a 7.5-cm-diameter soda-lime glass bulb filled with dry air. The thermopile output can be recorded by a self-balancing electronic potentiometer located 100 m or more from the recorder.

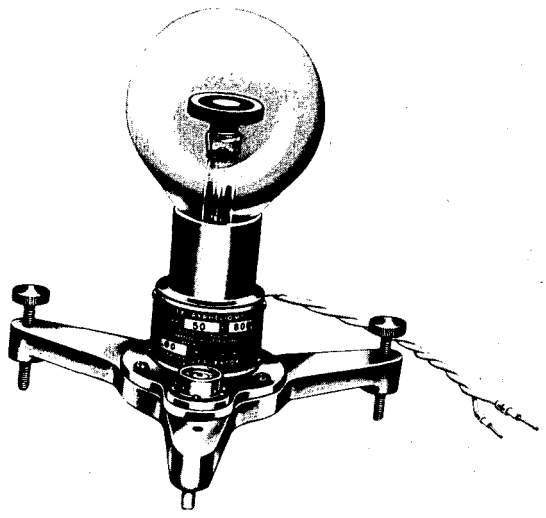

Fig. 6.20 — A pyranometer (pyrheliometer) (The Eppley Laboratory, Inc.).

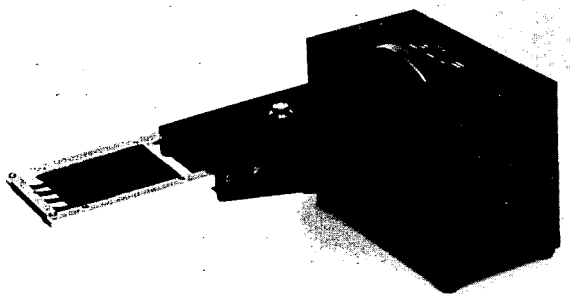

Fig. 6.21 — A net radiometer (Beckman & Whitley, Inc.).

The net radiation flux as measured by a net radiometer is determined from the output of a differential thermopile measuring the vertical temperature gradient across a horizontal Bakelite sheet. A schematic diagram of this type of net radiometer is shown in Fig. 6.22. The entire unit is mounted in front of a housing containing a blower that provides an airflow distributed equally across the top and bottom of the flux plate. This airflow equalizes convective heat losses and minimizes dust and dew accumulation. The net radiometer, however, cannot be used during rainfall since wetting of the top surface causes appreciable cooling and thus produces a spurious indication of radiation flux.

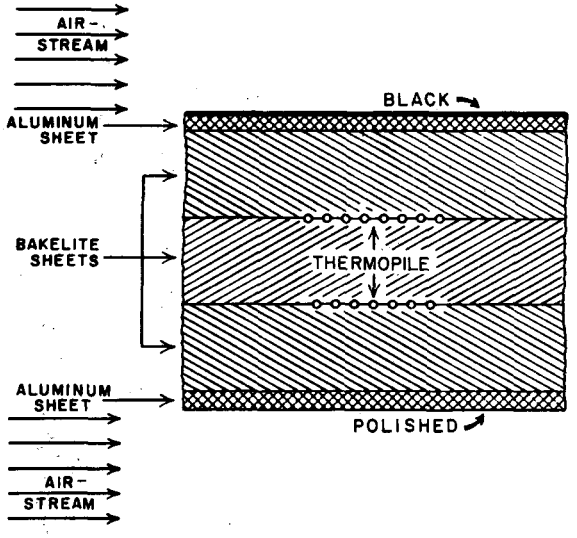

Fig. 6.22—A schematic drawing of a net radiometer. In this instance the thermopiles are cemented between aluminum faceplates (Beckman & Whitley, Inc.).

Radiation instruments should be located so that the sun is unobstructed during all times of the year. The pyranometer can be mounted on top of a building if a suitable ground location is unavailable. The mounting of the net radiometer, however, is more critical since the radiation received by both the bottom plate and the top plate is of concern. For this reason building roofs are not suitable as platforms for net radiometers. Both types of instruments must be mounted on a firm base and leveled.

6-7 PRECIPITATION MEASUREMENTS

Systems for measuring precipitation are of two general types. The first type is the simple nonrecording collector, usually a cylinder. Total precipitation amounts are determined by measuring the amount of accumulated precipitation with a graduated dipstick. The second type of system furnishes a continuous record of the amount of precipitation by utilizing mechanical and electrical devices. The major cause of inaccuracy in precipitation gauges is the aerodynamic flow in the vicinity of the gauge mouth. Warnick (1956) established that any moderate to strong flow of air past a gauge standing vertically above the ground will create eddy patterns that will divert a significant portion of the precipitation away from the intake of the gauge. In strong winds then the gauge itself and the pattern of upwind obstacles can produce deficiencies of 10% to 30% of the true precipitation fall. There are methods of minimizing this effect to some extent (as shown by Kurtyka, 1953), but it is not possible to eliminate the problem completely with any standard gauge.

One solution to the problem is to introduce an instrument as a simulated section of the ground surface in very uniform terrain, but the increased accuracy is seldom necessary in the atomic energy industry.

A second type of error results from the various forms that precipitation takes. Drops of rain are more readily recorded accurately, particularly as a function of time, than are similar amounts of snow, sleet, hail, and other frozen precipitation forms. It is possible to obtain gauges on special order that will melt the precipitation as it arrives on the gauge.

In a comprehensive review of rain gauges, Kurtyka (1953) shows that almost 200 types of gauges have been constructed and used. His report describes, illustrates, and gives excellent references to the various types found.

The most common type of rain gauge is a cylinder with a diameter of 20.32 cm (8 in.). At the top of the cylinder is a funnel-shaped intake below which there is a cylinder of much smaller diameter (Fig. 6.23). Rainfall collected at the mouth is then funneled into a smaller diameter cylinder so that, with the linear height of the precipitation magnified, even quite small amounts can be measured with a graduated rule. Within the limitations previously mentioned, this gauge is perfectly suitable for those purposes requiring only an integrated measure over a long period of time, i.e., 12 to 24 hr or more.

A modification of the standard rain gauge uses a spring-scale assembly that records essentially the weight of the water collected in a bucket system (Fig. 6.24). As the amount of catch increases, the bucket and its mounting platform are depressed, and the pen indicates the current weight of the bucket translated into amount of precipitation on a drum chart assembly. Depending upon the time scale of the clock mechanism used, such a gauge permits a reasonably accurate interpretation not only of the rate of rainfall but of the total amount

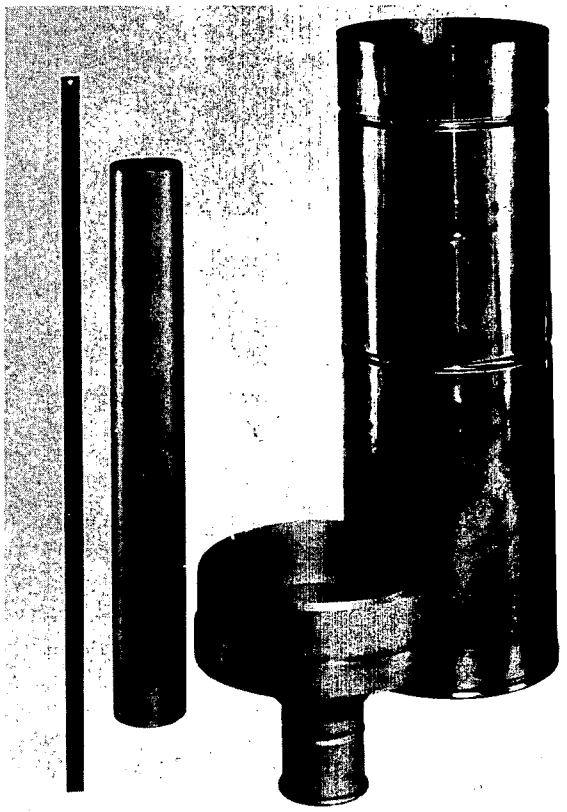

Fig. 6.23—A standard rain gauge. The precipitation is collected in the widemouthed funnel, which fits into the top of the large cylinder, and then passes into the narrow cylinder, which is mounted below the funnel. Precipitation depth is measured by a suitably graduated rule (Belfort Instrument Co.).

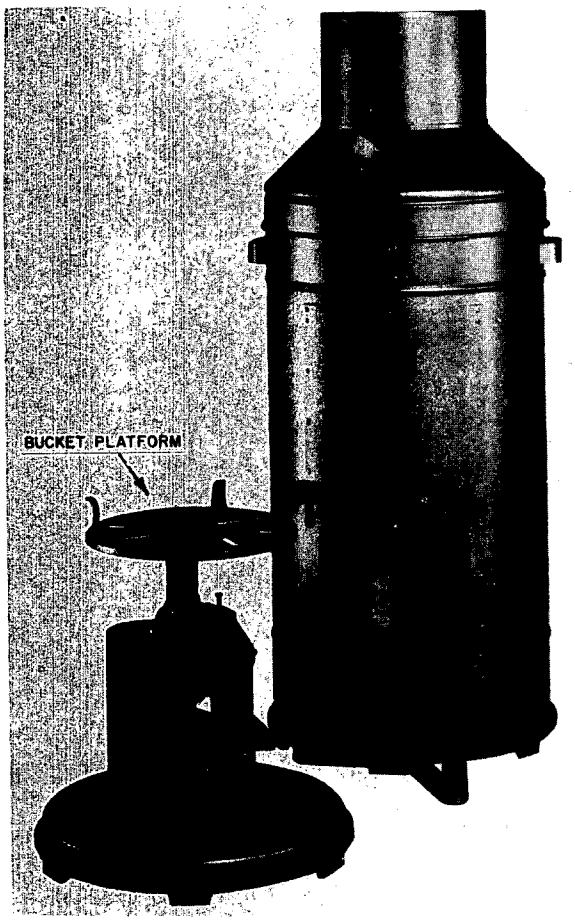

Fig. 6.24—A weighing rain gauge. Precipitation enters the top of the gauge and passes into a bucket (not shown) that rests on the bucket platform (foreground). A cumulative record of the depth of precipitation is recorded on the clock-driven drum (Belfort Instrument Co.).

deposited within any given time period. The main disadvantage of this type of gauge is the loss of precipitation by evaporation. Calibration is relatively simple with weights corresponding to equivalent amounts of liquid water.

Another precipitation-measuring system with time resolution is the tipping-bucket rain gauge (Fig. 6.25) in which the collection of some very small amount of precipitation causes a bucket assembly to become overbalanced and flip to the opposite side. As it does so, a magnetic switch or other type of switch produces an appropriate electrical pulse indicating the event. Recording of such information is relatively simple. An event pen (a pen that changes position by a fixed amount when energized and returns to its original position when deenergized) provides a continuous chart record of the occurrence of each unit of precipitation. Thus it is possible to define with rather high precision not only the total amount of precipitation in a given time period but variations of the short-term rate if the chart speed is fast enough. An event counter would indicate the total rainfall for a given period.

Precipitation itself may be of interest in certain atomic energy studies, such as evaluating fallout or, in isolated cases, determining the presence of radioactivity or other atmospheric pollutants. Generally speaking, such evaluation requires considerably larger volumes of water than are provided by the smaller standard gauges. For this reason several labora-

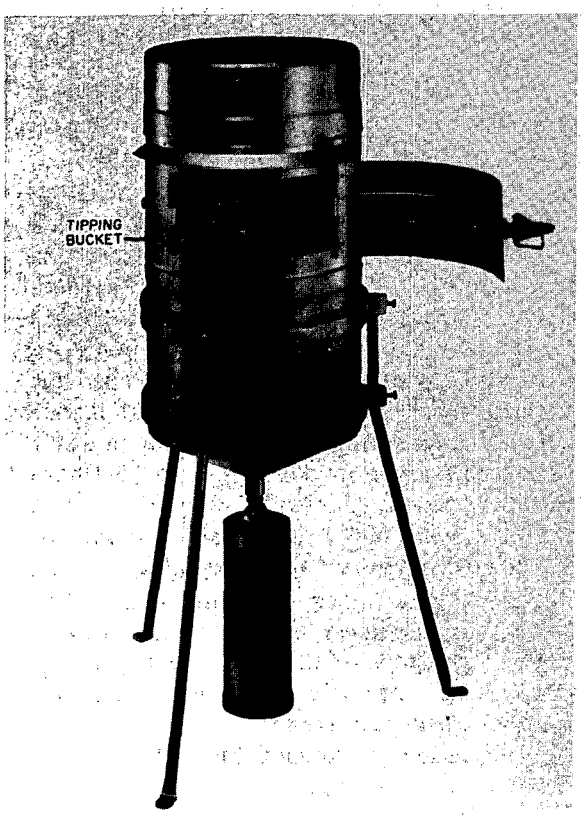

Fig. 6.25—A tipping-bucket rain gauge. The precipitation enters the top of the gauge and is funneled into one cell of the pivoting bucket. After being filled, the cell tips, the impulse of the tipping is counted, and the empty cell is positioned under the funnel (Belfort Instrument Co.).

tories and Atomic Energy Commission contractors have designed and constructed collectors with very large diameters and complex bucket-switching systems so that precipitation can be separated into short-term samples, each having a volume of the order of liters.

6-8 PRESSURE MEASUREMENTS

At atomic energy installations the need for atmospheric-pressure information arises when values of atmospheric density are required. Should a reactor mishap occur and radioactive gases be contained in a reactor shell or reactor building, information on 24-hr pressure variations would be useful in determining the breathing rate from the building to the external atmosphere.

The two most frequently used pressure-measuring instruments at atomic energy installations in the United States are the Fortin mercurial barometer (Fig. 6.26) and the aneroid microbarograph (Fig. 6.27).

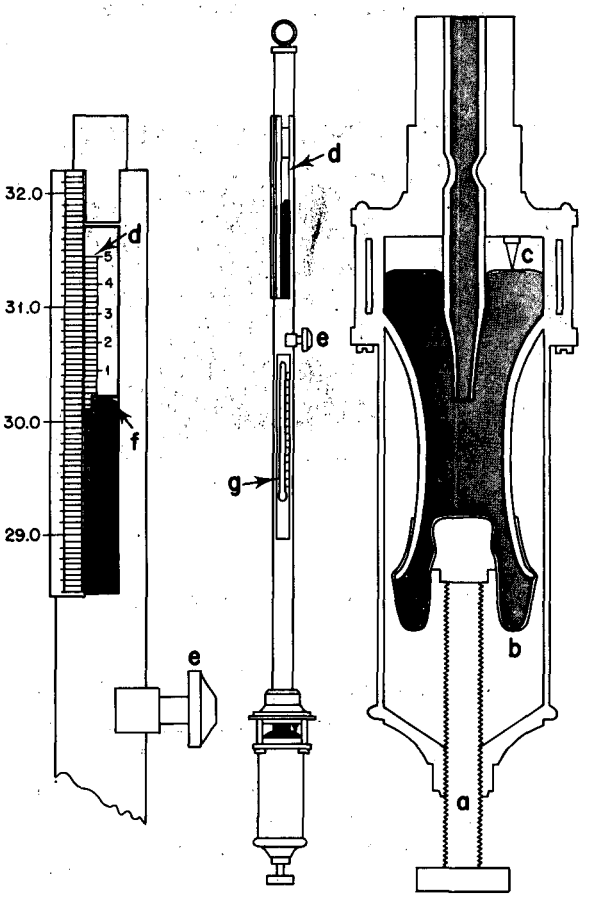

Fig. 6.26—Schematic drawing of a Fortin mercurial barometer: (center) the entire barometer, (right) the barometer cistern, and (left) the vernier scale. The level of the mercury in the cistern is adjusted by a screw (a) pressing on a leather bag (b) so that the top of the mercury meniscus just touches the index pointer (c). The sliding vernier (d) is adjusted by a thumbscrew (e) until the slide bottom is at the same level as the top of the mercury meniscus (f). The reading from a thermometer (g) is used to correct the height of the mercury column.

In the mercurial barometer the pressure of the atmosphere exerted on a cistern of mercury is balanced against the weight of a liquid-mercury column contained in a vertical glass tube that is sealed at the top but open at the bottom where the tube is submerged in the

cistern. In the Fortin barometer the mercury level in the cistern is raised and lowered by a screw until brought to a position just contacting a fixed ivory point. The height of the mercury column is read on a metal scale to the nearest 0.0025 cm. Readings must be corrected for variations in the gravitational constant associated with altitude and adjusted to a reference value of 980.665 cm^2/sec. The largest correction involves that of adjusting the mercury-column height to a standard of 0°C. In barometers of lower precision, an instrumental correction is frequently necessary.

Fig. 6.27—An aneroid microbarograph.

The pressure-sensing element of a microbarograph consists of one or more partially evacuated flexible metal bellows enclosing a spring. One end of the bellows is fixed; the motion of the other end responds to variations in atmospheric pressure. A mechanical linkage system, including springs for zero setting, is used to move a pen making a trace on a rotating spring-driven drum. In this country a frequently used instrument exaggerates the height change of a mercury column by a factor of 2.5.

The microbarograph also contains one or several dashpots of oil to damp rapid pressure oscillations due to gustiness (called pumping) of the wind or sudden indoor pressure changes due to opening and shutting of doors. Readings accurate to about 0.025 cm Hg can be obtained with commercially available microbarographs.

6-9 ATMOSPHERIC-MOISTURE MEASUREMENTS

In day-to-day operations at the national laboratories and other large atomic installations, a variety of uses can be found for information on atmospheric moisture. For example, measurements of wet-bulb temperatures are important in the design of cooling towers, and data on relative humidity are of concern to physicists working with high-voltage machines or biologists working with experimental animals. Relatively complete summaries of the underlying theory of and techniques for measuring atmospheric moisture are given by Middleton and Spilhaus (1953) and Spencer-Gregory and Rourke (1957), and in the *Handbook of Meteorological Instruments* (Great Britain, Meteorological Office, 1956). At Atomic Energy Commission installations, the most frequently used moisture-measuring systems are the wet- and dry-bulb psychrometer, the hair hygrometer, and the hygroscopic hygrometer.

The reduction in temperature of a wetted surface owing to evaporational cooling can be used to determine the amount of moisture in the atmosphere. The ambient-air temperature and pressure must also be known. This principle is used in the operation of the wet- and dry-bulb psychrometer, which commonly consists of two mercury-in-glass thermometers, the bulb of one being wrapped in clean muslin. The muslin is wet with distilled water, and the instrument is placed in an airstream of the order of 3 to 5 m/sec. Other forms of psychrometers in which the glass thermometers have been replaced by resistance thermometers, thermocouples, or thermistors have been used. These types lend themselves to remote and continuous recording through the use of self-balancing potentiometers or Wheatstone bridges.

Conversion of the wet- and dry-bulb readings to relative humidity or dew point is easily accomplished by using psychrometric tables or humidity slide rules.

Many schemes are used for providing an airstream past the wet-bulb thermometer. In the sling psychrometer the two thermometers are mounted side by side on a metal plate or in a metal frame and whirled by hand. Often the two thermometers mounted in this way are placed in the instrument shelter in front of a fan driven

by a hand crank. Spring-driven or electric motors have been used to create the airstream in the Assmann psychrometer.

For the last 150 years, the hair hygrometer has been widely used for both industrial and meteorological purposes although its defects have been loudly criticized from time to time. Its continued use is no doubt due to the fact that the instrument is simple in construction, lends itself easily to recording, and provides measurements that are of sufficient accuracy (about 5%) for ordinary usage, at least in air temperatures above freezing. When human or animal hairs have been carefully cleaned and the grease and oil have been removed by treatment in ethyl ether, they elongate about 2.5% as the relative humidity changes from 0 to 100%. The relation between elongation and relative humidity is logarithmic in the relative humidity range 20 to 100%, i.e., $L = a + b \log RH$, where RH is the relative humidity, L is the length of the hairs, and a and b are constants. The loss in speed of response with low temperatures, i.e., below freezing, may be a distinct shortcoming for some applications.

In the conventional hygrograph the humidity element consists of a harp of human hairs held under slight tension and connected through a logarithmic compensating linkage to a pen making an ink trace on a clock-driven drum. Frequently a single drum is used to record the pen traces of both a humidity and a thermal sensor. This kind of instrument is called a hygrothermograph. Daily or weekly calibration checks are required. Human hairs can function well for several years in areas free from dust and salt.

Salts, such as calcium chloride or lithium chloride, are hygroscopic and therefore absorb water vapor when placed in a moist atmosphere. Various types of hygrometers making use of this phenomenon have been devised. In these instruments the salt may be coated on a flat surface, such as a glass or plastic slide, or may be impregnated on a fabric or a single strand of fiber glass. The gravimetric hygrometer and the electrolytic hygrometer are examples of moisture-measuring instruments using hygroscopic salts.

In the gravimetric hygrometer the actual amount of water vapor absorbed is weighed by a sensitive balance. From this measurement the relative humidity can be determined if the temperature is known. In the electrolytic hygrometer the electrical resistance, either between two electrodes placed on a coated slide or between two points on an impregnated fiber, is measured by a bridge, an ohmmeter, or some other electronic device. Such resistance measurements can be related to the ambient relative humidity if the temperature is known. The radiosonde humidity element makes use of this principle.

The Foxboro Dewcel is a commonly used modified form of the electrolytic hygrometer. Its operation depends on the fact that for each value of water-vapor pressure of the surrounding air there is one temperature of the saturated solution at which equilibrium exists, i.e., the vapor pressure surrounding the lithium chloride salt surface equals that of the ambient vapor pressure. The instrument consists of a cylindrical tube about 10 cm long and 0.6 cm in diameter, covered by a wick of woven glass tape upon which gold or silver wires are wound in bifilar fashion. The tape is impregnated with lithium chloride, and the wires are connected to a 25-volt a-c power source. The conductivity between the parallel wires depends upon the amount of moisture absorbed by the hygroscopic lithium chloride. If the vapor pressure of the ambient atmosphere is greater than that in the immediate vicinity of the lithium chloride film, the vapor will be absorbed, and the conductivity between the wires will increase and allow more current to flow. The increase in current flow raises the temperature of the Dewcel element until the equilibrium vapor-pressure point is reached. If the vapor pressure of the ambient atmosphere is less than that surrounding the lithium chloride film, the reverse process takes place. Thus the Dewcel acts as an automatic self-regulating control mechanism in which the current flow between the heating wires is varied to maintain an equilibrium temperature from which the ambient vapor pressure can be determined. The thermal element can be a resistance thermometer or a liquid-expansion tube.

6-10 METEOROLOGICAL DATA-PROCESSING EQUIPMENT

The steady increase in the availability and the capability of data-processing and computing

equipment makes it advisable that the final recorded form of data from each meteorological installation be considered very carefully. Particularly when several instruments are to be involved, it is legitimate to question whether the data should be hand abstracted from simple chart recorders or whether the additional cost of a more-sophisticated recording mechanism is justified. Inasmuch as it may help the reader in his decision, several types of recording and auxiliary data-handling equipment are discussed.

Virtually all data from meteorological sensors recorded electrically are in the form of electrical voltage or current. In the initial design of a meteorological system, one must consider simultaneously the selection of the sensors, the recording technique, and the data-processing form.

In general, electrical voltages and currents are easily converted to a shaft-position change that lends itself readily to chart recording. Reliable shaft-position encoders are readily available to convert this type of analog information to digital form. Information from sensors having a digital output, such as the tipping-bucket rain gauge or an anemometer giving pulses for each unit of air passage, is readily recorded directly on magnetic tape or (with some processing) on paper punch tape. Ink-trace recordings utilizing time-of-event (chronograph) pens are often used for a pen-and-ink record, but the analysis is tedious.

6-10.1 Chart Recorders

One of the most common forms of recording in use today is the strip or circular chart on which one or more pens record the variables of interest usually as a function of time (Fig. 6.28). Although these recorders have various internal mechanisms for converting voltages and currents, shaft positions, or counts into the final pen movement, they share a number of common features:

1. All provide good resolution of the variable with time and permit easy inspection not only of existing conditions but also of conditions over previous hours or days. This advantage is not one to be overlooked in installations where it may frequently be necessary to evaluate recent meteorological changes and to utilize the information quickly. Figures 2.30 and 2.31 (Chap. 2) are illustrations of typical chart records.

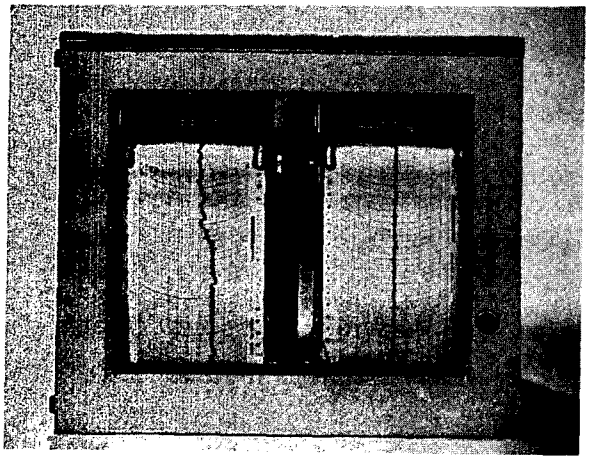

Fig. 6.28 — A pair of strip-chart recorders displaying simultaneous records of two variables (Esterline-Angus Instrument Co.).

2. Considerable effort is required to extract information from the chart records. Equipment available to simplify this task is described in a later section, but for the most part one would consider such equipment an analysis aid rather than a basic data-processing system.

3. The chart recorder, having been in use for many years, is a highly developed device, and the better equipment of this type has very high reliability. Many recorders have run without major maintenance for periods as long as 10 or even 15 years.

A partial solution to the data-abstraction problem is found in the addition of an integrating device, which can operate in conjunction with the recorders or be supplementary to them. The simplest form of such an integration device can be used with the tipping-bucket rain gauge or with the anemometer providing a pip for the same fixed unit of wind passage. For example, a counter can be added which will automatically summarize events over a period of time while the recorder provides the detail. In some recorders an event pen can count directly on the record. In others counting is accomplished externally.

Similar in principle to the counter system are more sophisticated integrators, such as the ball and disk integrator used by the Argonne National Laboratory (Moses and Kulhanek, 1962).

A somewhat different solution to the data-abstraction problem involves alteration of either

the input data or the recording mechanism to provide either integration or lagged response of the pen. The simplest form is the familiar resistance–capacitance network. Sensors with large thermal lag (such as resistance thermometers of large mass) are often used to make further integration unnecessary.

Lagging can also be accomplished mechanically or electromechanically, as is done in the Brookhaven system (Brown, 1959). Here, servomotors operating through 1000:1 gear ratios greatly slow the response of the recording system.

Implicit in the reduction of detail thus accomplished is the idea that the detail may not have been necessary. Here again, the decision regarding the recording form should precede and dictate the input wherever possible.

Hand abstraction of chart data can be accelerated considerably by the use of chart readers of one type or another. All these include mechanisms for the orderly advancing and inspection of the chart by the operator as well as simplified means of following the pen trace as a function of time. In typical systems the operator follows the pen trace with a stylus or with wheel-driven vertical and horizontal line markers, and at selected intervals the ink-trace reading is converted into digital form and recorded automatically on punch cards or tape.

Other chart readers actually follow the trace themselves photoelectrically and record either manually or automatically at set intervals of time or chart spacing.

6-10.2 Automatic Data-recording Systems

At the present time there are a number of automatic data-recording systems described in the literature. Some of these have been discussed by Brown (1959), Fritschen and van Bavel (1963), Gerhardt, Mitcham, and Straiton (1962), Moses and Kulhanek (1962), and Newstein (1963). Few systems can be adapted to general meteorological use, however, and none are offered commercially as shelf items.

Since most of the existing meteorological sensors are analog devices, the analog output must be converted to digital form prior to introduction into the programming and recording portions of the system. The digital output can be in the form of paper or plastic punched tape, magnetic tape, or cards.

There are many devices for converting analog information into digital form. Such devices have been used for many years, and reliable units are readily available commercially.

The choice of the final output form, as well as the intermediate conversion equipment, is always a difficult one and usually represents a compromise between cost, adaptability, and anticipated needs. In principle, however, each has advantages and disadvantages, but an automatic system will ordinarily represent a saving in time and money and will provide improved accuracy in the data-reduction process.

Experience has shown that the pen-and-ink recorder trace should be retained even though an automatic data-processing system is adopted. The visual record thus provided is extremely valuable both for providing information concerning the operation of the sensors and for avoiding the loss of data in the event the automatic data system malfunctions.

Magnetic tape is an increasingly popular method of recording data; information can be in either analog or digital form although usually the latter. Probably the most important advantages of magnetic tape recordings are an extremely high speed capability (which is generally needed only in research installations) and ease of storage. One reel of tape can store the data contained on about 125,000 cards. Magnetic tape can be used in any one of many computers, assuming appropriate programs exist, and therefore presents a minimum of problems in the final utilization.

Magnetic tape, however, has at least two disadvantages, the most important of which is the cost of the tape-handling units. A good system of this type is necessary to provide reliable operation and is likely to cost as much as or more than the rest of the automatic system. Also, direct readout is ordinarily difficult. The tape usually cannot be inspected and checked except by the computer with which it is utilized.

Midway between magnetic tape and punched cards is the paper-tape system, which has some of the advantages and some of the disadvantages of each. Moderately high-speed operation is possible with paper tape, and, with the latest punch drives available, as many as

150 digits can be recorded per second. Punch tape can be stored for years without deterioration. Also it has the advantage of providing a visual check of the information for errors, often with considerable ease (some tapes have the information printed on them at the same time the punches are made). A disadvantage is that punched tape is usually converted to cards or magnetic tape before computer analysis is performed. Although this additional step, together with diligent maintenance of the tape punch, is costly, punched tape often represents the least expensive way of automatically processing and storing data.

At the risk of making this section obsolete, the authors suggest that for general meteorological use in the atomic energy field the punched card is the most versatile and suitable system of all. It is by far the most-common data-storage form, and every computer has some provision for utilizing punched cards either directly or following simple conversion to magnetic tape. In addition, the punched card automatically segregates the data into time sections and provides for easy inspection and repair of inaccurate information. Most computer facilities have card-to-tape and tape-to-card equipment.

It is not possible to record at extremely great speeds directly on punch cards, but such speed is seldom necessary. The card is not without its flaws, however, the main one being the card structure itself. The standard punched card deteriorates fairly readily with or without use, and in short order a given deck will not pass through the handling machines. In some areas this problem requires special plasticized cards. Nevertheless card reproducers can ordinarily process a deck of standard cards that have been stored under room temperature and humidity conditions for 10 years or more even though they are not suitable for passage through the computer.

6-11 EQUIPMENT FOR DIFFUSION MEASUREMENTS

Although the direct measurement of atmospheric diffusion has played a central role in our understanding of this phenomenon, those persons involved in planning a nuclear installation are not likely to become involved in performing diffusion experiments. There are two reasons for this: first, the problems at most sites are not usually critical enough to warrant the great expense of a diffusion experiment and, second, should it be thought necessary to conduct such experiments, meteorological consultants will usually be employed for the operation and its evaluation. However, to present some background information on this subject, we will include a sketch of some of the techniques.

The diffusion characteristics of the atmosphere can be determined by measurements of purposely generated tracer materials. The experimenter, since he is dealing with the atmosphere, must be continually aware that he is working with a unique situation that will never recur in just the same way and that, if tracer tests are to have some general applicability, the results of the program must be amenable to both statistical and theoretical analysis. Otherwise the program is only an illustration of what the atmosphere did at a particular time and over a particular area. Tracer programs can be used either to illustrate individual situations or to accumulate data describing the expected variations of meteorological conditions in a particular area.

Chemical warfare groups were among the first to become interested in tracer techniques. Since the introduction of atomic energy and the development of the atomic industry, tracer techniques have been used extensively to explore atmospheric diffusion patterns in the areas around atomic operations. Both the chemical warfare and the atomic plant uses of tracers are examples of situations in which a tracer is used to approximate the diffusion of toxic materials.

A quantitative tracer-analysis program depends upon the controlled emission of relatively small amounts of a distinctive material to the atmosphere, its collection, and the careful analysis of the collected samples for minute amounts of the tracer.

Because of the usually minute amounts of tracer material in the samples, extreme care must be taken to guard against excessive background concentrations. A thorough analysis for background effects should be part of any comprehensive tracer program, and, if at all possible, techniques should be selected so that there is little or no background correction. Back-

ground effects can be caused by a number of factors. Some of the more important seem to be (1) contamination of equipment, clothes, and personnel with tracer material and its subsequent transfer to the sample, (2) mistaking natural materials for the tracer, (3) the redistribution of tracer that had been dispersed in a previous operation, (4) mistaking industrial effluents for the tracer, and (5) analysis errors caused by extraneous materials in reagents or equipment. From this list it can be seen that the background may depend upon the volume of air sampled and thus be related to the tracer concentration or it may be introduced as a single amount, such as might come from handling.

Aerosols rather than gases have been used most often in tracer studies. Since the purpose of most tracer programs is the determination of diffusion patterns applicable to the diffusion of gases, the question is often asked whether or not the diffusion of the particulate aerosol actually represents that of a gas. It is recognized that, if the gas and the particles were mixed and enclosed in still air, there would be a gradual settling out of the particles from the gas. In the open atmosphere, however, turbulence will cause gravitational settling to be an insignificant feature of the effluent distribution. Available data on these turbulent currents indicate that they are at least 100 times larger than the gravitational forces acting on the particles. Gravitational settling is thus an insignificant influence within the time scale of most tracer experiments. Several experimental programs substantiate this use of aerosols for gas tracing.

The results of particle-size determinations on a zinc sulfide tracer aerosol before and after dissemination are shown in Table 6.4. The field samples used in this check were collected at distances of 30 to 40 km from the source. These data show that there was no significant change in the particle-size distribution of the pigment between that which had not been dispersed and that which had been carried by the wind. If settling were a significant factor in the distribution of the aerosol, a difference would be expected. Webster and Duckworth (1959) and Leighton, Perkins, Grinnell, and Webster (1965) have presented studies on the relative transport of gases and aerosols.

Table 6.4—COMPARATIVE PARTICLE-SIZE DISTRIBUTIONS BEFORE AND AFTER DISSEMINATION*

Particle size, μ	Pigment sample, %	Field-collected sample,† %
0.5	8	‡
1.0	31	35
2.0	35	33
3.0	15	22
4.0	7	8
5.0	3	2
6.0	1	0

*From E. Robinson, Atmospheric Tracer Techniques Using Aerosols, presented at the Instrument Society of America Conference and Exhibit, San Francisco, 1960, Paper 11-SF60.

†Collected from 30 to 40 km from the source.

‡On the filter samples it was not possible to measure particles less than 1 μ in diameter, and thus all particles less than 1 μ are included in the 1-μ range.

6-11.1 Oil Fog Tracer Techniques

Smoke plumes from oil fog generators have been used in atmospheric diffusion studies for many years (Church, 1949, and Lowry, Mazzarella, and Smith, 1951). Most of these studies have utilized military oil fog generators, such as the M2 and M3A2, or copies of them. Such generators can conveniently produce large volumes of smoke for extended periods of time. The M2 generator produces smoke by forcing a mixture of oil and water into a coil located in a combustion chamber in which heat vaporizes the two liquids. The vapor escapes through a manifold into the air where rapid chilling condenses it into a fog of submicron droplets (War Department, 1944). In the M3A2 generator, smoke is produced when oil is injected into the engine tube of a pulse-jet engine where it is vaporized (Department of the Army, 1955). The most desirable drop size for these condensed smoke particles ranges from 0.5 to 1.0 μ. The average size of the condensing droplet is controlled by the concentration of condensing vapor and the rate of cooling. If the cooling is not rapid enough, large drops will form, and the smoke will be unsatisfactory. A properly generated smoke cloud is stable, and the life of the cloud is determined almost solely by meteorological conditions.

Three methods of analysis have been used for oil fog studies. The first was a photometric

method in which the concentration of smoke in small volumes of air was determined by the amount of light scattered by the aerosol particles (Church, 1949, and Lowry, 1951). The photometer was carried in a truck and moved around the downwind area. Samples from plumes aloft were obtained by lifting the photometer into the smoke with a captive balloon. These samplers could be used to record smoke density continuously, but equipment costs did not permit observations at a large number of points. Two more-economical methods were developed in which the amount of oil collected by a filter could be determined (Smith, Bartlett, and Potts, 1956, and Smith, Singer, Bartlett, and Marcus, 1957). In these methods the amounts of oil are determined either gravimetrically or fluorometrically. The fluorometric technique is based upon the fluorescent character of the oil used to produce the fog. When the oil collected by a filter sampler is dissolved in benzol, the amount of oil can be determined from the resulting fluorescence of the benzol solution.

6-11.2 Fluorescent Tracer Techniques

The Chemical Corps has developed techniques for using insoluble fluorescent pigments (FP) as tracer materials for diffusion studies. The materials selected were pigments of zinc sulfide or zinc cadmium sulfide from 1 to 5 μ in diameter. These particles can be detected by the green and yellow fluorescence, respectively, of the particles under ultraviolet illumination. The techniques developed included methods for quantitative dispersion of the dry pigment, the preparation of filter and impactor samplers, and optimum microscopic sample-analysis procedures. The FP technique has been described by Leighton, Perkins, Grinnell, and Webster (1965).

Other groups have used a modified fluorescent-pigment tracer. A number of tests were run in which the pigment was mixed with the oil and fed to an oil fog generator (Braham, Seely, and Crozier, 1952). Braham et al. used an airplane to sample the plumes and measured tracer concentrations as far as 160 km and as high as 3.0 km from the source. A moving-stage impactor permitted the tracer catch to be identified with certain parts of the flight path.

The fluorescent-pigment technique has also been used in diffusion tests at Hanford, Wash. (see Sec. 4-4.2.2, Chap. 4). A dispersion method was developed in which a water slurry of the pigment is dispersed by a high-volume insecticide fog generator, the TIFA (Todd Insecticidal Fog Applicator). This method of operation overcame some feed difficulties encountered with the dry dispersers. An even more significant development of the Hanford group has been the development of an instrumental technique for the analysis of fluorescent-pigment filter samples (Barad and Fuquay, 1962). This technique photometrically measures the scintillations of the pigment particles that are excited by alpha particles. The limit of sensitivity of this technique is about 10 to 20 particles on a 2.5-cm filter. Other Hanford developments include methods for handling filters where natural dust loadings are large enough to interfere with particle resolution. Without some instrumental technique the tracer samples can be evaluated only by rather tedious manual microscopic counting.

Satisfactory results require complete dispersion of discrete pigment particles. Since dispersion is at a given mass rate of emission and sample evaluation is in terms of numbers of particles, the sample catch can be equated to the emission only by assuming some predetermined size distribution to apply to the emitted tracer. Large errors can occur if there is inefficient dispersion or agglomeration of particles because the particle-size distribution would be unknown.

In 1957 a tracer technique was developed in which water-soluble fluorescent uranin dye was used as the tracer material (Robinson, MacLeod, and Lapple, 1959). The use of other fluorescent dyes has also been described (Dumbauld, 1962). Dispersion of these liquids is by a high-pressure air-aspirated spray nozzle with the concentrated liquid spray drying to form an aerosol of dye particles from 1 to 10 μ in diameter. Filter samplers are used, and analysis is made by dissolving the dye particles of the filters in distilled water and then measuring the fluorescence of the solution in a fluorometer. The fluorescence is proportional to the concentration of dye in the solution, and thus the amount of tracer material collected can be determined. An analytical sensitivity of 10^{-10} g, which is equivalent to a single 5-μ dye particle, has been achieved.

Dispersion of the uranin dye as a concentrated water solution permits close control to be maintained over the final aerosol-particle size distribution since it depends upon readily controlled conditions of nozzle geometry, air pressure, liquid flow rate, and solution concentration. The emission and analysis of the uranin are both in units of mass; so a particle-size-distribution step such as that needed in the pigment sample is unnecessary.

In the uranin-tracer developmental tests, natural dusts were present in the samples. No correlation was noted, however, between the dust in a sample and sample fluorescence. The experimental area did not have any urban pollution concentrations, however. Wholers, Lapple, Kass, and Johnson (1959) have reported on a fluorescent-dye tracer program and the problems encountered in an area around a phosphate-fertilizer operation, where a fluorescent background of apparent industrial origin did interfere with the use of uranin dye. The interference was overcome by using another fluorescent dye, Rhodamine B, as the tracer aerosol. Difficulties were also encountered in leaching the dye from the filters and with variations of pH that affected fluorescence. These difficulties emphasize the importance of adequate checks for background concentrations and environmental effects.

6-11.3 Other Aerosol Tracer Techniques

The usual absence of freezing nuclei effective at temperatures of −15 to −20°C and the ease with which large numbers of effective nuclei can be produced with silver iodide cloud-seeding techniques led Schaefer (1958) to use silver iodide as an atmospheric tracer material. The tracer plume was measured with a portable cloud chamber in which the concentration of ice crystals was visually estimated. Schaefer states that, because of temperature effects and the appearance of the crystals, little trouble may be expected in separating natural ice nuclei from the silver iodide nuclei. The rather cumbersome sampling procedure is a major limitation to its use in a large-scale program.

A tracer method using some aspects of nuclear technology has been used in a limited pilot-plant program (Haines, Cember, and Hemeon, 1956). In this method antimony oxide is dispersed, and the airborne material is collected on filters. The samples are exposed in an atomic pile and are analyzed for the induced radioactivity of the metallic antimony. In the tests run difficulties were encountered owing to low disperser efficiency and to relatively high background concentrations. Chemical-analysis steps were proposed to reduce background values. Even without these extra steps, the technique for handling the samples was more complex than the methods using pigment dye or oil aerosol and had the additional problem of requiring exposure in an atomic pile.

In England, Hay and Pasquill (1959) have used Lycopodium spores in diffusion tracer studies. The spores were released from a point source and collected downwind by natural impaction on exposed cylinders. Sample catches were evaluated by microscopically identifying the distinctive spore particles.

6-11.4 Gaseous Tracer Techniques

There have been a number of attempts to develop a tracer technique in which a gas could be used as the tracer material. Most have been unsuccessful, largely because of the limitation in the sensitivity of available analytical procedures. Although the aerosol tracer materials, such as the fluorescent pigments and dyes, can be detected in amounts of 10^{-10} g, the limit of sensitivity for most gaseous materials is about 10^{-7} g. However, two gases, Freon and sulfur dioxide, have been successfully used as tracers. A third material, tritiated ethane, was studied (Shapiro, Gibbs, Field, and Dillon, 1955), but a solution could not be found for high background interferences encountered. Mercury vapor has also been considered, but sufficiently sensitive analytical methods could not be found (Haines, Cember, and Hemeon, 1956).

Argonne National Laboratory developed techniques to use Freon 12 (dichlorodifluoromethane) as a tracer gas (Schultz, 1957), and further improvements have been reported by Collins, Bartlett, Turk, Edmonds, and Mark (1965). The gas was released from a cylinder through proper flowmeters and control valves. Evacuated flasks were used to collect the samples. The samples were analyzed for Freon by special techniques using a modified version of a com-

mercial halogen leak detector or gas-chromatograph techniques. Concentrations of 0.1 ppm can be measured with the leak detector and of 0.05 ppm in a 5-ml air sample with the gas chromatograph. Field tests have been successful, but further development is necessary. Collins et al. also mention that sulfur hexafluoride can be used when the analysis is carried out by gas chromatography.

Sulfur dioxide is a common air pollutant, and there are good methods for measuring it in the atmosphere, either instrumentally or chemically (Giever and Cook, 1960, and West and Gaeke, 1956). Sulfur dioxide has been used in extensive tracer diffusion studies conducted as part of Project Prairie Grass (see Sec. 4-4.2.1, Chap. 4). In this program liquid-filled bubbler samplers were used, and the results were obtained by conductivity analysis of the bubbler solution. Emission systems for compressed gases, such as sulfur dioxide or Freon, must be carefully designed to prevent large variations in the emission rate due to adiabatic cooling.

The advent and rapid growth of gas chromatography as an analytical technique has made available to the research meteorologist means for carrying out diffusion experiments on a scale and with a sensitivity and precision not previously attainable.

Gas chromatography is a technique for separating complex mixtures of volatile materials into their individual components. A carrier gas (usually nitrogen, argon, or helium) sweeps the mixture, injected as a pulse, through a long tubular column packed with an inert porous solid. A nonvolatile liquid coated on the porous packing material functions as a solvent for the several components of the mixture being separated. A component that is completely volatile and totally insoluble in this liquid will be swept through the column in the same time that it takes an element of the carrier gas to pass. Another component that is totally nonvolatile and completely soluble in this liquid will be dissolved in the liquid coating immediately upon entering the column and will never move from this point. Still other components will behave in intermediate fashions, depending on their volatilities and solubilities. In any mixture each component will possess its own combination of these properties of volatility and solubility, and the several components will therefore emerge from the column one by one in orderly procession. Selection of the best liquid phase and of column operating parameters, such as temperature, column length, and carrier-gas flow rate, ensures that degree of separation required for a specific problem with a minimum of effort.

A detector located at the end of the chromatographic column generates a minute electrical signal whenever the emerging carrier gas contains any other material. An amplifier and recorder convert this signal into a visual record. In such a record each component of a mixture is represented by a peak, and the quantity of each component present is proportional to the area under its peak.

An outstanding feature of gas chromatography is the sensitivity with which it can detect and measure a compound in the presence of an overwhelming quantity of one or many others. Present-day ionization detectors can measure parts-per-million concentrations of nearly any compound that may be encountered. This capability has often been extended to the parts-per-billion range. Parts-per-trillion sensitivity is far from unknown, and even this has been exceeded in a few special cases.

For further information regarding gas chromatography, the reader is referred to Burchfield and Storrs (1962). A review article by Altshuller (1963) bears closely on the present aspect and provides good bibliographic coverage.

An example of the direct application of gas chromatography to a meteorological problem is described in papers by Saltzman, Coleman, and Clemons (1966) and by Turk, Edmonds, Mark, Collins, and Bartlett (1965). These workers have demonstrated that certain selected materials, such as sulfur hexafluoride, can be used in atmospheric tracer tests. The sensitivity demonstrated is such that detailed mapping of trajectories extending over several hundreds of miles is considered feasible.

6-11.5 Tracer Techniques Based on Visible Plumes

In addition to the detailed studies possible with aerosol and gaseous tracers, diffusion information can be obtained from observations of visible plumes. This information can be either qualitative plume trajectory and behavioral data or detailed diffusion estimates

based on careful measurement of the visible plume.

Measuring the density of a photograph of visible smoke offers the possibility of directly estimating atmospheric diffusion (see Sec. 3-3.4.2, Chap. 3; Record, 1952; Ronne, 1959; and Högström, 1964). Stereoscopic techniques can be used to size individual smoke parcels in space (Clark, 1956). For visual studies smoke can be generated for short periods of time by smoke pots, flares, or other pyrotechnic devices and for extended periods by an oil aerosol generator, such as the Chemical Corps M2 model.

Visual tracer studies have involved both surface and elevated release points from either tethered balloons or a tower. Several smoke sources ignited simultaneously at different heights can be used to estimate the variations in diffusion conditions with altitude.

In one study program small black-powder charges carried aloft by a balloon were ignited, and the resultant smoke clouds were followed downwind (Sartor, Katz, and Katz, 1952). A radio-commanded smoke puffer for remote or balloon work has also been described (Randall and Clark, 1955).

Most smoke generators used in meteorological studies have been military types. The Army manual, *Military Chemistry and Chemical Agents* (Departments of the Army and Air Force, 1956), describes the several types of smoke that have been developed: titanium tetrachloride (FM), sulfur trioxide–chlorosulfonic acid solution (FS), aluminum-zinc oxide–hexachloroethane (HC), and white phosphorus (WP). The most satisfactory mixture is the HC. Disadvantages of the others are (1) that the high rate of hydrolysis of FM mixtures causes orifice clogging, etc., and corrosion is a definite problem, (2) that the FS mixture produces a sulfuric acid aerosol by absorption of moisture from the atmosphere and thus requires careful handling, and (3) that white phosphorus burns rapidly, is dangerous to handle, and is toxic.

The HC mixture burns with intense heat and smoke. By far the greater portion of the smoke is zinc chloride, which rapidly absorbs moisture from the air to form particles of effective screening size.

Colored smokes may be produced by volatilizing and condensing a mixture containing organic dyes. Standard military colors are red, green, and yellow. Smoke candles and smoke pots can be obtained from a number of commercial firms since they are used in various air-conditioning tasks and as emergency signals. Marine supply houses are also a possible source.

Tracer sampling techniques fall into two classes: those in which the air sample is drawn directly into the detecting instrument and those in which the tracer is removed from the air sample and held for analysis at a later time. The oil aerosol photometer is an example of the former; filters used with pigment tracers are examples of the latter.

Portable field analyzers, such as the photometer, do not need further explanation because their form is fixed once the tracer method is decided upon.

Filter or bubbler sampling units, on the other hand, offer a wide choice of units. It is likely that the developments to date in this field can supply a wide variety of situations. Numerous different sampling units are described in the literature in such publications as the *Journal of the Air Pollution Control Association, Archives of Environmental Health,* and the *American Industrial Hygiene Association Quarterly.* A useful but incomplete compilation of air-sampling units is found in the *Encyclopedia of Instrumentation for Industrial Hygiene* (Yaffe, Byers, and Hosey, 1956). Most references describing tracer techniques also include descriptions of the field samplers used in the program, and, since many tracer studies have used similar sampling techniques, designs can be adapted from one program to another.

6-12 ATMOSPHERIC MEASUREMENTS WITH BALLOONS

Most meteorological observations necessary for the nuclear-energy industry have been made from sensors mounted on short or tall masts or towers. Occasionally, when measurements above tower heights are necessary, balloons have been used either as the sensor or as a platform for sensors. Since balloon techniques require the services of at least one observer and frequently more than one, their use in a long-term observation program results in a considerable cost.

Three primary types of balloon systems are used for obtaining meteorological information.

The first of these systems is the buoyant free balloon. In this system the horizontal motion of the rising balloon is used to infer the wind-speed profile. The rising balloon can carry pressure, temperature, and humidity sensors that transmit readings by radio to a ground station. A complete outline of these various techniques as practiced by the U. S. Weather Bureau and most other national meteorological services can be found in the Weather Bureau publications *Manual of Winds-Aloft Observations*, Circular O, and *Manual of Radiosonde Observations*, Circular P, both of which are available through the Superintendent of Documents, U. S. Government Printing Office, Washington, D. C.

In the second type of balloon system, the balloon is tethered to a ground station, and the tether carries signals from sensors carried by the balloon. This system is sometimes called a wiresonde.

A multiconductor nylon-coated wire with braided fiber glass covering is often used both as the tether and the means for transmitting the signals. The data can be recorded automatically by a self-balancing bridge recorder or manually by an observer using a balancing bridge or reading the dials of other suitable electronic equipment. Atmospheric soundings using tethered systems have been made in the past at the Oak Ridge National Laboratory (Myers, 1952), at the National Reactor Testing Station (Humphrey, 1951), and more recently in England by Thompson (1962).

With the wiresonde a balloon or blimp with a volume of several tens of cubic meters is usually used. Commercially available blimps with a volume of 17.0 m^3 have been found very satisfactory. In this country helium is generally used as the inflating gas although hydrogen is also suitable. Measurements from tethered blimps at heights of 1500 m have been reported (F. B. Smith, 1961). Specially designed balloons with fins have desirable aerodynamic properties that provide greater stability and permit observations to somewhat greater heights than do conventional blimps.

The tethered-balloon technique is cumbersome and sometimes hazardous. During high winds the blimp is extremely hard to handle. Special precautions must be taken if there is danger of lightning or the buildup of static electricity. For this reason soundings are avoided beneath or near convective clouds. Ordinarily the equipment must be well grounded, and the blimp upon its return to the surface must be grounded before it is touched.

The third type of balloon used in meteorological investigations has been designed to float at a constant density level. The constant-density-level balloon, with which the data in Sec. 4-11 of Chap. 4 was obtained, is constructed by filling a balloon made of an inelastic film with a lighter-than-air gas mixture at a pressure considerably above that at the computed flight altitude. Changes in the temperature of the superpressured gas within the balloon will not result in an appreciable balloon-volume change. Thus the buoyancy force will remain relatively constant, and the balloon will respond only to ambient density changes and to the forces exerted by the three-dimensional wind field. Constant-density-level balloons used to date have not been capable of maintaining their height in precipitation.

Balloons can take a variety of shapes, but the tetrahedron shape has been most commonly used. The balloon in Fig. 6.29 has a nominal volume of about 1 m^3 and is made of Du Pont

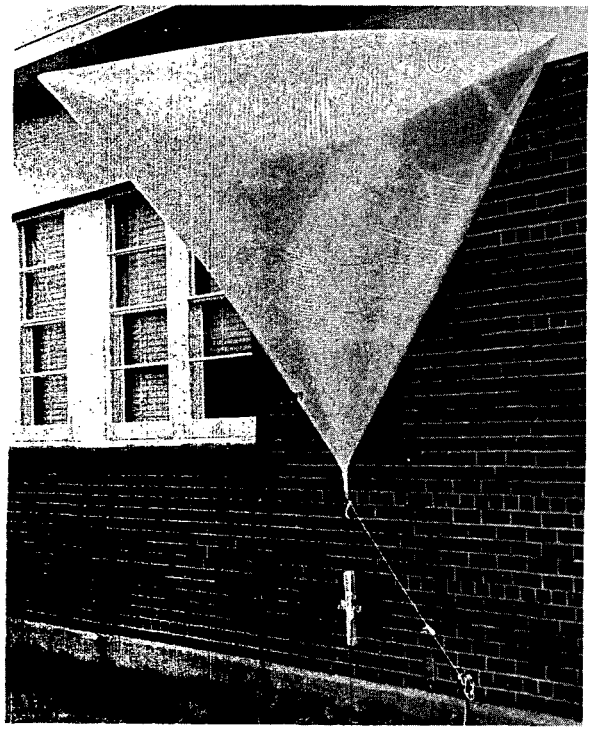

Fig. 6.29 — A superpressured constant-level tetrahedron balloon (tetroon).

Mylar, with a thickness of 2 mils (0.002 in.). Such balloons are called tetroons—a combination of the words tetrahedron and balloon. The tetroons are inflated to a superpressure of several tens of millibars above ambient pressure and at the floating level may have a superpressure of slightly under 100 mb. Mylar has a high stress-to-strain ratio; thus its volume changes little during its rise, i.e., a few percent for 100 mb superpressure (Fig. 6.30). From information concerning tetroon volume as a function of superpressure, the total weight of the system, and the variation of atmospheric density as a function of height, the tetroon floating level can be predicted. This level can be varied by adding or subtracting weights carried by the system. As with the wiresonde blimps, helium is ordinarily used as the inflating gas in the United States, but hydrogen is also suitable.

These balloons can be tracked by three different methods. The first consists of the double-theodolite technique with a base line exceeding 1 km. This, of course, suffers from the usual difficulties inherent in visual tracking, such as loss of the target in clouds and limitations in the length of the run. The second method involves tracking with radar. The balloon material can be metalized to serve as a passive reflector, or auxiliary reflectors can be used. The latter has been more satisfactory. A difficulty associated with tracking by reflection is the interference due to ground clutter at large distances when the elevation angle is low. The third and most successful technique uses a 403 MHz transponder attached to the tetroon. The difficulties experienced with the other two techniques are thereby eliminated. Both the X-band (3 cm) M33 and the S-band (10 cm) WSR-57 radars can be used in these measurements. The radar signal triggers the transponder to transmit its 403 MHz signal, which is received by the radar. The circuitry of the radar is modified to use this signal in providing data on the range and azimuth and elevation angles. The radar–transponder system can be used to track constant-level balloons to distances of well over 100 km even when the balloon floats at 1000 m or less.

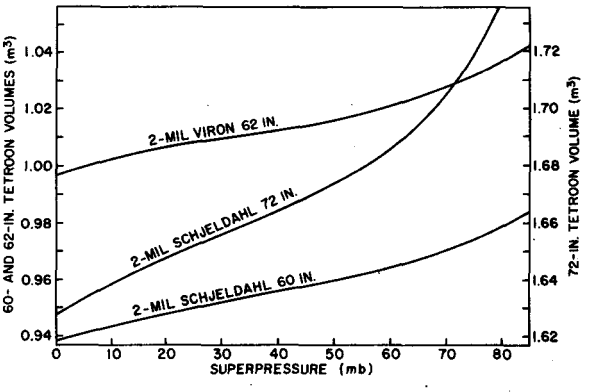

Fig. 6.30—Volume vs. superpressure curves for three different tetroons.

Chapter 7

Radioactive Cloud-dose Calculations

John W. Healy*

With Robert E. Baker†

LIST OF SYMBOLS

Symbols used frequently in Chaps. 7 and 8 are listed here. The equation or section number indicates the first appearance of the symbols. The noted units for each symbol are those that are typically used in the calculations discussed in the text although other units may be used in specific instances.

A	Atomic weight: relative weight of an atom based on a weight of 16 for oxygen, Eq. 7.14
B'	Breathing rate (m^3/sec), Eq. 7.98
B_x	Dose buildup factor (dimensionless), Eq. 7.74
b	A height above the ground (g/cm^2,m) for beta- and gamma-ray equations, respectively, Eqs. 7.26 and 7.65a
c	Energy-dependent parameter in equations for estimating beta dose (dimensionless), Eq. 7.25
c_m	Concentration of radioactive material in the muscle (μc/g), Eq. 7.123
c_g	Concentration of isotopes in foodstuffs (μc/g), Eq. 7.116
$c_.$	Concentration of radioactive material in the food of an animal (μc/g), Eq. 7.123
D	Dose to an organ (rad), Eq. 7.90
D'	Dose rate to an organ from internal irradiation (rad/sec), Eq. 7.88
${}_\beta D_d$	Beta dose (rad) at a depth, d (g/cm^2), in body tissue, Eq. 7.25
${}_\beta D_\infty$	Beta dose from an infinite cloud (rad), Eq. 7.19
${}_\beta D'_\infty$	Beta dose rate from an infinite cloud (rad/sec), Eq. 7.15
${}_\beta D'_{\infty b_1}$	Beta dose rate (rad/sec) at a height b_1(g/cm^2) above an infinite plane upon which w curies/m^2 of beta-emitting material has been deposited, Eq. 7.26
${}_\gamma D$	Gamma-ray dose (rad), Eq. 7.32
${}_\gamma D_0$	Gamma dose that would be received in the absence of shielding (rad), Eq. 7.32
${}_\gamma D'_r$	Gamma dose rate (rad/sec) at a distance r (m) from a point source, Eq. 7.33
${}_\gamma D'_\infty$	Gamma dose rate from an infinite cloud (rad/sec), Eq. 7.35
d	An effective depth (g/cm^2), Eq. 7.25
$\overline{E}$	Energy absorbed in an organ from one disintegration (Mev), Eq. 7.88
$E_i(\mu r)$	Exponential integral $\int_{\mu r}^{\infty} [\exp(-\mu r)/r]\, dr$ (dimensionless), Eq. 7.64
E_0	Maximum energy of the beta-ray spectrum (Mev), Eq. 7.25a
$\overline{E}_\beta$	Average beta energy per disintegration (Mev/dis), Eq. 7.15

*General Electric Company, Schenectady, New York.
†Division of Reactor Licensing, U. S. Atomic Energy Commission, Bethesda, Maryland.

$\bar{E}_\gamma$	Average gamma energy emitted at each disintegration (Mev)/dis), Eq. 7.33
${}_a\bar{E}_\gamma$	Average gamma energy absorbed in an organ per disintegration (Mev/dis), Eq. 7.89
${}_0\bar{E}_\gamma$	Average gamma energy emitted in an organ per disintegration (Mev/dis), Eq. 7.89
f_a	Fraction of a soluble radionuclide which is translocated to a critical organ (dimensionless), Eq. 7.87
f_w	Fraction of an ingested isotope deposited in a critical organ or in a specific tissue (dimensionless), Eq. 7.116
f_1	Fraction of radionuclide passing from the gastrointestinal tract to the blood (dimensionless), Eq. 7.87
f_2	Fraction of the total body radionuclide burden in the critical organ (dimensionless), Eq. 7.88
f_2'	Fraction of radionuclide passing from the blood to a critical body organ (dimensionless), Eq. 7.87
$f(\sigma_z,h,h_i)$, $f_1(\sigma_z,h,h_i)$, $f_2(\sigma_z,h,h_i)$	Factors used in equations describing diffusion beneath a capping inversion (dimensionless), Eqs. 7.51 and 7.52
$f_B(t)$	Function describing the rate of biological elimination of a mixture of radionuclides from an organ (dimensionless), Eq. 7.91
$f_R(t)$	Function describing the radioactive decay in a mixture of radionuclides in an organ (dimensionless), Eq. 7.91
G_1,G_2	Integrals used in the evaluation of the gamma dose from radioactive materials deposited on the ground, Eqs. 7.68 and 7.68a
h,h_i	Height of release and inversion base, respectively, (m), Fig. 7.17
I	Gamma-ray intensity (photons/m^2 sec), Eq. 7.64
I_1,I_2,I_T	Integrals used in the solution of the equations for gamma-ray dose from a cloud, Eqs. 7.41a and 7.41b and Sec. 7-5.2.2
$\bar{I}_1,\bar{I}_2,\bar{I}_T$	Integrals used in the solution of equations for gamma dose from a continuous release maintained over a long time period, Eqs. 7.61a and 7.61b and Sec. 7-5.2.5
k	Component in the buildup factor $(1 + k\mu x)$ for gamma rays where $k = (\mu-\mu_a)/\mu_a$ (dimensionless), Eq. 7.33
M	Mass of an organ (g), Eq. 7.88
M_e	Amount of food eaten per day (g/day), Eq. 7.116
M_g	Mass of edible portion of vegetation (g/m^2), Eq. 7.122
M_m	Total mass of muscle in an animal (g), Eq. 7.123
M_R	Mass of a radioactive material (g), Eq. 7.14
m	Slope of logarithmic plot of retention of radioactive material in the body or in an organ vs. time, Eq. 7.95
N	Number of atoms, Eqs. 7.1 and 7.8
N_0	The number of atoms in one gram atomic weight of a substance (6.02486×10^{23} atoms/gram atomic weight), Eq. 7.14
n	Slope of logarithmic plot of radioactivity from material in the body or in an organ vs. time, Eq. 7.95
$P_{\beta 1}$	Radioactive source term in power units for beta radiation (Mev/sec), Eq. 7.22
$P_{\beta 2}$	Radioactive source term in power units for beta radiation (erg/sec), Eq. 7.24
$P_{\gamma 1}$	Total gamma energy release rate from a source (Mev/sec), Eq. 7.44
$P_{\gamma 2}$	Total gamma energy release rate from a source (watts), Eq. 7.45
Q_0	Initial source strength (curie), Eq. 7.22 (also given as Q). Primes (Q′) indicate rate of source release (curies/sec)
Q_x	Amount of source material remaining in a cloud after a travel distance, x (curie), Eq. 7.22

q	Quantity of radioactive material used to express strength of a point source or quantity in the body (curie or μc); appears in various sections and in a variety of uses
qf_2	Quantity of radioactive material in a body organ (curie or μc), Eq. 7.88
R	A radial distance (m), Eq. 7.60
S	Source strength per unit area of an infinite plane (photons/m^2-sec), Eq. 7.64
s	Volume of a building (m^3), Eq. 7.83; also a distance between a receptor and a cloud centerline path (m), Sec. 7-5.2.2
T_B	Biological half-life (time), Eq. 7.92
$T_R, T_{½}$	Radioactive half-life (time), Eqs. 7.3 and 7.14
t	Time (sec, hr); appears in various sections and in a variety of uses
$\bar{u}$	Mean value of the wind component in the x-direction (m/sec); appears in numerous equations. In practice $\bar{u}$ is usually replaced by the average value of the wind speed indicated by an anemometer
V	Ventilation rate in a building (m^3/time), Eq. 7.83
v_d	Deposition velocity (m/sec), Eq. 7.28
w	Thickness of shielding afforded by building walls (g/cm^2), Eq. 7.74
α	Normalizing constant in the beta-dose estimation equations, Eq. 7.25
η	Factor change in building ventilation rate following cloud passage (dimensionless), Eq. 7.85
θ	Angular width of a sector (radians), Eq. 7.60
λ, λ_R	Disintegration or decay constant for model in which a constant fraction is removed per unit time (1/time), Eq. 7.1
λ_B	Biological elimination constant equal to $0.693/T_B$ (1/sec), Eq. 7.92
λ_R	Radioactive-decay constant equal to $0.693/T_R$ (1/sec), Eq. 7.92
λ_v	Fraction of an isotope removed from vegetation by radioactive decay, weathering, growth, etc. (1/day), Eq. 7.116
λ_W	Weathering constant for vegetation (1/day) Eq. 7.123
λ_1	Elimination constant for short component in lung retention (1/time), Eq. 7.104
λ_2	Elimination constant for long component in lung retention (1/time), Eq. 7.104
μ	Total gamma-ray absorption coefficient ($\mu = \mu_a + \mu_s$) (1/m or cm^2/g), Eq. 7.32
μ_a	Energy-absorption coefficient for gamma rays (1/m or cm^2/g), Sec. 7-5.1
μ_s	Scattering absorption coefficient for gamma rays (1/m or cm^2/g), Sec. 7-5.1
μ_x	Absorption coefficient for wall material (cm^2/g), Eq. 7.74
ν	Apparent absorption coefficient for beta radiation in tissue (cm^2/g), Eq. 7.25
ρ	Atmospheric density at ambient conditions of temperature and pressure (g/m^3), Eq. 7.17
ρ_0	Atmospheric density at S.T.P. (g/m^3), Eq. 7.17
σ_y, σ_z	Standard deviation of the distribution of material in a continuous plume in the y and z directions (m), Eq. 7.47
$\sigma_{xI}, \sigma_{yI}, \sigma_{zI}$	Standard deviations of the distribution of material in a puff (instantaneously generated cloud) (m), Sec. 7-5.2.2
τ	A time interval (sec, hr); appears in various sections and in a variety of uses
χ	The concentration at a point at a given instant (curie/m^3), Eq. 7.15
$\bar{\chi}$	Time-averaged concentration at a point (curie/m^3), Eq. 7.27
ψ	Exposure; the integral of concentration over a specified time interval ($\psi = \int_{t_0}^{t_0+t} \chi \, dt$ in typical units of curie sec/m^3), Eq. 7.19

ω Quantity of deposited radioactive material per unit area (curie/m^2), Eq. 7.26

7-1 INTRODUCTION

In previous chapters the transport and diffusion of materials released to the atmosphere and the mechanisms of removal have been discussed. In radiation-dosage calculations these concepts must be related to the effects that occur at the receptor, whether the receptor be man, animal, or property. Such effects are frequently a complex function of the actual atmospheric distribution of the material in time and space at the location of the receptor. This distribution depends upon the physical properties of the material emitted and the method of release as well as upon the meteorological situation following release. The effects usually depend upon many sociological and biological factors that vary considerably among individuals, groups, and entire populations.

The techniques of radiation-dosage calculation discussed in this chapter are presented as an introduction to some of the major elements in this field. As in any brief résumé of a technological discipline, many topics cannot be discussed and many subtleties are lost. Therefore this chapter must be viewed as a demonstration of the more important aspects of dosage calculation and not as a complete, self-contained working manual.

Releases of radioactive material to the atmosphere can occur almost instantaneously or over a long period of time. The resulting downwind exposure of people and objects to the airborne material will be of short or long duration, depending upon the release time, the wind speed, the nature of the radioactive material, the geometry of the source, and the spreading of the cloud as it travels. In many cases the effects of a radioactive cloud on the receptor are a function of the total radiation received from the cloud with variations in the concentration during the exposure period generally being of minor significance. In this circumstance the integral of the concentration vs. time curve at the point of receipt is a measure of the total effect. The important release parameter thus is the total quantity released without regard to the rate as long as the diffusion parameters remain constant.

An exception to this generalization will occur when the total radiation dose approximates that dose expected to have an immediate biological effect. For example, a gamma dose to the whole body that could be lethal if delivered within a few hours might be expected to produce less serious consequences if delivered over a period of days or weeks.

With many chemically toxic materials, the maximum allowable concentration in the atmosphere for long-term exposure differs by only one or two orders of magnitude from the concentration that can be expected to produce damage from short-term exposure. It is possible to produce damage by a single inhalation if the concentration is sufficiently high. Since the peak short-term concentration in a cloud can exceed the average concentration by several orders of magnitude (e.g., in high-concentration puffs that reach the ground from a stack during unstable conditions), it may be necessary to consider the effects of instantaneous peak concentrations as well as the effects of average concentrations.

In the event of an accidental release of radioactive materials to the atmosphere, the radiation dose received by people and animals can be considered in two phases: the initial or acute phase while the airborne material is passing the receptor and the latent or recovery phase following the passage of the cloud.

Radiation doses in the initial phase will include the external radiation from the cloud passage, some contribution (before recovery action is taken) from the materials deposited on the ground, body, or other surfaces, and the radiation from any material inhaled during cloud passage. These doses must be considered in conjunction with any other possible doses, such as those from the direct radiation from a nuclear excursion or from fission products retained in a containment vessel. Although the dose from inhaled material will be received over a period of time following the accident, it is included in the acute phase because the total amount inhaled will depend upon conditions in the cloud and not upon later actions.

The dose received in the latent phase will consist of external radiation from material deposited on the ground or other surfaces and

internal radiation from ingestion of foodstuffs or liquids that have become contaminated by the cloud passage. Possibly an additional internal dose could be received during this phase by inhalation of resuspended dust in the contaminated area or from the adherence of such dust to the body. This additional dose would be expected to be significant only in highly contaminated areas.

The doses received in the initial phase will depend upon the location of people or animals and the speed of evacuation as well as upon the quantity and physical characteristics of the material released and the meteorological situation causing the dispersal. The doses received in the latent phase will depend upon administrative actions taken to limit access and to provide protective devices and upon the limits chosen for such actions. The risk or probability of injury to people is therefore a function of the doses received in the initial phase before evacuation; property damage resulting from denying individuals access to or the use of their property will depend upon the residual contamination in the latent phase.

At short time periods after release, before appreciable mixing or diffusion has occurred, the physical limits of the cloud will be quite sharply defined. The cloud will have a limited size and steep concentration gradients. Consequently the effect of the release at near downwind locations may be quite critically affected by minor topographical features (i.e., buildings, hills, and trees), by minor fluctuations in meteorological variables (i.e., wind direction and wind speed), and by release parameters (i.e., finite size of source and rate of release).

As the cloud moves farther from the point of release, continued diffusion will cause the concentration gradients to decrease. At these greater distances the cloud will be relatively insensitive to local irregularities but will be affected by major topographical features, gross changes in meteorological conditions, and depletion by ground deposition en route. The combination of uncertainties in these several parameters can produce major uncertainties in the estimate of effects at all distances downwind.

The greatest overall uncertainty in estimating the effects of a release arises from the dynamic character of the atmosphere. Frequent shifts of wind direction and changes in stability and wind speed may cause the plume to move toward unanticipated areas. Present practice is to estimate the dose under several meteorological conditions, while varying the physical and chemical composition of the cloud over a reasonable range, in order to illustrate the potential influence of these factors on the results.

Radiation can be received by a downwind receptor in a variety of ways. The radiation received can be classed as external or internal according to the location of the radioactive material irradiating the tissue. External radiation is received from the radiations emitted as the cloud passes the receptors, from material deposited on surfaces in the region of the receptor, and from material deposited on the body as the cloud passes. As noted earlier, additional external radiation can be received directly from the devices originating the radioactive source.

Internal exposure can result from inhaling the radioactive material in the air as the cloud passes or by ingesting contaminated water or foodstuffs. In each case it is necessary to consider not only the dose to the organs serving as the portal of entry, such as the lungs or gastrointestinal tract, but also the dose to other organs of the body through metabolic transfer of the radioisotopes. Parameters describing the rate of uptake, such as breathing rate and retention in the lung, along with parameters describing the residence time in the specific organ and the transfer between organs must be included in the calculation. The final estimate of internal dose will inherently include the uncertainties in these parameters, as well as those involving the initial air concentration and the movement of the radioactive materials through the ecological systems in the area.

Radioactive material taken into the body b inhalation, by ingestion, or through a woun will continuously deliver a dose to the bod (or portions of it) until it has been removed b biological elimination or radioactive deca The total dose delivered to the person duri his lifetime by a specific intake is known a the dose commitment for the incident.

The calculational model presented here based upon the estimation of internal or e

ternal exposure from each important radiation type. The calculations start with the amount and nature of the material released, the air concentration integrated over the time of interest, and the deposition pattern as determined from meteorological conditions. In many cases an exact solution of the geometrical problem thus presented is not warranted by the accuracy with which other factors are known, and an approximate solution may be used.

Calculation of potential doses that could be received during the acute phase of an accidental release will provide an estimate of the time available to evacuate an area or to complete other emergency actions that will minimize or limit exposure to people in the area. The dose estimated for the latent phase will provide a basis for determining the stringency needed in recovery measures and the time period during which such measures may be required.

7-2 SOURCES OF AIRBORNE MATERIALS

An important concept in the relation between plant operations and potential effects on a receptor in the environs is the so-called "source term," which describes the quantities of material released to the atmosphere. Also important, although frequently not so well quantitized, are the physical and chemical characteristics of the material emitted and their influence on the subsequent behavior of the material.

In its broadest sense the source term includes a description of the mode of emission. The material may be released as an almost instantaneous puff or it may be released continuously; the initial source configuration may be represented by a point, a line, or a finite area or volume; the material may be less or more dense than air, or it may have an appreciable exit velocity. The effects of these source conditions on the ultimate disposition of the released materials is important and has been the subject of previous chapters.

Radioactive materials can be released to the atmosphere either routinely during normal operation or as a result of an abnormal operating condition or accident. In general, it is possible to determine the characteristics of routine wastes through direct observation of operating installations so that the source term under these conditions can be as well known as desired (although some uncertainty may exist in the design of a new facility). For abnormal operating conditions or accidents, however, there may be wide uncertainties as to both the quantity of material emitted and its physical and chemical characteristics.

It is general practice in the nuclear industry to treat off-gases to remove radioactive materials to a very low level during routine operation and to provide backup devices to minimize the probability of release in the event of abnormal conditions. Since it is impossible to remove all unwanted materials from the off-gases, it is necessary to select some limits as bases for equipment design. The lowest feasible concentration measurement is determined by instrument sensitivity and the statistical nature of radioactive disintegrations. Thus estimates of receptor effect are of prime importance in establishing safe and economical limits for discharge.

The quantities and types of radioactive materials reaching the atmosphere are a function of the type of installation, the specific design, and the operating mode. The actual source term can be determined only from the characterization of a particular installation. The following description of sources is general and intended to provide some orientation rather than specific numbers for use.

7-2.1 Classification of Airborne Materials

Atmospheric contaminants can be in the form of gases or particles. Gases are monomolecular distributions of the contaminant formed by evaporation or sublimation; particles are agglomerates of many molecules in crystalline or amorphous form and in the solid or liquid state.

In general, gases will mix in the same manner as the atmosphere in which they are dispersed although at high concentrations heavier gases may have a net settling force owing to the lower density of the surrounding mixture. The deposition characteristics of a gas will depend upon its chemical reactivity and, perhaps, on the difference between the boiling point of the source material and the ambient temperature of surfaces. Noble gases, such as xenon, krypton, or radon, will not deposit on

surfaces although they have limited solubility in water and other fluids. They are eliminated from the atmosphere primarily by radioactive decay. Other gases will deposit with varying degrees of efficiency. For example, elemental ^{131}I will deposit very strongly on many types of surfaces including vegetation when in the form of iodine vapor. Such gases will be eliminated from the atmosphere by deposition, by reaction with or adsorption on natural aerosol particles in the atmosphere, by photochemical reactions resulting in a more reactive compound, by washout with precipitation, or by biological processes. Since the removal rates of these processes depend upon the chemical form of the gas, predictions of interactions in the environs require data on the deposition tendency of the particular effluent and on its change with time under the environmental conditions of the atmosphere. Only a few materials have been studied to any appreciable degree; therefore such estimates require empirical verification.

Particles may be composed of liquids or solids. When in liquid form, they are referred to as mists or, in high concentrations of submicron particles, as fogs. Solid particulates may be dusts formed mechanically by grinding, crushing, and drilling; fumes may be formed by combustion, sublimation, and condensation; smokes are usually formed by combustion of organic material. In general, the particle sizes of fumes are less than 1 μ, smokes are usually less than 0.5 μ (Silverman, 1959) and may range as low as tens of Angstrom units. The general term "aerosol" is used to denote these disperse systems in air in analogy to the term "hydrosol" applied to disperse systems in water.

The fate of aerosols once they are released to the atmosphere depends to a large degree on the dynamic properties of the aerosol which, in turn, depend upon the particle size, shape, density, and, in some important cases, upon the absolute number of particles per unit volume. Among the more important processes influencing such particles are gravitational settling, agglomeration, and impaction. A discussion of some of this information is included in Sec. 5-3 as well as in the following paragraphs.

Gravity will act upon particles to provide a net settling force. Owing to the high surface area per unit mass of these small particles and the resulting high air resistance, the particles after a short time will reach a constant velocity at which the force of gravity is exactly balanced by the drag forces. This velocity is referred to as the terminal velocity of the particle. The drag forces will vary with the character of the flow around the particle and, hence, with the particle shape and velocity. Figure 7.1 illustrates the approximate terminal velocity for

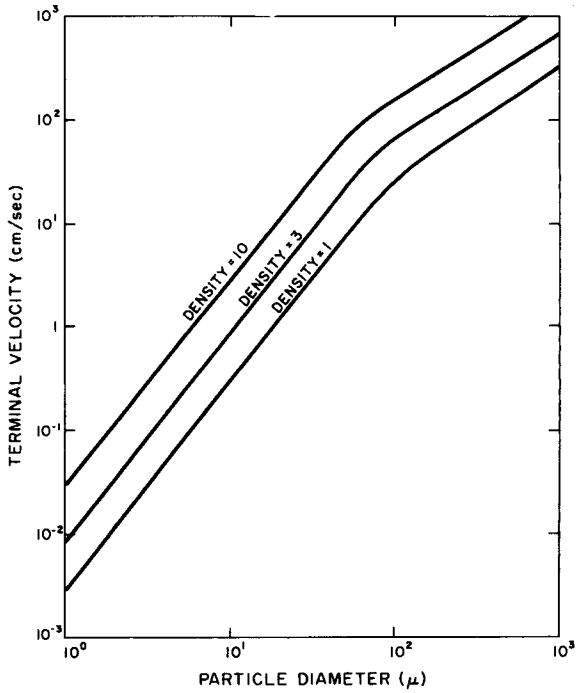

Fig. 7.1 — Terminal velocities for spheres of various sizes and densities in air at S.T.P.

spheres of several densities as calculated by equations given by Drinker and Hatch (1954). The decrease in slope above about 100 μ is in the intermediate region between streamline flow and turbulent flow where the equations result from approximate relations between the drag coefficient and the Reynolds number. For particles of other than spherical shape, the drag resistance of the air would generally be increased so that the terminal velocity for an irregular particle containing the same mass as the sphere would be smaller. In the atmosphere the forces exerted on small particles by turbulent motions are large compared with the force of gravity, and consequently such particles can remain suspended for long periods of time. The dependence of fall velocity on atmospheric den-

sity, interpreted in terms of height in the atmosphere, has been shown in Fig. 5.4.

Particles will increase in size by agglomeration when the number of particles per unit volume is very high as in the case of an aerosol generated by volatilization in a limited space. In a freshly formed fume, the particle sizes are very small so that agitation by Brownian movement causes frequent collisions and formation of larger particles through agglomeration. As the particle size increases, the rate of collision and agglomeration decreases, and the larger particles are removed by gravitational settling or, in an agitated atmosphere, by impaction on surfaces. Such flocs of particles frequently have bulk densities considerably lower than the theoretical density of the parent material. This process places an upper limit of about 10^5 to 10^6 particles/cm^3 on the number of particles that can exist in a stable aerosol, i.e., one that can last for a reasonable period of time (Magill, Holden, and Ackley, 1956). Agglomeration rate, shape, and bulk density may be affected by the composition of the fluid in which the process occurs, e.g., the presence of steam can have a marked effect. The agglomeration of radioactive material may be different from the agglomeration of stable material because the radiation field associated with the radioactive material will produce ions that can produce statically charged particles and thereby affect the forces of attraction between particles.

When a stream of air containing particles flows around an obstacle in its path, particle inertia will resist the change in motion. If the particle inertia is sufficiently high and the flow direction change is great enough, the particle will not swerve sufficiently to miss the object and will impact upon it. The efficiency of impaction (collision) is defined as the ratio of the number of impacting particles to the number that would have passed through the same area if the object had not been present. The overall collection efficiency of the object will depend upon both the impaction efficiency and the fraction of the impacting particles that are retained. Small particles or particles of lower density will have lower impaction efficiencies than will large or dense particles. Theory predicts that inertial forces for small particles are so low that collection by direct impact becomes negligible but that collection is enhanced for very small particles by diffusion. Deposition of very small particles may occur owing to electrostatic forces and adsorption. Inertial forces are believed to play an important part in deposition from turbulent mediums such as the atmosphere.

7-2.2 Characteristics of Radioactive Materials

The behavior of radioactive contaminants in the atmosphere is governed by their chemical and physical nature, i.e., the dynamics of transport, diffusion, deposition, and condensation will be nearly the same for these materials as for their nonradioactive counterparts. A reservation as to overall behavior is necessary since the radiation from a radioactive particle produces ionization in the surrounding air and leaves charges on particles and it is possible that this factor could change processes that are dependent upon charge effects. The radioactive properties of individual radioisotopes or particular mixtures of radioisotopes are of importance in determining the quantity and nature of the radioactive materials reaching the receptor as well as the resulting radiation dose.

7-2.2.1 Radioactive Decay. A radioactive atom is characterized by an unstable nucleus that tends to a more stable condition through the emission of a nuclear particle and/or a quantum of energy. If a charged particle is emitted, the resulting atom has a different atomic number and is therefore a different element. Such disintegrations occur according to the laws of chance. The decrease in the number of radioactive atoms in a time period is therefore

$$dN = -\lambda_R N\, dt \qquad (7.1)$$

where N is the number of radioactive atoms, dt is the time period, and λ_R is a proportionality constant called the disintegration constant with the units of reciprocal time. λ_R is a constant for a given radioactive species and represents the fraction of the atoms present which disintegrate per unit time. If Eq. 7.1 is integrated using the condition that $N = N_0$ at zero time, the familiar exponential radioactive-decay equation results.

$$N = N_0 \exp(-\lambda_R t) \quad (7.2)$$

From Eq. 7.2 it can be shown that one-half the radionuclei originally present will decay in a time given by

$$T_R = \frac{\ln 2}{\lambda_R} = \frac{0.693}{\lambda_R} \quad (7.3)$$

where T_R is the half-life of the radionuclide and is characteristic of the particular isotope.

In many cases the original radionuclide (parent) decays to a nucleus that is also unstable (daughter). The number of atoms of the daughter at some time after starting with an initial quantity of the parent (N_1^0 atoms) is given by

$$N_2 = N_1^0 \frac{\lambda_{R1}}{\lambda_{R2} - \lambda_{R1}} [\exp(-\lambda_{R1} t) - \exp(-\lambda_{R2} t)] \quad (7.4)$$

where the subscripts 1 and 2 refer to the parent nucleus and the daughter nucleus, respectively. Equation 7.4 indicates that, if the half-life of the parent is very long with respect to that of the daughter (i.e., if λ_{R1} is small with respect to λ_{R2}), an equilibrium condition is reached after some time, depending upon the half-life of the daughter, where the number of atoms of N_2 are such that the disintegration rate of the daughter equals the disintegration rate of the parent. Since the source of supply of the daughter atoms is the disintegration of the parent, the daughter atoms are, on the average, decaying at the same rate at which they are being supplied. Such a condition is known as secular equilibrium between the parent and the daughter.

$$\lambda_{R1} N_1 = \lambda_{R2} N_2 \quad (7.4a)$$

If the parent has a longer half-life than the daughter, $\exp(-\lambda_{R2} t)$ becomes negligible in comparison to $\exp(-\lambda_{R1} t)$ after some period of time. Equation 7.4 then reduces to

$$N_2 = N_1^0 \frac{\lambda_{R1}}{\lambda_{R2} - \lambda_{R1}} \exp(-\lambda_{R1} t) = N_1 \frac{\lambda_{R1}}{\lambda_{R2} - \lambda_{R1}} \quad (7.5)$$

If expressed as disintegration rate rather than number of atoms, Eq. 7.5 becomes

$$\lambda_{R2} N_2 = (\lambda_{R1} N_1) \frac{\lambda_{R1}}{\lambda_{R2} - \lambda_{R1}} \quad (7.6)$$

This is known as transient equilibrium since the amount of daughter to the parent is a constant although the absolute quantities of the two radioisotopes present are continuously decreasing with time at a rate determined by the decay constant of the parent. Note that the disintegration rate of the daughter exceeds that of the parent once this equilibrium is established.

Such chains in which radioactive daughters produce radioactive second daughters, third daughters, etc. can extend to many numbers. In the chain originating with ^{238}U, for example, there are 10 steps before stable ^{207}Pb is reached. Bateman (1910) gave equations for solving such a radioactive chain of any length with the condition that only the parent material is present at time zero.

$$N_n = N_1 [C_1 \exp(-\lambda_{R1} t) + C_2 \exp(-\lambda_{R2} t) + \ldots + C_n \exp(-\lambda_{Rn} t)] \quad (7.7)$$

where $$C_1 = \frac{\lambda_{R1} \lambda_{R2} \ldots \lambda_{R(n-1)}}{(\lambda_{R2} - \lambda_{R1})(\lambda_{R3} - \lambda_{R1}) \ldots (\lambda_{Rn} - \lambda_{R1})}$$

$$C_2 = \frac{\lambda_{R1} \lambda_{R2} \ldots \lambda_{R(n-1)}}{(\lambda_{R1} - \lambda_{R2})(\lambda_{R3} - \lambda_{R2}) \ldots (\lambda_{Rn} - \lambda_{R2})}$$

$$C_3 = \frac{\lambda_{R1} \lambda_{R2} \ldots \lambda_{R(n-1)}}{(\lambda_{R1} - \lambda_{R3})(\lambda_{R2} - \lambda_{R3}) \ldots (\lambda_{Rn} - \lambda_{R3})}$$

7-2.2.2 Activation. Radioactive materials can be produced by nuclear reactions caused by bombarding the nucleus with subatomic particles, such as energetic alpha particles, deuterons, electrons, or neutrons with considerably lower kinetic energy. Since the nuclear reactor depends upon a large number of neutrons being present during the chain reaction, radioactive materials will be produced in structural members as well as in coolant, gases, or any other material in the vicinity of the reactor core.

Of greatest interest at the present time are activation reactions caused by thermal neutrons, i.e., neutrons with kinetic energy equivalent to that caused by thermal energies, because most of the present generation of reactors operate with a preponderance of neutrons slowed to this energy and because the probability of a nucleus capturing a neutron with this energy is considerably higher than for more energetic

neutrons. Most of the thermal-neutron reactions are of the type in which the nucleus captures a neutron and immediately emits a gamma photon so that the end result is a nucleus of the same element as the parent t with a mass of one mass unit greater (n,γ reaction). With fast neutrons the reactions are more likely to produce prompt emission of a particle, such as an alpha particle or one or more neutrons.

Such reactions can be written symbolically as, for example, the reaction of a thermal neutron with ^{40}Ar:

$$^{40}Ar + n \rightarrow h\nu + {}^{41}Ar \xrightarrow[1.8\ hr]{\beta^-} {}^{41}K$$

This indicates that an ^{40}Ar nucleus has absorbed a neutron, emitted a quantum ($h\nu$) of gamma radiation, and produced an atom of ^{41}Ar. The ^{41}Ar is unstable and decays by emission of a beta particle with a half-life of 1.8 hr to a stable ^{41}K. Frequently the nucleus resulting from such a reaction is stable so that no radioactive material results.

The measure of the probability of a nucleus capturing a particle and undergoing the reaction is the activation cross section usually designated as σ_A. The cross section will vary with the energy of the bombarding particle and is different for each nucleus being bombarded. Cross sections are expressed in units of barns, which have the dimensions of 10^{-24} cm^2.

For a material exposed to a given neutron flux (in neutrons/cm^2-sec), the number of interactions, and thus the net number of atoms of radioactive material produced (dN_R), in time dt is

$$dN_R = (nv)\ \sigma_A N_T\ dt - \lambda_R N_R\ dt \qquad (7.8)$$

where N_T is the number of target atoms exposed and λ_R is the radioactive-decay constant. The second term accounts for the number of radioactive atoms lost by radioactive decay. Solution of this equation with the condition that the number of radioactive atoms present at the start of the irradiation is zero gives

$$N_R = \frac{(nv)\ \sigma_A N_T}{\lambda_R} [1 - \exp(-\lambda_R t)] \qquad (7.9)$$

Thus the number of atoms of radioactive material will increase at a decreasing rate that is dependent upon the half-life of the radioactive material until an equilibrium is attained between the rate of formation and the rate of decay. At equilibrium

$$N_R \lambda_R = (nv)\ \sigma_A N_T \qquad (7.10)$$

In other words, at equilibrium the rate of decay of the material produced is equal to the rate at which it is formed.

7-2.2.3 Fission. Fission is a special type of nuclear reaction in which the nucleus of the bombarded atom splits into two pieces and releases energy in the form of heat and radiations. Fission can be induced in most elements with an atomic number above about 30 by bombardment with sufficiently energetic particles. Only elements with atomic number above 90 can be fissioned by neutrons of low or moderate energy (<10 Mev) with appreciable cross sections. Some isotopes are fissionable with thermal neutrons (^{235}U, ^{233}U, and ^{239}Pu are most important); others, such as ^{238}U, require neutrons with an energy of 1 Mev or greater. Of particular interest is the fact that the fission process produces neutrons that in themselves can produce further fissions. Thus it is possible to arrange a mass of fissionable material so that these additional neutrons produce a chain reaction. Since the fission cross section is high for slow neutrons, a thermal reactor is designed to produce further fissions by absorbing much of the energy of the neutrons before they enter the fuel. In a fast reactor the neutrons are utilized with only slight degradation of energy so that the cross sections for fission are lower but the parasitic captures in structural or other materials are also lower. This permits more efficient use of the neutrons and greater freedom in choice of materials for construction.

In the fission process the nucleus is split asymmetrically into two fragments of different mass. In ^{235}U, for example, only about 0.01% of the fissions result in a symmetrical division producing two fragments of identical size.

The average frequency occurrence of each mass chain is referred to as the fission yield and varies to some extent with the energy of the bombarding neutrons and the mass and type of the fissionable nucleus. A fission-yield curve for ^{235}U for thermal neutrons is presented as a

function of the chain mass in Fig. 7.2 (Plutonium Project, 1946, Petruska, Thode, and Tomlinson, 1955, and Bolles and Ballou, 1959). Note that the total yield adds to 200% since the basis is the yield per 100 atoms fissioned, i.e., each fission will yield one atom on the lower part of the mass scale and one atom on the higher part. With high-energy neutrons as the bombarding particles, the pronounced dip between the high-mass and low-mass fractions tends to become less pronounced and practically disappears when 14-Mev neutrons are used.

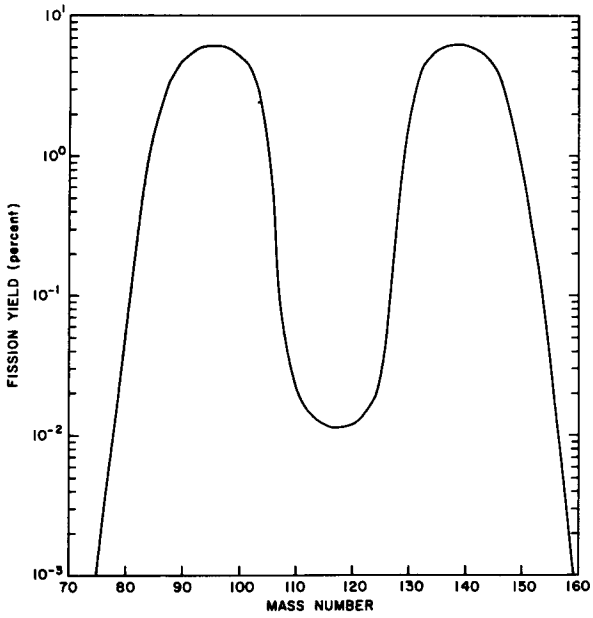

Fig. 7.2—Yield of fission-product mass chains from ^{235}U fission by thermal neutrons.

When ^{239}Pu fissions, the low-mass portion of the curve is displaced about four mass units from ^{235}U, but the higher mass region is only slightly affected. This has considerable significance in reactor operation because a sizable portion of the power may be produced by ^{239}Pu fissions in slightly enriched reactors. (The ^{239}Pu is produced by neutron capture in ^{238}U during operation.) As a result, the quantities of strontium and other fission products of similar mass number may be lower than would be estimated from ^{235}U fission, and the quantities of ruthenium and fission products of similar mass number may be higher.

The total amount of energy released per fission is about 200 Mev. Thus the production of 1 watt of thermal power in a reactor corresponds to a fission rate of 3.1×10^{10} fissions/sec, and a burst of 1 Mw-sec corresponds to a total of 3.1×10^{16} fissions. Since the energy of the explosion of 1 ton of TNT is taken as 10^9 calories (Glasstone, 1962), the fission of 1.3×10^{20} atoms will release an amount of energy equivalent to the explosion of 1 ton of TNT.

The formulas for computing the quantities of individual fission products present are similar to those for neutron activation and decay. For the first member of the chain,

$$\lambda_{R1}N_1 = \gamma F\,[1 - \exp(-\lambda_{R1}t)] \times \exp(-\lambda_{R1}T) \qquad (7.11)$$

where $\lambda_1 N_1$ = the disintegration rate of the first member
γ = the fission yield of the chain
F = fission rate in fissions per second
t = the time over which the fission rate occurs
T = the time since the fission rate stopped

Similarly, for the second member

$$\lambda_{R2}N_2 = \frac{\gamma F \lambda_{R1}\lambda_{R2}}{\lambda_{R2} - \lambda_{R1}} \left\{ \frac{[1 - \exp(-\lambda_{R1}t)]}{\lambda_{R1}} \times \exp(-\lambda_{R1}T) - \frac{[1 - \exp(-\lambda_{R2}t)]}{\lambda_{R2}} \times \exp(-\lambda_{R2}T) \right\} \qquad (7.12)$$

where λ_{R1} and λ_{R2} are the decay constants of the first and second members. These equations assume that the isotope is removed only by radioactive decay. In some cases, particularly with reactors with high neutron fluxes, some fission products with high neutron-capture cross sections may be eliminated by such capture.

Inspection of Eqs. 7.11 and 7.12 indicates that the short-lived isotopes will soon build to an equilibrium level where the rate of decay is equal to the rate of formation by fission. As in the radioactive-decay equations, the time required to reach such an equilibrium depends upon the half-life of the isotope produced. The longer lived isotopes, such as ^{90}Sr or ^{137}Cs, will continue to increase with the life of the core as the reactor operates. As a result, the mixture of fission products in a reactor is

weighted much more heavily toward the longer lived materials than are the fission products from a nuclear excursion or a nuclear detonation.

Way and Wigner (1951) by considering the statistics of fission and resulting fission products derived a useful rule of thumb for the quantities of radioactive materials produced. In their formulation the beta disintegration rate for times in excess of 10 sec following a single fission is given by

$$\beta(t) = 5.2 \times 10^{-6} t_d^{-1.2} \qquad (7.13)$$

where $\beta(t)$ is the number of beta particles emitted per second and t_d is the time since fission in days.

Figure 7.3 shows the total quantity of fission products remaining after a fission burst equivalent to an energy release of 10 tons of TNT (1.3×10^{21} fissions) or 42,000 Mw-sec as calculated by Bolles and Ballou (1959). For comparison the decay curve for the gross fission mixture from a typical power reactor operated at 1 Mw for a period of 1000 days at an average power of 10.4 Mw/ton of fuel is included. (Quantities have been normalized to the quantity produced per megawatt.) For the reactor curve the assumption that plutonium replaced ^{235}U was made in order to hold power constant, and it was assumed that 4% of the fissions were caused by fast neutrons.

Table 7.1 presents the inventory of specific fission products for (1) decay periods of 1 day and 90 days following reactor operation of 1095 days and (2) decay periods of 1 day and 100 days following a very-short-term excursion of 4,200 Mw-sec, an energy release one-tenth of that chosen for Fig. 7.3.

7-2.3 Nuclear Power

Nuclear power in this discussion is considered the application of the fission reaction in a nuclear reactor regardless of the purpose.

7-2.3.1 Fuel Cycle. The primary fuel for nuclear reactors is ^{235}U, an isotope which comprises about 0.72% by weight of natural uranium. In some reactors, such as military propulsion reactors, the ^{235}U is separated from the ^{238}U to provide a smaller, more compact source of power. In most reactors, however, the ^{235}U is used with a large quantity of ^{238}U either as slightly enriched uranium or, in the case of the heavy-water-moderated reactors and graphite-moderated reactors, as natural uranium in the proportions provided by nature.

In the majority of the U. S. reactors, the ^{238}U is enriched 2 to 5% to provide sufficient reactivity to operate with a less efficient but cheaper moderator such as ordinary water. The production of ^{239}Pu is induced by neutron capture in ^{238}U and subsequent decay of ^{239}U to ^{239}Pu. Plutonium-239 is in itself fissionable and can be used as a fuel to replace ^{235}U by separation at the end of the irradiation period and incorporation into a new fuel batch. In a similar fashion thorium introduced into the reactor can produce ^{233}U by capture of a neutron. Uranium-233 is also fissionable and can be used as a fuel.

In most thermal reactors the conversion reaction is relatively inefficient so that the discharged fuel contains only 20 to 50% as much ^{239}Pu or ^{233}U as the initial ^{235}U content. It is possible to raise the conversion to a factor greater than 100% (i.e., more fissionable material is produced than is used). This process is called breeding, and the fast reactors show the greatest promise for providing such multiplication of available fuel.

The entire fuel cycle starts with the mining of uranium (or thorium) and proceeds through the refining of the ore and concentrates to the desired uranium compound. At this point the fuel elements for reactors are fabricated with natural uranium; an enrichment step is interposed for those reactors requiring a higher ^{235}U percentage. After the fuel elements are used in the reactor, the remaining uranium and the plutonium are separated, sent to fuel fabrication, and recycled; fission products are processed for use or storage. A second input to the cycle can occur with thorium or depleted uranium used as targets to produce ^{233}U or additional plutonium.

The fuel cycle is illustrated in Fig. 7.4

7-2.3.2 Airborne Wastes from Fuel-element Fabrication. Uranium and thorium are mined in underground operations or in open pits. Since the uranium and thorium and their daughter products are radioactive, some radioactive wastes will be produced at all steps in the chain of producing fuel or targets. Both uranium and thorium have very long half-lives. Therefore the mass associated with a given quantity of

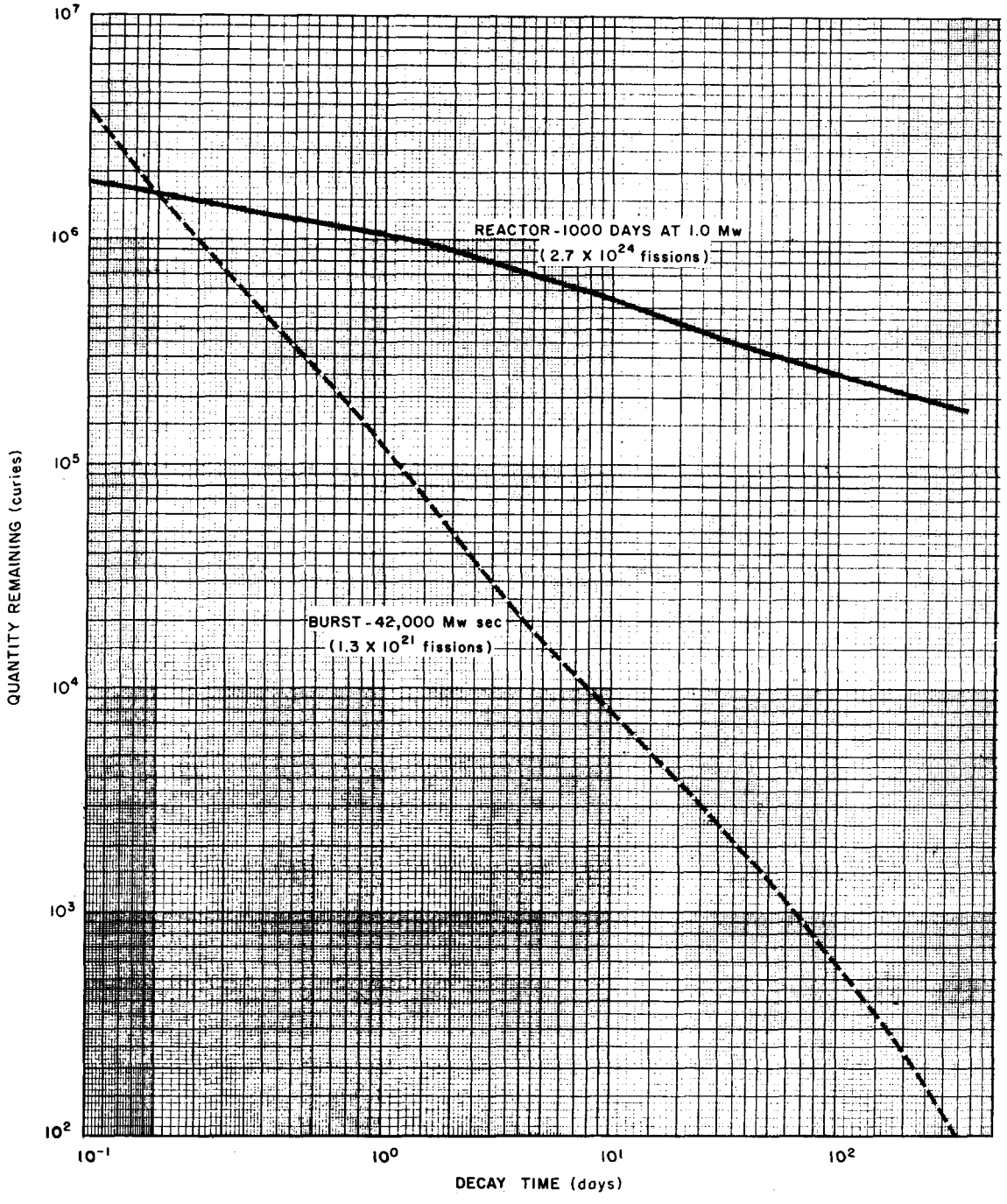

Fig. 7.3—Quantities of fission products remaining after very short and long term reactor operation.

Table 7.1—DECAY OF INDIVIDUAL FISSION PRODUCTS*

Isotope	Isotope half-life	Reactor (1095 days operation) Decay, curies/Mw 1 day	90 days	Excursion (4200 Mw-sec) Decay, curies 1 day	100 days
^{85}Kr	4.36 hr	140		38	
^{85}Kr	10.57 years	360	350	0.03	0.03
^{89}Sr	53 days	23,000	6,600	21	6.1
^{90}Sr	28 years	2,600	2,600	0.2	0.2
^{91}Sr	9.7 hr	5,300		700	
^{90}Y	64.8 hr	2,700	2,600	0.05	0.2
^{91}Y	51 min	3,500		300	
^{91}Y	58.3 days	30,000	11,000	21	8.3
^{92}Y	3.5 hr	1,100		330	
^{93}Y	10 hr	7,800		790	
^{95}Zr	65 days	50,000	19,000	270	97
^{97}Zr	17 hr	18,000		950	
^{95}Nb	90 hr	1,000	410	0.09	0.2
^{95}Nb	35 days	51,000	32,000	0.5	12
^{97}Nb	60 sec	17,000		950	
^{97}Nb	74 min	20,000		990	
^{99}Mo	68 hr	40,000		470	
^{99}Tc	6.04 hr	40,000			
^{103}Ru	39.8 days	40,000	8,600	24	4.4
^{105}Ru	4.5 hr	610		38	
^{106}Ru	1 year	19,000	16,000	0.4	0.3
^{103}Rh	57 min	40,000	8,600	24	4.4
^{105}Rh	45 sec	170		38	
^{105}Rh	36.5 hr	16,000		130	
^{106}Rh	30 sec	19,000	16,000	0.4	0.3
^{109}Pd	13.6 hr	2,600		4.1	
^{112}Pd	21 hr	330		2.1	
^{109}Ag	40 sec	2,600		4.1	
^{111}Ag	7.6 days	1,300			
^{112}Ag	3.2 hr	390		2.4	
^{121}Sn	27.5 hr	150		1.8	
^{125}Sn	9.4 days	420	0.6	0.7	
^{125}Sb	2.0 years	200	190	0.0005	0.007
^{127}Sb	93 hr	2,600		10	
^{128}Sb		820			
^{129}Sb	4.6 hr	180		30	
^{127}Te	105 days	580	340	0.015	0.05
^{127}Te	9.3 hr	2,800	330	8.7	5.1
^{129}Te	33.5 days	3,000	460	1.6	0.2
^{129}Te	74 min	3,100	460	31	0.02
^{131}Te	30 hr	2,600		45	
^{131}Te	25 min	580		46	
^{132}Te	77 hr	38,000		280	
^{130}I	12.6 hr	235			
^{131}I	8 days	28,000	13		0.02
^{132}I	2.4 hr	35,000		285	
^{133}I	20.5 hr	22,000		930	
^{135}I	6.68 hr	4,700		490	
^{131}Xe	≈12 days	270	4	0.05	
^{133}Xe	2.3 days	1,500		8.2	
^{133}Xe	5.27 days	55,000		160	
^{135}Xe	15 min	1,300		160	
^{135}Xe	9.2 hr	14,000		1300	
^{134}Cs	2.1 years	2,000	1,800		
^{136}Cs	12.9 days	910	8		
^{137}Cs	27 years	3,600	3,600	0.1	0.1
^{137}Ba	2.63 min	3,300	3,300	0.1	0.1
^{140}Ba	12.8 days	45,000	370	130	0.7
^{140}La	40.5 hr	49,000	420	44	0.8
^{141}La	3.7 hr	750		140	
^{141}Ce	32.8 days	48,000	7,200	51	6.7
^{143}Ce	33 hr	29,000		700	
^{144}Ce	290 days	38,000	30,000	4.9	3.9
^{142}Pr	119 hr	900			
^{143}Pr	13.7 days	46,000	550	44	1.0
^{144}Pr	17.5 min	38,000	30,000	4.9	3.9
^{145}Pr	4.5 hr	1,700		280	
^{147}Nd	11.3 days	19,000	72	67	0.2
^{147}Pm	2.6 years	7,600	7,400	0.04	0.6
^{148}Pm	42 days	620	140		
^{148}Pm	5.3 days	4,100	160		
^{149}Pm	54 hr	12,000		150	
^{151}Pm	27.5 hr	3,400		70	
^{153}Sm	47 hr	6,300		16	
^{156}Eu	14 days	4,800	78	0.2	0.04

*From Bolles and Ballou (1959), and private communication with I. F. Stuart and A. S. Szigeh, August 4, 1966.

radioactivity is high. Although this tends to minimize radiation problems, in the actual fuel the large quantities handled and the association with relatively short-lived daughter products, particularly in the early stages of refining, provide the potential for airborne release of radioactive material.

Airborne dusts containing the parent materials and daughter products are generated, but little is released to the atmosphere. The chief problem in the operation is with the gaseous radon daughter and its decay products. Extensive ventilation is required to limit the concentration in the mines to tolerable levels.

Uranium mill operations include crushing, grinding, and, in some mills, roasting. All these operations are potential sources of airborne dusts or gaseous daughter products. Usually equipment to clean the air is provided along with forced ventilation through stacks. A possible additional source of airborne radioactivity may be the wind pickup and transport of materials from mill stockpiles and tailing piles. Since the milling operations are carried out on the ore with the daughter products in equilibrium with the product, steps in the milling process produce the greatest likelihood that the more hazardous daughter products will be separated and released to the atmosphere.

After the milling operation the concentrates are subjected to further chemical and metallurgical purification to produce essentially pure uranium metal or uranium compounds. Since the majority of the daughter products have been removed earlier, airborne materials from these purification operations consist primariiy of dusts or fumes of uranium or thorium gen-

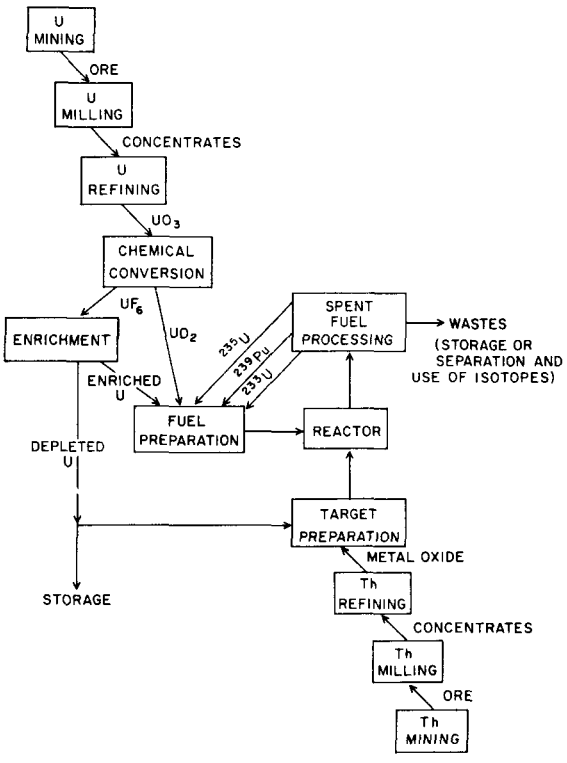

Fig. 7.4 — Nuclear fuel cycle.

erated by mechanical or chemical means. These can be controlled by conventional industrial ventilation and air-cleaning equipment. Similarly the fuel-fabrication steps are primarily mechanical, and dusts are essentially the uranium or thorium compounds involved in the process.

The enrichment step is accomplished by converting the uranium to UF_6 (which is gaseous at a slightly elevated temperature) and processing this compound in a gaseous-diffusion plant. The UF_6 is very reactive chemically and, if released, combines with water in the air to produce a cloud of UO_2F_2 and HF. Since impurities can affect the process, care is taken to minimize the possibilities of leaks. Accidental releases are possible, however, in which case the UF_6 would be converted to small particles of uranium compounds and gases that could disperse downwind. If a release occurs at the product end of the process, the higher concentrations of ^{234}U and ^{235}U will result in more radioactivity per unit mass (relative to natural uranium) and a somewhat greater radiation hazard. In the event of a large release, the chemical toxicity of the fluorine compounds may well be the major hazard.

7-2.3.3 Nuclear Reactors. Radioactive products that could be released to the atmosphere during reactor operation include the fissionable material and the fission and activation products. The actual releases during normal operation depend upon the design of the fuel and the cooling system, and wide variations are possible depending upon the reactor type and use. Reactors can be classified in a number of ways. For the purpose of this chapter, it appears useful to classify reactors by the relation between the cooling system and the atmosphere: the once through direct cycle, the direct cycle, and the indirect cycle. In the first type the coolant (usually air or water) flows through the reactor removing heat and is then discharged to the environment. In the second type the coolant circulates, but the vapor is used directly to drive the energy-recovery system with any entrained gases discharged through the turbine condenser. In the indirect-cycle type, the coolant passes through a heat exchanger and produces steam or other heated gas in the secondary loop which drives the energy-recovery system.

Table 7.2 listing some present or proposed reactors under these classifications indicates the variability of other characteristics possible.

Although corrosion and activation products must be considered a potential source for release of radioactive material during routine operations, the major problem is in maintaining the integrity of the fuel and cladding so that fission products do not escape to the coolant and then to the wastes or the environs. During irradiation the structural changes that occur cause the fuel to swell, thus producing cracks and breaks in the fuel material. With metal fuels operating temperatures are generally limited by phase changes. All of these changes tend to place stresses on the fuel cladding so that eventually the clad may break or lose its integrity. The fuel is designed to operate for a given period with only minimal failures, but even so the escaping fission products may make a major contribution to the radioactivity released in the effluents during normal operations.

In the reactors using once-through cooling systems, any activation or impurities in the coolant, as well as corrosion and fission products picked up by the coolant stream, will be

Table 7.2—REPRESENTATIVE REACTORS CLASSIFIED BY TYPE OF COOLING CYCLE

Use	Coolant	Moderator	Fuel form	Power, Mw(t)	Reactor
			Once Through		
Experimental	Air	Graphite	Metal	3.8	X-10*
^{239}Pu production	Air	Graphite	Alloy		Britain*
^{239}Pu production	Water	Graphite	Metal		Hanford
Experimental	Air	Graphite	Metal	20	Brookhaven
			Direct Cycle		
Power	Water	Water	Oxide	To 3000	Boiling-water reactors
Power	Water	Water	Oxide	700	Dresden 1
Power	Water	Water	Oxide	50	Vallecitos Boiling Water Reactor*
Power	Water	Water	Oxide	240	Humboldt Bay
Development (superheat)	Steam	Water	Oxide	12	EVESR, Vallecitos
Power (superheat)	Steam	Water	Oxide	38	BONUS
Power (superheat)	Steam	Water	Oxide	190	Pathfinder
Power	Heavy water	Heavy water	Oxide	575	Marviken (Sweden)
			Indirect Cycle		
Power	Water	Water	Oxide	To 3000	Pressurized-water reactors
				505	Shippingport
				600	Yankee
				615	Indian Point
Power and ^{239}Pu production	Water	Graphite	Metal		NPR, Hanford
Power	Heavy water	Heavy water	Oxide	694	Douglas Point (Canada)
Power	CO_2	Graphite	Alloy	1533	EDF-3 (France)
Power	CO_2	Graphite	Alloy	1453	Dungeness (United Kingdom)
Power	He	Graphite	Carbide	46	AVR (Germany)
Power	He	Graphite	Carbide	116	Peach Bottom
Power	Sodium		Alloy	200	Fermi
Experimental	Sodium		Oxide	20	Southwest Experimental Fast Oxide Reactor
Power	Organic	Organic	Alloy	46	Piqua

*Shut down.

discharged in the coolant. In the air-cooled reactors, for example, production of ^{41}Ar with a 110-min half-life produces a significant source of radioactive material that is released to the atmosphere. In the water-cooled reactors at Hanford, some discharge of noble gases to the atmosphere occurs through stacks or from the open cooling basins as the dissolved gases separate from the water. In the X-10 reactor, a series of fuel-cladding failures caused contamination of the channels and ducts so that a continuous discharge of fission products occurred. This was remedied by filtering the exit coolant. A particular source of possible effluent for the graphite-moderated reactors is the production of ^{14}C in the moderator and subsequent slow oxidation or exchange with the moderator coolant. Present use of once-through cooling systems is minimal for reactors of any significant power level owing to the preference to operate at higher temperatures and pressures to conserve expensive coolant and to minimize discharges of radioactive materials.

The direct-cycle plants are best illustrated by the present boiling-water reactors or the superheat reactors, either thermal (in the present generation) or fast (in the future). In these plants the steam or superheated steam flows directly from the reactor to the turbine after which it is condensed and returned to the reactor. A continuous demineralization system is used to remove most of the fission or corrosion products in the coolant. In these direct-cycle plants, some of the gaseous and volatile

radioactive materials carried with the steam are carried with the gases from the turbine condenser and exhausted to the atmosphere. Experience has shown that the phase separation at the surface of the boiling water in a boiling-water reactor is an efficient method of decontaminating the steam for all except the noble gases. For normal operating conditions separation factors of 500 to 1000 have been estimated for iodine. The majority of the more troublesome fission products remain in the system to be removed by the ion exchangers. Somewhat more possibility of escape to the atmosphere occurs with the direct-cycle superheat plants because the coolant is steam and no phase change occurs. Even in the event of serious fuel-cladding failures in the present experimental plants, however, the release to the steam is lower than could be expected and has been controlled by changing the faulty fuel, treating the exit air, or lowering the operating temperature of the faulty fuel.

In the direct-cycle reactor, the primary system is completely contained, and any gases generated are withdrawn for storage and subsequent release. In pressurized-water reactors, the volume of noncondensable gases is reduced because the hydrogen and oxygen produced by radiolytic decomposition are dissolved in the water at the high pressure of the primary system. In the reactors employing liquid sodium as a coolant, the capacity of the sodium to dissolve and retain fission products even at the high temperatures involved has been found to be quite efficient. In particular the sodium appears to retain the radioiodines with high efficiency.

In any of these systems, leaks of the primary coolant with the associated dissolved fission products or activation products produce a potential source of airborne particulates and gases that must be removed by the air-cleaning system before release to the atmosphere. It is difficult to ensure that a water system will remain leakproof at high pressure, and any leakage will result in flashing of the steam with dissolved materials suspended in the air. The liquid-sodium and the heavy-water systems seem to have additional problems in this regard: the liquid-sodium systems because of the necessity of preventing chemical reaction with the air and water and the heavy-water systems because of the expense of the coolant.

Potential consequences of reactor accidents may range from the trivial to the extremely serious. The very large inventory of radioactive materials in a large operating reactor in close association with an almost unlimited source of heat poses the main concern.

There are two types of accidents that could result in major releases of fission products from the core. Smaller variants of these possibly could result in smaller releases.

1. A nuclear excursion in which the chain reaction goes out of control owing to a large, unexpected insertion of reactivity. Sufficient heat is generated to melt or even vaporize the fuel in a short time and thereby release the fission products.

2. A loss of coolant to the fuel after some period of operation so that the residual heat generation by the highly radioactive fission products causes the fuel to melt and release fission products from the core.

In the ultimate accident such mechanisms could result in complete melting of the core and the bulk release of fission products. A more likely case, however, would involve only a portion of the core or the melting of a single fuel bundle after removal from the reactor.

In modern reactors the principles of redundancy and inherently safe design are used to minimize the probability of an accident. For example, dual-control instrument systems are used to minimize the possibility of failure, and the reactors are designed to lose reactivity with increasing temperature. Redundant emergency coolant systems are also provided. In addition, a containment or confinement system surrounds the reactor so that any fission products escaping from the core will be contained in the building and the release to the atmosphere will be minimal.

The source term for a reactor accident can vary greatly, depending upon the type of accident and the severity. The time period over which release occurs can also vary considerably, depending upon the pressures involved and the heat sources, heat sinks, and coolant capacity available. In the extreme case where a containment is filled with fission products, sudden failure of the containment could result in a ground-level puff release. If the containment remains intact, a continuous release extending over an appreciable period of time could be expected.

Quantitative data on the fission products that might be released to the atmosphere are meager owing to the uncertainties of the physical conditions expected in a given accident and the lack of experimental data on the behavior of the isotopes. In estimating the release to the atmosphere, both the release from the fuel and the subsequent behavior of the released materials in such processes as agglomeration, impaction, electrostatic attraction, absorption, adsorption, and desorption should be considered. Unfortunately present knowledge permits only qualitative consideration of these processes, and even this is speculative because the environment in which the accident occurs is poorly defined.

An effort is currently being made to obtain experimental data concerning the release and deposition of fission products. The processes involved are complex, however, and accidental conditions are difficult to simulate. Current estimates can be considered only as useful generalizations until much more data have been obtained.

Some fission products may be released from fuel at temperatures below melting if the cladding is destroyed. In general, the noble gases and iodines will comprise the major portion of this release. If the fuel is melted, essentially all the noble gases and most of the iodines will be released. The volatile solids, such as cesium, tellurium, and ruthenium, under oxidizing conditions may be released to about the same extent as iodine. The more refractory fission products, such as strontium and the rare earths, may be largely retained in the melt. In an accident serious enough to volatilize the fuel, however, the bulk of the fission products may be released from the fuel.

Immediately after release the fission products will tend to cool, and particle sizes may increase by agglomeration. The nongaseous fractions will be subject to deposition on surfaces. The extent of the deposition will depend upon the exact pathway of escape, the flow velocities, the temperatures, the characteristics of the atmosphere, and similar factors. Investigation of these factors has been primarily directed at ^{131}I in large reactor facilities. Here it is noted that some fraction of the iodine will rapidly deposit on walls and other surfaces and a smaller fraction will deposit at a much slower rate. Iodine appears in several combinations of chemical and physical form, and these probably change with time. These factors will produce a reduction in the quantities of material that may become airborne. However, the data are not available to estimate with any degree of certainty the quantity of material that will remain airborne following any reactor accident.

7-2.3.4 Separation Plants. After discharge from the reactor, the spent fuel still contains a significant quantity of ^{235}U plus quantities of ^{239}Pu in low-enrichment reactors and ^{233}U if thorium is present. Both ^{233}U and ^{239}Pu can be used as fuels if they are separated from the fission products and reworked into new fuel elements. This is accomplished by a chemical separation process in which either the uranium mixture is dissolved in acid and the uranium is then extracted with solvents or, in proposed processes, the uranium is volatilized by producing uranium hexafluoride and the plutonium and fission products are left to be treated separately.

Even though the fuel is stored for periods ranging from 100 days to 1 year or longer to provide time for radioactive decay, a large quantity of highly radioactive material is still present when the fuel reprocessing begins. During the initial step of dissolution or reaction to produce uranium hexafluoride, the noble gases and a part of the ^{131}I left after the decay period are released. The chief noble gas will be ^{85}Kr with a half-life of 10.76 years. Each ton of metal from a present-day power plant will contain about 5000 curies of ^{85}Kr that will be released to the atmosphere. If the cooling time is on the order of 100 days, significant quantities of ^{133}Xe with a 5.2-day half-life will also be released. Although the ^{85}Kr emits only a soft beta radiation with a minimum of gamma radiation, the ^{133}Xe radiation has a significant gamma component and can deliver external radiation to individuals in the environs.

Of the fission products released to the atmosphere, ^{131}I is of particular interest because of its rapid deposition and inclusion in the food cycles of the region. Since its half-life is 8 days, cooling periods of several hundred days permit time for it to essentially disappear by radioactive decay. If shorter cooling periods are used, various techniques are applied to

remove the iodine from the gaseous effluent before discharge to the atmosphere.

Tritium is also produced in fuel elements during power operations. More than 300 curies of ^{3}H per ton of fuel may be released during processing, and the bulk of it is discharged to the environs.

In addition to these radioisotopes, a general background of other fission products results from leaks and dusts that become airborne. Banks of high-efficiency particulate air (HEPA) filters are used in the ventilation system to maintain fission products at a reasonable level.

In some plants selected fission products are separated for use as radiation or radioisotope heat sources. Such special separations include ^{90}Sr, ^{137}Cs, and ^{144}Ce. The operations can also produce radioactive aerosols that must be controlled by filtration.

Other possible sources of airborne wastes are the storage tanks used for the waste fission products and the equipment used to immobilize the fission products by incorporating them in an insoluble medium. In some cases the heat generation in storage tanks due to the high fission-product concentration may be sufficient to cause boiling. Again, treatment of the exit air is necessary.

Generally, separations plants require massive shielding so that the accidents will not cause a loss of plant integrity or excessive exposure to employees. One potential accident of special concern is the redispersion of radioactive materials collected in one of the air-cleaning devices, e.g., a fire in a charcoal filter containing iodine or in an air filter containing other fission products.

7-2.4 Other Sources

The widespread use of radioisotopes in research, industry, and medicine has created a variety of potential sources ranging from a large number of applications involving small quantities of a few radioisotopes to a few large laboratories where many different radioisotopes are produced and used in large quantities. At each of these installations, at least potentially, a discharge of radioactive materials into the atmosphere can result in a multiple-source problem with low source strength. In general, controls on the amount emitted consist of air-treatment facilities and monitoring.

Shipments of radioisotopes or spent fuel might, in an accident, constitute another source of airborne radioactivity. Although shipping containers are designed to withstand most accidents, the use of air transportation or the potential for involvement of the shipment with large quantities of explosives poses the possibility that the shipping cask might be breached and a portion of the contents melted or vaporized.

The use of radioisotopes and reactors for auxiliary power sources and in propulsion systems has added a new dimension in accident potential because these systems often exist in unusual environments or operate under unusual stresses. The safety problems are further complicated by the uncertainties in predicting the dispersion of the material (particularly for space missions) and in evaluating the biological effects of the various fuel forms.

7-3 RADIOLOGICAL CONCEPTS

7-3.1 Radiations

The ionizing radiations of concern in potential problems with atmospheric waste disposal or a reactor accident are alpha radiation, beta radiation, and gamma radiation.

7-3.1.1 Alpha Radiation. Alpha radiations are particles that are physically identical with the nuclei of helium atoms and are ejected from the nucleus of certain radioactive atoms with a kinetic energy of 4 to 10 Mev. Alpha particles have a mass of approximately 4 amu (6.642×10^{-24} g) and a positive charge of two resulting in strong interactions with atoms encountered. In these interactions a portion of the alpha-particle energy is imparted to the electrons of the atoms of the material traversed with consequent ion-pair production (a negative electron and an associated positive ion). The large number of such ion pairs produced per unit of track length by the alpha particle (30,000 to 100,000 ion pairs per centimeter in air) cause a rapid loss of kinetic energy and, consequently, a short range. Alpha particles emitted from most radioactive materials will travel only 1 to 8 cm in air, depending upon their energies. Since alpha particles of these energies will generally be stopped by the inert surface layer of skin, alpha emitters present no problem of external radiation but can produce serious damage if emitted inside the body where such a protective layer does not exist.

7-3.1.2 Beta Radiation. Beta radiations are electrons emitted from the nucleus of a radioactive atom with an energy of 0.02 to 3.2 Mev which imparts a speed approaching that of light. Because of their lower mass and charge, ionizing interactions between beta particles and the atoms of other materials are more infrequent than for alpha particles (≤200 ion pairs per centimeter in air). The consequent lower rate of energy loss permits a longer range of up to several meters in air and several centimeters in tissue. External beta radiation is important because it will penetrate the protective layer of the skin and produce damage to the underlying sensitive tissues if the kinetic energy is above about 100 Kev. It will not penetrate to the deeper-seated organs of an animal as large as man; so damage is largely confined to the surface layers of the body, including exposed organs such as the eyes. The slowing of the high-speed beta-ray electrons in material (bremsstrahlung) gives rise to electromagnetic radiation, but generally such radiation is significant only with very intense and energetic beta-ray sources. Owing to the limited range of the beta radiation, the dose rate is sensitive to the local concentration, and wide variations can be encountered because of local shielding, pockets developed by increased deposition from eddies, or later translocation and concentration by runoff from a rain storm.

7-3.1.3 Gamma Radiation. Gamma radiations are electromagnetic rays emitted from the nucleus of radioactive atoms. They are indistinguishable from X rays, and both X rays and gamma rays are included in dose calculations. Interactions of gamma photons passing through matter are less frequent than for charged particles; consequently their penetrating ability is much greater. Such interactions occur at random with the drop-off in intensity of the primary beam following an exponential relation complicated by the reentry of certain scattered components into the beam. The relaxation length (distance to decrease the intensity by a factor of 1/e) for typical gamma rays (~0.7 Mev) is on the order of 100 m for air, 50 cm for water, and 5 cm for lead. As a result the gamma-ray dose at any location is a function of the distribution of the radioactive material over a relatively large area or volume.

7-3.2 Radiation Units

Special units have been defined to permit measurement of radiation relative to the effects it produces. The damage to tissue is related to the amount of energy deposited by the radiation in the tissue in the form of ionization and excitation of the molecules with subsequent degradation to heat. Therefore many of the radiation units are closely related to energy deposition.

7-3.2.1 Rad. The rad is the unit of absorbed dose and is defined as the deposition of 100 ergs/g of any absorbing material [International Commission on Radiological Units and Measurements, 1962]. The amount of energy delivered to a body will depend on the nature and degree of the interaction between the radiation and the body irradiated. It is therefore possible to have different absorbed doses in different materials subjected to the same radiation flux as, for example, when the same masses of lead and tissue are exposed to a gamma flux. An obsolete unit frequently found in older literature is the rep, which was defined as the absorption of 93 ergs/g in soft tissue.

7-3.2.2 Roentgen. The roentgen (r) is the unit of exposure (formerly, exposure dose). The past definition gave the roentgen as the quantity of X or gamma radiation such that the associated corpuscular emission per 0.001293 g of air (1 cm^3 at S.T.P.) produces, in air, ions carrying 1 esu of electricity of either sign (International Commission on Radiological Units and Measurements, 1959). A recent report (International Commission on Radiological Units and Measurements, 1962), defined exposure as the quotient $\Delta Q/\Delta M$, where ΔQ is the sum of the electrical charges on all the ions of one sign produced in air when all the electrons liberated by photons in a volume element of air with a mass of ΔM are completely stopped in air. The symbol Δ indicates that averaging must be done in a volume that is small enough so that a further reduction in its size would not appreciably change the measured value of the ratio but is still large enough so that it contains many interactions. The unit of exposure is given by

$$1\ r = 2.58 \times 10^{-4}\ \text{coulomb/kg}$$

Since the roentgen is a measure of the interaction of gamma radiation and air, the absorbed dose (in rads) will vary in different materials from the same exposure (in roentgens). With moderate-energy gamma rays (0.2 to 3 Mev), an exposure of 1 r will produce an absorbed dose in muscle of about 0.97 rads.

7-3.2.3 Dose Equivalent. The dose-equivalent concept is similar to the former RBE dose. All radiations do not produce identical biological effects for a given amount of energy delivered to tissue, i.e., for equal absorbed doses. In general, radiations with high specific ionization along their tracks will produce a greater effect, but the quantitative degree of difference will depend upon the biological change chosen for study. The relative biological effectiveness factor (RBE) is used to compare the effectiveness of absorbed doses of radiation delivered in different ways. It has been recommended (International Commission on Radiological Units and Measurements, 1962) that the term RBE be used only in radiobiological work and that the term quality factor (QF) be used for the linear-energy-transfer dependent factor for radiation-protection purposes. Where appropriate, provision is also made for other factors, such as the distribution factor. The dose equivalent (DE) is now defined as the product of the absorbed dose, the quality factor, the dose-distribution factor, and other necessary modifying factors. The concept of quality factor has a limited usefulness since the biological effectiveness depends on many factors, including the type and degree of biological damage, the absorbed-dose rate, the fractionation of the dose, and the conditions of delivery. It is not possible to determine an accurate value of the quality factor for a given radiation as compared to another which will describe all effects, such as lethality, carcinogenic action, damage to specific tissues, etc.

The dose equivalent is numerically equal to the product of the dose in rads and an agreed-upon conventional value of the quality factor which describes the effects of concern. The standard of comparison is X or gamma radiation having a linear energy transfer in water of 3.5 Kev/μ and a rate of about 10 rad/min.

The unit of dose equivalence is the rem. In addition to the uncertainties introduced by the concept of quality factor, the rem assumes values of the quality factor determined by convention rather than direct measurement. Such values are normally chosen on the basis of long-term effects that may occur over the lifetime of the individual and are therefore applicable to long-term effects rather than the more pronounced immediate effects from a large absorbed dose. For radiation from internal emitters, the following quality factors (QF) are used to convert from absorbed dose to dose equivalent:

Internal radiation	QF
β^-, β^+, γ, X	
$E_{max.} > 0.03$ Mev	1
$E_{max.} < 0.03$ Mev	1.7
α	10
Fission fragment and α recoil	20
Neutrons from spontaneous fission	8

In the case of exposure to mixed radiations, the dose equivalent is assumed to be equal to the sum of the dose equivalents (in rems) of each of the radiations involved.

7-3.2.4 Curie. The curie is the special unit of activity (International Commission on Radiological Units and Measurements, 1962). It was earlier the unit of quantity of radioactive material. The activity is given by $\Delta N/\Delta T$, where ΔN is the number of nuclear transformations that occur in the quantity of material of concern in time Δt. The symbol Δ indicates that averaging must be done in a time interval that is short enough so that a further reduction in the interval would not appreciably change the measured value of the ratio but is still long enough so that it contains many disintegrations. One curie is that quantity of a radioactive nuclide in which the number of disintegrations (transmutations) per second is exactly 3.7×10^{10}.

The curie is related to the mass of a radioactive material through the half-life and the number of atoms per unit mass (atomic weight). The mass of material associated with 1 curie varies widely. For example, one curie of ^{24}Na (half-life, 14.8 hr) weighs 10^{-15} g, 1 curie of ^{226}Ra (half-life, 1622 years) weighs 1 g, and 1 curie of ^{238}U (half-life, 4.5×10^9 years) weighs 3×10^6 g. The relation between the curies and the mass of a specific radionuclide is given by

$$q = \frac{\lambda_R M_R N_0}{A\,(3.7 \times 10^{10})} \qquad (7.14)$$

where q = number of curies
λ_R = disintegration constant (fraction of the atoms that decay per second) = $0.693/T_{1/2}$
$T_{1/2}$ = half-life of the radionuclide (sec)
M_R = mass of radionuclide (g)
N_0 = Avagadro's number: 6.03×10^{23} atoms/gram atomic weight
A = atomic weight of the radionuclide

Frequently there is some confusion about the use of the term "curie" when it is applied to mixtures of radionuclides. In this book the term will be used to describe the total disintegration rate of the mixture, i.e., the sum of the activities contributed by the specific radionuclides of the mixture when more than one radionuclide is involved. Many radionuclides emit more than one gamma ray per disintegration or a beta particle and one or more gamma ray per disintegration, and care must be exercised when determining the radiation flux from a source (in curies) or when determining the source (in curies) that produces a given flux.

The relation between the quantity of radioactive material (curie) and the radiation dose rate (rad/sec) is dependent upon the energy of the radiation emitted, the type of radiation emitted, the geometrical pattern between the radioactive material and the receptor, and the amount of absorbing material between the radioactive material and the receptor.

7-3.3 Radiation Measurements

Measurement devices used in radiation protection are designed to measure the radiation dose or dose rate or to measure the quantity of active material present by the rate at which radiation is emitted. Although a large number of measurement devices are available, the three in principal use are the ionization chamber, the particle counter, and the photographic film.

An ionization chamber in its simplest form consists of a pair of charged electrodes that collect ions formed within their electrical field. Many of the electrons actually entering the gas in the chamber are the result of secondary interactions in the chamber walls; consequently the chamber response is governed by the wall material. Properly designed and calibrated chambers are usually used for dose or dose-rate measurements because they provide an indirect measure of the energy deposited in the chamber.

Counters are designed to record the passage of a single particle, primary or secondary, through the sensitive volume of the counter. Gas-filled counters may simply collect the ionization produced by the radiation and amplify it to produce a pulse. Amplification may be produced by the acceleration of the electrons and their subsequent collisions with molecules in the gas to produce a pulse proportional to, but greater than, the initial pulse (proportional counter); or a large amplification may be produced by providing conditions such that the pulse spreads through the entire sensitive volume and a complete discharge between the electrodes results (Geiger-Mueller counter). A scintillation counter registers electrical pulses from a phototube. These pulses are initiated by the small flash of light produced by the radiation interacting with the phosphor or crystals in the vicinity of the tube.

Counters are usually used to determine the activity present by measuring the number of particles or photons emitted by the radioactive material. Scintillation or proportional counters can be used to determine dose or dose rates if the equipment is designed to measure the energy delivered to the receptor. Geiger counters are frequently used as radiation detectors because of their sensitivity and can be used to measure dose rate if they are calibrated for the energy and type of radiation to be measured.

Photographic film will darken upon exposure to radiation and can be used to give a measure of the quantity of radiation present. Although the film response is energy dependent for gamma rays below 0.5 Mev, this can be corrected by filters to about 0.2 Mev. Film is frequently used in measuring personnel exposure and in other dose measurements where a long integration time period is required or a permanent record is desired.

7-3.4 Effects of Radiation

The effects of a given dose of radiation depend upon a large number of factors, including the magnitude of the absorbed dose, the type of radiation, the penetrating power of the radia-

tion, the radiosensitivity of the organism for the effect involved, the rate at which the dose is delivered, the portion of the organism irradiated, and the specific organs involved.

The qualitative aspects of radiation effects are well known from past experience with human exposure and extensive studies with animals, but the quantitative relation between a dose delivered under given conditions and the resulting biological change is not so well defined for man. Only a few of the effects will be discussed here in order to illustrate the magnitudes of doses involved.

A massive exposure delivered in a relatively short time can produce immediate or acute effects, which in their most severe form can cause the death of the organism. For man it is estimated that a X- or gamma-radiation dose of 400 to 500 rads delivered to a major portion of the body in a short time interval will result in the death of about 50% of those so exposed within a few months (Braestrup and Wyckoff, 1958). Most mammals have about the same degree of sensitivity to the dose required to give 50% lethality in 30 days (LD 50) ranging from perhaps 275 r for swine to 800 r for the rabbit (Patt and Brues, 1954). Sublethal exposure of humans to doses above 100 to 200 r will produce nausea, vomiting, diarrhea, and malaise with the symptoms developing earlier for the higher exposures (Glasstone, 1962). A loss of hair might occur about 2 weeks after an exposure of greater than 300 r (Nickson and Bane, 1959).

Skin reactions will develop if the dose is sufficiently high. Such effects are of primary importance in exposure to beta radiation or low-energy gamma radiation which can deliver very high doses to the skin with comparatively small doses to the remainder of the body. Doses of 400 to 1500 rads to the skin will result in an erythema (reddening) in several days and possible loss of hair in about 2 weeks (Nickson and Bane, 1959). The hair will return, but there is a possibility that it will be gray. At the higher end of this dose range, there may be dry scaling of the surface layers in about 3 weeks. Above 1500 rads an erythema will develop, and raw moist areas will form. Above 5000 to 7000 rads, these areas may develop into areas that heal very slowly or not at all.

Late effects of radiation exposure are those which occur some time after the exposure or as a result of continued low-level exposure over a period of time. These effects are detected by statistical review of the incidence of the effect among those exposed compared to the incidence in a similar unexposed group; i.e., these effects are not an invariable result of exposure as with the acute effects but rather express themselves as an increase in probability of the individual's contracting a specific ailment. The degree of increase in probability depends upon the radiation dose, the time of exposure, the organs exposed, and other parameters.

The increased incidence of certain malignancies with radiation exposure has been well documented both in experimental animals and in man. The ingestion of radium by the dial painters in New Jersey between 1916 and 1925 claimed 41 victims over a period of about 20 years (Furth and Lorenz, 1945). Bone sarcomas developed in individuals, a few of whom had 20 μg of radium or more in their bodies. The increased incidence of leukemia among the Japanese surviving the nuclear detonations over Hiroshima and Nagasaki (Wald, 1958) and among certain patients treated with radiation (Court-Brown and Doll, 1957) has indicated that leukemia can be produced by single exposures on the order of 100 r. Similar results have been noted in a study of American radiologists who received radiation over a period of time during the days before the institution of present protection methods (March 1944). Similarly numerous skin cancers have developed among early workers with X rays where the majority of the exposure was to the hands. Direct evidence on the production of malignancies by lower doses is not available, and it is not known whether this is due to the difficulty of detecting a small increase over the normal incidence or to a possible threshold value of dose below which the effect will not occur.

Radiation is but one of the mutagenic agents to which man is exposed. Such agents can produce changes in the germ cells which can be passed to children and may produce abnormalities in future generations (World Health Organization, 1957). These effects will not appear in the person irradiated but may result in harmful changes in the future populations. Since such changes result from intermixing of the genes, an important criterion of possible radiation damage in addition to the exposure to the individual is the number of individuals

exposed. An estimate of the average dose over the reproductive lifetime of the individual which is required to double the mutation rate is between 10 and 100 rads (United Nations, 1958).

Other effects that occur later include cataract formation and shortening of the lifespan. Cataracts have been noted from single clinical exposures of over 175 r (Merriam and Facht, 1958). With the radiation delivered over a period of 3 months, the lowest exposure associated with a cataract was 550 r. Life shortening from radiation exposure has been noted in animals where no specific injury was responsible for the death. Evidence for such an effect in man has been presented for the early radiologists (Warren, 1956) but has been questioned owing to the difficulty of obtaining an adequate control group for comparison (Lewis, 1957).

7-3.5 Radiation Limits

Shortly after the discovery of X rays in 1895, evidence of the harmful effects of indiscriminate exposure to radiation began to accumulate, and recommendations for limitations of exposure were made. In 1928 the International Commission on Radiological Protection (ICRP) was organized under the auspices of the Second International Congress on Radiology. In 1929 the Advisory Committee on X-ray and Radium Protection was organized to develop recommendations in the United States. Following World War II, this Advisory Committee was reorganized as the National Committee on Radiation Protection (NCRP) with representatives from professional societies and governmental agencies, as well as individual experts. The recommendations developed by this group have served as the basis for most radiation-protection programs and, later, for rules and codes adopted by the various regulatory agencies in the United States. In 1959 the Federal Radiation Council (FRC) was formed to advise the President on radiation matters and to provide guidance for all federal agencies in the formulation of standards of protection against radiation damage.

Each of the groups that have recommended exposure limits has written lengthy reports that include a discussion of the factors taken into consideration in arriving at the recommendations and limits. These reports must be read fully and carefully to understand the recommendations as they were intended by the authors. Only deliberate study of the complete reports can provide the basis for judgment on the adequacy of a program for radiation protection. When limits are enumerated, they are intended as limits and not design criteria for an apparatus or activity. All groups have stressed the fact that there are multiple sources and modes of exposure and have assumed a linear relation between dose and effect. All groups have recommended keeping exposure to the minimum practical and have called for a balance of risk and benefit to justify those exposures which cannot be avoided. A balance of benefit and risk is difficult because they cannot be adequately reduced to a common denominator and considerable uncertainty is involved on both sides of the "scale". In the final analysis professional judgment is required, and the basis for the judgment should be sound.

7-3.5.1 Occupational Exposure. The original recommendations of the NCRP and the ICRP were aimed at controlling the exposures of individuals working with radiation and were primarily based upon effects that had been observed in early radiation workers. Following World War II a large body of information became available from the animal experiments performed in connection with the Manhattan Project. Review of these data, plus continued review of the extensive work since that time, has led to the present recommendations for the control of occupational exposure.

The maximum permissible doses (MPD) for radiation workers as recommended by the ICRP (International Commission on Radiological Protection, 1959) and NCRP (National Committee on Radiation Protection, 1958) are in basic agreement although there are some minor differences.

Organ	MPD (annual), rem
Gonads, red bone marrow, and whole body	5*
Skin, thyroid, and bone	30
Hands and forearms, feet and ankles	75
All other organs	15

*The cumulative dose of D = 5(N-18) rem should not be exceeded. Here D (rem) is the cumulative dose and N(years) is the age of the individual.

These exposure levels are well below those observed to cause damage, and they are not expected to cause appreciable bodily injury to a person continuously so exposed during his working years. However, the assumption that the relation between risk and dose is linear leads to the conclusion that any radiation will result in an increase in the risk for the development of certain somatic and genetic effects.

Limitations for internal emitters are based upon the radiation dose delivered to specific organs or, in the case of bone-seekers, are based upon a comparison with the energy delivered by radium. Radium is the only internal emitter for which the available experience with man is adequate to establish a maximum permissible limit from direct evidence of damage. In the derivation of limits for internal emitters, the maximum permissible quantity in an organ is calculated from the organ size, the energy release in the organ, and, where appropriate, the distribution of the isotope in the organ (National Committee on Radiation Protection and Measurement, 1959). This quantity of radioactive material in the organ provides the basic limitation because it describes the radiation actually received by the organ. As guides to the conditions that could result in exposure of the organ to the maximum permissible dose, secondary numbers called maximum permissible concentrations of the radioisotope in air and water are derived by considering the uptake and translocation of the isotope in the various organs.

To provide a standard basis of calculation, the ICRP has defined a so-called "standard man" in terms of the intake of air and water, retention of particulates, and organ weights (International Commission on Radiological Protection, 1959a). All maximum permissible concentrations refer to this idealized model. It should be noted that this standard man is a hypothetical individual and that specific people vary significantly from this standard.

Use of standard-man values does not provide an estimate of the greatest dose that might be experienced by any specific individual (or increment) of the general population, but it does, generally, provide an overestimate of the doses that might be experienced by the average industrial worker.

The uncertainties in the metabolic parameters are such that the estimation of the dose to individuals and the estimation of the resulting effects can be only order of magnitude at best. Important parameters of the standard man are given in Table 7.3.

Table 7.3—SELECTED PARAMETERS OF THE STANDARD MAN

Organ weights	
Total body	70,000 g
Skeleton:	
Without bone marrow	7,000 g
Red marrow	1,500 g
Yellow marrow	1,500 g
Contents of GI tract:	
Lower large intestine	150 g
Stomach	1,100 g
Small intestine	135 g
Upper large intestine	1,700 g
Liver	1,500 g
Lungs	700 g
Kidneys	300 g
Spleen	150 g
Testes	30 g
Thyroid	20 g
Water intake in food and fluids	2,200 g/day
Total air inhaled per day	2×10^7 cm^3

	Retention of particles*	
Distribution	Readily soluble compounds, %	Other compounds, %
Exhaled	25	25
Deposited in upper respiratory passages and later swallowed	50	50
Deposited in lungs	25†	25‡

	Constants for GI tract		
Portion	Mass of contents, g	Time of food arrival, hr	Time of food leaving, hr
Lower large intestine	150	13	31
Small intestine	1100	1	5
Upper large intestine	135	5	13
Stomach	250	0	1

*A new lung model is being developed to replace that described here. Current literature should be consulted for possible changes.

†Taken up into the body.

‡One-half eliminated from lungs and swallowed in first 24 hr. Remaining 12.5% retained in lungs with a half-life of 120 days except for plutonium and thorium for which the biological half-life is assumed to be one year and four years respectively.

With knowledge of the way the various radionuclides are assimilated by the body and intake values for the standard man assumed, one can calculate the concentrations of specific radionuclides in water or air which, if ingested or inhaled continuously by the individual during a

50-year working lifetime, would limit the critical organ exposure to the maximum permissible dose rate. For most radionuclides taken at a uniform rate over a 50-year period, the body will attain an equilibrium quantity of the radionuclide, i.e., balance between intake and elimination by both radiological decay and biological modes. However, certain long-lived radionuclides that are retained by the body for a long time (^{90}Sr, ^{238}Pu, ^{239}Pu, ^{240}Pu, ^{241}Pu, etc.) do not attain equilibrium in 50 years, and the quantity accumulated in the body will continue to increase. In either case the total quantity of the radionuclide in the body when the critical organ is being exposed at the MPD rate is the maximum permissible body burden. The concentrations of the radionuclides in air and water, calculated as described above, are the maximum permissible concentrations in air $(MPC)_a$ and water $(MPC)_w$, respectively. Typical values of the limits for several internal emitters for occupational exposure as derived by the NCRP and ICRP are given in Table 7.4 (National Committee on Radiation Protection and Measurement, 1959).

Table 7.4—NCRP LIMITS FOR SELECTED INTERNAL EMITTERS

Isotope	Critical organ	Body burden, μc	MPC (industrial worker, 168-hr week), μc/cm³	
			Water	Air
^{89}Sr	Bone	4	10^{-4}	10^{-8}
^{90}Sr	Bone	2	10^{-6}	10^{-10}
^{103}Ru	GI		8×10^{-4}	2×10^{-7}
	Kidney	20	3×10^{-2}	3×10^{-7}
^{106}Ru	GI		10^{-4}	3×10^{-6}
	Kidney	3	4×10^{-3}	5×10^{-8}
	Lung			2×10^{-9}
^{131}I	Thyroid	0.7	2×10^{-5}	3×10^{-9}
^{137}Cs	Total body	30	2×10^{-4}	2×10^{-6}
^{239}Pu	Bone	0.04	5×10^{-5}	6×10^{-13}

The critical organ in Table 7.4 is considered to be the organ that receives the highest radiation dose after the isotope is absorbed into the body and is therefore assumed to be the organ most likely to be damaged. In some cases, particularly when the isotope is in a form not readily assimilated into the body, the highest dose is received by the organs at the point of entry, i.e., usually the gastrointestinal tract or the lung. In such cases a maximum permissible concentration is derived on the basis of the estimated dose to these organs.

7-3.5.2 Exposure of Populations. Individuals not working with radiation can be exposed in a variety of ways: e.g., the radiation from cosmic rays or natural radioactive materials in the earth; medical or dental uses of X rays; television tubes; radium dials; fallout from nuclear detonations; waste disposal from nuclear plants; accidents with radiation sources. An estimate of the relative importance of some of these sources to the population as a whole is given in Table 7.5 (Parker, 1960).

Table 7.5—THIRTY-YEAR PER CAPITA DOSES IN THE UNITED STATES FROM RADIATION SOURCES OTHER THAN FALLOUT

Source	30-year dose	
	Gonad dose, rem	Bone dose,* rem
Natural radiation		
External		
Cosmic rays	0.9	0.9
Terrestrial radiation	2.1	2.1
Atmospheric radiation	0.06	0.06
Internal		
^{40}K	0.6	0.3
^{14}C	0.06	0.06
Rn–Th	0.06	0.06
Ra		1.2
Subtotal	~3.8	~4.7
Man-made radiation		
Diagnostic X ray	3.0†	1.4
X-ray therapy	0.36	‡
Internal isotopes	<0.03	‡
Luminous dials	0.03	‡
Television	<0.03	<0.03
Atomic energy workers	0.003	0.003
Medical workers	0.03	‡
Subtotal	~3.5	~1.4
Approximate total	7 to 8	5 to 7

*Taken here as the osteocyte dose. This principally affects the radium entry, which would be 0.05 rem for mean marrow dose.

†Additional studies on limited groups have given values on the order of 1.5 rems.

‡No estimate.

All groups that have made recommendations on radiation exposure of the general public have recommended values lower than those for occupational workers. A decrease by a factor of 10 for individuals in the vicinity of an area controlled because of the presence of radiation has been used by the NCRP (National Committee on Radiation Protection and Measurement, 1959) and the ICRP (International Commission on Radiological Protection, 1966). Further, the ICRP specifies that these limits

apply to the "appropriate critical group" within the general public which, because of age, diet, activities, etc., receives the highest dose in the particular environment. As an alternative to defining this group, the commission recommends applying an appropriate safety factor to the dose limits for the general public. The dose limit applied to the thyroid of children less than 16 years of age is 1.5 rem/year because of the damage susceptibility. A gonad dose limit of 5 rem in 30 years is specified for populations in consideration of genetic effects. The Federal Radiation Council (FRC) gives a radiation protection guide of 0.5 rem/year of whole-body radiation for individuals with an average of 0.17 rem/year for appropriate population groups to ensure that no individual exceeds 0.5 rem/year. In each case exposure from medical applications or natural background is omitted.

Controls on internal emitters must also consider the amount of radiation received by the gonads. The ICRP has suggested that the MPC of isotopes that irradiate the whole body or the gonads be reduced by 1/100, a factor that allows for concurrent external exposure when applied to whole populations. For other isotopes the commission recommends a reduction factor of 1/30.

The FRC (Federal Radiation Council, 1961) has published guides for normal use based on daily intake with three ranges of concern:

1. Range I would not be expected to result in a large fraction of the Radiation Protection Guide (RPG) for an appreciable fraction of the individuals. Only surveillance is needed.

2. Range II would not be expected to result in average exposures exceeding the RPG. Active surveillance and routine control are needed.

3. Range III exposures would be expected to exceed the RPG if continued for a sufficient period of time. Intake within this range must be evaluated in terms of the RPG, and, if necessary, appropriate positive control measures should be instituted.

Range limits for several isotopes as given by the FRC are listed in Table 7.6 (Federal Radiation Council, 1961).

7-3.5.3 Emergency Radiation Limits. The radiation limits given earlier are applicable to routine situations that are amenable to control of the exposure. Exposure to higher radiation levels does not mean that damage will result. In emergency situations, where the radiation rates are high, it may be impossible to control the exposure to any preset level either because the radiation is received before action is instituted or because action involving radiation exposure is required to save lives or otherwise control the situation. Firm limits to be followed in all such situations cannot be derived since any exposure under these conditions involves a judgment on the value of a given action as opposed to the possible damage that would result from the exposure. The NCRP, in a study of this situation, states: "It is obviously not possible to spell out every ... circumstance; and it is certainly not the prerogative of any committee to assign relative values to high-priority tasks on the one hand, and to the radiation exposure involved in doing so on the other hand" (National Committee on Radiation Protection and Measurements, 1962). The NCRP defines a radiation emergency as: "... an accident, or other event out of the ordinary, that threatens to expose people to more than 25 r in 1 week. It is not intended to include maintenance and reconstruction activities following a peacetime accident after the hazard to the general population has passed. It is expected that most radiation accidents in peace-

Table 7.6—RANGES OF TRANSIENT RATES OF INTAKE FOR USE IN GRADED SCALE OF ACTIONS

Isotope	Range I, μc/day	Range II, μc/day	Range III, μc/day
^{226}Ra	$\leq 2 \times 10^{-6}$	2×10^{-6} to 2×10^{-5}	2×10^{-5} to 2×10^{-4}
^{131}I	$\leq 1 \times 10^{-5}$	1×10^{-5} to 1×10^{-4}	1×10^{-4} to 1×10^{-3}
^{90}Sr	$\leq 2 \times 10^{-5}$	2×10^{-5} to 2×10^{-4}	2×10^{-4} to 2×10^{-3}
^{89}Sr	$\leq 2 \times 10^{-4}$	2×10^{-4} to 2×10^{-3}	2×10^{-3} to 2×10^{-2}

time can be handled satisfactorily under the principles set forth in Handbook 59" (National Committee on Radiation Protection and Measurement, 1962).

Limits per se are not pertinent to emergency conditions during which the risk of acute exposure and immediate harm is present. Instead, such situations must be guided by individuals acquainted with the risks involved and the importance of various tasks.

The FRC in reviewing the problem of emergency conditions noted that "Protective actions are appropriate when the health benefit associated with the reduction in dose that can be achieved is considered sufficient to offset the undesirable factors associated with the action" (Federal Radiation Council, 1964). The FRC also provided guidance in applying Protective Action Guides (PAG). They proposed:

> 1. If the projected dose exceeds the PAG, protective action is indicated.
> 2. The amount of effort that properly may be given to protective action will increase as the projected dose increases.
> 3. The objective of any action is to achieve a substantial reduction of the dose that would otherwise occur—not to limit it to some prespecified value.
> 4. Proposed protective actions must be weighed against their total impact. Each situation should be evaluated individually. As the projected dose becomes less, the value of protective actions becomes correspondingly less.
> 5. The Protective Action Guide is based on the assumption that the occurrence, in a particular area, of environmental contamination that would require protective action is an unlikely event. Circumstances that involve either repetitive occurrence or in which there appears a substantial probability of recurrence within a period of one or two years would require special considerations. . . . In contemplating the possibility of a future event, it is necessary to consider not only the possible magnitude but also the probability that the event will occur.

The FRC then recommends the use of a value of 30 rads to the thyroid of an individual as the PAG for ^{131}I. As an operational technique, it is considered that the PAG will not be exceeded if the average dose to the thyroid of a suitable sample of the population does not exceed 10 rads. A suitable sample is considered to consist of children about 1 year of age using milk from a reasonably homogeneous supply.

7-4 EXTERNAL BETA RADIATION

Because beta radiation has a limited range (1 to 10 m in air), the beta dose depends mainly upon the concentration of radioactive materials in the immediate vicinity of the individual. Since any variations in the local concentration will result in a corresponding variation in the dose, the prior estimates of beta doses can be regarded only as order of magnitude estimates of the average dose, particularly in those cases in which the radioactive materials settle very close to, or on, the person.

7-4.1 Beta Dose from Passing Clouds

A cloud of radioactive materials that decay through beta emission will constitute a source of beta radiation. The importance of this source will depend upon the energies of the radiations emitted, the size of the cloud, the concentration in the cloud, and the wind speed.

7-4.1.1 Beta Dose from Infinite Clouds. Consider a spherical cloud with a uniform concentration of a beta-emitting isotope and a radius equal to the range of the beta particles. Such a cloud would be considered an infinite cloud for a receptor at the center because any additional beta-emitting material beyond the cloud dimensions would not alter the flux of beta particles to the receptor. For such a cloud the beta dose rate can be calculated from equilibrium considerations provided the receptor volume is small and does not perturb the radiation field.

For an infinite uniform cloud containing χ curies of beta radiation per cubic meter, the beta dose rate in air at the cloud center is given by Eq. 7.15:

$$ {}_{\beta}D'_{\infty} = \frac{\overline{E}_{\beta}\ (1.6 \times 10^{-6})\ (3.7 \times 10^{10})\ \chi}{(1293)\ (100)} \qquad (7.15) $$

$$ {}_{\beta}D'_{\infty} = 0.457\ \overline{E}_{\beta}\ \chi \qquad (7.16) $$

where ${}_{\beta}D'_{\infty}$ = beta dose rate from an infinite cloud (rad/sec)
$\overline{E}_{\beta}$ = average beta energy per disintegration (Mev/dis)
1.6×10^{-6} = number of ergs per Mev
χ = concentration of beta-emitting isotope in the cloud (curie/m^3)
3.7×10^{10} = disintegration rate per curie (dis/sec curie)

1293 = density of air at S.T.P. (g/m^3)
100 = energy absorbed per gram of absorbing material per rad (erg/g-rad)

If the air is at other than standard density, Eq. 7.16 can be corrected by the ratio of the air densities, thus

$$ {}_{\beta}D'_{\infty} = 0.457\ \bar{E}_{\beta}\ \chi \left(\frac{\rho_0}{\rho}\right) \qquad (7.17) $$

where ρ_0 = density of air at S.T.P. (g/m^3) and ρ = density of air at reference conditions (g/m^3). Although applicable throughout, this correction factor for air density will not be repeated in subsequent equations.

By the time a cloud or plume has reached the receptor, the dimensions of the cloud are generally on the order of tens of meters. Under these conditions the cloud can be considered infinite in extent for any point within the cloud, and the error introduced by this approximation will be well within the uncertainties caused by other factors.

For these conditions of infinite cloud size, if $\chi_{(x,y,z,t)}$ is the instantaneous concentration of the cloud at the receptor location at time t (sec) after the release, the external beta dose rate ${}_{\beta}D'_{\infty(x,y,z,t)}$ to the receptor at any time t after release is given by

$$ {}_{\beta}D'_{\infty(x,y,z,t)} = 0.457\ \bar{E}_{\beta}\ \chi_{(x,y,z,t)} \qquad (7.18) $$

where $\chi_{(x,y,z,t)}$ has been corrected for depletion by ground deposition and radioactive decay en route.

The total direct beta dose ${}_{\beta}D_{\infty(x,y,z)}$ due to cloud passage is given by

$$ {}_{\beta}D_{\infty(x,y,z)} = 0.457\ \bar{E}_{\beta}\ \psi_{(x,y,z)} \qquad (7.19) $$

where $\psi_{(x,y,z)}$ = concentration time integral (curie sec/m^3) at the receptor location and is corrected for depletion en route
$= \int_{t_a}^{t} \chi_{(x,y,z,t)}\ dt$
t_a = time of cloud arrival (seconds since release)
t = time of cloud departure (seconds since release)

The meteorological formulas generally used to determine the cloud concentration or concentration time integral are developed for nonradioactive source material and do not include correction for ground deposition. When the source material is radioactive, correction factors must be included to account for the depletion by radioactive decay en route to the receptor. When a single radionuclide is involved, the correction is simply

$$ \left(\frac{Q_x}{Q_0}\right)_R = \exp\left(-\lambda_R \frac{x}{\bar{u}}\right) $$

where $(Q_x/Q_0)_R$ = the reduction in quantity of radioactive material due to radioactive decay
x = downwind distance between the point of release and the receptor location (m)
$\bar{u}$ = average wind speed during transit (m/sec)
λ_R = radioactive-decay constant (sec^{-1})

When the source term includes several radionuclides, a single exponential equation is inadequate, and a power function or other empirical decay factor may be required to describe the depletion by concurrent decaying of several radionuclides. In this case the correction factor may be indicated symbolically as

$$ \left(\frac{Q_x}{Q_0}\right)_R = f_R(t) $$

The correction factor for depletion due to ground deposition (see Sec. 5-3.2.2) is similar to Eq. 5.48,

$$ \left(\frac{Q_x}{Q_0}\right)_d = \exp\left[-\left(\frac{2}{\pi}\right)^{1/2} \left(\frac{v_d}{\bar{u}}\right) \int_0^x \frac{\exp\left(-h^2/2\sigma_z^2\right)}{\sigma_z}\, dx\right] $$

The total depletion correction term is the product of the two factors:

$$ \frac{Q_x}{Q_0} = \left(\frac{Q_x}{Q_0}\right)_R \left(\frac{Q_x}{Q_0}\right)_d $$

In this chapter, in which meteorological dispersion formulas are used to calculate radiation dose values, the symbols for cloud concentration (χ) and cloud concentration time integral (ψ) at the receptor location are assumed to include the appropriate depletion correction factors.

The value of $\bar{E}_\beta$ in Eqs. 7.15 and 7.19 is the average kinetic energy of the beta particles released per disintegration. Beta particles are emitted from radioactive material with a continuous spectrum of energies ranging from zero to a maximum value characteristic of the specific material. The average of the beta-ray spectrum varies from about 0.25 to 0.45 of the maximum energy for negative electrons, depending upon the atomic number of the radionuclide and the maximum energy (Hine and Brownell, 1956). In view of the accuracy with which other parameters are known, it is usually adequate to consider the average beta energy for a specific radionuclide to be one-third of the maximum beta-ray energy. In a cloud composed of a number of radioisotopes, it is necessary to obtain an overall average beta energy by considering the fraction of each species present and its average energy of emission.

Equations 7.15 and 7.19 describe the beta dose rate and dose resulting from an essentially infinite cloud where media of different absorbing characteristics are not present. In the actual case the presence of the body in the cloud causes a perturbation to the radiation field. Owing to the very limited range of beta particles in tissue, the beta dose to a body surrounded by a beta source will generally be limited by geometrical considerations to irradiation from half the cloud. Protruding organs, such as the nose, ears, and fingers, may, however, receive radiation from greater than a 2π solid angle. For this reason the beta dose or dose rate at the surface of a body immersed in an infinite cloud will be about one-half the equilibrium beta dose (or dose rate) of the full cloud. In addition, the surface of the earth provides a further perturbation in the radiation field. The dose rate at the surface is only one-half of that in an infinite cloud but increases to the full infinite-cloud dose at an elevation equal to the maximum range of the beta particles involved. Therefore dose rates will vary from the head to the foot of an individual with the highest dose rate at the head. This factor varies from 0.5 at the ground to 1.0 at heights greater than the range of the beta radiation. This correction factor will not be included in subsequent formulas although specific corrections can be made for particular elements of tissue if the radiation energy and height of concern are defined.

The surface body dose from beta emitters in the infinite cloud can be approximated as

$$ {}_\beta D_{\infty(x,y,z)} = (0.5)\,(0.457)\,\bar{E}_\beta\,\psi_{(x,y,z)} \qquad (7.20) $$

$$ {}_\beta D_{\infty(x,y,z)} = 0.23\,\bar{E}_\beta\,\psi_{(x,y,z)} \qquad (7.21) $$

where $\psi_{(x,y,z)}$ is the concentration time integral for the cloud (curie sec/m^3) corrected for depletion by ground deposition and radioactive decay en route. If the source (release of radioactive material) is known in terms of power units, e.g., $P_{\beta 1}$ (Mev/sec) or $P_{\beta 2}$ (erg/sec), the beta dose (rads) to the surface of the body from the passing infinite cloud can be given by

$$ {}_\beta D_{\infty\,(x,y,z)} = \frac{(0.5)\,(1.6\times 10^{-6})}{1293\times 100}\left(\frac{\psi_{(x,y,z)}}{Q}\right) P_{\beta 1} \qquad (7.22) $$

$$ {}_\beta D_{\infty\,(x,y,z)} = 6.2\times 10^{-12}\left(\frac{\psi_{(x,y,z)}}{Q}\right) P_{\beta 1} \qquad (7.23) $$

where $[\psi_{(x,y,z)}/Q]$ is the time-integrated dilution factor (sec/m^3) and $P_{\beta 1}$ is the source term (Mev/sec) emitted by the entire cloud at the time of release.

When the source term $P_{\beta 2}$ is in units of ergs per second, the equation for the beta dose becomes

$$ {}_\beta D_{\infty(x,y,z)} = 3.86\times 10^{-6}\left(\frac{\psi_{(x,y,z)}}{Q}\right) P_{\beta 2} \qquad (7.24) $$

Similar equations can be written for other beta power units, e.g., watts.

In Eqs. 7.20 through 7.24, the concentration and energy release rates depend upon the source characteristics and the amount of radioactive decay and ground deposition that has occurred between the time of release and the time of exposure. Whether the release occurs over a short period of time or is continuous, the change in quantity due to radioactive decay during the actual passage time of the cloud is generally small compared to the change during transit between the release point and the receptor. In this case a single correction term has been applied to ψ to correct for the radioactive decay.

In cases where the release consists of a mixture of radionuclides and the time of exposure to the radiation from a passing cloud is long with respect to the half-life of the radioactive material, it is desirable to correct for decay during passage. In this case the source term is not constant, and the concentration integration over time must include a term describing the time variation of the source, i.e., $\overline{E}_\beta\psi$ or $(\psi/Q)\ P_\beta$ must be replaced by $\int(\overline{E}_\beta\chi)dt$ or by $\int(P_\beta\chi/Q)dt$. This, in turn, may be evaluated from considerations of the individual radionuclides present by fitting an arbitrary mathematical function to the rate of decay and integrating or by calculating the dose rate at various times during cloud passage and averaging over the exposure time.

7-4.1.2 Depth Dose. The beta dose calculated in the preceding section is the dose received at the surface of the body or clothing. Before damage is produced, the radiation must penetrate the clothing and the normal inert layer of skin and reach the sensitive tissues underneath. A complete estimate of the beta-dose effects must evaluate the dose to the underlying tissues.

From measurements of the distribution of dose in air around a point source of beta radiation, Loevinger, Japha, and Brownell (1956) have derived an empirical equation that permits calculation of the dose as a function of the depth of penetration and energy of the beta radiation. The integration of this expression to give the dose above an infinite slab can be used to provide an estimate of the depth dose because the cloud will act as an infinite slab in contact with the body.

$$ {}_\beta D_d = {}_\beta D_\infty \alpha \left\{ c^2 \left[3 - \exp\left(1 - \frac{\nu d}{c}\right) - \frac{\nu d}{c} \times \left(2 + \ln \frac{c}{\nu d}\right)\right] + \exp(1 - \nu d)\right\} \qquad (7.25) $$

where the quantity in square brackets equals zero when $d \geq c/\nu$.

In Eq. 7.25 ${}_\beta D_d$ is the dose at a depth of d (g/cm^2 in the body) from a surface dose of ${}_\beta D_\infty$, and c is an energy-dependent parameter with the following values:

c = 2	0.17 Mev < E_0 < 0.5 Mev	
= 1.5	0.5 Mev ≤ E_0 < 1.5 Mev	
= 1	1.5 Mev ≤ E_0 < 3 Mev	(7.25a)

where E_0 is the maximum beta energy emitted and α is a normalizing constant given by

$$ \alpha = [3c^2 - (c^2 - 1)\ e]^{-1} \qquad (7.25b) $$

The values of α for various values of c are

c	α
1	0.333
1.5	0.297
2	0.260
3	0.190

In Eq. 7.25 ν is an apparent absorption coefficient derived from measurements in polystyrene with a correction for the electron density of tissue. It is expressed in units of square centimeters per gram so that the product νd is dimensionless.

$$ \nu = \frac{37.2}{(E_0 - 0.036)^{1.37}} \qquad (7.25c) $$

An additional term to correct for anomalous spectra with certain beta emitters has been omitted in Eq. 7.25c because the correction is not of significance for the accuracy of these calculations.

The dose at a given depth in the tissue will be strongly dependent upon the energy of the beta particles emitted. For a mixture of different emitters, it is necessary to evaluate the dose from each emitter separately or to calculate for various energy groupings and weight the result by the fractional occurrence of each group. Figure 7.5 illustrates the dose to be expected at various depths in tissue from exposure to a cloud with a concentration time integral (ψ) of 1.0 curie sec/m^3 and with the beta energies shown. For a sustained concentration of 1.0 curie/m^3, Fig. 7.5 will give the dose rate in rads per second from an infinite cloud. The depth is expressed in milligram per square centimeter, a unit that expresses the mass available for absorbing radiation to the thickness given. For tissue with a density of one, a thickness of 100 mg/cm^2 corresponds to a linear depth of 1 mm.

The inert thickness of the epidermis varies over the body but is usually considered to be 7 mg/cm^2. For most calculations the surface dose given by Eq. 7.21 will estimate the dose

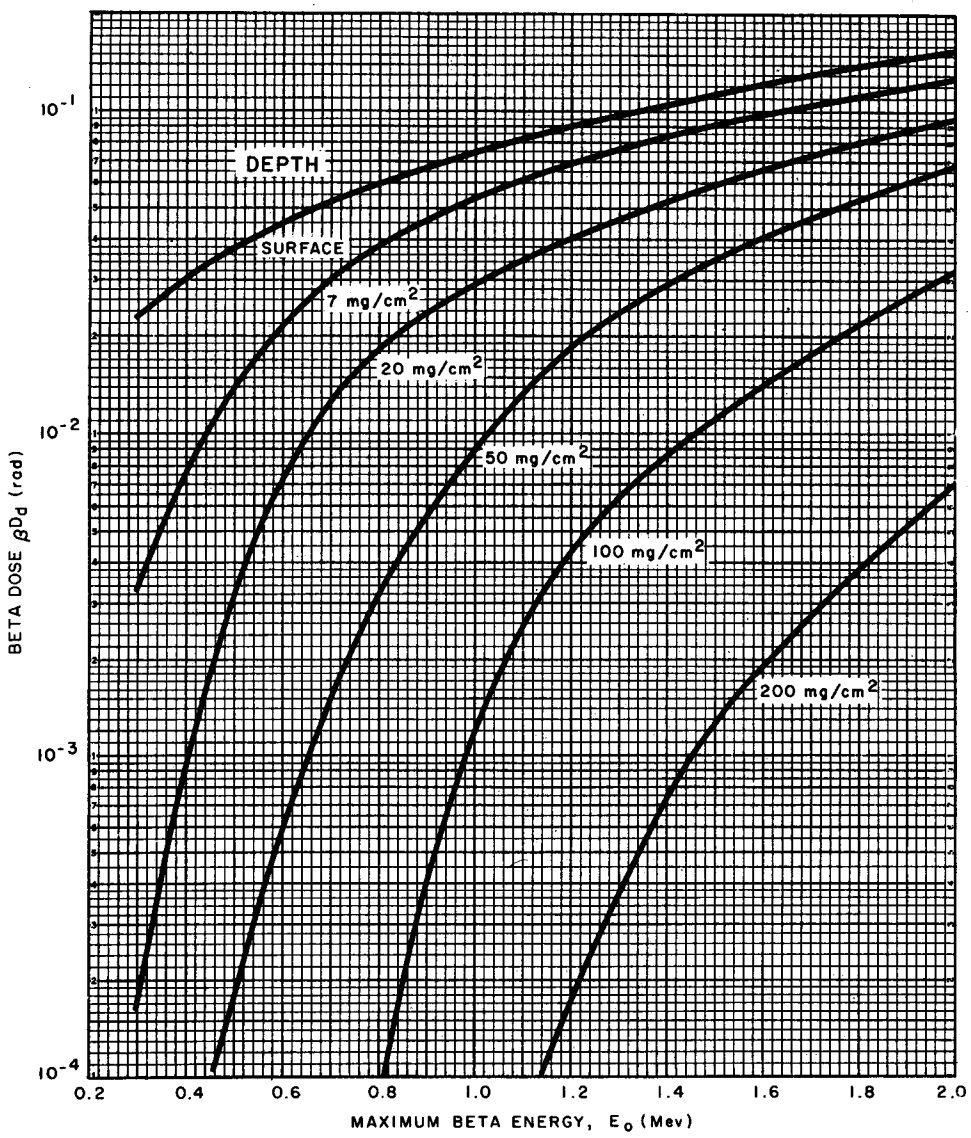

Fig. 7.5 — Beta doses at various depths in tissue produced by an exposure of 1.0 curie sec/m³ from an infinite cloud containing a beta-emitting radionuclide.

for the unclothed part of the body to within the accuracy of the knowledge of the local concentration.

7-4.2 Beta Dose from Material Deposited on the Ground

During the passage of the cloud, a portion of the radioactive material will be deposited on the ground by dry deposition, rainout, or washout. This material can consist of any of the radioactive materials in the cloud except the noble gases. In general, the pattern of deposition calculated from the dispersion equations will consist of a central line of high deposition with the amount per unit area decreasing on either side in a Gaussian distribution similar to the pattern of concentration in the cloud. In practice there will be localized dose rate variations due to runoff and puddling of rain water, increased deposition caused by eddies near obstructions, variable patterns from wind-shifts, deposition of large particles that cannot remain airborne, increased accumulation in oils or

greases, etc. The present knowledge of the detailed diffusion mechanisms for a particular terrain is not adequate to calculate these localized variations in any detail. The calculations of the radiation field above the ground provide the general area dose rates with the localized variations due to these factors superimposed upon this general field. In dry weather, differences in the rate of dry deposition due to particle sizes, physical form of the material, and other factors will cause fractionation; so the composition of the deposited material may vary with distance. In general, the beta dose from the separate fractions with different deposition constants must be evaluated separately and then summed.

The material deposited on the surface can be considered as a thin source that, because of the short range of the beta particles, is effectively infinite in the horizontal plane. Under these conditions the variation of dose rate above the ground is given by Loevinger, Japha, and Brownell (1956) as

$$ {}_{\beta}D'_{\infty(b,t)} = 0.0297\,\nu\bar{E}_{\beta}\,\alpha\omega\left[c\left(1+\ln\frac{c}{b\nu}\right) - \exp\left(1-\frac{b\nu}{c}\right)\right] + \exp\,(1-b\nu) \qquad (7.26) $$

where the expression in brackets equals 0 when $b > c/\nu$. The term ${}_{\beta}D'_{\infty(b,t)}$ is the beta dose rate (rad/sec) at height b (g/cm^2) above an infinite plane upon which ω curies/m^2 of beta-emitting material has been deposited (1 cm^3 of air weighs 1.293×10^{-3} g), ω is surface activity (curie/m^2), and values of the other parameters are as given previously.

Where the cloud is a plume of radioactive material from the release of a single radionuclide at a constant rate of Q'_0 (curies/sec) from an elevated point h_d(m) above the ground plane, the concentration of the established plume at a location (x,y,0), when corrected for depletion en route, is given in curies per cubic meter by

$$ \bar{\chi}_{(x,y,0)} = \frac{Q'_0}{\pi\bar{u}\sigma_y\sigma_z}\left(\frac{Q_x}{Q_0}\right)_d \exp\left(-\lambda_R\frac{x}{\bar{u}}\right) \times \exp-\left(\frac{y^2}{2\sigma_y^2}+\frac{h^2}{2\sigma_z^2}\right) \qquad (7.27) $$

The activity deposited on the surface, $\omega_{(x,y,0)}$ (curie/m^2) is given by

$$ \omega_{(x,y,0)} = \bar{\chi}_{(x,y,0)}\,v_d\int_0^{t_d}\exp\,(-\lambda_R t)\,dt \qquad (7.28) $$

where v_d is the deposition velocity (m/sec) and t_d is time interval of discharge (sec). The net activity on the ground after the first part of the plume reaches the point (x,y,0) will be given by

$$ \omega_{(x,y,0)} = \bar{\chi}_{(x,y,0)}\,v_d\frac{[1-\exp\,(-\lambda_R t_d)]}{\lambda_R} \qquad (7.29) $$

At times after the last of the plume has passed the point, the deposited activity of a single radionuclide will again decay according to the simple exponential, and the activity per unit surface area will be given by

$$ \omega_{(x,y,0,t)} = \bar{\chi}_{(x,y,0)}\,v_d \times\frac{[1-\exp\,(-\lambda_R t_d)]\,\exp\,(-\lambda_R t)}{\lambda_R} \qquad (7.30) $$

where t is the time interval (sec) after the last of the plume has passed the point (x,y,0).

For the special case of an instantaneous release of Q_0 curies, i.e., $t_d \to 0$, the quantity $[1-\exp\,(-\lambda_R t_d)] \to \lambda_R t_d$, and $Q_0 = Q'_0\Delta t$, Eq. 7.30 becomes

$$ \omega_{(x,y,0,t)} = \frac{Q_0 v_d\,(Q_x/Q_0)_d}{\pi\bar{u}\sigma_y\sigma_z}\exp\left[-\lambda_R\left(t+\frac{x}{\bar{u}}\right)\right] \times\exp-\left(\frac{y^2}{2\sigma_y^2}+\frac{h^2}{2\sigma_z^2}\right) \qquad (7.31) $$

where t is the time interval (sec) after the cloud center has passed the point (x,y,0).

Figure 7.6 presents the dose rate at several approximate distances above the ground (rounded off for simplicity) for a uniform deposition of 1.0 curie/m^2. For estimations of the total beta dose received during a given period of occupancy, the dose rate shown (with an appropriate correction for radioactive decay) should be multiplied by the time of occupancy or integrated over the appropriate time interval.

Note that the beta dose rate will vary when the material is deposited on surfaces other than the ground. For example, the dose rate from fission products on tall bushes, on buildings, or in regions of very rough terrain will differ from that calculated by Eq. 7.26, which is based upon a plane surface.

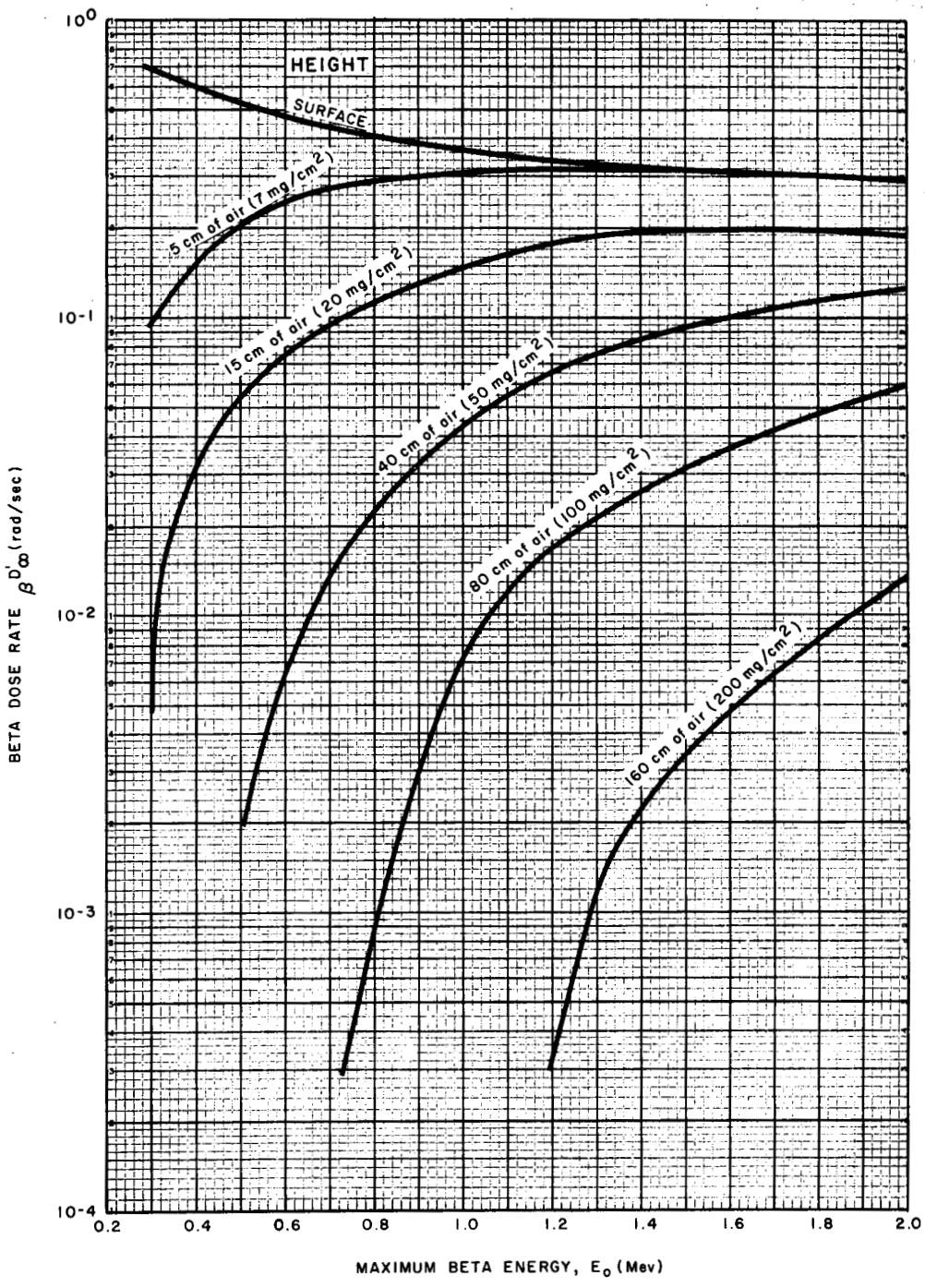

Fig. 7.6—Beta dose rate in air above a plane surface with a uniform contamination of 1.0 curie/m². Curves are labeled with the depth of air in terms of length and mass. The curves will apply to the dose rate in tissue if the density of tissue is substituted for the density of air.

7-4.3 Beta Dose Rates from Materials Deposited on the Body

Radioactive materials deposited directly on the skin can deliver relatively high beta doses because of their proximity to sensitive tissues. Although some gamma dose is usually associated with the beta dose, the longer range of the gamma radiation results in spreading the absorbed energy over a larger volume, whereas the short range of the beta particles results in intense energy deposition in the first few millimeters of the skin.

The physical form of the deposited material can range from a uniform coating over the entire surface to the random distribution of a few small very intensely radioactive particles, depending upon the characteristics of the material in the passing cloud. These single particles are usually found close to the point of discharge or, in the event of a contaminated surface, in dust resuspended by the action of the winds. Such particles act as discrete sources of radiation and provide very-high dose rates to the tissue in the immediate vicinity of the particle. One can estimate dose rates of 10^6 rad/hr at distances of 10μ from a 1 μc particle. The beta dose rate, however, drops rapidly with distance from the particle; so the total amount of tissue involved is very small. The significance of such estimated doses is not clear in determining the hazard because the available correlations with biological damage are poor. For this reason the equations for estimating the dose or dose rate from discrete particles are not included, and the reader is referred to the literature for material on the estimation of dose and effects (George, Healy, and Bustad, 1955; Loevinger, 1956; Passonneau, Brues, Hamilton, and Kisieleski, 1952).

The amount of radioactive material deposited on the body will vary over the body surfaces. It is to be expected that the greatest deposition will occur on the hair and on any oily spots on the body. The feet and legs may also become contaminated if the individual moves around in the contaminated area. The estimation of the quantities of material deposited on the body can be made only with poor accuracy, but for an average estimate it can be assumed that the deposition velocity for the transfer of radioactive material from the passing cloud to the body is the same as for transfer of material to the ground. The beta dose rate to the body can be calculated from Eq. 7.26, where b is the depth within the body rather than the height in air above the ground. In addition, the dose rate at various depths within the tissue can be obtained from Fig. 7.6 if the depth in tissue is expressed in units of mg/cm^2.

Figure 7.7 presents the approximate beta dose rate that would occur through the 7 mg/cm^2 protective layer of the skin immediately after cloud passage as a result of deposition velocities ($v_d = \omega/\psi$; see Sec. 5-3 of Chap. 5) ranging from the low values expected for small particles (and perhaps organic compounds of iodine) in light winds to the much higher values that might apply for iodine in the vapor state in moderate winds. The beta dose rate for beta emitters of various energies and for a considerable range of deposition velocities can be obtained directly from the graph.

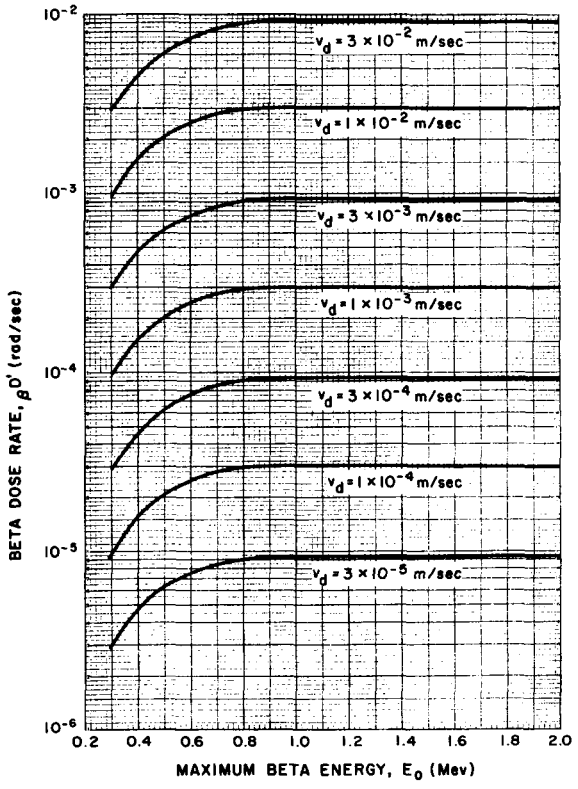

Fig. 7.7 — Approximate beta dose rate through the 7 mg/cm^2 of protective skin layer from materials deposited on the body for various deposition velocities following an exposure (ψ) of 1.0 curie sec/m^3 for various β energies.

In estimates of beta doses, the shielding effects and protection provided by clothing may be taken into account. The maximum beta dose will be delivered to the exposed surfaces of the skin. Clothing will attenuate the beta radiation dose because of its shielding effect and the fact that the clothing will hold the deposited material away from the skin.

7-5 EXTERNAL GAMMA RADIATION

Although the principles and methods of calculating the dose from extended sources of gamma radiation are well-known and straightforward, the solution for actual cases is the most complicated of the cloud-dosage calculations. As a result, the gamma dose from a passing cloud can be evaluated with good accuracy only for specific conditions.

With extended sources, such as cloud or ground deposits, the gamma dose in air at a given point depends upon the location of the radioactive materials for distances up to several hundred meters. The radiation field is therefore more uniform than with beta radiation because local variations in the material distribution are averaged over a much larger area or volume.

The use of the equations developed in this section (and in other sections) should be approached with considerable caution because many assumptions and approximations are necessary to obtain numerical solutions. Many factors in a specific application may cause significant differences between the measured doses or dose rates and those calculated by the formulas presented.

7-5.1 The Point Source

Calculations of the gamma dose from an extended source start with consideration of the radiation received at the receptor from a differential area or volume that can be regarded as a point source. This radiation is then integrated over the entire source with account being taken of the geometry of the source, variation in concentration, attenuation by interactions of the photons with matter in the path between source and receptor, and scattering of radiation from material outside the direct path to the receptor.

For a point source the geometrical considerations provide an inverse-square decrease in the dose with distance. Since the total radiation emitted (minus that absorbed) will pass through a sphere of radius equal to the distance between source and receptor, the flux passing through any area at that distance can be determined if the initial emission is known.

Gamma photons are absorbed in matter by three discrete processes: (1) the photoelectric effect in which the total energy of the photon is passed to an orbital electron with consequent ejection of the electron from the atom, (2) Compton scattering in which the photon undergoes an elastic collision with an electron with consequent ejection of the electron from the atom and a scattered photon of lower energy, and (3) pair production in which the photon in the electric field of a nucleus or an electron is converted to an electron and a positron. The photoelectric effect occurs with low-energy photons and high-atomic-number materials. For lead the photoelectric effect is important up to energies of about 1 Mev; for aluminum, up to about 0.1 Mev. The Compton effect is of importance in the energy range above the photoelectric effect and is the dominant absorption process for intermediate gamma energies (1 to 5 Mev for lead, 0.1 to 5 Mev for aluminum). Pair production occurs at higher energies with a threshold of 1.02 Mev, which is the energy equivalent of the mass of the positron and electron pair at rest.

For a narrow, collimated beam falling on an absorber, the gamma radiation is absorbed according to

$$ {}_{\gamma}D = {}_{\gamma}D_0 \exp(-\mu x) \qquad (7.32) $$

where ${}_{\gamma}D$ is the gamma-ray dose (rad), ${}_{\gamma}D_0$ is the gamma-ray dose (rad) that would be received without a shield of x thickness, and μ is the total gamma-ray absorption coefficient (1/m or cm^2/g). The absorption coefficient, μ, is a function of the specific shield material and energy of the radiation. A shield of thickness $x = 1/\mu$ would attenuate the beam by a factor of 1/e; this thickness is designated as the relaxation length. The product μx is frequently used as a dimensionless thickness of absorber. The units of μ may be reciprocal length (linear absorption coefficient) or reciprocal mass per unit area (mass absorption coefficient).

In the Compton scattering process, which predominates in the energy ranges and absorber atomic numbers of interest in calculations of cloud gamma dose, only a portion of the energy is absorbed and transferred to a short-range electron. The remainder is carried by scattered photons that, although removed from the beam under the conditions for which Eq. 7.32 is written, can contribute to the gamma dose received at some other point. The total cross section for this process is divided into two parts: μ_a represents the fraction of the total energy in the recoil electrons and thus represents the fraction of the energy absorbed near the site of the interaction and μ_s represents the fraction of the energy contained in the scattered photons. Thus $\mu = \mu_a + \mu_s$.

Contributions from scattered radiation in air or other materials not directly between the source and the receptor will cause the gamma dose calculated from Eq. 7.32 to be low for broad beams. Buildup factors to account for the increased radiation have been computed for several configurations and shielding materials (Goldstein and Wilkins, 1954). For air, Gamertsfelder (1960) has used a buildup factor of the form $(1 + k\mu x)$, where k is equal to $(\mu - \mu_a)/\mu_a$. This factor gives the correct value of energy absorption in an infinite radioactive medium but overestimates the scatter component from sources close to the receptor and underestimates the scatter from distant sources.

The gamma dose rate to air at a distance r meters from a point source of q (curies) can then be written as

$$ {}_{\gamma}D'_r = \frac{\mu_a\, q\, (3.7 \times 10^{10})\, \bar{E}_\gamma\, (1.6 \times 10^{-6})\, (1 + k\mu r)\, \exp(-\mu r)}{4\pi r^2\, (1293)\, (100)} \qquad (7.33) $$

$$ {}_{\gamma}D'_r = 0.0364\, \frac{\mu_a\, q\, \bar{E}_\gamma\, (1 + k\mu r)\, \exp(-\mu r)}{r^2} \qquad (7.33a) $$

where ${}_{\gamma}D'_r$ = dose rate (rad/sec) at a distance r (m)
μ_a = energy absorption coefficient for air (1/m)
μ = total absorption coefficient for air (1/m)
$k = (\mu - \mu_a/\mu_a)$
$\bar{E}_\gamma$ = average gamma energy emitted at each disintegration (Mev/dis)
3.7×10^{10} = disintegrations per second per curie
1.6×10^{-6} = ergs per Mev
1293 = density of air at S.T.P. (g/m^3)
100 = ergs per gram per rad

The gamma dose rate to tissue would be higher than that to air by the ratio of the electron densities in the two media. Over the energy range from 0.1 to 5.0 Mev, this ratio can be approximated as 1.11. The gamma dose rate to tissue is given by

$$ {}_{\gamma}D'_r = 0.0404\, \frac{\mu_a\, q\, \bar{E}_\gamma\, (1 + k\mu r)\, \exp(-\mu r)}{r^2} \qquad (7.34) $$

Values of the gamma absorption coefficients for air and the associated values of k are given in Fig. 7.8 as a function of gamma energy. If air density differs from the standard conditions of temperature and pressure used in developing the relationship, corrections must be made in applying these coefficients. The ratio (ρ_0/ρ) should be used as a correction factor for values of μ and μ_a.

7-5.2 Cloud Gamma Dose

For clouds with dimensions that are small compared to the range of the gamma radiation, a calculation of the gamma dose at a given point must take into account the radiation received from various parts of the cloud. The complexities of geometry, absorption, and buildup make a complete solution difficult and require the use of special integrals. Approximate solutions have been obtained by neglecting absorption or buildup. Holland (1956) has calculated the dose, assuming that all particles of the cloud pass the receptor with the mean wind velocity and isotropic turbulence so that $\sigma_y = \sigma_z$, where σ_y represents the standard deviation of width and σ_z the standard deviation of height for the Gaussian-shaped cloud. His calculations have been presented in the form of nomograms. Couchman (1960) has described a computer technique based on the Sutton form of the diffusion equations which provides for attenuation, buildup, and nonisotropic diffusion. Gamertsfelder (1960) has provided a general method for an isotropic cloud which will be used in the following discussion.

7-5.2.1 Infinite Cloud. If the dimensions of a homogeneous cloud of gamma-emitting material are large compared to the distance that the

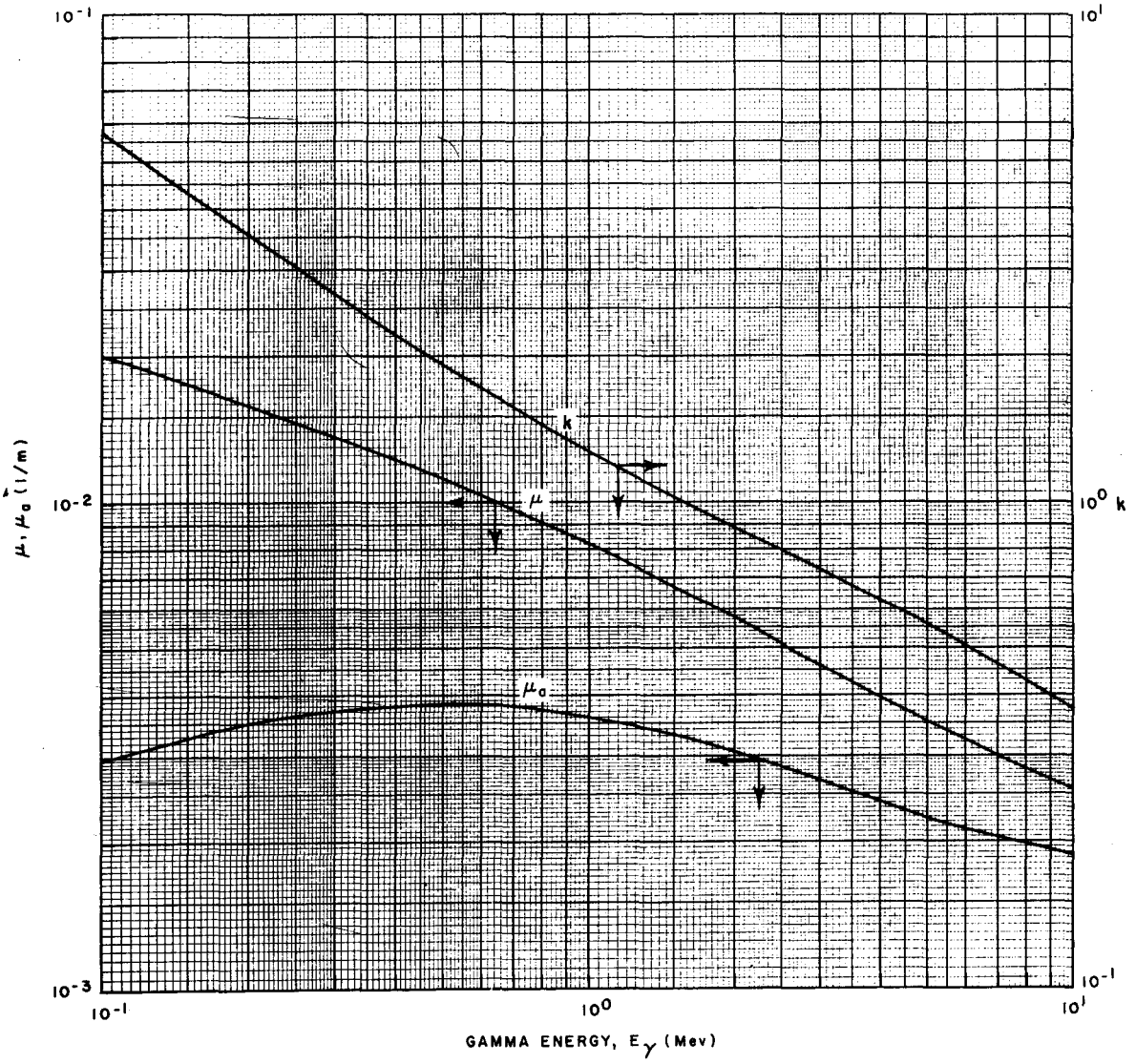

Fig. 7.8 — Absorption coefficients and values of the buildup constant for air at S.T.P.

gamma rays travel, an equilibrium condition occurs similar to that noted for beta radiation in Sec. 7-4.1.1. Under these conditions the rate of energy absorption per unit volume is equal to the rate of energy release per unit volume, and the gamma dose rate to air will be given by Eq. 7.17 if $\overline{E}_\beta$ is replaced by $\overline{E}_\gamma$, the average gamma energy released per disintegration, and a correction factor is included for the ratio of electron densities of tissue to those for air (a factor of 1.11).

$$ {}_\gamma D'_\infty = 0.507\, \overline{E}_\gamma\, \chi \left(\frac{\rho_0}{\rho}\right) \qquad (7.35) $$

where the dose rate is in rads per sec and (ρ_0/ρ) is the correction factor that can be applied when the air is at other than standard conditions. This factor will generally not be repeated in subsequent equations except in instances where it is required for clarity.

If the receptor is at ground level, the gamma dose calculated with Eq. 7.35 must be corrected for the fact that the radiation is received from only half the cloud owing to the presence of the ground (a factor of 0.5). For an actual cloud the assumption of an infinite cloud of gamma-emitting material can be made only after relatively long travel times when the di-

mensions of the cloud (σ) are large compared to $1/\mu$. When this is the case, the value of the gamma dose rate is given by

$$ {}_{\gamma}D'_{\infty(x,y,0,t)} = 0.25\ \bar{E}_{\gamma}\ \chi_{(x,y,0,t)} \qquad (7.35a) $$

where ${}_{\gamma}D'_{\infty(x,y,0,t)}$ is the gamma dose rate (rad/sec) to a person located at (x,y,0) at time t and $\sigma > 1/\mu$..

Equation 7.35a will yield the gamma dose rate for an established plume from the emission of gamma-emitting material at a constant rate of Q'_0 (curies/sec) if the plume concentration $\bar{\chi}_{(x,y,0)}$ (curies/m^3) is used. If the concentration time integral $\psi_{(x,y,0)}$ (curie sec/m^3) is used, the dose received during the cloud passage is given by

$$ {}_{\gamma}D_{\infty(x,y,0)} = 0.25\ \bar{E}_{\gamma}\ \psi_{(x,y,0)} \qquad (7.36) $$

Consistent with earlier definitions, the value of $\bar{\chi}$ and ψ must include the appropriate correction factors for depletion en route, i.e., $[(Q_x/Q_0)_d\ (Q_x/Q_0)_R]$.

7-5.2.2 Finite Cloud. Near the source of the plume, the gamma doses and dose rates will be less than those estimated by the infinite-cloud assumption. The following treatment of the smaller cloud is from unpublished work by Gamertsfelder (1960).

In Fig. 7.9 consider the gamma dose rate to a ground-level receptor at point (x_1, y_1, 0) and at time t if the gamma dose rate is due to the presence of q curies in a volume element of a cloud containing a total of Q curies and if the center of the cloud is moving with a velocity u (average velocity $\bar{u}$) in the x−z plane and is located at the point ($\bar{u}t$, 0, h) at the time t. For an isotropic cloud consisting of a single puff release, values of σ_{xI}, σ_{yI}, σ_{zI}, and σ_I are equal, i.e., $\sigma_{xI} = \sigma_{yI} = \sigma_{zI} = \sigma_I$. If perfect reflection at the ground plane is assumed, the gamma dose rate to a receptor located at (x_1, y_1, 0) from that part of the cloud which is reflected from the ground is the same as that which would be received if the cloud passed through the ground plane. Since the cloud concentration is symmetrical with respect to the line from (x_1, y_1, 0) to the cloud center at ($\bar{u}t$, 0, h), the dose rate from the entire cloud at time t is obtained by replacing the incremental source term, q, in Eq. 7.34 with the instantaneous cloud concentration times the elemental volume $\chi_{(x,y,z)}$ dV (which is equivalent) and integrating the volume element 2π r sin ϕ dϕ r dr over the entire cloud volume. The gamma dose rate to the receptor from the cloud at time t is given by

$$ {}_{\gamma}D'_{(x_1,y_1,0,t)} = 0.0404\mu_a\ \chi_{(x,y,z,t)}\bar{E}_{\gamma} \times \int_0^{\infty}\int_0^{\pi} \frac{(1 + k\mu r)\ \exp\ (-\mu r)}{r^2} \times 2\pi\ r^2\ \sin\ \phi\ d\phi\ dr \qquad (7.37) $$

In terms of the reference system given in Fig. 7.9, the general equation for the instantaneous isotropic cloud concentration, $\chi_{(x,y,z,t)}$, (curies/m^3) can be written

$$ \chi_{(x,y,z,t)} = \frac{Q_0(Q_x/Q_0)}{(2\pi)^{3/2}\ \sigma_I^3} \exp\left[-\frac{(m^2 + r^2 - 2\ mr\ \cos\ \phi)}{2\sigma_I^2}\right] \qquad (7.38) $$

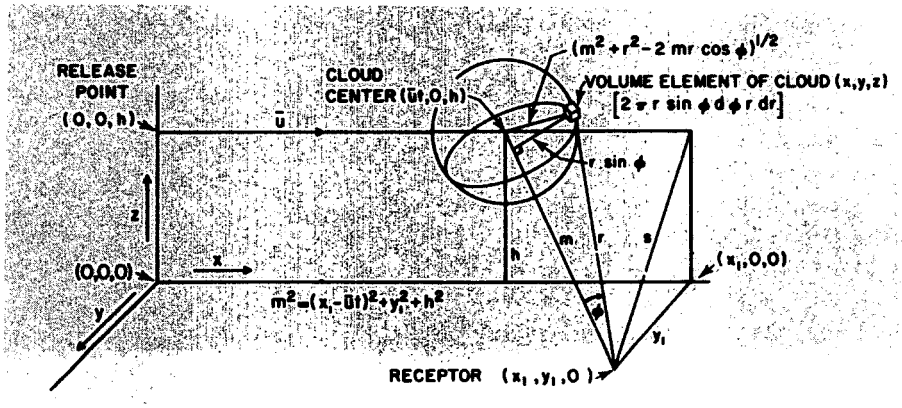

Fig. 7.9— Coordinate system for cloud gamma-dose calculations.

where Q_0 is the total number of curies of the radionuclide in the cloud at the time of release and (Q_x/Q_0) is the fraction of original source material which has not been deposited on the ground or removed by radioactive decay en route.

Replacing $\chi_{(x,y,z,t)}$ in Eq. 7.37 by the equivalent in Eq. 7.38 gives

$$ {}_{\gamma}D'_{(x_1,y_1,0,t)} = \frac{0.0404\ \mu_a\ \bar{E}_{\gamma} Q_0\ (Q_x/Q_0)}{(2\pi)^{3/2}\sigma_I^3} \times \int_0^{\infty}\int_0^{\pi} (1 + k\mu r)\ \exp\ (-\mu r) \times \exp\left[-\frac{(m^2 + r^2 - 2\cos\phi)}{2\sigma_I^2}\right] \times 2\pi\, r^2 \sin\phi\, d\phi\, dr \qquad (7.39) $$

$$ {}_{\gamma}D'_{(x_1,y_1,0,t)} = \frac{0.0404\ \mu_a\ \bar{E}_{\gamma} Q_0\ (Q_x/Q_0)}{(2\pi)^{1/2}\sigma_I} \int_0^{\infty} (1 + k\mu r)\ \exp\ (-\mu r) \times \left\{\frac{\exp\left[-\frac{(m-r)^2}{2\sigma_I^2}\right] - \exp\left[-\frac{(m+r)^2}{2\sigma_I^2}\right]}{mr}\right\} dr \qquad (7.40) $$

If σ_I and the cloud source-depletion correction factors for decay and ground deposition are considered to be constants when the center of the cloud is at a distance $\bar{u}t$ from the point of release for the effective time of cloud passage, the equation for the gamma dose may be written

$$ {}_{\gamma}D_{(x,y,0)} = \frac{0.0404\ \mu_a\ \bar{E}_{\gamma} Q_0\ (Q_x/Q_0)}{2\pi\ \sigma_I} \int_0^{\infty}\int_0^{\infty} (1 + k\mu r)\ \exp\ (-\mu r) \times \frac{\exp\left[-\frac{(m-r)^2}{2\sigma_I^2}\right] - \exp\left[-\frac{(m+r)^2}{2\sigma_I^2}\right]}{mr}\, dr\, dt \qquad (7.41) $$

If I_1 and I_2 are defined as

$$ I_1 = \frac{\bar{u}}{4(2\pi)^{1/2}\ \mu\sigma_I} \int_0^{\infty}\int_0^{\infty} \frac{\exp\ (-\mu r)}{mr} \times \left\{\exp\left[-\frac{(m-r)^2}{2\sigma_I^2}\right] - \exp\left[-\frac{(m+r)^2}{2\sigma_I^2}\right]\right\} dr\, dt \qquad (7.41a) $$

and

$$ I_2 = \frac{\bar{u}}{4(2\pi)^{1/2}\ \mu\sigma_I} \int_0^{\infty}\int_0^{\infty} \frac{\mu\ \exp\ (-\mu r)}{m} \times \left\{\exp\left[-\frac{(m-r)^2}{2\sigma_I^2}\right] - \exp\left[-\frac{(m+r)^2}{2\sigma_I^2}\right]\right\} dr\, dt \qquad (7.41b) $$

then Eq. 7.41 may be written as

$$ {}_{\gamma}D_{(x,y,0)} = \frac{0.1616\ \mu\ \mu_a\ \bar{E}_{\gamma} Q_0\ (Q_x/Q_0)\ (I_1 + kI_2)}{\bar{u}} \qquad (7.42) $$

Values of I_1 and I_2 were determined by graphical and numerical integrations. Specific values of I_1 and I_2 can be obtained from Figs. 7.10 and 7.11 for various values of $\mu\ \sigma_I$. In these figures values of I_1 and I_2 are presented as a function of $\mu\ \sigma_I$ and are given for various values of μs, where $\mu s = \mu(y^2 + h^2)^{1/2}$ and s is the distance between the receptor and the center line of the cloud path. Dashed lines show values of I_1 and I_2 as functions of fixed ratios between s and σ_I and thereby permit interpolation of I_1 and I_2 for values of μs other than those given.

The values of I_1 and I_2 can be applied to the case of the continuous source if the instantaneous values of cloud width (σ_I) are replaced by values for the continuous plume (σ).

Equation 7.36 was developed for an isotropic single-puff release of Q_0 curies of radioactive material. If the release were to occur at a constant rate (Q_0') over a period of time (t_d) so that $Q_0' t_d = Q_0$, then the governing meteorological variables to determine the concentration time integral, ψ, would be $\bar{u}$, σ_y, and σ_z. These sigma values would be larger than the instantaneous puff values, σ_I, because they would include the effects of meander of the plume at the receptor over the time interval of the release. Since the equation for the concentration time integral for the plume is identical in form to that for the puff release (see Chap. 3, Eq. 3.158), the only difference in the computed values of ψ would be due to the differences in the wind speed and the plume spread during the long and short time intervals. In both cases then the dose is proportional to ψ. Values for the continuous and instantaneous sigmas can be found in Chap. 4, Secs. 4-4.1.7, 4-4.3, and 4-10.3. The sigma values can be adjusted to the actual release

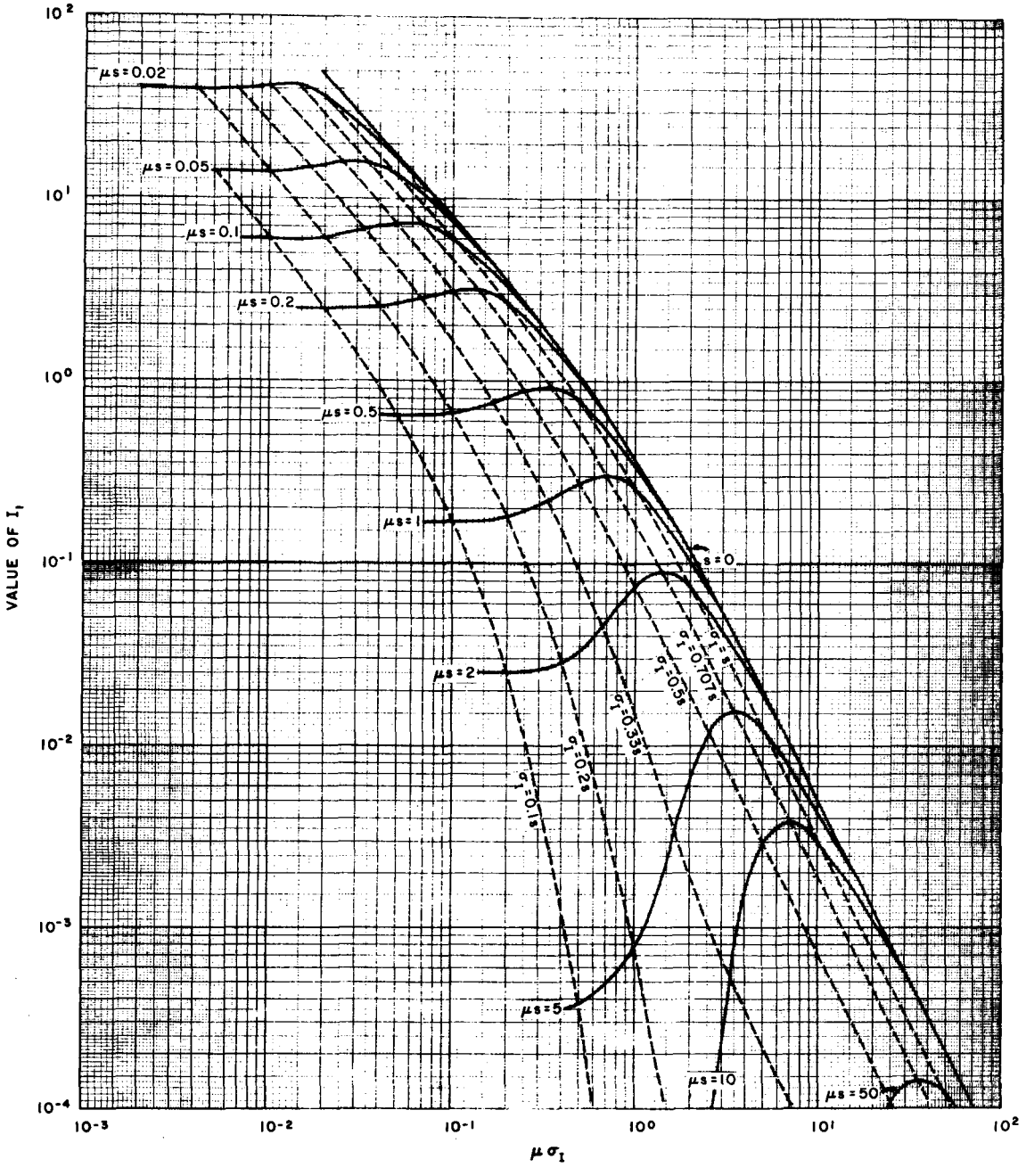

Fig. 7.10 — Values of the I_1 integral (see Eq. 7.41a). Values of σ or σ_1 can be used.

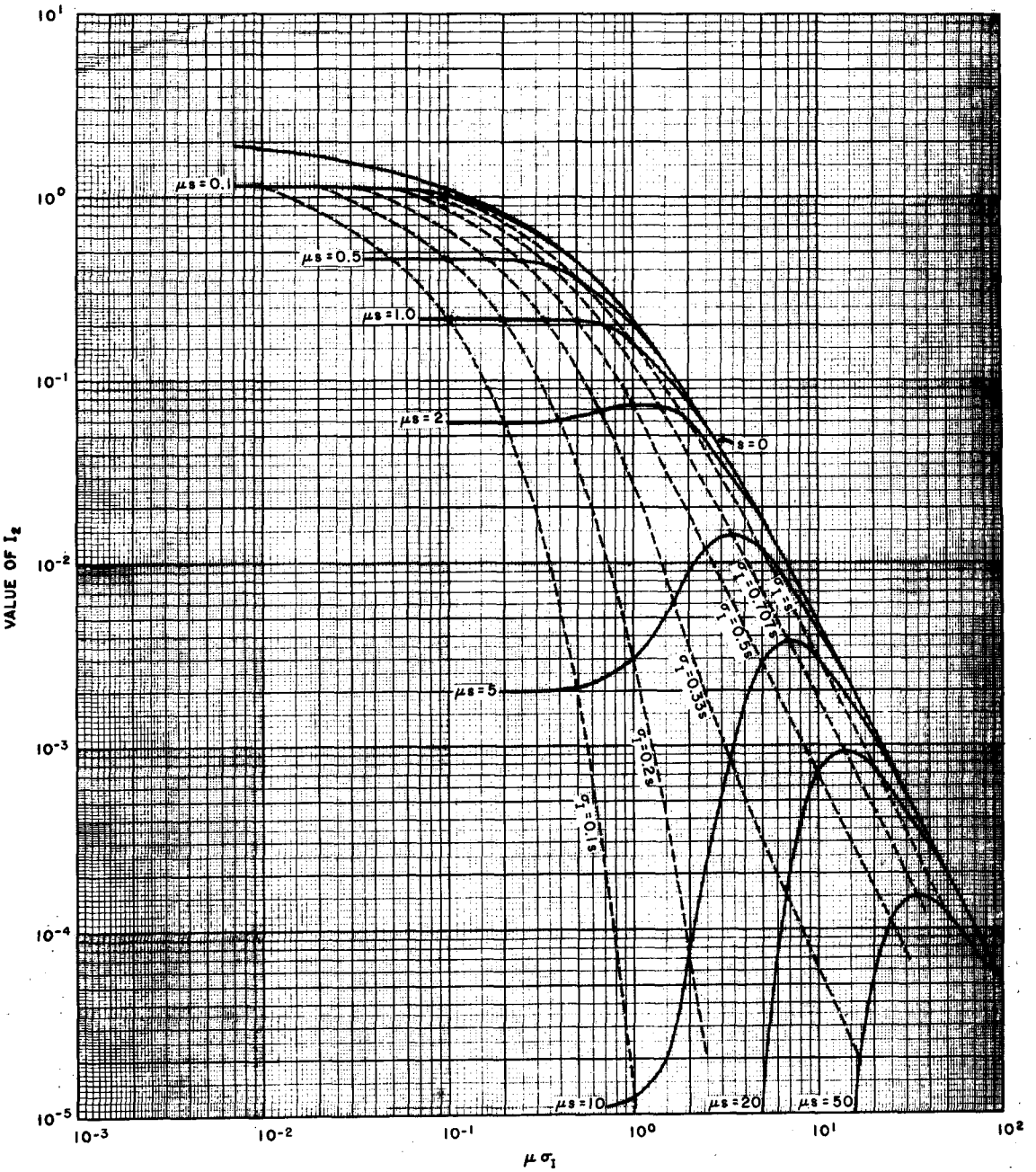

Fig. 7.11 — Values of the I_2 integral (see Eq. 7.41b). Values of σ or σ_I can be used.

interval over the range of a few minutes to a few hours by a power law such as is given in Chap. 2, Eq. 2.7.

The gamma dose rate ($_{\gamma}D'$), which is the time derivative of the dose ($_{\gamma}D$), will be proportional to the time derivative (Q_0') of the source (Q_0) if the plume has attained an equilibrium growth condition. Therefore Eq. 7.42 can be used to calculate the gamma dose rate from an established plume if the source release rate (Q_0') is used in place of the total source (Q_0) and if sigma values appropriate to the continuous source are used.

$$ {}_{\gamma}D'_{(x,y,0)} = \frac{0.1616\ \mu\ \mu_a\ \bar{E}_{\gamma} Q_0'\ (Q_x/Q_0)\ (I_1 + kI_2)}{\bar{u}} \qquad (7.43) $$

where $_{\gamma}D'_{(x,y,0)}$ is the gamma dose rate (rad/sec) from the established plume to a receptor on the ground plane at a point x (m) downwind and y (m) perpendicular to the plume center line in the horizontal plane and Q_0' is the source release rate at the time of release (curie/sec).

It is frequently more convenient to consider the power generated by the radioactive materials in the cloud at the point of interest. In this case the product $\bar{E}_{\gamma} Q_0$ can be replaced by the gamma power, P_{γ}, if suitable absorption coefficients can be assumed. Conversion of the constants in Eq. 7.42 gives

$$ {}_{\gamma}D_{(x,y,0)} = \frac{4.36 \times 10^{-12}\ \mu\ \mu_a P_{\gamma 1}}{\bar{u}} (I_1 + kI_2) \qquad (7.44) $$

where $P_{\gamma 1}$ is the total energy release rate in the cloud by gamma emission at the time of cloud passage (Mev/sec), i.e., it is corrected for depletion en route, and $_{\gamma}D$ is the gamma dose in rads. If $P_{\gamma 2}$ is in watts, Eq. 7.44 becomes

$$ {}_{\gamma}D_{(x,y,0)} = 27.3\ P_{\gamma 2} \frac{\mu\ \mu_a}{\bar{u}} (I_1 + kI_2) \qquad (7.45) $$

and the same depletion correction factors used before are applicable.

Values of $(I_1 + kI_2)$ can be computed as a single term, I_T, if the gamma energy and thus the absorption coefficients can be fixed. If it is assumed that the effective gamma energy in a cloud consisting of fission products is 0.7 Mev, then $\mu = 9.7 \times 10^{-3}$ and $\mu_a = 3.8 \times 10^{-3}$. The values of $I_T = (I_1 + kI_2)$ for this condition are given in Fig. 7.12.

The preceding equations apply to an isotropic cloud, i.e., $\sigma_{yI} = \sigma_{zI}$ or $\sigma_y = \sigma_z$. Since many of the present studies of diffusion result in a nonisotropic-cloud formulation, particularly with inversions, a method of calculation is required. Gamertsfelder (1960) noted that if $\sigma_y > \sigma_z$ the value of I_T for $\sigma_y > \sigma_z$ and σ_z small with respect to the height of the cloud center line is the same as if $\sigma_y = \sigma_z$. For a cloud which is effectively infinite in height ($\sigma_z \approx 700$ m), however, the value of I_T should be reduced by the fraction σ_z/σ_y to account for the reduced concentration caused by the horizontal spread. Gamertsfelder suggested that a correction factor at intermediate distances can be obtained by drawing a curve with correction factor on the abscissa and σ_z on the ordinate scales. The value of the correction factor should be unity for 0.7-Mev gamma rays at $\sigma_z \leq 0.035h$, and the curve should smoothly approach the value of σ_z/σ_y at $\sigma_z = 700$ m. This curve is shown in Fig. 7.13.

An alternative approach to the problem of correcting for a nonisotropic cloud which gives comparable answers is to use an average value of σ given by

$$ \sigma_{av.} = (\sigma_y \sigma_z)^{1/2} \qquad (7.46) $$

7-5.2.3 Ratio of Finite to Infinite Cloud Dose. Since it is relatively simple to estimate the gamma dose or dose rate from a cloud large enough to be considered infinite, it is frequently more convenient to apply correction factors to the dose calculations for infinite clouds to determine the dose from a cloud of finite size. The concentration time integral at a point on the path of the center of a cloud of finite size is given by

$$ \psi_{(x,0,h)} = \frac{Q_x}{\pi \bar{u}\ \sigma_y \sigma_z} \qquad (7.47) $$

If the concentration of an infinite cloud is numerically equal to the concentration time integral of the finite cloud, i.e., $\chi_{\infty} = \psi$, and the exposure time to the infinite cloud is 1 sec, the ratio of the gamma doses from the two clouds can be calculated by using Eqs. 7.36, 7.42, and 7.46.

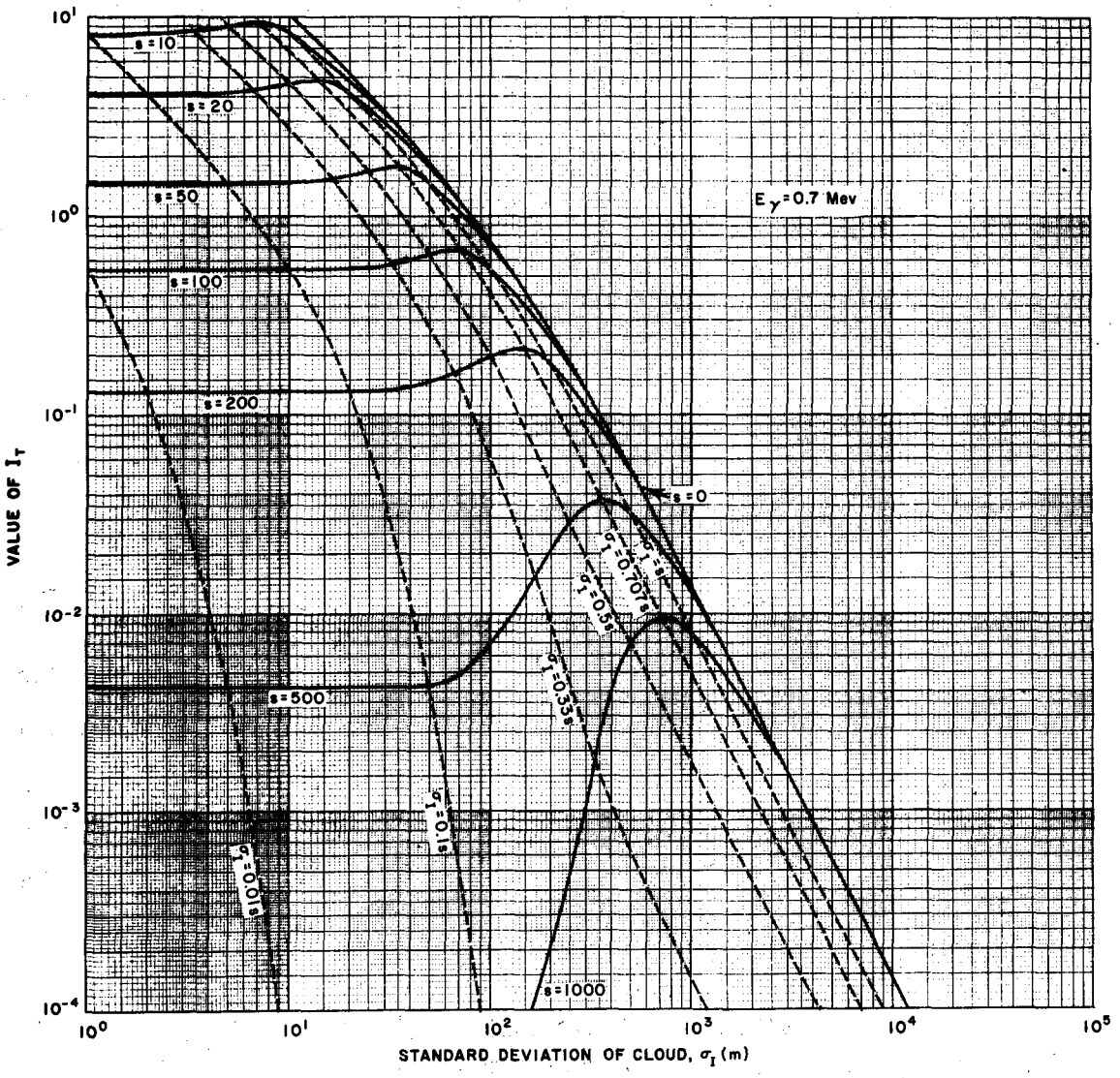

Fig. 7.12 — Values of I_T integral for E_γ = 0.7 Mev. Values of σ or σ_I can be used.

$$\frac{{}_\gamma D_{(x,y,0)}}{{}_\gamma D_{\infty(x,0,0)}} = \frac{0.1616 \frac{\mu\,\mu_a}{\bar{u}} \bar{E}_\gamma Q_x\,(I_1 + kI_2)}{0.25\,\bar{E}_\gamma\,(Q_x/\pi\bar{u}\,\sigma^2)} \qquad (7.48)$$

$$\frac{{}_\gamma D_{(x,y,0)}}{{}_\gamma D_{\infty(x,0,0)}} = 2.03\,\mu\,\mu_a\,\sigma^2\,(I_1 + kI_2) \qquad (7.48a)$$

Values of this ratio are given in Fig. 7.14 for 0.7-Mev gamma photons and values of the cloud-concentration standard deviation. Both the center-line dose and the dose at various distances from the center line in units of the cloud width, as measured by the standard deviation, are included. Note that for smaller plumes the gamma dose at a distance from the plume is controlled more by the penetrating nature of gamma radiation than by the concentration at the location. Figure 7.15 illustrates this by showing the ratio of the gamma dose at various distances from the center line to the center-line dose and comparing these values to the Gaussian function, which describes the decrease in concentration with distance from the plume. It is not until the plume width reaches a standard deviation of about 1000 m that the dose is reasonably described by the concentration function.

The ratio of finite to infinite cloud gamma dose at the center line of the plume is given for

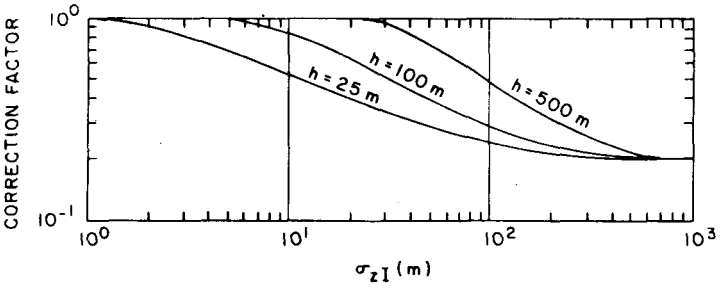

Fig. 7.13 — Correction curves for gamma dose from nonisotropic clouds.

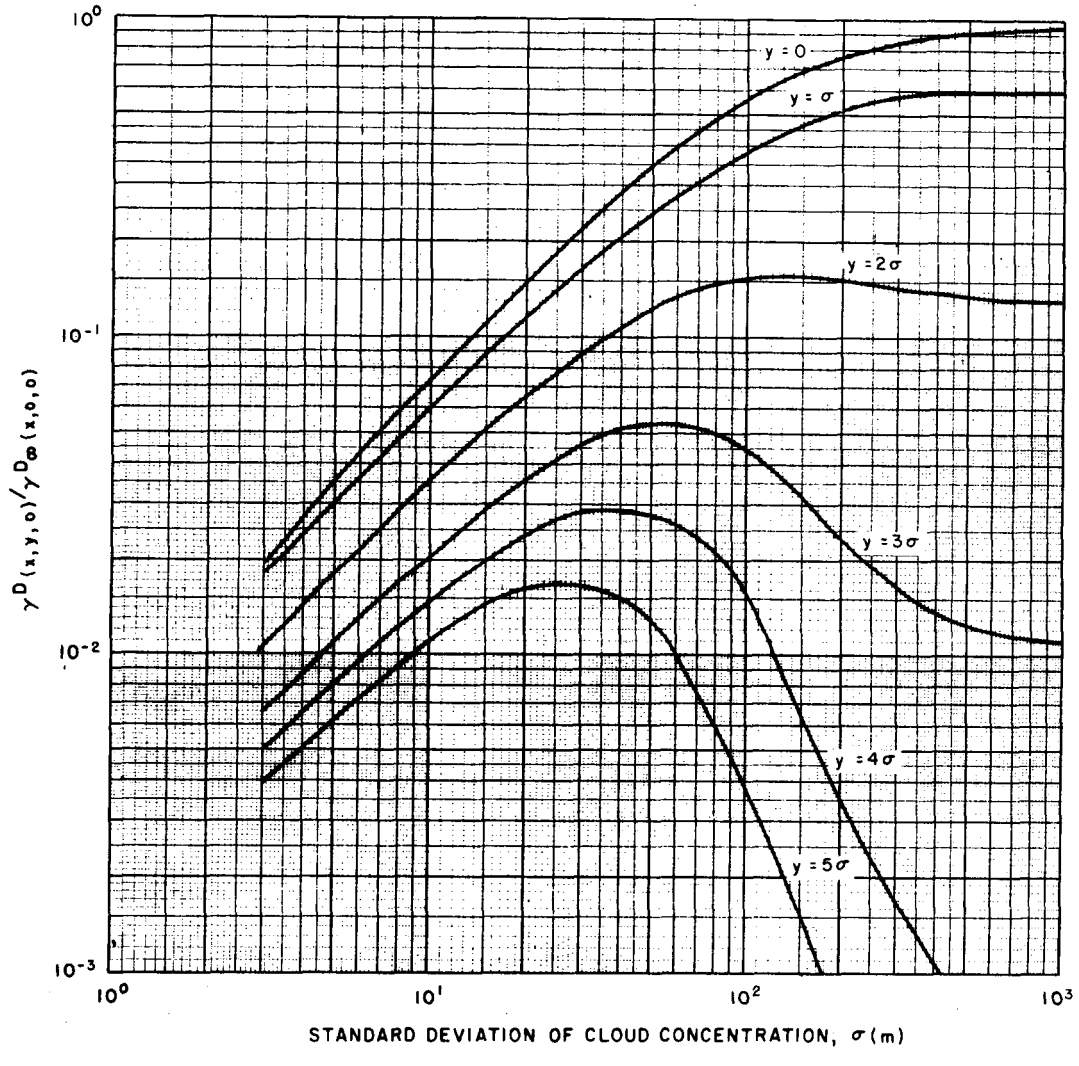

Fig. 7.14 — Ratio of the gamma dose in a finite cloud to the gamma dose in an infinite cloud having the same concentration as the center line of the finite cloud for 0.7-Mev gamma photons.

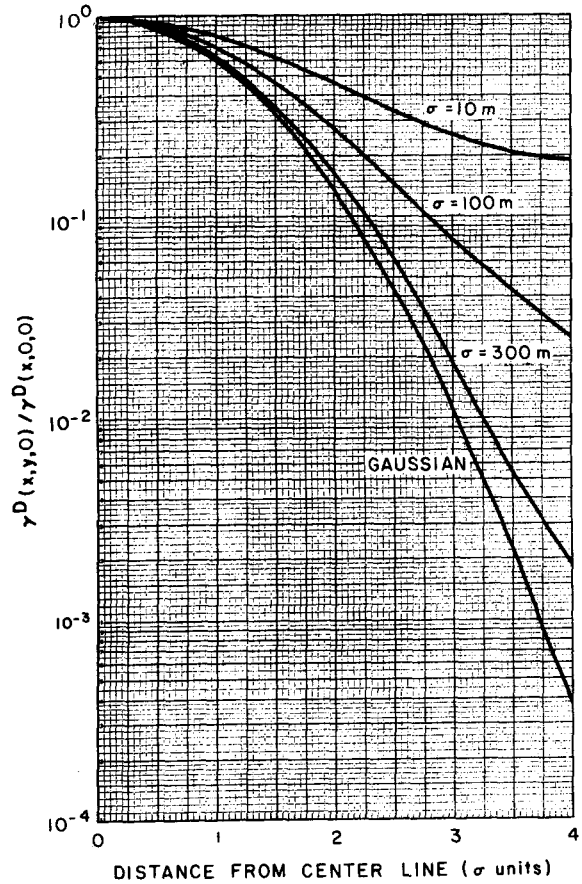

Fig. 7.15—Ratio of off-center-line to center-line doses from finite size clouds containing radionuclides emitting 0.7-Mev gammas compared to Gaussian concentration distribution.

three different gamma energies in Fig. 7.16. The spread in ratios is only a factor of 2 for energies that differ by a factor of 20.

7-5.2.4 Gamma Dose from Releases Under Capping Inversions. It is not uncommon to find that the vertical diffusion of the cloud released in a layer between the ground and an inversion base is restricted by the presence of the two boundaries. Just as the concentration is affected by the presence of the ground (the reflected component), it is also affected by the presence of the inversion layer. Capping inversions have been discussed in Chap. 3, Sec. 3-3.5, and values of the heights that might be expected have been presented by Holzworth (1964). Mounting evidence indicates that capping inversions occur frequently over cities at night, as well as over other rather limited geographical areas.

The concentration and concentration time integral of a cloud released in the layer between the ground and a capping inversion will be greater than similar values calculated with equations based upon the uniform infinite atmosphere. The magnitude of this difference will depend upon the relative magnitudes of the height of the inversion layer, the height of release of the source material, and the distance downwind from the release point. The following treatment of the problem, which is similar to that of Hewson, Gill, and Bierly (1959), makes use of the reference system shown in Fig. 7.17.

Consider a source Q_0 released at a point h meters above the ground and below the base of the inversion, h_i. As the cloud moves downwind, the source is depleted by ground deposition and radioactive decay, i.e., $Q_x = Q_0 (Q_x/Q_0)$. An observer located at the center of the cloud and moving with the cloud at the average wind speed $\bar{u}$ (m/sec) would observe that the upper and lower cloud limits follow the paths indicated by the solid and dashed lines of Fig. 7.17, respectively. The path lengths computed with the reference points (a,a′,b,b′, ...) are indicated in Table 7.7.

If an arbitrary index m = θ is used for the first two ground reflections, i.e., a,a′,b,b′, and

Table 7.7—HYPOTHETICAL CLOUD OBSERVATIONS UNDER CAPPING INVERSIONS

Reference points	Direction	Distance
	Upper Cloud Limit	
b	↓	$(2h_i - h - \Delta h)$
b′	↑	$(2h_i - h + \Delta h)$
d	↓	$(2h_i - h - \Delta h) + 2h_i$
.	.	.
.	.	.
.	.	.
n	↓	$(2h_i - h - \Delta h) + (a - 1)2h_i$
n′	↑	$(2h_i - h + \Delta h)\ (a + 1)2h_i$
	Lower Cloud Limit	
a	↓	$(h - \Delta h)$
a′	↑	$(h + \Delta h)$
c	↓	$(h - \Delta h) + 2h_i$
.	.	.
.	.	.
.	.	.
m	↓	$(h - \Delta h) + a2h_i$
m′	↑	$(h + \Delta h) + a2h_i$

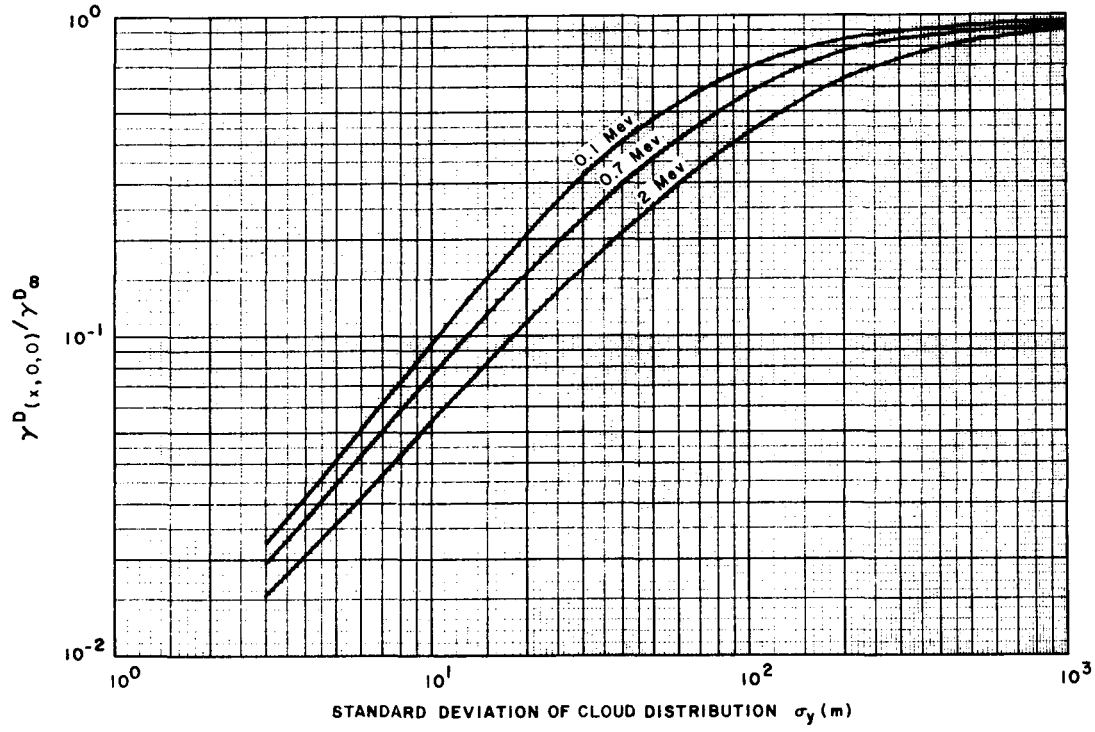

Fig. 7.16—Ratio of gamma dose at center line in a finite cloud of gamma-emitting radionuclides to dose in an infinite cloud with the same center-line concentrations.

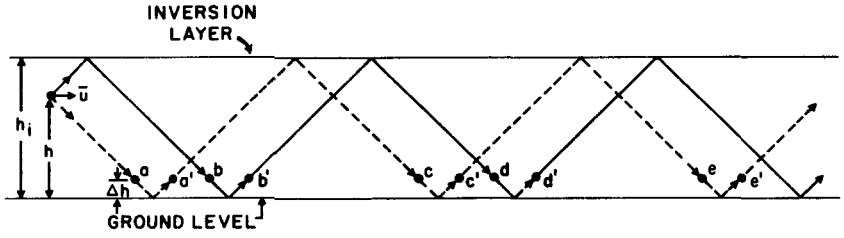

Fig. 7.17—Schematic drawing of the reference system used in the calculational model for the cloud concentration under a capping inversion.

m = 1 for the next two reflections, etc., the path lengths can be described in general terms:

Reference points	Distances
Lower Cloud	
(a,c,e, ... m)	$2mh_i + h - \Delta h$
(a′,c′,e′, ... m′)	$2mh_i + h + \Delta h$
Upper Cloud	
(b,d,f, ... n)	$(2m + 1)h_i - h - \Delta h$
(b′,d′,f′, ... n′)	$(2m + 1)h_i - h + \Delta h$

The concentration time integral at a point r meters from the center of an isotropic cloud can be described by

$$\psi_r = \psi_p \exp\left(-\frac{r^2}{2\sigma^2}\right) \qquad (7.49)$$

where ψ_p is the concentration time integral of the cloud center line (curie sec/m^3).

With the path lengths developed for the capping inversion, the concentration time integral

at a point x m downwind directly under the cloud path and Δh meters above the ground may be described by

$$\psi_{(x,0,\Delta h)} = \psi_p \sum_{m=0}^{\infty} \left\{ \exp - \left[\frac{2mh_i + h - \Delta h}{(2)^{1/2}\sigma_z}\right]^2 + \exp - \left[\frac{2mh_i + h + \Delta h}{(2)^{1/2}\sigma_z}\right]^2 + \exp - \left[\frac{(2m+1)h_i - h - \Delta h}{(2)^{1/2}\sigma_z}\right]^2 + \exp - \left[\frac{(2m+1)h_i - h + \Delta h}{(2)^{1/2}\sigma_z}\right]^2 \right\} \quad (7.50)$$

For the special case of the receptor at ground level, $\Delta h = 0$, the first and second exponential terms are equal and the third and fourth terms are equal; therefore Eq. 7.50 becomes

$$\psi_{(x,0,0)} = 2\psi_p \sum_{m=0}^{\infty} \left\{ \exp - \left[\frac{2mh_i + h}{(2)^{1/2}\sigma_z}\right]^2 + \exp - \left[\frac{(2m+1)h_i - h}{(2)^{1/2}\sigma_z}\right]^2 \right\} \quad (7.50a)$$

For the special case of the inversion layer at a very-high altitude, only the ground reflection is important, and Eq. 7.50 becomes

$$\psi_{(x,0,0)} = 2\psi_p \exp\left(-\frac{h^2}{2\sigma_z^2}\right) \quad (7.50b)$$

The terms $f(\sigma_z,h,h_i)$, f_1, and f_2 are defined as

$$f(\sigma_z,h,h_i) = \sum_{m=0}^{\infty} \left\{ \exp - \left[\frac{2mh_i + h}{(2)^{1/2}\sigma_z}\right]^2 + \exp - \left[\frac{2(m+1)h_i - h}{(2)^{1/2}\sigma_z}\right]^2 \right\} \quad (7.51)$$

and

$$f_1(\sigma_z,h,h_i) = \frac{h}{(2)^{1/2}\sigma_z} f(\sigma_z,h,h_i)$$

$$f_2(\sigma_z,h,h_i) = \frac{h^2}{2\sigma_z^2} f(\sigma_z,h,h_i) \quad (7.52)$$

When $(2)^{1/2}\sigma_z > h_i$, where the vertical equilibrium has been established by multiple reflections of the cloud between the two planes, Eq. 7.52 becomes

$$f_1(\sigma_z,h,h_i) = \frac{(\pi)^{1/2}h}{2h_i}$$

and

$$f_2(\sigma_z,h,h_i) = \frac{(\pi)^{1/2}h^2}{(2)^{3/2}\sigma_z h_i} \quad (7.52a)$$

When $(2)^{1/2}\sigma_z < h_i$, Eq. 7.52 becomes

$$f_1(\sigma_z,h,h_i) = \frac{h \exp(-h^2/2\sigma_z^2)}{(2)^{1/2}\sigma_z}$$

and

$$f_2(\sigma_z,h,h_i) = \frac{h^2 \exp(-h^2/2\sigma_z^2)}{2\sigma_z^2} \quad (7.52b)$$

With these functions the equations for the cloud concentrations become the following:

For an instantaneous point source released at h,

$$\chi_{(x,y,0,t)} = \frac{Q_x \sigma_{zI}}{\pi^{3/2}(2)^{1/2}\sigma_{xI}\sigma_{yI}h^2} f_2(\sigma_{zI},h,h_i) \times \exp\left\{-\left[\frac{(x-\bar{u}t)^2}{2\sigma_{xI}^2} + \frac{y^2}{2\sigma_{yI}^2}\right]\right\} \quad (7.53)$$

and, when $(2)^{1/2}\sigma_{zI} > h_i$,

$$\chi_{(x,y,0,t)} = \frac{Q_x}{2\pi\sigma_{xI}\sigma_{yI}h_i} \times \exp\left\{-\left[\frac{(x-\bar{u}t)^2}{2\sigma_{xI}^2} + \frac{y^2}{2\sigma_{yI}^2}\right]\right\} \quad (7.53a)$$

For a continuous point source with steady winds released at h,

$$\bar{\chi}_{(x,y,0)} = \frac{2Q'_x f_1(\sigma_z,h,h_i)}{\pi \bar{u} h (2)^{1/2}\sigma_y} \exp\left(-\frac{y^2}{2\sigma_y^2}\right) = \frac{2Q'_x \sigma_z f_2(\sigma_z,h,h_i)}{\pi \bar{u} h^2 \sigma_y} \exp\left(-\frac{y^2}{2\sigma_y^2}\right) \quad (7.54)$$

and, when $(2)^{1/2}\sigma_z > h_i$,

$$\bar{\chi}_{(x,y,0)} = \frac{Q'_x}{(2\pi)^{1/2}\sigma_y \bar{u} h_i} \exp\left(-\frac{y^2}{2\sigma_y^2}\right) \quad (7.54a)$$

Note that Eqs. 7.54 and 7.54a yield the concentration time integral when Q_x is substituted for Q'_x and appropriate values of σ are used.

For a continuous source release over long time periods (the equations for concentration and dosage from sources operating over long time periods are developed in Sec. 7-5.2.5.),

$$\bar{\chi}_{(R,\theta,0)} = \frac{2Q'_R\, f_1(\sigma_z,h,h_i)}{(\pi)^{1/2}\bar{u}\ R\ \theta\ h} \qquad (7.55)$$

and, when $(2)^{1/2}\sigma_z > h_i$,

$$\bar{\chi}_{(R,\theta,0)} = \frac{Q_R}{\bar{u}\ R\ \theta\ h_i} \qquad (7.55a)$$

These equations can be used to determine the amount of radioactive material inhaled during cloud passage and to calculate the direct dose to persons from the cloud passage. Values of $f_1(\sigma_z,h,h_i)$ and $f_2(\sigma_z,h,h_i)$ can be obtained from Figs. 7.18 and 7.19, where they are shown graphically as a function of σ_z/h for various ratios of h_i/h.

The equations previously developed for the direct dose from passing clouds can be written in terms of $f_1(\sigma_z,h,h_i)$ and $f_2(\sigma_z,h,h_i)$.

For the gamma dose from passage of a finite size cloud (see Eq. 7.42) where $(2)^{1/2}\,\mu\sigma_z > 10$, the values of I_1 and I_2 can be given accurately as

$$I_1 = I_2 = \frac{\exp\,(-s/2\sigma_I^2)}{2\mu\sigma_I^2} \qquad (7.56)$$

and the equation for the gamma dose can be written

$$_{\gamma}D_{(x,y,0)} = \frac{0.1616\ Q_0\ (Q_x/Q_0)\ \exp\,(-s^2/2\sigma_I^2)}{\bar{u}\ 2\sigma_I^2} \qquad (7.57)$$

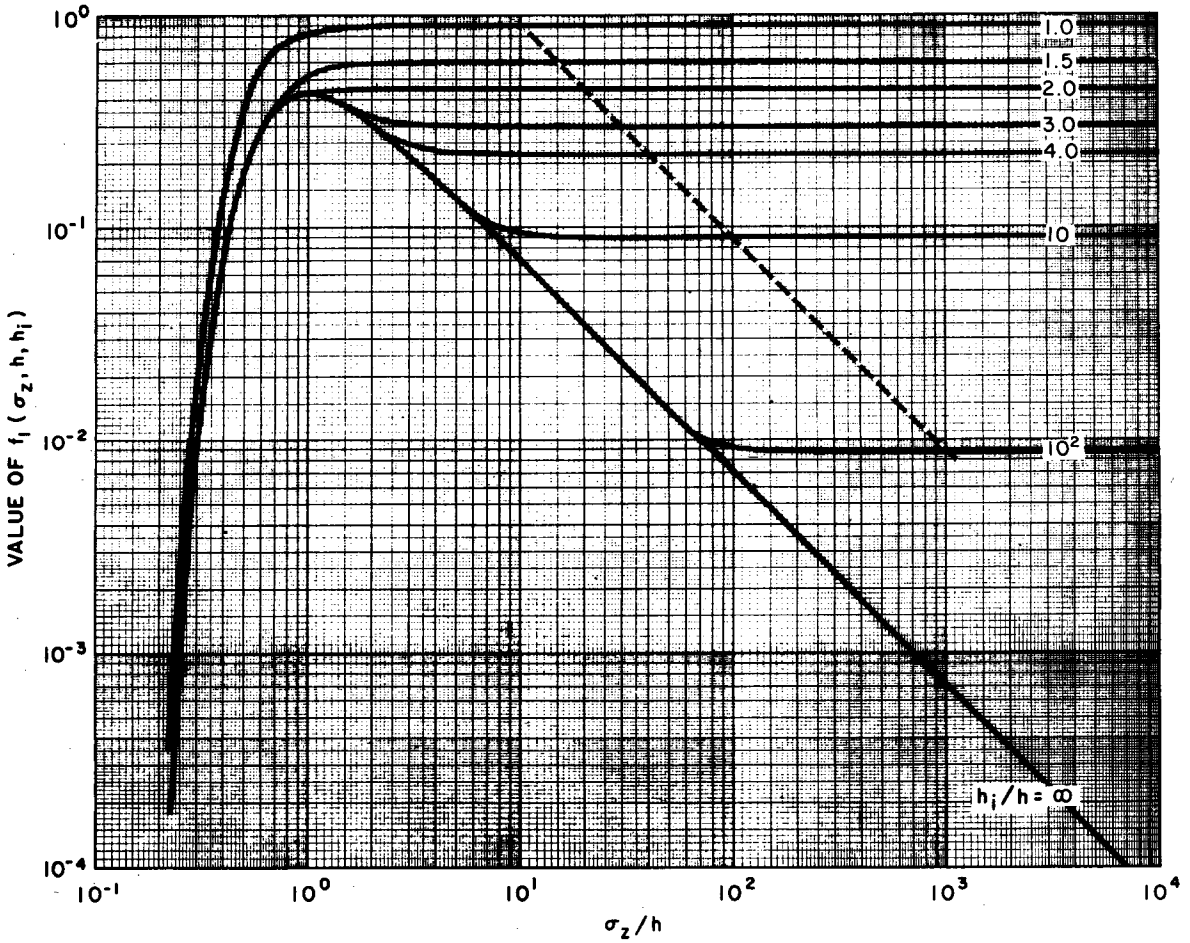

Fig. 7.18 — Values of $f_1(\sigma_z,h,h_i)$ as a function of σ_z/h for various ratios of h_i/h. (See Eq. 7.52).

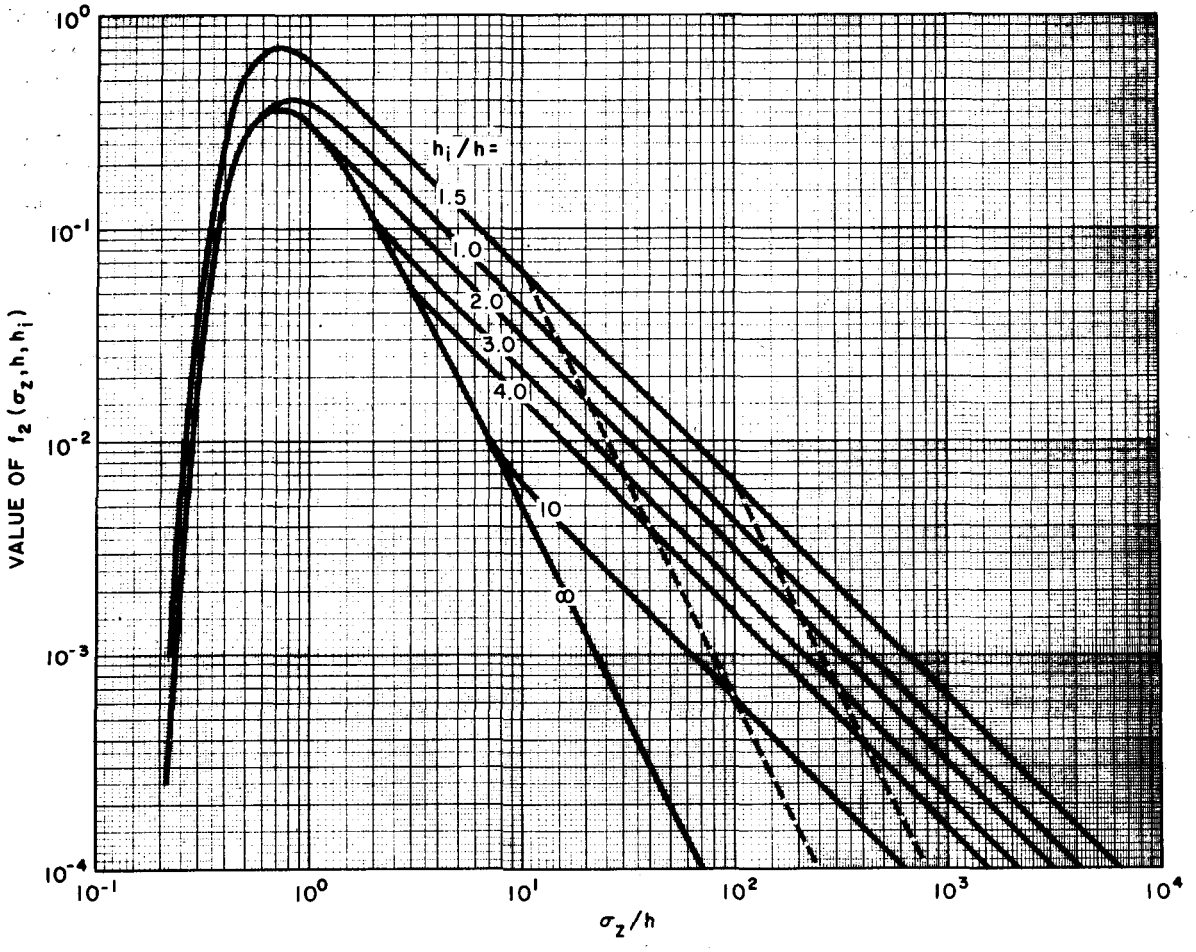

Fig. 7.19 — Values of $f_2(\sigma_z,h,h_i)$ as a function of σ_z/h for various ratios of h_i/h. (See Eq. 7.52).

where values of μ_a and μ are not involved.

In terms of the functions previously derived, this can be written

$$ {}_{\gamma}D_{(x,y,0)} = \frac{0.1616\, Q_x\, \bar{E}_\gamma \exp(-y^2/2\sigma_y^2)}{\bar{u}\, h^2} \times \frac{\sigma_z}{\sigma_y} f_2(\sigma_z,h,h_i) \quad (7.58) $$

In a similar manner the gamma dose from a prolonged release of Q'_0 (curies/sec) for t_d (sec) to a receptor in the sector wherein the release may be averaged over the sector width θ (for a fuller discussion of this, see Eqs. 7.60, 7.61, and 7.62) can be written

$$ {}_{\gamma}D_{(R,\theta,0)} = \frac{0.2865\, Q'_x t_d\, \bar{E}_\gamma}{\bar{u}\, R\, \theta\, h} f_1(\sigma_z,h,h_i) \quad (7.59) $$

This equation for a capping inversion yields results that are slightly high for cases where $\mu h_i < 2$, but, if $\mu h_i > 2$, the results are high by only a few percent and no correction is necessary.

7-5.2.5 Average Gamma Dose from Continuous Releases over Long Time Periods. During routine release of radioactive effluents from stacks, the gamma dose received in the vicinity over a long period of time is of interest for comparison with the radiation limits, which frequently permit averaging of the dose over time intervals of up to 1 year. Estimates of this dose prior to carrying out a disposal program permit the establishment of emission limits, which, in turn, indicate the plant features needed to meet these limits.

The average dose over such a long time period must consider the effects of shifting winds, as well as the more normal parameters for estimating turbulent diffusion. The frequency with which the wind blows in a given direction is given by the conventional wind rose, usually to an 8- or 16-point compass or to the nearest 10°. For an estimate of long-term average doses, the frequency of occurrence of each atmospheric stability class must be provided to augment the wind rose.

If it is assumed that a source of radioactive material is continuously emitted at a constant rate of Q_0' (curie/sec) at a height h (m) above the ground plane for a time period t_d (sec), the equilibrium concentration in the plume at a point (x,y,z) is given by Eq. 3.115 in Chap. 3.

$$\bar{\chi}_{(x,y,z)} = \frac{Q_x'}{2\pi\bar{u}\sigma_y\sigma_z}\exp\left(-\frac{y^2}{2\sigma_y^2}\right) \times\left\{\exp\left[-\frac{(z-h)^2}{2\sigma_z^2}\right]+\exp\left[-\frac{(z+h)^2}{2\sigma_z^2}\right]\right\}$$

where $Q_x' = Q_0'\,(Q_x/Q_0)$ is the activity release rate for a specific radionuclide corrected for depletion en route to the receptor and the coordinate system is the same as that used previously. The last exponential term in the equation represents the reflected component, i.e., that portion of the plume which has diffused to the ground plane and diffused back into the plume. For calculations of the direct gamma dose rate from the plume, the term for the reflected component will be retained in this form which, essentially, disregards the presence of the ground plane as a barrier but correctly describes the location of the reflected component source contribution with respect to a ground-level receptor.

The following treatment of the problem is based upon the work of Gamertsfelder (1960). Figure 7.20 shows the reference system used in the following discussion. If the direction of the emission shifts continuously and uniformly over a horizontal angle θ (radians) during the time period of concern, the concentration within the sector can be averaged in the horizontal direction across the sector. Integrating Eq. 3.115 in the y-direction from $-\infty$ to $+\infty$ and averaging the concentration over the width of the sector with R as the radial equivalent of x yields

$$\bar{\chi}_{(R,\theta,0)} = \frac{Q_R'}{(2\pi)^{1/2}\sigma_z\bar{u}\,R\,\theta}\left\{\exp\left[-\frac{(z-h)^2}{2\sigma_z^2}\right] + \exp\left[-\frac{(z+h)^2}{2\sigma_z^2}\right]\right\} \quad (7.60)$$

where $\bar{\chi}_{(R,\theta,0)}$ is the average concentration in the plume at a point R meters radially from the re-

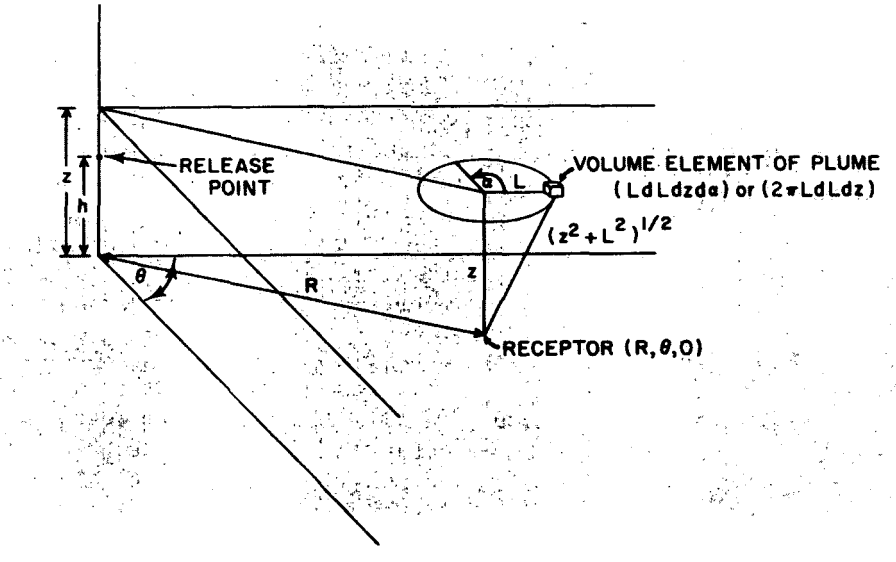

Fig. 7.20 — Reference system for long-term dosage equations.

lease point and z meters above the ground plane (curies/m^3) and θ is the angular width of the sector within which the plume is dispersed (radians).

In cases where the distance between the source and the receptor is sufficiently great so that the change in concentration with distance is relatively small over the relaxation length of the gamma rays, the plume, averaged over the sector, can be considered to be comprised of a series of infinite horizontal plane sources. The plane sources vary in concentration according to a Gaussian distribution centered about the plume center plane, i.e., centered about the height of release.

The gamma dose rate to tissue located a distance r (m) from a source increment of q curies was given by Eq. 7.34.

If a volume element of the source is located at a height z (m) above the ground plane and a horizontal distance L (m) from the receptor, the source is a distance $(L^2 + z^2)^{1/2}$ from the receptor. With this reference system shown in Fig. 7.20, a volume element of source in the plane is $2\pi L\, dL\, dz$. Substituting $(L^2 + z^2)^{1/2}$ for r in Eq. 7.34 and the expression for $\overline{\chi}_{(R,\theta,0)}$ of Eq. 7.60 for the incremental source q, the equation for the gamma dose rate from the plume can be written as

$$ {}_{\gamma}D'_{(R,\theta_1,0)} = \frac{0.0404\,\mu_a\,\overline{E}_{\gamma}Q'_x}{(2\pi)^{1/2}\,\bar{u}\,R\,\sigma_z\,\theta}\int_0^{\infty}\int_0^{\infty}\frac{1}{L^2+z^2} \times \left(\left[1+k\mu\,(L^2+z^2)^{1/2}\right]\left\{\exp\left[-\frac{(z-h)^2}{2\sigma_z^2}\right] + \exp\left[-\frac{(z+h)^2}{2\sigma_z^2}\right]\right\}\exp\left[-\mu\,(L^2+z^2)\right]\right) \times 2\pi\,L\,dL\,dz \qquad (7.61) $$

If I_1 and I_2 are defined as

$$ \bar{I}_1 = \frac{1}{(2)^{3/2}\,\sigma_z}\int_0^{\infty}\int_0^{\infty}\frac{1}{L^2+z^2}\left\{\exp\left[-\frac{(z-h)^2}{2\sigma_z^2}\right] + \exp\left[-\frac{(z+h)^2}{2\sigma_z^2}\right]\right\}\exp\left[-\mu\,(L^2+z^2)^{1/2}\right]\,L\,dL\,dz $$

$$ = \frac{1}{(2)^{3/2}\,\sigma_z}\int_0^{\infty}\left\{\exp\left[-\frac{(z-h)^2}{2\sigma_z^2}\right] + \exp\left[-\frac{(z+h)^2}{2\sigma_z^2}\right]\right\} \times \left\{\int_{\mu z}^{\infty}\frac{\exp\left[-\mu\,(L^2+z^2)^{1/2}\right]}{\mu\,(L^2+z^2)}\,d\left[\mu\,(L^2+z^2)^{1/2}\right]\right\}dz \qquad (7.61a) $$

$$ \bar{I}_2 = \frac{1}{(2)^{3/2}\,\sigma_z}\int_0^{\infty}\int_0^{\infty}\frac{1}{(L^2+z^2)^{1/2}}\left\{\exp\left[-\frac{(z-h)^2}{2\sigma_z^2}\right] + \exp\left[-\frac{(z+h)^2}{2\sigma_z^2}\right]\right\}\exp\left[-\mu\,(L^2+z^2)^{1/2}\right]\,\mu L\,dL\,dz $$

$$ = \frac{1}{(2)^{3/2}\,\sigma_z}\int_0^{\infty}\left\{\exp\left[-\frac{(z-h)^2}{2\sigma_z^2}\right] + \exp\left[-\frac{(z+h)^2}{2\sigma_z^2}\right]\right\}\exp\left(-\mu z\right)\,dz \qquad (7.61b) $$

Equation 7.61 can be written

$$ {}_{\gamma}D'_{(R,\theta,0)} = \frac{0.2865\,\mu_a\,Q'_x\overline{E}_{\gamma}}{\bar{u}\,R\,\theta}\left[\bar{I}_1 + k\bar{I}_2\right] \qquad (7.62) $$

Values of $\bar{I}_1$ and $\bar{I}_2$ are shown graphically in Figs. 7.21 and 7.22 as a function of $\mu\sigma_z$ for various release heights. The dashed lines permit interpolating for release heights not given specifically. Equation 7.62 and other equations derived from the model will yield values that somewhat overestimate the gamma dose rate (or dose) if $\mu\, r\, \theta < 2$ but yield quite accurate values when $\mu\, r\, \theta \geq 2$. The gamma dose rate can be multiplied by the time period of discharge, t_d (sec), to calculate the dose to the receptor. For a specific gamma energy, the term $[\bar{I}_1 + k\bar{I}_2]$ can be combined into a single term $\bar{I}_T$. Figure 7.23 presents the values of $\bar{I}_T$ for 0.7-Mev photons.

Equation 7.62 can be written as shown in Eq. 7.59 for the gamma dose from a prolonged release under a capping inversion. For a fuller discussion see Sec. 7-5.2.4 and Eq. 7.59.

Equation 7.62 can be used to calculate the long-term direct gamma dose to receptors in the general vicinity of a point where a source of radioactive material is released continuously at a uniform rate over an extended period of time. The direct gamma dose from such a source to an individual located at $(R,\theta_1,0)$, a distance R (m) from the point of release in a sector of width θ (radians) at ground level, can be calculated by evaluating Eq. 7.63.

$$ {}_{\gamma}D_{(R,\theta_1,0)} = \frac{0.2865\,\Delta t}{\theta R}\left[\sum_{i=1}^{l}\sum_{j=1}^{m}\sum_{k=1}^{n}\frac{P_{\sigma_{z(j,k,\theta_1)}}\,Q'_{R(i,j,k)}}{\bar{u}_j} \times \mu_{a_i}\,\overline{E}_{\gamma_i}\,(\bar{I}_1 + k\bar{I}_2)_{(i,j,k)}\right] \qquad (7.63) $$

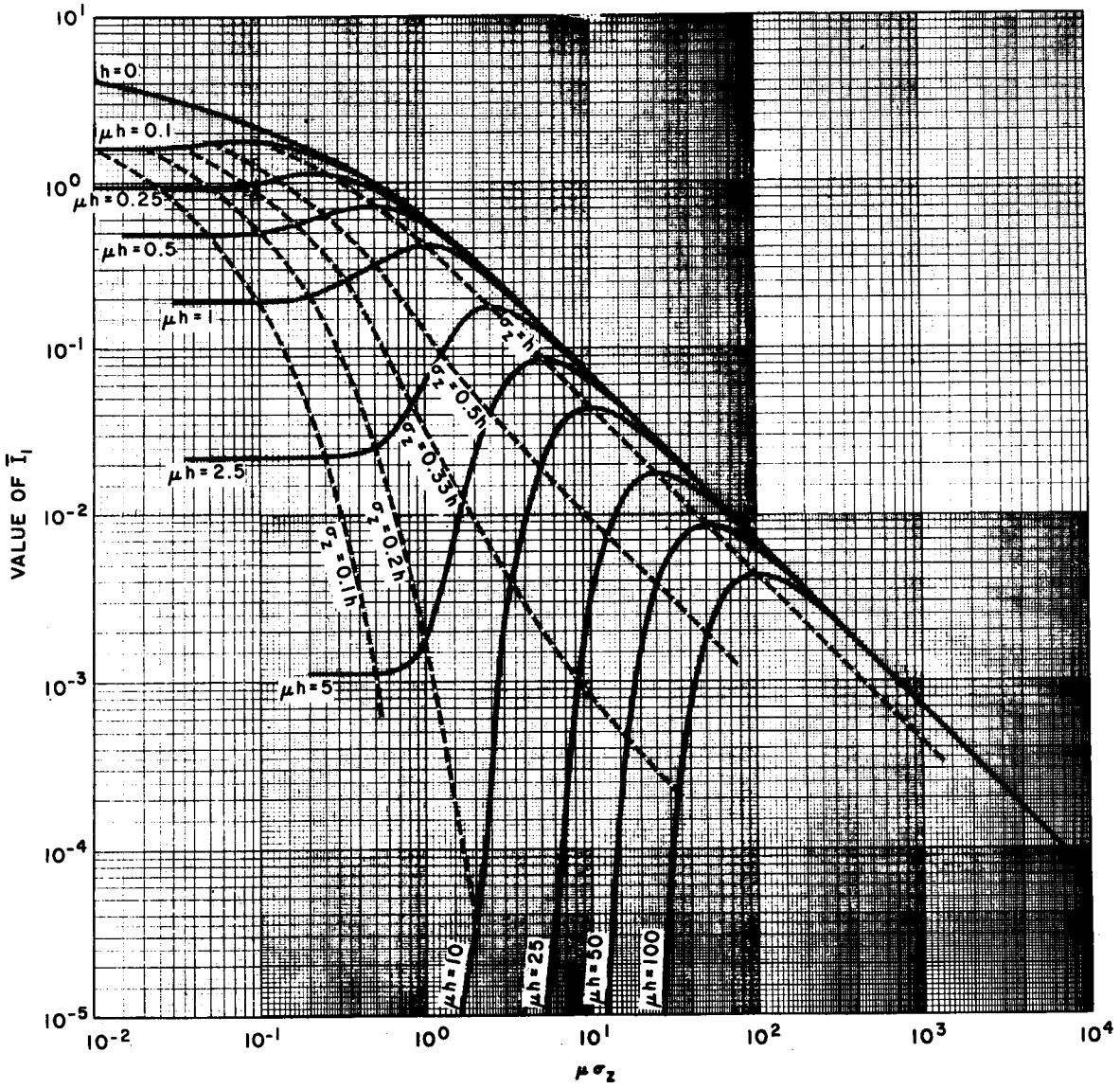

Fig. 7.21 — Values of the $\bar{I}_1$ integral (see Eq. 7.61a).

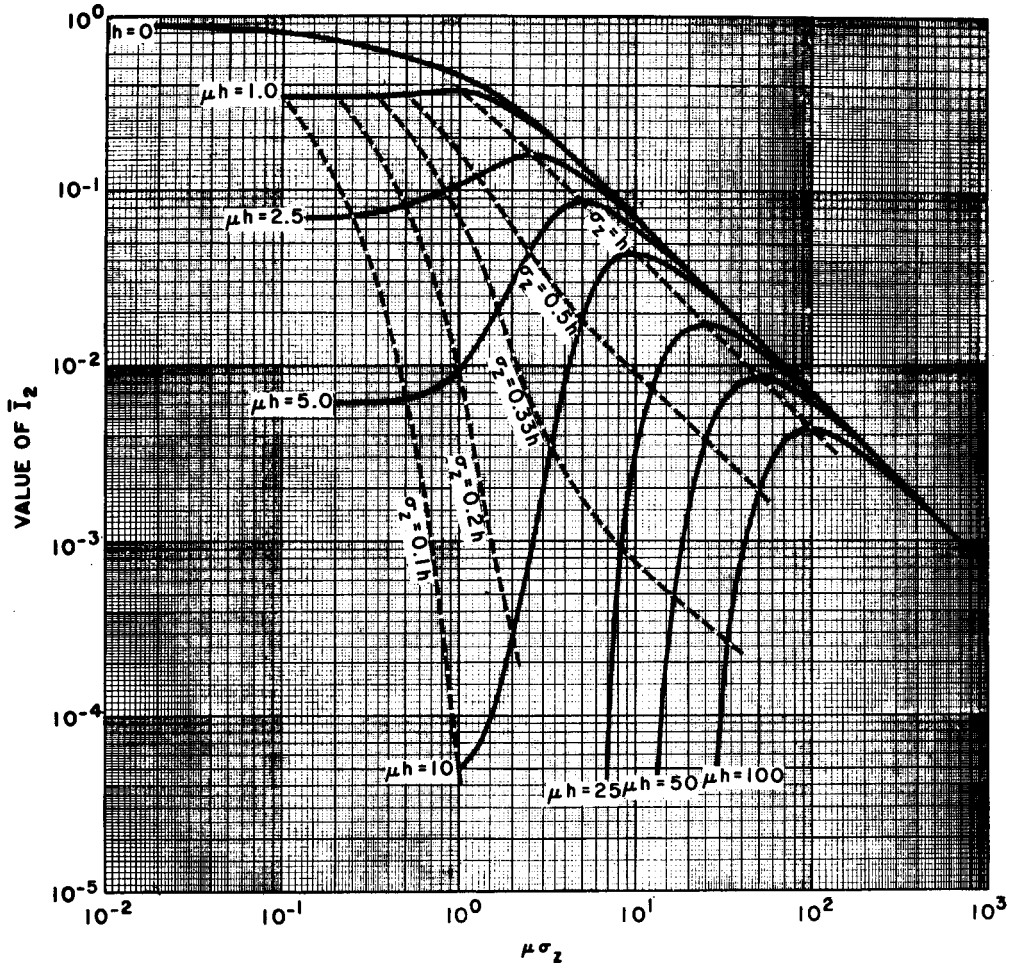

Fig. 7.22 — Values of the $\bar{I}_2$ integral (see Eq. 7.61b).

where $Q_{R(i,j,k)}$ = source term (release rate) of isotope type i corrected for depletion by ground deposition and radioactive decay en route to receptor location

$$= Q_0' \left[\exp\left(-\lambda_i \frac{R}{\bar{u}_j} \right) \right] (Q_x/Q_0)_{d_{j,k}}$$

(curie/sec)

$(Q_R/Q_0)_{d(j,k)}$ = depletion factor for ground deposition

$$= \exp\left[-\left(\frac{2}{\pi}\right)^{1/2} \frac{v_d}{\bar{u}_j} \times \int_0^R \frac{\exp\left(-\frac{h^2}{2\sigma_{z_k}}\right)}{\sigma_{z_k}} \, dR \right]$$

or equivalent Sutton form

$(\bar{I}_1 + k\bar{I}_2)_{i,j,k}$ = function of μ_i, σ_{z_k}, and $\bar{u}_j$

$\bar{u}_j$ = average of wind speed range j (m/sec)

σ_{z_k} = standard deviation of plume concentration in vertical plane for stability class k (m)

$P_{\sigma z(j,k,\theta_1)}$ = joint probability of wind speed and atmospheric stability into sector θ_1

Δt = exposure time interval (sec)

θ = angular width of sector θ_1 (radians)

R = distance from release point (m)

At long distances from the point of release, σ_z becomes large so that the cloud becomes uniform in concentration and can be regarded as an infinite cloud for which the gamma dose

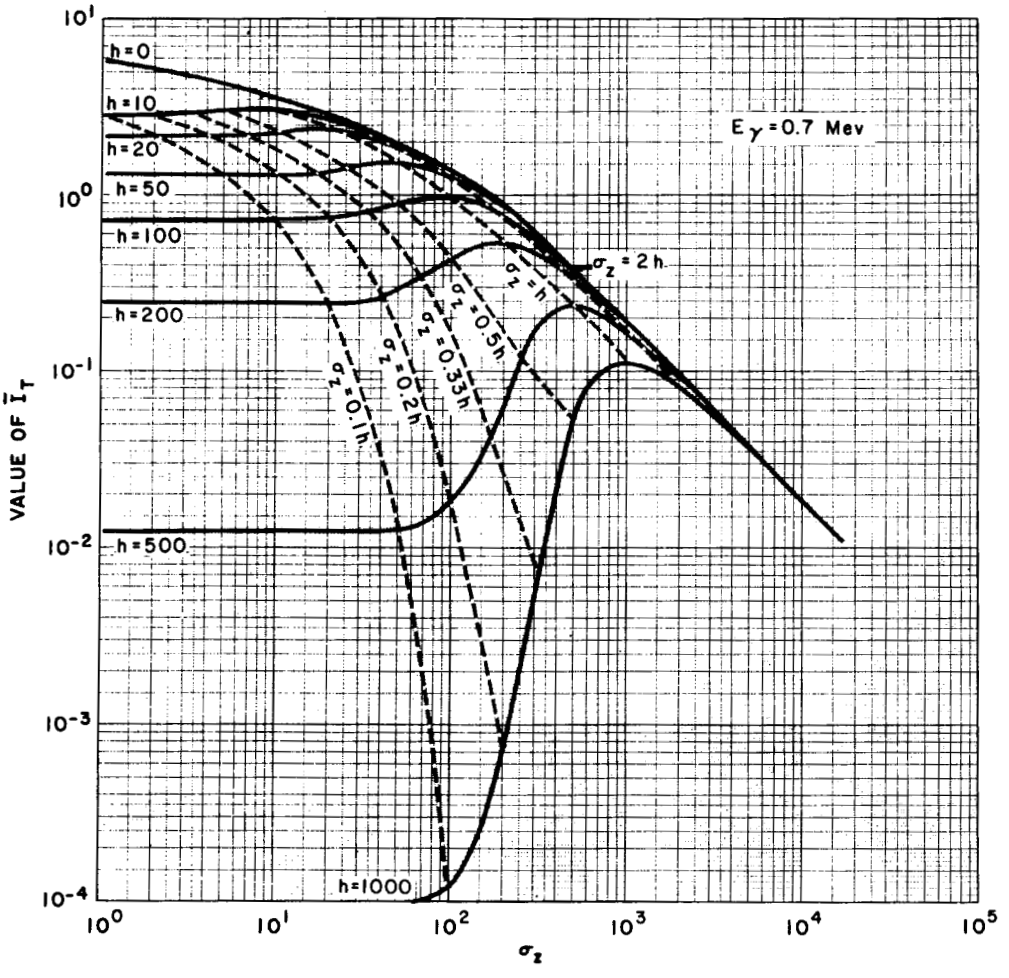

Fig. 7.23 — Values of the $\bar{I}_T$ integral for 0.7-Mev gamma radiation.

rate is given by Eq. 7.35a with the assumption that the value of χ used includes the reflected component of the cloud.

A receptor located on the line that defines the division between sectors would receive an intermediate dose between those doses calculated for the two sectors. In practice the doses for each of the sectors are calculated at several radial distances over the range of interest. The results are plotted on log graph paper (dose vs. distance); the radial distances in each sector are determined for several selected dose values (usually differing by factors of 10^1 or $10^{0.5}$), and these locations are plotted on circular coordinate paper for the center-line rays in each sector. Points representing the location of common dose values are then connected with a smooth curve to represent the dose isopleths. When the many approximations in developing the mathematical models and difficulty in obtaining input data are considered, more exact methods are not warranted.

7-5.3 Gamma Dose from Radioactive Materials Deposited on the Ground

A passing cloud of radioactive particles or halogens will deposit material on the ground by dry deposition, washout, or rainout. The radioactive materials on the ground will result in a gamma-radiation dose for a period of time after the cloud has passed. The ground pattern of these materials can be estimated by the methods indicated in other chapters. The persistence of the dose depends upon the radio-

active decay of the materials involved and the degree of cleanup by natural forces or by decontamination efforts.

7-5.3.1 The Infinite Plane Source. When the contamination is uniformly spread over a wide area, the intensity of the radiation is given by Eq. 7.64 for various distances above the ground.

$$I = \frac{S}{2} E_i(\mu r) + \frac{kS \exp(-\mu r)}{2} \qquad (7.64)$$

where I is the gamma-ray intensity (photon/m^2 sec), $E_i(\mu r)$ is the exponential integral $\int_{\mu r}^{\infty} [\exp(-\mu r)/r]\, dr$, and S is the source strength per unit area of the plane (photon/m^2 sec). The exponential integral, $E_i(\mu r)$, occurs in many shielding problems and is given in tabular form by Jahnke, Emde, and Lösch (1960). Equation 7.64 can be converted to dose rate units to give

$${}_{\gamma}D'_{\infty} = \frac{(I)\,(\overline{E}_{\gamma})\,(\mu_a)\,(1.6 \times 10^{-6})\,(1.11)}{(1293)\,(100)}$$

$${}_{\gamma}D'_{\infty} = 1.37 \times 10^{-11} I\, \overline{E}_{\gamma} \mu_a \qquad (7.65)$$

If I is replaced by its equivalent as given in Eq. 7.64 and one photon of average energy $\overline{E}_{\gamma}$ is assumed to be emitted per disintegration, the gamma dose rate is given by

$${}_{\gamma}D'_{\infty} = 0.254\, \omega\, \overline{E}_{\gamma} \mu_a \left[E_i(\mu b) + \frac{k \exp(-\mu b)}{2} \right] \qquad (7.65a)$$

where ${}_{\gamma}D'_{\infty}$ is the gamma dose rate (rad/sec) to a receptor located b meters above an infinite plane uniformly contaminated, and ω is the number of curies per square meter on the ground. The constant in the buildup factor has been divided by two to provide an approximate correction for the primary radiation that enters the ground and is scattered to the receptor with a much lower efficiency than that which enters the air.

Figure 7.24 presents the dose rate at several heights above the ground for radiation with energies from 0.1 to 2 Mev as obtained from Eq. 7.65.

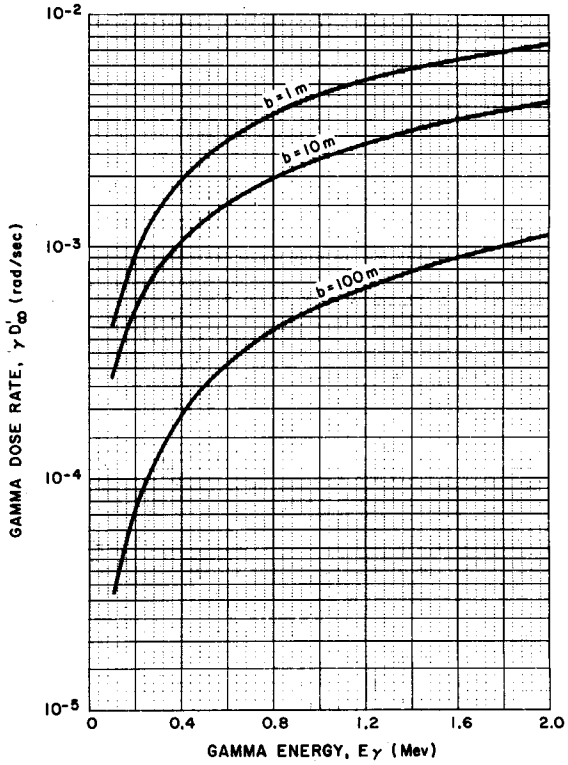

Fig. 7.24 — Gamma dose rate at heights of 1, 10, and 100 m above ground as given for infinite plane source of 1.0 curie/m^2.

7-5.3.2 The Finite Plane Source. If radioactive materials are deposited from a plume, either by dry deposition or by rainout or washout, the deposition pattern will consist of a maximum at the center line with the deposition decreasing with distance from the center line according to the Gaussian distribution of concentration in the cloud. This pattern can be described by

$$\omega_{(x,y,0,t)} = \omega_{(x,0,0,t)} \exp\left(-\frac{y^2}{2\sigma_y^2}\right) \qquad (7.66)$$

where $\omega_{(x,0,0,t)}$ is the deposition in curies per square meter at distance x on the cloud center line at a specific time and $\omega_{(x,y,0,t)}$ is the deposition at a distance y from the center line at the same time. Since the value of ω will vary as a function of time owing to radioactive decay or decontamination efforts, the equation for ω must include these considerations.

Gamertsfelder (1960) has derived an equation to give the gamma dose rate to tissue at a height b above the center line of the pattern.

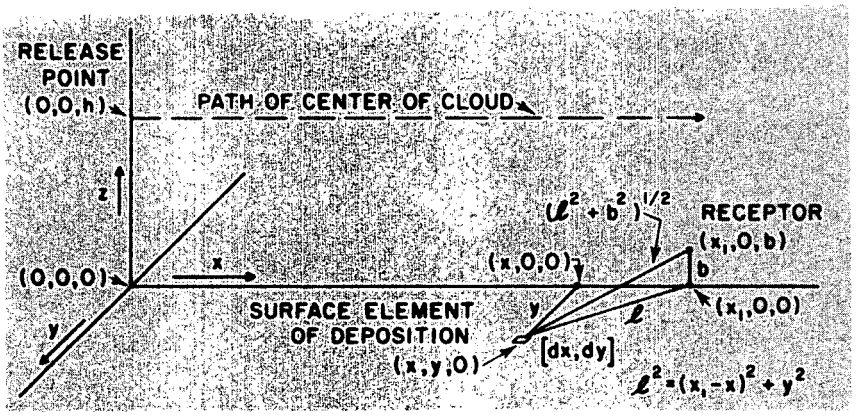

Fig. 7.25 — Reference system for equations involving deposition patterns of finite size.

From the equation for a point source, Eq. 7.34, and the coordinate system given in Fig. 7.25, the dose rate is given by

$$ {}_{\gamma}D_{(x_1,0,b,t)} = 0.0404\mu_a \bar{E}_{\gamma}\omega_{(x_1,0,0,t)} \times \int_{-\infty}^{\infty}\int_{0}^{\infty} \frac{[1+(k/2)\,\mu(l^2+b^2)^{1/2}]\,\exp[-\mu(l^2+b^2)^{1/2}]}{l^2+b^2} \times \exp\left(-\frac{y^2}{2\sigma_y^2}\right) dx\,dy \qquad (7.67) $$

where ${}_{\gamma}D_{(x_1,0,b,t)}$ is in rads per second at time t and k/2 is used in the buildup factor to allow for loss of scattered radiation from that part of the primary radiation that starts in a downward direction. With G_1 and G_2 defined as

$$ G_1 = \frac{1}{(2)^{1/2}\pi\mu\sigma_y}\int_{-\infty}^{\infty}\int_{0}^{\infty} \frac{\exp[-\mu(l^2+b^2)^{1/2}]\exp(-y^2/2\sigma_y^2)}{l^2+b^2} \times dx\,dy \qquad (7.68) $$

$$ G_2 = \frac{1}{(2)^{1/2}\pi\mu\sigma_y}\int_{-\infty}^{\infty}\int_{0}^{\infty} \frac{\mu\exp[-\mu(l^2+b^2)^{1/2}]\exp(-y^2/2\sigma_y^2)}{(l^2+b^2)} \times dx\,dy \qquad (7.68a) $$

Then

$$ {}_{\gamma}D_{(x_1,0,b,t)} = 0.36\,\omega_{(x,0,0,t)} \times \sigma_y\,\mu\mu_a\,\bar{E}_{\gamma}\left(G_1 + \frac{k}{2}G_2\right) \qquad (7.69) $$

For cases where the cloud is large with respect to the range of the gamma radiation ($\mu\sigma_y > 10$), the ground concentration is essentially uniform in all directions and the value of $\exp(-y^2/2\sigma_y^2)$ can be taken as unity for all values of y. Under these conditions the values of G_1 and G_2 can be written as

$$ G_1 = \frac{1}{(2)^{1/2}\mu\sigma_y}\int_0^{\infty}\frac{\exp[-\mu(l^2+b^2)^{1/2}]}{(l^2+b^2)}\,l\,dl = \frac{1}{(2)^{1/2}\mu\sigma_y}E_1[-\mu(l^2+b^2)^{1/2}] \qquad (7.70) $$

$$ G_2 = \frac{1}{(2)^{1/2}\mu\sigma_y}\int_0^{\infty}\frac{\mu\exp[-\mu(l^2+b^2)^{1/2}]}{(l^2+b^2)^{1/2}}\,l\,dl = \frac{1}{(2)^{1/2}\mu\sigma_y}\int_{\mu b}^{\infty}\frac{\exp(-\mu b)\,d(\mu b)}{(2)^{1/2}\mu\sigma_y} \qquad (7.71) $$

The exponential integral, $E_1[-\mu(l^2+b^2)^{1/2}]$, is as discussed earlier. These values for G_1 and G_2 provide the upper limits of the integrals. Values for smaller finite deposition patterns were obtained by Gamertsfelder by numerical evaluation of the integrals and are given in Figs. 7.26 and 7.27.

The ratio of the gamma dose rate above the center line of a deposition pattern smaller than an infinite plane to the dose rate above an infinite plane can be obtained from Eqs. 7.65 and 7.69. Figure 7.28 indicates this ratio for 0.7-Mev gamma photons. For most deposition patterns of interest, the correction factor for cloud size is comparatively small. Calculations for other energies indicate that Fig. 7.28 gives reasonable estimates of the ratio for energies up to 2 Mev but the difference may be 5% to 10% for the small pattern widths when the energy is as low as 0.1 Mev.

These equations provide an estimate of the gamma dose rate for a given amount of radio-

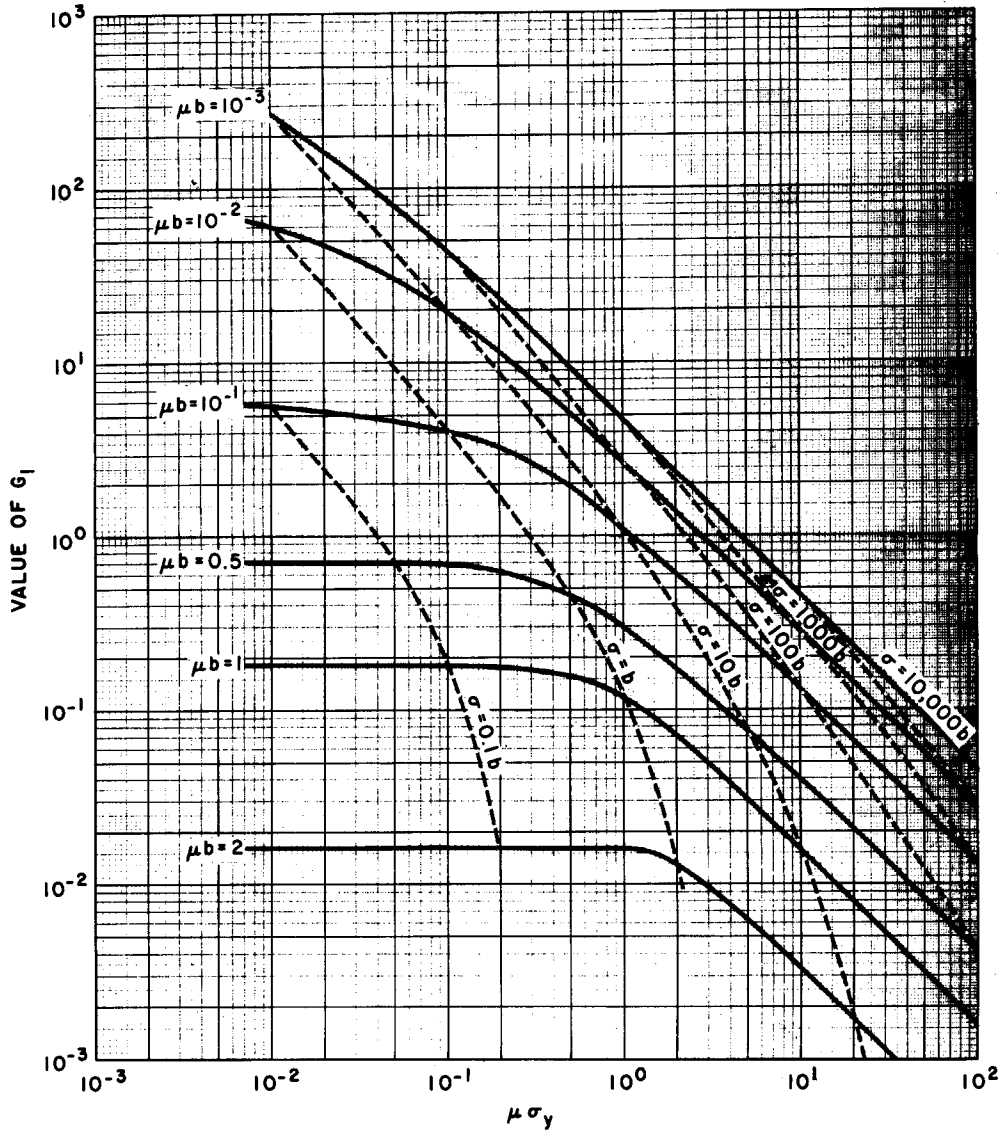

Fig. 7.26 — Values of the G_1 integral (see Eq. 7.68).

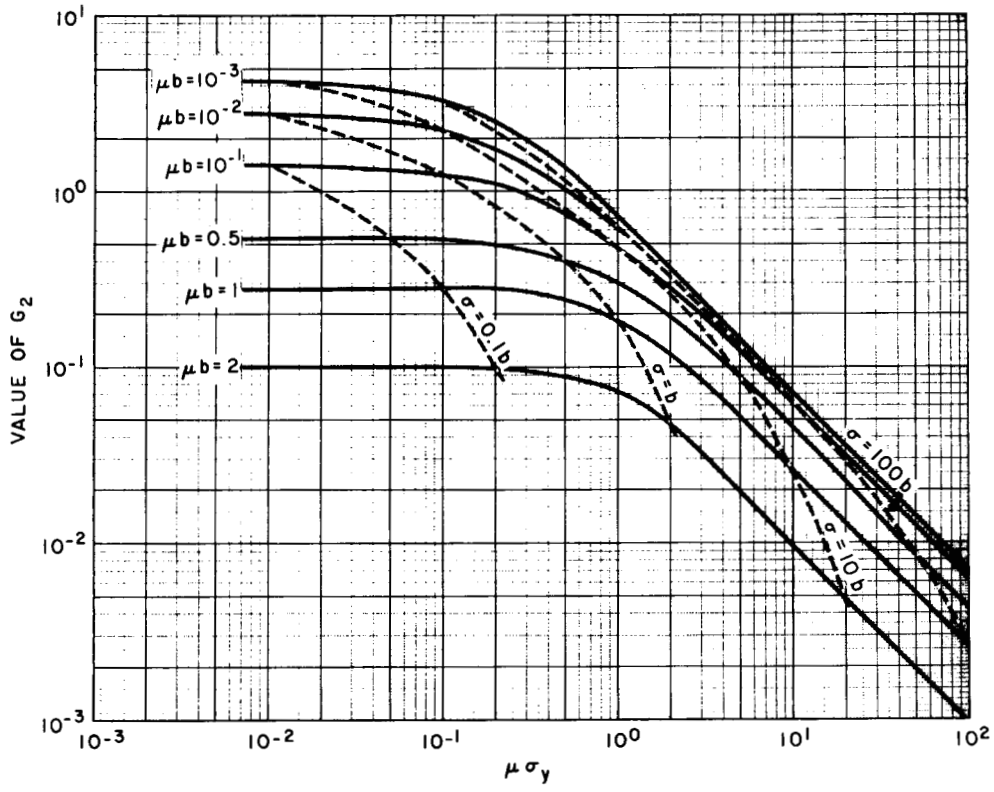

Fig. 7.27 — Values of the G_2 integral (see Eq. 7.68a).

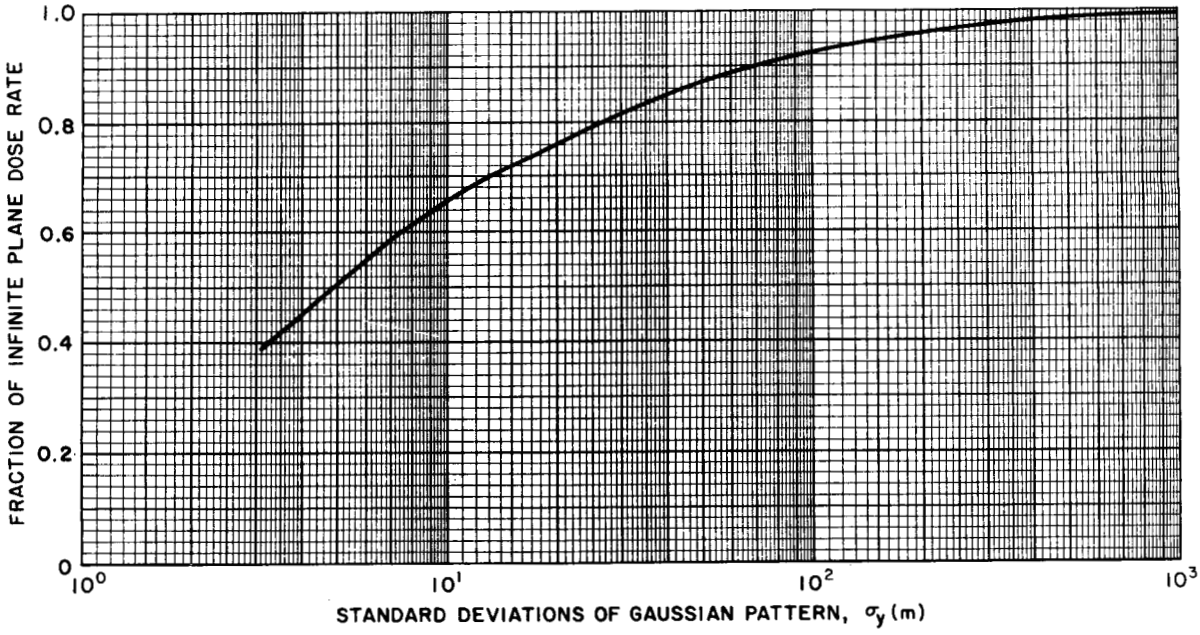

Fig. 7.28 — Ratio of the gamma dose rate from a Gaussian pattern of finite size to that from an infinite plane pattern with deposition equal to the center line of the finite Gaussian pattern.

active material on the ground at a specific time. If radioactive decay or weathering is of importance during the period of exposure, the total dose received must be corrected for the decrease in dose rate. In the simplest case, i.e., a release of a single isotope and subsequent deposition, the decrease can be described by a single exponential, and the dose rate at any given time (t sec) after the cloud has passed the receptor can be written as

$$ {}_{\gamma}D'_{(x_1,0,b,t)} = 0.36\ \omega_{(x,0,0,0)}\sigma_y\ \mu\mu_a\ \overline{E}_{\gamma} \times \left(G_1 + \frac{k}{2} G_2\right) \exp\ (-\lambda_R t) \qquad (7.72) $$

where $\omega_{(x,0,0,0)}$ is the center-line deposition based upon the source at the time of release and λ_R is the removal constant ($0.693/T_{1/2}$ with $T_{1/2}$ in seconds). Integrating from the cloud arrival time to the time at which the exposure estimate is desired gives the gamma dose equation for the finite deposition pattern.

$$ {}_{\gamma}D_{(x_1,0,b)} = 0.36\ \omega_{(x_1,0,0,t)}\ \sigma_y\ \mu\mu_a\ \overline{E}_{\gamma} \times \left(G_1 + \frac{k}{2} G_2\right) \left[\frac{1 - \exp\ (-\lambda_R t)}{\lambda_R}\right] \qquad (7.73) $$

In Eq. 7.73 ${}_{\gamma}D_{(x_1,0,b)}$ is in rads, and t is the time interval in seconds after arrival over which the dose estimate is desired.

For more complex rates of removal, such as a power function, similar integrations over time may be carried out, but the resulting integrals will probably not be as easily solved and tables of integrals or numerical solutions may be needed.

7-5.4 Protection by Structures

The computational methods presented have assumed that the receptor is in the open, usually in the center of a large flat plain. In most cases there will be some reduction of dose if the receptor is in a building. Although the integrals for estimating the dose received inside a building have not been evaluated exactly, some estimates of the protection factor expected can be obtained by assuming simple geometrical conditions for which analytical solutions can be found. The following methods of estimating the protection factors afforded by structures have been developed from methods suggested by Decker (1964).

7-5.4.1 Cloud Gamma Dose. A structure can provide protection both by the geometrical effect of limiting the distance of approach of the cloud and by shielding afforded by the walls. For geometrical protection it is assumed that the radioactive material does not enter the building (see, however, Sec. 7-5.4.3).

A rough estimate of the protection factor afforded by various structures can be obtained by assuming the cloud to be hemispherical in shape and uniform in concentration throughout and by using a hemisphere of radius a to approximate the building. Under these conditions the dose rate in the building will be given by

$$ {}_{\gamma}D' = (\text{constant})\ B_x \exp\ (-\mu_x w) \times \int_a^{r_1} \frac{(1 + k\mu r) \exp\ (-\mu r) 2\pi r^2}{4\pi r^2}\ dr \qquad (7.74) $$

where w = thickness of shielding afforded by building walls (g/cm^2)
μ_x = mass absorption coefficient for wall material (cm^2/g)
r = distance from receptor to elemental cloud volume (cm)
r_1 = cloud radius (m)
a = building radius (m)
μ = absorption coefficient for air (Fig. 7.8) (cm^2/g)
B_x = dose buildup factor (dimensionless)
constant = dose-rate conversion factor

The dose buildup factor is that appropriate for the shielding material and the energies and directions of radiation falling on the shield.

Integrating Eq. 7.74 and substituting $B_x = (1 + k_x \mu_x w)$ gives

$$ {}_{\gamma}D' = \frac{\text{constant}}{2\mu} (1 + k_x\mu_x w) \exp\ (-\mu_x w) [\exp\ (-\mu a) - \exp\ (-\mu r_1) - k(1 + \mu r_1) \exp\ (\mu r_1) + k\ (1 + \mu a) \exp\ (-\mu a)] \qquad (7.75) $$

If the building is not present, a and w equal zero, and Eq. 7.75 becomes

$$ {}_{\gamma}D' = \frac{\text{constant}}{2\mu} [1 - \exp\ (-\mu r_1) - k(1 + \mu r_1) \times \exp\ (-\mu r_1) + k] \qquad (7.76) $$

The protection factor (P.F.) provided by the building is then the ratio of Eqs. 7.75 and 7.76

$$\text{P.F.} = (1 + k_x \mu_x w) \exp(-\mu_x w) \times \left\{ [\exp(-\mu a) - \exp(-\mu r_1) - k(1 + \mu r_1) \times \exp(-\mu r_1) + k(1 + \mu a) \exp(-\mu a)] \times [1 - \exp(-\mu r_1) - k(1 + \mu r_1) \exp(-\mu r_1) + k]^{-1} \right\} \quad (7.77)$$

The term in the braces, $\{\}$, expresses the protection factor from the geometrical considerations, whereas the term outside the braces expresses the shielding factor. These two factors have been evaluated separately.

Figure 7.29 presents the geometric protection factor for buildings up to 50 m in effective radius and for clouds both infinite in extent and with a radius of 100 m. (Note that the 50-m building occupies 12.5% of the 100-m radius cloud; no correction was made for this.) It is apparent that the geometrical protection is insignificant for most residential buildings in a very large cloud but becomes somewhat more important as the cloud becomes smaller.

The values given in Fig. 7.29 are for an individual in the center of the building. If he is against one wall, the reduction in dose would be approximately one-half the reduction for a hemisphere twice as large. Thus, from Fig. 7.29, the reduction factor in the center of a 10-m-radius building for an infinite cloud is 0.96. If the receptor were against one wall, the reduction would be one-half that for a 20-m building, or $1.0 - 0.075/2 = 0.963$.

The shielding effectiveness was evaluated with the mass absorption coefficient for most construction materials considered to be about the same as that of air for the energies of interest. The mass absorption coefficients are given in Table 7.8 for materials and elements commonly used in construction (Wyckoff, 1959).

The attenuation through various thicknesses of material expressed as the dimensionless quantity μw was calculated from

$$\text{P.F.} = B_x \exp(-\mu_x w) \quad (7.78)$$

where B_x is the buildup factor for radiation passing through a thickness w of a material with an absorption coefficient μ_x. The factor B_x varies with the energy of the radiation, the atomic number of the shielding material, and the direction of the radiation falling on the shield. Figures 7.30 and 7.31 illustrate the buildup factors for various thicknesses of water, aluminum, and iron for 0.5- and 2.0-Mev photons originating as a point source and as a plane monodirectional source. The value for a point source in air as computed by $(1 + k\mu w)$ is given for comparison. In the present problem one would expect the source to be between the point source and the monodirectional plane source with a fraction of the photons falling on the shield degraded in energy to a value below that of the initial energy.

In view of these factors and the simplifying assumptions already made, the buildup factor for air was used in estimating the shielding-protection factor. This will underestimate the protection factor for low-shielding thickness of high atomic numbers but may overestimate it for thicker structures of low atomic numbers.

Figure 7.32 gives the protection factors for various thicknesses of shields for 0.3-, 0.7-, and 2-Mev gamma photons. For illustration, a building with 8-in.-thick brick walls and roof would have a shielding thickness of about 20 cm. For brick with a density of 1.9, the shielding mass thickness would be 38 g/cm^2. For 0.7-Mev

Table 7.8— MASS ABSORPTION COEFFICIENTS FOR AIR AND ELEMENTS FOUND IN CONSTRUCTION MATERIALS

Energy, Mev	Mass absorption coefficients, μ_x, cm^2/g						
	Air	Concrete	Iron	Calcium	Silicon	Aluminum	Oxygen
0.1	0.151	0.169	0.344	0.238	0.172	0.161	0.151
0.3	0.106	0.107	0.106	0.109	0.107	0.103	0.107
0.5	0.0868	0.0870	0.0828	0.0876	0.0869	0.0840	0.0870
0.6	0.0804	0.0804	0.0762	0.0809	0.0802	0.0777	0.0806
0.8	0.0706	0.0706	0.0664	0.0708	0.0706	0.0683	0.0708
1.0	0.0635	0.0635	0.0595	0.0634	0.0635	0.0614	0.0636
1.5	0.0517	0.0517	0.0485	0.0518	0.0517	0.0500	0.0518
2.0	0.0445	0.0445	0.0424	0.0451	0.0447	0.0423	0.0445

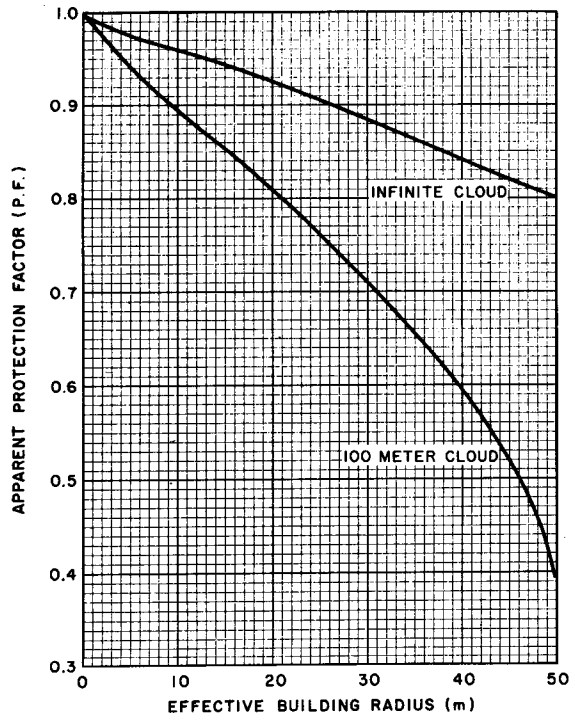

Fig. 7.29 — Apparent dose reduction (protection factor, P. F.) afforded by the geometrical configuration of buildings.

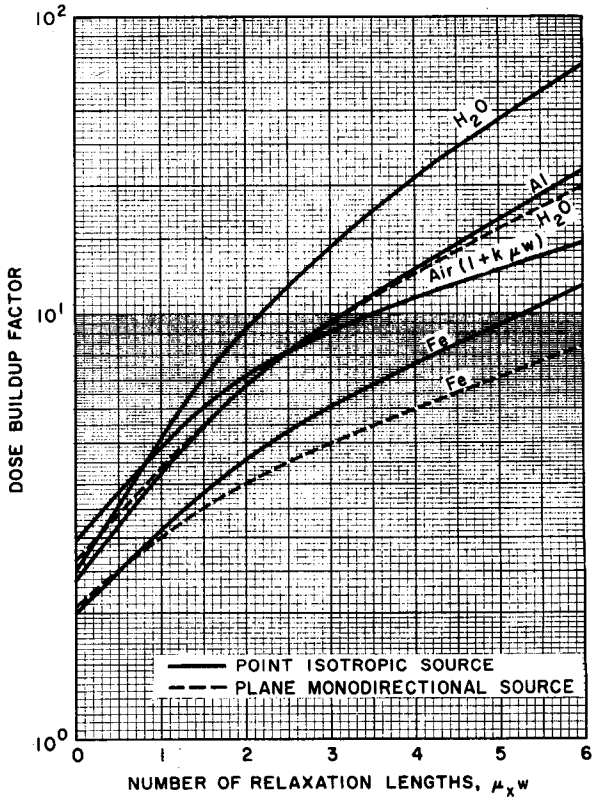

Fig. 7.30 — Buildup factors for 0.5-Mev gamma radiation.

gamma photons, with an absorption coefficient of 0.075 cm^2/g the thickness in μw units would be 2.85 or the estimated protection factor from shielding would be about 0.33. For buildings of lighter construction, such as most wooden residences, the shielding is negligible.

Most buildings have relatively thin roofs; so the shielding from material overhead is negligible. The overall protection factor can be estimated by considering the fraction of the solid angle subtended by the roof and the walls and applying the appropriate shielding and geometrical corrections. Figure 7.33 gives the fraction of a hemisphere which is subtended by the roof for buildings of the given ratio of effective diameter to height.

From these data one can estimate the order of magnitude of dose reduction expected according to structure. For the usual wooden residence, about 20 by 20 by 10 m, only the geometric factor would be of any significance. From Fig. 7.29 this would amount to 93% to 94% of the outside dose for an individual in the center of the ground floor. If the walls are of 8-in.-thick brick, about 70% of the solid angle would be shielded and about 30% open (Fig. 7.33). Thus in an infinite cloud an individual in the center of the first floor would be exposed to 0.93 $(0.7 \times 0.33 + 0.3) = 0.5$ of the cloud dose outside the building. If the individual were on the second floor halfway up the building (diameter/height ratio = 4), the angle subtended by the roof would be 0.55, and his protection factor would be 0.93 $(0.45 \times 0.33 + 0.55) = 0.65$. Actually the geometric protection factor would not be as great as 0.93 in the latter case because the effective radius is smaller. If the individual were directly under the roof, the building would offer little or no protection. As a further illustration, the protection factor offered in the center of the ground floor of a large industrial building 100 by 100 by 20 m with 8-in.-thick brick walls against a large cloud emitting 0.7-Mev photons would be [assuming a geometrical protection factor of 0.86 (35-m radius) and a roof fraction of 0.63]

$$P.F. = 0.86\ (0.37 \times 0.33 + 0.63) = 0.65$$

In addition, the presence of floors or equipment would increase the protection factor.

The foregoing methods lay no claim to accuracy, but they do illustrate the approximate protection available from a passing cloud. Except for small clouds it appears that the ordinary residence provides little reduction in dose and that for large clouds only massive buildings with complete shielding are effective.

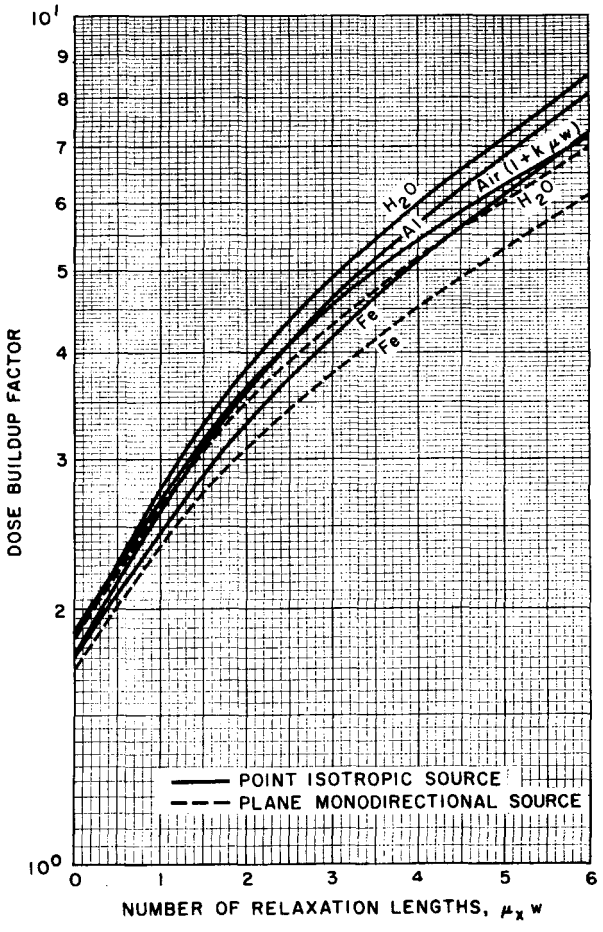

Fig. 7.31—Buildup factors for 2.0-Mev gamma radiation.

7-5.4.2 Radiation from Deposited Materials. The radiation dose rate at a height b above a uniformly contaminated area is given by Eq. 7.65a. If the building provides a clean area around the receptor of radius a (m), the dose rate from the material outside the clean area is given in units of rads per second by

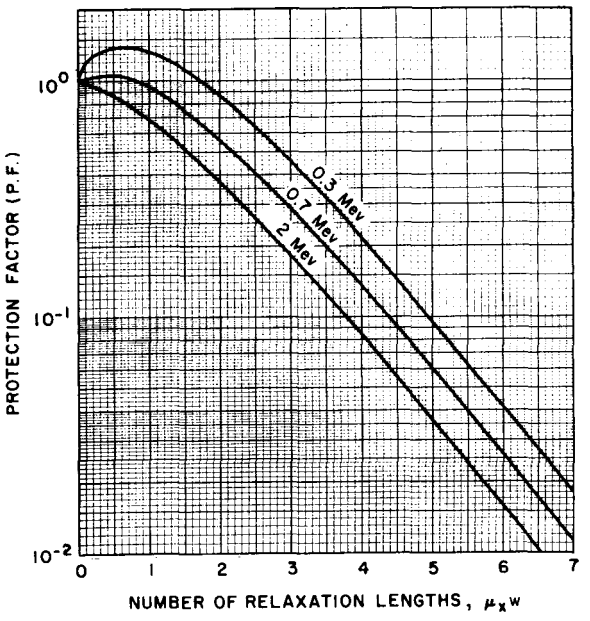

Fig. 7.32—Shielding protection factors.

$$_{\gamma}D' = 0.254\ \omega\bar{E}_{\gamma}\mu_a \left[E_i\ (\mu\sqrt{a^2+b^2}) + \frac{k}{2}\exp\ (-\mu\sqrt{a^2+b^2})\right] \quad (7.79)$$

The ratio of Eq. 7.79 to Eq. 7.65a then gives the geometrical protection factor

$$P.F. = \frac{E_i\ (\mu\sqrt{a^2+b^2}) + (k/2)\exp\ (-\mu\sqrt{a^2+b^2})}{E_i\ (\mu a) + (k/2)\exp\ (-\mu a)} \quad (7.80)$$

Figure 7.34 presents the reduction in dose at 1 m above grade and at 4 m above grade as compared to the dose 1 m above an infinite plane contaminated to a uniform level with radioactive materials emitting 0.7-Mev gamma rays. It can be seen that the reduction in dose on the second floor of an unshielded building is negligible.

This treatment ignores any deposition on the roof and sides of the building and the resulting radiation dose. This dose can be approximated by considering the roof to be a disk source at a distance b_1 meters from the receptor. If the shielding of the roof and floor materials is ignored, this dose rate is given by

$$_{\gamma}D' = 0.254\ \omega\bar{E}_{\gamma}\mu_a \left[E_i\ (\mu b_1) - E_i\ (\mu\sqrt{b_1^2+a^2}) + \frac{k}{2}\exp\ (-\mu b_1) - \frac{k}{2}\exp\ (-\mu\sqrt{b_1^2+a^2})\right] \quad (7.81)$$

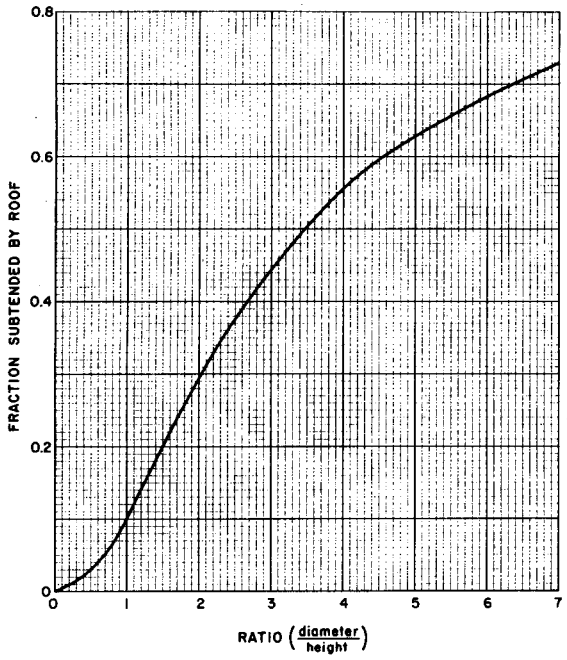

Fig. 7.33 — Fraction of hemisphere subtended by roof of building with various ratios of diameter to height.

where a is the diameter of the roof. The ratio of Eq. 7.81 to Eq. 7.65a will give the geometrical protection factor.

$$\text{P.F.} = \left[E_i(\mu b_1) - E_i\left(\mu\sqrt{b_1^2 + a^2}\right) + \frac{k}{2}\exp(-\mu b_1) - \frac{k}{2}\exp\left(-\mu\sqrt{b_1^2 + a^2}\right)\right] \times \left[E_i(\mu b) + \frac{k}{2}\exp(-\mu b)\right]^{-1} \quad (7.82)$$

Equation 7.82 was solved with account taken of the ratio of the dose received at various distances from the roof to the dose received 1 m above a uniformly contaminated infinite plane emitting 0.7-Mev gamma rays. These results are given in Fig. 7.35.

For an illustration of the protection afforded, consider a wood frame house 20 m square and 10 m high. From Fig. 7.34 the dose at the center of the ground floor will be about 40% of the infinite plane dose. At the ground floor the roof is 10 m away with a diameter of 20 m. From Fig. 7.35 this will contribute an additional 7% for a total of 47%. On the second floor where the roof is 3 to 5 m away, the roof will contribute 20%, and the dose from the sourrounding

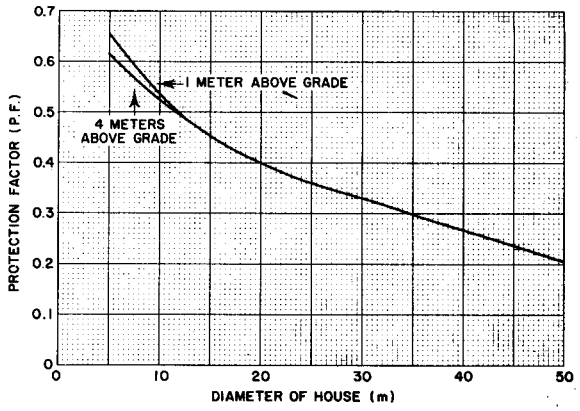

Fig. 7.34 — Geometrical protection from ground deposit of 0.7-Mev gamma radiation.

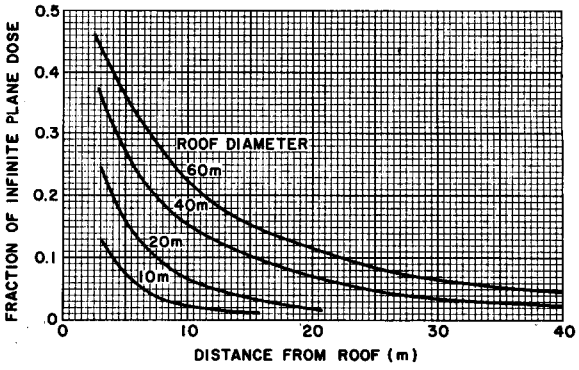

Fig. 7.35 — Radiation received from deposit on roof given as a fraction of dose at 1 m above an infinite plane for 0.7-Mev gamma radiation.

area is about the same. For this floor the protection factor drops to about 60% of the dose 1 m above an infinite plane. These calculations assume that the roof is contaminated to the same level as the surrounding area and that no radioactive material is adhering to the walls.

If the same house is made of 8-in.-thick brick, the radiation from the ground outside is reduced by a factor of 0.33 from Fig. 7.32, and the protection factor becomes about 0.2 on the ground floor and about 0.33 on the second floor.

7-5.4.3 Contamination Inside a Building. The previous geometrical protection factors are based upon the assumption that the building provides a noncontaminated area or volume around the individual. Most buildings unless specifically designed to be airtight have changes of air from leaks in the structure resulting from pressure

differences caused by wind velocities or by temperature differences in heated buildings. If windows or doors are open, interchange of air with the outside can be relatively rapid.

If a building is surrounded by a cloud of average concentration $\bar{\chi}$, the amount of activity, dq, entering is given by

$$dq = V\bar{\chi}dt - \frac{Vq}{s}dt \tag{7.83}$$

where V is the ventilation rate in cubic meters per time interval and s is the volume of the building (q/s is the concentration in the building). This equation assumes that the activity entering is uniformly mixed through the building upon entry. Solving Eq. 7.83 and using the condition that $q/s = 0$ at zero time gives the concentration in the building as

$$\frac{q}{s} = \bar{\chi}\left[1 - \exp\left(-\frac{V}{s}t\right)\right] \tag{7.84}$$

If V/s is one change per hour (a reasonably tight building with low winds), the concentration inside will build to 10% of that outside in 6 min, to 50% in 40 min, and to 90% in 2.3 hr. If $V/s = 6$, the concentration inside will build to 10% of that outside in 1 min, to 50% in 7 min, and to 90% in 23 min.

Since the total dose received depends upon the integral of the concentration vs. time curve, it is of interest to compare this integral inside the building with that outside for a transient cloud. If the time of cloud passage is taken as t_1 (with the time of cloud arrival as t_0), then the integrated concentration is given by

$$\left(\frac{q}{s}\right)_f = \int_0^{t_1} \bar{\chi}\left[1 - \exp\left(-\frac{V}{s}t\right)\right]dt + \int_0^{\infty} \left(\frac{q}{s}\right)_{t_1} \exp\left(-\frac{\eta V}{s}t\right)dt \tag{7.85}$$

where $(q/s)_{t_1}$ is the concentration in the building after the cloud passage. The ventilation rate after cloud passage is taken as $\eta V/s$, where η is a factor describing possible changes in the ventilation rate due to changes in wind speed or to deliberate actions, such as opening windows or turning on ventilation.

Solving and substituting for (q/s) at t_1 from Eq. 7.84 gives

$$\left(\frac{q}{s}\right)_f = \bar{\chi}\left\{t_1 - \frac{s}{V} \times \left[1 - \exp\left(-\frac{V}{s}t_1\right)\right]\left(1 - \frac{1}{\eta}\right)\right\} \tag{7.86}$$

Note that if the ventilation rate remains the same, $\eta = 1$, the integral concentration inside becomes $\bar{\chi}t_1$ *which is the same as that outside.* If the ventilation rate decreases (as, for example, by diminishing wind speed), the integral concentration inside is *greater than the concentration time integral outside.* Equation 7.86 indicates that a defensive measure against a transient cloud would consist in closing window and doors and sealing cracks during cloud passage and then increasing the ventilation rate as rapidly as possible after the cloud passage. This may be impractical since it depends upon a knowledge of the exact time of cloud arrival and the exact time when the bulk of the cloud has passed.

In practice the concentration inside may be lower than outside, depending upon the physical and chemical characteristics of the contaminant, since the incoming air as it passes through narrow cracks or small holes may deposit some materials because of inertial forces or chemical affinity. Note that in this case there will be localized areas of higher surface contamination. Megaw (1962), for example, measured the concentrations of ^{132}I as vapor inside and outside a hut with ventilation rates of 1.8 to 5.5 changes per hour and found integral concentrations inside ranging from about 20% to 70% of those outside. When the windows were open at one end of the hut, the ventilation rate increased to 5 to 8 changes per hour, and the integral concentrations inside were about 70% of those outside. Iodine vapor is known as a very strong depositing material; so the influence of deposition mechanisms would be expected to be strong.

Megaw also studied the penetration into the same hut of Aitken nuclei produced by burning paraffin-soaked sand. For ventilation rates ranging from 0.8 to 2.5 changes per hour, the integral concentrations inside ranged from 34% to 78% of those outside.

Although the above treatment indicates that high concentrations inside the building are possible, it is expected that the deposition inside buildings will be considerably less than that outside, both due to lower turbulence levels in-

side and due to the restriction on the source by the limited rate of entry to the building. The experiments by Megaw again confirm this expectation since the deposition inside was only a few percent of that outside. The deposition velocity outside ranged from 0.3 to 3.1 cm/sec and that inside ranged from 0.1 to 0.24 cm/sec.

7-6 DOSE FROM INHALED MATERIALS

Inhaling radioactive materials can result in radiation doses to (1) the lungs and upper respiratory tract from isotopes deposited in the passages, (2) the gastrointestinal tract (GI tract) from isotopes originally deposited in the respiratory tract and later removed by ciliary action and swallowed, and (3) other organs in which the isotopes may be deposited after they are absorbed into the bloodstream from either the lung or GI tract.

The radiation dose to each organ will depend upon the physical and chemical characteristics of the radionuclides in the cloud and the distribution and retention of these materials in the body. In general, the physical and chemical characteristics of the routine radioactive wastes normally emitted from a facility can be determined with reasonable accuracy, but the materials from an accidental release will not be well characterized in advance. Even with accurate characterization the metabolic parameters involved, such as retention in the lung, solubility in body fluids, and translocation to other organs, are not known well enough to do more than provide an estimate of the radiation dose involved. The primary mathematical models and parameters for the calculation of the doses from these internal sources has been set by the Internal Dose Subcommittees of the National Committee on Radiation Protection (National Committee on Radiation Protection and Measurement, 1959) and the International Commission on Radiological Protection (International Commission on Radiological Protection, 1959a).

7-6.1 Intake, Retention, and Translocation of Inhaled Radioactive Materials

The total amount of radioactive material inhaled by a person during cloud passage is determined by the product of the cloud concentration time integral ψ (curie sec/m^3) times the breathing rate B′ (m^3/sec) during cloud passage. Equations for ψ were developed in Chap. 3, and modifications to incorporate the effect of radioactive decay were developed earlier in this chapter.

The breathing rate for the standard man is given as 10 m^3/8-hr work day and 20 m^3/24-hr day. These are 3.48×10^{-4} m^3/sec and 2.31×10^{-4} m^3/sec, respectively. During times of extreme stress the breathing rate can be greater, and a breathing rate of 5×10^{-4} m^3/sec is frequently assumed for relatively short periods of time. The breathing rate selected depends upon the details of the situation considered.

Two biological factors are of importance in assessing the overall dose to the lung: the fraction of the inhaled material that is deposited and the time interval during which the deposited material is retained in the lung. The deposition and site of deposition, whether in the upper or lower pulmonary tract, will vary with particle size, shape, and density. Different amounts and different patterns of deposition will occur, depending upon whether an individual breathes through his nose or his mouth. The time of retention in the lung will depend upon the site of deposition and the solubility of the material in body fluids. Material deposited in the upper respiratory tract will be quickly cleared by ciliary action; that deposited deep in the lung will be removed primarily by solution into the bloodstream or, in some cases, by transfer of the particle across the lung alveoli. Standard assumptions concerning the fate of soluble and insoluble radioactive particles in the lung have been made by the ICRP (International Commission on Radiological Protection, 1959a) to facilitate dose estimates. These assumptions, which are given in Table 7.3, should be used only when specific data on the particular material of interest are not available.

As indicated in Table 7.3 inhaled material that is soluble in body fluids will be translocated via the GI tract and through the blood stream to other organs. The fraction of a soluble radionuclide which is translocated to the critical organ (generally the body organ that subsequently receives the highest dose from the material) is given by

$$f_a = (0.25 + 0.5\, f_1) f_2' \qquad (7.87)$$

where f_a is the fraction of a soluble radionuclide which is translocated to a critical organ, f_1 is the fraction of the radionuclide passing from the gastrointestinal tract to the blood, and f_2' is the fraction of radionuclide passing from the blood to the critical body organ.

When f_2' is not known, it is generally replaced by f_2, the fraction of the total body radionuclide burden in the critical organ.

When the material inhaled is either insoluble or slightly soluble, a portion of the GI tract or the lung is usually the critical organ. When better data for the inhalation of specific radioactive insoluble dust particles is not available, the value of f_a is assumed to be 0.12 in the case of the lungs. Some of the inhaled radioactive material is swallowed and irradiates the GI tract. If a portion of the GI tract is the critical tissue, the value of f_a is given as 0.62 for insoluble material and 0.5 for soluble material. Values of the various biological factors have been tabulated by the ICRP (International Commission on Radiological Protection, 1959a).

Although in many instances it is difficult to predict the biological fate of the source material released from a facility, radioiodine in most forms will be quickly absorbed from the lungs into the blood stream and translocated to the thyroid. The noble gases do not enter into the body metabolism but may be dissolved to some extent in body fluids or fat. Since the physical and chemical characteristics of the particles are generally unknown, the common practice is to make two dose calculations: one based on the assumption that the radioactive material is soluble and the other based upon the assumption that the material is insoluble.

7-6.2 Dose to a Body Organ from Internal Radiation

The dose rate to any body organ from internal irradiation is given by

$$D' = (qf_2)\frac{(3.7\times10^{10})\,\bar{E}\,(1.6\times10^{-6})}{100\,M}$$

$$= 5.92\times10^{2}\,(qf_2)\frac{\bar{E}}{M} \qquad (7.88)$$

where D' = dose rate to the organ from internal irradiation (rad/sec)
M = mass of the organ (g)
q = total quantity of radioactive material in the total body (curie)
f_2 = fraction of the total body radionuclide burden in the critical organ
qf_2 = quantity of radioactive material in the critical organ (curie)
3.7×10^{10} = disintegration rate (dis/sec) for 1 curie
$\bar{E}$ = energy absorbed in the organ from one disintegration (Mev)
1.6×10^{-6} = number of ergs per Mev
100 = number of ergs per gram per rad

The values of $\bar{E}$, the average energy absorbed in the organ per disintegration, can be taken as equal to the average energy released per disintegration for alpha and beta emitters because the ranges of these particles are small compared to the organ dimensions. For this reason nearly all the energy is released in the organ containing the radioactive material. For beta particles the average energy can be assumed to be one-third of the maximum energy, and the resulting error will be well within other uncertainties. If more precise information is needed, measured or calculated values can be found in the literature (Hine and Brownell, 1956). For most gamma photons the range in tissue will be considerably greater than the organ dimensions; so only a portion of the energy released will be absorbed in the organ. This fraction can be estimated by assuming the organ to be approximately spherical. Under these conditions the fraction absorbed will be approximately

$$_a\bar{E}_\gamma = {}_0\bar{E}_\gamma\,[1-\exp(-\mu_a r_0)] \qquad (7.89)$$

where $_a\bar{E}_\gamma$ = the average gamma energy absorbed per disintegration
$_0\bar{E}_\gamma$ = the average gamma energy emitted per disintegration
μ_a = the energy absorption coefficient for the gamma photon energy
r_0 = the effective diameter of the organ

For many of the calculations involving small organs, the gamma contribution to the dose can be neglected if mixed radiation is present. Total values of the average energy absorbed by various organs per disintegration for specific radionuclides are tabulated in the ICRP report (International Commission on Radiological Protection, 1959a).

The dose delivered to an organ by internal irradiation depends upon the retention of the radioactive material in the organ over the time period of concern. For the total dose it is necessary to integrate the quantity of radioactive material in the organ over the period of time of concern with proper allowance for accumulation, radioactive decay, and biological elimination. In the following discussion the intake is assumed to occur in a short time interval, e.g., exposure to a relatively small cloud from a puff release. Subsequently it will be shown that this assumption is not restrictive in most cases.

$$D = 5.92 \times 10^2 \frac{\overline{E}}{M} \int_{t_A}^{t_2} (qf_2)\, dt \qquad (7.90)$$

where D is the dose to the organ (rad), t_A is the time at which the irradiation starts (sec) ($t_A = x/\bar{u}$ for a puff release), and t_2 is the time to which the total dose is to be calculated (sec). (This assumes a negligible transit time for the radionuclide between intake and deposition in the organ.) The value of (qf_2) at a given time after uptake depends upon both the elimination by radioactive decay and the elimination by biological processes.

$$\int_{t_A}^{t_2} (qf_2)\, dt = (qf_2)_0 \int_{t_A}^{t_2} f_R(t)\, f_B(t)\, dt \qquad (7.91)$$

where $(qf_2)_0$ is the quantity of radioactive material in the organ initially (curie), $f_R(t)$ is the function chosen to describe the radioactive decay of the mixture in the organ, and $f_B(t)$ is the function chosen to describe the rate of biological elimination of the mixture from the organ.

In Eq. 7.91, $f_B(t)$ is frequently described by a single exponential function of time. For most radionuclides such an exponential is taken to describe only the long-term elimination with the assumption that the majority of the radiation dose is due to this long component. For many radionuclides the retention may be more accurately described by a series of several exponentials to describe different compartments or by a power function fitted to the retention curve over the period of interest (Healy, 1956).

The value of $f_R(t)$ for a single radionuclide is a single exponential function. For a group of radionuclides, the value of $f_R(t)$ can be represented over some time periods by a power function of the time. The well-known Way–Wigner equation for decay of fission products following a nuclear detonation or critical accident involving a short burst in which the fission products decay as $t^{-1.2}$ is a power function describing the gross decay of the mixture (Way and Wigner, 1948). For very long periods of reactor operation and decay times that are relatively short compared to the time of operation, the gross decay of the fission mixture is frequently approximated as $t^{-0.2}$. For the actual time of operation and fractionation chosen, several power functions can frequently be fitted to the gross-decay curve.

From these combinations of methods for expressing the radioactive decay and the biological elimination, it is possible to produce a number of different methods for calculating the quantity of radioactive material in the organ. The particular function chosen will depend upon the information available and the type of calculation to be performed. If both the retention and the radioactive decay are expressed by a single exponential,

$$\int_{t_A}^{t_2} (qf_2)\, dt = (qf_2)_0 \int_{t_A}^{t_2} [\exp(-\lambda_R t) \times \exp(-\lambda_B t)]\, dt \qquad (7.92)$$

where λ_R is the radioactive decay constant and equals $0.693/T_R$ (1/sec), λ_B is the biological elimination constant and equals $0.693/T_B$ (1/sec), and T_R and T_B are the radioactive and biological half-lives (sec).

Substituting $\tau = (t_2 - t_A)$ and integrating gives

$$\int_0^{\tau} (qf_2)\, dt = \frac{(qf_2)_0}{\lambda_B + \lambda_R} \times \{1 - \exp[-\tau(\lambda_B + \lambda_R)]\} \qquad (7.93)$$

where τ is the time interval for which the cumulative dose is evaluated (sec).

If, compared to the human lifetime, the residence time in the body is short owing to biological elimination or radioactive decay, then the total number of disintegrations in the organ (or dose instead of dose rate when Eq. 7.90 is involved) can be obtained by letting τ equal infinity.

$$\int_0^{\infty} (qf_2)\, dt = \frac{(qf_2)_0}{\lambda_B + \lambda_R} \qquad (7.94)$$

If both the retention and the radioactive decay are described by power functions, the integral can be expressed as

$$\int_{t_A}^{t_2} (qf_2)\, dt = (qf_2)_i \int_0^{\tau} t^{-n} t^{-m}\, dt \qquad (7.95)$$

where n is the slope of the logarithmic plot of radioactivity vs. time, m is the slope of the logarithmic plot of retention vs. time, and $(qf_2)_i$ is the quantity of radioactive material in the critical organ after exposure ceases. In this case

$$\int_{t_A}^{t_2} (qf_2)\, dt = \frac{(qf_2)_i\, \tau^{[1-(n+m)]}}{1-(n+m)} \qquad (7.96)$$

If the radioactive decay is expressed as a power function and the retention as an exponential, then the integral can be expressed as

$$\int_{t_A}^{t_2} (qf_2)\, dt = \int_0^{\tau} t^{-n} \exp(-\lambda_B t)\, dt \qquad (7.97)$$

In Eq. 7.97 the integral reduces to a gamma function if $n < 1$. If τ is taken as infinity, the integral is a complete gamma function. For evaluation of a time interval, τ, less than infinity, the integral is an incomplete gamma function and may be evaluated from Pearson's tables (Pearson, 1951). For values of $n > 1$, the integral must be evaluated by other means.

7-6.2.1 Critical Organ Dose Due to Finite Inhalation Exposure Time. A fraction of the radioactive material inhaled will be absorbed into the blood stream from either the lung or the GI tract and transferred to other organs, e.g., a significant fraction of the radioiodine absorbed into the blood will be deposited in the thyroid and a significant fraction of radiostrontium will be deposited in the bone. Experiments on the inhalation of water-insoluble silver iodide and strontium sulfate have indicated that the translocation process for these materials is as efficient as if the iodine or strontium were present as water-soluble compounds (Willard and Bair, 1958).

For an individual exposed to a uniform concentration of a nuclide for a finite period of time, the change in the quantity of the nuclide in the critical organ during the period of exposure is given by

$$d(qf_2) = B'\overline{\chi} f_a dt - (qf_2)\,\lambda\, dt \qquad (7.98)$$

where B' is the breathing rate (m^3/sec), f_a is the fraction of inhaled material that is translocated to the critical organ, and λ equals $\lambda_R + \lambda_B$ (sec^{-1}).

The cumulative dose in rads from the onset of plume inhalation until the exposure ceases is obtained by integrating the amount in the critical organ over the time of exposure and converting to dose.

$${}_1D = \frac{5.92 \times 10^2 \overline{E}}{M\lambda} f_a B' \overline{\chi}_{(x,y,0)} \times \left[\tau - \frac{1 - \exp(-\lambda\tau)}{\lambda}\right] \qquad (7.99)$$

where ${}_1D$ is the dose from onset of plume inhalation until exposure ceases (rad) and τ is time interval of exposure (sec).

If the exposure to the plume ceases after the time interval of τ seconds, the irradiation of the critical organ will continue owing to the burden in the critical organ at that time. The dose received in the time interval of τ_1 seconds immediately following the exposure is obtained by substituting the body burden at the end of the exposure period into Eq. 7.88 and integrating.

$${}_2D = \frac{5.92 \times 10^2\, \overline{E}}{M\lambda^2} f_a B'\, \overline{\chi}_{(x,y,0)} \times [1 - \exp(-\lambda\tau)]\,[1 - \exp(-\lambda\tau_1)] \qquad (7.100)$$

where ${}_2D$ is the dose received in time interval following exposure (rad) and τ_1 is the time interval following exposure (sec). The total cumulative dose delivered from the time that exposure to the plume started until some time after the end of exposure, i.e., $T = (\tau + \tau_1)$ seconds, is the sum ${}_1D + {}_2D$ (rads).

$$D_{co} = \frac{5.92 \times 10^2\, \overline{E}}{M\lambda^2} f_a B'\, \overline{\chi}_{(x,y,0)} \{\lambda\tau - \exp(-\lambda\tau_1) + \exp[-\lambda(\tau + \tau_1)]\} \qquad (7.101)$$

where D_{co} is the cumulative dose from the beginning of exposure to the plume until some time after the end of exposure (rad).

There is one observation concerning this development that deserves special consideration. When the irradiation time τ_1 (time interval after cloud exposure) is long compared to the effective half-life of the radioactive material, i.e.,

$\lambda\tau_1 \rightarrow \infty$, the total dose to the critical organ is given

$$_{\infty}D_{co} = \frac{5.92 \times 10^2\ \overline{E}}{M\lambda} f_a B' \psi_{(x,y,0)} \quad (7.102)$$

where $_{\infty}D_{co}$ is the total dose when irradiation time is long compared to half-life (rad) and $\psi_{(x,y,0)}$ equals $\overline{\chi}_{(x,y,0)}\tau$. The total dose (dose commitment) to the critical organ depends upon the amount of radioactive material inhaled without regard to the time required to inhale the amount.

7-6.2.2 Lung Dose. When the radioactive material inhaled is insoluble and the other characteristics of the material are unknown, the ICRP values for the standard man are used (see Table 7.3). In the following development for a short exposure time, a breathing rate of 5×10^{-4} m^3/sec (30 liters/min) will be used. This is higher than the breathing rate of the standard man to allow for a heightened respiratory rate during periods of exertion.

The quantity of insoluble material (in curies) deposited in the lungs immediately after cloud passage is given by

$$(qf_2)_0 = (5 \times 10^{-4})\ (0.25)\ \psi_{(x,y,0)} = 1.25 \times 10^{-4}\ \psi_{(x,y,0)} \quad (7.103)$$

where 5×10^{-4} is the breathing rate (m^3/sec).

The ICRP standard man allows for a decrease of 50% in the lung burden in the first day but does not specify the rate of this decrease or the form of the function. It will be arbitrarily assumed that the lung burden consists of two components, each consisting initially of 12.5% of the amount inhaled (to give a total initial retention of 25%). The long-lived component is eliminated with a half-life of 120 days; the short-lived component is eliminated with a half-life such that only about 1% of the initial quantity is present at the end of 1 day (T_B = 4 hr). Note that there will be additional exposure not accounted for in these equations from the radioactive material deposited in the nasal passages and the upper bronchi. Since this material will be removed rather rapidly by ciliary action and swallowed, the total dose received by these organs is taken to be less than the dose received by the lung.

It should be recognized that the preceding assumptions concerning the behavior of material in the lung represent a standardized model that is valuable for estimating the order of magnitude of the expected dose. Under some circumstances the deposition in the areas of the bronchi where the air flow changes direction can result in localized doses that are higher than the average dose to the lung. This is recognized as an important factor in the long-term exposure to the relatively short-lived daughters of radon among uranium miners.

There is some concern about the possible effects of one or a few intensely radioactive particles that may penetrate to the lung. Although the total quantity of radioactive material carried by this mechanism may be small enough so that the dose averaged over the entire lung appears insignificant, the actual dose in the immediate vicinity of these few particles may be very high (National Academy of Science–National Research Council, 1961). At the present time it is not possible to state whether these particles represent a greater or a smaller hazard than the same amount of material uniformly distributed through the lung. It may also be noted that defects in the ciliary mechanism may permit a particle to be retained in the upper respiratory tract and, perhaps, produce localized damage. Such defects do occur in a reasonable proportion of the populace. There is also considerable evidence that the transfer of particulate material to the lymph nodes results in a very high concentration in a relatively small mass of tissue (Thomas, 1965). Although available evidence would not justify basing damage estimates on the dose to the lymphatic system, neither can the dose to the lymphatic system be ignored.

The total retention in the lung can then be written as the sum of two exponentials

$$(qf_2) = (qf_2)_0\ [\exp(-\lambda_1 t) + \exp(-\lambda_2 t)]\ f_R(t) \quad (7.104)$$

where t = time interval since inhalation (sec)

λ_1 = elimination constant of the short component ($0.693/4$ hr^{-1}) = 4.8×10^{-5} sec^{-1}

λ_2 = elimination constant of the long component ($0.693/120 \times 24$ hr^{-1}) = 6.7×10^{-8} sec^{-1}

$f_R(t)$ = radioactive decay function

For individual radionuclides that decay by a single exponential, the total dose to the lung is then given by combining Eqs. 7.88, 7.92, 7.103, and 7.104 and allowing 50% of the material from Eq. 7.104 in each component.

$$D_L = \frac{\bar{E}\psi_{(x,y,0)}}{M}\left\{\frac{3.7\times10^{-2}}{\lambda_R+\lambda_1}[1-\exp-(\lambda_R+\lambda_1)\tau] + \frac{3.7\times10^{-2}}{\lambda_R+\lambda_2}[1-\exp-(\lambda_R+\lambda_2)\tau]\right\} \quad (7.105)$$

where D_L is the total dose to the lung (rad), τ is the time interval after cloud arrival over which the cumulative lung dose is desired (sec), and M is the mass of lung (g).

Equations 7.88, 7.97, 7.103, and 7.104 can be used to calculate the dose when the radioactive decay of the gross mixture of radioactive materials is described by a power function.

$$D_L = \frac{3.7\times10^{-2}\,\bar{E}\psi_{(x,y,0)}}{M}\left[\int_0^{t_2} t^{-n}\exp(-\lambda_1 t)\,dt + \int_0^{t_2} t^{-n}\exp(-\lambda_2 t)\,dt\right] \quad (7.106)$$

7-6.2.3 Dose to the Gastrointestinal Tract from Inhalation of Insoluble Radioactive Materials. ICRP standard man model is given in Table 7.3. When insoluble radioactive material is inhaled, 62.5% of the material is eliminated through the GI tract (50% deposited in the upper respiratory tract and later swallowed, plus one-half of the 25% initially deposited in the lungs). The 62.5% eliminated through the GI tract clears the respiratory system in 24 hr. If the exact rate of elimination from the respiratory system were defined, the dose to various portions of the GI tract could be obtained by integrating the dose rate over the time of passage through any portion of the GI tract. The mass content and residence time for various portions of the GI tract are given in Table 7.3 (International Commission on Radiological Protection, 1959a). The portion of the GI tract that receives the maximum dose will obviously depend upon the specific biological removal model assumed for the lung and the radiological half-life of the radioactive material. If the radioactive half-life of the material is relatively long, the dose to the lower large intestine (LLI) will be controlling because of the longer residence time in that portion. For short-lived material the greater dose may be received by the upper portions of the GI tract.

Since the exact model for the clearing of material from the respiratory system is not given, a number of calculational methods are possible. For the purpose of demonstrating a calculational technique, it will be assumed that the clearing will be exponential with a biological half-life of 4 hr. A single radionuclide will be considered, and the inhalation will be assumed to occur over a short period of time.

The amount of insoluble radioactive material inhaled and initially deposited in the respiratory system is given in curies by

$$(qf_2)_0 = 0.75\,B'\psi_{(x,y,0)} \quad (7.107)$$

The amount of material subject to removal via the GI tract is

$$(qf_2)_1 = 0.625\,B'\psi_{(x,y,0)} \quad (7.108)$$

The amount of material in this component remaining in the respiratory system is given by

$$(qf_2)_2 = 0.625\,B'\psi_{(x,y,0)}\exp(-\lambda t) \quad (7.109)$$

where λ equals $\lambda_B + \lambda_R$, λ_B is the biological elimination constant, and t is the time interval after intake by inhalation (sec). (Note that when $T_B = 4$ hr and $\lambda_B = 4.81\times10^{-5}$ sec^{-1} virtually all of the material is removed from the respiratory system in 24 hr. Figure 7.36 may be helpful in following this development. It indicates the quantity of material in various locations as a function of time, but, for simplicity, the decay corrections are not shown.) The total amount of material (in curies) swallowed in the time interval t is

$$(qf_2)_s = 0.625\,B'\psi_{(x,y,0)}[1-\exp(-\lambda t)] \quad (7.110)$$

Since this component is insoluble in body fluids, the quantity that entered the lower large intestine (LLI) will be the amount swallowed corrected for radioactive decay en route, i.e., 13 hr,

$$(qf_2)_{LLI} = 0.625\,B'\psi_{(x,y,0)}\exp(-4.67\times10^4\,\lambda_R)\times[1-\exp(-\lambda\tau)] \quad (7.111)$$

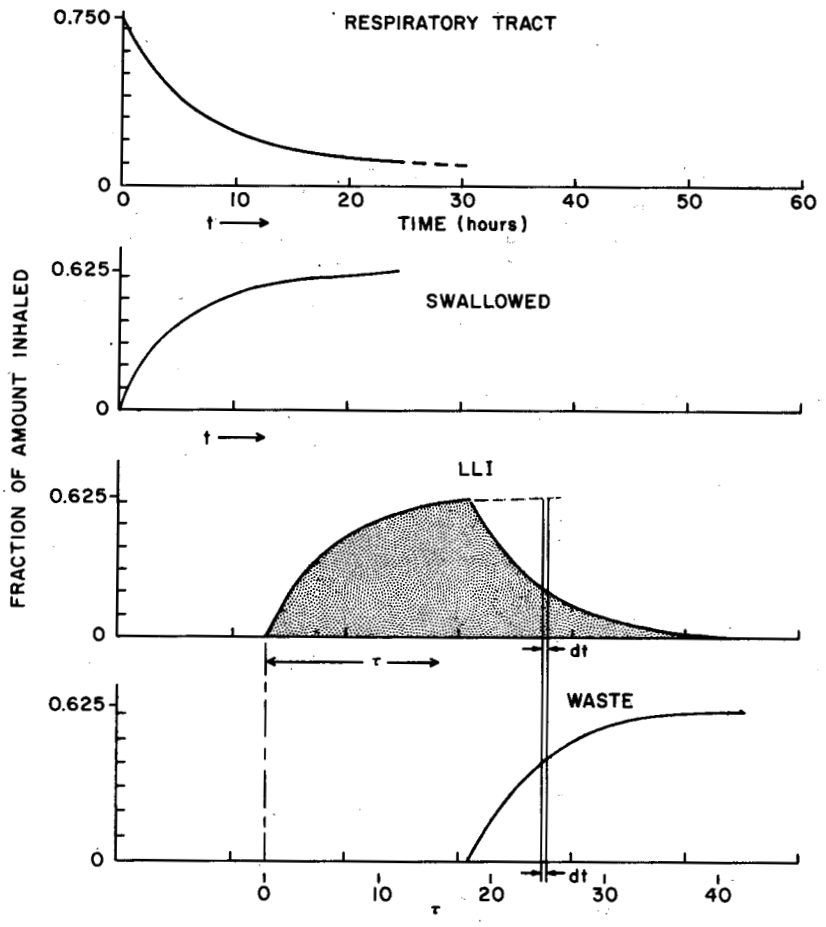

Fig. 7.36—Reference system for GI-tract dose considerations for inhaled insoluble materials.

where τ is the time interval (sec) after material enters LLI.

Material entering the LLI is retained 18 hr; therefore, if a continuous elimination is assumed, the amount in curies eliminated is given by

$$(qf_2)_{\text{Elim.}} = 0.625\ B'\psi_{(x,y,0)}\ \exp(-6.48\times10^4\,\lambda_R) \times\{1-\exp[-(\tau-6.48\times10^4)\lambda]\} \quad (7.112)$$

where $\tau \geq 6.48\times10^4$ sec. The amount in the LLI is obtained by subtracting Eq. 7.112 from Eq. 7.111 to give

$$(qf_2)_{LLI} = 0.625\ B'\psi_{(x,y,0)}\left(\exp(-4.67\times10^4\,\lambda_R) \times[1-\exp(-\lambda\tau)] - \exp(-6.48\times10^4\,\lambda_R) \times\{1-\exp[-(\tau-6.48\times10^4)\lambda]\}\right) \quad (7.113)$$

Integrating Eq. 7.113 with respect to time gives

$$\int_0^\infty (qf_2)_{LLI}\ dt = 4.05\times10^4\ B'\psi_{(x,y,0)} \times[\exp(-4.67\times10^4\,\lambda_R) - \exp(-6.48\times10^4\,\lambda_R)] \quad (7.114)$$

where $t \geq 50$ hours, $\tau \to \infty$, and the result is in terms of curie seconds.

The dose to the LLI from inhalation can be calculated by substituting Eq. 7.114 into Eq. 7.88.

$$D_{LLI} = \int_0^\infty D'\ dt = 5.92\times10^2\ \frac{\overline{E}}{\overline{M}} \times\int_0^\infty (qf_2)_{LLI}\ dt \quad (7.115)$$

$$D_{LLI} = 1.97\ \overline{E}\int_0^\infty (qf_2)_{LLI}\ dt \quad (7.115a)$$

where M = 150 g (content of LLI) and irradiation of the intestine walls is assumed to occur from one side only (0.5 geometry). As stated at the onset, this is but one method of solution and is intended only as a point of departure for better calculational methods.

7-7 DOSE FROM INGESTED MATERIALS

The deposition of radioactive materials from the atmosphere can result in general contamination of an area so that, in addition to the direct radiation, radiation can be received from the later ingestion of water or of foodstuffs grown in the area. This type exposure is often the one that provides the lowest limit for the release of wastes during normal operating conditions and the one that requires countermeasures over the greatest area for accident conditions, e.g., the confiscation of milk produced in the area around the reactor following the Windscale release of ^{131}I.

Such contamination can result either by direct deposition of the radioactive materials on the foodstuff or by incorporation of the radioactive material into the nutrients of a food chain. Because of the many uncertainties in the deposition process and the chemical and biological features of the food chains, direct estimates of the potential contamination are difficult and uncertain. For this reason much of the available information relates to experience with individual radioisotopes in a given environment, and generalization of the experience is available in only a few cases. Thus only general consideration will be given to dose estimates from these chains.

7-7.1 Contamination of Vegetation

Consideration of the mechanisms of contamination of vegetation is of importance because the vegetation may serve directly as a source of diet for man or it may serve as an entry into a food chain for another source of diet, e.g., the movement of iodine from contaminated pasture to the milk of cows.

7-7.1.1 Direct Deposition. The contamination of plants due to direct deposition on the foliage is a transitory problem in the sense that only a single crop is affected by this process and the contamination is reduced by radioactive decay, weathering, plant growth (and consequent dilution by uncontaminated vegetation), and, eventually, harvesting or a new cycle of growth. Materials deposited in this fashion provide a direct path of radiation without the time delay inherent in the root uptake and plant metabolism. As a result, this deposition is of importance for relatively short-lived radioisotopes that would be largely eliminated by radioactive decay before significant incorporation into the plant through the soil-uptake route. The importance of this mechanism for introducing radioactive materials into the diet will vary with the season of the year, i.e., it will be of less importance in some areas during the winter when crops are not growing and milk cows are usually fed with stored feed.

Available data on the distribution and retention of radioisotopes on vegetation are largely based upon studies of debris from nuclear weapons; so the data represent the behavior of the chemical and physical forms characteristic of this debris, as well as, in many cases, the integrated effects of deposition over a long time period. The behavior of this material depends upon the type of vegetation. It has been noted that the shape of wheat inflorescences tends to maximize particle entrapment (Eisenbud, 1963). About 2% of the ^{90}Sr deposited during the time the heads of the wheat plant were exposed was retained in the grain, and the whole crop retained about 3% of the deposited material (National Academy of Sciences–National Research Council, 1963). Less than 0.1% of the applied strontium was found in the wheat grain if the surface deposition occurred before the heads of the wheat developed. Rye grass grown in flats absorbed directly 23% of the ^{90}Sr.

Certain chemical forms of some radioisotopes can be absorbed through the plant foliage. About 4% of the strontium and 2% of the ruthenium applied to tomatoes is absorbed through the intact skin of the fruit (National Academy of Sciences–National Research Council, 1963). Gaseous ^{131}I will adsorb on plant leaves; about 35% to 40% penetrates the leaf epidermis, and about 2% moves to other parts of the plant. Stable iodine will not reduce the ^{131}I adsorption but does reduce the translocation (Selders and Hungate, 1956). The plant species is of importance in the absorption of elements. Wheat plants absorbed

85% of the applied strontium and 93% of the cesium, whereas cabbage absorbed only 5% to 6% of either of these elements.

The effectiveness of weathering as a mechanism for removing deposited materials has been estimated by the Federal Radiation Council (1965): "There is a wide range of measured values for the effective half-time of radionuclides on grass, most of which are close to 14 days." Unfortunately, since no references are given to the sources of these measured values and the types of contaminant are not indicated, it is difficult to assess the overall applicability of this half-time. It is noted, in the NAS–NRC report (National Academy of Sciences–National Research Council, 1963) that the washing effect of rain can reduce the foliar intake of strontium from material sprayed on the leaves by a factor as large as 6 and can reduce foliar intake of cesium to a lesser extent. It is not indicated whether a similar reduction occurs in the total contamination including adsorbed isotopes. Over 50% of the iodine in foliar contamination is removed by washing. Washing can also remove ions from within the plant. Sodium, potassium, and manganese are readily leached; calcium, magnesium, sulfur, potassium, and strontium are moderately leached; and iron, zinc, phosphorus, and chlorine are leached with difficulty. Thus some reduction in the amount of radioactive materials on the vegetation may occur during food preparation from such processes as washing, peeling, husking, and cooking.

A possible mechanism for uptake of materials not deposited directly on the foliage exists where there are root mats as in long-established pastures. Here the ^{90}Sr may be deposited directly on the roots and held long enough for some absorption to occur.

If the deposition occurs as a result of a single release, as in an accident, the vegetation contamination occurs in a relatively short time. Under conditions in which the vegetation serving directly as a source of food for man is harvested continually (as in a truck farm or a home garden), the uptake in the body can be estimated by using the uptake factor given by the ICRP (International Commission on Radiological Protection, 1959a) for water. (Note that this uptake factor may be different from that of water owing to the possible difference in chemical species of the radioisotope and the difference in chemical compounds associated with the radioisotope.) In this case the change in organ content can be written as

$$d(qf_2) = M_e\, f_w\, c_g \exp(-\lambda_v t)\, dt - (qf_2)(\lambda_R + \lambda_B)\, dt \quad (7.116)$$

where qf_2 = organ burden (μc)
M_e = quantity eaten (g/day)
f_w = fraction of ingested isotope that is deposited in the critical organ
c_g = concentration of isotopes in foodstuff (μc/g)
λ_v = fraction of isotope removed from the vegetation by decay, weathering growth, etc., (1/day)
λ_R = radioactive disintegration constan (1/day)
λ_B = fraction of isotope removed fror the critical organ per day by biolog ical processes (1/day)

Solving Eq. 7.116 with the condition that qf equals zero at time zero (time is measure after ingestion starts) gives

$$qf_2 = \frac{M_e f_w c_g}{\lambda_R + \lambda_B - \lambda_v}\{\exp(-\lambda_v t) - \exp[-(\lambda_R + \lambda_B)\tau]\} \quad (7.117)$$

where τ is the time interval after ingestion begins (days).

Equation 7.117 describes the quantity of radionuclide in the organ at any time after the start of ingestion. Substituting Eq. 7.117 for (qf_2) in Eq. 7.88 and integrating yields the equation for the total dose received over any time interval τ:

$$D = \frac{51\,\bar{E}\,M_e f_w c_g}{M(\lambda_R + \lambda_B - \lambda_v)}\left\{\frac{1-\exp(-\lambda\tau)}{\lambda_v} - \frac{1-\exp[-(\lambda_R+\lambda_B)\tau]}{\lambda_R+\lambda_B}\right\} \quad (7.118)$$

where the values of λ_v, λ_R, and λ_B are in units of 1/day.

For the special case in which removal from both the organ and the vegetation is by radioactive decay only, i.e., $\lambda_v = \lambda_R$ and $\lambda_B = 0$,

$$qf_2 = M_e\, f_w\, c_g\, \tau \exp(-\lambda_R \tau) \quad (7.119)$$

Substituting Eq. 7.119 for (qf_2) in Eq. 7.88 yields the dose received over the time period τ when removal is by radioactive decay only:

$$D = \frac{51\ \bar{E}\ M_e f_w c_g}{M\lambda_R^2}[1 - \exp(-\lambda_R\tau) \times (\lambda_R\tau - 1)] \quad (7.120)$$

where λ_R is in units of 1/day.

The dose rate to the GI tract can be estimated by comparing the total intake of the radioactive material ($M_e c_g$) with the total intake of water at the MPC calculated by the NCRP to give 300 mrem/week to the GI tract (National Committee on Radiation Protection and Measurement, 1959). The total dose over a period of time can be estimated by integrating the resulting dose rate over the time of interest.

If the crop is harvested as a whole, the quantity remaining on the edible portions at the time of harvesting will depend on the rate of removal by weathering, growth, etc. and the time since the contamination occurred. This quantity will then remain constant except for radioactive decay. The quantity of isotope accumulated in the critical organ of an individual eating M_e grams of this crop per day will then be

$$(qf_2) = \frac{M_e\ f_{w\,o}c_g \exp(-\lambda_v\tau_1)}{\lambda_R + \lambda_B} \times \{1 - \exp[-(\lambda_R + \lambda_B)\tau_2]\} \quad (7.121)$$

where ${}_oc_g$ is the initial deposition (μc/g), τ_1 is the time interval between deposition and harvest, and τ_2 is the time over which the crop is eaten.

With a continuous release, as in waste disposal, the rate of deposition when averaged over a long time period can be taken as essentially constant. Under these conditions the contamination levels in the foodstuffs will be given by

$$c_g = \frac{f\ v_d\ \bar{\chi}_{(x,y,0)}}{M_g(\lambda_R + \lambda_v)}\{1 - \exp[-(\lambda_R + \lambda_v)t]\} \quad (7.122)$$

where f = fraction of the deposited material which is on the edible portion
v_d = deposition velocity (m/sec)
M_g = mass of edible portion per unit area (g/m^2)
t = time over which the deposited material is accumulated (days), i.e., effective time of formation of the edible portions

The quantity in the critical organ of an individual eating the food can then be calculated for continuous intake over the contamination period or after harvesting as in the short-period release.

7-7.1.2 Uptake from the Soil. Soils can become contaminated from airborne materials by several processes:

1. Direct deposition on the soil.
2. Removal of material initially deposited on vegetation by weathering.
3. Seasonal cycling of vegetation cover.
4. Irrigation by water contaminated by direct fallout or by runoff from a contaminated area.

Once on the soils, the fate of the radioactive material depends upon the physical nature of the material and the chemical behavior of the radioisotopes. In general, soluble materials will be adsorbed to a variable degree by soil particles. This results in the gradual leaching of such materials as strontium or cesium through the soil. For example, ^{90}Sr from worldwide fallout was located primarily in the upper 2 in. of uncultivated soil during 1954 and 1955 (National Academy of Sciences–National Research Council, 1963).

The plant uptake will depend on the concentration of the radioisotope near the roots and on the availability of the radioisotope in ionic form. Of the long-lived fission products, strontium and cesium are most strongly absorbed. Since cesium is more tightly bound to the soils than strontium, it is usually regarded as less likely to be absorbed by plants. The uptake in a particular situation, however, can vary, depending upon the local conditions. Cesium uptake, for instance, is increased by the presence of ammonia or potassium because these ions free the adsorbed cesium from the soil (U. S. Atomic Energy Commission, 1961). In addition, bean plants that were grown under conditions dry to the wilting point contained five times the concentration of ^{137}Cs in stems when compared with those grown with the soil moisture kept at near field capacity.

Measurements of the uptake indicate that about 1% of the applied strontium and less than 0.1% of the other elements are taken up by single crops of plants; however, uptake of up to 4% to 8% has been noted in controlled pot ex-

periments. When expressed as the ratio of plant-tissue concentration to soil concentration, factors for fallout constituents have been reported as 0.05 for the alkaline earth group and 0.009 for the rare earths in barley. The average maximum uptake of cesium in experiments appears to be about 0.1% of the applied dose. However, in a complex situation represented by long-continued worldwide fallout from nuclear debris, the ratio of ^{137}Cs to ^{90}Sr in Chicago foodstuffs was higher than in the contaminating mixture even for root vegetables and during periods when the rate of fallout was comparatively low (Hardy and Rivera, 1964).

Strontium tends to accumulate in the above-ground portions of plants with the greatest concentration usually found in the older leaves. Cesium is distributed more uniformly through the plants. About 10% of all cesium found in plants is in the grain of wheat and oats.

The root system of the plant plays an important role in uptake. As a result, the depth of the contamination in the soil in relation to the root will also affect the uptake. Since grasses have a shallow root system, they will tend to absorb radioisotopes occurring near the surface. In a grass–clover mixture the strontium content was reduced 70% by plowing under the surface contamination. In other crops, cultivation tends to increase strontium uptake. Little variation in the availability of strontium has been observed over a period of years, and the uptake of strontium per unit of plant weight is fairly constant. The uptake of cesium increased under prolonged cropping, possibly because of some potassium depletion in the soil.

The organ burden of an individual eating such crops can be estimated from Eq. 7.121 and the estimated contamination level of the crop. The dose to the organ can then be obtained from Eq. 7.88.

Special dose considerations are frequently given to ^{90}Sr because of its metabolic similarity to calcium. Both strontium and calcium are incorporated into new bone in the same ratio as they exist in blood. The dose to the mineral portion of the bone and that to the marrow surrounded by the mineralized bone then depend upon the ^{90}Sr concentration in the calcified bone. The ratio of strontium to calcium in the blood, however, is not the same as the ratio of strontium to calcium in nature or even in the diet since there is some discrimination against the strontium. This discrimination is expressed as the Observed Ratio (OR) and is the ratio of the Sr/Ca in bone to the Sr/Ca in diet. Values of the OR are quoted as about 0.1 for the fetus, 1 at birth, 0.5 at the age of one year, and 0.25 for the adult (National Academy of Sciences–National Research Council, 1964). It is estimated that 10^{-3} μc of ^{90}Sr per gram of calcium uniformly distributed in adult bone would result in a dose of about 2.7 rads/year to the mineral bone and about 0.7 rads/year to the bone marrow (Federal Radiation Council, 1965). The dose to mineral bone of the fetus and infant may be about one-half of the value for adults because of the lower calcification although the dose to the bone marrow will be about the same as for the adult.

These concepts are applicable primarily to the ^{90}Sr intake over a long period of time. For short-term exposures, about 50% of the deposited radiostrontium is localized in areas of active bone formation, and the remainder is diffusely distributed in the bone in lower concentrations.

7-7.2 Contamination of Animal Products

Animals living in a contaminated region frequently will ingest radioactive materials to a much greater extent than humans. A portion of some of these radioisotopes will appear in the products used by man, such as meat, milk, eggs, etc. Chains of this nature that appear to be of the most importance are

$$^{131}I \rightarrow \text{vegetation} \rightarrow \text{cow} \rightarrow \text{milk}$$

$$\text{Sr} \rightarrow \text{vegetation} \rightarrow \text{cow} \rightarrow \text{milk}$$
$$\searrow \quad \nearrow$$
$$\text{soil}$$

$$^{137}Cs \rightarrow \text{vegetation} \rightarrow \text{cow} \rightarrow \text{milk}$$
$$\searrow \quad \nearrow \qquad\qquad \searrow$$
$$\text{soil} \qquad\qquad\qquad \text{meat}$$

There is some evidence that eggs may be of importance in such chains, particularly for ^{131}I.

Information on these chains and their importance has been developed both from experience and by experiment (Dunster, Howells, and Templeton, 1958); United Nations, 1962). Milk containing ^{131}I was the controlling factor in the environment following the Windscale release.

Here a deposition of about 1 $\mu c/m^2$ resulted in about 0.09 μc/liter of ^{131}I milk.

Knapp (1963) from a study of the ^{131}I milk concentrations resulting from nuclear fallout during periods of low and high deposition rates indicated that the concentration in milk is related to the quantity in the soil and the current rate of deposition by

$$\text{Milk concentration } (\mu c/\text{liter}) = \frac{1000}{9} \times (\text{total fallout on ground}) + 2600 \times (\text{deposition in the last month})$$

where the fallout is expressed in curies per square mile. The first term expresses the uptake in vegetation from material previously deposited and the second term describes the strontium present from current direct deposition.

If data are available on the uptake and retention (or excretion in milk) from a single administration of a radioisotope, the quantities in meat or milk can be estimated. For example, for a single contaminating event with ^{137}Cs followed by continued ingestion of the vegetation by cows, the average concentration in meat will be given by

$$\frac{dc_m}{dt} = \frac{M_e\, c_v\, f_w}{M_m} \exp(-\lambda_W t) - c_m \lambda_B \qquad (7.123)$$

where c_m = concentration of radioactive material in the animal's muscle ($\mu c/g$)
M_e = mass of food ingested by the animal per day (g/day)
c_v = concentration of cesium in the animal's food ($\mu c/g$)
f_w = fraction of the radioactive material eaten that goes to the muscle
M_m = total mass of the animal muscle (g)
λ_W = weathering constant for vegetation (1/day)
λ_B = elimination constant for the muscle (1/day)

Solving Eq. 7.123 gives

$$c_m = \frac{M_e\, c_v\, f_w}{M_m\,(\lambda_B - \lambda_W)} [\exp(-\lambda_W t) - \exp(-\lambda_B t)] \qquad (7.124)$$

7-7.3 Contamination of Water

Direct deposition into a stream or body of water is usually of minor importance compared with deposition on land because of the dilution and the relatively rapid removal of the contaminated portion by flushing. In special cases significant quantities of radioisotopes may deposit in sources of domestic water.

A special problem is the contamination of water supplies by runoff from land contaminated with reactor fission products by direct deposition or by decontamination efforts following an accident. For example, if 1 sq mile of land was contaminated so that the gamma reading at 1 m above the ground was about 5 r/hr, decontamination disposal to a stream with a flow of 5000 cu ft/sec would result in an average concentration of 10^{-6} to 10^{-5} $\mu c/cm^3$ over a 1-month period.

Potential doses from the direct ingestion of water can be estimated by comparison to the maximum permissible concentration in water given by the NCRP (National Committee on Radiation Protection and Measurement, 1959) with appropriate allowances made for the exposure time compared to the half-life of the contaminating radioisotope.

Food chains are again of importance in many bodies of water because some elements are concentrated strongly in the lower organisms and in fish or wild fowl that feed on these organisms (Davis, Perkins, Palmer, Hanson, and Cline, 1958). This may make fish or wild fowl a source of significant radiation dose if they are eaten by people, even though the water may be within maximum permissible limits for drinking purposes. In addition, this provides a mechanism for retaining some contamination in a body of water even after the major contaminated portion of the stream has passed.

Detailed studies have been made of several radioisotopes in particular environments (Dunster, 1958, Couchman, 1960, and Dunster, Howells, and Templeton, 1958), but these data have not been generalized to permit overall estimation of the effects in any environment. Estimates of the potential effects can be made only after detailed study of the data available and their application to the environment in question.

Chapter 8

Environmental Safety Analysis

James J. Fuquay*

8-1 INTRODUCTION

One facet of the complete environmental-safety examination of a nuclear plant is the analysis of the behavior of airborne effluents both from normal operations and from possible accidents and the estimation of the resulting exposure to radiations or noxious substances. Other facets include examination of the fate of liquid effluents and of the radiation dose that may result from direct gamma radiation from any source within the facility either during normal operation or following accidental release from primary shielding.

In general, such safety analyses are performed for one or more of the following purposes:

1. To provide operating limits for normal release of effluents.

2. To predict potential exposures from abnormal releases and to indicate the adequacy of design safeguards.

3. To provide a basis for planning action in case of abnormal release.

4. In unusual cases, to provide a basis for meteorological control of operations.

In estimations of average concentrations over the period of cloud passage at downwind locations, three main release-time-dependent mechanisms influence the effluent behavior:

1. A near-instantaneous release in which dilution occurs by the classical concepts of turbulent diffusion, i.e., the dilution rate is characterized by the turbulence within the volume as it travels downwind.

2. A short-term release period ranging from several minutes to, perhaps, several tens of hours in which the average concentration downwind is affected by both the turbulent dilution and the dispersive effect of large eddies that are too big to affect the turbulent mixing within the plume, i.e., wind meander.

3. A generally longer release period in which discrete changes in wind direction and speed occur so that the effective concentration at any point is a function of the first two mechanisms, as well as the fraction of the release time that the point is within the plume pattern.

The safety analysis and specific meteorological inputs vary widely, depending upon the purpose or purposes of the analysis and the individual plant characteristics. Even within a given category of nuclear installations, the types and quantities of material released and the rates and location of emission vary widely, particularly when possible accidents are being considered. These variations result from differences in containment or confinement design, materials, ventilation, and locations. For this reason it is difficult, if not impossible, to provide a detailed plan of computation that is applicable to all, or even to a majority, of the cases. The approach in this chapter has therefore been one of illustrating some types of computational procedures that can be used and considering the specific input data needed for the safety analysis. Calculations are made for each of the diffusion-time regimes that are of importance with different source characteristics.

In the practical case, particularly when the effects of accidents are being assessed, the

*Environmental and Radiological Sciences Department, Battelle–Northwest, Richland, Washington.

source may consist of a mixture of materials. In this case one can obviously obtain the answer by calculation for each material involved according to its individual emission characteristics and reaction in the environs. In most problems it is adequate to group materials according to their chemical and physical characteristics and their behavior after release to the atmosphere. Thus, in analyzing reactor accidents, the groups considered are frequently (1) the noble gases, which do not deposit on surfaces, (2) the very small particulates, which deposit only slightly, and (3) the iodines, which deposit strongly on nearly all surfaces if they are in vapor form or deposit only slightly if they are in organic compounds or attached to very small particles.

In establishing such groups, one must take care to see that the behavior of individual materials within the group is consistent. For example, if there is evidence that one isotope has a considerably different particle size distribution from another (perhaps because of a different method of formation), the evidence indicates that the rate of deposition from the airstream is different. Thus the distribution in the environment will differ.

The methods for estimating the types of atmospheric statistics used in dosage calculations vary widely among the various installations (see Chap. 4). Most of these methods are comparable, however, because of common initial assumptions, e.g., a multivariate normal material distribution. Final results using various of these models and methods are generally similar.

The analyses presented in this chapter are based on experience at Hanford (now Battelle–Northwest; see Sec. 4-4.2.2). This approach has been adopted because of the broad experience at this installation with a variety of different sources and because of the consistent treatment of a wide variety of problems on the basis of a large number of turbulence and diffusion investigations. Other techniques, e.g., for estimating cloud-spread rates, are equally applicable but have not generally been applied to so wide a range of operational problems.

Note that the calculations in this chapter have been carried out for distances considerably greater than those for which data are available. This was done intentionally to illustrate the magnitude of the computed quantities at great distances. Actual patterns would be considerably more irregular since the long-distance travel of a cloud becomes increasingly affected by large-scale fluctuations in the meteorological patterns and by changes in topography, circumstances not accounted for in the models used here.

Symbols used frequently in Chap. 8 are included in the List of Symbols given in Chap. 7.

8-2 INSTANTANEOUS RELEASE

For a demonstration of calculational methods, consider a puff release of $Q_0 = 10^6$ curies of each of three radioisotopes, ^{41}Ar, ^{137}Cs, and ^{131}I, from a 70-m stack during moderately stable conditions with a wind speed of 5 m/sec.

8-2.1 Ground-level Concentrations

For calculations of ground-level concentrations, a bivariate normal distribution was used as expressed in Eq. 8.1, which is identical to Eq. 3.158,

$$\psi_{(x,y,0)} = \frac{Q_x}{\pi \bar{u}\ \sigma_{yI}\sigma_{zI}} \exp - \left(\frac{y^2}{2\sigma_{yI}^2} + \frac{h^2}{2\sigma_{zI}^2}\right) \qquad (8.1)$$

where ψ is the integral of the concentration over a specified time interval in curie sec/m^3, Q_x is equal to $Q_0(Q_x/Q_0)_d \exp(-\lambda_R x/\bar{u})$ curies (the amount of radioactive material in the cloud at the downwind distance x meters), and $(Q_x/Q_0)_d$ is the correction for depletion of source from ground deposition.

First, calculations were made for the concentration time integral under the cloud center line at ground level, i.e., y = 0 and z = 0. With data from zinc sulfide tracer experiments performed at Hanford, Wash., empirical equations for σ_{yI} and σ_{zI} have been determined for moderately stable conditions. These equations, discussed in Sec. 4-4.2.2, are

$$\sigma_{yI}^2 = At - \frac{A^2}{2(\sigma_\theta \bar{u})^2}\left\{1 - \exp\left[\frac{-2(\sigma_\theta \bar{u})^2 t}{A}\right]\right\} \qquad (8.2)$$

where A is a constant related to the scale of turbulence and has a value of $13.0 + 232\ \sigma_\theta \bar{u}$, $\sigma_\theta \bar{u}$ equals 0.05, and t equals $x/\bar{u}$.

$$\sigma_{zI}^2 = a\left[1 - \exp(-k^2 t^2)\right] + bt \qquad (8.3)$$

where a, k^2, and b are functions of the degree of stability ($a = 97\ m^2$, $k^2 = 2.5 \times 10^{-4}\ sec^{-2}$, and $b = 0.33\ m^2/sec$).

The values of the standard deviation of cloud concentration as determined from Eqs. 8.2 and 8.3 for the horizontal direction, σ_{yI}, and the vertical direction, σ_{zI}, for various downwind distances are shown in Fig. 8.1. As the cloud proceeds downwind, the amount of radioactive

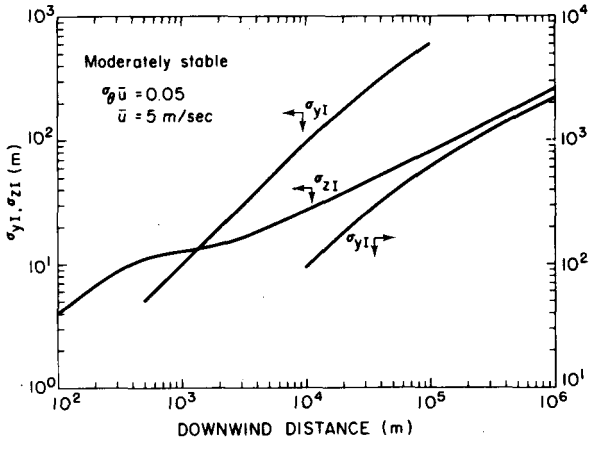

Fig. 8.1 — Standard deviations of cloud concentration distribution in the crosswind and vertical directions (instantaneous release).

material in the cloud will decrease owing to radioactive decay and, in the case of ^{137}Cs and ^{131}I, owing to ground deposition. The correction for radioactive decay was made for each isotope using Eq. 7.23, $(Q_x/Q_0)_R = \exp(-\lambda_R x/\bar{u})$, and the following decay constants:

Isotope	λ, sec^{-1}
^{41}Ar	1.05×10^{-4}
^{137}Cs	8.27×10^{-10}
^{131}I	9.96×10^{-7}

The correction for depletion from ground deposition was determined by the deposition integral as discussed in Sec. 5-3.2.2:

$$\left(\frac{Q_x}{Q_0}\right)_d = \exp\left[-\left(\frac{2}{\pi}\right)^{1/2}\left(\frac{v_d}{\bar{u}}\right) \times \int_0^x \frac{\exp(-h^2/2\sigma_{zI}^2)}{\sigma_{zI}}\,dx\right] \quad (8.4)$$

where $(Q_x/Q_0)_d$ is the fraction of the original material released which remains in the cloud after traveling x meters.

This equation can also be written in the Sutton form:

$$\left(\frac{Q_x}{Q_0}\right)_d = \exp\left[-\left(\frac{2}{\pi}\right)^{1/2}\left(\frac{v_d}{\bar{u}C_z}\right)\int_0^x (x)^{\frac{n-2}{2}} \times \exp\left(-\frac{h^2}{C_z^2 x^{2-n}}\right)dx\right] \quad (8.4a)$$

For this particular demonstration ($v_d/\bar{u}$) values of 2.2×10^{-4} and 3.4×10^{-3} were assumed for ^{137}Cs and ^{131}I, respectively. Values of ($v_d/\bar{u}$) depend on the physical and chemical characteristics of the source and the meteorological conditions prevailing. Therefore caution is required in selecting such values for a specific application. The values used here were somewhat arbitrarily selected. Equation 8.1 may be written for the ground-level concentration time integral at various distances directly under the path of the center of the cloud, i.e., y = 0, z = 0, as

$$\psi_{(x,0,0)} = \frac{Q_0}{\pi \bar{u}\,\sigma_{yI}\sigma_{zI}} \exp\left(-\lambda_R \frac{x}{\bar{u}}\right)\left(\frac{Q_x}{Q_0}\right)_d \times \exp\left(-\frac{h^2}{2\sigma_{zI}^2}\right) \quad (8.1a)$$

This equation was evaluated, and the results for the three radioisotopes are shown in Fig. 8.2.

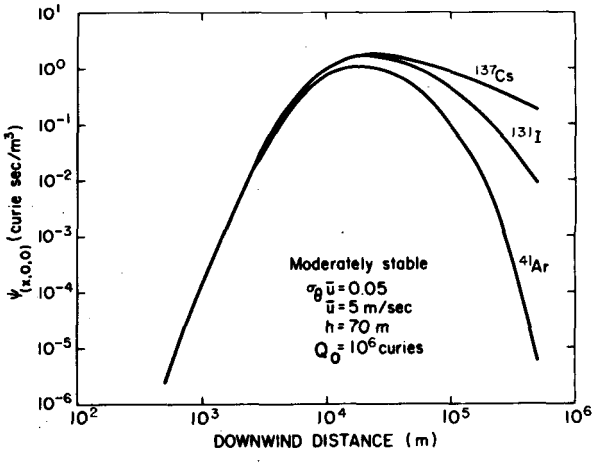

Fig. 8.2 — Cloud concentration time integral at ground level under the cloud center line (instantaneous release).

For the crosswind concentration time integral distribution, the following equation was evaluated at various downwind distances of $x = \bar{u}t$:

$$\psi_{(x,y,0)} = \psi_{(x,0,0)} \exp\left(-\frac{y^2}{2\sigma_{yI}^2}\right) \quad (8.5)$$

Isopleths of ψ (location of points of equal concentration time integral) were determined by solving for y for specific x values with the following equation:

$$y = (2)^{1/2} \left\{-\ln\left[\frac{\psi_{(x,y,0)}}{\psi_{(x,0,0)}}\right]^{1/2}\right\} \sigma_{yI} \quad (8.6)$$

Isopleths of ψ (curie sec/m^3) for the three radioisotopes are presented in Fig. 8.3.

8-2.2 Ground Deposition

The deposition of a specific isotope from the cloud on the ground along the path beneath the center of the cloud can be determined from

$$\omega_{(x,0,0,t_1)} = \psi_{(x,0,0)} v_d \exp(-\lambda_R t_1) \quad (8.7)$$

where ω is the quantity of deposited radioactive material in units of curies per square meter and the subscript $(x, 0, 0, t_1)$ indicates that the value is time dependent owing to radioactive decay.

For a puff release of a single isotope, the value of t_1 in the exponential in the decay correction factor represents the time interval after cloud passage. A correction factor has already been included in the formulation of ψ to correct for isotope decay en route to the receptor. In the following examples for determining ω and the associated gamma dose, the calculations were made for $t = (x/\bar{u})$ and $t_1 = 0$, and the subscripts for time dependence have been discarded.

With the values of $\psi_{(x,0,0)}$ and $v_d/\bar{u}$ given in Sec. 8-2.1, values of $\omega_{(x,0,0)}$ in curies per square meter were determined as presented in Fig. 8.4 for ^{137}Cs and ^{131}I. Argon-41 will not deposit because it is a stable gas.

In a manner similar to that used to determine $\psi_{(x,y,0)}$, the crosswind distribution of deposition, $\omega_{(x,y,0)}$, in curies per square meter, can be determined.

$$\omega_{(x,y,0)} = \omega_{(x,0,0)} \exp\left[-\frac{y^2}{2\sigma_{yI}^2}\right] \quad (8.8)$$

$$y = (2)^{1/2} \left\{-\ln\left[\frac{\omega_{(x,y,0)}}{\omega_{(x,0,0)}}\right]^{1/2}\right\} \sigma_{yI} \quad (8.9)$$

Isopleths of the ground deposition, $\omega_{(x,y,0)}$, obtained from this evaluation are presented in Fig. 8.5 for ^{137}Cs and ^{131}I.

8-2.3 External Gamma Dose from Cloud Passage

The equation for the gamma dose to a receptor from the passage of a cloud of finite size was developed in Sec. 7-5.2.2. Equation 7.42 as applied to a puff release was used to calculate the gamma dose in rads from the released 10^6 curies of each of the three radioisotopes ^{41}Ar, ^{137}Cs, and ^{131}I.

$$\gamma D_{(x,y,0)} = \frac{0.1616\ \mu\mu_a \bar{E}_\gamma Q_x (I_1 + kI_2)}{\bar{u}} \quad (8.10)$$

where Q_x is the source term corrected for depletion prior to arrival x meters downwind.

Spectral diagrams for each of the radioisotopes are shown in Fig. 8.6. These diagrams indicate schematically the decay mode, energies involved, and probable energy per emission. Average gamma energies have also been included. From the graph of μ and μ_a for various gamma energies shown in Fig. 7.8 and the spectral diagrams, the following values of $\bar{E}_\gamma$, μ, and μ_a were obtained for the three radioisotopes:

Isotope	$\bar{E}_\gamma$, Mev/dis	μ, 1/m	μ_a, 1/m
^{41}Ar	1.29	7.0×10^{-3}	3.4×10^{-3}
^{137}Cs	0.61	1.03×10^{-2}	3.9×10^{-3}
^{131}I	0.39	1.25×10^{-2}	3.85×10^{-3}

Corrections for cloud depletion due to ground deposition and radioactive decay were made and applied to Eq. 8.10. The values of I_1 and I_2 were obtained by using Figs. 7.10 and 7.11. For this demonstration a value of σ_I, needed to ascertain the values of I_1 and I_2, was determined by the following relations as explained in Sec. 7-5.2.2:

$$\sigma_I = (\sigma_{zI}\sigma_{yI})^{1/2}$$

$$\mu s = \mu(y^2 + h^2)^{1/2}$$

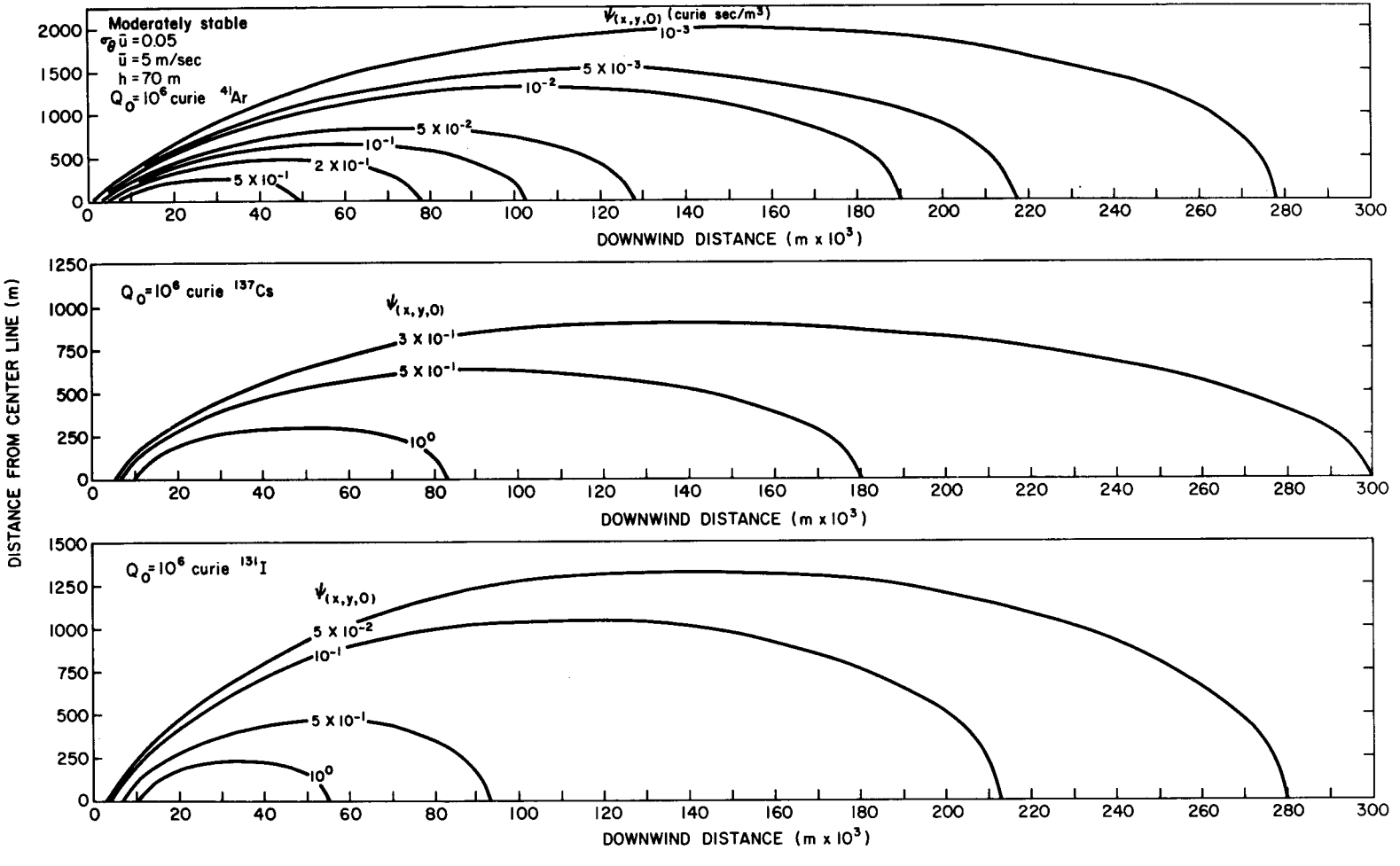

Fig. 8.3—Isopleths of cloud concentration time integral at ground level (instantaneous release).

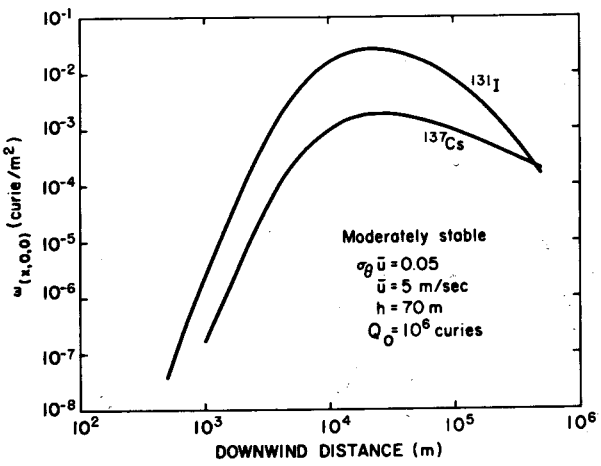

Fig. 8.4—Ground deposition directly under a cloud center line and immediately after cloud passage (instantaneous release).

The calculations of the gamma dose at various distances downwind under the path of the center of the cloud were made for y = 0 and s = h, and the appropriate values of μs and k are

Isotope	μs	k
^{41}Ar	0.50	1.2
^{137}Cs	0.70	1.6
^{131}I	0.875	2.3

With these values the gamma dose $_\gamma D_{(x,0,0)}$, presented in Fig. 8.7, was determined for each of the isotopes. Values of the dose to receptors at locations not directly under the cloud, i.e., $_\gamma D_{(x,y,0)}$, can be determined by substituting the appropriate y values into the equation $\mu s = \mu(y^2 + h^2)^{1/2}$ and evaluating Eq. 8.10.

8-2.4 External Gamma Dose Rate from Ground Deposition

Equations for the dose rate, $_\gamma D'_{(x,0,0)}$, from material deposited on the ground directly under a cloud center line were developed in Sec. 7-5.3.2. These equations dealt with the radiation from ground patterns of finite size at the time x/$\bar{u}$, i.e., immediately after cloud passage. The form of Eq. 7.72 used here is

$$_\gamma D'_{(x_1,0,b)} = 0.36\omega_{(x,0,0)}\,\sigma_y\,\mu\mu_a\,\bar{E}_\gamma \times\left(G_1 + \frac{k}{2}G_2\right) \quad (8.11)$$

The calculations of $\omega_{(x,0,0)}$ are explained in Sec. 8-2.2, and the results are presented in Fig. 8.4. From values of G_1 and G_2 given in Figs. 7.26 and 7.27, specific values of the gamma dose rate were obtained by using, in this case, the relation $\sigma_I = (\sigma_{yI}\sigma_{zI})^{1/2}$ and assuming the receptor height, b, to be 1 m above the ground. Results of these calculations are presented in Fig. 8.8 for ^{137}Cs and ^{131}I.

Isopleths of the gamma dose rate obtained with relations similar to those in Secs. 8-2.2 and 8-2.3 are shown in Fig. 8.9.

The gamma dose rate to a receptor at locations other than those directly under the path of the cloud center line (i.e., $_\gamma D'_{(x,y,b)}$) can be obtained by using the following equation:

$$_\gamma D'_{(x,y,b)} = {}_\gamma D'_{(x_1,0,b)}\,\exp\left(-\frac{y^2}{2\sigma_{yI}^2}\right) \quad (8.12)$$

8-3 INTERMEDIATE-LENGTH RELEASES

The release intervals defined here as intermediate in length range from 10 minutes or so to a few hours. Much of the diffusion experiment work over the last 10 years has been concentrated on this time scale, and a considerable body of data has accumulated.

For a demonstration of the calculational methods for intermediate-length releases, consider a continuous source of radioactive material with a uniform emission rate of Q'_0 = 1 curie/sec for a discharge period of 1 hr (t_d = 3600 sec) from a 70-m stack into a moderately stable atmosphere with an average wind speed of $\bar{u}$ = 5 m/sec. Again, the three radioisotopes ^{41}Ar, ^{137}Cs, and ^{131}I will be considered.

8-3.1 Ground-level Concentrations

When the release occurs over an intermediate time interval, the same equations for exposure, dosage, etc. used in Sec. 8-2.1 are applicable if proper values of σ_y and σ_z are used. The plume released over a 1-hr period can be expected to spread horizontally more than the cloud formed by a puff release. For the Hanford site the value of $\sigma_\theta\bar{u}$ = 0.2 was selected as representative for a 1-hr release under moderately stable conditions. Equations 8.2 and 8.3 were again used to determine σ_y and σ_z, respectively.

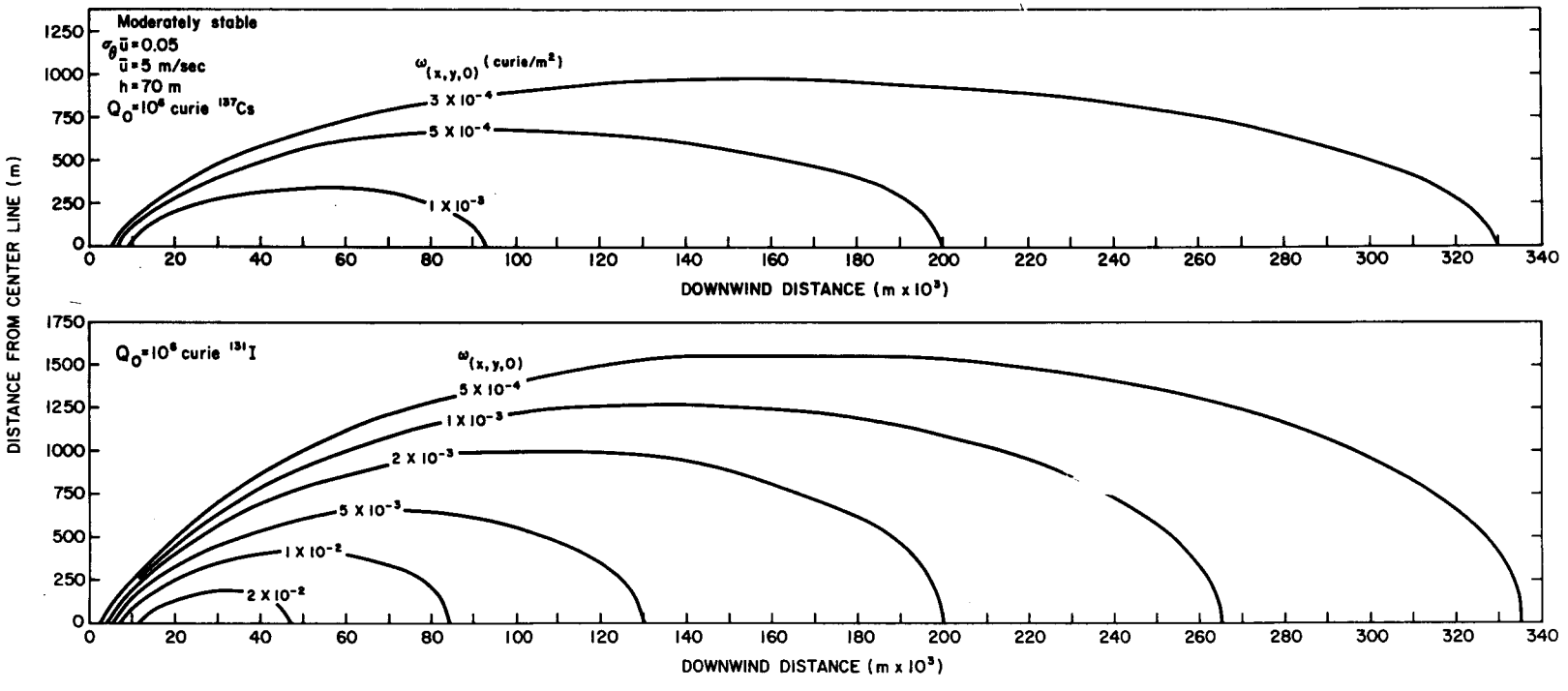

Fig. 8.5—Isopleths of ground deposition (instantaneous release).

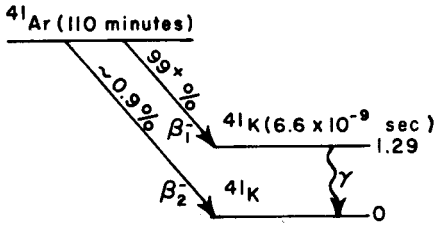

E_{β_1} = 1.20 Mev, p_1 = 0.99+ E_γ = 1.29 Mev, p = 0.99+

E_{β_2} = 2.48 Mev, p_2 = 0.009 $\bar{E}_\gamma$ = 1.28 Mev/dis

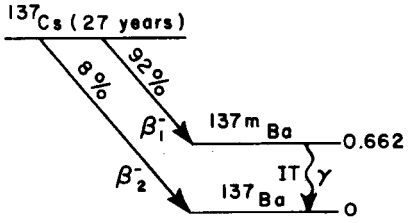

E_{β_1} = 0.51 Mev, p_1 = 0.92 E_γ = 0.662 Mev, p = 0.92

E_{β_2} = 1.17 Mev, p_2 = 0.08 $\bar{E}_\gamma$ = 0.608 Mev/dis

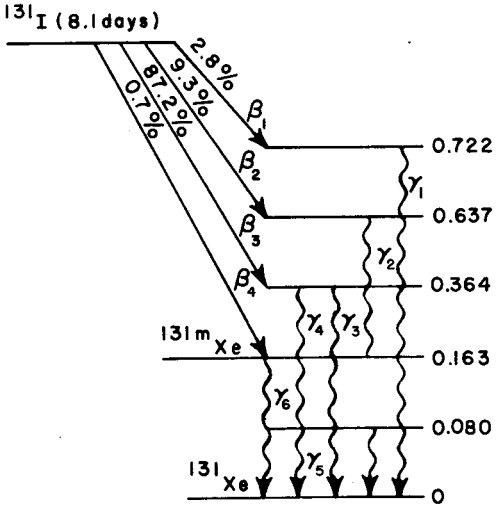

E_{β_1} = 0.250 Mev, p_1 = 0.028

E_{β_2} = 0.335 Mev, p_2 = 0.093

E_{β_3} = 0.608 Mev, p_3 = 0.872

E_{β_4} = 0.815 Mev, p_4 = 0.007

E_{γ_1} = 0.722 Mev, p_1 = 0.03

E_{γ_2} = 0.637 Mev, p_2 = 0.09

E_{γ_3} = 0.364 Mev, p_3 = 0.80

E_{γ_4} = 0.284 Mev, p_4 = 0.053

E_{γ_5} = 0.080 Mev, p_5 = 0.022

E_{γ_6} = 0.163 Mev, p_6 = 0.022

$\bar{E}_\gamma$ = 0.390 Mev/dis

Fig. 8.6 — Spectral diagrams for ^{41}Ar, ^{137}Cs, and ^{131}I.

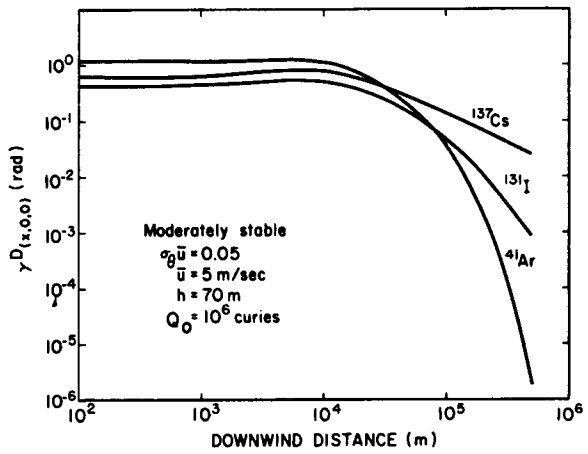

Fig. 8.7—Direct gamma dose from passing cloud to receptor under cloud center line (instantaneous release).

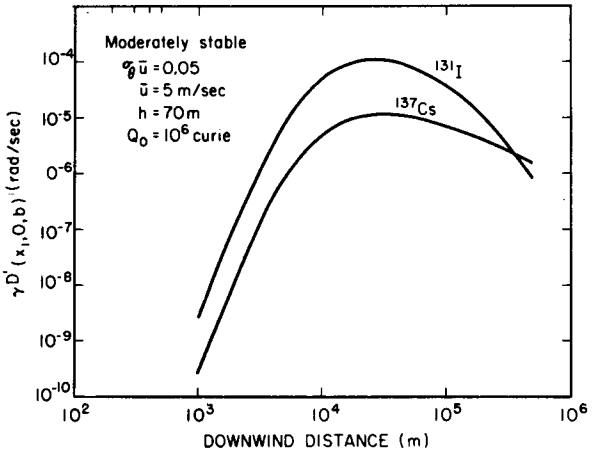

Fig. 8.8—Gamma dose rate from ground deposition under cloud center line immediately after cloud passage (instantaneous release).

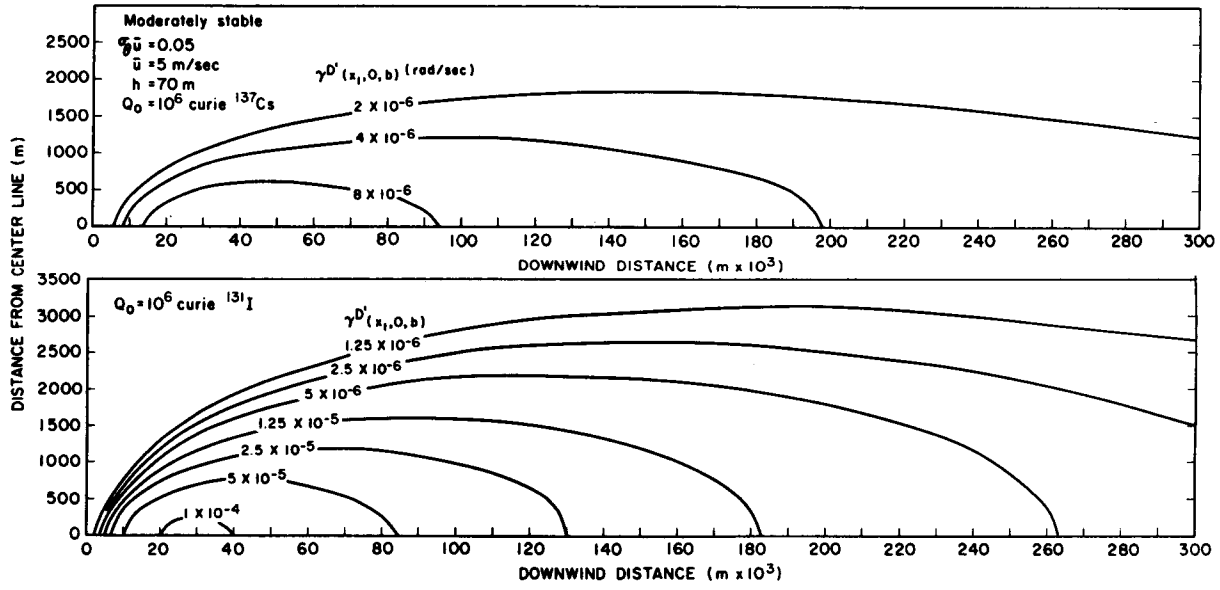

Fig. 8.9—Isopleths of gamma dose rate from ground deposition immediately after cloud passage (instantaneous release).

The bivariate normal distribution as given in Eq. 8.1 can be applied to continuous-release conditions. In this case Eq. 8.1 will yield the concentration time integral of the plume if the product of Q'_x (curie/sec) times t_d (sec) is substituted for Q_x (curies) of the puff release (both terms corrected for depletion en route to the point of reference). If the release rate Q'_x (curies/sec) is substituted for Q_x (curies), Eq. 8.1 will yield the concentration $\bar{\chi}$ (curies/m^3) of the established plume. These modifications of Eq. 8.1 are indicated as Eqs. 8.1a and 8.1b, respectively:

$$\psi_{(x,y,0)} = \frac{Q'_x t_d}{\pi \bar{u} \sigma_y \sigma_z} \exp -\left(\frac{y^2}{2\sigma_y^2} + \frac{h^2}{2\sigma_z^2}\right) \text{ curie sec/m}^3 \quad (8.1a)$$

$$\bar{\chi}_{(x,y,0)} = \frac{Q'_x}{\pi \bar{u} \sigma_y \sigma_z} \exp -\left(\frac{y^2}{2\sigma_y^2} + \frac{h^2}{2\sigma_z^2}\right) \text{ curies/m}^3 \quad (8.1b)$$

The source term Q_x in Eq. 8.1, or Q'_x as applied to the plume, is the amount of source material in the cloud or plume at the receptor downwind at distance x or at time x/$\bar{u}$ (sec). The source terms as measured at the time of release must be corrected for both ground deposition and radioactive decay in Eqs. 8.1a and 8.1b. The correction factors for depletion by ground deposition and radioactive decay are identical for both the puff release and the plume.

The values of $\bar{\chi}_{(x,0,0)}$ for the established plume determined with Eq. 8.1b are given in Fig. 8.10 for various downwind distances for the three isotopes.

The isopleths of the plume equilibrium concentration were determined from Eq. 8.6 with $\bar{\chi}$ substituted for ψ. These isopleths are shown in Fig. 8.11 for the three isotopes.

8-3.2 Ground Deposition

The rate of deposition from the established plume to the ground can be determined by using Eq. 7.30 for $t_d \to 0$ and including appropriate depletion factors en route. The total deposition for the 1-hr release was determined for points directly under the plume center line

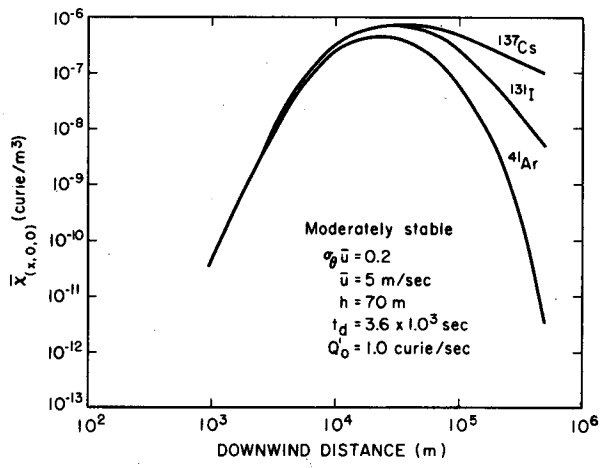

Fig. 8.10 — Equilibrium plume concentration at ground level under a cloud center line (intermediate release).

by using $\psi_{(x,0,0)}$ for the plume as discussed in Sec. 8-3.1. In the case of the plume, Eq. 7.30 was used.

For the special case of t = 0, the ground deposition $\omega_{(x,y,0,t)}$ is a maximum. Figure 8.12 shows the values of $\omega_{(x,0,0)}$ for ^{137}Cs and ^{131}I obtained with Eq. 7.30. Isopleths of ω can be determined for the short-term release in a manner similar to that used for the puff release.

8-3.3 External Gamma Dose Rate and Dose from Cloud Passage

Equation 7.43 yields the gamma dose rate from an established plume. This equation was used to calculate the gamma dose rate of the established plume directly under the plume center line, $_\gamma D'_{(x,0,0)}$, i.e., y = 0 and s (the distance from the receptor to the plume center line) = h. In evaluating Eq. 7.43 for the plume, values of I_1 and I_2 are functions of $\sigma = (\sigma_y \sigma_z)^{1/2}$, and the σ values for the plume were used. The dose rates from the plume are shown in Fig. 8.13 for the three isotopes. Dose rates for receptor points other than those directly under the plume center line can be obtained by evaluating I_1 and I_2 in Eq. 7.43 for $s = (h^2 + y^2)^{1/2}$.

The gamma dose received at a point during the plume passage can be obtained by multiplying the dose rate $_\gamma D'_{(x,y,0)}$ by the time interval of release t_d(sec). In this case t_d = 3600 sec.

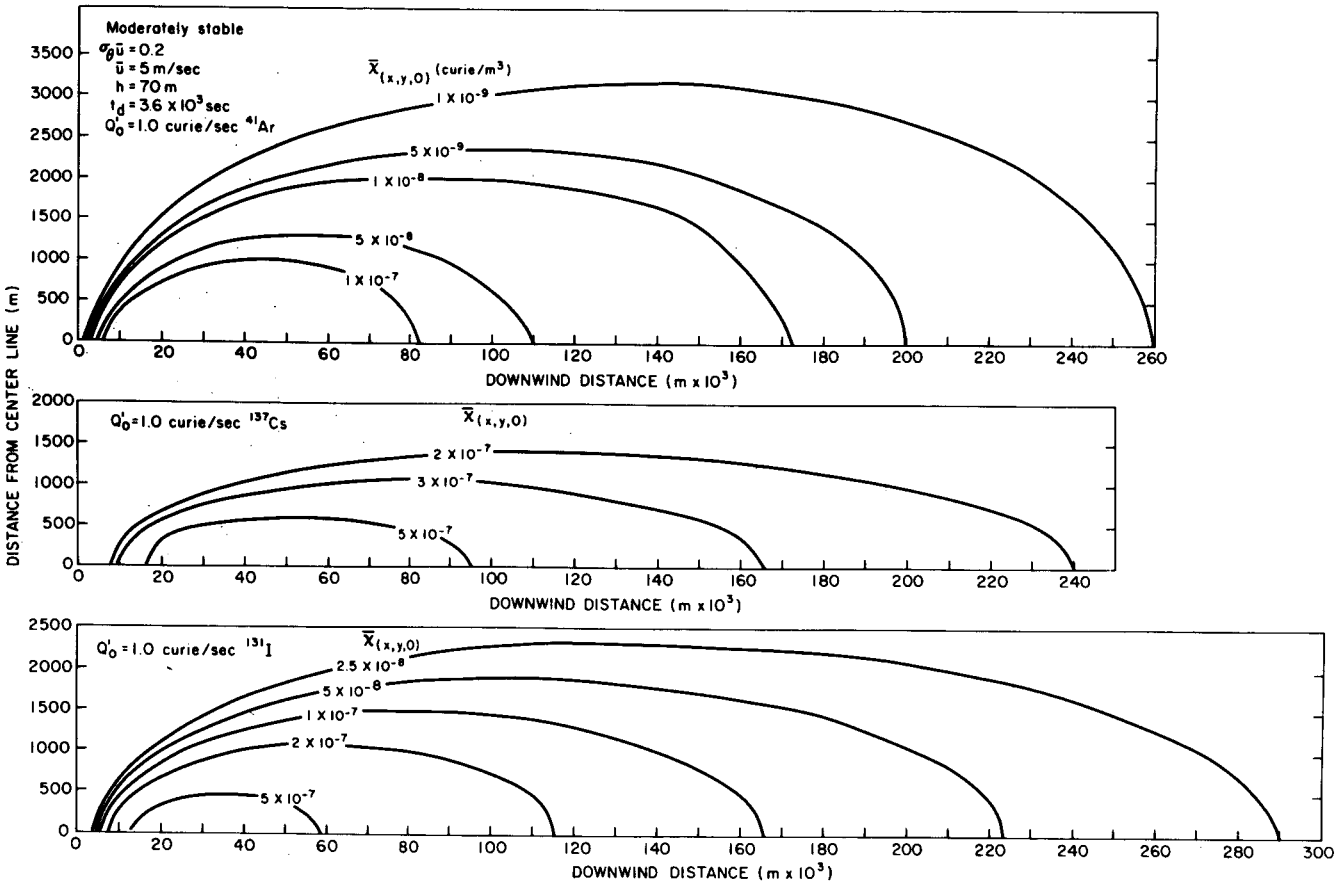

Fig. 8.11—Isopleths of plume concentration at ground level under the cloud (intermediate release).

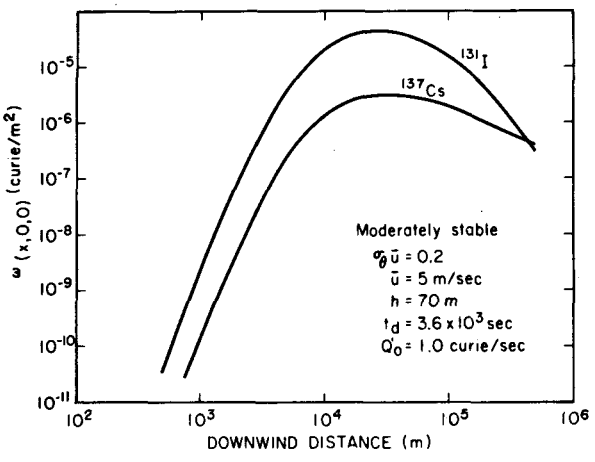

Fig. 8.12—Ground deposition directly under the plume center line immediately after cloud passage (intermediate release).

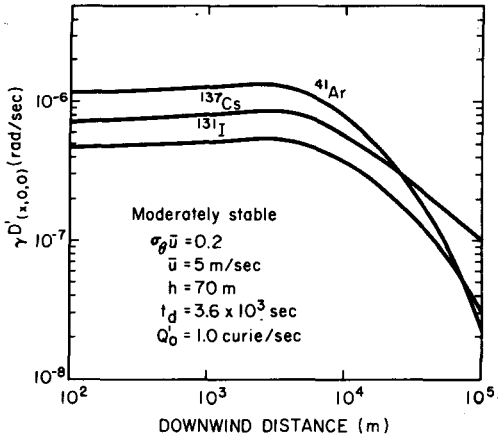

Fig. 8.13—Direct gamma dose rate from a plume to a receptor under the center line (intermediate release).

8-3.4 External Gamma Dose Rate from Ground Deposition

The gamma dose rate from ground deposition from the plume can be determined for any time if the appropriate modifications are made to the equations for the dose rate from ground deposition patterns of finite size (Sec. 7-5.3.2). For dose rates at points directly under the plume center line, Eq. 7.69 may be used.

With the appropriate σ value for the plume, Eq. 7.69 was evaluated for the release of ^{137}Cs and ^{131}I at the rate of 1 curie/sec and the deposition dose rates at t = 0 when the end of the plume had just passed the receptor points. These dose rates are shown in Fig. 8.14.

Isopleths for the gamma dose rate from the deposition described in the preceding paragraph can be determined using Eq. 8.12 in Sec. 8-2.4 with σ values appropriate to the intermediate-length release.

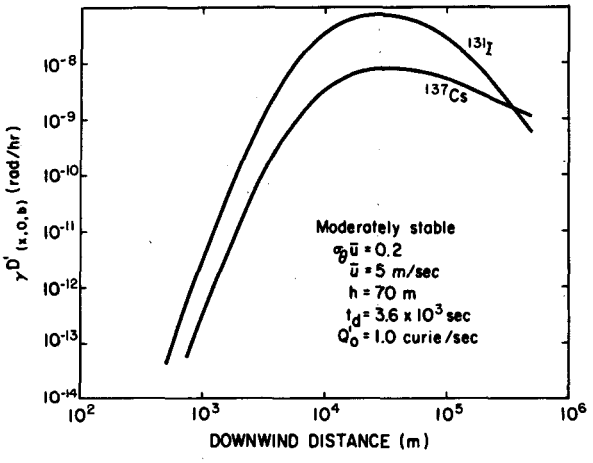

Fig. 8.14—Gamma dose rate from ground deposition under the plume center line during plume passage (intermediate release).

8-4 LONG-PERIOD RELEASE

Equations for evaluating doses from continuous releases at uniform rates over long periods of time (i.e., from days to years) were developed in Sec. 7-5.2.5. In addition to the information required for dispersion calculations, data on the joint frequency of occurrence of wind speed, wind direction, and stability are required.

Table 8.1 presents the percentage frequency distribution of wind speed and direction as determined from measurements taken at the 200-ft level of the Hanford meteorology tower for various stability classes in the 200-ft layer for 16 compass sectors.

The many individual calculations required to evaluate long-term release effects generally make the use of a computer mandatory. From the Hanford data shown in Table 8.1, the average air concentrations, deposition rate, direct dose rate from cloud passage, and dose rate from material deposited on the ground were determined with the assumption that ^{41}Ar, ^{137}Cs,

Table 8.1 — ANNUAL PERCENTAGE FREQUENCY DISTRIBUTION OF WIND SPEED AND DIRECTION AS A FUNCTION OF ATMOSPHERIC STABILITY AT HANFORD*

Wind speed, miles/hr	Atmospheric stability	Wind direction																		
		NNE.	NE.	ENE.	E.	ESE.	SE.	SSE.	S.	SSW.	SW.	WSW.	W.	WNW.	NW.	NNW.	N.	Variable	Calm	Total
0 to 3	Very stable	0.16	0.20	0.14	0.22	0.24	0.41	0.21	0.24	0.20	0.25	0.24	0.46	0.38	0.53	0.41	0.37	0.15	0.56	5.37
	Moderately stable	0.19	0.25	0.19	0.22	0.44	0.48	0.22	0.22	0.13	0.17	0.16	0.23	0.29	0.40	0.37	0.41	0.12	0.67	5.17
	Neutral	0.27	0.38	0.28	0.36	0.40	0.47	0.22	0.18	0.13	0.14	0.12	0.23	0.22	0.44	0.50	0.50	0.15	0.50	5.47
	Unstable	0.38	0.65	0.40	0.45	0.36	0.26	0.11	0.22	0.12	0.18	0.10	0.14	0.16	0.30	0.40	0.64	0.49	0.02	5.38
4 to 7	Very stable	0.18	0.19	0.11	0.15	0.16	0.31	0.22	0.22	0.21	0.35	0.44	0.93	1.03	1.04	0.65	0.35	0.02	0.00	6.57
	Moderately stable	0.16	0.12	0.12	0.16	0.22	0.40	0.22	0.18	0.18	0.22	0.26	0.46	0.58	0.81	0.49	0.33	0.01	0.00	4.92
	Neutral	0.10	0.13	0.10	0.10	0.15	0.25	0.13	0.11	0.07	0.10	0.12	0.18	0.30	0.66	0.31	0.16	0.02	0.00	2.98
	Unstable	0.70	0.77	0.43	0.50	0.43	0.56	0.35	0.47	0.46	0.49	0.38	0.39	0.42	1.09	0.97	1.20	0.28	0.00	9.88
8 to 12	Very stable	0.12	0.10	0.08	0.09	0.05	0.14	0.20	0.10	0.11	0.23	0.55	1.07	1.80	1.88	0.55	0.20	0.00	0.00	7.28
	Moderately stable	0.11	0.09	0.02	0.07	0.07	0.19	0.19	0.15	0.21	0.33	0.48	0.90	1.62	1.89	0.35	0.16	0.00	0.00	6.84
	Neutral	0.06	0.05	0.03	0.03	0.03	0.06	0.06	0.05	0.06	0.08	0.12	0.12	0.36	0.87	0.17	0.09	0.00	0.00	2.26
	Unstable	0.47	0.35	0.11	0.06	0.07	0.09	0.10	0.12	0.28	0.59	0.54	0.33	0.49	1.33	0.47	0.49	0.00	0.00	5.91
13 to 18	Very stable	0.04	0.03	0.02	0.02	0.00	0.05	0.08	0.02	0.03	0.11	0.25	0.41	1.05	1.64	0.22	0.07	0.00	0.00	4.04
	Moderately stable	0.08	0.03	0.02	0.01	0.02	0.09	0.13	0.14	0.26	0.60	0.84	1.07	2.81	2.71	0.18	0.12	0.00	0.00	9.10
	Neutral	0.06	0.01	0.01	0.01	0.00	0.03	0.03	0.05	0.07	0.15	0.20	0.14	0.28	0.51	0.07	0.04	0.00	0.00	1.66
	Unstable	0.25	0.15	0.04	0.00	0.00	0.03	0.03	0.04	0.19	0.53	0.64	0.26	0.59	1.00	0.10	0.12	0.00	0.00	3.97
19 to 24	Very stable	0.00	0.00	0.00	0.01	0.00	0.01	0.01	0.00	0.01	0.02	0.03	0.03	0.04	0.20	0.00	0.00	0.00	0.00	0.37
	Moderately stable	0.03	0.03	0.01	0.00	0.00	0.02	0.07	0.09	0.23	0.56	0.50	0.35	1.37	1.69	0.04	0.01	0.00	0.00	5.00
	Neutral	0.01	0.02	0.00	0.00	0.00	0.01	0.01	0.02	0.07	0.12	0.14	0.05	0.18	0.30	0.01	0.01	0.00	0.00	0.96
	Unstable	0.06	0.05	0.01	0.00	0.00	0.00	0.01	0.01	0.10	0.30	0.44	0.11	0.26	0.60	0.01	0.03	0.00	0.00	2.00
Over 24	Very stable	0.00	0.00	0.00	0.00	0.00	0.00	0.00	0.01	0.01	0.01	0.01	0.00	0.00	0.00	0.00	0.00	0.00	0.00	0.04
	Moderately stable	0.00	0.00	0.00	0.00	0.00	0.01	0.02	0.08	0.33	0.60	0.24	0.08	0.48	0.84	0.01	0.00	0.00	0.00	2.70
	Neutral	0.00	0.00	0.00	0.00	0.00	0.00	0.00	0.02	0.06	0.15	0.07	0.02	0.10	0.27	0.00	0.01	0.00	0.00	0.71
	Unstable	0.01	0.01	0.00	0.00	0.00	0.00	0.00	0.01	0.07	0.37	0.27	0.08	0.11	0.48	0.01	0.00	0.00	0.00	1.41
Total	Very stable	0.50	0.52	0.35	0.48	0.45	0.91	0.73	0.59	0.58	0.97	1.52	2.90	4.30	5.29	1.83	0.99	0.17	0.56	23.67
	Moderately stable	0.57	0.52	0.36	0.46	0.75	1.19	0.85	0.87	1.35	2.48	2.49	3.09	7.15	8.34	1.45	1.03	0.14	0.67	33.74
	Neutral	0.50	0.59	0.41	0.49	0.59	0.82	0.46	0.43	0.46	0.73	0.77	0.75	1.45	3.06	1.07	0.81	0.17	0.50	14.04
	Unstable	1.85	1.97	0.99	1.02	0.86	0.95	0.61	0.87	1.22	2.47	2.37	1.32	2.02	4.80	1.96	2.48	0.77	0.02	28.55

*Measured on Hanford tower at 200 ft during the period January 1955 through July 1961.

and ^{131}I were each released from a 70-m stack at a constant rate of 1.0 curie/sec for a period of 1 year.

8-4.1 Average Ground-level Concentration

The average ground-level air concentration is given by Eq. 7.60. For stable atmospheric stratifications, σ_z was calculated with Eq. 8.3 evaluated from the data in Table 8.2.

Table 8.2—VALUES OF DIFFUSION PARAMETERS FOR STABLE CONDITIONS AT HANFORD

Parameter	Degree of stability	
	Very stable	Moderately stable
a	34 m^2	97 m^2
b	2.5×10^{-2} m^2/sec	0.33 m^2/sec
k^2	8.8×10^{-4} sec^{-2}	2.5×10^{-4} sec^{-2}

The values for σ_z in meters during neutral and unstable conditions were determined by the Sutton form

$$\sigma_z = \frac{C_z x^{(1-n/2)}}{(2)^{1/2}}$$

where values of C_z are given in Table 8.3, $n = 0.25$ for neutral conditions, and $n = 0.20$ for unstable conditions.

Table 8.3—VERTICAL DIFFUSION PARAMETER VALUES (C_z) FOR NEUTRAL AND UNSTABLE ATMOSPHERES AS USED AT HANFORD

Wind speed, m/sec	Degree of stability	
	Neutral	Unstable
1.0	0.15	0.30
2.5	0.14	0.28
5.0	0.12	0.26
7.5	0.115	0.25
10.0	0.11	0.24
15.0	0.10	0.23

The value of Q'_R in Eq. 7.60 is the rate at which the source in the cloud passes the vertical plane perpendicular to the cloud path at the receptor point in the sector (that is, corrected for depletion en route per Eq. 5.48). Values of v_d used in evaluating the deposition integral depend upon the atmospheric stability during the dispersion and the characteristics of the source material. For this particular demonstration the values of $v_d/\bar{u}$ given in Table 8.4 were assumed. These values are somewhat arbitrary and may not be applicable to other situations.

Table 8.4—VALUES OF $v_d/\bar{u}$ USED IN DEPOSITION CALCULATIONS AT HANFORD

Atmospheric conditions	Particulates (^{137}Cs)	Halogens (^{131}I)
Strong inversion	1.5×10^{-4}	2.4×10^{-3}
Moderate inversion	2.2×10^{-4}	3.4×10^{-3}
Neutral	3.0×10^{-4}	4.6×10^{-3}
Unstable	6.0×10^{-4}	8.0×10^{-3}

Calculations of the average ground-level concentration, $\bar{\chi}_{(R,\theta,0)}$ (curie/m^3), were made for each of the 16 compass sectors by using the values of percentage frequency in Table 8.1. The concentrations were then added for each of the joint frequencies for a given isotope at several downwind distances in each sector. The isopleths of $\bar{\chi}$ about the release point are shown in Figs. 8.15, 8.16, and 8.17. The calculated values have been located on the center line of the individual sectors, and smooth curves have been drawn to connect common $\bar{\chi}_{(R,\theta,0)}$ values.

8-4.2 External Gamma Dose

The external doses for individuals at various locations in the vicinity of the release point were calculated with Eq. 7.63 and the data in Table 8.1.

Isopleths of the dose contributed by each of the radionuclides are shown in Figs. 8.18, 8.19, and 8.20 for the 1-year exposure period. The total dose from cloud passage would, of course, be the sum of the contributions by each radionuclide.

8-4.3 External Gamma Dose Rate from Ground Deposition

The dose rate from ground deposition will increase continuously during the period of release because the ^{137}Cs does not attain equilibrium in 1 year. The isopleths of dose rate from ^{137}Cs and ^{131}I sources computed for the end of the year are shown in Fig. 8.21. The time-integrated dose can be determined by integrating the activity on the ground over the period of concern and using this value as a source in Eq. 7.63.

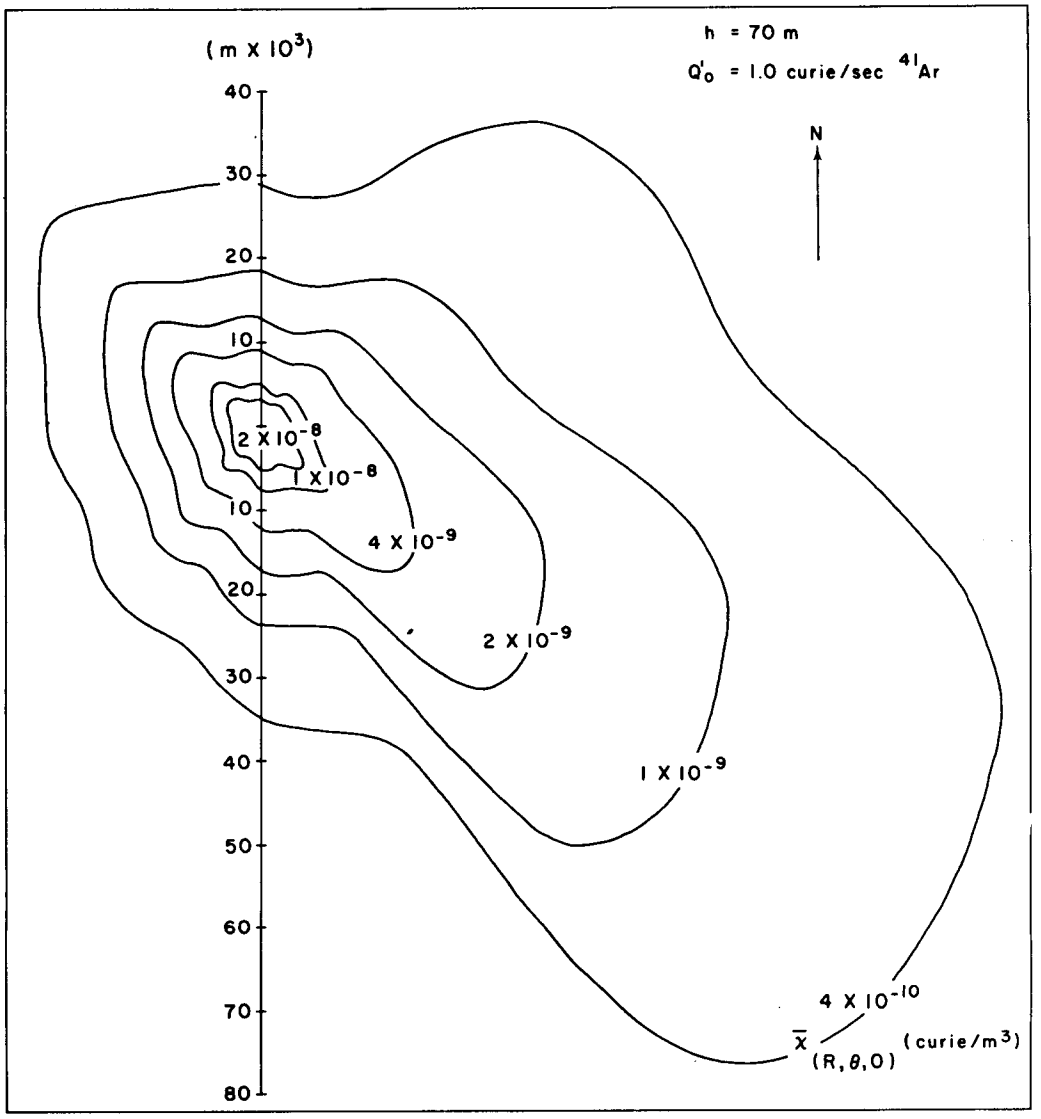

Fig. 8.15 — Isopleths of average cloud concentration of ^{41}Ar about the release point (long-period release).

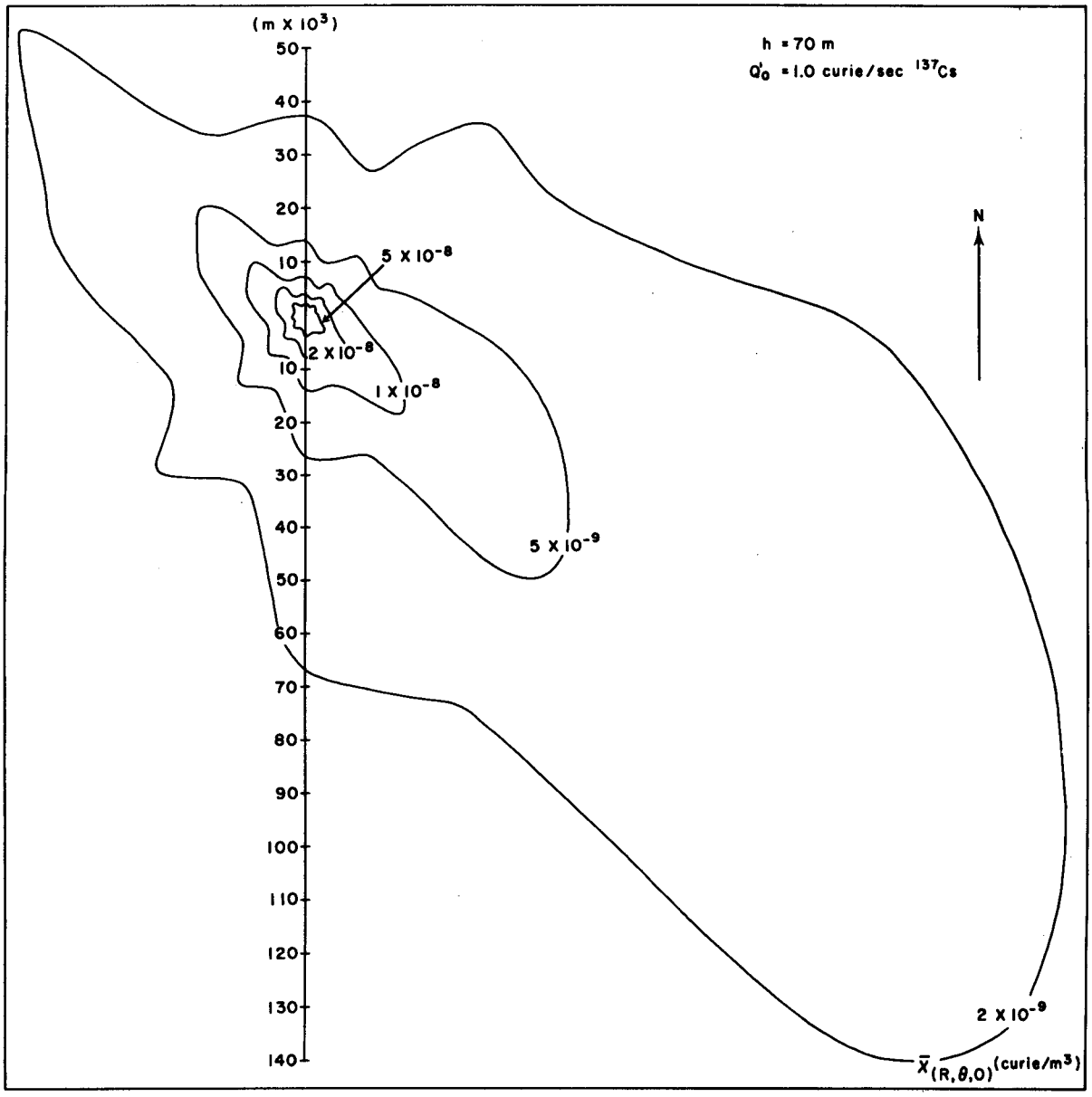

Fig. 8.16 — Isopleths of average cloud concentration of ^{137}Cs about the release point (long-period release).

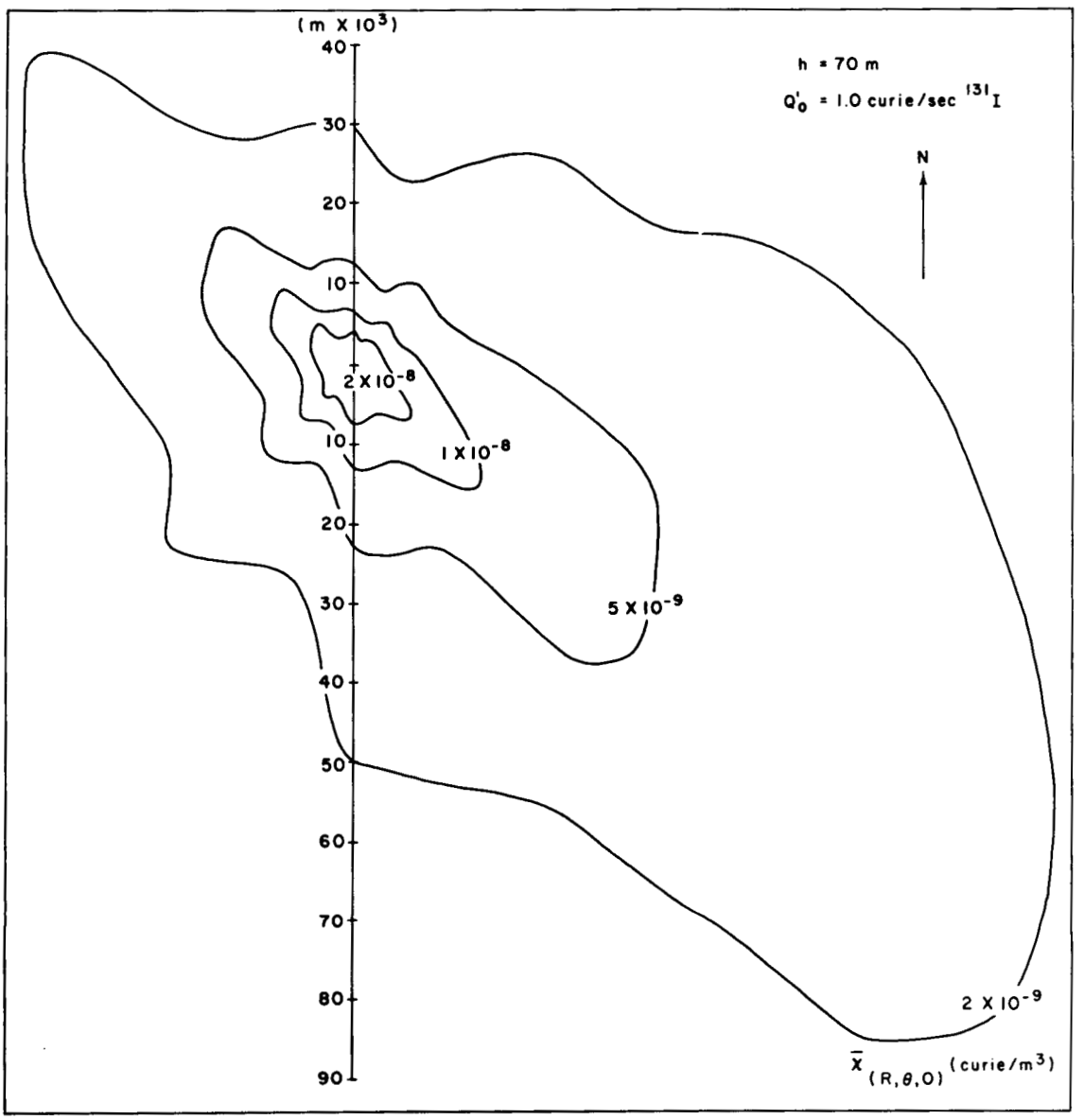

Fig. 8.17 — Isopleths of average cloud concentration of ^{131}I about the release point (long-period release).

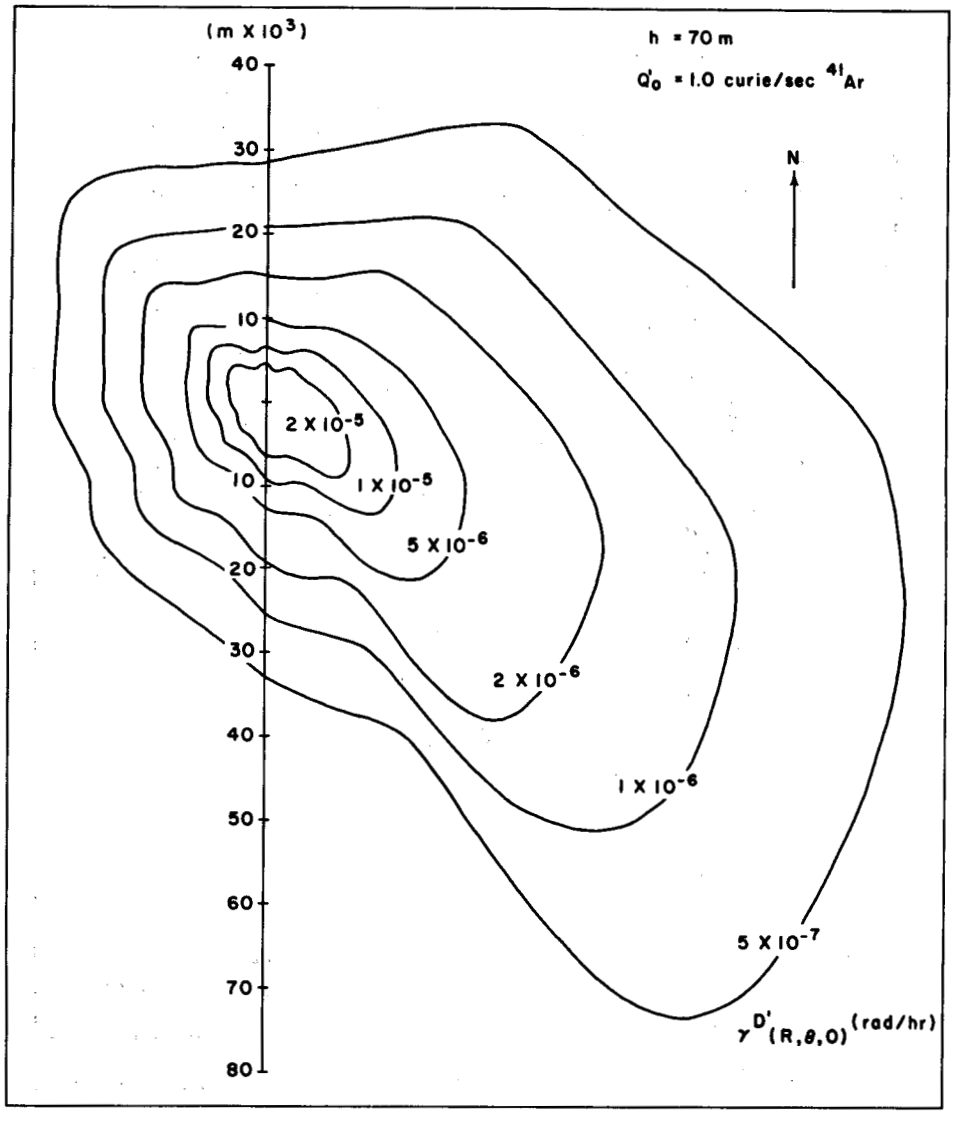

Fig. 8.18 — Isopleths of direct cloud gamma dose rate from ^{41}Ar (long-period release).

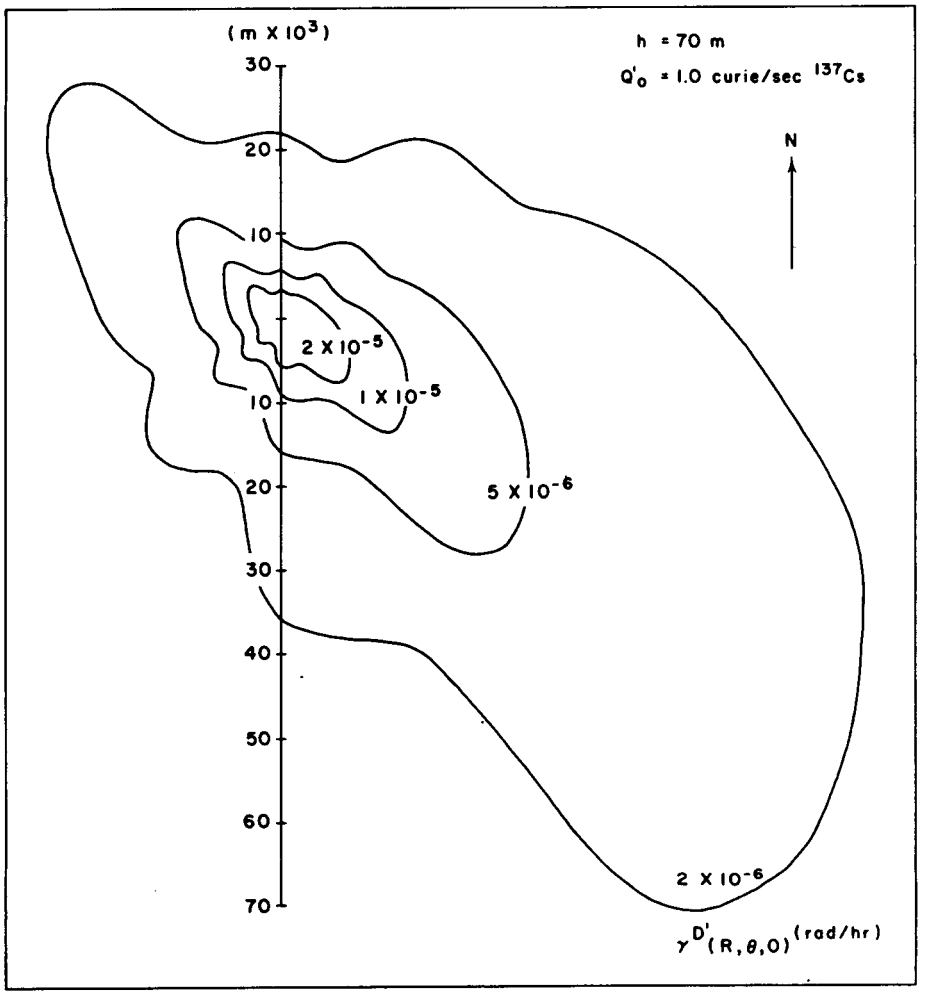

Fig. 8.19—Isopleths of direct cloud gamma dose rate from ^{137}Cs (long-period release).

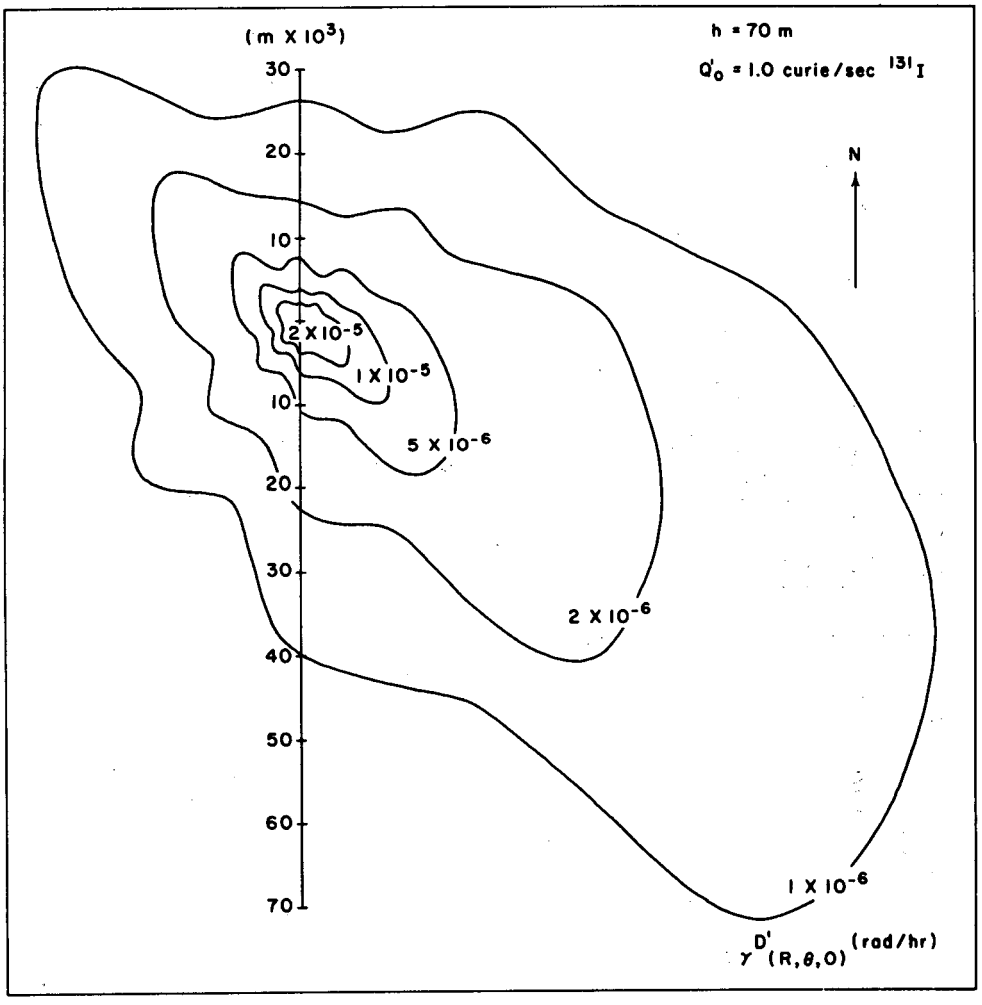

Fig. 8.20 — Isopleths of direct cloud gamma dose rate from ^{131}I (long-period release).

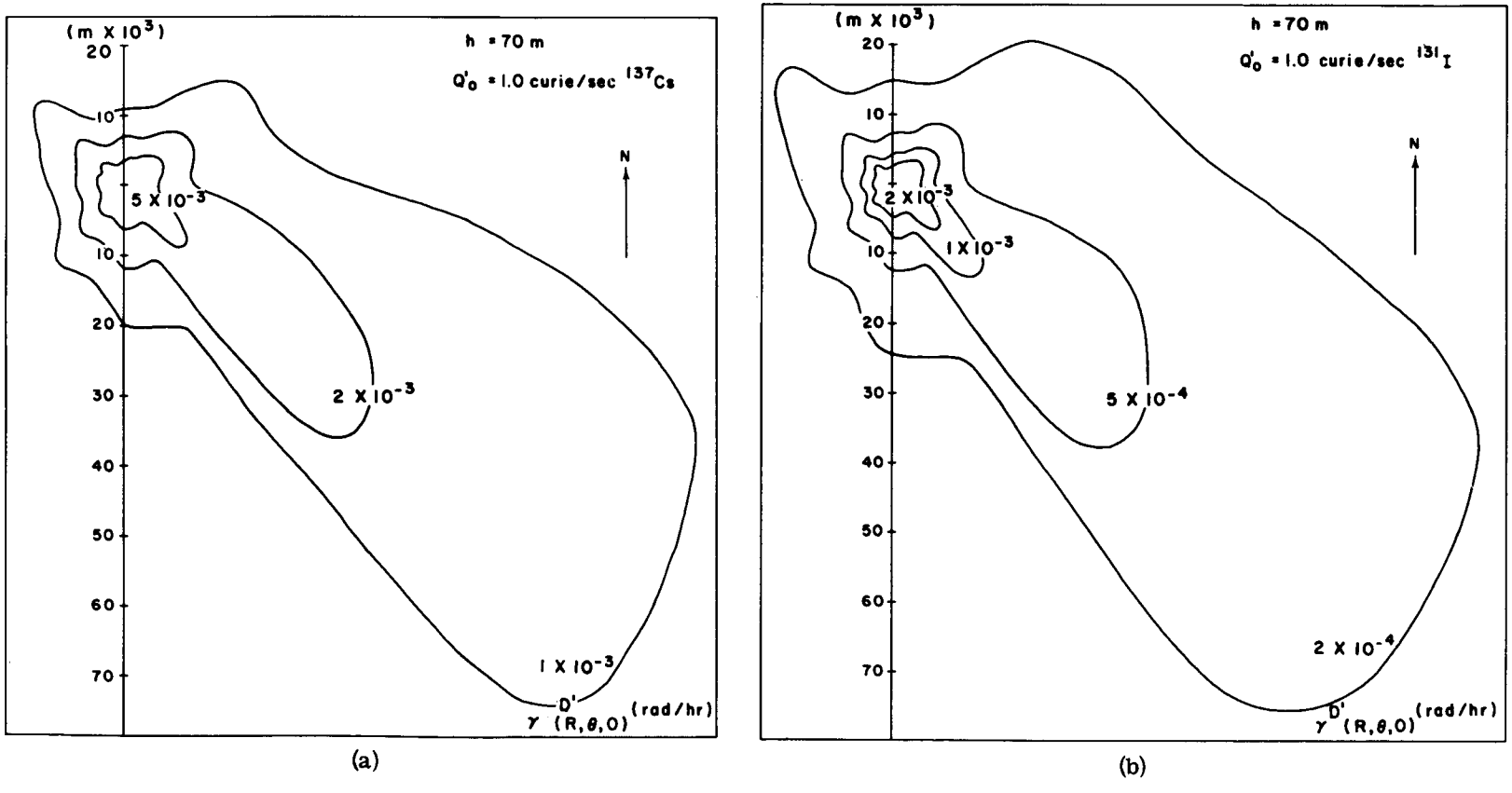

Fig. 8.21—Isopleths of dose rate from deposited material after 1 year (long-period release). (a) From ^{137}Cs source. (b) From ^{131}I source.

Appendix

This appendix contains four sections:

A-1. A listing of conversion factors.
A-2. A listing of commonly used diffusion equations.
A-3. Graphical and tabular aids.
A-4. A list of diffusion equations in the Sutton form.

The graphs in Sec. A-3 are presented as an illustration of what might be done with the diffusion equations rather than as a definitive collection. These graphs apply to continuous point source releases sampled for about 30 min. It is obviously impossible to present the many graphs that would result from considering various source configurations, release heights, and release lengths. In general, if a particular graph is needed repeatedly, it can be developed from the appropriate equation in rather short order.

Although the various forms of the diffusion equations presented by Sutton have not been discussed at great length in this volume, these equations are listed in Sec. A-4 of the Appendix. The nomenclature, as well as the chapter and section designations following the equations, refers to the 1955 edition of *Meteorology and Atomic Energy* where this material appeared in Appendix A.

The reader may find it useful to supplement this appendix with more detailed information. An excellent volume titled *Workbook of Atmospheric Dispersion Estimates* has been prepared (Turner, 1967). In addition to a variety of nomograms, conversion factors, and other helpful working information, the author presents detailed solutions to various forms of the diffusion equations covering a variety of situations.

Two comprehensive handbooks of use in diffusion meteorology as applied to chemical and radiological pollution problems are *Handbook of Air Pollution* (Sheehy, Achinger, and Simon, undated) and *Health Physics Handbook* (General Dynamics/Fort Worth, Tex., 1963). The former publication, in addition to extensive sections of dimensional conversion factors, has nomographic and tabular data on the properties of air, other gases, particulates, and pollutants of various types and also has sections directed toward the fields of medicine and mathematics. Although *Health Physics Handbook* is similarly extensive and contains a broad variety of conversion factors and nomograms, it deals entirely with working problems of the nuclear energy field and covers such topics as radiological monitoring, source and dose rate data, biological data, and shipping regulations.

An excellent guide for the estimation of diffusion is currently being prepared by a task group of the American Society of Mechanical Engineers. In addition to general discussions of diffusion meteorology, this guide will contain a number of working techniques for making first approximations of diffusion in simple situations.

A-1 CONVERSION FACTORS

LENGTH

1 m = 3.2808 ft
= 39.3701 in.
= 1.0936 yard
= 10^6 μ

1 km = 3280.84 ft
= 0.6214 statute mile
= 0.5396 nautical mile

1° latitude = 111.14 km
= 69.057 statute mile
= 60.0 nautical mile

1 in. = 2.540 cm

1 ft = 0.3048 m

1 statute mile = 0.8684 nautical mile
= 1.6093 km

AREA

1 sq in. = 6.4516 cm^2
= 0.007 sq ft

1 m^2 = 1550.0 sq in.
= 10.7639 sq ft

1 km^2 = 1.0764×10^7 sq ft
= 0.3861 statute $mile^2$

1 sq ft = 0.09290 m^2

1 sq statute mile = 2.590 km^2

VOLUME

1 m^3 = 999.972 liters
= 35.315 cu ft

1 liter = 61.0255 cu in.
= 0.2642 gal

1 cu ft = 28316.8 cm^3
= 28.316 liters
= 1728 cu in.

SPEED

1 m/sec = 1.9425 knots
= 2.2369 mph
= 3.2808 ft/sec
= 0.77742° latitude/day

1 knot = 1.1516 mph
= 1.6890 ft/sec
= 0.5148 m/sec

1 mph = 0.8684 knot
= 1.4667 ft/sec
= 1.6093 km/hr
= 0.4470 m/sec

1° latitude/day = 1.2863 m/sec
= 2.5 knots
= 2.8774 mph

1 ft/sec = 0.5921 knot
= 0.6818 mph
= 0.3048 m/sec

MASS

1 kg = 35.2740 oz
= 2.2046 lb

DENSITY

1 g/cm^3 = 62.4280 lb/cu ft

PRESSURE

1 standard atmosphere = 1013.25 mb
= 760 mm Hg
= 29.92 in. Hg
= 14.696 lb/sq in.
= 406.79 in. H_2O

ENERGY

1 Btu = 252 g-cal
= 1.055×10^{-3} Mw-sec

1 erg = 6.2421×10^{11} ev

1 ev = 1.60203×10^{-12} erg
= 1.60203×10^{-19} watt-sec

1 hp-hr = 2547 Btu

1 fission = 193.7 Mev
= 3.10×10^{-11} watt-sec

1 g-cal = 4.186 watt-sec

1 Mw = 3.413×10^6 Btu/hr

1 watt = 3.22×10^{10} fissions/sec

1 watt-sec = 9.480×10^{-4} Btu
= 6.2421×10^{18} ev
= 1×10^7 ergs
= 3.22×10^{10} fissions

RADIATION

1 barn = 10^{-24} cm^2

1 curie = 3.7×10^{10} disintegrations/sec
= 4.14×10^{-3} watt

1 rad = 100 ergs/g absorbing material

1 rem = 93 ergs/g

1 r = 1 esu charge/cm^3 (air)
= 2.09×10^9 ion pairs/cm^3
= 83.8 ergs/g (air)
= 93.0 ergs/g (tissue)

A-2 COMMONLY USED DIFFUSION EQUATIONS

List of Symbols

Symbols used in diffusion equations in Sec. A-2 are given here. (The dimensions mass, length, and time are abbreviated as M, L, and T, respectively.)

h	Height of source above the ground (L)
Q	Total amount of material released from a point source (M or other units of amount)
Q'	Rate of material emission from a continuous point source (M/T)
Q_L	Total amount of material emitted per unit length from a continuous line source (M/L)
Q'_L	Rate of material emission per unit length from a continuous line source (M/LT)
t	Time (T)
$\bar{u}$	Average value of the wind component in the x (along-wind) direction; in practical diffusion computations, $\bar{u}$ is usually assumed to be equal to the total horizontal wind speed as measured by an anemometer (L/T)
x,y,z	Positions in a Cartesian coordinate system that is usually oriented so that the x-axis is in the direction of the mean horizontal wind vector, the y-axis is crosswind, and the z-axis is vertical (L)
σ_y,σ_z	Standard deviation of the distribution of material in a plume in the y- and z-directions (L)
$\sigma_{xI},\sigma_{yI},\sigma_{zI}$	Standard deviation of the distribution of material in a puff in the x-, y-, and z-directions (L)
χ	The instantaneous value of the concentration (M/L^3)
$\bar{\chi}$	Time-averaged value of the concentration (M/L^3)
$\chi_{CWI},\bar{\chi}_{CWI}$	Crosswind integrated concentration (M/L^2)
$\bar{\chi}_F$	Fumigation concentration (M/L^3)
$\bar{\chi}_p$	Peak or center-line concentration value (M/L^3)
ψ	Exposure (MT/L^3); subscripts p and CWI have the same meaning as for concentration (also referred to as concentration time integral)

Diffusion Equations

1. Concentration from an instantaneous point source (Sec. 3-3.5.8):

$$\chi = \frac{Q}{2^{1/2}\pi^{3/2}\sigma_{xI}\sigma_{yI}\sigma_{zI}} \exp\left\{-\left[\frac{(x-\bar{u}t)^2}{2\sigma_{xI}^2}+\frac{y^2}{2\sigma_{yI}^2}+\frac{h^2}{2\sigma_{zI}^2}\right]\right\}$$

2. Exposure from an instantaneous point source (Sec. 3-3.5.8):

$$\psi = \frac{Q}{\pi \sigma_{yI} \sigma_{zI} \bar{u}} \exp\left[- \left(\frac{y^2}{2\sigma_{yI}^2} + \frac{h^2}{2\sigma_{zI}^2} \right) \right]$$

3. Average concentration from a continuous point source (Sec. 3-3.1):

$$\bar{\chi} = \frac{Q'}{2\pi \sigma_y \sigma_z \bar{u}} \exp\left(- \frac{y^2}{2\sigma_y^2} \right) \left\{ \exp\left[- \frac{(z-h)^2}{2\sigma_z^2} \right] + \exp\left[- \frac{(z+h)^2}{2\sigma_z^2} \right] \right\}$$

or, if the receptor is at ground level (z = 0).

$$\bar{\chi} = \frac{Q'}{\pi \sigma_y \sigma_z \bar{u}} \exp\left[- \left(\frac{y^2}{2\sigma_y^2} + \frac{h^2}{2\sigma_z^2} \right) \right]$$

which, if the center-line concentration from a surface source is of interest, reduces to

$$\bar{\chi}_p = \frac{Q'}{\pi \sigma_y \sigma_z \bar{u}}$$

4. Crosswind integrated average concentration from a continuous point source (Sec. 3-3.5.3):

$$\bar{\chi}_{CWI} = \left(\frac{2}{\pi} \right)^{1/2} \frac{Q'}{\sigma_z \bar{u}} \exp\left(- \frac{h^2}{2\sigma_z^2} \right)$$

5. Crosswind integrated concentration from an instantaneous point source (Sec. 3-3.5.8):

$$\chi_{CWI} = \frac{Q}{\pi \sigma_{xI} \sigma_{zI}} \exp\left\{ - \left[\frac{(x - \bar{u}t)^2}{2\sigma_{xI}^2} + \frac{h^2}{2\sigma_{zI}^2} \right] \right\}$$

6. Crosswind integrated exposure from an instantaneous point source (Sec. 3-3.5.8):

$$\psi_{CWI} = \left(\frac{2}{\pi} \right)^{1/2} \frac{Q}{\sigma_{zI} \bar{u}} \exp\left(- \frac{h^2}{2\sigma_{zI}^2} \right)$$

7. Concentration from an instantaneous infinite crosswind line source (Sec. 3-3.5.8):

$$\chi = \frac{Q_L}{\pi \sigma_{xI} \sigma_{zI}} \exp\left\{ - \left[\frac{(x - \bar{u}t)^2}{2\sigma_{xI}^2} + \frac{h^2}{2\sigma_{zI}^2} \right] \right\}$$

8. Exposure from an instantaneous infinite crosswind line source (Sec. 3-3.5.8):

$$\psi = \left(\frac{2}{\pi} \right)^{1/2} \frac{Q_L}{\sigma_{zI} \bar{u}} \exp\left(- \frac{h^2}{2\sigma_{zI}^2} \right)$$

9. Average concentration from a continuous infinite crosswind line source:

$$\bar{\chi} = \left(\frac{2}{\pi}\right)^{1/2} \frac{Q'_L}{\sigma_z \bar{u}} \exp\left(-\frac{h^2}{2\sigma_z^2}\right)$$

10. Average long-period concentration from a continuous point source (Sec 3-3.5.4):

$$\bar{\chi}_{\text{long-term av./sector}} = \left(\frac{2}{\pi}\right)^{1/2} \frac{0.01fQ'}{\sigma_z \bar{u}_{(2\pi x/n)}} \exp\left(-\frac{h^2}{2\sigma_z^2}\right)$$

where f is the percent of frequency with which the wind blows from a given sector, $2\pi x/n$ is the sector width for each of n sectors at the distance x, and Q', σ_z, and $\bar{u}$ are average values for the long time period.

11. Maximum ground-level concentration and exposure from elevated sources and distance to the maximum (Sec. 3-3.5.5): For elevated continuous point sources, the maximum ground-level concentration and its distance from the source can be determined directly from Fig. A.4 of Sec. A-3. Formulations in the Sutton framework are in Sec. A-4 of the Appendix. Concentration and exposure maximums for instantaneous sources can be determined from the σ_{yI} and σ_{zI} values in Table A.2 and the appropriate instantaneous-source equations.

12. Average fumigation (trapping) concentration from a continuous point source (Sec. 3-3.5.1):

$$\bar{\chi}_F = \frac{Q'}{(2\pi)^{1/2} \bar{u} H \sigma_y} \exp\left(-\frac{y^2}{2\sigma_y^2}\right)$$

where the plume lies below the level H, the height of the base of the inversion.

The above equations in the generalized Gaussian form can be converted to the corresponding Sutton form through the following identities:

$$\sigma_y^2 = \tfrac{1}{2} C_y^2 x^{2-n}$$

$$\sigma_z^2 = \tfrac{1}{2} C_z^2 x^{2-n}$$

where C_z and C_y are Sutton's virtual diffusion coefficients.

Formulas for the plume half-width and half-depth are

$$y_p = \left(2\sigma_y^2 \ln \frac{100}{p}\right)^{1/2}$$

$$z_p = \left(2\sigma_z^2 \ln \frac{100}{p}\right)^{1/2}$$

where p is the required percent of the axial concentration (see Sec. 3-3.5.6).

A-3 GRAPHICAL AND TABULAR AIDS

The following tables and graphs (Tables A.1 and A.2 and Figs. A.1–A.8) are based either on the Pasquill graphs in the version given by Hilsmeier and Gifford (1962) or on the discussion of instantaneous-source information in Chap. 4. The Pasquill curves can be relabeled in terms of σ_θ as noted in Secs. 4-4.3 and 4-4.4. No account was taken of the effect of a lid to vertical mixing in the construction of the continuous-source graphs. This should be considered as indicated in Sec. 3-3.5.1.2.

Table A.1—RELATION OF PASQUILL TURBULENCE TYPES TO WEATHER CONDITIONS

A—Extremely unstable conditions
B—Moderately unstable conditions
C—Slightly unstable conditions
D—Neutral conditions*
E—Slightly stable conditions
F—Moderately stable conditions

Surface wind speed, m/sec	Daytime insolation			Nighttime conditions	
	Strong	Moderate	Slight	Thin overcast or ≥ 4/8 cloudiness†	≤ 3/8 cloudiness
<2	A	A-B	B		
2	A-B	B	C	E	F
4	B	B-C	C	D	E
6	C	C-D	D	D	D
>6	C	D	D	D	D

*Applicable to heavy overcast, day or night.
†The degree of cloudiness is defined as that fraction of the sky above the local apparent horizon that is covered by clouds.

Table A.2—SUGGESTED VALUES OF σ_{yI}, σ_{zI}, AND $\psi_p\bar{u}/Q$ FOR INSTANTANEOUS RELEASES*†

Parameter	Conditions	Value at 100 m	Value at 4000 m	Approximate power function
σ_{yI}, m	Unstable	10.0	300	$0.14(x)^{0.92}$
	Neutral	4.0	120	$0.06(x)^{0.92}$
	Very stable	1.3	35.0	$0.02(x)^{0.89}$
σ_{zI}, m	Unstable	15.0	220	$0.53(x)^{0.73}$
	Neutral	3.8	50.0	$0.15(x)^{0.70}$
	Very stable	0.75	7.0	$0.05(x)^{0.61}$
$\psi_p\bar{u}/Q$, m^{-2}	Unstable	2.12×10^{-3}	4.81×10^{-6}	$4.20(x)^{-1.65}$
	Neutral	2.08×10^{-2}	5.30×10^{-5}	$35.5(x)^{-1.62}$
	Very stable	3.26×10^{-1}	1.30×10^{-3}	$330.0(x)^{-1.50}$

*See Sec. 4-10.3.
†The power functions are applicable in the given range of distances only.

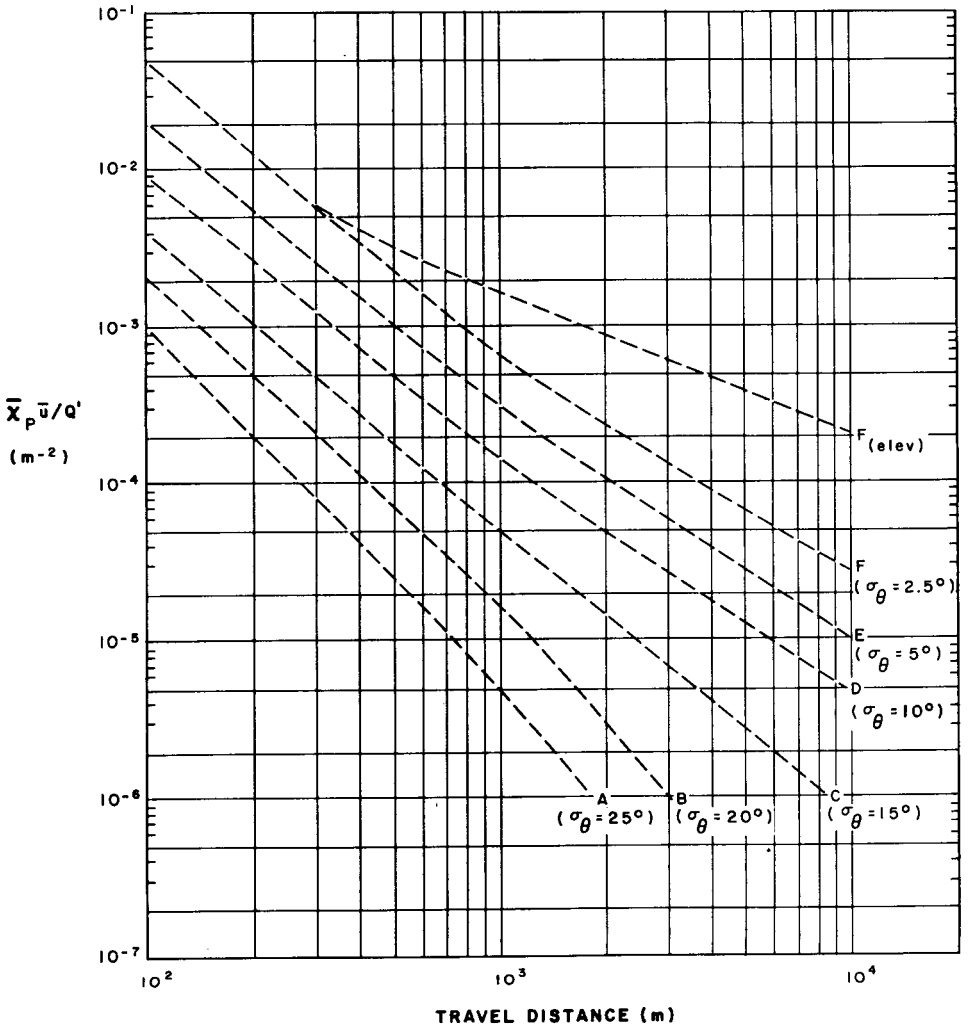

Fig. A.1—Normalized average axial concentration, $\bar{\chi}_p \bar{u}/Q'$, as a function of travel distance from a continuous source. A–F are Pasquill's diffusion categories.

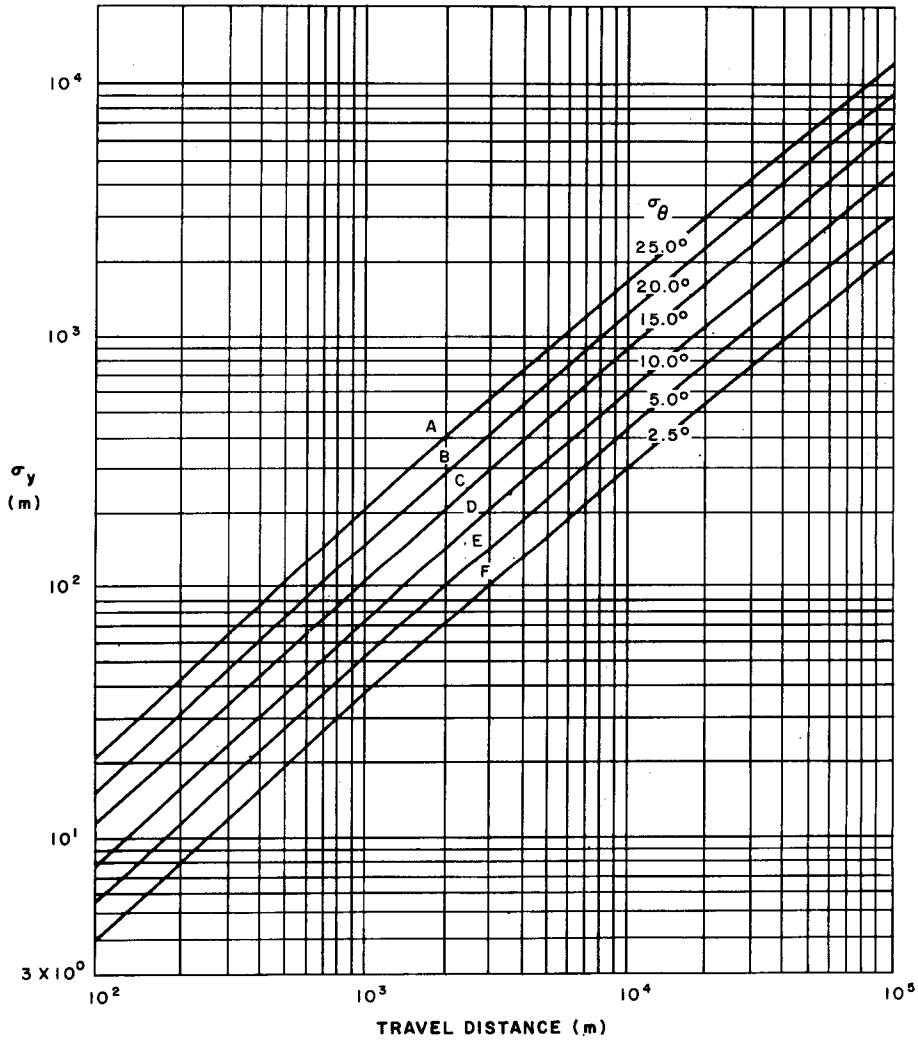

Fig. A.2 — Standard deviation of the lateral concentration distribution, σ_y, as a function of travel distance from a continuous source. A–F are Pasquill's diffusion categories.

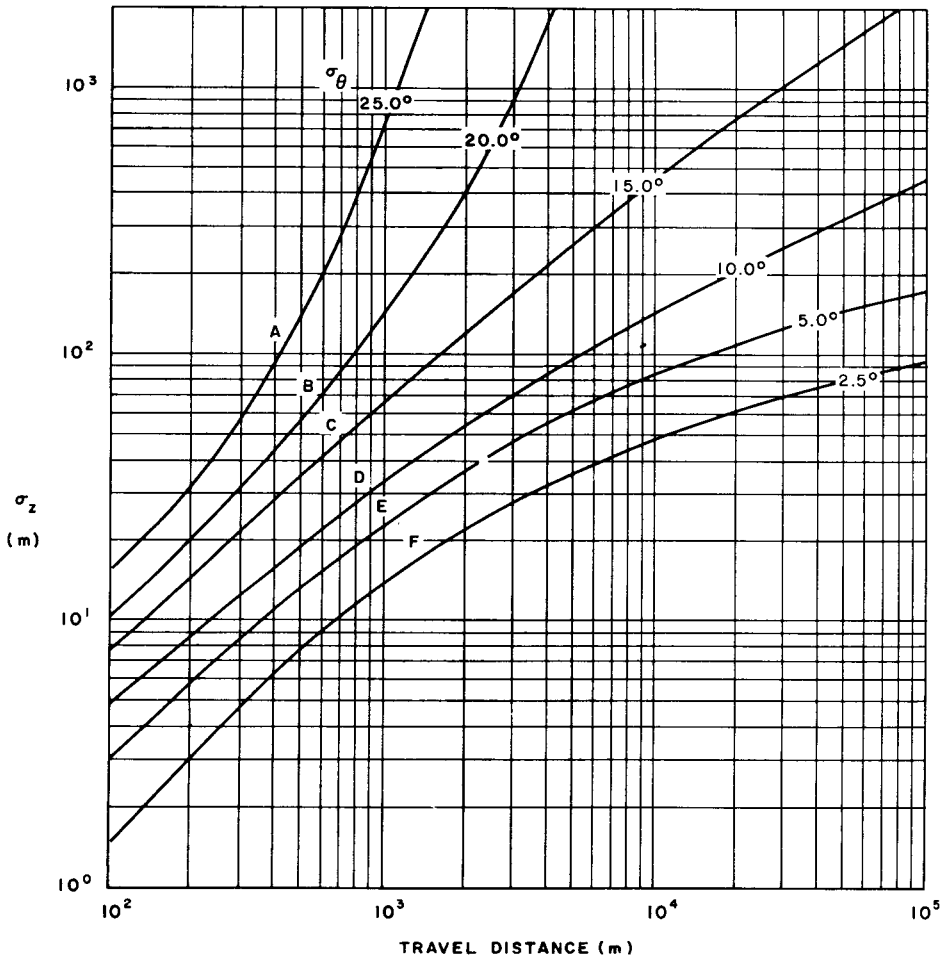

Fig. A.3—Standard deviation of the vertical concentration distribution, σ_z, as a function of travel distance from a continuous source. A–F are Pasquill's diffusion categories.

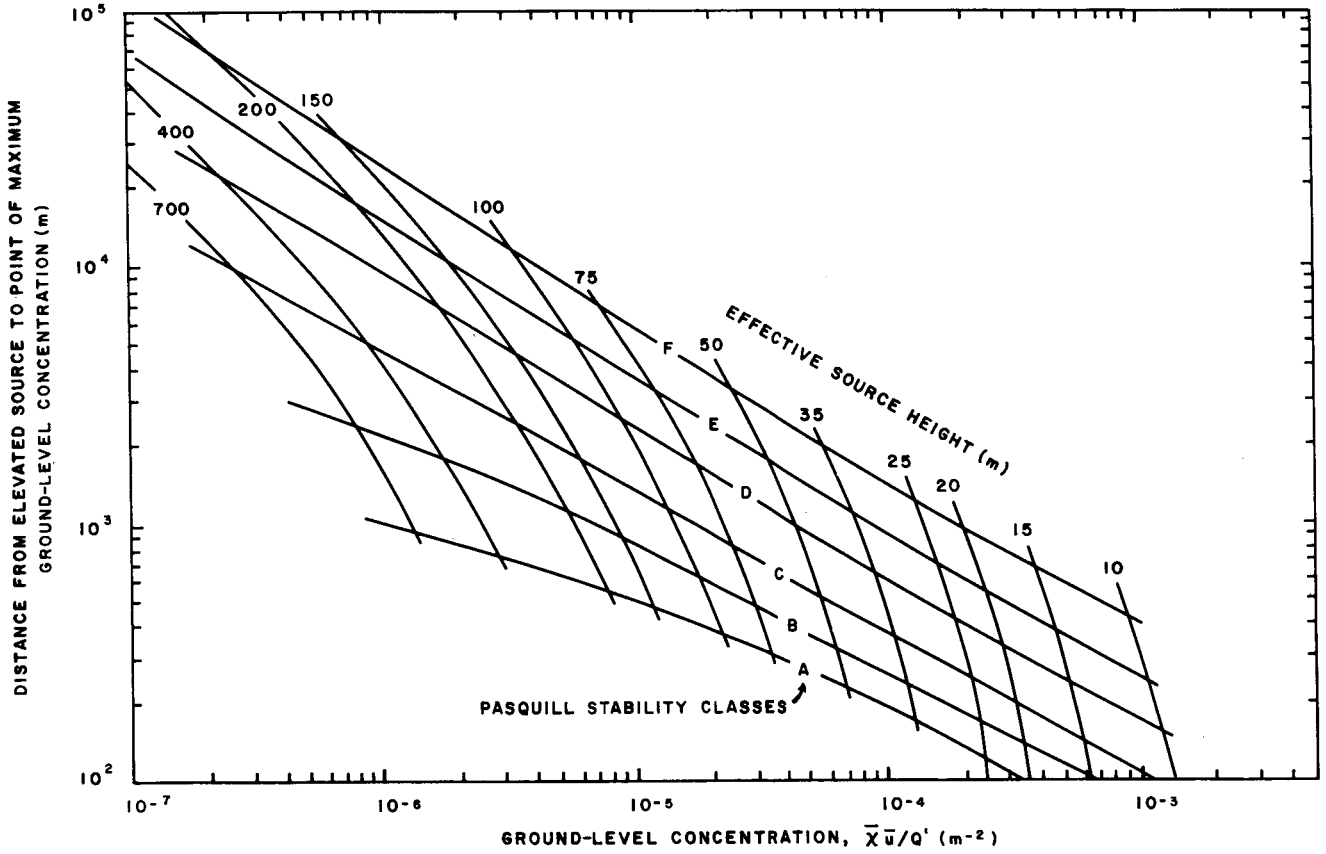

Fig. A.4—Distance from an elevated continuous source to point of maximum ground-level average concentration and values of maximum ground-level concentration for various effective source heights and stability categories (D.O. Martin, 1965).

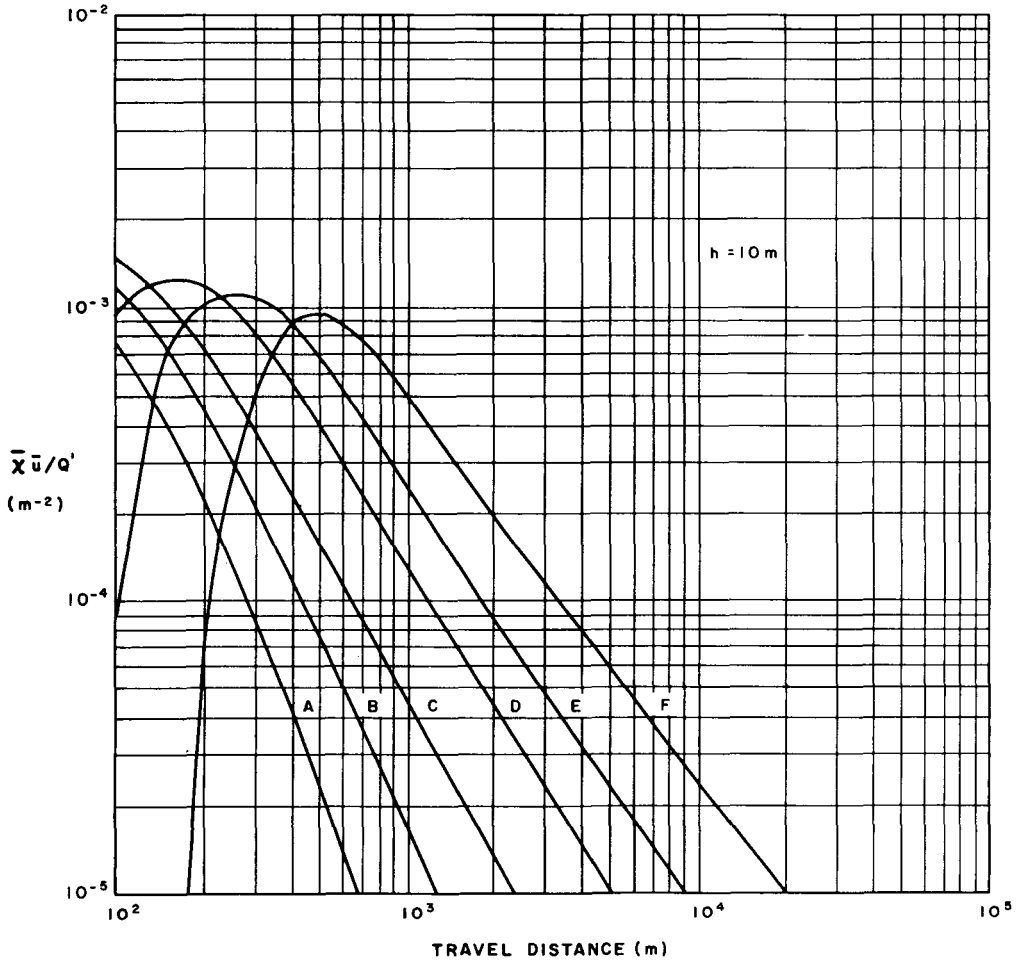

Fig. A.5—Normalized ground-level average concentration for an effective source height of 10 m as a function of distance from the source (Hilsmeier and Gifford, 1962). A–F are Pasquill's diffusion categories.

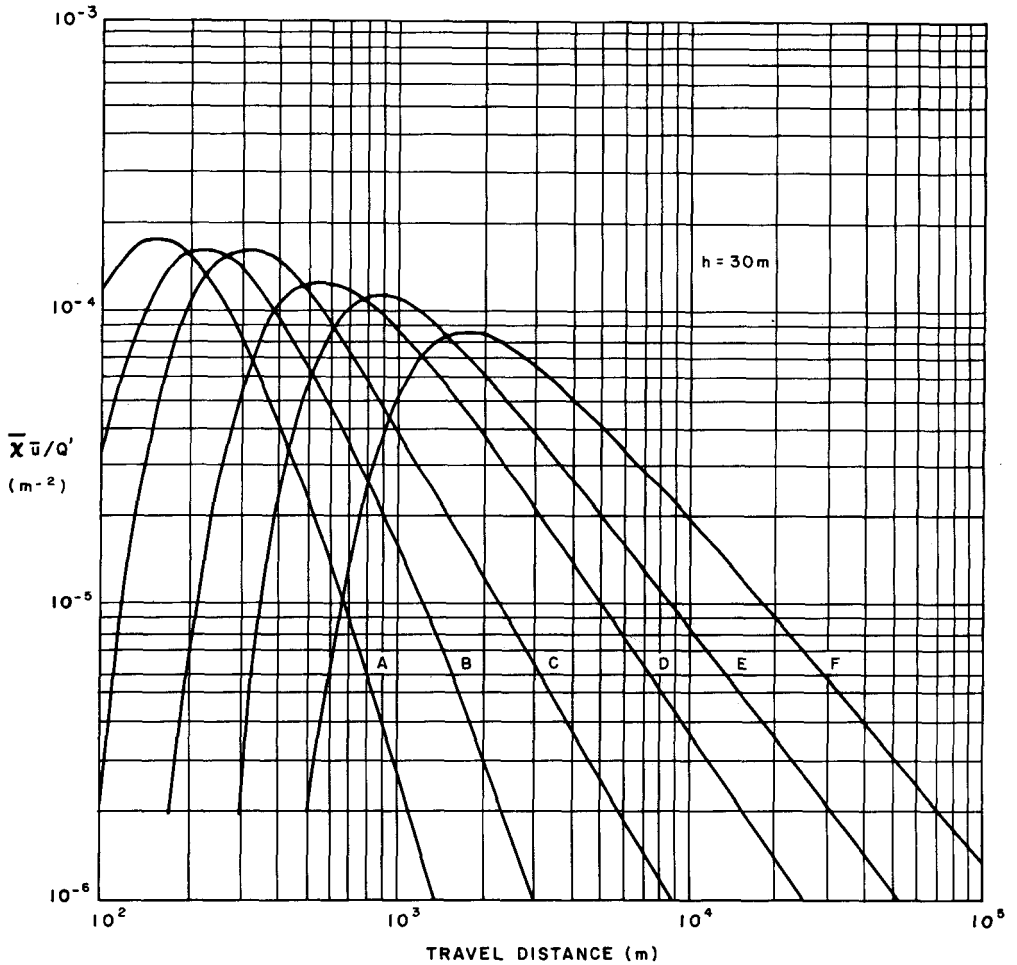

Fig. A.6—Normalized ground-level average concentration for an effective source height of 30 m as a function of distance from the source (Hilsmeier and Gifford, 1962). A–F are Pasquill's diffusion categories.

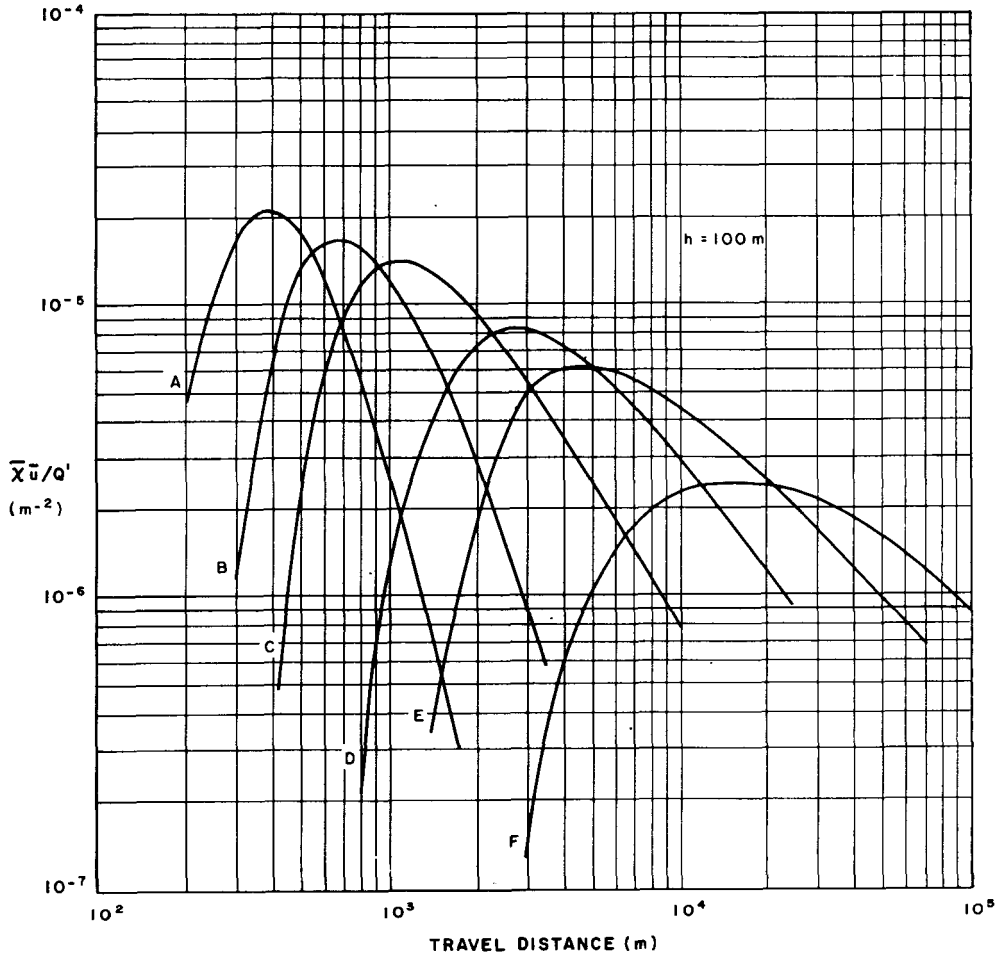

Fig. A.7—Normalized ground-level average concentration for an effective source height of 100 m as a function of distance from the source (Hilsmeier and Gifford, 1962). A–F are Pasquill's diffusion categories.

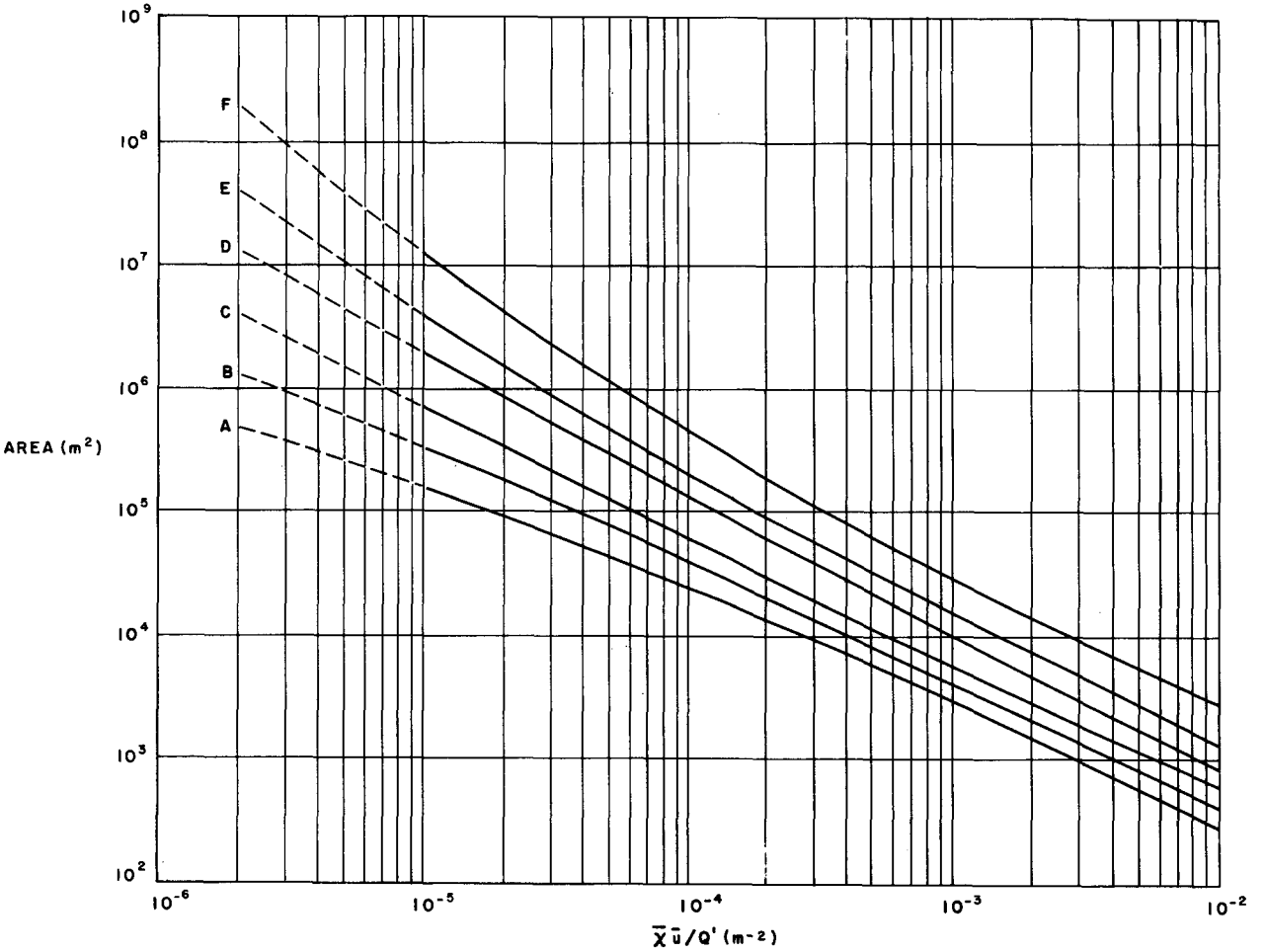

Fig. A.8—Areas with average ground-level concentration isopleths ($\bar{\chi}$) in terms of $\bar{\chi}\bar{u}/Q'$ for a ground-level source for various stability categories (Hilsmeier and Gifford, 1962). A–F are Pasquill's diffusion categories.

A-4 SUTTON EQUATIONS

This information has been taken directly from the original edition of *Meteorology and Atomic Energy* (U. S. Weather Bureau, 1955). Chapter and section designations, as well as nomenclature, refer to that volume.

A.1 GENERAL NOMENCLATURE

χ = concentration (grams per cubic meter, curies per cubic meter, etc.)
Q = source strength (instantaneous; grams, curies, etc.)
= emission rate (continuous; grams per second, curies per second, etc.)
= emission rate (continuous line source; grams per second per meter, etc.)
C_x, C_y, C_z = diffusion coefficients $[(\text{meters})^{n/2}]$ in the x, y, and z planes, respectively
C = generalized diffusion coefficient $[(\text{meters})^{n/2}]$ for isotropic turbulence, i.e., $C = C_x = C_y = C_z$
n = nondimensional parameter associated with stability
x, y, z = downwind, crosswind, and vertical coordinates measured from a ground point beneath a continuous source and from the center of the moving cloud in the instantaneous case (meters)
t = time (seconds)
$\bar{u}$ = mean wind speed (meters per second)
h = height of source or, alternatively, height of plume

A.2 CONCENTRATION

Continuous point source (see Chap. 4, Sec. 2.1):

$$\chi_{(x,y)} = \frac{2Q}{\pi C^2 \bar{u} x^{2-n}} \exp\left(-\frac{y^2 + h^2}{C^2 x^{2-n}}\right)$$

(Note that Q is doubled to allow for reflection by the ground.)

Instantaneous elevated point source (see Chap. 4, Sec. 1.6):

$$\chi_{(x,y)} = \frac{2Q}{\pi^{3/2} C^3 (\bar{u}t)^{3(2-n)/2}} \exp\left[-\frac{x^2 + y^2 + h^2}{C^2 (\bar{u}t)^{2-n}}\right]$$

Continuous infinite elevated crosswind line source (see Chap. 1, Sec. 2.2):

$$\chi_{(x)} = \frac{2Q}{\pi^{1/2} C \bar{u} x^{(2-n)/2}} \exp\left(-\frac{h^2}{C^2 x^{2-n}}\right)$$

A.3 FINITE VOLUME CORRECTION

Instantaneous source (see Chap. 4, Sec. 2.3):

$$(\bar{u}t)_0 = \left(\frac{2Q/\chi(0)}{\pi^{3/2}C^3}\right)^{2/3(2-n)} \qquad \text{(ground source)}$$

Continuous source:

$$x_0 = \left(\frac{2Q/\chi(0)}{\pi C^2 \bar{u}}\right)^{1/(2-n)} \qquad \text{(ground source)}$$

where x_0 or $(\bar{u}t)_0$ = distance upwind from a real source required to produce the required volume at the point (0,0,0) and $t = 0$

$\chi(0)$ = central concentration

A.4 FORMULAE FOR SPECIAL CASES

Instantaneous point source (see Chap. 4, Sec. 2.4):

$$d_{max} = \left(\frac{2h^2}{3C^2}\right)^{1/(2-n)}$$

$$\chi_{max} = \frac{2Q}{(2/3\ e\pi)^{3/2}h^3}$$

$$TID = \frac{2Q}{\pi C^2 \bar{u}(\bar{u}t)^{2-n}} \exp\left[-\frac{h^2}{C^2(\bar{u}t)^{2-n}}\right]$$

$$TID_{max} = \frac{2Q}{\pi e \bar{u} h^2}$$

$$d_{max\ dosage} = \left(\frac{h^2}{C^2}\right)^{1/(2-n)}$$

where d_{max} = distance, downwind from the source, of the maximum concentration

χ_{max} = concentration at d_{max}

TID = total integrated dosage (see Chap. 4, Sec. 2.6a)

Continuous point source (see Chap. 4, Secs. 2.4, 2.6a, and 2.6c):

$$d_{max} = \left(\frac{h^2}{C^2}\right)^{1/(2-n)}$$

$$\chi_{max} = \frac{2Q}{e\pi\bar{u}h^2} \qquad \text{[anisotropic, multiply by } (C_z/C_y)\text{]}$$

$$2y_0 = 2\left(\ln \frac{100}{p}\right)^{1/2} C_y x^{(2-n)/2}$$

$$z_0 = \left(\ln \frac{100}{p}\right)^{1/2} C_z x^{(2-n)/2}$$

$$\chi_{\text{fumigation conc.}} = \frac{Q}{(\pi)^{1/2} C_y \bar{u} H x^{(2-n)/2}}$$

$$\chi_{\text{av. conc. over long period}} = \frac{0.02Qf}{\pi^{1/2} C_z \bar{u} x^{2-(n/2)}} \times \exp\left(-\frac{h^2}{C_z^2 x^{2-n}}\right)$$

where p = percent of axial concentration
$2y_0$ = cloud width
z_0 = cloud height
H = height of inversion
f = wind direction frequency (percent) per radian

Bibliography

Altshuller, A. P., 1963, Gas Chromatography in Air Pollution Studies, *J. Gas Chromatog.*, 1(7): 6-20.

Anderson, E. R., L. J. Anderson, and J. J. Marciano, 1950, *A Review of Evaporation Theory and Development of Instrumentation*, Interim Report: Lake Mead Water Loss Investigations, U. S. Navy Electronics Laboratory, Report 159.

Angell, J. K., 1961, Use of Constant Level Balloons in Meteorology, *Advances in Geophysics*, Vol. 8, pp. 137-219, H. E. Landsburg and J. Van Meighem (Eds.), Academic Press Inc., New York.

———, 1962, On the Use of Tetroons for the Estimation of Atmospheric Dispersion on the Mesoscale, *Monthly Weather Rev.*, 90(7): 263-270.

———, 1963, A Summary of Tetroon Flights at Cardington, England, with Emphasis on Eulerian–Lagrangian Scale Estimates Derived Therefrom, U. S. Weather Bureau, unpublished.

———, 1964, Measurements of Lagrangian and Eulerian Properties of Turbulence at a Height of 2500 Feet, *Quart. J. Roy. Meteorol. Soc.*, 90(383): 57-71.

———, and D. H. Pack, 1960, Analysis of Some Preliminary Low-level Constant Level Balloon (Tetroon) Flights, *Monthly Weather Rev.*, 88(7): 235-248.

———, and D. H. Pack, 1961, Estimation of Vertical Air Motions in Desert Terrain from Tetroon Flights, *Monthly Weather Rev.*, 89(8): 273-283.

———, and D. H. Pack, 1962, Analysis of Low-level Constant Volume Balloon (Tetroon) Flights from Wallops Island, *J. Atmospheric Sci.*, 19(1): 87-98.

———, and D. H. Pack, 1965, Atmospheric Lateral Diffusion Estimates from Tetroons, *J. Appl. Meteorol.*, 4(3): 418-425.

Arie, M., and H. Rouse, 1956, Experiments on Two-dimensional Flow over a Normal Wall, *J. Fluid Mech.*, 1: 129-141.

aufm Kampe, H. J., and H. K. Weickmann, 1957, Physics of Clouds, *Meteorol. Monographs*, 3: 182-225.

Badgley, F. I., and R. G. Fleagle, 1952, *Photographic Study of Turbulence*, Occasional Report 2, Atmospheric Turbulence Study, Department of Meteorology and Climatology, University of Washington, Seattle, Wash.

Baines, W. D., 1963, Effects of Velocity Distribution on Wind Loads and Flow Patterns on Buildings, paper presented at International Conference on Wind Effects on Buildings and Structures, National Physical Laboratory, Teddington, Middlesex.

Baldwin, L. V., and W. R. Mickelsen, 1961, The Experimental Relation Between Turbulent Diffusion and Hot-wire Anemometer Measurements, paper presented at American Society of Civil Engineers Conference, New York, October 1961.

Ball, F. K., 1958, Some Observations of Bent Plumes, *Quart. J. Roy. Meteorol. Soc.*, 84(359): 61-65.

Barad, M. L., 1951, Diffusion of Stack Gases in Very Stable Atmosphere, *Meteorol. Monographs*, 1(4): 9-19.

———, (Ed.), 1958, Project Prairie Grass, A Field Program in Diffusion, *Geophysical Research Papers, No. 59*, Vols. I and II, Report AFCRC-TR-58-235, July 1958 (ASTIA Documents AD-152572 and AD-152573), Air Force Cambridge Research Center.

———, 1959, Analysis of Diffusion Studies at O'Neill, *Advances in Geophysics*, Vol. 6, pp. 389-396, F. N. Frenkiel and P. A. Sheppard (Eds.), Academic Press Inc., New York.

———, and J. J. Fuquay (Eds.), 1962, The Green Glow Diffusion Program, *Geophysical Research Papers, No. 73*, Vols. I and II, USAEC Report HW-71400 (Report AFCRL-62-251(I), January 1962, and Report AFCRL-62-251(II), April 1962), Air Force Cambridge Research Laboratories.

———, and J. J. Fuquay, 1962a, Diffusion in Shear Flow, *J. Appl. Meteorol.*, 1(2): 257-264.

———, and D. A. Haugen, 1959, A Preliminary Evaluation of Sutton's Hypothesis for Diffusion from a Continuous Point Source, *J. Meteorol.*, 16(1): 12-20.

———, D. A. Haugen, and J. J. Fuquay, 1960, A Diffusion-Deposition Model for In-flight Release of Fission Fragments, *Air Force Surveys in Geophysics, No. 123*, Report AFCRC-TN-60-400, Air Force Cambridge Research Center.

———, and B. Shorr, 1954, Field Studies of the Diffusion of Aerosols, *Am. Ind. Hyg. Assoc. Quart.*, 15(2): 136-140.

Barger, G. L. (Ed.), 1960, *Climatology at Work*, National Weather Records Center, U. S. Weather Bureau, Asheville, N. C.

Barry, P. J., 1964, *Estimation of Downwind Concentration of Airborne Effluents Discharged in the Neighborhood of Buildings*, Canadian Report AECL-2043, July 1964.

Batchelor, G. K., 1949, Diffusion in a Field of Homogeneous Turbulence. I. Eulerian Analysis, *Australian J. Sci. Res.*, 2: 437-450.

———, 1950, Application of the Similarity Theory of Turbulence to Atmospheric Diffusion, *Quart. J. Roy. Meteorol. Soc.*, 76(328): 133-146.

———, 1952, Diffusion in a Field of Homogeneous Turbulence. II. The Relative Motion of Particles, *Proc. Cambridge Phil. Soc.*, 48: 345-362.

———, 1954, Heat Convection and Buoyancy Effects in Fluids, *Quart. J. Roy. Meteorol. Soc.*, 80(345): 339-358.

———, 1959, Some Reflections on the Theoretical Problems Raised at the Symposium, *Advances in Geophysics*, Vol. 6, pp. 449-452, F. N. Frenkiel

and P. A. Sheppard (Eds.), Academic Press Inc., New York.

———, 1959a, Note on the Diffusion from Sources in a Turbulent Boundary Layer, unpublished.

———, 1964, Diffusion from Sources in a Turbulent Boundary Layer, *Arch. Mech. Stosowanej*, 3: 661-670.

Bateman, H., 1910, The Solution of a System of Differential Equations Occurring in the Theory of Radioactive Transformations, *Proc. Cambridge Phil. Soc.*, 15: 423-427.

———, 1956, Turbulent Flow, *Hydrodynamics*, Part III, H. Dryden, F. D. Murnaghan, and H. Bateman (Eds.), Dover Publications, Inc., New York.

Beattie, J. R., 1961, *An Assessment of Environmental Hazards from Fission Product Releases*, British Report AHSB(S)R-9.

Beaver, Sir Hugh (Chairman), 1954, *Report of Government Committee on Air Pollution*, Command Paper 9322, Her Majesty's Stationery Office, London.

Bernstein, A. B., and C. R. Hosler, 1959, Temperature Patterns Along the Atlantic and Gulf Coasts, *Monthly Weather Rev.*, 87(11): 395-400.

Best, A. C., 1950, The Size Distribution of Raindrops, *Quart. J. Roy. Meteorol Soc.*, 76(327): 16-36.

———, 1957, Maximum Gas Concentration at Ground Level from Industrial Chimneys, *J. Inst. Fuel*, 30(197): 329-338.

Bierly, E. W., and E. W. Hewson, 1962, Some Restrictive Meteorological Conditions To Be Considered in the Design of Stacks, *J. Appl. Meteorol.*, 1(3): 383-390.

Blackadar, A. K., H. A. Panofsky, G. E. McVehil, and S. H. Wollaston, 1960, *Structure of Turbulence and Mean Wind Profiles Within the Atmospheric Boundary Layer*, Report AFCRL-TR-60-422, Pennsylvania State University.

Blanc, Milton L., 1958, *Climatological Investigation of Soil Temperature*, Technical Note 20, WMO 72, T.P. 28, World Meteorological Organization, Geneva, Switzerland.

Bolles, R. C., and N. E. Ballou, 1959, Calculated Activities and Abundances of U^{235} Fission Products, *Nucl. Sci. Eng.*, 5: 156-185.

Booker, D. V., 1965, Exchange Between Water Droplets and Tritiated Water Vapour, *Quart. J. Roy. Meteorol. Soc.*, 91(387): 73-79.

Bosanquet, C. H., 1957, The Rise of a Hot Waste Gas Plume. *J. Inst. Fuel*. 30(197): 322-328.

———, W. E. Carey, and E. M. Halton, 1950, Dust Deposition from Chimney Stacks, *Proc. Inst. Mech. Engrs. (London)*, 162: 355-367.

———, and J. L. Pearson, 1936, The Spread of Smoke and Gases from Chimneys, Disperse Systems in Gases, *Trans. Faraday Soc.*, 32: 1249-1264.

Boussinesq, J., 1877, Essai sur la Théorie des Eaux Courantes, *Mémoires Présentés par Divers Savants à l'Académie des Sciences de l'Institut de France*, Paris, 23: 1-680.

Bowne, N. E., 1961, Some Measurements of Diffusion Parameters from Smoke Plumes, *Bull. Am. Meteorol. Soc.*, 42(2): 101-105.

Braestrup, C. B., and H. O. Wyckoff, 1958, *Radiation Protection*, Charles C Thomas, Publisher, Springfield, Ill.

Braham, R. R., B. K. Seely, and W. D. Crozier, 1952, A Technique for Tagging and Tracing Air Parcels, *Am. Geophys. Union, Trans.*, 33(6): 825-833.

Brazier, C. E., 1914, Recherches Expérimentales sur les Moulinets Anémométriques, *Annales du Bureau Central Météorologique de France*, pp. 157-300.

Brevoort, M. J., and U. T. Joyner, 1935, *Experimental Investigation of the Robinson-type Cup Anemometer* Technical Report 513, National Advisory Committee for Aeronautics, Langley Memorial Aeronautical Laboratory.

Bridgman, P. W., 1931, *Dimensional Analysis*, Yale University Press, New Haven, Conn.

Brier, G. W., 1950, The Statistical Theory of Turbulence and the Problem of Diffusion in the Atmosphere, *J. Meteorol.*, 7(4): 283-290.

Briggs, G. A., 1965, A Plume Rise Model Compared with Observations, *J. Air Pollution Control Assoc.*, 15(9): 433-438.

Brooks, F. A., 1961, Need for Measuring Horizontal Gradients in Determining Vertical Eddy Transfers of Heat and Moisture, *J. Meteorol.*, 18(5): 589-596.

Brown, R. M., 1959, An Automatic Meteorological Data Collecting System, *J. Geophys. Res.*, 64(12): 2369-2372.

Bryant, L. W., 1949, *The Effects of Velocity and Temperature of Discharge on the Shape of Smoke Plumes from a Funnel or Chimney in a Wind Tunnel*, British Report ACSIL-49/2482, pp. 1-14.

———, and C. F. Cowdrey, 1955, The Effects of Velocity and Temperature of Discharge on the Shape of Smoke Plumes from a Funnel or Chimney; Experiments in a Wind Tunnel, *Proc. Inst. Mech. Eng., (London)*, 169: 371-400.

Bryant, P. M., 1964, *Methods of Estimation of the Dispersion of Wind-borne Material and Data to Assist in Their Application*, British Report AHSB(RP)R-42.

Burchfield, H. P., and E. E. Storrs, 1962, *Biochemical Applications of Gas Chromatography*, Academic Press Inc., New York.

Burger, W., 1964, A Method for Considering the Influence of Buildings on the Diffusion of Stack Gas in the Atmosphere (in German), *Staub*, 24: 223-228.

Businger, J. A., 1959, A Generalization of the Mixing Length Concept, *J. Meteorol.*, 16(5): 516-523.

Butler, G. C., and P. J. Barry, 1962, Experience with Dilution Rate Factors from the AECL Reactor Stack, in *Reactor Safety and Hazards Evaluation Techniques*, Symposium Proceedings, Vienna, 1963, Vol. 2, pp. 401-411, International Atomic Energy Agency, Vienna, 1962 (STI/PUB/57).

Byutner, E. K., and F. A. Gisina, 1963, Effective Coefficient of Capture of Aerosol Particles by Rain and Cloud Droplets, JPRS-24,490, pp. 133-151; translated from *Trudy, Leningradskii Gidrometeorologicheskii Institut*, Vypusk 15 (*Proc. Leningrad Hydrometeorol. Inst.*, Vol. 15).

Calder, K. L., 1949, Eddy Diffusion and Evaporation in Flow over Aerodynamically Smooth and Rough Surfaces: A Treatment Based on Laboratory Laws of Turbulent Flow with Special Reference to Conditions in the Lower Atmosphere, *Quart. J. Mech. Appl. Math.*, 2: 153-176.

———, 1961, Atmospheric Diffusion of Particulate Material Considered as a Boundary Value Problem, *J. Meteorol.*, 18(3): 413-416.

———, 1963, Concerning Similarity Theory Applied to Diffusion in Turbulent Shear Flow, unpublished.

———, 1965, On the Equation of Atmospheric Diffusion, *Quart J. Roy. Meteorol. Soc.*, 91(390): 514-517.

Cermak, J. E., 1963, Lagrangian Similarity Hypothesis Applied to Diffusion in Turbulent Shear Flow, *J. Fluid Mech.*, 15(Part I): 49-64.

Chadam, J., 1962, On a Theory of Turbulent Diffusion, *Geophysics Research Directorate Research Note*, Report AFCRL-62-1107, Air Force Cambridge Research Laboratories.

Chamberlain, A. C., 1953, *Aspects of Travel and Deposition of Aerosol and Vapor Clouds*, British Report AERE-HP/R-1261.

———, 1959, Deposition of Iodine-131 in Northern England in October 1957, *Quart. J. Roy. Meteorol. Soc.*, 85(366): 350-361.

———, 1960, Aspects of the Deposition of Radioactive and Other Gases and Particles, *Intern. J. Air Pollution* 3(1-3): 63-88; also in *Aerodynamic Capture of Particles*, pp. 63-88, E. G. Richardson (Ed.), Pergamon Press, Inc., New York.

Chandrasekhar, S., 1943, Stochastic Problems in Physics and Astronomy, *Rev. Mod. Phys.*, 15: 1-89; reprinted in *Selected Papers on Noise and Stochastic Processes*, N. Wax (Ed.), Dover Publications, Inc., 1954.

Chien, N., Y. Feng, H-J Wang, and T-T Siao, 1951, *Wind Tunnel Studies of Pressure Distribution on Elementary Building Forms*, Iowa Institute of Hydraulic Research.

Church, P. E., 1949, Dilution of Waste Stack Gases in the Atmosphere, *Ind. Eng. Chem.*, 41(12): 2493-2493-c.

Clark, R. D. M., 1956, Photographic Technique for Measuring Diffusion Parameters, USAEC Report TID-7513 (Pt. 1), pp. 186-199. Division of Reactor Development.

Collins, G. F., F. E. Bartlett, A. Turk, S. M. Edmonds, and H. L. Mark, 1965, A Preliminary Evaluation of Gas Air Tracers, *J. Air Pollution Control Assoc.*, 15(3): 109-112.

Conover, John H., 1946, Tests of the Friez Aerovane in the Natural Wind at Blue Hill Observatory, *Bull. Am. Meteorol. Soc.*, 27(9): 523-531.

Convair, 1959, *Fission Products Field Release Test I*, Report NARF 59-32T (FZK-9-140; AFSWC-TR-59-44), U. S. Air Force Nuclear Aircraft Research Facility.

———, 1960, *Fission Products Field Release Test II*, Report NARF 60-10T (FZK-9-149; AFSWC-TR-60-26), U. S. Air Force Nuclear Aircraft Research Facility.

Cooper, R. D., and M. Lutzky, 1955, *Exploratory Investigation of Turbulent Wakes Behind Bluff Bodies*, Report DTMB-963, David W. Taylor Model Basin, Navy Department.

Corcoran, J. W., 1962, *Theoretical Analysis of Wind Vanes*, Report RD81, Beckman and Whitley, Inc., San Carlos, Calif.

———, and Daniel L. Esau, 1964, *Comparison of a Theoretical Model for Anemometer Cups with Experimental Data*, Meteorological Report 9, Beckman and Whitley, Inc., San Carlos, Calif.

Corrsin, S., 1959, Outline of Some Topics in Homogeneous Turbulent Flow, *J. Geophys. Res.*, 64(12): 2134-2150.

Coté, O., 1963, On the Question of Turbulence in the 100-120 km Region of the Atmosphere, paper presented at the American Meteorological Society Meeting, New York, January 1963; based on the report, *On the Question of Turbulence in the Upper Atmosphere*, GCA Technical Report 62-12-N, Geophysics Corporation of America, October 1962.

Couchman, J. C., 1960, *Determining External Dose from the Passage of a Radioactive Cloud*, Report FZM-2029, Convair, Ft. Worth, Tex.

———, 1961, Graphic and Tabular Aids for Reactor Hazard Evaluations, paper presented at Health Physics Society Meeting, Las Vegas, Nevada, June 12–16, 1961.

Court, A., 1961, Area-depth Rainfall Formulas, *J. Geophys. Res.*, 66(6): 1823-1831.

Court-Brown, W. M., and R. Doll, 1957, *Leukaemia and Aplastic Anemia in Patients Irradiated for Ankylosing Spondylitis*, Medical Research Council Special Report 295, Her Majesty's Stationery Office, London.

Cramer, H. E., 1957, A Practical Method for Estimating the Dispersal of Atmospheric Contaminants, *Proceedings of the First National Conference on Applied Meteorology*, pp. C-33 to C-55, American Meteorological Society, Hartford, Conn., October 1957.

———, 1959, Engineering Estimates of Atmospheric Dispersion Capacity, paper presented at the annual meeting of the American Industrial Hygiene Association, Chicago, Ill., April 1959.

———, G. M. DeSanto, R. K. Dumbauld, P. Morgenstern, and R. N. Swanson, 1964, *Meteorological Prediction Techniques and Data System*, Report GCA-64-3-G, Geophysical Corporation of America, Bedford, Mass.

———, G. C. Gill, and F. A. Record, 1957, Heated-thermocouple Anemometers and Light Bivanes — Massachusetts Institute of Technology, *Exploring the Atmosphere's First Mile*, pp. 233-242, H. H. Lettau and B. Davidson (Eds.), Pergamon Press Ltd., London.

———, F. A. Record, and H. C. Vaughan, 1958, *The Study of the Diffusion of Gases or Aerosols in the Lower Atmosphere*, Report AFCRC-TR-58-239, Department of Meteorology, Massachusetts Institute of Technology.

Crawford, T. V., and A. S. Leonard, 1962, Observations of Buoyant Plumes in Calm Stably Stratified Air, *J. Appl. Meteorol.*, 1(2): 251-256.

Crozier, W. D., and B. K. Seely, 1955, Concentration Distributions in Aerosol Plumes Three to Twenty-two Miles from a Point Source, *Am. Geophys. Union, Trans.*, 36: 42-52.

Csanady, G. T., 1955, Dispersal of Dust Particles from Elevated Sources, *Australian J. Phys.*, 8(4): 545-550.

———, 1961, Some Observations on Smoke Plumes, *Intern. J. Air and Water Pollution*, 4(1-2): 47-51.

Culkowski, W. M., 1958, Calculations of the Deposition of Aerosols from Elevated Sources, USAEC Report ORO-171, Oak Ridge Operations Office.

——— 1960, Estimates of Accumulated Exposures and Environmental Build-up of Radioactivity, in *Sixth AEC Air Cleaning Conference, July 7–9, 1959*, USAEC Report TID-7593, pp. 89-99, Division of Reactor Development.

———, 1961, Time Exposure Photography of Smoke Plumes, USAEC Report ORO-359, Weather Bureau, Oak Ridge, Tenn.

———, 1962, Analogue Devices for Dispersion Estimates, in *Seventh AEC Air Cleaning Conference, Oct. 10–12, 1961*, USAEC Report TID-7627, pp. 507-519, Division of Reactor Development.

———, 1963, Deposition and Washout Computations Based on the Generalized Gaussian Plume Model, USAEC Report ORO-599, Weather Bureau, Oak Ridge, Tenn.

Dalton, J., 1799, Experiments and Observations on the Power of Fluids to Conduct Heat; with Reference to Count Rumford's Seventh Essay on the Same Subject, *Memoires of the Manchester Lit. Phil. Soc.*, 5: 373-397.

Danielsen, E. F., 1964, *Project Springfield Report*, Report DASA-1517, Isotopes, Inc., Westwood, N. J.

Danovich, A. M., and S. G. Zeyger, 1963, Determining the Altitude of Rise of a Heated Contaminant in the Atmosphere, JPRS-28, 188, pp. 52-66; translated from *Trudy, Leningradskii Gidrometeorologicheskii Institut*, Vypusk 18 *(Proc. Leningrad Hydrometeorol. Inst.*, Vol. 18).

Das, P. K., 1950, The Growth of Cloud Droplets by Coalescence, *Indian J. Meteorol. Geophys.*, 1: 137-144.

Davidson, B., 1965, College of Engineering, New York University, personal communication.

———, and L. Herbach, 1962, *The Diffusion of Polydisperse Particulate Clouds*, U. S. Army Chemical Corps, Department of Defense.

Davidson, W. F., 1954, The Dispersion and Spreading of Gases and Dusts from Chimneys, in *Trans. Conf. Ind. Wastes, 14th Annual Meeting*, pp. 38-55, Industrial Hygiene Foundation of America.

Davies, D. R., 1954, A Note on the Two-dimensional Equation of Diffusion in the Atmosphere, *Quart. J. Roy. Meteorol. Soc.*, 80(345): 429-434.

Davies, R. W., and R. J. Diamond, 1954, A Mathematical Treatment of Turbulent Diffusion. II. Diffusion of Particle Pairs, Technical Report of O.A. 235, Office of Scientific Research, Air Research and Development Command.

———, R. J. Diamond, and T. B. Smith, 1954, A Mathematical Treatment of Diffusion, Technical Note 201, Report OSR-TN-54-62, Office of Scientific Research, Air Research and Development Command.

Davis, C. N., 1945, Definitive Equations for the Fluid Resistance of Spheres, *Proc. Phys. Soc. (London)*, 57(Part 4): 259-270.

Davis, J. J., R. W. Perkins, R. F. Palmer, W. C. Hanson, and J. F. Cline, 1958, Radioactive Materials in Aquatic and Terrestrial Organisms Exposed to Reactor Effluent Water, in *Proceedings of the Second United Nations International Conference on the Peaceful Uses of Atomic Energy, Geneva, 1958*, Vol. 18, pp. 423-428, United Nations, New York, 1958.

Deacon, E. L., 1949, Vertical Diffusion in the Lowest Layers of the Atmosphere, *Quart. J. Roy. Meteorol. Soc.*, 75(324): 89-103.

———, 1951, The Over-estimation Error of Cup Anemometers in Fluctuating Winds, *J. Sci. Instr.*, 28(8): 231-234.

Decker, R., 1964, Protection Afforded by a Building During Passage of a Radioactive Cloud, Division of Space Nuclear Systems, U. S. Atomic Energy Commission, unpublished.

DeMarrais, G., 1959, Wind Speed Profiles at Brookhaven National Laboratory, *J. Meteorol.*, 16(2): 181-190.

———, and N. F. Islitzer, 1960, Diffusion Climatology of the National Reactor Testing Station, USAEC Report IDO-12015, Weather Bureau, Idaho Falls, Idaho.

Department of the Army, 1955, Generator, Smoke, Mechanical, M3A2, Report TM 3-431, Superintendent of Documents, U. S. Government Printing Office, Washington, D. C.

Departments of the Army and the Air Force, 1956, Military Chemistry and Chemical Agents, Report TM 3-215 or Report AFM 335-7.

Drinker, P., and T. Hatch, 1954, *Industrial Dust, Hygienic Significance, Measurement and Control*, 2nd ed., McGraw-Hill Book Company, Inc., New York.

Dumbauld, R. K., 1962, Meteorological Tracer Technique for Atmospheric Diffusion Studies, *J. Appl. Meteorol.*, 1(4): 437-443.

Dunster, H. J., 1958, The Disposal of Radioactive Liquid Wastes into Coastal Waters, in *Proceedings of the Second United Nations International Conference on the Peaceful Uses of Atomic Energy, Geneva, 1958*, Vol. 18, pp. 390-399, United Nations, New York, 1958.

———, H. Howells, and W. L. Templeton, 1958, District Surveys Following the Windscale Incident, in *Proceedings of the Second United Nations International Conference on the Peaceful Uses of Atomic Energy, Geneva, 1958*, Vol. 18, pp. 296-308, United Nations, New York, 1958.

Durst, C. S., A. F. Crossley, and N. E. Davis, 1957, Horizontal Diffusion in the Atmosphere in the Light of Air Trajectories, paper of the Meteorological Research Committee (London), MRP 1058.

Edinger, J. G., 1952, A Technique for Measuring the Detailed Structure of Atmospheric Flow. *Geophysical Research Papers, No. 19*, Report AFCRC-TR-53-9, pp. 241-261, Air Force Cambridge Research Center.

Eisenbud, M., 1963, *Environmental Radioactivity*, McGraw-Hill Book Company, Inc., New York.

Elliott, W. P., 1959, The Areas Within Concentration Isopleths Downwind of Continuous Point Source, *Intern. J. Air Pollution*, 2(2): 115-126.

———, 1960, A Discussion of the Calder–Deacon Equation for Diffusion from a Continuous Point Source, *Geophysics Research Directorate Research Notes, No. 31*, Report AFCRC-TN-60-298, Air Force Cambridge Research Center.

———, and M. L. Barad, 1964, Operational Prediction of Diffusion Downwind from Line Sources, *Air Force Surveys in Geophysics, No. 156*, Report AFCRL-64-163, Air Force Cambridge Research Laboratories.

———, R. J. Engelmann and P. W. Nickola, 1961, Area-Dosage Relationships and Time of Tracer Arrival in the Green Glow Program, *Air Force Surveys in Geophysics, No. 134*, Report AFCRL-468, Air Force Cambridge Research Laboratories.

———, and P. W. Nickola, 1961, The Estimation of Areas Within Isopleths of Dosage Downwind of a Point Source, *Am. Ind. Hyg. Assoc. J.*, 22: 238-244.

Ellison, T. H., 1957, Turbulent Transport of Heat and Momentum from an Infinite Rough Plane, *J. Fluid Mech.*, 2(Part 5): 456-466.

———, 1959, Meteorology, *Sci. Progr.*, 47(187): 495-506.

Engelmann, R. J., 1963, Rain Scavenging of Particulates, USAEC Report HW-79382, Hanford Atomic Products Operation.

———, 1965, Rain Scavenging of Zinc Sulfide Particles, *J. Atmospheric Sci.*, 22(6): 719-729.

———, R. W. Perkins, D. I. Hagen, and W. A. Haller, 1966, Washout Coefficients for Selected Gases and Particulates, in *Proc. 59th Annual Meeting Air Pollution Control Assoc.*; also USAEC Report BNWL-SA-657, Battelle-Northwest, June 1966.

Estoque, M. A., and W. S. Yee, 1963, Air–Earth Interface Characteristics and the Atmospheric Boundary Layer, Report AFCRL-63-813, Air Force Cambridge Research Laboratories.

Evans, B. H., 1957, Natural Air Flow Around Buildings, Texas Engineering Experimental Station Research Report 59, College Station, Tex.

Facy, L., 1962, Radioactive Precipitations and Fallout, *Nuclear Radiation in Geophysics*, pp. 202-240, H. Israel and A. Krebs (Eds.), Springer-Verlag, Berlin.

Fail, R., J. A. Lawford, and R. C. W. Eyre, 1957, Low-speed Experiments on the Wake Characteristics of Flat Plates Normal to an Air Stream, *Aeronautical Research Council Reports and Memoranda*, No. 3120, Aeronautical Research Council, Great Britain.

Federal Radiation Council, 1961, *Background Material for the Development of Radiation Protection Standards, Staff Report 2*, Superintendent of Documents, U. S. Government Printing Office, Washington, D. C.

Federal Radiation Council, 1964, *Background Material for the Development of Radiation Protection Standards, Staff Report 5*, Superintendent of Documents, U. S. Government Printing Office, Washington, D. C.

Federal Radiation Council, 1965, *Background Material for the Development of Radiation Protection—Protective Action Guides for Strontium-89, Strontium-90, and Cesium-137, Staff Report 7*, Superintendent of Documents, U. S. Government Printing Office, Washington, D. C.

Fick, A., 1855, Uber Diffusion, *Ann. Physik Chem.*, [2]94: 59-86; see also, On Liquid Diffusion, *Phil. Mag.*, [4]10: 30-39.

Fletcher, N. H., 1962, *The Physics of Rain Clouds*, Cambridge University Press, Great Britain.

Frenkiel, F. N., 1948, On the Kinematics of Turbulence, *J. Aeron. Sci.*, 15(1): 57-64.

———, 1952, Application of the Statistical Theory of Turbulent Diffusion to Micrometeorology, *J. Meteorol.*, 9(4): 252-259.

———, 1952a, On the Statistical Theory of Turbulent Diffusion, *Geophysical Research Papers, No. 19, International Symposium on Atmospheric Turbulence in the Boundary Layer, Massachusetts Institute of Technology, June 4-6, 1951*, p. 415, Report AFCRC-TR-53-9, Air Force Cambridge Research Center.

———, 1953, Turbulent Diffusion: Mean Concentration Distribution in a Flow Field of Homogeneous Turbulence, *Advan. Appl. Mech.*, 3: 61-107.

———, and I. Katz, 1956, Studies of Small-scale Turbulent Diffusion in the Atmosphere, *J. Meteorol.*, 13(4): 388-394.

Friedman, I., L. Machta, and R. Soller, 1962, Water-vapor Exchange Between a Water Droplet and Its Environment, *J. Geophys. Res.*, 67(7): 2761-2766.

Fritschen, L. J., and C. H. M. van Bavel, 1963, Micrometeorological Data Handling System, *J. Appl. Meteorol.*, 2(1): 151-155.

Frost, R., 1948, Atmospheric Turbulence, *Quart. J. Roy. Meteorol. Soc.*, 74(321-322): 316-388.

Fuchs, M., and C. B. Tanner, 1965, Radiation Shields for Air Temperature Thermometers, *J. Appl. Meteorol.*, 4(4): 544-547.

Fuchs, N. A., 1964, *The Mechanics of Aerosols*, Pergamon Press, Inc., New York.

Fuquay, J., 1958, Meteorological Factors in the Appraisal and Control of Acute Exposures to Stack Effluents, in *Proceedings of the Second United Nations International Conference on the Peaceful Uses of Atomic Energy, Geneva, 1958*, Vol. 18, pp. 272-279, United Nations, New York, 1958.

———, 1960, Hanford Atomic Products Operation, personal communication.

———, 1963, Hanford Atomic Products Operation, personal communication.

———, C. L. Simpson, M. L. Barad, and J. H. Taylor, 1963, Results of Recent Field Programs in Atmospheric Diffusion, *J. Appl. Meteorol.*, 2(1): 122-128.

———, C. L. Simpson, and W. T. Hinds, 1964, Prediction of Environmental Exposures from Sources near the Ground Based on Hanford Experimental Data, *J. Appl. Meteorol.*, 3(6): 761-770.

Furth, J., and E. Lorenz, 1945, Carcinogenesis by Ionizing Radiation, in *Radiation Biology*, Vol. I, Part II, pp. 1145-1201, A. Hoellander (Ed.), McGraw-Hill Book Company, Inc., New York.

Gamertsfelder, C. G., 1960, Hazards Calculation Notebook, Aircraft Nuclear Propulsion Department, General Electric Co., unpublished.

Garbell, Maurice A., 1957, Fins for Meteorological Instruments, *J. Meteorol.*, 4(3): 82-90.

Gartrell, F. E., F. W. Thomas, S. B. Carpenter, F. Pooler, B. B. Turner, and J. M. Leavitt, 1964, *Full Scale Study of Dispersion of Stack Gases, a Summary Report*, Tennessee Valley Authority and Public Health Service, Chattanooga, Tennessee.

Gee, J. H., and D. R. Davies, 1963, A Note on Horizontal Dispersion from an Instantaneous Ground Source, *Quart. J. Roy. Meteorol. Soc.*, 89(382): 542-545.

Geiger, R., 1957, *The Climate near the Ground*, Harvard University Press, Cambridge, Mass.

General Dynamics/Fort Worth, Tex., 1963, Health Physics Handbook, Report OSP-379.

George, L. A., J. W. Healy, and L. K. Bustad, 1955, Irradiation of Pig Skin with Radioactive Particles,

Radiological Sciences Department Research and Development Activities, p. 9, USAEC Report HW-38198, Hanford Atomic Products Operation.

Georgii, H., and E. Weber, 1964, Investigations on Tropospheric Washout, Report AFCRL-64-816, Johann Wolfgang Goethe University.

Gerhardt, J. R., W. S. Mitcham, and A. W. Straiton, 1962, A 1400-foot Meteorological Tower with Automatic Data Readout, *Proc. Inst. Radio Engrs.*, 50: 2263-2271.

Giever, P. M., and W. A. Cook, 1960, Automatic Recording Instruments as Applied to Air Analysis, *Am. Med. Assoc. Arch. Ind. Health*, 21(3): 233-249.

Gifford, F. A., Jr., 1953, A Study of Low Level Air Trajectories at Oak Ridge, Tennessee, *Monthly Weather Rev.*, 81(7): 179-192.

———, 1955, A Simultaneous Lagrangian–Eulerian Turbulence Experiment, *Monthly Weather Rev.*, 83(12): 293-301.

———, 1955a, Atmospheric Diffusion from Volume Sources, *J. Meteorol.*, 12(3): 245-251.

———, 1957, Relative Atmospheric Diffusion of Smoke Puffs, *J. Meteorol.*, 14(5): 410-414.

———, 1958, Atmospheric Turbulent Diffusion of Puffs and Plumes, in *International Association of Meteorology and Atmospheric Physics, Report of Proceedings*, Publication IAMAP 11/b, p. 46, International Association of Meteorology and Atmospheric Physics.

———, 1959, Smoke Plumes as Quantitative Air Pollution Indices, *Intern. J. Air Pollution*, 2(1): 42-50.

———, 1959a, Statistical Properties of a Fluctuating Plume Dispersion Model, *Advances in Geophysics*, Vol. 6, pp. 117-138, F. N. Frenkiel and P. A. Sheppard (Eds.), Academic Press Inc., New York.

———, 1960, Peak to Average Concentration Ratios According to a Fluctuating Plume Dispersion Model, *Intern. J. Air Pollution*, 3(4): 253-260.

———, 1960a, Atmospheric Dispersion, *Nucl. Safety*, 1(3): 56-62.

———, 1961, Use of Routine Meteorological Observations for Estimating Atmospheric Dispersion, *Nucl. Safety*, 2(4): 47-51.

———, 1962, Diffusion in the Diabatic Surface Layer, *J. Geophys. Res.*, 67(8): 3207-3212.

———, 1962a, The Area Within Ground-level Dosage Isopleths, *Nucl. Safety*, 4(2): 91-92.

———, W. Culkowski, and W. Hilsmeier, 1963, Computation of Atmospheric Dispersion Parameters at Reactor Sites by a Smoke Plume Ratio Method, paper presented at the International Conference on Radioactive Pollution of Gaseous Media, Saclay, France.

———, and D. H. Pack, 1962, Surface Deposition of Airborne Material, *Nucl. Safety*, 3(4): 76-80.

Gill, G. C., 1959, Meteorological Instrumentation. Professional Notes, C. E. 199, Partial Bibliography on Anemometers and Calibration Devices: A Lecture by G. C. Gill Assisted by Floyd Elder, University of Michigan, Ann Arbor, Mich.

———, L. E. Olsson, and Motozo Suda, 1966, Errors in Measurements of Wind Speed and Direction Made With Tower- or Stack-mounted Instruments, Publication 06973-1-P, Department of Meteorology and Oceanography, College of Engineering, University of Michigan, Ann Arbor, Mich.

Glasstone, S. (Ed.), 1962, *Effects of Nuclear Weapons*, Superintendent of Documents, U. S. Government Printing Office, Washington, D. C.

Godson, W. L., 1958, The Diffusion of Particulate Matter from an Elevated Source, *Arch. Meteorol., Geophys. Biokimatol.*, 10: 305-327.

Golden, J., 1961, *Scale Model Techniques*. M. A. Thesis, Department of Meteorology and Oceanography, New York University.

Goldstein, H., and J. E. Wilkins, Jr., 1954, Calculations of the Penetration of Gamma Rays, Final Report, USAEC Report NYO-3075, Nuclear Development Associates, Inc.

Goldstein, S., 1951, On Diffusion by Discontinuous Movements, and on the Telegraph Equation, *Quart. J. Mech. Appl. Math.*, 4: 129-156.

Gomberg, H. J., 1958, A Quantitative Approach to Evaluation of Risk in Locating a Power Reactor on a Given Site, in *Proceedings of the Second United Nations International Conference on the Peaceful Uses of Atomic Energy, Geneva, 1958*, Vol. 11, pp. 57-65, United Nations, New York, 1958.

Gordon, D., 1963, Wind Persistence for Expanding Sectors, Environmental Meteorological Research Branch, Weather Bureau, Washington, D. C., unpublished.

Great Britain, Meteorological Office, 1956, Instruments for Surface Observations, in *Handbook of Meteorological Instruments, Part I*, Her Majesty's Stationery Office, London, England.

Greenfield, S. M., 1957, Rain Scavenging of Radioactive Particulate Matter from the Atmosphere, *J. Meteorol.*, 14(2): 115-125.

Gregory, P. H., 1945, The Dispersion of Airborne Spores, *Trans., British Mycological Society*, 28(Parts I and II): 26-72.

Griffiths, V., 1963, The Removal of Iodine from the Atmosphere by Sprays, British Report AHSB(S)-R-45.

Gunn, R., and G. D. Kinzer, 1949, The Terminal Velocity of Fall for Water Droplets in Stagnant Air, *J. Meteorol.*, 6(4): 243-284.

Guthrie, C. E., and J. P. Nichols, 1964, Theoretical Possibilities and Consequences of Major Accidents in U^{233} and Pu^{239} Fuel Fabrication and Radioisotope Processing Plants, USAEC Report ORNL-3441, Oak Ridge National Laboratory.

Hage, K. D., 1964, Particle Fallout and Dispersion Below 30 km in the Atmosphere, Report SC-DC-64-1463, Sandia Corporation.

Haines, G. F., H. Cember, and W. C. L. Hemeon, 1956, Stack Gas Tracer Technique Employing Neutron Activation Analysis, Final Report by Mellon Institute of Industrial Research, Pittsburgh, Pennsylvania, to American Petroleum Institute for Industrial Hygiene Foundation of America, Inc.

Halitsky, J., 1961, Wind Turbulence in the Lee of a Low Conical Mountain, *New York University Quarterly Progress Report No. 4, Local Wind Circulations*, New York University.

———, 1962, Diffusion of Vented Gas Around Buildings, *J. Air Pollution Control Assoc.*, 12(2): 74-80.

———, 1963, Gas Diffusion near Buildings, *ASHRAE (Am. Soc. Heating, Refrig. Air-cond. Eng.) Trans.*, 69: 464-484.

———, 1965, Estimation of Stack Height Required to Limit Contamination of Building Air Intakes, *Am. Ind. Hyg. J.*, 26: 106-116.

———, 1965a, Effect of Turbulence on Gas Diffusion Around Obstacles, New York University, unpublished.

———, 1966, A Method for Estimating Concentrations in Transverse Jet Plumes, *Air and Water Pollution*, 10(11-12): 821-843.

———, J. Golden, P. Halpern, and P. Wu, 1963, Wind Tunnel Tests of Gas Diffusion from a Leak in the Shell of a Nuclear Power Reactor and from a Nearby Stack, Geophysical Sciences Laboratory Report 63-2, Department of Meteorology and Oceanography, New York University.

———, G. A. Magony, and P. Halpern, 1965, Turbulence Due to Topographical Effects, Geophysical Sciences Laboratory Report TR 65-2, Department of Meteorology and Oceanography, School of Engineering and Science, New York University.

Halstead, M., 1943, A Stability-term in the Wind-gradient Equation, *Am. Geophys. Union, Trans.*, 24: 204-208.

Hamilton, G. F., 1962, Effect of Velocity Distribution on Wind Loads on Walls and Low Buildings, Technical Publication Series, TP 6205, Report of the University of Toronto Mechanical Engineers, University of Toronto, Toronto, Canada.

Hardy, E. P., Jr., and J. Rivera, 1964, Fallout Program Quarterly Report, June 1, 1964–September 1, 1964, USAEC Report HASL-149, New York Operations Office.

Haugen, D. A. (Ed.), 1959, Project Prairie Grass, A Field Program in Diffusion, *Geophysical Research Papers, No. 59*, Vol. III, Report AFCRC-TR-58-235 (ASTIA Document AD-217076), Air Force Cambridge Research Center.

———, 1959a, The Effects of Sampler Spacing on Basic Analysis of Concentration Data, *Geophysics Research Directorate Research Notes, No. 7*, Report AFCRC-TN-58-651, U. S. Air Force Cambridge Research Center.

———, 1960, A Study of a Lagrangian–Eulerian Relationship for Turbulent Diffusion in the Atmospheric Boundary Layer, paper presented at the 184th National Meeting of the American Meteorological Society, April 27-30, 1960, Washington, D. C.

———, 1963, Air Force Cambridge Research Laboratories, personal communication.

———, and J. J. Fuquay (Eds.), 1963, The Ocean Breeze and Dry Gulch Diffusion Programs, Vol. I, USAEC Report HW-78435 [Report AFCRL-63-791(I)], Air Force Cambridge Research Laboratories and Hanford Atomic Products Operation.

———, and J. H. Taylor (Eds.), 1963, The Ocean Breeze and Dry Gulch Diffusion Programs, Vol. II, Report AFCRL-63-791, Air Force Cambridge Research Laboratories.

Hawkins, J. E., and G. Nonhebel, 1955, Chimneys and the Dispersal of Smoke, *J. Inst. Fuel*, 28(178): 530-545.

Hawley, C. A., Jr., C. W. Sill, G. L. Voelz, and N. F. Islitzer, 1964, Controlled Environmental Radioiodine Tests at the National Reactor Testing Station, USAEC Report IDO-12035, Idaho Operations Office and Weather Bureau, Idaho Falls, Idaho.

Hay, J. S., and F. Pasquill, 1956, Measurements of the Short Range Diffusion of Airborne Particles at a Height of a Few Hundred Feet in the Atmosphere, Porton Technical Paper No. 561, Ministry of Supply, Directorate of Chemical Defense Research and Development, Chemical Defense Experimental Establishment, Porton, England.

———, and F. Pasquill, 1957, Diffusion from a Fixed Source at a Height of a Few Hundred Feet in the Atmosphere, *J. Fluid Mech.*, 2(Part 3): 299-310.

———, and F. Pasquill, 1959, Diffusion from a Continuous Source in Relation to the Spectrum and Scale of Turbulence, *Advances in Geophysics*, Vol. 6, pp. 345-365, F. N. Frenkiel and P. A. Sheppard (Eds.), Academic Press Inc., New York.

Healy, J. W., 1956, The Calculation of Maximum Permissible Concentrations for Long-lived Radioisotopes, *Radiation Res.*, 4(5): 367-372.

Heffter, J. L., 1965, The Variation of Horizontal Diffusion Parameters with Time for Travel Periods of One Hour or Longer, *J. Appl. Meteorol.*, 4(1): 153-156.

Herne, H., 1960, The Classical Computation of the Aerodynamic Capture of Particles by Spheres, *Aerodynamic Capture of Particles*, pp. 26-34, E. G. Richardson (Ed.), Pergamon Press, London.

Hewson, E. W., and G. C. Gill, 1944, Meteorological Investigations in Columbia River Valley near Trail, B. C., U. S. Bureau of Mines Bulletin 453, Superintendent of Documents, U. S. Government Printing Office, Washington, D. C.

———, G. C. Gill, and E. Bierly, 1959, Maximum Ground Concentrations in Relation to Stack Heights Under Various Meteorological Conditions at the Enrico Fermi Nuclear Power Plant near Monroe, Michigan, University of Michigan, Ann Arbor, Mich., unpublished.

———, G. C. Gill, and G. J. Walke, 1963, Smoke Plume Photography Study, Big Rock Point Nuclear Plant, Charlevoix, Michigan, *Progress Report No. 3*, Publication 04015-3-P, Department of Meteorology and Oceanography, University of Michigan, Ann Arbor, Michigan; see also G. J. Walke, E. W. Hewson, and G. C. Gill, 1965, A Better Way to Evaluate Nuclear-site Meteorology, *Nucleonics*, 23: 72-75.

Hill, G. R., M. D. Thomas, and J. M. Abersold, 1945, High Stacks Overcome Concentrations of Gases, *Mining Congr. J.*, 31: 21-34.

Hilsmeier, W. F., and F. A. Gifford, Jr., 1962, Graphs for Estimating Atmospheric Dispersion, USAEC Report ORO-545, Weather Bureau, Oak Ridge, Tenn.

Hilst, G. R., 1957, The Dispersion of Stack Gases in Stable Atmospheres, *J. Air Pollution Control Assoc.*, 7(3): 205-210.

———, and C. L. Simpson, 1958, Observations of Vertical Diffusion Rates in Stable Atmospheres, *J. Meteorol.*, 15(1): 125-126.

Hine, G. J., and G. L. Brownell (Eds.), 1956, *Radiation Dosimetry*, Chapter 16, pp. 693-799, Academic Press Inc., New York.

Hinzpeter, M., 1958, The Influence of Meteorological Parameters on the Propagation of Radioactive Fission Products in the Biosphere, in *Proceedings of the Second United Nations International Conference on the Peaceful Uses of Atomic Energy, Geneva, 1958*, Vol. 18, p. 284, United Nations, New York, 1958.

Högström, U., 1964, An Experimental Study on Atmospheric Diffusion, *Tellus*, 16(2): 205-251.

Holdredge, E. S., and B. H. Reed, 1956, Pressure Distribution in Buildings, *Texas Engineering Experimental Station Summary Report No. 1*, Agricultural and Mechanical College of Texas, Engineering Experimental Station.

Holland, J. Z., 1953, A Meteorological Survey of the Oak Ridge Area: Final Report Covering the Period 1948-52, USAEC Report ORO-99, Weather Bureau, Oak Ridge, Tenn.

———, 1956, Radiation from Clouds of Reactor Debris, in *Proceedings of the Second United Nations International Conference on the Peaceful Uses of Atomic Energy, Geneva, 1958*, Vol. 13, pp. 110-118, United Nations, New York, 1958.

Holzworth, G. C., 1964, Estimates of Mean Maximum Mixing Depth in the Contiguous United States, *Monthly Weather Rev.*, 92(5): 235-242.

———, E. K. Kauper, and T. B. Smith, 1962, Some Observed Low-level Air Trajectories over Los Angeles, California, *Monthly Weather Rev.*, 91(8): 387-392.

Hosler, C. R., 1961, Low-level Inversion Frequency in the Contiguous United States, *Monthly Weather Rev.*, 89(9): 319-339.

Humphrey, P. A., 1951, Atomic Energy Commission Meteorological Information Meeting: February 1-2, 1951, USAEC Report TID-399, pp. 14-16, Atomic Energy Commission, Oak Ridge, Tenn.

Inoue, E., 1960, On the Shape of Stack Plumes, *Meteorol. Res. Notes*, Division of Meteorology, National Institute of Agricultural Science, Japan, II(5): 332-339.

———, 1961, On the Blackness of Stack Smoke Plumes, *Tenki*, 8: 179-184.

International Commission on Radiological Protection, 1959, *Recommendations of the International Commission on Radiological Protection*, Pergamon Press, Inc., New York.

International Commission on Radiological Protection, 1959a, Report of Committee II on Permissible Dose for Internal Radiation, 1959, *Recommendations of the International Commission on Radiological Protection*, ICRP Publication 2, Pergamon Press, Inc., New York.

International Commission on Radiological Protection, 1960, Report of Committee II on Permissible Dose for Internal Radiation, *Health Phys.*, 3: 1-380.

International Commission on Radiological Protection, 1966, *Recommendations of the International Commission on Radiological Protection*, ICRP Publication 9, Pergamon Press, Inc., New York.

International Commission on Radiological Units and Measurements, 1959, National Bureau of Standards, Handbook 62, *Report of the International Commission on Radiological Units and Measurements (ICRU)*, Superintendent of Documents, U.S. Government Printing Office, Washington, D. C.

International Commission on Radiological Units and Measurements, 1962, *Radiation Quantities and Units*, National Bureau of Standards, Handbook 84 (ICRU Report 10a), Superintendent of Documents, U. S. Government Printing Office, Washington, D. C.

Islitzer, N. F., 1961, Short-range Atmospheric-dispersion Measurements from an Elevated Source, *J. Meteorol.*, 18(4): 443-450.

———, 1962, The Role of Meteorology Following the Nuclear Accident in Southeast Idaho, USAEC Report IDO-19310, Weather Bureau, Idaho Falls, Idaho.

———, 1965, Aerodynamic Effects of Large Reactor Complexes upon Atmospheric Turbulence and Diffusion, USAEC Report IDO-12041, Weather Bureau, Idaho, Falls, Idaho.

———, 1965a, Conference on AEC Meteorological Activities, May 19–22, 1964, pp. 57-64, USAEC Report BNL-914, Brookhaven National Laboratory.

———, and R. K. Dumbauld, 1963, Atmospheric Diffusion-deposition Studies over Flat Terrain, *Intern. J. Air Water Pollution*, 7(11-12): 999-1022.

———, and E. H. Markee, 1964, Puff Diffusion Measurements from Reactor Destructive Tests, paper presented at the American Meteorological Society National Conference on Micrometeorology, Oct. 13–16, 1964, Salt Lake City, Utah.

Jahnke, E., and F. Emde, revised by F. Lösch, 1960, *Tables of Higher Functions*, 6th ed., McGraw-Hill Book Company, Inc., New York.

Jensen, M., 1958, The Model-law for Phenomena in Natural Wind, *Ingenioeren*, 2: 121-128.

———, and N. Franck, 1965, Model-scale Tests in Turbulent Wind, Part II, Danish Technical Press, Copenhagen.

Jones, J. I. P., 1966, Presentations of Surface Wind and Turbulence Using the Cathode-ray Tube, *J. Appl. Meteorol.*, 5(1): 25-32.

———, and F. Pasquill, 1959, An Experimental System for Directly Recording the Statistics of the Intensity of Atmospheric Turbulence, *Quart. J. Roy. Meteorol. Soc.*, 85(365): 225-236.

Jordinson, R., 1956, Flow in a Jet Directed Normal to the Wind, *Aeronautical Research Council Reports and Memoranda*, No. 3074, Aeronautical Research Council, Great Britain.

Junge, C. E., 1963, *Air Chemistry and Radioactivity*, Academic Press Inc., New York.

Kahn, A. B., 1957, A Generalization of Average-correlation Methods of Spectrum Analysis, *J. Meteorol.*, 14(1): 9-17.

Kalinske, A. A., R. A. Jensen, and C. F. Schadt, 1945, Wind-tunnel Studies of Gas Diffusion in a Typical Japanese Urban District, OEMsr-1243, Informal Report 10.3-48, Iowa Institute of Hydraulic Research, State University of Iowa, Iowa City, Iowa.

———, R. A. Jensen, and C. F. Schadt, 1945a, Correlation of Wind Tunnel Studies with Field Measurements of Gas Diffusion, OEMsr-1243, Informal Report No. 10.3-48a, Iowa Institute of Hydraulic Research, State University of Iowa, Iowa City, Iowa.

Kao, S. K., 1960, The Effects of Thermal Stratification on Turbulent Diffusion from a Continuous Fixed Source, *Tellus*, 12(4): 359-363.

Katz, M., 1952, Application of Diffusion Theory to Dispersion of Stack Gas in the Atmosphere, Defence Research Chemical Laboratories Report 110, Defence Research Board, Canada, Ottawa, Canada.

Kazansky, A. B., and A. S. Monin, 1957, The Form of Smoke Jets, *Bull. Acad. Sci. USSR, Geophys. Ser.*, No. 8, pp. 56-70 (English translation of *Izvestiya Akademii Nauk SSSR, Seriya Geofizicheskaya*, 1957, No. 8, pp. 1020-1033).

———, and A. S. Monin, 1958, On the Turbulent Regime in the Near-surface Layer of Air at Unstable Stratification, *Bull. Acad. Sci. USSR, Geophys. Ser.*, No. 6, pp. 421-426 (English translation of *Izvestiya Akademii Nauk SSSR, Seriya Geofizicheskaya*, 1958, No. 6, pp. 741-751).

Keffer, J. F., and W. D. Baines, 1963, The Round Turbulent Jet in a Cross-wind, *J. Fluid. Mech.*, 15(4): 481-496.

Kelkar, V. N., 1959, Size Distribution of Raindrops. Part I. *Indian J. Meteorol. Geophys.*, 10(2): 125-136.

Kellogg, W. W., 1956, Diffusion of Smoke in the Stratosphere, *J. Meteorol.*, 13(3): 241-250.

———, R. R. Rapp, and S. M. Greenfield, 1957, Close-in Fallout, *J. Meteorol.*, 14(1): 1-8.

King, L. V., 1914, On the Convection of Heat from Small Cylinders in a Stream of Fluid: Determination of the Convection Constants of Small Platinum Wires with Applications to Hot-wire Anaemometry, *Phil. Trans. Roy. Soc. London, Ser.* A, 214: 373-432.

Kinzer, G. D., and W. E. Cobb, 1958, Laboratory Measurements and Analysis of the Growth and Collection Efficiency of Cloud Droplets, *J. Meteorol.*, 15(2): 138-148.

Knapp, H. A., 1963, Iodine-131 in Fresh Milk and Human Thyroids Following a Single Deposition of Nuclear Test Fallout, USAEC Report TID-19266, Division of Biology and Medicine.

Kolmogorov, A. N., 1941, Dissipation of Energy in Locally Isotropic Turbulence, *Compt. Rend. Acad. Sci. U. R. S. S.*, 32: 16.

Koschmieder, H., 1925, Zur Kenntnis des Stromfeldes in Lee, *Zeitschrift für Flugtechnik und Motorluftschiffahrt*, 16: 240-244.

Kurtyka, J. C., 1953, Methods of Measuring Precipitation for Use with the Automatic Weather Station, Report of Investigation No. 20, Illinois State Water Survey, Urbana, Ill.

Langmuir, I., 1948, The Production of Rain by a Chain Reaction in Cumulus Clouds at Temperatures Above Freezing, *J. Meteorol.*, 5(5): 175-192.

———, and K. B. Blodgett, 1945, Mathematical Investigations of Water Droplet Trajectories, Report No. RL-225, General Electric Research Laboratory, Schenectady, N. Y.

Leighton, P. A., W. A. Perkins, S. W. Grinnell, and F. X. Webster, 1965, The Fluorescent Particle Atmospheric Tracer, *J. Appl. Meteorol.*, 4(3): 334-348.

Leonard, B. P., Jr., 1957, A Modification of Sutton's Diffusion Equation for Anisotropic Diffusion, Report FZM-819, Convair, Ft. Worth, Tex.

Lettau, H., 1949, Isotropic and Non-isotropic Turbulence in the Atmospheric Surface Layer, *Geophysical Research Papers, No. 1*, Report NP-1761, Air Force Cambridge Research Laboratories.

———, 1952, On Eddy Diffusion in Shear Zones, *Geophysical Research Papers, No. 19*, Report AFCRC-TR-53-9, pp. 437-445, Air Force Cambridge Research Center.

———, 1962, Studies of the Three-dimensional Structure of the Planetary Boundary Layer, Final Report, Department of Meteorology, University of Wisconsin, Madison, Wis.

———, and B. Davidson (Eds.), 1957, *Exploring the Atmosphere's First Mile*, Vols. I and II, Pergamon Press, Inc., New York.

———, and J. E. Kutzbach, 1961, Investigations of the Modification of Wind Profiles by Artificially Controlled Surface Roughness, Annual Report to Army Electronic Proving Ground, Fort Huachuca, Arizona, pp. 71-114, Department of Meteorology, University of Wisconsin, Madison, Wis.

Leutheusser, H. J., 1964, The Effect of Wall Parapets on the Roof Pressure-coefficients of Block-type and Cylindrical Structures. Report TP-6404, Technical Publications Series, Department of Mechanical Engineering, University of Toronto.

———, 1965, Pressure Distribution on a Cube at Various Degrees of Boundary Layer Immersion, Report TP-6502, Technical Publication Series, Department of Mechanical Engineering, University of Toronto.

Levin, L. M., 1954, Size Distribution Function for Cloud-droplets and Raindrops, *Dok. Akad. Nauk, SSSR*, 94(6): 1045-1048 (translation T-263-R, Director, Science Information Service, Defence Research Board, Canada, 1958).

Lewis, E. B., 1957, Leukemia and Ionizing Radiation, *Science*, 125(3255): 965-972.

Lin, C. C., 1960, On a Theory of Dispersion by Continuous Movements, *Proc. Natl. Acad. Sci.*, 46: 566-570.

———, 1960a, On a Theory of Dispersion by Continuous Movements. II. Stationary Anisotropic Processes, *Proc. Natl. Acad. Sci.*, 46: 1147-1150.

———, and W. H. Reid, 1963, Turbulent Flow, Theoretical Aspects, *Handbuch der Physik*, Vol. 8, Part 2, pp. 438-523, Springer-Verlag, Berlin.

Lindackers, K. H., H. Bresser, and J. Albracht, 1965, Some Theoretical and Experimental Results Useful for Estimation of Inhalation Radiation Dose and Environmental Radioactive Contamination in *International Symposium on Fission Product Release and Transport Under Accident Conditions*, Apr. 5–7, 1965, Oak Ridge, Tennessee, p. 362, USAEC Report CONF-650407, Oak Ridge National Laboratory.

Liu, V. C., 1956, Turbulent Dispersion of Dynamic Particles, *J. Meteorol.*, 13(4): 399-405.

Loevinger, R., 1956, The Dosimetry of Beta Sources in Tissue, the Point Source Function, *Radiology*, 66(1): 55-62.

———, E. M. Japha, and G. L. Brownell, 1956, Discrete Radioisotope Sources, Chap. 16, *Radiation Dosimetry*, Academic Press Inc., New York.

Lord, G. R., W. D. Baines, and H. J. Leutheusser, 1964, On the Minimum Height of Roof-mounted Chimneys, Results of an Exploratory Wind-tunnel

Study, Report TP-6409 Technical Publication Series, Department of Mechanical Engineering, University of Toronto.

Lowry, P. H., 1951, Microclimate Factors in Smoke Pollution from Tall Stacks, *Meteorol. Monographs*, 1(1): 24-29.

———, D. A. Mazzarella, and M. E. Smith, 1951, Ground-level Measurements of Oil-fog Emitted from a Hundred-meter Chimney, *Meteorol. Monographs*, 1(4): 30-35.

Lucas, D. H., 1958, The Atmospheric Pollution of Cities, *Intern. J. Air Pollution*, 1(1-2): 71-86.

———, D. J. Moore, and G. Spurr, 1963, The Rise of Hot Plumes from Chimneys, *Intern. J. Air Water Pollution*, 7(6-7): 473-500.

———, G. Spurr, and F. Williams, 1957, The Use of Balloons in Atmospheric Pollution Research, *Quarterly J. Roy. Meteorol. Soc.*, 83(358): 508-516.

Lumley, J. L., 1957, Some Problems Connected with the Motion of Small Particles in Turbulent Fluid, Johns Hopkins University, Baltimore, Md., report to Mechanics Branch, Office of Naval Research, Washington, D. C.

———, and H. A. Panofsky, 1964, *The Structure of Atmospheric Turbulence*, Interscience Publishers, New York.

MacCready, P. B., Jr., 1962, The Inertial Subrange of Atmospheric Turbulence, *J. Geophys. Res.*, 67(3): 1051-1059.

———, 1964, Mean Wind Speed Measurements in Turbulence, paper presented at the American Meteorological Society National Conference on Micrometeorology, Oct. 13-15, 1964, Salt Lake City, Utah.

———, 1966, Mean Wind Speed Measurements in Turbulence, *J. Appl. Meteorol.*, 5(2): 219-225.

———, and Henry R. Jex, 1964, Response Characteristics and Meteorological Utilization of Propeller and Vane Sensors, *J. Appl. Meteorol.*, 3(2): 182-193.

———, T. B. Smith, and M. A. Wolf, 1961, Vertical Diffusion from a Low Altitude Line Source, Vols. I and II, Meteorology Research, Inc., Altadena, Calif.

McDonald, J. E., 1960, Rates of Descent of Fallout Particles from Thermonuclear Explosions, *J. Meteorol.*, 17(3): 380-381.

———, 1960a, An Aid to Computation of Terminal Velocities of Spheres, *J. Meteorol.*, 17(4): 463-465.

———, 1963, Rain Washout of Partially Wettable Insoluble Particles, *J. Geophys. Res.*, 68(17): 4993-5003.

Machta, L., 1958, Global Scale Dispersion by the Atmosphere, in *Proceedings of the Second United Nations International Conference on the Peaceful Uses of Atomic Energy, Geneva, 1958*. Vol. 18, pp. 519-523, United Nations, New York, 1958.

Magill, P. L., F. R. Holden, C. Ackley (Eds.), 1956, *Air Pollution Handbook*, McGraw-Hill Book Company, Inc., New York.

Markee, E. H., Jr., 1963, On the Relationships of Range to Standard Deviation of Wind Fluctuations, *Monthly Weather Rev.*, 91(2): 83-87.

Marshall, J. S., and W. McK. Palmer, 1948, The Distribution of Raindrops with Size, *J. Meteorol.*, 5(4): 165-166.

Martin, D. O., 1965, U. S. Weather Bureau Air Resources Field Research Office, Robert A. Taft Sanitary Engineering Center, Cincinnati, Ohio, unpublished.

Martin, J. E., 1965, The Correlation of Wind Tunnel and Field Measurements of Gas Diffusion Using Krypton-85 as a Tracer, Michigan Memorial Phoenix Project 272, University of Michigan, Ann Arbor, Mich.

Mason, B. J., 1957, *The Physics of Clouds*, Oxford University Press, London.

May, F. G., 1958, The Washout by Rain of Lycopodium Spores, British Report AERE-HP/R-2198.

Mazzarella, D. A., 1954, Wind-tunnel Tests on Seven Aerovanes, *Rev. Sci. Instr.*, 25: 63-68.

Meade, P. J., 1959, The Effects of Meteorological Factors on the Dispersion of Airborne Material, *Rassegna Internazionale Elettronica e Nucleare, 6 Rassegna, Rome, July, 1959, Atti del Congresso Scientifico, Sezione Nucleare*, Vol. II, pp. 107-130, Comitato Nazionale per le Ricerche Nucleari, Rome.

———, 1960, Meteorological Aspects of the Peaceful Uses of Atomic Energy, Technical Note 33, Part I, WMO-No. 97, TP.41, World Meteorological Organization, Geneva, Switzerland.

———, and F. Pasquill, 1958, A Study of the Average Distribution of Pollution Around Staythorpe, *Intern. J. Air Pollution*, 1(1-2): 60-70.

Megaw, W. J., 1962, The Penetration of Iodine into Buildings, *Intern. J. Air Water Pollution*, 6: 121-128 (March-April).

Merriam, G. R., and E. F. Facht, 1958, Radiation Dose to the Lens in Treatment of Tumors of the Eye and Adjacent Structures, Possibilities of Cataract Formation, *Radiology*, 71: 357-369.

Mickelsen, W. R., 1955, An Experimental Comparison of the Lagrangian and Eulerian Correlation Coefficients in Homogeneous Isotropic Turbulence, *NACA Washington Technical Note* No. 3570, National Advisory Committee for Aeronautics, National Aeronautics and Space Administration.

Middleton, W. E. K., 1965, *A History of Theories of Rain*, Franklin Watts, Inc., New York.

———, and A. F. Spilhaus, 1953, *Meteorological Instruments*, 3rd ed., University of Toronto Press, Toronto, Canada.

Miller, J. E., 1952, A Photographic Technique for Analyzing Turbulent Motions of Air, *Geophysical Research Papers*, No. 19, Report AFCRC-TR-53-9, pp. 293-301, Air Force Cambridge Research Center.

Monin, A. S., 1955, Diffusion with a Finite Speed, *Izvestiya Akademii Nauk SSSR, Seriya Geofizicheskaya*, No. 3, pp. 234-248.

———, 1959, Smoke Propagation in the Surface Layer of the Atmosphere, *Advances in Geophysics*, Vol. 6, pp. 331-344, F. N. Frenkiel and P. A. Sheppard (Eds.), Academic Press Inc., New York.

———, and A. M. Obukhov, 1953, Dimensionless Characteristics of Turbulence in the Layer of Atmosphere near the Ground, *Doklady Akademii Nauk SSSR*, 93: 257-267.

Moore, D. J., 1963, Fluctuations in Short-period Measurements of Surface SO_2 Concentrations, Laboratory Note RD/L/N.72/63, Central Electricity Research Laboratory, Great Britain.

Morton, B. R., 1959, The Ascent of Turbulent Forced Plumes in a Calm Atmosphere, *Intern. J. Air Pollution*, 1(3): 184-197.

_____, 1959a, Forced Plumes, *J. Fluid Mech.*, 5 (Part I): 378-383.

_____, G. I. Taylor, and J. S. Turner, 1956, Turbulent Gravitational Convection from Maintained and Instantaneous Sources, *Proc. Roy. Soc. (London), Ser. A*, 234: 1-23.

Moses, H., and R. Clark, 1956, Report on Biological, Medical, and Biophysics Programs. Part I. Semiannual Report of Radiological Physics Division. Part II. Quarterly Report of Biological and Medical Research Division, pp. 67-80, USAEC Report ANL-5518, Argonne National Laboratory.

_____, and H. G. Daubek, 1961, Errors in Wind Measurements Associated with Tower-mounted Anemometers, *Bull. Am. Meteorol. Soc.*, 42(3): 190-194.

_____, and F. C. Kulhanek, 1962, Argonne Automatic Meteorological Data Processing System, *J. Appl. Meteorol.*, 1(1): 69-80.

_____, and G. H. Strom, 1961, A Comparison of Observed Plume Rises with Values Obtained from Well-known Formulas, *J. Air Pollution Control Assoc.*, 11(10): 455-466.

_____, G. H. Strom, and J. E. Carson, 1964, Effects of Meteorological and Engineering Factors on Stack Plume Rise, *Nucl. Safety*, 6(1): 1-19.

Munn, R. E., and A. F. W. Cole, 1965, Turbulence and Diffusion in the Wake of a Building, paper presented at the First Canadian Conference on Micrometeorology, Toronto, Canada, April 1965.

Myers, R. F., 1952, A Low-level Temperature Sounding for Routine Use, *Bull. Am. Meteorol. Soc.*, 33(1): 7-12.

Nagabhushanaiah, H. S., 1961, Separation Flow Downstream of a Plate Set Normal to the Plane Boundary, Ph.D. Thesis, Colorado State University, Fort Collins, Colo.

National Academy of Sciences—National Research Council, 1961, Effect of Inhaled Radioactive Particles, Publication 848, Committee on the Pathologic Effects of Atomic Radiation.

_____, 1963, The Behavior of Radioactive Fallout in Soils and Plants, Publication 1092, Committee on Effects of Atomic Radiation on Agriculture and Food Supplies.

_____, 1964, Implications to Man of Irradiation by Internally-deposited Strontium-89, Strontium-90 and Cesium-137, Division of Medical Sciences, *Federal Radiation Council*, Washington, D. C.

National Committee on Radiation Protection, 1958, National Bureau of Standards, Handbook 59, *Permissible Dose from External Sources of Ionizing Radiation, Addendum: Maximum Permissible Radiation Exposures to Man.*

National Committee on Radiation Protection and Measurement, 1959, National Bureau of Standards, Handbook 69, *Maximum Permissible Body Burdens and Maximum Permissible Concentrations of Radionuclides in Air and in Water for Occupational Exposure.*

_____, 1962, *Exposure to Radiation in an Emergency*, Report No. 29, University of Chicago, Chicago, Ill.

Newstein, H. (Project Director), 1963, Design and Construction of Meteorological Instrumentation and Observation Systems on the 1,000 Ft Television Tower in Philadelphia, Pennsylvania, Progress Report I, Physics Department, Drexel Institute of Technology, Philadelphia, Penn.

Nickson, J. J., and H. N. Bane, 1959, Physiological Effects of Radiation, *Radiation Hygiene Handbook*, pp. 19-1 to 19-17, McGraw-Hill Book Company, Inc., New York.

Nishiwaka, Y., 1959, On the Method of Estimation of the Population Dose, Population, and Surface Area Covered by the Diffusion of Radioactive Clouds, *J. Atomic Energy Soc., Japan*, 1: 1-23 (translated as USAEC Report AEC-tr-4463).

Nonhebel, G., 1957, Discussion Before the Institute in London, 13th February, 1957, *J. Inst. Fuel*, 30: 336.

_____, 1960, *Recommendations on Heights for New Industrial Chimneys*, Institute of Fuel, London.

Obukhov, A. M., 1941, Distribution of Energy in the Spectrum of Turbulent Current, *Comptes Rendus de l'Academie des Sciences de l'URSS*, 32: 19, and *Izvestiya Akademii Nauk SSSR*, Seriya Geofizicheskaya, Nos. 4-5, pp. 453-466.

_____, 1959, Description of Turbulence in Terms of Lagrangian Variables, *Advances in Geophysics*, Vol. 6, pp. 113-116, F. N. Frenkiel and P. A. Sheppard (Eds.), Academic Press Inc., New York.

Ogura, Y., 1957, The Influence of Finite Observation Intervals on the Measurement of Turbulent Diffusion Parameters, *J. Meteorol.*, 14(3): 176-181.

Okubo, A., 1962, Horizontal Diffusion from an Instantaneous Point-source Due to Oceanic Turbulence, Report 32, Chesapeake Bay Institute, Johns Hopkins University, Baltimore, Md.

Owe Berg, T. G., 1963, *Investigation of Coalescence in Washout*, Report 0780-01(01)QP, Aerojet-General Corporation, Downey, Calif.

Ower, E., 1949, *The Measurement of Air Flow*, Chapman and Hall, Ltd., London.

Pacific Northwest Laboratory, 1967, Pacific Northwest Laboratory Annual Report for 1966 to the USAEC Division of Biology and Medicine. Volume II. Physical Sciences. Part I. Atmospheric Sciences, USAEC Report BNWI-481-1, pp. 43-52, Battelle—Northwest.

Pack, D. H., 1962, Air Trajectories and Turbulence Statistics from Weather Radar Using Tetroons and Radar Transponders, *Monthly Weather Rev.*, 90(12): 491-506.

_____, and J. K. Angell, 1963, A Preliminary Study of Air Trajectories in the Los Angeles Basin as Derived from Tetroon Flights, *Monthly Weather Rev.*, 91(10-11): 583-604.

Panofsky, H. A., 1962, Scale Analysis of Atmospheric Turbulence at 2 Meters, *Quart. J. Roy. Meteorol. Soc.*, 88(375): 57-69.

_____, A. K. Blackadar, and G. E. McVehil, 1960, The Diabatic Wind Profile, *Quart. J. Roy. Meteorol. Soc.*, 86(369): 390-398.

_____, and G. W. Brier, 1958, *Some Applications of Statistics to Meteorology*, Pennsylvania State University, University Park, Penn.

_____, and A. A. Townsend, 1964, Change of Terrain Roughness and the Wind Profile, *Quart. J. Roy. Meteorol. Soc.*, 90(384): 147-155.

Parker, H. M., 1960, Testimony on Radiation Protection Criteria and Standards: Their Basis and

Use, Hearings Before the Special Subcommittee on Radiation, Joint Committee on Atomic Energy, 86th Congress, Superintendent of Documents, U. S. Government Printing Office, Washington, D. C.

Pasquill, F., 1961, The Estimation of the Dispersion of Windborne Material, *Meteorol. Mag.*, 90(1063): 33-49.

_____, 1962, *Atmospheric Diffusion*, D. Van Nostrand Company, Ltd., London.

_____, 1962a, Some Observed Properties of Medium-scale Diffusion in the Atmosphere, *Quart. J. Roy. Meteorol. Soc.*, 88(375): 70-79.

_____, 1963, Atmospheric Turbulence, *Weather*, 28: 233-246.

Passonneau, J. V., A. M. Brues, K. A. Hamilton, and W. E. Kisieleski, 1952, Carcinogenic Effects of Diffuse and Point-source Beta Irradiation on Rat Skin: Final Summary, in Quarterly Report for August, September, and October, 1952; Division of Biological and Medical Research, p. 31, USAEC Report ANL-4932, Argonne National Laboratory.

Patt, H. M., and A. M. Brues, 1954, The Pathological Physiology of Radiation Injury in the Mammal. I. Physical and Biological Factors in Radiation Action, *Radiation Biology*, Chap. 14, A. Hollaender (Ed.), McGraw-Hill Book Company, Inc., New York.

Patterson, J., 1926, The Cup Anemometer, *Trans. Roy. Soc., Canada*, Sect. III, Ser. III, 20: 1-54.

Pearcey, T., and G. W. Hill, 1957, A Theoretical Estimate of the Collection Efficiencies of Small Droplets, *Quart. J. Roy. Meteorol. Soc.*, 83(355): 77-92 and 83(358): 555-556.

Pearson, K. (Ed.), 1951, Tables of the Incomplete Γ-Function, Department of Applied Statistics, University of London, University College, Cambridge, England.

Perkins, R. W., and R. J. Engelmann, 1966, Trace Element and Trace Radionuclide Composition of Snow and Rain, USAEC Report BNWL-SA-650, Battelle-Northwest.

Peterson, J. B., and S. H. J. Womack, 1937, Electrical Thermometers for Aircraft, National Bureau of Standards, Report 606, for National Advisory Committee for Aeronautics, National Aeronautics and Space Administration, Washington, D. C.

Petruska, J. A., H. G. Thode, and R. H. Tomlinson, 1955, The Absolute Fission Yields of Twenty-eight Mass Chains in the Thermal Neutron Fission of U^{235}, *Can. J. Phys.*, 33: 693-705.

Plutonium Project, 1946, Nuclei Formed in Fission; Decay Characteristics Fission Yields and Chain Relationships, *J. Am. Chem. Soc.*, 68: 2411-2442.

Pooler, F., 1965, Potential Dispersion of Plumes from Large Power Plants, Public Health Service Publication No. 999-AP-16, Robert A. Taft Sanitary Engineering Center, Cincinnati, Ohio.

Priestley, C. H. B., 1955, Free and Forced Convection in the Atmosphere near the Ground, *Quart. J. Roy. Meteorol. Soc.*, 81(348): 139-143.

_____, 1956, A Working Theory of the Bent-over Plume of Hot Gas, *Quart. J. Roy. Meteorol. Soc.*, 82(352): 165-176.

_____, 1959, *Turbulent Transfer in the Lower Atmosphere*, University of Chicago Press, Chicago.

_____, and F. K. Ball, 1955, Continuous Convection from an Isolated Source of Heat, *Quart. J. Roy. Meteorol. Soc.*, 81(348): 144-157.

_____, R. A. McCormick, and F. Pasquill, 1958, Turbulent Diffusion in the Atmosphere, Technical Note No. 24, WMO-No. 77. TP. 31, World Meteorological Organization, Geneva, Switzerland.

Randall, D. L., and A. B. J. Clark, 1955, A Radiocommand Control Buffer for Studying Airflow, *Bull. Am. Meteorol. Soc.*, 36(5): 224-227.

Rauch, H., 1962, Zur Schornstein-Ueberhöhung, Bericht des Meteorologischen Institutes an der Technischen Hochschule, Darmstadt, West Germany.

Raynor, G. S., and M. E. Smith, 1964, A Diffusion-deposition Tracer System, USAEC Report BNL-859, Brookhaven National Laboratory.

Record, F. A., 1952, Field Studies of Turbulence and Diffusion, *Geophysical Research Papers, No. 19*, Report AFCRC-TR-53-9, pp. 457-473, Air Force Cambridge Research Center.

_____, and H. E. Cramer, 1957, Preliminary Analysis of Project Prairie Grass Diffusion Measurements, *J. Air Pollution Control Assoc.*, 8(3): 240-248.

Reiter, E. R., 1964, Transport Processes in the Atmosphere Leading to Radioactive Fallout, Technical Paper 58, Progress Report 1, Colorado State University, Fort Collins.

Reynolds, O., 1895, On the Dynamical Theory of Incompressible Viscous Fluids and the Determination of the Criterion, *Phil. Trans. Roy. Soc., London, Ser.* A, 186(Part 1): 123-164.

Richardson, L. F., 1920, I. Some Measurements of Atmospheric Turbulence, *Phil. Trans. Roy. Soc. London, Ser.* A, 221: 1-28.

_____, 1926, Atmospheric Diffusion Shown on a Distance-Neighbour Graph, *Proc. Roy. Soc. (London), Ser.* A, 110: 709-737.

_____, and D. Proctor, 1925, Diffusion over Distances Ranging from 3 to 86 Kilometers, *Mem. Roy. Meteorol. Soc.*, 1(1): 1-16.

Roberts, O. F. T., 1923, The Theoretical Scattering of Smoke in a Turbulent Atmosphere, *Proc. Roy. Soc. (London), Ser.* A, 104: 640-654.

Robinson, E., 1960, Atmospheric Tracer Technique Using Aerosols, paper presented at the Instrument Society of America Conference and Exhibit, San Francisco, Calif.

_____, J. A. MacLeod, and C. E. Lapple, 1959, A Meteorological Tracer Technique Using Uranine Dye, *J. Meteorol.*, 16(1): 63-67.

Robinson, T. R., 1850, Description of an Improved Anemometer for Registering the Direction of the Wind, and the Space Which It Traverses in Given Intervals of Time, *Trans. Roy. Irish Acad.*, 22: 155-178.

Ronne, C., 1959, On a Method of Cloud Measurement for Aircraft Motion Picture Films, Reference 59-29, Woods Hole Oceanographic Institution, Mass., unpublished.

Rosinski, J., 1958, Scavenging of Particulate Matter in Connection with Nuclear-Powered Ships, Report No. 1, Theoretical Dissertation on Diffusion and Deposition of Radioactive Particulate Matter in Connection with Nuclear-powered Ships, USAEC Report AECU-4138, Armour Research

Foundation, Illinois Institute of Technology, Chicago.

Rounds, W., Jr., 1955, Solutions of the Two-dimensional Diffusion Equations, *Am. Geophys. Union Trans.*, 36: 395-405.

Rouse, H., and S. Ince, 1957, History of Hydraulics, Iowa Institute of Hydraulic Research, State University of Iowa. Iowa City.

Rumford, B. T., 1806, Inquiries Concerning the Mode of Propagation of Heat in a Liquid, *Nicholson's Journal*, 14: 355-363.

Rupp, A. F., S. E. Beall, L. P. Bornwasser, and D. H. Johnson, 1948, Dilution of Stack Gases in Cross Winds, USAEC Report AECD-1811 (CE-1620), Clinton Laboratories.

Saffman, P. G., 1962, The Effect of Wind Shear on Horizontal Spread from an Instantaneous Ground Source, *Quart. J. Roy. Meteorol. Soc.*, 88(378): 382-393.

———, 1963, Reply to Discussion, *Quart. J. Roy. Meteorol. Soc.*, 89(380): 293-295.

Saissac, J., 1958, Sur la Diffusion Atmospherique des Particules, *Compt. Rend.*, 247(17): 1371-1374.

Sakagami, J., 1961, Diffusion Experiments Using Balloons, *Nat. Sci. Rep., Ochanomizu Univ., Tokyo*, 12: 1-25.

Saltzman, B. E., A. I. Coleman, and C. A. Clemons, 1966, Halogenated Compounds as Gaseous Meteorological Tracers, *Anal. Chem.*, 38(6): 753-758.

Sanuki, M., 1950, Studies on Biplane Wind Vanes, Ventilator Tubes and Cup Anemometers, Part I, *Papers Meteorol. Geophys. (Tokyo)*, 1(1): 81-132.

———, S. Kimura, and M. Baba, 1960, Wind Tunnel Experiment on Two-directional Wind Vanes, *Papers Meteorol. Geophys. (Tokyo)*, 11(1): 23-29.

Sartor, J. D., I. Katz, and R. E. Katz, 1952, A Mobile Method for Measuring Atmospheric Diffusion, *Bull. Am. Meteorol. Soc.*, 33(5): 188-194.

Schaefer, V. J., 1958, The Use of Silver Iodide as an Air Tracer, *J. Meteorol.*, 15(1): 121-122.

Schlichting, H., 1960, *Boundary Layer Theory*, McGraw-Hill Book Company, Inc., New York.

Schmidt, F. H., 1957, On the Diffusion of Stack Gases in the Atmosphere, *Mededelingen Verhandelingen. Koninklijk Nederlandsch Meteorologisch Instituut*, Serie 102, No. 68.

———, 1960, On the Dependence on Stability of the Parameters in Sutton's Diffusion Formula, *Beiträge zur Physik der Atmosphäre*, 33: 112-122.

———, 1963, Derivation of the Graphs for the Determination of Plume Rise, USAEC Report AEC-tr-6365 (translated from report of Royal Netherland Meteorological Institute, De Bilt).

———, 1965, On the Rise of Hot Plumes in the Atmosphere, *Intern. J. Air Water Pollution*, 9(4): 175-198.

Schmidt, W., 1925, Der Massenaustausch in Freier Luft and Verwandte Erschéinungen, *Probleme der Kosmischen Physik*, Hamburg, Vol. 7, Verlag von Henri Grand.

Schrenk, O., 1929, Über die Trägheitsfehler des Schalenkreuz–Anemometers bei schwankender Windstärke, *Zeitschrift für Technische Physik*, 10(2): 57-66.

Schubauer, G. B., and G. H. Adams, 1954, Lag of Anemometers, National Bureau of Standards, Washington, D. C., unpublished.

Schultz, H. A., 1957, Measurement of Concentrations of Gaseous Halide Tracers in Air by Positive Ion Emission Techniques, *Anal. Chem.*, 29(12): 1840-1842.

Scorer, R. S., 1958, *Natural Aerodynamics*, Pergamon Press, London.

———, 1959, The Behavior of Chimney Plumes, *Intern. J. Air Pollution*, 1(3): 198-220.

———, 1959a, The Rise of Bent-over Hot Plumes, *Advances in Geophysics*, Vol. 6, pp. 399-411, F. N. Frenkiel and P. A. Sheppard (Eds.), Academic Press Inc., New York.

———, 1962, Comment (#11) during Symposium on the Dispersion of Chimney Gases, December 7, 1961, Royal Meteorological Society, *Intern. J. Air Water Pollution*, 6(3-4): 96-99.

———, and C. F. Barrett, 1962, Gaseous Pollution from Chimneys, *Intern. J. Air Water Pollution*. 6(1-2): 49-63.

Scriven, R. A., 1965, Properties of the Most Probable Ground Level Concentration from an Elevated Source, Laboratory Note RD/L/N61/65, Central Electricity Research Laboratory, Great Britain.

Selders, A. A., and F. P. Hungate, 1956, The Foliar Sorption of Iodine by Plants, USAEC Report HW-44890, Hanford Atomic Products Operation.

Sellers, W., 1962, A Simplified Derivation of the Diabatic Wind Profile, *J. Atmospheric Sci.*, 19(2): 180-181.

Shandorov, G. S., 1957, Flow from a Channel into Stationary and Moving Media (in Russian), *Zh. Tekh. Fiz.*, 27(1): 156-179 (1957).

Shapiro, E., J. Gibbs, E. Field, and T. Dillon, 1955, Development of a Tracer Technique, Report AFCRC-TR-55-290, Air Force Cambridge Research Center.

Shaw, Sir Napier, 1942, *Manual of Meteorology*, Vol. IV, Cambridge University Press, Great Britain.

Sheehy, J. P., W. C. Achinger, and R. A. Simon, undated, Handbook of Air Pollution, Robert A. Taft Sanitary Engineering Center, Cincinnati, Ohio.

Sherlock, R. H., and E. A. Stalker, 1941, A Study of Flow Phenomena in the Wake of Smoke Stacks, *Engineering Research Bulletin, No. 29*, Department of Engineering Research, University of Michigan, Ann Arbor, Mich.

———, and M. B. Stout, 1931, An Anemometer for a Study of Wind Gusts, *Engineering Research Bulletin No. 20*, Office of Research Administration, University of Michigan, Ann Arbor, Mich.

Shorr, B., 1952, Studies of Diffusion in the Atmosphere, Progress Report 1, Nucleonics Division, General Electric Company, Hanford, Wash.

———, 1953, Ground Level Concentrations in the Vicinity of a 185 Ft Stack, USAEC Report HW-27781, Hanford Atomic Products Operation.

Silverman, L., 1959, Control of Radioactive Air Pollution, *Radiation Hygiene Handbook*, pp. 22-1 to 22-45, H. Blatz (Ed.), McGraw-Hill Book Company, Inc., New York.

Simpson, C. L., 1961, Some Measurements of the Deposition of Matter and Its Relation to Diffusion from a Continuous Point Source in a Stable Atmosphere, USAEC Report HW-69292 REV, Hanford Atomic Products Operation.

Sims, A. L., E. A. Mueller, and G. E. Stout, 1965, *Investigation of the Quantitative Determination of Point and Areal Precipitation by Radar Echo Measurements*, Final Report, Illinois State Water Survey, University of Illinois, Urbana.

Singer, I. A., I. Kazuhiko, and R. Gonzalez del Campo, 1963, Peak to Mean Pollutant Concentration Ratios for Various Terrain and Vegetation Cover, *J. Air Pollution Control Assoc.*, 13(1): 40-42.

_____, and G. S. Raynor, 1957, Analysis of Meteorological Tower Data, April 1950–March 1952, USAEC Report BNL-461, Brookhaven National Laboratory.

Small, S. H., 1960, Wet and Dry Deposition of Fallout Materials at Kjeller, *Tellus*, 12(3): 308-314.

Smith, F. B., 1957, The Diffusion of Smoke from a Continuous Elevated Point-source into a Turbulent Atmosphere, *J. Fluid Mech.*, 2(Part 1): 49-76.

_____, 1959, The Turbulent Spread of a Falling Cluster, *Advances in Geophysics*, Vol. 6, pp. 193-210, F. N. Frenkiel and P. A. Sheppard (Eds.), Academic Press Inc., New York.

_____, 1961, An Analysis of Vertical Wind-fluctuations at Heights Between 500 and 5,000 Ft., *Quart. J. Roy. Meteorol., Soc.*, 87(372):180-193.

_____, 1962, The Effect of Sampling and Averaging on the Spectrum of Turbulence, *Quart. J. Roy. Meteorol. Soc.*, 88(376): 177-180.

_____, 1962a, The Problem of Deposition in Atmospheric Diffusion of Particulate Matter, *J. Atmospheric Sci.*, 19(5): 429-434.

_____, and P. F. Abbott, 1961, Statistics of Lateral Gustiness at 16 Meters Above the Ground, *Quart. J. Roy. Meteorol. Soc.*, 87(374): 549-561.

_____, and J. S. Hay, 1961, The Expansion of Clusters of Particles in the Atmosphere, *Quart. J. Roy. Meteorol. Soc.*, 87(371): 82-101.

Smith, M. E., 1956, The Variation of Effluent Concentrations from an Elevated Point Source, *A.M.A. Archives of Industrial Health*, 14: 56-68.

_____, 1959, A Potentiometer System for the Continuous Indication or Recording of Wind Direction, *J. Meteorol.*, 16(3): 335-337.

_____, F. E. Bartlett, and G. W. Potts, 1956, Filter Samplers for Field Use, Paper 56-8, *Proceedings of the Air Pollution Control Association, 49th Annual Meeting*, Buffalo, N. Y.

_____, and I. A. Singer, 1965, An Improved Method of Estimating Concentrations and Related Phenomena from a Point Source Emission, USAEC Report BNL-9700, Brookhaven National Laboratory.

_____, I. A. Singer, F. E. Bartlett, and L. Marcus, 1957, The Variation of Effluent Concentrations During Temperature Inversions, *J. Air Pollution Control Assoc.*, 7(3): 194-197.

Smith, T. B., E. K. Kauper, S. Berman, and F. Vukovich, 1964, Micrometeorological Investigation of Naval Missile Facility, Point Arguello, California, Volume I, Analysis, Volume II, Data Supplement, Report MRI64-FR-167, Meteorology Research Inc., Altadena, Calif.

_____, and M. A. Wolf, 1963, Vertical Diffusion from an Elevated Line Source over a Variety of Terrains, Meteorology Research, Inc., Altadena, Calif.

Spencer-Gregory, H. and E. Rourke, 1957, *Hygrometry*, Crosby Lockwood & Sons, Ltd., London.

Spilhaus, A. F., 1934, Analysis of the Cup Anemometer, Meteorological Course, Professional Notes 7, Massachusetts Institute of Technology, Cambridge, Mass.

Staley, D. O., 1956, The Diurnal Temperature Wave for Bounded Eddy Conductivity, *J. Meteorol.*, 13(1): 13-20.

Stern, A. C. (Ed.), 1962, *Air Pollution*, Vol. 1, pp. 118-195, Academic Press Inc., New York.

Stewart, N. G., H. J. Gale, and R. N. Crooks, 1954, The Atmospheric Diffusion of Gases Discharged from the Chimney of the Harwell Pile (BEPO), British Report AERE HP/R-1452.

_____, H. J. Gale, and R. N. Crooks, 1958, The Atmospheric Diffusion of Gases Discharged from the Chimney of the Harwell Reactor BEPO, *Intern. J. Air Pollution*, 1(1-2): 87-102(1958).

Strom, G. H., 1962, Atmospheric Dispersion of Stack Effluents, *Air Pollution*, Vol. 1, Chapter 6, pp. 118-195, A. C. Stern (Ed.), Academic Press Inc., New York.

Stümke, H., 1961, Zur Berechnung der Aufstiegshöhe von Rauchfahnen, *VDI-Forschungsh.*, 27: 38-43.

_____, 1963, Vorschlag einer empirischen Formel für die Schornsteinüberhöhung im AnschuluB und eine Überprüfung bekannter Formeln mit zusätzlichem Beobachtungs-material, Dem AusschuB II der VDI-Kommission "Reinhaltung der Luft" vorgelegt als wissenschaftliches Gutachten, Institut für Gasströmungen der Technischen Hochschule, Stuttgart, West Germany.

Sutton, O. G., 1932, A Theory of Eddy Diffusion in the Atmosphere, *Proc. Roy. Soc. (London), Ser. A*, 135: 143-165.

_____, 1949, *The Science of Flight*, Penguin Books Inc., Baltimore, Maryland.

_____, 1950, The Dispersion of Hot Gases in the Atmosphere, *J. Meteorol.*, 7(5): 307-312.

_____, 1953, *Micrometeorology*, McGraw-Hill Book Company, Inc., New York.

Swanson, R. N., and H. E. Cramer, 1965, A Study of Lateral and Longitudinal Intensities of Turbulence, *J. Appl. Meteorol.*, 4(3): 409-417.

Tanner, C. B., 1963, Basic Instrumentation and Measurements for Plant Environment and Micrometeorology, *Soils Bulletin 6*, University of Wisconsin, Madison, Wis.

Taylor, G. I., 1921, Diffusion by Continuous Movements, *Proc. London Math. Soc.*, [2]20: 196-202.

_____, 1938, The Spectrum of Turbulence, *Proc. Roy. Soc. (London), Ser. A*, 164: 453-465.

Taylor, J. H. (Ed.), 1965, Project Sand Storm, An Experimental Program in Atmospheric Diffusion, *Environmental Research Papers, No. 134*, Report AFCRL-65-649, Air Force Cambridge Research Laboratories.

_____, J. V. Nou, and G. L. Tucker, 1964, Preliminary Report on Project Sand Storm, Air Force Cambridge Research Laboratories.

Tchen, C. M., 1947, Mean Value and Correlation Problems Connected with the Motion of Small Particles Suspended in a Turbulent Fluid, *Mededelingen No. 51*, Lab. voor Aero-en Hydrodynamica der Technische Hogeschool, Delft, Netherlands.

Telegadas, K., and K. M. Nagler, 1960, Fallout Patterns from Operation Hardtack, Phase II, Weather Bureau, Washington, D. C.

Television Digest Inc., 1966, *Television Fact Book*, Washington, D. C.

Thomas, F. W., 1954, TVA Air Pollution Studies, *Air Repair*, 4: 7-12.

———, S. B. Carpenter, and F. E. Gartrell, 1963, Stacks—How High? *J. Air Pollution Control Assoc.*, 13(5): 198-204.

Thomas, R. G., 1965, Transport of Relatively Insoluble Materials from Lung to Lymph Nodes, Lovelace Foundation for Medical Education and Research, Albuquerque, N. Mex.

Thompson, N., 1962, Intensities and Spectra of Vertical Wind Fluctuations at Heights Between 100 and 500 Ft in Neutral and Unstable Conditions, *Quart. J. Roy. Meteorol. Soc.*, 88(377): 328-334.

Townsend, A. A., 1956, *The Structure of Turbulent Shear Flow*, Cambridge University Press, Great Britain.

Trimmer, J. D., 1950, *Response of Physical Systems*, John Wiley & Sons, Inc., New York.

Turk, A., S. M. Edmonds, H. Mark, G. F. Collins, and F. Bartlett, 1965, Use of Gas Tracers for Meteorological Studies, paper presented at American Chemical Society, Division of Water, Air, and Waste Chemistry, meeting held in Detroit, Mich., on April 5, 1965.

Turner, D. B., 1964, A Diffusion Model for an Urban Area, *J. Appl. Meteorol.*, 3(1): 83-91.

———, 1967, Workbook of Atmospheric Dispersion Estimates, Public Health Service Publication 999-AP-26, Robert A. Taft Sanitary Engineering Center, Cincinnati, Ohio.

United Nations, 1958, Report of the United Nations Scientific Committee on the Effects of Atomic Radiation, United Nations General Assembly, Official Records: 13th Session Supplement No. 17 (A/3838).

———, 1962, Report of the United Nations Scientific Committee on the Effects of Atomic Radiation, United Nations General Assembly, Official Records: 17th Session Supplement No. 16 (A/5216).

U. S. Atomic Energy Commission, 1961, *Atomic Energy Research: Life and Physical Sciences, Reactor Development, Waste Management*, Superintendent of Documents, U. S. Government Printing Office, Washington, D. C.

U. S. Weather Bureau, 1953: A Meteorological Survey of the Oak Ridge Area: Final Report Covering the Period 1948-52, USAEC Report ORO-99, Weather Bureau, Oak Ridge, Tenn.

———, 1955, Meteorology and Atomic Energy, USAEC Report AECU-3066.

Van der Hoven, I., 1963, A Diffusion-deposition Model for Particulate Effluents from Ground-tested Nuclear Engines, *Intern. J. Air and Water Pollution*, 7(11-12), pp. 1023-1032.

Van Vleck, L. D., and F. W. Boone, 1964, Rocket Exhaust Cloud Rise and Size Studies Hot Volume Sources, paper presented at the 225th National Meeting of the American Meteorological Society, January 29-31, 1964, Los Angeles, Calif.

Velez, C., 1961, Effect of the Height of the Source of Fission Products from a Small or Medium Power Reactor, in *Small and Medium Power Reactors*, Vol. II, Conference Proceeding, Vienna, 1960, pp. 95-107, International Atomic Energy Agency, Vienna (STI/PUB/30).

Wald, N., 1958, Leukemia in Hiroshima City Atomic Bomb Survivors, *Science*, 127(3300): 699-700.

Walker, E. R., 1963, Atmospheric Turbulence Characteristics Measured at Suffield Experimental Station, Defence Research Board Project No. D52-32-01-04, Suffield Experimental Station, Department of National Defence of Canada.

Walton, W. and A. Woolcock, 1960, The Suppression of Airborne Dust by Water Spray, *Aerodynamic Capture of Particles*, E. G. Richardson (Ed.), Pergamon Press, New York.

War Department, 1944, Generator, Smoke, Mechanical, M2 (50 Gallon) M3A2, Report TM 3-381, Washington, D. C.

Warnick, C. C., 1956, Influence of Wind on Precipitation Measurements at High Altitudes, Bulletin 10, University of Idaho Engineering Experiment Station, University of Idaho, Moscow, Idaho.

Warren, S., 1956, Longevity and Causes of Death from Irradiation in Physicians, *J. Am. Med. Assoc.*, 162: 464-468.

Way, K., and E. P. Wigner, 1948, The Rate of Decay of Fission Products, *Phys. Rev.*, 73: 1318-1330.

———, and E. P. Wigner, 1951, Rate of Decay of Fission Products, Paper 43 in *Radiochemical Studies: The Fission Products*, Book 1, edited by C. D. Coryell and N. Sugarman, National Nuclear Energy Series, Division 9, Volume 9, pp. 436-458, McGraw-Hill Book Company, Inc., New York.

Webb, E. K., 1962, Thermal Convection with Wind Shear, *Nature*, 193(4817): 840-842.

Webster, F. X., and F. S. Duckworth, 1959, Comparative Atmospheric Travel of a Gas and an Aerosol, paper presented at 177th National Meetinf of the American Meteorological Society, San Diego, Calif.

West, P. W., and G. C. Gaeke, 1956, Fixation of Sulfur Dioxide as Disulfitomercurate (II) and Subsequent Colorimetric Estimation, *Anal. Chem.*, 28(12): 1816-1819.

Wholers, H. C., C. E. Lapple, T. E. Kass, and K. R. Johnson, 1959, Fluorescent Dyes as Airborne Tracer Materials, paper presented at the Third Pacific Area National Meeting of the American Society for Testing Materials, San Francisco, Calif.

Wilkins, E. M., 1958, Observations on the Separations of Pairs of Neutral Balloons and Applications to Atmospheric Diffusion Theory, *J. Meteorol.*, 15(3): 324-327.

Willard, D. H., and W. J. Bair, 1958, Behaviour of I^{131} Following Its Inhalation as a Vapor and as a Particle, USAEC Report HW-58221, Hanford Atomic Products Operation.

Wippermann, F., 1961, Die Maximal-Konzentrationen eims sich in Turbulenter Strömung Ausbreitenden Gases, *Intern. J. of Air and Water Pollution*, 4(1-2): 1-23.

———, P. Gburcik, and W. Klug, 1962, On the Eulerian and Lagrangian Statistics of Very Large-scale Atmospheric Motions, *Technical Note* 1, Institut fuer Meteorologie, Technische Hochschule, Darmstadt, West Germany.

World Health Organization, 1957, *Effect of Radiation on Human Heredity*, World Health Organization, Geneva, Switzerland.

Wyckoff, H. O., 1959, Radiation Attenuation Data, *Radiation Hygiene Handbook*, pp. 8-1 to 8-69, H. Blatz (Ed.), McGraw-Hill Book Company, Inc., New York.

Yaffe, C. D., D. H. Byers, and A. D. Hosey (Eds.), 1956, *Encyclopedia of Instrumentation for Industrial Hygiene*, Institute of Industrial Health, University of Michigan, Ann Arbor, Mich.

Yaglom, A. M., 1965, Lagrangian Properties of Turbulence in a Diabatic Surface Layer and in Convective Jets, *Bull. Acad. Sci. USSR, Atmospheric and Oceanic Physics*, 1: 94-99 (English translation of *Izvestiya Akademii Nauk SSSR, Fizika Atmosfery I Okeana*, 1(2): 157-166).

Yamamoto, G., 1959, Theory of Turbulent Transfer in Non-neutral Conditions, *J. Meteorol. Soc. Japan*, 37(2): 60-70.

Yanskey, G. R., and N. F. Islitzer, 1962, The Area Within a Specified Isopleth of Air Concentration from Continuous Point Sources, Weather Bureau, Idaho Falls, Idaho, unpublished.

Yudine, M. I., 1946, Physical Mean-forming and the Laws of Turbulent Diffusion, *Comptes Rendus de l'Academie des Sciences de l'URSS*, 51: 103-106.

———, 1959, Physical Considerations on Heavy-particle Diffusion, *Advances in Geophysics*. Vol. 6, F. N. Frenkiel and P. A. Sheppard (Eds.), Academic Press Inc., New York.

Zimmerman, S. P., and K. S. W. Champion, 1963, Transport Processes in the Upper Atmosphere, *J. Geophys. Res.*, 68(10): 3049-3056.

Name Index

NAME INDEX

Subject Index

☆U.S. GOVERNMENT PRINTING OFFICE: 1978-740-306/276 REGION NO. 4

Notes

U. S. DEPARTMENT OF ENERGY CRITICAL REVIEW SERIES

As a continuing series of state-of-the-art studies published by the DOE Technical Information Center, the critical reviews are designed to evaluate the existing state of knowledge in a specific and limited field of interest, to identify significant developments, both published and unpublished, and to synthesize new concepts out of the contributions of many.

SOURCES OF TRITIUM AND ITS BEHAVIOR UPON RELEASE TO THE ENVIRONMENT
December 1968 (TID-24635) $6.00
D. G. Jacobs
Oak Ridge National Laboratory

REACTOR-NOISE ANALYSIS IN THE TIME DOMAIN
April 1969 (TID-24512) $6.00
Nicola Pacilio
Argonne National Laboratory
and Comitato Nazionale
per l'Energia Nucleare

PLUME RISE
November 1969 (TID-25075) $6.00
G. A. Briggs
Environmental Science Services
Administration

ATMOSPHERIC TRANSPORT PROCESSES
Elmar R. Reiter
Colorado State University
Part 1: Energy Transfers and Transformations
December 1969 (TID-24868) $6.00
Part 2: Chemical Tracers
January 1971 (TID-25314) $6.00
Part 3: Hydrodynamic Tracers
May 1972 (TID-25731) $3.00

THE ANALYSIS OF ELEMENTAL BORON
November 1970 (TID-25190) $3.00
Morris W. Lerner
New Brunswick Laboratory

AERODYNAMIC CHARACTERISTICS OF ATMOSPHERIC BOUNDARY LAYERS
May 1971 (TID-25465) $3.00
Erich J. Plate
Argonne National Laboratory
and Karlsruhe University

NUCLEAR-EXPLOSION SEISMOLOGY
September 1971 (TID-25572) $3.00
Howard C. Rodean
Lawrence Livermore Laboratory

BOILING CRISIS AND CRITICAL HEAT FLUX
August 1972 (TID-25887) $3.00
L. S. Tong
Westinghouse Electric Corporation

NEPTUNIUM-237 PRODUCTION AND RECOVERY
October 1972 (TID-25955) $3.00
Wallace W. Schulz and Glen E. Benedict
Atlantic Richfield Hanford Company

THE KINETICS OF THE OXIDATION–REDUCTION REACTIONS OF URANIUM, NEPTUNIUM, PLUTONIUM, AND AMERICIUM IN AQUEOUS SOLUTIONS
August 1975 (TID-26506) $5.45
T. W. Newton
Los Alamos Scientific Laboratory

PARTICLE-TRANSPORT SIMULATION WITH THE MONTE CARLO METHOD
October 1975 (TID-26607) $5.45
L. L. Carter and E. D. Cashwell
Los Alamos Scientific Laboratory

THE CHEMISTRY OF AMERICIUM
October 1976 (TID-26971) $6.00
Wallace W. Schulz
Atlantic Richfield Hanford Company

ICHIBAN: RADIATION DOSIMETRY FOR THE SURVIVORS OF THE BOMBINGS OF HIROSHIMA AND NAGASAKI
March 1977 (TID-27080) $4.75
John A. Auxier
Oak Ridge National Laboratory

AN INTRODUCTION TO TRAPPED-PARTICLE INSTABILITY IN TOKAMAKS
July 1977 (TID-27157) $4.75
Wallace M. Manheimer
Naval Research Laboratory

Available from the National Technical Information Service, U. S. Department of Commerce, Springfield, Virginia 22161.